

Contents

No. 1 JANUARY 1968

JULIAN J. BAUMEL AND LEROY GERCHMAN. The Avian Inter-carotid Anastomosis and its Homologue in other Vertebrates	1
RALPH M. STEINMAN. An Electron Microscopic Study of Ciliogenesis in Developing Epidermis and Trachea in the Embryo of <i>Xenopus laevis</i>	19
BRIAN CORRIN AND KURT ATERMAN. The Pattern of Glycogen Distribution in the Liver	57
WILLIAM K. ELWOOD AND MAURICE H. BERNSTEIN. The Ultrastructure of the Enamel Organ Related to Enamel Formation	73
TREVOR HEATH. Origin and Distribution of Portal Blood in the Sheep	95
ARTHUR T. HERTIG. The Primary Human Oocyte: Some observations on the fine structure of Balbiani's vitelline body and the origin of the annulate lamellae	107
TSUYOSHI ISHII AND REINHARD L. FRIEDE. Tissue Binding of Tritiated Norepinephrine in Pigmented Nuclei of Human Brain	139
G. KARPATI AND W. KING ENGEL. Histochemical Investigation of Fiber Type Ratios with the Myofibrillar ATP-ASE Reaction in Normal and Denervated Skeletal Muscles of Guinea Pig	145
E. L. RODRÍGUEZ ECHANDÍA, R. S. PIEZZI AND E. M. RODRÍGUEZ. Dense-core Microtubules in Neurons and Gliocytes of the Toad <i>Bufo arenarum</i> Hensel	157

No. 2 MARCH 1968

THOMAS M. CRISP AND HENRY C. BROWNING. The Fine Structure of Corpora Lutea in Ovarian Transplants of Mice Following Luteotrophin Stimulation	169
F. O. SIMPSON AND D. G. RAYNS. The Relationship Between the Transverse Tubular System and Other Tubules at the Z Disc Levels of Myocardial Cells in the Ferret	193

- DON M. LONG, THOMAS S. BODENHEIMER, J. FRANCIS HARTMANN AND IGOR KLATZO. Ultrastructural Features of the Shark Brain
- Y. CLERMONT AND E. BUSTOS-OBREGON. Re-examination of Spermatogonial Renewal in the Rat by Means of Seminiferous Tubules Mounted "in toto"
- T. S. BODENHEIMER AND M. W. BRIGHTMAN. A Blood-Brain Barrier to Peroxidase in Capillaries Surrounded by Perivascular Spaces
- KIMIE FUKUYAMA AND WILLIAM L. EPSTEIN. Protein Synthesis Studied by Autoradiography in the Epidermis of Different Species
- EDWARD C. ROOSEN-RUNGE AND JEAN LEIK. Gonocyte Degeneration in the Postnatal Male Rat
- JOANNA JENSEN HILL AND NANCY E. HENDERSON. The Vascularization of the Hypothalamic-Hypophyseal Region of the Eastern Brook Trout, *Salvelinus fontinalis*
- PASKO RAKIC AND RICHARD L. SIDMAN. Subcommissural Organ and Adjacent Ependyma: Autoradiographic study of their origin in the mouse brain
- DAVID N. MENTON. The Effects of Essential Fatty Acid Deficiency on the Skin of the Mouse
- MICHAEL N. SHERIDAN AND RUSSEL J. REITER. The Fine Structure of the Hamster Pineal Gland
- JOHN YOUSON AND H. VAN HEYNINGEN. Dense Granules (Lysosomes?) and Crystals in the Thyroids of Senile Rats ...
- RUTH GUSSEN. Articular and Internal Remodeling in the Human Otic Capsule

No. 3 MAY 1968

- ALLEN C. ENDERS. Fine Structure of Anchoring Villi of the Human Placenta
- ALLEN C. ENDERS AND WILLIAM A. WIMSATT. Formation and Structure of the Hemodichorial Chorio-allantoic Placenta of the Bat (*Myotis lucifugus lucifugus*)
- WILLIAM PARRY. The Embryonic Origin of the Abdominal (Ventrolateral) Musculature in the Albino Rat

CONTENTS

v

WILLIAM P. JOLLIE. Changes in the Fine Structure of the Parietal Yolk Sac of the Rat Placenta with Increasing Gestational Age	513
JOHN SCOTT MCKIBBEN AND ROBERT GETTY. A Comparative Morphologic Study of the Cardiac Innervation in Domestic Animals. I. The Canine	533
JOHN SCOTT MCKIBBEN AND ROBERT GETTY. A Comparative Morphologic Study of the Cardiac Innervation in Domestic Animals. II. The Feline	545
F. P. MOSS. The Relationship between the Dimensions of the Fibres and the Number of Nuclei during Normal Growth of Skeletal Muscle in the Domestic Fowl	555
F. P. MOSS. The Relationship between the Dimensions of the Fibres and the Number of Nuclei during Restricted Growth, Degrowth and Compensatory Growth of Skeletal Muscle	565
PALLE GAD AND SAM L. CLARK, JR. Involution and Regeneration of the Thymus in Mice, Induced by Bacterial Endotoxin and Studied by Quantitative Histology and Electron Microscopy	573
LYNN H. LARKIN AND RICHARD L. SCHULTZ. Histochemical and Autoradiographic Studies of the Formation of the Metrial Gland in the Pregnant Rat	607
BRIAN D. JOHNSTON. Nerve Endings in the Human Endocardium	621
ROGER O. LAMBSON AND JEROME E. COHN. Ultrastructure of the Lung of the Goose and its Lining of Surface Material	631
INDEX TO VOLUME 122	651

The Avian Intercarotid Anastomosis and its Homologue in other Vertebrates¹

JULIAN J. BAUMEL AND LeROY GERCHMAN²

Department of Anatomy
Creighton University School of Medicine, Omaha, Nebraska

ABSTRACT Intrasphenoid and intrasellar segments of the cerebral carotid arteries were dissected in 82 specimens of birds, representing 21 avian orders. The configuration and branching of these carotid segments and the intercarotid anastomosis were observed.

A well developed intercarotid anastomosis unites the two carotids directly caudal to the hypophysis in all birds examined except for five specimens of passeriform birds of the Suborder Tyranni. Three principal patterns occur: an H-type having a lengthy transverse anastomosis connecting the carotids; an X-type with the carotids anastomosing side-to-side; and an I-type with the carotids merged into a single longitudinal vessel. Patterns for each species are illustrated.

Since ordinarily birds lack a cerebral arterial circle comparable to that of mammals, the intercarotid anastomosis obviously serves as its substitute. Evidence of correlation between asymmetry of caudal rami of the cerebral carotids and form of the intercarotid anastomosis is presented.

A communication between cerebral carotids caudal to the hypophysis seems to be a deep-rooted vertebrate characteristic. An intercarotid anastomosis, apparently homologous to that of birds, occurs in a number of cartilaginous fishes, reptiles, and mammals. In mammals the intercarotid anastomosis is a communication between right and left posterior hypophyseal arteries.

Although the cervical and intracranial segments of the cerebral carotid arteries of birds have been studied extensively, the intrasphenoid segment of these arteries has received relatively little notice. The intrasphenoid carotid is interesting in that apparently most birds display some sort of intercarotid anastomosis, uniting the two carotids, placing them into open communication with one another directly caudal to the hypophysis. This anastomosis occurs either within the basis cranii or in the hypophyseal fossa of the cranial cavity. A connection between the cerebral carotids in this location appears to be a deep-rooted vertebrate characteristic, existing in representatives of other vertebrate classes (see Discussion).

The intercarotid anastomosis of birds permits one to inject the cervical portion of one carotid and routinely achieve bilateral filling of both the intra- and extracranial arteries via the anastomosis. Not only will the contralateral cranial arteries be filled, but in bicarotid birds the injection mass will flow recurrently in the other carotid to the aorta and the arteries of neck, trunk, and appendages.

This investigation is an outgrowth of a previous comparative study of the cerebral arteries of birds (Baumel, '67) in which essentially the same series of specimens were further dissected and studied. In addition to consideration of the intercarotid anastomosis, observations were made of the root(s) of the basilar artery, the external ophthalmic, sphenomaxillary, palatine, and internal ophthalmic branches of the internal carotid. The manner of origin of the basilar artery seems to be correlated with the intercarotid anastomosis. The last four mentioned branches of the internal carotid appear to be important channels of communication between intra- and extracranial arterial systems and will be treated in a separate paper.

HISTORY

Descriptions of the avian intercarotid anastomosis mostly have been incidental to studies of the hypophysis cerebri. Previously only three workers have compared

¹ This investigation was supported by PHS Research grant HE 05620-0251, National Heart Institute, Public Health Service.

² Present address: Department of Anatomy, Michigan State University, East Lansing, Michigan.

seal transverse anastomosis" (Assenmacher, '52). The true *internal ophthalmic artery*, when present in adult birds, is emitted from the intrasellar part of the cerebral carotid (Hafferl, Hughes, Wingstrand, Assenmacher).

This study is based on dissections of 82 specimens of birds representing 21 of the 26-28 usually recognized avian orders. A list of the species and numbers of specimens of each are set down in "Observations." All were adult in size except for immature specimens of the ostrich and rhea. The dissection procedure involved careful removal of brain by dorsal approach to expose the region of the sella turcica, leaving cranial and caudal rami of the cerebral carotids and the basilar artery in place on the floor of the cranial cavity. A drawing was made of the above arteries *in situ*. The next step was removal of the diaphragma sellae and dorsum sellae, exposing hypophysis, intrasellar portions of the carotids, intercarotid anastomosis and related cavernous venous sinuses. From this point the cerebral carotids on both sides were traced caudally in their intrasphenoid extents by excision of the inner table of bone of the middle and posterior cranial fossae, displaying the osseous carotid canal. The canal itself was opened, the cerebral carotids being traced posterolaterally to the external orifice of the canal where the external ophthalmic artery arises from the internal carotid. The external ophthalmic was secured and traced for a distance in its bony canal arching superior to the oval fenestra and columella. The above procedure necessitated destruction of much of the inner ear region. A second annotated drawing of each specimen was then made of the main branches, configuration, and relative sizes of the intercarotid anastomosis, the cerebral carotids with their principal intrasphenoid branches, and the root of the external ophthalmic artery.

The arteries of some of the specimens had been injected with neoprene latex. Many of the uninjected specimens had been fixed and stored in alcohol, rendering the vessels extremely friable, limiting the amount of manipulation possible during dissection. In uninjected specimens the arteries were differentiated from surround-

ing tissues by applying Mallory's aniline blue collagen stain, rinsing off the excess with tap water. This technique proved particularly helpful, especially with smaller specimens.

Most of the actual dissections were performed by the second author; observations, drawings, and annotations were joint efforts of both authors.

OBSERVATIONS

Carotid canal. Not only does the facial skeleton of birds demonstrate a remarkable range of shapes, but the neurocranium as well exhibits extremes of structural adaptations in relation to posture of the head and brain shape (see Cobb, '60; Duijm, '51). The basis cranii of most birds is transversed by a long, tubular osseous carotid canal (See Wingstrand, *op. cit.* for exceptions) whose external (caudal) orifice is usually located medial or posteromedial to the inferior margin of the external auditory meatus. The internal (rostral) end of each canal opens into the caudolateral angle of the floor of the sella turcica; however, in some birds (*Columba*, *Larus*, *Pelecanus*, *Falco*) the right and left canals fuse into a common canal which enters the median caudal aspect of the floor of the sella (fig. 1). The external end of the carotid canal develops in the suture between the exoccipital and basiparasphenoid bones, traversing the parasphenoid supported between inner and outer tables of bone by trabeculae of pneumatized cancellous bone. Jollie ('57) describes the development of the floor of the skull of the chicken, including remarks on formation of the sella turcica and carotid canals.

The length, form, and other features of the carotid canal vary, being dependent on the form of the skull base; this accounts for the diversity of patterns of the intrasphenoid portions of the carotids illustrated in this paper (figs. 3, 4, 5.). Likewise, the sella turcica is highly variable among the different groups of birds. For example, in certain birds (*Columba*, *Gavia*, *Buteo*, *Dendrocopos*, *Gallus*) the dorsum sellae is osseous; in other species (*Megaceryle*, *Chordeiles*) the dorsum sellae is fibrous, having a transverse bar of bone connecting the two sides at its superior margin. In yet other species (*Progne*, *Pipra*, *Elanoides*)

the anastomoses in series of different birds: Barkow (1829) set up four categories of intercarotid anastomoses of 14 species representative of 11 orders. Wingstrand's significant work ('51) on the structure of and development of the avian pituitary refers to the intercarotid anastomosis as "characteristic of birds." He summarizes the adult configuration of the anastomosis in more than 20 genera of a dozen orders of birds, describing three types. Unfortunately Barkow did not illustrate his findings; Wingstrand has drawn the anastomosis of several of his species. Green ('51) states that all birds investigated by him (5 species from four orders) were characterized by a broad H-shaped anastomosis of the carotids behind the pars distalis of the hypophysis.

Notwithstanding the apparent general occurrence of the intercarotid anastomosis in members of Class Aves, a number of works on avian vasculature neglect to mention its existence. The earliest account available referring to the anastomosis is Tiedemann's (1810). Studying wax injected specimens of a hawk, chicken, goose, and swan he observed in the sella turcica union of the brain artery of one side with that of the other side. Bauer (1825), a contemporary of Tiedemann, indicated the presence of the anastomosis in a species each of duck and hawk. The work of Barkow was cited above.

Other authors have dealt in a limited way with the intercarotid anastomosis of adult birds in descriptions of the carotids of birds collectively or of individual species; these follow in chronological order: Klinckowström (1890); Gadow (1895); Hofmann ('00); Hafferl ('21, '33); Shiina and Miyata ('32); Ask-Upmark ('35); Sapy ('41); Assenmacher ('53); Westpfahl ('61); Baumel ('62); Kitch ('62); Vitums *et al.* ('64, '65); and Cralley ('65). Starck ('55) described the anastomosis of the carotids in the fossil birds, *Diornis* and *Aepyornis* from markings in the skull base.

The course, relationships, and branching of the intrasphenoid segment of the internal carotids were presented by Gadow, Wingstrand, Assenmacher, and Vitums *et al.* (all cited above).

The two most outstanding works on the detailed embryonic development of the intercarotid anastomosis of birds are those of Rost ('40) for the pigeon and of Vitums and co-workers ('66) for the sparrow (see Discussion). Some attention to the early development of the anastomosis in other species is given by Hafferl ('21), Wingstrand (*op. cit.*) and Atwell ('39). Hughes' classic work ('34) on the development of the head vessels in the chick does not deal with the anastomosis.

TERMINOLOGY, MATERIALS AND METHODS

The common carotid artery of birds is a short vessel in the root of the neck. The internal (dorsal) carotid artery arises from the common carotid, ascending the intermediate length of the neck in the cervical carotid (hypophyseal) canal, an osseofibromuscular passage on the ventral aspect of the cervical vertebrae (Baumel, '64). Leaving the canal below the skull base, the internal carotid is located dorsal to the cervical viscera. Starting with this part of the artery Assenmacher ('53) defines its three distal segments as *retropharyngeal*, *intrasphenoid*, and *intracranial*—all self-explanatory. Wingstrand describes an *intrasellar* part of the internal carotids since these vessels first enter the cranial cavity in the sella turcica (hypophyseal fossa).

Just below its external orifice, or upon entering the cranial carotid canal (parabasal canal, Kesteven, '25) in the basis cranii, the internal carotid gives off the external ophthalmic (stapedial) artery. Following Barkow, Ask-Upmark, and Kitch, the cerebral carotid artery is the internal carotid distal to origin of the external ophthalmic artery. The palatine (sphenoid, Vidian) artery and the sphenomaxillary artery are branches of the intrasphenoid part of the cerebral carotid. Even though the maxillary artery has a palatine branch, it seems advisable to employ the term, palatine artery, since in many birds it is the companion of the palatine ramus of the facial nerve.

The intercarotid anastomosis of birds has also been designed as A. intercarotica (Sapy; Westpfahl), the intercarotic anastomosis (Wingstrand), and "subhypophy-

seal transverse anastomosis" (Assenmacher, '52). The true internal ophthalmic artery, when present in adult birds, is emitted from the intrasellar part of the cerebral carotid (Hafferl, Hughes, Wingstrand, Assenmacher).

This study is based on dissections of 82 specimens of birds representing 21 of the 26-28 usually recognized avian orders. A list of the species and numbers of specimens of each are set down in "Observations." All were adult in size except for immature specimens of the ostrich and rhea. The dissection procedure involved careful removal of brain by dorsal approach to expose the region of the sella turcica, leaving cranial and caudal rami of the cerebral carotids and the basilar artery in place on the floor of the cranial cavity. A drawing was made of the above arteries *in situ*. The next step was removal of the diaphragma sellae and dorsum sellae, exposing hypophysis, intrasellar portions of the carotids, intercarotid anastomosis and related cavernous venous sinuses. From this point the cerebral carotids on both sides were traced caudally in their intrasphenoid extents by excision of the inner table of bone of the middle and posterior cranial fossae, displaying the osseous carotid canal. The canal itself was opened, the cerebral carotids being traced posterolaterally to the external orifice of the canal where the external ophthalmic artery arises from the internal carotid. The external ophthalmic was secured and traced for a distance in its bony canal arching superior to the oval fenestra and columella. The above procedure necessitated destruction of much of the inner ear region. A second annotated drawing of each specimen was then made of the main branches, configuration, and relative sizes of the intercarotid anastomosis, the cerebral carotids with their principal intrasphenoid branches, and the root of the external ophthalmic artery.

The arteries of some of the specimens had been injected with neoprene latex. Many of the uninjected specimens had been fixed and stored in alcohol, rendering the vessels extremely friable, limiting the amount of manipulation possible during dissection. In uninjected specimens the arteries were differentiated from surround-

ing tissues by applying Mallory's aniline blue collagen stain, rinsing off the excess with tap water. This technique proved particularly helpful, especially with smaller specimens.

Most of the actual dissections were performed by the second author; observations, drawings, and annotations were joint efforts of both authors.

OBSERVATIONS

Carotid canal. Not only does the facial skeleton of birds demonstrate a remarkable range of shapes, but the neurocranium as well exhibits extremes of structural adaptations in relation to posture of the head and brain shape (see Cobb, '60; Duijm, '51). The basis cranii of most birds is transversed by a long, tubular osseous carotid canal (See Wingstrand, *op. cit.* for exceptions) whose external (caudal) orifice is usually located medial or posteromedial to the inferior margin of the external auditory meatus. The internal (rostral) end of each canal opens into the caudolateral angle of the floor of the sella turcica; however, in some birds (*Columba*, *Larus*, *Pelecanus*, *Falco*) the right and left canals fuse into a common canal which enters the median caudal aspect of the floor of the sella (fig. 1). The external end of the carotid canal develops in the suture between the exoccipital and basiparasphenoid bones, traversing the parasphenoid supported between inner and outer tables of bone by trabeculae of pneumatized cancellous bone. Jollie ('57) describes the development of the floor of the skull of the chicken, including remarks on formation of the sella turcica and carotid canals.

The length, form, and other features of the carotid canal vary, being dependent on the form of the skull base; this accounts for the diversity of patterns of the intrasphenoid portions of the carotids illustrated in this paper (figs. 3, 4, 5.). Likewise, the sella turcica is highly variable among the different groups of birds. For example, in certain birds (*Columba*, *Gavia*, *Buteo*, *Dendrocopos*, *Gallus*) the dorsum sellae is osseous; in other species (*Megasceryle*, *Chordeiles*) the dorsum sellae is fibrous, having a transverse bar of bone connecting the two sides at its superior margin. In yet other species (*Progne*, *Pipra*, *Elaenia*)

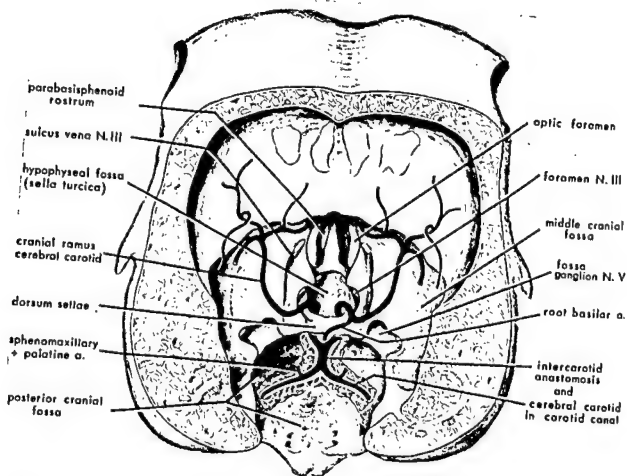


Fig. 1. Intercarotid anastomosis and cerebral carotids *in situ*. *Columba* (pigeon); calvaria removed; caudodorsal aspect of cranial cavity. Inferior part of dorsum sellae and inner table of bone of posterior cranial fossa cut away. Carotid canal opened to show arteries; canal supported by trabecular bone. Note fusion of right and left carotid canals forming a common canal caudal to hypophyseal fossa. Root of basilar artery-caudal ramus of cerebral carotid.

the dorsum sellae is completely fibrous (see also Wingstrand, *op. cit.*). Starck (*op. cit.*) illustrates well the sella of several birds.

Relationships. In addition to the cerebral carotid artery, the carotid canal also conducts the carotid vein which drains caudally into the posterior cephalic vein, thence into the jugular. Rostrally the carotid vein communicates with the cavernous venous sinuses in the sella turcica. The cerebral carotids and intercarotid anastomosis are partially or completely surrounded by the carotid vein and the transverse communication between right and left cavernous sinuses. The intersellar portion of each cerebral carotid rostral to the anastomosis is ordinarily situated medial

to the cavernous sinus, coursing between hypophysis and sinus. In some birds the sinus actually surrounds the carotids. The internal carotid nerve is described as coursing within the carotid canal (Cords, '04; Hsieh, '51; Wingstrand, *op. cit.*) accompanying the cerebral carotids. Observations on this nerve have been made only for the pigeon. In this form the nerve appears to run in its own osseous tube attached to the anterolateral aspect of the carotid canal. The palatine ramus of the facial nerve also runs in its proper canal lateral to the rostral end of the carotid canal.

The intrasphenoid part of the cerebral carotid artery in birds generally has consistent relationships to a number of other

structures. The caudal half of the carotid canal lies in the medial wall of the middle ear cavity. The rostral half of each carotid canal lies dorsal to the auditory tube and ventral to the medial end of the bony cochlea (and lagena). In birds having carotid canals merged rostrally, the common canal, which the anastomosis occupies, lies just dorsal to the rostral ends of the auditory tubes or their antrum.

Within the sella turcica the intercarotid anastomosis and cerebral carotids themselves groove the hypophysis caudally and laterally. As the carotids ascend out of the sella they pierce the diaphragma sellae, the duplication of dura roofing over the hypophyseal fossa, partially separating fossa from general cranial cavity.

Branches of intrasphenoid and intrasellar segments of cerebral carotids. The major branches of the cerebral carotids arising within the carotid canal are the palatine and sphenomaxillary arteries (figs. 3, 4, 5, 6). These vessels arise from the cerebral carotid on either side of the hypophyseal fossa, coursing into the floor of the orbit in their proper osseous canals which are offsets of the carotid canal. In certain birds these arteries are represented by a single stem designated the sphenomaxillary + palatine artery (fig. 1).

The external (orbital) orifices of the canal(s) for the palatine and sphenomaxillary arteries are located on either side of the root of the rostromaxillary bone directly caudal to the orbital process of the quadrate bone and the pterygoid bone.

Intrasellar branches of cerebral carotids. Wingstrand (*op. cit.*) notes that small arteries spring from the intercarotid anastomosis or the carotids just caudal to it which supply "immediate surroundings." This probably refers to osseous and dural rami. Such rami were not regularly searched for. Observations of several acrylic injected, macerated pigeon heads fail to show such rami. Wingstrand asserts that in some species one or two inferior hypophyseal arteries invariably arise from the region of the intercarotid anastomosis for supply of the neural lobe of the hypophysis. The nature and condition of the arteries in most of the specimens did not permit a search for these minute vessels.

They have, however, been identified in well injected pigeon specimens.

The internal ophthalmic artery, when present in adult birds, arises from the intrasellar segment of the cerebral carotid (figs. 3, 4, 5.), extending out of the hypophyseal fossa into the orbit via its own foramen. Even though it traverses the fossa lateral to the hypophysis, it does not contribute to the vascular supply of this organ (Wingstrand).

Types of intercarotid anastomoses. All birds examined possess well developed intercarotid anastomoses with the exception of specimens of the Suborder Tyranni of the passerine birds. Three principal patterns or types of anastomoses were found (fig. 2): an H-type in which the anastomosis is a transverse vessel of some length connecting the two carotids; an X-type in which the carotids communicate by a side-to-side anastomosis; and an I-type in which the two carotids merge into a single vessel of considerable length. Inasmuch as the types intergrade, it is sometimes impossible to define an extremely short transverse anastomosis as either X or H; in these borderline specimens the anastomosis was simply designated as "X-H." Likewise, there were borderline examples intermediate between X- and I-types. This distinction was also resolved arbitrarily; i.e., if the anastomosis were broad, resembling two carotids apposed side-to-side, no matter what the length of the union, it was classed as an X-type. Only if the carotids merged to form a distinctly unpaired, lengthy, cylindrical anastomosis was it considered as I-type.

The anastomotic segment of both the H-type and the X-type are situated within the hypophyseal fossa proper. Only the rostral end of an I-type (or elongated X-type) intercarotid anastomosis is located within the fossa, the caudal end of the anastomosis occupying the median carotid canal inferocaudal to the fossa. All of the illustrations in this paper portray the I-type anastomosis as if it were on the same plane as the cerebral carotids in the posterior parts of the carotid canals. Actually the plane of the I-type anastomosis varies in different birds from almost perpendicular to the plane of the floor of the posterior cranial fossa (*Pelecanus*, *Eudocimus*,

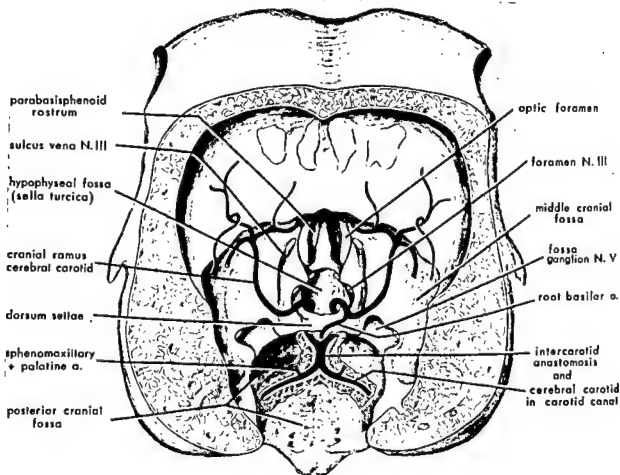


Fig. 1. Intercarotid anastomosis and cerebral carotids *in situ*. *Columba* (pigeon); calvaria removed; caudodorsal aspect of cranial cavity. Inferior part of dorsum sellae and inner table of bone of posterior cranial fossa cut away. Carotid canal opened to show arteries; canal supported by trabecular bone. Note fusion of right and left carotid canals forming a common canal caudal to hypophyseal fossa. Root of basilar artery-caudal ramus of cerebral carotid.

the dorsum sellae is completely fibrous (see also Wingstrand, *op. cit.*). Starck (*op. cit.*) illustrates well the sella of several birds.

Relationships. In addition to the cerebral carotid artery, the carotid canal also conducts the *carotid vein* which drains caudally into the posterior cephalic vein, thence into the jugular. Rostrally the carotid vein communicates with the cavernous venous sinuses in the sella turcica. The cerebral carotids and intercarotid anastomosis are partially or completely surrounded by the carotid vein and the transverse communication between right and left cavernous sinuses. The intersellar portion of each cerebral carotid rostral to the anastomosis is ordinarily situated medial

to the cavernous sinus, coursing between hypophysis and sinus. In some birds the sinus actually surrounds the carotids. The *internal carotid nerve* is described as coursing within the carotid canal (Cords, '04; Hsieh, '51; Wingstrand, *op. cit.*) accompanying the cerebral carotids. Observations on this nerve have been made only for the pigeon. In this form the nerve appears to run in its own osseous tube attached to the anterolateral aspect of the carotid canal. The palatine ramus of the facial nerve also runs in its proper canal lateral to the rostral end of the carotid canal.

The intrasphenoid part of the cerebral carotid artery in birds generally has consistent relationships to a number of other

TABLE 1 (Continued)

List of species and number of specimens dissected. Type of intercarotid anastomosis found for all specimens is indicated. See text for description of types.
0, no intercarotid anastomosis

Avian order and species	Type of intercarotid anastomosis				
	O	H	X	X-H	I
Strigiformes					
<i>Strix varia</i> (owl)					2
<i>Otus asio</i> (owl)			1		
<i>Bubo virginianus</i> (owl)			1		
Caprimulgiformes					
<i>Chordeiles minor</i> (nighthawk)		2		1	
Apodiformes					
<i>Selasphorus sasin</i> (hummingbird)		1			
<i>Calypte costae</i> (hummingbird)		1			
Coraciiformes					
<i>Megaceryle alcyon</i> (kingfisher)					2
Piciformes					
<i>Dendrocopos pubescens</i> (woodpecker)		1			
<i>Sphyrapicus varius</i> (woodpecker)		1			
<i>Pteroglossus sanguineus</i> (toucan)				3	
Passeriformes					
<i>Sayornis phoebe</i> (flycatcher)		1			
<i>Elaenia martinica</i> (flycatcher)		1			
<i>Pipra mentalis</i> (manakin)		1			
<i>Thamnophilus punctatus</i> (antbird)		1			
<i>Dendrocincla homochroa</i> (woodcreeper)		1			
<i>Passer domesticus</i> (house sparrow)			1		
<i>Cyanocitta cristata</i> (jay)			1		
<i>Toxostoma rufum</i> (thrasher)			1		
<i>Progne subis</i> (swallow)			1		
<i>Sturnus vulgaris</i> (starling)			1		

Columba) to a plane of about 45° with the floor of the posterior fossa (*Larus c.*).

Figures 3, 4, and 5 portray the most common configurations of intercarotid anastomoses for the various species dissected. Also illustrated are the palatine, sphenomaxillary, and internal ophthalmic arteries.

The clear-cut H-type of anastomosis is of greatest frequency in the series, occurring in almost half (35) of the specimens. The remaining specimens having anastomoses comprise three groups of about equal size. I-type, 15 specimens; X-type, 13 specimens, and the borderline X-H types, 18 specimens; five specimens lack an anastomosis. Owing to the unequal numbers of specimens in the different taxa of birds, the above statistics are meaningful only in a general way. Furthermore, some individual variation of the anastomosis within a species is evident, for example,

three specimens of *Fulica* are H-types; three are borderline X-H types (fig. 4). Two specimens of *Eudocimus* are X-types; two are X-H types (fig. 3). Four pigeon specimens are I-types; one is an H-type, etc. Particularly in species represented by only one or two specimens should one be cautious in accepting that a certain type of anastomosis is characteristic of that species.

In a few cases specimens representing several families of an order are present in the series. In these there is little evidence that a specific type of anastomosis is characteristic of that order. For example, in the Order Pelecaniformes the anhinga (Family Anhingidae) has an H-type; the cormorant (Phalacrocoracidae) shows X and X-H patterns; the pelican (Pelecanidae) has the I-type. There is, however, some uniformity in the Passeriformes: representatives of five different families of the Suborder

TABLE 1

List of species and number of specimens dissected. Type of intercarotid anastomosis found for all specimens is indicated. See text for description of types.
0, no intercarotid anastomosis

Avian order and species	Type of intercarotid anastomosis				
	O	H	X	X-II	I
Sphenisciformes					
<i>Pygoscelis adeliae</i> (penguin)		2			
<i>Spheniscus demersus</i> (penguin)			1		
Struthioniformes					
<i>Struthio camelus</i> (ostrich)		1			
Rheiformes					
<i>Rhea americana</i> (rhea)		1			
Gaviiformes					
<i>Gavia immer</i> (loon)			1		
Podicipediformes					
<i>Podilymbus podiceps</i> (grebe)				1	
Procellariiformes					
<i>Procellaria aequinoctialis</i> (shearwater)				1	
<i>Diomedea cauta</i> (albatross)				1	
<i>Diomedea immutabilis</i> (albatross)			1		
Pelecaniformes					
<i>Pelecanus occidentalis</i> (pelican)					2
<i>Phalacrocorax auritus</i> (cormorant)			1	1	
<i>Anhinga anhinga</i> (anhinga)		1			
Ciconiiformes					
<i>Eudocimus albus</i> (ibis)			2	2	
<i>Hydranassa caerulea</i> (heron)			1		
Anseriformes					
<i>Anser anser</i> (goose)		1	1		
<i>Catriana moschata</i> (duck)		2			
Falconiformes					
<i>Falco sparverius</i> (falcon)					2
<i>Accipiter cooperi</i> (hawk)		1			
<i>Buteo lineatus</i> (hawk)		1			
<i>Buteo borealis</i> (hawk)			1		
Galliformes					
<i>Gallus gallus</i> (chicken)		3			
<i>Phasianus cholchicus</i> (pheasant)			1		
Gruiformes					
<i>Fulica americana</i> (coot)		3		3	
Charadriiformes					
<i>Larus delawarensis</i> (gull)				2	
<i>Larus californicus</i> (gull)			1		1
<i>Erolia alpina</i> (sandpiper)				2	
<i>Erolia minutilla</i> (sandpiper)		1			
Columbiformes					
<i>Columba livia</i> (pigeon)		1			4
Psittaciformes					
<i>Melopsittacus undulatus</i> (parakeet)		3			
Cuculiformes					
<i>Coccyzus americana</i> (cuckoo)					2

TABLE 1 (Continued)

List of species and number of specimens dissected. Type of intercarotid anastomosis found for all specimens is indicated. See text for description of types.
O, no intercarotid anastomosis

Avian order and species	Type of intercarotid anastomosis				
	O	H	X	X-H	I
Strigiformes					2
<i>Strix varia</i> (owl)			1		
<i>Otus asio</i> (owl)			1		
<i>Bubo virginianus</i> (owl)					
Caprimulgiformes					
<i>Chordeiles minor</i> (nighthawk)		2		1	
Apodiformes					
<i>Selasphorus sasin</i> (hummingbird)		1			
<i>Calypte costae</i> (hummingbird)		1			
Coraciiformes					2
<i>Megaceryle alcyon</i> (kingfisher)					
Piciformes					
<i>Dendrocopos pubescens</i> (woodpecker)		1			
<i>Sphyrapicus varius</i> (woodpecker)		1			
<i>Pteroglossus sanguineus</i> (toucan)				3	
Passeriformes					
<i>Sayornis phoebe</i> (flycatcher)		1			
<i>Elaenia martinica</i> (flycatcher)		1			
<i>Pipra mentalis</i> (manakin)		1			
<i>Thamnophilus punctatus</i> (antbird)		1			
<i>Dendrocincla homochroa</i> (woodcreeper)		1			
<i>Passer domesticus</i> (house sparrow)			1		
<i>Cyanocitta cristata</i> (jay)			1		
<i>Toxostoma rufum</i> (thrasher)			1		
<i>Progne subis</i> (swallow)			1		
<i>Sturnus vulgaris</i> (starling)			1		

Columba) to a plane of about 45° with the floor of the posterior fossa (*Larus c.*).

Figures 3, 4, and 5 portray the most common configurations of intercarotid anastomoses for the various species dissected. Also illustrated are the palatine, sphenomaxillary, and internal ophthalmic arteries.

The clear-cut H-type of anastomosis is of greatest frequency in the series, occurring in almost half (35) of the specimens. The remaining specimens having anastomoses comprise three groups of about equal size. I-type, 15 specimens; X-type, 13 specimens, and the borderline X-H types, 18 specimens; five specimens lack an anastomosis. Owing to the unequal numbers of specimens in the different taxa of birds, the above statistics are meaningful only in a general way. Furthermore, some individual variation of the anastomosis within a species is evident, for example,

three specimens of *Fulica* are H-types; three are borderline X-H types (fig. 4). Two specimens of *Eudocimus* are X-types; two are X-H types (fig. 3). Four pigeon specimens are I-types; one is an H-type, etc. Particularly in species represented by only one or two specimens should one be cautious in accepting that a certain type of anastomosis is characteristic of that species.

In a few cases specimens representing several families of an order are present in the series. In these there is little evidence that a specific type of anastomosis is characteristic of that order. For example, in the Order Pelecaniformes the anhinga (Family Anhingidae) has an H-type; the cormorant (Phalacrocoracidae) shows X and X-H patterns; the pelican (Pelecanidae) has the I-type. There is, however, some uniformity in the Passeriformes: representatives of five different families of the Suborder

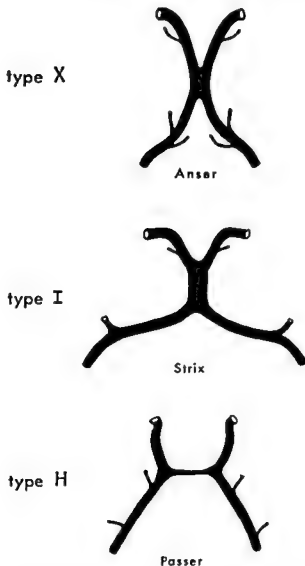


Fig. 2 Types of intercarotid anastomoses of birds. The H-type anastomosis is a transverse vessel of some length; in the X-type the carotids communicate by a side-to-side anastomosis; in the I-type anastomosis the two carotids merge into a single vessel of considerable length. See text for further details and for comments on intergrading types.

Passerines all possess the H-type anastomosis; representatives of four different families of the Suborder Tyranni all lack an intercarotid anastomosis (see Discussion).

Attention is directed to two unique patterns observed in the series. The right half of the intercarotid anastomosis of *Anhinga* (fig. 3) is divided into two vessels which join the right cerebral carotid independently. The internal ophthalmic artery of the left side springs from the anastomosis rather than from the cerebral carotid as its counterpart does contralaterally. The intercarotid anastomosis of the hummingbird, *Calypte* (fig. 5), is doubled—one transverse vessel located, as usual, caudal

to the hypophysis, the other rostral to the hypophysis. The unusual rostral anastomosis in *Calypte* may be related to the findings in the specimens of Tyranni, pre-

Figs. 3-5 Configuration of intercarotid anastomosis, intrasphenoid and intrasellar segments of cerebral carotids of the various species of birds studied (see table 1). Patterns are drawn with intrasphenoid segment at bottom; dorsocaudal aspect. Hypophysis occupies a position just above anastomosis. Patterns not drawn to scale. In some cases two patterns are illustrated for a species (see Observations). Also drawn are palatine, sphenomaxillary, and internal ophthalmic branches of the carotids. Internal ophthalmic arteries are not present in all species. In some species the palatine and sphenomaxillary arteries are represented by a single vessel on each side.



Spheniscus



Pygoscelis



Struthio



Rhea



Gavia



Podilymbus



Diomedea i.



Diomedea c.



Procellaria



Anhinga



Phalacrocorax



Pelecanus



Eudocimus



Eudocimus



Hydrocnassa

Figure 3

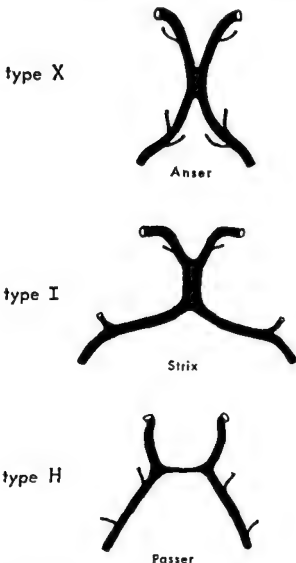


Fig. 2 Types of intercarotid anastomoses of birds. The H-type anastomosis is a transverse vessel of some length; in the X-type the carotids communicate by a side-to-side anastomosis; in the I-type anastomosis the two carotids merge into a single vessel of considerable length. See text for further details and for comments on intergrading types.

Passeres all possess the H-type anastomosis; representatives of four different families of the Suborder Tyranni all lack an intercarotid anastomosis (see Discussion).

Attention is directed to two unique patterns observed in the series. The right half of the intercarotid anastomosis of *Anhinga* (fig. 3) is divided into two vessels which join the right cerebral carotid independently. The internal ophthalmic artery of the left side springs from the anastomosis rather than from the cerebral carotid as its counterpart does contralaterally. The intercarotid anastomosis of the hummingbird, *Calypte* (fig. 5), is doubled—one transverse vessel located, as usual, caudal

to the hypophysis, the other rostral to the hypophysis. The unusual rostral anastomosis in *Calypte* may be related to the findings in the specimens of Tyranni, pre-

Figs. 3-5 Configuration of intercarotid anastomosis, intrasphenoid and intrasellar segments of cerebral carotids of the various species of birds studied (see table 1). Patterns are drawn with intrasphenoid segment at bottom; dorsocaudal aspect. Hypophysis occupies a position just above anastomosis. Patterns not drawn to scale. In some cases two patterns are illustrated for a species (see Observations). Also drawn are palatine, sphenomaxillary, and internal ophthalmic branches of the carotids. Internal ophthalmic arteries are not present in all species. In some species the palatine and sphenomaxillary arteries are represented by a single vessel on each side.



Spheniscus



Pygoscelis



Struthio



Rhea



Gavia



Podilymbus



Diomedea i.



Diomedea c.



Procellaria



Anhinga



Phalacrocorax



Pelecanus



Eudocimus



Eudocimus



Hydranassa

Figure 3

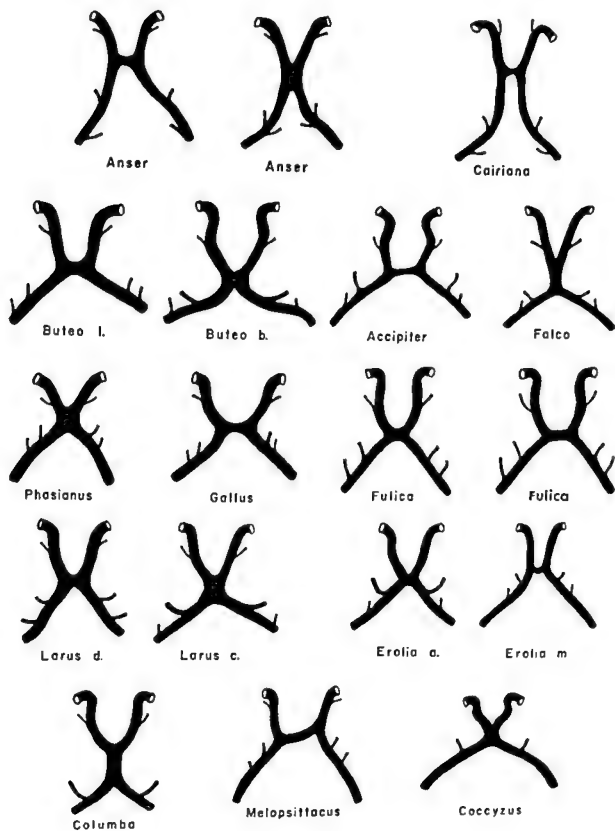


Figure 4

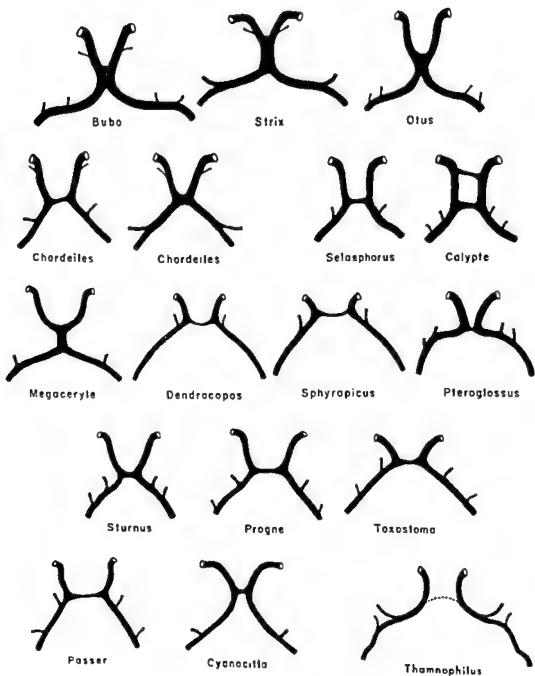


Figure 5

viously mentioned, which lack an anastomosis. In these specimens no trace of an intercarotid anastomosis could be found in the usual position caudal to the hypophysis; however, what appeared to be a vestigial, atrophied channel was noted in all specimens lying rostral to the hypophysis in the same position as the rostral anastomosis in *Calypte*. This "vestige" is attached to the anterior aspect of each cerebral carotid arching rostrally and superiorly (see *Thamnophilus*, fig. 5), surrounded by a transversely disposed venous sinus which united the two cavernous sinuses rostral to the hypophysis. No lumen could be detected in this vestige, even by examination of the interior of the carotids opposite the attachment of the vestige on the outside of the vessel. Study of well-injected young specimens or embryos of these forms are needed to clarify this matter. The anastomosis rostral to the hypophysis is comparable in position to the anastomosis of teleost fishes (see Discussion).

Basilar artery (fig. 6). The origin of the basilar artery was recorded in all specimens. It is rather well established that the basilar is usually formed asymmetricaly in most birds; i.e., in adults the basilar is the prolongation of the caudal ramus of the cerebral carotid on only one side (Beddard, '05; Wingstrand, *op. cit.*; Hughes, *op. cit.*; Baumel, '62; Vitums *et al.*, '65). Only in one specimen each of the following was the basilar artery formed symmetricaly by union of equisized caudal rami of both carotids: *Procellaria*, *Buteo b.*, *Accipiter*, *Falco*, *Fulica*, *Sayornis*, *Elaenia*, *Pipra* and *Dendrocincla*. In several other specimens the basilar was formed by both caudal rami, with one ramus distinctly larger than the other, the smaller ramus ranging from minute to one-half the caliber of the dominant ramus. This occurred in specimens of *Anhinga*, *Cairiana*, *Falco*, *Fulica*, *Larus d.*, *Strix*, *Bubo*, *Otus*, *Pteroglossus*, and *Toxostoma*. In all remaining remaining specimens the basilar was formed unilaterally as the continuation of either left or right caudal rami of the cerebral carotids. (See Discussion for comment on the relationship between basilar artery and intercarotid anastomosis.)

DISCUSSION

Considering that there are more than 8500 living species of birds, it is almost superfluous to remark that the present series is indeed a small sample on which to base generalities on the avian intercarotid anastomosis. Recollecting the great number of deletions and variations of patterns occurring in the cervical parts of the avian carotid arteries (Glenny, '55), it is actually amazing that the presence of an intercarotid anastomosis comprises such a consistent feature of the vasculature of birds. Incidentally, there seems to be no correlation of types of intercarotid anastomoses with the bicarotid or unicarotid condition seen in different birds. Almost certainly groups of birds other than the Tyranni will be found which lack an intercarotid anastomosis.

The absence of the anastomosis in members of the Suborder Tyranni of the perching birds was first noted by Wingstrand (*op. cit.*) in *Leptastentura* and *Elaenia*, with only a minute channel in *Xolmis*. Members of this group were the last to be examined in the series. Having noted an anastomosis in all specimens previously dissected, these writers frankly questioned Wingstrand's observations; specimens of Tyranni were obtained in order to verify or refute him. As noted above, species of four separate families of Tyranni lack a definitive anastomosis, possessing only questionable rudimentary vestiges. This bears out Wingstrand completely, enhancing his speculation that lack of the anastomosis is characteristic of Tyranni. Wingstrand ('41) and Rahn and Painter ('41) described the unique, attenuated, rostrocaudally compressed hypophysis displayed in series of Tyranni. The possibility exists that the shape and form of the hypophysis in these forms is related to the absence of the anastomosis.

Anastomoses of other birds. Although Barkow (*op. cit.*) described a plexiform intercarotid anastomosis consisting of numerous fine channels as one of his four types, no such arrangement has been seen in this series in which practically all of the H-shaped anastomoses consist of discrete, single channels. For exceptions, see above for *Calypte* and *Anhinga* (figs. 3, 5).

Very few direct comparisons of the intercarotid anastomoses of the birds in Bar-

kow's, Wingstrand's and the present series are permitted since in only a few cases were the same species studied. Barkow described fine, plexiform transverse anastomoses in *Podiceps* and *Anas*; combination plexiform communications plus a short transverse anastomosis in *Anser*; only a short transverse anastomosis in *Fulica*, *Gallus*, *Falco*, and *Corvus*; and a short common stem anastomosis in *Strix*, *Columba*, *Ciconia*, *Ardea*, *Cuculus*, and *Oedipodius*. Wingstrand described a long transverse anastomosis in passerine birds (except *Tyranni*), *Picus*, *Encognathus*, *Caprimulgus*, *Gallus*, *Sephanoides*, and *Apus*; a lengthy longitudinal anastomosis in *Columba*, *Melanitta*, *Anser*, *Larus*, *Strix*, *Diomedea*, *Priocella*, and *Procellaria*; a short longitudinal anastomosis in *Pelecanoides* and *Milvago*; and minute or absent anastomosis in species of *Tyranni* (see above).

Birds generally do not possess a cerebral arterial circle (of Willis) comparable to that of mammals since the basilar artery ordinarily is not formed by union of both caudal rami of the cerebral carotids (see above) and a communications anterior between the anterior cerebral arteries is rare (Baumel, '67; Kitch, *op. cit.*). The intercarotid anastomosis obviously serves as an admirable substitute. Since the anastomosis of some avian species is literally huge by contrast with the carotids themselves, the avian intercarotid anastomosis may be a more effective collateral channel than the usual mammalian arterial circle. Even in H-type anastomoses wherein the communication is of relatively smaller dimensions than in the X- and I-types, the caliber of the anastomotic segment in most specimens is at least one-half that of the cerebral carotids which it joins. Only in a few of the H and X-H types is the anastomosis rather constricted, having a relatively small lumen *Phalacrocorax*, *Podilymbus*, *Pteroglossus* (figs. 3, 5).

Ostensibly the form and size of the anastomoses are of functional significance. The X- and I-type anastomoses appear of greatest potential value as collateral circulatory pathways by forming broad communication between the two carotids, most likely providing some mixing of the blood conducted by them. Even in some H and X-H types the anastomotic segment cannot

be considered as merely a latent or potential communication; the angulation of the communication and relative sizes of the intrasellar parts of the carotids indicates that in some specimens during life there was shunting of blood from one carotid to the other via the anastomoses (see below).

That the intercarotid anastomosis functions as a collateral channel is demonstrated by a specimen of cormorant (*Phalacrocorax*) in which the intrasellar part of the left carotid was occluded and atrophied, represented by only a sizeable connective tissue remnant. Blood from the left carotid of necessity was shunted across the anastomosis to the right carotid which supplied both sides of the brain by means of a communication between the two caudal rami of the cerebral carotids at the rostral end of the basilar artery.

It is noteworthy that the specimens of *Tyranni*, all lacking an intercarotid anastomosis, do have symmetrical roots of the basilar artery from both caudal rami of the carotids; this appears to have compensated for the absent intercarotid anastomosis in these forms. Wingstrand (*op. cit.*) also noted persistence of both roots of the basilar artery in two additional species of *Tyranni*.

As mentioned above, (see "Basilar artery") a number of specimens exhibit bilateral formation of the basilar artery in addition to an intercarotid anastomosis. Wingstrand speculated on the possible interrelationship of the anastomosis and the development of the asymmetry of caudal rami of the carotids: "If one of the two ways from the intercarotid anastomosis to the a. basilaris offers less resistance to the blood, more blood will choose this way. Now it seems probable that an acceleration of the blood stream through a vessel causes an increase of the diameter (cf. review in Hughes, '34), and the pre-existing small difference between the two rami posteriores will thus rapidly be multiplied." Eleven specimens in the present series provide evidence which bears out Wingstrand's contention. These specimens were all H- or X-H types in which the anastomotic segment was not transversely oriented but was angled somewhat obliquely so that one end of the anastomosis was located at a higher level than the other. From the angle

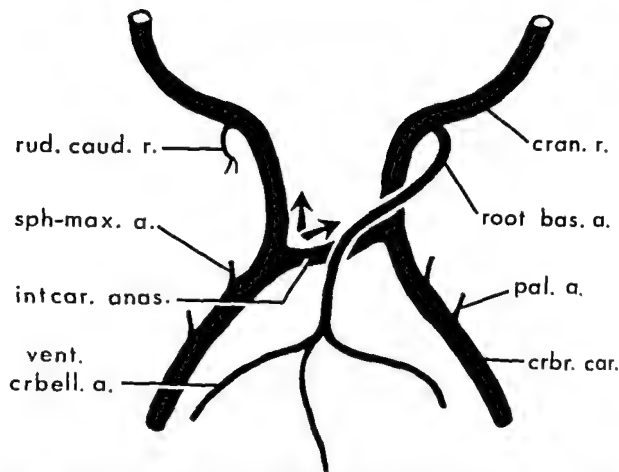


Fig. 6 Schema showing correlation of obliquity of intercarotid anastomosis with side of origin of basilar artery. *Mclopsittacus* (parakeet), caudodorsal aspect. In 11 of 12 II-type specimens showing a comparable exaggerated obliquity of the anastomotic segment, the dominant caudal ramus of the carotids (root of basilar artery) was found on the side to which blood flow was apparently delivered across the anastomosis. Angle of branching of left cerebral carotid indicates that the blood stream was split (arrows). See text for details. Cran. r., cranial ramus; crbr. car. a., cerebral carotid artery; intcar. anas., intercarotid anastomosis; pal. a., palatine artery; root bas. a., root basilar artery; rud. caud. r., rudimentary caudal ramus; sph-max. a., sphenomaxillary artery; vent. crbell. a., ventral cerebellar artery.

of branching it is assumed that the blood stream was split on the side of the more proximal end of the anastomotic segment, routing a part of that carotid's stream across the anastomosis to the opposite carotid which probably received a larger volume of blood than its counterpart. The side of each specimen having the dominant caudal ramus of the carotid was noted and compared with the angulation of the anastomotic segment. In 11 of 12 cases the dominant caudal ramus was on the side to which the anastomosis directed extra blood (see fig. 6). The above specimens, exemplifying this haemodynamic influence on vessel development, show persistent exaggerated configurations. Of specimens

which do not show a persistent obvious angulation of the anastomosis, all that can be said about the development of asymmetry of their caudal rami is that only subtle differences in embryonic blood flow are required to influence asymmetry of the caudal rami. Hughes (*op. cit.*) states that the basilar artery is formed equally by the left and right caudal rami up to the three day stage of incubation in the chick embryo, with asymmetry occurring the fourth and fifth days. Vitums *et al.* ('66) assert that the symmetrical development of the right and left caudal rami persists for most of the embryonic period (10 days) in the White-crowned sparrow, followed by development of asymmetry.

Intercarotid anastomoses in other vertebrates. A communication between the cerebral carotids caudal to the hypophysis appears to be a deep-rooted vertebrate characteristic, reaching its zenith of development in birds both in size and in its widespread distribution throughout Class Aves.

The occurrence of an intercarotid anastomosis has been described in both cartilaginous and bony fishes. Goodrich ('58), citing the work of Allis ('11), states that in the shark, *Chlamydoselachus*, the two lateral dorsal aortae unite in a median sinus cephalicus ventral to the tip of the notochord in the very early embryo, persisting in the adult, forming a circulus cephalicus behind the pituitary body. Grodzinski (46b) describes in *Scyllium*, *Mustellus*, and *Torpedo* the right and left internal carotids merging to form an unpaired vessel which enters the cranial cavity beneath the caudal end of the hypophysis. In *Raja* Grodzinski notes that the carotids cross one another without anastomosing; however, Hofmann (*op. cit.*) indicates that the two carotids communicate at the base of the skull in both *Raja* and *Acanthus* where the two vessels cross.

Goodrich (*op. cit.*) says that the usual definitive condition in teleost fishes is the coming together and fusion of the internal carotids to complete a circulus cephalicus. Since the union of the carotids is anterior to the pituitary, Goodrich asserts that the anastomosis is not homologous to that of the selachians. Grodzinski (46a) illustrates this location of the fused carotids rostral to the hypophysis in *Salmo*. According to Goodrich, Spencer (1892) notes a circulus cephalicus behind the hypophysis in adult Dipnoi (lungfish). Grodzinski states that in the Chondrostei both *Acipenser* and *Polyodon* lack the intercarotid anastomosis.

No references have been uncovered which cite the occurrence of an intercarotid anastomosis in amphibians. Wingstrand says that the anastomosis is not found in amphibians, ascribing this to the very exceptional course of the carotids in these animals. In *Rana* the cerebral artery enters the skull by the oculomotor foramen (Gaupp, 1893). The papers of Green ('47) and Roope ('38) which deal with the vessels of the amphibian hypophysis fail to mention an intercarotid anastomosis.

Roope does note a ramus communicans posterior, single or double, forming a connecting link between the two cerebral carotids in *Amblysatoma*; however, this ramus arises from the root of the cranial division of the carotid on each side and does not seem to be homologous with the avian intercarotid anastomosis or the circulus cephalicus of selachians. Neither Hofmann (*op. cit.*), Francis ('34), nor Ask-Upmark reports an intercarotid anastomosis for either *Rana* or *Salamandra*.

In reptiles an intercarotid anastomosis corresponding to that of birds is rather common. Ask-Upmark (*op. cit.*) and Green ('51) describe an H-shaped anastomosis in *Alligator*. Shindo ('14) reports a large transverse anastomosis on the lower surface of the hypophysis of *Crocodilus*. Both Green and Shindo indicate the presence of a transverse anastomosis behind the pituitary in the Chelonians: *Chelydra*, *Chrysemys*, *Trionyx*, *Terrepene*, and *Emys*. In the lizards Wingstrand (*op. cit.*) states that the anastomosis was lacking in most of the lacertilians in his collection, existing only in three specimens of *Chamaeleon*. Shindo does not mention the intercarotid anastomosis in *Lacerta* although he does describe minute hypophyseal rami of the carotids. Green ('51) does not refer to the anastomosis in *Anolis* nor does O'Donoghue ('21) for *Sphenodon*. Wingstrand denies the existence of an intercarotid anastomosis in snakes based on his observations in *Vipera* and *Tropidonotus*. On the other hand, Ask-Upmark states that in the ophiidians of his series, *Drymarchon*, *Lampropeltis*, and *Bothrops*, the dorsal carotid artery enters the cranial cavity joining its contralateral partner at the base of the brain. His diagram shows the I-shaped anastomosis.

Wingstrand errs in stating that an intercarotid anastomosis is lacking in "all mammals." To the contrary, it has been reported for numerous mammalian species, although it does not attain sizeable dimensions as in fish, reptiles, and birds, ordinarily consisting of cross anastomoses between the inferior (posterior) hypophyseal arteries. In human foetuses of five to nine months de la Torre and Netsky ('60) state, "The inferior hypophyseal artery is directed medially toward the posterior part

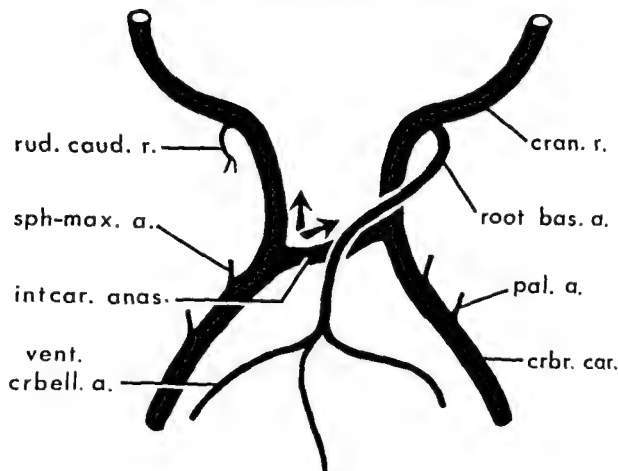


Fig. 6 Schema showing correlation of obliquity of intercarotid anastomosis with side of origin of basilar artery. *Melopsittacus* (parakeet), caudodorsal aspect. In 11 of 12 H-type specimens showing a comparable exaggerated obliquity of the anastomotic segment, the dominant caudal ramus of the carotids (root of basilar artery) was found on the side to which blood flow was apparently delivered across the anastomosis. Angle of branching of left cerebral carotid indicates that the blood stream was split (arrows). See text for details. Cran. r., cranial ramus; crbr. car. a., cerebral carotid artery; intcar. anas., intercarotid anastomosis; pal. a., palatine artery; root bas. a., root basilar artery; rud. caud. r., rudimentary caudal ramus; sph-max. a., sphenomaxillary artery; vent. crbell. a., ventral cerebellar artery.

of branching it is assumed that the blood stream was split on the side of the more proximal end of the anastomotic segment, routing a part of that carotid's stream across the anastomosis to the opposite carotid which probably received a larger volume of blood than its counterpart. The side of each specimen having the dominant caudal ramus of the carotid was noted and compared with the angulation of the anastomotic segment. In 11 of 12 cases the dominant caudal ramus was on the side to which the anastomosis directed extra blood (see fig. 6). The above specimens, exemplifying this haemodynamic influence on vessel development, show persistent exaggerated configurations. Of specimens

which do not show a persistent obvious angulation of the anastomosis, all that can be said about the development of asymmetry of their caudal rami is that only subtle differences in embryonic blood flow are required to influence asymmetry of the caudal rami. Hughes (*op. cit.*) states that the basilar artery is formed equally by the left and right caudal rami up to the three day stage of incubation in the chick embryo, with asymmetry occurring the fourth and fifth days. Vitums *et al.* ('66) assert that the symmetrical development of the right and left caudal ramal persists for most of the embryonic period (10 days) in the White-crowned sparrow, followed by development of asymmetry.

Intercarotid anastomoses in other vertebrates. A communication between the cerebral carotids caudal to the hypophysis appears to be a deep-rooted vertebrate characteristic, reaching its zenith of development in birds both in size and in its widespread distribution throughout Class Aves.

The occurrence of an intercarotid anastomosis has been described in both cartilaginous and bony fishes. Goodrich ('58), citing the work of Allis ('11), states that in the shark, *Chlamydoselachus*, the two lateral dorsal aortae unite in a median sinus cephalicus ventral to the tip of the notochord in the very early embryo, persisting in the adult, forming a circulus cephalicus behind the pituitary body. Grodzinski (46b) describes in *Scyllium*, *Mustellus*, and *Torpedo* the right and left internal carotids merging to form an unpaired vessel which enters the cranial cavity beneath the caudal end of the hypophysis. In *Raja* Grodzinski notes that the carotids cross one another without anastomosing; however, Hofmann (*op. cit.*) indicates that the two carotids communicate at the base of the skull in both *Raja* and *Acanthus* where the two vessels cross.

Goodrich (*op. cit.*) says that the usual definitive condition in teleost fishes is the coming together and fusion of the internal carotids to complete a circulus cephalicus. Since the union of the carotids is anterior to the pituitary, Goodrich asserts that the anastomosis is not homologous to that of the selachians. Grodzinski (46a) illustrates this location of the fused carotids rostral to the hypophysis in *Salmo*. According to Goodrich, Spencer (1892) notes a circulus cephalicus behind the hypophysis in adult Dipnoi (lungfish). Grodzinski states that in the Chondrostei both *Acipenser* and *Polyodon* lack the intercarotid anastomosis.

No references have been uncovered which cite the occurrence of an intercarotid anastomosis in amphibians. Wingstrand says that the anastomosis is not found in amphibians, ascribing this to the very exceptional course of the carotids in these animals. In *Rana* the cerebral artery enters the skull by the oculomotor foramen (Gaupp, 1893). The papers of Green ('47) and Roope ('38) which deal with the vessels of the amphibian hypophysis fail to mention an intercarotid anastomosis.

Roope does note a ramus communicans posterior, single or double, forming a connecting link between the two cerebral carotids in *Amblystoma*; however, this ramus arises from the root of the cranial division of the carotid on each side and does not seem to be homologous with the avian intercarotid anastomosis or the circulus cephalicus of selachians. Neither Hofmann (*op. cit.*), Francis ('34), nor Ask-Upmark reports an intercarotid anastomosis for either *Rana* or *Salamandra*.

In reptiles an intercarotid anastomosis corresponding to that of birds is rather common. Ask-Upmark (*op. cit.*) and Green ('51) describe an H-shaped anastomosis in *Alligator*. Shindo ('14) reports a large transverse anastomosis on the lower surface of the hypophysis of *Crocodylus*. Both Green and Shindo indicate the presence of a transverse anastomosis behind the pituitary in the Chelonians: *Chelydra*, *Chrysemys*, *Trionyx*, *Terrepena*, and *Emys*. In the lizards Wingstrand (*op. cit.*) states that the anastomosis was lacking in most of the lacertilians in his collection, existing only in three specimens of *Chamaeleon*. Shindo does not mention the intercarotid anastomosis in *Lacerta* although he does describe minute hypophyseal rami of the carotids. Green ('51) does not refer to the anastomosis in *Anolis* nor does O'Donoghue ('21) for *Sphenodon*. Wingstrand denies the existence of an intercarotid anastomosis in snakes based on his observations in *Vipera* and *Tropidonotus*. On the other hand, Ask-Upmark states that in the ophiidians of his series, *Drymarchon*, *Lampropeltis*, and *Bothrops*, the dorsal carotid artery enters the cranial cavity joining its contralateral partner at the base of the brain. His diagram shows the I-shaped anastomosis.

Wingstrand errs in stating that an intercarotid anastomosis is lacking in "all mammals." To the contrary, it has been reported for numerous mammalian species, although it does not attain sizeable dimensions as in fish, reptiles, and birds, ordinarily consisting of cross anastomoses between the inferior (posterior) hypophyseal arteries. In human foetuses of five to nine months de la Torre and Netsky ('60) state, "The inferior hypophyseal artery is directed medially toward the posterior part

of the sella turcica where it anastomoses with its contralateral counterpart to form the intercarotid anastomoses." Parkinson ('64) describes the constant anastomosis of the right and left inferior hypophyseal arteries in the region of the posterior floor of the sella turcica in a large series of adult humans. In a primate other than man Kassel and Langfitt ('65) have observed a large transverse artery joining the two carotids at the level of the hypophysis in seven of their specimens of the rhesus monkey, *Macaca*.

From personal observations and the works of Martinez ('65) and Hurliman ('13) the domestic cat possesses an intercarotid artery brought about by union of the posterior hypophyseal arteries. According to Miller *et al.* ('64) the dog has an arteria intercarotica posterior which lies caudal to the hypophysis, yielding a posterior hypophyseal artery. De la Torre and Netsky (*op. cit.*) also describe and illustrate a prominent "intercarotid anastomosis" in the dog derived by union of the posterior hypophyseal arteries.

Among the ungulates Baldwin ('64) mentions communications between the right and left carotid retia in the ox both anterior and posterior to the pituitary. In the sheep he says that only a few small interconnecting vessels pass posterior to the pituitary body between the paired carotid retia. Sisson and Grossman ('63) describe an intercarotid artery, lying in the intercavernous sinus, behind the pituitary body of the horse. Hofmann (*op. cit.*) also mentions a strong transverse anastomotic branch uniting the two internal carotids in the horse; Ask-Upmark likewise describes an anastomosis in the same position for the tapir, *Tapirella*. According to the last author a connection exists between the two intracranial carotid retia in the cetacean, *Phocaena*.

As previously mentioned the inferior hypophyseal arteries of many birds arise from the region of the intercarotid anastomosis (Wingstrand, *op. cit.*). Inasmuch as the intercarotid anastomosis of most of the mammals cited above consists of a communication between the inferior hypophyseal arteries caudal to the hypophysis, within the sella turcica, it is reasonable to assume that the avian and mammalian

intercarotid anastomoses are homologous vessels.

Embryology of intercarotid anastomosis. In his description of the embryonic development of the pigeon intercarotid anastomosis (Rost, '40) noted that in earlier stages the two carotids are completely separated, lying at the sides of the hypophyseal anlage. At five days the internal carotids bend mesad coming closer to one another behind the anlage. In embryos of seven days a weakly formed transverse anastomosis is formed which is strengthened in the further course of development. In embryos of nine to ten days the carotids are almost completely fused together. Rost emphasized that in none of his early embryos was there an indication of capillary union between the carotids before development of the transverse connection. Rost also noted incomplete fusion of the carotids in some of his specimens. This condition in which the anastomosis was an H-type rather than the usual I-type has been seen in adult pigeons only once by the present writers.

For the embryo of the sparrow, *Zonotrichia*, Vitums and co-workers ('66) describe the two carotids converging toward the rostral part of Rathke's pouch at the 3-4 day stage with an early appearance of the intercarotid anastomosis at about the 4-day stage. At 5-7 days of incubation the internal carotids are connected by a distinct anastomosis located at the boundary of the developing rostral and caudal lobes of the pars distalis of the hypophysis. In post-natal life the anastomosis changes in position to lie in relationship to the caudoventral aspect of the caudal lobe of pars distalis. The adult anastomosis of *Zonotrichia* is the H-type as seen in all the specimens of the Suborder Passeres in this study. Wingstrand (*op. cit.*) has described the time of appearance of the intercarotid anastomosis in *Gallus* and *Larus* as has Hafferl ('21) for the plover, *Vanellus*. Assenmacher ('52) describes the influence of the intercarotid anastomosis on the developing hypophysis of ducks stating that the hinge or angulation of the hypophysis takes form in the concavity of the large transverse anastomosis at the sixth day of development.

That a fundamental intimate relationship between hypophysis and internal carotids exists throughout the gnathostome vertebrates is well known. In his discussion of the morphology of the base of the skull Goodrich (*op. cit.*) points out that the internal carotids and the anlage of the adenohypophysis enter the basis cranii through the primitive fenestra hypophyseos in the chondrocranium which is subsequently closed off leaving only the persistent carotid foramina. The manner in which the fenestra is obliterated by cartilage or bone apparently results in a shifting together of the carotids in some forms leading to the close relationship or actual apposition and merging of the carotids. Perhaps the pattern of closure of the fenestra has predisposed toward the phylogenetic and ontogenetic development of an intercarotid anastomosis best exemplified in birds.

ACKNOWLEDGMENTS

Many individuals and their institutions were extremely helpful in donating and lending the specimens employed in this study. The authors are sincerely grateful to Dr. Pierce Brodkorb, Mr. Charles H. Trost, and Mr. David W. Johnson of the University of Florida; Dr. Richard Liveridge, Museum, Port Elizabeth, Union of South Africa; Dr. Richard L. Zusl, Division of Birds, U. S. National Museum; Dr. Larry Z. McFarland, University of California (Davis); Dr. George E. Hudson, Washington State University; Drs. George R. Toney, Robert Wood, Verne Peckham of the Office of Antarctic Programs, National Science Foundation; Dr. Carl L. Hubbs of Scripps Institution of Oceanography; Dr. Glen E. Woolfenden, University of South Florida; Dr. David B. Slauterback, University of Wisconsin; and Dr. Robert Lasiewski, University of Michigan.

LITERATURE CITED

- Allis, E. P. 1911 Pseudobranchial and carotid arteries in *Chlamydoselachus anguineus*. *Anat. Anz.*, 39: 511-519.
- Ask-Upmark, E. 1935 The carotid sinus and the cerebral circulation. *Berlingska Boktryckeriet*, Lund.
- Assenmacher, L. 1952 La vascularisation du complexe hypophysaire chez le canard domestique. *Arch. d'Anat. micros. et Morph. exper.*, 41: 69-106.

- 1953 Etude anatomique du système artériel cervicocéphalique chez l'oiseau. *Arch. Anat. Hist. et Embry.*, 35: 181-202.
- Atwell, W. J. 1939 The morphogenesis of the hypophysis cerebri of the domestic fowl during the second and third weeks of incubation. *Anat. Rec.*, 73: 57-72.
- Baldwin, B. A. 1964 The anatomy of the arterial supply to the cranial regions of the sheep and ox. *Am. J. Anat.*, 115: 101-117.
- Barkow, H. 1829 Anatomisch-physiologische Untersuchungen, vorzüglich über das Schlagadersystem der Vögel. *Arch. f. Anat. u. Physiol.*, Heft 4.
- Bauer, F. 1825 Disquisitiones circa nonnullarum avium systema atherosum. *Inaug. Diss.*, Berolini.
- Baumel, J. I. 1962 Asymmetry of encephalic arteries in the pigeon (*Columba livia*). *Anat. Anz.*, 111: 91-102.
- 1964 Vertebral-dorsal carotid artery interrelationships in the pigeon and other birds. *Anat. Anz.*, 113: 113-130.
- 1967 The characteristic asymmetrical distribution of the posterior cerebral artery of birds. *Acta Anat.*, 67: 523-549.
- Beddard, F. E. 1905 A contribution to the knowledge of the arteries of the brain in the Class Aves. *Proc. Zool. Soc. London.*, 1: 102-117.
- Cobb, S. 1960 Observations on the comparative anatomy of the avian brain. *Perspec. Biol. Med.*, 3: 383-408.
- Cords, E. 1904 Beiträge zur Lehre vom Kopf-nervensystem der Vögel. *Anat. Hefte*, 26: 49-100.
- Crallay, J. C. 1965 The vascular anatomy of the starling, *Sturnus vulgaris* Linnaeus. *Ph.D. Diss.*, Univ. Ill.
- de la Torre, E., and M. G. Netsky. 1960 Study of persistent primitive maxillary artery in human fetus; some homologies of cranial arteries in man and dog. *Am. J. Anat.*, 106: 185-195.
- Duijrn, M. 1951 On the head posture in birds and its relation to some anatomical features. I and II. *Proc. Konink. Nederlandse Akad. v. Wetens.*, Series C, 54: 3-24.
- Francis, E. T. B. 1934 The anatomy of the salamander. Clarendon Press, Oxford.
- Gadow, H. 1891 In: *Bronn's Klassen und Ordnungen des Thierreichs*. Bd. VI, Abt. 4, Vögel, Leipzig.
- Glenny, F. H. 1955 Modifications of pattern in the aortic arch system of birds and their phylogenetic significance. *Proc. U. S. Natl. Mus.*, 104: 525-621.
- Goodrich, E. S. 1958 Studies on the structure and development of vertebrates. Dover Publ., New York.
- Green, J. D. 1947 Vessels and nerves of amphibian hypophyses. A study of the living circulation and of the histology of the hypophysial vessels and nerves. *Anat. Rec.*, 99: 21-54.
- 1951 The comparative anatomy of the hypophysis, with special reference to its blood supply and innervation. *Am. J. Anat.*, 88: 225-312.

- Grodzinski, Z. 1946a The main vessels of the brain in Rainbow Trout (*Salmo trideus* Gibb.) Bull. Internatl. Acad. Polon. Sci. and Lettres, Series B: 1-21.
- 1946b The blood vessels in the brain of elasmobranchs. Bull. Internatl. Acad. Polon. Sci. and Lettres, Series B: 23-85.
- Hafferl, A. 1921 Zur Entwicklungsgeschichte der Kopfarterien beim Kiebitz (*Vanellus cristatus*). Anat. Hefte, 59: 520-576.
- 1933 In: Bolk, Göppert, Kallius, Lubosch, Handbuch der vergleichenden Anatomie der Wirbeltiere, Bd. VI, Urban u. Schwarzenberg, Berlin u. Wien.
- Hofmann, M. 1900 Zur vergleichenden Anatomie der Gehirn- und Rückenmarksarterien der Vertebraten. Ztschr. f. Morph. u. Anthropol., 2: 247-322.
- Hsieh, T. M. 1951 The sympathetic and parasympathetic nervous systems of the fowl. Ph.D. Diss., Univ. Edinburgh.
- Hughes, A. F. W. 1934-35 On the development of the blood vessels in the head of the chick. Phil. Trans. Roy. Soc. London, Series B, 224: 75-129.
- Hurlimann, R. 1912-13 Die arteriellen Kopfgefäße der Katze. Internatl. Monatsch. Anat. Physiol., 29: 371-442.
- Jollie, M. T. 1957 The head skeleton of the chicken and remarks on the anatomy of this region in other birds. Jour. Morph., 100: 389-436.
- Kassell, N. F., and T. W. Langfitt 1965 Variations in the circle of Willis in *Macaca mulatta*. Anat. Rec., 152: 257-264.
- Kesteven, H. L. 1925 The parabasal canal and nerve foramina and canals in the bird skull. Jour. Roy. Soc. New South Wales, 59: 108-123.
- Kitoh, J. 1962 Comparative and topographical anatomy of the fowl. XII. Observations on the arteries with their anastomoses in and around the brain in the fowl (in Japanese). Jap. J. Vet. Sci., 24: 141-150.
- Klinckowström, A. 1890 Quelques recherches morphologiques sur les artères du cerveau des vertébrés. Bih. Sven. Vet.-Akad. Hand., 15: 1-26.
- Martínez, P. 1965 Le système artériel de la base du cerveau et l'origine des artères hypophysaires chez le chat. Acta Anat., 61: 511-546.
- Miller, M. E., G. C. Christensen, and H. E. Evans 1964 Anatomy of the dog. W. B. Saunders Co., Philadelphia.
- O'Donoghue, C. H. 1921 VI. The blood vascular system of the Tuatara, *Sphenodon punctatus*. Phil. Trans. Roy. Soc. London, Series B, 210: 175-252.
- Parkinson, D. 1964 Collateral circulation of cavernous carotid artery: anatomy. Can. J. Surg., 7: 251-268.
- Rahn, H., and B. T. Painter 1941 A comparative histology of the bird pituitary. Anat. Rec., 79: 297-312.
- Roofe, P. G. 1938 The blood vascular system of the hypophysis of *Amblystoma tigrinum*. J. Comp. Neur., 69: 249-254.
- Rost, H. 1940 Die Entwicklung der Hypophyse der Haustauben und ihre rassetypische Ausbildung bei der Römertaube. Zeltsch. Wiss. Zool., 152: 221-276.
- Sapy, B. 1941 Über das arteriensystem der Hausvögel. Inaug. Diss., Budapest. (In Hungarian, German summary).
- Shiina, J., and D. Miyata 1932 Studies on the cerebral arteries of birds. I. the arterial supply on the brain surface of some kinds of birds. Acta Anat. Nipponica, 5: 13-28 (In Japanese).
- Shindo, T. 1914 Zur vergleichenden Anatomie der arteriellen Kopfgefäße der Reptilien. Anat. Hefte, 51: 267-356.
- Sisson, S., and J. D. Grossman 1963 The anatomy of the domestic animals, 4th ed., rev. W. B. Saunders, Philadelphia.
- Spencer, W. B. 1892 Contribution to our knowledge of *Ceratodus*. Part I. The blood vessels. Macleay Memorial Vol. 1892.
- Starck, D. 1955 Die endokraniale Morphologie der Ratte, besonders der Apterygidae und Dinornithidae. Morph. Jahrb., 96: 13-72.
- Tiedemann, D. F. 1810 Anatomie und Naturgeschichte der Vögel. Bd. 1. Mohr u. Zimmer, Heidelberg.
- Vitums, A., S.-I. Mikami, A. Oksche, and D. S. Farner 1964 Vascularization of the hypothalamo-hypophysial complex in the White-crowned Sparrow, *Zonotrichia leucophrys gambelii*. Zeltsch. f. Zellforsch., 64: 541-569.
- Vitums, A., S.-I. Mikami and D. S. Farner 1965 Arterial blood supply to the brain of the white-crowned Sparrow, *Zonotrichia leucophrys gambelii*. Anat. Anz., 116: 309-326.
- Vitums, A., K. Ono, A. Oksche, D. S. Farner and J. R. King 1966 The development of the hypophysial portal system in the White-crowned Sparrow, *Zonotrichia leucophrys gambelii*. Zeltsch. f. Zellforsch., 73: 335-366.
- Westpfahl, U. 1961 Dar Arteriensystem des Haushuhnes. Wiss. Zeltsch. Humboldt-Univ. Berlin, Math.-Nat. R., 10: 93-124.
- Wingstrand, K. G. 1951 The structure and development of the avian pituitary. C. W. K. Gleerup, Lund.

An Electron Microscopic Study of Ciliogenesis in Developing Epidermis and Trachea in the Embryo of *Xenopus laevis*¹

RALPH M. STEINMAN²

Department of Anatomy, Harvard Medical School, Boston, Massachusetts

ABSTRACT This paper describes the ultrastructural phenomena occurring during the differentiation of cilia in the epidermis and trachea of *Xenopus laevis*. The sequence of developmental events seems to begin with the *de novo* formation of clusters of small, dense "procentriole precursor bodies" which are apparently transformed into procentrioles under the influence of dense amorphous masses here termed "procentriole organizers." The procentriole so formed is a cylinder 150 mμ in diameter with nine single microtubules in its wall which probably give rise to the nine "triplet" microtubules in the wall of the definite centrioles (200 mμ in diameter). The appearance of multiple centrioles in the apical cytoplasm is correlated with disappearance of procentriole precursor bodies and procentrioles. Smooth-surfaced vesicles seemingly produced in the well developed Golgi zones may contribute to the development of the ciliary membrane. Following their formation in the supranuclear cytoplasm, the centrioles or presumptive basal bodies align with their longitudinal axes perpendicular to the apical plasmalemma. A ciliary shaft then appears distal to each basal body and simultaneously small, dense bodies like those termed "procentriole precursor bodies" reappear. At this time we call the dense bodies, "axonemal precursor bodies," because they probably provide material for the synthesis of new axial microtubules at the tip end of the growing cilium. Centriolar rootlets develop during centriolar alignment and ciliary shaft formation from a distinct, low electron-opaque, precursor substance.

From 1875 to 1925, light microscopists extensively investigated the behavior of centrioles during mitosis (van Beneden and Neyt, 1887; Boveri, '01; Schreiner, '05; Heuthner, '33) and ciliogenesis (Benda, '01; Ikeda, '06; Helvenstine, '21-'22; Jordan and Helvenstine, '22; Kindred, '27; Rényi, '24; Walter, '29). These workers concluded that the centrioles found in most cells, and the basal bodies of cilia, possessed similar staining and fixation properties (Helvenstine, '21-'22; Kindred, '27) and could be interconverted (v. Lenhossek, 1898; Henneguy, 1897). In mitosis and ciliogenesis, it was inferred that centrioles could replicate because, in both instances, four or more centrioles appeared in a cell which previously contained but two. Since the multiplication of centrioles occurred at a different time than that of the nucleus, cytologists postulated that centrioles were autonomous cytoplasmic organelles capable of self-replication. They were aware (Heuthner, '33), however, that centrioles apparently could be formed *de novo* in parthenogenetically stimulated oocytes and certain flagellating plant cells. More re-

cently, Lwoff ('50) suggested centrioles represented plasmagenes which, like nuclear genes, were capable of both self-replication and synthesis of specific proteins such as cilia and various centriolar appendages.

Electron microscopists have confirmed the structural similarity of ciliary basal bodies and other centrioles (de Harven and Bernhard, '56) and their associated fibers or microtubules (Porter et al., '64). The first investigators of the ultrastructure of ciliogenesis, however, suggested that centrioles formed *de novo* rather than by replication of preexisting centrioles. Renaud and Swift ('64), and Mizukami and Gall ('66), have now shown that in *Allomyces*, *Marsilia* and *Zamia*, small cylinders or "procentrioles" develop into centrioles in the absence of any preexisting centriolar structure. Stockinger and Cireli ('65) and Cireli ('66) did not report the existence of procentrioles in developing mammalian respiratory passages, but they did find an-

¹Supported by grants HD-00143 and 2T1GM406 from the United States Public Health Service.

²Supported by a John H. Parker Bequest, Harvard University, and a Wislocki Fellowship, Department of Anatomy.

other type of supposed centriolar precursor, clusters of tiny electron-opaque bodies. Dirksen and Crocker ('66), Sorokin and Adelstein ('67), and Sorokin ('67) have seen similar clusters in their studies of mammalian ciliogenesis. In this paper, evidence will be presented that both the clusters of electron-opaque bodies and the procentrioles are involved in the synthesis of centrioles in the ciliating cells of embryonic amphibian epidermis and trachea. Events will also be described that apparently are involved in the differentiation of the other main ciliary components: axial filaments, rootlets and ciliary membrane.

MATERIALS AND METHODS

Xenopus laevis embryos (Nieuwkoop and Faber, '56, stages 19-44) were fixed in glutaraldehyde for 10-30 minutes at room temperature. Generally one of the two following mixtures was used: 3% glutaraldehyde in 0.05 M phosphate buffer at pH 7.4 (Byers and Porter, '64); 5% glutaraldehyde and 4% paraformaldehyde, with 0.075% CaCl₂ in 0.1 M cacodylate at pH 7.4 (Karnovsky, '65). After fixation in glutaraldehyde, the tissues were washed briefly in phosphate or cacodylate buffer, postfixed in 1.3% osmium tetroxide in 0.05 M phosphate at 4°C for one hour, dehydrated in alcohol, flat-embedded in Araldite (R. P. Cargille Labs, Inc., Cedar Grove, Illinois), and sectioned with a glass knife for study in the light and electron microscopes (RCA EMU 3F and Siemens Elmiskop I). The 0.5-1 μ sections were stained with 0.5% toluidine blue in 0.5% borax, while sections on grids were stained with 0.2-0.5% lead citrate alone (Venable and Coggeshall, '65) or preceded by saturated uranyl acetate.

To obtain ventral epidermis, dorsal and head portions of the embryo were removed with a razor blade held in a hemostat. The remainder of the embryo hardened in a few minutes, after which the endoderm was dissected away with fine forceps. This left a sheet of epidermis and underlying lateral mesoderm which could be easily oriented during subsequent processing. To obtain trachea, the embryo was again immersed in a drop of glutaraldehyde fixative on a wax plate, and a transverse section was made just anterior to the midgut. The

head portion alone was prepared for sectioning.

RESULTS

The earliest cilia to appear in the embryo of *X. laevis* develop in the epidermis (fig. 2) following closure of the neural folds (N.F. stages 20, 21). In the case of trachea (fig. 3), the first cilia do not develop until after the embryo has hatched (N.F. stages 42, 43). The general cytology of ciliating epidermis and trachea will be described separately and then the specific ultrastructural events involved in the formation of cilia in the two tissues will be considered together.

General cytology of ciliating epidermis

At the end of neurulation (N.F. stage 20), the ectoderm is already an organized stratified epithelium consisting of basal cuboidal cells and two kinds of superficial columnar cells (fig. 2). One type, representing about three-quarters of the superficial cells, contains numerous pigment granules and apical mucous droplets. The other cell type is more basophilic and contains no mucous droplets, little or no pigment and many centrioles in the apical cytoplasm. Often this cell lies beneath the actual surface of the epidermis. The presence of numerous centrioles permits the conclusion that it is this basophilic, non-pigmented cell which will form cilia. It does so very rapidly, for it is only a matter of an hour or two before the typical ciliated embryonic epidermis is observed (N.F. stage 22).

The most prominent feature of the epidermal mucous cell (fig. 4) is the presence of cytoplasmic organelles associated with secretory activity. Both the Golgi apparatus and the rough endoplasmic reticulum are well developed. The cell also contains a fibrillar terminal web, numerous mitochondria scattered throughout the cytoplasm, and a striking number of particles 200-300 Å in diameter which probably represent ribosomes and glycogen (Hay, '66). Like other embryonic cells at this stage of amphibian development, the mucous cell contains protein and lipid forms of yolk platelets (Wishnitzer, '66). Not more than one centriolar pair is observed per cell. In

one case, this pair was located at the cell surface and was associated with a rudimentary cilium (fig. 6). Single poorly developed cilia have been noted on a number of other "unciliated" cell types (Sorokin, '62; Adams and Hertig, '64).

The centriole-rich basophilic cell does not contain large amounts of endoplasmic reticulum, but does possess a well developed Golgi complex. A few secretory vacuoles may be found, but they are smaller and have a less dense content than the secretory droplets in mucous cells. In the more mature ciliated cell (fig. 5), the centrioles occur near the cell surface as basal bodies associated with cilia. At this time, secretory vacuoles of the type described above are plentiful in the cortical cytoplasm. Numerous mitochondria occur in the apical zone of the cell below the secretory vacuoles, and the Golgi zone is found between the mitochondria and the nucleus. Ribosomes, glycogen particles and yolk platelets are plentiful, occurring throughout the cytoplasm in the progenitor as well as in the more mature ciliated cell.

Ciliated epidermal cells contain relatively few cilia (fig. 5), compared with tracheal cells. The structure of the cilia is not unusual (fig. 7). The ciliary shaft is bounded by an extension of the cell membrane and contains the usual axoneme of nine, plus two axial microtubules that are continuous with, or abut on, the microtubular wall of the centriole or basal body. The interior of the centriole at its distal end is closed by a bilayered basal plate from which short fine filaments descend into the centriolar cavity (fig. 7, fig. 8, arrows). A typical striated foot extends laterally from the basal body (figs. 7, 9) and two types of striated rootlet bundles extend basally (fig. 7). A prominently striated, thick rootlet runs obliquely below and to the side of the centriole, while the other rootlet is thin and descends more deeply into the cell to reach the mitochondrial zone.

General cytology of ciliating trachea

The epithelium of the differentiating trachea, both immediately prior to and following the development of cilia, is pseudo-stratified and columnar in nature (fig. 3). Unlike the case in the epidermis, all of the epithelial cells in the trachea contain mu-

cous droplets prior to ciliogenesis. The mucous vacuoles in those cells in which centriole formation is beginning (fig. 10) are similar to those found in nonciliated cells. Secretory droplets are observed infrequently once centrioles are formed in abundance in the progenitors of ciliated cells (e.g., fig. 21). They are rarely seen following the appearance of ciliary shafts (compare figs. 29 and 31 with fig. 24). The impression is obtained, then, that some of the young mucous epithelial cells originally lining the trachea are converted into ciliated cells, in contrast to the case in the epidermis where typical mucous cells developed independently of their ciliated neighbors.

The ciliated cell in the trachea resembles its epidermal counterpart in the structure of its cilia, the presence of a polarized apical mitochondrial zone, and the abundance of glycogen and ribosomal particles. Yolk platelets are less prominent at this stage. Cilia are much more numerous on the cells of the trachea and thus are more closely packed along the cell surface than was the case in the skin. The Golgi complex is well developed in the progenitor cells that contain multiple centrioles, but is not prominent in the differentiated cell with cilia. The fine structure of the mucous cell in the trachea is almost identical to that of the epidermal mucous cell.

The ultrastructural events that are unique to the development of cilia are similar in both epidermis and trachea. They are presented here in a sequence which appears to represent the chronological order of ciliogenesis *in vivo*.

Procentrioles

Several investigators (Gall, '61; Andre and Bernhard, '64; Renaud and Swift, '64; Mizukami and Gall, '66) have suggested that small dense "cylinders" (140-160 m μ in diameter, 100-120 m μ in length) are precursors to centrioles, and they have given them the name, "procentrioles." Procentrioles of this type are consistently found in amphibian ciliating epidermis and trachea (figs. 10, 16-19).

The wall of the procentriole contains up to nine microtubules which are surrounded by an amorphous dense material (figs. 17, 19). Occasionally the interior of the pro-

centriole seems to contain a central tubule (arrow, fig. 19) from which fine filaments radiate toward the microtubules of the wall, an image which Mizukami and Gall ('66) have likened to a "hub and spoke." The procentrioles tend to occur in groups of four or more (figs. 15, 16) called "generative clusters," by Dirksen and Crocker ('66). An electron-opaque mass, which we have termed the "procentriole organizer," usually occurs in the center of each group of developing (figs. 14, 15) or developed (figs. 16, 17, 33) procentrioles. This so-called "organizer" is absent or much smaller once centrioles appear (fig. 22). On only two occasions, have we observed procentrioles in association with a structure resembling a centriole (fig. 18).

Procentriole-precursor bodies

Clusters of much smaller, seemingly spherical electron-opaque bodies (about 800 Å in diameter) are found in the supranuclear cytoplasm of cells which possess the cylindrical procentrioles (figs. 10, 11). The ground cytoplasm in which the bodies appear to be embedded is relatively lacking in ribosomes and glycogen particles. In one case only, a mature centriole was observed in association with these bodies (fig. 12). Sometimes the dense bodies are observed outside the cluster.

Dense bodies of this same type have been seen during mammalian ciliogenesis by Stockinger and Cireli ('65) and Cireli ('66) who postulated that they constitute precursor material for the *de novo* synthesis of centrioles. They were not observed to occur in groups of nine (Stockinger and Cireli, '65) in our study, however. We think that these bodies are involved in the formation of procentrioles rather than centrioles directly, and have therefore termed them, "procentriole-precursor bodies." They are frequently seen within groups of partially formed procentrioles (figs. 14, 15), whereas they are rarely associated with fully formed groups of procentrioles (figs. 16, 17). Moreover, microtubules like those in procentrioles are often found in certain dense aggregates within the cluster of "precursor bodies" (figs. 11, 13). These dense areas containing microtubules may represent the first step in a transformation of procentriole precursor bodies. It is difficult,

however, to obtain micrographs which conclusively demonstrate the conversion of the precursor bodies into procentrioles.

Formation of centrioles

It is equally difficult to prove that procentrioles are converted into centrioles, although this interpretation has been suggested by certain investigators (Gall, '61; André and Bernhard, '64; Renaud and Swift, '64; Mizukami and Gall, '66). Cells containing centrioles (fig. 21) infrequently possess procentrioles, suggesting that the latter structures have been consumed in centriole production. The procentriole to centriole transformation may be very rapid and therefore difficult to follow in static pictures of fixed material. We have seen, on one occasion, a structure which could represent an intermediate stage between a procentriole and a centriole (fig. 20). The wall of this structure contained both double (fig. 20**) and single microtubules (fig. 20*), some of which had filamentous flanges extending from them (fig. 20, arrows). Possibly the centriolar microtubular triplets are formed by the extension and rounding up of these flanges as Cameron ('65) suggested for microtubule production in *Tenebrio* sperm. The amorphous material that is found in the procentriolar wall (figs. 17, 19) could also be utilized in the differentiation of centriolar triplets.

A cell is observed in both epidermis and trachea which seems intermediate in morphology between the cell containing precursor bodies and procentrioles, and the cell with mature cilia (fig. 21). This cell type was first seen in ciliating tissues by Leeson ('61). Numerous centrioles occupy the supranuclear cytoplasm. The centrioles are similar to the basal bodies of mature cilia in size, wall and internal structure, but they are not associated with axial filaments, basal feet, or rootlets. Numerous smooth vesicles (about 150 mμ in diameter) are intermingled with the centrioles, and the Golgi apparatus is well developed (fig. 22), in spite of the fact that secretory droplets are not usually observed in tracheal cells at this time. It appears that at this stage, the ciliating cell has synthesized its full complement of centrioles. Not only are procentrioles and precursor bodies generally absent, but also there are no signs

of centriolar replication by fission or budding as suggested by light microscopists (Benda, '01; Ikeda, '06; Helvenstine, '22; Rényi, '24; Jordan and Kindred, '27; Walter, '29).

Alignment of centrioles

Following their formation in the supranuclear cytoplasm, centrioles seem to ascend and align beneath the apical cell surface (figs. 23, 28, 29). Presumably there is a distinct delay between the time that centrioles are produced and the time that they begin to migrate to the cell surface, because it is easy to find cells containing unaligned centrioles in both skin and trachea (fig. 21). It also seems likely that movement of centrioles to the surface is a distinct step preceding the formation of ciliary shafts. Only twice have axial filaments been found extending from centrioles in the deeper cytoplasm (fig. 30), although we have found several instances of short cilia protruding from the cell surface (figs. 24-27, 29, 31). Although alignment of centrioles at the cell surface almost inevitably precedes ciliary shaft formation, centrioles evidently do not all ascend to the cell surface simultaneously. The cells at this time contain basal bodies associated with cilia of varying lengths, as well as unaligned centrioles in the supranuclear cytoplasm (fig. 29).

Axonemal precursor bodies

Cells which are forming ciliary shafts possess numerous electron-opaque masses (figs. 24, 28, 29, 31) similar to the procentriole-precursor bodies previously described, even though such bodies were absent in the intermediate cell type containing unaligned centrioles (fig. 21). The cells with developing ciliary shafts, however, lack procentrioles, and the new precursor clusters do not possess the dense aggregates presumed to represent an early stage in the transformation of precursor bodies into procentrioles (figs. 10, 12). Because of the likely possibility that the electron-opaque masses supply material for the production of ciliary axial filaments, we have called them at this stage, "axonemal precursor bodies." These bodies can appear in clusters (figs. 24, 28, 31), but frequently they are scattered about the apical cytoplasm, some-

times in close association with aligning centrioles (figs. 28, 29, 31).

Structure of short cilia

In glutaraldehyde-fixed material, even the shortest of developing cilia contain, throughout their length, axial filaments connected to centrioles (figs. 24-26, 29, 31). Short cilia in osmium-fixed material may seem to lack axial filaments (fig. 27). This fixation lability of developing shaft microtubules is comparable to that of the many other cytoplasmic microtubules that require glutaraldehyde for their convincing demonstration (Ledbetter and Porter, '63). The fixation lability of the earliest axial filaments may account for the empty appearance of the short cilia described in previous studies of ciliogenesis (Sotelo and Trujillo-Cenoz, '59; Tokuyasu and Yamada, '59; Eakin and Westfall, '61; Nilsson, '64). In no case was axial filament formation preceded by the appearance of a microvillus above the centriole as suggested by Rhodin ('66).

We frequently find that the axial filaments of short cilia insert into a cap of electron-opaque material (figs. 24-26) which differs from the striated density (fig. 31) seen at the tips of fully grown cilia. The electron opacity of the growing tip is similar to that of the axonemal precursor bodies and it may be that the cilium grows from the tip end by conversion of axonemal precursor material into axial filaments. We found no evidence for direct formation of ciliary axial filaments by basal bodies as suggested by Lwoff ('50).

Formation of rootlets

In the main part, ciliary rootlets are formed at the same time that centrioles align with the cell surface and ciliary shafts appear (figs. 28, 29). Rootlets seem to be derived from a distinct precursor material of low electron opacity. This substance occurs in patches in cells containing centrioles (fig. 32) and occasionally in cells containing procentrioles and precursor bodies (fig. 33). Electron-opaque foci which are found within this material (figs. 32, 33), may represent a stage in the transformation into rootlet fibrils. A striated fibrillar component was observed within

the rootlet precursor material in a few instances (fig. 33).

DISCUSSION

Since both mucous-secreting and ciliated cells are found in many ciliated epithelia, some controversy has existed in the literature as to whether or not the two cell types are interconvertible. Stockinger ('63) has suggested that mucous cells in mammalian nasal passages undergo metaplasia to ciliated cells. Our results support this hypothesis in the case of embryonic trachea. We observed early stages of ciliogenesis in cells whose cytology is otherwise identical to that of the young mucous cells which initially line the lumen of this organ. The mucous droplets present in immature ciliated cells disappear when fully formed cilia appear at later stages. Although mucous cells as well as ciliated cells are present in developing epidermis, mucous cells do not seem to be involved in the process of ciliogenesis in this tissue. Here, ciliogenesis seems to occur in relatively undifferentiated epidermal cells. Not only do the ciliated cells in the epidermis develop independently of the true mucous cells, but also they may even continue a secretory activity of their own at later stages of development. They retain a few cisternae of rough-surfaced endoplasmic reticulum, hypertrophied Golgi zones and numerous secretory vacuoles that are smaller with a less dense content than that of vacuoles in the adjacent mucous cells. In spite of these differences in cell types of origin, centrioles (basal bodies), axial filaments (axoneme), ciliary rootlets, and the ciliary membrane develop in the same manner in both epidermis and trachea. Our observations suggest a sequence in which these structures are formed, and indicate that the development of the ciliary components is associated with the appearance of distinct precursors in the supranuclear cytoplasm of ciliating cells. The results are summarized diagrammatically in figure 1.

Formation of centrioles — the role of procentrioles

The presence of procentrioles in ciliating epithelia indicate that these tiny dense cylinders might be universally involved in centriole formation. A number of electron

microscopists have found procentrioles in various cell types in which centriole formation was occurring. Procentriole clusters were observed by Gall ('61) in the multiflagellate spermatids of the snail, *Viviparus*. Renaud and Swift ('64) have suggested that a preexisting procentriole develops into a centriole during the transformation of the water mold, *Allomyces*, from the vegetative to the gametophyte phase. Flagellation in the fern, *Marsilia*, and the cycad, *Zamia*, also involves the appearance of procentrioles (Mizukami and Gall, '66). Finally, procentrioles have been found in the development of mitotic centrioles (André and Bernhard, '64).

Certain light microscopists felt that both ciliary (Benda, '01; Ikeda, '06; Jordan and Helvestine, '22; Rényi, '24; Kindred, '27; Walter, '29; Lwoff, '50) and mitotic (van Beneden and Neyt, 1887; Heidenhain 1894; Boveri, '01; Schreiner and Schreiner, '05; Huettner, '33) centrioles replicated to form other centrioles either by fission of a preexisting centriole or by the production of a centriolar "bud" which elongated to form a centriole. Although electron-microscope studies of centriole formation have not uncovered any evidence for centriolar fission, the ultrastructural similarity between the tiny procentriole and larger centriole suggests that the procentriole could

Fig. 1 This diagram depicts the suggested sequence of events involved in the development of cilia in *Xenopus laevis*. Dense procentriole precursor bodies are transformed into procentrioles, possibly under the influence of dense procentriole organizers (top left). The procentriole is a small cylinder with nine single microtubules in its wall, and a hub and spoke structure in its interior. The next stage in ciliogenesis involves the appearance of a cell type containing numerous centrioles (top right), presumably produced from the procentrioles. The centrioles have nine microtubular triplets in their walls, and are larger than the procentrioles. Procentrioles and precursor bodies are absent in these cells, but smooth vesicles and rootlet precursor areas (not shown here) do occur. The centrioles move to the cell surface (lower half of diagram), where they align with their longitudinal axes perpendicular to the apical plasmalemma. Ciliary shafts and new clusters of axonemal precursor bodies now appear. The axial filaments probably elongate utilizing dense material in the tip of the cilium, which may be derived from the axonemal precursor bodies. Centriolar rootlets begin to appear at this stage and smooth vesicles are abundant (not shown here).

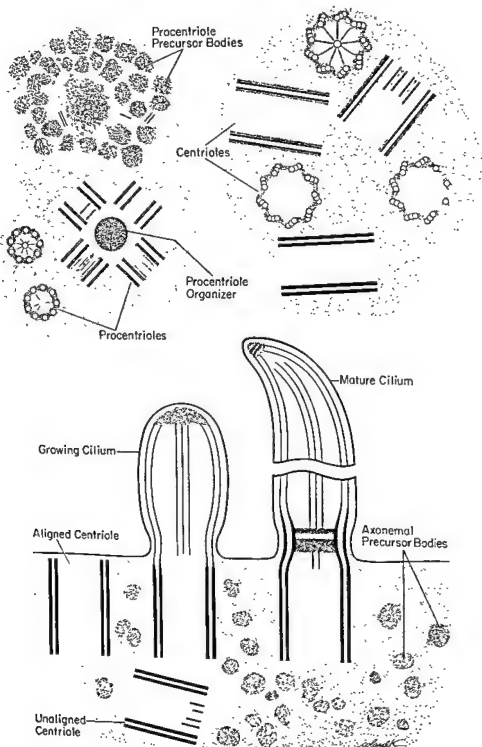


Figure 1

correspond to the hypothetical centriolar bud. Both organelles have the shape of a dense cylinder, but the procentriole is smaller in diameter (140–160 $\mu\mu$) and length (100–120 $\mu\mu$) than the centriole (200 \times 300–500 $\mu\mu$). The wall of the procentriole contains nine single microtubules, and its inner cavity is occupied by a central microtubule from which fine filaments radiate toward the wall microtubules (the "hub and spoke" pattern). The wall of the centriole possesses nine triplets of microtubules, but only the proximal portion of the inner cavity contains the hub and spoke structure. Gall ('61) concluded that the procentriole will constitute the proximal part of the centriole to which it seems to give rise.

The procentriole-precursor bodies

Our results support those of several recent workers (Stockinger and Cireli, '65; Cireli, '66; Dirksen and Crocker, '66; Sorokin and Adelstein, '67; Sorokin, '67) who postulated that clusters of tiny electron-opaque masses serve as precursors to centrioles during ciliogenesis in mammalian respiratory passages. We have seen essentially the same material in cells containing procentrioles, and at this stage these dense bodies are generally independent of fully developed or preexisting centrioles. We have not observed the amorphous low-electron-opaque material which enmeshes the precursor bodies (or "proliferative elements") in the micrographs of Dirksen and Crocker ('66). These workers employed osmium fixation, and it may be that the glutaraldehyde we employed preserves enough of the background cytoplasm so that the latter cannot be distinguished from the background material within the precursor clusters.

We have named these tiny electron-opaque masses "procentriole-precursor bodies." Two lines of evidence suggest that these bodies are involved in procentriole formation. First, the so-called procentriole-precursor bodies are most likely to be associated with procentrioles in areas in which the procentriole cluster is incomplete. Secondly, profiles of microtubules, similar to those found in the procentriole wall, are observed in electron-opaque aggregates within the clusters of precursor

bodies. Possibly these dense regions represent a very early step in the conversion of the procentriole-precursor bodies into procentrioles. Dense precursor bodies of this type could be involved in the manufacture of procentrioles in nonciliated cells as well. Structures similar to procentriole-precursor bodies can be seen in Gall's micrographs of *Viviparus* spermatid development and the author apparently considers them to be immature procentrioles. Also, pericentriolar "satellites," which seem to be identical with precursor bodies, could be involved in the production of centrioles prior to mitosis (Bessis and Breton-Gorius, '58; Murray et al., '65).

Procentriole organizer

An interesting new structure has been seen in the middle of procentriole clusters. It is a large electron-opaque mass which we have called a "procentriole organizer." This tentative name reflects the possible involvement of the structure in organizing procentriole precursor bodies into procentrioles. Consistent with this possible function is the occurrence of the procentriole organizer in areas where procentriole synthesis seems to be taking place, i.e., in regions containing both procentrioles and procentriole precursor bodies. It is equally possible, however, that organizer masses are somehow employed in the conversion of procentrioles into centrioles. Indeed, the organizers are invariably present amidst procentriole clusters but they are infrequently seen in cells containing fully differentiated centrioles. Procentriole organizers may be present during centriole formation in *Marsilia* and *Zamia*. Here, the blepharoplast structures at both poles of the nucleus are converted to annuli whose walls contain numerous procentrioles and whose cores contain electron dense areas which may correspond to our organizer bodies (Mizukami and Gall, '66; fig. 30). Although the bulk of centrioles in our material are apparently formed *de novo*, i.e., without the direct association of the preexisting centriolar pair, it is possible that the latter can perform a function similar to procentriole organizers. We have observed three cases in which an apparently preexisting centriole occupies the position of a procentriole organizer. The preexisting

centrioles themselves may be all that is required in those cases of centriologenesi in which a small number of new centrioles are being formed, e.g., in mitosis (André and Bernhard, '64; Murray et al., '65) and in snail spermatid flagellation (Gall, '61). The procentriole organizer may then constitute a specialization required for centriole production in cells whose demand for new centrioles exceeds the supply of pre-existing ones, or in cells which lack pre-existing centrioles.

Formation of axial filaments (axoneme)

Few speculations on the initiation of ciliary shaft formation are to be encountered in the literature. Sorokin ('62) and others (e.g. Renaud and Swift, '64; Allen, '65; Satir, '65) state that in the case of certain solitary cilia, axial filaments develop from centrioles located deep in the cytoplasm. The elongating shaft seems to be surrounded by a membranous sheath which eventually fuses with the cell membrane. On the other hand, the single cilia of embryonic chick ependymal cells (Sotelo and Trujillo-Cenoz, '59) and various photoreceptors (Tokuyasu and Yamada, '59; Eakin and Westfall, '61; Nilsson, '64) seem to develop directly on the cell surface after alignment of the centrioles beneath the apical plasmalemma. In ciliating skin and trachea, we too have observed centrioles arranged directly beneath and perpendicular to the cell surface. Very short cilia, which are likely in a state of growth, extend into the lumen from these centrioles. The initial stimulus for ciliary shaft formation may result from contact of the distal end of the centriole with the apical membrane. We have rarely seen axial filaments developing from centrioles deep in the cytoplasm.

Cells which are forming ciliary shafts contain dense (800 Å) bodies which resemble the material referred to as procentriole-precursor bodies. We will refer to these as "axoneme precursor bodies" to indicate the temporal phase of development in which they occur. Precursor bodies appear in two phases then: the first begins with the synthesis of procentrioles and ends with the formation of cells containing centrioles; the second phase commences with axial filament development and ends

when the cell has mature cilia. The precursor bodies in the cells forming ciliary shafts probably are not involved in procentriole manufacture, because cells developing axonemes do not contain procentrioles. The fact that the second phase of precursor body development begins at the time when cilia begin to grow out from the cell surface and finishes by the time all the cilia have differentiated is taken as evidence that these precursor bodies contain material for the developing ciliary shafts. The dense precursor bodies seem to follow the centrioles as they move to the cell surface to initiate the development of the axoneme. It may seem unreasonable to think that the same kind of precursor material could give rise to both centriole and axoneme, yet both structures are composed of microtubules in a similar organization. Other cell types contain cytoplasmic microtubules which may be related to dense masses that are similar in size and electron opacity to our precursor bodies. (de Thé, '64; Gonatas and Robbins, '65; Trelstad et al., '67; Hamilton, in preparation). De Thé has suggested that such dense masses, the pericentriolar satellites, are involved in microtubule formation.

We have found that the axial filaments of short cilia insert into a cap of electron-opaque material at the ciliary tip. The rather granular material at the tips of developing cilia differs from the striated densities found at the tips of mature cilia. In electron opacity, it is similar to axoneme precursor bodies. It is possible, then, that the cilium elongates by accumulation of precursor material at the tip of the ciliary shaft and conversion there into axial filaments. Autoradiographic studies (Rosenbaum and Child, '67), have demonstrated an incorporation of amino acids into the tip end of regenerating flagella of *Euglena gracilis*, although these authors could not determine if the axoneme membrane or some other shaft component was being labeled.

Formation of rootlets

The precursor material seemingly involved in rootlet formation differs considerably from the electron-opaque precursor bodies observed near procentrioles and growing ciliary shafts. The rootlet precur-

sor substance appears to be of uniform low electron opacity, and can be found near centrioles, procentrioles or precursor bodies. The evidence that rootlets develop from the relatively large patches of low electron absorbing material is two-fold. First, bundles of rootlets have been seen within the large patches. Secondly, the so-called rootlet precursor disappears at the time that rootlets differentiate. It is to be noted that the large precursor patches can be found in cells which do not yet contain centrioles. The rootlet precursor might accumulate into the large patches as it is synthesized and later can divide into portions that become associated with individual centrioles. Indeed the centrioles may attract the precursor and/or influence its transformation into actual rootlets.

Formation of ciliary membrane

There must be a considerable amount of plasma membrane synthesized during ciliogenesis, since the long axial filament complex of each cilium is enclosed by a typical plasmalemma. New cell membrane may be derived from the numerous smooth-surfaced vesicles which are seen in the apical cytoplasm at the time that multiple centrioles appear. Williams et al. ('60) report the occurrence of similar vesicles during *Tetrahymena* ciliogenesis. Other workers (Sorokin, '62; Renaud and Swift, '64) have suggested that vesicles, 50–250 μ in diameter, fuse to form the intracellular sheath for developing solitary cilia or flagella. This so-called sheath is said to become the membrane of the cilium upon coalescence with the cell surface. Porter and Machado ('60), and Whaley et al. ('66), have observed that the cell membrane involved in plant cell cytokinesis is derived from a fusion of smooth vesicles in the equatorial plate. There are other possible roles for vesicles in ciliating cells, however. Graf and Stockinger ('66) claim that acetylcholinesterase is localized in the smooth reticulum of ciliated cells. If acetylcholine is involved in ciliary excitation (Augustinsson and Gustafson, '49), smooth vesicles may function in the metabolism of this transmitter. Of course, small vesicles could also be associated with pinocytosis or secretion. It seems unlikely that all of the smooth vesicles are precursors of secre-

tory droplets, however, as they are found in tracheal cells which no longer contain mucous granules, and in skin cells at a stage in which the number of mucous vacuoles is extremely small.

The origin of vesicles in ciliating cells is unknown. Sorokin ('62) considered the Golgi apparatus as the source of vesicles used in the differentiation of the sheath of solitary cilia. The Golgi complex was also implicated (Whaley and Mollenhauer, '63; Whaley et al., '66) in the production of vesicles involved in equatorial plate formation in dividing plant cells. Palade ('59) has suggested that the high ratio of surface area to volume of the Golgi lamellae makes this organelle suitable for membrane storage and formation, and we find that Golgi lamellae in ciliating cells often do assume considerable lengths. Certainly, ciliogenesis provides an excellent opportunity for future study of the relation between cell membrane and Golgi complex.

ACKNOWLEDGMENTS

It was a most enjoyable and instructive experience for the author to be guided by Drs. Elizabeth D. Hay and Jean-Paul Revel through the bulk of his training in electron microscopy and his study of ciliogenesis. The author also profited from the advice of Drs. Don W. Fawcett, S. Ito, R. E. Coggeshall, and A. L. Jones.

LITERATURE CITED

- Adams, E. C., and A. T. Hertig 1964 Electron microscopic observations on the development of cytoplasmic organelles in oocytes of primordial and primary follicles. *J. Cell Biol.*, 21: 397–427.
- Allen, R. A. 1965 Isolated cilia in inner retinal neurones in the retinal pigment epithelium. *J. Ultra. Res.*, 12: 730–747.
- André, J., and W. Bernhard 1964 The centriole and the centriolar region. *Excerpta Med. Int. Cong. Ser.*, 77: 9.
- Augustinsson, K. B., and T. Gustafson 1949 Cholinesterase in developing sea urchin eggs. *J. Cell. and Comp. Physiol.*, 34: 311–321.
- Benda, C. 1901 Ueber neue Darstellungsmethoden der Centralkörperchen und die Verwandtschaft der Basalkörper der Cilien mit Centralkörperchen. *Arch. für Anat. und Physiol. Abt.*, 147–157.
- Bessis, M. M., and J. Breton-Gorius 1958 Sur une structure inframicroscopique pericentriolaire. Etude au microscope électronique sur des leucocytes de mammifères. *Compt. Rendues Soc. Biol.*, 246: 1289–1291.

- Boveri, T. 1901 Ueber die Natur der Centrosomen. Jena. Z. für Natur., 35: 1-220.
- Byers, B., and K. R. Porter 1964 Oriented microtubules in elongating cells of the developing lens rudiment after induction. Proc. Nat. Acad. Sci., U. S., 52: 1091-1099.
- Cameron, M. L. 1965 Some details of ultrastructure in the development of flagellar fibers of the *Tenebrio* sperm. Can. J. Zool., 43: 1005-1010.
- Cirelli, E. 1966 Elektronenmikroskopische Analyse der prä- und postnatalen Differenzierung des Epithels der oberen Luftwege der Ratte. Z. für Mikr. Anat. Forsch., 74: 132-178.
- Dirksen, E. R., and T. T. Crocker 1966 Centriole replication in differentiating ciliated cells of mammalian respiratory epithelium. An electron microscope study. J. Micr., 5: 639-644.
- Eakin, R. M., and J. A. Westfall 1961 The development of photoreceptors in the stirnorgan of the tree frog, *Hyla regilla*. Embryologia, 6: 84-98.
- Gall, J. G. 1961 Centriole replication: A study of spermatogenesis in the snail, *Viviparus*. J. Biochem. and Biophys. Cytol., 10: 163-209.
- Gonatas, N. K., and E. Robbins 1965 The homology of spindle tubules and neurotubules in the chick embryo retina. Protoplasma, 59: 377-391.
- Graf, J., and L. Stockinger 1966 Endoplasmatisches Retikulum und Reizleitung im Flimmerepithel; Darstellung der Cholinesterase. Z. für Zellforsch. und Mikr. Anat., 72: 184-192.
- Hamilton, D. W. In preparation.
- de Harven, E., and W. Bernhard 1956 Etude au microscope électronique de l'ultrastructure du centriole chez les vertébrés. Z. für Zellforsch. und Mikr. Anat., 45: 378-398.
- Hay, E. D. 1966 Polygranular arrays of glycogen that mimic polyribosomes in *Xenopus* eggs and embryos. J. Cell Biol., 31: 45A.
- Heidenhain, M. 1894 Neue Untersuchungen über die Centrialkörper und ihre Beziehungen zum Kern und Zellenprotoplasma. Schultze Archiv. für Mikr. Anat., 43: 423-758.
- Helvenstine, F., Jr. 1921-1922 Amitosis in the ciliated cells of the gill filaments of *Cyclops*. J. Morph., 36: 103-117.
- Hennequy, L. F. 1897 Sur les rapports des cils vibratiles avec les centrosomes. Arch. Anat. Micr., Paris, 1: 481-496.
- Heutner, A. F. 1933 Continuity of the centrioles in *Drosophila melanogaster*. Z. für Zellforsch. und Mikr. Anat., 19: 119-135.
- Ikeda, R. 1906 Ueber das Epithel im Nebenhoden des Menschen. Anat. Anz., 29: 76-82.
- Jordan, H. E., and F. Helvenstine, Jr. 1922 Cilogenesis in the epididymis of the white rat. Anat. Rec., 25: 7-17.
- Karnovsky, M. J. 1965 A formaldehyde-glutaraldehyde fixative of high osmolality for use in electron microscopy. J. Cell Biol., 27: 137A.
- Kindred, J. E. 1926-1927 Cell division and cilogenesis in the ciliated epithelium of the pharynx and esophagus of the tadpole of the green frog, *Rana clamitans*. J. Morph., 43: 267-297.
- Ledbetter, M. C., and K. R. Porter 1963 A "microtubule" in plant cell fine structure. J. Cell Biol., 19: 239-250.
- Leeson, T. S. 1961 The development of the trachea in the rabbit with particular reference to its fine structure. Anat. Anz., 110: 214-223.
- Lenhossek, M. v. 1898 Ueber Flimmerzellen. Verhandl. der Anat. Gesell., 12: 106-128.
- Lwoff, A. 1950 Problems of morphogenesis in ciliates. J. Wiley, New York.
- Mizukami, J., and J. Gall 1966 Centriole replication II: Sperm formation in the fern, *Marsilea*, and the cycad, *Zamia*. J. Cell Biol., 29: 97-111.
- Murray, R. C., A. S. Murray and A. Pizzo 1965 The fine structure of mitosis in rat thymic lymphocytes. J. Cell Biol., 26: 601-619.
- Nilsson, S. E. G. 1964 Receptor cell outer segment development and ultrastructure of the disk membranes in the retina of the tadpole (*Rana pipiens*). J. Ultrastruct. Res., 11: 581-620.
- Nieuwkoop, P. D., and J. Faber 1956 Normal Table of *Xenopus laevis* (Daudin). North Holland Publishing, Amsterdam.
- Palade, G. F. 1959 Functional changes in the structure of cell components. In: Subcellular Particles. T. Hayashi, ed. Ronald Press, New York, pp. 64-83.
- Porter, K. R., M. C. Ledbetter and S. Baudens-husen 1964 The microtubule in cell fine structure as an accompaniment of cytoplasmic movements. Excerpta Med. Int. Cong. Ser., 77: 36-37.
- Porter, K. R., and R. D. Machado 1960 Studies on the endoplasmic reticulum. IV. Its form and distribution during mitosis in cells of onion root tip. J. Biophys. Biochem. Cytol., 7: 167-180.
- Renaud, F. L., and H. Swift 1964 The development of basal bodies and flagella in *Allomyces arbusculus*. J. Cell Biol., 23: 339-354.
- Rényi, G. 1924 Die Entwicklung des Flimmerapparates. Z. für Anat. und Entwicklung., 73: 349-357.
- Rhodin, J. A. G. 1966 Ultrastructure and function of human tracheal mucosa. Amer. Rev. Resp. Dis., 93: no. 3, Part II, 1-15.
- Rosenbaum, J. L., and F. M. Child 1967 Flagellar regeneration in protozoan flagellates. J. Cell Biol., 34: 327-344.
- Schreiner, A., and K. E. Schreiner 1905 Über die Entwicklung der männlichen Geschlechtszellen von *Myxine glutinosa* (L.). II. Die Centriolen und ihre Vermehrungsweise. Arch. de Biol., 21: 315-355.
- Satir, P. 1965 Structure and function in cilia and flagella. Protoplasmatologia, 3: 1-52.
- Sorokin, S. 1962 Centrioles and the formation of rudimentary cilia by fibroblasts and smooth muscle cells. J. Cell Biol., 15: 363-377.
- Sorokin, S. 1968 Reconstruction of centriole formation and cilogenesis in mammalian lungs. J. Cell Sci. (in press).
- Sorokin, S. P., and S. J. Adelstein 1967 Failure of 1100 rads X-radiation to affect cilogenesis and centriolar formation in cultured rat lungs. Radiation Res., 31: 748-759.

sor substance appears to be of uniform low electron opacity, and can be found near centrioles, pro-centrioles or precursor bodies. The evidence that rootlets develop from the relatively large patches of low electron absorbing material is two-fold. First, bundles of rootlets have been seen within the large patches. Secondly, the so-called rootlet precursor disappears at the time that rootlets differentiate. It is to be noted that the large precursor patches can be found in cells which do not yet contain centrioles. The rootlet precursor might accumulate into the large patches as it is synthesized and later can divide into portions that become associated with individual centrioles. Indeed the centrioles may attract the precursor and/or influence its transformation into actual rootlets.

Formation of ciliary membrane

There must be a considerable amount of plasma membrane synthesized during ciliogenesis, since the long axial filament complex of each cilium is enclosed by a typical plasmalemma. New cell membrane may be derived from the numerous smooth-surfaced vesicles which are seen in the apical cytoplasm at the time that multiple centrioles appear. Williams et al. ('60) report the occurrence of similar vesicles during *Tetrahymena* ciliogenesis. Other workers (Sorokin, '62; Renaud and Swift, '64) have suggested that vesicles, 50-250 m μ in diameter, fuse to form the intracellular sheath for developing solitary cilia or flagella. This so-called sheath is said to become the membrane of the cilium upon coalescence with the cell surface. Porter and Machado ('60), and Whaley et al. ('66), have observed that the cell membrane involved in plant cell cytokinesis is derived from a fusion of smooth vesicles in the equatorial plate. There are other possible roles for vesicles in ciliating cells, however. Graf and Stockinger ('66) claim that acetylcholinesterase is localized in the smooth reticulum of ciliated cells. If acetylcholine is involved in ciliary excitation (Augustinsson and Gustafson, '49), smooth vesicles may function in the metabolism of this transmitter. Of course, small vesicles could also be associated with pinocytosis or secretion. It seems unlikely that all of the smooth vesicles are precursors of secre-

tory droplets, however, as they are found in tracheal cells which no longer contain mucous granules, and in skin cells at a stage in which the number of mucous vacuoles is extremely small.

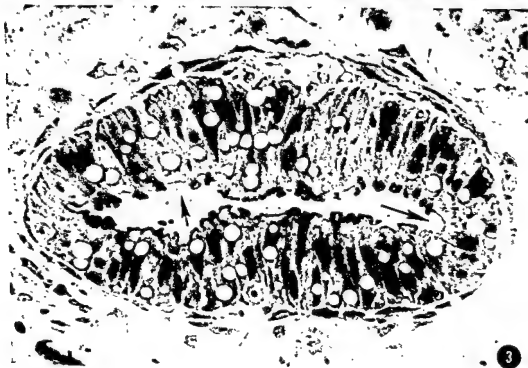
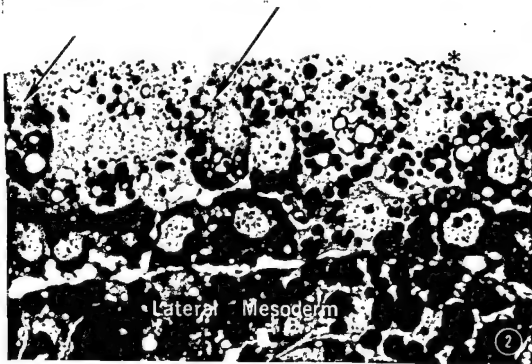
The origin of vesicles in ciliating cells is unknown. Sorokin ('62) considered the Golgi apparatus as the source of vesicles used in the differentiation of the sheath of solitary cilia. The Golgi complex was also implicated (Whaley and Mollenhauer, '63; Whaley et al., '66) in the production of vesicles involved in equatorial plate formation in dividing plant cells. Palade ('59) has suggested that the high ratio of surface area to volume of the Golgi lamellae makes this organelle suitable for membrane storage and formation, and we find that Golgi lamellae in ciliating cells often do assume considerable lengths. Certainly, ciliogenesis provides an excellent opportunity for future study of the relation between cell membrane and Golgi complex.

ACKNOWLEDGMENTS

It was a most enjoyable and instructive experience for the author to be guided by Drs. Elizabeth D. Hay and Jean-Paul Revel through the bulk of his training in electron microscopy and his study of ciliogenesis. The author also profited from the advice of Drs. Don W. Fawcett, S. Ito, R. E. Coggeshall, and A. L. Jones.

LITERATURE CITED

- Adams, E. C., and A. T. Hertig 1964 Electron microscopic observations on the development of cytoplasmic organelles in oocytes of primordial and primary follicles. *J. Cell Biol.*, 21: 397-427.
- Allen, R. A. 1965 Isolated cilia in inner retinal neurones in the retinal pigment epithelium. *J. Ultra. Res.*, 12: 730-747.
- André, J., and W. Bernhard 1964 The centriole and the centriolar region. *Excerpta Med. Int. Cong. Ser.*, 77: 9.
- Augustinsson, K. B., and T. Gustafson 1949 Cholinesterase in developing sea urchin eggs. *J. Cell. and Comp. Physiol.*, 34: 311-321.
- Benda, C. 1901 Ueber neue Darstellungsmethoden der Centrialkörperchen und die Verwandtschaft der Basalkörper der Cilien mit Centrialkörperchen. *Arch. für Anat. und Physiol. Abt.*, 147-157.
- Bessis, M. M., and J. Breton-Gorius 1958 Sur une structure inframicroscopique pericentriolaire. Etude au microscope électronique sur des leucocytes de mammifères. *Compt. Rendues Soc. Biol.*, 246: 1280-1291.



- Sotelo, J. R., and O. Trujillo-Cenoz 1959 An electron microscope study on the development of ciliary components of the neural epithelium of the chick embryo. *Z. für Zell. Mikr. Anat.*, 49: 1-12.
- Stockinger, L. 1963 Beiträge zur Entwicklung und Ultrastruktur des Flimmersaumes. *Anat. Ges. Verhandl.*, 59: 443-466.
- Stockinger, L., and E. Cireli 1965 Eine Bisher Unbekannte art der Zentriolenvermehrung. *Z. für Zell. Mikr. Anat.*, 68: 733-740.
- de Thé, G. 1964 Cytoplasmic microtubules in different animal cells. *J. Cell Biol.*, 23: 265-275.
- Tokuyasu, K., and E. Yamada 1959 The fine structure of the retina studied with the electron microscope. IV. Morphogenesis of outer segments of retinal rods. *J. Biochem. Biophys. Cytol.*, 6: 225-230.
- Trelstad, R. L., E. D. Hay and J. P. Revel 1967 Cell contact during early morphogenesis in the chick embryo. *Dev. Biol.*, 16: 78-106.
- van Beneden, E., and A. Neyt 1887 Nouvelle recherches sur la fécondation et la division mitotique chez l'*Ascaride mégalocéphale*—communication préliminaire. *Bull. Acad. Roy. Belg. Serie 3*, 14: 215-290.
- Venable, J. H., and R. Coggeshall 1965 A simplified lead citrate stain for use in electron microscopy. *J. Cell Biol.*, 25: 407-408.
- Walter, L. 1929 Ciliogenesis in a cystically dilated hydatid of Morgagni. *Anat. Rec.*, 42: 177-187.
- Whaley, W. G., and H. H. Mollenhauer 1963 The Golgi apparatus and cell plate formation—a postulate. *J. Cell Biol.*, 17: 216-221.
- Whaley, W. G., J. E. Dauwalder and J. E. Kephart 1966 The Golgi apparatus and an early stage in cell plate formation. *J. Ultra. Res.*, 15: 169-180.
- Williams, N. E., E. Anderson, R. Kessel and H. W. Beams 1960 Electron microscope observations on synchronously dividing *Tetrahymena*. *J. Protozool.*, Suppl., 7: 27.
- Wischnitzer, S. 1966 The ultrastructure of the cytoplasm of the developing amphibian egg. *Adv. in Morphogenesis*, 5: 131-179.

PLATE 1

EXPLANATION OF FIGURES

- 2 A light micrograph of ectoderm and underlying lateral mesoderm in an embryo, following closure of the neural folds (stage 20, N.F.). The ectoderm consists of a columnar superficial layer and a cuboidal basal layer. The superficial layer contains many mucous cells, which are rich in pigment granules (e.g., beneath asterisk), and a number of more basophilic cells, which have little or no pigment. These columnar basophilic cells (arrows) often possess numerous centrioles in the supranuclear cytoplasm, whereas the deeper cuboidal basophilic cells do not. All of the cells have dense yolk platelets and hollow-appearing lipid droplets whose content is probably not well preserved in our preparations. $\times 525$.
- 3 A light micrograph of trachea after ciliogenesis is well underway (stage 43, N.F.). A loose mesenchyme surrounds the pseudostratified epithelium. Two cell types lining the lumen of the trachea are easily distinguished. The ciliated cells (arrows) have distinct tufts of cilia extending from a row of basal bodies, while the mucous cells are characterized by densely staining mucous vacuoles. Hollow-appearing lipid droplets are still prominent in most *Xenopus laevis* cells at stage 43. $\times 650$.

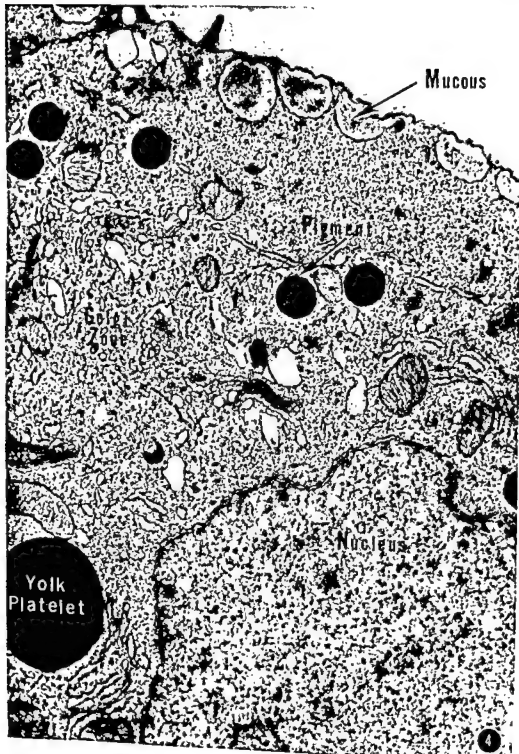


PLATE 2

EXPLANATION OF FIGURE

- 4 An electron micrograph of a mature mucous cell in the epidermis. The cortical cytoplasm contains mucous droplets and ill defined tonofilaments that seem to comprise a terminal web. The presence of a well developed apical Golgi zone, and abundant rough endoplasmic reticulum in other parts of the cell, are consistent with the secretory activity of this cell type. Some of the many pigment granules that characterize skin mucous cells are shown in the figure. Glycogen and ribosomal particles are abundant. $\times 22,000$.

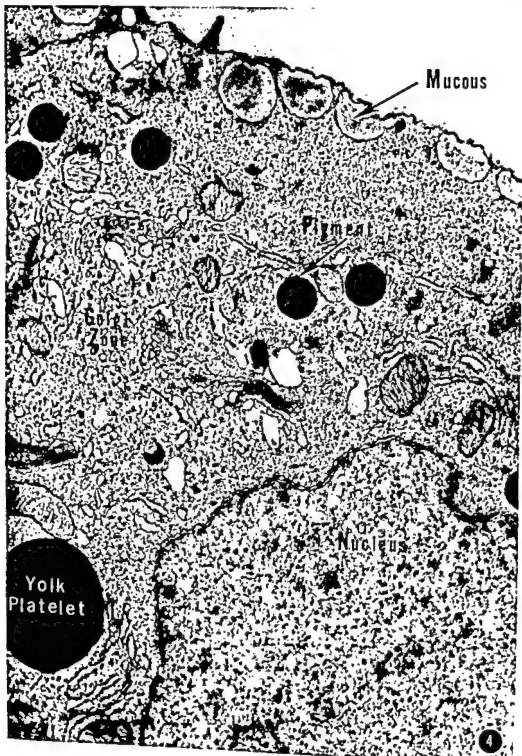


PLATE 3

EXPLANATION OF FIGURES

- 5 The organelles of ciliated cells are strikingly polarized in the sense that the centrioles, mitochondria, and Golgi elements form discrete bands in the supranuclear cytoplasm. Centriolar rootlets (arrow) descend into the underlying mitochondrial zone. No ciliary shaft seems to have developed yet in association with the centriole labeled by the asterisk. The cytoplasm is replete with glycogen and ribosomal particles, and a well developed nucleolus can be seen in the basal nucleus. In the epidermis, the cortical cytoplasm of ciliated cells contains secretory droplets of unknown nature. $\times 11,000$.
- 6 This electron micrograph portrays an instance in which the centriolar pair of an epidermal mucous cell was situated next to the apical plasmalemma. A very rudimentary cilium seems to be associated with one of the centrioles. Usually the centrioles occupy a deeper position in the cytoplasm of mucous cells. A few cytoplasmic microtubules course near the centrioles (arrow). $\times 29,000$.

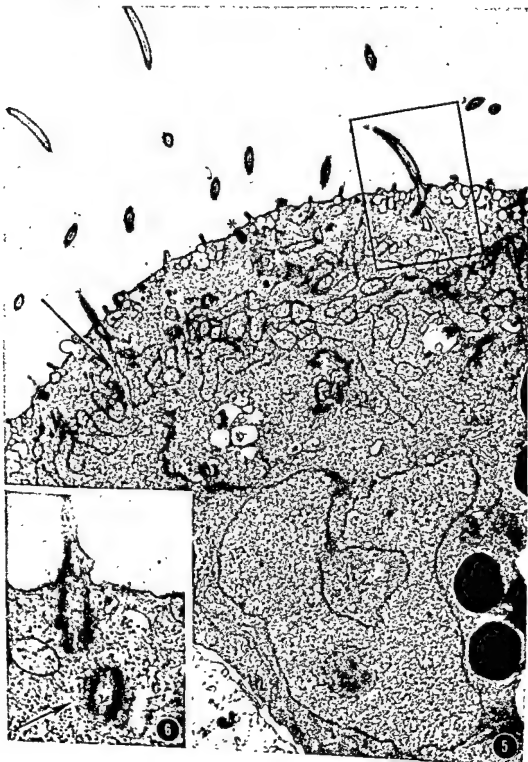


PLATE 4

EXPLANATION OF FIGURES

- 7-9 A high-power view (fig. 7) of the cilium outlined by the rectangle in figure 5, illustrates the principal components of a typical cilium. The ciliary shaft is bound by an extension of the cell membrane and contains longitudinally arranged microtubules which are continuous with, or abut on, the microtubules of the centriole. The ciliary shaft and centriole are separated by a bilayered basal plate from which fine filaments (arrow) descend into the centriolar interior. These filaments are shown in cross-section in figure 8 (arrow). The basal foot extending laterally from the basal body can be seen (arrow) in cross-section in figure 9. Two bundles of striated rootlets descend basally from the centriole. A short, broad group of rootlet fibers extends obliquely, and a long thin bundle reaches deep into the mitochondrial zone. Figure 7, $\times 50,000$. Figure 8, $\times 100,000$. Figure 9, $\times 90,000$.



PLATE 5

EXPLANATION OF FIGURE

- 10 An electron micrograph of the supranuclear cytoplasm of several cells lining the lumen of a trachea. Ciliogenesis is just beginning. Many of these cells contain clusters of the electron-opaque masses which we have termed "procentriole-precursor" bodies. Two such clusters are encircled. Procentrioles are also found in cells which possess the precursor bodies. At this stage of differentiation, the immature ciliated cells of the trachea contain the same kind of secretory droplet as do the nonciliated mucous cells. The Golgi apparatus (lower left corner of figure) has lengthy lamellae. Mitochondria and abundant glycogen and ribosomal particles are also evident. $\times 26,000$.

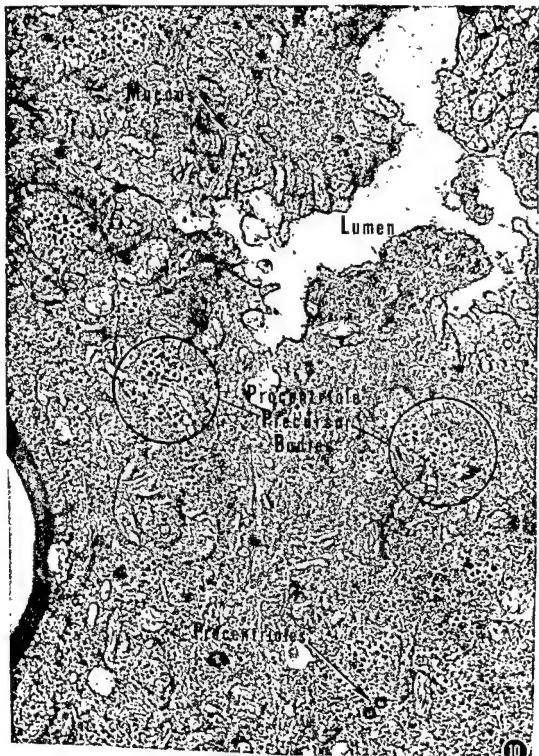


PLATE 6

EXPLANATION OF FIGURE

- 11 A higher power view of two clusters of procentriole precursor bodies. The sectioned diameter of individual precursor bodies varies from 300–800 Å, which is to be expected if each body is spherical in form with a maximum diameter of 800 Å. A few smooth vesicles and cytoplasmic particles are found within the precursor clusters. The glutaraldehyde fixative which we employed does not clearly demarcate from the rest of the cytoplasm a distinct matrix material seen by other workers as enmeshing the precursor bodies. Frequently, amorphous electron-opaque areas (double-edged arrow) are associated with the clusters of precursor bodies. $\times 52,000$.



PLATE 7

EXPLANATION OF FIGURES

- 12 Procentriole-precursor bodies are rarely associated with centrioles but, in one instance in trachea, this association was observed. $\times 85,000$.
- 13 The amorphous dense areas found near procentriole-precursor cluster (fig. 11, double-edged arrow) appear at higher magnification to contain microtubules. The arrows point to cross-sections of two such tubular structures, each 250 Å in diameter. It is possible that these amorphous areas are intermediate stages in the formation of procentrioles from the precursor bodies (see text). $\times 130,000$.
- 14 The encircled structure in this electron micrograph is probably a developing procentriole, whereas the electron-opaque body (arrow) appears to be a procentriole organizing body. The remaining electron-opaque material may be similar to that shown in figure 13. $\times 84,000$.
- 15 The dense organizer is more clearly seen in this micrograph from trachea. Developing procentrioles are closely associated with the organizer, while procentriole-precursor bodies lie on the left of the figure. $\times 80,000$.

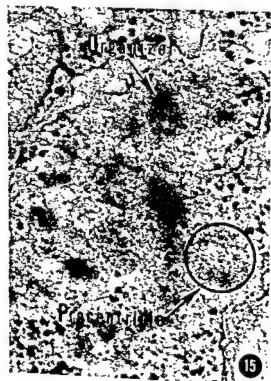
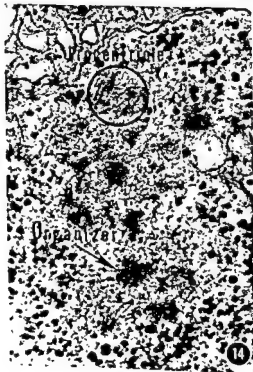
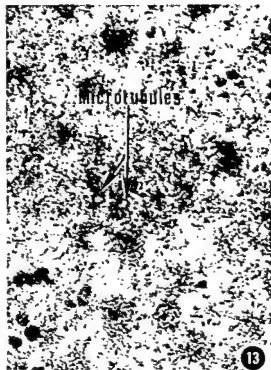
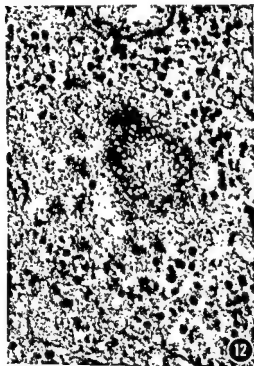


PLATE 8

EXPLANATION OF FIGURES

- 16-17 Additional electron micrographs of sections through groups of pro-centrioles reveal again the dense structures called "procentriole organizers." At the top of figure 16, the procentrioles are seen to be arranged at right angles around the organizing body. The circle in figure 17 contains a procentriole cut in cross-section demonstrating the single microtubules which form the procentriolar wall. Figure 16, $\times 50,000$. Figure 17, $\times 75,000$.
- 18 This electron micrograph depicts one of two cases in which a large centriole-like structure was observed to be surrounded by a group of procentrioles. That this central structure is a centriole in this unusual case is suggested by its dimensions and the presence of what are apparently microtubular triplets in its wall. $\times 70,000$.
- 19 Several procentrioles are seen here cut in cross-section. One procentriole has a central tubule (arrow) from which fine filaments radiate to the wall. This is the so-called "hub and spoke" arrangement found in procentrioles and the proximal portion of centrioles. The procentriole walls are seen to contain nine single microtubules, some of which are indicated by an asterisk. $\times 90,000$.
- 20 The structure depicted here may be an intermediate in the conversion of a procentriole into a centriole. Single (*) and doublet (**) microtubules are seen. Flanges (arrows), which may represent incomplete microtubules, extend from some of the formed microtubules. $\times 95,000$.

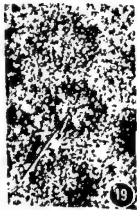
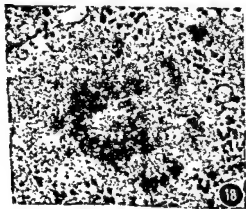
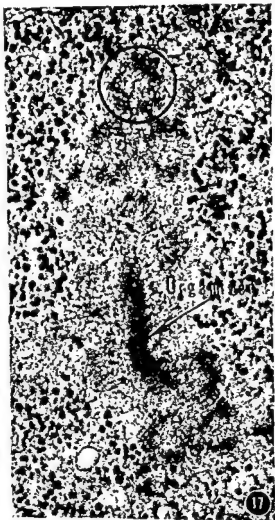
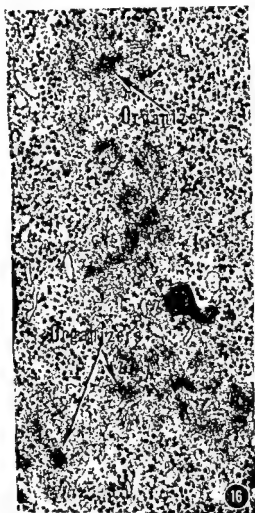


PLATE 9

EXPLANATION OF FIGURES

- 21 A cell type in which the supranuclear cytoplasm is filled with formed centrioles is common in tissues which are forming cilia. The centrioles (see circles) contain typical triplets of microtubules at this stage of development. Many smooth-surfaced vesicles are associated with the centrioles, but precursor bodies, procentrioles, organizers, and rootlets are infrequently found in this cell type. The tracheal lumen is in the upper righthand corner of this figure. $\times 28,000$. Circular inset, $\times 90,000$.
- 22 The Golgi apparatus is invariably well developed and associated with many smooth vesicles at the stage of ciliogenesis depicted in figure 21. Secretory droplets generally are not found in trachea by this time. $\times 39,000$.

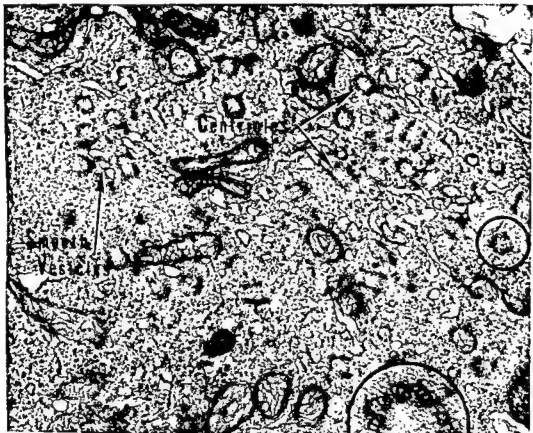


PLATE 9

EXPLANATION OF FIGURES

- 21 A cell type in which the supranuclear cytoplasm is filled with formed centrioles is common in tissues which are forming cilia. The centrioles (see circles) contain typical triplets of microtubules at this stage of development. Many smooth-surfaced vesicles are associated with the centrioles, but precursor bodies, procentrioles, organizers, and rootlets are infrequently found in this cell type. The tracheal lumen is in the upper righthand corner of this figure. $\times 28,000$. Circular inset, $\times 90,000$.
- 22 The Golgi apparatus is invariably well developed and associated with many smooth vesicles at the stage of ciliogenesis depicted in figure 21. Secretory droplets generally are not found in trachea by this time. $\times 39,000$.

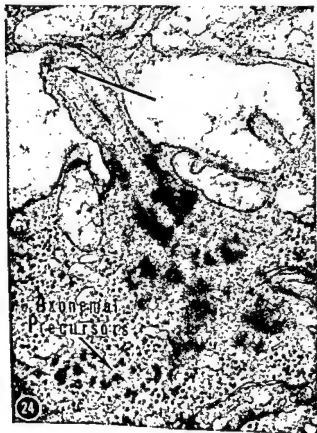
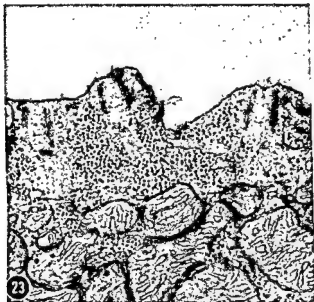


PLATE 10

EXPLANATION OF FIGURES

- 23 Three centrioles are shown aligned beneath the apical plasma-lemma of an epidermal cell in this electron micrograph. The amorphous, low-electron-opaque material beneath each centriole at this stage may contain precursor substance for rootlet formation. $\times 40,000$.
- 24 This electron micrograph shows a short cilium, probably just after the onset of ciliary shaft formation. The axial microtubules which extend throughout the length of the ciliary shaft seem to be connected to the centriolar microtubules. Because a basal plate is not present at this stage, the plate is probably not involved in the initiation of ciliary shaft formation as has been suggested by previous workers. The growing ciliary tip characteristically contains an amorphous material (arrow). Clusters of so-called "axonemal precursor bodies" and condensing centriolar rootlets appear beneath the centriole. This cell is unusual in that it contains mucous droplets at a relatively late stage of development. $\times 55,500$.
- 25-26 These longitudinal sections through growing cilia demonstrate again the presence of microtubules throughout the length of short cilia and the absence of basal plates at these early stages. The tips of the immature cilia contain amorphous material (arrows) which is similar in electron opacity to axonemal precursor bodies. Figure 25, $\times 78,500$. Figure 26, $\times 61,000$.
- 27 Immature cilia fixed in osmium tetroxide show little or no development of axial filaments, probably because the initial axial microtubules are less stable in such fixatives than the fully formed axoneme. $\times 66,000$.

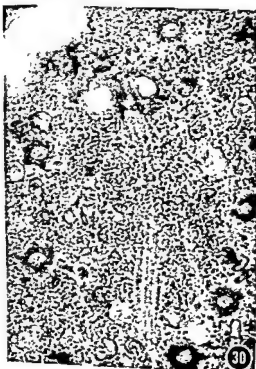
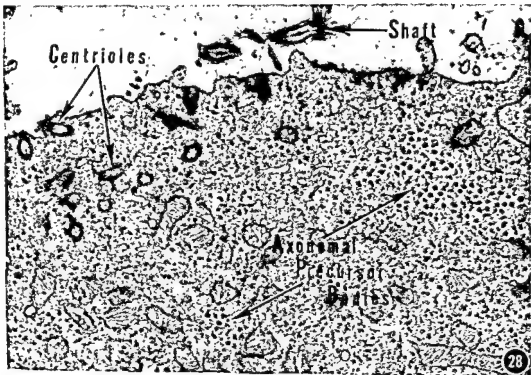


PLATE 11

EXPLANATION OF FIGURES

- 28 The axonemal precursor bodies which are typical of late stages of ciliogenesis are shown to good advantage in this electron micrograph from trachea. Procentrioles are not found at this stage, and the precursor bodies are not associated with structures thought to be intermediate stages in procentriole development (figs. 10, 12). It seems likely that, at this time, the dense precursor bodies are involved in ciliary shaft synthesis. Rootlets are forming in association with several of the centrioles. $\times 21,000$.
- 29 Another electron micrograph of a tracheal cell, forming ciliary shafts. This cell contained short cilia of different lengths associated with apical centrioles. Other centrioles apparently are moving to the cell surface. Axonemal precursor bodies and smooth vesicles are dispersed amidst the centrioles which in some cases already possess developing rootlets. $\times 22,000$.
- 30 This micrograph depicts one of two instances in which ciliary axial filaments were observed lying free in the apical cytoplasm beneath the plasmalemma. $\times 33,500$.

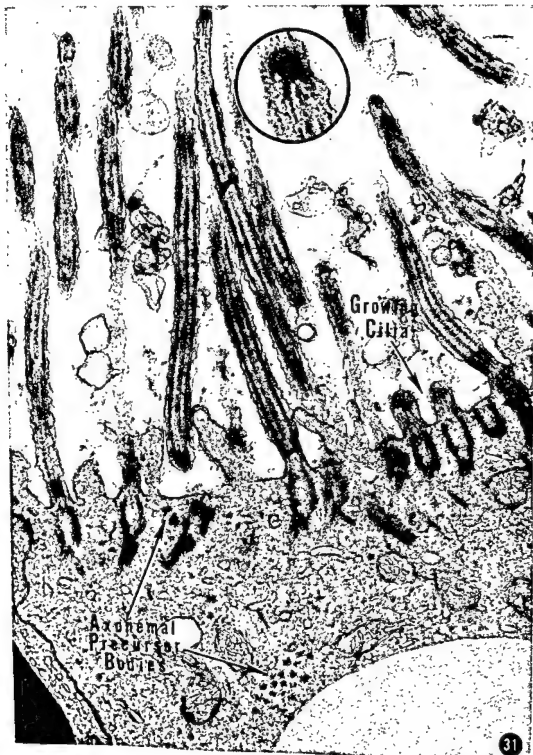


PLATE 12

EXPLANATION OF FIGURE

- 31 Ciliogenesis is practically complete in this tracheal cell. The tips of mature cilia are tapered and contain a distinctly striated material (circular inset). Growing cilia are also present in this cell, and axonemal precursor bodies can be found as might be expected. This block of glutaraldehyde-fixed tissue was treated with ribonuclease prior to postfixation with osmium tetroxide. The various ciliary components and precursors are resistant to digestion by this enzyme. Glycogen particles remain in the cytoplasm. $\times 29,000$. Inset, $\times 75,000$.

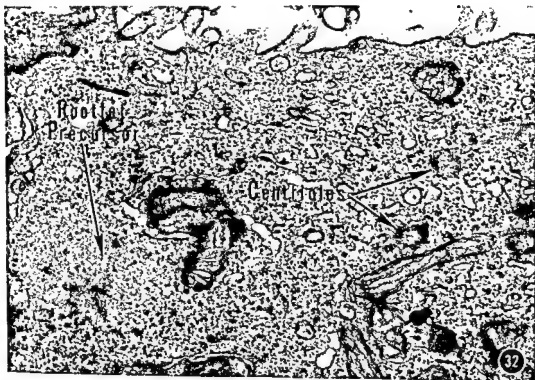


PLATE 13

EXPLANATION OF FIGURES

- 32 Rootlet precursor material is well shown in this electron micrograph. Small electron-opaque foci are found within these precursor patches. Ciliary shafts have not developed yet in this tracheal cell, although it contains centrioles and smooth vesicles. $\times 33,500$.
- 33 A fibrillar, rootlet-like, component is seen in a patch of rootlet precursor material in this electron micrograph. This cell is relatively young because it contains several small groups of procentrioles around procentriole organizer bodies. Rootlets do not generally begin to form, however, until the newly developed centrioles migrate to the apical plasmalemma. $\times 48,000$.

The Pattern of Glycogen Distribution in the Liver¹

BRIAN CORRIN AND KURT ATERMAN

*Department of Pathology, St. Thomas' Hospital, London, S.E.1., England
and Department of Pathology, Dalhousie University and
Children's Hospital, Halifax, Nova Scotia*

ABSTRACT The behaviour of glycogen in the rat liver under conditions of fasting, refeeding, and cortisone administration has been investigated in a combined chemical and histochemical study. In contrast to the observations of others the distribution of glycogen in the liver was found to be reasonably uniform. Histochemically, the periodic acid-Schiff reaction was considered to be the method of choice for the assessment of glycogen, particularly at low levels. In sections from frozen dried liver, however, reasonably good results could also be obtained with Best's carmine stain, although this stain was not very sensitive at the lower, and was thought to be too dense for accurate visual assessment at the higher levels of glycogen. As far as the intralobular distribution of glycogen was concerned, no fixed zones of "glycogen deposition" and "glycogen withdrawal" were found, since the intralobular gradient could be altered by varying the experimental conditions. This observation led to the postulate of a "glycogenic wave," which not only helps to explain some of the contradictory findings in the literature on the localization of glycogen in the liver, but which can also be reconciled with the traditional concept of the liver lobule. The "heterogeneity of the cell population" in the liver lobule was considered to be a function of time rather than of fixed anatomical features.

In the voluminous literature on the behaviour of glycogen in the liver two questions seem to have loomed large in the thinking and writing of earlier workers:

1. Is the distribution of glycogen in the liver sufficiently uniform for a sample to be considered representative of the whole?

2. Is it possible to localize glycogen within the liver lobule, and within the liver cell, with sufficient accuracy to detect a regular pattern of glycogen deposition and withdrawal?

Both these questions have retained much of their clinical and theoretical interest. With the increasingly widespread use of needle biopsies of the liver it is, of course, very pertinent to ask the very question which von Wittich raised in 1875 when he found that the left lobe of the liver of rabbits contained more glycogen than the rest of the liver. He already then considered the possibility that this difference might be an expression of the body's response to the operative interference, but concluded nevertheless that the distribution of glycogen in the liver was unequal. This conclusion was accepted by some (Barfurth, 1885), but rejected by other workers (Seegen and Kratschmer, 1880; Cramer, 1888; Külz, 1886; Schöndorf, '03; Grube, '05). Paulesco ('13) simply states

that glycogen deposition in dogs fed after a fast is not "absolutely uniform." Scheiff ('31) found the glycogen content at the edge of the liver to be higher than in the middle of a lobe, and reported in the liver of rabbits, dogs and tortoises differences between lobes ranging from 0.5% to 37.8% which he attributed to differences in the blood supply of the various lobes. Hédon and Loubatières ('38) also found differences of 18% between different parts of the same lobe, and of 45% between the glycogen content of the surface of different lobes of the dog's liver. Bareillier and Gajin ('38) thought that the glycogen distribution was uniform, but Deane, Nesbitt and Hastings ('46), on the basis of photometric estimations of the glycogen content of histological preparations, reported occasionally significantly different levels in two different lobes. Whereas Uzan and Dziri ('51) found differences of 2% to 60% in the glycogen level of two pieces of the liver of guinea pigs, Gomori and Goldner ('47) even warned that there may be a difference of "up to several hundred percent" between samples of the same rabbit's liver. Discrepancies of this magnitude always suggest a need for further in-

¹ Send reprint requests to Professor K. Aterman, Children's Hospital, Halifax, Nova Scotia.

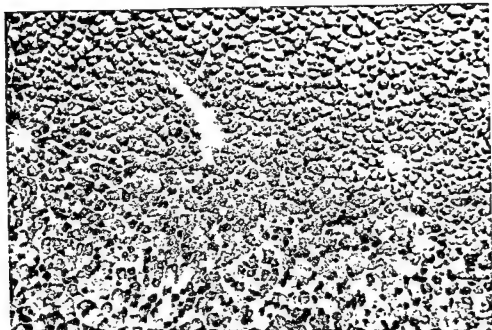


Fig. 1 Section of liver showing the displacement artefacts in the distribution of glycogen caused by the conventional liquid fixatives. Note the zonation of glycogen and its variable degree of clumping. A reliable assessment of the amount of glycogen present becomes a rather difficult undertaking. Alcoholic Bouin, 7 μ , PAS (no counterstain), $\times 80$. Glycogen appears black.

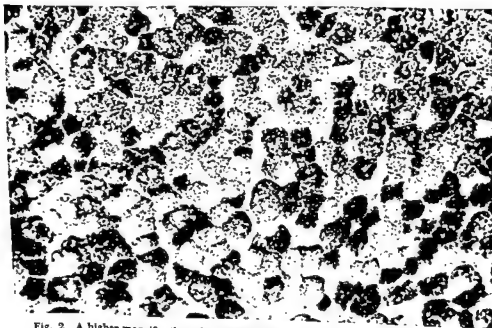


Fig. 2 A higher magnification of same section shown in figure 1 to illustrate the marked variability of appearance on the cellular level. $\times 400$.

vestigation, if only to see if some light could be thrown on the reasons for these discrepancies. This is the more pertinent as already Macleod and Pearce ('10, '11), who had reviewed the older literature, had attributed the large variations in the glycogen levels reported by some of the earlier workers to methodological errors.

The introduction of the method of freezing and drying by Gersh ('48) into cytology and histochemistry has made it possible to localize intracellular glycogen much more precisely, and permits therefore a more accurate and much needed quantitative assessment of the now widely used Periodic Acid-Schiff (PAS) reaction for glycogen. To our knowledge only Kugler and Wilkinson ('60), under different conditions, have attempted such an assessment of the sensitivity of this reaction. It was, therefore, considered of interest to undertake such a study, and to combine it with a reinvestigation of some related problems which had been so widely debated by earlier workers. Inevitably, there arose the question of the distribution of glycogen in the liver, not only with regard to the variability of the glycogen levels in the different lobes of the same liver, but also as far as the pattern of glycogen deposition within each liver lobule was concerned. It seemed particularly desirable to study the latter question since many, if not all, of the previously published reports attempting to localize the deposition of glycogen in one zone of the liver lobule, and the removal of it in another, were open to the objection of dealing with material that was not free from artefacts of fixation, preparation and staining. That the customary methods of fixation by slowly penetrating fluids significantly alter the localization of glycogen had probably already been recognized in 1872 by Bock and Hoffmann, and by Barfurth (1885), and is illustrated in figures 1 and 2, which clearly show how difficult an accurate quantitative assessment of glycogen in such specimens must be. For further illustrations of this point the paper by Trott ('61) should be consulted. It is therefore conceivable that at least some of the categorical statements found in the literature concerning the biological behaviour of glycogen in the liver may be based more

on the study of artefacts than on real differences. These objections do not apply to the same extent and at the same level to sections of liver prepared by the method of freezing and drying of Altmann-Gersh, which seems to be the method of choice for light microscopical studies of intracellular glycogen. It was therefore decided to study the following four main problems by modern histochemical means:

1. Is the glycogen in the liver reasonably uniformly distributed or is there, as has been suggested by some, a large variation from area to area? If so, what determines this variation?
2. How does the histochemical assessment of the amount of glycogen seen in sections compare with the glycogen content found by chemical determination? How sensitive is the PAS reaction by comparison with Best's carmine method for glycogen?
3. How are the changes seen in the appearance of the liver cells in sections stained by routine histological stains related to the level of glycogen in the liver? The distinction between "dark" and "light" cells, and their dependence on the glycogen content of the liver have been briefly described in an earlier paper (Aterman, '60), and will be presented elsewhere in greater detail. Here interest will be centered on the level of glycogen at which these cellular changes could be clearly seen.
4. In which parts of the liver lobule is glycogen deposited or withdrawn, and can a definite pattern of change be distinguished?

METHODS

The level of glycogen in the liver of 89 male and female white rats of an inbred strain, weighing from 50-340 gm, was determined chemically and histochemically. The animals were fed and treated in a variety of ways. Some animals had free access to the stock rat cake diet throughout the experiment whilst others were fasted for varying intervals up to 24 hours, and others again were fed for periods ranging from 40 minutes to 12 hours after a fast of 8 or of 24 hours. A protein-free diet, described elsewhere (Aterman and Darlington, '59), or adrenocortical steroids, both factors known to increase the level of glycogen in the liver, (Elman, Smith

at about -30°C , embedded in paraffin, cut at $6-7\ \mu$, and stained after deparaffinization, and denaturation in absolute alcohol, with hematoxylin-eosin, Best's carmine and the Periodic Acid-Schiff reagent (PAS). Coating the sections with celloidin before staining, as recommended by some workers, was not considered necessary, since unpublished studies had shown that in frozen-dried material this procedure does in no way enhance the histochemical demonstration of glycogen. The intensity of glycogen seen was estimated on a scale ranging from 1 to 6. Quarter fractions were chosen in preference to 0, since histochemically it did not seem that the liver was ever completely devoid of glycogen. Since glycogen was only rarely distributed in a uniform manner throughout the liver lobule (figs. 3, 4), it became necessary to pay attention not only to the intensity of the stain, but also to the area of the liver lobule occupied by the more intensely stained zone, expressed as an estimated $1/3$, $2/3$, $7/8$, etc. of the liver lobule. The product of these two figures, the in-

tensity of staining and the area so stained, was called the "score." It is apparent that this method of assessment cannot take account of the staining found in the rest of the liver lobule — a distinct disadvantage — but in our opinion it is nevertheless more accurate than the customary assessment on a 0-6 scale only, which ignores the translobular gradient.

RESULTS

It has already been pointed out that improved technique and experience gained in preliminary experiments had reduced the variability of the results to some extent, but some differences were always found in the glycogen content of the median and left lateral lobes of the livers of normally fed rats who had not been interfered with in any way. These differences, however, did not follow a consistent pattern. Of 16 rats in one experiment, for instance, the glycogen content was higher in the median lobe in nine, and in the left lobe in seven animals. Since all animals were killed at the same time of day, in order to avoid

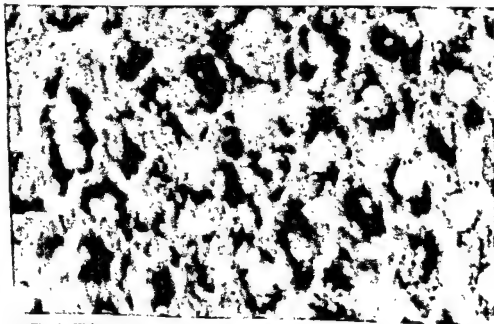


Fig. 4 Higher magnification of same section shown in figure 3 to illustrate the intra-cellular distribution of glycogen. $\times 1000$. By comparison with figures 1 and 2, this photograph and that of figure 3 present less contrast, because the artefactual clumping of the glycogen has been avoided. The amount of glycogen can, however, be more easily estimated

and Sachar, '43; Kosterlitz, '47; Wang, Hegsted, Lapi, Zamcheck and Black, '49; Seifter, Muntwyler and Harkness, '50; Schmid-Bircher, '54, Tardini, '55), were given for periods of 2-6 days, the dose of the steroids ranging from 5 mg to 30 mg/100 gm body weight per day. Some of these rats were also fasted for 24 hours. These procedures made it possible to obtain a wide spread of the level of glycogen levels in the liver, with values ranging from approximately 0.17 gm to 9.4 gm glycogen per 100 gm wet weight of liver.

All rats were lightly anesthetized with ether. The abdomen was rapidly opened, a small piece of liver was removed with a sharp razor blade and immediately immersed in chilled isopentane for histochemical studies; an adjacent piece was removed as quickly as possible, weighed in a tared tube containing 30% KOH, and placed in a boiling water bath for 20 minutes. Preliminary experiments on over 40 animals had shown that with practice the

procedure could be significantly speeded up, with a distinct improvement in the results. The anesthesia, sampling and weighing took no longer than 3-5 minutes. In each animal two samples were taken from the median lobe and two from the left lateral lobe. Biopsies were taken first from the edge of the liver and then from the middle of the lobe and the order in which the lobes were sampled was alternated in each animal. In the later phases of the experiment, when reasonably uniform results were obtained, this procedure of multiple sampling was abandoned. The glycogen content of the digests was estimated by the method of Seifter, Dayton, Novic and Muntwyler ('50), and duplicate estimates were performed on the diluted digest of each piece.

For the histochemical studies the method of freezing and drying of Altmann-Gersh (Gersh, '48) was used. Small pieces of liver were plunged into liquid isopentane chilled to -175°C , dried in a vacuum



Fig. 3 Section of liver prepared by freezing and drying. The displacement artefacts on the lobular and intracellular level have been avoided, and the glycogen is more uniformly distributed. Note, however, that individual cell variation can still be seen, although it is not pronounced. It is considered to represent a true, not artefactual, feature. The empty area in the centre represents a portal tract. Glycogen appears black. Frozen-dried, 7μ , PAS (no counterstain), $\times 550$.

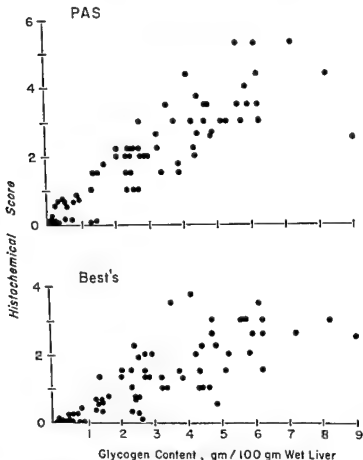


Fig. 5 A comparison of the histochemical "score" in frozen-dried sections stained by the PAS and the Best's carmine method. Note the greater scatter of values obtained with Best's stain.

ter of the individual results obtained was greater, and the sensitivity, particularly to small and to large amounts of glycogen, was less than with the PAS method. The lowest level at which it was thought that glycogen could be detected with the PAS stain in the present series was in the region of 0.16 gm/100 gm; it was certainly seen at 0.33 gm %. This, however, applied only to distinct glycogen granules, not to the general faint pink background stain which was always present in the sections stained by the Hotchkiss-McManus method, and whose intensity and variability was very difficult to assess. The background stain may represent submicroscopic particles of glycogen, or it may correspond to that frac-

tion of glycogen called "desmoglycogen" by some workers (Willstätter and Rohdewald, '34; Kugler and Wilkinson, '60).² With Best's carmine stain, the results were much less reliable in these lower regions, and barely a few granules could be seen in one animal at 0.3 gm %. On occasion the stain was still negative at 0.4 gm %

² That this background represents glycogen is made probable by experimental studies on the restoration of the liver after partial hepatectomy in rats that had been fasted before and after the operation (Aterman, '52). Even within a short interval after hepatectomy PAS-stained sections of the lobes that had been left behind appeared distinctly paler than those of the lobes removed at operation. This is interpreted as an expression of the rapid mobilization of residual traces of glycogen in the fasting animal by the additional stress of the operation. The difference was more distinctly seen by this comparison than if sections of the lobes removed by hepatectomy were compared with and without digestion by saliva.

the effect of possible diurnal rhythm fluctuations, (Deuel, Butts, Hallman, Murray and Blunden, '38), the absence of a significant preponderance of one lobe over another suggested that the differences obtained were due either to chance or to experimental error, but not to any physiologically determined variability. This point was further investigated in rats from whom two adjacent pieces were taken from both median and left lateral lobes. Some of these results are presented in table 1. It can be seen that the differences between duplicate determinations from two pieces of one lobe were larger than the differences between the average glycogen contents of the two lobes, and that the highest difference between the average glycogen contents of the median and of the left lateral lobes of the liver was, in terms of the average content of both lobes, only 28.1%. The figures presented here differ therefore considerably from the data given by, for instance, Gomori et al. ('47) who found differences of "up to several hundred per

cent" in the glycogen content of different portions of the liver; they support the contention of other workers that the glycogen content of the liver is reasonably uniform.

The sensitivity of the two main glycogen stains currently in use was assessed by a comparison of the "score" obtained in sections stained by the PAS method and by Best's carmine stain. A better correlation between the chemical and the histochemical assessment could be obtained with the PAS method than with Best's stain. This feature is brought out clearly if the individual scores are plotted against the level of glycogen (fig. 5). With the PAS stain a somewhat linear distribution could be obtained up to a level of about 6 gm % or so. Higher values were difficult to assess, and were more liable to error because of the intensity of the stain which, from a certain level on, apparently is no longer adequately estimated by the eye. Stains with Best's carmine by comparison showed that, although a reasonable assessment could be obtained by this method, the scat-

TABLE 1
The distribution of glycogen in rat liver

Glycogen (Grams/100 Grams wet liver)								
Rats	Left lobe ¹			Median lobe ²			Difference of mean glycogen contents of left and median lobes	Difference in % of average glycogen content of whole liver
	Piece 1	Piece 2	Largest difference	Piece 1	Piece 2	Largest difference		
A	4.09 3.98	4.16 3.94	0.22	3.55 3.62	4.17 4.00	0.62	0.59	15.0
B	2.61 2.33	2.13 2.27	0.48	1.87 1.92	2.15 1.62	0.53	0.44	20.4
C	2.25 2.20	2.19 2.32	0.13	2.67 2.68	2.08 2.20	0.60	0.16	6.8
D	2.08 2.00	2.15 2.26	0.26	2.25 2.15	2.17 2.03	0.22	0.03	1.4
E	1.19 1.09	1.36 1.30	0.27	1.45 1.39	1.53 1.45	0.14	0.22	16.4
F	0.74 0.80	1.25 0.79	0.51	1.39 1.32	1.13 0.89	0.50	0.29	28.1
G	0.19 0.16	0.14 0.13	0.06	0.15 0.15	0.21 0.16	0.06	0.01	6.2
H	0.15 0.11	0.15 0.12	0.04	0.17 0.15	0.11 0.14	0.06	0.01	7.2
I	0.15 0.13	0.19 0.17	0.06	0.20 0.20	0.19 0.17	0.03	0.03	17.6

¹ Piece 1 is from the edge of the lobe.
² Piece 2 is from the middle of the lobe.

gm %, the cells in the central zone of the liver lobule contained more glycogen than those in the periportal region. After fasts of 9, 12, 14.5 and 24 hours the liver glycogen levels fell to 0.14–0.38 gm %, but if the histological picture was studied it became apparent that the glycogen tended to disappear more rapidly from the central zone of the lobule, so that at some stages of this gradual depletion a distinctly periportal glycogen distribution was obtained which, however, was no longer seen in the present series if the animal had been fasted for more than fourteen and one-half hours (table 2). It would be of great interest to study in detail the pattern and the rate of disappearance of liver glycogen in the

period between fourteen and one-half and 24 hours, the next time interval chosen here, since at 24 hours no distinct distribution of the scanty histochemically demonstrable material could be detected. Only an irregular distribution of odd glycogen granules was noted at the low levels of glycogen found at the end of the 24 hour period of fasting in that in some animals glycogen was present in the intermediate zone, in others in the central and in yet others occasionally even perhaps in the periportal zone. This irregular distribution after what must be for a small animal a rather long period of fasting suggests that after a certain level of glycogen depletion any regular pattern, which may be noted in the fed or partially starved animal, may be overshadowed by the rapid synthesis of glycogen wherever and whenever possible. This interpretation received some support by a re-examination of slides from an earlier experiment in which rats had been starved for periods longer than 24 hours (Aterman, '52); under these conditions the amount of histochemically demonstrable glycogen in the liver was distinctly increased by comparison with the liver of animals fasted for about 24 hours, but the distribution of the glycogen clumps and granules was irregular and no distinct zonal localization could be made out. Attention should be drawn to this observation since herein may lie a clue to some of the contradictory opinions found in the literature.

The effect of refeeding on the distribution of glycogen in the liver is shown in table 3. If rats that had been starved for 24 hours were killed at varying intervals

TABLE 2
The withdrawal of glycogen from the liver during fasting

Fasted for (hours)	G. Glycogen %	Predominant site in lobule
0 (Controls)	1.4–4.4	Central
9	2.6	Periportal
9	2.5	Periportal
9	1.5	Periportal
9	0.9	Periportal
12	2.6	Periportal
12	1.5	Periportal
12	1.4	Periportal
14½	0.8	Periportal
14½	0.6	Periportal
14½	0.4	Periportal
24	0.4	Central
24	0.3	Irregular
24	0.3	Central
24	0.2	Irregular
24	0.2	Even "emptiness", only scattered granules
24	0.2	Even "emptiness"
24	0.2	Even "emptiness,"
24	0.1	Even "emptiness"

TABLE 3
The deposition of glycogen in the liver after 24 hours fast

G %	Fed for (hours)	Predominant site in lobule
0.14–0.33	0	Even "emptiness"
0.8	0 hours, 40 minutes	Early central
0.5	0 hours, 45 minutes	Early central
1.3	1 hour, 5 minutes	Scattered, intermediary
0.6	1 hour, 11 minutes	Central to intermediary
1.5	1 hour, 38 minutes	Early central
1.0	1 hour, 45 minutes	Early central
1.7	2 hours, 0 minutes	Central
2.0	2 hours, 50 minutes	Central
1.3	4 hours, 0 minutes	Central
2.0	4 hours, 0 minutes	Central

and even at 0.6 gm %. The increase in the "score" obtained with the increase in the glycogen level tended to flatten out sooner in sections stained by Best's carmine than was the case with the PAS method, presumably as the result of the rather dense stain obtained at the higher levels of glycogen which renders discrimination of intensity variations by the eye rather difficult. It is apparent from these considerations that both on theoretical and practical grounds the PAS stain should be considered the method of choice for the demonstration of hepatocellular glycogen. It should, however, be added that adequate preparations could be obtained with Best's stain in frozen-dried material, so that the value of this stain as a confirmatory test should be kept in mind, particularly if one is not dealing with very small amounts of glycogen.

The changes which the liver cell undergoes with changes in the level of glycogen have been the subject of a controversy centering on the existence of the so-called "dark" and "light" cells. These have been briefly described elsewhere (Aterman, '60) and the thesis has been advanced that a "light" cell was one containing sufficient glycogen to produce a displacement of the basophilic nucleic acids which now assume the appearance of "basophile inclusions," whereas in the "dark" cells the paucity of glycogen allows a uniform distribution of these basophile elements. Here it is merely of interest to draw attention to some quantitative aspects of these changes. Most of the liver cells appeared dark and evenly stained in haematoxylin-eosin sections until the amount of glycogen in the liver exceeded a level of about 0.7 gm %. This was about twice the level at which distinct glycogen granules could be demonstrated histochemically, but clearly this level was not yet adequate to affect the uniform distribution of cytoplasmic basophil material which determines the "dark" appearance of the liver cells. At higher levels of glycogen, however, distinct basophilic clumps appeared in the hepatocellular cytoplasm which now became increasingly lighter. At approximately 5 gm % of glycogen the basophilic substance appeared pushed against the nuclear and the cell membranes, so that most liver cells ac-

quired the characteristic "plant cell-like" appearance which represents the other end of the spectrum of hepatocellular changes described. This change, however, could in some areas already be found at a level of 3.6 gm %, or even perhaps at 3.3 gm %, thus emphasizing the fact that the characteristic changes which the appearances of the liver cell undergoes with fluctuations of the glycogen level are not clearly and rigidly definable in quantitative terms, but are best thought of as a "spectrum" of changes gradually merging into each other. This was clearly seen in one rat treated with cortisone and then fasted for 24 hours before death, in whom a chemically determined glycogen level of 3.9 gm % corresponded to cell changes ranging from early plant-like cells with cytoplasmic rimming in the portal region to cells with fine chromidia in the central zone of the liver lobule, with the cells in the intermediate zone containing coarse basophilic clumps — changes well in keeping with the histochemically demonstrable lobular gradient of hepatocellular glycogen, with most glycogen in this animal being present in the cells of the periportal zone.

Some interesting findings became apparent when the zonal distribution during glycogen withdrawal and deposition was systematically studied — a subject which has provoked much debate (Bock and Hoffmann, 1872; Rosenberg, '10; Arndt, '27; Forsgren, '28; Pfuhl, '32; Clara, '34; Sunder, '37; Bareillier and Gajin, '38; Milette, '38; Chipps and Duff, '42; Deane, '44, '46; Eger and Klärner, '48; Ekman and Holmgren, '49; Wang, Hegsted, Lapi, Zamcheck and Black, '49; Cazal, '55; Ehrenbrand, '55; Novikoff, '59; Eger, '61). A detailed review of the contradictory findings is probably unnecessary, and it may be sufficient to state merely that most workers consider glycogen to be deposited in one zone of the liver lobule and withdrawn from another. The controversy is mainly concerned with the question of which zone is which. In the series studied here a distinct zonal distribution of glycogen was indeed found in the liver of most animals, but no simple, and certainly no rigid, pattern could be made out. In the normal animals with free access to food, whose liver glycogen levels ranged from 1.4 to 4.4

still found in the liver despite the complete absence of food and, significantly, a persistence of the predominantly periportal distribution of glycogen was noted.

One final observation must be described, particularly when the high glycogen levels induced by corticosteroids are mentioned. It was repeatedly observed in sections from the liver of animals so treated that within the glycogen-rich zones there were minor differences in the glycogen content of individual cells, so that a cell containing much glycogen could be seen next to another cell which, while it also contained much glycogen, nevertheless showed a less intense stain with fewer coarse granules. While the variations of individual cells were quite easily seen they were, however, not on the level of one cell containing much and an adjacent cell containing little or no glycogen, so that in a zone of "much" glycogen this assessment applied to almost all cells in that zone, any differences seen being only those of a greater or lesser degree. The variability increased, however, in the zones of transition to areas containing less glycogen and, a finding noted in other series of experiments, in areas adjacent to regions of distinct cell injury. It was not possible, in the sections studied here, to correlate the minor variations in the glycogen content of individual cells with any distinct factor such as, for instance, the width of capillaries since, as had been pointed out, differences could be seen in adjacent cells. This problem obviously requires more detailed study, but is mentioned here since it represents another factor which, on the one hand, contributes to the difficulty of assessing correctly the glycogen content of the liver and, on the other, underlines the value of adequate histochemical studies.

DISCUSSION

It is reassuring to find that the wide variations in the glycogen content of different parts of the liver claimed to exist, for instance, by Gomori and Goldner ('47), were not found in the studies presented here. While there are distinct variations present, they are not of the magnitude which would render the assessment of liver glycogen from single samples a futile un-

dertaking. The fact that in the course of preliminary experiments an improvement in the results was noted with increasing experience, and the fact that it is difficult to advance any acceptable physiological basis for the extreme differences found by some workers for samples from the same liver, suggest that, to some extent at least, the variability is associated more with the techniques of sampling and the methods of determination used than with the true distribution of glycogen in the liver. To what extent variations in the blood supply play a part is open to question. A difference in the blood supply of the left and right halves of the liver has been claimed by some older workers (see Emery, '52) as well as by, for instance, Himsworth ('50). De Baker ('56), has pointed out that the difference is not of great magnitude. So far no evidence has been offered to show that there is a causal connection between the glycogen level of a segment of the liver and the source of its blood supply. These considerations have led us to assume that the glycogen content of the liver is, on the lobar level, fairly uniform, in agreement with De Baker's ('56) conclusion in a somewhat different context, that there is "little evidence to support the existence of different functional states in different areas of the same liver."

There would be little need to comment on the question of which stain should be used for the proper histochemical assessment of glycogen, had not some workers considered that a comparison of chemical and histochemical results "may be entirely misleading" (Goldschmidt, Vars and Ravdin, '39). The data presented here show that this view is not justifiable and that, as had also been concluded by Bareiller and Gajin, ('38), Fitzpatrick, Lerner and Landing ('48) and by Eger and Klärner ('48), within limits it is possible to correlate the histochemical with the chemical assessment fairly well, although a precise correlation cannot be hoped for. The difficulties encountered in such an attempt are as much due to the variable pattern of the distribution of glycogen as to the subjective nature of the visual assessment. The pessimistic view of Goldschmidt et al. ('39), shared by other workers (Grafflin, Marble and Smith, '41; Elman et al., '43;

of time after they had been allowed to feed freely again, it was found that at first, shortly after the meal, no distinct zonal localization of the newly formed glycogen could be made out, but that the rather small amounts were irregularly distributed. This irregular pattern seemed to be more a function of time than of the actual amount of glycogen involved, for after an interval of about one hour or so after the feeding a centrilobular pattern of distribution seemed to emerge which, while questionable at first, became gradually more distinct.

In one group of rats a fast of 8 hours was followed by a period of nine hours during which the rats had free access to food before the liver was examined. The glycogen levels in this group were rather high, ranging from 4.5–5.9 gm %, and an interesting histochemical picture was noted, the significance of which is not quite clear but which may be interpreted in the light of the previous findings. The glycogen, present in rather large amounts throughout most of the liver lobule, nevertheless seemed to have either a faint periportal or a rather distinct centrilobular preponderance. More important, however, was the fact that there was a distinct difference in the appearance of the cells, stained for PAS-stainable glycogen, in these two zones. Whereas the cells of the central zone presented a diffusely pink,

homogenous appearance, the cells of the periportal zone showed distinct clumps of glycogen against a rather paler background, and in some cells these glycogen clumps seemed to have a perisinusoidal arrangement. If, on the basis of the findings described earlier, it is assumed that during the period of fasting glycogen has been withdrawn from the central zone, so that a periportal distribution remains, and that during the period of refeeding the newly formed glycogen is deposited in the now empty central zone, the intriguing possibility emerges that perhaps a pattern of glycogen deposition and mobilization may be distinguished histochemically on the cellular level. The impression of a cellular difference was heightened by the interposition of an intermediary zone containing less glycogen, thus accentuating the stronger staining central and periportal areas. It should, however, be emphasized that more work on impeccably fixed and stained material will be required to verify these observations.

The feeding of a protein-free diet for six days or, more clearly, the administration of various levels of cortisone for four days, produced a rise in the level of liver glycogen, which now assumed a distinct periportal distribution (table 4). If now animals, that had been treated with cortisone, were fasted for 24 hours a high glycogen content (3.9 gm–4.7 gm %) was

TABLE 4
The effect of cortisone or of a protein-free diet on the level and the distribution of glycogen in the liver

Treatment	G. % Glycogen	Predominant site in lobule
5 mgm Cortisone/100 gm body wt \times four days	5.7	Periportal
5 mgm Cortisone/100 gm body wt \times four days	6.2	Periportal
5 mgm Cortisone/100 gm body wt \times four days	7.3	Periportal
10 mgm Cortisone/100 gm body wt \times four days	6.0	Periportal
10 mgm Cortisone/100 gm body wt \times four days	6.3	Periportal
10 mgm Cortisone/100 gm body wt \times four days	6.3	Periportal
30 mgm Cortisone/100 gm body wt \times four days	8.3	Periportal
30 mgm Cortisone/100 gm body wt \times four days	9.1	Periportal
30 mgm Cortisone/100 gm body wt \times four days	9.5	Periportal
Protein free diet for six days	2.4	Periportal
Protein free diet for six days	3.3	Periportal
Protein free diet for six days	3.6	Periportal
Protein free diet for six days	4.2	Periportal
Protein free diet for six days	4.5	Periportal
Protein free diet for six days	4.9	Periportal

more an expression of a rhythmic variation than of a firm division.⁸ This was clearly demonstrated in the experiments presented here when the pattern of glycogen withdrawal and glycogen deposition was studied. It was then noted that glycogen, which in the fasting animal tended to disappear first from the central zone of the liver lobule, was also deposited in that zone when the animal was fed again. In the normal animal glycogen tends to be more prominent in the central zone of the liver lobule, yet when such an animal is given one of the adrenal glucocorticoids in amounts which raise the level of glycogen in the liver, the predominant localization of glycogen becomes periportal. It is apparent, therefore, not only that the liver cells in the whole lobule are capable of functioning in a more or less similar manner, but that there may be a serious misconception in the thinking of those workers who, for instance like Eger ('61), would like to attribute glycogen storage to one, and glycogen withdrawal to another, zone of the liver lobule. From the data presented here it seems possible to advance another, perhaps more physiological, explanation based on the concept of a "glycogenic wave" (fig. 4). Glycogen is not stored here and released there, but those cells that are *now* storing glycogen will *later* be releasing it, whereas those cells that already have given up glycogen and are *now* "empty" will be ready to start the cycle again. This interpretation recalls the very similar views of Ekman and Holmgren ('49), and is well in keeping with, for instance, the observation that the fed rat whose liver, in the experiments studied here, had a centrilobular glycogen distribution pattern, on fasting released the glycogen in that zone so that, as the wave progressed, a periportal pattern emerged — the result partly of the central loss of glycogen and partly of the synthetic activity in the previously "empty" or glycogen-poor periportal zone. Refeeding, on the other hand, finds the central zone prepared for "synthesis" and "storage," and a predominantly centrilobular picture emerges with a spread from that zone. By suitably spacing the periods of fasting and refeeding it is possible to develop an overlap of these "waves" so that a different

pattern of intracellular glycogen distribution is found, as described above. Since in the normal active animal glycogen is constantly needed, it is difficult to find a liver in which some degree of zonation cannot be detected, thus accounting for the almost constant presence of "light" and "dark" cells in the liver, since the appearance of the liver cell in routine stains is determined by the amount of its glycogen. It is probable that many of the contradictory reports in the literature on the "site" of deposition and of withdrawal of glycogen can be explained by this postulate of a progressive "wave," whose "wave length," incidentally, it must be possible to alter quite radically by various experimental stimuli. If, for instance, one assumes that fasting for more than 15 hours represents a severe stress for the animals so that glycogen will be produced at random in the lobules by gluconeogenesis, one can account for the irregular emergence of glycogen granules in the liver lobule during the prolonged starvation as described earlier on, and even during the earliest stages of refeeding. Once, however, the most urgent needs of the body are covered and "storage" can set in in the presence of sufficient exogenous material, the "wave" reappears, as was noted about one hour after refeeding. Conversely, if the "wave length" is prolonged by the accumulation of raised glycogen levels under the influence of corticosteroids, the fed animal thus treated will differ from the fed animal that has not been given corticosteroids by a periportal instead of a central distribution pattern, merely by virtue of the fact that, presumably, depletion in one zone will take longer in the presence of the initially higher levels of glycogen induced by steroids. It is apparent that this concept, if it can be substantiated by further experimentation, could offer a better understanding of the contradictory data in the literature as well as of the workings of the liver lobule itself. This raises one final point. The concept of the liver lobule has in recent years been re-examined, notably by Rappaport ('63) who has advanced an alternative concept based on

⁸ Novikoff ('59) has already alluded to this in a footnote by pointing out that "diurnal variations and other factors" had not been taken into account.

Spatz and Segal, '65), must have been determined to a large extent by the manner of preparation of their sections since in conventionally fixed material Best's carmine stain, then used exclusively, can be misleading, (Siegmund, '39; Elman, Smith and Sachar, '43). The comments by Trott ('61) are highly pertinent in this connection. Even with Best's carmine stain, however, other workers have arrived at different conclusions (Fitzpatrick et al., '48). In sections fixed by freezing and drying glycogen can, however, be demonstrated much more brilliantly and abundantly also by Best's method than in conventionally fixed material of the same liver. It can, therefore, not be emphasized strongly enough that for a proper understanding of the behaviour of glycogen, certainly at the cellular level, optimally fixed specimens are an absolute prerequisite, to the extent that in improperly prepared material the choice of staining method becomes a secondary consideration. Here, undoubtedly, lies another key to the many contradictions found in the literature. Once, however, satisfactory fixation has been obtained, the Periodic Acid-Schiff stain becomes the method of choice, both on theoretical and on practical grounds, for the demonstration of glycogen in the liver. Best's carmine stain will find a use mainly as a confirmatory stain or for purposes of comparison.

The combination of good fixation and a sensitive stain brought out a feature which had already been noted by earlier (Barfurth, 1885; Rosenberg, '10; Arndt, '26) as well as by more recent workers (Schneider, Joel and Clark, '56; Kleinfeld, '57), but to which attention should also be drawn here: The degree of variation in the glycogen content of individual liver cells. With the emphasis on the zonal distribution of glycogen in the liver one has come to think of the cells in a particular lobular zone as behaving in a rather uniform fashion, so that the differences seen on the cellular level between adjacent cells come somewhat as a surprise. While the cells of one zone are clearly part of a group by comparison with those of the other zone, always keeping in mind the gradual nature of the transition, they also seem to behave as "individuals." To the

biologist individual variability should not, of course, be surprising. The relevance of the observations of the older workers—apparently Luchsinger had commented on it already in 1875—may, however, have been obscured by the ever present possibility that they may have studied and described artefacts of preparation (Pfuhl, '32). It is therefore of interest to point out that in the present series some degree of hepatocellular variability was still noticed even though the method of freezing and drying used was free of the customary artefacts of fixation.

One of the most interesting and long lasting controversies in the literature on the physiology and pathology of the liver has been the question of the lobular distribution and variability of hepatocellular organelles and substances. Already Beale (1856) had considered the possibility that there may be differences in the formation of bile by different liver cells, and from time to time other workers subsequently advanced similar views with regard to other substances. In recent years this debate has received a new impetus by the concept of "cell heterogeneity" revived, in modern form, by Novikoff ('59), Shank, Morrison, Cheng, Karl and Schwartz ('59) and Eger ('61). As far as glycogen is concerned, the observations presented here do not lend much support to this concept, if by cell heterogeneity is meant that different cells of the liver lobules behave differently, depending on the zone in which they are situated. That at any given time there are differences in the distribution of glycogen on the zonal level cannot be denied. Attention should, however, be drawn not only to the variability on the individual cell level described above, but also to the fact that the intralobular differences found to some extent appear to be a function of time. Hence it should be clearly understood that the concept of cell heterogeneity in the liver lobule should be qualified by the statement "at time Tx," and should not be taken to mean a rigid division into cell "types" depending perhaps on fixed anatomical, circulatory or other factors. Potentially, at least as far as glycogen is concerned, all the liver cells are capable of storage and release, and the differences seen at any given time are

wave will explain some of the discordant statements in the literature concerning the site of glycogen release and storage. This view was discussed in relation to the concept of "cell heterogeneity" in the liver lobule. Attention was also drawn to the individual variability of the histochemical appearance of the liver cells within a given zone. It was finally pointed out that in optimally fixed specimens chemical and histochemical comparative studies can lead to conclusions which can be interpreted on the basis of the conventional liver lobule.

LITERATURE CITED

- Arndt, H. J. 1926 Experimentelle morphologische Untersuchungen über den Glykogen- und Fettstoffwechsel in ihren gegenseitigen Beziehungen. *Verh. Deutsch. Ges. Path.*, 21: 297-303.
- 1927 Vergleichende morphologische und experimentelle Untersuchungen über den Kohlehydrat- und Fettstoffwechsel der Gewebe. *Beitr. Path. Anat.*, 79: 69-116, 523-558.
- Aterman, K. 1952 Some local factors in the restoration of the rat's liver after partial hepatectomy: Glycogen; The Golgi apparatus; sinusoidal cells; the basement membrane of the sinusoids. *Arch. Path.*, 53: 197-208.
- Aterman, K. 1960 The dark and the light cells of the liver. Presented at the Seventh International Anatomical Congress, New York. (*Anat. Rec.*, 136: 157.)
- Aterman, K., and D. Darlington 1959 A re-examination of the effect of vitamin B₁₂ concentrate on the hepatic injury produced by carbon tetrachloride. *Brit. J. Nutr.*, 13: 163-177.
- Bareillier, G., and G. Gajin 1938 Contribution à l'étude de la charge histologique et chimique en glycogène des foies de chiens perfusés. *Ann. Anat. Pathol.*, 15: 426-434.
- Barfurth, D. 1885 Vergleichende histochemische Untersuchungen über das Glykogen. *Arch. Mikrosk. Anat.*, 25: 259-404.
- Beale, L. S. 1856 Lectures on the minute anatomy of the liver. *Med. Times Gaz.*, 13: 82-85.
- Bock, C., and F. A. Hoffmann 1872 Über das mikrochemische Verhalten der Leberzellen. *Virchow's Arch. Path. Anat.*, 56: 201-211.
- Cazal, P. 1955 Histopathologie du foie: Le diagnostic des affections hépatiques. Étude iconographique. Masson & Co., Paris.
- Chippis, H. D., and G. L. Duff 1942 Glycogen infiltration of the liver cell nuclei. *Am. J. Path.*, 78: 645-655.
- Clara, M. 1934 Der Bau der Gallenkapillaren unter physiologischen und experimentellen Bedingungen — Morphologische und experimentelle Untersuchungen an der Kaninchenleber. IV. *Ztschr. Mikr. Anat. Forsch.*, 35: 1-56.
- Cramer, A. 1888 Beiträge zur Kenntniss des Glykogens. *Ztschr. f. Biol.*, 24: 68-104.
- Deane, H. W. 1944 A cytological study of the diurnal cycle of the liver of the mouse in relation to storage and secretion. *Anat. Rec.*, 88: 39-65.
- Deane, H. W., F. B. Neshitt and A. B. Hastings 1946 Improved fixation for histological demonstration of glycogen and comparison with chemical determination in the liver. *Proc. Soc. Exp. Biol. Med.*, 63: 401-406.
- de C. Baker, H. 1956 A spiral valve in the hepatic portal vein. *Nature*, 178: 1003-1004.
- 1956 Ischaemic necrosis in the rat liver. *J. Path. Bact.*, 71: 135-143.
- Deuel, Jr., H. J., J. S. Butts, L. F. Hallman, S. Murray and H. Blunden 1938 Studies on Ketosis. XIII. Diurnal changes in liver glycogen. *J. Biol. Chem.*, 123: 257-265.
- Eger, W. 1961 Zur Struktur und Funktion des Lebergewebes. *Arzt. Sammelblätter*, 50: Heft 1.
- Eger, W., and Ch. Klärner 1948 Über Glykogenbildung und Glykogenablagerung in der menschlichen Leber. *Virchow Arch. Path. Anat.*, 315: 135-146.
- Ehrenbrand, F. 1955 Leberstudien bei experimenteller Hyperthyreose. *Anat. Anz.*, 101: 315-356.
- Ekman, Carl-Axel, and H. Holmgren 1949 The effect of alimentary factors on liver glycogen rhythm and the distribution of glycogen in the liver lobule. *Anat. Rec.*, 104: 199-216.
- Elman, R., M. G. Smith and L. A. Sachar 1943 Correlation of cytological with chemical changes in the liver as influenced by diet, particularly protein. *Gastroenterol.*, 1: 24-33.
- Emery, J. L. 1952 Degenerative changes in the left lobe of the liver in the newborn. *Arch. Dis. Child.*, 27: 558-561.
- Fitzpatrick, T. B., J. Lerner and B. H. Landing 1948 The estimation of hepatic glycogen content from sections by Best's carmine method. *Bull. Int. Assoc. Med. Mus.*, 28: 96-103.
- Forsgren, E. 1928 Mikroskopische Untersuchungen über die Gallenbildung in den Leberzellen. *Ztschr. Zellforsch.*, 6: 647-688.
- Gersh, I. 1948 Application in pathology of the method of fixation by freezing and drying of tissues. *Bull. Internat. Assoc. Med. Mus.*, 28: 179-185.
- Goldschmidt, S., H. M. Vars and I. S. Ravdin 1939 The influence of the foodstuffs upon the susceptibility of the liver to injury by chloroform, and the probable mechanism of their action. *J. Clin. Invest.*, 18: 277-289.
- Gomori, G., and M. G. Goldner 1947 The uneven distribution of glycogen in the liver. *Proc. Soc. Exper. Biol. Med.*, 66: 163-164.
- Grafflin, A. L., A. Marble and R. M. Smith 1941 Note on histological estimation versus chemical analysis of liver glycogen. *Anat. Rec.*, 81: 495-497.
- Grube, K. 1905 Über die Verteilung des Glykogens in der Leber. *Arch. Ges. Physiol.*, 107: 483-489.
- Hédou, L., and A. Loubatières 1938 Dosage du glycogène dans de petits fragments de foie excisés au bistouri électrique: Degré de précision de la technique. Répartition du glycogène dans le foie du chien. *Bull. Soc. Chim. Biol.*, 20: 910-922.

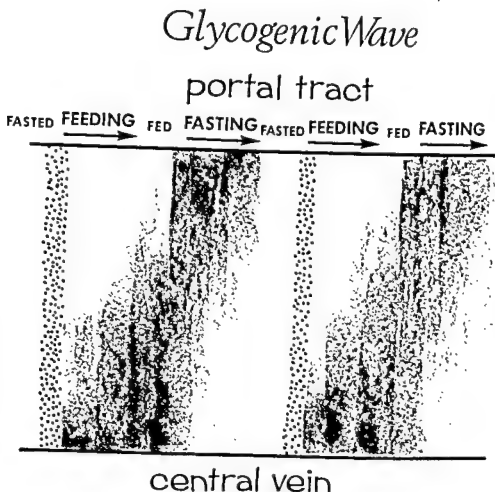


Fig. 6 A schematic representation of the "glycogenic wave."

the liver acinus. While the data presented here in no way contradict Rappaport's views, it is of great interest to see that they offer an intelligible interpretation of the organizational pattern of the liver based on the conventional and convenient concept of the liver lobule.

SUMMARY

The chemically and histochemically demonstrable level of glycogen in the liver has been studied in rats fasted and refed for various intervals of time. Particular attention was paid to the question of whether glycogen is or is not uniformly distributed in the various lobes, and whether a distinct pattern of glycogen deposition and withdrawal could be established. In addition the sensitivity of the Periodic Acid-Schiff stain for glycogen was assessed by comparing it not only with the level of

chemically determined glycogen, but also with the conventional demonstration of glycogen by Best's carmine in frozen-dried sections. It was concluded that glycogen was fairly uniformly distributed and that variations in its level were probably related to the techniques of sampling and determination. The PAS method for demonstrating glycogen was considered to be the method of choice because of its greater sensitivity and technical reliability, although Best's carmine in frozen-dried sections also reflected to a fair degree the chemically determined level. No fixed zones of glycogen deposition or withdrawal in the liver lobules could be distinguished, but the zonal distribution found at any given time was considered to be an expression of a "glycogenic wave." It is probable that this assumption of a rhythmically recurring

The Ultrastructure of the Enamel Organ Related to Enamel Formation

WILLIAM K. ELWOOD¹ AND MAURICE H. BERNSTEIN

Departments of Anatomy and Restorative Dentistry, University of Kentucky, Lexington, Kentucky and Department of Anatomy, Wayne State University, Detroit, Michigan

ABSTRACT The ultrastructure of the cells of the enamel organ related to enamel formation was studied using the lower incisors of adult male rats. In the region of enamel deposition, stratum intermedium cells are stabilized by a system of intercellular bridges and intracellular fibrils. The mitochondria in these cells are positioned toward the extracellular channels through which any direct intercellular exchange between the capillaries and ameloblasts must occur. Tentatively, the mitochondrial arrangement is considered to be related to the movements of electrolytes and water across the capillary-ameloblast interval.

In the region of transition, enamel deposition ceases and the ergastoplasm of the ameloblasts is removed, apparently by cytosegresomes, with an accompanying reduction in the height of the ameloblasts. Here, vesicles containing stippled material are infrequent compared to their occurrence in ameloblasts concerned with enamel deposition. Other vesicles, characteristically found in ameloblasts related to maturing enamel, first appear in the transition region and seem to originate from the cell membrane abutting on the enamel.

In the region of maturation, cytosomes are common in the Golgi region whereas vesicles and mitochondria predominate in the distal ends of the ameloblasts. The papillary cells contain an unusually large number of mitochondria, elaborate microvilli and vesicles, which suggests that these cells are extremely active, presumably in the movement of materials related to enamel maturation.

The changes in structure of the papillary cells, which occur concomitantly with those of the ameloblasts during enamel formation, are indicative of interrelated functional changes and strongly support the concept of ameloblasts and papillary cells acting together as a functional unit.

For nearly a century, evidence has accumulated that developing enamel differs from fully formed enamel in hardness, staining characteristics, transmission of polarized light and acid solubility (Hoppe, 1862; von Ebner, '06; Beust, '28; Chase, '32, '35). Recent investigations have shown more specifically that the mineral and organic content of young and mature enamel differs significantly (Deakins and Volker, '41; Deakins, '42; Deakins and Burt, '44; Weinmann, Wessinger and Reed, '42; Eastoe, '60, '63). From such observations the concept developed that amelogenesis (enamel formation) is a 2-phase process. First, young or immature enamel is deposited; second, enamel matures. The maturation of enamel is characterized by a decrease in water and organic content concomitant with a marked increase in inorganic material (Marsland, '51, '52; Eastoe, '63; Burgess and Maclaren, '65).

The various stages of enamel formation may be conveniently studied in a continuously forming and erupting tooth, such as the rat incisor. Here, amelogenesis is in progress during most of the life span of the animal. This is not true of the molars of the rat which, like human teeth, exhibit a relatively brief period of enamel formation (Schour and Massler, '49). Once enamel development is complete, the enamel organ usually degenerates and is lost when the tooth erupts. (See fig. 1 for a comparison of the rat incisor with the developing human incisor.)

The enamel or dental organ (ectodermal in derivation) is responsible for the formation of enamel. Excluding the generative end of the incisor, the enamel organ is composed of two main types of cells, the

¹This investigation was supported in part by United States Public Health Service Grants DT-54 and NB 02010 when the principal investigator was affiliated with the Henry Ford Hospital, Detroit, Michigan.

- Himsworth, H. P. 1950 The liver and its diseases. Second Ed. Blackwell, Oxford.
- Kleinfeld, R. G. 1957 Early changes in rat liver and kidney cells induced by thioacetamide. *Cancer Res.*, 17: 954-962.
- Kosterlitz, H. W. 1947 The effects of changes in dietary protein on the composition and structure of the liver cell. *J. Physiol.*, 106: 194-210.
- Kugler, J. H., and W. J. Wilkinson 1960 Glycogen fractions and their role in the histochemical detection of glycogen. *J. Histochem. Cytochem.*, 8: 195-199.
- Külz, R. 1886 Zur quantitativen Bestimmung des Glykogens. *Ztschr. Biol.*, 22: 161-193.
- Luchsinger, B. 1888 Experimentelle und kritische Beiträge zur Physiologie und Pathologie des Glykogens. Dissertation. Zürich 1875 S. 63. (Quoted by A. Cramer) *Ztschr. f. Biol.*, 24: 68-104.
- Macleod, J. J. R., and R. G. Pearce 1910-1911 Studies in experimental glycosuria — VI. The distribution of glycogen of the liver under various conditions. Post mortem glycogenolysis. *Am. J. Physiol.*, 27: 341-365.
- Milletti, M. 1938 Citologia della cellula epatica nel corso della iperglicemia sperimentale. *Ztschr. Zellforsch.*, 28: 210-237.
- Novikoff, A. B. 1959 Cell heterogeneity within the hepatic lobule of the rat (staining reactions). *J. Histochem. Cytochem.*, 7: 240-244.
- Paulesco, N. C. 1913 Chez un chien alimenté, le glycogène est-il distribué d'une façon égale dans tous les lobes du foie? *C. R. Soc. Biol. (Paris)*, 74: 629-630.
- Pfuhl, W. 1932 Die Leber. In: W. von Möllendorff (ed.), *Handbuch der Mikr. Anat. d. Mensch.*, Bd. V/2, S. 235, 1932. Springer, Berlin.
- Rappaport, A. M. 1963 Acinar units and the pathophysiology of the liver. In: The liver, morphology, biochemistry, physiology. Ed.: Ch. Rouiller, V. I: 265. Acad. Press, New York.
- Rosenberg, O. 1910 Histologische Untersuchungen über das Leberglykogen. *Beitr. Path. Anat.*, 49: 284-312.
- Scheiff, W. 1931 Untersuchungen über die chemische Zusammensetzung der verschiedenen Leberlappen: Ein Beitrag zur Stoffwechselphysiologie der Leber: *Pfluegers Arch. Ges. Physiol.*, 226: 481-499.
- Schmid-Bircher, M. 1954 Histologische Organveränderungen beim Kaninchen durch hohe Cortisondosen. *Beitr. Path. Anat.*, 114: 136-150.
- Schneider, E. M., W. Joel and M. L. Clark 1956 Use of histochemical stains in needle biopsy of the liver. I. Neutral polysaccharide stain. *Gastroenterol.*, 30: 373-381.
- Schöndorff, B. 1903 Ueber den Maximalwerth des Gesamtglykogengehalts von Hunden. *Arch. f. d. Ges. Physiol.*, 99: 191-242.
- Seegen, J., and F. Kratschmer 1880 Ueber Zuckerbildung in der Leber. *Pfluegers Arch. Ges. Physiol.*, 22: 214-239.
- Seifter, S., S. Dayton, B. Novic and E. Muntwyler 1950 Estimation of glycogen with Anthrone reagent. *Arch. Biochem.*, 25: 191-200.
- Seifter, S., E. Muntwyler and D. M. Harkness 1950 Some effects of continued protein deprivation, with and without methionine supplementation on intracellular liver components. *Proc. Soc. Exper. Biol.*, 75: 46-50.
- Shank, R. E., G. Morrison, C. H. Cheng, I. Karl and R. Schwartz 1959 Cell heterogeneity within the hepatic lobule (Quantitative Histochemistry). *J. Histochem. Cytochem.*, 7: 237-239.
- Siegmund, H. 1939 Glykogenspeicherungs Krankheit. Pathologisches Referat. Verhldg. Deutsch. Ges. Path., 31st Tagung, Gustav Fischer, Jena, 150-187.
- Spatz, M., and St. Segal 1965 Transplacental galactose toxicity in rats. *J. Ped.*, 67: 438-446.
- Sunder, L. 1937 Untersuchungen über das Verhalten der Speichersubstanzen (Glykogen, Fett, Eiweiss) und der Gallengranula bei normaler und einseitiger Fütterung in der Leber der weissen Maus. *Z. Mikr. Anat. Forsch.*, 41: 541-557.
- Tardini, A. 1955 Le Modificazioni della sostanza basofila citoplasmatica e la cariologia della cellula epatica quali indici della funzionalità cellulare e del metabolismo proteico nelle varie malattie del fegato. *Arch. Inst. Biochim. Ital.*, 17: 24-83.
- Trott, J. R. 1961 An evaluation of methods commonly used for the fixation and staining of glycogen. *J. Histochem. Cytochem.*, 9: 703-710.
- Uzan, M., and A. Dziri 1951 Sur l'inégale répartition du glycogène et des graisses dans le foie. *Arch. Mal. Appar. Dig.*, 40: 199-201.
- Wang, Ch-Fa, D. M. Hegsted, A. Lapi, N. Zamcheck and M. B. Rohdewald 1934 Progressive changes in liver composition, function, body fluids and liver cytology during protein depletion in the rat and the effect of choline upon these changes. *J. Lab. Clin. Med.*, 34: 953-964.
- Willstätter, R., and M. Rohdewald 1934 Über den Zustand des Glykogens in der Leber, im Muskel und in Leukocyten. (Zur Kenntniss der Proteinbindung physiologisch wichtiger Stoffe). *Ztschr. f. physiol. Chem.*, 225: 103-124.
- v. Wittich 1875 Zur Statistik des Leberglykogens. *Centralbl. Med. Wissensch.*, 13: 113-118.

shaped process from one cell into an adjacent cell.

Cytosome and cytosegresome are used, as defined by Ericsson ('64). A cytosome is an inclusion body limited by a single membrane, and varies in largest dimension from 0.3–3.0 μ . A cytosegresome is a body, "containing well recognizable cytoplasmic organelles, limited by a single or a double outer membrane." Because of the subjective judgment required to decide whether a "well recognizable cytoplasmic organelle" is present, some inclusion bodies are difficult to classify.

OBSERVATIONS

Region of Enamel Deposition

Light microscopy

The ameloblasts are tall (about 70 μ) and slender, with proximally disposed nuclei. They possess proximal and distal terminal bars. The stratum intermedium cells form a layer one cell thick, adjacent to the proximal ends of the ameloblasts. Capillaries contact the cells of the stratum intermedium. Between such contacts, one or two rows of outer papillary cells overlie the stratum intermedium cells. The extracellular space is extensive in the papillary layer.

Electron microscopy

Ameloblasts

The distal ends of the ameloblasts present extended cell processes directly related to an irregular enamel surface (fig. 2). Single-membrane vesicles containing a stippled material are prominent in the distal processes. A similar stippled material lies extracellularly adjacent to the distal surface of the ameloblasts and is intimately related to developing apatite crystals. The stippled material also is encountered between ameloblasts beyond the distal terminal bars. Well developed endoplasmic reticulum occupies much of the distal ends of the cells and is arranged parallel to the long axis of the cell (fig. 2). It extends mainly from the Golgi region to the level of the distal terminal bars, a distance of about 10–15 μ . In the Golgi region (fig. 3), vesicles are present which contain stippled material, similar to that seen

in the distal ends of the ameloblasts. Similar vesicles are occasionally present in the proximal part of the ameloblasts. Mitochondria are perinuclear.

Specific junctions are not present between the ameloblasts from the enamel to the distal terminal bars. From the distal terminal bars to the nuclear level, the plasma membranes of adjacent ameloblasts lie in close apposition. On a level with the distal ends of the nuclei, the ameloblasts are separated by a definite extracellular space. Between nuclei, the extracellular space is reduced and a few desmosomes occur. Proximal to the nuclei, the extracellular space is increased but is again reduced at the proximal terminal bars. Interdigitations of the cell membranes are common in association with the proximal terminal bars (figs. 4, 5). Vesicles, which are considered to be pinocytotic, are present where the proximal surfaces of the ameloblasts are exposed to the extracellular space of the papillary layer.

Papillary cells

(A) *Stratum intermedium cells.* The cells of the stratum intermedium lie either between the ameloblasts and a capillary or between the ameloblasts and the outer papillary cells (fig. 4). The nuclei of the stratum intermedium cells are somewhat rectangular in cross-section. The mitochondria are disposed lateral to the nuclei, toward adjacent stratum intermedium cells. The Golgi apparatus is located both on the side of the nucleus facing the ameloblasts and on the opposite side. Single-membrane vesicles are found in the cytoplasm toward the ameloblasts. The endoplasmic reticulum is sparse and not confined to any particular region of the cell.

The stratum intermedium cells contact only a small area of the proximal surface of the ameloblasts (figs. 4, 5). Contact may appear fortuitous, or exhibit a snug junction sometimes together with an interlock. Few desmosomal units are formed at papillary-ameloblast junctions. The stratum intermedium cells are interconnected by numerous intercellular bridges (figs. 4, 5). Snug junctions may occur together with desmosomes to constitute part of the intercellular bridges. Fibrillar material is present in the cytoplasm and is oriented in

ameloblasts and the so-called papillary cells (Williams, 1896). The ameloblasts form a simple columnar layer adjacent to the enamel and are immediately responsible for enamel formation. Histologists have noted that the ameloblasts associated with young enamel differ from those adjacent to mature enamel, in their width, height, and distribution of mitochondria (Marsland, '51; Pindborg and Weinmann, '59; Reith, '60, '61). This alteration in structure of the ameloblasts implies a modification in their function.

The papillary cells separate the ameloblasts from the nearest capillary bed. This interposition may permit them to modify and control the metabolic exchange necessary for enamel formation. In the region of young enamel deposition, the papillary cells closest to the ameloblasts form a stratum intermedium. Further incisally, in the region of maturing enamel, all cells of the papillary layer are similar and a stratum intermedium no longer can be distinguished (Elwood and Bernstein, '64, '65). Here, as with the ameloblasts, the change in structure of the papillary cells suggests a functional alteration.

In 1952, Marsland stated that the ameloblasts and the cells that separate them from the capillaries should be considered together as a functional unit concerned with enamel deposition, in the basal region, and with enamel maturation, more incisally. Stimulated by this concept, the present ultrastructural investigation was conducted to examine the cells of the enamel organ as a functional unit in the process of amelogenesis.

MATERIALS AND METHODS

Male rats (200–400 gm) were anesthetized with nembutal. The bone of the mandible overlying the labial aspect of the incisors was removed, using a dental handpiece with a diamond disc. The enamel organs and adjacent tissues were fixed *in situ* about five minutes, with 2% osmium tetroxide in a balanced physiological salt solution (Pease, '64). Then the animals were sacrificed and the incisors together with the enamel organs were removed and placed in fresh fixative at 4°C for one hour. During the subsequent hour, the tissues were placed in fresh cold fixative and were

permitted to reach room temperature. The tissues were dehydrated in graded concentrations of ethanol and acetone and embedded in Araldite or Vestopal. Thin sections were cut with glass knives on a Sorvall ultramicrotome and mounted on formvar-coated copper grids. The sections were stained in uranyl acetate for 20–60 minutes followed by a lead citrate stain for 20 minutes. The specimens were examined in a RCA EMU-3 or Hitachi HS-6 electron microscope.

Sections, 1 μ -thick, were cut from the blocks prepared for electron microscopy, stained with cobalt sulfide by the method of Moe, Behnke, and Rostgaard ('62) and examined by phase contrast microscopy.

Terminology

The formative end of the tooth will be referred to as *basal*, and the erupting end as *incisal*. The ends of the ameloblasts facing the enamel will be called *distal*, and the opposite ends (facing the papillary cells), *proximal*.

In the basal region, stratum intermedium cells will be designated where they can be distinguished from the other papillary cells. The rest of the papillary cells lying between the stratum intermedium and the connective tissue will be called the *outer papillary cells*. In the more incisal region where stratum intermedium cells no longer can be distinguished from the outer papillary cells, all cells of the papillary layer will be referred to as *papillary cells*.

The various junctions described between cells include "snug" junctions, terminal bars, and interlocks. A close union is exhibited between many of the cells. Although it may be assumed that tight (zonula or macula occludens) and intermediate (zonula adhaerens) junctions (Farquhar and Palade, '63) constitute part of many of these unions, they cannot be distinguished satisfactorily in the electron micrographs. Hence, for ease of communication, such regions are referred to as "snug" junctions. "Terminal bar" refers to a snug junction which girds a cell together with an associated dense band of cytoplasmic material. An "interlock" is a configuration made by the projection of a mushroom-

Region of Maturation

Light microscopy

The ameloblasts are about 40 μ in length. Terminal bars are not evident. The stratum intermedium cells are no longer distinguishable from the outer papillary cells. The cells of the papillary layer form parallel ridges which lie at right angles to the longitudinal axis of the tooth (fig. 13). Each ridge separates adjacent capillaries. The capillaries are separated from the ameloblasts by a layer of papillary cells (see fig. 14 for a comparable electron micrograph). The extracellular space present in the papillary layer is less evident in this region than in the basal region.

Electron microscopy

Ameloblasts

The distal ends of the ameloblasts present a more even surface facing the enamel than in the basal region. At several sites along the distal surface, there is a suggestion of a "fuzzy" coating of the cell membrane. Large vesicles associated with numerous smaller ones, some of which are in communication with the cell surface, are the predominant structures at the distal ends of the ameloblasts. Single-membrane vesicles containing stippled material are found infrequently. A thin layer of similar stippled material lies extracellularly between the distal surface of the cells and the apatite crystals (fig. 15).

The endoplasmic reticulum distal to the Golgi complex is greatly reduced in amount, and possesses fewer ribosomes than that present in the ameloblasts in the basal region. Mitochondria are scattered throughout the cytoplasm of the ameloblasts but are more concentrated between the distal end of the cell and the Golgi region. The Golgi region lies distal to the nucleus, together with some cytosomes and a few vesicles containing stippled material (fig. 16). Distal to the Golgi complex, most of the vesicles of stippled material lie peripherally, between the mitochondria and the cell wall. An electron-opaque substance thought to be lipid is occasionally observed in the ameloblast cytoplasm, proximal to the Golgi region. The substance is irregular in

outline and does not appear to be membrane-bound.

Evidence for a proximal terminal bar system persisting in the region of enamel maturation is inconclusive. Distal terminal bars are absent. Otherwise, ameloblasts are united by an occasional snug junction, interlock or desmosome.

An extracellular space separates one ameloblast from another. Distally, the space is bounded by the enamel. Proximally, it may be continuous with the extracellular space of the papillary layer, provided the proximal terminal bar system is discontinuous. A few microvilli extend from the lateral walls of the ameloblasts into this space.

Papillary cells

The papillary cells interposed between the ameloblasts and the capillaries have nuclei disposed toward the ameloblasts and a rich accumulation of mitochondria toward the capillaries (fig. 14). The papillary cells constituting the papillary ridges contain centrally located nuclei and mitochondria concentrated toward the capillaries or connective tissue. Many microvilli project from each papillary cell into the extracellular space. An occasional cytosome, irregularly shaped mass of electron-opaque material or vesicle containing stippled material, is found in the cytoplasm of the papillary cells. Numerous vesicles are seen in the cytoplasm along the periphery of the cells (fig. 17). Golgi complexes may be located on the lateral sides of a papillary cell as well as toward the ameloblasts. A fibrillar material is present in some of the cells of the papillary layer.

The papillary cells contact a larger area of the proximal surface of the ameloblasts than they did in the basal region of the tooth. These contacts include an increased number of snug junctions and a decreased number of desmosomes (fig. 17). At junction sites, a process from one cell frequently indents the wall of the companion cell creating an appearance similar to a ball and socket joint. Sections through the crown of one of these junctions may be seen as an island of cytoplasm from one cell surrounded by the cytoplasm of another. The papillary cells contact the basement membrane of the capillaries or con-

line with the fibrillar components of desmosomal junctions. This is especially noticeable in the cytoplasm near the ameloblasts and on the opposite side.

(B) *Outer papillary cells.* The nuclei of the outer papillary cells tend to be ovoid or truncated. The mitochondria are disposed toward the connective tissue as well as lateral to the nuclei. The amount and distribution of free ribosomes and endoplasmic reticulum are similar to that seen in the stratum intermedium cells.

A basement membrane complex, formed by the union of a capillary basement membrane with that of the enamel organ, separates the stratum intermedium and papillary cells from capillary endothelial cells by 3,000–5,000 Å (figs. 4, 6). In the intervals between capillaries, only the basement membrane (about 500 Å thick) of the enamel organ separates the outer papillary cells from the adjacent connective tissue (fig. 7). Both stratum intermedium and outer papillary cells abut against the basement membrane of the enamel organ and spread out to cover almost the entire surface. Contacts between outer papillary cells or between outer papillary and stratum intermedium cells are limited to an infrequent snug junction or desmosome. The endothelial cells are especially thin, often measuring 200 Å or less, where they lie closest to the ameloblasts (fig. 6).

Region of Transition

Light microscopy

The ameloblasts are intermediate in height (about 55–60 μ) between those overlying young enamel and those overlying maturing enamel. The papillary cells situated between the ameloblasts and capillaries appear transitional between the stratum intermedium cells basally and the homologous papillary cells incisally. The nuclei are rounded but have not yet moved from a central position to lie close to the ameloblasts. Intercellular bridges are present but reduced in number from those connecting the stratum intermedium cells. The most notable feature in this region is the appearance of osmiophilic globules in both the ameloblasts and the papillary cells,

which vary in size from less than 1 μ to more than 5 μ in diameter (fig. 8).

Electron microscopy

Ameloblasts

The distal surface of the ameloblasts facing the enamel is relatively even. Single-membrane vesicles containing stippled material are less abundant in the distal ends of the cells here than basally. Vesicles lacking stippled material, which predominate more incisally, make their appearance in the zone of transition. Stippled material also lies extracellularly adjacent to the cell surface and the apatite crystals (fig. 9). Distal to the Golgi region, the endoplasmic reticulum is arranged generally parallel to the long axis of the ameloblasts. It is reduced in amount, however, compared with that present in the more basally situated ameloblasts (figs. 2, 9). In the Golgi region, cytosomes and vesicles containing stippled material are found. Also in the Golgi zone and proximal to it, very large cytogesomes occur which enclose ribosome-studded membranes, smooth membranes, and granular and amorphous material (figs. 10, 11, 12). Electron-opaque material with irregular outlines is present in the Golgi region and proximal to it and is similar to that observed in the ameloblasts and papillary cells located more incisally. Adjacent ameloblasts exhibit extensive snug junctions near the distal ends (figs. 9, 10) and remain in close apposition to the proximal ends.

Papillary cells

The papillary cells occlude a larger area of the ameloblasts' proximal surface from the extracellular space than they do in either the more basal or incisal regions. Both snug and desmosomal junctions are formed between ameloblasts and papillary cells. Cytogesomes and electron-opaque masses of irregular shape, similar to those seen in the ameloblasts, are found commonly in the cytoplasm of those papillary cells which lie close to the ameloblasts. Amorphous material is more abundant in the extracellular space in the region of transition than either more basally or incisally.

moglobin. These authors point out the work of others, which provides indirect evidence that the tight junctions may be impermeable, in addition, to electrolytes and water. Consequently, the transport of material from the extracellular space of the papillary layer across the ameloblasts to the enamel may be inferred to be intracellular.

The arrangement of the organelles in the ameloblasts is such that material moving from their proximal to their distal ends first passes through a mitochondrial zone (containing the nucleus), next the Golgi zone, and finally a zone of highly organized endoplasmic reticulum. Vesicles containing stippled material appear chiefly in two locations, in the Golgi region and in the distal end of the cell. The vesicles in the Golgi region are usually larger and less dense than their distal counterparts. The intervening region, rich in rough-surfaced endoplasmic reticulum, contains few vesicles.

The abundant, well ordered, rough-surfaced endoplasmic reticulum must certainly be responsible for the elaboration of protein precursors utilized in the enamel matrix formation. This ergastoplasm develops in the ameloblasts concerned with young enamel deposition, but is virtually absent from the ameloblasts related to maturing enamel, whose final thickness has been obtained. The vesicles containing stippled material, however, are not related to the organelles in the characteristic manner observed in protein-secreting glandular cells. In such cells, the Golgi region lies between the organized rough-surfaced endoplasmic reticulum and the secretory surface (Ito, '63; Kurosumi, '61). The cell product is formed in the endoplasmic reticulum basally, "packaged" in single-membrane vesicles at the level of the Golgi apparatus, and extruded from the apical end of the cell (Caro and Palade, '64; Palade, Siekevitz and Caro, '61; Siekevitz and Palade, '60). In the ameloblasts, on the other hand, the rough-surfaced endoplasmic reticulum rather than the Golgi region lies closest to the extrusive end of the cell. In this respect, the ameloblasts resemble the liver cell, plasma cell, neuron and other cells which produce and eliminate protein continuously and do not ex-

hibit an accumulative secretory phase (Junqueira, '65).

Region of Transition

In this region, the ameloblasts and papillary cells show structural changes which accord with a conversion from the production of young enamel to activities concerned with enamel maturation. The ameloblasts cease to synthesize enamel matrix and the final thickness of enamel is complete. Large amounts of rough-surfaced endoplasmic reticulum are removed, apparently by cytosegresomes. The fate of the cytosegresomes is not known but it is suggested that their contents may be degraded enzymatically and eventually reach the extracellular space of the papillary layer and blood stream. It is in this region that the ameloblasts are decreased in height from 70 to 40 μ (Pindborg and Weinmann, '59). This reduction in height may be explained, at least in part, by a loss of volume with the removal of the enamel matrix-synthesizing apparatus.

The large cytosegresomes containing fragments of endoplasmic reticulum and free ribosomes together with other granular material undoubtedly represent the globular structures reported by Saunders, Nuckolls and Frisbie ('42), Marsland ('52), and Symons ('62). The ultrastructural findings of the present study concur with the histochemical report by Symons ('62) that ribonucleic acid is present in the globules.

Region of Maturation

During maturation, the transport of minerals continues from the capillaries, across the papillary cells and ameloblasts, to the enamel; whereas water and organic substances lost from the maturing enamel move in the opposite direction. The papillary cells possess elaborate microvilli which project into the extracellular space, contain numerous vesicles and are extremely rich in mitochondria. Similar structural characteristics noted for the salt glands of marine birds (Komnick, '65) appear to be related to the active transport of electrolytes. A similar function is suggested for the papillary cells. In cells of the kidney tubules (Pease, '56) and striated ducts of the salivary glands (Tandler, '63), mito-

nective tissue by numerous finger-like processes or folds. An occasional snug junction may occur between papillary cells along the basement membrane. Gaps, however, commonly exist between adjacent processes, permitting direct communication between the basement membrane and the extracellular space.

DISCUSSION

Region of Enamel Deposition

In the basal region of the incisor, material supplied by the closest capillaries is utilized by the ameloblasts to produce young enamel. The electron micrographs show that metabolites must cross an endothelial cell and then a basement membrane complex as a first step in their passage from the lumen of a capillary toward the ameloblasts. Next, the material passes into a stratum intermedium cell, outer papillary cell or enters the extracellular space of the papillary layer. Inasmuch as the stratum intermedium and outer papillary cells cover most of the surface of the basement membrane, the most probable route of transport is through the cytoplasm of these cells. A limited passage, however, is possible directly from the basement membrane to the extracellular space of the papillary layer at the junctions between the outer papillary or stratum intermedium cells. Finally, the metabolites enter the ameloblasts from the stratum intermedium cells or extracellular space. It was noted that a relatively small area of the proximal surface of the ameloblasts was occluded by stratum intermedium cell contacts. This suggests that metabolic exchange occurs chiefly between the ameloblasts and the extracellular space.

The stratum intermedium cells exhibit an arrangement of the Golgi substance, mitochondria and the intracellular fibrils indicative of a specific functional orientation. The Golgi complex, present on two opposite sides of the nucleus, is most extensive on the side facing the ameloblasts. Here, single-membrane vesicles occur. These vesicles may be secretory, destined for extrusion toward the ameloblasts, or they may be pinocytotic in origin. The mitochondria are disposed lateral to the

nucleus and form a perinuclear ring in each stratum intermedium cell. This position of the mitochondria places them adjacent to the extracellular channels, through which any direct intercellular exchange between the capillaries and ameloblasts must occur. Tentatively, the mitochondrial arrangement is considered to be related to the movement of electrolytes and water across the capillary-ameloblast interval. The intracellular fibrils lie mainly in planes above and below the nucleus and appear to be related to desmosomes formed with adjacent stratum intermedium cells. These fibrils may act to protect the configuration of the stratum intermedium cells against the shearing forces of gnawing and eruption.

The results of several other investigations strongly suggest that stratum intermedium cells participate in enamel formation. The microincineration studies of Hampp ('40) show the stratum intermedium cells to possess a high mineral content. Fullmer ('63) found a correlation in appearance of dehydrogenase activity, the degree of activity, and the kinds of dehydrogenase activities in the stratum intermedium cells and ameloblasts. An abundance of alkaline phosphatase in the stratum intermedium has been reported by many individuals (Mori, Takada and Okamoto, '61; Sasso and Castro, '57) and a relation to the mineralization of enamel has been suggested. Pourtois ('62, '63) describes an ATP, ADP, AMP dephosphorylating enzyme which appears in the stratum intermedium cells and later progresses along the lateral walls of the ameloblasts to the developing enamel. This enzyme, Pourtois points out, could make available for utilization in enamel formation all of the phosphate ions from adenosine nucleotides (Pourtois, '63).

The ameloblasts in this region show both proximal and distal terminal bars. Direct communication of material from the extracellular space of the papillary layer to the enamel is unlikely inasmuch as tight and intermediate junctions probably constitute, at least in part, the terminal bar complexes. The work of Farquhar and Palade ('63) showed that tight junctions associated with terminal bars block extracellular passage of molecules such as he-

papillary cells, concomitant with those in the ameloblasts during enamel formation. The mutual structural modifications are indicative of interrelated functional changes and strongly support the concept of ameloblast and papillary cells acting together as a functional unit.

LITERATURE CITED

- Beust, T. 1928 Intrafollicular enamel development. *J. Amer. Dent. Ass.*, 15: 2021-2031.
- Burgess, R. C., and C. M. Maclaren 1965 Proteins in developing bovine enamel. In: *Tooth Enamel*. M. V. Stack and R. W. Fearnhead, eds. Williams and Wilkins, Baltimore, pp. 78-82.
- Caro, L. G., and G. E. Palade 1964 Protein synthesis, storage, and discharge in the pancreatic exocrine cell. *J. Cell Biol.*, 20: 473-493.
- Chase, S. W. 1932 Histogenesis of the enamel. *J. Amer. Dent. Ass.*, 19: 1275-1289.
- 1935 The nature of the enamel matrix at different ages. *J. Amer. Dent. Ass.*, 22: 1343-1352.
- Deakins, M., and J. F. Volker 1941 Amount of organic matter in enamel from several types of human teeth. *J. Dent. Res.*, 20: 117-121.
- Deakins, M. 1942 Changes in the ash, water and organic content of pig enamel during calcification. *J. Dent. Res.*, 21: 429-435.
- Deakins, M., and R. L. Burt 1944 The deposition of calcium, phosphorus and carbon dioxide in calcifying dental enamel. *J. Biol. Chem.*, 156: 77-83.
- Decker, J. D. 1963 A light and electron microscope study of the rat molar enamel organ. *Arch. Oral Biol.*, 8: 301-310.
- Eastoe, J. E. 1960 Organic matrix of tooth enamel. *Nature (Lond.)*, 187: 411-412.
- 1963 The amino acid composition of proteins from the oral tissues — II. The matrix proteins in dentine and enamel from developing human deciduous teeth. *Arch. Oral Biol.*, 8: 633-652.
- Ebner, V. von 1906 Über die histologischen Veränderungen des Zahnschmelzes während der Erhärtung insbesondere beim Menschen. *Arch. Mikr. Anat.*, 67: 18-81.
- Elwood, W. K., and M. H. Bernstein 1964 Ultrastructural evidence of papillary cell function in amelogenesis. *J. Applied Physics.*, 35: 3086.
- 1965 Ultrastructure of the cells of the papillary layer in the rat incisor. *Anat. Rec.*, 151: 486.
- Ericsson, J. L. E. 1964 Absorption and decomposition of homologous hemoglobin in renal proximal tubular cells. *Acta Path. Micro. Scand. Suppl.* 168.
- Farquhar, M. G., and G. E. Palade 1963 Junctional complexes in various epithelia. *J. Cell Biol.*, 17: 375-412.
- Fullmer, H. M. 1963 Dehydrogenases in developing teeth of rats. *J. Histochem. Cytochem.*, 11: 641-644.
- Hampp, E. G. 1940 Mineral distribution in the developing tooth. *Anat. Rec.*, 77: 273-291.
- Hoppe, F. 1862 Untersuchungen über die Constitution des Zahnschmelzes. *Arch. path. Anat. u. physio. Klin. med.*, 24: 13-32.
- Ito, S., and R. J. Winchester 1963 The fine structure of the gastric mucosa in the bat. *J. Cell Biol.*, 16: 541-577.
- Junqueira, L. C. U. 1965 Aspects of the biology of the animal cell secretion. In: *Funktionelle und morphologische Organisation der Zelle II Sekretion und Exkretion*. Springer-Verlag, Berlin, pp. 27-35.
- Kallenbach, E. 1966 Electron microscopy of the papillary layer of rat incisor enamel organ during enamel maturation. *J. Ultrastructure Res.*, 14: 518-533.
- Kornick, H. 1965 Funktionelle Morphologie von Salzdrüsenzellen. In: *Funktionelle und morphologische Organisation der Zelle II Sekretion und Exkretion*. Springer-Verlag, Berlin, pp. 289-314.
- Kurosuni, K. 1961 Electron microscopic analysis of the secretion mechanism. In: *International Review of Cytology*. C. H. Bourne and J. F. Danielli, eds. Academic Press, New York and London, 11: 1-124.
- Loewenstein, W. R., and Y. Kanno 1964 Studies on an epithelial (gland) cell junction. I. Modifications of surface membrane permeability. *J. Cell Biol.*, 22: 565-586.
- Marchesi, V. T., and R. J. Barnett 1963 The demonstration of enzymatic activity in pinocytotic vesicles of blood capillaries with the electron microscope. *J. Cell Biol.*, 17: 547-556.
- Marsland, E. A. 1951 Histological investigation of amelogenesis in rats. I. Matrix formation. *Brit. Dent. J.*, 91: 251-261.
- 1952 Histological investigation of amelogenesis in rats. II. Maturation. *Brit. Dent. J.*, 92: 109-119.
- Moe, H., O. Behnke and J. Rostgaard 1962 Staining of osmium fixed vestibular embedded tissue sections for light microscopy. *Acta Anat.*, 48: 142-148.
- Mori, M., K. Takada and J. Okamoto 1961 Comparative distribution of alkaline and acid phosphatase activities in the developing teeth. *J. Osaka Univ. Dent. Sch.*, 1: 67-83.
- Palade, G. E., P. Siekevitz and L. G. Caro 1961 Structure, chemistry and function of the pancreatic exocrine cells. In: *Ciba Foundation Symposium on the Exocrine Pancreas: Normal and Abnormal Functions*. A. V. S. de Reuck and M. P. Cameron, eds. Little, Brown, Boston, pp. 23-49.
- Pease, D. C. 1956 Infolded basal plasma membranes found in epithelia noted for their water transport. *J. Biophys. Biochem. Cytol.*, 2: 203-208, Suppl. 2.
- 1964 Histological techniques for electron microscopy. Academic Press, New York, pp. 38-39.
- Pindborg, J. J., and J. P. Weinmann 1959 Morphologic and functional correlations in the enamel organ of the rat incisor during amelogenesis. *Acta Anat.*, 36: 367-381.

chondria are found concentrated near the cell wall across which electrolytes and water are actively carried into the cell. In the papillary cells, the localization of mitochondria toward the capillaries may indicate a similar activity in the transport of material from the capillaries toward the ameloblasts. Kallenbach ('66) suggests that the papillary cells act to concentrate electrolytes.

The vesicles lie mostly in the periphery of the papillary cell and appear to arise from the plasma membrane. One might expect to find a high ATPase activity localized in these vesicles as has been reported for pinocytotic vesicles in endothelial cells engaged in active transport (Marchesi and Barnett, '63). Pourtois ('62) describes a similar enzyme in the stratum intermedium cells of the mouse. Based on the presence of a "cytoplasmic fuzz" on the pinocytotic vesicles, Kallenbach ('66) considers that the papillary cells may be involved in specific (enamel?) protein uptake.

The passage of metabolites between the basement membrane complex and the ameloblasts is possible via the extracellular space of the papillary layer or, intracellularly, through the papillary cells. The junctions of the papillary cells with the ameloblasts occlude a greater area of the proximal surface of the ameloblasts and form many more desmosomal units than observed basally in the region of young enamel formation. The extensive junctions and increase in desmosomes may serve to stabilize the ameloblast to papillary cell relations in the region of maturing enamel. Loewenstein and Kanno ('64) reported that small ions and fluorescein move rather freely from one cell to the next across epithelial cell junctions. A similar function has been suggested by Kallenbach ('66) for the junctions between papillary cells. The junctions between the papillary and ameloblast cells may also serve as sites of free ion-movement.

The ameloblasts contain numerous vesicles in their distal ends which apparently arise from the plasma membrane facing the enamel. Similar vesicles are first seen in the region of transition. Thus, these vesicles appear in relation to enamel from which water and organic components are being removed. This coincidence suggests

that the vesicles may be a means by which the ameloblasts transport water and organic components from the enamel toward the papillary layer. The mitochondria concentrated near the vesicles may play an important role in the movement of materials necessary for maturation. A suggestion of a "fuzzy" coating is seen at several sites on the surface of the cell membrane facing the enamel. It is reminiscent of the amorphous or filamentous coating related to protein adsorption (Roth and Porter, '64; Ericsson, '64). Such a structure on the distal surface of the ameloblasts could be important in the removal of proteinaceous substances from the enamel during maturation.

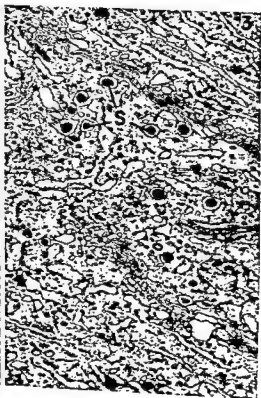
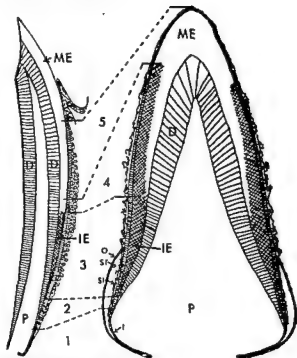
The extensive distal cytoplasmic processes described by Reith ('61, '63) for ameloblasts overlying maturing enamel were not seen in the present investigation. Reith ('61) suggests the ameloblasts to be transporting cells by virtue of the mitochondrial concentrations in their distal ends, noting further that the distal borders of the cells are PAS- and alkaline phosphatase-positive, as are epithelial absorptive cells of the intestines and the brush borders of the proximal tubule cells of the kidney.

The irregularly shaped osmiophilic material observed principally in the enamel organ related to enamel maturation appears similar to the lipid inclusions reported by Decker ('63) in the rat molar enamel organ. This material may represent a transient lipid storage.

At the present time, the function of the extracellular space is not understood. It is considered likely, however, that the volume of the space may vary readily with changes in ionic and osmotic forces, either natural or artificial. It is not yet possible to describe in detail the movement of the apatite constituents, organic material and water between the capillaries and the enamel. However, the ultrastructure of the enamel organ possesses characteristics which are in accord with the basic movements of the organic and inorganic constituents and water required for the formation of young enamel and its maturation.

The results of the present study of the ultrastructure of the enamel organ show changes to occur in the structure of the

I.



- Pourtois, M. 1962 Contribution à l'étude des bourgeons, dentaires chez la souris. II. Phases de cytodifférenciation, d'élaboration organique et de minéralisation. *Arch. Biol.*, 73: 225-309.
- 1963 Aspects histochimiques du développement des bourgeons dentaires. Ninth ORCA Congress, Pergamon Press, London, pp. 201-207.
- Reith, E. J. 1960 The ultrastructure of ameloblasts from the growing end of the rat incisors. *Arch. Oral Biol.*, 2: 253-262.
- 1961 The ultrastructure of ameloblasts during matrix formation and the maturation of enamel. *J. Biophys. Biochem. Cytol.*, 9: 825-840.
- 1963 The ultrastructure of ameloblasts during early stages of maturation of enamel. *J. Cell Biol.*, 18: 691-696.
- Roth, T. F., and K. R. Porter 1964 Yolk protein uptake in the oocyte of the mosquito *Aedes Aegypti* L. *J. Cell Biol.*, 20: 313-332.
- Sasso, W. S., and N. M. Castro 1957 Histochemical study of amelogenesis and dentinogenesis. *Oral Surg., Oral Med., Oral Path.*, 10: 1323-1329.
- Saunders, J. B. de C. M., J. Nuckolls and H. E. Frisbie 1942 Amelogenesis. A histologic study of the development, formation and calcification of the enamel in the molar tooth of the rat. *J. Amer. Coll. Dent.*, 9: 107-136.
- Schour, I., and M. Massler 1949 The rat in laboratory investigation. E. J. Farris and J. Q. Griffith, eds. Lippincott, Philadelphia, pp. 104-165.
- Siekevitz, P., and G. E. Palade 1960 A cytochemical study on the pancreas of the guinea pig. V. In vivo incorporation of leucine- ^{14}C into the chymotrypsinogen of various cell fractions. *J. Biophys. Biochem. Cytol.*, 7: 619-644.
- Symons, N. B. B. 1962 Globular structures associated with the completion of the enamel matrix in the rat. *J. Dent. Res.*, 41: 55-60.
- Tandler, B. 1963 Ultrastructure of the human submaxillary gland II. The base of the striated duct cells. *J. Ultrastructure Res.*, 9: 65-75.
- Weinmann, J. P., C. D. Wessinger and G. Reed 1942 Correlation of chemical and histological investigations on developing enamel. *J. Dent. Res.*, 21: 171-182.
- Williams, J. L. 1896 Formation and structure of dental enamel. *D. Cosmos*, 38: 101-127.

PLATE 1

EXPLANATION OF FIGURES

- 1 The diagram, on the left, represents a longitudinal section of a rat incisor; on the right, a developing human incisor. Corresponding segments based on the Pindborg-Weinmann division of the enamel organ are indicated. 1, region of odontogenic epithelial proliferation; 2, enamel organ abutting on dentin; 3, region of enamel deposition; 4, area of enamel maturation; 5, enamel organ overlying mature enamel. The region of "transition" dealt with in this paper is not assigned a specific zone by Pindborg and Weinmann, but corresponds closely to their "initial stages of maturation" in which "matrix globules" are found in the ameloblasts. In this figure, the region of transition may be considered as the junctional region between 3 and 4. The present investigation is concerned with three regions, enamel deposition (3), transition (junction of 3 and 4), and maturation (4). The rat incisor differs from the human tooth in three major respects: (a) the rat incisor is continuously forming and erupting, (b) a brown pigment is deposited in the final coat of enamel in the rat, and (c) enamel is formed only on the labial aspect of the incisor of the rat. Several minor differences between the rat incisor and the developing human tooth include the formation of high papillary ridges in the rat enamel organ and the limitation of the occurrence of the four distinct enamel-organ strata (outer dental epithelium, stellate reticulum, stratum intermedium, and inner dental epithelium) to the extreme basal end. The minor differences develop with the continued maintenance and activity of the enamel organ in the rat. D, dentin; I, inner dental epithelium; IE, immature enamel; ME, mature enamel; O, outer dental epithelium; P, pulp; SI, stratum intermedium; SR, stellate reticulum.
- 2 Oblique section through the distal ends of three ameloblasts engaged in enamel deposition, and the immature enamel associated with them. ER, rough-surfaced endoplasmic reticulum; IE, immature enamel; S, stippled material; TB, terminal bar. $\times 11,000$.
- 3 Oblique section (right side is distal) through the Golgi region of ameloblasts engaged in enamel deposition. Numerous vesicles contain a stippled material similar to that observed in the distal ends of the cells in figure 2. S, stippled material. $\times 27,000$.

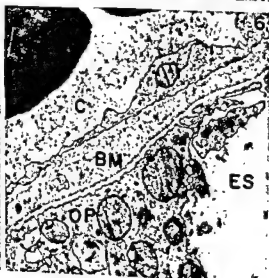


PLATE 2

EXPLANATION OF FIGURES

- 4 Low-power survey electron micrograph showing the interrelations of the cells of the papillary layer, the proximal ends of the ameloblasts, and a capillary. A, ameloblast; BM, basement membrane complex; C, capillary; ES, extracellular space; OP, outer papillary cell; SI, stratum intermedium cell; TB, terminal bar. $\times 8,000$.
- 5 Junction of the proximal ends of ameloblasts with stratum intermedium cells. This electron micrograph is of the section cut next to the one seen in figure 4. The neighboring components lie in the lower right quadrant of the preceding figure. A, ameloblast; F, fibrils; SI, stratum intermedium cell; TB, terminal bar. $\times 16,000$.
- 6 An enlargement of the basement membrane complex and related structures shown in figure 4. The papillary cells spread out to occlude most of the surface of the basement membrane from the extracellular space of the papillary layer. BM, basement membrane complex; C, capillary; ES, extracellular space; OP, outer papillary cell. $\times 22,000$.

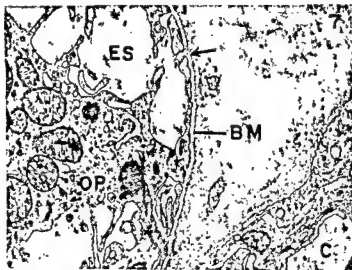


PLATE 3

EXPLANATION OF FIGURES

- 7 Junction between outer papillary cells and the connective tissue which overlies the enamel organ. The outer papillary cells exhibit processes that spread out on a thin basement membrane. The arrow indicates an opening between the outer papillary cells where the basement membrane is in direct contact with the extracellular space. BM, basement membrane; C, capillary; ES, extracellular space; OP, outer papillary cell. $\times 23,000$.
- 8 Phase-contrast photomicrograph of the enamel organ in the region of transition. Basal to this, the enamel organ is related to young enamel deposition; incisally it is related to maturing enamel. Many osmiophilic globules are evident in the ameloblasts and papillary cells. A, ameloblast; C, capillary; CT, connective tissue; E, enamel; OG, osmiophilic globules; P, papillary cell. $\times 600$.
- 9 An electron micrograph of the junction of the ameloblasts with the enamel in the region of transition. Compared with the more basally located ameloblasts (fig. 2), the amount of endoplasmic reticulum is decreased, mitochondria appear in the distal ends of these cells, and a more even junction with the enamel is observed. The distal terminal bars disappear in this region, and extracellular space appears between the ameloblasts. Figures 9 and 10 are contiguous; continuity of the structures may be discerned by matching the asterisks. E, enamel; ER, rough-surfaced endoplasmic reticulum; ES, extracellular space; S, stippled material; V, vesicles. $\times 24,000$.

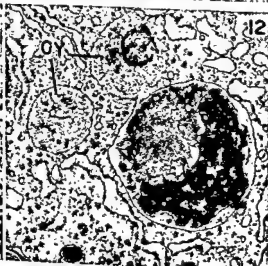


PLATE 4

EXPLANATION OF FIGURES

- 10 In the region of transition, cytosegresomes are numerous and frequently large. They are found chiefly in an area extending from and including the Golgi region of the ameboblasts to the closest capillary network of the papillary layer. The electron micrograph shows cytosegresomes lying slightly distal to the Golgi apparatus. Detail of the cytosegresomes is better seen in figures 11 and 12. Cs, cytosegresomes; L, lipid inclusion; S, stippled material. $\times 18,000$.
- 11, 12 Enlargements of the cytosegresomes shown in figure 10. The cytosegresomes contain mainly granular material and smooth and ribosome-studded membrane fragments. Two cytosomes lie close to the cytosegresome in figure 12. Cy, cytosome. $\times 31,000$.

13

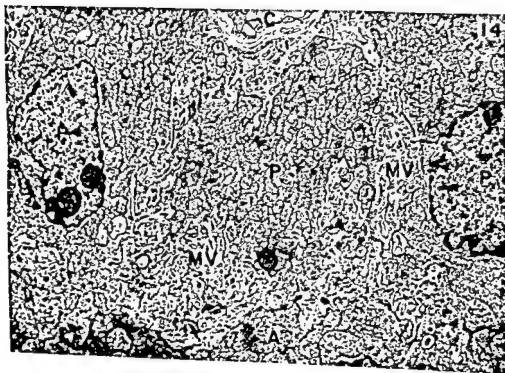
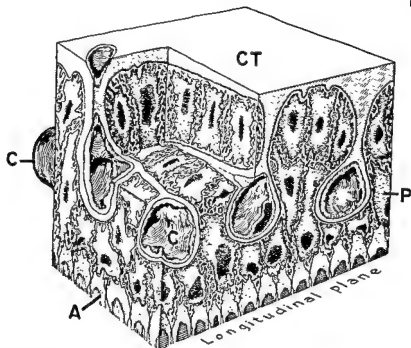


PLATE 5

EXPLANATION OF FIGURES

- 13 Three-dimensional diagram showing the appearance of the papillary ridges overlying maturing enamel. A capillary lies between each ridge and is separated from the ameloblasts by papillary cells. A, ameloblast; C, capillary; CT, connective tissue; P, papillary cell.
- 14 A low-power survey electron micrograph of a longitudinal section through papillary cells, a capillary, and the proximal ends of the ameloblasts. The cytoplasm of the papillary cells is packed with mitochondria. Microvilli project into the extracellular channels. A, ameloblast; C, capillary; Mv, microvilli; P, papillary cell. $\times 800$.

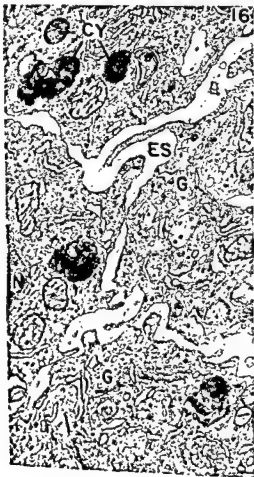
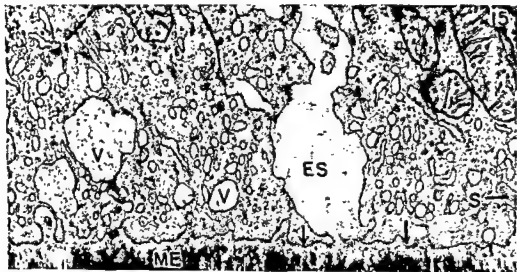


PLATE 6

EXPLANATION OF FIGURES

- 15 The junction of ameloblasts with maturing enamel. Numerous vesicles appear to be arising at the distal surface of the ameloblasts. Mitochondria accumulate close to these vesicles. An occasional vesicle containing stippled material is found in this region. Distal terminal bars are absent. There is a suggestion of a "fuzzy" coating at several sites of the cell membrane facing the enamel (arrows). ES, extracellular space; ME, maturing enamel; S, stippled material; V, vesicle. $\times 32,000$.
- 16 This electron micrograph is of a cross-section of ameloblasts through the Golgi region which lies between the nucleus and the more distal mitochondria-rich zone. Several cytosomes are present. Extracellular space separates these ameloblasts which overlie maturing enamel. ES, extracellular space; G, Golgi apparatus; Cy, cytosomes; N, nucleus. $\times 23,000$.
- 17 The junction between ameloblasts and papillary cells in this electron micrograph lies in the region of the termination of enamel maturation. Many fine granules (50-70 Å in diameter) presumed to be related to the formation of pigment in the final coats of enamel are present in the ameloblasts but not in the papillary cells. Bundles of intracellular fibrils become evident in the ameloblasts of this region and prominent in the papillary cells. Many vesicles, probably of pinocytotic origin, are found in the peripheral cytoplasm of the papillary cells. A, ameloblast; ES, extracellular space; F, fibrils; P, papillary cell. $\times 23,000$.

Origin and Distribution of Portal Blood in the Sheep¹

TREVOR HEATH²

*Veterinary School, University of Melbourne,
Parkville, N.2, Victoria, Australia*

ABSTRACT In sheep, the gastrosplenic and mesenteric veins converge at an angle of about 140° to form the portal vein, which is joined, along its right ventral border, by the gastroduodenal vein. At the porta, right and left branches of the portal vein diverge at an angle of 65–70° to supply separate areas that join along a line between the fossa for the gall bladder, and the middle of the left branch. Right dorsal branches leave the portal vein or its right branch near the point of bifurcation.

When ¹²⁵I-albumin that had been heated was injected into the right ruminal vein and entered the portal stream in the gastrosplenic vein, no significant differences existed in the levels of radioactivity between the areas supplied by the different portal branches. When the ¹²⁵I-albumin entered the portal stream from either the gastroduodenal or mesenteric veins, the area supplied by the right branch contained a significantly higher level of radioactivity than the remainder of the liver. When corrections were made for an unequal distribution of blood, it was found that blood from the gastrosplenic vein was distributed preferentially to the left branch, blood from the gastroduodenal vein to the right branch, and that blood from the mesenteric vein enters the right and left branches in preference to the right dorsal branches of the portal vein.

The anatomic arrangement of the tributaries of the portal vein may affect the distribution within the liver of blood derived from the various contributing organs (Seregé, '02; Himsworth, '50; Barnett and Cochrane, '56). Some workers have found that in dogs blood from the spleen, stomach and part of the colon flows to the left lobe, and that from most of the small intestine flows to the right lobe of the liver (Bartlett, Corper and Long, '14; Copher and Dick, '28; Hahn, Donald and Grier, '45). These workers studied the distribution within the liver of either emulsified olive oil, trypan blue or radioactive phosphoric acid that had been injected into one of the portal tributaries. Other workers, who injected radioactive iodine-labelled rose bengal into portal tributaries and measured its intrahepatic distribution with scintillation counters placed on the body surface, found no differences between the two sides of the liver in the distribution of the isotope (Cole, Krohmer, Bonte and Schatten, '56). In all these experiments the dogs were anaesthetised, and alterations in the relative positions of the portal vessels may have contributed to the variations between the results (c.f. Bradley, '63).

Variations between species in the anatomic arrangement of the portal vessels

may cause variations in the intrahepatic distribution of blood derived from different tributaries (Barnett and Cochrane, '56). In ruminant animals, the venous drainage from the cranial portion of the gut is much more extensive than in nonruminants (c.f. Horowitz and Venzke, '66), and the different portal tributaries probably vary in their relative importance. Some evidence is available to suggest that the distribution within the liver of blood from these tributaries differs from that described in other species (Himsworth, '50; Garner and Singleton, '53).

The anatomic arrangement of the tributaries and branches of the portal vein of sheep is described in this paper. A description is also given of experiments that were designed to determine whether blood from each of these tributaries is preferentially distributed to a particular branch of the portal vein in conscious, standing sheep.

MATERIALS AND METHODS

Anatomy of the portal vessels

Latex casts and angiograms were used to study the anatomy of the portal venous sys-

¹ Presented in part at meetings of the Australian Physiological Society (May, 1967) and the Victorian Division of the Australian Veterinary Association (July, 1967).

² Present address: School of Physiology, University of New South Wales, Kensington, New South Wales, Australia.

the liver stopped 40–60 seconds after the beginning of the injection. The sheep were destroyed with pentobarbitone sodium and measurements made of the distribution of radioactivity throughout the liver.

Student's "t" test, coupled with an analysis of variance, was used to determine whether significant differences existed between different areas of the liver in the distribution of radioactivity. These tests are described in detail in the Observations section.

OBSERVATIONS

Anatomy of the portal vessels

The portal vein in sheep is a dorso-ventrally flattened vessel, 1.5–3 cm long, formed by the confluence of the gastrosplenic and mesenteric veins (figs. 2, 3). A third tributary, the gastroduodenal vein, enters the right ventral border of the portal vein at almost a right angle, and conveys blood from the abomasum, duodenum, pancreas and omentum (figs. 2, 3). Although all the venous blood from some abdominal organs enters the portal vein through a single tributary, either two or all three tributaries may convey blood from

some organs (fig. 2, table 1). Significant variations do exist between different sheep in the arrangement of the different veins that contribute blood to the portal vein.

The gastrosplenic vein, which is formed from the splenic and left gastric veins, flows caudally and to the right for about 1 cm before it joins the mesenteric vein (figs. 2, 3). The left gastric vein, the smaller of the two tributaries of the gastrosplenic vein, also flows caudally and to the right, and conveys blood from the abomasum, omasum, reticulum and the left face of the rumen. The splenic vein is formed by the confluence of tributaries within the spleen, and is joined by veins from the pancreas, greater omentum and right face of the rumen. The epiploic and right ruminal veins extend in a cranial direction and join the caudal border of the splenic vein shortly before its junction with the left gastric vein (fig. 2).

The mesenteric vein, which is smaller than the gastrosplenic vein, receives blood from the pancreas, terminal duodenum, and the jejunum, ileum and large intestine (fig. 2). The terminal segment of the mesenteric vein extends cranially and slightly to the

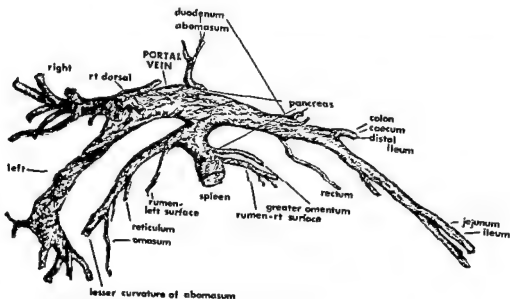


Fig. 2 Origin and distribution of portal vessels in the sheep. The cast from which this drawing was made was prepared by injecting neoprene latex into the mesenteric vein.

tem in merino and crossbred ewes and wethers. Each sheep was destroyed and bled out, then 100–150 ml neoprene latex (Dunlop Rubber Company, Melbourne, Australia) was injected into the mesenteric vein through a PVC cannula. The latex filled the intrahepatic branches of the portal vein and flowed in a retrograde direction along most of the portal tributaries. The abdominal organs were left in their normal positions, and the sheep were stored at 4°C for several days to allow the latex to solidify. The cast was then dissected out, and the traces of organic matter that remained were removed by soaking in 10% sodium hydroxide.

The livers of some sheep were removed immediately after death, and the branches of the portal vein were filled with mercury. A General Electric Patrician X-ray unit was used to take radiographs of these livers. Non-screen film was used without a grid.

Distribution of portal blood

Human serum albumin labelled with ^{131}I (The Radiochemical Centre, Amersham, England) and previously heated was injected into one of the tributaries of the portal vein, then the circulation through the liver was occluded and measurements made of the distribution of radioactivity throughout the liver. Three series, each of five experiments were conducted: in one series the ^{131}I -albumin was injected into the mesenteric vein, in another into the gastroduodenal vein, and in the third series of experiments the ^{131}I -albumin was injected into the right ruminal vein.

Before each experiment, the sheep was anaesthetised with halothane ("Fluothane," Imperial Chemical Industries, Melbourne, Australia) and an incision made parallel to and just behind the last rib on the right side. Either the mesenteric vein draining the mid-jejunum, the gastroduodenal vein near the pylorus, or the right ruminal vein was isolated. A PVC cannula (O.D. 0.96 mm) was inserted into the lumen of the vein through a small side branch, and did not appear to obstruct the flow of blood through the vein. A second piece of PVC tubing was placed loosely around the hepatic artery and portal vein, and did not touch the walls of the vein. This tube was designed as a snare, and both ends were led

out of the incision through a larger tube. The flank incision was closed, then a tube was placed in the right jugular vein and the sheep allowed to regain its feet.

The sheep was then restrained gently in the standing position and 20 μC ^{131}I -albumin in 1 ml of normal saline was injected through the cannula into one of the portal tributaries. This ^{131}I -albumin, which had been heated at 55–60°C for ten minutes before injection, was washed into the vein with 2 ml normal saline. The snare around the portal vein and hepatic artery was immediately pulled tight and the flow of blood into the liver stopped 15–30 seconds after the beginning of the injection. The sheep was destroyed a few seconds later by the injection of 20 ml of 30% pentobarbitone sodium through the jugular cannula.

The liver was removed and 63 cylindrical segments, each 18 × 1–2 mm, were removed from predetermined areas (fig. 1). These segments were dried overnight at 50°C, then their content of radioactivity was measured in a Geiger-Müller end-window counter. The level of radioactivity in each segment was expressed in counts/min/g of dried liver.

In another series of experiments, ^{131}I -albumin was injected into the jugular vein in five sheep, and the flow of blood into

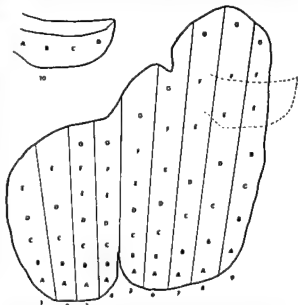


Fig. 1 Segments of the liver taken for radioactivity analysis after the injection of ^{131}I -albumin into the jugular vein or tributaries of the portal vein.

the liver stopped 40–60 seconds after the beginning of the injection. The sheep were destroyed with pentobarbitone sodium and measurements made of the distribution of radioactivity throughout the liver.

Student's "t" test, coupled with an analysis of variance, was used to determine whether significant differences existed between different areas of the liver in the distribution of radioactivity. These tests are described in detail in the Observations section.

OBSERVATIONS

Anatomy of the portal vessels

The portal vein in sheep is a dorso-ventrally flattened vessel, 1.5–3 cm long, formed by the confluence of the gastrosplenic and mesenteric veins (figs. 2, 3). A third tributary, the gastroduodenal vein, enters the right ventral border of the portal vein at almost a right angle, and conveys blood from the abomasum, duodenum, pancreas and omentum (figs. 2, 3). Although all the venous blood from some abdominal organs enters the portal vein through a single tributary, either two or all three tributaries may convey blood from

some organs (fig. 2, table 1). Significant variations do exist between different sheep in the arrangement of the different veins that contribute blood to the portal vein.

The gastrosplenic vein, which is formed from the splenic and left gastric veins, flows caudally and to the right for about 1 cm before it joins the mesenteric vein (figs. 2, 3). The left gastric vein, the smaller of the two tributaries of the gastrosplenic vein, also flows caudally and to the right, and conveys blood from the abomasum, omasum, reticulum and the left face of the rumen. The splenic vein is formed by the confluence of tributaries within the spleen, and is joined by veins from the pancreas, greater omentum and right face of the rumen. The epiploic and right ruminal veins extend in a cranial direction and join the caudal border of the splenic vein shortly before its junction with the left gastric vein (fig. 2).

The mesenteric vein, which is smaller than the gastrosplenic vein, receives blood from the pancreas, terminal duodenum, and the jejunum, ileum and large intestine (fig. 2). The terminal segment of the mesenteric vein extends cranially and slightly to the

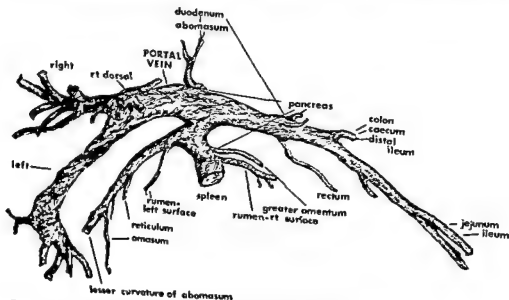


Fig. 2 Origin and distribution of portal vessels in the sheep. The cast from which this drawing was made was prepared by injecting neoprene latex into the mesenteric vein.

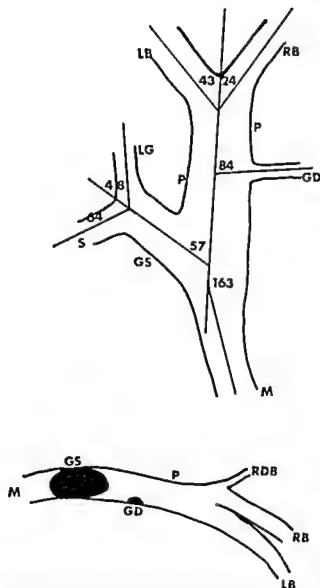


Fig. 3 Relative disposition of the tributaries and branches of the portal vein. Neoprene latex casts of the tributaries and branches of the portal vein were prepared in five sheep. The angles of convergence and divergence were measured after projection of the vessels onto a horizontal plane (upper figure) or a vertical plane (lower figure) through the long axis of the vein. P, portal vein; LB, left branch; RB, right branch; RDB, right dorsal branches; GD, gastroduodenal V; M, mesenteric V; GS, gastrosplenic V; S, splenic V; LG, left gastric V.

left and approaches the gastrosplenic vein at an angle of about 140° (fig. 3).

Valves were not observed in either the portal vein or its three tributaries. A large number of valves were present in the smaller veins, but these were relatively inefficient and in most cases did not impede the flow of latex along the veins.

The portal vein enters the liver at the porta, and immediately receives small veins from the gall bladder and cystic duct. It immediately divides at an angle of $65-70^\circ$ into the left and right branches that supply the ventral lobe and the ventral part of the dorsal lobe of the liver (figs. 2, 3, 6). Right dorsal branches that supply blood to the caudate lobe and the dorsal part of the dorsal lobe emerge from the dorsal surface of either the portal vein at the point of bifurcation, or the proximal part of the right branch (figs. 2, 3, 6).

The right branch proceeds ventrally and gives rise to 3 or 4 major branches and a variable number of minor branches (fig. 6). These vessels supply a wedge-shaped segment of liver tissue: the apex of the wedge is at the depression for the gall bladder and the base along the line of the left branch of the portal vein (fig. 6). The ventral margin of this segment lies along a line between the depression for the gall bladder, and the midpoint of the left branch of the portal vein. This line does not correspond to the line of division between the dorsal and ventral lobes. Generally no vessels that can be seen in angiograms cross this line, but in one liver a relatively large branch extended into the area supplied by the left branch.

The left branch, which is considerably larger than the right branch of the portal vein, curves ventrally and to the left within a deep depression on the liver surface. A number of small branches leave the cranial surface of the left branch, and supply that portion of the liver in the region of the

TABLE 1
Tributaries through which blood from different abdominal organs enters the portal vein

Blood from → enters portal vein in ↓	Spleen fore- stomachs	Abomasum	Duodenum	Jejunum ileum large intestine	Pancreas
Mesenteric V.			×	×	×
Gastroduodenal V.		×	×		×
Gastrosplenic V.	×	×			×

TABLE 2

Distribution of radioactivity in the liver after injection of ^{131}I -albumin into jugular vein, and portal tributaries

^{131}I -albumin injected into	Mean cpm/g DW in area of			Remainder ¹	Total	Error mean square ²	Degrees of freedom
	Left ¹	Right ¹	Right dorsal ¹				
Jugular V.	2527	2834	2868	2435	2625	211,582	248
Mesenteric V.	3473	3989	3133	3397	3505	1,086,313	248
Gastroduodenal V.	2579	4006	2917	2928	2960	3,442,497	248
Right ruminal V.	2412	2473	2236	2171	2357	595,272	248
Total no. of segments	155	60	50	50	315		

¹ Area supplied by right dorsal branches of portal vein contains segments 8E-G, 9E-G, 10A-D, and area supplied by right branch contains segments 7A-D, 8A-D, 9A-D (fig. 1); left branch supplies all segments in strips 1-5.

² Samples 6A-G, and 7E-G, were from intermediate regions between identifiable drainage areas.

³ Estimated during analysis of variance.

caudal vena cava. At the level of the umbilical fissure, the left branch divides into dorsal, intermediate and ventral rami (fig. 6). The ventral ramus divides into two vessels that supply the liver tissue on either side of the umbilical fissure, and the dorsal and intermediate rami, which may arise from the common trunk, supply the remainder of the ventral lobe (fig. 6).

Distribution of portal blood

Estimates were made of the mean levels of radioactivity within each series in the areas supplied by the right dorsal, right and left branches of the portal vein (table 2). It was considered that the right dorsal branches supplied segments 8 E-G, 9 E-G and 10 A-D, the right branch segments 7 A-D, 8 A-D and 9 A-D and that the left branch supplied all the segments in strips 1-5 (figs. 1, 6). Student's "t" test was used to estimate the significance of the differences between the mean levels of radioactivity in the different areas ($\bar{x}_i - \bar{x}_j$). The "t" values were calculated by substituting the mean values, the error mean square (EMS), estimated in an analysis of variance (table 2), and the total number of segments in each area (N_i, N_j) in equation (1).

$$t = \frac{\bar{x}_i - \bar{x}_j}{\sqrt{\text{EMS}(N_i^{-1} + N_j^{-1})}} \quad \dots \quad (1)$$

When the ^{131}I -albumin was injected into the right ruminal vein, no significant differences were apparent between the levels of radioactivity in the different areas (fig. 4). When the ^{131}I -albumin was injected

into either the mesenteric vein or the gastroduodenal vein, the mean levels of radioactivity in the areas supplied by the left branch and the right branch did not differ significantly, but these levels were significantly less than those in the area supplied by the right branch of the portal vein (fig. 4, table 3).

In these experiments, the ^{131}I -albumin would not have had time to escape from the blood vessels, and the unequal distribution of radioactivity must have been due to variations either in the amount of blood represented in each gram of dried liver, or in the concentration of ^{131}I -albumin in this blood, or in both these parameters. An attempt was made to determine the relative importance of each of these parameters in contributing to the variations in the distribution of radioactivity observed in each series. Initially, ^{131}I -albumin was injected into the jugular vein in an effort to produce a uniform concentration of radioactivity in the blood entering the liver. When measurements were made of the distribution of radioactivity in the livers from the jugular series, it was found that although the areas supplied by the right and right dorsal branches contained a fairly uniform level, these areas did contain a significantly higher level of radioactivity than the area supplied by the left branch (fig. 4, table 3). These results indicated that the volume of blood represented in each gram of dried liver did vary throughout the organ.

The intrahepatic distribution of radioactivity in each of the mesenteric, gastroduodenal and right ruminal series was then

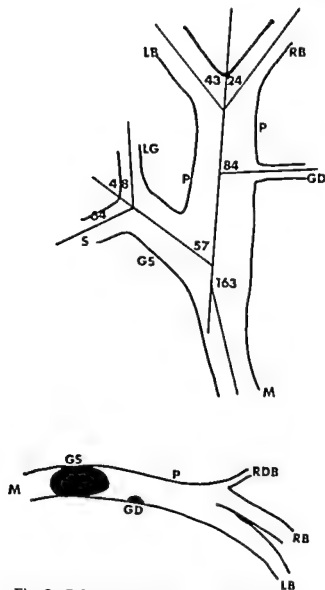


Fig. 3 Relative disposition of the tributaries and branches of the portal vein. Neoprene latex casts of the tributaries and branches of the portal vein were prepared in five sheep. The angles of convergence and divergence were measured after projection of the vessels onto a horizontal plane (upper figure) or a vertical plane (lower figure) through the long axis of the vein. P, portal vein; LB, left branch; RB, right branch; RDB, right dorsal branches; GD, gastroduodenal V; M, mesenteric V; GS, gastrosplenic V; S, splenic V; LG, left gastric V.

left and approaches the gastrosplenic vein at an angle of about 140° (fig. 3).

Valves were not observed in either the portal vein or its three tributaries. A large number of valves were present in the smaller veins, but these were relatively inefficient and in most cases did not impede the flow of latex along the veins.

The portal vein enters the liver at the porta, and immediately receives small veins from the gall bladder and cystic duct. It immediately divides at an angle of $65-70^\circ$ into the left and right branches that supply the ventral lobe and the ventral part of the dorsal lobe of the liver (figs. 2, 3, 6). Right dorsal branches that supply blood to the caudate lobe and the dorsal part of the dorsal lobe emerge from the dorsal surface of either the portal vein at the point of bifurcation, or the proximal part of the right branch (figs. 2, 3, 6).

The right branch proceeds ventrally and gives rise to 3 or 4 major branches and a variable number of minor branches (fig. 6). These vessels supply a wedge-shaped segment of liver tissue: the apex of the wedge is at the depression for the gall bladder and the base along the line of the left branch of the portal vein (fig. 6). The ventral margin of this segment lies along a line between the depression for the gall bladder, and the midpoint of the left branch of the portal vein. This line does not correspond to the line of division between the dorsal and ventral lobes. Generally no vessels that can be seen in angiograms cross this line, but in one liver a relatively large branch extended into the area supplied by the left branch.

The left branch, which is considerably larger than the right branch of the portal vein, curves ventrally and to the left within a deep depression on the liver surface. A number of small branches leave the cranial surface of the left branch, and supply that portion of the liver in the region of the

TABLE 1
Tributaries through which blood from different abdominal organs enters the portal vein

Blood from → enters portal vein in ↓	Spleen fore- stomachs	Abomasum	Duodenum	Jejunum ileum large intestine	Pancreas
Mesenteric V.					
Gastroduodenal V.		×	×	×	×
Gastrosplenic V.	×	×			×

TABLE 2

Distribution of radioactivity in the liver after injection of ^{131}I -albumin into jugular vein, and portal tributaries

^{131}I -albumin injected into	Mean cpm/g DW in area of			Remainder *	Total	Error mean square *	Degrees of freedom
	Left †	Right †	Right dorsal †				
Jugular V.	2527	2834	2888	2435	2625	211,582	248
Mesenteric V.	3473	3989	3133	3397	3505	1,086,313	248
Gastroduodenal V.	2579	4006	2917	2928	2960	3,442,497	248
Right ruminal V.	2412	2473	2236	2171	2357	595,272	248
Total no. of segments	155	60	50	50	315		

* Area supplied by right dorsal branches of portal vein contains segments 8E-G, 9E-G, 10A-D, and area supplied by right branch contains segments 7A-D, 8A-D, 9A-D (fig. 1); left branch supplies all segments in strips 1-5.

† Samples 6A-G, and 7E-G, were from intermediate regions between identifiable drainage areas.

* Estimated during analysis of variance.

caudal vena cava. At the level of the umbilical fissure, the left branch divides into dorsal, intermediate and ventral rami (fig. 6). The ventral ramus divides into two vessels that supply the liver tissue on either side of the umbilical fissure, and the dorsal and intermediate rami, which may arise from the common trunk, supply the remainder of the ventral lobe (fig. 6).

Distribution of portal blood

Estimates were made of the mean levels of radioactivity within each series in the areas supplied by the right dorsal, right and left branches of the portal vein (table 2). It was considered that the right dorsal branches supplied segments 8 E-G, 9 E-G and 10 A-D, the right branch segments 7 A-D, 8 A-D and 9 A-D and that the left branch supplied all the segments in strips 1-5 (figs. 1, 6). Student's "t" test was used to estimate the significance of the differences between the mean levels of radioactivity in the different areas ($\bar{x}_1 - \bar{x}_2$). The "t" values were calculated by substituting the mean values, the error mean square (EMS), estimated in an analysis of variance (table 2), and the total number of segments in each area (N_1, N_2) in equation (1).

$$t = \frac{\bar{x}_1 - \bar{x}_2}{\sqrt{[\text{EMS}(N_1-1 + N_2-1)]/4}} \quad \dots (1)$$

When the ^{131}I -albumin was injected into the right ruminal vein, no significant differences were apparent between the levels of radioactivity in the different areas (fig. 4). When the ^{131}I -albumin was injected

into either the mesenteric vein or the gastroduodenal vein, the mean levels of radioactivity in the areas supplied by the left branch and the right branch did not differ significantly, but these levels were significantly less than those in the area supplied by the right branch of the portal vein (fig. 4, table 3).

In these experiments, the ^{131}I -albumin would not have had time to escape from the blood vessels, and the unequal distribution of radioactivity must have been due to variations either in the amount of blood represented in each gram of dried liver, or in the concentration of ^{131}I -albumin in this blood, or in both these parameters. An attempt was made to determine the relative importance of each of these parameters in contributing to the variations in the distribution of radioactivity observed in each series. Initially, ^{131}I -albumin was injected into the jugular vein in an effort to produce a uniform concentration of radioactivity in the blood entering the liver. When measurements were made of the distribution of radioactivity in the livers from the jugular series, it was found that although the areas supplied by the right and right dorsal branches contained a fairly uniform level, these areas did contain a significantly higher level of radioactivity than the area supplied by the left branch (fig. 4, table 3). These results indicated that the volume of blood represented in each gram of dried liver did vary throughout the organ.

The intrahepatic distribution of radioactivity in each of the mesenteric, gastroduodenal and right ruminal series was then

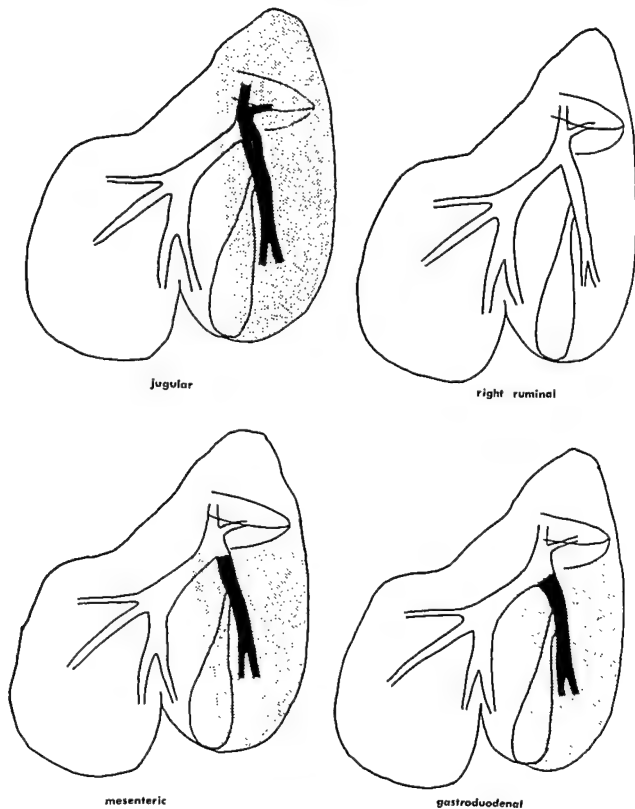


Fig. 4 Distribution of radioactivity within the liver after the injection of ^{125}I -albumin into either the jugular, mesenteric, gastroduodenal or right ruminal veins. Within each series, the shaded area, supplied with blood by the blackened branch of the portal vein, contained a significantly higher level of radioactivity than the unshaded area.

TABLE 3

Comparison of levels of radioactivity between areas supplied by different branches of the portal vein¹

¹²⁵ I-albumin injected into	Comparison within series ²				Comparison with jugular series ³			
			t	P			t	P
Jugular V	RD	∇ R	0.39	> 10 ⁻¹				
	RD+R	L	5.62 *	< 10 ⁻⁷				
Mesenteric V	L	∇ RD	1.62	> 10 ⁻¹	L	∇ R	1.20	> 10 ⁻¹
	R	L+RD	5.39 *	< 10 ⁻⁶	L+R	RD	4.30 *	< 10 ⁻⁴
Gastroduodenal V	RD	∇ L	1.12	> 10 ⁻¹	L	∇ RD	0.001	> 10 ⁻¹
	R	L+RD	4.94 *	< 10 ⁻⁴	R	RD+L	3.84 *	< 10 ⁻³
Right ruminal V	R	∇ RD	1.61	> 10 ⁻¹	R	∇ RD	1.86	> 10 ⁻¹
	L	RD+R	0.49	> 10 ⁻¹	L	RD+R	6.86 *	< 10 ⁻³

¹ The right dorsal branch of the portal vein is designated "RD," the right branch "R" and the left branch "L."² "t" values were calculated by substituting data from table 2 into equation (ii).³ "t" values calculated by substituting data derived from table 2 into equations (ii) and (iii).

* Highly significant difference.

compared with that in the jugular series to determine whether ¹²⁵I-albumin, injected into a portal tributary (T), was uniformly distributed throughout the blood that entered the right, right dorsal and left branches of the portal vein. In this comparison, the difference obtained in each of the mesenteric, gastroduodenal and right ruminal series between the mean level of radioactivity in the areas supplied by two of the portal branches (1, 2) was calculated ($\bar{x}_n - \bar{x}_m$). This difference was compared with the corresponding difference obtained in the jugular series ($\bar{x}_n - \bar{x}_m$). The variance of the difference between these differences, equal to the sum of the respective variances ($V\bar{x}_n + V\bar{x}_m + V\bar{x}_n + V\bar{x}_m$), was estimated from the error mean squares and sample numbers (table 2), and "t" was estimated from equation (ii).

$$t = \frac{(\bar{x}_n - \bar{x}_m) - (\bar{x}_n - \bar{x}_m)}{\sqrt{(EMS_e + EMS_f) \left(\frac{1}{N_e-1} + \frac{1}{N_f-1} \right)}}$$
 (ii)

A similar, independent test was used to compare these two areas with the area of distribution of the third branch of the portal vein. In this test, the "t" variable was estimated by substituting values from table 2 into equation (iii).

$$t = \frac{(\bar{x}_n + \bar{x}_m - 2\bar{x}_l) - (\bar{x}_n + \bar{x}_m - 2\bar{x}_l)}{\sqrt{(EMS_e + EMS_f) \left(\frac{1}{N_e-1} + \frac{1}{N_f-1} + \frac{4}{N_l-1} \right)}}$$
 (iii)

The number of degrees of freedom of each error mean square used in these tests was so large (248) that the "t" variables closely approximated normal variables and it was

possible to estimate the probabilities from tables of the normal distribution (Fisher and Yates, '63).

These tests revealed that when the ¹²⁵I-albumin was injected into the mesenteric vein, the concentration of radioactivity in the blood did not differ significantly between the right and left branches of the portal vein (fig. 5, table 3). The concentration in these branches, however, was significantly higher than that in the blood that entered the right dorsal branches. In the gastroduodenal series, the initial comparison between the right dorsal and left branches revealed a striking uniformity of concentration, but this was significantly less than that in the right branch (fig. 5, table 3). When the ¹²⁵I-albumin was injected into the right ruminal vein, the concentration of radioactivity in the right and right dorsal branches did not differ significantly, but this was significantly lower than that in the left branch of the portal vein (fig. 5, table 3).

Similar tests were used to determine whether significant differences either in the total level of radioactivity or in the concentration of radioactivity in the blood existed between the areas supplied by each of the three rami of the left branch (fig. 6). When the ¹²⁵I-albumin was injected into the gastroduodenal vein, the area supplied by the left ventral ramus contained a significantly higher level of radioactivity than the remainder of the left lobe ($P < 10^{-7}$). In this series, the blood in the left ventral

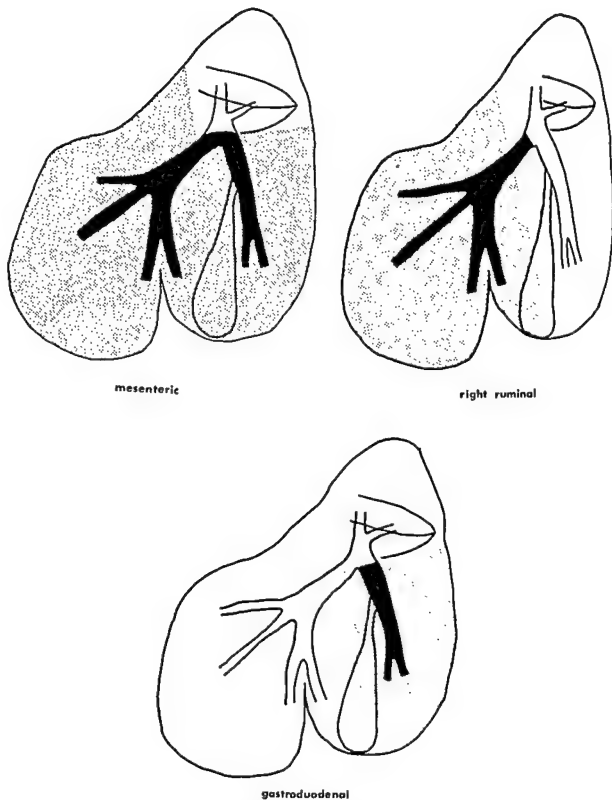


Fig. 5 Distribution within the liver of blood derived from the mesenteric, gastroduodenal or right ruminal veins. The blood derived from each of these tributaries is preferentially distributed, through the blackened branch of the portal vein, to the shaded area of the liver.

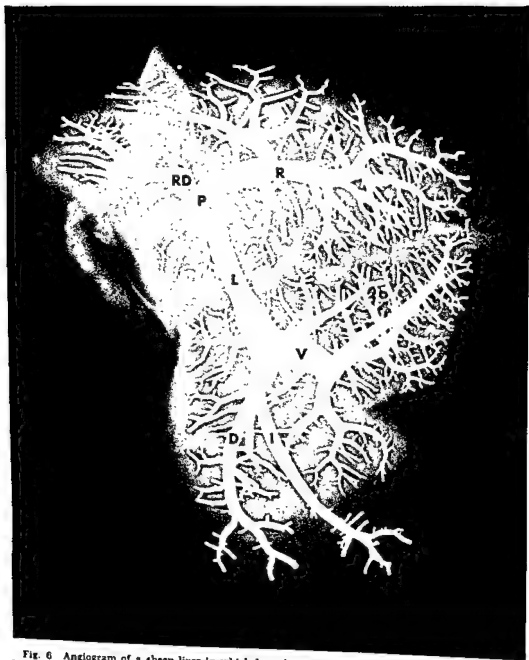


Fig. 6 Angiogram of a sheep liver in which branches of the portal vein were filled with mercury. Left (L) and right (R) branches of the portal vein separate at the porta (P) and supply separate areas that join along a line between the fossa for the gall bladder (GB) and the middle of the left branch. The left branch divides, at the level of the umbilical fissure, into dorsal (D), intermediate (I) and ventral (V) rami. Right dorsal branches (RD) emerge from either the portal vein or the right branch, and supply the caudate lobe and the dorsal area of the dorsal lobe.

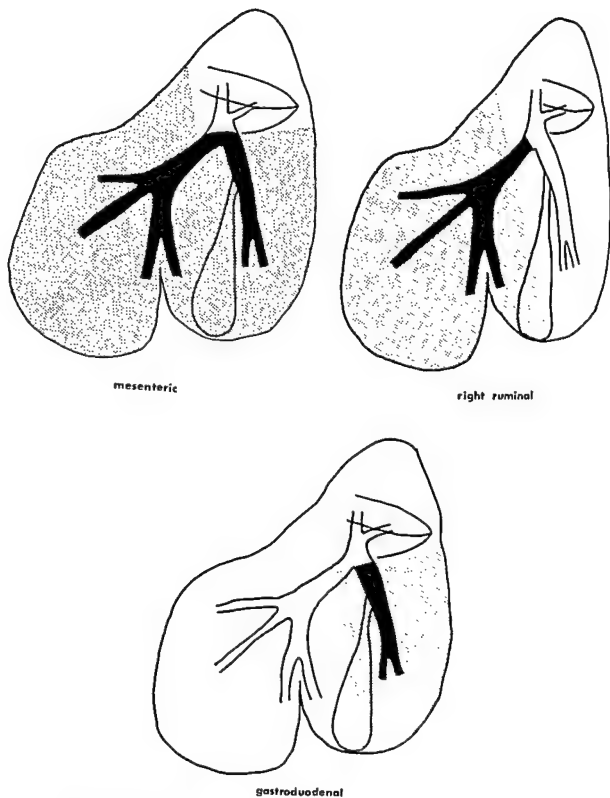


Fig. 5 Distribution within the liver of blood derived from the mesenteric, gastroduodenal or right ruminal veins. The blood derived from each of these tributaries is preferentially distributed, through the blackened branch of the portal vein, to the shaded area of the liver.

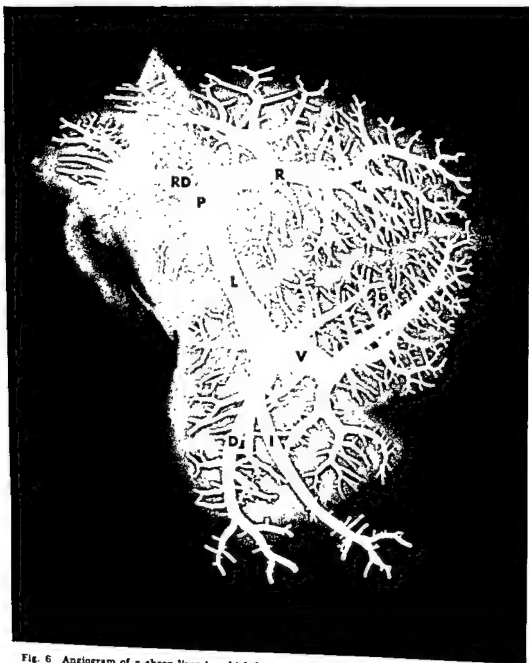


Fig. 6 Angiogram of a sheep liver in which branches of the portal vein were filled with mercury. Left (L) and right (R) branches of the portal vein separate at the porta (P) and supply separate areas that join along a line between the fossa for the gall bladder (CB) and the middle of the left branch. The left branch divides, at the level of the umbilical fissure, into dorsal (D), intermediate (I) and ventral (V) rami. Right dorsal branches (RD) emerge from either the portal vein or the right branch, and supply the caudate lobe and the dorsal area of the dorsal lobe.

ramus also contained a significantly higher concentration of radioactivity ($P = 10^{-1}$) than the blood in the dorsal and intermediate rami of the left branch.

Comparisons were also made between the marginal and central areas of each lobe. In the jugular and right ruminal series, the marginal areas of both right ($P < 5.10^{-1}$, 10^{-3} respectively) and left lobes ($P < 10^{-4}$, 10^{-2} respectively) contained significantly higher levels of radioactivity than the respective central areas. In the right ruminal series, the blood in the marginal areas of both right ($P < 5.10^{-1}$) and left lobes ($P < 2.10^{-3}$) also contained significantly higher concentrations of radioactivity than the central areas.

DISCUSSION

In the sheep liver, the line of division between the dorsal and ventral lobes (Sisson and Grossman, '53) does not correspond to the line of separation between the areas supplied with blood by the right and left branches of the portal vein. It has been known for many years that a similar condition exists in the liver of man and the dog (Bartlett, Corper and Long, '14; McIndoe and Counseller, '27; Hjortsjö, '51), and in 1953 Garner and Singleton suggested that this may apply in the sheep liver, but provided no clear evidence to support their suggestion. Garner and Singleton considered that the right branch is the direct continuation of the portal vein of the sheep as it is in man (Bartlett, Corper and Long, '14; Elias, '63), and that the left branch diverges at about a right angle. In the sheep examined in this study, both right and left branches diverged from the line of the portal vein, and the total angle of divergence was less than a right angle (fig. 3). It is not likely, however, that the angle of divergence of the portal branches will affect the distribution within the liver of blood derived from the different portal tributaries (c.f. Barnett and Cochrane, '56).

The results obtained by Barnett and Cochrane ('56) in an *in vitro* system indicate that the disposition of the portal tributaries themselves is likely to affect the intrahepatic distribution of blood derived from the different tributaries. In ruminant animals, the exact arrangement of the por-

tal tributaries may vary depending on the degree of distension of the rumen. Although some variations in ruminal distension may occur under normal conditions, major variations may occur during anaesthesia (Wright and Hall, '61). This may explain the variability in the results of Garner and Singleton ('53) who injected colloidal chromic phosphate into the spleen of anaesthetised sheep and goats and studied the distribution of radioactivity within the liver.

The exact arrangement of the tributaries of the portal vein does vary considerably between different species of animals. In the human, dog and goat, the gastrosplenic vein conveys blood into the portal vein in a generally cranial direction (Bartlett, Corper and Long, '14; Miller, Christensen and Evans, '64; Horowitz and Venzke, '66), but in the sheep it extends caudally and to the right at its termination (figs. 2, 3). In the sheep, the gastrosplenic vein is the largest tributary of the portal vein, but in the dog it is only about one-half to two-thirds as large as the vein that drains the intestines (Miller, Christensen and Evans, '64).

The intrahepatic distribution of blood from the different portal tributaries in sheep varies from that described in other animals. When ^{125}I -albumin entered the portal stream in the gastrosplenic vein of standing, conscious sheep, there were no significant differences between the levels of radioactivity in the areas supplied by the right and left branches of the portal vein. However, when these results were corrected for variations in the total amount of blood represented in each gram of dried liver, it was found that the blood from the gastrosplenic vein had flowed preferentially into the left branch of the portal vein. The difference between the amount flowing to the left and right branches was much less than that found by Hahn, Donald and Grier ('45) in the anaesthetised dog. When these authors injected labelled phosphoric acid into the splenic vein, they found that the left margin of the liver contained up to 45 times more radioactivity per gram than the right margin. When the injection was made into a branch of the mesenteric vein, the level of radioactivity in the right section of

he liver was about three times as high as that in the left section (Hahn, Donald and Grier, '45). In the conscious sheep, the urea supplied by the right branch of the portal vein also contained a higher level of radioactivity than that supplied by the left branch when ^{14}C -albumin was injected into the mesenteric vein (table 3). However, this was due almost entirely to variations between the areas supplied by the right and left branches in the amount of blood represented in each gram of dried liver. There was no evidence that blood that drained from the intestines in the mesenteric vein of sheep was preferentially distributed to either the right or left branches of the portal vein. The blood from the proximal duodenum and abomasum that entered the portal vein in the gastroduodenal vein was preferentially distributed to the right branch, but some blood from the abomasum also entered the portal vein in the gastrosplenic vein, and this was preferentially distributed to the left branch of the portal vein. It may be concluded that no major variations exist between the right and left branches of the portal vein in the distribution of blood derived from the abomasum and intestines of sheep.

ACKNOWLEDGMENTS

This study was supported by USPHS grant 1 RO5 TW00190-01. Mr. C. K. Herbert, and Miss B. Laby and Mr. J. S. Maritz of the Department of Statistics, University of Melbourne, were of considerable assistance during the analysis of the results. Mr. D. J. Meehan and Mr. A. J. Forman provided valuable technical assistance.

LITERATURE CITED

- Barnett, C. H., and W. Cochrane 1936 Flow of viscous liquids in branched tubes With reference to the hepatic portal vein. *Nature, Lond.*, 177: 740-742.
- Bartlett, F. K., H. J. Corper and E. R. Long 1914 The independence of the lobes of the liver. *Am. J. Physiol.*, 35: 36-50.
- Bradley, S. E. 1963 The hepatic circulation. In: *Handbook of Physiology*. Section 2, Circulation Volume II. W. F. Hamilton and Philip Dow, eds. American Physiological Society, Washington, D. C., pp. 1387-1438.
- Cole, J. W., J. Krohmer, F. J. Bonte and W. Schatten 1956 An experimental study of intrahepatic distribution of portal blood. *Surg. Gynec. Obst.*, 102: 543-544.
- Copher, G. H., and B. M. Dick 1928 "Stream line" phenomena in the portal vein and the selective distribution of portal blood in the liver. *Arch. Surg.*, 17: 408-419.
- Elias, H. 1963 Anatomy of the liver. In: *The Liver Morphology Biochemistry Physiology*. Volume 1. Ch. Rouiller ed. Academic Press, New York and London, pp. 41-59.
- Fisher, R. A., and F. Yates 1963 Statistical tables for biological, agricultural and medical research. Oliver and Boyd, London.
- Garner, R. J., and A. G. Singleton 1953 Laminar flow in the portal vein of the sheep and goat. *J. Comp. Path.*, 63: 300-303.
- Hahn, P. F., W. D. Donald and R. C. Grier, Jr. 1945 The physiological bilaterality of the portal circulation. Streamline flow of blood into the liver as shown by radioactive phosphorus. *Am. J. Physiol.*, 143: 105-107.
- Himsworth, H. P. 1950 The liver and its diseases. Second edition. Blackwell Scientific Publications, Oxford, pp. 26-28.
- Hjortsjö, C.-H. 1951 The topography of the intrahepatic duct systems. *Acta Anat.*, 11: 599-615.
- Horowitz, A., and W. C. Venzke 1966 Distribution of blood vessels to the postdiaphragmatic digestive tract of the goat: celiac trunk-gastroduodenal and splenic tributaries of the portal vein. *Am. J. Vet. Res.*, 27: 1293-1315.
- McIndoe, A. H., and V. S. Counseller 1927 The bilaterality of the liver. *Arch. Surg.*, 15: 589-612.
- Miller, M. E., G. C. Christensen and H. E. Evans 1964 Anatomy of the Dog. W. B. Saunders Company, Philadelphia and London.
- Seregé, H. 1902 Sur la teneur en urée de chaque lobe du foie en rapport avec les phases de la digestion. *Compt. rend. Soc. Biol.*, 54: 200-202.
- Sisson, S., and J. D. Grossman 1953 Anatomy of the Domestic Animals. W. B. Saunders Company, Philadelphia and London.
- Wright, J. G., and L. W. Hall 1961 Veterinary Anaesthesia and Analgesia. Ballière, Tindall and Cox, London.

ramus also contained a significantly higher concentration of radioactivity ($P = 10^{-2}$) than the blood in the dorsal and intermediate rami of the left branch.

Comparisons were also made between the marginal and central areas of each lobe. In the jugular and right ruminal series, the marginal areas of both right ($P < 5.10^{-3}$, 10^{-2} respectively) and left lobes ($P < 10^{-4}$, 10^{-3} respectively) contained significantly higher levels of radioactivity than the respective central areas. In the right ruminal series, the blood in the marginal areas of both right ($P < 5.10^{-3}$) and left lobes ($P < 2.10^{-3}$) also contained significantly higher concentrations of radioactivity than the central areas.

DISCUSSION

In the sheep liver, the line of division between the dorsal and ventral lobes (Sisson and Grossman, '53) does not correspond to the line of separation between the areas supplied with blood by the right and left branches of the portal vein. It has been known for many years that a similar condition exists in the liver of man and the dog (Bartlett, Corper and Long, '14; McIndoe and Counseller, '27; Hjortsjö, '51), and in 1953 Garner and Singleton suggested that this may apply in the sheep liver, but provided no clear evidence to support their suggestion. Garner and Singleton considered that the right branch is the direct continuation of the portal vein of the sheep as it is in man (Bartlett, Corper and Long, '14; Elias, '63), and that the left branch diverges at about a right angle. In the sheep examined in this study, both right and left branches diverged from the line of the portal vein, and the total angle of divergence was less than a right angle (fig. 3). It is not likely, however, that the angle of divergence of the portal branches will affect the distribution within the liver of blood derived from the different portal tributaries (c.f. Barnett and Cochrane, '56).

The results obtained by Barnett and Cochrane ('56) in an *in vitro* system indicate that the disposition of the portal tributaries themselves is likely to affect the intrahepatic distribution of blood derived from the different tributaries. In ruminant animals, the exact arrangement of the por-

tal tributaries may vary depending on the degree of distension of the rumen. Although some variations in ruminal distension may occur under normal conditions, major variations may occur during anaesthesia (Wright and Hall, '61). This may explain the variability in the results of Garner and Singleton ('53) who injected colloidal chromic phosphate into the spleen of anaesthetised sheep and goats and studied the distribution of radioactivity within the liver.

The exact arrangement of the tributaries of the portal vein does vary considerably between different species of animals. In the human, dog and goat, the gastrosplenic vein conveys blood into the portal vein in a generally cranial direction (Bartlett, Corper and Long, '14; Müller, Christensen and Evans, '64; Horowitz and Venzke, '66), but in the sheep it extends caudally and to the right at its termination (figs. 2, 3). In the sheep, the gastrosplenic vein is the largest tributary of the portal vein, but in the dog it is only about one-half to two-thirds as large as the vein that drains the intestines (Miller, Christensen and Evans, '64).

The intrahepatic distribution of blood from the different portal tributaries in sheep varies from that described in other animals. When ^{125}I -albumin entered the portal stream in the gastrosplenic vein of standing, conscious sheep, there were no significant differences between the levels of radioactivity in the areas supplied by the right and left branches of the portal vein. However, when these results were corrected for variations in the total amount of blood represented in each gram of dried liver, it was found that the blood from the gastrosplenic vein had flowed preferentially into the left branch of the portal vein. The difference between the amount flowing to the left and right branches was much less than that found by Hahn, Donald and Grier ('45) in the anaesthetised dog. When these authors injected labelled phosphoric acid into the splenic vein, they found that the left margin of the liver contained up to 4.5 times more radioactivity per gram than the right margin. When the injection was made into a branch of the mesenteric vein, the level of radioactivity in the right section of

The Primary Human Oocyte: Some observations on the fine structure of Balbiani's vitelline body and the origin of the annulate lamellae ^{1,2}

ARTHUR T. HERTIG

Department of Pathology, Harvard Medical School, Boston, Massachusetts

ABSTRACT The ultrastructural details of human oocytes from four primordial follicles and one early primary follicle are presented. A fifth primordial follicle is represented by a paraffin section stained by hematoxylin and eosin. The paranuclear Balbiani vitelline body, consisting of a centrosome surrounded by endoplasmic reticulum, Golgi complexes, compound aggregates, annulate lamellae, and mitochondria is described. The annulate lamellae arise as an evagination from the outer leaflet of the nuclear envelope and interdigitate with folds of the endoplasmic reticulum which also is continuous with the outer leaflet of the nuclear envelope. Structural aspects of annulate lamellae are discussed in relationship to current ideas of nuclear membrane ultrastructure and to their possible role in nucleo-cytoplasmic transfer. A biographical note on the life of Edouard Gérard Balbiani is presented.

The conspicuous paranuclear mitochondrial mass surrounding the centrosome of vertebrate and invertebrate oocytes has been studied by light microscopists for many years. According to Henneguy (1887) it was described in the spider oocyte by von Wittich in 1845 and was named the "Dotterkern" by Carus in 1848. Balbiani described it in detail in oocytes of spiders and myriapods (1864a, b). He summarized his extensive observations in 1893. This structure was designated by Henneguy — Balbiani's student — as "Balbiani's vesicle" in 1887 and as the "yolk body of Balbiani" in 1893. Van der Stricht in his classic monograph of 1923 on the developmental stages of oocytes in mammals distinguishes clearly between the central vitelline or Balbiani body and the surrounding vitellogenic or mitochondrial bed. Aykroyd ('38), following the example of Brambell, whose 1925 paper she quotes, designated these areas as the "pallial layer" and "couche vitellogène" respectively. These authors believed that in the past Balbiani's name has been applied indiscriminately to either or both the components of this paranuclear complex. Beams and Sheehan ('41) designate it as the "yolk nucleus complex" whereas Raven ('61) believes that it should be called Balbiani's vitelline body. We agree with this latter designation and apply that term to

the entire paranuclear complex of apparently interrelated organelles in human oocytes within primordial and early transitional primary follicles. Four of the oocytes from primordial follicles illustrated here were included in a larger group previously reported in detail (Hertig and Adams, 67). One previously unpublished primordial oocyte is illustrated and, in addition, one oocyte from an early transitional primary follicle (H35-2) will be described (table 1).

During the preparation of this paper and the address based upon it, the author became interested in the life and works of Edouard Gérard Balbiani, the cytologist, comparative embryologist and supplier of medical eponyms. A biographical summary of this remarkable man is included here.

Edouard Gérard Balbiani (fig. 17) came from an Italian family of ancient lineage. During the reign of Francis the First his ancestors left Italy to reside in various European countries. Edouard descended from the German branch; his banker father having emigrated to Haiti. Balbiani was born, apparently in Port-au-Prince, about 1823. His classical schooling

¹ The present communication forms the historical and scientific basis of the address given by the author after the banquet of the American Association of Anatomists in Kansas City, Mo., April 6, 1967 entitled: "Human Oocytes, Past Present and Future; a Resurrection of Balbiani's Body."

² This work was supported in large part by U.S.P.H.S. grant HD-00137.

Balbani described at magnifications of 100-150, the irregularly convoluted or folded cord of 15 μ in diameter with its dark cross striations and discoid pale expansions. The relationship of the "cordon" to the nucleoli is seen in all three of his drawings (fig. 19). The cross striations were stained by methyl green although the intervening areas and rings were unstained. Carmine and hematoxylin, however, left the bands only slightly stained but stained the rings and the nucleoli intensely. It is ironic that Balbani refused to speculate (1881b) on the function of the "cordon" and never returned to it in any of his subsequent publications. Nevertheless, he was the first to describe the morphologic counterpart of the gene concept as formulated by the geneticists.

It is of interest that both Mendel's and Balbani's observations lay unnoticed for many years. By 1915 the location of 50 genes for the four single chromosomes of *Drosophila* had been mapped (Morgan et al., '15, as cited by Hughes, '59). It was not until 1933, however, that Heitz and Bauer realized that the giant chromosomes of dipterous larvae, described by Balbani in 1881 under the light microscope, were equivalent to the interphase chromosomes of ordinary cells. This led Painter and others to compare the band patterns of giant chromosomes to established genetic maps in larval *Drosophila*. There also emerged the chemical nature of Balbani's rings or puffs (Beermann, '52; Beermann and Bahr, '54; Clever and Karlson, '60).

The bands contain DNA whereas the puffs or rings contain RNA (Beermann and Clever, '64).

Henneguy ('00) summarized Balbani's failure to understand the significance of his classic observations in these words, "... if he did not fully profit in terms of scientific renown from his discoveries it is because he made them too soon."

MATERIALS AND METHODS

The ovarian material was obtained at elective operation from four fertile women whose essential clinical data are shown in table 1. Since this is, in essence, the summary of a speech, the interested reader is referred to our previous paper for the details of preparation of our material (Hertig and Adams, '67).

OBSERVATIONS

Light microscopy

If the plane of section happens to pass through the center of the nucleus and through the center of the cytocentrum, Balbani's vitelline body is clearly seen in the conventional histologic sections (fig. 2) as well as in electron micrographs (fig. 3). Stained by hematoxylin and eosin it is a pale, crescent shaped eosinophilic complex applied closely to the nuclear membrane as shown in figure 2. The cytocentrum appears as a dark sphere surrounded by a pale halo and flanked by dark granules.

With Sudan black stain, sudanophilia is present throughout Balbani's vitelline

TABLE 1
Clinical data from patients whose oocytes appear in this study

No.	Age	Para	Grav	Indication for operation	Endometrial phase	Figures	No. oocytes
H-35	28	V	VII	Carcinoma in situ of Cervix uteri	Mid-proliferative	6, 7, 8 9, 10, 11 12 and 14	2
H-43	37	VIII	XII	Caesarean section	Term (35 3/7 weeks) pregnancy	13	1
H-48	34	V	VI	Carcinoma in situ of Cervix uteri	19-20th day	2, 3, 4	2
H-57	34	I	III	Pelvic pain, menorrhagia, 2 ectopic pregnancies	25th day	15	1

took place in Frankfurt-am-Main and in Paris. There he went on to study law, natural science and medicine; obtaining his M.D. in 1854 (Henneguy, '00; Boyer, '48; Bibliographie Anatomique, 1899; Nature, 1899).

Balbani immediately embarked upon a scientific career. He was a patient, skillful dissector and manipulator of living cells and unicellular organisms which he observed for hours; recording the effect upon them of various reagents. He developed techniques of microdissection and coined the term "merotomy." During his first study of the ciliated infusoria he observed their fission and conjugation. Believing that such animals were complete and that the macronucleus was an ovary and the micronucleus a "testicle," he totally misunderstood the process of mitosis. According to Hughes, (plate X, fig. G., '59) the original plates of Balbani's 1861 paper, however, show several phases of mitotic division; the spindle fibers and chromosomes unfortunately being interpreted as a bundle of spermatozoa. Thus, although Balbani was the first to observe and record the vital process of mitosis, it remained for Bütschli in 1876 to interpret correctly the role of the micronucleus in the sexual reproduction of ciliates. Balbani's skills brought him to the attention of Claude Bernard who appointed him in 1867 as Director of Histological Studies of the Laboratory of Physiology at the Museum of Natural Sciences. He held this post until 1873 when he succeeded Coste in the Professorship of Comparative Embryology at the Collège de France.

The complex, subsequently to be called the "yolk body of Balbani" by Henneguy in 1893, was first studied by Balbani in spiders and myriapods (1864a, b). His interpretation of these structures was obscured by his belief in the hermaphroditism which he thought he had established for the ciliates. In applying such concepts to the germ cells of metazoa he attributed a role in the formation of the "germ" to the yolk nucleus. Later (1893) he was to regard the "yolk nucleus" (Dotterkern) as homologous to the Nebenkern (centrosome of Plater) of germinal cells and of the centrosome of somatic cells. He believed that the yolk nucleus originated from the

nucleus of the immature oocyte and that during its formation, a more or less thick layer of yolk condensed around it. (It is now clear that what he was observing was the centrosome with its surrounding mass of organelles, undoubtedly Golgi bodies and mitochondria. Please refer to figure 1, an intact oocyte from the myriapod, *Geophilus longicornis* drawn by Balbani himself and figure 18, the microscope with which he presumably studied such oocytes.)

As an applied scientist he identified the causative sporozoan of the silk-worm disease, *pebrine*, whose cure added to Pasteur's growing fame. Balbani also worked out the life cycle of the root louse, *Phylloxera vastatrix*, with its parthenogenetic generations, which was infesting the French vineyards (Henneguy, '00; Boyer, '48). Although Balbani recommended decortication ("décortilage des cepes") of the vine stocks, and application of insecticides to the roots to control the overwintering louse eggs, the more practical solution to this pressing problem lay elsewhere. Resistant root stocks of *Vitis rupestris* were imported from American vineyards and upon these were grafted the native French *Vitis vinifera* (Amerine, '66).

Perhaps Balbani's greatest cytological achievement lay in his discovery and description of the giant chromosome with its surrounding puffs or rings in the larval salivary glands of the midge, *Chironomus plumosus* (fig. 19). He named this structure a "cordon" (Balbani, 1881a, b) and it is later referred to as a "filament nucléaire" (Bibliographie Anatomique, 1899). It is not clear whether it was accepted as a chromosome or not, even though Balbani himself (1876) explicitly identified it as being homologous with the filaments which he had earlier observed in the nuclei of dividing cells in the ovary of the grasshopper, *Stenobothrus pratensis*. He also related the "cordon" to the nuclear filaments of cells in karyokinesis as described in the salamander by Pfützner (1881). [The term "mitosis" was introduced in 1882 by Flemming and the term "chromosome" by Waldeyer in 1888. It was of historic interest that at this time Miescher (1871) and Altmann (1889) were doing their pioneer work on the nucleic acids.]

ous or granular material (figs. 4, 8). The vacuoles contain a homogeneous material. These compound aggregates vary in size and appearance (fig. 4): some are membrane-bound while others are not; some are ballooned and appear to have imbibed a clear fluid in which the elements of the aggregates are dispersed. Similar structures are frequently seen in the peripheral cytoplasm of the oocyte and in the cytoplasm of the follicular (figs. 3, 11) and cortical cells of the surrounding ovarian tissue. Evidence for the possible transport, either from oocyte to follicle or vice versa, of the material in the compound aggregates has been presented previously (Hertig and Adams, '67).

Annulate lamellae may be attached or immediately adjacent to the nucleus (figs. 12-16) or be free within Balbiani's vitelline body. In the latter situation it may be adjacent to the cytocentrum (figs. 7, 8) or be within the surrounding mass of mitochondria (fig. 4). These structures may be stacked (figs. 12, 14, 16) or concentric (figs. 13, 15). They consist of smooth surfaced paired membranes which at their periphery are connected to the more granular endoplasmic reticulum, the latter in turn closely associated with mitochondria. These paired membranes mimic or duplicate the two leaflets of the nuclear membrane. The pores of the latter are often in register with some of those of the attached lamellae although the lamellae have more pores per unit of membrane than does the nuclear envelope. Within the pores of the nuclear envelope and connected lamellae are cores of moderately dense material, presumably the extended or expanded material of the "pore-complex" (Watson, '59). Close inspection of some of the annuli seen in a fortunate plane of section suggests that this material within the pore is a hollow cylinder rather than a solid band or rod (figs. 14, 15). Moreover, its external diameter seems to be somewhat larger than that of the pore and its internal diameter slightly less than that of the pore. The appearance of such annulate lamellae, whether attached, detached, stacked or concentric is one of a multilaminated structure duplicating the nuclear envelope and apparently precisely aligned so that the pores are in register. That the

"pore complex" of these annulate lamellae duplicates that of the nuclear membrane is shown by their similarity when they are sectioned in a tangential plane (figs. 4, 8).

When annulate lamellae are in the coiled form and are immediately adjacent to the nuclei, the cytoplasm within the coil will occasionally (twice in our experience) show multiple collections of moderately fine, dense, almost amorphous material surrounded by finer, more widely dispersed, halos (fig. 15). These appear to be morphologically similar, and maybe analogous to the material within the pore complex of the nuclear membrane and annulate lamellae. In another oocyte from a primordial follicle similar deposits were found within the cytoplasmic center of comparable concentric annulate lamellae. These were illustrated in a previous paper (fig. 32 in Hertig and Adams, '67) although another section through this same structure, illustrated here in figure 13, does not contain them.

By a fortunate plane of section through one primordial oocyte the continuity of the annulate lamellae with the outer leaflet of the nuclear envelope could be clearly demonstrated (figs. 12, 14, 16). The outer leaflet evaginates into an expanded perinuclear space forming a series of folds which are at first single and then double. The latter feature owes its origin to the invagination of the primary fold by secondary folds derived from the endoplasmic reticulum. The latter also arises from the external nuclear leaflet. Thus there is formed a very striking replication of the external nuclear leaflet which, in its early stage is connected to both the nucleus and the endoplasmic reticulum. A simplified diagrammatic reconstruction of annulate lamellae, in the act of formation, is to be seen in figure 16.

The granulosa cells of the primordial follicle are of variable thickness and density. A crescent-shaped cap of thicker cells appears at one side (fig. 3). The early or transitional primary follicle, however, has cuboidal epithelium (figs. 5-7). Neither of these closely related stages shows evidence of mitotic activity in the follicular epithelium. The latter contains dense vesicular compound aggregates (fig.

body. This apparently represents the phospholipid of the complex, since there was no detectable difference between Sudan black preparations of frozen and of paraffin sections. The PAS stain reveals a pale center and a darker periphery, possibly associated with compound aggregates.

Electron microscopy

These oocytes have a spherical nucleus of 22 to 24 μ in diameter with a typical envelope whose double leaflet is interrupted by pores containing electron dense material (figs. 4, 8, 9, 12, 13, 14, 15, 16).

Closely packed, parallel spiral fibrillae are occasionally seen attached to but apparently not arising from, the outer leaflet of the nuclear membrane (fig. 8). There is a suggestive evidence that the nuclear pores may be more closely spaced in conjunction with these fibrils than elsewhere. These clusters of closely packed fibrillae are also seen occasionally in the cytoplasm. Arising from the outer nuclear leaflet are profiles of endoplasmic reticulum (figs. 9, 12, 14, 16) and stacks of annulate lamellae (figs. 12, 13, 14, 16). These will be described more in detail later.

The cytocentrum (centrosome) at the center of Balbiani's body (figs. 3, 4, 7, 8) is conspicuous as a cluster of organelles with a spherical dense center and lighter periphery. Mitochondria are conspicuous by their absence in the center and scarcity at the periphery. The prominent center, measuring up to 4.5 μ in diameter (probably the counterpart of the dense structure seen by H and E stain in fig. 2) is composed of electron opaque deposits embedded within a matrix of fine fibrils. These dense granules may become periodically aligned to form radiating fibrils which apparently merge with peripheral coarse fibers measuring up to 0.13 μ in diameter. Their maximum length is not possible to estimate. In oocytes of primordial follicles, (fig. 4) the peripheral coarse fibers appear in favorable serial sections to be straight and to be interwoven as a basket-like network about the periphery of the cytocentrum. In the early primary follicle (fig. 8) they appear more curved so that they conform to the contour of the cytocentrum. Vesicles either in discrete aggregates or dispersed among the amor-

phous deposits are also characteristic of the cytocentrum (fig. 4). At the periphery of the cytocentrum there is a network of vesicular or tubular endoplasmic reticulum which becomes continuous with that in the more peripheral areas of Balbiani's body (figs. 4, 8). No centrioles were seen within the cytocentrum in spite of careful search. Microtubules can be found throughout Balbiani's vitelline body and also less frequently in the peripheral cytoplasm.

Surrounding the cytocentrum are multiple Golgi complexes, prominent compound aggregates, a mass of mitochondria and a single stack or coil of annulate lamellae. Endoplasmic reticulum that is sparsely granular is found throughout this area. The ovoid or spherical mitochondria measure 0.5 to 1.8 μ and contain prominent arched cristae. They are frequently clustered in rosette fashion, about a dense somewhat reticulated mass (Hertig and Adams, '67). In some oocytes in primordial follicles, the mitochondria appear to be entirely localized within Balbiani's vitelline body (fig. 3) whereas in other oocytes a variable number together with Golgi complexes and elements of endoplasmic reticulum are sparsely distributed around the entire circumference of the nucleus (Hertig and Adams, '67).

In oocytes of both primordial and early transitional primary follicles the endoplasmic reticulum is intimately associated with the mitochondria in Balbiani's vitelline body (figs. 4, 8). In the stage of early transitional primary follicle illustrated, the endoplasmic reticulum is also prominent as a basket-like shell at the periphery of Balbiani's body (figs. 7, 8). The membranes of this shell appear to be formed by multiple evaginations from the outer leaflet of the nuclear membrane (fig. 9). In this primary stage, the concentration of Golgi complexes appears to have shifted from the periphery of the cytocentrum (fig. 4) to the periphery of Balbiani's body where their membranes are in continuity with those of the endoplasmic reticulum (figs. 8, 10).

The large, electron-opaque compound aggregates at the periphery of the cytocentrum or within the mitochondrial mass are composed of vacuoles surrounded by finely divided, electron-opaque membran-

gested the need for further study of some cyclical hormonal effect upon the oocyte nucleus and its adjacent organelles.

Wilson's ('66) radioautographic studies on the localization of estradiol-17B-1,2-H³ on the lampbrush chromosomes of the ova from the newt *Triturus viridescens* seem germane in this regard. She showed that "radioactivity is concentrated in the areas of the loops which have been demonstrated to correspond to the areas of RNA transcription in these cells." She concluded that this result (and others) "are compatible with the concept that these steroid hormones may be bound selectively to the sites of gene transcription in the nuclei of target tissues."

Ancla and DeBrux ('65) in reporting the ultrastructure of the endometrium from a series of 40 patients, most of them infertility problems, said, "annulate lamellae may appear before ovulation but are more frequently seen during the secretory phase if there is hyperestrogenism." This observation suggests some relationship of annulate lamellae to the endocrine events in the human menstrual cycle.

It is not surprising that the oocytes in primordial human follicles and in one early primary follicle, (Adams and Hertig, '65), should have annulate lamellae since later stages of human oocyte development contain annulate lamellae (Wartenberg and Stegner, '60) and the early pronucleus stage of the human fertilized ovum contains such structures both in the cytoplasm and pronuclei (Zamboni et al., '66).

The interested reader is referred to the original articles of the various authors who have made significant observations on the origin, form and possible function of this amazing structure which simulates the nuclear membrane so precisely. Swift ('56) originally named these structures annulate lamellae but pointed out that others had seen them before. According to Swift they were probably first seen by McCulloch in 1952 in *Arbacia*. Afzelius ('55) considered them fragments of nuclear membrane of the sea urchin oocyte. Palade ('52) observed them in the rat spermatid; Dalton and Felix ('54) in the mouse epididymis; and Gay ('55) in *Drosophila*. It was Swift ('56) who pointed out their basophilia and presumed high RNA con-

tent. He observed and described annulate lamellae in the oocytes of the surf clam, *Spisula solidissima*; the pulmonate helixid snail, *Otala lactea*; the spermatocytes of the Sprague-Dawley rat of four months; and the larval pancreas of *Amblystoma*. His succinct summary is worth recording here. "These structures are alike in possessing numerous rings or annuli; resembling those in the nuclear membrane. Thus the name 'annulate lamellae' has been proposed for them. It is suggested that they may function in the transfer of specificities from nucleus to cytoplasm."

Rebhun ('56a, b, '61) and Ruthman ('58) have stressed the basophilia of these structures. Ruthman has studied them cytochemically in the spermatocyte of the crayfish. Although annulate lamellae are strongly basophilic, they are relatively free of ribosome-like particles. Ruthman observed that annulate lamellae connect with endoplasmic reticulum. This is in agreement with our findings in human oocytes and suggests a potential mechanism for the transfer of material from nuclear-derived membranes to the cytoplasm via the endoplasmic reticulum.

The favorable chance finding of masses within the cytoplasm surrounded by a coil of annulate lamellae (fig. 15) further suggests that this structure, replicating nuclear membrane, is transporting or elaborating material that simulates that found within the pore complex of the nuclear membrane.

Annulate lamellae have been described in oocytes of the sea urchin *Psammechinus miliaris* by Afzelius ('55); of the sand dollar *Dendraster excentricus* by Merriam ('59); of the surf clam *Spisula solidissima* and the pulmonate snail *Otala lactea* by Rebhun ('56a, b, '61); of the newt *Triturus viridescens* by Wischnitzer ('58) and of the tunicate *Ciona intestinalis* by Mancusco ('64).

The latter author cites literature which shows that annulate lamellae also occur in germ cells of other forms as well as in other types of cells but are to be seen in cells having the "common characteristic of a particularly active metabolism."

Kessel, in a classic series of papers, has reported his investigations on the origin of annulate lamellae in oocytes of such di-

11) which are indistinguishable from those seen within Balbiani's vitelline body (figs. 3, 4, 7, 8, 10). Such deposits or structures are also to be seen in cortical and even serosal cells of the ovary. The granulosa cells are characterized by villous projections which only slightly indent the ooplasm of the enclosed oocyte (fig. 11). Such microvilli are most prominent between adjacent granulosa cells at the granulosa-oocyte junction.

DISCUSSION

Balbani's vitelline body has been observed for well over a hundred years and extensively studied by light microscopists in both invertebrate and vertebrate oocytes. Raven ('61) summarizing the voluminous comparative observations on oocytes has this to say about primordial stage, "the earliest oocyte often contains a distinct cytocentrum, situated on one side against the nuclear membrane, sometimes in an indentation of the latter. It consists of one or two small granules, the centrioles, surrounded by a sphere of dense cytoplasm, the *archoplasm* or *idiosome*. Sometimes there is an indication of astral radiations in the latter. The *archoplasm* is often encircled by a ring of Golgi bodies, which in turn is surrounded by a dense cloud of mitochondria. The whole structure thus outlined is known as Balbiani's vitelline body, often wrongly called yolk nucleus."

Rebhun ('65a), in reporting on the ultrastructure and basophilia of the periodic lamellae and nuclear envelope, cites literature from 1919 to 1949 and says, "The mitochondria and Golgi apparatus in the early germ cell are located in a perinuclear ring or crescent so closely applied to the nuclear membrane as to appear attached to it." He emphasizes that as the oocyte increases in size these structures migrate throughout the ooplasm. This dispersal of organelles has also been noted by Akyroyd ('38) and Beams and Sheehan ('41).

As a pathologist, examining routine hematoxylin and eosin sections of ovaries, the author has seen an occasional Balbiani vitelline body in an ovo-testes of an 8-months stillborn; in newborns and in a child of 18 months. Judging from such routine observations over the years, oocytes at this stage of human development are

apparently undergoing atresia or "degeneration" (pathologist's terminology) in great numbers. That this actually is so is shown by Baker's ('63) precise quantitative and cytological studies of germ cells in human ovaries from the early fetal stage through seven years of age. The difficulty of finding a Balbiani vitelline body in routine sections of any ovary prepared in a pathology laboratory is compounded of many factors; the generally poor fixation of the large watery oocyte, the random plane of section and the question: do oocytes in primordial follicles of the adult continue to undergo atresia?

By electron microscopy the paranuclear complex of organelles forming Balbiani's vitelline body is particularly striking in the oocytes of adult human primordial follicles. Comparable though less striking paranuclear aggregates are also found in other mammalian species. They are regarded as large Golgi complexes in the rat (Sotelo, '59); guinea pig (Anderson and Beams, '60; Adams and Hertig, '64); the rabbit (Blanchette, '61; Zamboni and Mastrolanni, '66); the hamster (Odor, '65; Weakley, '66). Fetal human ovaries containing oocytes in early meiotic prophase show a paranuclear concentration of mitochondria and Golgi complexes (Lanzavecchia and Mangioni, '64; Stegner and Wartenberg, '63).

All of the oocytes in primordial follicles studied by Hertig and Adams ('67) contained similar arrangements of the organelles within Balbiani's vitelline body. In some oocytes, however, the annulate lamellae were attached to the nuclear membrane and in others they were free in the cytoplasm. It was noted that those oocytes with annulate lamellae attached to the nuclear membrane also had some mitochondria, Golgi complexes and elements of the endoplasmic reticulum dispersed around the entire circumference of the nuclear membrane, whereas in those with detached annulate lamellae these organelles appeared to be more concentrated in or near Balbiani's vitelline body. Furthermore the prevalence of attached annulate lamellae together with the dispersal of some organelles around the nucleus in ovaries removed during the estrogen dominant or follicular phase of the menstrual cycle sug-

gested the need for further study of some cyclical hormonal effect upon the oocyte nucleus and its adjacent organelles.

Wilson's ('66) radioautographic studies on the localization of estradiol-17B-1,2-H³ on the lampbrush chromosomes of the ova from the newt *Triturus viridescens* seem germane in this regard. She showed that "radioactivity is concentrated in the areas of the loops which have been demonstrated to correspond to the areas of RNA transcription in these cells." She concluded that this result (and others) "are compatible with the concept that these steroid hormones may be bound selectively to the sites of gene transcription in the nuclei of target tissues."

Ancla and DeBrux ('65) in reporting the ultrastructure of the endometrium from a series of 40 patients, most of them infertility problems, said, "annulate lamellae may appear before ovulation but are more frequently seen during the secretory phase if there is hyperestrogenism." This observation suggests some relationship of annulate lamellae to the endocrine events in the human menstrual cycle.

It is not surprising that the oocytes in primordial human follicles and in one early primary follicle, (Adams and Hertig, '65), should have annulate lamellae since later stages of human oocyte development contain annulate lamellae (Wartenberg and Stegner, '60) and the early pronucleus stage of the human fertilized ovum contains such structures both in the cytoplasm and pronuclei (Zamboni et al., '66).

The interested reader is referred to the original articles of the various authors who have made significant observations on the origin, form and possible function of this amazing structure which simulates the nuclear membrane so precisely. Swift ('56) originally named these structures annulate lamellae but pointed out that others had seen them before. According to Swift they were probably first seen by McCulloch in 1952 in *Arbacia*. Afzelius ('55) considered them fragments of nuclear membrane of the sea urchin oocyte. Palade ('52) observed them in the rat spermatid; Dalton and Felix ('54) in the mouse epididymis; and Gay ('55) in *Drosophila*. It was Swift ('56) who pointed out their basophilia and presumed high RNA con-

tent. He observed and described annulate lamellae in the oocytes of the surf clam, *Spisula solidissima*; the pulmonate helioid snail, *Otala lactea*; the spermatocytes of the Sprague-Dawley rat of four months; and the larval pancreas of *Amblystoma*. His succinct summary is worth recording here. "These structures are alike in possessing numerous rings or annuli; resembling those in the nuclear membrane. Thus the name 'annulate lamellae' has been proposed for them. It is suggested that they may function in the transfer of specificities from nucleus to cytoplasm."

Rebhun ('56a, b, '61) and Ruthman ('58) have stressed the basophilia of these structures. Ruthman has studied them cytochemically in the spermatocyte of the crayfish. Although annulate lamellae are strongly basophilic, they are relatively free of ribosome-like particles. Ruthman observed that annulate lamellae connect with endoplasmic reticulum. This is in agreement with our findings in human oocytes and suggests a potential mechanism for the transfer of material from nuclear-derived membranes to the cytoplasm via the endoplasmic reticulum.

The favorable chance finding of masses within the cytoplasm surrounded by a coil of annulate lamellae (fig. 15) further suggests that this structure, replicating nuclear membrane, is transporting or elaborating material that simulates that found within the pore complex of the nuclear membrane.

Annulate lamellae have been described in oocytes of the sea urchin *Psammechinus miliaris* by Afzelius ('55); of the sand dollar *Dendraster excentricus* by Merriam ('59); of the surf clam *Spisula solidissima* and the pulmonate snail *Otala lactea* by Rebhun ('56a, b, '61); of the newt *Triturus viridescens* by Wischnitzer ('58) and of the tunicate *Ciona intestinalis* by Mancusco ('64).

The latter author cites literature which shows that annulate lamellae also occur in germ cells of other forms as well as in other types of cells but are to be seen in cells having the "common characteristic of a particularly active metabolism."

Kessel, in a classic series of papers, has reported his investigations on the origin of annulate lamellae in oocytes of such di-

verse forms as *Necturus* ('63), the echinoderm *Thyone birareus* ('64) and various tunicates ('65). He has shown that annulate lamellae probably arise by blebbing of the external lamella of the nuclear envelope; the blebs subsequently aligning themselves to simulate a segment of nuclear membrane. Such contiguous flattened vesicles then arrange themselves parallel to their fellows, thus forming stacks of annulate lamellae; the annulae of which are in register. Kessel ('65) indicates there is some morphologic evidence that the annuli are patent. The outer nuclear leaflet of the tunicate oocyte also contributes to the formation of the vesicular and granular endoplasmic reticulum.

Annulate lamellae have also been seen in a variety of somatic cells. For a recent review see the report by Frasca et al. ('67) who found these structures in normal bronchial cells from 17 of 90 human males.

The mechanism of origin of annulate lamellae of oocytes in various specimens is to be sure somewhat different but the morphologic, and presumably functional features are comparable; the replication of nuclear envelope material which ultimately lies within the cytoplasm. Whether, as Swift suggested in 1956, annulate lamellae are involved in nucleocytoplasmic transfer is still unknown (Gall, '64). Nevertheless there is no doubt that in the human primordial oocyte the annulate lamellae are continuous with and appear to arise from the nuclear envelope, interdigitate with the endoplasmic reticulum (fig. 16) and appear to be cast off periodically into the ooplasm. It would seem that this transfer to the cytoplasm of enormous amounts of stacked replicated nuclear membrane with its pore complexes or annulae in perfect register might be an ideal mechanism for transfer of genetic information by some form of RNA.

The transfer of material from nucleus to cytoplasm and vice versa has been investigated by many techniques. For a recent complete symposium on the nucleus, the reader is referred to the collection of articles collectively entitled "The Nuclear Membrane and Nucleoplasmic Interchange" by Feldherr and Harding, Gall, Goldstein, Loewenstein and Mirsky ('64)

respectively. In discussing the fine structure of the nuclear envelope, Gall concludes that "there is both circumstantial and direct evidence of an association between the nuclear envelope and membrane systems of the cytoplasm, and it is possible that transport of materials may involve the membranes."

Loewenstein ('64) summarizes his and his colleagues' elegant microelectrical measurements of nuclei from the giant salivary glands of *Drosophila* and *Chironomus* and from oocytes of amphibia (*Xenopus* and *Triturus*); the starfish (*Asterias*); the seaworm (*Nereis*); the clam (*Spisula*); and the coelenterate (*Hydractinia*). The gland cell nuclei are much less permeable than those of oocytes although the ultrastructural morphology of these nuclei give no clue as to reason for such electrophysical discrepancy. That the pores *per se* in nuclear membranes do not offer free communication between the nucleoplasm and ooplasm of gland nuclei is shown by the fact that a simple "porous" membrane would have a resistance of $10^{-3} \Omega \text{ cm}^2$, three orders of magnitude smaller than the observed membrane resistance in gland cell nuclei," (Loewenstein and Kano, '63). Nevertheless the oocyte nuclei tested by Loewenstein behave "merely like a small droplet of nucleoplasm without the additional surface resistance of a membrane."

Kessel ('66) has reported morphologic evidence of nucleocytoplasmic exchange in the oocytes of the tunicate, *Ciona intestinalis*. He demonstrates the transfer of Feulgen negative material from nucleoplasm to ooplasm directly through the nuclear pores. His superb pictures are of interest in that the material as it lies within the pores (and presumably is going through the pores) is similar in appearance to this non-granular pore material — cylinders or stacked annuli — of the human oocyte. Nevertheless the adjacent material in the nucleoplasm and in the cytoplasm (Kessel, fig. 3) is obviously coarsely granular and suggests "a subsequent transformation of this material into particulate ribosomes." Anderson and Beams ('56) first observed direct transfer of nuclear material to the cytoplasm in the nuclei of oocyte nurse cells of the true Reduviid bug *Rhodnius prolixus* (their fig. 2). The nuclear pores

are 400 Å and contain hour-glass shaped aggregates of granular material which appears identical to the Feulgen negative material of the nucleolus.

Fawcett ('66a,b) emphasizes very succinctly that the nuclear pore is a complicated structure and subject to variation in different animal forms. It is usually regarded as being round although Gall ('67) gives evidence that it may be octagonal in such diverse forms as the starfish (*Henricia*), frog (*Rana*) and newt (*Triturus*). These observations may well be related to those of Wischnitzer ('58) who demonstrated 8 "microcylinders" within the tubes or annuli associated with each nuclear pore. Callan and Tomlin ('50) first described annuli associated with nuclear pores in the newt, *Triturus cristatus*, and the toad *Xenopus laevis* using the technique of spreading the nuclear envelopes onto grids followed by shadow casting and examination under the electron microscope. Students of the nuclear pore are generally agreed that there is a cylinder or annulus associated with each pore. They are moreover in general agreement that it is amorphous, moderately electron-opaque and without discrete particles of 150 Å size consistent with RNP granules although dense bodies in the center of the pore are often noted. Such cylinders are about 1000–1500 Å in diameter but may be smaller. The pore is variable but is about 800–1000 Å in diameter and formed by the fusion of the two nuclear leaflets. The latter are about 75 Å in thickness and separated by a perinuclear cisterna or space about 150 Å in width. What these observers are not agreed upon, however, is the precise relationship of the cylinders or annuli to the pores. Gall ('64) has summarized in a diagram the conclusions of the various observers. Thus Afzelius ('55) believes that the cylinder or annulus is entirely beyond the pore; Watson ('55, '59) believes that the less dense center of the hollow cylinder coincides with the pore diameter resulting in an "intranuclear channel;" Wischnitzer ('58) believes that the cylinder is entirely within the pore, whereas Gall ('64) believes that the cylinder extends beyond the pore but its lumen is smaller than that of the pore. Watson ('59) designates the cylindrical formation

penetrating the nuclear envelope as a "pore complex."

It is of interest to us that the distribution of the pore material (equivalent to the cylinders, superimposed annuli or pore complexes) in our human oocyte nucleus appears to agree with the views of Gall ('64). The external diameter of the annulus is slightly larger than, but the internal diameter slightly smaller than, the nuclear pore. Although we have not studied the annuli, appearing as slightly electron-opaque cores or suggestive hollow cylinders in the nuclear envelope (figs. 13, 15) or in the annulate lamellae (figs. 12–15), at higher magnifications than 42,000, it would appear that this pore material extends into the nucleoplasm and out into the cytoplasm (figs. 13, 15). This is so whether the pore material is associated with a bare nuclear envelope or the registered stacks of attached or detached annulate lamellae. Such pore material appears to be equivalent to the cylinders described in oocytes of lower forms. The question is now a very simple one. Is this annulus or cylinder or pore material — Watson's "pore complex" — indeed a potential or actual mechanism for the transfer of genetic information from nucleoplasm to cytoplasm? The answer is obviously unknown but the circumstantial evidence is in favor of an affirmative answer.

That nature has many potentially if not actually different mechanisms for transference of genetic information to the cytoplasm must be obvious to all (even to the newcomer in ultrastructure as is the author). It is of more than passing interest, however, that annulate lamellae — a potential mechanism for the transfer of a genetic message — should appear in the human oocyte, be prominent in the oocytes of lower forms but seemingly absent in oocytes of all of the laboratory mammals thus far studied. The student of evolution could certainly make something of this strange and interesting phenomenon!

ACKNOWLEDGMENTS

The author is grateful to many persons for their various contributions to this after dinner speech and to its definitive published form. The after dinner speech drew upon the skills of Stuart Little, a mouse

described by E. B. White, drawn by Garth Williams and published by Harper and Row. Stuart helped the author to explore the perinuclear space and the nuclear pore-complex. Dr. A. James French made available a series of lantern slides depicting the famous Mary Toft, "The Rabbet Lady of Godalming," a hoax perpetrated during the early eighteenth century and immortalized by Hogarth in one of his prints. This material, appropriate and fun to assemble for the speech, does not, however, seem suitable for a scientific article. The preparation of the speech was fun but the preparation of this manuscript has been hard work. To Donald Duncan, medical classmate and long time friend, I am grateful for his invitation to give the banquet address.

Without the superb interpretive and technical work of Miss Eleanor C. Adams, my long time colleague and collaborator, this material would not have been available for ultrastructural study. Her technical associates, Miss Harriet Jopson and Mrs. Barbara Barton, have also contributed significantly. Our research photographer, Mrs. Audrey Hadfield, printed the micrographs as well as the other illustrations. Miss Adams' group also did much searching of the pertinent literature on Balbiani's vitelline body and also on the annulate lamellae.

Dr. Stephen M. Shea of this department diligently searched the scientific and biographic literature concerning Balbiani and his several significant contributions. The resume of Balbiani's life is a much condensed version prepared by Dr. Shea.

I am grateful to the editorial staff on the *Journal of Cell Biology* (The Rockefeller University Press) for permission to use a small portion of the material published by Hertig and Adams in the August 1967 issue of that journal (Vol. 34; pp. 647-675). None of the pictures here used is identical to any of those in our other paper. Figure 3 is a survey micrograph of a primordial oocyte, a portion of which appears as figure 10 in the JCB article. Similarly figure 12 is from the same stack of attached annulate lamellae as appears in figure 27 of the JCB article, although the cropping is somewhat different in the two illustrations. Figure 13 is from the same stack of coiled annulate lamellae as in fig-

ures 29-32 of the JCB article but is from a different serial section.

Dr. Morris J. Karnovsky has made many helpful criticisms during the interpretive and preparatory phases of this paper.

And finally my thanks are due to Mrs. Nancy Cote for her patience and typing skills during the preparation of this manuscript.

LITERATURE CITED

- Adams, E. C., and A. T. Hertig 1964 Studies of guinea pig oocytes; I. Electron microscopic observations on the development of cytoplasmic organelles in oocytes of primordial and primary follicles. *J. Cell Biol.*, 21: 397-427.
- 1965 Annulate lamellae in human oocytes in primordial and primary follicles. Abstract Fifth Annual Meeting American Society for Cell Biology III. Demonstrations, p. 119A.
- Afzelius, B. A. 1955 The ultrastructure of the nuclear membrane of the sea urchin oocyte as studied with the electron microscope. *Exp. Cell Res.*, 8: 147-158.
- Altman, R. 1889 Ueber Nucleinsäuren. *Arch. Anat. Physiol.*, pp. 524-539.
- Amerine, M. A. 1966 In search of good wine. *Science*, 154: 1621-1628.
- Ancla, M., and J. DeBrux 1965 Occurrence of intranuclear tubular structures in the human endometrium during the secretory phase, and of annulate lamellae in hyperestrogenic states. *Obst. and Gyn.*, 26: 23-33.
- Anderson, E., and H. W. Beams 1956 Evidence from electron micrographs for the passage of material through pores in the nuclear membrane. *J. of Biophys. and Biochem. Cytol.*, 2: (no. 4) Suppl., 439-444.
- 1959-1960 Cytological observations on the fine structure of the guinea pig ovary with special reference to the oögonium, primary oocyte, and associated follicle cells. *J. Ultrastruct. Res.*, 3: 432-446.
- Aykroyd, O. E. 1938 The cytoplasmic inclusions in the oögenesis of man. *Zeitschr. f. Zellforsch. u. mikr. Anat.*, 27: 691-710.
- Baker, T. G. 1963 A quantitative and cytological study of germ cells in human ovaries. *Proc. Roy. Soc. B.*, 158: 417-433.
- Balbani, E. G. 1861a,b,c,d Recherches sur les phénomènes sexuels des Infusoires. *J. de la Physiol. de Brown-Séquard.*, 4: 102-130, 194-220, 431-448, 465-520.
- 1864a Sur la constitution du germe dans l'oeuf animal avant la fécondation. *C. R. Acad. Sciences*, 58: 584-588.
- 1864b Sur la constitution du germe dans l'oeuf animal avant la fécondation. Comparaison avec l'ovule végétal. *C. R. Acad. Sciences*, 58: 621-625.
- 1876 Sur les phénomènes de la division du noyau cellulaire. *C. R. Acad. Sciences*, 83: 831-834.

- 1881a,b Sur la structure de noyau des Cellules salivaires chez les larves de *Chironomus*. *Zoolog. Anzeig.*, 4: 637-641, 662-666.
- 1893 Centrosome et "Dotterkern." *J. Anat. Physiol.*, 29: 145-180.
- Beams, H. W., and J. F. Sheehan 1941 The yolk nucleus complex of the human ovum. *Anat. Rec.*, 81: 545-554.
- Beermann, W. 1952 Chromosomenkonstanz und spezifische Modifikationen der Chromosomenstruktur in der Entwicklung und Organdifferenzierung von *Chironomus tentans*. *Chromosoma*, 5: 139-198.
- Beerman, W., and G. Bahr 1954 The submicroscopic structure of the Balbiani ring. *Exp. Cell Res.*, 6: 193-201.
- Beermann, W., and U. Clever 1964 Chromosome puffs. *Scientific American*, 210: 50-58.
- Bibliographie Anatomique, 1899 7: 151-152.
- Blanchette, E. J. 1961 A study of the fine structure of the rabbit primary oocyte. *J. Ultrastruct. Res.*, 5: 349-363.
- Boyer, J. 1948 Dictionnaire de Biographie Française. Librairie Letouzay et Ané T.4 Paris 1414-1416.
- Brambell, F. W. R. 1925 Oogenesis in the fowl. *Phil. Trans. Royal Soc. Lond.*, 113-150.
- Bütschli, O. 1876 Studien über die ersten Entwicklungsvorgänge der Eizelle, die Zellteilung und die Conjugation der Infusorien. *Abhandl. heraus. v.d. Senckenbergischen naturforsch. Gesellschaft*, 10: 213-457.
- Callan, H. G., and S. G. Tomlin 1950 Experimental studies on amphibian oocyte nuclei. I. Investigation of the structure of the nuclear membrane by means of the electron microscope. *Proc. Roy. Soc. London B.*, 137: 367-378.
- Carus, J. V. 1850 Ueber die Entwicklung des Spinnweibes. *Z. f. wiss. Zool.*, 2: 97-104.
- Clever, U., and P. Karlson 1960 Induktion von Puff-Veränderungen in den Speicheldrüsen-chromosomen von *Chironomus tentans* durch Ecdyson. *Exp. Cell Res.*, 20: 623-626.
- Dalton, A. J., and M. Felix 1954 Cytologic and cytochemical characteristics of the Golgi substance of epithelial cells of the epididymis in situ, in homogenates and after isolation. *Am. J. Anat.*, 94: 171-207.
- Fawcett, D. W. 1966a An Atlas of Fine Structure. The Cell: Its Organelles and Inclusions. W. B. Saunders Company, Philadelphia and London.
- 1966b On the occurrence of a fibrous lamina on the inner aspect of the nuclear envelope in certain cells of vertebrates. *Am. J. Anat.*, 119: 129-146.
- Feldherr, C. M., and C. V. Harding 1964 The permeability characteristics of the nuclear envelope at interphase. In: *Protoplasmatologia, Handbuch der Protoplasmaforschung, Band V, 2, The Nuclear Membrane and Nucleocytoplasmic Interchange*, Vienna, Springer-Verlag, pp. 35-50.
- Flemming, W. 1882 Zellsubstanz, Kern, und Zellteilung. Leipzig.
- Frasca, J. M., O. Auerbach, V. R. Parks and W. Stoekenius 1967 Electron microscopic observations of bronchial epithelium. I. Annulate lamellae. *Expt. Mol. Path.*, 6: 261-273.
- Gall, J. G. 1964 Electron microscopy of the nuclear envelope. In: *Protoplasmatologia, Handbuch der Protoplasmaforschung, Band V, 2, The Nuclear Membrane and Nucleocytoplasmic Interchange*, Vienna, Springer-Verlag, pp. 4-25.
- 1967 Octagonal nuclear pores. *J. Cell Biol.*, 32: 391-400.
- Gay, H. 1955 Nucleo-cytoplasmic relations in salivary gland cells of *Drosophila*. *Proc. Nat. Acad. Sc.*, 41: 370-375.
- Goldstein, L. 1964 Combined nuclear transplantation and isotope techniques for the study of nuclear activities. In: *Protoplasmatologia, Handbuch der Protoplasmaforschung, Band V, 2, The Nuclear Membrane and Nucleocytoplasmic Interchange*, Vienna, Springer-Verlag, pp. 51-71.
- Heitz, E., and H. Bauer 1933 Beweise für die Chromosomennatur der Kernschleifen in den Knäuelkernen von *Bibio hortulanus* L. *Z. Zellforsch.*, 17: 67-82.
- Hennequy, F. 1887 Note sur la vésicule de Balbiani. *C. R. Soc. Biol.*, 39: 68-69.
- 1893 Le corps vitellin de Balbiani dans l'oeuf des vertébrés. *J. Anat. Physiol.*, 29: 1-29.
- 1900 E. G. Balbiani. Notice biographique. *Arch. Anat. Microscop.*, 3: 1-36.
- Hertig, A. T., and E. C. Adams 1967 Studies on the human oocyte and its follicle: I. Ultrastructural and histochemical observations on the primordial follicle stage. *J. Cell Biol.*, 34: 647-675.
- Hughes, A. 1959 A History of Cytology. Abelard-Schuman, London and New York.
- Kessel, R. G. 1963 Electron microscope studies on the origin of annulate lamellae in oocytes of *Necturus*. *J. Cell Biol.*, 19: 391-414.
- 1964 Electron microscope studies on oocytes of an echinoderm, *Thyone briareus*, with special reference to the origin and structure of the annulate lamellae. *J. Ultrastruct. Res.*, 10: 498-514.
- 1965 Intracellular and cytoplasmic annulate lamellae in tunicate oocytes. *J. Cell Biol.*, 24: 471-487.
- 1966 An electron microscope study of nuclearcytoplasmic exchange in oocytes of *Ciona intestinalis*. *J. Ultrastruct. Res.*, 15: 181-196.
- Lanzavecchia, G., and C. Mangioni 1964 Etude de la structure et des constituants du follicule humain dans l'ovaire foetal I. Le follicule primordial. *J. de Microscopie*, 3: 447-464.
- Loewenstein, W. R. 1964 Permeability of the nuclear membrane as determined with electric methods. In: *Protoplasmatologia, Handbuch der Protoplasmaforschung, Band V, 2, The Nuclear Membrane and Nucleocytoplasmic Interchange*, Vienna, Springer-Verlag, pp. 26-34.
- Loewenstein, W. R., and Y. Kanno 1963 Some electrical properties of a nuclear membrane examined with a microelectrode. *J. Gen. Physiol.*, 46: 1123-1140.
- Mancuso, V. 1964 Ultrastructural changes in the cytoplasm of *Ciona intestinalis* oocytes.

- Acta Embryologiae et Morphologiae Experimentalis, 7: 269-295.
- McCulloch, D. 1952 Fibrous structures in the ground cytoplasm of the *Arbacia* egg. *J. Exp. Zool.*, 119: 47-64.
- Merriam, R. W. 1959 The origin and fate of annulate lamellae in maturing sand dollar eggs. *J. Biophys. and Biochem. Cytol.*, 5: 117-121.
- Miescher, F. 1871 Ueber die chemische Zusammensetzung der Eiterzellen. *Hoppe-Selyer's med. chem. Untersuch.*, 4: 441.
- Mirsky, A. E. 1964 The nuclear membrane and nucleocytoplasmic interchange. Preface, In: *Protoplasmatologia, Handbuch der Protoplasmaforschung, Band V, 2, The Nuclear Membrane and Nucleocytoplasmic Interchange*, Vienna, Springer-Verlag, pp. 1-3.
- Morgan, T. H., A. H. Sturtevant, H. J. Muller and C. B. Bridges 1915 *The Mechanism of Mendelian Heredity*. H. Holt and Co., New York.
- Nature, 1899, 60: 399.
- Odor, D. L. 1965 The ultrastructure of unlaminar follicles of the hamster ovary. *Am. J. Anat.*, 116: 493-522.
- Painter, T. S. 1933 A new method for the study of chromosome rearrangements and the plotting of chromosome maps. *Science*, 78: 585-586.
- Palade, G. E. 1955 Studies on the endoplasmic reticulum. II. Simple dispositions in cells in situ. *J. Biophys. and Biochem. Cytol.*, 1: 567-581.
- Pflüger, W. 1881 Über den feineren Bau die bei der Zelltheilung auftretenden fadenförmigen Differenzierung des Zellkerns. *Morpholog. Jahrbuch*, 7: 289-311.
- Raven, C. P. 1961 *Oogenesis. The Storage of Developmental Information*. Pergamon Press. The Macmillan Co., New York.
- Rebhun, L. I. 1956 Electron microscopy of basophilic structures of some invertebrate oocytes. I. Periodic lamellae and the nuclear envelope. *J. Biophys. and Biochem. Cytol.*, 2: 93-104.
- 1956 Electron microscopy of basophilic structures of some invertebrate oocytes. II. Fine structure of the yolk nuclei. *J. Biophys. and Biochem. Cytol.*, 2: 159-170.
- 1961 Some electron microscope observations on membranous basophilic elements of invertebrate eggs. *J. Ultrastruct. Res.*, 5: 208-225.
- Ruthman, A. 1958 Basophilic lamellar systems in the crayfish spermatocyte. *J. Biophys. Biochem. Cytol.*, 4: 267-274.
- Sotelo, J. R. 1959 An electron microscopic study on the cytoplasmic and nuclear components of rat primary oocytes. *Zeitschr. f. Zellforsch.*, 50: 749-765.
- Stegner, H. E., and H. H. Wartenberg 1963 Elektronenmikroskopische Untersuchungen an Eizellen des Menschen in verschiedenen Stadien der Oogenese. *Arch. f. Gynäk.*, 199: 151-172.
- van der Stricht, O. 1923 Etude comparée des ovules des mammifères aux différentes périodes de l'ovogenèse, d'après les travaux du laboratoire d'histologie et d'embryologie de l'université de Gand. *Arch. Biol.*, 33: 229-300.
- Swift, H. 1956 The fine structure of annulate lamellae. *J. Biophys. and Biochem. Cytol.*, 2 (no. 4): Supplement, 415-418.
- Waldeyer, W. 1888 Ueber Karyokinese und ihre Beziehungen zu den Befruchtungsvorgängen. *Arch. f. mikro. Anat.*, 32: 1-122.
- Wartenberg, H., and H. E. Stegner 1960 Über die Elektronenmikroskopische Feinstruktur des menschlichen Ovarialeles. *Zeitschr. f. Zellforsch.*, 52: 450-474.
- Watson, M. L. 1955 The nuclear envelope. Its structure and relation to cytoplasmic membranes. *J. Biophys. and Biochem. Cytol.*, 1: 257-270.
- 1959 Further observations on the nuclear envelope of the animal cell. *J. Biophys. and Biochem. Cytol.*, 6: 147-156.
- Weakley, B. S. 1966 Electronmicroscopy of the oocyte and granulosa cells in the developing ovarian follicles of the golden hamster (*Mesocricetus auratus*). *J. Anat.*, 100: 503-534.
- Wilson, J. D. 1966 The intranuclear localization of testosterone and estradiol. Second Int. Congr. on Hormone Steroids, Milan, 23-28 May. E. B. Romanoff, and L. Martini (eds.), Abstract 70, p. 45, 1966 Int. Congr. Series No. 111, Excerpta Medica Foundation.
- Wischnitzer, S. 1958 An electron microscope study of the nuclear envelope of amphibian oocytes. *J. Ultrastruct. Res.*, 1: 201-222.
- von Wittich, W. H. 1845 *Dissertatio sistens observationes quaedam de Araneorum ex ovo evolutione*. Halis, Saxonium, (Halle, Germany).
- Zamboni, L., and L. Mastrolanni, Jr. 1966 Electron microscopic studies on rabbit ova: I. The follicular oocytes. *J. Ultrastruct. Res.*, 14: 95-117.
- Zamboni, L., D. R. Mishell, J. H. Bell and M. Baca 1966 Fine structure of the human ovum in the pronuclear stage. *J. Cell Biol.*, 30: 579-600.

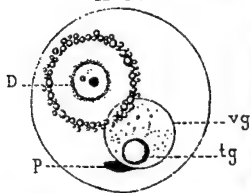
PLATE 1

EXPLANATION OF FIGURES

Figures 1-3 represent three epochs in the investigation of Balbiani's vitelline body.

- 1 A drawing made by Balbiani himself of the oocyte of the miriapod, *Geophilus longicornis*. His original legend says, "Figure 18. Ovule de *G. longicornis*, observé en mars. Outre la vésicule germinative *vg*, il renferme un volumineux noyau vitellin *D*, composé d'un corps central sphérique, entouré d'une épaisse couche de protoplasma vitellin homogène (*archoplasma*); *tg*, tache germinative; *p*, prolongement stoloniforme de la vésicule germinative qui a donné naissance au noyau vitellin (voir mon Memoire in *Zool. Anz.*, 1883, nos. 155 et 156)." Translated it becomes "Oocyte of *G. longicornis*, observed in the month of March. Besides the germinal vesicle *vg*, it contains a voluminous yolk nucleus *D*, composed of a central spherical body, surrounded by a thick layer of homogeneous vitelline protoplasm (*archoplasm*); *tg* germinal spot; *p* beak-like prolongation of the germinal vesicle which has given birth to the yolk nucleus (see my memoir in *Zool. Anzeiger*, 1883, numbers 155 and 156)." From plate III, Balbiani (1893).
- 2 A paraffin section of a primordial human oocyte from the left ovary of a patient whose endometrial histology was that of the nineteenth to twentieth day. Note the characteristic crescent-shaped paranuclear complex known as Balbiani's vitelline body, closely applied to the spherical nucleus. The cytocentrum (centrosome) is the dark spot surrounded by a halo which in turn is flanked by massed mitochondria. Case H-48, hematoxylin and eosin $\times 1200$.
- 3 Another primordial human oocyte from the right ovary (corpus luteum side) of the same patient as figure 2, oriented in much the same position to show the ultrastructural components of Balbiani's vitelline body. A higher power detail of a section, two grids beyond this one is to be seen in figure 4. The granulosa cells are of variable thickness and density. No mitoses are present. Note cytocentrum surrounded by dense fibers, the surrounding halo of endoplasmic reticulum, the dense, vacuolated, compound aggregates, the massed mitochondria and the dispersed vesicular endoplasmic reticulum. Case H-48, Oocyte no. 1 $\times 2400$.

XVIII



E.G. Balbiani del.

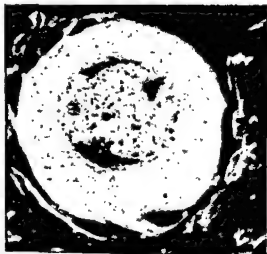


PLATE 2

EXPLANATION OF FIGURE

- 4 A nearby section (2 grids removed) to that seen in figure 3. Note nuclear envelope to right; the prominent dense, vacuolated compound aggregates with and without surrounding membranes; the cytocentrum composed of dense granules and closely packed vesicles with peripheral dense fibers; the surrounding halo of smooth endoplasmic reticulum; the scattered Golgi complexes; the annulate lamellae (upper left) cut tangentially and therefore resembling the nuclear pores and annulae; and the clusters of mitochondria intimately connected with endoplasmic reticulum. Case H-48, Oocyte no. 1 $\times 10,000$.

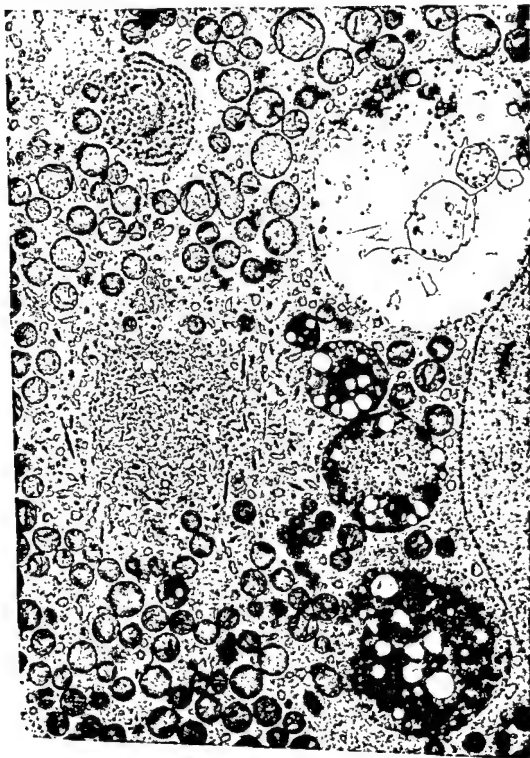


PLATE 3

EXPLANATION OF FIGURES

Figures 5-7 show the evolution of techniques used to study the organelle complex of human oocytes designated as Balbiani's vitelline body.

- 5 A primary human follicle from van der Stricht's classic monograph of 1923, figure 6, plate VII. (The definitions are translated from his description.) This represents a section of a small follicle from the ovary of an adult woman, fixed in concentrated aqueous sublimate solution and stained by iron hematoxylin. Note the several parts of the Balbiani vitelline body as seen in light microscopic preparation. (Courtesy of Archives de Biologie, Brussels, Belgium, published by Masson and Cie, Paris and Liege.)
- 6 Photograph by phase microscopy of thick epon section from a comparable human early primary follicle removed from a patient on the tenth day of her menstrual cycle. Note similarity of Balbiani's vitelline body to that drawn in figure 5. The ultrastructure of this same oocyte is to be seen in figures 7-11. Case H-35, Oocyte no. 2, phase microscopy $\times 950$.
- 7 A survey electron micrograph of the same early transitional primary oocyte seen in figure 6. Note cuboidal granulosa cells which, however, do not yet show mitotic activity. The paranuclear complex of Balbiani's vitelline body is well seen below the nucleus. Case H-35, Oocyte no. 2 $\times 2700$.

HUMAN
 OOCYTE

Planche VII. from
 O. Van der Stricht
 Arch. Biol. 33:229
 1923

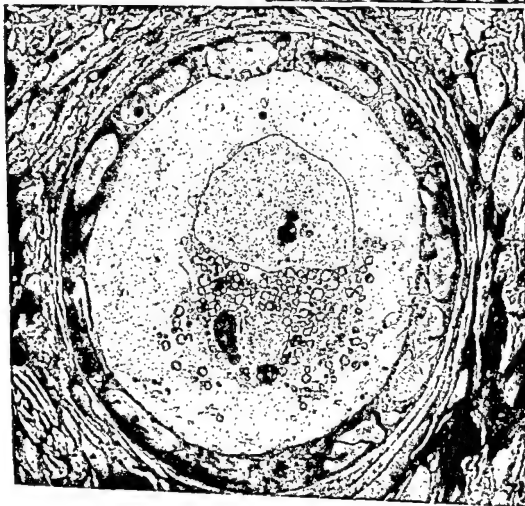
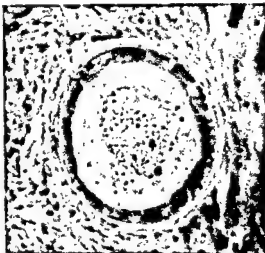
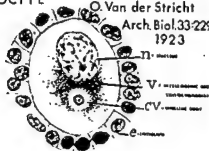


PLATE 4

EXPLANATION OF FIGURE

- 8 A more detailed micrograph of the section adjacent to that seen in figure 7. The nuclear membrane is at upper right. Note cluster of closely packed spiral fibrils attached to the nuclear envelope. The cytocentrum, at center, is composed of dense granules, some arranged periodically on fine fibers, and small vesicles, with a peripheral zone of endoplasmic reticulum and dense fibers. Surrounding the cytocentrum are massed mitochondria and compound aggregates. A stack of annulate lamellae is cut somewhat tangentially. Note the prominent endoplasmic reticulum in close association with multiple Golgi complexes at periphery of Balbiani's vitelline body. See figures 9-11 for higher powered details of this primary oocyte. Case H-35, Oocyte no. 2 \times 10,500.

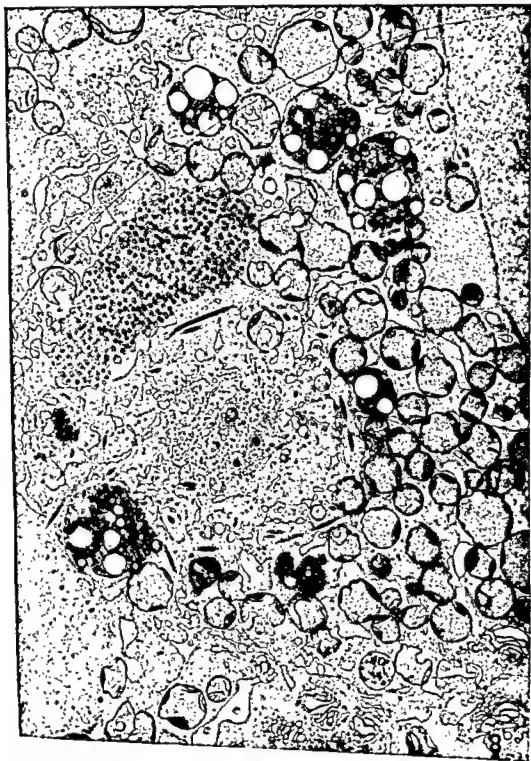


PLATE 5

EXPLANATION OF FIGURES

- 9 The edge of the paranuclear cluster of mitochondria surrounded by a network of endoplasmic reticulum continuous with the outer leaflet of the nuclear envelope. The nuclear envelope is at the right, the cytoplasm at upper part of micrograph. Note close affiliation of endoplasmic reticulum, to both margin of mitochondrial mass and to individual mitochondria. Note concentration of microtubules, cut in cross section, along the network of endoplasmic reticulum that encloses Balbiani's vitelline body at this stage of development of the oocyte. The endoplasmic reticulum has relatively few RNP particles. Case H-35, Oocyte no. 2 \times 13,500.
- 10 A detail of the meshwork of sparsely granular endoplasmic reticulum forming a meshwork surrounding Balbiani's vitelline body and in continuity with the numerous prominent Golgi complexes. Note prominent, longitudinally oriented microtubules. Note compound aggregate at top and the membrane bound mass of granules at bottom. Case H-35, Oocyte no. 2 \times 13,500.
- 11 Two granulosa cells below and oocyte above. Note dilated, sparsely granular endoplasmic reticulum of oocyte; multiple villi of granulosa cells, the pinocytic vesicle attached to oolemma at far right of micrograph; and the dark vesicular compound aggregate within the cytoplasm of the granulosa cell to the right. Case H-35, Oocyte no. 2 \times 1,500.

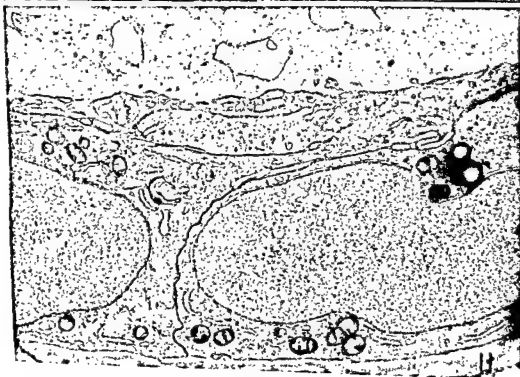
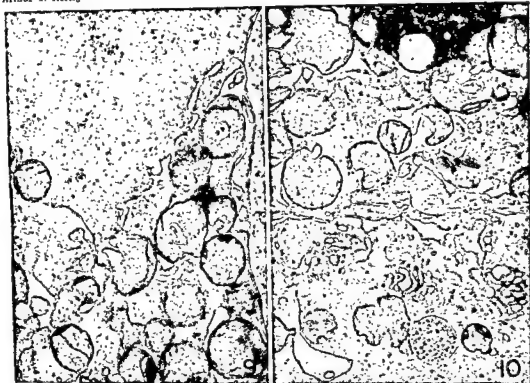


PLATE 6

EXPLANATION OF FIGURES

Figures 12-14 show details of the origin from and/or attachment of annulate lamellae to the nucleus of two primordial oocytes.

- 12 The nucleus is at the left. The external leaflet of the nuclear envelope has evaginated by multiple folds into the expanded perinuclear cisterna seen best at the lower portion of the micrograph and in somewhat more detail in figure 14. Note that the fold nearest the nucleus is single whereas the next four folds are double. The reason for this is the secondary invagination by folds of the endoplasmic reticulum, also continuous with the external leaflet of the nuclear envelope. This feature is best seen at the top of the micrograph. Note several connections of this large stack of annulate lamellae with the endoplasmic reticulum in the adjacent cytoplasm. Note that many annuli of the lamellae are in register and that occasional annuli are in continuity with those of nuclear membrane. The three-dimensional drawing of those several interrelationships is shown in figure 16. Case H-35, Oocyte no. 4 \times 22,000.
- 13 A concentric stack of annulate lamellae apparently in the process of peeling off from the nucleus seen in the upper part of the picture. Note pore material or annuli within the nuclear pores as well as within the annulate lamellae. Case H-43 Oocyte no. 1 \times 21,000.
- 4 A high power detail of the edge of a stack of annulate lamellae continuous with the external leaflet of the nuclear envelope. The entire stack is seen in figure 12. Note expanded perinuclear cisternae; one single folded lamina next to nucleus; four double folded laminae; and communication of annulate lamellae with endoplasmic reticulum. Note further that the pores and electron-opaque annuli of the annulate lamellae are in register within the stack and occasionally connect with the nuclear pores. Case H-35, Oocyte no. 4 \times 33,000.

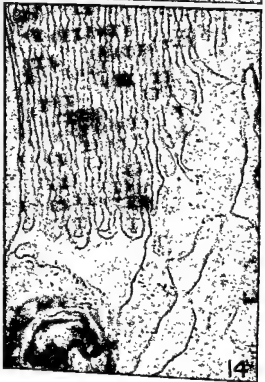
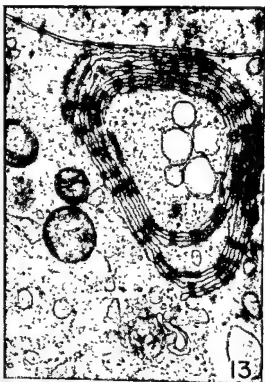
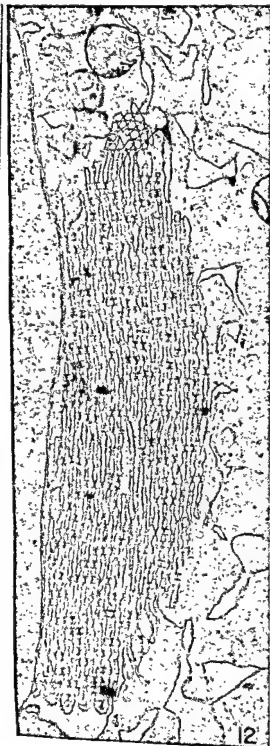


PLATE 6

EXPLANATION OF FIGURES

Figures 12-14 show details of the origin from and/or attachment of annulate lamellae to the nucleus of two primordial oocytes.

- 12 The nucleus is at the left. The external leaflet of the nuclear envelope has evaginated by multiple folds into the expanded perinuclear cisterna seen best at the lower portion of the micrograph and in somewhat more detail in figure 14. Note that the fold nearest the nucleus is single whereas the next four folds are double. The reason for this is the secondary invagination by folds of the endoplasmic reticulum, also continuous with the external leaflet of the nuclear envelope. This feature is best seen at the top of the micrograph. Note several connections of this large stack of annulate lamellae with the endoplasmic reticulum in the adjacent cytoplasm. Note that many annuli of the lamellae are in register and that occasional annuli are in continuity with those of nuclear membrane. The three-dimensional drawing of those several interrelationships is shown in figure 16. Case H-35, Oocyte no. 4 \times 22,000.
- 13 A concentric stack of annulate lamellae apparently in the process of peeling off from the nucleus seen in the upper part of the picture. Note pore material or annuli within the nuclear pores as well as within the annulate lamellae. Case H-43 Oocyte no. 1 \times 21,000.
- 14 A high power detail of the edge of a stack of annulate lamellae continuous with the external leaflet of the nuclear envelope. The entire stack is seen in figure 12. Note expanded perinuclear cisternae; one single folded lamina next to nucleus; four double folded laminae; and communication of annulate lamellae with endoplasmic reticulum. Note further that the pores and electron-opaque annuli of the annulate lamellae are in register within the stack and occasionally connect with the nuclear pores. Case H-35, Oocyte no. 4 \times 33,000.

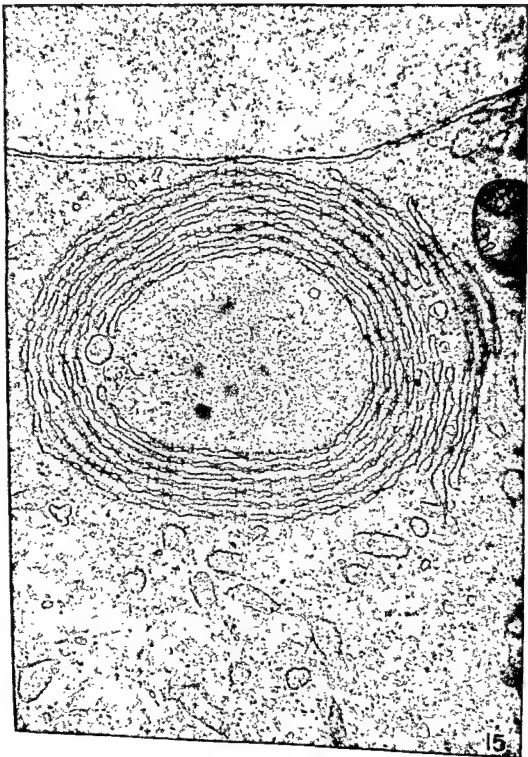


PLATE 7

EXPLANATION OF FIGURE

- 15 A coiled stack of annulate lamellae from a primordial oocyte. The nuclear membrane is at the top of the picture and the ooplasm below. Note nuclear pores, at least four of which show core material extending into both the nucleoplasm and ooplasm. Within the coiled annulate lamellae are numerous pores, often in register and containing electron-opaque material in the form of a cylinder. Note the numerous masses of amorphous material, possibly representing concentrations of core material, lying within the ooplasm enclosed by the coiled annulate lamellae. The sparsely granular endoplasmic reticulum, apparently connected with the annulate lamellae, is dispersed throughout the ooplasm. Case II-57, Oocyte no. 1, $\times 31,250$.

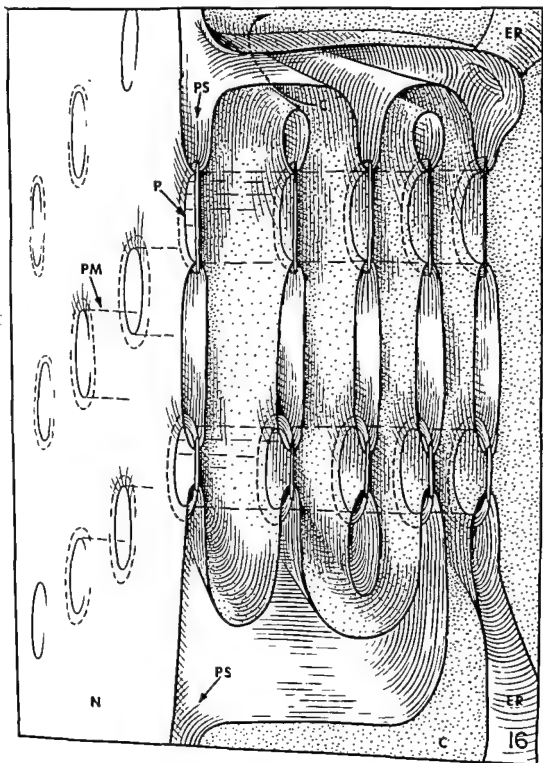
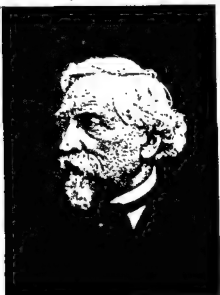


PLATE 8

EXPLANATION OF FIGURE

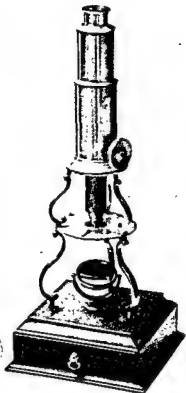
- 16 A three-dimensional drawing by Mr. Joshua Clark, made from a sketch by the author. The drawing is oriented in the same position as figures 12 and 14 from which the drawing was made. Illumination is represented as being from the left, exposing the inner surface of the nuclear envelope (N). The pore material (PM) or annulus is indicated by a dotted line. The pore (P) contains a diaphragm formed by coalescence of the two nuclear leaflets. Only two evaginated folds of outer nuclear leaflet in the expanded perinuclear cisterna or space (PS) are shown; the one nearest the nucleus is single whereas the more distal one, containing an invagination of the endoplasmic reticulum (ER) is double. The cytoplasm (C) is stippled. Note multiple connections of annulate lamellae with endoplasmic reticulum and/or the outer nuclear leaflet. Case H-35, Oocyte no. 4, magnified about 50,000 diameters.



1873-1899

Arthur T. Hertig

17



18



Fig. 2.



Fig. 3.



Fig. 4.

19



20



21

PLATE 9

EXPLANATION OF FIGURES

Figures 17-21 represent some aspects of the life and work of Professor Edouard Gérard Balbiani.

- 17 A photograph of Balbiani. (Courtesy of Mme. Matte, librarian of the College de France.)
- 18 Microscope used by Balbiani, now in the museum of The Faculty of Medicine of the University of Paris. (Courtesy of Dr. Guido Majno and photographed by Gabriel of Paris.)
- 19 Line drawings, made by Balbiani, of giant chromosomes with puffs from salivary glands of the larval midge, *Chironomus plumosus* (Balbiani, 1881).
- 20 A giant chromosome IV from the larval salivary glands of the midge *Chironomus tentans*. This structure, originally photographed in color after staining for DNA and counterstained green for protein. The bands (or genes) are positive for DNA, the puffs contain protein and RNA as seen in figure 21. (Courtesy of Dr. Ulrich Clever. From Beermann and Clever, Scientific American, 210: 50-58, '64.)
- 21 A giant larval salivary chromosome IV of the midge *Chironomus tentans*, stained for RNA by toluidine blue. The puff is positive for RNA whereas the bands contain DNA. (Courtesy of Dr. Claus Pelling. From Beermann and Clever, Scientific American, 210: 50-58, '64.)

Tissue Binding of Tritiated Norepinephrine in Pigmented Nuclei of Human Brain¹

TSUYOSHI ISHII AND REINHARD L. FRIEDE

Institute of Pathology, Western Reserve University, Cleveland, Ohio

ABSTRACT Regional binding of norepinephrine to tissue structures occurs in sections of brain tissue incubated *in vitro* with tritiated norepinephrine, followed by radioautography. The binding probably represents one of the mechanisms involved in the uptake and storage of catecholamines by nerve cells. Applying this method to a study of human brains showed excessively strong binding of norepinephrine at the surface membranes of pigmented nerve cells in the substantia nigra, nucleus coeruleus, nucleus dorsalis vagi, and others. Such excessive binding was not found in nonpigmented nuclei in the human brain nor in rat brain. The arrangement of sites of binding at the cell membranes strongly suggested synaptic endings. Melanin pigmentation of nerve cells may be related to the amount of catecholamine-containing synapses at the surface of the neurons.

Adrenergic neurons, or nerve terminals respectively, possess a mechanism for the active uptake and storage of catecholamines from the surrounding fluid. The nature of the uptake mechanism is not clearly understood. According to Giachetti and Shore ('66), two mechanisms seem to be involved in the uptake. A specific mechanism, ATP dependent and inhibited by reserpine, is located in the synaptic vesicles; it was studied extensively by v. Euler and Lishajko ('63a-d, '64) and v. Euler et al. ('63). In addition, there appears to be a nonspecific mechanism of uptake, insensitive to reserpine, and presumably located in the cell membranes. Furthermore, binding of catecholamines occurs in a specific fraction of human plasma — in a catecholamine binding protein (Mirkin et al., '66).

The uptake mechanism for catecholamines can be used experimentally to demonstrate catecholamine-storing structures in the tissue, e.g. after intraventricular injection (Aghajanian and Bloom, '66; Aghajanian et al., '66; Fuxe and Ungerstedt, '66). With fluorescent microscopy, Hamberger and Hamberger ('66) showed uptake of catecholamines by nerve fibers near brain lesions in animals in which the intrinsic catecholamines had been depleted by large doses of reserpine. Jonsson ('67) found that catecholamines and related compounds are bound to proteins — after treatment with formalin vapor; the binding was the result of the enclosure or ad-

sorption on the protein network formed by the fixation. Experiments with rat brain sections incubated *in vitro* showed by radioautography that tritiated norepinephrine is bound to tissue sections in regionally characteristic patterns; we also found that the binding mechanism survived limited cold formalin fixation (Ishii and Friede, '67).

The method used for *in vitro* binding of norepinephrine to tissue sections of rat brain was applied to human material. The findings in pigmented nuclei were especially surprising and are reported in this paper. These observations are of special significance because there are no pigmented nuclei in the brains of the readily available laboratory animals, and because material of pigmented nuclei of human brain never reaches the laboratory in a condition suitable for microchemical studies or for fluorescence microscopy.

MATERIALS AND METHODS

The tissues for this study were obtained from nine human autopsies of cases without involvement of the central nervous system, ranging in age between 29 and 93 years. The brains were obtained and studied 4 to 16 hours after death. No variations that could be attributed to the length of time between death and investigation was noted.

¹ This investigation was supported by grant NB 6239 from the National Institute of Neurological Diseases and Blindness.

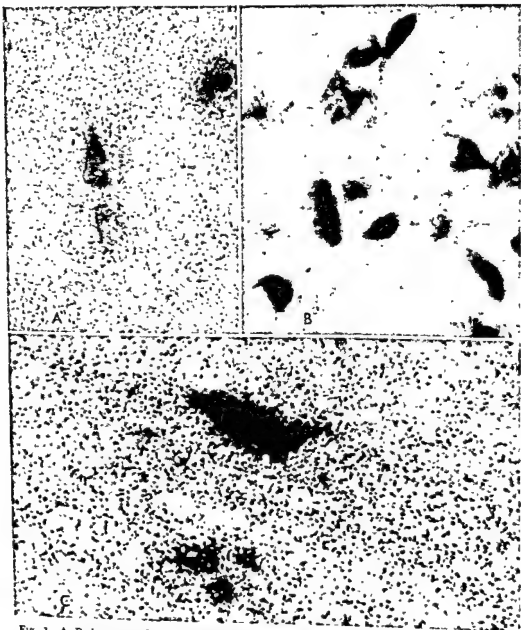


Fig. 1 A. Radioautographic demonstration of selective binding of norepinephrine at pigmented cells in the substantia nigra 145 \times . B. Negative control in a dichromated, emulsion-coated section. 145 \times . C. Enlargement shows binding at one side of pigmented nerve cell. The structures in the lower half of the picture were considered to be cross-sections of dendrites. 450 \times .

lateral to the oculomotor nucleus (Olszewski and Baxter, '59).

The intense pericellular binding of norepinephrine occurred only at nerve cells

containing the argyrophil pigment that is commonly identified as melanin. Nerve cells with deposits of lipofuscin never showed pericellular binding, regardless of

Our method for the demonstration of *in vitro* binding of tritiated catecholamines in rat brain is given in detail in a recent report (Ishii and Friede, '67), including the trials leading to the development of the procedure. The method is therefore described only briefly here.

Slices of brain of a few mm thickness were fixed in cold, neutral formalin at 4°C for 6 to 8 hours. Frozen sections were cut at 30 μ and washed thoroughly in Ringer's solution for three hours to remove all traces of formalin. The sections were incubated for one to one and one-half hours at room temperature with constant agitation in a medium containing 10 ml of Tyrode's solution, and 0.1 ml of tritiated norepinephrine solution containing 3.4 μ g/ml with a specific activity of 2.5 c/mM. The excess of unbound catecholamine was removed by washing for two minutes in chilled Ringer's solution. The length of this washing period was determined by trial and error. Loss of norepinephrine during subsequent tissue preparation was prevented by postfixation in a 10% solution of dichromate for four hours, precipitating the norepinephrine. The sections were then thoroughly washed in Ringer's solution for four hours, mounted, dried, coated with Kodak NTB-2 emulsion and exposed for four weeks.

Three sets of controls were used: emulsion-coated blank slides, untreated tissue sections coated with emulsion, and tissue sections that were not incubated but were fixed in dichromate. All controls were negative. The binding of norepinephrine was resistant to reserpine in 10^{-4} /M concentration.

The method used for our study is relatively simple and gave uniform, reproducible results. There were only two minor technical difficulties. In the large and thick sections (up to 30 \times 40 mm) used for human material, an occasional tearing and partial defoliation of the emulsion occurred in the white matter. This was thought to be related to changes in the myelin lipids produced by dichromate. The problem was remedied by incubating many sections and discarding those with artefacts. The other difficulty was the precipitation of unbound label, forming clusters at the edges of the sections or at random in the tissue.

This artefact was a problem only when either higher concentrations of norepinephrine were used in the medium or when the time for washing after incubation was too short. It was negligible or absent at the concentration and with the time for washing given in this report.

RESULTS

Pigmented nuclei

All pigmented nuclei showed very intense binding of norepinephrine, exceeding markedly the binding in any other region or nuclei of the brain; all controls were negative (fig. 1B). The binding occurred at the surface of the cells, and no binding was noted in the cytoplasm or in the melanin granules. Some of the pigmented cells were entirely encompassed by intense binding; others showed intense binding in circumscribed, sharply delineated zones at the surface of the cell (fig. 2A). The zones of intense norepinephrine binding were found mostly at the cell body, but they sometimes extended for some distance upon major dendrites. The regional distribution of zones of binding at the cell membrane suggested groups of synaptic buttons.

In the substantia nigra and the nucleus coeruleus intense binding of norepinephrine occurred at the vast majority of cells. Some pigmented cells without binding were seen, but these were thought to represent incomplete specimens extending into an adjacent tissue sections. Very little binding occurred at nonpigmented cells of the portion of the substantia nigra. The correlation between pigmentation of nerve cells and intense pericellular binding of norepinephrine was even more striking in populations. The dorsal vagal nucleus, for example, showed only a few scattered pigmented nerve cells in its lateral portion. These cells always showed intense pericellular binding of norepinephrine. The binding in the rest of the nucleus was much weaker or minimal (fig. 2B). Similar observations were made in the midbrain where scattered pigmented nerve cells occurred in the nucl. paranigralis; in the nucl. parabrachialis, near the substantia nigra; and, in the nucl. intracapsularis.

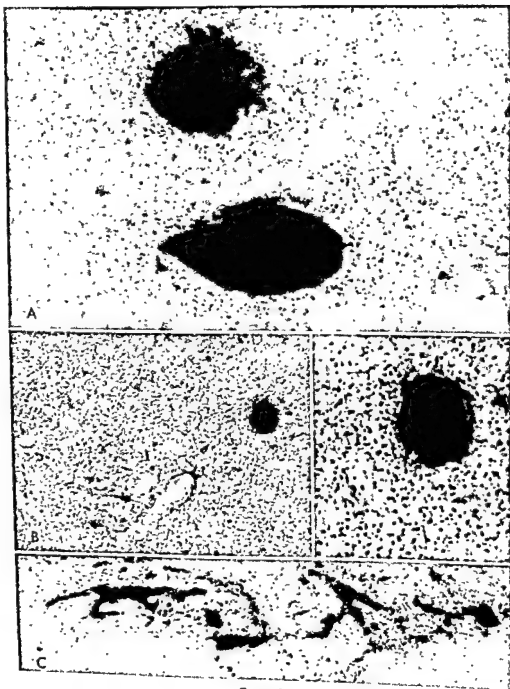


Figure 2

the extent of lipofuscin deposition; the latter was quite marked in some of our cases with advanced age.

Melanophores

The correlation between pigmentation and binding of norepinephrine prompted further studies of the melanophores in the meninges, which were numerous in six of our cases. These cells were usually more slender with thinner branches than the perikarya of neurons; hence, distinction between pericellular and intracellular binding was more difficult. Melanophores usually showed conspicuous binding of norepinephrine (fig. 2C), some apparently throughout their cytoplasm. There was some variation among cells, however; and, cells without binding were seen occasionally.

Binding in nonpigmented nuclei

Binding of norepinephrine occurred in many nonpigmented nuclei of the brain, although always much less than at pigmented nerve cells. Such binding was seen in a pericellular arrangement, similar to that at pigmented cells, or it was diffusely distributed throughout the neuropil. The latter condition generally prevailed. We were unable to localize binding to specific structures in the neuropil, such as at axons or axon terminals. Regions with relatively marked binding in the neuropil were: the subependymal glial layer, especially at the dorsal circumference of the oral portion of the aqueduct; the hypothalamic gray matter, tuber cinereum, nucl. paraventricularis, and the gray matter at the floor of the fourth ventricle; the caudate nucleus; and the substantia gelatinosa of the dorsal horn of the spinal cord. The distribution of marked binding in these regions of human brain corresponded to that of regions in which a high content of catecholamines was found biochemically (Sano et al., '59; and other authors). White matter generally showed less binding than gray matter; slight differences were noted among individual fiber tracts.

Binding in rat brain

The exceptional behavior of pigmented neurons in the human brain prompted us to compare the same regions in a species in which the neurons contain little or no

melanin. Our previous material on rat brains (Ishii and Friede, '67) showed somewhat more than average binding of norepinephrine in the neuropil of the substantia nigra and the nucl. coeruleus. However, the exceptionally intense pericellular binding of norepinephrine was not found in rat brains; hence, it appeared to be characteristic for the pigmented cells of human brain.

DISCUSSION

Several exceptional chemical features have been reported for either the substantia nigra or for the nucl. coeruleus, or for both; for example, a high concentration of copper, large amounts of dopamine or of substance P, monoamines in the cells — demonstrated by fluorescence microscopy — a high content of vitamin C, etc. (for survey see Friede, '66). However, none of these exceptional chemical properties was found in pigmented nuclei only, and none was shown to correlate consistently with the presence of pigmentation. The present observations appear to be unique in this regard and may enable one to understand the occurrence of melanin in only a few nuclei of the human brain. It is of particular interest that pigmentation was found to be related to properties of pericellular structures rather than to features of cytoplasm of the pigmented neurons. A more specific interpretation of our data is hampered by the lack of basic knowledge on the nature of the mechanism of binding and storing of catecholamines in nerve cells.

Fig. 2 A. Areas of binding at the surface of two pigmented neurons in the nucleus coeruleus; a third, nonpigmented cell with minimal binding is seen at the right. The picture had to be printed at low contrast to permit distinction between the silver grains and the melanin granules; these are readily distinguishable by their color under the microscope. 960 \times . B. A single pigmented nerve cell in the lateral portion of the dorsal vagal nucleus shows intense pericellular binding of norepinephrine which is absent in the rest of the nucleus. 120 \times . The zone of binding is confined to a portion of the cell surface, as shown in the high power enlargement of the same cell at right. 450 \times . C. Binding of norepinephrine in melanophores in the meninges, binding in melanophores may occur at the cell surface and in the cytoplasm. 380 \times .

Histochemical Investigation of Fiber Type Ratios with the Myofibrillar ATP-ASE Reaction in Normal and Denervated Skeletal Muscles of Guinea Pig¹

G. KARPATI² AND W. KING ENGEL³

Medical Neurology Branch, National Institute of Neurological Diseases and Blindness, Bethesda, Maryland

ABSTRACT The myofibrillar ATPase histochemical reaction was utilized to determine the proportion of the two basic histochemical fiber types in three "mixed" skeletal muscles of guinea pig after denervation. In five normal control animals, there was no significant difference in the proportion of fiber types on the two sides. In 12 experimental animals, from 6-27 weeks after right sciatic neurectomy, the intensity of the myosin ATPase activity was not appreciably altered in the denervated muscle fibers but the type II (dark) fibers underwent preferential atrophy. The fiber type ratio between denervated and control sides in the experimental animals was not significantly different from the same values in the normal control animals. This allowed the conclusion that, up to 27 weeks after denervation, the histochemical typing of a fiber by the myofibrillar ATPase reaction probably reflects the original fiber type. This reaction is the preferred method for fiber typing in denervated guinea pig muscle, especially since most other histochemical reactions show markedly reduced activity of muscle enzymes after denervation and are unsuitable for fiber typing. The soleus, which normally contains only type I fibers, showed numerous type II fibers at 27 weeks after denervation and this was interpreted as a dedifferentiating process.

Prolonged deprivation of a skeletal muscle of its motor nerve results in progressively severe morphological and biochemical changes in the muscle. Some of these changes have been studied in mammals by experimental denervation, using histochemical and cytochemical techniques (Nachmias and Padykula, '58, Golarz and Bourne, '61, '62, Hogenhuis and Engel, '65; Romanul and Hogan, '65; Smith, '65, Engel, Brooke and Nelson, '65), which allow detection of subtle changes in individual muscle fibers. Since it was shown by histochemical methods that "mixed" skeletal muscles of man and animals normally contain two basic types of muscle fibers (Nachmias and Padykula, '58, Dubowitz and Pearce, '60, 60a; Engel, '62) attention has been focused on the qualitative and quantitative differences between the two fiber types in various pathologic conditions (Engel). In most normal mammalian skeletal muscles, one set of fibers (termed type I) contains high activity of most oxidative enzymes and low activity of muscle amylophosphorylase, myofibrillar A-band adenosinetriphosphatase⁴ and menadione-mediated α -glycero-

phosphate dehydrogenase, whereas the other set of fibers (termed type II) shows opposite characteristics (Dubowitz and Pearce, '60a; Engel, '62). A small portion of muscle fibers appears to be of intermediate type regarding the activity of some of these enzyme reactions. The soleus of the adult guinea pig is a "uniform" muscle, containing exclusively type I fibers.

In a previous histochemical study of experimentally denervated guinea pig muscle (Hogenhuis and Engel, '65), it was demonstrated that the activity of a number of enzymes of the glycolytic pathway and Krebs cycle show a progressive decline at a characteristic rate for the individual enzyme. By the end of 11 weeks following denervation, the activity of most of the studied enzymes was markedly diminished and, with these reactions, it was no longer possible to differentiate between histochemical fiber types. How-

¹ This study was supported in part by the Muscular Dystrophy Association of Canada.

² Postdoctorate Research Fellow, The Muscular Dystrophy Association of Canada.

³ Chief, Medical Neurology Branch, National Institutes of Neurological Diseases and Blindness, Bethesda, Maryland 20014

⁴ Subsequently abbreviated as myofibrillar ATPase.

The most logical interpretations of our findings appear to be that pigmented nerve cells have an exceptionally large number of catecholamine-discharging synapses; and, that the abundance of discharged catecholamines results in pigment formation in the cells. These assumptions would be consistent with the observation that the pigment content of substantia nigra can be increased *in vitro* by exposing it to excessive concentrations of epinephrine (Friede, '53). It seems more logical to assume that regional synaptic patterns, rather than a primary metabolic changeover in these nerve cells, are responsible for the occurrence of a few scattered pigmented neurons such as found in the nucl. dorsalis vagi. The very marked pigmentation of the substantia nigra and nucl. coeruleus in primates could be explained by the presence of extremely numerous catecholamine-containing synapses at the neurons. A few melanin granules can be detected in these nuclei in most mammalian species if searched for with scrutiny (Marsden, '61). This observation would be consistent with the assumption that there are relatively fewer catecholamine-containing synapses in nonprimates.

LITERATURE CITED

- Aghajanian, G. K., and F. E. Bloom 1966 Electronmicroscopic autoradiography of rat hypothalamus after intraventricular H^3 -norepinephrine. *Science*, 153: 308-309.
- Aghajanian, G. K., F. E. Bloom, R. A. Lovell, M. H. Sheard and D. X. Freedman 1966 The uptake of 5-hydroxytryptamine- 3H from the cerebral ventricles: Autoradiographic localization. *Biochem. Pharmacol.*, 15: 1401-1403.
- Friede, R. L. 1953 Über die mutmassliche Bedeutung des Melanins in der Substantia nigra. *Naunyn-Schmiedeberg's Arch. Exp. Path. Pharmacol.*, 218: 286-289.
- 1966 "Topographic Brain Chemistry." Academic Press, New York.
- Fuxe, K., and U. Ungerstedt 1966 Localization of catecholamine uptake in rat brain after intraventricular injection. *Life Sci*, 5 1817-1824.
- Giachetti, A., and P. A. Shore 1966 Studies *in vitro* of amine uptake mechanisms in heart. *Biochem. Pharm.*, 15: 607-614.
- Hamberger, A., and B. Hamberger 1966 Uptake of catecholamines and penetration of trypan blue after blood-brain barrier lesions: A histochemical study. *Z. f. Zellforsch.*, 70 385-392.
- Ishii, T., and R. L. Friede 1967 Distribution of catecholamine-binding mechanism in rat brain. *Histochemie*, 9: 126-135.
- Jonsson, G. 1967 Binding of catecholamines and related compounds to proteins after for maldehyde gas treatment. *Histochemie*, 8 122-130.
- Marsden, C. D. 1961 Pigmentation in the nucleus substantiae nigrae of mammals. *J. Anat. (London)*, 95: 256-261.
- Mirkin, B. L., D. M. Brown and R. A. Ulfstrom 1966 Catecholamine binding protein: Binding of tritium to a specific protein fraction of human plasma following *in vitro* incubation with tritiated noradrenaline. *Nature*, 212: 1270-1271.
- Olszewski, J., and D. Baxter 1959 Cytoarchitecture of the Human Brain Stem. Lippincott, Philadelphia, Pennsylvania.
- Sano, I., T. Gamo, Y. Kakimoto, K. Taniguchi, M. Takesada and K. Nishinuma 1959 Distribution of catechol compounds in human brain. *Biochim. Biophys. Acta*, 32: 586-587.
- v. Euler, U. S., and F. Lishajko 1963a Catecholamine release and uptake in isolated adrenergic nerve granules. *Acta Physiol. Scand* 57: 468-480.
- 1963b Influence of PH on uptake and release of noradrenaline in adrenergic nerve granules. *J. Neurochem.*, 10: 145-149.
- 1963c Effect of reserpine on the uptake of catecholamines in isolated nerve storage granules. *Int. J. Neuropharmacol.*, 2: 127-134.
- 1963d Effect of adenine nucleotides on catecholamine release and uptake in isolated adrenergic nerve granules. *Acta Physiol Scand* 59: 454-461.
- 1964 Uptake of L- and D-isomers of catecholamines in adrenergic nerve granules. *Acta Physiol. Scand.*, 60: 217-222.
- v. Euler, U. S., F. Lishajko and L. Stjärne 1966 Catecholamines and adenosine triphosphate in adrenergic nerve granules. *Acta Physiol Scand* 59: 495-496.

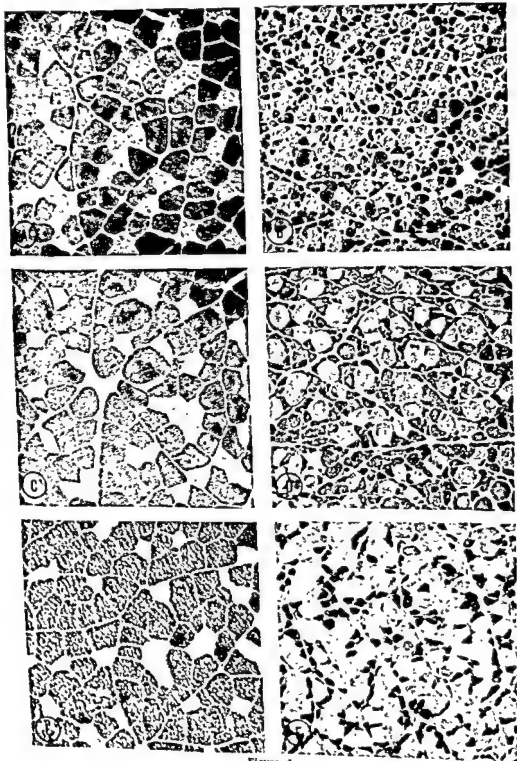


Figure 1

ever, with the myofibrillar ATPase reaction, the activity of the individual muscle fibers could readily be discerned and the two fiber types identified even 11 weeks after denervation. This observation and experience with human muscle biopsy material (Engel, '65) suggested that amongst the available cytochemical reactions in use at present the myofibrillar ATPase reaction would be the method of choice in determining histochemical fiber types in various pathologic conditions of muscle.

The objective of the present study was to determine the ratio of type I to type II fibers at various stages of denervation in several mixed muscles of the guinea pig, by the myofibrillar ATPase reaction, and to ascertain if the ratio remains constant or changes. A constant and normal ratio of the two fiber types in denervated muscle would probably indicate that the myofibrillar ATPase reaction reflects the original fiber type even in severely affected atrophic muscle, and would prove the value of this histochemical test in determining fiber types in denervated skeletal muscle.

METHODS

Young adult male guinea pigs of the Hartley strain weighing about 400 gms were kept on a standard diet of chow and fresh vegetables *ad libitum* in cages with a smooth metal floor covered copiously with sawdust. Twelve animals were denervated under intraperitoneal pentobarbital sodium anesthesia (25 mg/kg) by exposing the right sciatic nerve from a posterior thigh approach and blunt dissection of the hamstrings. A 2-2.5 cm segment of the nerve was resected from the greater trochanter to the popliteal fossa. Removal of the long segment was designed to prevent regeneration of the nerve leading to reinnervation of the calf muscles. The left side served as one type of control, and here a sham operation was performed with the identical maneuvers of the right side but the nerve was not resected. Self-cannibalism of the foot on the denervated side was prevented by blunting the front teeth. Two animals at each interval were sacrificed by an overdose of intraperitoneal pentobarbital so-

dium at 6, 8, 10, 12 and 27 weeks after denervation, and the following muscles were removed *in toto* on both sides while the animal was still alive: large (medial) head of gastrocnemius; small (lateral) head of gastrocnemius, plantaris and soleus. It was of paramount importance to examine and count the fibers on the whole cross-section of the muscle at a standard level to eliminate the bias of fiber type predominance in certain areas. From the midpoint of the muscle belly of the denervated and control muscles an 8 mm-thick cylindrical segment was mounted for transverse section so that the denervated and control muscle of the same animal (right and left side, respectively) were on the same chuck. The mounting medium was 7% gum tragacanth jelly, and freezing was done by immersing the chuck into isopentane (2-methyl butane) chilled to -160°C with liquid nitrogen. Ten μ -thick cryostat sections were prepared in a routine manner (Engel and Brooke, '65). The myofibrillar ATPase reaction was performed by the method of Padykula and Herman ('55). For the purpose of general survey, the sections were also stained by the modified trichrome stain (Engel and Cunningham, '63) and the NADH-tetrazolium reductase reaction (Novikoff, Shin and Drucker, '61). Sections of a given muscle from the denervated and control side from the same animal were stained in the same incubating medium at the same time and mounted next to each other on glass slides with Permount. The stained sections were photographed and reproduced on enlarged photographic prints to provide sufficient magnification ($\times 150$) to identify and count the different fiber types. All the counting was made by one investigator (GK) with the naked eye. On every photograph, the type I (light) fibers were counted first and the type II (dark) fibers second, and each counted fiber was

Fig. 1 Myofibrillar ATPase, fresh-frozen, $\times 100$, large head of gastrocnemius. A, C, E, are control sides; B, D, F are denervated sides at 6, 12, and 27 weeks, respectively, after denervation. Preferential atrophy of type II (dark) fibers is obvious, although the type I (light) fibers also show some atrophy. The intensity of the reaction is not diminished in denervated fibers.

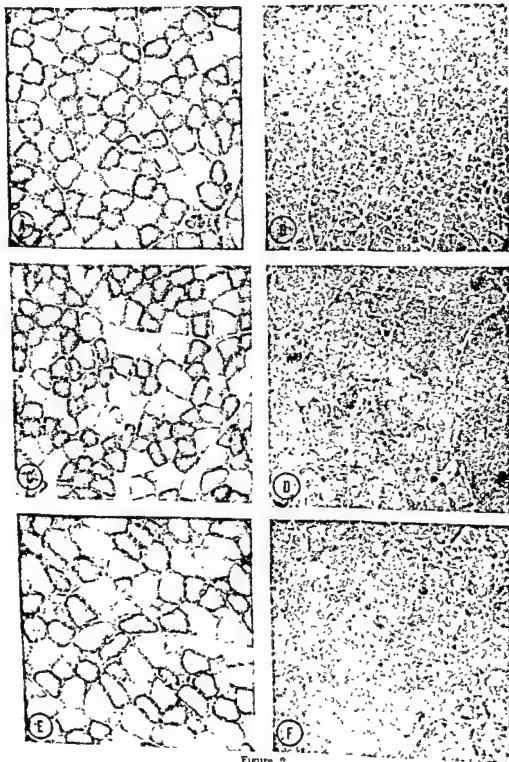


Figure 2

checked with a pen mark. A very small portion of fibers which appeared darker than the type I fibers, but not quite as dark as the type II fibers were consistently counted as type II fibers.

In addition to the controls of the non-denervated side of the experimental animals, five completely normal guinea pigs of the same size and sex were also studied to determine if there is any significant difference of fiber type ratio between the right and left sides in normal animals. The fiber type ratio difference between denervated and control side of the experimental animals was then contrasted to the difference in the normal controls for each muscle and a conclusion was drawn as to whether there was any statistically significant difference. Sections from the muscles of the right and left side of normal control animals were prepared in the identical manner described for the experimental animals.

RESULTS

A total of 520,149 fibers were counted in 102 muscles. The morphological changes of the denervated muscle fibers were identical with those of the previous study (Hogenhuis and Engel, '65). There was a striking preferential atrophy of the type II fibers, whose diameter decreased 5-10 times in excess of the type I fibers, as shown with the myofibrillar ATPase reaction (fig. 1). This has been termed type II fiber atrophy (Engel). With the NADH-tetrazolium reductase reaction, as early as three weeks after denervation, there was sufficient loss of activity so the fiber types could no longer be distinguished (fig. 2). Lack of neuronal regeneration was evidenced by the absence of stainable axons.

The fiber type ratios in the normal control and denervated animals were expressed as percentage of type II fibers in the total number of fibers counted on the cross-section of a given muscle.

$$\text{Ratio} = \frac{N_{II}}{N_I + N_{II}} \times 100$$

N_I = number of type I fibers
 N_{II} = number of type II fibers

I. Normal controls

Results are summarized in table 1. The maximum difference in a given animal

between the right and left sides is 4% in all three muscles. From this it appears that in none of the three muscles is there any significant difference of fiber type ratio between right and left sides. It is suggestive, however, that there are certain ratios of type I to II fibers characteristic for the large (medial) and small (lateral) head of gastrocnemius and plantaris muscles. The plantaris appears to contain the least type I fibers, i.e., the highest type II ratios, and the small head of the gastrocnemius the most. The large head of the gastrocnemius is intermediate

II. Denervated animals

Results are summarized in table 2. The maximum difference in a given animal between the right (denervated) and the left (control) side is 10% in both heads of the gastrocnemius and 7% in the plantaris muscle.

In tables 3 and 4, the differences of fiber type ratios between right and left in the 5 control and 12 denervated animals are summarized. The figures are shown with a sign, positive being arbitrarily designated as preponderance on the right side. There does not appear to be a trend toward a type of change as the length of postdenervation time increases.

The statistical significance between the means of the difference of right and left side in control and denervated animals was analyzed by the *t* test (Hill, '56) which revealed no significant difference ($p > 0.05$).

Absolute number of fibers. Comparing the right and left sides of the control animals, the absolute number of fibers (both histochemical types) shows an average difference of 15% in the large head of the gastrocnemius, 10% in the small head of gastrocnemius and 25% in the plantaris. In the small head of the gastrocnemius, the preponderance was on the left side whereas, in the other two muscles, it was on the right. In the denervated

Fig. 2 NADH-tetrazolium reductase, fresh-frozen, $\times 100$, large head of gastrocnemius. A, C, E are control muscles; B, D, F are denervated muscles at 6, 12 and 27 weeks respectively, following denervation. In the denervated muscle, there is marked decrease of the intensity of the reaction, so that fiber types are not discernible.

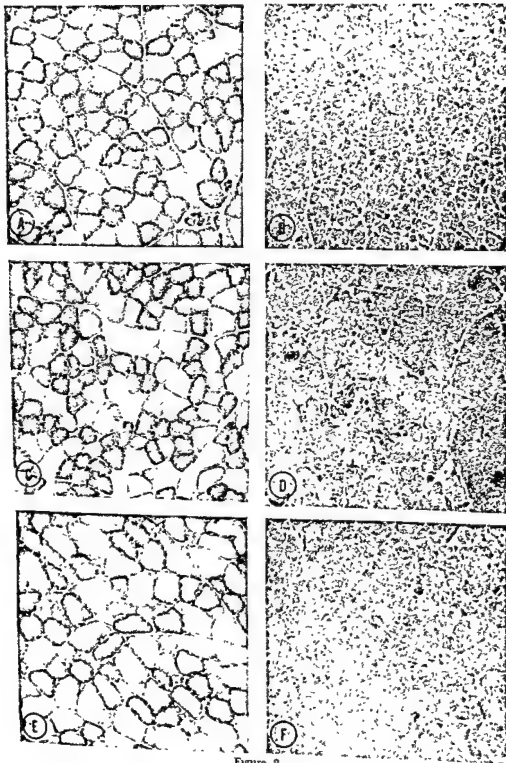


Figure 2

checked with a pen mark. A very small portion of fibers which appeared darker than the type I fibers, but not quite as dark as the type II fibers were consistently counted as type II fibers.

In addition to the controls of the non-denervated side of the experimental animals, five completely normal guinea pigs of the same size and sex were also studied to determine if there is any significant difference of fiber type ratio between the right and left sides in normal animals. The fiber type ratio difference between denervated and control side of the experimental animals was then contrasted to the difference in the normal controls for each muscle and a conclusion was drawn as to whether there was any statistically significant difference. Sections from the muscles of the right and left side of normal control animals were prepared in the identical manner described for the experimental animals.

RESULTS

A total of 520,149 fibers were counted in 102 muscles. The morphological changes of the denervated muscle fibers were identical with those of the previous study (Hogenhuis and Engel, '65). There was a striking preferential atrophy of the type II fibers, whose diameter decreased 5-10 times in excess of the type I fibers, as shown with the myofibrillar ATPase reaction (fig. 1). This has been termed type II fiber atrophy (Engel). With the NADH-tetrazolium reductase reaction, as early as three weeks after denervation, there was sufficient loss of activity so the fiber types could no longer be distinguished (fig. 2). Lack of neuronal regeneration was evidenced by the absence of stainable axons.

The fiber type ratios in the normal control and denervated animals were expressed as percentage of type II fibers in the total number of fibers counted on the cross-section of a given muscle.

$$\text{Ratio} = \frac{N_{II}}{N_I + N_{II}} \times 100$$

N_I = number of type I fibers
 N_{II} = number of type II fibers

I. Normal controls

Results are summarized in table 1. The maximum difference in a given animal

between the right and left sides is 4% in all three muscles. From this it appears that in none of the three muscles is there any significant difference of fiber type ratio between right and left sides. It is suggestive, however, that there are certain ratios of type I to II fibers characteristic for the large (medial) and small (lateral) head of gastrocnemius and plantaris muscles. The plantaris appears to contain the least type I fibers, i.e., the highest type II ratios, and the small head of the gastrocnemius the most. The large head of the gastrocnemius is intermediate.

II. Denervated animals

Results are summarized in table 2. The maximum difference in a given animal between the right (denervated) and the left (control) side is 10% in both heads of the gastrocnemius and 7% in the plantaris muscle.

In tables 3 and 4, the differences of fiber type ratios between right and left in the 5 control and 12 denervated animals are summarized. The figures are shown with a sign, positive being arbitrarily designated as preponderance on the right side. There does not appear to be a trend toward a type of change as the length of postdenervation time increases.

The statistical significance between the means of the difference of right and left side in control and denervated animals was analyzed by the *t* test (Hill, '56) which revealed no significant difference ($p > 0.05$).

Absolute number of fibers. Comparing the right and left sides of the control animals, the absolute number of fibers (both histochemical types) shows an average difference of 15% in the large head of the gastrocnemius, 10% in the small head of gastrocnemius and 25% in the plantaris. In the small head of the gastrocnemius, the preponderance was on the left side whereas, in the other two muscles, it was on the right. In the denervated

Fig. 2 NADH-tetrazolium reductase, fresh-frozen, $\times 100$, large head of gastrocnemius. A, C, E are control muscles; B, D, F are denervated muscles at 6, 12 and 27 weeks respectively, following denervation. In the denervated muscle there is marked decrease of the intensity of the reaction, so that fiber types are not discernible.

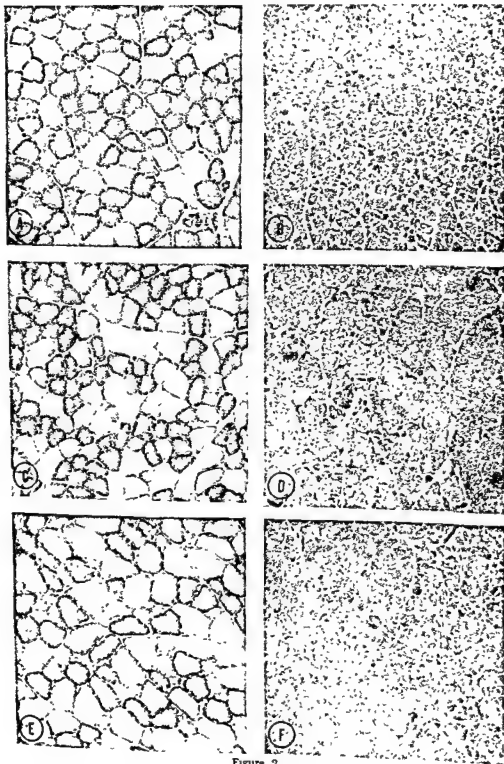


Figure 2

TABLE 1
Comparative ratios of type II fibers between right and left sides in the three studied muscles in five control animals. In tables 1-4, the ratios are expressed as percentage of type II fibers in the total number of fibers

	Gastrocnemius				Plantaris	
	Large head		Small head			
	Right	Left	Right	Left	Right	Left
C ₁	84	88				
C ₂	83	84	77	73		
C ₃	88	87	78	81	87	88
C ₄	81	80	87	85	86	85
C ₅	88	86	73	78	92	98
			83	87	90	89
					88	87
Mean \pm S.D.	85 \pm 2.8	85 \pm 2.8	80 \pm 6.3	80 \pm 4.1	88 \pm 2.2	88 \pm 1.6

TABLE 2
Comparative ratios of type II fibers between denervated (right) and control (left) sides in the three studied muscles in ten denervated animals. Index number of D designates weeks after denervation. A and B are separate animals

Gastrocnemius							
Large head				Small head		Plantaris	
	Right	Left	Right	Left	Right	Left	
D ₄ A	79	85					
D ₄ B	85	80	79	75			
D ₄ A	83		81		86	86	
D ₄ B	84	84	89	81	89	90	
D ₁₀ A	83	86	90	82	85	85	
D ₁₀ B	86	81	81	83	87	85	
D ₁₂ A		86	86	73			
D ₁₂ B	77	84	85	85	91	90	
D ₁₇ A	86	78	87	75	87	87	
D ₁₇ B	77	85	87	81	90	83	
	77	87	73	78	76	82	
			83	75	89	89	
Mean \pm S.D.	81.7 \pm 3.2	83.6 \pm 2.6	83.4 \pm 4.5	78.8 \pm 3.5	86.7 \pm 4.2	86.4 \pm 2.6	

animals, the same difference in the large head of the gastrocnemius was 35%, in the small head of gastrocnemius 40%, and in the plantaris 40%, but all preponderant on the right. This is a somewhat paradoxical finding in an atrophic muscle, and an explanation is offered in the discussion.

Soleus. The soleus muscle exhibited unique features after denervation. As previously mentioned, this muscle is histochemically uniform, containing only type I fibers in the adult guinea pig so normally the fiber type ratio cannot be considered. (In other species, e.g., cat, rabbit, rat and mouse, scattered type II fibers occur). Up to 12 weeks after denervation, there is a uniform decrease of the diameter of fibers, but the muscle still contains only type I fibers with the myofibrillar

ATPase reaction. However, at 27 weeks a number of scattered type II fibers were detected with the same reaction (fig. 3).

DISCUSSION

Histochemical studies of experimentally denervated mammalian skeletal muscle utilizing the myofibrillar ATPase reaction are few (Nachmias and Padykula, '58; Hogenhuis and Engel, '65; Golarz and Bourne, '62; Engel, Brooke and Nelson, '65). Light microscopic (Engel, '62; Padykula and Gauthier, '63) and ultrastructural (Tice and Barnett, '62) evidence has been reported that the histochemical reaction for ATPase activity by the method of Padykula and Herman ('55), which we employed in this study, is demonstrating the ATPase activity of myosin. Other authors have used different histochemical

TABLE 3

Difference of ratio of type II fibers between right and left sides in the three studied muscles in five control animals. Positive sign has been arbitrarily assigned to indicate preponderance on the right.

	Gastrocnemius		Plantaris
	Large head	Small head	
C ₁	-4	+4	-1
C ₂	-1	-3	+1
C ₃	+1	+2	+4
C ₄	+1	-5	+1
C ₅	+2	-4	+1
Mean \pm S.D.	-0.2 \pm 2.3	-1.2 \pm 3.9	+1.2 \pm 1.7

TABLE 4

Difference of ratio of type II fibers between right (denervated) and left (control) sides in the three studied muscles in ten denervated animals. Index number of D designates weeks after denervation. A and B are separate animals. Positive sign has been arbitrarily assigned to indicate preponderance on the right side.

	Gastrocnemius		Plantaris
	Large head	Small head	
D ₄ A	-6	+4	0
D ₄ B	+5	0	-1
D ₄ A	-1	+7	0
D ₆ B	-2	+7	+2
D ₁₀ A	+2	+8	+1
D ₁₀ B	0	+1	0
D ₁₃ A	-7	+10	0
D ₁₃ B	+8	+6	+7
D ₁₇ A	-8	-5	-6
D ₁₇ B	-10	+8	0
Mean \pm S.D.	-1.9 \pm 3.88	+4.6 \pm 4.62	+0.3 \pm 3.16

techniques, e.g., oxidative enzyme and amylophosphorylase reactions for the study of experimentally denervated muscle (Bajusz, '64; Hogenhuis and Engel, '65; Romanul and Hogan, '65; Smith, '65). They are in agreement that the activity of the oxidative enzymes used and of amylophosphorylase is significantly reduced in early stages of denervation and the difference between the muscle fiber types is no longer discernible. Bajusz ('64) has shown with the haematoxylin-phloxin stain in denervated cat and mouse muscle that more rapid atrophy of the "agranular white" fibers takes place than the "granular red" fibers. He concluded

from his findings that the "red" fibers display relative independence of neural control. Since his "white" fibers which underwent preferential atrophy probably correspond to type II fibers with the myofibrillar ATPase reaction, his conclusions are in harmony with the results of the present study as well as with the findings of another study (Engel, Brooke and Nelson, '65).

In the present study, our findings revealed no significant diminution of the relative activity of myofibrillar ATPase in individual muscle fibers up to six months after denervation. In view of this, a brief review of the biochemical studies concerning ATPase activity of myosin in denervated muscles is of interest.

Michelazzi *et al.* ('55) studied myofibrillar ATPase activity in denervated guinea pig gastrocnemius and found progressive decline starting at 12 hours and continued up to 48 hours, when it reached 70% decrease of the activity of the control muscle based on wet weight. Fisher ('48) demonstrated that, after 35 days, there was a 95% decrease of myosin ATPase activity in skeletal muscle but, at the same time, the "soluble," though possibly mitochondrial, ATPase activity increased.

Other authors found no decrease of ATPase activity in denervated skeletal muscle. Beznak ('49) found an increase of total ATPase activity in rat muscle from 1-10 weeks after sciatic denervation, but the myosin ATPase was not determined selectively. Bargellini and colleagues ('60) demonstrated no significant fall of myosin ATPase activity in denervated guinea pig muscles up to one month after denervation. They also pointed out that alteration of the solubility characteristics of myosin in denervated muscle could give rise to incomplete extraction and thus falsely lower ATPase activity. Nachmias and Padykula ('58), in a combined histochemical and biochemical study, mentioned increased activity of ATPase two weeks after denervation in rat skeletal muscles, but the biochemical data were not described in detail. Kohn ('64), in a recent study on the fate of protein degradation in denervated muscles of the rat (up to 13 days),

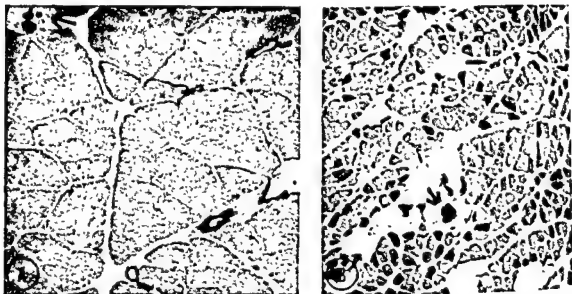


Fig. 3 (A) Myofibrillar ATPase, fresh frozen, $\times 100$. Soleus on the control side shows uniform type I extrafusal fibers. A muscle spindle on the section (arrow) contains three type II fibers and one type I. (B) Same animal, contralateral soleus, 27 weeks after denervation. A number of type II fibers are scattered amongst the lighter, type I fibers. Diameter of both fiber types is markedly reduced compared to the control side. There is some increase of adipose tissue indicated by optically empty spaces. Arrow indicates a relatively preserved spindle.

showed that the loss of myofibrillar proteins was not disproportionate to the rest of the muscle proteins in reference to wet weight. He found no alteration of ATPase activity of the remaining myosin. In agreement with the preceding study, the experiments of M. Barany *et al.* ('65) revealed that despite the marked absolute loss of myosin in denervated (up to 19 days) "fast" and "slow" muscles of rabbit, the Ca^{++} -activated ATPase activity of the remaining myosin was not significantly different from the normal controls. These findings would be in harmony with the present histochemical finding of no significant decrease of myosin ATPase activity in the denervated (atrophic) fibers, indicating that the remaining myofibrils, in spite of the greatly diminished fiber size, are sufficiently active to give a strong reaction.

At the present time, the reason for the different intensity of the myofibrillar ATPase activity in the two fiber types is not known. Gergely and colleagues ('65) demonstrated biochemically about four times higher myofibrillar ATPase activity in "white" skeletal muscles than in "red" muscles. M. Barany *et al.* ('65) found that the ATPase activity of the

"fast" muscle myosin was 2-3 times higher than the myosin from "slow" muscle. Since, in "white" ("fast") mammalian skeletal muscles, there is predominance of the histochemical type II fibers (which have higher myofibrillar ATPase activity than the type I fibers) the foregoing biochemical studies appear to be in accord with our histochemical data.

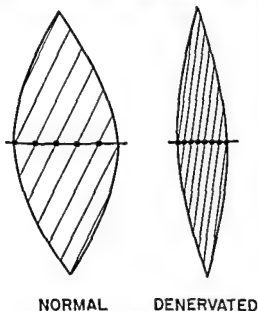
Ultrastructural studies of denervated rat skeletal muscle by Pellegrino and Franzini demonstrated that "in rather advanced stages of neuromuscular atrophy the reduction of the myofibril diameter was due to a loss of filaments at the periphery with complete preservation of the normal pattern inside the fibrils" (Pellegrino and Franzini, '63). This finding would be compatible with the expectation that the remaining thick filaments of the myofibrils retain normal relative ATPase activity. This point is also supported by light-microscopic findings (Adams, Denny-Brown and Pearson, '62), demonstrating that, in denervation, myofibrils show a progressive decrease but those remaining at a given stage fill the sarcolemmal tube and retain their cross-striation several months after denervation.

From the present study, we conclude that the constant ratio of type II to type I fibers in normal and denervated muscle indicates that denervated fibers retain their original distinctive histochemical characteristics with the myofibrillar ATP-ase reaction. Other possibilities which could give rise to similar experimental results should be considered. In figure 4, some of the possibilities are summarized. If a change of one histochemical fiber type to another had taken place during denervation, this change would have to have been offset by a quantitatively comparable change of the other fiber type in the opposite direction, for the ratio of the two fiber types remained constant. We feel that this is a much less likely possibility than the one postulated, i.e., that no change of histochemical fiber types takes place. If preferential "absorption" or splitting of one histochemical fiber type had taken place, a similar change of the

same degree in the same direction must have occurred in the other fiber type so that the ratio between the fiber types remained constant. Or within one fiber type, a rate of "absorption" would have to have been paralleled by an equal rate of splitting to keep the ratio constant. These two possibilities also seem unlikely.

The increase of the absolute number of fibers counted in the denervated muscles requires an explanation. Even 27 weeks after denervation, there were no significant "degenerative" changes aside from some fatty replacement in certain fasciculi. Although marked fiber splitting (to an equal degree in the two types) could account for the increased total fiber counts, there was no evidence of fiber splitting present in the sections. A more plausible explanation is illustrated in figure 5. In pennate muscles, such as the ones studied, the direction of the fibers between origin and termination in the atrophic state more closely approximates the direction of the long axis of the muscle, while normally they are oblique and of larger diameter. Hence, in the atrophic muscle, a transverse section across the belly of the muscle would transect more fibers than normally. Since in this study all muscle fibers were counted on the entire cross-section of the muscles at their proximodistal midpoint, an increased number of fibers could be obtained in atrophic muscles.

The unique features of the soleus fibers at 27 weeks after denervation are of par-



TYPE I FIBERS

TYPE II FIBERS

Increase

Decrease

1. Splitting

1. Absorption

2. Change from II ← 2. Change to I

Decrease

Increase

1. Absorption

1. Splitting

2. Change to II → 2. Change from I

Fig. 4 This diagram illustrates the direction of muscle fibers in a pennate muscle such as the gastrocnemius. In the denervated muscle, the angle between the long axis of the fiber and the long axis of the muscle is diminished as compared to the normal muscle. Therefore a transverse section across the midportion of the muscle transects more fibers in the denervated than in the normal muscle.

Fig. 5 Potential factors which might affect fiber type ratios in denervated muscles.

ticular interest. Guttman ('62) reported "heterogeneous atrophy" in denervated rabbit soleus with larger and smaller fibers, which might have been of different histochemical types, but in the rabbit soleus there are normally some scattered type II fibers. In our study, reinnervation was ruled out by the absence of stainable axons in the denervated muscles. Therefore we regard the appearance of the numerous scattered type II fibers as a process of dedifferentiation. This view is supported by our observation that the soleus in neonatal guinea pig is a mixed muscle and only becomes uniform by 4-6 weeks of age. Neonatal denervation prevents the soleus from becoming uniform in terms of histochemical fiber type (Karpati and Engel, '66).

ACKNOWLEDGMENTS

The authors wish to acknowledge the help of Dr. Wayne Tobin in the early phases of the study. The assistance of Mr. D. Tyson in microphotography is appreciated.

LITERATURE CITED

- Adams, R. D., D. D. Denny-Brown and C. M. Pearson 1962 *Diseases of Muscle*. Hoeber Medical Book, p. 141.
- Bajusz, E. 1964 "Red" skeletal muscle fibers: relative independence of neural control. *Science*, 145: 938-939.
- Barany, M., K. Barany, T. Reckard and A. Vulpe 1965 Myosin of fast and slow muscles of the rabbit. *Arch. Biochem. Biophys.*, 109: 185-191.
- Bargellini, P., V. Galucci and A. Corsi 1960 L'attività adenosintrifosfatase delle miofibrille del muscolo scheletrico dopo denervazione. *Sperimentale*, 110: 241-249.
- Beznak, M. 1949 The ATP splitting ability of denervated muscle. *First Congr. Biochem. Cambridge, Abst. Commun.*, pp. 601-602.
- Chappell, J. B., and S. V. Parry 1953 The respiratory and adenosintrifosfatase activities of skeletal-muscle mitochondria. *Biochem. J.*, 55: 586-595.
- Close, R. 1964 Dynamic properties of fast and slow skeletal muscles of the rat during development. *J. Physiol.*, 173: 74-95.
- Dubowitz, V., and A. G. Pearse 1960 Comparative histochemical study of oxidative enzyme and phosphorylase activity in skeletal muscle. *Histochemie (Berlin)*, 2: 105-117.
- 1960a Reciprocal relationship of phosphorylase and oxidative enzymes in skeletal muscle. *Nature*, 185: 701-702.
- Engel, W. K. 1962 The essentiality of histo- and cytochemical studies of skeletal muscle in the investigation of neuromuscular disease. *Neurology*, 12: 778-794.
- 1963 Adenosine triphosphatase of sarcoplasmic reticulum triads and sarcolemma identified histochemically. *Nature*, 200: 558-559.
- Histochemistry of neuromuscular disease—significance of muscle fiber types, eighth International Congress of Neurology, Vienna, 5-10 IX, Tom. II, pp. 67-101.
- 1965 Diseases of the neuromuscular junction and muscle. In: *Neurohistochemistry* C. W. M. Adams, ed. Elsevier, pp. 622-672.
- Engel, W. K., and M. H. Brooke 1965 Muscle Biopsy as a clinical diagnostic aid in Neurological Diagnostic Techniques. W. S. Fields, ed. Charles C Thomas, pp. 1-57.
- Engel, W. K., M. H. Brooke and P. H. Nelson 1965 Histochemical studies of denervated or tenotomized cat muscle: Illustrating difficulties in relating experimental animal conditions to human neuromuscular disease. *Ann. N.Y. Acad. Sci.*, 138: 160-186.
- Engel, W. K., and G. G. Cunningham 1963 Rapid examination of muscle tissue. An improved trichrome method for fresh frozen biopsy sections. *Neurology*, 13: 919-923.
- Fisher, E. 1948 Some enzyme systems of denervated muscle. *Arch. Phys. Med.*, 29: 291-300.
- Gergely, J., D. Pragay, A. T. Scholz, J. C. Seldel, F. A. Streter and M. M. Thompson 1965 Comparative studies on white and red muscle. In: *Molecular Biology of Muscular Contraction*. S. Ebashi et al., eds. Elsevier, pp. 145-159.
- Golarz, M. N., and G. H. Bourne 1961 Induction and accentuation of phosphatase activity in the nucleoli of muscle nuclei by denervation and injected nucleotides. *Exp. Cell. Res.*, 25: 691-693.
- 1962 Effects of denervation and treatment with nucleotides on phosphatase reactions in muscle of rats. *Acta Neuropath.*, 1: 463-473.
- Guttman, E., and J. Zelena 1962 Morphologic changes in denervated muscle. In: *The Denervated Muscle*. E. Guttman, ed. Publishing House of the Czechoslovak Academy of Sciences, Prague, pp. 57.
- Hill, A. B. 1956 *Principles of Medical Statistics*. Lancet, p. 146.
- Hogenhuis, L. A. H., and W. K. Engel 1965 Histochemistry and cytochemistry of experimentally denervated guinea pig muscle. *Acta Anat.*, 60: 39-65.
- Karpati, G., and W. K. Engel 1966 A new aspect of the trophic function of motor nerve: influence of the cytochemical features of the skeletal muscle cell. (Abstract) *Neurol.*, 17: 298.
- Kielley, W. W. 1961 Myosine adenosine triphosphatase. In: *The Enzymes*. P. D. Boyer, H. Lardy and K. Myrback, eds. Academic Press, N. Y., Vol. 5, pp. 159-168.
- Kohn, R. R. 1964 Mechanism of protein loss in denervation muscle atrophy. *Am. J. Path.*, 45: 435-447.
- Michelazzi, L., M. A. Mor and M. U. Dianzani 1955 Adenosine triphosphate concentration in

- guinea pig muscle after denervation. *Experimenta*, 13: 117-118.
- Muscatello, U., E. Andersson-Cedergren, G. F. Arzone and A. von der Decken 1961 The sarcotubular system of frog skeletal muscle. A morphological and biochemical study. *J. Biophys. Biochem. Cytol.*, 10 (4) Suppl: 201-218.
- Nachmias, V. T., and H. A. Padykula 1958 A histochemical study of normal and denervated red and white muscles of the rat. *J. Biophys. and Biochem. Cytol.*, 4: 47-53.
- Novikoff, A. B., W. Y. Shin and F. Drucker 1961 Mitochondrial localization of oxidative enzymes: staining results with two tetrazolium salts. *J. Biophys. Biochem. Cytol.*, 9: 47-61.
- Padykula, H. E., and E. Herman 1955 The specificity of the histochemical method for adenosine triphosphatase. *J. Histochem. Cytochem.*, 3: 170-183.
- Padykula, H. A., and G. F. Gauthier 1963 Cytochemical studies of adenosine triphosphatases in skeletal muscle fibers. *J. Cell Biol.*, 18: 87-107.
- Pellegrino, C., and C. Franzini 1963 An electron microscope study of denervation atrophy in red and white skeletal muscle fibers. *J. Cell Biol.*, 17: 327-349.
- Romanul, F. C. A., and E. L. Hogan 1965 Enzymatic changes in denervated muscle. *Arch. Neurol.*, 13: 263-273.
- Samaha, F. J., and J. Gergely 1965 N^+ and K^+ stimulated ATPase in human striated muscle. *Arch. Biochem.*, 109: 76-79.
- Smith, B. 1965 Changes in the enzyme histochemistry of skeletal muscle during experimental denervation and reinnervation. *J. Neurol. Neurosurg. Psychiat.*, 28: 89-103.
- Tice, L. W., and R. J. Barnett 1962 Fine structural localization of adenosinetriphosphatase activity in heart myofibrils. *J. Cell Biol.*, 15: 401-416.

Dense-core Microtubules in Neurons and Gliocytes of the Toad *Bufo arenarum* Hensel¹

E. L. RODRÍGUEZ ECHANDÍA,² R. S. PIEZZI³ AND E. M. RODRÍGUEZ⁴
Instituto de Histología y Embryología, U.N.C., Mendoza, Argentina

ABSTRACT Numerous microtubules of nerve cells and gliocytes in the toad are found, in electron micrographs, to contain a dense core. Such content is granular in nature, the granules being irregularly disposed in the lumen of the microtubules. Comparative observations on dense-core microtubules in peripheral and central nerve cells indicate that they are consistent cell components in the entire nervous system of the toad. The functional significance of the granular content of the microtubules is discussed.

An increasing amount of evidence indicates at present that minute tubular structures are a universal component of cells. Microtubules were observed in neurons (De Robertis and Bennett, '55; Palay, '56) and have been found in almost all nerve cells analyzed so far with the electron microscope; their functional significance, however, is still a matter of discussion. They were first regarded as elements of the endoplasmic reticulum, presumably concerned with the genesis of the synaptic vesicles in nerve terminals (Palay, '56). However, the fact that the endoplasmic reticulum, but not the microtubular system, is a unit, membrane-bounded organelle indicates that reticulum and tubules are distinct entities. In this regard, it might be relevant to quote here the opinion of Gray ('64): "This does not exclude the possibility that the axonal tubules contribute to the formation of the synaptic vesicles and their contents, but suggests that the origin of the membranous envelope itself must lie in some other source." The neurotubules, on the other hand, are regarded by others as cytoskeletal structures, an interpretation that also applies to neurofilaments in general, as well as to the microtubular component of other cell types (Ledbetter and Porter, '63; Porter et al., '64; Fawcett and Witebsky, '64).

As far as fine structure is concerned, the neurotubules of a variety of vertebrate and invertebrate nerve cells are described in the literature as slender cylinders of undetermined length, and 200–250 Å across. They are constructed of a dense wall enclosing

an adielecronic lumen. This work presents, instead, a description of microtubules with an electron-dense core which we have found in neurons and gliocytes of the toad. It is hoped that these observations will contribute to the understanding of the physiological role of neurotubules. Peters and Vaugh ('67) have described neurotubules with a dense central core but did not investigate longitudinal sections as done in this study.

MATERIAL AND METHODS

Adult toads (*Bufo arenarum* Hensel) were anesthetized with ether. In the first group of animals, the kidney and adrenal were surgically exposed and the abdominal cavity was filled with fixative. The fixative used was a combination of formaldehyde and glutaraldehyde according to Karnovsky ('65). After this preliminary *in situ* fixation, the kidney-adrenal was removed and placed in the fixative at room temperature for two additional hours; during this time, the adrenal gland was cut into small blocks under a dissecting microscope. The material was then washed in pure buffer and postfixed in 1% osmium tetroxide.

In a second group of animals, the brain was fixed by slowly perfusing 20 ml of the same fixative through the third ventricle. The hypothalamus, median eminence and neural stalk were then dissected out and

¹ This study was supported by RG 58028 School grant from the Rockefeller Foundation.

² Member of the Scientific Research Career of the "Consejo Nacional de Investigaciones Científicas y Técnicas" of Argentina.

³ Fellows of the "Consejo Nacional de Investigaciones Científicas y Técnicas."

related to the neurohypophysis. The pituitary stalk, the median eminence and the hypothalamus were chosen, therefore, as the material in which to investigate the occurrence of an endotubular content in the central nervous system of the toad.

From such analysis, it was found that electron micrographs of these areas also contain a significant population of dense-core microtubules that conform to the description of the ones in adrenal nerve endings (figs. 4, 5, 10). They are intermingled with the other organelles in the perikaryon and cell processes of hypothalamic secretory neurons as well as in nerve fibers of the median eminence and neural stalk (figs. 3, 4, 5). It is of particular interest that, in addition to dense-core microtubules in nerve cells, such components also occur in intervening glial processes, as well as in dark arborescent gliocytes of the neural stalk (fig. 5, lower inset). These observations indicate that dense-core microtubules are not exclusively confined to neurons and that they are consistent components of cells in the whole nervous system of the toad.

DISCUSSION

In summary, examination of peripheral and central neurons and gliocytes of the toad has shown that a variable population of dense-core microtubules is a consistent component of their cytoplasm. The above-mentioned results of Bern and collaborators ('66), have already drawn attention to the presence of dense-core microtubules in gliocytes of the pars nervosa in the sparrow. The striking resemblance between the dense-core microtubules of the sparrow and those of the toad indicates that they are not a rare organelle to be found only in cells of a single class of vertebrates.

The comparative analysis of longitudinally and cross-sectioned nerve fibers shows that their dense core is granular in nature, at least after the above-described method of preparation. The functional significance of these findings, however, cannot be decided at present. The two main alternatives are: (1) The granular content may be a structural component of the neurotubules; or (2) it may be a visible expression of an endotubular flow of materials. Certainly, neither of these speculations

can be definitely substantiated by the information at hand, but a brief discussion of the distribution of granules within the lumen of the microtubuli may throw some light upon the problem. Electron micrographs comprising longitudinally oriented neurotubules show, in general, that the intraluminal granules are relatively few and irregularly arranged. Since most tubules in longitudinal sections appear devoid of content, it is reasonable to expect a majority of them to look empty in cross-sections also. This is in fact the case. In some nerve endings, however, most tubules enclose granular aggregations which may indicate storage of electron-dense material within the neurotubules. On the other hand, such an irregular distribution of the intraluminal granules seems to preclude their identification as macromolecular units involved in the construction of the neurotubule itself since, if such were the case, one should find a regular, or even a periodical, granule-to-granule relationship. If the endoluminal granules are indeed an expression of the migration of electron-dense cellular products, the findings reported here could be in good agreement with the current concept of centrifugal axonal transport of materials newly synthesized in the endoplasmic reticulum (Taylor, and Weiss, '65). In this context, we would like to call attention also to the results of Droz ('64), who reported, on the basis of electron microscopic radioautographs, that labeled proteins migrate along the axons "over packed neurofilaments and neurotubules, and to a lesser extent, over the axolemmal membrane." The alternative, that the intraluminal granules are the expression of endotubular flow, is currently the object of experimental research.

ACKNOWLEDGMENT

The authors wish to thank Dr. M. H. Burgos and Dr. F. Sacerdote for critical reading of the manuscript.

LITERATURE CITED

- Bern, H. A., S. R. Nishioka, L. R. Mewaldt and D. S. Farner 1966 Photoperiodic and osmotic influences on the ultrastructure of the hypothalamic neurosecretory system of the white-crowned sparrow, *Zonotrichia leucophrys gambelii*. *Z. Zellforsch.*, 69: 198-227.
- De Robertis, E., and H. S. Bennett 1955 Some features of the submicroscopic morphology of

immersed in the fixative for 40 minutes; the next steps were identical to the ones outlined for the first group. In each case, the specimens were dehydrated in ethanol and embedded in Epon 812 (Luft, '61). Sections were made with a Porter-Blum ultramicrotome, collected on Athene slit grids covered with a carbon film (Robertson, '59), stained with uranyl acetate-methanol and lead citrate (Venable and Coggeshall, '65) and studied in a Siemens Elmiskop I electron microscope.

OBSERVATIONS

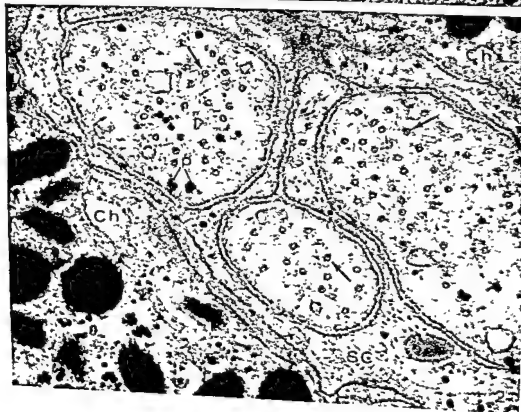
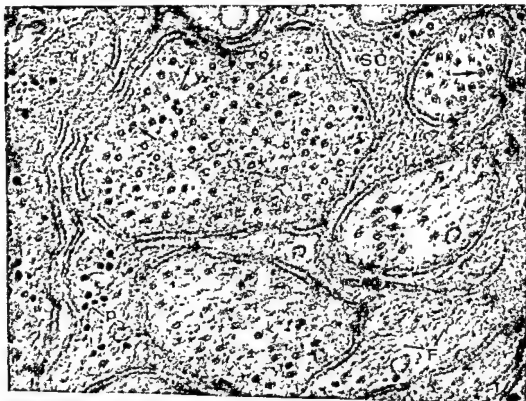
The microtubules in adrenal endings of the splanchnic nerve. Numerous splanchnic nerve endings are known to innervate the adrenal chromaffin cells of the toad. The interstices between such cells are in turn filled with a significant population of axons, which appear in sections as packages of irregular profiles, each enclosed by a single layer of a satellite cell process. In these areas, the axoplasm is pale in general, and contains microtubules, bundles of filaments, a few mitochondria and scattered particles of the glycogen type (figs. 1, 2). The axons may be seen, on occasion, making synaptic contact with the plasmalemma of the chromaffin cells; they contain the typical annular and granular varieties of synaptic vesicles, and a few neurotubules (Piezzi, '67). In this description, the adrenal endings of the splanchnic nerve would not seem to differ from what is known of other nerve endings. Nevertheless, the unusual fine structure of the tubular component deserves to be analyzed in detail. Most tubules lie in the direction of the axons and may extend into synaptic endings. Electron micrographs of cross-sectioned adrenal terminals comprise, in general, two distinctive types of microtubular profiles; one conforms to the typical empty cylinders found in nerve cells of a variety of species; the other, which we propose to call the "dense-core neurotubule," is the main object of the present work. Though the most abundant tubular component in these endings is the familiar empty neurotubule, certain fibers, which we have chosen to illustrate in figures 1 and 2, contain a fair number of the structures in question.

Figures 6-10 are high-power micrographs, showing that the wall of the neurotubules is not a 75 Å-thick trilaminar unit membrane but an intimate aggregation of well defined condensations about 50 Å across. It is interesting that a significant variability in the total number of condensations making up the tubular wall does occur in these images. Most neurotubules, on the other hand, contain centroluminal material, in the form of a single condensation, 30-50 Å wide, this being the most frequent expression of such content. Figures 7 and 8, however, illustrate tubules with two or even three such condensations.

Turning now to high-power views of longitudinally oriented neurotubules (fig. 9), we find that their wall appears somewhat less clearly defined than the wall of cross-sectioned units, while the lumen looks denser. These differences are due to the fact that longitudinal views of tubuli are full images of these 200 Å thick organelles, since most of them lie entirely within the depth of the 300-600 Å-thick Epon sections. Moreover, cytoplasmic particles are seen frequently superimposed on the images of the longitudinally oriented neurotubules. At times, however, distinctive condensations, so small as to be easily overlooked in low-power micrographs, can be recognized in the center of their lumen (fig. 9, arrows). They correspond to the dense core seen in cross-section units. Only a few of such "granules" can be found in most longitudinal views of the tubules; they are irregularly distributed along the axis of the lumen. In a minority of nerve fibers, however, the microtubules contain rosaries of granules, as illustrated in figure 9.

From such a comparative analysis of longitudinal and cross-sections of adrenal nerve endings it seems clear that: (1) the dense core of the neurotubule is granular in nature; and (2) the number of endotubular granules varies from one nerve ending to another.

The microtubules in nerve fibers of the hypothalamus, median eminence and neural stalk. Since Bern et al. ('66) have shown dense-core microtubuli in gliocytes of the pars nervosa in the sparrow, we thought it pertinent to analyze the neurotubules in areas which are morphologically



- synapses in the frog and earthworm. *J. Biophys. Biochem. Cytol.*, 1: 361-372.
- Droz, B. 1964 Continuous elaboration of axoplasmic components by nerve cell bodies as revealed by means of electron microscopic radioautography. *Eleventh International Congress of Cell Biology. Excerpta Medica*, 17 A.
- Fawcett, D. W., and F. Witebsky 1964 Observations on the ultrastructure of nucleated erythrocytes and thrombocytes with particular reference to the structural basis of their discoidal shape. *Z. Zellforsch.*, 62: 785-806.
- Gray, E. G. 1964 Tissue of the central nervous system. In: *Electron Microscopic Anatomy* S. M. Kurtz, ed. Academic Press, New York, pp. 369-417.
- Ledbetter, M. C., and K. R. Porter 1963 A "microtubule" in plant cell fine structure. *J. Cell Biol.*, 19: 239-250.
- Karnovsky, M. J. 1965 A formaldehyde-glutaraldehyde fixative of high osmolality for use in electron microscopy. *J. Cell Biol.*, 27: 137-138 A.
- Luft, J. H. 1961 Improvements in epoxy resin embedding methods. *J. Biophys. Biochem. Cytol.*, 9: 409-414.
- Palay, S. 1956 Synapses in the central nervous system. *J. Biophys. Biochem. Cytol.*, 2: 193-202.
- Peters A., and J. E. Vaughn 1967 Microtubules and filaments in the axons and astrocytes of early postnatal rat optic nerves. *J. Cell Biol.*, 32: 113-119.
- Piezzi, R. S. 1966 Two types of synapses in the chromaffin tissue of the frog. *Acta Physiol. Lat. Amer.*, 16: 282-285.
- Porter, K. R., M. C. Ledbetter and S. Badenhausen 1964 The microtubule in cell fine structure as an accompaniment of cytoplasmic movements. *Eleventh International Congress of Cell Biology. Excerpta Medica*, 36 A.
- Robertson, J. D. 1959 The electron microscope In: *Tools of Biological Research*. H. J. B. Atkins, ed. Blackwell Sci. Publ. Oxford, pp. 72-121.
- Taylor, A. C., and P. Weiss 1965 Demonstration of axonal flow by the movement of tritium-labeled protein in mature optic nerve fibers. *Proc. Nat. Acad. Sci.*, 54: 1521-1527.
- Venable, J., and R. Coggeshall 1965 The use of simple lead citrate stain in electron microscopy. *J. Cell Biol.*, 25: 407-408.

PLATE 1

EXPLANATION OF FIGURES

- 1, 2 Electron micrographs of cross-sectioned nerve fibers from the adrenal gland illustrating abundant dense-core microtubules (arrows). SC, Satellite cell processes containing numerous filaments (F); p, dense particles of the glycogen type; Bl, basement lamina; Ch, chromaffin cells. $\times 80,000$.

E. L. Rodríguez Echandía, R. S. Pierzi and E. M. Rodríguez

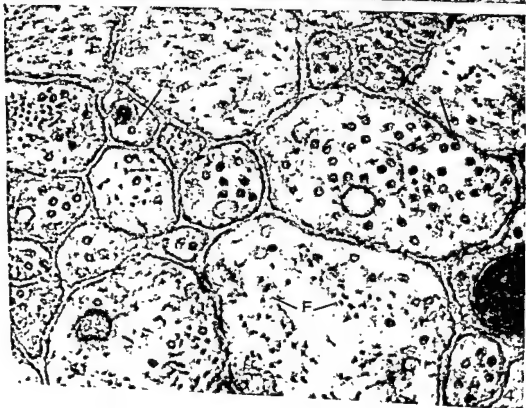


PLATE 2

EXPLANATION OF FIGURES

Perikaryon and cell processes of hypothalamic neurons.

- 3 Low-power view of the juxtannuclear perikaryon showing numerous longitudinally oriented microtubules (m), one of which is reproduced at high magnification in figure 10. M, mitochondria; GC, Golgi complex; N, nucleus; NG, neurosecretory granules; NF, nerve fibers. $\times 24,000$.
- 4 Hypothalamic nerve fibers (cross-section) illustrating dense-core microtubules in their interior (arrows). F, filaments. $\times 110,000$.



PLATE 3

EXPLANATION OF FIGURES

Electron micrographs of the neural stalk.

- 5 Low-power view of the neural stalk illustrating dark arborescent gliocytes (G); a round plasma cell (PC) and close-packing nerve fibers (NF) which contain neurosecretory granules (arrows). $\times 8,800$.

Upper Inset: At higher magnification, the nerve fibers, in this area are found to contain dense-core microtubules (arrow). $\times 80,000$.

Lower Inset: A portion of the cytoplasm of one of the dark gliocytes shown in the figure 5. Dense-core microtubules (arrow) can be also found in these cells. $\times 160,000$.

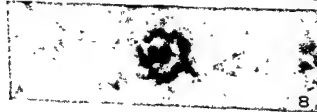
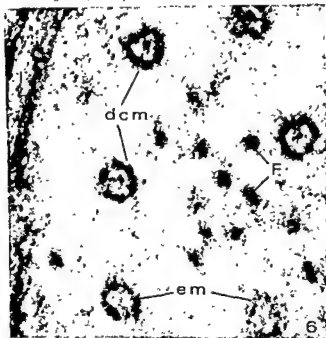


PLATE 4

EXPLANATION OF FIGURES

A group of selected micrographs illustrating dense-core microtubules at high magnification.

- 6 Cross-sectioned nerve fiber from adrenal, containing dense-core microtubules (dcm); empty microtubules (em) and groups of filaments (F). The wall of the microtubules is an aggregation of small condensations. The cell boundary is a typical trilaminar unit membrane. I, interstice. $\times 400,000$.
- 7 Cross-sectioned nerve fiber from adrenal illustrating dense-core microtubules, one of which contains two distinctive granules (arrow). Note that significant variability in the number of condensations building a wall of the microtubule does occur in these images. $\times 600,000$.
- 8 Cross-sectioned microtubules containing three distinctive granules. $\times 600,000$.
- 9 Nerve fiber from adrenal illustrating abundant longitudinally oriented microtubules. They contain central granules (arrows), most of which are irregularly disposed in the center of the lumen. $\times 120,000$.
- 10 High-power micrograph of a longitudinally oriented microtubule in the perikaryon of an hypothalamic neuron. It contains a rosary of granules. $\times 600,000$.

The Fine Structure of Corpora Lutea in Ovarian Transplants of Mice Following Luteotrophin Stimulation¹

THOMAS M. CRISP,² AND HENRY C. BROWNING

Departments of Anatomy, University of Texas Medical Branch, Galveston, Texas, and The University of Texas Dental Branch, Houston, Texas

ABSTRACT Lutein cells from non-functional white corpora lutea of ovulation and functional hyperemic corpora following exogenous luteotrophin stimulation were studied in ovarian isografts of the mouse with the aid of the light and electron microscope. Luteal tissue of white corpora consisted of small parenchymal cells, some intercellular material and a meager vascular bed. Luteal tissue from hyperemic corpora lutea possessed a rich sinusoidal plexus which supplied the hypertrophied lutein cells. At the fine structural level, lutein cells from functional, hyperemic corpora were distinguished from non-functional lutein cells in having a reduced lipid content, well-developed Golgi complex, abundant tubulo-vesicular elements of agranular and granular endoplasmic reticulum, non-motile cilia and a more elaborate folding of the cell membrane into microvillous projections bordering the subendothelial space. The functional significance of these morphological changes of luteal tissue in response to luteotrophin was discussed and correlated with recent biochemical findings of steroidogenic tissue. It was concluded that the presence of luteotrophin following luteinization in mouse ovarian transplants results in numerous morphological changes of luteal tissue which are indicative of progesterone synthesis and secretion.

Ovariectomized mice, bearing intraocular ovarian isologous transplants, show normal vaginal cycles and repeated development of vesicular follicles which luteinize to form white corpora lutea of ovulation or estrus (Browning, Sadler and White, '59). Red corpora lutea, displaying a sinusoidal hyperemia, develop in ovarian transplants during pseudopregnancy (White and Browning, '62), during lactation (Sadler and Browning, '61), in the presence of an anterior pituitary transplant (Browning and White, '62) and as a result of the administration of exogenous luteotrophic hormone (LTH) but not of follicle stimulating (FSH) or luteinizing (LH) hormones (Browning, Larke and White, '62). Further, luteotrophic hormone is essential for development of functional hyperemic corpora in hypophysectomized mice with LH having a synergistic action with it (Browning et al., '65). Evidence of function of hyperemic corpora lutea (i.e., secretion of progesterone) is based on the fact that deciduomata can be induced only when such corpora are present (Browning, Larke and White, '62).

Sadler and Browning ('61), using paraffin embedded material, have compared lutein cells taken from hyperemic corpora with those taken from non-functional corpora lutea. However, there has been no description or comparison of the fine structure of such corpora. On the other hand, Enders and Lyons ('64), and more recently, Rennels ('66), have studied active and inactive luteal tissues of prepubertal rats following gonadotrophin administration. These workers have described differences in the fine structure of cytoplasmic organelles between such lutein tissues. In general, active lutein cells were distinguished from inactive lutein cells in having: (1) a reduced lipid content, (2) well-developed mitochondria exhibiting tubular cristae and a more electron-dense intramitochondrial matrix, (3) abundant tubulo-vesicular elements of agranular endoplasmic reticulum and (4) numerous and

¹This work supported by NIH Training grant ST1 GM 459 and in part by U.S.P.H.S. Research grant CA02830.

²Present Address: Department of Anatomy, Georgetown University Schools of Medicine, Dentistry, Washington, D. C.

The Fine Structure of Corpora Lutea in Ovarian Transplants of Mice Following Luteotrophin Stimulation¹

THOMAS M. CRISP,¹ AND HENRY C. BROWNING

Departments of Anatomy, University of Texas Medical Branch, Galveston, Texas, and The University of Texas Dental Branch, Houston, Texas

ABSTRACT Lutein cells from non-functional white corpora lutea of ovulation and functional hyperemic corpora following exogenous luteotrophin stimulation were studied in ovarian isotransplants of the mouse with the aid of the light and electron microscope. Luteal tissue of white corpora consisted of small parenchymal cells, some intercellular material and a meager vascular bed. Luteal tissue from hyperemic corpora lutea possessed a rich sinusoidal plexus which supplied the hypertrophied lutein cells. At the fine structural level, lutein cells from functional, hyperemic corpora were distinguished from non-functional lutein cells in having a reduced lipid content, well-developed Golgi complex, abundant tubulo-vesicular elements of agranular and granular endoplasmic reticulum, non-motile cilia and a more elaborate folding of the cell membrane into microvillous projections bordering the subendothelial space. The functional significance of these morphological changes of luteal tissue in response to luteotrophin was discussed and correlated with recent biochemical findings of steroidogenic tissue. It was concluded that the presence of luteotrophin following luteinization in mouse ovarian transplants results in numerous morphological changes of luteal tissue which are indicative of progesterone synthesis and secretion.

Ovariectomized mice, bearing intraocular ovarian isologous transplants, show normal vaginal cycles and repeated development of vesicular follicles which luteinize to form white corpora lutea of ovulation or estrus (Browning, Sadler and White, '59). Red corpora lutea, displaying a sinusoidal hyperemia, develop in ovarian transplants during pseudopregnancy (White and Browning, '62), during lactation (Sadler and Browning, '61), in the presence of an anterior pituitary transplant (Browning and White, '62) and as a result of the administration of exogenous luteotrophic hormone (LTH) but not of follicle stimulating (FSH) or luteinizing (LH) hormones (Browning, Larke and White, '62). Further, luteotrophic hormone is essential for development of functional hyperemic corpora in hypophysectomized mice with LH having a synergistic action with it (Browning et al., '65). Evidence of function of hyperemic corpora lutea (i.e., secretion of progesterone) is based on the fact that deciduomata can be induced only when such corpora are present (Browning, Larke and White, '62).

Sadler and Browning ('61), using paraffin embedded material, have compared lutein cells taken from hyperemic corpora with those taken from non-functional corpora lutea. However, there has been no description or comparison of the fine structure of such corpora. On the other hand, Enders and Lyons ('64), and more recently, Rennels ('66), have studied active and inactive luteal tissues of prepubertal rats following gonadotrophin administration. These workers have described differences in the fine structure of cytoplasmic organelles between such lutein tissues. In general, active lutein cells were distinguished from inactive lutein cells in having: (1) a reduced lipid content, (2) well-developed mitochondria exhibiting tubular cristae and a more electron-dense intramitochondrial matrix, (3) abundant tubulo-vesicular elements of agranular endoplasmic reticulum and (4) numerous and

¹ This work supported by N.I.H. Training grant 5T1 GM 459 and in part by U.S.P.H.S. Research grant CA02830.

² Present Address: Department of Anatomy, Georgetown University Schools of Medicine, Dentistry, Washington, D. C.

well-developed villous processes of the cell surface bordering the perivascular space. These morphological observations correlate well with recent biochemical findings on enzymes associated with mitochondrial and microsomal fractions which are important in the biosynthesis of sex steroid hormones (Toren, Menon, Forchielli and Dorfman, '64; Blanchette, '66a; Chesterton, '66; Davenport and Mallette, '66).

The present report concerns observations on the two types of corpora lutea taken from female mice bearing intraocular ovarian isografts. More specifically, we wish to report fine structural differences of luteal cells taken from red hyperemic corpora, representing functionally active tissue, with that from white corpora lutea of ovulation or estrus, representing non-functional luteal tissue. A preliminary report has been presented in abstract (Crisp, '65).

MATERIALS AND METHODS

Two months old BALB/c virgin female mice were ovariectomized. At this time they also received bilateral intraocular transplants of one-eighth of an isologous ovary (Browning, Sadler and White, '59). Three weeks after transplantation vaginal smears and ovarian transplant morphology (made under a dissecting binocular microscope at 20 \times) were followed daily to confirm the re-establishment of normal estrous cycles. Mature vesicular follicles appeared during late proestrous and estrous stages, subsequently followed by luteinization on the first day of metestrus. After exhibiting a brief period of hyperemia such corpora lutea of ovulation became white in color. White corpora lutea failed to support decidual maturation following uterine trauma (White and Browning, '62). These non-functional corpora were studied in the present investigation. Two mice, possessing two to four non-functional corpora within each intraocular ovarian graft were killed on the first day the transplant exhibited white corpora lutea.

Functional, red corpora lutea were obtained experimentally by the daily injection of 5 μ g LH¹ given intraperitoneally and 40 μ g LTH² administered subcutaneously beginning on the first day of metestrus

when corpora exhibited an ephemeral hyperemia. Two mice, possessing two to four hyperemic corpora within each graft, were killed on the fourth day of hormone injection.

Ovarian transplants containing either red or white corpora lutea were dissected from the anterior chamber of the eye of anesthetized mice and placed in cold phosphate-buffered 6% glutaraldehyde solution at pH 7.4 (Sabatini, Bensch and Barnett, '63). Glutaraldehyde, as the initial fixative, maintained the coloration of the hyperemic corpora, thus facilitating recognition of the luteal tissue during dissection of the ovarian transplant. Using a dissecting microscope, individual corpora were first isolated and then cut into small pieces approximately one-fourth the size of an original corpus. The cut pieces were immediately transferred to vials containing cold s-collidine-buffered 1% osmium tetroxide solution at pH 7.4 as described by Bennett and Luft ('59). Sucrose was added to the latter fixative in a concentration of 0.045 gm/ml and calcium chloride at 0.2 gm/ml.

Following a two hour fixation period, tissues were dehydrated quickly in ascending grades of cold ethyl alcohols and embedded in Epon 812 according to the method of Luft ('61). The material was sectioned with glass knives on a Porter-Blum ultramicrotome. Sections displaying gold interference colors with fluorescent lighting were mounted, unsupported, on number 200 mesh copper grids and stained with lead citrate (Reynolds, '63) or uranyl acetate and lead citrate. Sections were examined in an RCA EMU 3 G electron microscope using 50 KV accelerating voltages. Epoxy sections for light microscopy, approximately one-half to one micron in thickness, were stained with toluidine blue (Trump et al., '61).

RESULTS

A. *Light microscopic observations.* A comparison of functional and non-functional luteal tissue was made and marked

¹ LH-NIH-S-3, Lutalizing hormone generously supplied by the Endocrine Study Section National Institutes of Health.

² LTH-NIH-P-5-3, Luteotrophic, Prolactin, Lactogenic or Mammatrophic hormone supplied by Endocrine Study Section.

differences in tissue morphology between red and white corpora lutea were observed at both the light and electron microscopic levels. The newly-formed white corpus of ovulation consisted of a compact mass of lutein cells, some amorphous intercellular material and a relatively meager vascular bed (fig. 1). In any one section of this tissue few erythrocytes were present within the vascular spaces. The luteal cells were small (approximately $10\ \mu$ in diameter), and possessed a small amount of cytoplasm. These cells contained large lipid droplets of varying diameters. The lipid droplets were partially extracted with organic solvents during processing for electron microscopy and consequently appeared as light spherical bodies with dark rims. The nuclei of these cells were approximately $6\ \mu$ in diameter, irregularly shaped and possessed several clumps of chromatin material.

Hyperemic corpora lutea, on the other hand, consisted of hypertrophied lutein cells and a rich vascular bed (fig. 2). The sinusoidal plexus was engorged with erythrocytes and its endothelial cell lining was readily discernible in sections of luteal tissue. The lutein cells from luteotrophin-stimulated, hyperemic corpora were more than twice as large as those cells from non-functional corpora lutea. These active lutein cells had diameters of approximately 20 to $25\ \mu$. Some of the lutein cells of red corpora lutea appeared to lack lipid droplets, while others contained small droplets of uniform diameter dispersed throughout the cytoplasm. The nuclei of these hypertrophied cells were large ($8.5\ \mu$ in diameter) and well-rounded.

B. Electron microscopic observations. At the fine structural level, lutein cells of white corpora lutea differed from lutein cells of hyperemic corpora in a number of aspects. The small inactive luteal cells possessed oval to round-shaped mitochondria exhibiting tubulo-vesicular cristae which almost completely filled the interior of the organelle, thus leaving little intramitochondrial matrix (figs. 3, 4, 5). Another major component of luteal cells from non-functional corpora was the large number of lipid droplets. These droplets were quite variable in size and appearance.

Sometimes the central core of osmiophilic lipid material was absent, leaving a peripheral or cortical rim of lipid material intact (figs. 3, 4). At other times the lipid was better preserved and the central core of lipid was retained (fig. 5). In general, the preservation of lipid droplets was better in lutein cells of white corpora than in those cells of functional hyperemic corpora.

The endoplasmic reticulum of the small inactive luteal cell was sparse. It consisted of a few, short anastomosing tubules (approximately 30 to $60\ m\mu$ in diameter). Both granular and smooth-surfaced forms were present in about equal amounts (figs. 3, 5). The cisterna of agranular endoplasmic reticulum sometimes communicated with those tubules that possessed attached ribonucleoprotein particles. In some instances the agranular form of this organelle appeared vesicular rather than tubular (fig. 5).

Regions of Golgi membranes and associated vesicles were observed near the nucleus of these luteal cells. Occasionally small membrane-bound granules (approximately $150\ m\mu$ in diameter) were also observed.

Lutein cells of non-functional, white corpora possessed abundant fine granular material within their cytoplasm. These granules were considered to be free ribosomes, sometimes dispersed singly throughout the lutein cell cytoplasm (fig. 3). In some sections these granules were clustered together and therefore thought to represent polyribosomes (fig. 5).

Another characteristic of luteal cells of non-functional corpora was the minimal folding and relatively smooth cell margin associated with the narrow perivascular space (fig. 4). In some sections, apposition between adjacent lutein cells was relatively smooth and close (fig. 5). Occasionally one cell interdigitated with a neighboring cell. Desmosomes were never observed between luteal cells of white corpora. In many sections a definite intercellular space was observed. This space contained an amorphous intercellular ground substance and fine fibrillar material (fig. 3) and was continuous with the subendothelial space.

Besides exhibiting a cellular hypertrophy, active lutein cells from hyperemic corpora lutea possessed fewer lipid droplets than lutein cells of white corpora. In addition, the lipid droplets showed a reduced diameter and an increased tendency for lipid extraction, particularly the central core of the droplet (figs. 6, 8). Occasionally small osmiophilic inclusions (150 to 300 μ in diameter), which were considered to be lipid droplets, were seen within the microvillous projections bordering the subendothelial space (fig. 7).

Mitochondria of lutein cells from gonadotrophin-stimulated corpora lutea were round to oval in shape and possessed tubulovesicular cristae. In general no difference in the fine structure of mitochondria of lutein cells from either white or red corpora was detected.

The Golgi apparatus of active lutein cells was prominent and appeared more extensive in these cells than those of nonfunctional corpora (figs. 6, 8). In some sections this complex incompletely invested the nucleus. Like lutein cells of white corpora, membrane-bound granules (200–300 μ in diameter) were also present in active luteal tissue of hyperemic corpora.

Probably the most striking difference between active and inactive lutein cells was the increased amount of smooth-surfaced and granular forms of the endoplasmic reticulum in the luteal cells of hyperemic corpora. These elements of endoplasmic reticulum sometimes appeared as slender tubules in parallel array (figs. 6, 8, 11). In addition, the smooth-surfaced variety of this organelle consisted of anastomosing tubules or small dilated vesicles. The increase in both the agranular and granular endoplasmic reticulum following gonadotrophic hormone stimulation occurred throughout the cytoplasm, but some areas of the cell exhibited more abundant elements of this organelle than others. The smooth-surfaced form of the endoplasmic reticulum was frequently and intimately related with mitochondria (fig. 11).

Characteristic of active lutein cells was the presence of numerous microvillous projections of these cells into the subendothelial space (fig. 7). Further, the perivascular space was more extensive in hyperemic

corpora, accommodating these cytoplasmic projections. A definite basement membrane was present between the endothelium of the sinusoid and the perivascular space (fig. 7). Apposition of functional luteal cells was usually close and sometimes smooth. Occasionally increased densities were present in regions of very close apposition of adjacent lutein cells (fig. 8).

A common finding in many lutein cells of active hyperemic corpora was the presence of non-motile cilia, exhibiting the 9 + 0 pattern. Usually a single ciliary process projected from a basal body or distal centriole into the intercellular space (fig. 10). Occasionally a cilium was associated with a proximal centriole exhibiting the nine triplet fibrils (fig. 9). Cilia were never observed in inactive luteal cells.

DISCUSSION

Since the early work of Deansley ('30b), the corpus luteum of pregnancy or pseudopregnancy was distinguished from the corpus luteum of ovulation in the mouse by the increased vascular bed of functionally active corpora lutea. Confirmation of this finding by direct visualization of corpora lutea in intraocular ovarian transplants enabled Browning and co-workers to correlate the vascularity of the corpus luteum with luteotrophic activity. The present report provided further evidence for relating luteotrophic action with increases in the sinusoidal capillary plexus of active luteal tissue. Upon sections of glutaraldehyde-osmic acid fixed hyperemic corpora exhibited increased regions of blood-filled sinusoids which probably corresponded to the "islands of red blood cells" seen by Sadler and Browning ('61), in their paraffin embedded material. In tissue hyperemia presumably accounts for the red coloration of such corpora seen *in situ*. In marked contrast, sections of nonfunctional, white corpora lutea of ovulation possessed a meager vascular bed. This difference in vascularity is in keeping with the endocrine activity exhibited by these two types of corpora lutea, the highly vascularized tissue being associated with cells that are actively engaged in secretion of progesterone (Sadler and Browning, '61; Browning, Larke and White, '62).

The increase in size of the lutein cells stimulated with luteotrophin has been used by Wolthuis ('63), as a direct assay of this hormone. He found an almost linear inverse relationship between the number of lutein cell nuclei per unit area and the logarithm of the dose of LTH. In the present study, four injections of 40 μ g LTH daily, beginning on the first day of metestrus, more than doubled the average lutein cell diameter. The size of lutein cells taken from the two types of corpora in this study agreed remarkably with the earlier report of Deansley ('30a), for mouse lutein cells of corpora of ovulation and cells of corpora lutea of mid-pregnancy.

In general, the fine structural differences observed between functional and non-functional luteal tissue of mouse ovarian transplants agreed with those observations reported by Enders and Lyons ('64) and Rennels ('66), in their studies of active and inactive luteal tissue of the gonadotrophin-treated immature rat.

Lutein cells of hyperemic corpora lutea possessed a reduced lipid content and showed a greater degree of lipid extraction of these inclusions than did the lutein cells of nonfunctional, white corpora. If the lipid droplets seen in lutein cells of white corpora represent a storage or reservoir of cholesterol or some other precursor of progestational hormone, as has been suggested by Blanchette ('66b), in her study of rabbit lutein tissue, then the reduced lipid content of mouse lutein cells following LTH stimulation might represent mobilization of cholesterol toward progesterone synthesis. This idea is in agreement with the studies of Everett ('45), ('47), who showed that LH was responsible for cholesterol deposition or storage in corpora lutea while LTH caused utilization or depletion of luteal cholesterol in the rat.

No difference in the fine structure of mitochondria of lutein cells from either white or hyperemic corpora was observed in the present investigation. In addition, "cup-shaped" forms of this organelle were never seen in lutein cells of either red or white corpora. These observations were in marked contrast to that reported for the rat by Enders and Lyons ('64) and confirmed by Rennels ('66), who noted that

active lutein cells possessed mitochondria exhibiting a more electron-dense matrix than did those of mitochondria from inactive lutein cells. Further, Rennels ('66), showed that active lutein cells possessed a more elaborate system of tubular cristae of mitochondria and suggested that changes in the structure of this organelle along with increases in the smooth-surfaced endoplasmic reticulum might be related to increases in enzymes responsible for the conversion of cholesterol to progesterone. While it is well established that the "cholesterol side-chain cleavage" enzyme resides in mitochondrial fractions of rat testicular tissue (Toren, Menon, Forchielli and Dorfman, '64), it is not known whether this enzyme is associated with mitochondria of mouse lutein tissue. In a recent study on the fine structure of mouse interstitial cells (BALB/c strain), Christensen and Fawcett ('66), suggested the need to establish, biochemically, the presence of the "cholesterol side-chain cleavage" enzyme system within mitochondria of mouse Leydig cells. It is conceivable that species differences might occur and thus account for the failure to observe fine structural differences in mitochondria in the present study. However, this failure does not necessarily eliminate the participation of this organelle in the biosynthesis of steroid hormones.

The increase in both granular and agranular types of endoplasmic reticulum of lutein cells taken from mice following luteotrophin administration was most striking. While lutein cells of white corpora exhibited reduced, but approximately equal quantities of the rough and smooth-surfaced forms of this organelle, the lutein cells of functional, hyperemic corpora possessed much greater amounts of the agranular form of endoplasmic reticulum than that of the granular variety. The abundance of agranular endoplasmic reticulum in lutein cells of functional red corpora lutea and its scarcity in lutein cells of non-functional white corpora is in agreement with the observations of Enders and Lyons ('64) and Rennels ('66), for the rat. The biochemical study of Chesterton ('66), indicated that the conversion of labelled mevalonic acid to cholesterol was

Besides exhibiting a cellular hypertrophy, active lutein cells from hyperemic corpora lutea possessed fewer lipid droplets than lutein cells of white corpora. In addition, the lipid droplets showed a reduced diameter and an increased tendency for lipid extraction, particularly the central core of the droplet (figs. 6, 8). Occasionally small osmiophilic inclusions (150 to 300 $m\mu$ in diameter), which were considered to be lipid droplets, were seen within the microvillous projections bordering the subendothelial space (fig. 7).

Mitochondria of lutein cells from gonadotrophin-stimulated corpora lutea were round to oval in shape and possessed tubulovesicular cristae. In general no difference in the fine structure of mitochondria of lutein cells from either white or red corpora was detected.

The Golgi apparatus of active lutein cells was prominent and appeared more extensive in these cells than those of nonfunctional corpora (figs. 6, 8). In some sections this complex incompletely invested the nucleus. Like lutein cells of white corpora, membrane-bound granules (200–300 $m\mu$ in diameter) were also present in active luteal tissue of hyperemic corpora.

Probably the most striking difference between active and inactive lutein cells was the increased amount of smooth-surfaced and granular forms of the endoplasmic reticulum in the luteal cells of hyperemic corpora. These elements of endoplasmic reticulum sometimes appeared as slender tubules in parallel array (figs. 6, 8, 11). In addition, the smooth-surfaced variety of this organelle consisted of anastomosing tubules or small dilated vesicles. The increase in both the agranular and granular endoplasmic reticulum following gonadotrophic hormone stimulation occurred throughout the cytoplasm, but some areas of the cell exhibited more abundant elements of this organelle than others. The smooth-surfaced form of the endoplasmic reticulum was frequently and intimately related with mitochondria (fig. 11).

Characteristic of active lutein cells was the presence of numerous microvillous projections of these cells into the subendothelial space (fig. 7). Further, the perivascular space was more extensive in hyperemic

corpora, accommodating these cytoplasmic projections. A definite basement membrane was present between the endothelium of the sinusoid and the perivascular space (fig. 7). Apposition of functional luteal cells was usually close and sometimes smooth. Occasionally increased densities were present in regions of very close apposition of adjacent lutein cells (fig. 8).

A common finding in many lutein cells of active hyperemic corpora was the presence of non-motile cilia, exhibiting the 9 + 0 pattern. Usually a single ciliary process projected from a basal body or distal centriole into the intercellular space (fig. 10). Occasionally a cilium was associated with a proximal centriole exhibiting the nine triplet fibrils (fig. 9). Cilia were never observed in inactive luteal cells.

DISCUSSION

Since the early work of Deansley ('30b), the corpus luteum of pregnancy or pseudopregnancy was distinguished from the corpus luteum of ovulation in the mouse by the increased vascular bed of functionally active corpora lutea. Confirmation of this finding by direct visualization of corpora lutea in intraocular ovarian transplants enabled Browning and co-workers to correlate the vascularity of the corpus luteum with luteotrophic activity. The present report provided further evidence for relating luteotrophic action with increases in the sinusoidal capillary plexus of active luteal tissue. Epon sections of glutaraldehyde-osmic acid fixed hyperemic corpora exhibited increased regions of blood-filled sinusoids which probably corresponded to the "islands of red blood cells" seen by Sadler and Browning ('61), in their paraffin embedded material. This tissue hyperemia presumably accounts for the red coloration of such corpora seen *in situ*. In marked contrast, sections of non-functional, white corpora lutea of ovulation possessed a meager vascular bed. This difference in vascularity is in keeping with the endocrine activity exhibited by these two types of corpora lutea, the highly vascularized tissue being associated with cells that are actively engaged in secretion of progesterone (Sadler and Browning, '61; Browning, Larke and White, '62).

The increase in size of the lutein cells stimulated with luteotrophin has been used by Wolthuis ('63), as a direct assay of this hormone. He found an almost linear inverse relationship between the number of lutein cell nuclei per unit area and the logarithm of the dose of LTH. In the present study, four injections of 40 μ g LTH daily, beginning on the first day of metestrus, more than doubled the average lutein cell diameter. The size of lutein cells taken from the two types of corpora in this study agreed remarkably with the earlier report of Deansley ('30a), for mouse lutein cells of corpora of ovulation and cells of corpora lutea of mid-pregnancy.

In general, the fine structural differences observed between functional and non-functional luteal tissue of mouse ovarian transplants agreed with those observations reported by Enders and Lyons ('64) and Rennels ('66), in their studies of active and inactive luteal tissue of the gonadotrophin-treated immature rat.

Lutein cells of hyperemic corpora lutea possessed a reduced lipid content and showed a greater degree of lipid extraction of these inclusions than did the lutein cells of nonfunctional, white corpora. If the lipid droplets seen in lutein cells of white corpora represent a storage or reservoir of cholesterol or some other precursor of progesterone hormone, as has been suggested by Blanchette ('66b), in her study of rabbit lutein tissue, then the reduced lipid content of mouse lutein cells following LTH stimulation might represent mobilization of cholesterol toward progesterone synthesis. This idea is in agreement with the studies of Everett ('45), ('47), who showed that LH was responsible for cholesterol deposition or storage in corpora lutea while LTH caused utilization or depletion of luteal cholesterol in the rat.

No difference in the fine structure of mitochondria of lutein cells from either white or hyperemic corpora was observed in the present investigation. In addition, "cup-shaped" forms of this organelle were never seen in lutein cells of either red or white corpora. These observations were in marked contrast to that reported for the rat by Enders and Lyons ('64) and confirmed by Rennels ('66), who noted that

active lutein cells possessed mitochondria exhibiting a more electron-dense matrix than did those of mitochondria from inactive lutein cells. Further, Rennels ('66), showed that active lutein cells possessed a more elaborate system of tubular cristae of mitochondria and suggested that changes in the structure of this organelle along with increases in the smooth-surfaced endoplasmic reticulum might be related to increases in enzymes responsible for the conversion of cholesterol to progesterone. While it is well established that the "cholesterol side-chain cleavage" enzyme resides in mitochondrial fractions of rat testicular tissue (Toren, Menon, Forchielli and Dorfman, '64), it is not known whether this enzyme is associated with mitochondria of mouse lutein tissue. In a recent study on the fine structure of mouse interstitial cells (BALB/c strain), Christensen and Fawcett ('66), suggested the need to establish, biochemically, the presence of the "cholesterol side-chain cleavage" enzyme system within mitochondria of mouse Leydig cells. It is conceivable that species differences might occur and thus account for the failure to observe fine structural differences in mitochondria in the present study. However, this failure does not necessarily eliminate the participation of this organelle in the biosynthesis of steroid hormones.

The increase in both granular and agranular types of endoplasmic reticulum of lutein cells taken from mice following luteotrophin administration was most striking. While lutein cells of white corpora exhibited reduced, but approximately equal quantities of the rough and smooth-surfaced forms of this organelle, the lutein cells of functional, hyperemic corpora possessed much greater amounts of the agranular form of endoplasmic reticulum than that of the granular variety. The abundance of agranular endoplasmic reticulum in lutein cells of functional red corpora lutea and its scarcity in lutein cells of non-functional white corpora is in agreement with the observations of Enders and Lyons ('64) and Rennels ('66), for the rat. The biochemical study of Chesterton ('66), indicated that the conversion of labelled mevalonic acid to cholesterol was

associated in part with the microsomal fraction of rat liver. Further, Blanchette ('66a), and Davenport and Mallette ('60), have shown that microsomal fractions of rat and rabbit ovaries, respectively, exhibited $\Delta^1-3\beta$ -hydroxysteroid dehydrogenase activity, an important enzyme in the conversion of pregnenolone to progesterone. Thus the presence of agranular endoplasmic reticulum in luteal tissue of the mouse is in keeping with the general idea that this morphological entity is associated with enzymes necessary for the biosynthesis of a steroid hormone, and that increases in this organelle in response to LTH stimulation presumably reflects increases in the biosynthesis of progesterone or its precursors.

It was interesting to note that luteotrophin increased the amount of the rough-surfaced variety of endoplasmic reticulum in addition to that of the agranular form. It is generally agreed that the extensive presence of this organelle (at least the ribosomal portion) is associated with protein synthesis. Perhaps the increased occurrence of this organelle in LTH-stimulated lutein cells indicates increased synthesis of steroidogenic enzymes or other proteins concerned with the general increased metabolism of active luteal tissue. It was of further interest to note the presence of abundant free ribosomes, singly or in clusters, concomitant with the paucity of a well-developed vacuolar system. Conceivably under the influence of luteotrophin the ribonucleoprotein material of non-functional white corpora lutea might represent the site of new membrane formation which gives rise to the abundant endoplasmic reticulum observed in lutein cells of functional corpora.

The Golgi apparatus of active lutein cells was more extensive than that observed in lutein cells of white corpora. This observation was in agreement with Rennels ('66), who also observed a greater development of Golgi complexes in active lutein cells of the rat. While membrane-bound granules were sometimes seen in association with Golgi membranes in both types of luteal cells in the present study, it was not apparent that lipid droplets were being formed from this complex, as men-

tioned by Yamada and Ishikawa ('60), in their study of mouse corpora lutea of late pregnancy.

Active lutein cells were distinguished from inactive ones by the greater folding of the cell surface along the perivascular space. This increase in the surface area by the microvillous projection of functional luteal tissue concomitant with the increased vascular bed of such tissue correlates well with the known secretory activity of this endocrine tissue. While small lipid droplets were sometimes seen within the cell protrusions along the subendothelial space, no good morphological evidence at the fine structural level for a "secretory product" was observed. Further, we have never observed the penetration of lutein cell cytoplasm into the sinusoidal lumen as reported by Yamada and Ishikawa ('60), in mouse luteal tissue and recently by Brenner ('66), in monkey adrenocortical tissue.

The presence of cilia in cells of the corpus luteum following administration of gonadotrophic hormone and their apparent absence in inactive luteal cells was an unexpected observation. Previous reports of cilia in steroid-producing cells have been made, but to the authors' knowledge, this is the first report of such a finding in luteal tissue. Enders and Lyons ('64), observed centrioles in luteal cells of the rat ovary and Rhodin ('63), demonstrated them in mouse lutein cells, but neither author mentioned cilia associated with such organelles. Crabo ('63), observed a "small flagellum" protruding from a centriole of an interstitial cell from a rabbit testis, and Adams and Hertig ('64), observed a rudimentary cilium projecting from a centriole in follicular cells in their study of guinea pig oocytes. Recently, Wheatley ('67), studied cilia and centrioles of rat adrenocortical cells. In the latter study centrioles having the appearance of basal bodies were found in cells of the inner cortical zones, but unlike the cells of the zona glomerulosa, no cilia were observed in those regions. The function of these solitary, nonmotile processes in luteal tissue or any other endocrine tissue remains an enigma. Barnes ('61), in her study of ciliated secretory cells of the pars distalis of the mouse, cor-

related an increased frequency of cilia with increased metabolic and hormonal activity of the gland. Perhaps the presence of cilia in luteal cells that are known to be functionally active (i.e., secreting progesterone) might represent a similar phenomenon and thus add further support to the hypothesis of Barnes ('61), that nonmotile cilia probably represent a degenerate and functionally modified structure.

LITERATURE CITED

- Adams, E. C., and A. T. Hertig 1964 Studies on guinea pig oocytes. Electron microscopic observations on the development of cytoplasmic organelles in oocytes of primordial and primary follicles. *J. Cell Biol.*, 21: 397-427.
- Barnes, B. G. 1961 Ciliated secretory cells in the pars distalis of the mouse hypophysis. *J. Ultrastruct. Res.*, 5: 453-467.
- Bennett, H. S., and J. H. Luft 1959 α -Collidine as a basis for buffering fixatives. *J. Biophys. and Biochem. Cytol.*, 6: 113-114.
- Blanchette, E. J. 1966a The fine structure of the endoplasmic reticulum of "luteinized" ovarian cells and isolated microsomes in relation to Δ^4 -3 β -hydroxysteroid dehydrogenase activity. *Anat. Rec.*, 154: 318.
- 1966b Ovarian steroid cells: II. The lutein cell. *J. Cell Biol.*, 31: 517-542.
- Brenner, R. M. 1966 Fine structure of adrenocortical cells in adult male Rhesus monkeys. *Am. J. Anat.*, 119: 429-454.
- Browning, H. C., W. A. Sadler and W. D. White 1959 Isologous and homologous transplants of ovarian tissue in the anterior eye chambers of intact and castrated male and female mice of inbred strains. *Am. J. Anat.*, 105: 81-116.
- Browning, H. C., and W. D. White 1962 Luteotropic activity in mice bearing anterior pituitary transplants. *Texas Rep. Biol. Med.*, 20: 570-586.
- Browning, H. C., G. A. Larke and W. D. White 1962 Action of purified gonadotropins on corpora lutea in the cyclic mouse. *Proc. Soc. Exp. Med. Biol.*, 111: 686-690.
- Browning, H. C., A. L. Brown, T. M. Crisp and W. E. Gibbs 1965 Response of ovarian iso-grafts to purified FSH, LH, and LTH in partially and completely hypophysectomized mice. *Texas Rep. Biol. Med.*, 23: 715-728.
- Chesterton, C. J. 1966 The subcellular site of cholesterol synthesis in rat liver. *Biochem. Biophys. Res. Commun.*, 25: 205.
- Christensen, A. K., and D. W. Fawcett 1966 The fine structure of testicular interstitial cells in mice. *Am. J. Anat.*, 118: 551-572.
- Crabo, B. 1963 Fine structure of the interstitial cells of the rabbit testes. *Z. f. Zellforsch.*, 61: 587-604.
- Crisp, T. M. 1965 Observations on the fine structure of lutein cells in mice. *Anat. Rec.*, 151: 340.
- Davenport, G. A., and L. E. Mallette 1966 Some biochemical properties of rabbit ovarian hydroxysteroid dehydrogenases. *Endocrinology*, 78: 672-678.
- Deansley, R. 1930a The corpora lutea of the mouse, with special reference to fat accumulation during the oestrus cycle. *Proc. Roy. Soc. B.*, 106: 578-595.
- 1930b The development and vascularization of the corpus luteum in the mouse and rabbit. *Proc. Roy. Soc. B.*, 107: 60-76.
- Enders, A. C., and W. R. Lyons 1964 Observations on the fine structure of lutein cells. II. The effects of hypophysectomy and mammothrophic hormone in the rat. *J. Cell Biol.*, 22: 127-141.
- Everett, J. W. 1945 The microscopically demonstrable lipids of cyclic corpora lutea in the rat. *Am. J. Anat.*, 77: 293-323.
- 1947 Hormonal factors responsible for deposition of cholesterol in the corpus luteum of the rat. *Endocrinology*, 41: 364-377.
- Luft, J. H. 1961 Improvements in epoxy resin embedding methods. *J. Biophys. and Biochem. Cytol.*, 9: 409-414.
- Muta, T. 1958 The fine structure of the interstitial cell in the mouse ovary studied with electron microscope. *Kurume Med. J.*, 5: 167-185.
- Renness, E. G. 1966 Observations on the ultrastructure of luteal cells from PMS and PMS-HCG treated immature rats. *Endocrinology*, 79: 373-386.
- Reynolds, E. S. 1963 The use of lead citrate at high pH as an electron-opaque stain in electron microscopy. *J. Cell Biol.*, 17: 203-212.
- Rhodin, J. A. G. 1963 An atlas of ultrastructure. W. B. Saunders Co., Philadelphia and London, 122-123.
- Sabatini, D. D., K. G. Bensch and R. J. Barnett 1963 Cytochemistry and electron microscopy. The preservation of cellular ultrastructure and enzymatic activity by aldehyde fixation. *J. Cell Biol.*, 17: 19-58.
- Sadler, W. A., and H. C. Browning 1961 Gonadotropin secretion in lactating mice. *Proc. Soc. Exp. Biol. and Med.*, 106: 558-562.
- Toren, D., K. M. J. Menon, E. Forchelli and R. I. Dorfman 1964 *In vitro* enzymatic cleavage of the cholesterol side-chain in rat testis preparations. *Steroids*, 3: 381-390.
- Trump, B. F., E. A. Smuckler and E. P. Benditt 1961 A method for staining epoxy sections for light microscopy. *J. Ultrastruct. Res.*, 5: 343-348.
- Wheatley, D. N. 1967 Cilia and centrioles of the rat adrenal cortex. *J. Anat.*, 101: 223-237.
- White, W. D., and H. C. Browning 1962 Evidence for the periodic release of pituitary luteotropic during the estrus cycle of the mouse. *Texas Rep. Biol. Med.*, 20: 484-493.

Wolthuis, O. L. 1963 An assay of prolactin based on a direct effect of this hormone on cells of the corpus luteum. *Acta Endocr.*, 42: 364-379.

Yamada, E., and T. M. Ishikawa 1960 The fine structure of the corpus luteum in the mouse ovary as revealed by electron microscopy *Kyushu J. Med. Sci.*, 11: 235-257.

PLATE 1

EXPLANATION OF FIGURES

- 1 Photomicrograph of one micron thick section of Epon-embedded mouse corpus luteum of ovulation. This tissue is composed of numerous, small luteal cells possessing irregularly shaped nuclei and sparse amounts of cytoplasm. Numerous large lipid droplets, appearing as white spherical bodies within the cell cytoplasm, can be observed in this figure. The vascular bed is meager but obvious at the small arrows indicating sectioned erythrocytes. Toluidine blue stain. $\times 800$.
- 2 Photomicrograph of luteal tissue from hyperemic corpus luteum of a mouse receiving gonadotrophic hormones. This micrograph is of the same magnification as the above figure. Tissue from hyperemic corpora is composed of luteal cells possessing large, round nuclei and abundant cytoplasm. These hypertrophied cells are supplied by a rich sinusoidal plexus lined by endothelial cells (at arrows). Numerous erythrocytes engorge these dilated sinusoidal spaces (S) and probably contribute to the red color of the functional corpus luteum. Some luteal cells in section appear to lack lipid droplets while others possess uniform and smaller deposits than those seen in the above figure. Toluidine blue stain. $\times 800$.

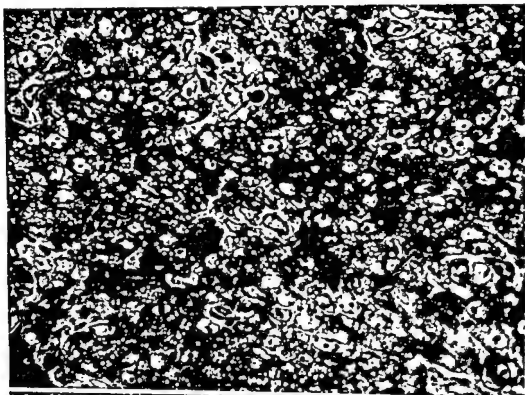


PLATE 2

EXPLANATION OF FIGURE

- 3 Electron micrograph of parts of several luteal cells from a mouse corpus luteum of ovulation. These cells possess rounded mitochondria (M) with tubulo-vesicular cristae and numerous lipid droplets (L), many of which have been partially extracted during processing. Elements of endoplasmic reticulum with attached ribosomes are evident, while the smooth-surfaced variety of this organelle is sparse. Note the fine granular nature of the lutein cell cytoplasm. These granules are thought to be free ribosomes. Some fibrillar material (arrows) can be observed in the intercellular space. Lead citrate. $\times 12,200$.

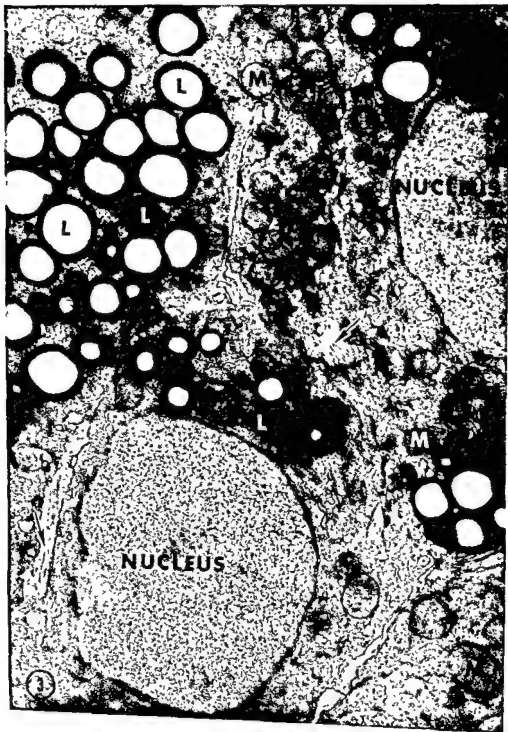


PLATE 3

EXPLANATION OF FIGURE

- 4 Electron micrograph of luteal cells from a mouse corpus luteum of ovulation in association with an endothelial cell lining the lumen of a sinusoid. The apposition of these luteal cells with the endothelium along the narrow subendothelial space (at arrows) is relatively smooth. (See fig. 9 for comparison). Lead citrate, $\times 13,200$.

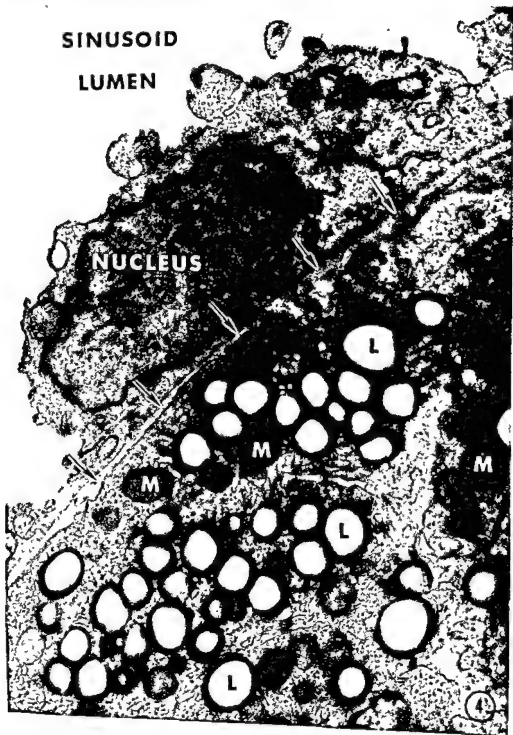


PLATE 3

EXPLANATION OF FIGURE

- 4 Electron micrograph of luteal cells from a mouse corpus luteum of ovulation in association with an endothelial cell lining the lumen of a sinusoid. The apposition of these luteal cells with the endothelium along the narrow subendothelial space (at arrows) is relatively smooth. (See fig. 9 for comparison). Lead citrate. $\times 13,200$.



PLATE 4

EXPLANATION OF FIGURE

- 5 Electron micrograph of parts of several luteal cells from a corpus luteum of ovulation. The mitochondria (M) are rounded and possess numerous, vesicular cristae and little matrix. Lipid droplets (L) are seen in the lower right corner of the figure. The lipid core of these inclusions has been preserved. Elements of granular endoplasmic reticulum are present at arrows. The smooth-surfaced endoplasmic reticulum is sparse. Note the free ribosomes (occurring singly and in clusters) within the cytoplasm. Uranyl acetate and lead citrate. $\times 22,400$.

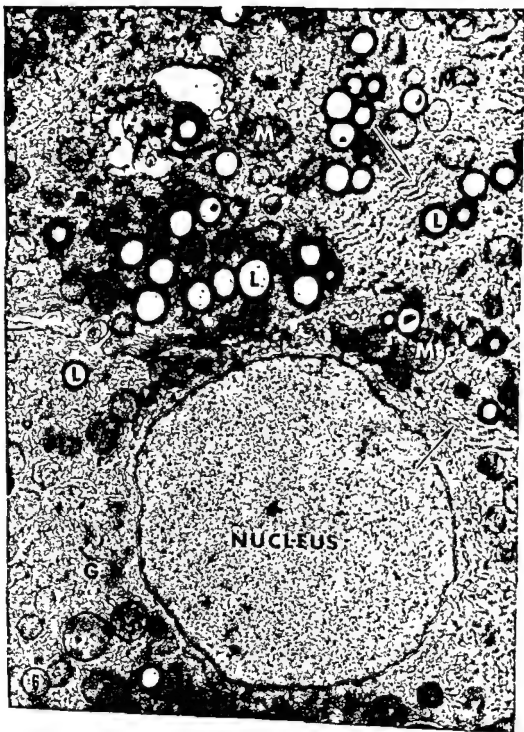


PLATE 5

EXPLANATION OF FIGURE

- 6 Electron micrograph of parts of several luteal cells from a hyperemic corpus luteum following gonadotrophin stimulation. Mitochondria (M) with tubulo-vesicular cristae and small, partially-extracted lipid droplets (L) are seen throughout the cytoplasm. A prominent Golgi apparatus (G) is seen to the left of the large, rounded nucleus. In addition to the granular type of endoplasmic reticulum (at arrows), note the abundant smooth-surfaced endoplasmic reticulum appearing as vesicles and short, interconnecting tubules throughout the luteal cell cytoplasm. Lead citrate. $\times 13,600$.

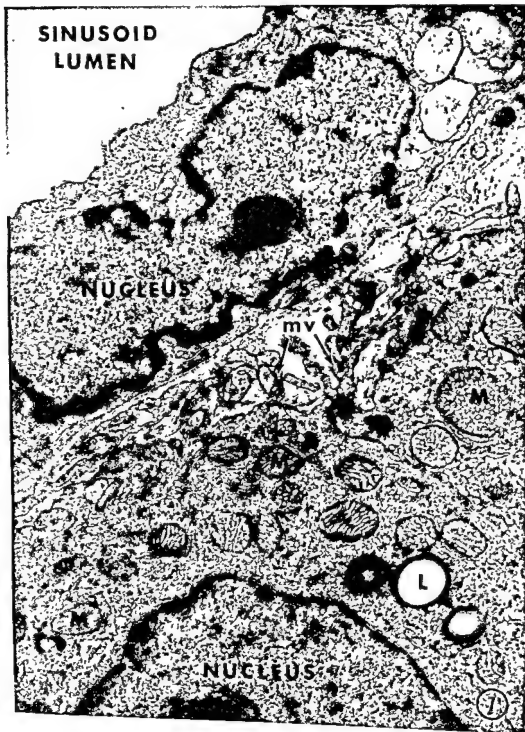


PLATE 6

EXPLANATION OF FIGURE

- 7 Luteal cells from hyperemic corpus luteum associated with a sinusoidal endothelial cell. Note the microvillous projections (mv) of the luteal cells within the subendothelial space and the presence of small lipid inclusions within the upper cell near to the perivascular space. Uranyl acetate and lead citrate. $\times 18,500$.

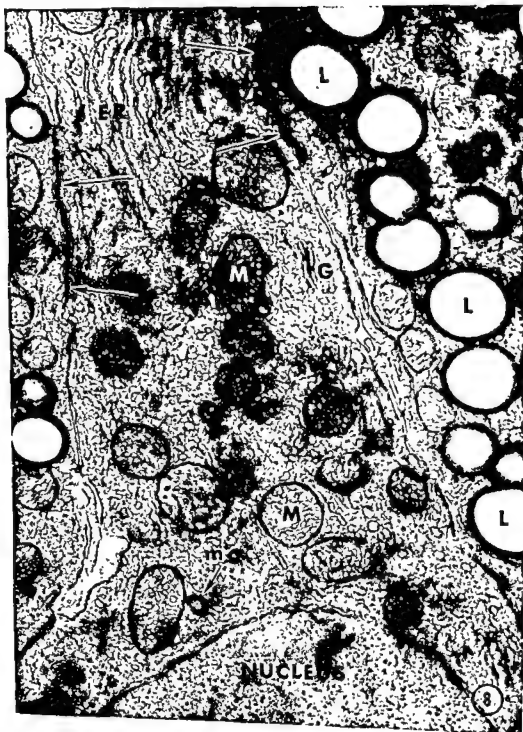


PLATE 7

EXPLANATION OF FIGURES

- 8 Portions of three luteal cells from a hyperemic corpus luteum. The mitochondria are large, round and possess tubulo-vesicular cristae. There is an increase in both granular (ER) and agranular endoplasmic reticulum following gonadotrophic hormone stimulation. Golgi membranes (G) are seen. The lipid droplets appear to be easily extractable. Occasionally a membrane-bound granule (mg), having a different and less dense matrix from a lipid granule, is also seen within the cytoplasm. Increased densities in closely apposed cell membranes of active luteal tissue are seen at long arrows. Lead citrate. $\times 21,900$.

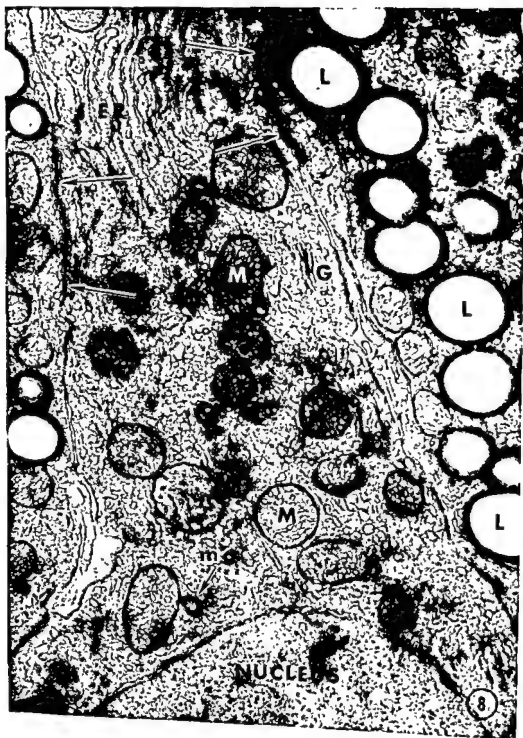
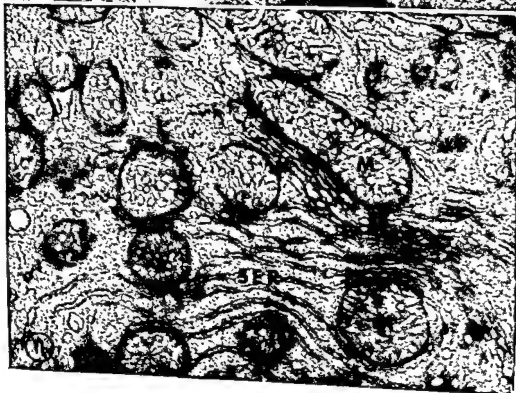


PLATE 8

EXPLANATION OF FIGURES

- 9 Portion of a luteal cell from a hyperemic corpus luteum to demonstrate a cilium. The ciliary process (C) originates from a basal body (BB) and projects toward the free surface in the upper left corner of the figure. In this electron micrograph a proximal centriole (PC), exhibiting the nine triplet fibrils, is seen in cross-section to the right of the associated basal body. Uranyl acetate and lead citrate. $\times 52,800$.
- 10 Longitudinal section of a single cilium projecting into the intercellular space. Cilia such as that seen in this electron micrograph have been observed only in luteal cells from hyperemic corpora of mice given luteotrophin. Lead citrate. $\times 25,900$.
- 11 Portion of luteal cell from a hyperemic corpus luteum demonstrating the rich array of smooth-surfaced endoplasmic reticulum (SER) and the close association of this organelle with mitochondria. Some elements of this reticulum exhibit both tubular and vesicular forms; other elements of the reticulum have areas of attached ribosomes. Lead citrate. $\times 34,300$.



The Relationship Between the Transverse Tubular System and Other Tubules at the Z Disc Levels of Myocardial Cells in the Ferret

F. O. SIMPSON¹ AND D. G. RAYNS

Wellcome Medical Research Institute and the Electron Microscope Laboratories of the Department of Pathology and the New Zealand Medical Research Council, University of Otago Medical School, Dunedin, New Zealand

ABSTRACT Apart from cytoplasmic microtubules, which exist in cardiac muscle as in most other tissues, there are two tubular systems in mammalian myocardial cells—the transverse (T) tubules which are invaginations of the sarcolemma (i.e., plasma membrane and basement membrane) and the finer tubules which appear to be separate from the transverse system and which have hitherto been known as longitudinal (L) tubules. Because so many of these finer tubules are transversely orientated it seems better to call them simply "sarcotubules." The sarcotubular system is best envisaged as a three-dimensional network extending throughout the cell, with specialized areas of flattened sarcotubular sacs at points of contact with the plasma membrane or its extensions in the transverse tubular system. A particularly constant element of the sarcotubular system is found encircling the myofibrils at the Z regions.

The structure of the tubules in striated muscle cells has been extensively investigated in recent years. In skeletal muscle cells of fish or amphibia, in which the transverse tubular system (T system) lies at Z disc levels (as in mammalian myocardium), it is now well established (Franzini-Armstrong, '64; Huxley, '64; Page, '64; Franzini-Armstrong and Porter, '65; Peachey, '65) that the T tubules communicate with the extra-cellular space and lie in close apposition to the Z discs. In such cells the terminal cisternae of the sarcotubular system (longitudinal tubular system, L system) surrounding each myofibril segment are closely applied to the adjacent transverse tubules (Fahrenbach, '65; Franzini-Armstrong, '64; Peachey, '65). It is generally agreed (e.g., A. F. Huxley, '64; Franzini-Armstrong, '64; Peachey, '65; Smith, '66) that the T tubules probably act as a conducting mechanism for the intracellular spread of electrical activity from the surface to the interior of the cell and that the L tubules are involved in some way with the contraction process, their main function perhaps being to release and recapture calcium ions (Costantin et al., '65; Pease et al., '65).

The extent to which the structure in mammalian cardiac muscle is similar to this is debatable. There can be no doubt

that the transverse tubular system in mammalian myocardium is in communication with the extracellular space (Lindner, '57; Simpson and Oertel, '61, '62; Nelson and Benson, '63; Simpson, '65; Forssmann and Girardier, '66; Rayns et al., '67) but the relationship of the sarcotubular system to the T tubules has not yet been fully defined. In Porter and Palade's classic study ('57) of the endoplasmic reticulum, the appearances in rat cardiac muscle were interpreted as showing in all essentials the type of relationship described above for amphibian skeletal muscle, and in a recent extensive review (Smith, '66), mainly devoted to skeletal muscle, it is stated that "it seems likely that the cytological relationship between the invaginated T system and intracellular cisternae of the reticulum occurring in skeletal fibers is duplicated in vertebrate heart muscle." However, in the myocardial cells of the cat (Fawcett, '65), the ox (Simpson, '65) and the rat (Forssmann and Girardier, '66) it has been noted that the standard description of a triad is not entirely appropriate. Further, in the ox (Simpson, '65) a small "circumferential Z tubule" was noted lying in close apposition to the circumference of

¹Supported by a research grant from the New Zealand Medical Research Council

the Z discs. This tubule appeared to be single, to communicate with other "circumferential Z tubules" and to communicate also with longitudinal elements of the sarcoplasmic reticulum. This circumferential Z disc tubule thus intervened laterally between the transverse tubules and the Z discs. In the present study, we have investigated further the relationship of the tubular systems in mammalian cardiac muscle cells.

METHODS

Small portions of ferret heart muscle were obtained under ether anesthesia, fixed for four hours in 4% glutaraldehyde in phosphate buffer at pH 7.6, washed in phosphate buffer, post-fixed in 1% osmium tetroxide in veronal acetate buffer at pH 7.6 for four hours, dehydrated through alcohols and embedded in Epon. Thin longitudinal sections were mounted on grids without supporting film, counter-stained with a saturated solution of uranyl acetate and with lead citrate (Reynolds, '63) and viewed in a Hitachi HU11A electron microscope.

OBSERVATIONS

Transverse tubular system. The transverse tubules were readily apparent, either as invaginations of the sarcolemma at the level of the Z discs, or as tubule profiles between the myofibrils at the Z disc levels (figs. 1, 2, 4-9). The basement membrane material within the transverse tubules often appeared to fill the lumen (figs. 1, 2, 6, 11). In some instances the plasma membrane of the wall of the T tubule showed buddings similar to pinocytotic vesicles (figs. 8c, 10) but no connection between T tubules and other tubules could be found.

The profiles of the T tubules usually appeared flattened with a width which was fairly constant at 500-800 Å. The flattening may have been partly artefact as the cells were mainly in a contracted state.

Sarcotubular system. This appeared in the sections as a three-dimensional network of fine tubules, cut in different planes. Some of these tubules, lying in a mainly longitudinal direction (figs. 1, 4, 6), clearly formed a lace-like network round the myofibrils as has been frequently de-

scribed in many types of striated muscle and these tubules can appropriately be termed longitudinal or L tubules. However, other elements of the sarcotubular system were clearly running in a transverse direction across the cell, almost exclusively at the Z levels (figs. 1-4, 6, 8). These transversely running tubules, which could readily be distinguished from the T tubules because of their much smaller size, appeared in the sections in the following forms.

(1) Round profiles, about 200 to 400 Å in diameter, lying close to the myofibrils at the Z levels (figs. 1, 2, 3, 6, 7). Such profiles were very common, and they were interpreted as cross sections of fine tubules running circumferentially round the myofibrils at the Z levels. Such tubules were demonstrated in transversely sectioned myocardial cells in a previous study (Simpson, '65) in which they were referred to as "circumferential Z tubules." For sake of brevity they will now be referred to as Z tubules.

(2) Profiles of single, longitudinally cut tubules (about 200 to 400 Å in diameter) running transversely across the between adjacent myofibrils at Z level and communicating with the Z tubules (figs. 1, 3, 6, 8). These transversely running elements therefore appeared to connect adjacent Z tubules together across the cell. They occurred as simple single tubules only at those places where no T tubule was present.

All figures, apart from figure 13, are electron micrographs of longitudinal sections of papillary muscle cells, fixed in glutaraldehyde, post fixed in osmium and counterstained with lead citrate. CM, cytoplasmic microtubule; C, connecting tubule between neighbouring myofibrils; Fs, flattened sac; L, longitudinal element of sarcotubular system; M, M line; Mf, myofibril; Mit, mitochondrion; P, pinocytotic vesicle; S, sarcotubule; T, transverse tubule; Z, Z disc; Z tubule.

Fig. 1 Cross sectioned Z tubules (Zt) are seen lying close to the Z discs (Z). A transversely running connecting tubule (Ct) lies between adjacent Z tubules at a point where no T tubule is present. Where a T tubule is present (T) it is flanked above and below by flattened sacs of the sarcotubular system. These flattened sacs are connected to the Z tubules on either side. (The T tubule in this particular instance is ble.) $\times 52,000$.



Figure 1

the Z discs. This tubule appeared to be single, to communicate with other "circumferential Z tubules" and to communicate also with longitudinal elements of the sarcoplasmic reticulum. This circumferential Z disc tubule thus intervened laterally between the transverse tubules and the Z discs. In the present study, we have investigated further the relationship of the tubular systems in mammalian cardiac muscle cells.

METHODS

Small portions of ferret heart muscle were obtained under ether anesthesia, fixed for four hours in 4% glutaraldehyde in phosphate buffer at pH 7.6, washed in phosphate buffer, post-fixed in 1% osmium tetroxide in veronal acetate buffer at pH 7.6 for four hours, dehydrated through alcohols and embedded in Epon. Thin longitudinal sections were mounted on grids without supporting film, counterstained with a saturated solution of uranyl acetate and with lead citrate (Reynolds, '63) and viewed in a Hitachi HU11A electron microscope.

OBSERVATIONS

Transverse tubular system. The transverse tubules were readily apparent, either as invaginations of the sarcolemma at the level of the Z discs, or as tubule profiles between the myofibrils at the Z disc levels (figs. 1, 2, 4-9). The basement membrane material within the transverse tubules often appeared to fill the lumen (figs. 1, 2, 6, 11). In some instances the plasma membrane of the wall of the T tubule showed buddings similar to pinocytotic vesicles (figs. 8c, 10) but no connection between T tubules and other tubules could be found.

The profiles of the T tubules usually appeared flattened with a width which was fairly constant at 500-800 Å. The flattening may have been partly artefact as the cells were mainly in a contracted state.

Sarcotubular system. This appeared in the sections as a three-dimensional network of fine tubules, cut in different planes. Some of these tubules, lying in a mainly longitudinal direction (figs. 1, 4, 6), clearly formed a lace-like network round the myofibrils as has been frequently de-

scribed in many types of striated muscle and these tubules can appropriately be termed longitudinal or L tubules. However, other elements of the sarcotubular system were clearly running in a transverse direction across the cell, almost exclusively at the Z levels (figs. 1-4, 6, 8). These transversely running tubules, which could readily be distinguished from the T tubules because of their much smaller size, appeared in the sections in the following forms.

(1) Round profiles, about 200 to 400 Å in diameter, lying close to the myofibrils at the Z levels (figs. 1, 2, 3, 6, 7). Such profiles were very common, and they were interpreted as cross sections of fine tubules running circumferentially round the myofibrils at the Z levels. Such tubules were demonstrated in transversely sectioned myocardial cells in a previous study (Simpson, '65) in which they were referred to as "circumferential Z tubules." For the sake of brevity they will now be referred to as Z tubules.

(2) Profiles of single, longitudinal cut tubules (about 200 to 400 Å in diameter) running transversely across the cell between adjacent myofibrils at Z levels and communicating with the Z tubules (figs. 1, 3, 6, 8). These transversely running elements therefore appeared to connect adjacent Z tubules together across the cell. They occurred as simple single tubules only at those places where no T tubule was present.

All figures, apart from figure 13, are electron micrographs of longitudinal sections of papillary muscle cells, fixed in glutaraldehyde, post fixed in osmium and counterstained with lead citrate. CM, cytoplasmic microtubules; Fs, flattened sac; L, longitudinal tubule; M, M line; Mf, m; Mit, mitochondrion; P, pinocytotic vesicle; Ct, cotubule; T, transverse tubule; Z, Z disc; Z tubule.

Fig. 1 Cross sectioned Z tubules (Zt) seen lying close to the Z discs (Z). A transverse running connecting tubule (Ct) lies between adjacent Z tubules at a point where no T tubule is present. Where a T tubule is present (T) it is flanked above and below by flattened sacs of the sarcotubular system. These flattened sacs are connected to the Z tubules on either side. (The T tubule in this particular instance lies at the top of the field.) $\times 52,000$.



Figures 2 and 3

(3) Pairs of parallel membranes, 250 Å apart (centre to centre spacing), lying usually both above and below the T tubules, but sometimes on only one side of a T tubule. These membranes were interpreted as representing sectioned flattened sacs rather than longitudinally-sectioned tubules because the structures persisted through several serial sections (figs. 6, 7, 8). The relationship between these flattened sarcotubular sacs and the adjacent T tubule was very close, with a space of only about 250 Å between the centre of the T tubule membrane and the centre of the nearer membrane of the flattened sac (figs. 1, 2, 4-8). Occasionally an electron-dense line could be seen between the T tubule and the flattened sac (figs. 2, 4, 5, 7) but no cross bridges were seen between the adjacent membranes such as those demonstrated in analogous places in other muscle cells (Revel, '62; Fahrenbach, '65). Another and more striking electron-dense line was consistently seen within the lumen of the flattened sacs, i.e., between the pairs of parallel membranes (figs. 2, 4-7). (The whole unit of T tubule and flattened sacs represents, of course, a triad," but this term will not be used, for reasons to be discussed later.)

(4) Tubular elements connecting the flattened sacs to the Z tubules lateral to the T tubule. Such connections were frequently seen in random longitudinal sections (figs. 1, 2, 4, 5), but their nature was more clearly demonstrated in serial sections (figs. 6, 7). The two flattened sacs and their lateral connections to a Z tubule at either side could be seen in some sections to form a complete ring round a T tubule (fig. 1). This apparently occurred when the lateral connections between the flattened sacs and the Z tubules were all present in the same plane of section. However, the four connections (i.e., two at each side) were usually not all present in a given section, and it appeared that the connecting elements were less extensive than the flattened sacs. In serial sections, also, these connecting elements usually did not persist through more than two or three sections, and sometimes they could be seen in only one section (figs. 6, 7). The appearances in serial sections occasionally suggested that a flattened sac might have

more than one connection to a neighbouring Z tubule (e.g., fig. 7), but confirmation of this will depend on longer series of sections. The exact extent of the flattened sacs has also not been definitely determined.

(5) Connections between flattened sacs and longitudinally-running elements. Occasionally evidence was obtained suggesting that a flattened sarcotubular sac communicated directly with a longitudinally-sectioned tubule (figs. 2, 4, 8). However, such connections appeared much less common than the lateral connections to the tubules.

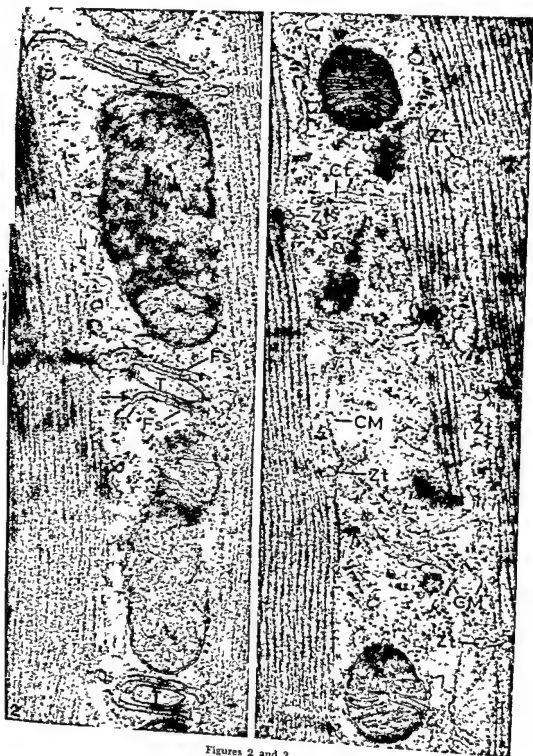
(6) Tubules lying under the plasma membrane of the cell and communicating with the Z tubules of the most peripheral myofibrils (figs. 9a-c, 10, 12). At some points these tubules take on the same appearance as that of the flattened sacs lying against the T tubules, i.e., they were electron-dense, the lumen was reduced, and an electron-dense line was present in the lumen.

This description has implied that the arrangement of the tubular systems is very regular one. It is perhaps not surprising, however, that minor deviations from the standard morphology do occur, such as a single (instead of paired) flattened sarcotubular sac (fig. 4) and double (instead of single) T tubules (fig. 1). The interesting structural variant was seen in places where the T tubule occupied a usual position, e.g., ran longitudinally over one sarcomere length or failed to connect with a Z disc level; at such places the sarcotubular elements which lay along the T tubule took on a flattened appearance regardless of their orientation (fig. 11).

Cytoplasmic microtubules. Microtubules were occasionally observed (fig. 3).

Fig. 2 Further examples of T tubules flanked by flattened sacs (Fs). An electron-dense line is present between the apposed membranes of each sac and also between the sacs and the T tubule. While the flattened sacs seem in some cases to lie transversely, one (arrow) seen connecting up with a longitudinally-running tubule rather than with a Z tubule. $\times 56,000$.

Fig. 3 Space between myofibrils. Z (Zt), transversely running connecting (Ct), and cytoplasmic microtubules (C) can be seen. $\times 45,000$.



Figures 2 and 3



Fig. 4 The T tubules have been more longitudinally sectioned in this instance, and the flattened sacs (Fs) cover only part of their surface. The sarcotubular network (S) is seen to connect up with one flattened sac (arrow). In another instance a flattened sac is seen to connect up with a Z tubule (Zt). $\times 48,000$.



Fig. 5 High power view of a cross-sectioned T tubule flanked by flattened sacs. The electron dense lines in the "lumen" of the sacs and between the sacs and the T tubule can be seen. Note cross sectioned Z tubules (Zt), both showing lateral connections. $\times 105,000$.

have previously been reported to be present also in cat Purkinje cells (Page, '67).

DISCUSSION

The relationships of the various tubules described are clearly very complicated, and a more extensive series of serial sections will be required before a definitive three-dimensional picture of the distribution of tubules in myocardial cells can be built up. However, it is clear from the present evidence that the arrangement of tubules in mammalian myocardial cells has certain special features.

The previous description of the circumferential Z tubule (Simpson, '65) has been confirmed. This tubule is so consistently found in both longitudinal (present study) and transverse (Simpson, '65) sections of myocardial cells that it seems to require a special name, and we are in this paper referring to it as the "Z tubule." *A Z tubule therefore is a tubule found in mammalian myocardial cells, 200–400 Å in diameter, encircling the myofibril at the Z level and closely applied to it.*

It is in fact surprising that this tubule has not been the subject of comment by other authors, and we believe that examples of Z tubules can be seen in various published electron micrographs of longitudinally-sectioned myocardial cells (Stenger and Spiro, '61; Karnovsky, '64; Forssmann and Girardier, '66). Page ('67) has recently commented on a sarcotubular element running transversely at the Z level in cat Purkinje cells, and cross-sectioned Z tubules are clearly seen in his micrographs. Once the Z tubule is recognised it is readily identifiable, and it seems unlikely to be an artefact of fixation or embedding.

We have shown examples of communication: (a) between a Z tubule and a neighbouring Z tubule; (b) between a Z tubule and the longitudinally-running tubules encircling the sarcomeres above and below the Z tubule; (c) between a Z tubule and the flattened sacs lying above and below a neighbouring T tubule; (d) between a Z tubule and other fine tubules lying under the plasma membrane at the edge of the cell. The Z tubules at one particular Z level are thus linked together across the cell by communicating tubules, so that

they can be considered to represent a system of transversely-orientated tubules at the Z level — additional to and more extensive than the T system, composed of much narrower tubules than the T system and bearing a very close spatial relationship to the T tubules through the medium of the flattened sarcotubular sacs.

There are therefore two distinct systems of tubules at the Z levels, and the question arises of whether the Z tubules might supplant the T system as the favoured candidate for the role of transmission of the activating impulse into the cell. Such a role seems unlikely because the Z tubules have no communication with the extra-cellular space, and because they communicate directly with the flattened sacs (which are analogous to the lateral elements of the triads of skeletal muscle). To postulate a depolarization-transmitting role for the Z tubules would therefore seem unreasonable, as this would both ignore the T tubules and would imply an excitation-coupling mechanism not analogous to any other known type of striated muscle.

It seems more reasonable to assume that the transverse connections between Z tubules are required because of the incomplete distribution of T tubules, the ramifications of which do not extend between all myofibrils. Thus some Z tubules appear not to have direct connections to a flattened sac and may therefore require communication with other Z tubules which do have such connection.

We have shown that there is only one tubule encircling a Z region of a myofibril and that it seems to communicate with the longitudinally-running tubules surrounding the sarcomeres above and below the Z region in question. Clearly, if this is the case then in mammalian cardiac muscle the system of tubules is not subdivided on the sarcomere basis but must be continuous throughout the length of the cell.

We have used the term "flattened sacs" for the structures lying close to the T tubules because it is more accurately descriptive than such terms as "terminal cisternae" or "lateral element of the triad" which have been used for skeletal muscle. "Terminal cisterna" is quite inappropriate because the sac is flattened and therefore hardly qu-

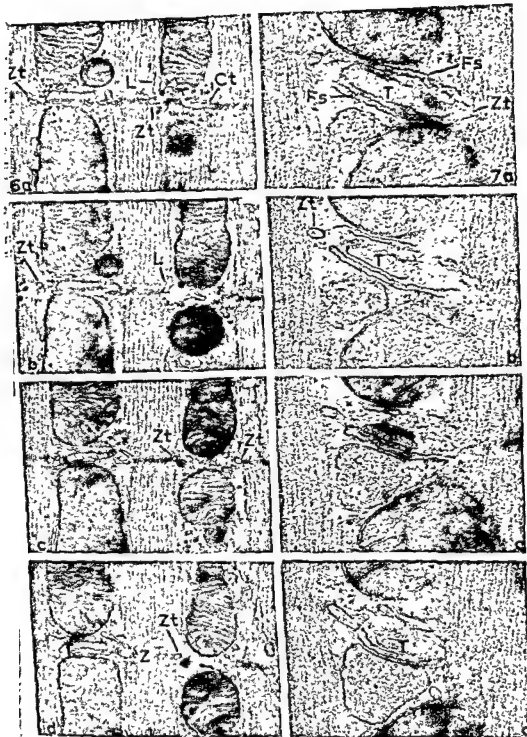


Fig. 6a-d Series of sections showing arrangement of sarcotubules where a T tubule is present (on left) and where no T tubule is present (on right). Note connection between Z tubule and longitudinal element (L) of sarcotubular system, and connection (Ct) between adjacent Z tubules. ×28,000.

Fig. 7a-d Series of sections showing arrangement of sarcotubules round a T tubule. Connections between the flattened sacs (Fs) and the adjacent Z tubules (Zt) are seen. ×58,000.

fies as a "cisterna," and also because the sac communicates at each side with adjacent Z tubules so that it is in no sense "terminal." "Lateral element of triad" has the disadvantage that although the "triad" has been a useful concept in the past, it is essentially a two-dimensional concept, descriptive of the appearances in a single section and originating at a time when the elements of the triad were considered to be vesicles rather than tubules. In cardiac muscle, especially, the relationships of the finer tubules to the T tubules are so complex that it seems essential to try to think of them in three-dimensional terms.

On the basis of our present findings therefore, we envisage the finer tubules to be parts of a single system, and we shall refer to this as the "sarcotubular system" (after the manner of Page, '67); this term does not include the sarcolemmal invaginations which make up the T system, and it avoids the use of the term "longitudinal" which is inappropriate for mammalian cardiac muscle. An attempt to depict the sarcotubular system is shown in figure 13: while we believe the general concept to be correct, there are a number of details which remain uncertain — particularly the extent of flattened sacs, the number of connections between the sacs and the other tubules, and the extent of the ramifications of the sarcotubular system under the sarcolemma. Essentially the sarcotubular system is a three-dimensional network of fine tubules, extending throughout the cell between the myofibrils and mitochondria, forming a lacework around the myofibril sarcomeres and having a particularly constant relationship to the Z region of the myofibrils, each of which is surrounded by a sarcotubular element. Specialisation of the sarcotubules occurs whenever they lie in contact with the plasma membrane of the cell, or its extensions in the transverse tubular system, as has also been pointed out by others (Rostgaard and Behnke, '64; Essner et al., '65; Page, '67). This morphological specialisation at points of contact with the plasma membrane consists of a widening and flattening of the sarcotubule, with a loss of lumen and the appearance of an electron-dense line between the apposed membranes forming the walls of the flattened sarcotubular sac. This type of

structure has also been described in detail by other authors (Rostgaard and Behnke, '64; Essner et al., '65; Forssmann and Girardier, '66; Page, '67) and has been shown to coincide with sites of ATPase activity (Rostgaard and Behnke, '64; Essner et al., '65) and calcium-binding activity (Hasselbach, '64; Costantin et al., '65; Pease et al., '65).

The structure of the tubular system in mammalian myocardial cells thus differs from that in other striated muscle cells. The main differences appear to be that in myocardial cells:

(1) the T tubules are much larger (Simpson and Oertel, '62; Nelson and Benson, '63; Simpson, '65; Rayns et al., '67) than in most vertebrate skeletal muscle cells; (2) there is an element of the sarcotubular system closely applied to the Z region of the myofibrils; (3) the structures analogous to the terminal cisternae are flattened instead of dilated, and (4) there is general continuity throughout the cell of all the elements making up the sarcotubular system.

To interpret these morphological differences in terms of function is not easy, but it seems justifiable to speculate on whether some at least of the differences are related to differences in the handling of calcium ions during excitation and recovery. If the entry of calcium ions from extra-cellular fluid occurs on a larger scale in mammalian myocardial than skeletal muscle cells (Naylor, '67), then it is possible that this is connected with the larger lumen of the transverse tubules in myocardial cells — on the presumption that extra-cellular fluid will have easier access to the lumen of the T tubules in myocardial cells.

The significance of the special arrangement of the sarcotubular system in mammalian myocardial cells is obscure. The most likely function of the sarcotubules is to handle calcium ions (Hasselbach, '61; Costantin et al., '65; Pease et al., '65; Naylor, '67) but it is not known whether they do this on a two-way basis or merely capture calcium ions at the end of action. The difference in structure between most of the sarcotubules and the specialised "flattened sacs" is known to reflect a difference in function (Rostgaard and Behnke, '64; Essner et al., '65), and it

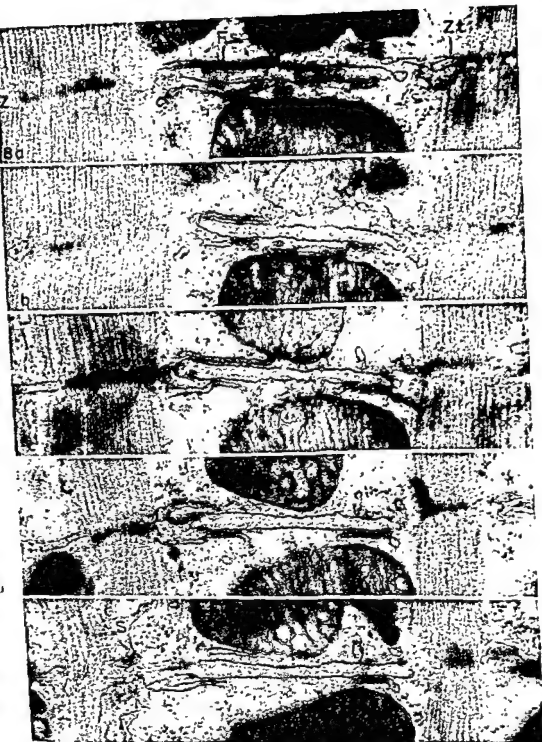


Fig. 8a-e Series of sections showing arrangement of sarcotubules seen when a T tubule is more longitudinally sectioned. (Fig. 8c is part of fig. 4.) The connections between the flattened sacs and Z tubules appear to be less readily seen in this situation. Pinocytotic vesicles (P) appear to be present in figure 8c. $\times 48,000$.

fies as a "cisterna," and also because the sac communicates at each side with adjacent Z tubules so that it is in no sense "terminal." "Lateral element of triad" has the disadvantage that although the "triad" has been a useful concept in the past, it is essentially a two-dimensional concept, descriptive of the appearances in a single section and originating at a time when the elements of the triad were considered to be vesicles rather than tubules. In cardiac muscle, especially, the relationships of the finer tubules to the T tubules are so complex that it seems essential to try to think of them in three-dimensional terms.

On the basis of our present findings therefore, we envisage the finer tubules to be parts of a single system, and we shall refer to this as the "sarcotubular system" (after the manner of Page, '67); this term does not include the sarcolemmal invaginations which make up the T system, and it avoids the use of the term "longitudinal" which is inappropriate for mammalian cardiac muscle. An attempt to depict the sarcotubular system is shown in figure 13: while we believe the general concept to be correct, there are a number of details which remain uncertain — particularly the extent of flattened sacs, the number of connections between the sacs and the other tubules, and the extent of the ramifications of the sarcotubular system under the sarcolemma. Essentially the sarcotubular system is a three-dimensional network of fine tubules, extending throughout the cell between the myofibrils and mitochondria, forming a lacework around the myofibril sarcomeres and having a particularly constant relationship to the Z region of the myofibrils, each of which is surrounded by a sarcotubular element. Specialisation of the sarcotubules occurs whenever they lie in contact with the plasma membrane of the cell, or its extensions in the transverse tubular system, as has also been pointed out by others (Rostgaard and Behnke, '64; Essner et al., '65; Page, '67). This morphological specialisation at points of contact with the plasma membrane consists of a widening and flattening of the sarcotubule, with a loss of lumen and the appearance of an electron-dense line between the apposed membranes forming the walls of the flattened sarcotubular sac. This type of

structure has also been described in detail by other authors (Rostgaard and Behnke, '64; Essner et al., '65; Forssmann and Girardier, '66; Page, '67) and has been shown to coincide with sites of ATPase activity (Rostgaard and Behnke, '64; Essner et al., '65) and calcium-binding activity (Hasselbach, '64; Costantin et al., '65; Pease et al., '65).

The structure of the tubular system in mammalian myocardial cells thus differs from that in other striated muscle cells. The main differences appear to be that in myocardial cells:

(1) the T tubules are much larger (Simpson and Oertel, '62; Nelson and Benson, '63; Simpson, '65; Rayns et al., '67) than in most vertebrate skeletal muscle cells; (2) there is an element of the sarcotubular system closely applied to the Z region of the myofibrils; (3) the structures analogous to the terminal cisternae are flattened instead of dilated, and (4) there is general continuity throughout the cell of all the elements making up the sarcotubular system.

To interpret these morphological differences in terms of function is not easy, but it seems justifiable to speculate on whether some at least of the differences are related to differences in the handling of calcium ions during excitation and recovery. If the entry of calcium ions from extra-cellular fluid occurs on a larger scale in mammalian myocardial than skeletal muscle cells (Naylor, '67), then it is possible that this is connected with the larger lumen of the transverse tubules in myocardial cells — on the presumption that extra-cellular fluid will have easier access to the lumen of the T tubules in myocardial cells.

The significance of the special arrangement of the sarcotubular system in mammalian myocardial cells is obscure. The most likely function of the sarcotubules is to handle calcium ions (Hasselbach, '64; Costantin et al., '65; Pease et al., '65; Naylor, '67) but it is not known whether they do this on a two-way basis or merely recapture calcium ions at the end of contraction. The difference in structure between most of the sarcotubules and the specialised "flattened sacs" is known to reflect a difference in function (Rostgaard and Behnke, '64; Essner et al., '65), and it may

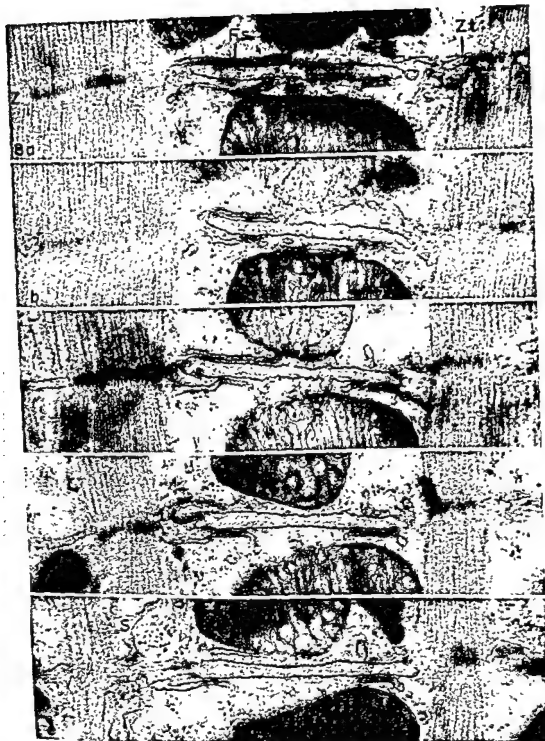


Fig. 8a-e Series of sections showing arrangement of sarcolemma seen when a T tubule is more longitudinally sectioned. (Fig. 8e is part of fig. 4.) The connections between the flattened sacs and Z tubules appear to be less readily seen in this situation. Pinocytotic vesicles (P) appear to be present in figure 8c $\times 48,000$.



Fig. 9a-c Series of sections showing the edges of two cells. The space between the cells is small; it and the T tubule invaginations (T) are almost filled with basement membrane-like material. Sarcotubules (S) branch out from Z tubule region (Zt) and one lies close to the plasma membrane (arrow). $\times 60,000$.

Fig. 10 Further example of a flattened sarcotubular sac (Fs) lying against the plasma membrane of a T tubule invagination and apparently joining a Z tubule (Zt). $\times 1$



Fig. 11 Example of a longitudinally-running T tubule (T). The sarcotubule lying beside it has taken on the typical "flattened sac" appearance (Fs). $\times 64,000$.

Fig. 12 Further example of sarcotubular elements at the edge of the cell branching out from the Z tubule and lying close to the plasma membrane. One sarcotubule appears to be making contact with M line (Mt) of the myofibril $\times 54,000$.

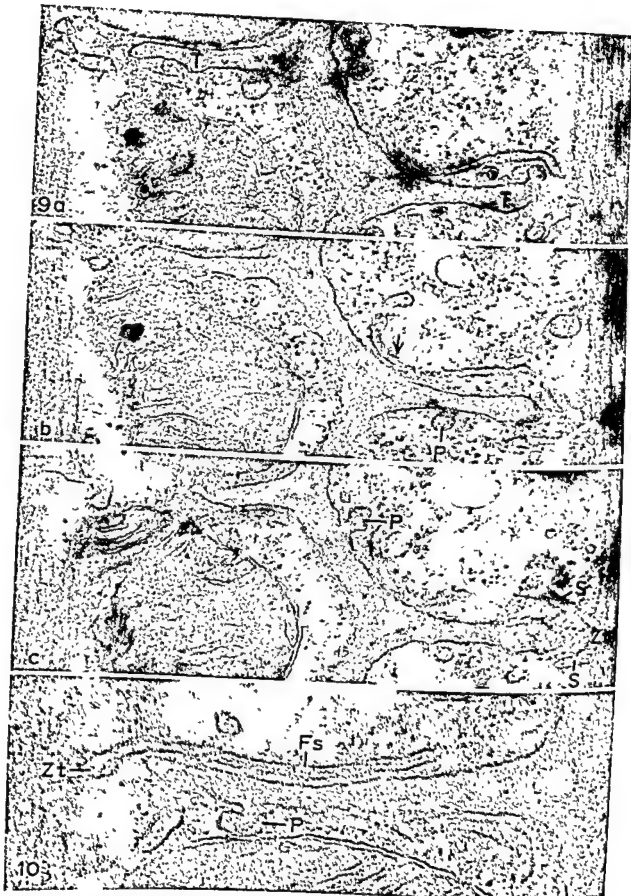


Fig. 9a-c Series of sections showing the edges of two cells. The space between the cells is small; it and the T tubule invaginations (T) are almost filled with basement membrane-like material. Sarcotubules (S) branch out from Z tubule region (Zt) and one lies close to the plasma membrane (arrow). $\times 60,000$.

Fig. 10 Further example of a flattened sarcotubular sac (Fs) lying against the plasma membrane of a T tubule invagination and apparently joining a Z tubule (Zt). $\times 1$



Fig. 11 Example of a longitudinally-running T tubule (T). The sarcotubule lying beside it has taken on the typical "flattened sac" appearance (Fs). $\times 64,000$

Fig. 12 Further example of sarcotubular elements at the edge of the cell branching out from the Z tubule and lying close to the plasma membrane. One sarcotubule appears to be making contact with M line (M) of the myofibril. $\times 54,000$.

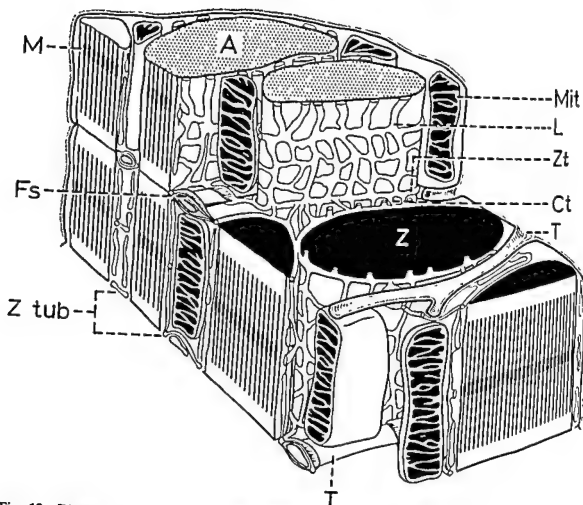


Fig. 13 Diagram representing the three dimensional distribution of the sarcotubular system in ferret myocardium.

be that the unspecialised parts of the system merely act as conduits for the calcium ions on their way to and/or from the specialised flattened sacs. If, however, any considerable quantities of calcium ions have to be expelled from the cell at the end of contraction (Winegrad, '61; Langer, '64), then it may perhaps be that such expulsions occur at specialised points such as the "junctional" areas of contact between the flattened sarcotubular sacs and the plasma membrane of the cell. At such places, the concentration of calcium ions within the cell could possibly provide a gradient across the junctional membranes, thus facilitating calcium expulsion. No obvious function for the Z tubules can be discerned at the moment other than a collecting and distributing one for calcium ions—i.e., a link in the chain of sarcotubules throughout the cell. It may however eventually prove that there is some

significance in the extremely close relationship between Z tubules and the Z regions of the myofibrils. The only other known type of muscle which has an extra set of tubules at the Z regions is the crab muscle studied by Peachey ('66), but these tubules are large and open to the exterior, and they seem scarcely analogous to the myocardial Z tubules.

ACKNOWLEDGMENTS

The authors wish to acknowledge with gratitude the technical assistance of Miss Janet Ledingham, and to thank Professor A. Wynn Williams of the Department of Pathology for use of the Hitachi HU11 electron microscope.

LITERATURE CITED

- Costantin, L. L., C. Franzini-Armstrong and R. J. Podolsky 1965 Localisation of calcium-accumulating structures in striated muscle fibres. *Science*, 147: 158-159.

- Easner, E., A. B. Novikoff and N. Quintana 1965 Nucleoside phosphatase activities in rat cardiac muscle. *J. Cell. Biol.*, 25: 201-216.
- Fahrenbach, W. H. 1965 Sarcoplasmic reticulum: ultrastructure of the triadic junction. *Science*, 147: 1308-1309.
- Fawcett, D. W. 1965 Observation on the T-system and cell to cell contacts in cardiac muscle. In: *Proc. 8th Internat. Anatom. Kongress Wiesbaden*. Georg Thieme Verlag, Stuttgart, pp. 37-38.
- Forssmann, W. G., and L. Girardier 1966 Untersuchungen zur Ultrastruktur des Rattenherzmuskels mit besonderer Berücksichtigung des sarcoplasmatischen Retikulums. *Z. Zellforsch.*, 72: 249-275.
- Franzini-Armstrong, C. 1964 Fine structure of sarcoplasmic reticulum and transverse tubular system in muscle fibres. *Fed. Proc.*, 23: 887-895.
- Franzini-Armstrong, C., and K. R. Porter 1964 Sarcolemmal invaginations and the T-system in fish skeletal muscle. *Nature*, 202: 355-357.
- Hasselbach, W. 1964 Relaxation and the sarco-tubular calcium pump. *Fed. Proc.*, 23: 909-912.
- Huxley, A. F. 1964 Muscle. *Ann. Rev. Physiol.*, 26: 131-152.
- Huxley, H. E. 1964 Evidence for continuity between the central elements of the triads and extracellular space in frog sartorius muscle. *Nature*, 202: 1067-1071.
- Karnovsky, M. J. 1964 The localization of cholinesterase activity in rat cardiac muscle by electron microscopy. *J. Cell. Biol.*, 23: 217-240.
- Langer, G. A. 1964 Kinetic studies of calcium distribution in ventricular muscle of the dog. *Circulation Res.*, 15: 393-405.
- Lindner, E. 1957 Die submikroskopische Morphologie des Herzmuskels. *Z. Zellforsch.*, 45: 702-746.
- Nayler, W. G. 1967 Calcium exchange in cardiac muscle: a basic mechanism of drug action. *Amer. Heart J.*, 73: 379-394.
- Nelson, D. A., and E. S. Benson 1963 On the structural continuities of the transverse tubular system of rabbit and human myocardial cells. *J. Cell. Biol.*, 16: 297-313.
- Page, E. 1967 Tubular systems in Purkinje cells of the cat heart. *J. Ultrastruct. Res.*, 17: 72-83.
- Page, S. 1964 The organization of the sarcoplasmic reticulum in frog muscle. *J. Physiol.*, 175: 10P-11P.
- Peachey, L. D. 1965 The sarcoplasmic reticulum and transverse tubules of the frog's sartorius. *J. Cell. Biol.*, 25: no. 3, part 2, 209-231.
- 1966 The role of transverse tubules in excitation-contraction coupling in striated muscle. *Ann. N.Y. Acad. Sci.*, 137: 1025-1037.
- Pease, D. L., D. J. Jenden and J. N. Howell 1965 Calcium uptake in glycerol-extracted rabbit psoas muscle fibres. II. Electron microscopic localization of uptake sites. *J. Cell. and Comp. Physiol.*, 65: 141-154.
- Porter, K. R., and G. E. Palade 1957 Studies on the endoplasmic reticulum. III Its form and distribution in striated muscle cells. *J. Biophys. Biochem. Cytol.*, 3: 269-300.
- Rayns, D. G., F. O. Simpson and W. S. Bertaud 1967 Mammalian myocardial cells. Surface array of transverse tubule apertures. *Science*, 156: 656-657.
- Revel, J. P. 1962 The sarcoplasmic reticulum of the bat cricothyroid muscle. *J. Cell. Biol.*, 12: 571-588.
- Reynolds, E. S. 1963 The use of lead citrate at high pH as an electron-opaque stain in electron microscopy. *J. Cell. Biol.*, 17: 208-212.
- Rostgaard, J., and O. Behnke 1965 Fine structural localisation of adenine nucleoside phosphatase activity in the sarcoplasmic reticulum and the T system of rat myocardium. *J. Ultrastruct. Res.*, 12: 579-591.
- Simpson, F. O. 1965 The transverse tubular system in mammalian myocardial cells. *Am. J. Anat.*, 117: 1-18.
- Simpson, F. O., and S. J. Oertels 1961 Relationship of the sarcoplasmic reticulum to sarcolemma in sheep cardiac muscle. *Nature*, 189: 758-759.
- 1962 The fine structure of sheep myocardial cells; sarcolemmal invaginations and the transverse tubular system. *J. Cell. Biol.*, 12: 81-100.
- Smith, D. S. 1966 The organization and function of the sarcoplasmic reticulum and T-system of muscle cells. *Progr. Biophys. Molec. Biol.*, 16: 109-142.
- Stenger, R. J., and D. Spiro 1961 The ultrastructure of mammalian cardiac muscle. *J. Biophys. Biochem. Cytol.*, 9: 325-352.
- Winegrad, S. 1961 The possible role of calcium in excitation-contraction coupling of heart muscle. *Circulation*, 24: 523-529.

Ultrastructural Features of the Shark Brain

DON M. LONG,¹ THOMAS S. BODENHEIMER,²
J. FRANCIS HARTMANN,³ AND IGOR KLATZO¹

¹Section on Clinical Neuropathology, Branch of Surgical Neurology, National Institute of Neurological Diseases and Blindness. ²Section on Neurocytology, Laboratory of Neuroanatomical Sciences, National Institute of Neurological Diseases and Blindness, National Institutes of Health, Public Health Service, Department of Health, Education and Welfare, Bethesda, Maryland. ³The Department of Neurology, Presbyterian-St. Luke's Hospital, and Department of Neurology and Neurosurgery, University of Illinois, Chicago, Illinois.

ABSTRACT The ultrastructural characteristics of elasmobranch central nervous system have not been previously reported. This study presents a general assessment of aldehyde perfused brain and spinal cord in three species of shark: tiger, hammerhead and Atlantic nurse. The same distinct cell types are present in the shark that exist in mammals and similar criteria may be used for their differentiation. Neurons have frequently round nuclei with a prominent nucleoli; cytoplasm is abundant and filled with formed elements; somatic synapses and subsurface cisterns are rare. Astrocytes are smaller, and have less cytoplasm and slightly fewer organelles. Glial fibrils occur, but are not invariably present. Separating astrocytes from neurons is the most difficult identification problem. Oligodendroglia are smaller, and have denser cytoplasm and a dark nucleus. The striking feature of capillary morphology is the presence of an appreciable perivascular space containing collagen; many tortuous evaginations of this space occur into surrounding glial processes which completely invest the capillaries. Astrocyte cell bodies frequently lie immediately next to vessels, and capillaries are occasionally totally surrounded by a single astrocyte process, thus being endocellular. Smaller pericapillary processes may be either astrocytic or ependymal. Dendrites, synapses, axons, and myelin have no obvious special characteristics. Sodium, visualized by precipitation techniques, is prominent in the astroglia and neurons.

Interest in comparative neuroanatomical studies has been increasing in recent years. This resurgence can be related both to the advent of the electron microscope, and the presence of certain unique structural features in lower forms which may be explored in ways not possible in related mammalian systems. Thus, studies on the giant axon of the squid (Cole and Hodgkin, '39) have provided basic information on nervous transmission, while investigations on the leech (Kuffler and Potter, '64) and aplysia (Rosenbluth, '67) have clarified some aspects of glial-neuronal interrelationship.

Nieuwenhuys ('64, '67) has been laying the foundation for such studies in lower vertebrates by providing compendia of the older literature supplemented by new light-microscopic observations. The electron microscope has been utilized to investigate the nervous system of several invertebrates, and most lower vertebrate classes. Although the light-microscopic cellular morphology of the shark brain has been briefly

described (Klatzo, '67), elasmobranch ultrastructure has received essentially no attention. One report which deals with fine structural changes in shark brain thought to be secondary to traumatic edema has appeared, but lacks adequate normal comparisons (Bakay and Lee, '66).

The recent interest in various aspects of elasmobranch biology has been expressed in two symposia ('62, '66) on this subject. Interesting data concerning some functional aspects of shark central nervous system have been reported on the production, composition, and circulation of the cerebrospinal fluid (Oppelt, Patlak, Zubrod and Rall, '64; Rasmussen and Rasmussen, '67; Klatzo and Steinwall, '65), and the striking resistance to injury of the blood-brain barrier in these animals (Klatzo and Steinwall, '65).

Exact delineation of the functional differences which may exist in elasmobranchs requires assessment of normal ultrastructure. Therefore, this study was undertaken

to provide a generalized, preliminary view of the fine cytocharacteristics and cellular relationships in shark brain, and to establish a basis on which to evaluate future experimentation on this ancient animal, some species of which have remained unchanged by evolution for over 15 million years. Our observations are of general characteristics of neurons, glia, and capillary systems; more restricted studies of special cells such as occur in anterior spinal horns, cerebellum, and mesencephalic trigeminal nucleus have not been carried out. The ependyma, pial surface, and choroid plexus have also been left for future study.

MATERIAL AND METHODS

This study was based on material prepared for light and electron microscopy from ten sharks: one 100-pound hammerhead shark, *Sphyrna zygaena*; two 200-pound tiger sharks, *Galeocerdo cuvieri*; one 150-pound nurse shark, *Ginglymostoma cirratum*; and six young nurse sharks under three pounds. The sharks were provided by the Marine Station of the Department of Marine Biology, University of Puerto Rico, La Parguera, Puerto Rico; fixation and tissue processing were carried out at this facility.

The fixative employed was a combination of glutaraldehyde and formaldehyde in shark buffer. The shark buffer consisted of a mammalian phosphate or cacodylate solution with added urea and NaCl to bring the osmotic strength to 670 mM/L, which is equivalent to the osmolality of shark plasma. The shark buffers were prepared in concentrated form (X 2) as follows:

NaH ₂ PO ₄ ·H ₂ O	4.52%	83 ml	} (488 mM/L)
NaOH	5.04%	17 ml	
Urea		4.4 gm	(720 mM/L)
NaCl		0.8 gm	(138 mM/L)
Sodium cacodylate		64 gm	(400 mM/L)
Urea		4.4 gm	(720 mM/L)
NaCl		1.2 gm	(220 mM/L)
H ₂ O		100 ml	

Concentrated (immersion) and dilute (perfusion) fixative solutions were made up according to the method of Karnovsky ('65) and Reese and Karnovsky ('67). To mix 100 ml of dilute fixative, 50 ml of shark buffer (X 2) and 2.5 ml of 50% glutaraldehyde were added to a solution

of 1 gm of paraformaldehyde in 47.5 ml of H₂O. For the concentrated fixative, 40 ml of shark buffer (X 2) and 10 ml of glutaraldehyde were added to 4 gm of paraformaldehyde in 50 ml of H₂O. The pH of these solutions was brought to about 7.2. The osmolality of the dilute solution, not including the contribution of the fixatives, is 673 mM/L, whereas that of the concentrated solution is somewhat less.

Fixation of the small sharks by perfusion was uniformly successful. The sharks were anesthetized by immersion in a 0.05% solution of MS-222 (Sandoz). The dilute solution (100–500 ml) was perfused via the conus arteriosus from a height of five feet. The brains were then removed, sliced coronally (1–2 mm), and immersed in the concentrated solution.

Fixation of large adults was less successful. The sharks were pulled out of the pen onto a platform in nets, and anesthetized by spraying about 500 ml of 1–2% MS-222 in sea water into the external gill slits. Briskly running sea water was pumped through the gills via a hose in the mouth to insure adequate oxygenation. One brain was fixed by immersion of slices in the concentrated fixative or in 1% osmium tetroxide in shark buffer. One perfusion was done by slicing off the tail and inserting a cannula (PE 360) up the caudal artery into the dorsal aorta. In another shark, a cannula was placed in the conus arteriosus. The most successful fixation was accomplished by perfusing both the conus and the caudal artery with the solution, but, even in this shark, only the spinal cord and olfactory bulbs were grossly free of blood. For the large sharks, 40 liters of the dilute fixative were used for perfusion, from a height of six feet.

Following the perfusion, the brains were sliced into the concentrated fixative. After 6–16 hours in the concentrated fixative, the specimens were washed for 1–2 hours in shark buffer, postfixed in 1% osmium tetroxide in shark buffer for 1–3 hours, and dehydrated and embedded in araldite or epon. Some tissue, prior to dehydration, was stained with uranyl acetate (Reese and Karnovsky, '67). Sections were stained with lead citrate (Venable and Coggeshall, '65) and examined in RCA EMU-3E and EMU-3F electron microscopes.

For ultrastructural localization of sodium, tissue was obtained from one adult and two young sharks. Fixation was by immersion in 1% unbuffered osmium for one-half-hour followed by one-half-hour in an osmium-antimony mixture. One animal was fixed by perfusion with an aldehyde-potassium phosphate buffer solution, prior to osmication. The tissue was then processed according to the method previously described by Hartmann ('66).

Tissue for light microscopy was left in fixative for several weeks and then embedded in paraffin. Luxol-fast-blue-Nissl and PTAH stains were employed in all animals. Gold chloride, silver carbonate, PAS, reticulin, and hematoxylin-eosin preparations were utilized in special instances.

RESULTS

The following observations were made from examination of material from various parts of the CNS of two adult tiger sharks, one adult hammerhead shark, and one adult and six immature nurse sharks. The descriptions are of general characteristics which occur throughout the nervous system. A brief resumé of the preliminary light microscopy will be presented for orientation, followed by the fine structure of the parenchyma and its capillaries.

Light microscopy

Neurons. The cellular morphology of shark nerve cells and their individual regional characteristics has been reported previously (Klatzo, '67). Shark neurons, although varying greatly in size, are basically similar to mammalian nerve cells. They usually possess large, spherical nuclei with prominent nucleoli and well developed Nissl bodies. A striking feature is glial satellitosis, which primarily occurs in central and frontodorsal regions of the telencephalon (fig. 1A). Glial cells are clustered around individual neurons. Satellitosis is less prominent in young sharks; neurons with only one or two neighboring glial cells are common. Neurons frequently occur in intimate spatial relationship to blood vessels, especially in the mesencephalic trigeminal nucleus and medulla. In the spinal cord, small neurons are found interspersed between myelinated fibers of lateral tracts (fig. 1D). Identification of

these cells as neurons and not astrocytes is based on the presence of a large nucleus, prominent nucleolus, and distinct peripheral zone of Nissl substance.

Glia. All three glial cell types (astrocytes, oligodendrocytes and microglia) are easily identified by specific metallic impregnations. In Cajal's gold chloride preparations, astrocytes are found in characteristic relationship to blood vessels, pial surfaces, and neurons. Astrocytes appear to lie with cell bodies directly applied to vascular walls (fig. 1B), with slender processes extending eccentrically into the nervous parenchyma without discernible formation of the vascular end feet characteristic of mammalian brain. The astroglia also line the pial surface with processes descending into the neuropil, again without prominent foot-plates. Many of the glial cells clustered about neurons (fig. 1A) can be identified by the specific gold chloride stain as astrocytes. All three configurations are most prominent in anterior forebrain.

Hortega's silver methods reveal that oligodendrocytes and microglia closely resemble the corresponding mammalian forms. Oligodendrocytes are the most common constituent of the perineuronal and perivascular glial clusters.

Blood vessels. In addition to the perivascular cuffing of glial cells and the intimate relationship of blood vessels and neurons observed in some areas, the striking feature of the vessels themselves is the richness of the connective tissue investiture. Fine reticulin fibers are regularly demonstrated in the walls of capillaries (fig. 1C). Another interesting feature is the presence of abundant glycogen in the smooth muscle cells of the arterioles and small arteries.

Electron microscopy

Neurons. The complexes consisting of a neuron and surrounding glia are readily apparent in ultrathin sections. However, only two or three cells, in addition to the neuron, are usually present (fig. 2). The nerve cell is usually prominent because of its size. The nucleus is frequently round but may be irregular in outline (figs. 3, 4). Two nucleoli are commonly present,

to provide a generalized, preliminary view of the fine cytocharacteristics and cellular relationships in shark brain, and to establish a basis on which to evaluate future experimentation on this ancient animal, some species of which have remained unchanged by evolution for over 15 million years. Our observations are of general characteristics of neurons, glia, and capillary systems; more restricted studies of special cells such as occur in anterior spinal horns, cerebellum, and mesencephalic trigeminal nucleus have not been carried out. The ependyma, pial surface, and choroid plexus have also been left for future study.

MATERIAL AND METHODS

This study was based on material prepared for light and electron microscopy from ten sharks: one 100-pound hammerhead shark, *Sphyrna zygaena*; two 200-pound tiger sharks, *Galeocerdo cuvieri*; one 150-pound nurse shark, *Ginglymostoma cirratum*; and six young nurse sharks under three pounds. The sharks were provided by the Marine Station of the Department of Marine Biology, University of Puerto Rico, La Parguera, Puerto Rico; fixation and tissue processing were carried out at this facility.

The fixative employed was a combination of glutaraldehyde and formaldehyde in shark buffer. The shark buffer consisted of a mammalian phosphate or cacodylate solution with added urea and NaCl to bring the osmotic strength to 670 mM/L, which is equivalent to the osmolality of shark plasma. The shark buffers were prepared in concentrated form (X 2) as follows:

NaH ₂ PO ₄ ·H ₂ O	4.52%	83 ml	} (489 mM/L)
NaOH	5.04%	17 ml	
Urea		4.4 gm	(720 mM/L)
NaCl		0.8 gm	(138 mM/L)
Sodium cacodylate		64 gm	(400 mM/L)
Urea		4.4 gm	(720 mM/L)
NaCl		1.2 gm	(220 mM/L)
H ₂ O		100 ml	

Concentrated (immersion) and dilute (perfusion) fixative solutions were made up according to the method of Karnovsky ('65) and Reese and Karnovsky ('67). To mix 100 ml of dilute fixative, 50 ml of shark buffer (X 2) and 2.5 ml of 50% glutaraldehyde were added to a solution

of 1 gm of paraformaldehyde in 47.5 ml of H₂O. For the concentrated fixative, 40 ml of shark buffer (X 2) and 10 ml of glutaraldehyde were added to 4 gm of paraformaldehyde in 50 ml of H₂O. The pH of these solutions was brought to about 7.2. The osmolality of the dilute solution, not including the contribution of the fixatives, is 673 mM/L, whereas that of the concentrated solution is somewhat less.

Fixation of the small sharks by perfusion was uniformly successful. The sharks were anesthetized by immersion in a 0.05% solution of MS-222 (Sandoz). The dilute solution (100–500 ml) was perfused via the conus arteriosus from a height of five feet. The brains were then removed, sliced coronally (1–2 mm), and immersed in the concentrated solution.

Fixation of large adults was less successful. The sharks were pulled out of the pen onto a platform in nets, and anesthetized by spraying about 500 ml of 1–2% MS-222 in sea water into the external gill slits. Briskly running sea water was pumped through the gills via a hose in the mouth to insure adequate oxygenation. One brain was fixed by immersion of slices in the concentrated fixative or in 1% osmium tetroxide in shark buffer. One perfusion was done by slicing off the tail and inserting a cannula (PE 360) up the caudal artery into the dorsal aorta. In another shark, a cannula was placed in the conus arteriosus. The most successful fixation was accomplished by perfusing both the conus and the caudal artery with the solution, but, even in this shark, only the spinal cord and olfactory bulbs were grossly free of blood. For the large sharks, 40 liters of the dilute fixative were used for perfusion, from a height of six feet.

Following the perfusion, the brains were sliced into the concentrated fixative. After 6–16 hours in the concentrated fixative, the specimens were washed for 1–2 hours in shark buffer, postfixed in 1% osmium tetroxide in shark buffer for 1–3 hours, and dehydrated and embedded in araldite or epon. Some tissue, prior to dehydration, was stained with uranyl acetate (Reese and Karnovsky, '67). Sections were stained with lead citrate (Venable and Coggeshall, '65) and examined in RCA EMU-3E and EMU-3F electron microscopes.

Neuropil. The neuropil in these animals is not remarkably different from that in other species. Cell processes are tightly packed, and a small 100–200 Å space exists between them. Macroglial processes which are not perivascular are difficult to recognize; in general, they are irregular in outline and may contain glycogen or fibrils, but not tubules. Synaptic terminals are very common and they seem to have the general configuration described in other species (figs. 8, 9). In the spinal cord, synapses containing dense-cored vesicles are occasionally evident (fig. 10). The majority of synapses occur in the fine neuropil; synapses on cell bodies and large dendrites are uncommon. Dendrites are often seen in longitudinal section; they are large with well developed tubular systems and frequently contain elongated mitochondria (fig. 9).

Capillaries. The CNS capillaries of sharks demonstrate several unusual features, which are most pronounced in the immature nurse sharks. The endothelium is continuous, as in other species, without fenestrations (Maynard, Schultz, and Pease, 57). Particularly in the young sharks, there are large numbers of endothelial vesicles, which occasionally communicate with the luminal or contraluminal cell surface. The endothelial junctions in the young sharks are unusually straight, with little or no overlapping of the adjoining cells (fig. 16). Often, there is a thickening of the apposed membranes at the junction. The adult has some of these straight junctions (fig. 15), and others which are longer or more tortuous. Pericytes line about 50% of the capillary surface, with a narrow gap between the pericyte and endothelial cell.

The most striking feature of capillary morphology is the presence of a collagen-containing perivascular space which, in our material, varies from 0.08–2.6 μ in width (figs. 11, 12, 13, 14). This space is wider and more densely packed with collagen in the adult sharks, and occasionally contains connective cell processes (figs. 13, 20). There are separate, ill defined, endothelial basement membranes on either side of the space. A prominent feature of many capillaries, particularly in the young sharks, is the occurrence of

evaginations of the perivascular space into the adjacent glial processes (figs. 12, 13). These certainly correspond to the radial "spokes" seen in the light microscope (Horstmann, '64), and can project as much as 1.5 μ into the perivascular tissue. The glial basement membrane is reflected into these "spokes," and their core consists of the collagen-containing material of the perivascular space which is visualized in reticulin-staining methods of light microscopy (fig. 1C). These evaginations are felt to be tubular in shape because they are seen as narrow projections in all planes of section through the capillary. They never extend completely across the perivascular glial processes into the surrounding neuropil.

Glial cytoplasm is interposed between the perivascular space and the nervous elements over the entire surface of the capillary. The cytoplasm is similar to that in mammals becoming clear and "watery" when fixation is not optimal. Junctions between neighboring processes are long and tortuous (figs. 13, 14), which has made it impossible to determine if they provide open channels from perivascular space to neuropil. Several features of this glial investment are of particular interest. First, it is not uncommon for the glial cell body to lie immediately against the capillary (fig. 11). These cells correspond in appearance to the astrocytes described previously. Occasionally, a process leaves the glial cell and stretches away from the capillary into the neuropil. Cell bodies appearing similar to these pericapillary somata, but removed from the pericapillary space by a narrow process of another cell are also common (fig. 4).

In immature sharks, a capillary is occasionally totally invested by a single glial cell process rather than two or more as in the mammal (fig. 12). In sections demonstrating this arrangement, there are no intercellular junctions whatsoever in the perivascular glial layer. Endoastrocytic capillaries have not been seen in the adult material but, in both young and adult sharks, each glial cell process tends to cover a greater portion of the capillary than in the mammal. Occasionally, the processes form a double layer around part

eccentrically abutting the nuclear membrane.

Cytoplasm is abundant and filled with organelles which have the general characteristics described for mammals. Rough-surfaced endoplasmic reticulum characteristically is found palisading peripherally near the cell membrane (fig. 5). This may occur in the perikaryon, but is more typical in proximal portions of dendrites. Subsurface cisterns occur but are rare. Free ribosomes are common. Neurofilaments have not been seen with certainty. Glycogen is not a component of neuron cytoplasm in our material.

Besides size, typical cytoplasmic components, and nuclear configuration, it is also possible to identify neurons by their frequent cell processes (fig. 3). One or two dendrites are commonly seen arising from these cells. The dendrites are broad processes whose chief identifying feature is an extensive tubular system such as characterizes dendrites in other species. Synapses are not commonly seen upon nerve cell bodies or large dendritic trunks (fig. 4). The neurons which by light microscopy are closely related to blood vessels are actually separated from the vascular wall by a glial process (fig. 4).

Astrocytes. The mammalian astrocyte was originally characterized as a "watery cell" with few organelles (Farquhar and Hartmann, '57). Improved methods of fixation have shown greater numbers of intracytoplasmic elements, but these cells are still distinguished by a relatively smaller complement of organelles in most species.

In the shark, astrocytes vary in size, but usually are smaller than neurons (fig. 6). The general outline is round, oval, or slightly elongated. The nuclei are pleomorphic, and frequently round or lobular, but may be angular, and are very close to neuronal nuclei in density. Nucleoli occur, but less commonly than in neurons. There is a moderate amount of cytoplasm, though consistently less than in nerve cells, and the cytoplasmic matrix is slightly less dense. Glycogen is not commonly found in cell bodies. Glial fibrils are far more common in adult animals than in the infants, and are more frequent in myelinated areas than in the forebrain.

Oligodendroglia. In myelinated areas of brain stem and spinal cord, cells occur which are identical in appearance with mammalian oligodendroglia. These glia are insinuated between myelin sheaths in large numbers, but do not form the characteristic interfascicular rows of mammals. Astrocytes are rare in such areas. These oligodendrocytes are smaller than astrocytes and vary greatly in shape from round to irregularly angular (fig. 7). Nuclear chromatin is densely clumped and the nucleus is much darker than that of the astrocyte. The cytoplasmic matrix is extremely dense. There are many free ribosomes. An extensive microtubular system may often be seen. Multiple sizes and shapes of dense bodies occur.

In the forebrain, the small darker cells are not so common and are not so obviously oligodendroglia. They are again variable in shape, frequently being quite irregular. The nuclear chromatin is less densely clumped, and the typical large organelle complement is not always present. Satellite oligodendroglia often are applied directly to the neuronal membrane. These cells are elongated in shape; the nucleus is dense with clumped chromatin, and there is a very thin rim of dense cytoplasm. Free ribosomes are common, as are microtubules. There is another type of cell which appears to be an oligodendrocyte but which differs from the majority of dark cells. This cell has a typical nucleus and cell body, but has one or two large, broad processes which, except for their denser cytoplasm, resemble dendrites. Characteristically, these processes have well developed microtubular systems. No major differences between oligodendrocytes in adult and young animals are apparent. Oligodendrocytes in perivascular clusters seem to be separated from the vessel wall by an interposed astrocyte process.

Microglia. Cells definitely identifiable as microglia were not seen. It is possible that some of the dark cells, particularly those with extensive dense body formations, could belong to this cell type (Villegas and Fernandez, '66). This problem will require further clarification, since these cells have been identified by light microscopy (Klatzo, '67).

number. Whereas it is seldom difficult to distinguish the oligodendroglia from astroglia, their differentiation from small neurons is less certain. This is especially true in brainstem and spinal cord where very small neurons are scattered through myelinated regions (fig. 1D). Cells of this nature have been described in other species as "dark" neurons (Mugnaini, '65), variant oligodendrocytes (Kruger and Maxwell, '67) or microglia (Villegas and Fernandez, '66). It is most prudent to say that, in the shark, the identity of these cells cannot be established with certainty in some instances.

In spite of these ambiguities, it is possible to identify astrocytes, oligodendroglia, and neurons in the shark by essentially the same criteria that are commonly utilized for separating these forms in mammals. Therefore, from a morphological standpoint, it appears there exists an homology between glial and neural elements in elasmobranchs, several other submammalian vertebrates, and mammals.

The pericapillary architecture of the shark CNS differs in several respects from the mammalian arrangement (Donahue and Pappas, '61; Maynard, Schultz, and Pease, '57). The endothelial layer presents only one variation of note, the frequent lack of interdigitation between adjacent endothelial cells with consequent shortening of the gap running from lumen to basement membrane (figs. 15, 16). The occurrence of a connective tissue space around parenchymal capillaries has been previously described only in the urodele amphibian, *Necturus* (Bodenheimer and Brightman, '67).

The total investment of CNS capillaries by glial cytoplasm is now a well established finding in mammals (Wolff, '63; Mugnaini and Walberg, '64). With the exception of some examples in teleosts (Kruger and Maxwell, '67), this rule seems to hold for lower vertebrates also. However, in certain specialized areas such as the neurohypophysis, other elements impinge directly upon the pericapillary space (Palay, '57). In the shark, glial cytoplasm is consistently present between the capillary and the neuropil, but there are some unusual features of this glial tunic. These are the

evaginations of the pericapillary space into the glial cytoplasm, the frequent occurrence of glial cell bodies in a juxtacapillary position, and the occasional capillaries ensheathed in a single glial process (figs. 12, 13, 14). The physiological significance of these variations is obscure. Neither the evaginations nor the capillaries invested by an uninterrupted glial sheath have been described in other species. The proximity of astroglial cell bodies to capillaries is unusual but not unknown; however, the frequency of this arrangement in the shark, particularly in the young specimens, is striking (fig. 11). This relationship was clearly noted in the light microscope by Horstmann ('54) and Klatzo ('67). Mugnaini and Walberg ('64) found occasional glial cell bodies in a pericapillary location in mammals, and Donahue and Pappas ('61) encountered this relationship more often in immature rats than in adults. This configuration is also present in *Mytilus* (Mugnaini and Walberg, '65).

The interesting question of the role of ependymal and astrocytic processes in the formation of vascular end feet in lower vertebrates has been discussed by Kruger and Maxwell ('66, '67). In the elasmobranch, Horstmann ('54) showed that vascular end feet are formed by both astrocytes and ependymal cells. However, the identification and description of ependymal processes in the shark and their differentiation from astrocyte processes, has not been attempted here. The fibrillar perivascular processes described may derive either from astrocytes or ependyma (Achúcarro, '15).

Finally, a brief word must be said concerning the blood-brain barrier. In mammals, the barrier to the protein, horseradish peroxidase, is situated in the endothelium (Reese and Karnovsky, '67). In the urodele amphibian, with pericapillary spaces identical to those of the shark, the barrier to peroxidase is likewise in the endothelium (Bodenheimer and Brightman, '67). In mammals, the perivascular glial processes do not enclose the capillaries by a continuous zone of tight junctions (Kuffler and Nicholls, '67; Reese and Karnovsky, '67); and, in the mammal and urodele, the gaps between glial and end feet are permeable to peroxidase (Bright-

of the capillary rather than the usual single investment.

In certain parts of the brain, the pericapillary glia contains tightly packed filaments, reminiscent of mammalian "glial" filaments, but far more extensive in array (fig. 13). These filamentous glial processes have been seen in scattered areas of the adult and young shark brain and spinal cord, both around capillaries and at the pial surface. They can only rarely be traced to cell bodies, and may constitute ependymal rather than astrocytic processes (Fleischhauer, '58).

Myelin and axons. Unmyelinated axons are common and can be recognized by their round or tubular shape and the presence of axon filaments. We have not attempted an extensive study of myelin in these animals. However, the general configuration of myelinated axons is similar to other species (figs. 18, 19).

Sodium distribution. Sodium antimonate was precipitated widely throughout the forebrain. As in mammals, the precipitate was found in astrocytes in large quantities and in smaller amounts in neurons and their processes (fig. 17). The high osmolarity of elasmobranch body fluids is not completely explained. This sodium pattern seems to give some support to the postulate that two cell populations with different ionic concentrations exist in the shark, one high in Na^+ and the other in K^+ (Murdaugh et al., '65). As judged by the immersion-fixation-pyroantimonate technique the astrocytes of the forebrain contain large amounts of sodium. However, the relevance of this demonstration to the actual ionic concentration of the living cell has not been completely established, and the technique is not quantitative (Hartmann, '66).

DISCUSSION

Much of the descriptive material presented does not require further elaboration, but there are two aspects relating to neuroglial cells which are worthy of some discussion. First, is the problem of glial cell identification and, second, are the questions raised by the arrangement of glia around capillaries.

The difficulty in characterizing the different varieties of glial cells in sub-

mammalian vertebrates is well known (Achúcarro, '15; Kruger and Maxwell, '67). In the shark, most parenchymal cells conform to the accepted appearance for neurons, astrocytes, and oligodendroglia (Palay and Palade, '55; Schultz, Maynard, and Pease, '57; Mugnaini and Walberg, '64). However, many others are not distinctly separated by these arbitrary categories. The ultrastructural classification of cells in submammalian brains is accomplished by comparison with light-microscopic findings with respect to appearance and location, and by comparison with mammalian observations. Mugnaini and Walberg ('64) have reviewed the characteristics of mammalian glia. Recently Kruger and Maxwell ('67) have discussed glial-cell identification in teleosts and reptiles, and found the principal problem to be the distinction of astrocytes from oligodendrocytes. In the shark, the chief difficulty is that of distinguishing the glial cells from neurons, rather than differentiating them from each other. Differences between the cell bodies of astrocytes and small neurons are few. Many cell bodies applied to blood vessels are quite certainly astrocytes, on the basis of gold chloride stains (fig. 1B). Clusters of cells around large neurons can also be identified as astrocytes in gold or Nissl material (fig. 1A). On an ultrastructural level size, the presence of ample cytoplasm, a large complement of organelles, well developed granular endoplasmic reticulum, free ribosomes, and processes containing these inclusions usually characterize neurons (figs. 2, 3, 4). Somatic synapses (fig. 4) and subsurface cisterns, when present, positively identify neurons. Unfortunately, these two features are rare in the shark, and glycogen is not solely confined to astrocytes in submammalian species (Kruger and Maxwell, '67; Bodenheimer and Brightman, '67). Many astrocytes and small neurons simply look alike, especially in the young sharks. If specific identifying characteristics such as synapses of subsurface cisterns are not present, some cells cannot be definitely categorized.

Most elasmobranch oligodendrocytes display the characteristic mammalian appearance and, in contrast to teleosts (Kruger and Maxwell, '67), are plentiful in

- Schultz, R. L., E. A. Maynard and D. C. Pease
1957 Electron microscopy of neurons and
neuroglia of cerebral cortex and corpus cal-
losum. *Am. J. Anat.*, 100: 369-408.
- Venable, J. H., and R. Coggeshall 1965 A
simplified lead citrate stain for use in electron
microscopy. *J. Cell Biol.*, 25: 407-408.

- Villegas, G. M., and J. Fernandez 1966 Perme-
ability to thorium dioxide of the intercellular
spaces of the frog cerebral hemisphere. *Exp.*
Neurol., 15: 18-36.
- Wolff, J. 1963 Beiträge zur Ultrastruktur der
Kapillaren in der normalen Grosshirnrinde. *Z.*
Zellforsch., 60: 409-431.

man, '67; Bodenheimer and Brightman, '67). Without the use of tracers in the shark, it is impossible to determine if the same situation holds. However, it is likely that it does, and that the unusual features of pericapillary glial architecture described do not affect the blood-brain barrier to protein. Klatzo and Steinwall ('65) noted an unusual resistivity of the elasmobranch blood-brain barrier to certain lesions, as compared with mammals and teleost fishes (Bernstein and Streicher, '65). Whether this is due to a difference in the capillary endothelium, the variation of perivascular glial cell architecture, or other factors cannot be decided from this preliminary view of the normal ultrastructure.

LITERATURE CITED

- Achúcarro, N. A. 1915 De l'évolution de la néurologie, et spécialement de ses relations avec l'appareil vasculaire. *Trab. Lab. Invest. Biol. (Madrid)*, 13: 169-212.
- Bakay, L., and J. C. Lee 1966 Ultrastructural changes in the edematous central nervous system. III Edema in shark brain. *Arch. Neurol.*, 14: 644-660.
- Bernstein, J. J., and E. Streicher 1965 The blood brain barrier of fish. *Exp. Neurol.*, 11: 464-473.
- Bodenheimer, T. S., and M. W. Brightman 1967 Perivascular space and the blood-brain barrier to peroxidase. *Anat. Rec.*, 157: 351.
- Brightman, M. W. 1967 Intracerebral movement of proteins injected into the blood and cerebrospinal fluid. *Anat. Rec.*, 157: 219.
- Cole, K. S., and A. L. Hodgkin 1939 Membrane and protoplasm resistance in the squid giant axon. *J. Gen. Physiol.*, 22: 671-687.
- Donahue, S., and G. D. Pappas 1961 The fine structure of capillaries in the cerebral cortex of the rat at various stages of development. *Am. J. Anat.*, 108: 331-347.
- Farquhar, M. G., and J. F. Hartmann 1957 Neuroglial structure and relationships as revealed by electron microscopy. *J. Neuropath. Exp. Neurol.*, 16: 18-39.
- Fleischhauer, K. 1958 Über die Feinstruktur der Faseraglia. *Z. Zellforsch.*, 47: 548-556.
- Gilbert, P. W., ed. 1963 *Sharks and Survival*. Heath, Boston.
- Gilbert, P. W., R. Matheson, and D. P. Rall, eds. 1967 *Sharks, Skates and Rays*. Johns Hopkins Press, Baltimore.
- Hartmann, J. F. 1966 High sodium content of cortical astrocytes. *Arch. Neurol.*, 15: 633-642.
- Horstmann, E. 1954 Die Faseraglia des Schachiergehirns. *Z. Zellforsch.*, 39: 588-617.
- Karnovsky, M. J. 1965 A formaldehyde-glutaraldehyde fixative of high osmolality for use in electron microscopy. *J. Cell Biol.*, 27: 137A.
- Klatzo, I. 1967 Cellular morphology of the lemon shark brain. In: *Sharks, Skates and Rays*. P. W. Gilbert, R. F. Mathewson, and D. P. Rall, eds. Johns Hopkins Press, Baltimore, pp. 341-360.
- Klatzo, I., and O. Steinwall 1965 Observations on cerebrospinal fluid pathways and behaviour of the blood-brain barrier in sharks. *Acta Neuropath.*, 5: 161-175.
- Kruger, L., and D. S. Maxwell 1966 The fine structure of ependymal processes in the telost optic tectum. *Am. J. Anat.*, 119: 479-493.
- 1967 Comparative fine structure of vertebrate neuroglia: Teleosts and reptiles. *J. Comp. Neurol.*, 129: 115-142.
- Kuffler, S. W., and J. G. Nicholls 1966 The physiology of neuroglial cells. *Ergebn. d. Physiol.*, 57: 1-90.
- Maynard, E. A., R. L. Schultz and D. C. Pease 1957 Electron microscopy of the vascular bed of rat cerebral cortex. *Am. J. Anat.*, 100: 409-433.
- Mugnaini, E. 1965 "Dark cells" in electron micrographs from the C.N.S. of vertebrates. *J. Ultra. Res.*, 12: 235.
- Mugnaini, E., and F. Walberg 1961 Ultrastructure of neuroglia. *Ergebn. Anat. Entwickl. Gesch.*, 37: 193-236.
- 1965 The fine structure of the capillaries and their surroundings in the cerebral hemispheres of *Myxine glutinosa* (L.). *Z. Zellforsch.*, 66: 333-351.
- Murdaugh, H. V., E. D. Robin, P. Soteres and E. Weiss 1965 Intracellular electrolyte patterns in the dogfish: II Muscle and brain. *Bull. Mt. Desert Island Biol. Lab.*, 5: 14-15.
- Nieuwenhuys, R. 1964 Comparative anatomy of the spinal cord. *Prog. Brain Res.*, 11: 1-57.
- 1967 Comparative anatomy of efferent centers and tracts. *Prog. Brain Res.*, 23: 1-64.
- Oppelt, W. W., C. S. Padak, C. G. Zubrod and D. P. Rall 1964 Ventricular fluid production rates and turnover in elasmobranchii. *Comp. Biochem. Physiol.*, 12: 171-174.
- Palay, S. L. 1957 Fine structure of neurohypophysis. In: *Ultrastructural and Cellular Chemistry*. P. Hoerber, New York.
- Palay, S. L., and G. E. Palade 1955 The fine structure of neurons. *J. Biophys. Biochem. Cytol.*, 1: 69-89.
- Rasmussen, L. E., and R. A. Rasmussen 1967 Comparative protein and enzyme profiles of the cerebrospinal fluid, extracellular fluid, nervous tissue, and sera of elasmobranchii. In: *Sharks, Skates and Rays*. P. W. Gilbert, R. F. Mathewson, and D. P. Rall, eds. Johns Hopkins Press, Baltimore, pp. 361-379.
- Reese, T. S., and M. J. Karnovsky 1967 Fine structural localization of a blood-brain barrier to exogenous peroxidase. *J. Cell Biol.*, (in press).
- Rosenbluth, J. 1967 Functions of glial cells. Presented to the Fifty-Sixth Annual Meeting of the International Academy of Pathology, March 12-15. Washington, D.C.



PLATE 1

EXPLANATION OF FIGURES

- 1A Adult nurse shark. Telencephalon. A neuron surrounded by satellite glial cells. Cresyl violet—Luxol blue stain; $\times 1100$.
- 1B Adult nurse shark. Telencephalon. A striking arrangement of astrocytic cells lying with cell-bodies in juxtaposition to a blood vessel and sending processes eccentrically into the parenchyma. Cajal's gold chloride stain; $\times 480$.
- 1C Adult tiger shark. Telencephalon. Capillaries showing network of connective tissue fibers (arrow). Hortega's reticulin stain; $\times 620$.
- 1D Adult tiger shark. Spinal cord. A small neuron (arrow) between myelinated nerve fibers in the lateral columns of the cord. Cresyl violet—Luxol blue stain; $\times 1200$.

Don M. Long, Thomas S. Bodenheimer, J. Francis Hartmann and Igor Klatzo

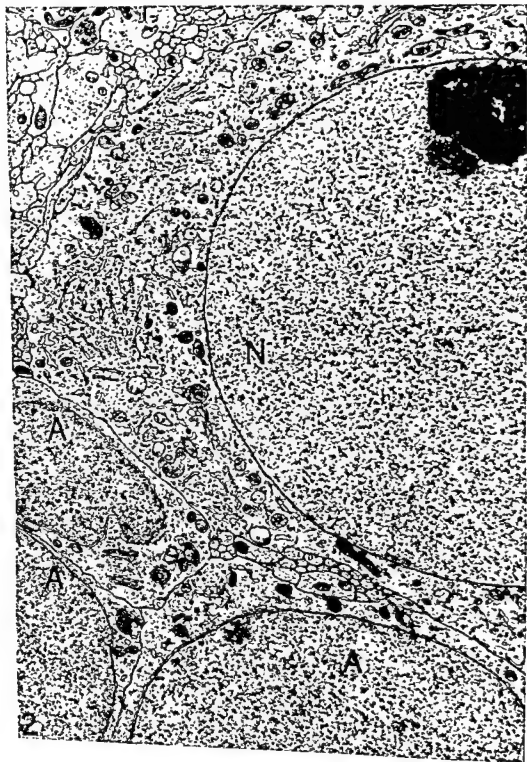


PLATE 2

EXPLANATION OF FIGURE

- 2 Typical neuron-glial complex from forebrain. The neuron (N) is larger, with more cytoplasmic organelles. Portions of three cells, probably all astrocytes (A), are seen in proximity. $\times 10,400$.

Don M. Long, Thomas S. Bodenheimer, J. Francis Hartmann and Igor Klatzo

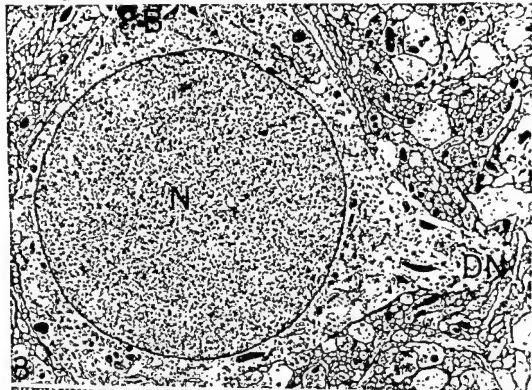


PLATE 3

EXPLANATION OF FIGURES

- 3 Small neuron (N) from periventricular region of forebrain. Several dense bodies (B) are present in the cytoplasm, and three dendritic (DN) origins are visible. $\times 15,200$.
- 4 Small neuron (N) in pericapillary position. Such a cell could easily seem to abut the capillary directly at low magnification but, with the electron microscope, glial processes (AP) are clearly interposed between the two. Capillary lumen (L). $\times 10,400$.

Don M Long, Thomas S. Bodenheimer, J Francis Hartmann and Igor Klotz

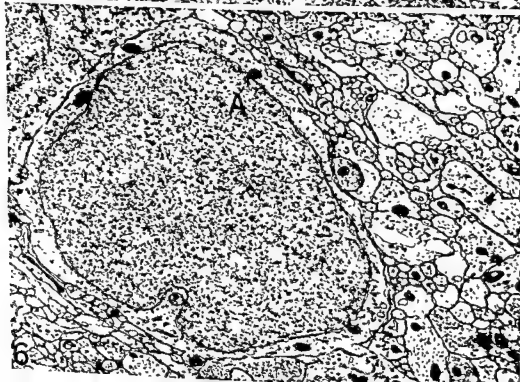
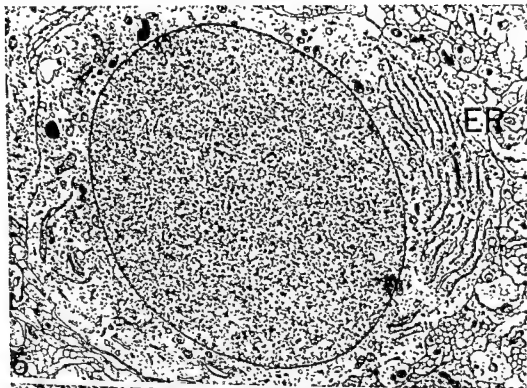


PLATE 4

EXPLANATION OF FIGURES

- 5 This figure illustrates the difficulty encountered in identifying some cells. The number of free ribosomes and amount of granular endoplasmic reticulum favor identification as a neuron, but definite differentiation from an astrocyte is not possible. Note palisading of endoplasmic reticulum (ER). $\times 10,400$.
- 6 Astrocyte (A) from forebrain of young shark. Sparser cytoplasm and fewer organelles identify this cell. $\times 15,200$.

Don M. Long, Thomas S. Bodenheimer, J. Francis Hartmann and Igor Klotz

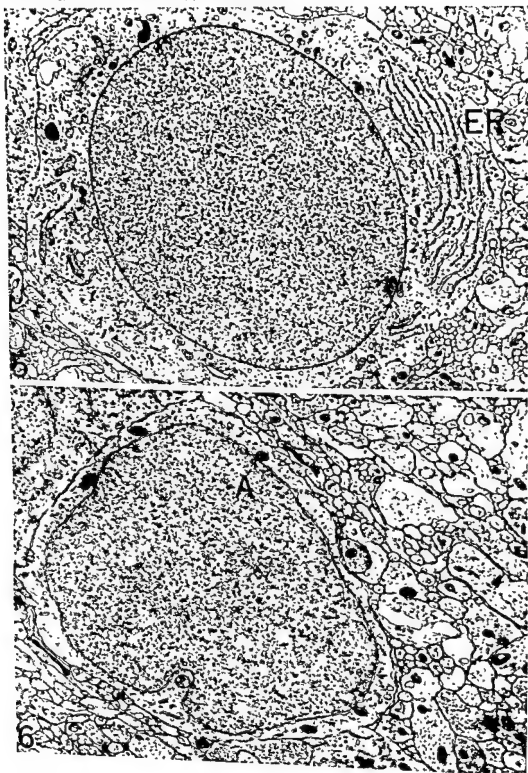


PLATE 5

EXPLANATION OF FIGURES

- 7 Oligodendrogliaocyte (O) near capillary in medulla of young shark. Several dense bodies (B) are present in the cytoplasm. A portion of a small neuron (N) is seen. $\times 12,800$.
- 8 Synapse (SN) from forebrain of young shark. Many uniform synaptic vesicles (V) are present. $\times 49,200$.

Don M. Long, Thomas S. Bodenheimer, J. Francis Hartmann and Igor Klatzo

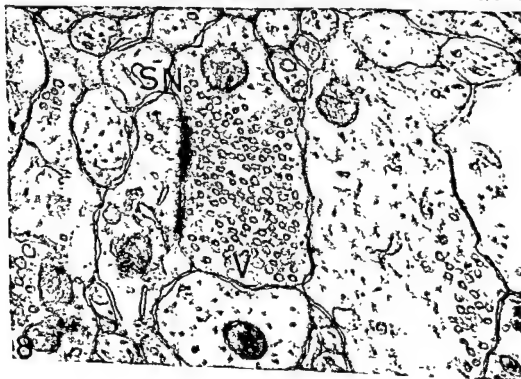
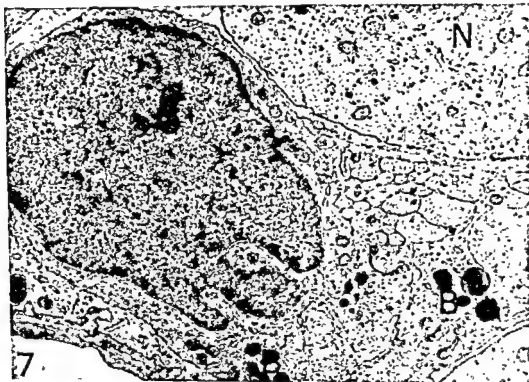


PLATE 6

EXPLANATION OF FIGURES

- 9 A large branching dendrite (DN) occupies the center of the field. Tubules, mitochondria, and free ribosomes are evident. $\times 15,200$.
- 10 Synapse from spinal cord of adult shark. Dense-cored vesicles (DV) are prominent. $\times 24,600$.
- 11 Astrocyte (A) perikaryon in typical juxtacapillary location. Cytoplasm (CY) is excessively clear due to less than optimal fixation. Capillary basement membrane (BM) and a pericyte (P) are demonstrated also. $\times 17,600$.

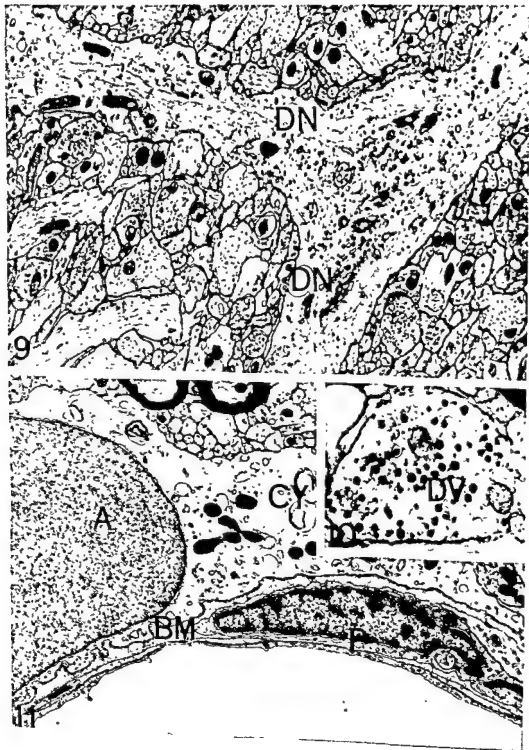


PLATE 6

EXPLANATION OF FIGURES

- 9 A large branching dendrite (DN) occupies the center of the field. Tubules, mitochondria, and free ribosomes are evident. $\times 15,200$.
- 10 Synapse from spinal cord of adult shark. Dense-cored vesicles (DV) are prominent. $\times 24,600$.
- 11 Astrocyte (A) perikaryon in typical juxtacapillary location. Cytoplasm (CY) is excessively clear due to less than optimal fixation. Capillary basement membrane (BM) and a pericyte (P) are demonstrated also. $\times 17,600$.

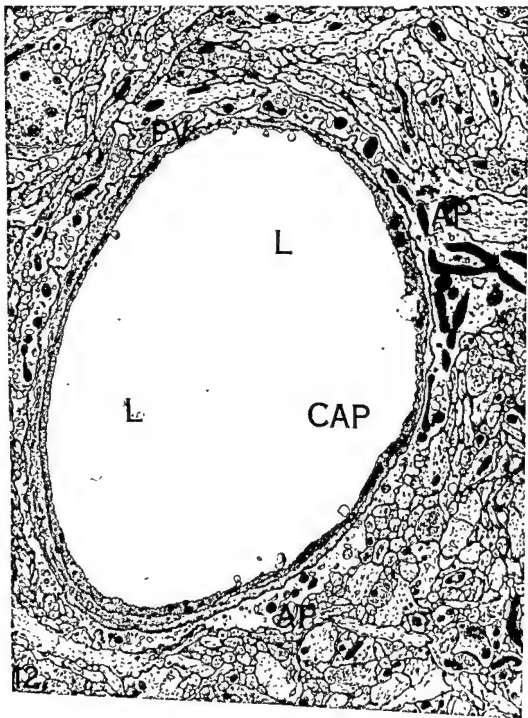


PLATE 7

EXPLANATION OF FIGURE

- 12 Uninterrupted perivascular glial sheath from forebrain of young shark. The astrocyte process (AP) on the right can be traced completely around the capillary (CAP) without an evident junction. Collagen-filled pericapillary space (PV) is present with some evaginations. Lumen (L) appear in center. $\times 10,400$.

Don M Long, Thomas S. Bodenheimer, J. Francis Hartmann and Igor Klatzo

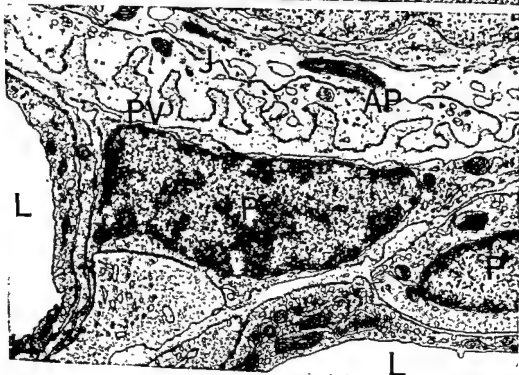
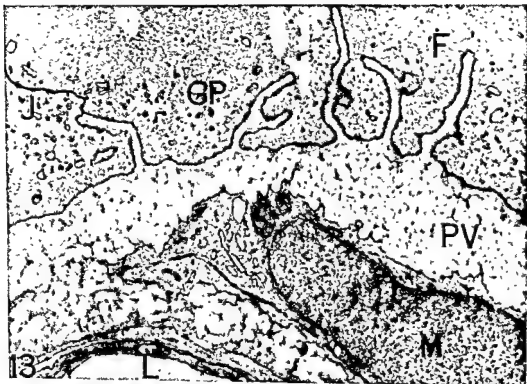


PLATE 8

EXPLANATION OF FIGURES

- 13 Capillary in spinal cord of adult shark. Lumen of capillary (L). Perivascular space (PV) is wide, filled with collagen and invaginates the pericapillary glial processes (GP). Glial processes contain packed filaments (F). Glial junctions (J) frequently connect with the tips of perivascular space evaginations. A portion of a mesothelial cell (M) is shown in the perivascular space. $\times 31,000$.
- 14 Capillary in forebrain of young shark near branching point. Lumen (L). Two pericyte nuclei (P) are evident. Two glial processes (AP) form a double layer of perivascular end feet separated by a tortuous junction (J). Pericapillary space (PV) has numerous evaginations. The nucleus of another glial cell lies beyond the double layer of glial cytoplasm. $\times 24,800$.

Don M. Long, Thomas S. Bodenheimer, J. Francis Hartmann and Igor Klatzo

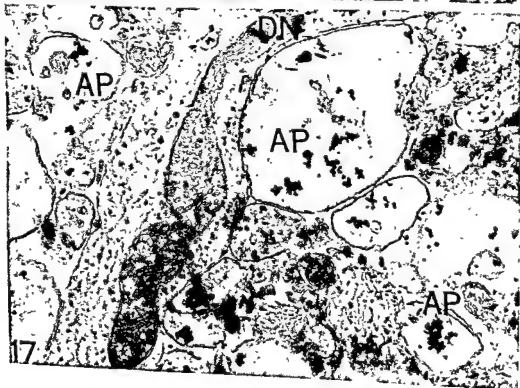
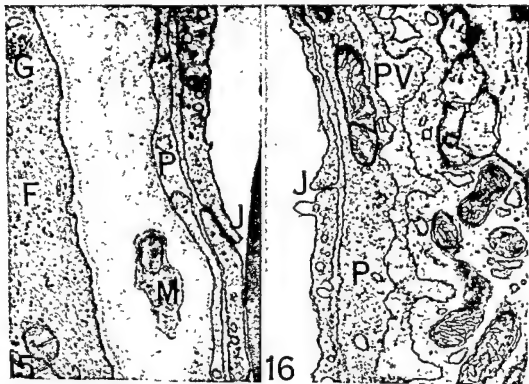
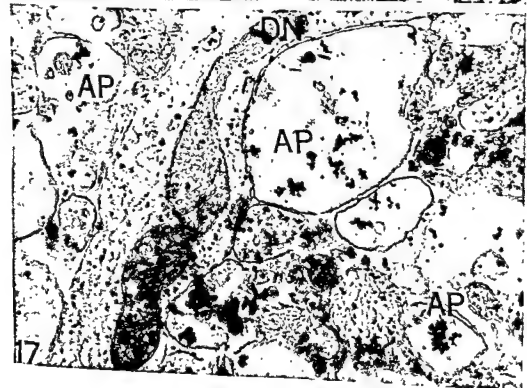
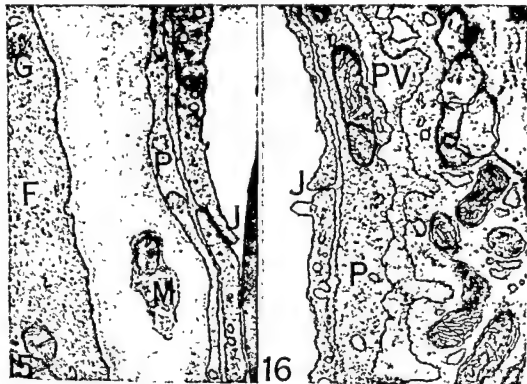


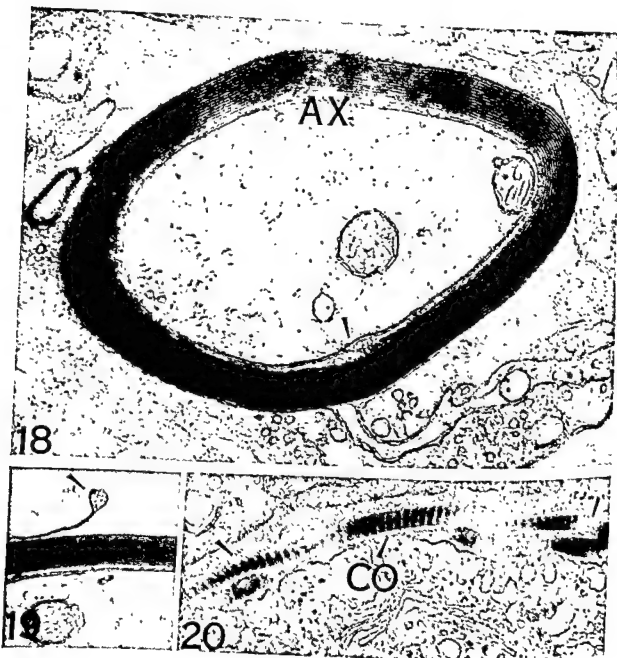
PLATE 9

EXPLANATION OF FIGURES

- 15 Interendothelial junction (J) in capillary in adult shark spinal cord. A pericyte (P) and mesothelial cell (M) process are seen. The perivascular glial process is packed with filaments (F) and contains glycogen granules (G). $\times 43,400$.
- 16 Interendothelial junction (J) in capillary from forebrain of young shark. Pericyte process (P) is visible. Typical collagen-filled evaginated pericapillary space (PV) is present. $\times 43,400$.
- 17 Several astrocyte processes (AP) from forebrain of adult shark contain sodium antimonate. The dendrite (DN) and its mitochondria have less precipitate. $\times 22,370$.

Don M Long, Thomas S. Bodenheimer, J Francis Hartmann and Igor Klatzo





EXPLANATION OF FIGURES

- 18 Typical myelinated axon from forebrain of adult shark. Myelin (MY). Axon (AX). Cytoplasmic tongue, seemingly analogous to internal mesaxon (arrow). $\times 40,500$.
- 19 Myelin from forebrain of adult shark. Cytoplasmic tongue, seemingly analogous to external mesaxon (arrow). $\times 34,000$.
- 20 Oblique section of capillary to demonstrate typical banding of collagen (CO, arrows) located in perivascular space. $\times 34,000$.

Re-examination of Spermatogonial Renewal in the Rat by Means of Seminiferous Tubules Mounted "in toto"

Y. CLERMONT AND E. BUSTOS-OBREGON¹

Department of Anatomy, McGill University, Montreal, Canada

ABSTRACT Observations on dissected tubules, fixed in Carnoy, stained with hematoxylin and mounted "in toto" revealed that there were five distinct classes of type A spermatogonia. The type A₁ found in stages II-VIII of the cycle of the seminiferous epithelium had round, pale-stained nuclei, typically arranged in linear clusters of four or eight along the tubular wall. They all divided at stage IX to produce type A₁ cells. These in turn divided at stage XII to produce type A₂ spermatogonia. The type A₂ and A₃ cells had large ovoid nuclei containing globular masses of deeply stained chromatin and were randomly distributed in the space between Sertoli nuclei. The type A₃ spermatogonia divided at stage XIV to produce type A₄ cells. These had smaller nuclei, sometimes lobulated, containing more deeply stained chromatin granulation, free in the nucleus or adhering to the nuclear membrane. They divided in stage I of the cycle to yield two classes of spermatogonia: intermediate type and new type A₁. Hence, type A₁-type A₄ spermatogonia were considered as "renewing stem cells." The fifth class of type A spermatogonia (A₅) was found at all stages of the cycle. Rare, isolated or in pairs, they had oval nuclei with deeply stained chromatin granulations. Seldom seen to divide, they did not appear to be actively involved in cell renewal and were tentatively considered as "reserve stem cells."

The renewal of the spermatogonial stem cell population has been investigated in several mammalian species and, amongst these, the rat has received the greatest attention (see reviews by Roosen-Runge, '62; Clermont, '67). It was soon observed that, between the initial spermatogonial stem cell and the spermatocytes, several intermediate generations of spermatogonia were being produced. In the rat, five distinct generations of spermatogonia were described, three of type A, one of intermediate type and one of type B spermatogonia (Clermont and Leblond, '53). It was also indicated that at each cycle of the seminiferous epithelium, while spermatocytes were being generated, some new spermatogonial stem cells were produced and set aside to serve in the production of future generations of spermatogonia and spermatocytes. It was also demonstrated that the new stem cells arose from the proliferating type A spermatogonia, before the production of the more differentiated intermediate and type B spermatogonia. More recently, Clermont ('62) suggested that the new stem cells were produced by divisions of the third generation of type A spermatogonia.

The main data used in these investigations (Roosen-Runge and Giesel, '50; Roosen-Runge, '51; Clermont and Leblond, '53; Clermont, '62) were average cell counts

obtained after enumerating large numbers of spermatogonia in tubular cross-sections. Therefore, on account of the statistical nature of these results, the exact time of formation and the source of the new stem cells remained a matter of speculation. In the present study, information bearing on this particular subject was obtained by a different experimental approach: the spermatogonial population, instead of being studied in transverse sections of seminiferous tubules, was analyzed in dissected tubules mounted "in toto." In such studies, the spermatogonia were complete and maintained in position along the tubular wall. Therefore, the topographical distribution of spermatogonial nuclei along the tubular limiting membrane, as well as their morphological characteristics could be more easily observed than in sections. New information on the nuclear morphology and the topographical arrangement of type A spermatogonia thus helped to clarify several aspects of the mode of development and renewal of spermatogonia in the rat.

MATERIALS AND METHODS

Testes from anesthetized adult Sprague-Dawley rats were removed through an abdominal incision and placed in cold 0.9%

¹ Present address: Catedra de Biología, Escuela de Medicina, Universidad de Chile, Santiago, Chile.

NaCl solution. The tunica albuginea was cut open and carefully detached from the underlying seminiferous tubules. Using fine sewing needles, the tubules were dissected apart. Pieces of such tubules, 2-4 cm long, were then fixed in Carnoy for 60 minutes. After fixation, the tubules were placed in three consecutive baths containing, respectively, 70%, 50% and 30% ethanol. The tubules were kept 10-15 minutes in each. Lastly, the tubules were immersed in distilled water. The tubules were then placed in a Petri dish containing hematoxylin (Harris) for 15-20 seconds, after which they were thoroughly washed in distilled water. After dehydration in 35%, 50%, 70% and 100% ethanol, the tubules were cleared in xylol, mounted on a glass slide in Malinol² and covered, without applying pressure, with a coverslip. The above method of preparation of tubules was essentially similar to the one already used by Roosen-Runge ('55).

It should be noted that the tubules were stained with hematoxylin only; the periodic acid-Schiff-hematoxylin technique which has been used on sections of rat testis to identify the 14 stages of the cycle of the seminiferous epithelium (identification based on the recognition of the steps of development of the PA-Schiff-positive acrosomic system of the spermatids; Leblond and Clermont, '52a,b) could not be applied to whole tubular mounts. The deep staining of the limiting membrane with the Schiff reagent prevented identification of the underlying spermatogonia or spermatids. However, since it was essential to relate the various types of spermatogonia to the stages of the cycle in order to understand the evolution in time of the spermatogonial population, identification of the stages was done by using criteria proposed by Clermont and Perey ('57) for sections stained with hematoxylin-eosin. These criteria were provided by the morphological characteristics of the nuclei of spermatogonia, spermatocytes and spermatids.

One histological feature which facilitated the identification of the stages of the cycle was their orderly distribution along the tubule in a sequence known as the "wave of the seminiferous epithelium" (Perey, Clermont and Leblond, '61). Thus, in whole mount preparations, when the

stage of the cycle of a given segment of tubule was determined, then the stages of the cycle of adjacent segments could be predicted.

RESULTS

It was found convenient, for reasons that will become clear later, to start the description of spermatogonia at stages II-III of the cycle. At these stages, the intermediate spermatogonia formed the predominant spermatogonial type. This cell showed an ovoid nucleus containing flakes of chromatin, many of them attached to the nuclear membrane (figs. 1, 8). They were randomly distributed between Sertoli cells.

In addition, two classes of type A spermatogonia respectively referred to as type A₀ and A₁, were found at stages II-III. Since these had not been recognized in sections, their features will be described in detail. The type A₀ spermatogonium was characterized by an ovoid nucleus with a small nucleolus and, in addition to a few larger clumps of chromatin, a finely granular and well stained chromatin. The overall staining of the nucleus was therefore relatively dark (when compared to the type A₁) (figs. 1, 4, 5). Type A₀ spermatogonia made up only about one-fifth of the total type A cell population at stages II-III (table 1). They usually occurred singly but

TABLE 1

Cell type	Stages of the cycle	No. of frames ¹ scored	Average no. of cells per frame
A ₀	II-VIII	120	0.54 ²
A ₁	II-VIII	120	2.05
In	II-IV	30	12.9
B	V	40	25.8
Pl	VII	50	49.7

¹ A frame is an area of the tubular limiting membrane delimited by a square ocular grid and having a surface of 10,000 μ^2 .

² The type A₀ thus constitute 21% of the type A cell population (A₀ + A₁) during these stages of the cycle.

were occasionally found in pairs. The type A₁ spermatogonium was characterized by a nucleus with a circular outline. The chromatin was very finely granular and lightly stained. One or more hemispherical nucleoli were seen applied to the nuclear mem

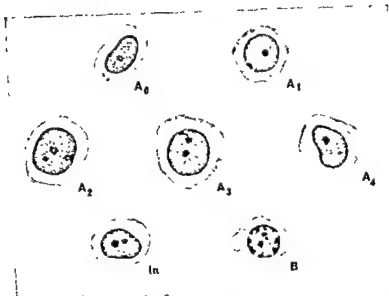


Fig. 1 Series of drawings illustrating the various types of spermatogonia as seen in dissected tubules fixed in Carnoy, stained with hematoxylin and mounted "in toto." These cells were found at the following stages of the cycle of the seminiferous epithelium: A_0 , at stages I–XIV; A_1 , at stages I–IX; A_2 , at stages IX–XII; A_3 , at stages XII–XIV; A_4 , at stages XIV–I; In, at stages I–IV; B, at stages IV–VI.

brane (figs. 1, 6, 7, 8). These cells, more abundant than the type A_0 spermatogonia (table 1), showed a characteristic topographical arrangement along the tubular wall. They formed linear clusters of four, but more commonly of eight nuclei (figs. 6, 7). Strings of 12 or 16 type A_1 nuclei were also present. In these linear clusters, the cells were adjacent to each other and were not separated by Sertoli cell nuclei. They appeared to occupy a corridor-like space limited by Sertoli cells (figs. 6, 7).

At stage IV of the cycle, while there was no apparent modification of type A_0 and A_1 spermatogonia, large groups of dividing intermediate spermatogonia were observed which gave rise to type B spermatogonia. The latter cells, present during stages IV, V and early VI of the cycle, were characterized by spherical nuclei which showed the features described in sections, i.e., characteristic large crusts of chromatin attached to the nuclear membrane and to a centrally located nucleolus (fig. 1). Fairly numerous, these cells were randomly distributed between Sertoli cell nuclei. Very large clusters of type B spermatogonia in

division were found at stage VI of the cycle. Such mitoses produced a large number of preleptotene (also called resting) spermatocytes. These were distributed in the spaces seen between Sertoli cell nuclei in late stage VI and in stages VII and VIII of the cycle (figs. 4–7). They entered the leptotene step of the meiotic prophase in stage IX of the cycle.

From stage IV to stage VIII of the cycle, there was no modification in the topographical arrangement, number and cytological appearance of type A_0 and A_1 spermatogonia. As stage IX of the cycle was approached, however, an increase in the nuclear diameter of type A_1 spermatogonia took place. An occasional isolated mitosis or even a pair of mitotic figures was observed during stages IV, V or VI. They were tentatively identified, on account of their isolation, as mitoses of type A_0 spermatogonia.

During stage IX of the cycle, type A_1 spermatogonia, in groups of four or eight, were seen to undergo mitoses. At late stage IX and in stages X and XI of the cycle, type A_1 spermatogonia were no longer pres-

ent. Instead, another type referred to as *type A₁* spermatogonia was found. The latter obviously arose from the type *A₁* during the peak of mitosis at stage IX. The type *A₁* spermatogonium was characterized by a large ovoid nucleus containing several globular masses of well stained chromatin, free in the nuclear sap or attached to the nuclear membrane; the rest of the chromatin, however, remained finely granulated and pale stained (figs. 1, 9). These nuclei were not arranged in clusters, but were widely dispersed along the limiting membrane, with Sertoli cell nuclei separating them. Type *A₁* spermatogonia, which showed no modification in number and cytological appearance, were present in association with type *A₁* spermatogonia.

At stage XII of the cycle, the type *A₁* spermatogonia divided. That the type *A₁* cells were the proliferating elements was indicated by the fact that all transitions were observed between type *A₁* cell interphasic and prophasic nuclei. During this peak of mitosis, groups of degenerating nuclei of type *A₁* cells were frequently seen, the onset of degeneration taking place during prophase.

At stage XIII of the cycle, the spermatogonia present, in addition to the unchanging type *A₁* cells, were referred to as *type A₂* spermatogonia. These elements, which were numerous, had the same nuclear characteristics as those described for type *A₁* spermatogonia, i.e., nuclei containing a background of pale-stained finely granulated chromatin and some deeply stained globular chromatin masses (figs. 1, 10).

Spermatogonial mitoses were again observed in midstage XIV of the cycle and found to be divisions of type *A₂* spermatogonia, as judged from the transitions seen between interphasic and mitotic nuclei of the latter cells. During this peak of mitosis, some type *A₂* spermatogonia underwent degeneration. The daughter cells arising from type *A₂* spermatogonial divisions were referred to as *type A₃* spermatogonia. They showed smaller nuclei than that of type *A₂* spermatogonia and more of the deeply stained chromatin granulations. Some of this chromatin accumulated on the nuclear membrane which then became more clearly delineated (figs. 1, 11). Occasionally one could observe, in type *A₃* sper-

matogonia, a constriction of the nuclear membrane which gave the nucleus a bilobed appearance.

Present in late stage XIV and early stage I, the type *A₃* spermatogonia divided in midstage I of the cycle. These divisions were, like the cells themselves, distributed at random between Sertoli cell nuclei. Some degenerating type *A₃* cells were identified during this peak of mitosis. Type *A₃* spermatogonia, unchanged in appearance and number, were present along the tubular wall in association with type *A₁* cells.

In late stage I of the cycle, i.e., immediately following the peak of mitosis just mentioned, the situation previously described for stages II and III of the cycle was found again. That is, in addition to the rare and isolated type *A₁* spermatogonia, type *A₁* spermatogonia were arranged in linear clusters of four or eight in presence of numerous intermediate spermatogonia; all type *A₃* spermatogonia had disappeared.

DISCUSSION

Following an analysis of quantitative data on spermatogonia and an examination of the topographical arrangement of dividing type *A* cells in stage IX of the cycle, a model was proposed for the development of spermatogonia in the rat (Clermont, '62). According to this model, illustrated in figure 2, there would be three generations of type *A* spermatogonia, dividing respectively in stages IX, XII and XIV-I of the cycle. Divisions of the last generation of type *A* spermatogonia would then produce intermediate spermatogonia and a pair of new type *A* spermatogonia. The latter cells, after a long period of dormancy (from stage I to stage IX of the cycle) would initiate another series of spermatogonial divisions. Meanwhile, all intermediate spermatogonia would divide in stage IV to produce type *B* spermatogonia, which in turn would divide in stage VI of the cycle to yield spermatocytes.

From the present series of observations on whole tubular mounts, it became evident that the mode of development of spermatogonia must be somewhat different from the model just described because, firstly, there were six rather than five successive peaks of spermatogonial mitoses

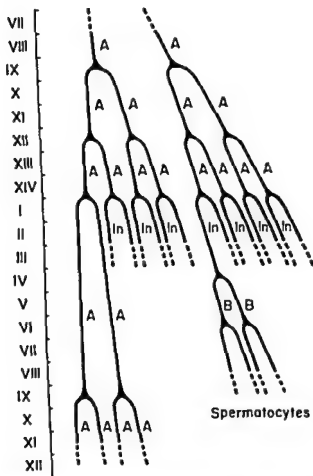


Fig. 2 Model proposed by Clermont ('62) to describe the behavior of spermatogonia in the rat. The Roman numerals on the left of the diagram indicate the stages of the cycle. Lettering: A, type A spermatogonia; In, intermediate spermatogonia; B, type B spermatogonia. According to this diagram, a pair of initial stem cells would start proliferating in stage IX of the cycle and the daughter cells would divide successively in stages XII and XIV-I of the cycle. Following this third peak of divisions, one type A spermatogonia would produce a new pair of initial stem cells which, after a period of dormancy, would start proliferating again. The other type A spermatogonia would yield intermediate spermatogonia, which in turn produce type B spermatogonia, which finally give rise to primary spermatocytes.

and, secondly, five instead of three classes of type A spermatogonia along the tubular wall.

Regarding the peaks of divisions, it was clear from the present series of observations that the mitotic peak previously located in stages XIV and I of the cycle was in fact constituted of two distinct peaks, one located in midstage XIV (involving

type A₁ spermatogonia) and the other located in midstage I (involving type A₂ spermatogonia). Huckins ('65), working on sections of testes from growing rats had already noticed the existence of these two distinct peaks of mitoses. Therefore, six instead of five successive spermatogonial divisions take place in the rat in a sequence that closely resembles that described in

the mouse by Monesi ('62), i.e. four divisions of type A, one of intermediate and one of type B spermatogonia.

While, in sections, no clear cytological distinction could be made between the various generations of type A spermatogonia, in whole tubules, five distinct classes of type A cells could be disclosed. It should be noted here that, in whole tubular mounts, the nuclei of the spermatogonia, complete and facing the limiting membrane lend themselves to a more direct observation than in sections, in which nuclear fragments were usually seen laterally. It is of importance at this point to review the criteria used to distinguish these five classes of type A spermatogonia.

The type A₁ spermatogonia were relatively rare elements but were found in all stages of the cycle. Characterized by ovoid nuclei containing dust-like chromophylic chromatin, they were isolated (figs. 4-6) or, if seen in pairs, the two members of the pair were separated by one or more Sertoli cell nuclei. (This feature distinguished them readily from the type A₂ spermatogonia, with which they have some morphological resemblance.) These elements rarely divided; the occasional isolated mitoses seen along the basement membrane were tentatively identified as divisions of such isolated cells. On account of their apparently low proliferative activity, the type A₁ spermatogonia were referred to as "reserve stem cells."

This appellation appeared justified in view of recent observations on the spermatogonial population following X-irradiation (Dym and Clermont, '67). In this study, it was found that, following a single dose of 250r, the number of type A (A₁ + A₂) spermatogonia in stages II-VIII of the cycle was reduced, eight days after irradiation, to 18% of normal values. Analysis of whole tubular mounts at this time interval revealed that the radioresistant elements were the type A₁ cells, while the type A₂ had disappeared altogether. From 13 days after irradiation onwards, the type A₁ spermatogonia reappeared along the tubular wall. It was concluded from this observation that the radioresistant type A₁ cells repopulated the seminiferous tubules with type A₂ cells. If this interpretation is correct, the type A₁ cells could, under cer-

tain circumstances, be called upon to rebuild the spermatogonial population and thus constitute a group of "reserve stem cells."

The type A₂ spermatogonia were found exclusively from stage I to stage IX of the cycle. Their pale discoid nuclei, arranged in linear clusters of four, eight or more, distinguished them from all other type A spermatogonia. They all divided in stage IX of the cycle; the groups of four or eight mitotic figures seen then were taken to be a clear demonstration of this assertion. Furthermore, quantitative data on type A₂ spermatogonia (Clermont and Leblond, '53; Clermont, '62) have shown that, during the stage IX-peak of mitoses, the number of these cells doubled.

The next two classes of spermatogonia, respectively labeled as type A₃ and A₄, could not be distinguished from each other on the basis of their nuclear morphology, although they both could be readily distinguished from the other classes of type A cells (fig. 1). They were found from late stage IX to early stage XIV of the cycle. The existence of two rather than a single generation of spermatogonia during these stages was based on the presence of a sharply demarcated peak of divisions during stage XII of the cycle. Cell counts have shown, however, that there was no duplication of the number of spermatogonia during this peak of mitosis (2.4 in stages X-XI versus 3.1 in stage XIII; Clermont, '62). But, it should be recalled that an abundance of degenerating type A spermatogonia were found during stage XII. Therefore the low yield of type A₃ spermatogonia must be due to the loss by degeneration of type A₃ spermatogonia at the time of their mitoses.

The type A₃ spermatogonia were presumably those dividing during stage XIV of the cycle, to be replaced by the type A₂ spermatogonia. The latter elements, which were fairly abundant along the tubular limiting membrane, had nuclei smaller than that of type A₁ cells and showing a more chromophylic chromatin granulation along the nuclear membrane. Several of them showed a bilobed nucleus, suggestive of cellular motion. These bilobed nuclei have already been well described by Regaud ('01) who interpreted them as ami-

totic nuclei. In fact these type A_4 cells divided mitotically in stage I of the cycle and were replaced by two categories of cells: intermediate, and type A_1 spermatogonia.

This last observation on whole tubules was taken to be a clearcut indication that the new type A_1 spermatogonia arose from the fourth spermatogonial divisions, i.e., divisions of type A_4 cells. This finding there-

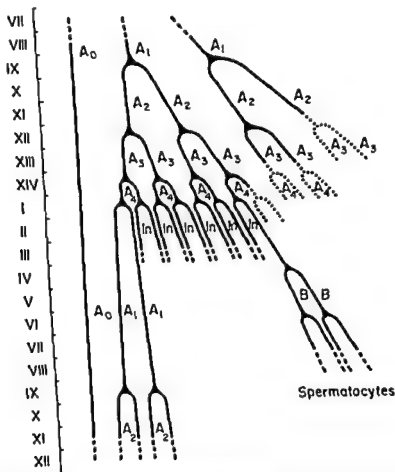


Fig. 3 Diagram representing the mode of proliferation and renewal of spermatogonia in the rat based on observations made on dissected tubules mounted "in toto" and on quantitative data on the spermatogonial population (Clermont and Leblond, '63; Clermont, '62). Roman numerals indicate the stages of the cycle. Lettering A_0 , A_1 – A_4 , the various classes of type A spermatogonia; In and B, intermediate and type B spermatogonia. According to this model, there are two main categories of type A spermatogonia, the "reserve stem cells" (A_0) and the "renewing stem cells" (A_1 – A_4). The type A_0 spermatogonia were represented as a straight unbranched line (on the left) to indicate that they do not proliferate to any significant extent in adult rats. On the side of the cells of the renewing series, a pair of initial stem cells (A_1) start proliferating in stage IX of the cycle to give successively types A_2 , A_3 and A_4 spermatogonia, each one of these dividing respectively in stages XII, XIV and I of the cycle. In stage I, dividing type A_4 spermatogonia produce a new pair of type A_1 spermatogonia and 12 intermediate spermatogonia. Some type A_1 , A_3 and A_4 spermatogonia on the right hand side of the diagram, were shown to disappear by degeneration at the time of division — dotted lines — thus explaining the low yield of intermediate spermatogonia per initial stem cell (A_1 :In = 1:6). Each intermediate spermatogonium divides to produce type B spermatogonia which in turn gives rise to spermatocytes. No degeneration takes place during these last two spermatogonial divisions.

fore clarified the exact time of formation of the new initial stem cells, which until now had been a matter of speculation.

The fact that the new type A_1 cells were always found in groups composed of even numbers of cells (usually 8) was taken to be a confirmation of the conclusion previously reached by Clermont ('62) that the new initial stem cells (A_1) were formed as a result of "equivalent" rather than "differential" mitoses of the progenitor cells (A_1). This conclusion differs from the one reached by Hilscher ('64) who stated that, in the rat, new stem cells were the product of "differential" mitoses.

Since the type A_1 - A_1 spermatogonia were, at each cycle of the seminiferous epithelium, actively engaged in proliferation and renewal, they were referred to as "renewing stem cells." The term "stem" was applied to all four generations of type A cells because they retained the capacity to yield the undifferentiated type A_1 spermatogonia. In contrast, the intermediate and type B spermatogonia should be considered as "differentiated" elements since they were committed to produce spermatocytes.

A new model to illustrate the mode of proliferation and renewal of spermatogonia of the rat may now be proposed (fig. 3). This model was based on the present observations on whole tubules as well as on previously published quantitative data on the spermatogonia (Clermont and Leblond, '53; Clermont, '62). According to this model, the reserve stem cell or type A spermatogonium was represented as a straight line running through successive cycles (fig. 3, left). The absence of branching of this line was meant to suggest that these cells do not proliferate to any significant extent in normal adult rats. However, the possibility that the type A cells divide sporadically to yield cells of the renewing series remains. The "renewing stem cells" (A_1 - A_1) starting with a pair of type A_1 cells were shown to divide consecutively four times in stages IX, XII, XIV and I of the cycle. Following this fourth peak of mitoses, intermediate and new type A_1 spermatogonia were produced; the latter cells arose in a pair as a result of an equivalent mitosis of a type A_1 cell. In the tubules, four adjacent type A_1 cells usually divide to yield eight new type A_1 cells, while

the other type A cells in the neighbourhood yield intermediate-type spermatogonia.

On this model, the number of intermediate spermatogonia produced by a pair of initial stem cells was shown to be equal to 12 (fig. 3, solid lines). This was done to be in accord with the ratio of type A₁ to intermediate cells, approximately equal to 1:6, obtained in previous quantitative studies (see also table 1). This relatively low yield of intermediate spermatogonia was taken to be the result of degeneration, not only of type A_1 cells as mentioned above, but also of type A_2 and A_3 cells during their respective peaks of mitosis. While the degenerations of the type A_2 spermatogonia had been reported before (Clermont, '62), the degeneration of type A_3 and A_4 spermatogonia had been clearly identified only in the present investigation of whole tubular mounts. Therefore the importance of such degenerations, which affected selectively these three classes of spermatogonia, would be greater than initially suspected. (The yield of intermediate spermatogonia or of spermatocytes, since intermediate and type B spermatogonia do not degenerate, would be only approximately 45% of the number obtained if all spermatogonia had divided without degenerating.)

Thus, according to this schematic representation of the mode of development of spermatogonia, there would be two main classes of spermatogonial stem cells: the "reserve stem cells" (A_1), the role of which remains to be clarified further; and the "renewing stem cells" (A_1 - A_1), which simultaneously produce new stem cells of the renewing series (A_1) and the "differentiated" spermatogonia which yield spermatocytes.

ACKNOWLEDGMENTS

This work was supported by a grant from Population Council Inc. Dr. E. Bustos-Obregon was a fellow of the Rockefeller Foundation. The help of Dr. C. P. Leblond and Mr. M. Dym in the preparation of the manuscript is acknowledged.

LITERATURE CITED

- Clermont, Y. 1962 Quantitative analysis of spermatogenesis of the rat: a revised model for the renewal of spermatogonia. *Am. J. Anat.* 111 111-129.

- 1967 Cinétique de la spermatogénèse chez les mammifères. Arch. Anat. Micro. Morph. Exp. (in press).
- Clermont, Y., and C. P. Leblond 1953 Renewal of spermatogonia in the rat. Am. J. Anat., 93: 475-502.
- Clermont, Y., and B. Perey 1957 The stages of the cycle of the seminiferous epithelium of the rat. Practical definitions in PA-Schiff-hematoxylin and hematoxylin-eosin stained sections. Rev. Can. Biol., 16: 451-462.
- Dym, M., and Y. Clermont 1967 Effects of X-rays on type A spermatogonia in the rat. Anat. Rec., 157: 238 (Abstr.)
- Hilscher, W. 1964 Beiträge zur Orthologie und Pathologie der "Spermatogoniogenese" der Ratte. Beitr. path. Anat., 130: 69-132.
- Huckins, C. 1965 The initiation of spermatogenesis in the testis of the Wistar albino rat. Ph D. Thesis. McGill University.
- Leblond, C. P., and Y. Clermont 1952a Definition of the stages of the cycle of the seminiferous epithelium in the rat. Ann. N. Y. Acad. Sci., 55: 548-573.
- 1952b Spermiogenesis of rat, mouse, hamster and guinea-pig as revealed by the "periodic acid-fuchsin sulfurous acid" technique. Am. J. Anat., 90: 167-215.
- Monesi, V. 1962 Autoradiographic study of DNA synthesis and the cell cycle in spermatogonia and spermatocytes of mouse testis using tritiated thymidine. J. Cell Biology, 14: 1-18.
- Perey, B., Y. Clermont and C. P. Leblond 1961 The wave of the seminiferous epithelium in the rat. Am. J. Anat., 108: 47-77.
- Regaud, C. 1901 Etude sur la structure des tubes séminifères et sur la spermatogénèse chez les mammifères. Arch. d'Anat. Micro., 4: 101-156; 231-380.
- Roosen-Runge, E. C. 1951 Quantitative studies on spermatogenesis in the albino rat. II. The duration of spermatogenesis and some effects of colchicine. Am. J. Anat., 88: 163-176.
- 1955 Untersuchungen über die Degeneration Samenbildender Zellen in der normalen Spermatogenese der Ratte. Z. Zellforsch., 41: 221-235.
- 1962 The process of spermatogenesis in mammals. Biol. Rev., 37: 343-377.
- Roosen-Runge, E. C., and L. O. Giesel 1950 Quantitative studies on spermatogenesis in the albino rat. Am. J. Anat., 87: 1-30.

PLATE 1

EXPLANATION OF FIGURES

All photographs were taken on dissected tubules, fixed in Carnoy, stained with hematoxylin and mounted "in toto." The photographs were taken through the limiting membrane focussing on the spermatogonial layer.

- 4-5 Two photographs showing isolated type A_0 spermatogonia (A_0) amongst the nuclei of Sertoli cells (S) and preleptotene primary spermatocytes (PI). The nuclei of type A_0 cells were ovoid and contained a chromophylic granulation. Seen here in stage VII, they were found in all stages of the cycle. $\times 600$.
- 6 Photograph showing a group of four type A_1 spermatogonia (arrows). These cells have a discoid nucleus with pale-stained chromatin. Note the linear arrangement of these nuclei. These cells seen here in stage VII of the cycle as indicated by the presence of preleptotene spermatocytes (PI) were found from late stage I to stage IX of the cycle. Sertoli cell nuclei (S) are clearly visible. $\times 600$.
- 7 Photograph showing the typical linear arrangement of type A_1 spermatogonia (arrows). Seven cells were in focus, the last one of the series of eight was out of focus and was not included in the photograph. $\times 600$.
- 8 Photograph showing type A_1 spermatogonial nuclei (A_1) in presence of a nucleus of an intermediate spermatogonium (In) in stages II-III of the cycle. Note the pale-stained granular chromatin in the discoid nuclei of type A_1 cells in contrast with the chromophilic chromatin in the ovoid nucleus of the intermediate spermatogonium. $\times 900$.
- 9 Photograph showing the nucleus of a type A_2 spermatogonium (A_2). These nuclei are larger than those of type A_1 and contain some chromophilic chromatin granulations in addition to the pale-stained chromatin seen in the rest of the nucleoplasm. These were found in stages X-XI of the cycle. A Sertoli cell nucleus is indicated (S). $\times 900$.
- 10 Photograph showing the nucleus of a type A_3 spermatogonium (A_3). Similar to the type A_2 spermatogonia, they were found in stages XIII of the cycle. $\times 900$.
- 11 Photograph showing two nuclei of type A_4 spermatogonia. They have smaller nuclei than those of types A_2 and A_3 spermatogonia and contain more of the chromophilic chromatin, some adhering to the nuclear membrane. They were found in late stage XIV and early stage I of the cycle. $\times 800$.

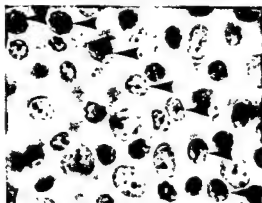
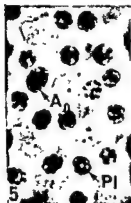
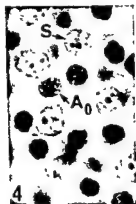


PLATE 1

EXPLANATION OF FIGURES

All photographs were taken on dissected tubules, fixed in Carnoy, stained with hematoxylin and mounted "in toto." The photographs were taken through the limiting membrane focussing on the spermatogonial layer.

- 4-5 Two photographs showing isolated type A_0 spermatogonia (A_0) amongst the nuclei of Sertoli cells (S) and preleptotene primary spermatocytes (PI). The nuclei of type A_0 cells were ovoid and contained a chromophylic granulation. Seen here in stage VII, they were found in all stages of the cycle. $\times 600$.
- 6 Photograph showing a group of four type A_1 spermatogonia (arrows). These cells have a discoid nucleus with pale-stained chromatin. Note the linear arrangement of these nuclei. These cells seen here in stage VII of the cycle as indicated by the presence of preleptotene spermatocytes (PI) were found from late stage I to stage IX of the cycle. Sertoli cell nuclei (S) are clearly visible. $\times 600$.
- 7 Photograph showing the typical linear arrangement of type A_1 spermatogonia (arrows). Seven cells were in focus, the last one of the series of eight was out of focus and was not included in the photograph. $\times 600$.
- 8 Photograph showing type A_1 spermatogonial nuclei (A_1) in presence of a nucleus of an intermediate spermatogonium (In) in stages II-III of the cycle. Note the pale-stained granular chromatin in the discoid nuclei of type A_1 cells in contrast with the chromophilic chromatin in the ovoid nucleus of the intermediate spermatogonium. $\times 900$.
- 9 Photograph showing the nucleus of a type A_2 spermatogonium (A_2). These nuclei are larger than those of type A_1 and contain some chromophilic chromatin granulations in addition to the pale-stained chromatin seen in the rest of the nucleoplasm. These were found in stages X-XI of the cycle. A Sertoli cell nucleus is indicated (S). $\times 900$.
- 10 Photograph showing the nucleus of a type A_3 spermatogonium (A_3). Similar to the type A_2 spermatogonia, they were found in stages XIII of the cycle. $\times 900$.
- 11 Photograph showing two nuclei of type A_4 spermatogonia. They have smaller nuclei than those of types A_2 and A_3 spermatogonia and contain more of the chromophilic chromatin, some adhering to the nuclear membrane. They were found in late stage XIV and early stage I of the cycle. $\times 800$.

A Blood-Brain Barrier to Peroxidase in Capillaries Surrounded by Perivascular Spaces

T. S. BODENHEIMER AND M. W. BRIGHTMAN

Laboratory of Neuroanatomical Sciences, National Institute of Neurological Diseases and Blindness, National Institutes of Health, Public Health Service, U. S. Department of Health, Education, and Welfare, Bethesda, Maryland

ABSTRACT Some investigators have hypothesized that the absence of a blood-brain barrier in specialized regions of the mammalian central nervous system is related to the occurrence of a pericapillary connective tissue space that can accommodate more substance than the usual narrow extracellular space in the remainder of the cerebral parenchyma. The capillaries of the urodele brain are well suited to test this hypothesis. All of the cerebral capillaries examined electron-microscopically in *Necturus maculosus* are surrounded by a collagen-containing space, about 0.5 μ wide, which is delimited by an endothelial and a glial basement membrane. In *Ambystoma tigrinum*, some capillaries have perivascular spaces whereas others are surrounded by a single basement membrane shared by endothelium and glia and therefore resemble mammalian vessels exhibiting barrier phenomena. In both *Necturus* and *Ambystoma*, horseradish peroxidase administered intravenously one-half to two hours before fixation did not cross the brain capillary endothelium. The bulk of the protein remained in the vessel lumen, although some was incorporated by membrane-bound inclusions within the endothelium, and none ever reached the perivascular basement membrane, space or parenchyma. The amphibian cerebral endothelium is, like the mammalian endothelium, the locus for the barrier to the entry of peroxidase from blood to parenchyma. Thus, the mere occurrence of a pericapillary space is not necessarily coincident with the absence of a blood-brain barrier.

A barrier situated somewhere between the blood vessel lumen and the brain parenchyma appears to exclude intravascularly injected substances such as proteins (Brown '61; Klatzo et al., '62) and dyes bound to proteins (Tschirgi, '50). The site of the barrier to exogenous peroxidase has recently been localized to the cerebral endothelium of the mouse brain (Reese and Karnovsky, '67). There are, however, several special regions of the mammalian brain, including the choroid plexus, neurohypophysis, area postrema, and pineal body, into which intravascularly-injected substances can enter freely. A structural feature common to these regions is the connective tissue space surrounding their capillaries. These pericapillary spaces have been associated with the absence of a blood-brain barrier (BBB), (Wislocki and Leduc, '52; Dempsey and Wislocki, '55; Brown, '61). One hypothesis (Dobbing, '63) attempting to relate these observations assumes that all cerebral vascular endothelium allows the passage of material from blood into brain, but that the usual narrow extracellular clefts around brain capillar-

ies and elsewhere throughout the parenchyma are too small to accommodate much of the material. The large perivascular spaces of the special regions would, however, provide a substantial extracellular compartment in which the substances could accommodate.

The brain of *Necturus* is peculiarly suited to test the validity of relating pericapillary spaces to the absence of a BBB, inasmuch as all of the cerebral capillaries are surrounded by connective tissue spaces. The present findings demonstrate that in *Necturus*, peroxidase cannot pass across the endothelial layer in significant amounts, and therefore the association of a perivascular space with the lack of a BBB is unwarranted.

MATERIALS AND METHODS

Necturus maculosus (mud-puppy) specimens ranged from 60–200 gm in weight, and *Ambystoma tigrinum* (salamander), both aquatic and terrestrial, from 40–100 gm.¹ The aquatic animals could be anes-

¹ Lemberger Co., Oshkosh, Wisconsin.

veloped Golgi apparatus near the nucleus, glycogen, fine filaments, tubules, vesicles, and multi-vesicular bodies. Large membrane-bounded dense bodies are often present, at times within peg-like evaginations of the endothelium (figs. 8, 9). One occasionally sees "pinocytotic" pits on both the luminal and the contraluminal cell membranes. The appositions between endothelial cells are longer and more extensively overlapping than in the mammal (fig. 6). This feature has made it impossible to determine whether or not these intercellular gaps are all closed by tight junctions as in mammals (Reese and Karnovsky, '67). The junctions are presumed to be tight because peroxidase was excluded from them and from the perivascular basement membrane.

Over a large part of the endothelial surface of each vessel one or more pericytes intervene between the endothelial cells and the perivascular space (figs. 3, 6, 7-9). Though their overlapping processes cover a considerably greater portion of the capillary surface than in the mammal, they do not form a continuous layer. Their cytoplasm is very similar to that of the endothelial cell. Between pericytes and endothelial cells is a narrow cleft containing basement membrane material as in mammals (figs. 3, 6, 8, 9).

Perivascular space

The remarkable feature of the *Necturus* brain capillaries, contrasting them graphically with their mammalian counterparts, is the constant occurrence of a connective-tissue space surrounding them (figs. 2, 3, 5-8, 10, 11). This space is usually about 0.5 μ in width, varying from 0.2-1.0 μ , and is bounded by endothelium or pericytes on one side and a layer of the parenchyma consisting of thin glial processes on the other. Both the endothelial and the glial sides of the perivascular space are coated by a basement membrane, a condensation of dense, amorphous material lying just outside the cell membrane; the one on the glial side is remarkably straight, approximately 300 Å wide, denser and more clearly defined than that on the endothelial side (figs. 2, 3, 5, 6, 9). Within the perivascular space is an amorphous substance of light to moderate density, and

loosely packed collagen fibers with their characteristic periodicity. Occasionally, cell processes within the space contain dense-core vesicles about 600 Å in diameter. These are probably mesothelial cells, but it is difficult to rule out the possibility that they are nerve fibers.

Parenchyma

The parenchymal side of the perivascular space is lined by a continuous layer of glial cell processes, which often thin out into slips of tissue only 300-400 Å wide (figs. 3, 5, 6). These glial feet appear to surround the entire vessel surface. Their cytoplasm contains glycogen, and the thin, wispy filaments also characteristic of mammalian astrocytes. Between the parenchymal glial processes and between perivascular glial end feet, are intercellular clefts about 150 Å in width. As in the mammalian brain, these patent clefts are in some places almost obliterated by "gap" junctions (figs. 6, 11) (Brightman and Reese, '67), whereas at other sites they form wider, open channels extending from the pericapillary space to the neuropil.

The cellular elements of the urodele brain are tightly packed, as in other species, and are separated by the usual 100-200 Å gap (figs. 3, 4, 10). The nerve cell bodies, dendrites and axons have the general cytological characteristics of mammalian neurons. Synapses display the usual array of vesicles in the presynaptic cytoplasm. In contradistinction to mammals, however, all nervous elements, cell bodies, axons, dendrites, and synaptic endings contain varying amounts of particulate glycogen (figs. 5, 6, 11).

The problem of glial cell identification has not been dealt with here and it is as yet undetermined whether ependymal cells, astrocytes, or both provide the processes leading to capillaries and to the pial surface. However, true astrocytes seem to exist in the urodele brain as in brains of other lower vertebrates (Kruger and Maxwell, '67). Glial cytoplasm cannot always be distinguished from dendritic cytoplasm, as both contain glycogen and both tend to develop lucent, "watery" cytoplasm if fixation is not optimal. Bundles of wispy filaments, when they occur, are helpful in recognizing glial processes (figs. 6, 9).

thetized very satisfactorily by immersion in 0.6% MS 222.² The terrestrial forms were anesthetized (with difficulty) by intraperitoneal injection of 0.5–1.0 ml of 1% MS 222. Fixation was accomplished almost entirely by perfusion, using chiefly the formaldehyde-glutaraldehyde mixture developed for mammals by Karnovsky ('65a) and Reese and Karnovsky ('67). The osmolality of the buffer was not adjusted to account for the lower plasma tonicity of urodeles.

Immersion fixation or fixation by perfusion of the cerebral ventricles, using a concentrated glutaraldehyde-formaldehyde solution (Karnovsky, '65) or osmium tetroxide in sodium phosphate, gave poor results except for the brain stem. Fixation by vascular perfusion was generally more complete in the immediate vicinity of blood vessels. *Ambystoma* was best perfused via the conus arteriosus, whereas *Necturus* gave better results with a cannula in the dorsal aorta after ligating the external gills. The pressure was best applied by injecting the solution rapidly with a syringe rather than with a gravity drip; 40–80 ml of a dilute formaldehyde-glutaraldehyde solution (Reese and Karnovsky, '67) were used for a 100 gm animal, injected at about 40 ml per minute. Following perfusion, the brain was placed into the concentrated fixative for 8–16 hours, washed with 0.1 M cacodylate buffer, post-fixed in 1% osmium tetroxide in 0.1 M cacodylate for 2–4 hours, dehydrated and embedded in Araldite or Maraglas. Some blocks, following osmication, were stained in uranyl acetate (Reese and Karnovsky, '67).

Two *Ambystoma* and three *Necturus* were injected intraperitoneally with 1.0 ml per day of a 2% solution of trypan blue for one to seven days. One *Necturus* was given 0.5 ml intravascularly and killed after four hours.

Six *Necturus* were injected intravascularly with from 20–35 mg of Type II horseradish peroxidase (Sigma),³ and one with 6 mg of Type VI peroxidase. After 30 minutes to two and one-half hours, these animals were fixed by vascular or ventricular perfusion. Two of these seven mud puppies were kept in water warmed to 30–35°C for the 30 minutes between peroxidase injection and fixation. Three *Ambystoma*

were injected with from 5–10 mg of Type II peroxidase, and were maintained for 30–40 minutes at room temperature before fixation.

One *Ambystoma* and two *Necturus* were given 2–4 mg of Type II peroxidase into the cerebral ventricle, and were fixed after 30 minutes by immersion or vascular perfusion.

All of the peroxidase-treated material was left in fixative for 8–16 hours and then washed in 0.1 M sodium cacodylate buffer. Some of the brains were then soaked in 15% sucrose and sectioned at about 120 μ in a cryostat. Others were not frozen, but instead cut into slices approximately 0.5 mm thick with a razor blade. All slices were then washed in Tris buffer, and further processed for peroxidase activity according to Karnovsky ('65b).

Thin sections of this material were stained with lead citrate (Venable and Coggeshall, '65) and examined in RCA EMU-3E and AEI-6B microscopes.

RESULTS

The intramedullary vessels of *Necturus* consist solely of hairpin capillary loops; the arterial and venous limbs accompanying one another within a single sheath (fig. 1B) (Craigie, '38, '40). These non-anastomosing loops are formed from pial vessels of the same caliber which simply dip down into the brain substance (figs. 1A, 2). The brain of *Ambystoma* contains both capillary loops and a branching, anastomosing capillary network (Craigie, '39; Herrick, '48). This presents the possibility for an interspecies comparison of the two main types of vascular organization in vertebrate brains. The fine structure is best described by starting with the endothelium and working outward to the perivascular nervous tissue. Thereafter the capillaries of the pia will be considered. The more pertinent findings in *Necturus* will be described first in some detail.

Parenchymal endothelium

The endothelial lining is thin but continuous and lacks fenestrations (figs. 9–11). The cytoplasm contains a we

² Sandoz Pharmaceuticals, Hanover, N. J.
³ Sigma Chemical Co., St. Louis, Mo.

However, when the endothelium was circumvented by injecting the protein into the cerebral ventricles, peroxidase passed across the ependyma to enter the 150–200 Å-wide clefts between glial and neuronal processes (fig. 11). The protein ultimately passed between glial end-feet along the common interglial clefts and the narrow ones of the gap junctions (Brightman and Reese, '67) depicted in figure 11. Peroxidase then permeated the glial basement membrane to enter and fill the perivascular space (fig. 11). From this space, protein was able to penetrate the clefts between adjacent endothelial cells but only as far as the "tight" junction. This retrograde filling of the inter-endothelial cleft is the converse of the distribution that follows injection of protein into the blood stream.

DISCUSSION

The results of this study indicate that the parenchymal capillaries of the brain of *Necturus* are surrounded by a collagen-containing connective-tissue space, and that no appreciable amount of horseradish peroxidase is able to cross the endothelium of these vessels to reach this space. The implication of these results is that, contrary to a currently held view, the BBB to proteins does occur in the presence of collagenous extracellular tissue.

Perivascular space

The history of the concept of the perivascular space is long and confused, and can best be grasped by a reading of Woollam and Millen's review ('54). These authors, who corroborated the work of Patek ('44), concluded that the true perivascular space in mammals lies between the tunica adventitia of the vessel and the layer of glial processes surrounding the vessel, and that this space communicates freely with the subarachnoid space. Most importantly, the perivascular space does not reach down to the level of the CNS capillary, but only accompanies the larger vessels. The absence of a pericapillary space in mammals, except in certain regions previously mentioned, has been repeatedly confirmed by electron microscopy (Maynard et al., '57; Donahue and Pappas, '61; Wolff, '63). An analysis of the fine structural relations of

the perivascular space in the hamster demonstrated that the space is obliterated before reaching the capillary level by fusion of the vascular and glial basement membranes (Nelson et al., '61).

There are, however, capillaries in the mammalian brain which do have a perivascular space. These spaces occur in regions which lack the BBB such as the neurohypophysis (Palay, '57; Hartmann, '58), the area postrema (Rivera-Pomar, '66; Kuffler and Nicholls, '66), and the pineal body (Wolfe, '65; Anderson, '65). In addition, there is a wide collagenous stroma surrounding the capillaries of the choroid plexus, another area lacking the BBB (Wislocki and Ladman, '58).

In contrast to the mammalian condition just described, at least one sub-mammalian form, *Necturus*, has a connective tissue space around all of its parenchymal capillaries. Colloidal tracers injected into the subarachnoid space of *Necturus* readily fill these pericapillary spaces (Brightman, '53). Moreover, peroxidase injected into the cerebral ventricles of *Necturus*, after passing extracellularly through the neuropil, permeates the basement membrane lining the glial border of the pericapillary space, thereby filling the space. Thus it is clear that a space has been demonstrated electron-microscopically, and this space can accommodate large molecules.

Endothelium and the blood-brain barrier

There are essentially three modern theories pertinent to this discussion concerning the site of a BBB to protein. First is the theory that substances are able to cross the capillary endothelium, but are impeded from entering the parenchyma by the layer of perivascular glial end feet (Schaltenbrand and Bailey, '28; Tschirgi, '52). The hypothesis of a glial barrier was strongly reinforced by the observation that brain capillaries are entirely invested by glial processes (Wolff, '63) and that the junctions between the adjoining glial processes are sealed (Gray, '61; Peters, '62). However, it is now clear that there is no continuous barrier of tight interglial junctions around capillaries (Kuffler and Nicholls, '66; Reese and Karnovsky, '67). The patency of the clefts between perivascular glial end feet has been demonstrated by

In *Ambystoma*, some of the capillaries have a perivascular space identical to that in *Necturus*. Others exhibit the mammalian architecture in having no pericapillary space, but rather a single basement membrane shared by the endothelium or pericytes and glial processes (fig. 4). In *Ambystoma*, capillary loops without perivascular spaces closely resemble the capillary loops of the opossum (Bubis, '62). No correlation could be made between the occurrence of a perivascular space and the type of capillary (loop or network), the size of the capillary, the region of the brain, or the distance from the pial surface. The endothelium, pericytes, and perivascular glial processes of *Ambystoma* are indistinguishable from those elements in *Necturus*.

Pial capillaries

In both species, the parenchymal capillaries are continuous with pial vessels which, morphologically, are capillaries rather than arterioles or venules (figs. 1, 2). Thus, in the urodele, many vessels lying within the subarachnoid space are capillaries whereas, in the mammal, none of the pericerebral vessels are capillaries (Millen and Woollam, '61). The pial capillaries have an endothelium and a discontinuous layer of pericytes identical to those of the parenchymal vessels (fig. 9). The basement membrane is a poorly defined, diffuse condensation of material merging into the collagenous bundles of the pia-arachnoid tissue. Occasional mesothelial cells are seen in the neighborhood of these vessels, sometimes containing large pigment granules.

The pial surface of the brain, on which these vessels run, is structurally identical with the neuropil surrounding parenchymal capillaries. There is a continuous layer of glial cells resting on a very straight basement membrane which borders the subarachnoid space. Both the glial layer and the basement membrane are continuous with the perivascular glial end-feet and their basement membrane at places where the vessels dip into the brain substance (fig. 2).

Tracer studies

In both species, trypan blue stained the connective tissues of the body shortly after administration. Some structures, like the gastrointestinal tract and sheaths around large blood vessels were strongly stained whereas the somatic muscles were only faintly tinted. The brain was grossly unstained, as was the urogenital system (including ovaries, oviducts and kidneys) in *Necturus*. The dura mater of both urodeles and the pineal body of *Ambystoma* were stained, but the choroid plexus of both species had scarcely any coloration. Route of injection and length of exposure to the dye did not alter the results.

Intravenous horseradish peroxidase does not cross the endothelial cells of the central nervous system (CNS) capillaries of *Necturus* or *Ambystoma* in discernible amount, regardless of the concentration of the protein, its duration of exposure, the temperature of the environment, or the route of fixation. In immersion-fixed material, the peroxidase filled the lumen (fig. 7) but, in perfused vessels, the reaction product was either totally washed out or was limited to a thin coating of the luminal surface of the endothelium (figs. 8-10), (perhaps bound to an endocapillary layer; Luft, '66). Peroxidase was only occasionally found in endothelial organelles, and the pictures provided for illustration are taken from areas with greater than average uptake. The protein could be found in pinocytotic vesicles, vacuoles and multivesicular bodies of the endothelium (figs. 8-10). It is important to note that in both the pial and parenchymal extensions of the capillaries, peroxidase-laden vesicles occurred, not only at the luminal surface, but near the contraluminal plasmalemma as well (fig. 8). Furthermore, peroxidase never moved beyond the luminal opening of inter-endothelial junctions. No detectable amounts of protein were ever found beyond the vessel wall within the perivascular space. The distribution of peroxidase just described indicates that the protein cannot pass between endothelial cells at the amount which is pinocytosed in the lumen, leaving no discernible protein to enter the perivascular space.

- Brightman, M. W. 1953 Perivascular spaces in the brains of *Necturus maculosus rafinesque* and *Mus norvegicus albinus*. *Anat. Rec.*, 117: 427-448.
- 1965 The distribution within the brain of ferritin injected into the cerebrospinal fluid compartments. II. Parenchymal distribution. *Am. J. Anat.*, 117: 193-220.
- 1967 Intracerebral movement of proteins injected into the blood and cerebrospinal fluid. *Anat. Rec.*, 157: 219.
- Brightman, M. W., and T. S. Reese 1967 Astrocytic and ependymal junctions in the mouse brain. *J. Cell Biol. Proceedings*. (In press.)
- Broman, T. 1949 The permeability of the cerebrospinal fluid vessels in normal and pathological conditions. Copenhagen: Ejnar Munksgaard. Chap. I, pp. 7-20.
- Brown, P. 1961 Albumin, connective tissue, and the blood-brain barrier. *Bull. Johns Hopkins Hosp.*, 108: 161-170.
- Bubis, J. J. 1962 The blood vessels in the central nervous system of the opossum. Fifth International Congress for Electron Microscopy. S. S. Breese, Jr., ed. Academic Press, New York, 2: N-12.
- Craigie, E. H. 1938 The comparative anatomy and embryology of the capillary bed of the central nervous system. *Assoc. Res. Nerv. Ment. Dis.*, 18: 3-28.
- 1939 Vascularity in the brains of tailed amphibians. I. *Ambystoma tigrinum* (green). *Proc. Amer. Philos. Soc.*, 81: 21-27.
- 1940 Vascularity in the brains of tailed amphibians. II. *Necturus maculosus rafinesque*. *Proc. Amer. Philos. Soc.*, 82: 395-410.
- Dawson, H. 1956 Physiology of the Ocular and Cerebrospinal Fluids. J. and A. Churchill Ltd., London, Chapter 6, pp. 152-189.
- Dawson, H., and E. Spaziani 1959 The blood-brain barrier and the extracellular space of the brain. *J. Physiol. (Lond.)*, 149: 135-143.
- Dempsey, E. W., and C. B. Wislocki 1955 An electron microscopic study of the blood-brain barrier in the rat, employing silver nitrate as a vital stain. *J. Biophys. Biochem. Cytol.*, 1: 245-256.
- DeRobertis, E., and H. M. Gerschenfeld 1961 Submicroscopic morphology and function of glial cells. *Internat. Rev. of Neurobiol.*, 3: 1-65.
- Dobbing, J. 1963 The blood-brain barrier: Some recent developments. *Cuy's Hosp. Reports*, 112: 267-286.
- Donahue, S., and G. D. Yappas 1961 The fine structure of capillaries in the cerebral cortex of the rat at various stages of development. *Am. J. Anat.*, 108: 331-347.
- Edström, R. 1964 Recent developments of the blood-brain barrier concept. *Int. Rev. Neurobiol.*, 7: 153-190.
- Gray, E. G. 1961 Electron Microscopy in Anatomy. J. D. Boyd, F. R. Johnson, and J. D. Lever, eds. Williams and Wilkins Co, Baltimore. Chap. 6, 54-73.
- Hartman, J. E. 1958 Electron microscopy of the neurohypophysis in normal and histamine-treated rats. *Zeit. f. Zellforsch.*, 48: 291-308.
- Herrick, C. J. 1948 The brain of the Tiger Salamander. University of Chicago Press, Chicago. Chap. II, 18-27.
- Karnovsky, M. J. 1965a A formaldehyde-glutaraldehyde fixative of high osmolality for use in electron microscopy. *J. Cell Biol.*, 27: 137A.
- 1965b Vesicular transport of exogenous peroxidase across the capillary endothelium into the T system of muscle. *J. Cell Biol.*, 27: 49A.
- King, L. S. 1938 Some aspects of the hematoencephalic barrier. *Assoc. Res. Nerv. Ment. Dis.*, 18: 150-177.
- Klatzo, I., J. Miguel, and R. Otenasek 1962 The application of fluorescein labeled serum proteins (FLSP) to the study of vascular permeability in the brain. *Acta Neuropath.*, 2: 144-160.
- Kruger, L., and D. S. Maxwell. 1967 Comparative fine structure of vertebrate neuroglia: teleosts and reptiles. *J. Comp. Neur.*, 129: 115-141.
- Kuffler, S. W., and J. G. Nicholls 1966 The physiology of neuroglial cells. *Ergebnisse der Physiologie*, 57: 1-80.
- Latansky, A., and F. J. Wald 1963 The extracellular space in the toad retina as defined by the distribution of ferrocyanide — a light and electron microscope study. *J. Cell Biol.*, 15: 463-479.
- Luft, J. H. 1966 Fine structure of capillary and endocapillary layer as revealed by ruthenium red. *Fed. Proc.*, 25: 1773-1783.
- Maynard, E. A., R. L. Shultz, and D. C. Pease 1957 Electron microscopy of the vascular bed of rat cerebral cortex. *Am. J. Anat.*, 100: 409-433.
- Millen, J. W., and D. H. Woollam 1961 Observations on the nature of the pia mater. *Brain*, 84: 514-520.
- Munger, B. L. 1966 Intercellular spaces in the posterior pituitary as related to the type of preservation. *J. Cell Biol.*, 31: 79A.
- Nelson, E., K. Blinzinger, and H. Hager 1961 Electron microscopic observations on subarachnoid and perivascular spaces of the Syrian hamster brain. *Neur.*, 11: 285-295.
- Palay, S. L. 1957 The fine structure of the neurohypophysis. *Prog. in Neurobiology*. S. Korey, and H. Nurnberger, eds. P. Hoeber, New York. Chap. II, 31-49.
- Patek, P. R. 1944 The perivascular spaces of the mammalian brain. *Anat. Rec.*, 88: 1-24.
- Peters, A. 1962 Plasma membrane contacts in the central nervous system. *J. Anat., Lond.*, 96: 237-248.
- Reese, T. S., and M. J. Karnovsky 1967 Fine structural localization of a blood brain barrier to exogenous peroxidase. *J. Cell Biol.*, 34: 207-217.
- Rivera-Pomar, J. M. 1966 Die Ultrastruktur der Kapillaren in der Area Postrema der Katze. *Zeit. f. Zellforsch.*, 75: 542-554.
- Rodriguez, L. A. 1955 Experiments on the histologic locus of the hemato-encephalic barrier. *J. Comp. Neur.*, 102: 27-45.
- Rosenbluth, J., and S. L. Wissig 1964 The distribution of exogenous ferritin in toad spinal ganglia and the mechanism of its uptake by neurons. *J. Cell Biol.*, 23: 307-325.

the movement of peroxidase through the clefts in the brain of the mouse (Brightman, '67) and of *Necturus*. The perivascular glia are, therefore, unlikely to present an effective barrier to different substances that are able to cross the endothelium.

Second, after the electron-microscopic demonstration of a surprisingly small CNS extracellular space, many have ascribed the BBB phenomenon to the lack of a sizable extracellular compartment into which substances could diffuse (Maynard et al., '57; DeRobertis and Gerschenfeld, '61; Brown, '61; Dobbing, '63; Edstrom, '64; Munger, '67). This view, which might be termed the "no-extracellular-space" theory, is also, in our opinion, no longer tenable. It has been repeatedly shown that the CNS extracellular fluid, though small in amount, functions as does extracellular fluid in other organs. Thus, substances which fail to enter the brain *in vivo* enter *in vitro*, presumably into an extracellular space (Davson and Spaziani, '59) but probably also enter into cells unavoidably damaged in such preparations. Crystalloids (Lasansky and Wald, '63) and large colloidal particles (Rosenbluth and Wissig, '64; Brightman, '65) are capable of traversing the intercellular clefts, and peroxidase is among these particles (Brightman, '67). In addition, it has been convincingly shown (Kuffler and Nicholls, '66) that it is through extracellular clefts rather than glial cytoplasm that ionic movements take place. Thus, there is a milieu in which extracellular substances can move about in the CNS.

A corollary to the "no extracellular space" theory would be that only in areas of the nervous system containing collagenous connective tissue spaces is there no BBB. King ('38) ascribed the lack of a barrier to trypan blue in the choroid plexus, area postrema, neurohypophysis, and pineal to the presence in these areas of collagen. Dempsey and Wislocki ('55) showed that silver is deposited only in these same regions, and correlated this with the occurrence of a collagenous perivascular space. Brown ('61) drew the same conclusion using the tracer I^{131} -albumin.

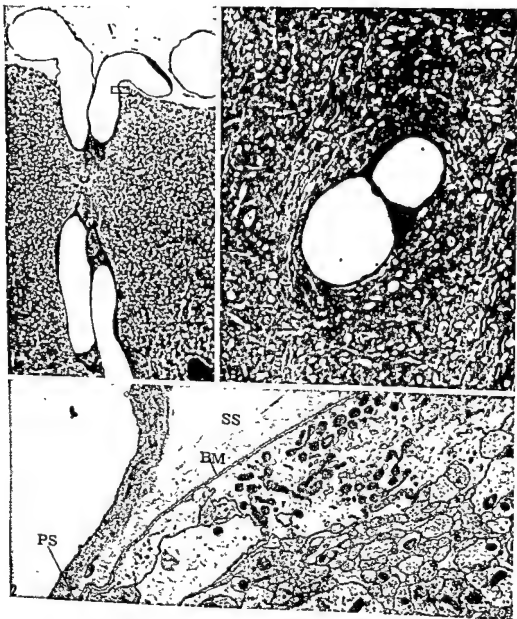
Protein-bound trypan blue, protein-complexed silver, albumin, and peroxidase are all of colloidal dimensions. In *Necturus*,

peroxidase is unable to pass from the brain capillary lumen in spite of the presence of collagenous tissue around the capillaries. In contrast, our results further demonstrate that the pericapillary space and CNS extracellular clefts can accommodate peroxidase entering from the cerebral ventricles. On the basis of these findings, the BBB to protein can no longer be explained by a lack of extracellular space.

The third theory places the barrier within the capillary endothelium (Spatz, '33; Broman, '49; Rodriguez, '55; Davson, '56). That the endothelium stands as a physical barrier to peroxidase has been demonstrated recently by Reese and Karnovsky ('67). The locus of the barrier appears to be the junction between adjacent endothelial cells. In comparison, the capillaries of cardiac muscle have interendothelial junctions that are open, permitting the protein to traverse the capillary wall (Karnovsky, '65b) whereas, in cerebral endothelium, the junctions are closed to peroxidase (Reese and Karnovsky, '67). In the choroid plexus of the mouse (Brightman, '67) and the rat (Becker et al., '67), peroxidase can cross the vessel walls and it would not be surprising if there is passage across comparable vessels in the other CNS areas lacking the BBB. Nevertheless, it is still not known which feature of the endothelium of these specialized regions differentiates it from that of ordinary brain capillaries. One characteristic of most of these areas is the presence of endothelial fenestrations (Palay, '57; Wolfe, '65; Rivera-Pomar, '66). However, these structures are not present in the ovine and bovine pineal gland (Anderson, '65); and, though it is as yet uncertain, the fenestrations of the choroid plexus appear to be impermeable to peroxidase (Brightman, '67). Whatever the vascular structures may be that subserve the transport of protein, it is the endothelium rather than any extravascular element which determines whether or not peroxidase can pass from blood to brain.

LITERATURE CITED

- Anderson, E. 1965 The Anatomy of bovine and ovine pineals. *J. Ultra. Res.*, Supp. 8, pp. 1-80.
Becker, N. A., A. B. Novikoff and H. M. Zimmerman 1967 Fine structural observations of the uptake of intravenously injected peroxidase by the rat choroid plexus. *J. Histochem. Cytochem.*, 15: 160-165.



- Schaltenbrand, G., and P. Bailey 1928 Die perivaskuläre Pia- und Glia-membran des Gehirns. *J. Psychol. u. Neur.*, 35: 199-276.
- Spatz, H. 1933 Die Bedeutung der vitalen Färbung für die Lehre vom Stoffaustausch zwischen dem Zentral-nervensystem und dem übrigen Körper. *Archiv f. Psychiat. u. Nervenkrank.* 101: 267-358.
- Tschirgi, R. D. 1950 Protein complexes and the impermeability of the blood-brain barrier to dyes. *Am. J. Physiol.*, 163: 756P.
- 1952 Blood-brain barrier. *The Biology of Mental Health and Disease*. P. B. Hoeber, Inc., New York. Chap. 4, 34-53.
- Venable, J. H., and R. Coggeshall 1965 A simplified lead citrate stain for use in electron microscopy. *J. Cell Biol.*, 25: 407-408.
- Wislocki, G. B., and A. J. Ladman 1958 The fine structure of the mammalian choroid plexus. In: *Ciba Foundation Symposium on the Cerebrospinal Fluid*. G. Wolstenholme, and C. O'Connor, eds. Little, Brown and Co., Boston, 55-79.
- Wislocki, G. B., and E. H. Leduc 1932 Vital staining of the hemato-encephalic barrier by silver nitrate and trypan blue, and cytological comparison of the neurohypophysis, pineal body, area postrema, intercolumnar tubercle, and supraoptic crest. *J. Comp. Neur.*, 36: 371-413.
- Wolfe, D. E. 1965 The epiphyseal cell: an electron-microscopic study of its intercellular relationships and intracellular morphology in the pineal body of the albino rat. *Prog. in Brain Res.*, 10: 332-376.
- Wolff, J. 1963 Beiträge zur Ultrastruktur der Kapillaren in der normalen Grosshirnrinde. *Zeit. f. Zellforsch.*, 60: 409-431.
- Woollam, D. H. M., and J. W. Millen 1954 Perivascular spaces of the mammalian central nervous system. *Biol. Rev.*, 29: 251-283.

PLATE 1

EXPLANATION OF FIGURES

- 1A Light micrograph of a pial capillary dipping into the brain of *Necturus* to form a typical capillary loop. The inset corresponds to figure 2. Toluidine blue stain. Forebrain. $\times 300$.
- 1B Cross-section of a capillary loop. The perivascular space cannot usually be visualized by light microscopy. Toluidine blue. $\times 800$.
- All subsequent figures are electron micrographs of sections stained with lead citrate.
- 2 Electron micrograph of the area indicated by the inset of figure 1A. A pial capillary merges into a parenchymal capillary. The subarachnoid space (SS) around the pial limb narrows to form the pericapillary space (PS). The well defined pial basement membrane (BM) is continuous with the perivascular glial membrane. Diencephalon. $\times 10,000$.

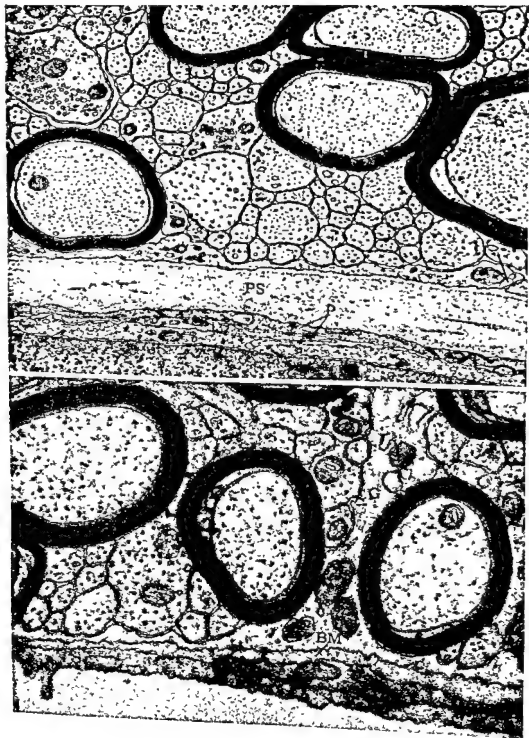


PLATE 2

EXPLANATION OF FIGURES

- 3 *Necturus*. The capillary lumen is not shown. Below is the nucleus and cytoplasm of an endothelial cell and of a pericyte (P). The perivascular space (PS) contains collagen fibers and is bordered by a poorly defined endothelial basement membrane and a distinct glial one. A thin glial sheet intervenes between parenchyma and PS. One interglial cleft occurs at the extreme right (arrow) and a synaptic contact at the upper left. Medulla oblongata. $\times 25,000$.
- 4 *Ambystoma*. A capillary lumen lies at the bottom and is enclosed by endothelium and pericyte (P). The lack of a perivascular space and the sharing of basement membrane by glial and endothelial cells and by pericytes is characteristic of the mammalian architecture. A glial process (G) forms an extensive, thin end foot interposed between capillary and parenchyma. Medulla. $\times 42,000$.

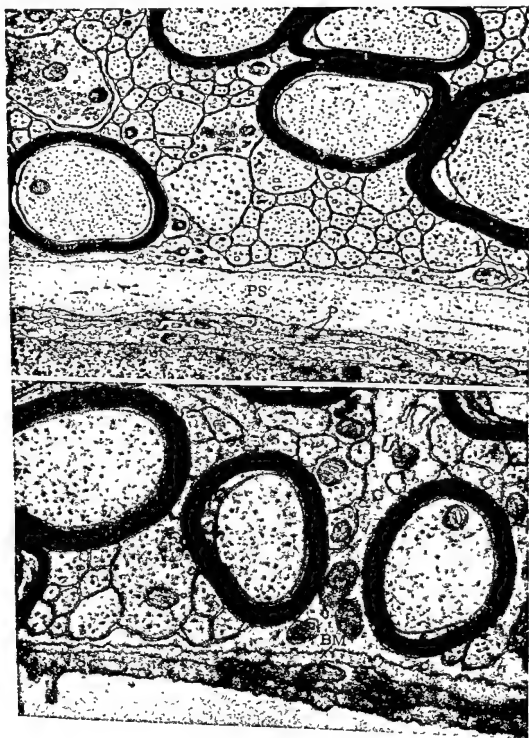


PLATE 3

EXPLANATION OF FIGURES

All subsequent micrographs are of sections from the medulla oblongata of different *Necturus*. The capillary lumen appears at the bottom of each figure.

- 5 Pericapillary region around an endothelial cell with its nucleus, includes the perivascular space (PS) and a glial sheet (G) separating the space from synaptic boutons (arrows) containing glycogen. $\times 21,000$.
- 6 Endothelial junction (J) is part of an interendothelial apposition that is always long and tortuous. Several pericytes processes (arrows) occur and the perivascular space (PS) separates them from the surrounding glia. $\times 42,000$.



PLATE 3

EXPLANATION OF FIGURES

All subsequent micrographs are of sections from the medulla oblongata of different *Necturus*. The capillary lumen appears at the bottom of each figure.

- 5 Pericapillary region around an endothelial cell with its nucleus, includes the perivascular space (PS) and a glial sheet (G) separating the space from synaptic boutons (arrows) containing glycogen. $\times 21,000$.
- 6 Endothelial junction (J) is part of an interendothelial apposition that is always long and tortuous. Several pericytes processes (arrows) occur and the perivascular space (PS) separates them from the surrounding glia. $\times 42,000$.



PLATE 4

EXPLANATION OF FIGURES

- 7 Capillary from a specimen injected intravascularly with 20 mg of peroxidase and fixed by immersion two hours later. The capillary is surrounded by a wide perivascular space (PS) but the granular reaction product is confined to the capillary lumen (lower half of the figure). $\times 13,500$.



PLATE 5

EXPLANATION OF FIGURES

Figures 8 to 10 Pericapillary region of a *Necturus* injected intravascularly with 30 mg peroxidase and fixed by vascular perfusion two-and-one-half hours later.

- 8 The reaction product has been washed out of the capillary lumen (bottom), except for some adhering to the luminal membrane. Several peroxidase-containing endothelial vesicles lie close to the contraluminal plasmalemma. No peroxidase has entered the pericyte (P), perivascular space (PS) or the parenchymal clefts. $\times 50,000$.

Inset: Reaction product occurs within a vesicle almost touching the contraluminal endothelial cell membrane. None has reached the perivascular basement membrane or space (PS). $\times 50,000$.

- 9 Pial capillary. Reaction product coats the luminal surface of the endothelial cell and appears within vesicles and a multivesicular body in the endothelial cytoplasm. No peroxidase appears in the subarachnoid space outside the vessel. An interglial apposition (upper left) faces a well defined basement membrane (BM) that forms a continuous boundary of the subarachnoid space (SS). $\times 37,000$.

Inset: An endothelial peg contains a dense body, characteristic of the endothelium, and vesicles filled with reaction product. $\times 30,000$.



PLATE 6

EXPLANATION OF FIGURES

- 10 Peroxidase has been incorporated by two endothelial vesicles (arrows). No reaction product occurs in the perivascular space (PS) or in the cerebral extracellular spaces. $\times 45,000$.
- 11 Pericapillary region of a *Necturus* injected with 4 mg of peroxidase into the cerebral ventricles for 20 minutes then fixed by cardiac perfusion. Peroxidase has entered the cerebral extracellular clefts, moved through an interglial gap junction (GJ) and across the glial basement membrane to fill the perivascular space (PS). Protein then passed into the interendothelial cleft until stopped by what is presumably a tight junction (arrow). The collagen within the PS appears to have been negatively "stained" by the reaction product. The large granules within the endothelial cell (bottom) represent particulate glycogen. $\times 86,000$.

Inset: Reaction product fills both the median cleft of a gap junction (arrow) between two glial end feet, and the perivascular space (bottom). $\times 160,000$.

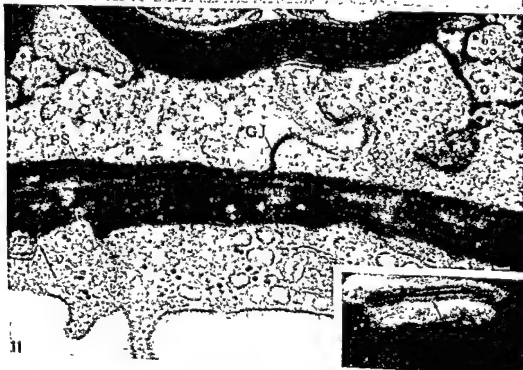
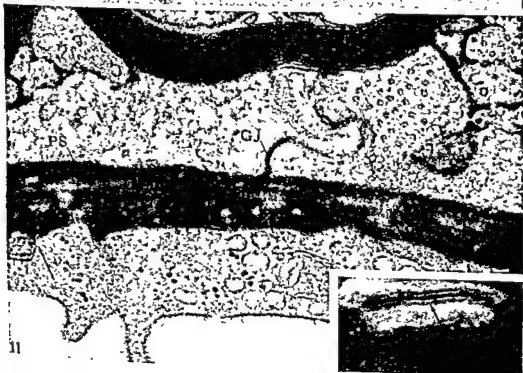


PLATE 6

EXPLANATION OF FIGURES

- 10 Peroxidase has been incorporated by two endothelial vesicles (arrows). No reaction product occurs in the perivascular space (PS) or in the cerebral extracellular spaces. $\times 45,000$.
- 11 Pericapillary region of a *Necturus* injected with 4 mg of peroxidase into the cerebral ventricles for 20 minutes then fixed by cardiac perfusion. Peroxidase has entered the cerebral extracellular clefts, moved through an interglial gap junction (GJ) and across the glial basement membrane to fill the perivascular space (PS). Protein then passed into the interendothelial cleft until stopped by what is presumably a tight junction (arrow). The collagen within the PS appears to have been negatively "stained" by the reaction product. The large granules within the endothelial cell (bottom) represent particulate glycogen. $\times 86,000$.

Inset: Reaction product fills both the median cleft of a gap junction (arrow) between two glial end feet, and the perivascular space (bottom). $\times 160,000$.



Protein Synthesis Studied by Autoradiography in the Epidermis of Different Species

KIMIE FUKUYAMA¹ AND WILLIAM L. EPSTEIN²

Division of Dermatology, Department of Medicine, University of California School of Medicine, San Francisco, California

ABSTRACT This paper reports autoradiographic studies of protein synthesis related to epidermal cornification in several different species. A high concentration of injected histidine appeared in granular cells of man, the monkey, guinea pig, hairless mouse, and newborn rat, indicating that synthesis of relatively histidine-rich protein is involved in formation of keratohyalin granules. Two steps in the cornification process: synthesis of this histidine-rich protein, in addition to protein synthesized in the lower layers of the epidermis are postulated in epidermis containing keratohyalin granules. In the epidermis of the turtle, which does not contain keratohyalin granules, concentration of histidine is not observed, suggesting that protein of the cornified layer in this species seems to be synthesized as a 1-stage process.

In man and the newborn rat, injected histidine- H^3 has been shown by autoradiography to be incorporated preferentially into the granular layer of the epidermis, whereas methionine- H^3 concentrates more in the basal and spinous layers (Fukuyama and Epstein, '65, '66, '67). In time, the radioactivity which appeared in the different layers of the epidermis reached the cornified layer. We considered therefore that proteins of different composition are synthesized in epidermal cells during the process of migration and differentiation; relatively, methionine, and leucine-rich protein is synthesized in the lower area of the epidermis and histidine-rich protein is added to cells in the granular layer, before they cornify completely.

The number of cells and layers of the epidermis is different in various parts of the body and in different species. The time needed for the basal cells to differentiate to granular cells is about ten days in man (Epstein and Maibach, '65) and about three days in newborn rats (Fukuyama and Bernstein, '61) and hairless mice (Epstein et al., '66). These differences suggest that the metabolic processes related to cornification in epidermal cells are different in different species. In fact, the size and distribution of keratohyalin granules vary considerably among species and, furthermore, in the epidermis of turtles and birds and in pathological parakeratotic lesions, the cornified layer forms without kerato-

hyalin granules (Spearman, '65). Accordingly, an attempt has been made by us to study the sites of incorporation of tritium-labeled amino acids in the epidermis of several different species, to investigate protein synthesis in the different types of cornification.

MATERIALS AND METHODS

Five-10 μ C of histidine- H^3 monohydrochloride (Spec. Act. 3.42 C/mM) and methionine-methyl- H^3 (Spec. Act. 35.8 mC/mM), or leucine-4.5- H^3 (Spec. Act. 5.0 C/mM) was injected intradermally in man, monkeys (*Rhesus maccus*), guinea pigs (Hartley strain), hairless mice, and turtles (*Pseudemys scripta elegans* and *Graptemys pseudogeographica Kohnii*), and biopsies were taken from the site of injection 30 minutes later. Four to five-day-old rats (Sprague-Dawley strain) were injected with 15 μ C of histidine- H^3 , leucine- H^3 , and methionine- H^3 intraperitoneally and, 30 minutes after injection, a biopsy was secured from the back sides of the animals. Tissues were fixed in formalin-acetic acid-alcohol and processed for autoradiography, as described previously (Fukuyama and Epstein, '66).

¹ Dr. Fukuyama is Assistant Professor in Residence, Division of Dermatology, University of California School of Medicine, San Francisco, California.

² Dr. Epstein is Associate Professor and Chairman, Division of Dermatology, University of California School of Medicine, San Francisco, California.

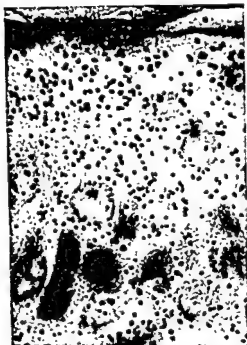


Fig. 2 Incorporation of leucine- H^3 into human epidermis at 30 minutes after injection. Labels distributed diffusely throughout the epidermis.

again greater in the upper area, especially over keratohyalin granules, when compared with that in the basal layer, but the differences in grain count between the basal and granular layers were not as significant as those observed in the epidermis of man. Radioactivity from injected methionine- H^3 was demonstrated mainly in the spinous and basal layers.

3. *Guinea pig and hairless mouse.* Histidine- H^3 and methionine- H^3 were injected separately in the dorsal skin of the side of six animals in each species. Both the 1-month-old guinea pig and the 3-month-old hairless mouse have a thin epidermis, 3-4 cells layers thick, and there are 1-2 layers of cells which possess easily recognized keratohyalin granules. Although injected histidine- H^3 was localized over keratohyalin granules, a considerable number of grains appeared also in the basal layer, and the ratio of grain counts in the granular layer as compared with the basal layer was rather low. Methionine- H^3 concentrated in the lower area of the epidermis, as observed in other species.

4. *Newborn rat.* In the newborn rat, the epidermis is thicker on the dorsal side than in the adult rat, consisting of 5-6 layers of relatively larger cells. The cells in the upper three layers contain large rounded keratohyalin granules. As previously reported (Fukuyama et al., '65), intraperitoneally injected histidine- H^3 primarily incorporated in the upper area, whereas methionine- H^3 and leucine- H^3 concentrated more in the lower area. A high concentration of radioactivity was observed over or adjacent to keratohyalin granules after injection of histidine- H^3 .

5. *Turtle.* The thighs of four turtles were used in this study. The epidermal cells of this region have large nuclei and are highly pigmented. In the upper layer, the number of nuclei is decreased, but no keratohyalin granules appear in the cytoplasm. Since pigment interferes with investigation of protein synthesis related to keratinization, as well as with identification of grains, tissues were treated with potassium permanganate and oxalic acid to bleach the pigment before filming. In incorporation of both histidine- H^3 and leucine- H^3 resulted in a much higher concentration in the lower area of the epidermis (figs. 3, 4). The pattern of distribution of grains was very similar between the two amino acids- H^3 .

DISCUSSION

Incorporation of histidine- H^3 , leucine- H^3 , and methionine- H^3 was observed in the epidermis of all species used in this study and radioactivity was detected in both the nucleus and cytoplasm. As previously discussed, the radioactivity demonstrated in autoradiography indicates localization of newly synthesized protein containing administered amino acids- H^3 (Leblond et al., '57, Droz and Warshawsky, '62). The amount of radioactive protein synthesized may be influenced by the pool size of each amino acid present in cells, which may result in a different intensity in labeled cells; but the number of grains appearing in different cells of the epidermis has been considered to represent a rate of incorporation of the specific amino acid into peptide chains in the area (Hooper and Bernstein, '65).

The number of silver grains was counted, using a Whipple eyepiece micrometer disc under $\times 1280$ – 1600 magnification. Since the number of grains actually appearing in the sections varied considerably from one animal to another, a ratio of counts in 200 squares (approximately $20 \times 2000 \mu$) in the lowermost and uppermost areas of each specimen was compared separately. The lower area used in the grain counts covered almost only basal cells in all species. But the upper area contained only granular cells in the newborn rat and guinea pig; whereas it consisted of granular cells and upper spinous cells in man and monkeys, because their granular cells are not always thick enough to cover the test area.

RESULTS

Radioactivity was detected over the epidermis of man, the monkey, guinea pig, hairless mouse, newborn rat, and turtle, after injection of histidine- H^3 , and methionine- H^3 . Concentration of grains, however, appeared in the lowermost area, and the uppermost area varied significantly depending upon the tracers and the species of animal used in the study. The number of grains counted in the uppermost area was compared with that of the lowermost area in the same section. This data is summarized in table 1.

1. *Man*. The skin of the upper arm from 12 volunteers was studied. Incorporation of histidine- H^3 in the granular layer was 3.7 times higher than in the basal layer (fig. 1). A concentration of silver grains over or adjacent to keratohyalin granules was striking, except in 10.4% of the granular cells, as reported previously (Fukuyama and Epstein, '67). Injection of leucine- H^3 resulted in labeling of the upper area slightly more than the lower area, but specific association of grains with kerato-



Fig. 1 Incorporation of histidine- H^3 into human epidermis at 30 minutes after injection. Grains concentrated over granular cells.

hyalin granules was not noted (fig. 2). The grains were distributed diffusely and many of the counts resulted from a high degree of labeling in the adjacent upper spinous cell layer. Following injection of methionine- H^3 , the ratio of grain counts in the upper layer to those of the basal layer was 88%, and almost no labels were seen over keratohyalin granules.

2. *Monkey*. Two sites each in the thigh area of three monkeys were injected with histidine- H^3 and methionine- H^3 . The epidermis consisted of 3–4 cell layers, groups of very fine keratohyalin granules were present in the outermost layer. Incorporation of histidine- H^3 was

TABLE 1

Ratio of grain counts made at 30 minutes after injection of amino acids- H^3 in the granular layer of different species. Number of grains appearing in the basal layer is taken as one

Amino acid	Human	Monkey	Guinea pig	Hairless mouse	Newborn rat	Turtle
Histidine- H^3	3.9	1.9	1.6	1.8	3.7	0.6
Leucine- H^3	1.5	—	—	—	0.5	—
Methionine- H^3	0.9	0.5	0.7	0.8	1.1	0.5

tron-microscopic observation on the epidermis containing keratohyalin granules supports the idea that keratohyalin granules play an active role in cell cornification (Brody, '59). Two sites of protein synthesis appear to correspond to sites of formation of tonofibrils and keratohyalin granules. Ultrastructural changes in the epidermis of the turtle should yield more information on the cornification process which occurs without keratohyalin granules, but we have not found any published reports on this subject as yet.

ACKNOWLEDGMENT

This study was supported in part by research grant no. 10 from the Academic Senate — San Francisco Division, Committee on Research, University of California School of Medicine, San Francisco.

LITERATURE CITED

- Droz, B., and H. Warshawsky 1963 Reliability of the radioautographic technique for the detection of newly synthesized protein. *J. Histochem. Cytochem.*, 11: 426-435.
- Epstein, J. H., K. Fukuyama and R. L. Dobson 1966 Ultraviolet light carcinogenesis. Presented at the fifteenth International Biometeorological Congress, New Brunswick, N. J. (in press).
- Epstein, W. L., and H. I. Maibach 1965 Cell renewal in human epidermis. *Arch. Derm.*, 92: 462-468.
- Fukuyama, K., and I. A. Bernstein 1961 Autoradiographic studies of the synthesis of deoxyribonucleic acid in the skin of young rats. *J. Invest. Derm.*, 36: 321-326.
- Fukuyama, T., Nakamura and I. A. Bernstein 1965 Differentially localized incorporation of amino acids in relation to epidermal keratinization in the newborn rat. *Anat. Rec.*, 152: 525-535.
- Fukuyama, K., and W. L. Epstein 1966 Epidermal keratinization: Localization of isotopically labeled amino acids. *J. Invest. Derm.*, 47: 551-560.
- 1967 Synthesis of RNA and protein during epidermal cell differentiation in man. *Arch. Derm.* (in press).
- Hoover, J. K., and I. A. Bernstein 1966 Protein synthesis related to epidermal differentiation. *Proc. Nat. Acad. Sci.*, 56: 594-598.
- Leblond, C. P., N. B. Everett and B. Simmons 1957 Sites of protein synthesis as shown by radioautography after administration of S^{35} -labeled methionine. *Am. J. Anat.*, 101: 225-271.
- Spearman, R. I. C. 1966 The keratinization of epidermal scales, feathers, and hairs. *Biol. Rev.*, 41: 59-94.

After methionine- H^3 injection, the radioactivity appeared more concentrated in the lower area of the epidermis in all species. Leucine- H^3 injection resulted in a similar observation in rats and turtles, but rather high counts were obtained in the upper layer of the epidermis of man. Labels were not obviously associated with keratohyalin granules in any species after injection of methionine- H^3 or leucine- H^3 . Even in the upper layers of the epidermis in man, where relatively high counts were obtained, labels located diffusely in the cytoplasm of granular cells and upper spinous cells, demonstrating many unlabeled keratohyalin granules.

Injected histidine- H^3 resulted in intensive labeling of the granular layer in man, the monkey, guinea pig, hairless mouse, and newborn rat. The resolution allowed by light microscopy is not sufficient to deal with specific subcellular sites of protein synthesis from injected histidine- H^3 , but



Figure 4



Figure 3

Figs. 3 and 4 Incorporation of histidine- H^3 (fig. 3) and leucine- H^3 (fig. 4) into turtle epidermis. There are no keratohyalin granules and grains

labels in the granular cells are definitely accumulated on or near keratohyalin granules. A relationship between keratohyalin granules and concentration of histidine- H^3 was further emphasized in turtles, by the fact that the grain count was low in the upper part of this epidermis where no keratohyalin granules were present. These results suggest that histidine incorporates into polypeptide chains during the differentiation process involving the formation of keratohyalin granules.

Labels appeared over keratohyalin granules, after histidine- H^3 injection had moved into the cornified layer in newborn rats, as well as leucine- H^3 and methionine- H^3 , which initially labeled cells in the lower layers (Fukuyama and Bernstein, '65). Two steps in the cornification process: synthesis of histidine-rich protein in granular cells besides a protein chain synthesized in the lower layers of the epidermis can be postulated to occur in the epidermis possessing keratohyalin granules. However, epidermis without keratohyalin granules (as in the turtle) seems

iron-microscopic observation on the epidermis containing keratohyalin granules supports the idea that keratohyalin granules play an active role in cell cornification (Brody, '59). Two sites of protein synthesis appear to correspond to sites of formation of tonofibrils and keratohyalin granules. Ultrastructural changes in the epidermis of the turtle should yield more information on the cornification process which occurs without keratohyalin granules, but we have not found any published reports on this subject as yet.

ACKNOWLEDGMENT

This study was supported in part by research grant no. 10 from the Academic Senate — San Francisco Division, Committee on Research, University of California School of Medicine, San Francisco.

LITERATURE CITED

- Droz, B., and H. Warshawsky 1963 Reliability of the radioautographic technique for the detection of newly synthesized protein. *J. Histochem. Cytochem.*, 11: 426-435.
- Epstein, J. H., K. Fukuyama and R. L. Dobson 1966 Ultraviolet light carcinogenesis. Presented at the fifteenth International Biometeorological Congress, New Brunswick, N. J. (in press).
- Epstein, W. L., and H. I. Malbach 1965 Cell renewal in human epidermis. *Arch. Derm.*, 92: 462-468.
- Fukuyama, K., and I. A. Bernstein 1961 Autoradiographic studies of the synthesis of deoxyribonucleic acid in the skin of young rats. *J. Invest. Derm.*, 36: 321-326.
- Fukuyama, T., Nakamura and I. A. Bernstein 1965 Differentially localized incorporation of amino acids in relation to epidermal keratinization in the newborn rat. *Anat. Rec.*, 152: 525-535.
- Fukuyama, K., and W. L. Epstein 1966 Epidermal keratinization: Localization of isotopically labeled amino acids. *J. Invest. Derm.*, 47: 551-560.
- 1967 Synthesis of RNA and protein during epidermal cell differentiation in man. *Arch. Derm.* (in press).
- Hoober, J. K., and I. A. Bernstein 1966 Protein synthesis related to epidermal differentiation. *Proc. Nat. Acad. Sci.*, 56: 594-598.
- Leblond, C. P., N. B. Everett and B. Simmons 1957 Sites of protein synthesis as shown by radioautography after administration of S^{35} -labeled methionine. *Am. J. Anat.*, 101: 225-271.
- Spearman, R. I. C. 1966 The keratinization of epidermal scales, feathers, and hairs. *Biol. Rev.*, 41: 59-94.

Gonocyte Degeneration in the Postnatal Male Rat¹

EDWARD C. ROOSEN-RUNGE AND JEAN LEIK

*Department of Biological Structure, University of Washington,
Seattle, Washington*

ABSTRACT The cell population of the sex cords in rat testes from day 1 to day 10 after birth was investigated by means of microscopic observation and quantitation, and with the electron microscope. Certain gonocytes, rare during the first 2 days, more frequent thereafter, were found in various stages of pyknosis. In electron micrographs these were characterized mainly by condensed and sometimes fragmented nuclei and cytoplasmic vacuoles and vesicles. The mitochondria remained typical of gonocytes in all but the most advanced stages of necrosis. Degenerating cells were eventually surrounded by single supporting cells and apparently phagocytized by them. Gonocytes which appeared "swollen," "fuzzy" and pale staining under the microscope were considered normal pre-mitotic cells or possibly in some cases altered by artifacts of fixation. No evidence was produced microscopically or electron microscopically that cells of this type are degenerative. In many gonocytes, the electron microscope revealed some swollen mitochondria with irregular cristae, "B-bodies" in varying numbers and occasional membrane breakage. The evidence was considered insufficient to interpret these as signs of impending cell death.

Quantitative determinations of the numbers of gonocytes at various stages indicate that approximately one third of the cells are lost between day 1 and 4 post-partum. In Sprague-Dawley rats gonocytic mitoses resume on day 4. There is evidence that degeneration of gonocytes continues until day 7 or 8. The total number of cells dying may possibly be accounted for by the number of pyknotic cells observed. Incidental data are reported concerning the growth of sex cords and the proliferation of supporting cells. Comparison with results in the literature lead to the general conclusion that there is excellent evidence that many gonocytes die during the first postnatal week, but that many of the morphological criteria for dying cells used by previous investigators lack validity when rigorously examined.

The development of seminiferous tubules immediately preceding the onset of spermatogenesis has been the object of detailed scrutiny for 70 years or more. It has been studied very frequently in the rat. In fact, there are few examples in the history of histological research of so many investigators examining such a small population of cells during a brief period of development in the same species. The following review is restricted to the literature on the development of the rat testis from birth to approximately day 10. Nowadays, such a review no longer needs to deal with the question of the origin of germ cells (Everett, '45) which has been answered unequivocally by Clermont and Perey ('57), Sapsford ('62), Beaumont and Mandl ('63), Huckins ('65) and others, to the effect that spermatogonia are the direct offspring of primordial germ cells found in the fetus, and represent a cell line different from that of the supporting (Sertoli) cells. Degeneration of gonocytes no longer implies the

complete extinction of a whole generation of germ cells. The literature remains contradictory, however, on the quantity and morphology of degenerating gonocytes and on the cause of their death.

Following cursory observations of the subject by Bouin (1895) and Popoff ('09), Hoven ('14) saw in rat testes, 3 to 8 days after birth, a considerable number of germ cells which he interpreted as degenerating because, in his material fixed in Flemming's solution and stained with Iron-Hematoxylin, their chromatin appeared irregularly clumped. Hoven did not mention any cytoplasmic features of degeneration, nor did he depict the degenerating cells. By day 10, they had almost entirely disappeared except for a few at the basement membrane which were described as "hardly distinguishable from the epithelial cells." Firket ('20) who fixed in Flemming's, Regaud's and other mixtures, came to the conclusion that all gonocytes died a

¹ Research was supported by USPHS grant HD-00471 and in part by HE-02698

few days after birth and that spermatogonia were subsequently formed from epithelial cells. He described the degenerating cells as undergoing hypertrophy "in which cytoplasm and nucleus seem to be filled with water; the chromatin is shrivelled into four or five irregular blocks staining weakly and lying next to the nuclear membrane; the mitochondria loose their sharp outline and seem to be dissolved in the general cytoplasm." Rauh ('25) did not consider degeneration of gonocytes an important phenomenon although he saw some germ cells of huge size. He described mitoses of germ cells which appeared in his strain of rats on the seventh postnatal day resulting in spermatogonia. Hargitt ('26) observed shrunken cells with pyknotic nuclei in postnatal rat testes and once again came to the conclusion that degeneration leads to the disappearance of all gonocytes by the sixth day after birth. Rauh ('29) contradicted him clearly and re-emphasized that spermatogonia arise by mitosis of gonocytes, but he also stated that "there is no doubt that primordial spermatogonia in degenerating condition are found." Although Rauh's demonstration of healthy gonocytes was thorough and lucid, his results apparently escaped the attention of Allen ('49) who studied the degenerating cells in much detail and came once again to the emphatic conclusion that *all* primordial germ cells degenerate by the postnatal age of nine days. In preparations fixed with modified Bouin's or Flemming's fluid, the degenerating cells first appeared shrunken and their nuclei pyknotic. Later, the nuclear remnants appeared pale and the cells were "lost in the central plasma of the tubule." In addition, Allen described a large cell which, in his view, originated from the basal cells and which also degenerated, often in mitotic failure.

Clermont and Perey ('57), for the first time, quantitated the cell population in the postnatal seminiferous tubules and demonstrated, in Sherman albino rats that some gonocytes start dividing at four days of age and give rise to spermatogonia, but "many" gonocytes fail to divide and degenerate. The changes which they considered suggestive of degeneration in material fixed in Helly's fluid were a swollen nucleus with pale, finely granulated chromatin dispersed

in the nuclear sap, poorly stained nucleoli and a wrinkled or broken nuclear membrane. In addition, some large mitoses appeared abnormal and degenerative. Sapsford ('62) in a non-quantitative study reached similar conclusions but challenged the view that nuclear swelling in gonocytes is indicative of degeneration. He considered the enlargement of nuclei as part of the normal process of differentiation of the gonocyte. According to Sapsford, "degenerative changes similar to those seen in irradiated cells (intense eosinophilia of nucleus and cytoplasm followed by shrinkage and dissolution) were observed in some of the enlarged cells in the normal testis."

Roosen-Runge ('62), for the first time, attempted to determine absolute numbers of gonocytes during the postnatal period. He found approximately 75,000 gonocytes per testis at birth and 50,000 on day 5. He considered his findings evidence for the death of approximately one-third of the germ cells present at birth. Beaumont and Mandl ('63) in a more extensive quantitative study found 60,000-70,000 gonocytes per testis at birth and approximately 25,000 at six to six and one-half days afterwards. They assumed that the decrease was due to "(a) the elimination of degenerating cells and (b) the transformation of gonocytes into definitive germ cells." Among the gonocytes observed microscopically between four and six and one-half days after birth, many appeared normal. Others showed changes including complete disappearance of the nuclear membrane and dispersal of the nuclear contents. This was interpreted as "almost certainly" lysis. It is of considerable interest that measurements of normal and "degenerating" nuclei failed to show any consistent difference between the two although Beaumont and Mandl felt, as had many observers before them, that the degenerating gonocytes undergo both nuclear and cytoplasmic swelling in Bouin fixed specimens. Huckins ('63, '65) has recently added a number of new observations to the often described phenomena of degeneration of gonocytes. Quantitative analyses caused her to conclude that in the Wistar rat approximately 75% of the primordial germ cell population at the time of birth are doomed

to death. Degeneration usually occurred in clusters and adjacent gonocytes frequently fused into "bizarre and multinucleate forms before degenerating." Huckins suggested that viable and non-viable gonocytes may be distinguished by the degree of basophilia of their cytoplasm, the viable cells staining vigorously with toluidine blue while non-viable ones show a decrease and finally a complete loss in basophilic material. Roosen-Runge ('64) was not able to demonstrate this difference.

Franchi and Mandl ('64) were the first to use the electron microscope in investigating normal and degenerating gonocytes in neonatal male rats. In specimens one and one-half to two days after birth, they found very few cells which showed a swollen endoplasmic reticulum and enlarged mitochondria. At five days of age, definite signs of degeneration were seen and at six days, the apical region of the supporting cells often contained debris which was interpreted as rests of necrotic gonocytes. Leik and Roosen-Runge ('66) confirmed many of these electronmicroscopic observations but were less convinced that they could be interpreted as degeneration.

In summary, data concerning the behavior of the male gonocyte population in the rat during the first ten days of postnatal life are available in impressive detail. It has become certain that gonocytes produce the first spermatogonia in the second half of the first week after birth. Furthermore, all investigators agree that at least some gonocytes degenerate and disappear during the first week. The quantity of these dying cells, however, is variously estimated or counted, from "some" to "approximately 75%." Microscopic observations have produced conflicting results on the characteristics of degenerating gonocytes. Electron microscopic studies have not yet decided these conflicts. The following paper constitutes a re-investigation of the problem directed particularly to an evaluation of existing opinions, by means of qualitative and quantitative, microscopic and electron microscopic methods. Incidentally, some new data on the development of supporting cells and the growth parameters of sex cords were collected.

MATERIALS AND METHODS

Rats of Sprague-Dawley stock were fed Purina Chow with supplementary vitamin rich feedings. Most of the qualitative and all of the quantitative histological investigations were carried out on a series of animals of seven age groups: day 1 (within 16 hours after birth), day 3 (46-52 hours), day 4 (72-76 hours), day 5 (4-4½ days), day 6 (5-5¼ days), day 8 (7¼-7¾ days), and day 10 (9-9¾ days). A rat designated "one day old" in this paper is at least 24 hours old; a rat "on day 1" or "of the day 1 age group" is not yet one day old.

Histologically, at least three animals from three different litters were studied in each age group. In each animal, only one testis was analyzed quantitatively. Beaumont's and Mandl's ('63) and our own results (unpublished) indicate that variability between the two testes of an animal can be safely neglected. After weighing, the testes were fixed in Stieve's solution, embedded in paraffin and sectioned serially at 6 μ . As the thickness of the sections enters into the determination of cell numbers, it was measured for each slide. Deviations of more than 1 μ (which were infrequent) were considered in the calculations. The standard staining method was a combination of gallocyanin and PAS-reaction, which differentiated cytoplasmic and nuclear features of normal and degenerating cells in a clear manner. Supplementary slides were stained with Feulgen, Methyl-Green Pyronin and Iron-Hematoxylin. Certain cytological observations were made on material embedded in Epoxy resin, sectioned one to one and one-half micra thick and stained with Richardson's stain.

Diameters of sex cords were measured in each age group. In 45 round or approximately round cross sections of cords, two diameters, perpendicular to each other, were recorded and the mean calculated. Standard deviations were found to be between 6% and 9.6% of the mean in ten series selected as samples.

The relative volume of sex cords was determined by Chalkley's method as described previously (Roosen-Runge, '55a). The weight of the testes in mg was equated

to volume in 0.1 ml without correction for density.

Cell numbers were determined by counting nuclei per cross section of sex cords in 90 cross sections under oil immersion, two sections from every tenth or twentieth section of the testis. There is an acute danger that subjective criteria in selecting cross sections will influence the results. The eye of the observer tends to favor sex cords which look "nice," have an "average" size or an "interesting" morphology. In order to avoid this danger as much as possible, cross sections were selected under very low magnification and counted under oil immersion without further consideration of suitability or special interest. Crude counts were adjusted according to Abercrombie's

formula: $T = C \times \frac{S}{S+D}$ where T is the

true count, C the crude count, S the thickness of the section and D the average nuclear diameter (60–100 nuclei).

Once the number of cells per cross section of a certain thickness is known, the absolute number can be derived after the length of the sex cords has been calculated from their volume and diameter.

$$L = \pi \frac{V}{r^2}$$

For electron microscopy, a variety of fixing fluids was used including OSO, Acrolein or glutaraldehyde followed by OsO₄, and a K₂Cr₂O₇-OsO₄ mixture. We believe this formulation is attributable to R. Weber. Fixing solutions were buffered with bicarbonate, cacodylate, collidine, phosphate or veronal systems to pH 7.3. In some cases sucrose or CaCl₂ was added to the fixing fluid. The most satisfactory results were obtained with a modified Weber's mixture (5% OsO₄; 1 part: 3% K₂Cr₂O₇; 1 part: veronal buffer, 0.056 M; 2 parts) to which 0.2 M sucrose was added and with cacodylate buffered OsO₄ (5% OsO₄; 2 parts: cacodylate buffer, 0.18 M; 1 part). Whole testes (or portions thereof in older specimens) were immersed in ice cold fixative for one-half hour, dehydrated in ethanol and embedded in Epon according to the Method of Luft ('61), sectioned and stained with uranyl acetate and/or Millonig's or Reynold's lead solution.

RESULTS

In the following paragraphs, results concerning the morphology and quantitation of degenerative cells are presented. For more details on the structure of the developing sex cords, the reader is referred, for instance, to the excellent description of Rauh ('25) and the illustrations of Clermont and Perey ('57).

Day 1: Germ cells and supporting cells are easily distinguished in microscopic preparations and in electron micrographs (figs. 1, 2, 8; 9, 12). Gonocytes are relatively large and their cytoplasm slightly basophilic. The nuclei are usually spherical, rarely oblong, with a diameter of 9.7 μ (average of 40 nuclei measured in each of three testes). A few large nuclei (diameter 13 μ and more) were seen. There are one to three prominent, spherical nucleoli which show a narrow Feulgen positive rim around a Feulgen negative, basophilic center. Ultrastructurally, such a differentiation is not apparent, the nucleolus being composed of a loose nucleolonema of uniform density (fig. 14). Occasionally amorphous material is seen in the interstices. In the cytoplasm, electron micrographs demonstrate sparse endoplasmic reticulum and scattered clusters of free ribosomes. The mitochondria are characteristically large with cristae in somewhat irregular array (figs. 8, 9). Two types of inclusions are regularly encountered in electron micrographs: large, granular masses of unidentified content (fig. 8) corresponding to the "A-bodies" of Franchi and Mandl ('64) and membrane-bound bodies of various sizes (fig. 8) containing granules, flocculent dense material, membrane whorls and small vesicles, corresponding to the "B-bodies" of Franchi and Mandl. The Golgi zone which is ultrastructurally unremarkable, microscopically stains strongly with PAS in 5–10% of the cells. Gonocytes are usually separated from the limiting membrane of the cord by supporting cells but an occasional cell is found in contact with the periphery even in electron micrographs. In microscopic preparations, careful focusing reveals that approximately 10% of all gonocytes touch the basement membrane with at least a small part of their surface.

The supporting cells (figs. 1, 2, 3) are more numerous, smaller, more basophilic and frequently found in mitosis in contrast to the gonocytes which were never observed to divide at this stage. The nuclei are somewhat irregularly ovoid. In electron micrographs, a small amount of granular endoplasmic reticulum and many free ribosomes are seen (figs. 8, 12). The mitochondria are smaller by one-half to one-third than those of the gonocytes but their cristae are often similarly irregular. Even small portions of supporting cells can be identified easily by their ultrastructural characteristics.

Day 3: The appearance of gonocytes and supporting cells do not essentially differ from that on day 1, except for some observations on degenerative cells which will be described below.

Day 4: Under the microscope gonocytes appear pale staining and somewhat "swollen," but the nuclear diameter was only insignificantly increased (10.1 μ). The degree of basophilia of the cytoplasm varied somewhat more than at earlier stages but it was not possible to establish types of gonocytes on this basis. In electron micrographs of 4- and 5-day testes gonocytes were frequently seen to extend long processes between the supporting cells to the periphery of the cord (fig. 9, arrow). Mitoses were not found until day 5, but in one out of three animals of day 4 a few spermatogonia of Type A were identified by their smaller, irregularly spheroid or ovoid nucleus with two or three nucleoli of lightly irregular outline. These nucleoli are even more characteristic in electron micrographs (fig. 17) where the nucleolonema is not of uniform density.

In addition to typical gonocytes and spermatogonia, less typical germ cells occur in small numbers. Some are elongated with ovoid and occasionally lobed nuclei. These were interpreted as moving gonocytes. Other cells with many of the characteristics of gonocytes have rod-shaped nucleoli and appear to be between gonocytes and spermatogonia in size. Such cells showed so much variability, however, that a single transitional "type" could not be established.

Day 5: Mitoses of gonocytes are frequently seen and spermatogonia of Type A

occur regularly in most specimens. Gonocytes not in mitosis and not frankly degenerating (see below) appear morphologically very similar to those on day 1. After day 5 gonocytes of this "normal" type become progressively rare, but a few were still seen on day 10. At this time they are always lying near the center of the cord which begins to develop a lumen on day 8.

Observations on degenerating gonocytes

Early in this investigation the question arose which gonocytes could be identified unequivocally as "degenerating." After careful consideration which will be elaborated in the discussion, the microscopic definition of a degenerating cell was restricted to cells which showed varying degrees of condensation and fragmentation of the nucleus, i.e. pyknosis, and varying degrees of granulation and vacuolization of the cytoplasm. Cells of this type could be arranged in a sequence of increasing signs of necrosis, beginning with a fairly large clumped nucleus and plentiful cytoplasm filled with granules and vacuoles (fig. 4) and ending with a small fragment, parts of which were strongly basophilic (fig. 7). The fragments had little recognizable cytoplasm. Pyknotic cells and cell rests microscopically often appeared to lie within supporting cells (fig. 6) as did structures resembling gonocyte nucleoli in outline, size and stainability. Pyknotic cells were often found in groups of two or more cells.

In each age group pyknotic cells and cell rests were counted in 120 cross sections of sex cords. There were 3 at day 1, nine at day 3, 13 on day 4, 12 on day 5, 8 on day 6 and 18 on day 8. The irregular size and the fragmentation of these rests does not permit the application of the same quantitative method which was used to calculate cell numbers from the counts per cross section, but some crude estimates were made which represent maximum numbers. The total number of pyknotic cells per testis was certainly not more than 2,500 on day 1 and 30,000 on day 8, but the last estimate may be considerably too high because on day 8, cell fragments are much more frequent than whole pyknotic cells. A few large mitotic

to volume in 0.1 ml without correction for density.

Cell numbers were determined by counting nuclei per cross section of sex cords in 90 cross sections under oil immersion, two sections from every tenth or twentieth section of the testis. There is an acute danger that subjective criteria in selecting cross sections will influence the results. The eye of the observer tends to favor sex cords which look "nice," have an "average" size or an "interesting" morphology. In order to avoid this danger as much as possible, cross sections were selected under very low magnification and counted under oil immersion without further consideration of suitability or special interest. Crude counts were adjusted according to Abercrombie's

formula: $T = C \times \frac{S}{S+D}$ where T is the

true count, C the crude count, S the thickness of the section and D the average nuclear diameter (60–100 nuclei).

Once the number of cells per cross section of a certain thickness is known, the absolute number can be derived after the length of the sex cords has been calculated from their volume and diameter.

$$L = r \frac{V}{r^3}$$

For electron microscopy, a variety of fixing fluids was used including OsO_4 , Acrolein or glutaraldehyde followed by OsO_4 , and a $\text{K}_2\text{Cr}_2\text{O}_7$ - OsO_4 mixture. We believe this formulation is attributable to R. Webor. Fixing solutions were buffered with bicarbonate, cacodylate, collidine, phosphate or veronal systems to pH 7.3. In some cases sucrose or CaCl_2 was added to the fixing fluid. The most satisfactory results were obtained with a modified Webor's mixture (5% OsO_4 ; 1 part: 3% $\text{K}_2\text{Cr}_2\text{O}_7$; 1 part: veronal buffer, 0.056 M; 2 parts) to which 0.2 M sucrose was added and with cacodylate buffered OsO_4 (5% OsO_4 ; 2 parts: cacodylate buffer, 0.18 M; 1 part). Whole testes (or portions thereof in older specimens) were immersed in ice cold fixative for one-half hour, dehydrated in ethanol and embedded in Epon according to the Method of Luft ('61), sectioned and stained with uranyl acetate and/or Milonig's or Reynold's lead solution.

RESULTS

In the following paragraphs, results concerning the morphology and quantitation of degenerative cells are presented. For more details on the structure of the developing sex cords, the reader is referred, for instance, to the excellent description of Rauh ('25) and the illustrations of Clermont and Perey ('57).

Day 1: Germ cells and supporting cells are easily distinguished in microscopic preparations and in electron micrographs (figs. 1, 2, 8, 9, 12). Gonocytes are relatively large and their cytoplasm slightly basophilic. The nuclei are usually spherical, rarely oblong, with a diameter of 9.7μ (average of 40 nuclei measured in each of three testes). A few large nuclei (diameter 13μ and more) were seen. There are one to three prominent, spherical nucleoli which show a narrow Feulgen positive rim around a Feulgen negative, basophilic center. Ultrastructurally, such a differentiation is not apparent, the nucleolus being composed of a loose nucleolonema of uniform density (fig. 14). Occasionally amorphous material is seen in the interstices. In the cytoplasm, electron micrographs demonstrate sparse endoplasmic reticulum and scattered clusters of free ribosomes. The mitochondria are characteristically large with cristae in somewhat irregular array (figs. 8, 9). Two types of inclusions are regularly encountered in electron micrographs: large, granular masses of unidentified content (fig. 8) corresponding to the "A-bodies" of Franchi and Mandl ('64) and membrane-bound bodies of various sizes (fig. 8) containing granules, flocculent dense material, membrane whorls and small vesicles, corresponding to the "B-bodies" of Franchi and Mandl. The Golgi zone which is ultrastructurally unremarkable, microscopically stains strongly with PAS in 5–10% of the cells. Gonocytes are usually separated from the limiting membrane of the cord by supporting cells but an occasional cell is found in contact with the periphery even in electron micrographs. In microscopic preparations, careful focusing reveals that approximately 10% of all gonocytes touch the basement membrane with at least a small part of their surface.

TABLE 2
Counts and numbers of cells in sex cords of postnatal rats

Counts and numbers of cells in sex cords of postnatal rats

Age	Gonocytes			Spermatogonia, Type A			Supporting cells			Mitotic index
	Counts/X-section		No. per testis $\times 10^4$	Counts/X-section		No. per testis $\times 10^4$	Counts/X-section		No. per testis $\times 10^4$	
	Crude	Adjusted		Crude	Adjusted		Crude	Adjusted		
days ¹										
1a	1.95	0.77	7.9	—	—	—	17.5	8.8	90	1.25
1b	1.87	0.73	7.5	—	—	—	18.6	9.2	95	0.85
1c	1.46	0.56	7.3	—	—	—	18.0	9.2	119	0.30
3d	1.23	0.47	6.3	—	—	—	22.1	11.4	153	1.85
3e	0.90	0.20	5.4	—	—	—	25.5	12.8	351	2.03
3f	0.80	0.30	4.4	—	—	—	23.8	11.9	176	1.91
4e	0.68	0.25	6.0	—	—	—	26.5	13.2	313	1.94
4f	0.30	0.12	2.6	—	—	—	25.6	13.2	296	1.92
4g	0.80	0.25	6.4	0.13	0.05	1.2	24.9	12.4	321	2.50
5e	0.35	0.12	4.3	0.15	0.06	2.2	27.8	13.2	462	2.03
5f	0.43	0.14	4.1	0.08	0.04	1.1	29.1	13.7	407	2.26
5h	0.53	0.17	5.0	—	—	—	26.5	13.1	390	1.27
6e	0.30	0.11	3.8	0.12	0.05	1.8	32.7	16.3	555	2.01
6f	0.32	0.11	5.3	0.25	0.11	4.9	32.1	15.3	710	1.64
6g	0.23	0.09	3.5	0.22	0.10	4.0	30.5	15.3	630	1.35
8a	0.12	0.04	1.6	0.38	0.17	6.1	33.9	17.0	620	1.48
8d	0.13	0.05	2.4	0.67	0.30	14.1	32.7	16.4	780	1.85
8i	0.08	0.03	1.4	0.83	0.37	16.4	33.8	16.9	755	2.03
10d	0.03	0.01	0.7	1.00	0.44	28.0	39.8	20.0	1270	1.63
10g	—	—	—	1.63	0.70	60.7	41.7	20.4	1770	1.59
10h	0.02	0.006	0.4	0.95	0.42	28.5	39.1	19.5	1340	2.02

¹ The exact age limits are explained under Materials and Methods. Letters identify litters.

TABLE 3
Average numbers of cells per testis in postnatal rats

Age	Gonocytes	Spermatogonia A-type	Spermatogonia Intermediate-B type	Supporting cells
days				
1	76,000	—	—	1,010,000
3	54,000	—	—	2,270,000
4	50,000	4,000*	—	3,100,000
5	44,000	11,000	—	4,200,000
6	42,000	36,000	—	6,320,000
8	18,000	122,000	—	7,180,000
10	4,000	353,000	37,000*	14,600,000

* 1 case only.

the growth parameters of testis and sex cords and the cell counts used in calculating the numbers of cells per testis at various stages. The third table is a brief summary of the most pertinent data.

Incidentally, table 1 demonstrates that the weight of the testis rises rapidly. It doubles during the first three days of life and triples during the first 5. This increase is due to a growth of the sex cords more than of interstitial tissue. The sex cords constitute approximately one third of the

testis on day 1, approximately two-thirds on day 10. Their growth is almost entirely in length for the first six postnatal days. Only on day 8 and 10 is there evidence of an appreciable, although relatively small, increase in diameter of the sex cords. The growth in length, however, is directly proportional to the increase in weight of the testis.

The data in table 2 indicate that until day 5 the growth of the sex cords is due entirely to multiplication of supporting cells.

figures with irregular, sometimes clumped chromosomal configurations were observed at day 5 and 6. Their size and the appearance of their cytoplasm suggested that they were gonocytes. They were considered degenerating.

In electron micrographs pyknotic cells were easily identified although they did not occur frequently. In some cases, the pictures closely paralleled those obtained by microscopy (compare figs. 6, 15). The necrotic cells in figures 10 and 11 were examples of what was considered a fairly early stage of degeneration. The main features in such cases are a "patchy" granulation of the nucleus, swelling of the nuclear membrane, dilated endoplasmic reticulum and an accumulation of ribosomes in large, irregular masses. Some, but not all, of the mitochondria appear swollen. Cells of this type, like normal gonocytes (for instance in figs. 12, 14) are bordered by several supporting cells (figs. 10, 11, 12). The degenerating cell in figure 12 shows a somewhat more condensed nucleus. The cytoplasmic organelles are more

closely packed but otherwise are similar to those in figures 10 and 11. The cell in figure 13 demonstrates an added degree of density of nuclear and cytoplasmic material. Large segments of the nuclear membrane are intact, however, and its pores are clearly visible. Mitochondria, flattened cisternae and large aggregations of ribosomes can be discerned. The mitochondria are of a size range found in normal gonocytes. The cell is completely enclosed by one supporting cell, at least in the section depicted.

Figures 14 and 15 illustrate examples of frankly necrotic remains of cells, possibly gonocytes, engulfed by supporting cells. Degeneration has proceeded too far for the identification of cell type or of specific organelles but some structures resemble, for instance, nucleoli (fig. 15) or mitochondria (fig. 14, Nr).

Quantitation

The quantitative results are presented in tables 1-3. The first two of these contain

TABLE 1
Weight of testis and growth parameters of the sex cords of postnatal rats

Age	Weight	Sex cords			
		Vol. of testis	Abs. vol.	Diameter	Length
<i>days</i> ¹	<i>mg</i>	<i>%</i>	<i>10³ ml</i>	<i>μ</i>	<i>cm</i>
1a	2.5	41	1.0	45.7	61.8
1b	2.8	36	0.9	45.9	61.5
1c	3.7	32	1.2	42.5	79.2
3d	3.2	46	1.5	46.7	83.1
3e	6.0	49	2.9	47.8	165
3f	3.8	44	1.7	49.0	89.0
4e	7.0	46	3.2	53.7	142
4f	5.8	47	2.7	50.8	135
4g	5.8	51	2.9	49.4	155
5e	7.0	48	3.4	47.0	195
5f	7.0	52	3.6	50.7	178
5h	6.3	51	3.2	48.1	177
6e	11.0	50	4.0	49.8	204
6f	9.0	53	4.8	47.8	265
6g	8.5	51	4.6	48.5	247
8a	8.2	55	4.5	51.2	219
8d	11.5	53	6.1	52.0	286
8i	10.7	53	5.7	51.1	268
10d	15.7	64	10.0	58.0	382
10g	19.2	62	10.9	54.2	518
10h	16.7	63	10.5	56.4	411

¹ The exact age limits are explained under Materials and Methods. Letters identify litters.

TABLE 2
Counts and numbers of cells in sex cords of postnatal rats

Age	Gonocytes			Spermatogonia, Type A			Supporting cells			Mitotic index
	Counts/X-section		No. per testis $\times 10^4$	Counts/X-section		No. per testis $\times 10^4$	Counts/X-section		No. per testis $\times 10^4$	
	Crude	Adjusted		Crude	Adjusted		Crude	Adjusted		
<i>days</i> ¹										
1a	1.95	0.77	7.9	—	—	—	17.5	8.8	90	1.25
1b	1.87	0.73	7.5	—	—	—	18.6	9.2	85	0.85
1c	1.46	0.56	7.3	—	—	—	18.0	9.2	119	0.30
3d	1.23	0.47	6.3	—	—	—	22.1	11.4	153	1.85
3e	0.90	0.20	5.4	—	—	—	25.5	12.8	351	2.03
3f	0.80	0.30	4.4	—	—	—	23.8	11.9	176	1.91
4e	0.68	0.25	6.0	—	—	—	26.5	13.2	313	1.94
4f	0.30	0.12	2.6	—	—	—	25.6	13.2	296	1.92
4g	0.80	0.25	6.4	0.13	0.05	1.2	24.9	12.4	321	2.50
5e	0.35	0.12	4.3	0.15	0.06	2.2	27.8	13.2	462	2.03
5f	0.43	0.14	4.1	0.08	0.04	1.1	29.1	13.7	407	2.26
5h	0.53	0.17	5.0	—	—	—	26.5	13.1	390	1.27
6e	0.30	0.11	3.8	0.12	0.05	1.8	32.7	16.3	555	2.01
6f	0.32	0.11	5.3	0.25	0.11	4.9	32.1	15.3	710	1.64
6g	0.23	0.09	3.5	0.22	0.10	4.0	30.5	15.3	630	1.35
8a	0.12	0.04	1.6	0.38	0.17	6.1	33.9	17.0	620	1.48
8d	0.13	0.05	2.4	0.67	0.30	14.1	32.7	16.4	780	1.85
8i	0.08	0.03	1.4	0.83	0.37	16.4	33.8	16.9	755	2.03
10d	0.03	0.01	0.7	1.00	0.44	28.0	39.8	20.0	1270	1.63
10g	—	—	—	1.63	0.70	60.7	41.7	20.4	1770	1.59
10h	0.02	0.006	0.4	0.95	0.42	28.5	39.1	19.5	1340	2.02

¹ The exact age limits are explained under Materials and Methods. Letters identify litters.

TABLE 3
Average numbers of cells per testis in postnatal rats

Age	Gonocytes	Spermatogonia A-type	Spermatogonia Intermediate-B type	Supporting cells
<i>days</i>				
1	76,000	—	—	1,010,000
3	54,000	—	—	2,270,000
4	50,000	4,000 *	—	3,100,000
5	44,000	11,000	—	4,200,000
6	42,000	36,000	—	6,320,000
8	18,000	122,000	—	7,180,000
10	4,000	353,000	37,000 *	14,600,000

* 1 case only.

the growth parameters of testis and sex cords and the cell counts used in calculating the numbers of cells per testis at various stages. The third table is a brief summary of the most pertinent data.

Incidentally, table 1 demonstrates that the weight of the testis rises rapidly. It doubles during the first three days of life and triples during the first 5. This increase is due to a growth of the sex cords more than of interstitial tissue. The sex cords constitute approximately one third of the

testis on day 1, approximately two-thirds on day 10. Their growth is almost entirely in length for the first six postnatal days. Only on day 8 and 10 is there evidence of an appreciable, although relatively small, increase in diameter of the sex cords. The growth in length, however, is directly proportional to the increase in weight of the testis.

The data in table 2 indicate that until day 5 the growth of the sex cords is due entirely to multiplication of supporting cells.

Only on day 6 does the total germ cell population become larger than it was at birth. Spermatogonia were present in one out of three animals on day 4, and in two out of three on day 5. The first divisions of gonocytes obviously did not occur any earlier than 72 hours and not later than 108 hours after birth in this strain of rats. It is important to observe that gonocytes decline in numbers before the formation of spermatogonia begins. This will be discussed later.

DISCUSSION

Until Roosen-Runge ('62) and Beaumont and Mandl ('63) determined the numbers of gonocytes present at various stages, the evidence for degeneration was derived entirely from microscopic observations of gonocyte morphology. All major histological accounts were, however, in agreement that at least some germ cells die before they transform into spermatogonia. On the other hand, three very different sets of phenomena were considered as evidence for degeneration: (1) condensation and clumping of chromatin combined with shrinkage and fragmentation of the nucleus, i.e. pyknosis (for example, Hoven, Hargitt, Allen), (2) swelling of cells and nuclei accompanied by loss of stainability of nuclear contents and cytoplasm and by breakage of membranes, i.e. hypertrophy and lysis (for example, Firket, Allen, Clermont and Perey), and (3) abnormal mitoses (Allen, Sapsford). In addition, Huckins ('65) described adjacent gonocytes fusing "into bizarre and multinucleate forms before disintegrating." A few authors have mentioned the occurrence of several types of degeneration, but most were concerned with only one or the other.

In the following paragraphs, the evidence for degenerative phenomena will be examined in detail. The evidence of pyknosis is least arguable. Pyknotic cells are easily identified and generally believed to be dying or dead. In our studies, various degrees of condensation and fragmentation of the nucleus accompanied by distinct cytoplasmic changes were observed microscopically and electron microscopically. These could be arranged into a sequence ending with small, dense cell

rests lying within supporting cells (figs. 6, 7, 15). The microscopic impression that such necrotic cells were gonocytes and not supporting cells was confirmed in many cases by their ultrastructural features. However, the most advanced stages of necrosis could not be identified as to cell type. The occasional death of a supporting cell, therefore, cannot be excluded although there is quantitative evidence that this does not occur frequently. Pyknosis is relatively rare when compared with other cell types which might be considered degenerative (Franchi and Mandl, '64). Our data, however, permit very crude estimates of maximum numbers which show that pyknosis alone might possibly account for the number of dying gonocytes indicated by the counts of normal cells.

Our investigations leave a gap with regard to very early and subtle changes which may lead to pyknotic (or any other) cell death. Even those cells which were considered the least advanced on the path toward death (fig. 10) showed relatively gross alterations. It is probable that initial signs of morbidity occur and proceed very rapidly. Pyknotic cells become significantly more frequent between day 3 and 4 which suggests that cells may pass from an unrecognized stage of morbidity to a grossly necrotic one within less than 24 hours, but possibly much more rapidly. On the other hand, the highly condensed and fragmented final stages of pyknosis may remain conspicuous for two days or more, as is suggested by the amount of pyknotic cells and cell rests present on day 8.

The interpretation of "swollen," pale and more or less poorly defined gonocytes is much more problematical. Some authors have accepted such cells without discussion as plainly degenerating (for example, Firket, '20). Beaumont and Mandl ('63) have carefully, but inconclusively, considered the possibility that such cells may be the result of fixation artefacts. They suggested that "gonocytes may be particularly sensitive to osmotic and other changes during the last two to three days of fetal life and the first few days after birth. They seem to be able to withstand fixation in buffered osmic acid, but apparently incur considerable damage in fixatives (such as Bouin's aqueous fluid) used for routine

histological purposes." In our histological material, fixed in acid, mercuric chloride containing solution, the majority of gonocytes particularly after day 3 appeared rather "empty," pale staining and somewhat fuzzy in outline (fig. 3). Initially, we did feel tempted to interpret some of these cells as "abnormal" but eventually we became convinced that they represented a normal range of developing cells.

Franchi and Mandl ('64) have described "lysis" in cells observed with the electron microscope. They described breakage of nuclear and cell membranes and dispersal of the cytoplasm. In our material, membrane breakage occurred in an irregular manner here and there. The phenomenon was not different from that observed often with fixation short of the very best. There was no evidence that it indicated degenerative changes. On the other hand, Franchi and Mandl have stated that "the cell membranes in neighboring somatic cells also fragment in the vicinity of the gonocyte," an observation which throws some doubt on the degenerative nature of the defects.

Sapsford ('62) regarded enlargement and decrease in stainability as signs of normal development of germ cells previous to the resumption of mitotic activity. He reinforced this conclusion by a quantitative investigation ('64) in which the size of nuclei was measured and statistically evaluated. This appeared to demonstrate that the nuclei of all gonocytes enlarged before spermatogenesis begins. Sapsford ('65) showed that this normal enlargement is correlated with an increase in synthesis of both DNA and nuclear protein. He also found some excessively hypertrophic nuclei during the 5- to 8-day period which he regarded as due to an abnormal accumulation of DNA and protein synthesized by nuclei which failed to complete mitosis. It appears that the "normal" increase in nuclear size does not exclude the possibility that in some cells an enlargement of the nucleus is concomitant with or due to degenerative processes. Beaumont and Mandl ('63) determined that gonocytes progressively increase in size at least during the period from one to four and one-half days after birth, but considering the period from four to six and one-half days, they stated: "Although qualita-

tive observations suggest that degenerative gonocytes undergo both nuclear and cytoplasmic swelling, measurements of normal and degenerating nuclei failed to show any consistent difference between the two." Our own measurements, while far less extensive than Sapsford's, indicate some increase in size of gonocytic nuclei from day 1 to day 4, which is of doubtful statistical significance. Nuclear measurements are subject to considerable methodological error, and differences, particularly when expressed as area or volume of the nucleus, may appear larger than is warranted by the degree of accuracy inherent in measurements with an eyepiece micrometer or on photographic enlargements. There remains, therefore, some doubt about the amount of nuclear enlargement in normal gonocytes, but the data available suffice to demonstrate that the so-called "hypertrophy" of gonocytes is not by itself a useful criterion for cellular degeneration.

The degeneration during mitosis which has been particularly well described by Allen ('49) was seen so rarely in our preparations that its relative importance could not be evaluated. It should be kept in mind, however, that all gonocytes which degenerate during the first postnatal week may well be in a specific pre-mitotic or early mitotic state.

Several features have been reported by which viable and non-viable gonocytes may be distinguished in pre-necrotic stages. The suggestion has been made repeatedly (Beaumont and Mandl, Huckins, etc.) that only those gonocytes remain viable which gain access to the periphery of the sex cords, and conversely that hypertrophic lysing cells are found only in the center of the cords. Early spermatogonia are always situated at the basement membrane where they originated by mitoses of gonocytes, although mitoses have been repeatedly observed in "unattached" gonocytes and frankly degenerating gonocytes do occasionally occur in peripheral positions (fig. 5). Microscopic and electron microscopic observations reveal that many gonocytes make contact with the periphery only by means of long narrow cytoplasmic processes which are easily missed unless serial sections are available. The correlation of viability and position within the sex cord

Only on day 6 does the total germ cell population become larger than it was at birth. Spermatogonia were present in one out of three animals on day 4, and in two out of three on day 5. The first divisions of gonocytes obviously did not occur any earlier than 72 hours and not later than 108 hours after birth in this strain of rats. It is important to observe that gonocytes decline in numbers before the formation of spermatogonia begins. This will be discussed later.

DISCUSSION

Until Roosen-Runge ('62) and Beaumont and Mandl ('63) determined the numbers of gonocytes present at various stages, the evidence for degeneration was derived entirely from microscopic observations of gonocyte morphology. All major histological accounts were, however, in agreement that at least some germ cells die before they transform into spermatogonia. On the other hand, three very different sets of phenomena were considered as evidence for degeneration: (1) condensation and clumping of chromatin combined with shrinkage and fragmentation of the nucleus, i.e. pyknosis (for example, Hoven, Hargitt, Allen), (2) swelling of cells and nuclei accompanied by loss of stainability of nuclear contents and cytoplasm and by breakage of membranes, i.e. hypertrophy and lysis (for example, Firket, Allen, Clermont and Perey), and (3) abnormal mitoses (Allen, Sapsford). In addition, Huckins ('65) described adjacent gonocytes fusing "into bizarre and multinucleate forms before disintegrating." A few authors have mentioned the occurrence of several types of degeneration, but most were concerned with only one or the other.

In the following paragraphs, the evidence for degenerative phenomena will be examined in detail. The evidence of pyknosis is least arguable. Pyknotic cells are easily identified and generally believed to be dying or dead. In our studies, various degrees of condensation and fragmentation of the nucleus accompanied by distinct cytoplasmic changes were observed microscopically and electron microscopically. These could be arranged into a sequence ending with small, dense cell

rests lying within supporting cells (figs. 6, 7, 15). The microscopic impression that such necrotic cells were gonocytes and not supporting cells was confirmed in many cases by their ultrastructural features. However, the most advanced stages of necrosis could not be identified as to cell type. The occasional death of a supporting cell, therefore, cannot be excluded although there is quantitative evidence that this does not occur frequently. Pyknosis is relatively rare when compared with other cell types which might be considered degenerative (Franchi and Mandl, '64). Our data, however, permit very crude estimates of maximum numbers which show that pyknosis alone might possibly account for the number of dying gonocytes indicated by the counts of normal cells.

Our investigations leave a gap with regard to very early and subtle changes which may lead to pyknotic (or any other) cell death. Even those cells which were considered the least advanced on the path toward death (fig. 10) showed relatively gross alterations. It is probable that initial signs of morbidity occur and proceed very rapidly. Pyknotic cells become significantly more frequent between day 3 and 4 which suggests that cells may pass from an unrecognized stage of morbidity to a grossly necrotic one within less than 24 hours, but possibly much more rapidly. On the other hand, the highly condensed and fragmented final stages of pyknosis may remain conspicuous for two days or more, as is suggested by the amount of pyknotic cells and cell rests present on day 8.

The interpretation of "swollen," pale and more or less poorly defined gonocytes is much more problematical. Some authors have accepted such cells without discussion as plainly degenerating (for example, Firket, '20). Beaumont and Mandl ('63) have carefully, but inconclusively, considered the possibility that such cells may be the result of fixation artefacts. They suggested that "gonocytes may be particularly sensitive to osmotic and other changes during the last two to three days of fetal life and the first few days after birth. They seem to be able to withstand fixation in buffered osmic acid, but apparently incur considerable damage in fixatives (such as Boulin's aqueous fluid) used for routine

TABLE 5

Comparison of diameters and total length of sex cords as determined by different authors

	Sex cords					
	Diameter in μ			Length in cm		
	Day 1	4	8	1	4	8
Clermont and Percy ('57)	51	63	67	—	—	—
Beaumont and Mandl ('63)	approx. 80	—	—	—	150	250
Huckins ('65)	29.5	34.3	36.5	37.4	—	62.5
Roosen-Runge and Leik	44.7	51.3	48.5	7.5	144	235

TABLE 6

Comparison of dates of resumption of gonocyte mitoses after birth, as observed by different authors

	Strain of rats	Days after birth
Rauh	Albino Rat	5-6
Sapsford	Albino Rat	6-7
Clermont and Percy	Sherman	3-4
Beaumont and Mandl	Birmingham Colony	4
Huckins	Wistar	6.5-7
Roosen-Runge and Leik	Sprague-Dawley	3-4

is taking place. On this question the results in the literature differ widely as shown by the brief compilation in table 6. The most probable explanation for the differences appears to lie in the different strains of animals used. It should be pointed out, however, that spermatogonia are a more reliable indicator for the time at which gonocytic mitoses have begun than the mitotic figures themselves. Spermatogonia are not only twice as frequent but also of much longer duration than the cell divisions which produce them. In our specimens, spermatogonia were found generally earlier than gonocytic mitosis. Table 4 shows that during the period between birth and the time when mitoses or spermatogonia were first seen Beaumont and Mandl and Roosen-Runge and Leik found a decrease in gonocytes of 30-40%, Huckins of 75%.

As soon as gonocytes resume their mitotic activity, their stock is rapidly diminished by their conversion into spermatogonia. Huckins found no evidence that gonocytes continued to degenerate once the first mitoses had begun. Beaumont and Mandl, on the contrary, observed gonocytes in "degeneration" for several days after this. In the present investigation also the evidence points clearly to a continuation of the degenerative process until day 7 or

8. From this it may be concluded that the total number of dying gonocytes is considerably higher than the number of cells degenerating before mitosis begins. It is difficult, however, to arrive at a meaningful estimate of the total number mainly because the speed of the process of degeneration is not known. It is probably a safe assumption that more than half of the gonocytes present at birth die within the nine days following.

Cell death in normal development is a regular, if not a well-investigated phenomenon (Saunders, '66). In the life of germ cells, it occurs at several, well-characterized periods beginning possibly in very early embryonic life (Mintz, '60) and ending with certain stages of spermiogenesis (Roosen-Runge, '55b). The events described in the present paper possess the same features which identify "morphogenetic cell death" (Saunders and Fallon, '66) in many other cases: they occur at a definite developmental stage and their morphological features are quite specific. It may also be characteristic that they are phagocytized. It is possible that the events are associated with a particular stage of the mitotic cycle (DNA synthesis?) as has been described for many cell deaths in normal development (Glücksmann, '51).

can, therefore, not be regarded as established. Similarly, the correlation with basophilia which was suggested by Huckins ('64) appears doubtful. Roosen-Runge ('64) was unable to confirm the occurrence of two classes of gonocytes on this basis. If they existed, the electron microscope should demonstrate two types of germ cells, one with little and one with much ribosomal material, but neither Franchi and Mandl ('64) nor the present investigators have been able to establish this.

Can certain changes in the ultrastructure of cellular organelles be regarded as degenerative? Franchi and Mandl ('64), fully aware of the great hazards of interpreting the morphology of fixed material, suggested that "B-bodies," particularly of the large "B₁" variety which have some of the characteristics of lysosomes, "may play an important part in the autolysis of some gonocytes," but subsequently ('66), they found that B-bodies persisted longer in cells which proved viable after irradiation. They observed swollen mitochondria with disarranged internal structure and a swollen endoplasmic reticulum in a few germ cells during the first three days and more frequently after the fourth day post-partum. In the present investigation, "B-bodies" and unusual mitochondria were observed in all gonocytes in varying amounts. The differences in distribution could not be quantitated. They did not appear to be correlated with any other characteristics of the cells.

The uncertainty of identifying cells in early stages of degeneration precludes a direct estimate of the numbers of cells which die. On the other hand, the determination of the numbers of normal cells at different stages promises to circumvent

observational difficulties and should indirectly yield information on the quantity of dying cells. Quantitation has been accomplished in three separate investigations (Roosen-Runge, '62; Beaumont and Mandl, '63; Huckins, '65). Several variations of essentially the same method were employed. Cells were counted in representative sections and the total number per testis calculated by determining the dimensions of the sex cords in which the cells occur. Although different strains of rats were used, the results were strikingly similar (table 4). The agreement is, in fact, better than might be expected when inherent errors of the method are considered. The wet weight of the testis is a relatively imprecise datum, although our determinations are within 10% of those of Beaumont and Mandl. The diameter of the sex cords can be measured quite accurately, but table 5 demonstrates surprising discrepancies between the results of different authors. The differences in the calculated length of sex cords presumably are due in part but not completely to differences in diameter. The inherent inaccuracy of measurements of nuclear diameters has been mentioned before. The thickness of sections which enters into the calculation of numbers of cells per section also cannot be measured with great accuracy. Under these circumstances, it is most important that all results appear to agree on an overall decline in the numbers of gonocytes throughout the first week after birth (table 4).

Any decrease in the number of gonocytes is presumably due to cell death as long as the cells do not divide or differentiate. It is, therefore, of great importance to know when the first postnatal mitosis

TABLE 4

Comparison of approximate numbers of gonocytes per testis as determined by different authors

	Numbers of gonocytes				
	Day 1	4	5	6	8
Beaumont and Mandl ¹	50-60,000	50-60,000	35-45,000	25-30,000	—
Huckins ²	75,000	70,000	58,000	55,000	26,000
Roosen-Runge and Leik	75,000	50,000	44,000	42,000	18,000

¹ Combined rough estimates from three somewhat different methods.

² Numbers originally given per external sex cord were multiplied by 32 for the purpose of this table on the assumption that there are approximately 32 cords per testis.

- 1955b Untersuchungen über die Degeneration samenbildender Zellen in der normalen Spermatogenese der Ratte. *Z. Zellf.*, 41: 221-235.
- 1962 Quantitative analysis of seminiferous tubules in the Sprague-Dawley rat, 1-10 days after birth. *Am. Zool.*, 2: 322 (abstract).
- 1964 The degeneration of pre-spermatogonial germ cells in the rat after birth. *Anat. Rec.*, 148: 328 (abstract).
- Sapsford, C. S. 1962 Changes in the cells of the sex cords and the seminiferous tubules during development of the testis of the rat and mouse. *Austral. J. Zool.*, 10: 178-192.
- 1964 Changes in the size of germ cell nuclei during the development of the testis of the ram and rat. *Austral. J. Zool.*, 12: 127-149.
- 1965 The synthesis of DNA and nuclear protein by gonocytes in the testes of normal and X-irradiated rats. *Austral. J. Biol. Sci.*, 18: 653-664.
- Saunders, J. W. 1966 Death in embryonic systems. *Science*, 154: 604-612.
- Saunders, J. W., and J. F. Fallon 1966 Cell death in morphogenesis. 25th Symp. Soc. develop. biol., 289-314.

Note added in proof: Two recent publications contain some pertinent, largely confirmatory information. Hilscher and Makoski ('68), applying autoradiography with H^3 -thymidine in an unidentified strain of rats, found that "part of the gonocytes degenerate, above all during the first postnatal days," and that spermatogenesis begins on day 3-6 after the gonocytes have gone through a G1-period of 6-9 days. Novi and Saba ('68), in an electron microscopic study of the seminiferous tubules in the postnatal *italico* rat, described no degenerating gonocytes. In their figure 8, however, a "round-shaped lipid inclusion" is seen within a supporting cell on day 7, which could well represent the remains of a germ cell. We cannot confirm their finding that the gonocyte in migratory stages just prior to transforming into a spermatogonium as a rule shows a cytoplasm strongly increased in density. On the other hand, we also have seen supporting cells with "lighter" cytoplasm, which are rare in our material. The work of Black ('68a) has provided additional evidence that cell rests found in the seminiferous tubules in postnatal stages are usually the remains of germ cells. In a strain of guinea pigs in which only the gonocytes are characterized by virus-like particles in the rough endoplasmic reticulum (Black, '68b), necrotic cells in the seminiferous tubules after birth are identifiable by these particles in the majority of cases.

- Hilscher, W., and H. -B. Makoski 1968 Histologische und autoradiographische Untersuchungen zur "Prä-spermatogenese" und "Spermatogenese." *Z. Zellforsch.*, 86: 327-350.
- Novi, Anna M., and Paolo Saba 1968 An electron microscopic study of the development of rat testis in the first 10 postnatal days. *Z. Zellforsch.*, 86: 313-326.
- Black, Virginia H. 1968a Personal communication.
- 1968b Fine structure of the tubule cells in the fetal guinea pig testis. *Anat. Rec.*, 160: 317 (abstract).

Cell deaths of the morphogenetic type are probably "aspects of genetic programming" (Saunders and Fallon). When considered in this way, the wave of gonocytic degeneration which occurs at the critical period just preceding the onset of spermatogenesis, fits into a large pattern of developmental processes.

CONCLUSIONS

Comparison of the data presented in this paper with those in the literature leads to the following conclusions:

(1) The similarity of the results of three different laboratories on the numbers of gonocytes present at various stages of postnatal development, provides strong evidence for the loss of at least half of the cells during the first week after birth, despite the obvious imprecision of the quantitative methods employed.

(2) Pyknotic gonocytes are regularly observed in the sex cords of postnatal rats. This process of cellular necrosis may be identified in some detail by means of the electron microscope. Pyknotic gonocytes are probably phagocytized by supporting cells. The sequence of events in this type of cell death is similar to that described for "morphogenetic cell death" by Saunders and Fallon ('66), and gonocyte degeneration may be regarded as belonging in this class of "normal" phenomena.

(3) It is possible that other types of gonocytic necrosis exist. A few of the cells die in mitosis. Cells which have previously been described as "swollen" or "lysing," however, cannot be identified as degenerating with any degree of certainty. Their microscopic and submicroscopic characteristics are in many cases those of normal pre-mitotic development and may, in other cases, be due to artifacts.

(4) It is not possible at present to distinguish microscopically or electron microscopically between viable and non-viable germ cells at an early stage. The earliest changes are probably nuclear. They are probably not in the lysosomes, the mitochondria or the endoplasmic reticulum. This is in general agreement with the findings of Saunders and Fallon on cells which die in normal morphogenesis.

LITERATURE CITED

- Allen, E. 1949 Studies on degenerating sex cells in immature mammals. I. An analysis of degeneration in primordial and large germ cells in male albino rats aged 1-9 days. *J. Morph.*, 85: 405-421.
- Beaumont, H. M., and A. M. Mandl 1963 A quantitative study of primordial germ cells in the male rat. *J. Embryol. exp. Morph.*, 11: 715-740.
- Bouin, P. 1895 De quelques phenomenes de degenerescence cellulaire dans le testicule jeune des mammiferes. *Bibliogr. anat.*, 3: 176-196.
- Clermont, Y., and B. Perey 1957 Quantitative study of the cell population of the seminiferous tubules in immature rats. *Am. J. Anat.*, 100: 241-267.
- Everett, N. B. 1945 The present status of the germ cell problem in vertebrates. *Biol. Rev.*, 20: 45-55.
- Firket, J. 1920 On the origin of germ cells in higher vertebrates. *Anat. Rec.*, 18: 309-316.
- Franchi, L. L., and A. M. Mandl 1964 The ultrastructure of germ cells in fetal and neonatal male rats. *J. Embryol. exp. Morph.*, 12: 289-308.
- 1966 The ultrastructure of male germ cells in rat X-irradiated at birth. *Proc. Roy. Soc. B*, 165: 136-154.
- Glücksmann, A. 1951 Cell deaths in normal vertebrate ontology. *Biol. Rev.*, 26: 59-86.
- Hargitt, G. T. 1926 The formation of the sex glands and germ cells of mammals. II. The history of the male germ cells in the albino rat. *J. Morph.*, 42: 253-306.
- Hoven, H. 1914 Histogenèse du testicule des mammiferes. *Anat. Anz.*, 47: 90-109.
- Huckins, C. 1963 Changes in gonocytes at the time of initiation of spermatogenesis in the rat. *Anat. Rec.*, 145: 243 (abstract).
- 1965 The initiation of spermatogenesis in the testis of the Wistar albino rat. Ph.D. Thesis, McGill University.
- Leik, J., and E. C. Roosen-Runge 1966 Electron microscopic observations on degenerative phenomena in the gonocytes of male rats three to five days after birth. *Anat. Rec.*, 154: 376 (abstract).
- Luff, J. 1961 Improvements in epoxy resin embedding methods. *J. biophys. biochem. Cytol.*, 9: 409-414.
- Mintz, B. 1960 Embryological phases of mammalian gametogenesis. *J. Cell. and Comp. Physiol.*, 56: suppl. 1: 31-48.
- Popoff, N. 1909 L'ovule male et le tissu interstitiel du testicule chez les animaux et chez l'homme. *Arch. bibl.*, 24: 433-500.
- Rauh, W. 1925 Ursprung der männlichen Keimzellen und die chromatischen Vorgänge bis zur Entwicklung der Spermatozyten. *Z. Anat. Entwickl.*, 76: 561-577.
- 1929 Das Chondrium in den ersten Keimzellen der Ratte. *Z. Anat. Entwickl.*, 89: 271-309.
- Roosen-Runge, E. C. 1955a Quantitative studies on spermatogenesis in the albino rat. III. Volume changes in the cells of the seminiferous tubules. *Anat. Rec.*, 123: 385-398.

- 1955b Untersuchungen über die Degeneration samenbildender Zellen in der normalen Spermatogenese der Ratte. *Z. Zellf.*, 41: 221-235.
- 1962 Quantitative analysis of seminiferous tubules in the Sprague-Dawley rat, 1-10 days after birth. *Am. Zool.*, 2: 322 (abstract).
- 1964 The degeneration of pre-spermatogonial germ cells in the rat after birth. *Anat. Rec.*, 148: 328 (abstract).
- Sapsford, C. S. 1962 Changes in the cells of the sex cords and the seminiferous tubules during development of the testis of the rat and mouse. *Austral. J. Zool.*, 10: 178-192.
- 1964 Changes in the size of germ cell nuclei during the development of the testis of the ram and rat. *Austral. J. Zool.*, 12: 127-149.
- 1965 The synthesis of DNA and nuclear protein by gonocytes in the testes of normal and X-irradiated rats. *Austral. J. Biol. Sci.*, 18: 653-664.
- Saunders, J. W. 1966 Death in embryonic systems. *Science*, 154: 604-612.
- Saunders, J. W., and J. F. Fallon 1966 Cell death in morphogenesis. 25th Symp. Soc. develop. biol., 289-314.

Note added in proof: Two recent publications contain some pertinent, largely confirmatory information. Hilscher and Makoski ('68), applying autoradiography with H^3 -thymidine in an unidentified strain of rats, found that "part of the gonocytes degenerate, above all during the first postnatal days," and that spermatogenesis begins on day 3-6 after the gonocytes have gone through a G1-period of 6-9 days. Novi and Saba ('68), in an electron microscopic study of the seminiferous tubules in the postnatal *italico* rat, described no degenerating gonocytes. In their figure 8, however, a "round-shaped lipid inclusion" is seen within a supporting cell on day 7, which could well represent the remains of a germ cell. We cannot confirm their finding that the gonocyte in migratory stages just prior to transforming into a spermatogonium as a rule shows a cytoplasm strongly increased in density. On the other hand, we also have seen supporting cells with "lighter" cytoplasm, which are rare in our material. The work of Black ('68a) has provided additional evidence that cell rests found in the seminiferous tubules in postnatal stages are usually the remains of germ cells. In a strain of guinea pigs in which only the gonocytes are characterized by virus-like particles in the rough endoplasmic reticulum (Black, '68b), necrotic cells in the seminiferous tubules after birth are identifiable by these particles in the majority of cases.

- Hilscher, W., and H. -B. Makoski 1968 Histologische und autoradiographische Untersuchungen zur "Prä-spermatogenese" und "Spermatogenese." *Z. Zellforsch.*, 86: 327-350.
- Novi, Anna M., and Paolo Saba 1968 An electron microscopic study of the development of rat testis in the first 10 postnatal days. *Z. Zellforsch.*, 86: 313-326.
- Black, Virginia H. 1968a Personal communication.
- 1968b Fine structure of the tubule cells in the fetal guinea pig testis. *Anat. Rec.*, 160: 317 (abstract).

PLATE 1

EXPLANATION OF FIGURES

Photomicrographs of sex cords of postnatal rats. Magnification $\times 1290$.

- 1 Six-micron section, paraffin embedded; Iron-Hematoxylin. 1-day. Two characteristic gonocytes are seen in the center of the sex cord. The periphery is almost entirely taken up by supporting cells.
- 2 One-and-one-half-micron section, epoxy embedded; Richardson's stain. 3-days. Four gonocytes are seen among the supporting cells. The one at right makes extensive contact with the basement membrane. Arrow points to Leydig cell.
- 3 Six-micron section, paraffin embedded; Hemalum-PAS stain. 8-days. Two spermatogonia (arrows) are seen in typical peripheral position. One supporting cell (below) is in mitosis.
- 4 One-micron section, epoxy embedded; Richardson's stain. 1-day. Arrow points to a degenerating gonocyte lying between two normal ones. The nucleus is greatly altered and poorly outlined, but the nucleolus appears unchanged. Cytoplasmic granules appear somewhat clumped in the vicinity of the nucleus.
- 5 One-micron section, epoxy embedded; Richardson's stain. 1-day. A large degenerating gonocyte is seen in peripheral location, a rare phenomenon. The nucleus is condensed. The cytoplasm shows vacuoles and large and small granular aggregations. Compare with electron micrograph, figure 10.
- 6 One-and-one-half-micron section, epoxy embedded; Richardson's stain. 4-day. Arrows point to two pyknotic cell rests. The left one is apparently the same type of structure which is shown in the electron micrograph in figure 15.
- 7 Six-micron section, paraffin embedded; Hemalum-PAS stain. 5-days. Arrows point to two small pyknotic cell rests which are surrounded by supporting cell cytoplasm. The spherical bodies are only partly basophilic.

CONOCYTE DEGENERATION IN THE POSTNATAL MALE RAT
Edward C. Roosen-Runge and Jean Leik

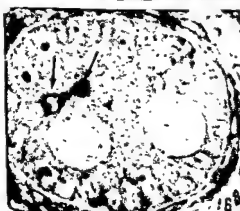
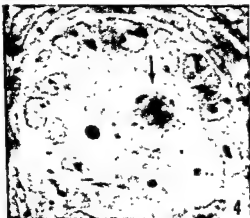
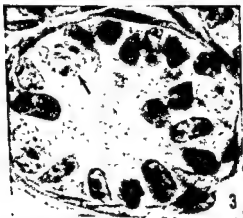
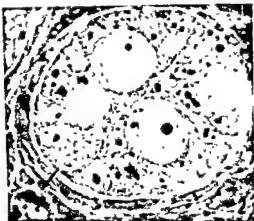
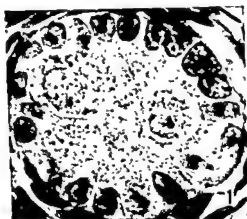


PLATE 1

EXPLANATION OF FIGURES

Photomicrographs of sex cords of postnatal rats. Magnification $\times 1290$.

- 1 Six-micron section, paraffin embedded; Iron-Hematoxylin. 1-day. Two characteristic gonocytes are seen in the center of the sex cord. The periphery is almost entirely taken up by supporting cells.
- 2 One-and-one-half-micron section, epoxy embedded; Richardson's stain. 3-days. Four gonocytes are seen among the supporting cells. The one at right makes extensive contact with the basement membrane. Arrow points to Leydig cell.
- 3 Six-micron section, paraffin embedded; Hemalum-PAS stain. 8-days. Two spermatogonia (arrows) are seen in typical peripheral position. One supporting cell (below) is in mitosis.
- 4 One-micron section, epoxy embedded; Richardson's stain. 1-day. Arrow points to a degenerating gonocyte lying between two normal ones. The nucleus is greatly altered and poorly outlined, but the nucleolus appears unchanged. Cytoplasmic granules appear somewhat clumped in the vicinity of the nucleus.
- 5 One-micron section, epoxy embedded; Richardson's stain. 1-day. A large degenerating gonocyte is seen in peripheral location, a rare phenomenon. The nucleus is condensed. The cytoplasm shows vacuoles and large and small granular aggregations. Compare with electron micrograph, figure 10.
- 6 One-and-one-half-micron section, epoxy embedded; Richardson's stain. 4-day. Arrows point to two pyknotic cell rests. The left one is apparently the same type of structure which is shown in the electron micrograph in figure 15.
- 7 Six-micron section, paraffin embedded; Hemalum-PAS stain. 5-days. Arrows point to two small pyknotic cell rests which are surrounded by supporting cell cytoplasm. The spherical bodies are only partly basophilic.

GONOCYTE DEGENERATION IN THE POSTNATAL MALE RAT
Edward C. Roosen-Runge and Jean Leik

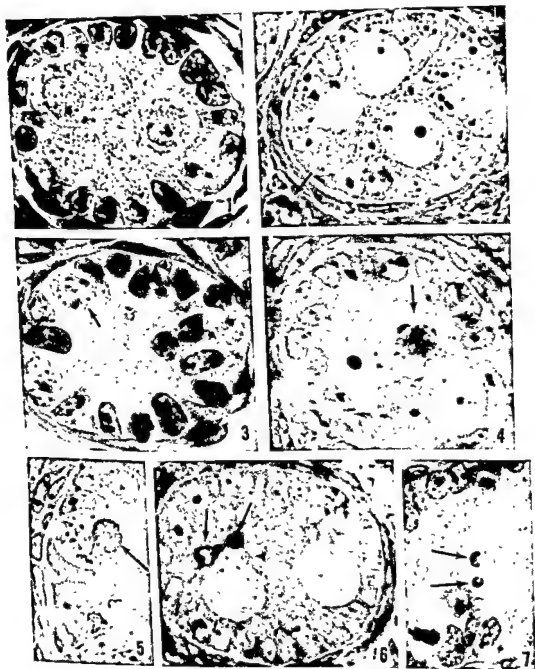


PLATE 2

EXPLANATION OF FIGURES

- 8 Normal gonocyte (G) and supporting cell (S) from testis of 1-day-old rat. Note "A" and "B" bodies. Uranyl acetate and Millonig's lead. 8850 \times .
- 9 Normal gonocyte (G) from testis of 5-day-old rat illustrating pseudopodial connection with the basement lamella (arrows). Uranyl acetate and Reynold's lead. 5650 \times .

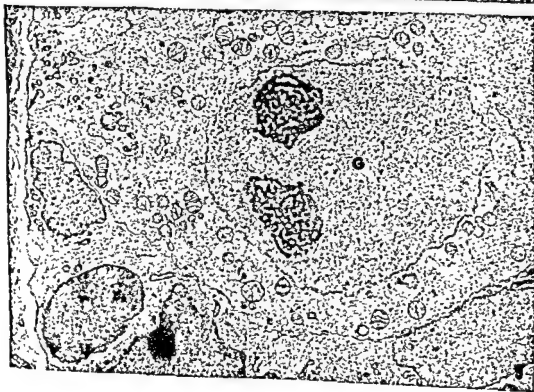


PLATE 2

EXPLANATION OF FIGURES

- 8 Normal gonocyte (G) and supporting cell (S) from testis of 1-day-old rat. Note "A" and "B" bodies. Uranyl acetate and Millonig's lead. 8850 \times .
- 9 Normal gonocyte (G) from testis of 5-day-old rat illustrating pseudopodial connection with the basement lamella (arrows). Uranyl acetate and Reynold's lead. 5650 \times .

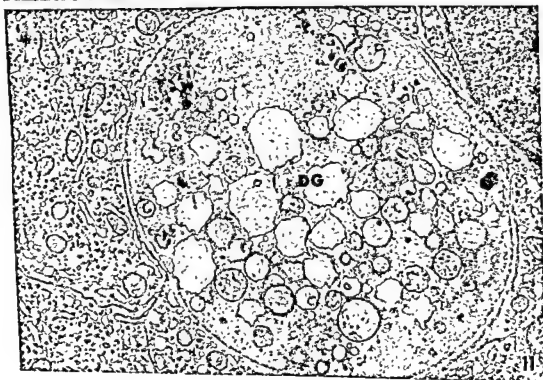


PLATE 3

EXPLANATION OF FIGURES

- 10-11 Degenerating gonocytes (DG) from testis of 1-day-old rat. Uranyl acetate and Reynold's lead. 13,400 \times .

GONOCYTE DEGENERATION IN THE POSTNATAL MALE RAT

Edward C. Roosen-Runge and Jean Leik

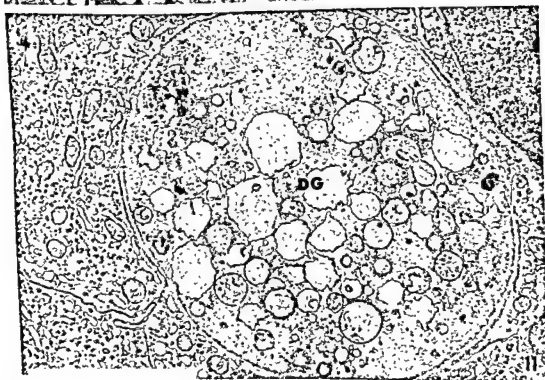


PLATE 4

EXPLANATION OF FIGURES

- 12 Degenerating (DG) and normal gonocyte (G) from testis of 1-day-old rat. Note particularly differences in nuclei. Uranyl acetate and Reynold's lead. 7500 \times .
- 13 Degenerating gonocyte (DG) from testis of 4-day-old rat. Arrows indicate nuclear pores. Uranyl acetate and Millonig's lead. 9900 \times .

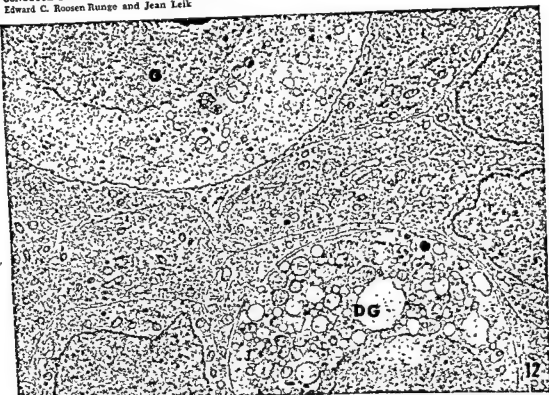


PLATE 4

EXPLANATION OF FIGURES

- 12 Degenerating (DG) and normal gonocyte (G) from testis of 1-day-old rat. Note particularly differences in nuclei. Uranyl acetate and Reynold's lead, 7500 \times .
- 13 Degenerating gonocyte (DG) from testis of 4-day-old rat. Arrows indicate nuclear pores. Uranyl acetate and Millonig's lead, 9900 \times .

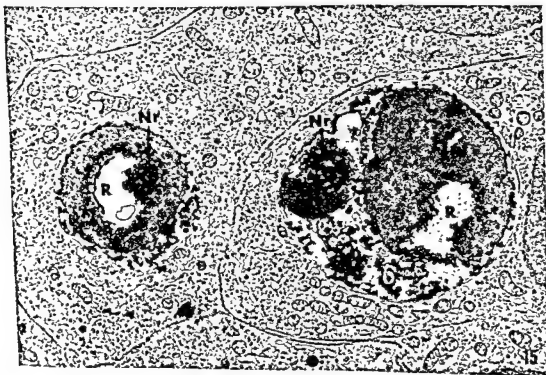


PLATE 5

EXPLANATION OF FIGURES

- 14 Normal gonocyte (G) and cell rest or debris (R) surrounded by supporting cell. Arrows indicate possible mitochondrial remains (Mr). Uranyl acetate. 7050 X.
- 15 Cell rests or debris (R) in testis of 4-day-old rat. Each rest is completely surrounded by one supporting cell (in this section). Arrows indicate possible nucleolar remains (Nr). Uranyl acetate and Mil-lonig's lead. 11,300 X.

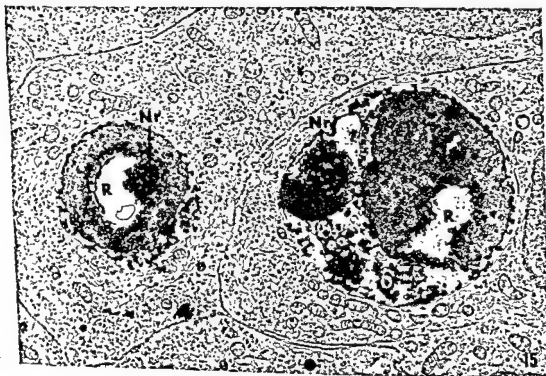
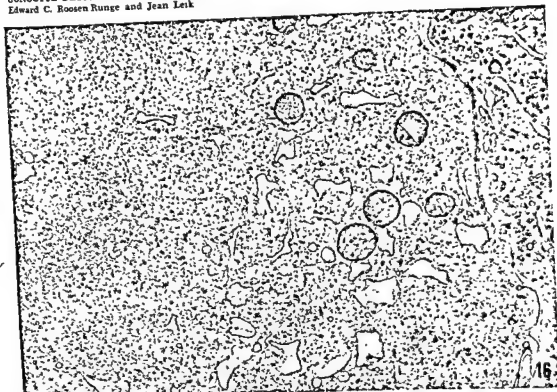


PLATE 6

EXPLANATION OF FIGURES

- 16 Portion of dividing gonocyte from testis of 7-day-old rat. Note swollen endoplasmic reticulum. Uranyl acetate and Reynold's lead. 18,500 X.
- 17 Spermatogonium (SG) in testis of 5-day-old rat. Note difference in nucleolar configuration from gonocyte (G), figure 14. Uranyl acetate and Reynold's lead. 7200 X.

CONOCYTE DEGENERATION IN THE POSTNATAL MALE RAT
Edward C. Roosen Runge and Jean Leik

The Vascularization of the Hypothalamic-Hypophyseal Region of the Eastern Brook Trout, *Salvelinus fontinalis*

JOANNA JENSEN HILL¹ AND NANCY E. HENDERSON

Department of Biology, University of Calgary, Calgary, Alberta, Canada

ABSTRACT The hypophysis of the brook trout is irrigated by blood vessels which originate from the internal carotid arteries. These are: (1) branches of the ventral hypothalamic arteries that give rise to an extensive capillary plexus in the neurohypophysis from which vessels extend into all regions of the adenohypophysis; (2) branches of the caudal hypothalamic artery that irrigate the saccus vasculosus and continue anteriorly to supply the ventral areas of the meta-adenohypophysis; (3) a caudal hypophyseal artery which vascularizes a portion of the meta-adenohypophysis however, this vessel is not always present; (4) a pair of small arteries which supply the peripheral regions of the gland directly from the carotids.

Most of the neurosecretory fibers of the preoptic-hypophyseal tract terminate close to capillaries in the neurohypophysis. A few axons extend into meso-adenohypophyseal tissue. It is suggested that the secretory activities of the pro-, meso- and meta-adenohypophyses are governed by hypothalamic factors that are chiefly transmitted to the gland cells via the vascular system (indirect control). However, the activity of the meso-adenohypophysis may also be regulated by factors which are transmitted directly to the cells from the endings of neurosecretory fibers which have traversed the neurohypophysis (direct control). The distribution and abundance of neurosecretion in the ventral hypophysis suggest the possibility of storage of hypothalamic products within this region.

It is generally assumed that the secretory activity of the teleost hypophysis is controlled by releasing factors that originate in hypothalamic centers however, the regulating mechanism is not understood. Some workers (e.g., Dodd and Kerr, '63) argue that neurosecretory axons terminate close to the glandular cells and that adenohypophyseal activity is under direct neural control (neuro-glandular linkage). Others (e.g., Green, '51) maintain that hypothalamic factors are transmitted to the gland cells via the vascular system and hence adenohypophyseal secretion is under indirect neural control (neuro-vascular-glandular linkage).

One reason for this controversy is a lack of detailed information on the micro-anatomy of the hypothalamic-hypophyseal area in teleosts. While there are a number of excellent descriptions of the cytology of the hypophysis and of the hypothalamic neurosecretory centers and tracts, comparatively little attention has been given to the vascularization of the hypophysis. With the exception of Barrington's ('60) work on *Phoxinus phoxinus* the published

reports are lacking in clarity and detail and they have frequently been accompanied by inadequate illustrations. Both Barrington ('60) and Dodd and Kerr ('63) have stressed the need for further anatomical studies of the teleost gland, particularly of a comparative nature.

In this paper, attention is centered on the vascularization of the hypothalamic-hypophyseal area of the brook trout. Comments on the hypothalamic centers are to be considered preliminary since work is continuing on this aspect.

METHODS

Adult brook trout of both sexes were collected from several rivers in southern Alberta. Each fish was decapitated just behind the opercula and the left side of the skull lateral to the neurocranium was removed. The dorsal portions of the skull and the corpora bigemina (optic lobes) were also cut away to expose the cavities of the latter and the head was immersed

¹ Submitted in partial fulfillment of the requirements for the degree of Master of Science at the University of Calgary.

in fixative for 15 minutes. To dissect the brain from the skull, the myodome was cleared of eye muscles and cranial tissue was chipped away from the sides of the brain. This exposed the hypophysis lying in the sella turcica of the parasphenoid bone which protrudes into the myodome. The olfactory tracts and cranial nerves were cut. There is a small aperture in the posterior aspect of the capsule housing the hypophysis and a probe was placed against this opening and used to gently push the hypophysis out of the capsule. It was then possible to lift the brain out of the cranium without damaging the short infundibular stalk.

Complete serial sections were made of the brains from 14 fish. Nine of the brains were fixed in mercuric formol, cut either longitudinally or frontally at 6 μ , and stained according to Bargmann's modification of the chrome-alum-haematoxylin and phyloxine method of Gomori (CAHP) or with Gomori's aldehyde-fuchsin (AF) or Heidenhain's azan. In addition to demonstrating neurosecretory material, sections stained by these methods were found to be particularly helpful when tracing details of the hypophyseal vascularization. Two brains were fixed in formol saline and

stained with Heidenhain's haematoxylin. To demonstrate nerve tracts, three were preserved in Bodian's formol-acetic acid-alcohol, cut at 25 or 50 μ and stained according to Bodian's protargol S method (as outlined by the suppliers of protargol, Winthrop Laboratories, New York).

A Leitz Prado micro-projector, equipped with a microscope slide attachment, was used to map the major blood vessels and hypothalamic centers. Drawings were made by combining tracings of the images of a number of serial sections projected consecutively on a screen. The detailed illustrations are reconstructions made by combining camera lucida drawings of consecutive sections viewed under phase contrast.

RESULTS

1. Vascularization

a. *Cephalic vascularization.*¹ The anterior arteries of the brook trout are illustrated in figure 1.

The dorso-lateral aortae enter the cranium through the hypophyseal foramina after which they are referred to as the in-

¹ Wherever possible, the nomenclature used is taken from the *Traité de Zoologie*, tome XIII (Grasse, '58), and from *Studies on the Structure and Development of Vertebrates* (Goodrich, '58).

Abbreviations

a, arteriole
ah, adenohypophysis
bas, basilar artery
bld sp, blood space
bc, "border cell" region
cap, connective tissue capsule
cap pl, capillary plexus
c hyp, caudal hypophyseal artery
c hyth, caudal hypothalamic artery
c mes, central mesencephalic artery
dla, dorso-lateral aorta
ebr, efferent branchial arteries
ehy, efferent hyoidian artery
eps, efferent pseudobranchial artery
hyp, hypophysis
hyth, hypothalamus
h com, horizontal commissure
hf, position of hypophyseal foramen
ib-rvh, inferior branch of right ventral hypothalamic artery
ic, internal carotid artery
ir, infundibular recess
l, loops of inferior branch of ventral hypothalamic artery
li, artery to lobus inferior
lic, left internal carotid artery

lob in, lobus inferior
m, meninx
med obl, medulla oblongata
meso-ah, meso-adenohypophysis
meta-ah, meta-adenohypophysis
mda, median dorsal aorta
nh, neurohypophysis
nlt, nucleus lateralis tuberis
npo, nucleus preopticus
ns, neurosecretory granules
on, orbito-nasal artery
op, optic nerve and tract
oph, ophthalmic artery
or, orbital artery
p cer, posterior cerebral artery
p-hyp, preoptic-hypophyseal tract
pro-ah, pro-adenohypophysis
ric, right internal carotid artery
rvh, right ventral hypothalamic artery
s, stalk
sac v, saccus vasculosus
sb-rvh, superior branch of right ventral hypothalamic artery
sl, blood sinus
v, veins or venules
III v, third ventricle

in fixative for 15 minutes. To dissect the brain from the skull, the myodome was cleared of eye muscles and cranial tissue was chipped away from the sides of the brain. This exposed the hypophysis lying in the sella turcica of the parasphenoid bone which protrudes into the myodome. The olfactory tracts and cranial nerves were cut. There is a small aperture in the posterior aspect of the capsule housing the hypophysis and a probe was placed against this opening and used to gently push the hypophysis out of the capsule. It was then possible to lift the brain out of the cranium without damaging the short infundibular stalk.

Complete serial sections were made of the brains from 14 fish. Nine of the brains were fixed in mercuric formol, cut either longitudinally or frontally at 6 μ , and stained according to Bargmann's modification of the chrome-alum-haematoxylin and phyloxine method of Gomori (CAHP) or with Gomori's aldehyde-fuchsin (AF) or Heidenhain's azan. In addition to demonstrating neurosecretory material, sections stained by these methods were found to be particularly helpful when tracing details of the hypophyseal vascularization. Two brains were fixed in formol saline and

stained with Heidenhain's haematoxylin. To demonstrate nerve tracts, three were preserved in Bodian's formol-acetic acid-alcohol, cut at 25 or 50 μ and stained according to Bodian's protargol S method (as outlined by the suppliers of protargol, Winthrop Laboratories, New York).

A Leitz Prado micro-projector, equipped with a microscope slide attachment, was used to map the major blood vessels and hypothalamic centers. Drawings were made by combining tracings of the images of a number of serial sections projected consecutively on a screen. The detailed illustrations are reconstructions made by combining camera lucida drawings of consecutive sections viewed under phase contrast.

RESULTS

1. Vascularization

a. *Cephalic vascularization.** The anterior arteries of the brook trout are illustrated in figure 1.

The dorso-lateral aortae enter the cranium through the hypophyseal foramina after which they are referred to as the in-

* Wherever possible, the nomenclature used is taken from the *Traité de Zoologie*, tome XIII (Grassé, '58), and from *Studies on the Structure and Development of Vertebrates* (Goodrich, '58).

Abbreviations

a, arteriole
ah, adenohypophysis
bas, basilar artery
bid sp, blood space
bc, "border cell" region
cap, connective tissue capsule
cap pl, capillary plexus
c hyp, caudal hypophyseal artery
c hyth, caudal hypothalamic artery
c mes, central mesencephalic artery
dla, dorso-lateral aorta
ebr, efferent branchial arteries
ehy, efferent hyoidian artery
eps, efferent pseudobranchial artery
hyp, hypophysis
hyth, hypothalamus
h com, horizontal commissure
hf, position of hypophyseal foramen
ib-rvh, inferior branch of right ventral hypothalamic artery
ic, internal carotid artery
ir, infundibular recess
l, loops of inferior branch of ventral hypothalamic artery
li, artery to lobus inferior
lic, left internal carotid artery

lob in, lobus inferior
m, meninx
med obl, medulla oblongata
meso-ah, meso-adenohypophysis
meta-ah, meta-adenohypophysis
mda, median dorsal aorta
nh, neurohypophysis
nlt, nucleus lateralis tuberis
npo, nucleus preopticus
ns, neurosecretory granules
on, orbito-nasal artery
op, optic nerve and tract
oph, ophthalmic artery
or, orbital artery
p cer, posterior cerebral artery
p-hyp, preoptic-hypophyseal tract
pro-ah, pro-adenohypophysis
ric, right internal carotid artery
rvh, right ventral hypothalamic artery
s, stalk
sac v, saccus vasculosus
sb-rvh, superior branch of right ventral hypothalamic artery
sl, blood sinus
v, veins or venules
III v, third ventricle

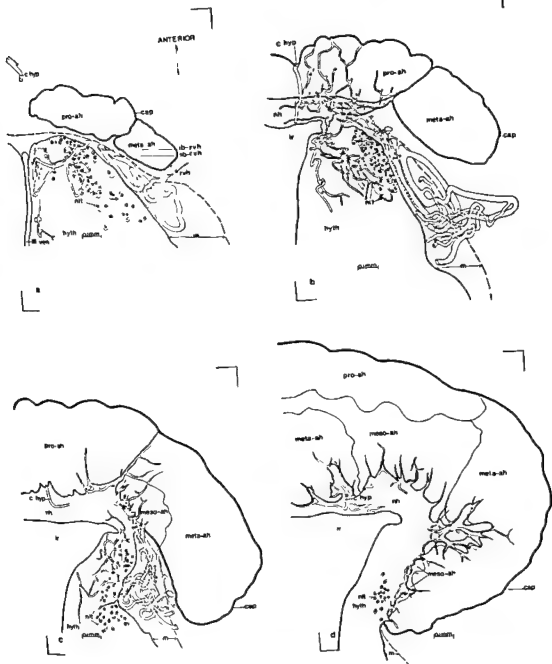


Fig 4a-d Details of the vascularization of the right half of the hypothalamic-hypophyseal area. Reconstructions from consecutive frontal sections; a and d illustrate the dorsal and ventral limits of the vascular supply of the hypophysis via the ventral hypothalamic artery. External limit of the meninx is indicated by a broken line.

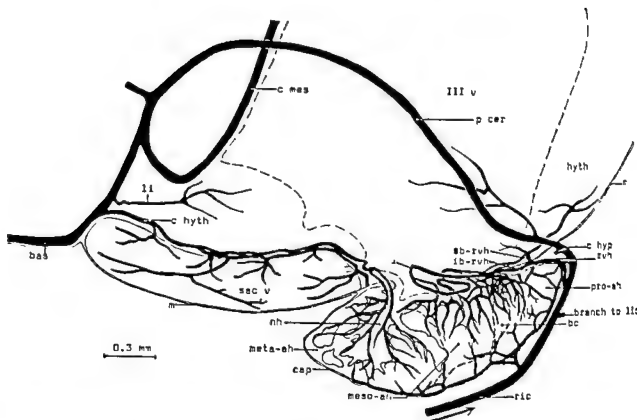


Fig. 3 Drawing of the vascularization of the hypophysis and saccus vasculosus; para-sagittal view. The extent of the third ventricle is shown by a broken line. The pro- and meso-adenohypophyses are adenohypophyseal cells.

the dorsal surface of the lobus inferior just below the corpora bigemina. In its course it gives off a branch which penetrates the hypothalamus and passes to a lateral extension of the third ventricle.

Upon reaching the posterior part of the lobus inferior, lateral to the saccus vasculosus, the posterior cerebral gives rise to a small vessel which continues along the ventral edge of the corpora bigemina. The posterior cerebral turns medially and sends off a large branch which passes dorsally and unites at the midline with its mate of the opposite side to form the central artery of the mesencephalon. The latter vessel continues upward to vascularize the dorsal part of the brain.

The posterior cerebral joins with the corresponding vessel of the opposite side and continues caudad as a single, medial basilar artery. This vessel courses along the ventral surface of the medulla oblongata and passes through the foramen magnum after which it is called the spinal artery.

A caudal hypothalamic artery of variable origin is found in the connective tissue surrounding the dorsal part of the saccus vasculosus (fig. 3). The path of this artery is described below.

b. Ventral hypothalamic arteries. These vessels extend posteriorly over the dorsal surface of the pro-adenohypophysis where, upon nearing the stalk, each bifurcates to form superior and inferior branches. The course of the right ventral hypothalamic artery is illustrated in figure 3 and in more detail in figure 4a-d.

The superior branch enters the hypothalamus and passes medially toward the third ventricle. Here it divides forming a system of capillaries some of which continue in the walls of the third ventricle while others run posteriorly and appear to end in ventral hypothalamic tissue near the cells of the nucleus lateralis tuberis. More importantly, a few capillaries run anteroventrally to pass down the hypophyseal stalk

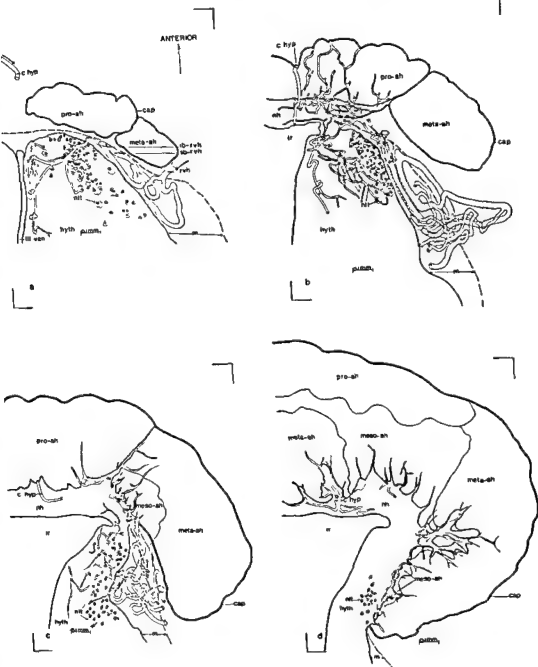


Fig. 4a-d Details of the vascularization of the right half of the hypothalamic-hypophyseal area. Reconstructions from consecutive frontal sections; a and d illustrate the dorsal and ventral limits of the vascular supply of the hypophysis via the ventral hypothalamic artery. External limit of the meninx is indicated by a broken line.

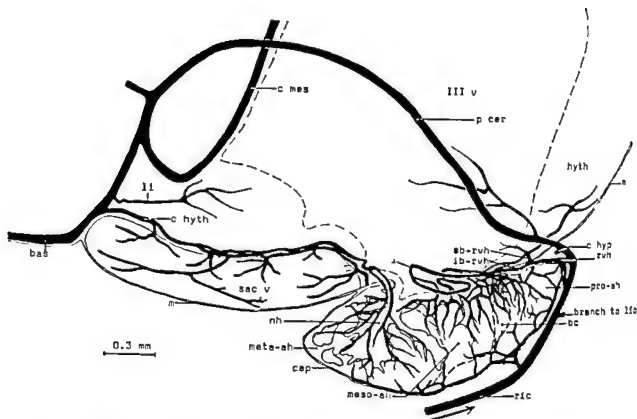


Fig. 3 Drawing of the vascularization of the hypophysis and saccus vasculosus; para-sagittal view. The extent of the third ventricle is shown by a broken line. The pro- and meso-adenohypophyses are adenohypophyseal cell.

the dorsal surface of the lobus inferior just below the corpora bigemina. In its course it gives off a branch which penetrates the hypothalamus and passes to a lateral extension of the third ventricle.

Upon reaching the posterior part of the lobus inferior, lateral to the saccus vasculosus, the posterior cerebral gives rise to a small vessel which continues along the ventral edge of the corpora bigemina. The posterior cerebral turns medially and sends off a large branch which passes dorsally and unites at the midline with its mate of the opposite side to form the central artery of the mesencephalon. The latter vessel continues upward to vascularize the dorsal part of the brain.

The posterior cerebral joins with the corresponding vessel of the opposite side and continues caudad as a single, medial basilar artery. This vessel courses along the ventral surface of the medulla oblongata and passes through the foramen magnum after which it is called the spinal artery.

A caudal hypothalamic artery of variable origin is found in the connective tissue surrounding the dorsal part of the saccus vasculosus (fig. 3). The path of this artery is described below.

b. *Ventral hypothalamic arteries.* These vessels extend posteriorly over the dorsal surface of the pro-adenohypophysis where, upon nearing the stalk, each bifurcates to form superior and inferior branches. The course of the right ventral hypothalamic artery is illustrated in figure 3 and in more detail in figure 4a-d.

The superior branch enters the hypothalamus and passes medially toward the third ventricle. Here it divides forming a system of capillaries some of which continue in the walls of the third ventricle while others run posteriorly and appear to end in ventral hypothalamic tissue near the cells of the nucleus lateralis tuberis. More importantly, a few capillaries run anteroventrally to pass down the hypophyseal stalk

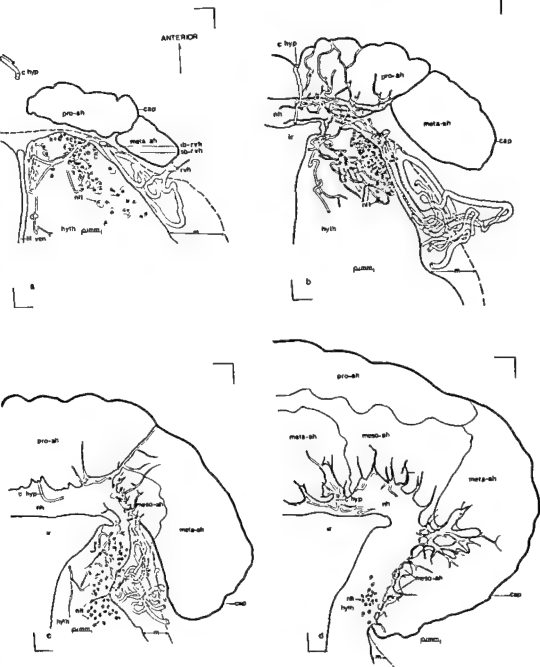


Fig. 4a-d Details of the vascularization of the right half of the hypothalamic-hypophyseal area. Reconstructions from consecutive frontal sections; a and d illustrate the dorsal and ventral limits of the vascular supply of the hypophysis via the ventral hypothalamic artery. External limit of the meninx is indicated by a broken line.

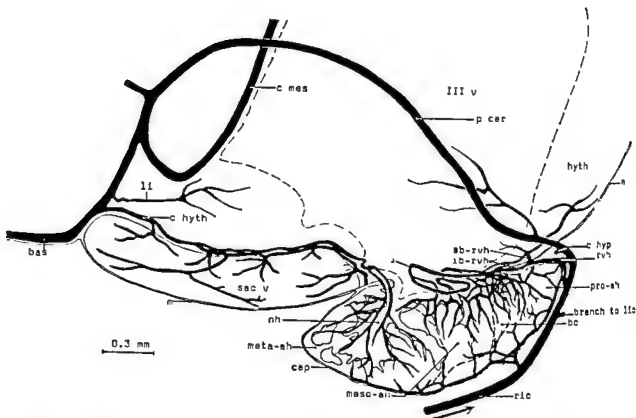


Fig. 3 Drawing of the vascularization of the hypophysis and saccus vasculosus; para-sagittal view. The extent of the third ventricle is shown by a broken line. The pro- and meso-adenohypophyses are adenohypophyseal cell.

the dorsal surface of the lobus inferior just below the corpora bigemina. In its course it gives off a branch which penetrates the hypothalamus and passes to a lateral extension of the third ventricle.

Upon reaching the posterior part of the lobus inferior, lateral to the saccus vasculosus, the posterior cerebral gives rise to a small vessel which continues along the ventral edge of the corpora bigemina. The posterior cerebral turns medially and sends off a large branch which passes dorsally and unites at the midline with its mate of the opposite side to form the central artery of the mesencephalon. The latter vessel continues upward to vascularize the dorsal part of the brain.

The posterior cerebral joins with the corresponding vessel of the opposite side and continues caudad as a single, medial basilar artery. This vessel courses along the ventral surface of the medulla oblongata and passes through the foramen magnum after which it is called the spinal artery.

A caudal hypothalamic artery of variable origin is found in the connective tissue surrounding the dorsal part of the saccus vasculosus (fig. 3). The path of this artery is described below.

b. *Ventral hypothalamic arteries.* These vessels extend posteriorly over the dorsal surface of the pro-adenohypophysis where, upon nearing the stalk, each bifurcates to form superior and inferior branches. The course of the right ventral hypothalamic artery is illustrated in figure 3 and in more detail in figure 4a-d.

The superior branch enters the hypothalamus and passes medially toward the third ventricle. Here it divides forming a system of capillaries some of which continue in the walls of the third ventricle while others run posteriorly and appear to end in ventral hypothalamic tissue near the cells of the nucleus lateralis tuberis. More importantly, a few capillaries run anteroventrally to pass down the hypophyseal stalk

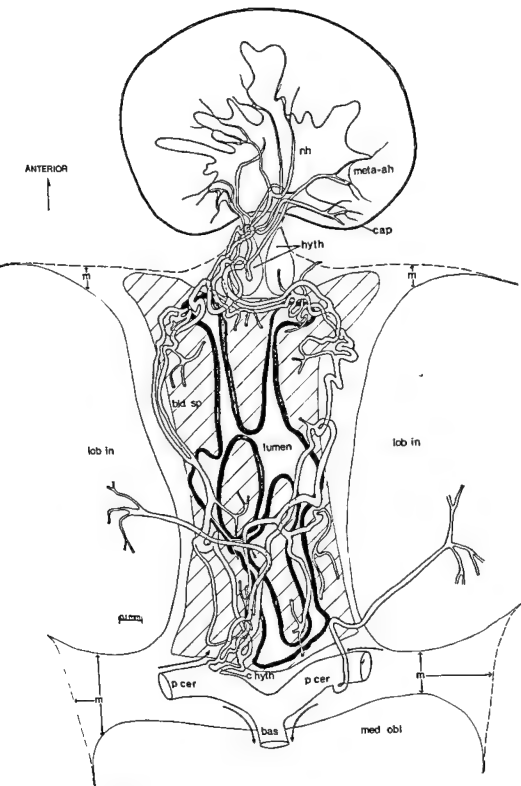


Fig. 5. Vascularization of the saccus vasculosus and meta-adenohypophysis by the caudal hypo-

and contribute to an extensive vascular plexus that lies in the neurohypophysis.

The inferior branch extends posterolaterally in the meninx covering the hypothalamus. This vessel passes caudally almost the length of the hypophysis before turning about itself and running anteriorly. During its forward path it breaks up into numerous arterioles which loop back and forth among themselves many times before ultimately entering the neurohypophysis (fig. 8).

The configuration of the loops is best understood from figure 4a-d. They are not always confined to the connective tissue, but occasionally may extend out of the meninx and run over the surface of the hypophysis. From the loops, a few vessels pass medially into the hypothalamus and either unite with capillaries from the superior branch or are distributed among the cells of the nucleus lateralis tuberis.

After looping, the arterioles enter the neurohypophysis and give rise to an extensive capillary plexus, most of which is localized in the anterior portion adjacent to pro-adenohypophyseal tissue (figs. 4, 9). As previously mentioned, some capillaries from the superior branch contribute to this network. From the plexus, numerous capillaries extend ventrally to give rise to the rich blood supply of the pro-adenohypophyseal and "border cell" regions. The meso-adenohypophysis is also vascularized by capillaries from this plexus, but to a much lesser extent than the pro-adenohypophysis. Some of these capillaries extend through the meso-adenohypophyseal tissue to vascularize the anterior region of the meta-adenohypophysis.

c. *Caudal hypothalamic artery.* Both the origin and the branching of the caudal hypothalamic artery are subject to considerable variation. This artery may originate from one of the two posterior cerebrals as illustrated in figure 5, or it may arise from the basilar artery. It has two main branches which extend rostrally on either side in the connective tissue dorsal to the saccus vasculosus.

The branches of the caudal hypothalamic artery send off small vessels which penetrate the connective tissue surrounding the saccus vasculosus and enter the

prominent blood spaces of this organ. These branches appear to be the sole source of arterial blood to the saccus vasculosus.

At the anterior end of the saccus, the two main branches of the artery move medially and divide into a few arterioles. These continue anteriorly and enter neurohypophyseal tissue adjacent to the meta-adenohypophysis. Capillaries from the arterioles extend ventrally into the meta-adenohypophysis and form the principle arterial supply to the cells of this region.

A pair of small arteries irrigate the posterior portions of the lobi inferiores. These vessels originate from either the caudal hypothalamic artery or from one of its branches or, as indicated in figures 3 and 5, from the posterior cerebrals.

d. *Venous drainage.* The distribution of vessels composing the drainage system of the hypophysis is highly variable. The general pattern is illustrated in figure 6.

Only a few veins and venules occur in the neurohypophysis and they pass ventrally to join with the venous channels of the adenohypophysis. Numerous venules arise among the follicles of the pro-adenohypophysis and these collect into a pair of lateral sinuses situated in the anterior part of the gland. From the sinuses, veins extend radially out of the hypophysis and form a prominent venous network covering the anterior surface of the gland. The vessels of this plexus converge to form a pair of large, mid-lateral veins which extend ventrally over the surface of the hypophysis and probably convey blood to the large sinus which lies on the floor of the sella turcica. The venous channels of the meso- and meta-adenohypophyses, though less numerous than those of the pro-adenohypophysis, usually open into the anterior sinuses. A few extend peripherally and run over the surface of the gland to join with the mid-lateral veins.

2. Hypothalamic nuclei and the preoptic-hypophyseal tract

The ventral hypothalamus contains two pairs of centers which are or could be neurosecretory, the nucleus preopticus and the nucleus lateralis tuberis.

The preoptic nucleus is found in the wall of the third ventricle, anterior and

possible to discern the limits of the cytoplasmic extensions of the tuberal cells.

A summary of the vascular supply of the adenohypophysis and the sites of endings of neurosecretory axons is given in table 1.

DISCUSSION

1. Vascularization of the hypothalamic-hypophyseal area

The chief arterial supply to the hypophysis and the ventral hypothalamus in the brook trout is from a pair of ventral hypothalamic arteries which arise from the internal carotids where the latter arch over the anterior tip of the pro-adenohypophysis. According to Barrington ('60), these areas in *Phoxinus phoxinus* are vascularized by a median artery originating from the internal carotids at the level of the anterior edge of the optic chiasma. In *Phoxinus*, this artery forms an intrameningeal ring vessel around the stalk of the hypophysis. From the ring vessel, branches extend either dorsally into the floor of the infundibular recess or ventrally into the hypophysis.

In the brook trout each ventral hypothalamic artery divides to form a superior and an inferior branch.

The superior branch passes to the ventral hypothalamus and gives rise to capillaries, some of which lie near the preoptic-hypophyseal tract. A few of the vessels continue into the stalk and contribute to the capillary plexus which is concentrated in the anteroventral region of the neurohypo-

physis. A similar, although usually more extensive, vascular connection between the ventral hypothalamus and hypophysis has been reported as occurring in *Corydora paltatus* (Miller, '44), *Rhodeus amarus* (Bretschneider and de Wit, '47), *Phoxinus phoxinus* (Barrington, '60), and *Channa punctatus* (Belsare, '65). Only Belsare ('65) has definitely suggested that the vascular link between the two areas is functionally comparable to the portal vessels in the median eminence of tetrapods; however, Miller ('44) and Barrington ('60) do not rule out such a possibility, while Bretschneider and de Wit ('47) merely comment that the connection may be important. Observations on the vessels connecting the ventral hypothalamus with the hypophysis in the brook trout do not support Belsare's ('65) suggestion since, not only are few capillaries involved, but also there is no evidence that neurosecretory axons terminate on or near these vessels. The functional significance of the vessels is unknown, but conceivably they might provide a pathway for the transport of products from the nucleus lateralis tuberculi to the hypophysis. In contrast to the above reports, Follenius ('65) states that the hypophyseal vascularization is independent of that of the hypothalamus in the nine species he studied.

Numerous arterioles originate from the inferior branches of the ventral hypothalamic arteries in the brook trout. After forming an intricate system of loops within

TABLE 1
Summary of the vascularization of the adenohypophysis and sites of neurosecretory axon endings

	Pro-adenohypophysis and "border cell" area	Meso-adenohypophysis	Meta-adenohypophysis
Vascularization from internal carotid arteries			
Ventral hypothalamic arteries	+	+	+
Caudal hypothalamic artery	—	—	+
Caudal hypophyseal artery (if present)	—	—	+
Peripheral arteries	+	+	+
Terminations of hypothalamic neurosecretory fibres			
In adenohypophysis	—	+	— ¹
In neurohypophysis adjacent to capillaries vascularizing adenohypophyseal regions	+	+	+

¹ Neurosecretory axons do not appear to penetrate into the meta-adenohypophysis however, some neurosecretion was seen about the venous channels in this region.

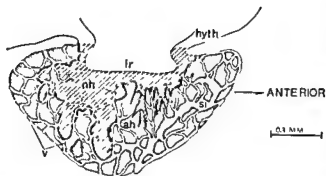


Fig. 6 Drawing of the venous channels within the hypophysis; sagittal view.

dorsal to the optic chiasma (fig. 7). The granular inclusions of its cells stain positively with both CAHP and AF. Fibers from the nucleus converge to form the preoptic-hypophyseal tract which extends ventrally to the base of the hypothalamus and passes through the nucleus lateralis tubercis. The fibers then enter the infun-

dibular stalk to extend radially in all directions within the neurohypophysis.

In the anterior part of the hypophysis, neurosecretion is localized about the walls of the rich capillary plexus lying above the pro- and meso-adenohypophyses and the "border cells." Also, a few neurosecretion-laden axons extend into the meso-adenohypophysis. Large aggregations of neurosecretory granules occur about the periphery of the neurohypophyseal projections into the meta-adenohypophysis lying close to the glandular cells. A few neurosecretory granules were observed on or in the walls of the venules and veins in this area of the gland.

The nucleus lateralis tubercis lies on either side of the infundibular recess in the ventral hypothalamus (fig. 10). The cells of this nucleus do not stain positively with either CAHP or AF. It has not been

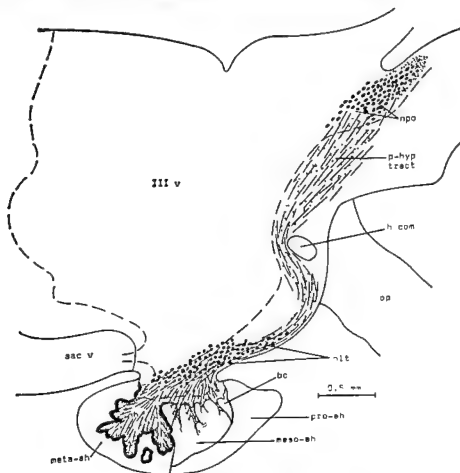


Fig. 7 Drawing of the hypothalamic nuclei, preoptic-hypophyseal tract and sites of neurosecretion within the hypophysis; para-sagittal view. The broken line indicates the extent of the third ventricle.

possible to discern the limits of the cytoplasmic extensions of the tuberal cells.

A summary of the vascular supply of the adenohypophysis and the sites of endings of neurosecretory axons is given in table 1.

DISCUSSION

1. Vascularization of the hypothalamic-hypophyseal area

The chief arterial supply to the hypophysis and the ventral hypothalamus in the brook trout is from a pair of ventral hypothalamic arteries which arise from the internal carotids where the latter arch over the anterior tip of the pro-adenohypophysis. According to Barrington ('60), these areas in *Phoxinus phoxinus* are vascularized by a median artery originating from the internal carotids at the level of the anterior edge of the optic chiasma. In *Phoxinus*, this artery forms an intrameningeal ring vessel around the stalk of the hypophysis. From the ring vessel, branches extend either dorsally into the floor of the infundibular recess or ventrally into the hypophysis.

In the brook trout each ventral hypothalamic artery divides to form a superior and an inferior branch.

The superior branch passes to the ventral hypothalamus and gives rise to capillaries, some of which lie near the preoptic-hypophyseal tract. A few of the vessels continue into the stalk and contribute to the capillary plexus which is concentrated in the anteroventral region of the neurohypo-

physis. A similar, although usually more extensive, vascular connection between the ventral hypothalamus and hypophysis has been reported as occurring in *Corydora palaiatus* (Miller, '44), *Rhodeus amarus* (Bretschneider and de Wit, '47), *Phoxinus phoxinus* (Barrington, '60), and *Channa punctatus* (Belsare, '65). Only Belsare ('65) has definitely suggested that the vascular link between the two areas is functionally comparable to the portal vessels in the median eminence of tetrapods; however, Miller ('44) and Barrington ('60) do not rule out such a possibility, while Bretschneider and de Wit ('47) merely comment that the connection may be important. Observations on the vessels connecting the ventral hypothalamus with the hypophysis in the brook trout do not support Belsare's ('65) suggestion since, not only are few capillaries involved, but also there is no evidence that neurosecretory axons terminate on or near these vessels. The functional significance of the vessels is unknown, but conceivably they might provide a pathway for the transport of products from the nucleus lateralis tubercis to the hypophysis. In contrast to the above reports, Follenius ('65) states that the hypophyseal vascularization is independent of that of the hypothalamus in the nine species he studied.

Numerous arterioles originate from the inferior branches of the ventral hypothalamic arteries in the brook trout. After forming an intricate system of loops within

TABLE 1
Summary of the vascularization of the adenohypophysis and sites of neurosecretory axon endings

	Pro-adenohypophysis and "border cell" area	Meso-adenohypophysis	Meta-adenohypophysis
Vascularization from internal carotid arteries			
Ventral hypothalamic arteries	+	+	+
Caudal hypothalamic artery	—	—	+
Caudal hypophyseal artery (if present)	—	—	+
Peripheral arteries	+	+	+
Terminations of hypothalamic neurosecretory fibres			
In adenohypophysis	—	+	— ¹
In neurohypophysis adjacent to capillaries vascularizing adenohypophyseal regions	+	+	+

¹ Neurosecretory axons do not appear to penetrate into the meta-adenohypophysis however, some neurosecretion was seen about the venous channels in this region.

the meninx they enter the neurohypophysis and give rise to a well developed capillary plexus which is chiefly localized in the anterior region close to the adenohypophysis. Many workers, including Kerr ('42), Miller ('44), Green ('51), Barrington ('60), Follenius and Porte ('62), Jasiński ('62), Dodd and Kerr ('63), Follenius ('65) and Lagios ('65), have also described a rich capillary plexus between the neuro- and adenohypophyses. Few authors have commented on its possible significance, but Follenius and Porte ('62) and Dodd and Kerr ('63) suggest that the vascular arrangement within the neurohypophysis may represent a portal system.

2. Hypothalamic centers and innervation of the hypophysis

In the brook trout, neurosecretory granules are present close to the capillaries of the neurohypophyseal plexus which border the pro- and meso-adenohypophyses. In addition, neurosecretory axons pass into meso-adenohypophyseal tissue. Large accumulations of neurosecretory material are found adjacent to the meta-adenohypophysis.

In a number of teleosts, neurosecretory material has been observed among both meso- and meta-adenohypophyseal cells (Da Lage, '55; Legait and Legait, '57; Stahl and Leray, '62. Legait and Legait ('57), Da Lage ('58) and Knowles, Vollrath and Nishioka ('67) state that neurosecretory fibers also extend into the pro-adenohypophysis however, Stahl and Leray ('62) report that neurosecretion is not present within this region.

While much has been written about the nucleus lateralis tuberis, little is known of the nature and function of the cells comprising it. Palay ('45), Billenstien ('63) and Szabó and Molnar ('65) refer to centers in the tuberal area as being neurosecretory. There is some argument as to whether the secretory product is discharged into the third ventricle (Hild, '50; Brehm, '58; Polenov, '60; Stahl and Leray, '62) or whether it is conveyed to the adenohypophysis by axonal transport (Billenstien, '63). A number of workers such as Billen-

stien ('63) have suggested that the nucleus may be concerned with gonadotropin secretion.

From this study, there is no evidence thus far to indicate that the tuberal center is neurosecretory or that its cells possess long axons which contribute to the hypophyseal tract. Morphologically, they resemble the "granule cells" described by Barrington ('60) in *Phoxinus phoxinus*. The "granule cells" lie scattered about a capillary bed in the floor of the infundibular recess and Barrington suggests they may be secretory and discharge their product into the third ventricle and the vascular system.

It is generally agreed that the preoptic nucleus is neurosecretory. Follenius ('63) and Szabó and Molnar ('65) have commented that the nucleus may play a role in regulating reproductive activity.

3. Regulation of adenohypophyseal activity

There are three schools of thought regarding the regulation of adenohypophyseal activity in teleost fishes.

a. Green ('51) suggests that if humoral transmission occurs from the neuro- to the adenohypophysis, that the vascular plexus between the two provides an effective arrangement for transmission. Thus he argues that control of the adenohypophysis by the nervous system may be indirect via a neuro-vascular pathway. According to Stahl and Leray ('62) neurosecretion from the tuberal nucleus is distributed to the adenohypophysis by the diencephalic capillary system.

b. Dodd and Kerr ('63) claim that the interdigitation of the neurohypophysis with the adenohypophysis is of prime importance in the regulation of adenohypophyseal secretion. They maintain that this interdigitation provides a large surface area for contact between glandular and neural tissues and that the two are close enough together to allow the active contents released from the endings of neurosecretory cells to act directly on the glandular cells and so control or regulate their secretions. Other workers who favour the hypothesis of direct neural (axonal) control are Bretschneider and de Wit ('47), Da Lage

('55, '58), Legait and Legait ('57, '59), Bargmann and Knoop ('60), and Knowles, Vollrath and Nishioka ('67).

c. Wingstrand ('59) and Follenius and Porte ('62) propose that neural control of adeno-hypophyseal activity may operate via nerve fibers which make direct contact with the glandular cells and/or indirectly via the vascular plexus in the neurohypophysis. Further details of this dual mechanism have been reported by Follenius ('65) based on his electron microscope study of *Perca fluviatilis* and *Salmo irideus*. In these fishes, neurosecretory fiber endings were observed on capillaries of the neurohypophyseal vascular network and also on the basement membrane which separates the neuro- and adeno-hypophyses. No fibers were found penetrating the glandular lobes. Follenius concluded that the adeno-hypophyseal cells bordering the neurohypophysis are probably under direct neural control while the more distant cells, particularly in the pro- and meso-adeno-hypophyses, may be regulated indirectly via a vascular relay from the neurohypophyseal network.

On the basis of the results obtained in this study, it is interesting to speculate on the possible mechanisms regulating the secretory activity of the adeno-hypophysis in the brook trout. The following interpretation suggests that the controlling pathway may not be the same for all of the three regions and agrees with the postulate that both direct and indirect routes exist in teleosts.

Vessels from the capillary plexus in the neurohypophysis pass among the pro-adeno-hypophyseal follicles and the "border cells." Although accumulations of hypothalamic neurosecretory material occur about the plexus, no neurosecretory fibers were observed immediately adjacent to or among the cell clusters. Thus, the secretory activity of the cells in these areas may be regulated by hypothalamic factors transmitted to them by way of the vascular plexus in the neurohypophysis.

The portion of the capillary plexus vascularizing the meso-adeno-hypophysis is also surrounded by neurosecretory material, but, in addition, neurosecretory axons pass among the cells of this region. This

suggests that the activity of the meso-adeno-hypophysis may be controlled by factors which are transmitted to the glandular cells directly from neurosecretory fibers and/or indirectly by way of the capillary plexus.

Neurosecretion accumulates close to the meta-adeno-hypophysis where it surrounds the walls of capillaries supplying this region. Neurosecretory axons do not penetrate into the meta-adeno-hypophysis. Thus, it is possible that the function of this area is regulated by factors transmitted by the vascular system.

The extremities of the wide, blunt-tipped projections of the neurohypophysis into the meta-adeno-hypophysis contain an abundance of neurosecretion and indeed may act as a reservoir for this material. Neurosecretory material is also present near the venous channels in the ventral meta-adeno-hypophysis. While some of the hypothalamic products may have local effects on adeno-hypophyseal function, perhaps others have systemic effects. If so, it is possible that some of the neurosecretion observed in the posterior portion of the gland is a storage form of a peripherally acting hormone or hormones.

Most of the arterial supply to the adeno-hypophysis originates from a capillary plexus in the ventral neurohypophysis. The meta-adeno-hypophyseal region is also vascularized by branches of the caudal hypothalamic artery. If we are correct in stating that most of the neurosecretory axons terminate in the neurohypophysis adjacent to blood vessels, we suggest that the neuro-vascular arrangement in the brook trout is functionally equivalent to that of the median eminence and hypophyseal portal vessels of tetrapods.

The neural, vascular and glandular relations of the brook trout merit investigation at the electron microscope level. It would be of particular interest to learn the extent to which the results presented here are compatible with the concept of dual innervation proposed by Knowles ('65). Knowles and his colleagues have marshalled considerable evidence in support of the idea that the intrinsic endocrine cells of the hypophysis of lower vertebrates are regulated by two kinds of neurosecre-

the meninx they enter the neurohypophysis and give rise to a well developed capillary plexus which is chiefly localized in the anterior region close to the adenohypophysis. Many workers, including Kerr ('42), Miller ('44), Green ('51), Barrington ('60), Follenius and Porte ('62), Jasiński ('62), Dodd and Kerr ('63), Follenius ('65) and Lagios ('65), have also described a rich capillary plexus between the neuro- and adenohypophyses. Few authors have commented on its possible significance, but Follenius and Porte ('62) and Dodd and Kerr ('63) suggest that the vascular arrangement within the neurohypophysis may represent a portal system.

2. Hypothalamic centers and innervation of the hypophysis

In the brook trout, neurosecretory granules are present close to the capillaries of the neurohypophyseal plexus which border the pro- and meso-adenohypophyses. In addition, neurosecretory axons pass into meso-adenohypophyseal tissue. Large accumulations of neurosecretory material are found adjacent to the meta-adenohypophysis.

In a number of teleosts, neurosecretory material has been observed among both meso- and meta-adenohypophyseal cells (Da Lage, '55; Legait and Legait, '57; Stahl and Leray, '62. Legait and Legait ('57), Da Lage ('58) and Knowles, Vollrath and Nishioka ('67) state that neurosecretory fibers also extend into the pro-adenohypophysis however, Stahl and Leray ('62) report that neurosecretion is not present within this region.

While much has been written about the nucleus lateralis tuberis, little is known of the nature and function of the cells comprising it. Palay ('45), Billenstien ('63) and Szabó and Molnar ('65) refer to centers in the tuberal area as being neurosecretory. There is some argument as to whether the secretory product is discharged into the third ventricle (Hild, '50; Brehm, '58; Polenov, '60; Stahl and Leray, '62) or whether it is conveyed to the adenohypophysis by axonal transport (Billenstien, '63). A number of workers such as Billen-

stien ('63) have suggested that the nucleus may be concerned with gonadotropin secretion.

From this study, there is no evidence thus far to indicate that the tuberal center is neurosecretory or that its cells possess long axons which contribute to the hypophyseal tract. Morphologically, they resemble the "granule cells" described by Barrington ('60) in *Phoxinus phoxinus*. The "granule cells" lie scattered about a capillary bed in the floor of the infundibular recess and Barrington suggests they may be secretory and discharge their product into the third ventricle and the vascular system.

It is generally agreed that the preoptic nucleus is neurosecretory. Follenius ('63) and Szabó and Molnar ('65) have commented that the nucleus may play a role in regulating reproductive activity.

3. Regulation of adenohypophyseal activity

There are three schools of thought regarding the regulation of adenohypophyseal activity in teleost fishes.

a. Green ('51) suggests that if humoral transmission occurs from the neuro- to the adenohypophysis, that the vascular plexus between the two provides an effective arrangement for transmission. Thus he argues that control of the adenohypophysis by the nervous system may be indirect via a neuro-vascular pathway. According to Stahl and Leray ('62) neurosecretion from the tuberal nucleus is distributed to the adenohypophysis by the diencephalic capillary system.

b. Dodd and Kerr ('63) claim that the interdigitation of the neurohypophysis with the adenohypophysis is of prime importance in the regulation of adenohypophyseal secretion. They maintain that this interdigitation provides a large surface area for contact between glandular and neural tissues and that the two are close enough together to allow the active contents released from the endings of neurosecretory cells to act directly on the glandular cells and so control or regulate their secretions. Other workers who favour the hypothesis of direct neural (axonal) control are Bretschneider and de Wit ('47), Da Lage

- chez quelques téléostéens. Étude au microscope électronique. C. R. Soc. Biol., Paris, 151: 1943-1946.
- Legait, E., et H. Legait 1959 Recherches sur l'ultrastructure de l'adénohypophyse. C. R. Ass. Anat., 45: 519-522.
- Miller, R. N. 1944 The hypophysis of the teleost, *Corydora pallatus*. J. Morph., 74: 331-345.
- Palay, S. L. 1945 Neurosecretion. VII. The preoptic-hypophysial pathway in fishes. J. Comp. Neur., 82: 129-143.
- Pickford, G. E., and J. W. Atz 1957 The Physiology of the Pituitary Gland of Fishes. New York Zoological Society, N. Y.
- Polenov, A. L. 1960 The preoptic hypophyseal Gomeripositive neurosecretory system of the sazan and carp. Dokl. Akad. Nauk SSSR (En Transl. Biol. Sci. Sec.), 129: 1029-1033.
- Stahl, A., and C. Leray 1962 The relationship between diencephalic neurosecretion and the adenohypophysis in teleost fish. Mem. Soc. Endo., No. 12: 149-163.
- Szabó, S., et B. Molnar 1965 L'activité neurosécrétrice des noyaux hypothalamiques durant le cycle ovarien chez le barbeau méridional (*Barbus meridionalis petényi* Heck.). Rev. Roum. Endocrin., 2: 35-40.
- Wingstrand, K. G. 1959 Attempts at a comparison between the neurohypophysial region in fishes and tetrapods, with particular regard to amphibians. In: Comparative Endocrinology. A. Gorbman, ed. John Wiley & Sons, Inc., New York.

tory fibers. In *Anguilla* and *Conger* (Knowles and Vollrath, '66) both kinds of fibers penetrate the adenohypophysis but the fiber terminals are separated from the intrinsic endocrine cells by narrow vascular channels into which the neurosecretory products are thought to be discharged. In *Hippocampus*, (Knowles, Vollrath and Nishioka, '67), the two types of fibers invade all parts of the adenohypophysis and, in this teleost, appear to make direct secretomotor junctions with the glandular cells.

ACKNOWLEDGMENTS

This project was supported by grants from the National Research Council of Canada.

We are grateful to Mr. A. C. Sinclair, Superintendent, Calgary Trout Hatchery, who supplied the brook trout and to Mrs. G. Dubé for her capable assistance with the histological preparations. We thank Dr. P. K. Anderson and Dr. H. A. Bern for their constructive criticisms of the manuscript.

LITERATURE CITED

- Bargmann, W., and A. Knoop 1960 Über die morphologischen Beziehungen des neurosekretorischen Zwischenhirnsystems zum Zwischenlappen der Hypophyse. (Licht- und elektronenmikroskopische Untersuchungen). Z. Zellforsch., 52: 256-277.
- Barrington, E. J. W. 1960 Some features of the vascularization of the hypothalamus and pituitary stalk in the minnow *Phoxinus phoxinus* L. Proc. Zool. Soc. Lond., 135: 551-558.
- Belsare, D. K. 1965 Vascular supply of the pituitary gland in *Channus punctatus*, Block. Nature, 206: 211.
- Billenstien, D. C. 1963 Neurosecretory material from the nucleus lateralis tuberis in the hypophysis of the eastern brook trout, *Salvelinus fontinalis*. Z. Zellforsch., 59: 507-512.
- Brehm, H. v. 1958 Über jahreszyklische Veränderungen im Nucleus lateralis tuberis der Schleie (*Tinca vulgaris*). Z. Zellforsch., 49: 105-124.
- Bretschneider, L. H., and J. J. D. de Wit 1947 Sexual Endocrinology of Non-mammalian Vertebrates. Elsevier Publishing Co., Inc., Amsterdam.
- Da Lage, C. 1955 Innervation neurosécrétoire de l'adénohypophyse chez l'hippocampe. C. R. Assoc. Anat., 85: 361-367.
- 1958 Recherches sur le complexe hypophysaire de l'hippocampe. Arch. Anat. Micr. Morph. Exp., 47: 401-445.
- Dodd, J. M., and T. Kerr 1963 Comparative morphology and histology of the hypothalamo-neurohypophysial system. Symp. Zool. Soc. Lond., No. 9: 5-27.
- Follenius, E. 1961 Comparaison des relations vasculaires hypothalamo-hypophysaires chez quelques espèces de téléostéens. C. R. Acad. Sci., Paris, 253: 1015-1017.
- 1963 Étude comparative de la cyologie fine du noyau préoptique (NPO) et du noyau latéral du tuber (NLT) chez la truite (*Salmo irideus* Gibb.) et chez la perche (*Perca fluviatilis*). Comparaison des deux types de neurosécrétion. Gen. and Comp. Endocrinol., 3: 66-85.
- 1965 Bases structurales et ultrastructurales des corrélations diencéphalo-hypophysaires chez les sélaginiens et les téléostéens. Arch. Anat. Micr., 54: 195-216.
- Follenius, E., and A. Porte 1962 Appearance, ultrastructure and distribution of the neurosecretory material in the pituitary gland of two teleost fishes, *Lebistes reticulatus* R. and *Perca fluviatilis* L. Mem. Soc. Endo., No. 12: 51-63.
- Goodrich, E. S. 1958 Studies on the Structure and Development of Vertebrates. Dover Publications, Inc., New York.
- Grassé, P. P. 1958 Traité de Zoologie, tome XIII. Masson et Cie., Paris.
- Green, J. D. 1951 The comparative anatomy of the hypophysis, with special reference to its blood supply and innervation. Amer. J. Anat., 88: 225-311.
- Hild, W. 1950 Zur Frage der Neurosekretion im Zwischenhirn der Schleie (*Tinca vulgaris*) und ihrer Beziehungen zur Neurohypophyse. Z. Zellforsch., 35: 33-46.
- Jasiński, A. 1962 Structure and vascularization of the pituitary body of Teleosts. Part II. The rainbow-trout (*Salmo irideus* Gibb.), perch-pike (*Lucioperca lucioperca* L.), burbot (*Lota lota*), and pond-loach (*Misgurnus fossilis* L.). Acta Biol. Crac., Zool., 5: 67-93.
- Kerr, T. 1942 A comparative study of some teleost pituitaries. Proc. Zool. Soc. Lond., 112A: 37-56.
- Knowles, Sir Francis 1965 Evidence for a dual control, by neurosecretion, of hormone synthesis and hormone release in the pituitary of the dogfish, *Scylliorhinus stellaris*. Phil. Trans. Roy. Soc. Lond., Ser. B, 249: 435-456.
- Knowles, Sir Francis, and L. Vollrath 1966 Neurosecretory innervation of the pituitary of the eels *Anguilla* and *Conger*. Phil. Trans. Roy. Soc. Lond., Ser. B, 250: 311-342.
- Knowles, F., L. Vollrath and R. S. Nishioka 1967 Dual neurosecretory innervation of the adenohypophysis of *Hippocampus*, the sea-horse. Nature, 214: 309.
- Lagios, M. D. 1965 Seasonal changes in the cytology of the adenohypophysis, testes, and ovaries of the black surfperch, *Embiotoca jacksoni*, a viviparous perciform fish. Gen. and Comp. Endocrinol., 5: 207-221.
- Legait, H., et E. Legait 1957 Terminaisons neurosécrétoires au niveau de l'adénohypophyse

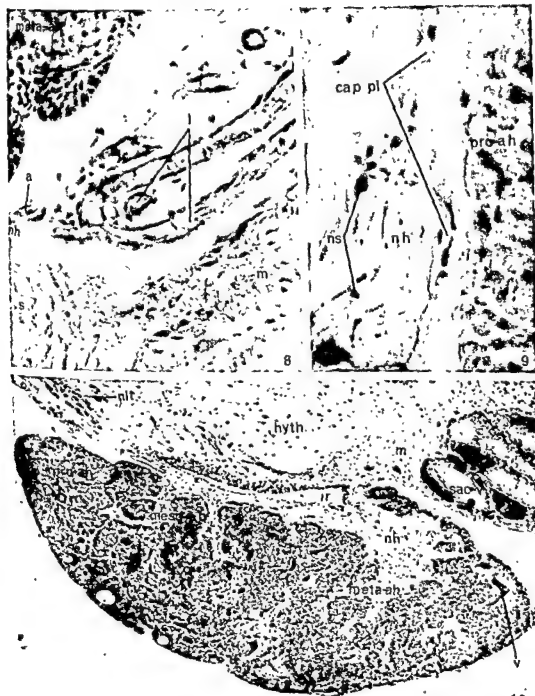


PLATE 1

EXPLANATION OF FIGURES

- 8 Loops of the arterioles formed by the inferior branch of the ventral hypothalamic artery; note vessel entering the neurohypophysis. CAHP, $\times 445$.
- 9 Capillary plexus of the neurohypophysis adjacent to the pro-adenohypophysis; note neurosecretory granules close to vessels. CAHP, $\times 985$.
- 10 Hypophysis and ventral hypothalamus; sagittal view. Heidenhain's azan, $\times 80$.

VASCULARIZATION OF TROUT HYPOPHYSIS

Joanna Jensen Hill and Nancy E. Henderson



Subcommissural Organ and Adjacent Ependyma: Autoradiographic study of their origin in the mouse brain¹

PASKO RAKIC AND RICHARD L. SIDMAN

Department of Neuropathology, Harvard Medical School,
Boston, Massachusetts

ABSTRACT Morphogenesis and time and place of cell origin of the subcommissural organ and adjacent ependyma in the mouse brain was investigated by light microscopy and autoradiography. Pregnant mice were injected systematically at different stages of gestation and their offspring killed after various periods. Cells of the subcommissural organ arise (undergo final replication of nuclear DNA) from embryonic days 11 to 15 at the diencephalomesencephalic junction in close association with the primordial fibers of the posterior commissure. The ependymal cells of the caudal part of the third ventricle first arise at approximately the same embryonic stage as the subcommissural cells and continue to proliferate through embryonic day 18.

The subcommissural organ is suitable for semiquantitative analysis because its cells are of one type, their number is small, they arise over a short time span and once formed, they persist indefinitely. Some cells exposed to thymidine- H^3 in utero at the time of final DNA replication were strongly labeled at adulthood, as expected, but others were weakly labeled. Calculations suggested that significant numbers of these weakly labeled cells should be assigned to the nondividing class i.e., had their birthdays on the day of thymidine- H^3 injection. Errors are introduced if the usual practice is followed of assigning birthdays on the basis of the heavily labeled population exclusively.

The subcommissural organ, a specialized part of the ependyma of the brain, is composed of columnar epithelial cells roofing the Sylvian aqueduct at its junction with the third ventricle. It cells are especially tall in the region of the mesocoelic recess, an outpocketing of the dorsal wall of the aqueduct in the vicinity of the posterior commissure. A subcommissural organ and mesocoelic recess are found in the brains of all vertebrates that have been examined, except the adult human. Present in human fetuses, these structures gradually diminish in size in the neonatal period and have disappeared or remained as vestiges in adulthood (Rakic, '65). By contrast, the subcommissural organ is prominent in adult rodents (Talanti, '58).

Histological properties of the subcommissural organ have been studied at length, especially with reference to a possible glandular secretory function (Bauer-Jokl, '17; Jordan, '25; Wislocki and Leduc, '52, '54, '56, Wislocki and Roth '58; Talanti, '58, and others). The epithelial cells contain numerous secretory granules, particu-

larly in their apical cytoplasm, and droplets and amorphous threads with similar staining properties are found extracellularly at the ventricular surface. Electron microscopic observations in calf (Isomaki, '65) and rabbit (Schmidt and D'Agostino, '66) were interpreted to indicate also basal secretion by the columnar epithelial cells and suggested an endocrine function for the subcommissural organ. Gilbert ('56, '57, '58) and Brown and Afifi ('65) have investigated a possible role of the subcommissural organ in water metabolism and control of thirst.

These studies indicate that the subcommissural organ differs from adjacent parts of the ependyma and the question arises, whence do the differences originate? The time and place of origin of cells in the intact developing mammalian brain can be determined by autoradiography after exposure of proliferating cells to thymidine- H^3 . The generally accepted basis of

¹ Supported by grant NB-04782 from the National Institutes of Health, U. S. Public Health Service, Bethesda, Maryland.

a Zeiss microscope fitted with a Wild drawing tube (Angevine, '65). The labeled nuclei in postnatally-killed specimens were classed somewhat arbitrarily as "strongly" or "weakly" labeled. Those designated as "strongly labeled" were covered with silver grains to about the same extent as the most strongly labeled neurons in adjacent parts of the diencephalon in the same sections. Typically they were completely covered with grains (usually more than 30 per nucleus) and the grains often were confluent. "Weakly labeled" nuclei were overlaid with at least five grains and formed a more heterogeneous population which included cells that had divided two or more times subsequent to labeling, and cells that were weakly labeled for other reasons, to be considered in the Discussion.

All counts and plots were made on specimens cut in the coronal plane in order to insure comparable orientation of the subcommissural organ. All cells in five consecutive sections through the same region in each specimen were drawn at a magnification of 400 \times . The subcommissural organ was outlined and strongly radioactive nuclei were plotted as solid circles, weakly labeled ones as open circles. The absolute numbers of labeled cells per section were counted on these plots rather than directly on the microscopic slides. To check the possibility that our criteria of classification might have changed during the study, a number of slides were replotted at different times. The percentages of labeled ependymal cells were obtained by classifying 500 consecutive cells in each specimen as "labeled" or "unlabeled."

The labeled embryos were fixed by immersion in 10% acrolein in 0.9% saline and prepared for autoradiography by the same methods used for the adult brain. Serial sections were cut at 10 μ in the sagittal plane. The slides were stained with toluidine blue after development of the autoradiographic emulsion.

RESULTS

Morphological studies

Comparison of subcommissural and ependymal cells in the adult. In the

mouse, as in other rodents (Wislocki and Leduc, '52), the subcommissural organ lies in the roof of the aqueduct immediately ventral and rostral to the posterior commissure at the junction of the aqueduct and third ventricle (fig. 1). In the transverse and sagittal planes its diameter is less than 275 μ . The organ is composed of pseudostratified columnar epithelial cells that collectively form a sheet curved so as partially to envelop the aqueduct in its hilum (fig. 2). The dorsally-positioned cells are taller than the lateral ones, and in most the nucleus lies in the basal half of the cell. The basal surfaces of the subcommissural cells and the myelinated fibers of the posterior commissure dorsal to them are in close apposition. At the ventral edge of the organ the transition is abrupt from the tall subcommissural cells to the low cuboidal ependymal cells that line the adjacent ventrally-directed part of the third ventricle (fig. 2). Anteriorly, however, the epithelial cells of the subcommissural organ diminish progressively in height so that there is a gradual transition to ordinary ependyma. Within the limits of light microscopic criteria, all the cells appeared to be of one class.

Form of the subcommissural organ in embryos. The close association of subcommissural organ and posterior commissure is evident from early developmental stages. Neither structure is recognizable in our material before the tenth embryonic day (fig. 3A). On the tenth and eleventh days the primordial fiber bundles of the posterior commissure are already prominent at the junction of mesencephalon and diencephalon, and the primitive ependyma below these bundles is thinner than it is at more anterior or posterior levels (fig. 3B,C). This thinned area is the presumptive subcommissural organ.

Essentially the same picture is seen on the twelfth embryonic day (fig. 3D). The primitive ependyma is relatively thin beneath the posterior commissure but the cells individually exhibit no features that would distinguish them from their neighbors in adjacent parts of the primitive ependyma. Some cells with nuclei positioned close to the ventricular surface are

the method is that exogenous thymidine is incorporated almost exclusively into DNA, so that only cells synthesizing DNA (several hours before cell division in most instances) become labeled. The radioactive precursor is available for DNA synthesis for less than one hour, and therefore only one population of cells becomes labeled. The radioactivity is retained indefinitely by the labeled cell but is halved and distributed about equally to the daughter cells with each subsequent cell division.

A practical difficulty in the application of these principles is how to assess the significance of weakly labeled cells in adult specimens. Cells that incorporated thymidine- H^3 in their final period of nuclear DNA synthesis may appear strongly or weakly labeled when examined at later times. Accurate delineation of the time span during which a given cell population arises calls not only for enumeration of the strongly labeled cells but also for calculation of the percentage of weakly labeled cells that were in their final replication cycle at the time of exposure to thymidine- H^3 . In the present study our purpose is twofold: (1) to describe histogenesis of the subcommissural organ, and (2) to examine closely the general validity of the autoradiographic method for determining the time of cell origin on the basis of the distribution of heavily labeled cells in adult animals that had been pulse-labeled with thymidine- H^3 during the developmental period. The subcommissural organ is suitable for this purpose because its cells are all of one type, their number is small, and once they have formed during a brief embryonic period, they persist for the life of the mouse.

MATERIALS AND METHODS

Histological studies

Adult specimens. The structure of the subcommissural organ was studied in several adult C57BL/6J mice about 60 days old. The vascular system of each animal was perfused with 15 ml of 4% glutaraldehyde in 0.1 M Sorenson's phosphate buffer, pH 7.4. In one specimen the whole brain was embedded in celloidin and sectioned sagittally at 20 μ for study of the relations between subcommissural

organ, ventricular system, and posterior commissure. In other specimens, the brain was removed from the skull 45 minutes after perfusion and a 1 mm block of tissue containing the subcommissural organ was washed in buffer at pH 7.4, immersed in 2% OsO_4 at room temperature for one hour, dehydrated in graded methanol solutions, and embedded in Epon. Transverse sections were cut at 1-2 μ in thickness and were stained with toluidine blue at alkaline pH for light microscopic study.

Embryonic specimens. F1 embryos of SJL/J male and BALB/cGn female mice were fixed and stained in bulk by Cajal's reduced silver methods (Ramon y Cajal and Castro, '33) on the eleventh, twelfth, fourteenth, and sixteenth days of gestation. Whole embryos were embedded in polyester wax and were sectioned serially at 16 μ . Also, toluidine blue-stained sections of 9 to 18 day embryos prepared for autoradiography, as described below, were examined with reference to the morphogenesis of the subcommissural organ.

Autoradiographic studies

Thymidine- H^3 (Specific activity 3.0 C/mM; 5 μ C/g body weight) was injected once at various stages from the ninth day of pregnancy to postnatal day 20 (gestation lasts 19 days in these mice). Thymidine- H^3 was injected intraperitoneally or intravenously into the mother during gestation, or it was injected subcutaneously into the young mouse postnatally. The labeled animals were killed at various embryonic stages after injection or at two months to two years postnatally.

Brains of adult mice were fixed by perfusion with 10% acrolein in 0.9% saline, dehydrated with methanol:methyl Cellosolve (1:1 v/v), embedded in polyester wax, serially sectioned in one of the cardinal planes at 5 or 8 μ , mounted on slides, and coated in the dark with Kodak NTB 2 or NTB 3 radiosensitive emulsion. The slides were kept at -70°C in a Dry Ice chest for three weeks or longer, subsequently developed with Kodak Dektol and stained through the emulsion with toluidine blue.

Autoradiograms were studied and the positions of the labeled cells plotted with



Fig. 2 Microphotograph of the subcommissural organ in coronal plane. PC, posterior commissure. Arrows indicate the junction of the subcommissural organ and ependyma lining the caudal part of the third ventricle. Fixation by perfusion with 4% glutaraldehyde, postfixation in 2% OsO_4 , embedded in EPON, sectioned at $1\ \mu$, and stained with alkaline toluidine blue $\times 350$.

From the sixteenth embryonic day onward, no mitotic activity is seen. The cells become even taller (fig. 3G) and by the seventeenth embryonic day the organ has attained its adult form. No further changes

have been observed up to an age of two years.

Autoradiographic studies
Birthdays of subcommissural cells.
The "birthday" of a cell may be defined as

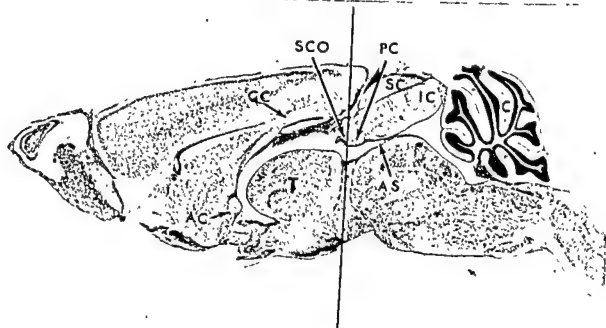


Fig. 1 Relations of ventricular system, subcommissural organ, and posterior commissure in mid-sagittal section of adult mouse brain. The slightly oblique section does not pass through the caudal part of the third ventricle, but its position is demarcated with dashed lines. The solid vertical line indicates the plane of section used for the autoradiographic study of subcommissural organ and ependyma. Abbreviations: AC, anterior commissure; AS, aqueduct of Sylvius; C, cerebellum; CC, corpus callosum; IC, inferior colliculus; PC, posterior commissure; SC, superior colliculus; SCO, subcommissural organ; T, thalamus. Cresyl violet stain. $\times 12.5$.

in mitosis, while the more deeply situated cells are intermingled with the fiber bundles of the posterior commissure.

On the thirteenth embryonic day the position of the subcommissural organ is more readily recognized because a slight indentation appears in the ventricular surface in the region of the posterior commissure, though the cells still show no indications of the tall columnar form that they will assume later.

The invagination of the ventricular surface becomes more evident on the fourteenth embryonic day (fig. 3E). The cell nuclei are still close to the ventricular surface, and mitotic figures are seen occasionally (fig. 4A). Numerous cells are interposed between fiber bundles of the posterior commissure. For the first time cells at the ventricular surface contain small vacuoles in their apical cytoplasm. In silver-stained preparations, an accumulation of apparently structureless threads

and particles known collectively as Reissner's fiber (Reissner, 1860; Jordan, '25) is seen in the aqueduct of Sylvius, in contact with the surface of the subcommissural organ (fig. 4B). The apical cytoplasm itself is similarly stained, evidence in support of the view that Reissner's fiber is a secretory product of the subcommissural cells (Wislocki and Leduc, '52 and '54). This morphological evidence indicates that secretion is under way on the fourteenth embryonic day.

On the fifteenth embryonic day the subcommissural organ is almost completely formed and is large relative to other diencephalic and mesencephalic structures (fig. 3F). The presence of an occasional mitotic figure indicates that cell proliferation continues, albeit to a lesser extent than at earlier stages. Most of the epithelial cells now are elongated, and their nuclei lie in a basal position.

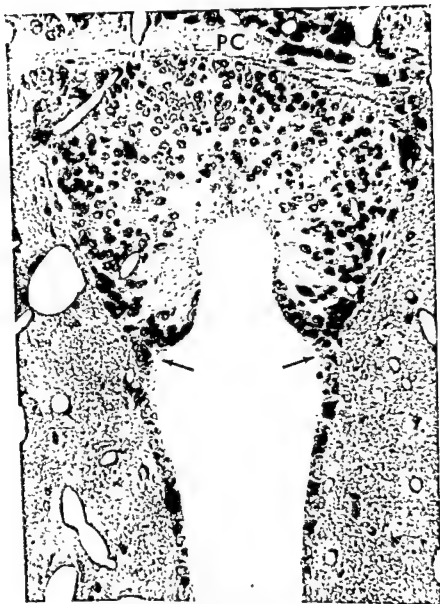


Fig. 2 Microphotograph of the subcommissural organ in coronal plane. PC, posterior commissure. Arrows indicate the junction of the subcommissural organ and ependyma lining the caudal part of the third ventricle. Fixation by perfusion with 4% glutaraldehyde, postfixed in 2% OsO_4 , embedded in EPON, sectioned at $1\ \mu$, and stained with alkaline toluidine blue $\times 350$.

From the sixteenth embryonic day onward, no mitotic activity is seen. The cells become even taller (fig. 3G) and by the seventeenth embryonic day the organ has attained its adult form. No further changes

have been observed up to an age of two years.

Autoradiographic studies

Birthdays of subcommissural cells.
The "birthday" of a cell may be defined as

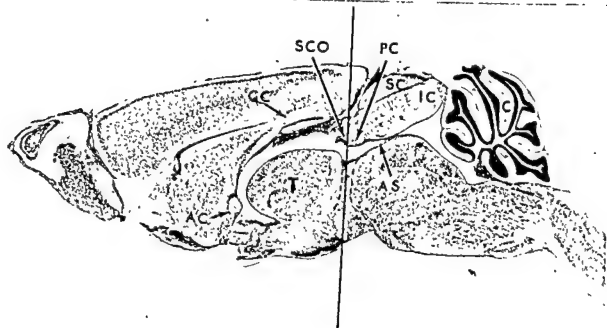


Fig. 1 Relations of ventricular system, subcommissural organ, and posterior commissure in mid-sagittal section of adult mouse brain. The slightly oblique section does not pass through the caudal part of the third ventricle, but its position is demarcated with dashed lines. The solid vertical line indicates the plane of section used for the autoradiographic study of subcommissural organ and ependyma. Abbreviations: AC, anterior commissure; AS, aqueduct of Sylvius; C, cerebellum; CC, corpus callosum; IC, inferior colliculus; PC, posterior commissure; SC, superior colliculus; SCO, subcommissural organ; T, thalamus. Cresyl violet stain. $\times 12.5$.

in mitosis, while the more deeply situated cells are intermingled with the fiber bundles of the posterior commissure.

On the thirteenth embryonic day the position of the subcommissural organ is more readily recognized because a slight indentation appears in the ventricular surface in the region of the posterior commissure, though the cells still show no indications of the tall columnar form that they will assume later.

The invagination of the ventricular surface becomes more evident on the fourteenth embryonic day (fig. 3E). The cell nuclei are still close to the ventricular surface, and mitotic figures are seen occasionally (fig. 4A). Numerous cells are interposed between fiber bundles of the posterior commissure. For the first time cells at the ventricular surface contain small vacuoles in their apical cytoplasm. In silver-stained preparations, an accumulation of apparently structureless threads

and particles known collectively as Reissner's fiber (Reissner, 1860; Jordan, '25) is seen in the aqueduct of Sylvius, in contact with the surface of the subcommissural organ (fig. 4B). The apical cytoplasm itself is similarly stained, evidence in support of the view that Reissner's fiber is a secretory product of the subcommissural cells (Wislocki and Leduc, '52 and '54). This morphological evidence indicates that secretion is under way on the fourteenth embryonic day.

On the fifteenth embryonic day the subcommissural organ is almost completely formed and is large relative to other diencephalic and mesencephalic structures (fig. 3F). The presence of an occasional mitotic figure indicates that cell proliferation continues, albeit to a lesser extent than at earlier stages. Most of the epithelial cells now are elongated, and their nuclei lie in a basal position.

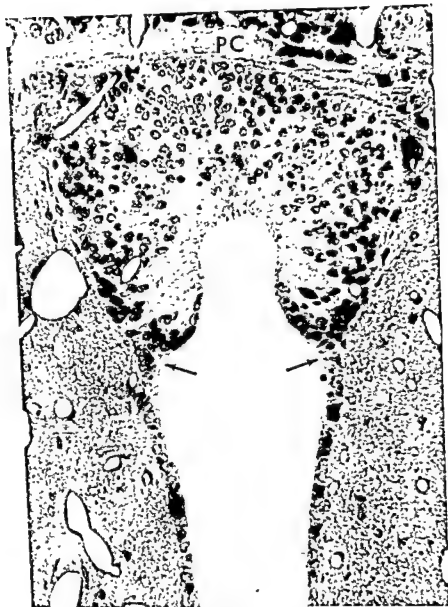


Fig 2 Microphotograph of the subcommissural organ in coronal plane. PC, posterior commissure. Arrows indicate the junction of the subcommissural organ and ependyma lining the caudal part of the third ventricle. Fixation by perfusion with 4% glutaraldehyde, postfixed in 2% OsO_4 , embedded in EPON, sectioned at $1\ \mu$, and stained with alkaline toluidine blue $\times 350$

From the sixteenth embryonic day onward, no mitotic activity is seen. The cells become even taller (fig. 3G) and by the seventeenth embryonic day the organ has attained its adult form. No further changes

have been observed up to an age of two years.

Autoradiographic studies

Birthdays of subcommissural cells. The "birthday" of a cell may be defined as

the last day on which nuclear DNA is replicated in that cell line. If exposed to thymidine- H^3 at any time during the final period of DNA synthesis, the parent cell becomes labeled. It then divides and distributes labeled DNA equally between the two daughter cells, which in turn remain heavily labeled for life and are recognized in autoradiograms of adult specimens. If a given progenitor cell is exposed to thymidine- H^3 at some stage prior to the final division, we would expect the progeny examined at adulthood to be more weakly labeled, and the number of silver grains per nucleus to be inversely proportional to the number of cell divisions in that lineage between the time of thymidine- H^3 injection and the time of death. Conversely, if thymidine- H^3 were injected later than the birthday, the cell in question should be unlabeled. These points are exemplified in Angevine's ('65) study of histogenesis in the hippocampal formation and Ruben's ('67) analysis of inner ear development.

In the mouse exposed to thymidine- H^3 on embryonic day 9 (E9) and killed 90 days postnatally, a diffuse light dusting of silver grains was seen over the subcommissural cells. While labeling was above background, no cell nucleus was covered with four or more grains and therefore none was classed as labeled (table 1, Specimen no. T 9.5.1).

In the animal injected on the tenth day of gestation and killed at adulthood, an average of 23 weakly labeled cells was counted in each of 5 successive sections (table 1). Almost all other cell nuclei were overlaid with one to three silver grains and were scored as unlabeled. No cells were strongly labeled (fig. 5).

In the animal injected on the eleventh embryonic day and killed eight months after birth, an average of 124.0 weakly labeled subependymal cells per section was counted, more than twice the number found at any other stage (table 1, fig. 6A). For the first time, heavily labeled cells were present, an average of 6.4 per section; these cells had their birthdays on E11. Another specimen exposed to thymidine- H^3 on embryonic day 11 and examined 2.5 months after birth contained a large

number of heavily labeled cells per section and was judged to have been some hours older at the time of injection of thymidine- H^3 than the specimen just described.

In the four animals injected on the twelfth and thirteenth days of gestation and killed postnatally, the number of heavily labeled cells was at a maximum, and the number of weakly labeled cells was decreased (table 1, figs. 5, 6B-D, 7A). The distribution of labeled cells within the subcommissural organ varied somewhat from section to section, but no consistent regional pattern was recognized.

In the animal injected on the fourteenth day of gestation and killed postnatally the number of both weakly and strongly labeled cells was decreased. The strongly labeled cells slightly outnumbered the weakly labeled ones, averaging 12 and 9.4 per section respectively (table 1, fig. 5, 7B).

In the two animals injected at E15 the number of labeled cells decreased further (fig. 7C), and in the mice injected on the sixteenth to nineteenth embryonic days or in the first three postnatal weeks, no labeled cells were found in the subcommissural organ (table 1, fig. 7D).

Site of origin of subcommissural cells. The evidence given above indicates that the first subcommissural cells arise (i.e., undergo final nuclear DNA replication) early on the eleventh day of gestation, and the last ones on embryonic day 15. Most of the cells form on embryonic days 11 through 13. Since the anlage of the subcommissural organ is recognizable already on day 11, it is possible to ascertain the embryonic source of subcommissural cells by injecting thymidine- H^3 once at times between the eleventh and fifteenth

Fig 3 Morphogenesis of the subcommissural organ and mesocoelic recess. Microphotographs (left) and drawings (right) of the diencephalo-mesencephalic junction at different stages from embryonic days 10 (E10) to 16 (E16). All specimens were cut in the sagittal plane. Abbreviations: MR, mesocoelic recess; PC, posterior commissure; SCO, subcommissural organ. $\times 100$. A. 9-day embryo. Inserted in right upper corner is a drawing of the whole embryo at lower magnification, for orientation. B. 10-day embryo. C. 11-day embryo. D. 12-day embryo. E. 14-day embryo. F. 15-day embryo. G. 16-day embryo.

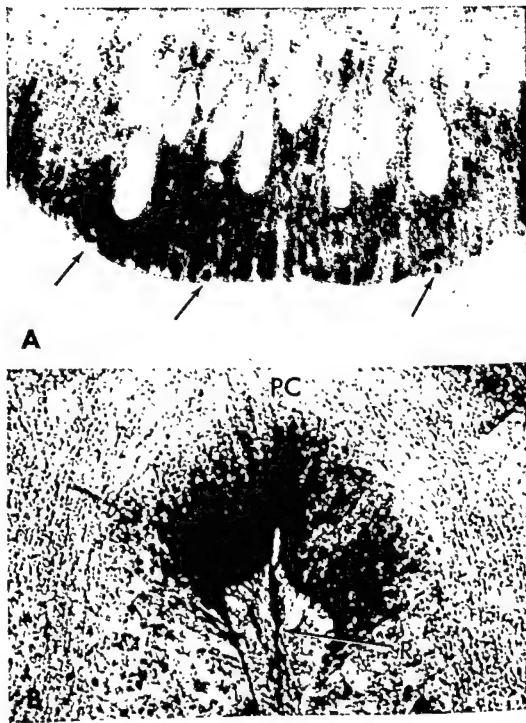


Fig. 4A Sagittal section through subcommissural organ of 14-day mouse embryo. Unstained fiber bundles of posterior commissure viewed in cross-section indent the upper regions of the subcommissural organ. Mitotic figures are at the ventricular surface (arrows). Toluidine blue. $\times 600$.

Fig. 4B Coronal section through subcommissural organ of 14-day mouse embryo. Reissner's fiber has already formed. Material with similar staining properties occupies the apical parts of the subcommissural cells and protrudes from them into the lumen of the aqueduct of Sylvius. Abbreviations: PC, posterior commissure; R, Reissner's fiber. Cajal's reduced silver stain. $\times 400$.

TABLE 1

Relative numbers of labeled cells in adult subcommissural organ after thymidine- H^3 injection at different embryonic stages

Specimen number ¹	Injected on embryonic day ²	Column a Weakly labeled cells ³	Column b Strongly labeled cells ³	Column c Total
T. 9.5.1	E9	0.0	0.0	0.0
T.10.1.3	E10	23.0 \pm 5.7	0.0	23.0
A.11.1.3	E11	124.2 \pm 7.6	6.4 \pm 2.4	130.6
A.12.1.3	E12	52.0 \pm 8.0	34.0 \pm 3.8	86.0
A.13.1.1	E13	41.0 \pm 5.9	34.5 \pm 5.1	75.5
T.14.1.2	E14	9.4 \pm 1.2	12.0 \pm 2.4	21.4
A.15.9.3	E15	4.4 \pm 0.7	4.2 \pm 0.7	8.6
A.16.9.3	E16	0.0	0.0	0.0

¹ Specimen numbers beginning with A or T are described further by Angevine ('65) and Pierce ('66) respectively

² All animals were killed as adults.

³ Mean number of labeled subcommissural cells in five successive sections in the coronal plane, \pm one standard error

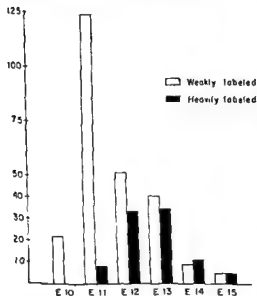


Fig 5 Mean number of weakly and heavily labeled cells in coronal sections through adult subcommissural organ in six mice, each exposed once to thymidine- H^3 on E10 (embryonic day 10), E11, E12, E13, E14, or E15.

days of gestation and killing the animals one hour to a few days after injection.

In embryos exposed to thymidine- H^3 on the eleventh or twelfth days of gestation and killed one hour later, nuclei of interphase cells engaged in DNA synthesis were labeled, and most of them lay in the half of the primitive ependyma furthest from the ventricular surface (fig. 8A).

Eight hours after injection the labeled nuclei had moved to positions near the ventricular surface (fig. 8B), where most of the mitotic figures are found. Virtually every mitotic figure was labeled at this time, indicating that most cells in mitosis at the time of fixation had been synthesizing DNA eight hours earlier when the thymidine- H^3 was injected. This migratory behavior of cell nuclei in the presumptive subependymal organ is the same as found in other regions of the primitive ependyma (Sidman, Feder and Miale, '59; Sidman, '61).

Nuclei of cells labeled on embryonic day 11 were found during the subsequent few days at various depths in the developing subcommissural organ, but the majority of the heavily labeled ones lay in the basal part of the organ, furthest from the ventricular surface (fig. 8C). Counts of labeled cells were not made since these embryonic specimens were cut in the sagittal plane and could not be compared readily with the coronal sections of the adult specimens. However, our impression is that few if any cells entered the incipient subcommissural organ from adjacent regions of the primitive ependyma or from other sites. Likewise, few cells appeared to leave the organ. The cells were generated locally, the postmitotic labeled population becoming somewhat less concentrated with time as the organ grew in size. Cells arising on embryonic day 13 behaved similarly.

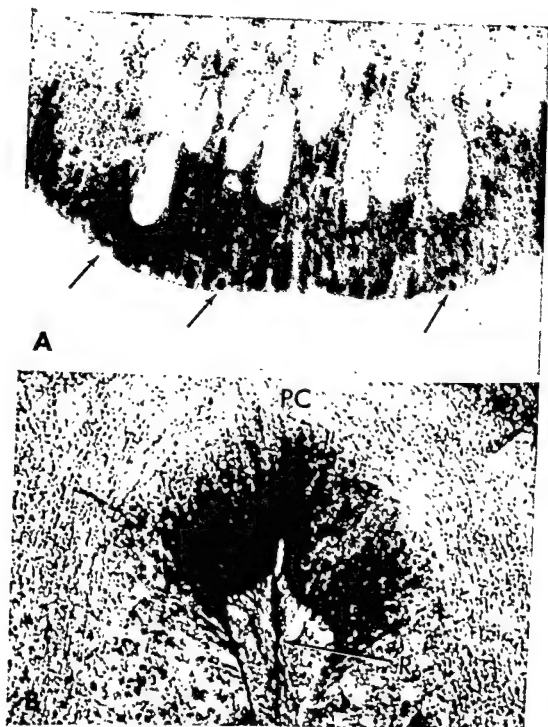


Fig. 4A Sagittal section through subcommissural organ of 14-day mouse embryo. Unstained fiber bundles of posterior commissure viewed in cross-section indent the upper regions of the subcommissural organ. Mitotic figures are at the ventricular surface (arrows). Toluidine blue. $\times 600$.

Fig. 4B Coronal section through subcommissural organ of 14-day mouse embryo. Reissner's fiber has already formed. Material with similar staining properties occupies the apical parts of the subcommissural cells and protrudes from them into the lumen of the aqueduct of Sylvius. Abbreviations: PC, posterior commissure; R, Reissner's fiber. Cajal's reduced silver stain. $\times 400$.

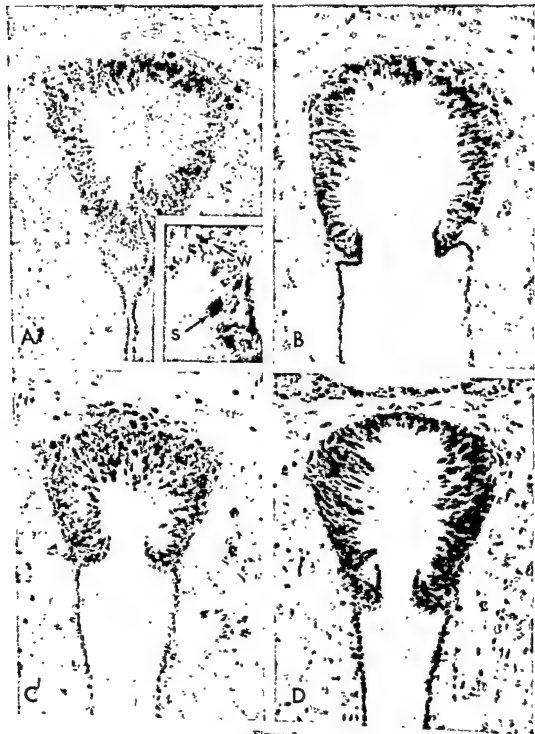


Figure 6

TABLE 2

Percentage of labeled cells in the ependymal lining of the caudal part of the third ventricle

Specimen number ¹	Injected on embryonic day ²	Labeled cells per 100 cells ³	
		Weakly labeled	Strongly labeled
T.10.1.3	E10	0	0
T.11.1.3	E11	19	0
T.12.1.3	E12	20.6	3.4
T.12.1.2	E13 (Early)	33.6	6.5
T.13.1.4	E13 (Late)	19.0	8.2
T.14.1.3	E14	17.2	4.4
T.15.1.2	E15	13.0	4.6
T.16.2.2	E16	6.0	0.9
A.17.6.1	E17	0	1.6
A.18.7.4	E18	0	1.4

¹ Specimen numbers beginning with A or T are described further by Angevine ('65) and Pierce ('66) respectively.

² All animals were killed as adults.

³ In each specimen 500 ependymal cells were examined in five successive sections.

Birthdays of ependymal cells. The same coronal sections of adult mouse brain that were prepared after the mother had been injected once with thymidine- H^3 on the tenth to eighteenth days of gestation and that were used for study of the subcommissural organ, served also for determining the percentages of labeled cells lining the caudal part of the third ventricle (table 2 and fig. 10). The appearance and distribution of strongly and weakly labeled ependymal cells in these adult specimens are illustrated in figs. 9A-D. From data on the initial date of thymidine- H^3 injection that yielded heavily labeled cells in adult specimens, one concludes that the earliest ependymal cells went through their final period of nuclear DNA synthesis on embryonic day 12, about one day later than the earliest cells of the adjacent subcommissural organ. Ependymal cells continued to form throughout the remainder of the embryonic period. Many of the ependymal cells, like those of the subcommissural organ, were still strongly labeled in mice killed at two years of age.

DISCUSSION

Birthday and site of origin of subcommissural and ependymal cells

Almost all cells of the subcommissural organ in the mouse arise in the primitive ependymal zone of the rostral midbrain between embryonic days 11 to 15 inclusive. We found no evidence that subcommissural cells arise elsewhere and then migrate

to the ependymal zone. On the contrary, the area of the primitive ependyma immediately ventral to the posterior commissure is distinguished from neighboring zones by its thinness already on the eleventh day of gestation, and many of its constituent cells have their birthdays on that day. The number of cells that become permanently labeled when thymidine- H^3 is injected on this and subsequent embryonic days is compatible with the increasing size of the subcommissural organ and few if any cells are seen to enter or leave the organ during the developmental period. It is open to speculation whether or not the intimate relationship between the developing subcommissural cells and the fibers of the posterior commissure is more than coincidental.

The human subcommissural organ acquires recognizable form during the fifth and sixth lunar months of gestation but has disappeared by birth or soon

Fig. 6 Labeled cells in autoradiograms of coronal sections through the subcommissural organ and adjacent ependyma of adult mice that have each been exposed once to thymidine- H^3 at different embryonic stage. $\times 223$. A. Animal exposed to thymidine- H^3 on embryonic day 11 and killed as adult. Insert in right lower corner high power microphotograph to illustrate weakly (W) and strongly (S) labeled cells. B. Animal exposed to thymidine- H^3 early on embryonic day 12 and killed as adult. C. Animal exposed to thymidine- H^3 late on embryonic day 12 and killed as adult. D. Animal exposed to thymidine- H^3 early on embryonic day 13 and killed as adult.

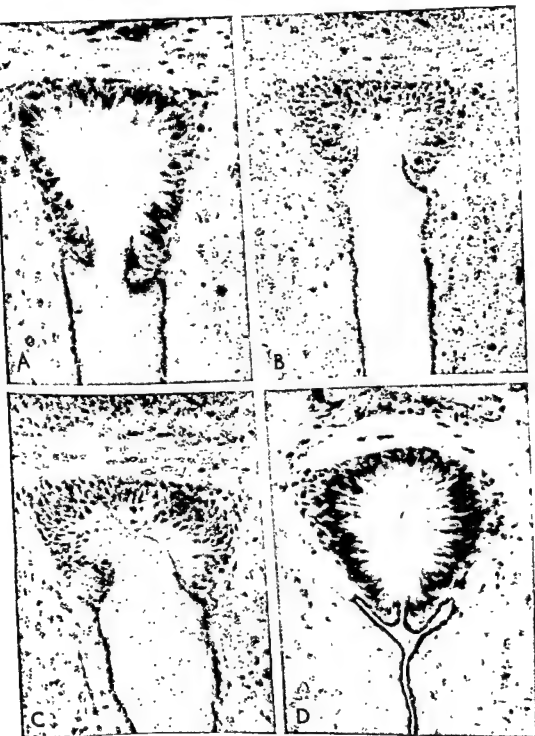


Figure 7

afterwards in most cases (Rakic, '65). By contrast, the mouse's subcommissural organ persists during adult life and retains the cells formed in the embryonic period for two years without significant diminution of labeled DNA. As further confirmation of the stability of subcommissural cells in the mouse, injection of thymidine- H^3 at various postnatal stages did not lead to labeling of nuclei in the subcommissural organ. These results indicate that the subcommissural cells, along with neurons, skeletal muscle cells and some other cell types must be classified in the "non-renewal" category (Leblond, '64).

Precursors of neurons, astrocytes, ependymal cells, and subcommissural cells all proliferate in the primitive ependymal zone, which is an embryonic germinal tissue lining the entire ventricular system. While the time period during which cells proliferate in the primitive ependyma varies extensively from region to region, the general behavior of the proliferating cells is fairly uniform. At the earliest stages, when all daughter cells are destined to remain in the expanding primitive ependyma itself, the nuclei of virtually all cells undergo a "to-and-fro" migration; they synthesize DNA while positioned at a distance from the ventricular surface, move toward that surface prior to mitosis, and return to the initial position following mitosis (Sidman, Miale, and Feder, '59). The cells at this stage show no signs of differentiation (Fujita and Fujita, '64; Herman and Kaufman, '66). Shortly thereafter, the first cells leave the primitive ependyma to initiate formation of the mantle layer. They appear to be neuroblasts (e.g., Langman, Guerrant, and Freeman, '66). These cells will not divide again under normal circumstances. Shortly thereafter, the first glial cells are recognizable at the margin of primitive ependyma and mantle layer; unlike most neuroblasts, these glial cells continue to multiply in the mantle and marginal layers and in the tissues derived later from these embryonic zones, but the cells apparently do not engage in the nuclear migrations that characterized their predecessors (Sidman, unpublished observations). Gliogenesis in rodents continues well into the postnatal

period, particularly in the cerebrum (Altman, '66), but in the upper parts of the brainstem, under consideration here, many glial cells have their birthdays earlier, during the eleventh to fifteenth days of gestation (Johnston and Angevine, '66).

In the present study we find that subcommissural cells arise in about the same embryonic time span as the nearby neurons of the upper brainstem. The subcommissural cell precursors exhibit the same to-and-fro nuclear migration in the primitive ependyma that is characteristic of neuronal and glial precursor cells, even though the subcommissural organ will acquire a very different structure and function. By contrast, the precise mode of origin of the ependymal cells remains elusive, for their precursors cannot be distinguished from other labeled cells in and near the primitive ependyma.

While the subcommissural and ependymal cells have a similar origin, they are not identical. The subcommissural cells arise over a slightly more restricted time period in close spatial relationship to fibers of the posterior commissure, and show morphological evidence of specialized secretory activity as early as the fourteenth day of gestation. From that time on the subcommissural cells are relatively tall, contain prominent and unusual secretory vesicles, and presumably function somewhat differently from ependymal cells. Neither population shows autoradiographic evidence of cell turnover during postnatal life.

The time lag between final cell division and appearance of specific morphological features of subcommissural secretory cells is about 48 hours, from embryonic days 11 and 12, when the early cells are in final division, to embryonic days 14 and 15, when they acquire specific morphological features (cylindrical shape with

Fig. 7 Continuation of figure 6. $\times 223$. Labeled cells in coronal sections of subcommissural organ of adult mice injected at different embryonic stages. $\times 223$. A. Adult animal exposed to thymidine- H^3 late on embryonic day 13. B. Adult animal exposed to thymidine- H^3 on embryonic day 14. C. Adult animal exposed to thymidine- H^3 on embryonic day 15. D. Adult animal exposed to thymidine- H^3 on embryonic day 16.

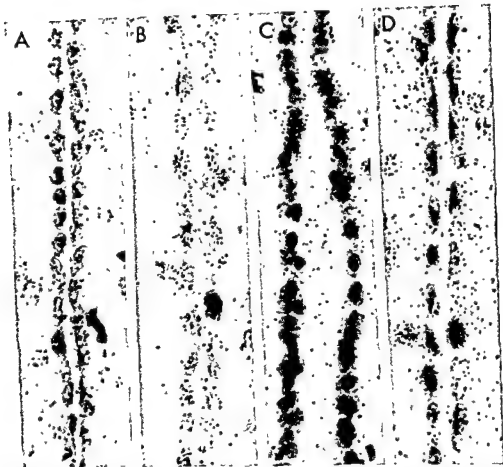


Fig. 9. Labeled cells in the ependyma lining the caudal part of the third ventricle. $\times 600$. A. Adult animal that had been exposed to one injection of thymidine- H^3 on embryonic day 11. B. Adult animal exposed to thymidine- H^3 on embryonic day 12. C. Adult animal exposed to thymidine- H^3 on embryonic day 13. D. Adult animal exposed to thymidine H^3 on embryonic day 14

basal nucleus and apical secretory granules). The hiatus between time of origin and time of morphological differentiation is much longer for certain other cell populations in the nervous system, e.g., Purkinje cells of the cerebellum (Miale and Sidman, '61).

Assessment of heavily labeled and lightly labeled cells

Since the subcommissural organ is small, has clear anatomical boundaries, and forms over only a few days, it is useful for the semiquantitative analysis of cell proliferation in a developing organ. As indicated in the Introduction, a major

problem is to assess whether or not some of the lightly labeled cells in adult specimens were engaged in their final period of DNA replication at the time of exposure to thymidine- H^3 . To render the following argument clear, it should be emphasized that the determination of cell birthdays is largely a statistical matter; the time and place of origin can be described for a population of labeled cells but cannot be determined accurately for any particular cell since individual cells are traced neither from one point in time to the next nor from one location to another. On a population basis, the intensity of labeling yields information about times and rates

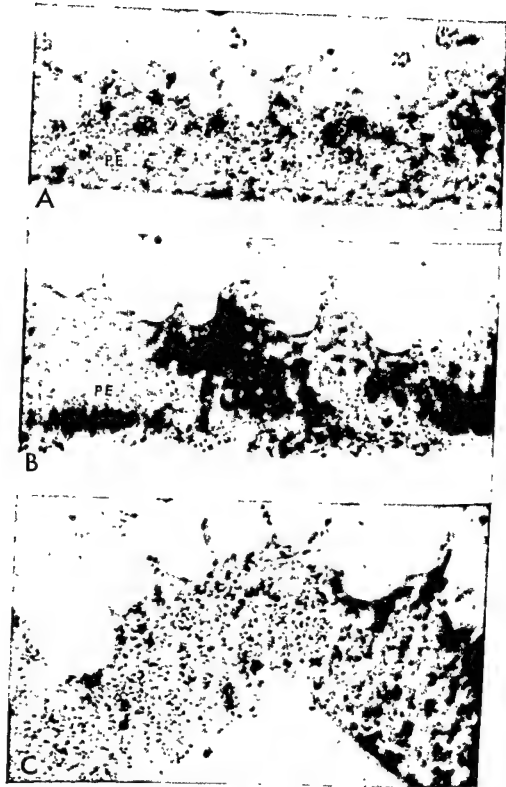


Fig. 8 Autoradiograms of the diencephalo-mesencephalic junction of three embryos exposed to thymidine- H^3 on embryonic day 11 (E11) and killed at various times after injection. $\times 360$. A. Mother injected at E11 and embryo killed one hour later. The numerous labeled nuclei lie almost exclusively in the deeper half of the primitive ependymal layer (PE). B. Mother injected at E11 and embryo killed eight hours later. Most of the labeled nuclei have moved to the half of the primitive ependyma (PE) nearest to the ventricular surface. All mitotic figures at the ventricular surface are labeled. C. Mother injected on embryonic day E11 and embryo killed 47 hours later. The subcommissural organ has enlarged considerably during the two days since the injection. Labeled nuclei are located at all levels of the subcommissural organ, but the most strongly labeled nuclei lie furthest from the ventricular surface.

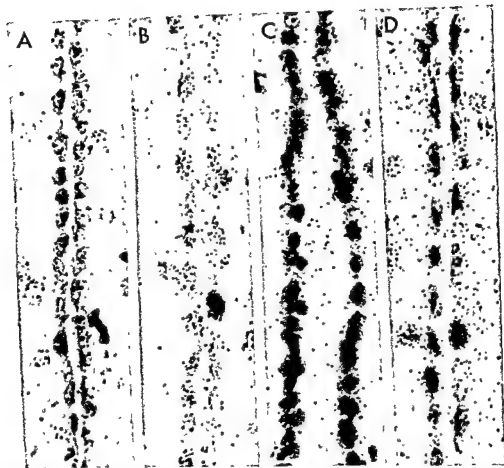


Fig. 9 Labeled cells in the endyma lining the caudal part of the third ventricle. $\times 600$. A. Adult animal that had been exposed to one injection of thymidine- H^3 on embryonic day 11. B. Adult animal exposed to thymidine H^3 on embryonic day 12. C. Adult animal exposed to thymidine- H^3 on embryonic day 13. D. Adult animal exposed to thymidine- H^3 on embryonic day 14.

basal nucleus and apical secretory granules). The hiatus between time of origin and time of morphological differentiation is much longer for certain other cell populations in the nervous system, e.g., Purkinje cells of the cerebellum (Miale and Sidman, '61).

Assessment of heavily labeled and lightly labeled cells

Since the subcommissural organ is small, has clear anatomical boundaries, and forms over only a few days, it is useful for the semiquantitative analysis of cell proliferation in a developing organ. As indicated in the Introduction, a major

problem is to assess whether or not some of the lightly labeled cells in adult specimens were engaged in their final period of DNA replication at the time of exposure to thymidine- H^3 . To render the following argument clear, it should be emphasized that the determination of cell birthdays is largely a statistical matter; the time and place of origin can be described for a population of labeled cells but cannot be determined accurately for any particular cell since individual cells are traced neither from one point in time to the next nor from one location to another. On a population basis, the intensity of labeling yields information about times and rates

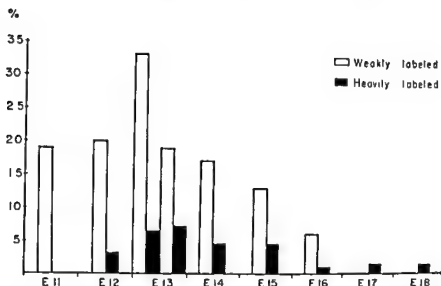


Fig. 10 Percentages of weakly and heavily labeled cells (labeled cells per 100 cells) in the same coronal sections of adult mouse brains utilized for figure 5. An additional E13 specimen is plotted here, as well as E16, E17 and E18 specimens. Scoring was based on examination of 500 consecutive cells in each specimen.

of cell genesis particularly if a series of specimens is available, each one exposed to thymidine- H^3 at a different embryonic stage.

In the case of the subcommissural organ, specimens exposed to thymidine- H^3 on the ninth or tenth days of gestation and examined at adulthood showed weak labeling, an indication that the subcommissural cell precursors probably were not yet in final division. With exposure to thymidine- H^3 on one of the subsequent several days, the numbers and relative proportions of weakly and strongly labeled cells changed systematically (fig. 5).

If the intensity of labeling was determined solely by the number of cell divisions in the interval between thymidine- H^3 injection and death, the number of weakly labeled cells in an adult specimen that had been exposed to thymidine- H^3 at any particular developmental stage should equal the sum of strongly labeled cells in a series of adult specimens each of which had been exposed once to thymidine- H^3 during one of the subsequent cell generation cycles. For example, if the cell generation time was 24 hours and cells were formed on embryonic days 11 through 15, the number of weakly labeled cells in an adult specimen injected on embryonic day 11 should equal the sum of strongly

labeled cells in adult specimens each of which had been injected on one of the subsequent four embryonic days. Similarly, the number of weakly labeled cells in the E12-adult specimen should equal the sum of strongly labeled cells in the E13-adult plus E14-adult plus E15-adult specimens; the number of weakly labeled cells in the E13-adult specimen should equal the number of strongly labeled cells in the E14-adult plus E15-adult specimens, and so on. On the final day during which cells become labeled, all cells should be strongly labeled.

These theoretical values are unlikely to be realized very often for a number of reasons, among them that the rate of DNA synthesis may not be uniform among different cells or throughout the synthesis period for a given cell; that some cells will be engaged in DNA synthesis for only part of the time that labeled precursor is available; that the size of the pool of DNA precursors molecules may not be constant; that activity of the kinase enzyme that catalyzes phosphorylation of exogenous thymidine may vary among cells; that the rate of degradation of exogenous thymidine may fluctuate; that nuclear size may vary among the cells (the grain counts are influenced by the concentration of DNA and by the ratio of nuclear diameter to section thickness); and that the

temporal spacing of the thymidine- H^3 injections is unlikely to match the cell generation cycles. A further factor of great importance is that younger embryos through the tenth and even the eleventh days tend to be less intensely labeled in general, the reasons being incompletely developed route of access through the placenta for thymidine- H^3 and perhaps the presence of larger pools of DNA precursors diluting the administered thymidine- H^3 at these early stages.

From a consideration of these limitations, one would predict that some cells would appear weakly labeled even though they had incorporated thymidine- H^3 during their final period of DNA synthesis. This prediction is borne out in the E15-adult specimen, where an average of four weakly labeled cells and four heavily la-

beled ones were recorded per section although none of them was destined to divide again (table 1 and fig. 5). These weakly labeled cells, along with the heavily labeled ones, must represent the population that was engaged in final nuclear DNA synthesis on E15. How many of the weakly labeled cells in adult specimens that had been exposed to thymidine- H^3 on earlier embryonic days also represent cells that were in final period of DNA synthesis? By calculating backwards from E15 one day at a time ("calculated" columns of table 3), it could be assumed that the average of 8.6 labeled cells per section in the E15-adult specimen must have been represented by 4.3 weakly labeled cells in the E14-adult specimen. By subtraction, the number of weakly labeled cells in final division in the E14-adult specimen was $9.4 - 4.3 =$

TABLE 3

Calculations based on relative numbers of labeled cells in adult subcommissural organs after thymidine- H^3 injection at different embryonic stages

Injected on embryonic day	Column a weakly labeled cells	Column b strongly labeled cells	Column c (equals a + b) total	Calculated			
				Dividing cells	Nondividing cells		
				Column d (equals c/2 in the row below) weakly labeled cells	Column e (equals a - d) weakly labeled cells	Column f (equals Col. b) strongly labeled cells	Column g (equals e + f) total
E9	0.0	0.0	0.0				
E10	23.0	0.0	23.0	(65.3)			
E11	124.2	6.4	130.6	43.0	81.2	6.4	87.6
E12	52.0	34.0	86.0	37.8	14.2	34.0	48.2
E13	41.0	34.5	75.5	10.7	30.3	34.5	64.8
E14	9.4	12.0	21.4	4.3	5.1	12.0	17.1
E15	4.4	4.2	8.6	0.0	4.4	4.2	8.6
E16	0.0	0.0	0.0	0.0	0.0	0.0	0.0
Total		91.1					226.3

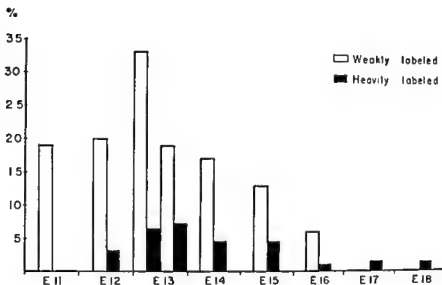


Fig. 10 Percentages of weakly and heavily labeled cells (labeled cells per 100 cells) in the same coronal sections of adult mouse brains utilized for figure 5. An additional E13 specimen is plotted here, as well as E16, E17 and E18 specimens. Scoring was based on examination of 500 consecutive cells in each specimen.

of cell genesis particularly if a series of specimens is available, each one exposed to thymidine- H^3 at a different embryonic stage.

In the case of the subcommissural organ, specimens exposed to thymidine- H^3 on the ninth or tenth days of gestation and examined at adulthood showed weak labeling, an indication that the subcommissural cell precursors probably were not yet in final division. With exposure to thymidine- H^3 on one of the subsequent several days, the numbers and relative proportions of weakly and strongly labeled cells changed systematically (fig. 5).

If the intensity of labeling was determined solely by the number of cell divisions in the interval between thymidine- H^3 injection and death, the number of weakly labeled cells in an adult specimen that had been exposed to thymidine- H^3 at any particular developmental stage should equal the sum of strongly labeled cells in a series of adult specimens each of which had been exposed once to thymidine- H^3 during one of the subsequent cell generation cycles. For example, if the cell generation time was 24 hours and cells were formed on embryonic days 11 through 15, the number of weakly labeled cells in an adult specimen injected on embryonic day 11 should equal the sum of strongly

labeled cells in adult specimens each of which had been injected on one of the subsequent four embryonic days. Similarly, the number of weakly labeled cells in the E12-adult specimen should equal the sum of strongly labeled cells in the E13-adult plus E14-adult plus E15-adult specimens; the number of weakly labeled cells in the E13-adult specimen should equal the number of strongly labeled cells in the E14-adult plus E15-adult specimens, and so on. On the final day during which cells become labeled, all cells should be strongly labeled.

These theoretical values are unlikely to be realized very often for a number of reasons, among them that the rate of DNA synthesis may not be uniform among different cells or throughout the synthesis period for a given cell; that some cells will be engaged in DNA synthesis for only part of the time that labeled precursor is available; that the size of the pool of DNA precursors molecules may not be constant; that activity of the kinase enzyme that catalyzes phosphorylation of exogenous thymidine may vary among cells; that the rate of degradation of exogenous thymidine may fluctuate; that nuclear size may vary among the cells (the grain counts are influenced by the concentration of DNA and by the ratio of nuclear diameter to section thickness); and that the

- Isomaki, A. M., E. Kivalo and S. Talanti 1965 Electron-microscopic structure of the subcommissural organ in the calf (*Bos taurus*) with special reference to secretory phenomena. *Ann. Acad. Scient. Fenn.*, 111: 1-64.
- Johnston, A. M., and J. B. Angevine 1966 Autoradiographic study of neuron origin in the diencephalon in the mouse. *Anat. Rec.*, 154: 363.
- Jordan, H. 1925 The structure and staining reactions of the Reissner's fiber apparatus, particularly the subcommissural organ. *Am. J. Anat.*, 34: 427-444.
- Langman, J., R. L. Guerrant and B. G. Freeman 1966 Behavior of neuroepithelial cells during closure of the neural tube. *J. Comp. Neur.*, 127: 339-411.
- Leblond, C. P. 1964 Classification of cell populations on the basis of their proliferative behavior. *Natl. Cancer Inst., Monograph* 14: 119-150.
- Miale, I. L., and R. L. Sidman 1961 An autoradiographic analysis of histogenesis in the mouse cerebellum. *Exptl. Neurol.*, 4: 277-296.
- Pierce, E. T. 1966 Histogenesis of the nuclei griseum pontis, corporis pontobulbaris and reticularis tegmenti pontis (Bechterew) in mouse. An autoradiographic study. *J. Comp. Neur.*, 126: 219-239.
- Rakic, P. 1965 Mesocoelic recess in the human brain. *Neurology*, 15: 708-715.
- Ramon y Cajal, S., and F. de Castro 1933 Elementos de técnica micrographica del sistema nervioso. *Tipografia Artistica*, Madrid, p. 103.
- Reissner, T. 1860 Beiträge zur Kenntniss vom Bau des Rückenmarkes von *Petromyzon fluviatilis*. *Arch. Anat. Physiol.*, pp. 445-588.
- Ruben, R. J. 1967 Development of the inner ear of the mouse: An autoradiographic study of terminal mitosis. *Acta Oto-laryng. Supp.*, 220: 1-44.
- Sidman, R., I. L. Miale and N. Feder 1959 Cell proliferation and migration in the primitive ependymal zone; an autoradiographic study of histogenesis in the nervous system. *Exptl. Neurol.*, 1: 322-333.
- Sidman, R. 1961 Histogenesis of mouse retina studied with thymidine- H^3 . In: *Structure of the Eye* (G. Smelser, ed.) Academic Press, New York, pp. 487-506.
- Schmidt, W. R., and A. N. D'Agostino 1966 The subcommissural organ of the adult rabbit: An electron microscopic study. *Neurology*, 16: 373-379.
- Talanti, S. 1958 Studies on the subcommissural organ in some domestic animals. *Ann. Med. Exp. Biol. Fenn., Supplement* 9: 1-97.
- Wislocki, G. B., and E. H. Leduc 1952 The cytology and histochemistry of the subcommissural organ and Reissner's fiber in rodents. *J. Comp. Neur.*, 97: 515-544.
- 1954 The cytology of the subcommissural organ, Reissner's fiber, periventricular glial cells and posterior collicular recess of the rat's brain. *J. Comp. Neur.*, 101: 238-309.
- Wislocki, G. B., E. H. Leduc and A. J. Mitchell 1956 On the ending of Reissner's fiber in the filum terminale of the spinal cord. *J. Comp. Neur.*, 104: 493-518.
- Wislocki, G. B., and W. D. Roth 1958 Selective staining of the human subcommissural organ. *Anat. Rec.*, 130: 125-134.

5.1 cells per section. There were also 12.0 heavily labeled cells per section in that specimen. The total of 21.4 labeled cells per section in turn must have been generated by 11 weakly labeled cells in the E13-adult specimens, and so on as charted in columns d to f of table 3. In this way, the weakly labeled population of each day can be assigned to dividing and nondividing categories.

A striking conclusion that emerges from these calculations is that 38% (87.6/226.3) of the subcommissural cells arise on E11, even though relatively few cells were strongly labeled (the usual criterion for the "birthday") in the E11-adult specimen. If only the strongly labeled cells had been considered in assigning birthdays, the conclusion would have been reached that a mere 7% (6.4/91.1) of the subcommissural cells arise on embryonic day 11. The numerical values calculated in table 3 are probably inaccurate, for they depend on the precision of the low counts in the E15-adult specimen and also imply a constant cell generation cycle of 24 hours. However, the general conclusion seems inescapable that the weakly labeled population of cells must be grouped into nondividing and dividing categories before the relative number of cells arising on each day of development can be estimated accurately.

Certain other errors skew the numbers. The lightly labeled population is underestimated if some cells are subthreshold; for example, the calculated value of 65 weakly labeled cells in the E10-adult specimen (table 3, column d) was grossly under-represented in the actual counts because the concentration of thymidine- H^3 reaching embryonic cell nuclei is relatively low at E10, a very early developmental stage. Further, in the interval between E10 and adulthood many cells will have dropped below our arbitrary threshold of five silver grains per nucleus due to numerous divisions. Another numerical error arises if cells that have divided more than once are classed in the "heavily labeled" category, as is likely when long exposure times are used in preparing the autoradiograms; most of the slides in the present study were exposed for long times

to facilitate the tracing of cell migration paths in other parts of the nervous system. Finally, sampling errors occur. For example, we found no labeled ependymal cells in the specimen injected with thymidine- H^3 on E18 and killed at adulthood, but occasional cells forming at this time or later might have been recognized if more than 500 cells had been counted in each specimen.

Despite these limitations, it appears that the autoradiographic method offers a reasonable, semiquantitative account of the day-to-day proliferative behavior of cells during embryonic formation of a circumscribed, stable organ. Additional new methods for the calculation of cell turnover rates based on labeling indices and grain counts in thinly sectioned autoradiograms have been presented in the course of studies on Schwann cell proliferation in the peripheral nervous system of the neonatal mouse (Asbury, '67).

LITERATURE CITED

- Altman, J. 1966 Proliferation and migration of undifferentiated precursor cells in the rat during postnatal gliogenesis. *Exptl. Neurol.*, 16: 263-278.
- Angewine, J. 1965 Time of neuron origin in the hippocampal region; an autoradiographic study in the mouse. *Exptl. Neurol.*, Supplement 2: 1-70.
- Asbury, A. K. 1967 Schwann cell proliferation in developing mouse sciatic nerve. A radioautographic study. *J. Cell Biol.*, 34: 735-743.
- Bauer-Jokl, M. 1917 Über das sogenannte Subcommissuralorgan. *Arb. a.d. Neurol. Inst. a.d. Univ. Wien.*, 22: 41-79.
- Brown, D., and A. K. Afti 1965 Histological and ablation studies on the relation of the subcommissural organ and rostral midbrain to sodium and water metabolism. *Anat. Rec.*, 153: 255-264.
- Fujita, H., and S. Fujita 1964 Electron microscopic studies on the differentiation of the ependymal cells and the glioblast in the spinal cord of domestic fowl. *Z. Zellforsch.*, 64: 262-272.
- Gilbert, G. J. 1956 The subcommissural organ. *Anat. Rec.*, 126: 253-266.
- 1957 The subcommissural organ: A regulator of thirst. *Am. J. Physiol.*, 191: 243-247.
- 1958 Subcommissural organ secretion in the dehydrated rat. *Anat. Rec.*, 132: 563-568.
- Herman, C., and S. L. Kauffman 1966 The fine structure of the embryonic mouse neural tube with special reference to cytoplasmic microtubules. *Devel. Biol.*, 13: 145-162.

- Isomaki, A. M., E. Kivalo and S. Talanti 1965 Electron-microscopic structure of the subcommissural organ in the calf (*Bos taurus*) with special reference to secretory phenomena. *Ann. Acad. Scient. Fenn.*, 111: 1-64.
- Johnston, A. M., and J. B. Angevine 1966 Autoradiographic study of neuron origin in the diencephalon in the mouse. *Anat. Rec.*, 154: 363.
- Jordan, H. 1925 The structure and staining reactions of the Reissner's fiber apparatus, particularly the subcommissural organ. *Am. J. Anat.*, 34: 427-444.
- Langman, J., R. L. Guerrant and B. G. Freeman 1966 Behavior of neuroepithelial cells during closure of the neural tube. *J. Comp. Neur.*, 127: 339-411.
- Leblond, C. P. 1964 Classification of cell populations on the basis of their proliferative behavior. *Natl. Cancer Inst., Monograph 14*: 119-150.
- Miale, I. L., and R. L. Sidman 1961 An autoradiographic analysis of histogenesis in the mouse cerebellum. *Exptl. Neurol.*, 4: 277-296.
- Pierce, E. T. 1966 Histogenesis of the nuclei griseum pontis, corporis pontobulbaris and reticularis tegmenti pontis (Bechterew) in mouse. An autoradiographic study. *J. Comp. Neur.*, 126: 219-239.
- Rakic, P. 1965 Mesocoelic recess in the human brain. *Neurology*, 15: 708-715.
- Ramon y Cajal, S., and F. de Castro 1933 Elementos de tecnica micrographica del sistema nervioso. *Tipografia Artistica, Madrid*, p. 103.
- Reissner, T. 1860 Beiträge zur Kenntniss vom Bau des Rückenmarkes von *Petromyzon fluviatilis*. *Arch. Anat. Physiol.*, pp. 445-588.
- Ruben, R. J. 1967 Development of the inner ear of the mouse: An autoradiographic study of terminal mitosis. *Acta Oto-laryng. Supp.*, 220: 1-44.
- Sidman, R., I. L. Miale and N. Feder 1959 Cell proliferation and migration in the primitive ependymal zone; an autoradiographic study of histogenesis in the nervous system. *Exptl. Neurol.*, 1: 322-333.
- Sidman, R. 1961 Histogenesis of mouse retina studied with thymidine-H³, In: *Structure of the Eye* (G. Smelser, ed.) Academic Press, New York, pp. 487-506.
- Schmidt, W. R., and A. N. D'Agostino 1966 The subcommissural organ of the adult rabbit: An electron microscopic study. *Neurology*, 16: 373-379.
- Talanti, S. 1958 Studies on the subcommissural organ in some domestic animals. *Ann. Med. Exp. Biol. Fenn., Supplement 9*: 1-97.
- Wislocki, G. B., and E. H. Leduc 1952 The cytology and histochemistry of the subcommissural organ and Reissner's fiber in rodents. *J. Comp. Neur.*, 97: 515-544.
- 1954 The cytology of the subcommissural organ, Reissner's fiber, periventricular glial cells and posterior collicular recess of the rat's brain. *J. Comp. Neur.*, 101: 238-309.
- Wislocki, G. B., E. H. Leduc and A. J. Mitchell 1956 On the ending of Reissner's fiber in the filum terminale of the spinal cord. *J. Comp. Neur.*, 104: 493-518.
- Wislocki, G. B., and W. D. Roth 1958 Selective staining of the human subcommissural organ. *Anat. Rec.*, 130: 125-134.

The Effects of Essential Fatty Acid Deficiency on the Skin of the Mouse^{1,2}

DAVID N. MENTON³

*Division of Biological and Medical Sciences,
Brown University, Providence, Rhode Island*

ABSTRACT Mice raised from weaning on a diet free of essential fatty acids (EFA) developed a syndrome involving scaliness and inelasticity of the skin with extensive loss of hair. Histologically, the epidermis of EFA-deficient mice became noticeably thicker within as few as ten days on the diet and reached a maximum thickness in all strata of the epidermis by 50 days. Animals on the same diet supplemented with 50 mg of purified linoleic acid every other day developed none of the symptoms of deficiency. Mitotic counts on whole-mounted epidermal sheets split from the foot pads of EFA-deficient and linoleic acid-supplemented mice revealed significantly greater mitotic activity in the deficient animals. Histochemical activity for succinic dehydrogenase and cytochrome oxidase was more intense and extensive in the lower stratum Malpighii of the deficient animals than in controls. Acid phosphatase activity also was more intense in the stratum granulosum of deficient animals. These observations are interpreted to indicate that in the mouse cellular proliferation and differentiation of the epidermis are accelerated by essential fatty acid deficiency.

A dietary requirement for certain unsaturated fats, such as linoleic acid, was first reported in rats by Burr and Burr ('29). These authors described a syndrome associated with fat deficiency that included abnormally scaly skin, loss of hair, inflammation and swelling in the hind feet, and necrosis of the tail. All of these could be reversed by the addition of a small amount of fat, such as lard, to the diet. Subsequently, a requirement for essential fatty acids (EFA) has been demonstrated in many species, including man (reviewed by Aaes-Jørgensen, '61).

The histology of the skin of an EFA-deficient animal was first described in the rat by Williamson ('41). The epidermis was thicker and showed "greater differentiation" than that of a normal rat. More detailed studies were carried out by Ramalingaswami and Sinclair ('51, '53) on rats, and by Hansen et al. ('51) on dogs. These investigators reported scaling and hypertrophy of the epidermis, keratotic plugging of hair follicles and sebaceous glands, fragmentation of dermal collagen and round-cell infiltration of the dermis. In addition, there is an increase in the rate of transepidermal water loss (Basnayake and Sinclair, '54; Macmillan and Sinclair, '58; Vinson et al., '61).

The epidermal hypertrophy resulting from EFA-deficiency has been attributed variously to (1) failure of the stratum corneum to shed normally, (2) slow and incomplete keratinization, and (3) increased production of cells in the stratum basale. According to the classification of Messier and Leblond ('60), the epidermis is a renewing tissue; i.e., cells are lost at a rate which equals cellular proliferation in a special germinative area. Epidermal hyperplasia of deficient animals could, therefore, result from either an increase in mitotic activity or a diminution in epidermal differentiation and exfoliation. Hansen et al. ('51) reported parakeratosis (nuclei in stratum corneum) in deficient dogs, indicating an incomplete differentiation of the stratum corneum. Ramalingaswami and Sinclair ('53) and Vinson et al. ('61) observed no obvious differences in mitotic activity in the epidermis between normal and deficient rats, whereas Hansen et al. ('51) and Kingery and Kellum ('65) reported an apparent increase in mitotic

¹Supported by Research Training grant STL-GM-00582-05 from the United States Public Health Service.

²The data contained in this paper are from a thesis submitted by the author to the Graduate School of Brown University in partial fulfillment of the requirements for the degree of Doctor of Philosophy.

³Present address: Department of Anatomy, Washington University School of Medicine, St. Louis, Missouri.

After this the epidermis was gently dissected away from the dermis. The epidermal sheets were then placed in Serra's fixative for one hour and stained by the Feulgen technique. Finally the stained epidermal sheets were placed between microscope slides to prevent curling, dehydrated, cleared, and mounted with the basal layer up to facilitate observing the mitotic figures. Mitotic figures were counted with the oil immersion lens in 40 randomly selected fields from each foot pad. Each field was delimited by an ocular reticle that divided the field into 36 squares to facilitate counting.

OBSERVATIONS

Body weight. The average weights of 48 EFA-deficient and 51 linoleic acid-supplemented male mice, evaluated at weekly intervals, are shown in figure 1. The weights of females were similar but slightly lower. During the first four weeks on the diet, deficient animals gained weight at least as fast as supplemented controls, but from four weeks on, they fell behind in growth and reached a plateau during the fifth to sixth week. After ten weeks the deficient

animals began to lose weight and most had died by 20 weeks. Surprisingly, deficient animals ate voraciously until death. Most striking, however, was the increase in daily water consumption, nearly twice that of the supplemented controls, by 120 days on the diet (fig. 2). The growth and water consumption of supplemented animals was almost the same as that of animals fed standard laboratory feed.

Deficient mice were infertile, whereas linoleic acid-supplemented mice produced normal litters. Post mortem examination of deficient animals revealed fatty infiltration of the liver, especially during the first 40 to 50 days. Unlike the findings of Ramalingaswami and Sinclair ('53) in rats, there was little subcutaneous or coelomic fat in deficient mice. Mice that were on the deficient diet for over 60 days had distended stomachs filled with undigested or partially digested food.

Gross changes in the skin. The first evidence of EFA deficiency developed after 30 days on the diet, as a general matting and disorientation of the fur. These changes usually appeared sooner in females than in males.

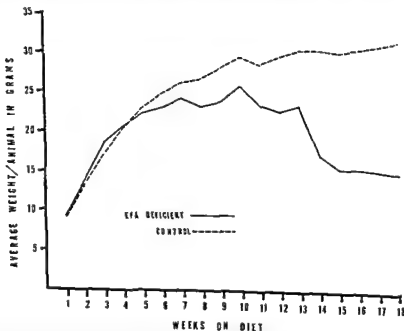


Fig. 1 Average growth curves of mice on a diet deficient in essential fatty acids and controls supplemented with linoleic acid.

activity in the epidermis of deficient dogs and rats. None of those authors reported making counts of mitotic figures.

This investigation was undertaken to evaluate the effects of essential fatty acid deficiency on the mitotic activity of the epidermis and to define further the effects of the deficiency on the morphology and histochemistry of the skin of mice.

MATERIALS AND METHODS

Caging and diet. Two hundred mice of the inbred BUA strain were used in the course of this study. Siblings of the same sex were housed in plastic cages with two to four animals per cage. A coarse wire screen, elevated one inch above the floor, was provided to minimize coprophagy, because Sinclair ('30) reported that feces from rats on fat-deficient diets may contain polyenoic fatty acids. Animals were kept in an air-conditioned room where the temperature was maintained at $78 \pm 2^\circ\text{F}$ and the relative humidity at about 45%. Lighting was controlled automatically for a 12-hour light period each 24 hours.

The EFA-deficient diet used in this study was based on that of Aaes-Jørgensen et al. ('56) (table 1). Litters were weaned and placed on the diet when the young weighed about ten grams. Half of each litter was fed the EFA-deficient diet and the other half was fed the deficient diet plus a supplement of 50 mg of highly purified linoleic acid administered every other day by

gavage. All animals received water and diet *ad libitum*, were weighed weekly, and were inspected frequently for gross manifestations of EFA deficiency.

Histology and histochemistry. Histologic and histochemical examinations were made of skin from the ear, back, belly, foot pad, tail, and throat from both deficient and linoleic acid-supplemented male and female mice. Specimens for histologic study were taken from 12 litters killed at ten-day intervals from ten to 120 days on the diet. Enzymatic activity was studied in three litters that were on the diet 25, 40 and 80 days. All animals were killed by cervical fracture at about 3:00 PM, the hair was clipped where necessary and the appropriate specimens of skin excised. Tissues for histologic study were fixed in Bouin's fluid and paraffin sections were stained with Delafield's hematoxylin and eosin, Van Gieson's connective tissue stain, Verhoeff's stain for elastic fibers, and Laidlaw's diamine silver carbonate method for reticular fibers. Tissues for histochemical study were frozen in dry ice or fixed in cold chlorohydrate formalin (Fishman and Baker, '56) and frozen sections were cut 40μ thick in a cryostat, dried briefly on slides, and processed for succinic dehydrogenase (Farber and Louviere, '56), cytochrome oxidase (Burstone, '60), acid phosphatase (Burstone, '58), and for metachromasia with toluidine blue.

Mitotic counts. Mitotic activity was evaluated in nine pairs of male EFA-deficient and linoleic acid-supplemented siblings that were on the diet for 10, 25, 30, 35, 40, 50, 70, 80 and 90 days respectively. All animals were given 0.1 mg of desacetylmethylcolchicine (derivative of colchicine; Colcemide, Ciba) in 0.25 ml of 0.85% saline subcutaneously five hours before killing at 3:00 PM, in order to arrest mitotic division during the peak of diurnal mitotic activity (Cooper and Franklin, '40). The hairless foot pad was used in order to avoid the possible effect of hair growth on mitotic activity (Chase et al., '53). The epidermis of the right hind foot pad was split from the dermis by a modification of the technique of Staricco and Pinkus ('57). Immediately after excision, the entire foot pad was placed in 0.2 M sodium bromide at 40°C for one-half hour.

TABLE 1

Percentage composition of the essential fatty acid-deficient diet

	%
Casein and vitamin mixture ¹	20.5
Sucrose	46.0
Salt mixture no. 2 ²	5.0
Choline methionine tartrate	0.5
Hydrogenated arachis oil ³	28.0

¹ The casein and vitamin mixture consisted of the following amounts of vitamins per 1000 gm of vitamin free casein: biotin, 2.5 mg; folic acid, 2.5 mg; p-aminobenzoic acid, 1750 mg; thiamine hydrochloride, 250 mg; pyridoxine hydrochloride, 250 mg; riboflavin, 250 mg; calcium pantothenate, 250 mg; nicotinic acid, 400 mg; inositol, 750 mg; ascorbic acid, 250 mg; vitamin B₁₂, 7.5 μ g; menadione, 5 mg; alpha-tocopherol, 250 mg; vitamin A₁, 1 mg; and vitamin D₃ (Calciferol), 0.2 mg. The lipid-soluble vitamins were dissolved in ether and sprayed over the casein-vitamin mixture.

² From Nutritional Biochemical Company, Cleveland, Ohio.

³ STA NUTS XX, Durkee Famous Foods, Chicago, Illinois.

TABLE 2
The development of cutaneous manifestations of EPA-deficiency

Days on diet	Gross appearance	Stratum corneum	Stratum granulosum	Stratum Malpighi	Adnexa	Dermis
Control	Normal	Normal thickness	Indefinite	1-2 layers	Normal	Normal
10	Normal	Normal thickness	Indefinite	Occasional slight thickening	Normal	Normal
20	Normal	Slightly thickened	1-2 layers, some granules	2-3 layers	Normal	Slightly thickened
30	Fur dull, slightly dishevelled Slight inelasticity	Twice as thick as control	2 layers many granules	3-4 layers Increased intercellular space Many mitotic figures	Outer root sheath of hair thickened Slightly hypertrophic sebaceous glands	Thickened and edematous Cellular infiltration Abundant elastic fibers
40	Fur matted Hair loss Scaliness Moderate inelasticity	Three times as thick as control	3-4 layers packed with granules	4-5 layers Wide intercellular space High mitotic activity	Few growing hair follicles Hypertrophic sebaceous glands	Greatly thickened Extensive cellular infiltration
50	Hair loss Fur wet and matted Scaling Loss of elasticity	Threes to four times as thick as control	Same as above	6-7 layers with wide intercellular spaces, larger separations in basal layer	No growing hair follicles	Same as above

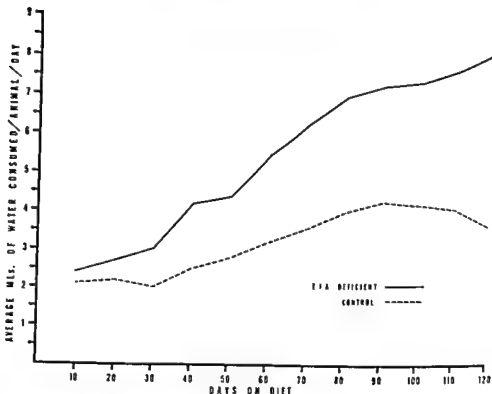


Fig. 2 Average water consumption of mice on a diet deficient in essential fatty acids and controls supplemented with linoleic acid.

After 40 days on the deficient diet, cutaneous changes became more pronounced. There was loss of the normal hair sheen, darkening and wrinkling of the ears, and an increase in the visibility of their blood vessels. Skin lost elasticity as indicated by the appearance of a fold of skin between the fore and hind limbs when animals were suspended by their tails (fig. 4).

After 50 days on the diet, the skin of the deficient animals developed a scaly appearance and transverse creases in the ventral thoracic and abdominal skin (fig. 4). Hair loss was especially noticeable on the back (fig. 5) and in those areas such as the throat and head, which were continuously abraded by the food cups. Plucked hair did not regrow.

As the deficiency progressed, hair loss and scaling became more extensive and the fur appeared constantly wet (fig. 5). Deficient animals frequently scratched themselves, and even the most inconspicuous wounds failed to heal. There was a leathery inelasticity of the skin that made it difficult to pick the animals up by the nape of the neck, and the skin could be torn readily with a probe. Erythema was

observed occasionally in the conjunctiva and in the anogenital region.

Histology of the skin. No appreciable difference developed between control mice supplemented with linoleic acid and mice fed Purina Laboratory Chow, or between males and females. During 50 days on the EFA-deficient diet, the epidermis of all areas studied became progressively more hyperplastic with a concomitant thickening and cellular infiltration of the dermis (table 2).

The first histologically detectable alterations developed in the ears. Within ten days on the diet, the epidermis appeared slightly thicker than that of control mice, which had one or two layers of cells in the stratum Malpighii and one or two layers of cells in the stratum granulosum. After 20 days on the deficient diet, the stratum Malpighii of the ear was three layers thick with two or three layers in the stratum granulosum (figs. 6, 7). Cells of the stratum Malpighii were separated by a slightly wider space than in the normal ear and the stratum corneum of deficient animals was at least twice as thick as that of controls. At 20 days epidermal thickening

TABLE 2
The development of cutaneous manifestations of EFA-deficiency

Days on diet	Gross appearance	Stratum corneum	Stratum granulosum	Stratum Malpighi	Adnexa	Dermis
Control	Normal	Normal thickness	Indefinite	1-2 layers	Normal	Normal
10	Normal	Normal thickness	Indefinite	Occasional slight thickening	Normal	Normal
20	Normal	Slightly thickened	1-2 layers, some granules	2-3 layers	Normal	Slightly thickened
30	Fur dull, slightly dishevelled Slight inelasticity	Twice as thick as control	2 layers many granules	3-4 layers Increased intercellular space Many mitotic figures	Outer root sheath of hair thickened Slightly hypertrophic sebaceous glands	Thickened and edematous Cellular infiltration Abundant elastic fibers
40	Fur matted Hair loss Scaliness Moderate inelasticity	Three times as thick as control	3-4 layers packed with granules	4-5 layers Wide intercellular space High mitotic activity	Few growing hair follicles Hypertrophic sebaceous glands	Greatly thickened Extensive cellular infiltration
50	Hair loss Fur wet and matted Scaling Loss of elasticity	Three to four times as thick as control	Same as above	6-7 layers with wide intercellular spaces, larger separations in basal layer	No growing hair follicles	Same as above

was also noticeable for the first time in other areas such as the back, belly, lip and throat.

By 30 days on the deficient diet, epidermis from all areas examined was considerably more hyperplastic than at 20 days and had a well-developed stratum granulosum. The ear epidermis, for example, had four layers of cells in the stratum Malpighii, three layers in the stratum granulosum, and a thick stratum corneum (compare figs. 8, 9). Hyperplasia was especially pronounced around hair follicles. The outer root sheaths of hair follicles also were thickened above the level of the sebaceous glands. An uncommonly large number of mitotic figures, limited to the basal layer, was apparent in the epidermis of deficient animals (fig. 9). Mitotic figures also appeared with greater frequency in the slightly hypertrophic sebaceous glands of deficient mice than in controls. The dermis of the deficient animals was slightly hypertrophic and infiltrated with cells (fig. 9).

By 40 days on the diet, epidermis of the ear and foot pad had reached maximum thickness, with six or seven layers of cells in the stratum Malpighii and three or four in the stratum granulosum. The stratum Malpighii of the belly and back was four or five cell layers thick with three or four layers of cells in the stratum granulosum (compare figs. 10, 11). The well-defined granular layer of the epidermis of deficient animals was filled with basophilic keratohyalin granules (fig. 12), whereas the epidermis from these areas in control animals lacked a granular layer. The cells of the stratum Malpighii from deficient mice were widely separated and of a pricked type (fig. 12). Growing hair follicles were rarely observed at 40 days on the deficient diet. The dermis from deficient animals was much thicker than in control animals and had an intense infiltration of round cells, among which lymphocytes and mast cells were particularly abundant. The latter cells were filled with metachromatic granules after staining with toluidine blue. Collagenous bundles appeared swollen and disoriented, and elastic and reticular fibers were abundant in the dermis of deficient mice. Subcutaneous fat was diminished. Hypertrophy of the sebaceous glands and

paucity of hypodermal fat were observed in all skin specimens (compare figs. 10, 11).

No further increase in epidermal thickness occurred after 50 days on the deficient diet, at which time all skin specimens had six or seven layers of cells in the stratum Malpighii and three or four layers of cells in the stratum granulosum. Large spaces frequently appeared between the cells of the basal layer (fig. 13). Cellular invasion of the dermis was particularly pronounced in the abraded areas of the throat of deficient mice. Keratinized material often closely invested the hair shafts in the region of the follicle and distal to the sebaceous gland. Even at this late stage of deficiency, no parakeratosis was present in the stratum corneum. Growing hair follicles never were observed in deficient animals after 90 days on the diet.

If deficient animals were given supplements of linoleic acid after 50 days on the diet, all manifestations of the deficiency disappeared within 30 days. For example, hair growth, in both plucked and denuded areas, began by at least 15 days and was complete by 30 days. Supplementing the deficient diet with oleic acid, an unsaturated but non-essential fatty acid, delayed but did not prevent the manifestations of EFA-deficiency.

Mitotic activity in skin. Within 30 days on the diet, the epidermis from deficient animals appeared to have an increased number of mitotic figures. In epidermal sheets split from the foot pads of deficient and supplemented animals, the population of mitotic figures was not homogeneously distributed, but occurred in clusters. Figure 14 shows the typical "C" mitotic figures produced by Colcemide treatment, at the magnification at which they were counted. Mitotic counts revealed a higher incidence of mitotic figures (1% level of significance) in deficient mice than in supplemented controls from as early as ten days to as late as 80 days on the diet, after which mitotic activity in deficient animals fell to normal levels (fig. 3).

Histochemical observations. Histochemical changes in both succinic dehydrogenase and cytochrome oxidase were evident in skin of deficient mice within 25 days on the diet. In supplemented controls, homogeneously distributed reaction products of

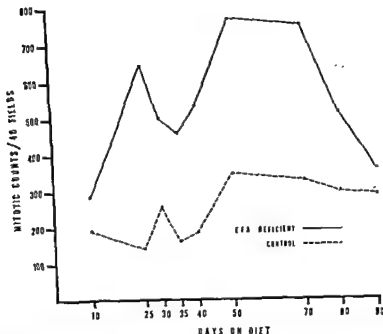


Fig. 3 Average counts of mitotic figures in 40 randomly selected fields in foot pad skin of mice on a diet supplemented or deficient in essential fatty acids, injected with Colcemide five hours prior to death.

succinic dehydrogenase and cytochrome oxidase were moderately concentrated in the stratum basalis and diminished toward the stratum corneum. Sebaceous glands had a granular deposit of reaction products (fig. 15) and the panniculus carnosus had intense enzyme activity (fig. 16). In the epidermis of mice on the deficient diet for 25 days, there was an increase in the breadth and intensity of the reactive zone for both enzymes. This became more pronounced after 40 days when intense activity was observed in the entire Malpighian and granular layers, being most intense in the lower three layers of cells in the stratum Malpighii (compare figs. 15, 16). At 80 days on the diet, hyperplastic epidermis in all skin areas still showed activities for both enzymes more intense than in controls (compare figs. 17, 18).

Unlike succinic dehydrogenase and cytochrome oxidase, acid phosphatase was limited to the transitional zone between the stratum granulosum and the stratum corneum in epidermis of control mice (fig. 19). At 25 days, differences between acid

phosphatase activity in the deficient and control animals were minimal, but at 40 days there was a striking increase in breadth and intensity of the acid phosphatase zone (compare figs. 19, 20). The reaction product in deficient mice filled the entire stratum granulosum and extended into the lower stratum corneum. Acid phosphatase activity also was evident in sebaceous glands, in the more centrally located cells near the excretory duct in both deficient and control animals, but was more intense in the deficient animals (figs. 19, 20). Acid phosphatase activity decreased in intensity in the epidermis of deficient animals after 80 days on the diet.

DISCUSSION

Although many investigators have started weanling animals on fat-deficient diets at a given age, it seemed apparent in the course of this study that the weight of mice at weaning affected the time of appearance of deficiency symptoms more than the age; i.e., small weanlings developed symptoms earlier than relatively

was also noticeable for the first time in other areas such as the back, belly, lip and throat.

By 30 days on the deficient diet, epidermis from all areas examined was considerably more hyperplastic than at 20 days and had a well-developed stratum granulosum. The ear epidermis, for example, had four layers of cells in the stratum Malpighii, three layers in the stratum granulosum, and a thick stratum corneum (compare figs. 8, 9). Hyperplasia was especially pronounced around hair follicles. The outer root sheaths of hair follicles also were thickened above the level of the sebaceous glands. An uncommonly large number of mitotic figures, limited to the basal layer, was apparent in the epidermis of deficient animals (fig. 9). Mitotic figures also appeared with greater frequency in the slightly hypertrophic sebaceous glands of deficient mice than in controls. The dermis of the deficient animals was slightly hypertrophic and infiltrated with cells (fig. 9).

By 40 days on the diet, epidermis of the ear and foot pad had reached maximum thickness, with six or seven layers of cells in the stratum Malpighii and three or four in the stratum granulosum. The stratum Malpighii of the belly and back was four or five cell layers thick with three or four layers of cells in the stratum granulosum (compare figs. 10, 11). The well-defined granular layer of the epidermis of deficient animals was filled with basophilic keratohyalin granules (fig. 12), whereas the epidermis from these areas in control animals lacked a granular layer. The cells of the stratum Malpighii from deficient mice were widely separated and of a pricked type (fig. 12). Growing hair follicles were rarely observed at 40 days on the deficient diet. The dermis from deficient animals was much thicker than in control animals and had an intense infiltration of round cells, among which lymphocytes and mast cells were particularly abundant. The latter cells were filled with metachromatic granules after staining with toluidine blue. Collagenous bundles appeared swollen and disoriented, and elastic and reticular fibers were abundant in the dermis of deficient mice. Subcutaneous fat was diminished. Hypertrophy of the sebaceous glands and

paucity of hypodermal fat were observed in all skin specimens (compare figs. 10, 11).

No further increase in epidermal thickness occurred after 50 days on the deficient diet, at which time all skin specimens had six or seven layers of cells in the stratum Malpighii and three or four layers of cells in the stratum granulosum. Large spaces frequently appeared between the cells of the basal layer (fig. 13). Cellular invasion of the dermis was particularly pronounced in the abraded areas of the throat of deficient mice. Keratinized material often closely invested the hair shafts in the region of the follicle and distal to the sebaceous gland. Even at this late stage of deficiency, no parakeratosis was present in the stratum corneum. Growing hair follicles never were observed in deficient animals after 90 days on the diet.

If deficient animals were given supplements of linoleic acid after 50 days on the diet, all manifestations of the deficiency disappeared within 30 days. For example, hair growth, in both plucked and denuded areas, began by at least 15 days and was complete by 30 days. Supplementing the deficient diet with oleic acid, an unsaturated but non-essential fatty acid, delayed but did not prevent the manifestations of EFA-deficiency.

Mitotic activity in skin. Within 30 days on the diet, the epidermis from deficient animals appeared to have an increased number of mitotic figures. In epidermal sheets split from the foot pads of deficient and supplemented animals, the population of mitotic figures was not homogeneously distributed, but occurred in clusters. Figure 14 shows the typical "C" mitotic figures produced by Colcemide treatment, at the magnification at which they were counted. Mitotic counts revealed a higher incidence of mitotic figures (1% level of significance) in deficient mice than in supplemented controls from as early as ten days to as late as 80 days on the diet, after which mitotic activity in deficient animals fell to normal levels (fig. 3).

Histochemical observations. Histochemical changes in both succinic dehydrogenase and cytochrome oxidase were evident in skin of deficient mice within 25 days on the diet. In supplemented controls, homogeneously distributed reaction products of

This apparent maximum limit to the thickness of the living portion of the epidermis may be due to the availability of nutrients and oxygen, in view of the lack of blood vessels in the epidermis. The epidermal hyperplasia seems to be accounted for by the high mitotic activity observed in the basal layer of deficient mice. The sharp decline in mitotic activity after 70 days on the deficient diet was perhaps due to the moribund condition of the animals at the latter stage of deficiency.

It may seem surprising that the epidermal hyperplasia of EFA deficiency is accompanied by cessation of hair growth, but these two activities also seem to be relatively independent in normal animals, where the cyclical rhythm of hair growth is accompanied by little corresponding variation in the growth of the epidermis (Bulough and Laurence, '58). That portion of the outer root sheath of the hair follicle just above the sebaceous gland has a mitotic rate similar to that of the surrounding epidermis and can be considered a stable element of the follicle, while the outer root sheath of the hair follicle just below the sebaceous gland is a rather transient structure that varies with the hair growth cycle (Montagna, '62). Consistent with this, the portion of the outer root sheath above the sebaceous gland was hyperplastic in EFA-deficient mice, while the portion below the sebaceous gland was not.

The wide intercellular spaces in the stratum Malpighii of the EFA-deficient mice have been reported previously in rats (Panos and Finerty, '53) and in dogs (Hansen et al., '51). These spaces may be artifacts, but they do indicate that the Malpighian cells of deficient animals are more easily separated than those of controls. Although the thickened stratum corneum of deficient mice does not appear different from that of control mice histologically, an altered adhesiveness of the cells there, similar to that indicated by widened intercellular spaces in the stratum Malpighii, might play a role in the increased trans-epidermal water loss characteristic of EFA deficient animals.

The increase in histochemically demonstrable succinic dehydrogenase and cytochrome oxidase activity in the epidermis of deficient mice correlated well with the

increased epidermal mitotic rate. Biological oxidation-reduction reactions catalyzed by these enzymes represent a major source of energy to the epidermis (Decker and Andersen, '65). Montagna and Formisano ('55) have reported a close correlation between succinic dehydrogenase activity and epidermal mitotic rate, as well as growth and differentiation, in various areas of human skin. Although caution must be exercised in assigning quantitative values to histochemical activities, the differences observed in both the intensity and distribution of the reaction products of these enzymes between the epidermis of deficient and control animals were striking and consistently reproducible.

It would be attractive to propose that the acid phosphatase observed in the stratum granulosum and in the center of sebaceous acini is associated with autolytic activity in these areas. Diengdoh ('64) has presented some evidence that the acid phosphatase in the stratum granulosum of mouse epidermis is membrane-bound as is typical of lysosomes. There has been, however, no cytochemical demonstration of lysosomes in the mouse epidermis by electron microscopy. The details regarding the sudden transformation of living epidermal cells of the stratum Malpighii into the dead cells of the stratum corneum are not well understood. It is possible that lysosomes or free acid hydrolases in the granular layer may be involved in the degradation of cell organelles during the process of keratinization. Bejdl ('54) on the other hand, has suggested that acid phosphatase works in concert with esterase in lipid metabolism in the epidermis and he has correlated the deposition of lipid in the stratum lucidum with the disappearance of acid phosphatase in this region. While it is not possible to resolve the function of acid phosphatase in the epidermis on the basis of this study, there does seem to be a correlation between the hyperplasia of EFA-deficiency and acid phosphatase activity. Similarly, Braun-Falco ('58) has reported an increase in acid phosphatase activity in the stratum corneum of psoriatic skin where an increase in epithelial proliferation is also known to exist.

From the time of their discovery, the essential fatty acids have been considered

larger ones regardless of age. Therefore, in the experiments reported here, mice were weaned and placed on the experimental diets when they reached a weight of 10 ± 2 gm, being usually 19 to 22 days of age.

The EFA-deficient diet employed in this study contained all required vitamins, minerals, and salts, together with casein and hydrogenated peanut oil. The hydrogenated peanut oil had an iodine number of about one and supplied much of the caloric requirement without providing the essential fatty acids, all of which are polyunsaturated (Aaes-Jørgensen, '61). Fat-free diets have also been used in many studies to induce EFA-deficiency, but such diets often include an inordinate quantity of sucrose to meet caloric requirements. Interestingly, signs of deficiency develop earlier on a diet containing saturated fat than on a fat-free diet (Peifer and Holman, '59). Burr ('42) suggested that hydrogenated oils accelerate the development of the deficiency because of the increased demand for essential fatty acids in a high fat diet. The saturated fat used in this study may have had unknown effects in addition to EFA-deficiency; nevertheless, a bi-daily supplement of 50 mg of linoleic acid completely prevented the development of those changes noted in deficient animals. Furthermore, signs of deficiency were reversible when deficient animals were supplemented with linoleic acid after as long as 50 days on the deficient diet.

Inelasticity of skin was one of the earliest grossly evident signs of EFA deficiency. Because the dermis imparts most of the strength and elasticity to skin, the thickened and structurally altered dermis of the deficient animals may have been responsible for this inelasticity.

Hair loss was apparent only after 40 days on the deficient diet, although it probably began earlier; much hair may be lost before it becomes grossly apparent. Hair growth in normal mice occurs in a cyclic pattern of waves passing anteroposteriorly and ventrodorsally over the body (Chase and Eaton, '59). Plucking hair is a strong stimulus for growth in resting follicles (Chase, '58). The observed diminution or absence of hair growth in deficient mice and inability of follicles to respond to

plucking could be interpreted as the result of poor general nutrition rather than as a specific effect of EFA-deficiency. However, the rapidity with which hair growth was resumed after supplementation of deficient animals suggests a direct involvement of EFA.

Blood vessels were more obvious in the ears of deficient mice than in controls. Kramár and Levine ('53) have presented evidence that blood vessels are more permeable and fragile in EFA-deficient mice. Perhaps the vasodilation that accompanies increased permeability accounts for both the increased visibility of the vessels and the edema observed in the dermis.

The earliest histologic change in the skin of deficient mice was an increase in the thickness of the stratum Malpighii, followed by the development of a well-defined stratum granulosum and thickening of the stratum corneum. Hansen et al. ('51) also reported the development of rete ridges and parakeratosis in the stratum corneum of EFA-deficient dogs, but parakeratosis was not observed in deficient mice and ridging of the epidermis occurred only at the mucocutaneous junction of the lip and to a lesser extent in the foot pad. In normal animals, a prominent stratum granulosum is found in those regions that have a relatively thick stratum corneum and is presumably related to the rate of keratinization (Lever, '61). However, when cellular proliferation is abnormally accelerated as, for example, in psoriasis or exfoliative dermatitis, the stratum corneum is greatly thickened, but the granular layer is poorly developed. Apparently, keratinization is incomplete in these diseases, as indicated by persistence of nuclear remnants in the stratum corneum (parakeratosis). In contrast, the epidermal hyperplasia of EFA-deficient mice seems to be associated with complete keratinization, as indicated by the greatly thickened stratum granulosum and lack of nuclear remnants in the stratum corneum.

Regardless of the normal epidermal thickness in any given area, the stratum Malpighii and stratum granulosum of all areas in deficient mice eventually attained a thickness of eight or nine cell layers by about 50 days on the diet and persisted at this thickness during the life of the animal.

This apparent maximum limit to the thickness of the living portion of the epidermis may be due to the availability of nutrients and oxygen, in view of the lack of blood vessels in the epidermis. The epidermal hyperplasia seems to be accounted for by the high mitotic activity observed in the basal layer of deficient mice. The sharp decline in mitotic activity after 70 days on the deficient diet was perhaps due to the moribund condition of the animals at the latter stage of deficiency.

It may seem surprising that the epidermal hyperplasia of EFA deficiency is accompanied by cessation of hair growth, but these two activities also seem to be relatively independent in normal animals, where the cyclical rhythm of hair growth is accompanied by little corresponding variation in the growth of the epidermis (Bulough and Laurence, '58). That portion of the outer root sheath of the hair follicle just above the sebaceous gland has a mitotic rate similar to that of the surrounding epidermis and can be considered a stable element of the follicle, while the outer root sheath of the hair follicle just below the sebaceous gland is a rather transient structure that varies with the hair growth cycle (Montagna, '62). Consistent with this, the portion of the outer root sheath above the sebaceous gland was hyperplastic in EFA-deficient mice, while the portion below the sebaceous gland was not.

The wide intercellular spaces in the stratum Malpighii of the EFA-deficient mice have been reported previously in rats (Panos and Finerty, '53) and in dogs (Hansen et al., '51). These spaces may be artifacts, but they do indicate that the Malpighian cells of deficient animals are more easily separated than those of controls. Although the thickened stratum corneum of deficient mice does not appear different from that of control mice histologically, an altered adhesiveness of the cells there, similar to that indicated by widened intercellular spaces in the stratum Malpighii, might play a role in the increased trans-epidermal water loss characteristic of EFA deficient animals.

The increase in histochemically demonstrable succinic dehydrogenase and cytochrome oxidase activity in the epidermis of deficient mice correlated well with the

increased epidermal mitotic rate. Biological oxidation-reduction reactions catalyzed by these enzymes represent a major source of energy to the epidermis (Decker and Andersen, '65). Montagna and Formisano ('55) have reported a close correlation between succinic dehydrogenase activity and epidermal mitotic rate, as well as growth and differentiation, in various areas of human skin. Although caution must be exercised in assigning quantitative values to histochemical activities, the differences observed in both the intensity and distribution of the reaction products of these enzymes between the epidermis of deficient and control animals were striking and consistently reproducible.

It would be attractive to propose that the acid phosphatase observed in the stratum granulosum and in the center of sebaceous acini is associated with autolytic activity in these areas. Diengdoh ('64) has presented some evidence that the acid phosphatase in the stratum granulosum of mouse epidermis is membrane-bound as is typical of lysosomes. There has been, however, no cytochemical demonstration of lysosomes in the mouse epidermis by electron microscopy. The details regarding the sudden transformation of living epidermal cells of the stratum Malpighii into the dead cells of the stratum corneum are not well understood. It is possible that lysosomes or free acid hydrolases in the granular layer may be involved in the degradation of cell organelles during the process of keratinization. Bejdl ('54) on the other hand, has suggested that acid phosphatase works in concert with esterase in lipid metabolism in the epidermis and he has correlated the deposition of lipid in the stratum lucidum with the disappearance of acid phosphatase in this region. While it is not possible to resolve the function of acid phosphatase in the epidermis on the basis of this study, there does seem to be a correlation between the hyperplasia of EFA-deficiency and acid phosphatase activity. Similarly, Braun-Falco ('58) has reported an increase in acid phosphatase activity in the stratum corneum of psoriatic skin where an increase in epithelial proliferation is also known to exist.

From the time of their discovery, the essential fatty acids have been considered

to play a structural role in cells. Sinclair ('32) showed that they are in a very stable form in the body and are retained even during starvation. Essential fatty acids are incorporated into phospholipids, which in combination with proteins comprise the basic structure of cell membranes. When the essential fatty acids are lacking in the diet other non-essential fatty acids apparently are substituted in both free lipids and membranous structures. DeTomas et al. ('63) for example, have reported abnormal phospholipids in EFA-deficiency, in which 5, 8, 11-eicosatrienoic acid apparently was substituted for arachidonic acid. Abnormal phospholipids are believed to produce structural and functional changes in liver mitochondria of EFA-deficient rats (Levin et al., '57; Macmillan and Sinclair, '58; Wilson and Leduc, '63). Alterations of both membrane structure and extracellular lipids might also influence the integrity of the stratum corneum and be a contributing factor in the striking increase in transepidermal water loss reported in deficient animals. Although the water barrier is known to reside in the stratum corneum (Blank, '53), there is little information regarding the specific chemical composition of the epidermal barrier. Free lipids and protein-lipid complexes seem to be important, and may serve both as cementing and barrier substances (Onken and Moyer, '63). Accordingly, deficiency of essential fatty acids could interfere with the synthesis of the lipid materials of the water barrier and lead to increased transepidermal water loss.

Dermatologists have long been aware that cutaneous lesions involving hyperkeratosis and rapid proliferation of epidermal cells are often accompanied by a several-fold increase in transepidermal water loss (Rothman, '54). This increased loss has been attributed, at least in part, to water freed by dehydration of Malpighian cells during the accelerated process of keratinization (Felsner and Rothman, '45). However, the volume of water lost would appear to exceed by far the amount available from this source. Instead of proposing that hyperplasia and hyperkeratinization increase transepidermal water loss, it may be more profitable to explore the possibility that the reverse is true, at least in EFA

deficiency. That is, if lack of essential fatty acids interferes with the synthesis of the lipids of the water barrier of the epidermis, then increased transepidermal water loss could be a direct result of the deficiency. Accordingly, increased permeability of the epidermis might precede and, indeed, be the stimulus for hyperplasia. Hyperplasia could then be viewed as a homeostatic mechanism for attempting to reduce transepidermal water loss. In preliminary experiments, maintenance of EFA-deficient mice in a humid environment that diminishes transepidermal water loss has reduced the degree of hyperplasia observed in the epidermis (Menton, '67).

ACKNOWLEDGMENTS

The author extends his thanks to Professors Richard Ellis and Elizabeth Leduc of Brown University for their helpful suggestions and encouragement during this work.

LITERATURE CITED

- Aaes-Jørgensen, E. 1961 Essential Fatty Acids. *Physiol. Rev.*, 41: 1-51.
- Aaes-Jørgensen, E., J. P. Funch, P. F. Engel and H. Dan 1956 The role of fat in the diet of rats. 9. Influence on growth and histological findings of diets with hydrogenated arachis oil or no fat, supplemented with linoleic acid or raw skim milk, and of crude casein compared with vitamin test casein. *Brit. J. Nutr.*, 10: 292-304.
- Basnayake, V., and H. M. Sinclair 1954 Skin permeability in deficiency of essential fatty acids. *J. Physiol.*, 126: 55-56.
- 1956 The effect of deficiency of essential fatty acids upon the skin. In: *International Conference on Biochemical Problems of Lipids*. G. Popjak and E. LeBreton, eds., London: Butterworth.
- Bejdl, W. 1954 Die saure Phosphatase in Haut und Vagina des Menschen und ihre Bedeutung für die Verhornung. *Z. Zellforsch. Mikroskop. Anat.*, 40: 389-400.
- Blank, I. H. 1953 Further observations on factors which influence the water content of the stratum corneum. *J. Invest. Derm.*, 21: 259-271.
- Braun-Falco, O. 1958 The histochemistry of psoriasis. *Ann. N. Y. Acad. Sci.*, 73: 936-976.
- Bullough, W. S., and E. B. Laurence 1958 The mitotic activity of the follicle. In: *The Biology of Hair Growth*. W. Montagna and R. A. Ellis, eds., Academic Press, New York.
- Burr, G. O. 1942 Significance of the essential fat acids. *Fed. Proc.*, 1: 224-233.
- Burr, G. O., and M. M. Burr 1929 A new deficiency disease produced by the rigid exclusion of fat from the diet. *J. Biol. Chem.*, 82: 345-367.

- Burstone, M. S. 1958 Histochemical demonstration of acid phosphatases using naphthol AS-phosphates. *J. Natl. Cancer Inst.*, 21: 523-540.
- 1960 Histochemical demonstration of cytochrome oxidase with new amine reagents. *J. Histochem. Cytochem.*, 7: 63-70.
- Chase, H. B. 1958 Physical factors which influence the growth of hair. In: *The Biology of Hair Growth*. W. Montagna and R. A. Ellis, eds., Academic Press, New York.
- Chase, H. B., and G. Eaton 1959 The growth of hair follicles in waves. *Ann. N. Y. Acad. Sci.*, 83: 365-368.
- Chase, H. B., W. Montagna, and J. D. Malone 1953 Changes in the skin in relation to the hair growth cycle. *Anat. Rec.*, 116: 75-81.
- Cooper, Z. K., and H. C. Franklin 1940 Mitotic rhythm in the epidermis of the mouse. *Anat. Rec.*, 78: 1-8.
- Decker, R. H., and R. L. Anderson 1965 Oxidative phosphorylation in the epidermis of man and the hairless mouse. *J. Invest. Derm.*, 45: 168-172.
- DeTomas, M. E., R. R. Brenner and R. O. Peluffo 1963 Position of eicosatrienoic acid in phosphatidylcholine and phosphatidylethanolamine from rats deficient in essential fatty acids. *Biochem. Biophys. Acta*, 70: 472-474.
- Diengdoh, J. V. 1964 The demonstration of lysosomes in mouse skin. *Quart. J. Micro. Sci.*, 105: 73-78.
- Farber, E., and C. D. Louviere 1956 Histochemical localization of specific oxidative enzymes. IV. Soluble oxidation-reduction dyes as aids in the histochemical localization of oxidative enzymes with tetrazolium salts. *J. Histochem. Cytochem.*, 4: 347-356.
- Fishman, W. H., and J. R. Baker 1956 Cellular localization of β -glucuronidase in rat tissues. *J. Histochem. Cytochem.*, 4: 570-585.
- Hansen, A. E., S. G. Holmes and H. F. Wiese 1951 Fat in the diet in relation to nutrition of the dog IV. Histological features of skin from animals fed diets with and without fat. *Texas Repts. Biol. Med.*, 9: 555-570.
- Kingery, F. A., and R. E. Kellum 1965 Essential fatty acid deficiency. Histochemical changes in the skin of rats. *Arch. Derm.*, 91: 272-279.
- Kramár, J., and V. E. Levine 1953 Influence of fats and fatty acids on the capillaries. *J. Nutr.*, 50: 149-160.
- Lever, W. F. 1961 *Histopathology of the Skin*. 3rd edition, J. B. Lippincott Company, Philadelphia.
- Levin, E., R. M. Johnson and S. Albert 1957 Mitochondrial changes associated with essential fatty acid deficiency in rats. *J. Biol. Chem.*, 228: 15-21.
- Macmillan, A. L., and H. M. Sinclair 1958 The structural function of essential fatty acids. In: *Essential Fatty Acids*. H. M. Sinclair, ed., Academic Press, New York.
- Menton, D. N. 1967 The relationship of trans-epidermal water loss to the epidermal hyperplasia produced by essential fatty acid deficiency. *Anat. Rec.*, 157: 287. (Abstract).
- Messier, B., and C. P. Leblond 1960 Cell proliferation and migration as revealed by radioautography after injection of thymidine- H^3 into male rats and mice. *Am. J. Anat.*, 106: 247-285.
- Montagna, W. 1962 *The Structure and Function of Skin*. Academic Press, New York.
- Montagna, W., and V. Formisano 1955 Histology and cytochemistry of human skin. VII. The distribution of succinic dehydrogenase activity. *Anat. Rec.*, 122: 65-78.
- Onken, H. D., and C. A. Moyer 1963 The water barrier in human epidermis. Physical and chemical nature. *Arch. Derm.*, 87: 584-590.
- Panos, T. C., and J. C. Finerty 1953 Effects of a fat-free diet on growing female rats, with special reference to the endocrine system. *J. Nutr.*, 49: 397-424.
- Peifer, J. J., and R. T. Holman 1959 Effect of saturated fat upon essential fatty acid metabolism of the rat. *J. Nutr.*, 68: 155-168.
- Ramalingaswami, V., and H. M. Sinclair 1951 Pathological changes in the rat in deficiency of essential fatty acids. *Brit. J. Nutr.*, 5: x.
- 1953 The relation of deficiencies of vitamin A and of essential fatty acids to follicular hyperkeritosis in the rat. *Brit. J. Derm.*, 65: 1-22.
- Sinclair, H. M. 1932 The metabolism of the phospholipids. V. The relationship between the amount of fat ingested and the degree of unsaturation of the phospholipids and neutral fat in the tissues of the rat. *J. Biol. Chem.*, 96: 103-125.
- Sinclair, R. G. 1930 Some observations on the growth of rats on "fat-free" and fat-containing diets. *Proc. Soc. Exp. Biol. Med.*, 27: 1059-1062.
- Staricco, R. G., and H. Pinkus 1957 Quantitative and qualitative data on the pigment cells of adult human epidermis. *J. Invest. Derm.*, 28: 33-45.
- Vinson, L. J., D. R. Choman, W. R. Koehler, M. D. Lehman, T. Masurat and E. J. Singer 1961 Basic studies in percutaneous absorption. Semi-annual report to the Army Chem. Ctr., Edgewood, Md. July-Dec.
- Williamson, R. 1941 A note on the epidermis of the rat on a fat-free diet. *Biochem. J.*, 35: 1003-1005.
- Wilson, J. W., and E. H. Leduc 1963 Mitochondrial changes in the liver of essential fatty acid-deficient mice. *J. Cell Biol.*, 16: 281-296.

Abbreviations

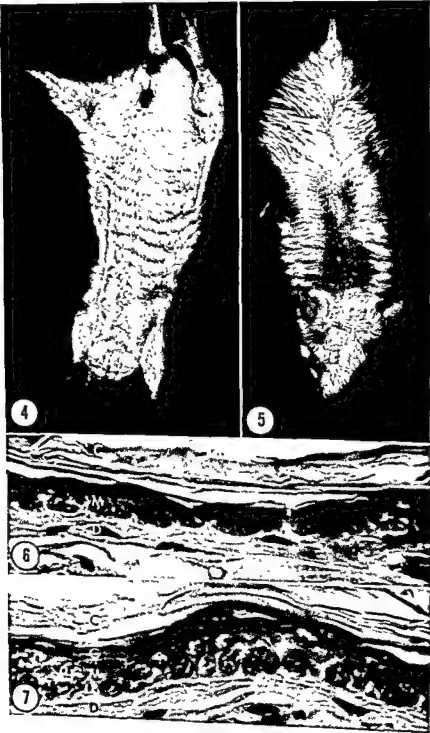
C, stratum corneum	M, stratum Malpighi
G, stratum granulosum	D, dermis

Figures 6-11 are comparisons of skin from EFA-deficient and linoleic acid-supplemented control, male littermate mice. Hematoxylin and eosin staining.

PLATE 1

EXPLANATION OF FIGURES

- 4 Mouse on EFA-deficient diet for 50 days. There are permanent horizontal creases in the ventral skin of the trunk. When the mouse is suspended by the tail, vertical folds extend tightly from forelimbs to hind limbs on each side. These changes are attributed to loss of normal elasticity of the skin. $\times 1$.
- 5 Mouse on EFA-deficient diet for 60 days. Note extensive hair loss and scaldiness in the middle of the back. The hair is matted and wet. $\times 1$.
- 6-7 Skin of a supplemented (fig. 6) and deficient mouse (fig. 7), on diet for 20 days. The epidermis of the deficient animal is hyperplastic and has a well-developed stratum granulosum. $\times 1,500$.



Abbreviations

C, stratum corneum	M, stratum Malpighi
G, stratum granulosum	D, dermis

Figures 6-11 are comparisons of skin from EFA-deficient and linoleic acid-supplemented control, male littermate mice. Hematoxylin and eosin staining.

PLATE 1

EXPLANATION OF FIGURES

- 4 Mouse on EFA-deficient diet for 50 days. There are permanent horizontal creases in the ventral skin of the trunk. When the mouse is suspended by the tail, vertical folds extend tightly from forelimbs to hind limbs on each side. These changes are attributed to loss of normal elasticity of the skin. $\times 1$.
- 5 Mouse on EFA-deficient diet for 60 days. Note extensive hair loss and scaliness in the middle of the back. The hair is matted and wet. $\times 1$.
- 6-7 Skin of a supplemented (fig. 6) and deficient mouse (fig. 7), on diet for 20 days. The epidermis of the deficient animal is hyperplastic and has a well-developed stratum granulosum. $\times 1,500$.

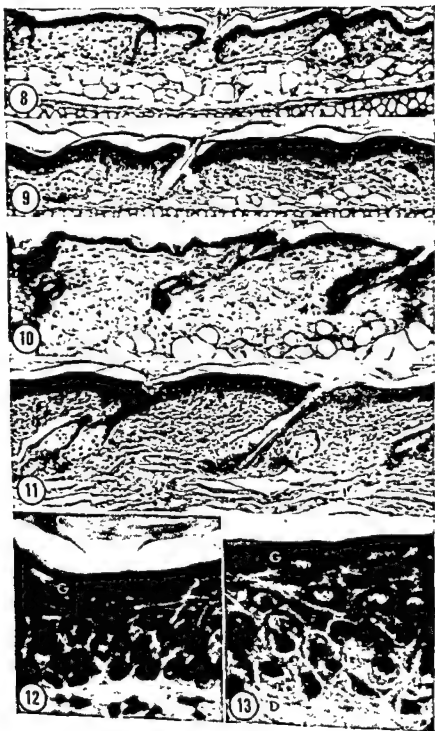
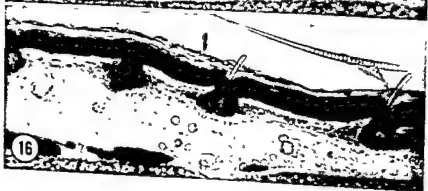
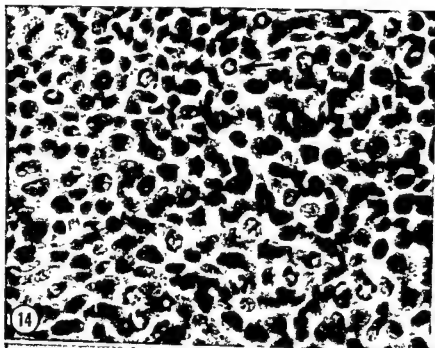


PLATE 2

EXPLANATION OF FIGURES

- 8-9 Ear skin from a supplemented (fig. 8) and deficient mouse (fig. 9) that were on the diet 30 days. Compared with the supplemented animal, the epidermis of the deficient animal is much thicker and has several mitotic figures in the basal layer (arrows). Cellular infiltration in the thickened dermis of the deficient animal is pronounced, and there is little hypodermal fat. $\times 225$.
- 10-11 Skin from the abdomen of a supplemented (fig. 10) and deficient mouse (fig. 11) that were on the diet 40 days. Compared with the supplemented animal, the epidermis of the deficient animal is much thicker, sebaceous glands appear hypertrophic, there is intense infiltration of round cells among the fragmented collagen of the thickened dermis, and hypodermal fat is absent. $\times 225$.
- 12 Higher magnification of the abdominal skin from the deficient animal of figure 11. Control skin from this area has only one or two layers in the stratum Malpighii and no demonstrable stratum granulosum, whereas the stratum Malpighii of the deficient animal is approximately four cell layers thick with two or three layers of cells in the stratum granulosum. $\times 1,500$.
- 13 Skin from the back of a deficient mouse that was on the diet 70 days. Intercellular spaces are particularly wide in the basal layer and the stratum granulosum is full of keratohyalin granules. $\times 1,500$.



Figures 15-20 are histochemical comparisons of enzyme activity in the skin of EFA-deficient and linoleic acid-supplemented control, male litter-mate mice.

PLATE 3

EXPLANATION OF FIGURES

- 14 The basal surface of a whole-mounted sheet of epidermis split from the foot pad of a deficient mouse five hours after injection of Colcemide. The "C" mitotic figures are readily distinguished from non-dividing cells (arrow). Fixed in Serra's fixative, stained with Feulgen reaction. $\times 1,000$.
- 15-16 Cytochrome oxidase activity in the ear skin of a supplemented (fig. 15) and deficient mouse (fig. 16), that were on the diet 40 days. The reaction product is confined to the stratum Malpighii, which is broader and more intensely reactive in the deficient animal than in the control. The stratum corneum is well-preserved in frozen sections which allow an appreciation of the thickened stratum corneum of the deficient animal. A granular reaction product occurs in the sebaceous glands of both animals. $\times 400$.

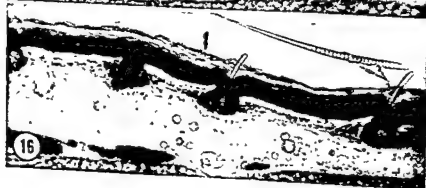
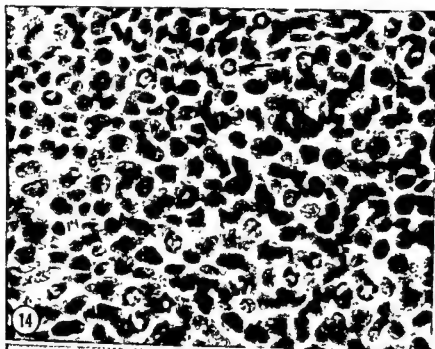


PLATE 4

EXPLANATION OF FIGURES

- 17-18 Succinic dehydrogenase in skin from the back of a supplemented (fig. 17) and a deficient mouse (fig. 18), that were on the diet 80 days. The zone of reaction product is much thicker and more intense in the deficient animal than in the control. Note the greatly thickened stratum corneum in the deficient animal. $\times 500$.
- 19-20 Acid phosphatase activity in the ear of a supplemented (fig. 19) and deficient mouse (fig. 20), that were on the diet 40 days. In the supplemented control, reaction product occurs in the thin transitional zone between the strata corneum and granulosum. In the deficient animal there is an increase in reaction product which occupies the entire stratum granulosum and lower stratum corneum. Acid phosphatase activity is also evident in the center of the acini and excretory ducts of the sebaceous glands and is more intense in the deficient animal. $\times 225$.



The Fine Structure of the Hamster Pineal Gland¹

MICHAEL N. SHERIDAN AND RUSSEL J. REITER

*Department of Anatomy, School of Medicine and Dentistry,
University of Rochester, Rochester, New York*

ABSTRACT The pineal gland of the hamster has been examined with the electron microscope. The gland is composed of two types of parenchymal cells, a "light" and a "dark" cell. Blood vessels are infrequently encountered and display little perivascular space. Axons, nerve endings, pineal cell processes, and occasional glial processes ramify within the parenchyma of the gland.

The parenchymal cells display abundant mitochondria, many with a tubular internum. Smooth and rough surfaced endoplasmic reticulum, a Golgi apparatus and lipid droplets are regular features of both cell types. Vesicles of varying size and containing electron dense centers are present in the cell body.

Parenchymal cells branch extensively and are characterized by the presence of microtubules in addition to the usual organelles encountered in the cell body. Pineal cell process terminations regularly show accumulations of vesicles with electron dense granulations.

With recent years the pineal gland has received renewed attention. In spite of these efforts its function remains unsolved. Most of the studies have been aimed at the pineal gonadal relationships and there is widespread agreement that the pineal possesses antigonadotropic properties. This idea was strengthened when a substance, melatonin, was isolated from beef pineal (Lerner, Case, Takahashi, Lee and Mori, '58) and was shown to produce effects in the rat similar to pineal extracts. In that melatonin is synthesized in the rat pineal gland and that it produces effects on the gonads, Wurtman and Axelrod ('65) considered this substance to be a pineal hormone. The inhibitory effects of melatonin on the gonads have not been reproducible by all workers (Chu, Wurtman, and Axelrod, '64; Ebels, and Prop, '65).

Thus far, most of the work concerning pineal physiology has utilized the rat which over the years has been highly inbred for reproductive purposes and is classified a continuous breeder. The hamster on the other hand has not been inbred to this extent and even under laboratory conditions its breeding ability varies with season. Since the activity of the pineal gland is photosensitive and there is a postulated relationship between pineal activity and seasonal breeding, it might be expected that the relationships of the pineal gland

would be more pronounced in the hamster than in the rat. Reiter, Hoffman and Hester ('66) recently showed that short photoperiods or blinding in the Syrian hamster produces atrophy of the reproductive organs and that this effect is reversed by removal of the pineal gland.

The fine structure of the mammalian pineal gland has been investigated in several species. Among these have been the rat (see Arstila, '67, for literature review), cattle and sheep (Anderson, '60, '65), rabbit (Wartenberg and Gusek, '65) and the cat (Duncan and Micheletti, '66). Because of the lack of the fine structural description of the hamster pineal gland and the marked effect which this gland exerts on the reproductive organs in this species, this organ has been subjected to a fine structural study. The results presented here have been previously reported in preliminary form (Sheridan, '67).

MATERIALS AND METHODS

Syrian hamsters, both albino and agouti, were anesthetized with ether between 9:00 and 10:00 AM, the thorax transected and the calvaria removed. The pineal gland remained attached to the calvaria, nestled in a depression at the confluence of sinuses. The pineal was flooded with fixa-

¹Supported by a General research grant (FR05403) from the NIDDK, NIH.

tive and removed from this cavity with the aid of a dissecting microscope.

The gland was usually cut in half transferred to fresh cold fixative. Fixation was prolonged for two hours at approximately 2°C in 1% OsO₄ in veronal-acetate buffer with sucrose (0.045 gm/ml) or 1.33% OsO₄ in collidine buffer.

Glutaraldehyde fixation was used on several occasions followed by OsO₄. Tissues were quickly dehydrated in cold ethanol to 95%, allowed to come to room temperature and further dehydrated through absolute ethanol. Prior to infiltration in either Maraglas (Freeman and Spurlock, '62), Epon (Luft, '61) or Dow epoxy Resin (Lockwood, '64) the tissues were passed through propylene oxide to aid infiltration. Infiltration was for several hours to overnight in a 50:50 mixture of propylene oxide and epoxy resin. They were then transferred to fresh resin in Beem capsules and cured at 60°C for 24 hours.

Thin sections were stained with uranyl acetate followed with lead hydroxide. Microscopic examination was with an RCA EMU-3H electron microscope.

RESULTS

The results reported here are based on pineals derived from normal agouti hamsters; the albino was found to possess basically the same pineal morphology. The morphology of the pineal cell was essentially the same regardless of the fixative employed. Glutaraldehyde in various buffers followed by OsO₄ did not enhance the morphology. The illustrations included in this report are taken from specimens all of which were fixed initially in osmium tetroxide.

The most frequently encountered cell in the pineal of the golden hamster is the parenchymal cell (fig. 1). This cell presents an overall low density appearance and will be referred to as a "light cell." The nucleus is centrally located and contains a prominent nucleolus. Nuclear morphology is typical, demonstrating peripheral chromatin and a double nuclear membrane with abundant nuclear pores. Occasionally a diaphragm fills the pore (fig. 1 Inset). These light cells are large and branched with processes evidently

ramifying at distances far from the cell body. Occasionally encountered are smaller cells of greater density which are not as extensively branched (fig. 1). This cell may represent a pineal parenchymal cell in a different functional state or these may be oligodendrocytes. The predominant differences between this smaller "dark cell" and the "light cell" are the presence of a greater concentration of granular endoplasmic reticulum and the accumulation of a larger number of lipid droplets (fig. 1).

Both types of parenchymal cells have the usual organelles. A Golgi apparatus is juxta-nuclear (fig. 3) and consists of flattened agranular stacks of membranes. At the peripheries of this organelle, vesicles and vacuoles are regularly encountered; occasionally, these demonstrate a content of variable density (figs. 3, 4).

The endoplasmic reticulum takes two forms (figs. 2, 4). One form consists of flattened sacs with 150 Å ribonucleoprotein particles attached to the cytoplasmic surfaces (fig. 2); this is especially prominent in the dark cell (fig. 1). The predominant form of reticulum in the light cell is the agranular variety (fig. 4). This ramifies throughout the cytoplasm and presents anastomosing and branching tubular profiles; cell areas are occasionally encountered in which this form of endoplasmic reticulum is especially concentrated.

The organelle presenting the most variability is the mitochondrion. This structure varies in size, shape and internal organization, the two extremes being small mitochondria with little internal structure and large mitochondria with a highly packed internum. Mitochondrial profiles are present throughout the cytoplasm and are spherical to elongate. Size varies from 0.2 to 1.5 μ in diameter. All mitochondria are bounded by two membranes approximately 75 Å thick. The inner membrane reflects inward in the smaller mitochondria as cristae or plates with some tubules (figs. 2, 3). In the majority of the larger mitochondria the internum is packed with what is interpreted as tubules (figs. 2, 5, 6, 9). Profiles of these tubules present cross, oblique and occasional longitudinal sections (figs. 5, 6). The density of the mitochondrial

matrix of the larger, tubule-containing organelles is greater than that of the matrix of the smaller.

Bizarre mitochondrial profiles are occasionally seen (figs. 6, 7). Mitochondria have been observed in which a central portion becomes attenuated, attaching and separating two normal appearing extremities (fig. 7). This central attenuation may or may not contain internal tubules; however, if they are observed they usually parallel the long axis of the attenuated portion producing profiles as in figure 6. This attenuated part is apparently responsible for encircling other structures and producing the cup-shaped mitochondria described by Christensen and Chapman ('59) in the testicular interstitial cell of the rat. Assuming a cup-shaped mitochondrial morphology, a mitochondrion nestled in area "A" in figure 6 would produce the profile in area "B" if sectioned at right angles to the present plane of section.

Lipid is present in droplet form in both parenchymal cell types, being much more abundant in the dark cell (fig. 1). The droplets assume a variety of appearances. Usually, however, they are not adequately preserved regardless of the fixation employed and remain as vacuoles of low density; occasionally, a peripheral rim of lipid remains. The usual droplet is round to oval but irregular shapes are encountered.

Centrioles are infrequently encountered; when present, they are usually associated with the Golgi apparatus with one member of the centriole pair being situated at right angles to the other. They possess the usual structure. Vesicle-studded lamellae are occasionally identified and appear similar to synaptic ribbons (fig. 10), (Smith and Sjostrand, '61). Concentric membrane lamellae have been seen; the one seen in figure 8 appears to be associated with the cell membrane of a light cell.

Parenchymal cells are founded by a membrane approximately 75 Å thick (figs. 2, 3, 4, 12). The intercellular space is about 200 Å wide and occasionally enlargements of this are seen (figs. 9, 12); attachment plaques (macula adherens) are present (fig. 2). Vesicles are frequently associated with the cell membrane with

some evidence of fusion having taken place between the two (fig. 12).

As previously mentioned, the light cell possesses processes that ramify for considerable distances. At points of emergence of the processes from the cell body there are accumulations of microtubular components (fig. 8). These structures are of indefinite length and measure approximately 200 Å in diameter; their tubular nature is best appreciated when the process is observed in cross-section (fig. 9).

Cell processes can be confused with axons. It is possible, however, to distinguish the two since axonal profiles contain a greater density of microtubules (fig. 16), and mitochondria of the type specific for the pineal parenchymal cell are also seen in its processes (fig. 9). A comparison of pineal cell processes with axons is made in figure 16.

Numerous electron dense structures are present in both light and dark pineal cells. Many of these possess a granular internal structure and are bounded by a single membrane of 75 Å thickness; they vary widely in size (0.1–0.4 μ) and have been designated lysosome-like bodies (fig. 2). These structures probably correspond to the "grumose" bodies described by Wolfe ('65). Other dense bodies of smaller dimensions (0.07–0.1 μ diameter) are also regularly encountered in the parenchymal cell (figs. 4, 8, 10). These are bounded by a 75 Å membrane with the internum usually homogeneous.

Near their terminations pineal cell processes accumulate numerous vesicles, many of which contain electron dense deposits (fig. 11). The terminations of the processes vary from one to several micra in diameter. Identification of these structures is difficult because of the presence of postganglionic sympathetic nerve endings which also contain vesicles similar to those of pineal cell processes. It is possible to distinguish these on the basis of mitochondrial morphology and dense-cored vesicles. Mitochondria are occasionally encountered in the pineal cell endings similar to those in the cell body. Similarly, vesicle morphology in the pineal process is like that in the cell body. Postganglionic sympathetic nerve endings possess vesicles with

tive and removed from this cavity with the aid of a dissecting microscope.

The gland was usually cut in half transferred to fresh cold fixative. Fixation was prolonged for two hours at approximately 2°C in 1% OsO₄ in veronal-acetate buffer with sucrose (0.045 gm/ml) or 1.33% OsO₄ in collidine buffer.

Glutaraldehyde fixation was used on several occasions followed by OsO₄. Tissues were quickly dehydrated in cold ethanol to 95%, allowed to come to room temperature and further dehydrated through absolute ethanol. Prior to infiltration in either Maraglas (Freeman and Spurlock, '62), Epon (Luft, '61) or Dow epoxy Resin (Lockwood, '64) the tissues were passed through propylene oxide to aid infiltration. Infiltration was for several hours to overnight in a 50:50 mixture of propylene oxide and epoxy resin. They were then transferred to fresh resin in Beem capsules and cured at 60°C for 24 hours.

Thin sections were stained with uranyl acetate followed with lead hydroxide. Microscopic examination was with an RCA EMU-3H electron microscope.

RESULTS

The results reported here are based on pineals derived from normal agouti hamsters; the albino was found to possess basically the same pineal morphology. The morphology of the pineal cell was essentially the same regardless of the fixative employed. Glutaraldehyde in various buffers followed by OsO₄ did not enhance the morphology. The illustrations included in this report are taken from specimens all of which were fixed initially in osmium tetroxide.

The most frequently encountered cell in the pineal of the golden hamster is the parenchymal cell (fig. 1). This cell presents an overall low density appearance and will be referred to as a "light cell." The nucleus is centrally located and contains a prominent nucleolus. Nuclear morphology is typical, demonstrating peripheral chromatin and a double nuclear membrane with abundant nuclear pores. Occasionally a diaphragm fills the pore (fig. 1 Inset). These light cells are large and branched with processes evidently

ramifying at distances far from the cell body. Occasionally encountered are smaller cells of greater density which are not as extensively branched (fig. 1). This cell may represent a pineal parenchymal cell in a different functional state or these may be oligodendrocytes. The predominant differences between this smaller "dark cell" and the "light cell" are the presence of a greater concentration of granular endoplasmic reticulum and the accumulation of a larger number of lipid droplets (fig. 1).

Both types of parenchymal cells have the usual organelles. A Golgi apparatus is juxta-nuclear (fig. 3) and consists of flattened agranular stacks of membranes. At the peripheries of this organelle, vesicles and vacuoles are regularly encountered; occasionally, these demonstrate a content of variable density (figs 3, 4).

The endoplasmic reticulum takes two forms (figs. 2, 4). One form consists of flattened sacs with 150 Å ribonucleoprotein particles attached to the cytoplasmic surfaces (fig. 2); this is especially prominent in the dark cell (fig. 1). The predominant form of reticulum in the light cell is the agranular variety (fig. 4). This ramifies throughout the cytoplasm and presents anastomosing and branching tubular profiles; cell areas are occasionally encountered in which this form of endoplasmic reticulum is especially concentrated.

The organelle presenting the most variability is the mitochondrion. This structure varies in size, shape and internal organization, the two extremes being small mitochondria with little internal structure and large mitochondria with a highly packed internum. Mitochondrial profiles are present throughout the cytoplasm and are spherical to elongate. Size varies from 0.2 to 1.5 µ in diameter. All mitochondria are bounded by two membranes approximately 75 Å thick. The inner membrane reflects inward in the smaller mitochondria as cristae or plates with some tubules (figs. 2, 3). In the majority of the larger mitochondria the internum is packed with what is interpreted as tubules (figs. 2, 5, 6, 9). Profiles of these tubules present cross, oblique and occasional longitudinal sections (figs. 5, 6). The density of the mitochondrial

pineal cell-nerve ending relationships. Milofsky ('57) early studied the fine structure of the rat pineal and identified processes containing granulated vesicles which he interpreted to belong to the pineal cell. DeRobertis, and Pellegrino de Iraldi ('61) later identified granule-containing vesicles in what they believed to be pineal processes in the perivascular space. Later, Wolfe, Potter, Richardson and Axelrod ('62) recognizing the innervation of the pineal to be from the superior cervical ganglia (Kappers, '60), administered tritiated noradrenalin and observed localization associated with granulated vesicles in what they interpreted to be nerve endings. On the basis of their experiments, Wolfe et al. ('62) concluded that the granulated vesicles resided in nerve endings. Pellegrino de Iraldi, Zieher and DeRobertis ('65) later removed the superior cervical ganglia in the rat and agreed with Wolfe et al. ('62) acknowledging their first interpretation to be incorrect. Others have obtained similar results in the rat (Rodin and Turner, '65), and recently Duncan and Michelletti ('66) saw similar depletion in the cat after this procedure.

The results reported here derived from the pineals of untreated hamster, would suggest that granulated vesicles not only reside in nerve endings but are present also in parenchymal processes. This observation is not in agreement with the statement of Pellegrino de Iraldi et al. ('65) that all granulated vesicles reside in nerve endings and that "pinealocytes have some processes, but they only have clear vesicles of different sizes which are found in the cytoplasm." However, Pellegrino de Iraldi ('66) recognized granules in a similar location in the hamster to those of this report.

This difference might be accounted for on the basis of species variation. However, at least one species of rat (Long-Evans strain) (Arstila, '67) shows granulated vesicles in pineal cell processes similar to those reported here. The conclusion that terminals of pineal cell processes contain granulated vesicles is reached for the following reasons: (1) the processes of pineal cells could be identified because they possessed mitochondria, microtubules

and other features similar to those found in the cell body; (2) these processes contained granules of similar size and consistency to those observed in the cell body; and (3) the size of the vesicles and granules of the pineal processes are generally larger than the vesicles and granules of the nerve endings.

Two types of granulated vesicles have been observed, one with a core 0.075–0.10 μ in diameter and one whose core is less than 200 \AA in diameter. The diameter of the entire smaller vesicle is approximately 500 \AA and the larger ranges from 0.08–0.12 μ . The vesicles of small diameter with dense cores have not been observed in the pineal cell body or processes. These are known to be present in postganglionic sympathetic nerve endings, (Richardson, '62). Previous published micrographs of nerve endings in the pineal of other species have contained vesicles with cores of these dimensions, (Rodin and Turner, '65). Therefore, the identification of nerve endings here has been restricted to those endings which possess the smaller granulated vesicles.

Earlier reports dealing with pineal fine structure in species other than the hamster have indicated that granulated vesicles are associated exclusively with nerve endings. This conclusion was reached because (1) granulated vesicles disappeared after removal of the superior cervical ganglia (Pellegrino de Iraldi et al., '65; Rodin and Turner, '65); (2) tritiated adrenalin was localized by autoradiography at the electron microscopic level over granulated vesicles presumed to be nerve endings (Wolfe et al., '62) and (3) depletion of granulated vesicles observed after reserpine application (Pellegrino de Iraldi et al., '65; Clementi, Muller and Zanoboni, '64; Clementi, Fraschini, Muller and Zanoboni, '65).

It has been shown that the function of the pineal in the blinded hamster at least in part is dependent upon the presence of an intact superior cervical ganglion (Reiter and Hester, '66). If the superior cervical ganglia are removed the antigonadotropic effects of the pineal are abolished. If the granulated vesicles associated with this cell represent the functional secretory products, then removal of

two different types of dense cores. A small dense core measuring less than 200 Å in diameter is present in many vesicles (figs. 12, 16). This dense-cored vesicle has not been encountered in the cell body or in the termination of a pineal cell process. Nerve endings do possess vesicles with dense cores of greater diameter as well, but vesicles with small cores are the predominant form.

In addition to the parenchymal cell the gland contains blood vessels of varying sizes (figs. 13, 14). Blood vessels are encountered infrequently in the hamster pineal gland. A perivascular space is usually present containing connective tissue fibrils (figs. 15, 16), parenchymal cell processes (fig. 16), nerve bundles (fig. 13), nerve endings and occasionally glial cell processes (fig. 14). The endothelial cells of the blood vessels rest on a basement membrane of usual thickness (figs. 13, 14). A basement membrane cannot be identified consistently on the surfaces of the parenchymal cells. Endothelial pores were not detected.

Nerve endings and pineal cell terminations are located primarily in the perivascular space, but both have been found to terminate apparently in proximity to parenchymal cells.

Glial cells are occasionally found. Their processes ramify in the perivascular space and are characterized by their component of fibrils (fig. 16).

Bundles of nerve fibers are frequently seen in the perivascular space and at the periphery of the gland (figs. 13, 15). These usually consist of unmyelinated axons associated with a Schwann cell, but occasionally a myelinated axon is encountered (fig. 15).

DISCUSSION

The results reported here are based on studies of the untreated golden hamster. The pineal cell in this species, in most respects, is similar to other species reported previously. There are, however, several areas of difference which may be related to the physiology of the gland.

The most striking difference in the hamster pineal is the presence of a mitochondrial form first reported by Pellegrino de

Iraldi ('66) which has not generally been reported for pineals of other species. A recent report has described a similar, but rarely encountered, mitochondrion in the pineal gland of the Long-Evans rat (Arstila, '67). The large mitochondrion packed with tubules is not unique to the pineal gland, but has previously been associated with cells that produce steroids (Belt and Pease, '56). The mitochondrion in the pineal cell does not present the orderly packed array of internal tubules that one sees in the adrenal cortex, for instance, but instead the tubules are highly tortuous. Attention was recently drawn to pineal mitochondria in the cat when Duncan and Micheletti ('66) wrote "it seems reasonable to assume that there is something unusual about the mitochondria in the pinealocyte." This concern was precipitated by an appearance suggesting poor fixation. While the exact significance of the tubule-packed mitochondrion is not known, it appears that its presence may be only associated with those species which demonstrate marked pineal inhibitory effects on the gonads. This mitochondrion has been observed in the agouti and albino hamsters but not in the Chinese hamster (unpublished observations). Neither has it been reported in the rat (Long-Evans excepted), cat, nor any of the other species examined. Lin ('65) also noted a peculiar mitochondrial morphology in some of his specimens of pineal glands derived from the Long-Evans strain. He observed a peculiar microcylindrical structure which perhaps represents a variant of the tubule reported here.

Using the present criteria of measurement, the pineal of the rat and Chinese hamster does not demonstrate the marked gonadal inhibitory effects which are readily apparent in the Syrian hamster. Since the tubular type mitochondria have heretofore usually been associated with steroid secreting organs, attempts were made to identify a steroid in this tissue. Thin layer chromatography of chloroform extracts of pineal glands has failed to identify a steroid which might be correlated with the presence of the tubular mitochondria.

Many of the earlier fine structural studies have been concerned primarily with the

pineal cell-nerve ending relationships. Milofsky ('57) early studied the fine structure of the rat pineal and identified processes containing granulated vesicles which he interpreted to belong to the pineal cell. DeRobertis, and Pellegrino de Iraldi ('61) later identified granule-containing vesicles in what they believed to be pineal processes in the perivascular space. Later, Wolfe, Potter, Richardson and Axelrod ('62) recognizing the innervation of the pineal to be from the superior cervical ganglia (Kappers, '60), administered tritiated noradrenalin and observed localization associated with granulated vesicles in what they interpreted to be nerve endings. On the basis of their experiments, Wolfe et al. ('62) concluded that the granulated vesicles resided in nerve endings. Pellegrino de Iraldi, Zieher and DeRobertis ('65) later removed the superior cervical ganglia in the rat and agreed with Wolfe et al. ('62) acknowledging their first interpretation to be incorrect. Others have obtained similar results in the rat (Rodin and Turner, '65), and recently Duncan and Michel-etti ('66) saw similar depletion in the cat after this procedure.

The results reported here derived from the pineals of untreated hamster, would suggest that granulated vesicles not only reside in nerve endings but are present also in parenchymal processes. This observation is not in agreement with the statement of Pellegrino de Iraldi et al. ('65) that all granulated vesicles reside in nerve endings and that "pinealocytes have some processes, but they only have clear vesicles of different sizes which are found in the cytoplasm." However, Pellegrino de Iraldi ('66) recognized granules in a similar location in the hamster to those of this report.

This difference might be accounted for on the basis of species variation. However, at least one species of rat (Long-Evans strain) (Arstila, '67) shows granulated vesicles in pineal cell processes similar to those reported here. The conclusion that terminals of pineal cell processes contain granulated vesicles is reached for the following reasons: (1) the processes of pineal cells could be identified because they possessed mitochondria, microtubules

and other features similar to those found in the cell body; (2) these processes contained granules of similar size and consistency to those observed in the cell body; and (3) the size of the vesicles and granules of the pineal processes are generally larger than the vesicles and granules of the nerve endings.

Two types of granulated vesicles have been observed, one with a core 0.075-0.10 μ in diameter and one whose core is less than 200 A in diameter. The diameter of the entire smaller vesicle is approximately 500 A and the larger ranges from 0.08-0.12 μ . The vesicles of small diameter with dense cores have not been observed in the pineal cell body or processes. These are known to be present in postganglionic sympathetic nerve endings (Richardson, '62). Previous published micrographs of nerve endings in the pineal of other species have contained vesicles with cores of these dimensions (Rodin and Turner, '65). Therefore, the identification of nerve endings here has been restricted to those endings which possess the smaller granulated vesicles.

Earlier reports dealing with pineal fine structure in species other than the hamster have indicated that granulated vesicles are associated exclusively with nerve endings. This conclusion was reached because (1) granulated vesicles disappeared after removal of the superior cervical ganglia (Pellegrino de Iraldi et al., '65; Rodin and Turner, '65); (2) tritiated adrenalin was localized by autoradiography at the electron microscopic level over granulated vesicles presumed to be nerve endings (Wolfe et al. '62) and (3) depletion of granulated vesicles observed after reserpine application (Pellegrino de Iraldi et al., '65; Clementi, Muller and Zanoboni, '64; Clementi, Frschini, Muller and Zanoboni, '65).

It has been shown that the function of the pineal in the blinded hamster at least in part is dependent upon the presence of an intact superior cervical ganglion (Reiter and Hester, '66). If the superior cervical ganglia are removed the androgenotropic effects of the pineal are abolished. If the granulated vesicles associated with this cell represent the functional secretory products, then removal

two different types of dense cores. A small dense core measuring less than 200 Å in diameter is present in many vesicles (figs. 12, 16). This dense-cored vesicle has not been encountered in the cell body or in the termination of a pineal cell process. Nerve endings do possess vesicles with dense cores of greater diameter as well, but vesicles with small cores are the predominant form.

In addition to the parenchymal cell the gland contains blood vessels of varying sizes (figs. 13, 14). Blood vessels are encountered infrequently in the hamster pineal gland. A perivascular space is usually present containing connective tissue fibrils (figs. 15, 16), parenchymal cell processes (fig. 16), nerve bundles (fig. 13), nerve endings and occasionally glial cell processes (fig. 14). The endothelial cells of the blood vessels rest on a basement membrane of usual thickness (figs. 13, 14). A basement membrane cannot be identified consistently on the surfaces of the parenchymal cells. Endothelial pores were not detected.

Nerve endings and pineal cell terminations are located primarily in the perivascular space, but both have been found to terminate apparently in proximity to parenchymal cells.

Glial cells are occasionally found. Their processes ramify in the perivascular space and are characterized by their component of fibrils (fig. 16).

Bundles of nerve fibers are frequently seen in the perivascular space and at the periphery of the gland (figs. 13, 15). These usually consist of unmyelinated axons associated with a Schwann cell, but occasionally a myelinated axon is encountered (fig. 15).

DISCUSSION

The results reported here are based on studies of the untreated golden hamster. The pineal cell in this species, in most respects, is similar to other species reported previously. There are, however, several areas of difference which may be related to the physiology of the gland.

The most striking difference in the hamster pineal is the presence of a mitochondrial form first reported by Pellegrino de

Iraldi ('66) which has not generally been reported for pineals of other species. A recent report has described a similar, but rarely encountered, mitochondrion in the pineal gland of the Long-Evans rat (Arstula, '67). The large mitochondrion packed with tubules is not unique to the pineal gland, but has previously been associated with cells that produce steroids (Belt and Pease, '56). The mitochondrion in the pineal cell does not present the orderly packed array of internal tubules that one sees in the adrenal cortex, for instance, but instead the tubules are highly tortuous. Attention was recently drawn to pineal mitochondria in the cat when Duncan and Micheletti ('66) wrote "it seems reasonable to assume that there is something unusual about the mitochondria in the pinealocyte." This concern was precipitated by an appearance suggesting poor fixation. While the exact significance of the tubule-packed mitochondrion is not known, it appears that its presence may be only associated with those species which demonstrate marked pineal inhibitory effects on the gonads. This mitochondrion has been observed in the agouti and albino hamsters but not in the Chinese hamster (unpublished observations). Neither has it been reported in the rat (Long-Evans excepted), cat, nor any of the other species examined. Lin ('65) also noted a peculiar mitochondrial morphology in some of his specimens of pineal glands derived from the Long-Evans strain. He observed a peculiar microcylindrical structure which perhaps represents a variant of the tubule reported here.

Using the present criteria of measurement, the pineal of the rat and Chinese hamster does not demonstrate the marked gonadal inhibitory effects which are readily apparent in the Syrian hamster. Since the tubular type mitochondria have heretofore usually been associated with steroid secreting organs, attempts were made to identify a steroid in this tissue. Thin layer chromatography of chloroform extracts of pineal glands has failed to identify a steroid which might be correlated with the presence of the tubular mitochondria.

Many of the earlier fine structural studies have been concerned primarily with the

- Del Rio Hortega, P. 1932 Pineal Gland. In: W. Penfield's Cytology and Cellular Pathology of the Nervous System. Hoeber, New York, pp. 673-703.
- DeRobertis, E., and A. Pellegrino de Iraldi 1961 Plurivesicular secretory processes and nerve endings in the pineal gland of the rat. *J. Biophys. and Biochem. Cytol.*, 10: 361-372.
- Duncan, D., and G. Micheletti 1966 Notes on the fine structure of the pineal organ of cats. *Texas Rep Biol. and Med.*, 24: 576-587.
- Ebels, I., and N. Prop 1965 A study of the effect of melatonin on the gonads, the oestrous cycle and the pineal organ of the rat. *Acta Endocrinologica*, 49: 567-577.
- Freeman, J. A., and B. O. Spurlock 1962 A new epoxy embedment for Electron Microscopy. *J. Cell Biol.*, 13: 437-443.
- Kappers, J. Ariens 1960 The development, topographical relations and innervation of the epiphysis cerebri in the albino rat. *Z. Zellforsch.*, 52: 163-215.
- 1965 Survey of the innervation of the epiphysis cerebri and the accessory pineal organ of vertebrate. *Progress Brain Research*, 10: 87-153.
- Lerner, A. B., J. D. Case, Y. Takahashi, T. H. Lee and W. Mori 1958 Isolation of melatonin, the pineal gland factor that lightens melanocytes. *J. Amer. Chem. Soc.*, 80: 2587.
- Lin, H. S. 1965 Microcylinders within mitochondrial cristae in the rat pinealocyte. *J. Cell Biol.*, 25: 435-443.
- Lockwood, W. R. 1964 A reliable and easily sectioned epoxy embedding medium. *Anat. Rec.*, 150: 129-140.
- Luft, J. H. 1961 Improvements in epoxy resin embedding methods. *J. Biophys. Biochem. Cytol.*, 9: 409-414.
- Milofsky, A. H. 1957 The fine structure of the pineal in the rat with special reference to parenchyma. *Anat. Rec.*, 127: 435-436.
- Pellegrino de Iraldi, A., L. M. Zieher and E. DeRobertis 1963 Ultrastructure and pharmacological studies of nerve endings in the pineal organ. *Prog. Brain Res.*, 10: 389-421.
- Pellegrino de Iraldi, A. 1966 Granular vesicles in pinealocytes of the hamster. *Anat. Rec.*, 154: 481.
- Reiter, R. J., and R. J. Hester 1966 Interrelationships of the pineal gland, the superior cervical ganglia and the photoperiod in the regulation of the endocrine systems of hamsters. *Endocrinology*, 79: 1168-1170.
- Reiter, R. J., R. A. Hoffman and R. J. Hester 1966 The role of the pineal gland and of environmental lighting in the regulation of the endocrine and reproductive systems of rodents. U.S. Army Edgewood Arsenal Tech. Report 4032. Med Res. Laboratory, U.S. Army Edgewood Arsenal, Md. 51 pp.
- Richardson, K. C. 1962 The fine structure of autonomic nerve endings in smooth muscle of the rat vas deferens. *J. Anat.*, 96: 427-442.
- Rodin, A. E., and R. A. Turner 1965 The relationship of intravesicular granules to the innervation of the pineal gland. *Lab. Invest.*, 14: 1644-1651.
- 1966 The perivascular space of the pineal gland. *Texas Reports Biol. and Med.*, 24: 153-163.
- Sheridan, M. N. 1967 Fine structure of the hamster pineal gland. *Anat. Rec.*, 157: 320.
- Shore, P. A., S. L. Silver and B. B. Brodie 1955 Interaction of reserpine, serotonin and lysergic acid diethylamine in brain. *Science*, 122: 284-285.
- Smith, C. A., and F. S. Sjostrand 1961 A synaptic structure in the hair cells of the guinea pig cochlea. *J. Ultrastructure Research*, 5: 184-192.
- Wartenberg, H., and W. Gusek 1965 Licht und elektronmikroskopische Beobachtungen über die struktur der epiphysis cerebri des kaninchens. *Progress Brain Research*, 10: 269-316.
- Wolfe, D. E. 1965 The epiphyseal cell: an electron microscopic study of its intercellular relationships and intracellular morphology in the pineal body of the albino rat. *Progress Brain Research*, 10: 332-386.
- Wolfe, D. E., L. T. Potter, K. C. Richardson and J. Axelrod 1962 Localizing tritiated norepinephrine in sympathetic axons by electron microscope autoradiography. *Science*, 138: 440-442.
- Wurtman, R. J., and J. Axelrod 1965 The formation, metabolism and physiological effects of melatonin in mammals. *Progress Brain Research*, 10: 520-529.

these ganglia would be expected to produce a disappearance of granulated vesicles in nerve endings and possibly the granulated vesicles in the pineal cell also. Pellegrino de Iraldi ('66) was unable to deplete the granulated vesicles located in the pineal cell of the hamster after removal of the superior cervical ganglia. Bertler, Falk and Owman ('64) have shown that there is a reduction in fluorescence after ganglionectomy apparently in the nerves and associated nerve endings with some decrease in the parenchymal cell fluorescence. Arstila ('67) was unable to show complete disappearance of granulated vesicles from the rat pineal parenchymal cell after similar treatment.

Reserpine is known to deplete biogenic amines in the central nervous system (Shore, Silver and Brodie, '55). Several investigations have shown reserpine-induced depletion of granulated vesicles presumably from the nerve endings as well as pineal cells and their processes. Arstila ('67) was, however, unable to deplete the granulated vesicles from the pineal cell processes, but showed an almost complete disappearance of granulated vesicles from the nerve endings. He, therefore, concluded that all such structures did not reside in nerve endings. Likewise, Pellegrino de Iraldi ('66) was unable to deplete the pineal cell of the hamster of its granules after reserpine and concluded that these structures represented secretory products. Evidence presented here supports a similar conclusion. Because of the location of granulated vesicles in pineal cell processes and nerve endings it appears that this organ would be a poor choice for assaying the effects of drugs on sympathetic nerve endings at the electron microscopic level as previously suggested (Pellegrino de Iraldi et al., '65).

Blood vessels have been encountered in the Syrian hamster infrequently. When they were encountered the perivascular space appeared to be less extensive than reported for other species (Rodin and Turner, '66; Duncan and Micheletti, '66). Since the early 1930's (Del Rio Hortega, '32) this organ has been accepted as possessing glandular organization. Recently, it has come to be considered as

an endocrine organ (Wurtman and Axelrod, '65) possessing physiological properties which substantiate this classification, especially in the hamster, (Reiter et al., '66).

Myelinated axons have been seen and demonstrated at the light microscope level. Kappers ('65) states that "epiphyseal afferent nerve fibers originating within the organ and coursing to the brain are absent." Kappers ('65) also reports central myelinated fibers originating from the habenular commissure and entering the pineal gland. In the gland these fibers make a 180° turn to leave the organ without synapsing and again enter the habenular commissure. The myelinated fibers of this report are believed to be peripheral and not central fibers in that a distinct Schwann cell has always been seen. These axons may represent stray meningeal afferents or preganglionic sympathetic fibers.

LITERATURE CITED

- Anderson, E. 1960 Some cytological observations on the fine structure of a mammalian pineal organ. *Anat. Rec.*, 136: 328.
- 1965 The anatomy of bovine and ovine pineals. Light and electron microscopic studies. *J. Ultrastruct. Res.*, Suppl. 8: 1-80.
- Arstila, A. U. 1967 Electron microscopic studies on the structure and histochemistry of the pineal gland of the rat. *Neuroendocr.* Suppl. 2: 1-101.
- Belt, W. D., and D. C. Pease 1956 Mitochondrial structure in sites of steroid secretion. *J. Biophys. and Biochem. Cytol.*, 2: 369-374.
- Bertler, A., B. Falk and C. Owman 1964 Studies on 5-hydroxytryptamine stores in the pineal gland of the rat. *Acta Physiol. Scand.*, 63: 1-18.
- Christensen, A. K., and G. B. Chapman 1959 Cup-shaped mitochondria in interstitial cells of the albino rat testis. *Exp. Cell Research*, 18: 576-579.
- Chu, E. W., R. J. Wurtman and J. Axelrod 1964 An inhibitory effect of melatonin on the estrous phase of the estrous cycle of the rodent. *Endocrinology*, 75: 238-242.
- Clementi, F., F. Fraschini, E. Muller and A. Zanoboni 1965 The pineal gland and the control of electrolyte balance and of gonadotropic secretion. Functional and morphological observations. *Progress Brain Research*, 10: 585-603.
- Clementi, F., E. Muller and A. Zanoboni 1964 Pineal function and modification of its ultrastructural aspects. *Proc. 2nd International Congress of Endocrinology (London)*, pp. 364-374.

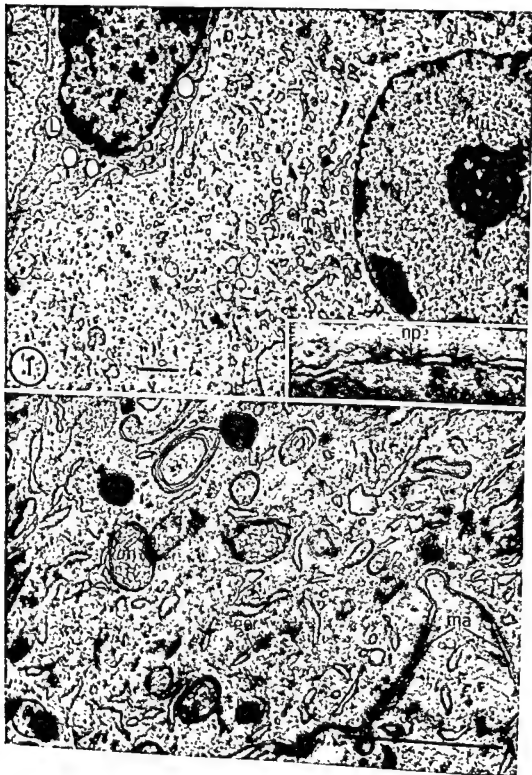


PLATE 1

EXPLANATION OF FIGURES

- 1 A survey electron micrograph depicting two cells encountered within the parenchyma of the hamster pineal. The cell of greater density has a higher concentration of lipid (L) and granular endoplasmic reticulum. Mitochondria (m) are evident in both cells. A nucleus (N) with a prominent nucleolus (NU) is evident in the lighter cell. $\times 10,000$ Inset: A higher magnification of the nuclear membrane from the light cell nucleus of figure 1. The double nature of the nuclear membrane is evident and it possess prominent nuclear pores (np). 1% OsO_4 in veronal acetate with sucrose/maraglas. $\times 60,000$.
- 2 An area showing cytoplasmic structure of two adjacent parenchymal cells. Maculae adherens (ma) are present. Mitochondrion (m) with a tubular internum, granular endoplasmic reticulum (ger) and membrane-bound dense structures, presumably lysosomes (Ly) are constant features of the pineal cell. 1% OsO_4 in veronal acetate with sucrose/maraglas. $\times 42,000$.

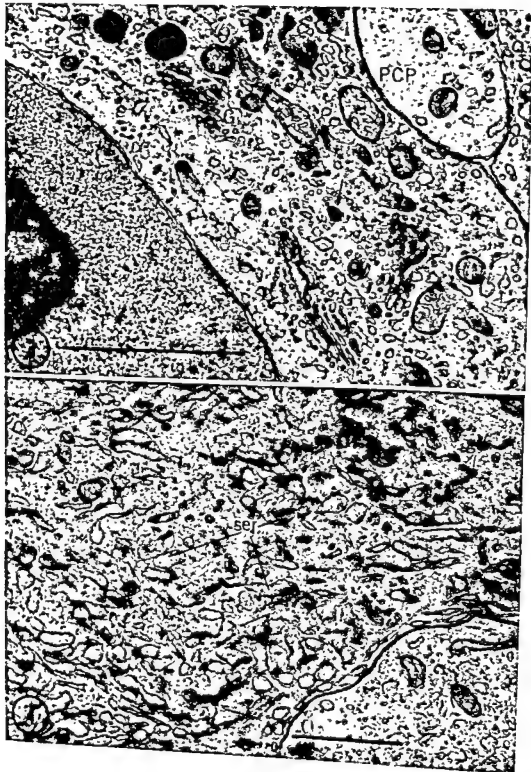


PLATE 2

EXPLANATION OF FIGURES

- 3 A Golgi apparatus (G) is present in a juxta-nuclear position. Some of the vesicles and larger vacuoles present contain electron dense deposits (arrow). A pineal cell process (PCP) is present in the upper right quadrant of the micrograph between two adjacent parenchymal cells. 1% OsO_4 in veronal acetate with sucrose/Epon. $\times 49,000$.
- 4 Smooth endoplasmic reticulum (ser) frequently occupies cytoplasmic areas often more compact than shown here. Vesicles with electron dense granulations are evident (gV). 1% OsO_4 in veronal acetate with sucrose/maraglas. $\times 29,000$.

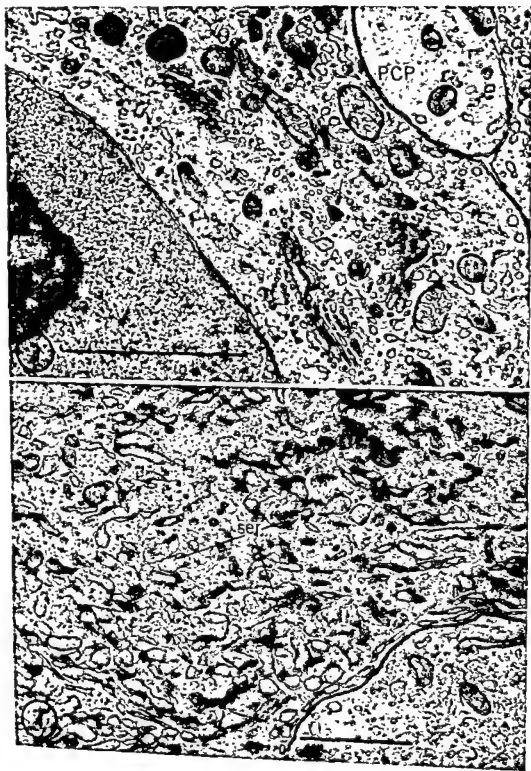


PLATE 2

EXPLANATION OF FIGURES

- 3 A Golgi apparatus (G) is present in a juxta-nuclear position. Some of the vesicles and larger vacuoles present contain electron dense deposits (arrow). A pineal cell process (PCP) is present in the upper right quadrant of the micrograph between two adjacent parenchymal cells. 1% OsO_4 in veronal acetate with sucrose/Epon. $\times 49,000$.
- 4 Smooth endoplasmic reticulum (ser) frequently occupies cytoplasmic areas often more compact than shown here. Vesicles with electron dense granulations are evident (gV). 1% OsO_4 in veronal acetate with sucrose/maraglas. $\times 29,000$.

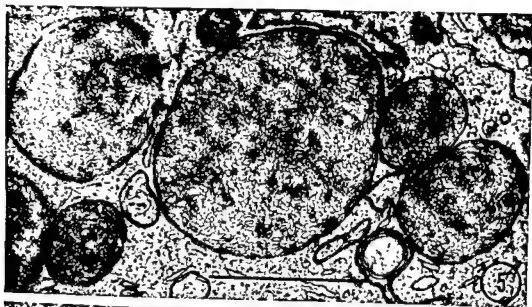


PLATE 3

EXPLANATION OF FIGURES

- 5 Mitochondria with a highly packed internum of tubules as shown here are regularly encountered in the pineal cell. 1% OsO_4 in veronal acetate with sucrose/maraglas. $\times 43,000$.
- 6 Mitochondrial profiles such as these shown, are frequent. A configuration as in area "B" would be obtained by sectioning area "A" at right angles to its present plane provided it contained a mitochondrion nestled in its cavity. 1% OsO_4 in veronal acetate with sucrose/maraglas. $\times 50,000$.
- 7 Mitochondrial forms such as this probably account for the cup-shaped form in figure 6. 1% OsO_4 in veronal acetate with sucrose/maraglas. $\times 69,000$.

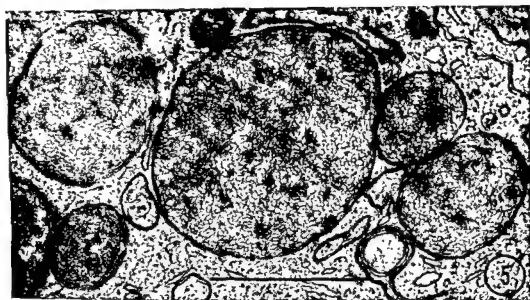


PLATE 4

EXPLANATION OF FIGURES

- 8 A pineal cell process (PCP) appears to be emerging from the pineal body (PCB). Microtubules (mt) approximately 200 Å in diameter appear to "sweep" into the process from the cell body. Granulated vesicles (gV) are present in the cell body. 1% OsO₄ in veronal acetate with sucrose/maraglas. \times 40,000.
- 9 Pineal cell processes cut in both cross and long section (PCP) are shown. Microtubules (mt) are evident. 1% OsO₄ in veronal acetate with sucrose/maraglas. \times 51,000.

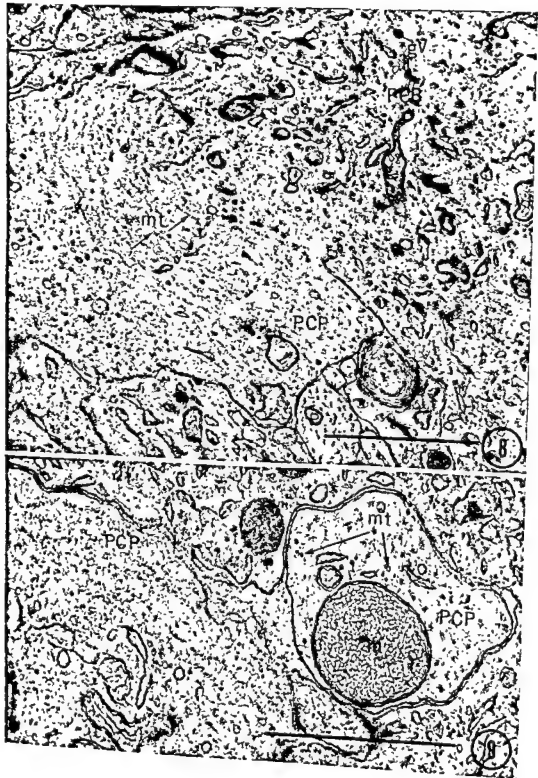


PLATE 5

EXPLANATION OF FIGURES

- 10 A pineal cell process is shown containing numerous vesicles, many of which contain granules (gV). Mitochondria (m) and smooth endoplasmic reticulum (ser) are present. A vesicle-crowned lamella (VCL) is present in a cell body. 1% OsO₄ in veronal acetate with sucrose/maraglas. $\times 31,000$.
- 11 A pineal cell process ending (PPE) is either located between two or surrounded by a single pineal cell. The ending contains numerous granulated vesicles all of the large-cored variety. 1% OsO₄ in veronal acetate with sucrose/DER. $\times 32,000$.
- 12 Two nerve endings (NE) are present adjacent to a pineal cell (PCB). Some of the vesicles of the nerve endings contain granules all of which are of the small-cored variety. 1% OsO₄ in veronal acetate with sucrose/maraglas. $\times 52,000$.

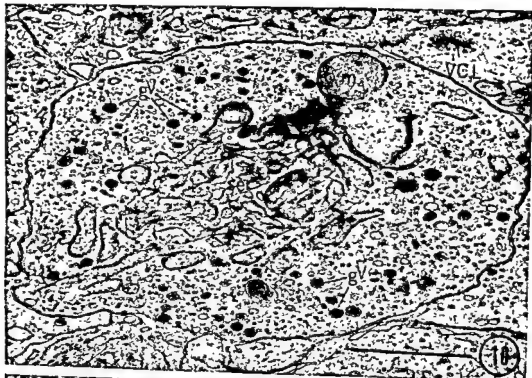


PLATE 6

EXPLANATION OF FIGURES

- 13 A capillary consisting of an endothelial cell (EC) resting on a basement membrane (BM) is present within the parenchyma of the gland. A red blood cell (RBC) occupies the lumen. Non-myelinated axons associated with a Schwann cell (SC) are present in the perivascular space. 1.33% OsO_4 in collidine/DER. $\times 15,000$.
- 14 A glial process (GP) occupying the perivascular space. The endothelial cell (EC) of the blood vessel shows numerous pinocytotic vesicles. 1.33% OsO_4 in collidine/DER. $\times 28,500$.
- 15 Most of the nerve bundles and fibers encountered in the pineal gland are non-myelinated axons (*). The occasional myelinated axon (AX) is seen. A Schwann cell is present in the lower part of the micrograph displaying a prominent nucleus (SN). 1% OsO_4 in veronal acetate with sucrose/Epon. $\times 18,000$.
- 16 Axons (*) and pineal cell processes (PCP) can be compared in this micrograph. The higher concentration of microtubules in the axons is readily apparent. A basement membrane (BM) surrounds axon bundles. Schwann cell cytoplasm (SC) and a nerve ending (NE) are indicated. 1% OsO_4 in veronal acetate with sucrose/maraglas. $\times 15,000$.



Dense Granules (Lysosomes?) and Crystals in the Thyroids of Senile Rats

JOHN YOUSON AND H. VAN HEYNINGEN
*Department of Anatomy, McGill University,
Montreal, Canada*

ABSTRACT While all follicular cells display some dense "lysosome-like" granules (0.1–2.5 μ), they are more numerous and complex in animals of 14 months or older. There are various types of granules which share some morphological features, but vary in the extent to which they accumulate dense membranous fragments and droplets (0.02–0.4 μ) within their matrices.

Crystalline inclusions are also found in the follicular cells of these older animals, and morphological similarities to dense granules suggest that the crystals may be derived from the granules.

Various types of granules have been classified in the thyroid follicular cells as to size (van Heyningen, '65), electron density (Wissig, '63; Wetzel et al., '65), acid phosphatase activity (Wetzel et al., '65) and glycoprotein content (van Heyningen, '65).

The largest of these are colloid droplets (1.0–3.0 μ), having a similar electron density to the luminal colloid. They contain periodic acid-reactive carbohydrate (van Heyningen, '65) and may show acid phosphatase activity under certain conditions (Wetzel, '65).

The smallest granule type (0.02–0.2 μ), the apical vesicles, are slightly more electron-dense than colloid droplets and the luminal colloid. They contain periodic acid-reactive carbohydrates (van Heyningen, '65, Youson, '66; Rambourg and Leblond, '67), but have not been shown to contain acid phosphatase.

Granules usually intermediate in size (0.1–2.5 μ) between colloid droplets and apical vesicles are also more electron-dense than both. They have been termed "dense granules" (Wetzel et al., '65), "medium-sized globules" (van Heyningen, '65), "zymogen-like granules" (Nadler et al., '64), "lysosomes" (Novikoff and Vorbrodt, '63, Wollman et al., '64) and "cytosomes" (Seljelid, '67) because they have been shown to contain acid phosphatase. Most investigators believe that these granules contain enzymes which act in the breakdown of the thyroglobulin molecule to release thyroxine.

When making a comparative morphological study of the thyroid follicular cells of rats of various ages, it was noticed that there was a large accumulation of these 0.1–2.5 μ granules in senile animals. It is the purpose of this paper to show the many forms in which these granules appear and also to report the presence of crystalline bodies within the senile rat thyroid.

MATERIALS AND METHODS

Male Sherman rats obtained from Rockland Farms Inc., Rockland County, N. Y., were classified into three groups of five on the basis of age. The weights of the animals were also recorded. One group of 40–45-day-old animals weighed between 150–200 gms. A second group of 14–16-month-old animals weighed 400–500 gms. while a final group consisted of 24-month-old animals weighing 550–600 gms.

The animals were anesthetized and the right lobe of the thyroid was fixed "in situ" for five minutes with 1% osmium tetroxide buffered to pH 7.2 with veronal acetate (Palade, '52). The animals were then killed by thoracotomy and the right lobe removed. Next, the tissue was sliced into small pieces and further fixation was performed in chilled veronal-buffered osmium tetroxide for 1–2 hours. After fixation, the tissues were dehydrated in a graded series of ethyl alcohol and propylene oxide before embedding in Epon 812 (Luft, '61). Ultrathin sections (silver to gold) were cut on a Porter-Blum microtome

In the electron microscope, the smaller or "dense" granules appeared to be of various types, perhaps because of the presence of dense membrane-fragments and small droplets within their matrix (fig. 2). Despite these irregularities, these granules all contained certain features in common. First, they all contained a matrix of similar density and granularity (figs. 4, 13, A-F). The density, although somewhat variable, was always much more pronounced than that of the luminal colloid. The matrix, in addition, usually contained particles of 70 Å (fig. 8). Second, they were bound by a single unit membrane which frequently appeared discontinuous (figs. 7, 13, A-F). Third, beneath the unit membrane there was a "halo," that is a space which did not take up stain (figs. 7, 13, A-F). This "halo" was usually of constant thickness but, like the membrane, did not extend completely around the matrix of the granule. Hence, any granule with these three features, whether or not it included dense material, was termed a dense granule.

Many types of dense granules were observed, due to their association with dense materials (fig. 13). The simplest type of dense granule showed a hazy, heavily stained material in the matrix abutting against the halo but never extending into it (figs. 4, 5). The amount of this material varied from practically none (fig. 4) to extending entirely around the matrix at the level of the halo (fig. 5). Other granules contained, in addition to hazy membrane-like material, small droplets of 0.02–0.4 μ diameter within their matrix (fig. 6). Sometimes these droplets appeared to be partly outside of the granule (fig. 5) but higher magnification showed that bleb-like extension of the granule completely included the droplets in the granule matrix. Finally, other granules contained hazy, heavily stained material within their matrix which almost obscured the entire granule matrix. However, the granule could still be identified by the characteristic halo, which usually was seen at some point inside of the unit membrane (fig. 4).

The dense granules did not appear to be localized within any specific region of the follicular cell, but occasionally groups

of the smaller ones could be seen close to the Golgi regions (fig. 4).

The crystal-like structures appeared in the electron microscope as a dense square or elongated oblong structure (figs. 9–11). They varied in width from 0.3–0.7 μ and in length from 2.0–8.0 μ . The matrix of the crystals was not homogeneous (fig. 9) but was interrupted by vacuoles or droplets and blotchy areas free of any matrix. The crystals were enclosed within a membrane, were of various shapes probably due to the plane of section, and contained a periodicity of 90–100 Å (fig. 12). The droplets were similar to those seen in some dense granule types (fig. 6). Sometimes the droplets appear as clear vacuoles, for their content had been leached out in the preparation of the tissue (figs. 10, 12). When the droplets within the crystals appeared to have been leached out, a similar leaching was noted in the droplets within the dense granules. There was no specific localization of these crystals within the follicular cell.

DISCUSSION

Axelrad and Leblond ('55) gave descriptions of the follicular epithelium of the thyroid glands of 24–36-month-old female Sherman albino rats fed on adequate iodine diets, and noted accumulation of spherical droplets within the follicular cells. In unstained preparations, these droplets showed a yellowish tinge and the suggestion was made that the droplets may be "wear and tear" pigments. Erdheim ('03) and Dogliotti and Nizzi-Nuti ('35) in the aged human thyroid, and Payne ('49, '52) in the aged fowl noted similar accumulations of granules. Recently, van Heyningen ('65) illustrated rat follicular cells packed with toluidine blue-staining granules, termed "medium-sized globules." The animals used in this study ranged from adult to senile. This present study is a portion of an investigation in which similar findings to the above were noted. That is, there appears to be an increase in granules of 0.1–2.5 μ diameter in the rat follicular cells with age (Youson, '66).

The obvious question to follow is the nature of these dense granules. In the light microscope, Axelrad and Leblond ('55), van Heyningen ('65) and Seljelid

and mounted on naked copper grids. Sections were stained with either lead hydroxide (Karnovsky, '61), lead citrate (Reynolds, '63) or doubly stained with uranyl acetate (Watson, '58) and Reynolds' lead.

In addition, 0.5–1.0 μ sections were stained with 1% toluidine blue in saturated sodium borate for light microscopy.

Approximately 5–10 blocks were examined for each animal.

RESULTS

The thyroid follicular cells of albino rats over 14 months of age were similar in general appearance to the description of the cells by earlier investigators (fig. 1). Namely, they were low to high cuboidal cells, pyramidal in shape, with a truncated apex. At their apex, they contained projections of cytoplasm, the microvilli, which were highly irregular in their shape, number and distribution (fig. 3). Their round and sometimes irregularly shaped nucleus was basally located and contained a prominent nucleolus. As is typical of thyroid follicular cells, the ergastoplasm was com-

posed of highly distended cisternae of the endoplasmic reticulum with irregularly distributed ribosomes along its wall. The Golgi apparatus appeared above and to one side of the nucleus and consisted of rather distended saccules and "microvesicles." Finally, mitochondria were round to elongated in shape and were distributed irregularly throughout the cell.

The majority of thyroid follicular cells of animals over 14 months of age were characterized by the presence of a large number of granules from 0.1–2.5 μ in diameter within their cytoplasm (figs. 2, 3). In 0.5 μ sections stained with toluidine blue, these granules stained a deep purple (fig. 1). The larger granules (1.0–2.5 μ) were found singly or in groups of two or three (fig. 3), while the smaller granules (0.1–1.0 μ) usually occurred in large clusters (fig. 2). In addition to these granules, the 0.5 μ sections indicated the presence of elongated structures resembling crystals (fig. 1, cs). These crystal-like structures stained with the same intensity as the granules and were not oriented in any specific manner within the cell.



Fig. 1 Thyroid gland of 24-month-old rat. Osmium-fixation, Epon-embedding, toluidine blue stain. $\times 1,100$.

Follicular cells containing numerous 1.5–2.5 μ dark granules (lg) as well as small numbers of dark granules, 0.1–0.8 μ (sg). In addition, a few follicular cells contain homogeneous crystal-like structures, 2.0–8.0 μ in length (cs). Short forms of crystals are also seen in close proximity to these elongated forms (arrow). Pale-staining colloid droplets (cd) are seen in a few cells only.

of old rats. Membrane fragments and droplets could be due to the engulfment of these particles by the granule or by enzymatic changes within the granule itself. On the other hand, Seljelid ('67) suggests that "cytosomes" come from the Golgi region and "cytosegrosomes" (the more complex granules) from wrappings of the endoplasmic reticulum around exhausted organelles.

The earliest report of crystals in the thyroid gland appears to be that of Zeiss (1877) who mentioned the presence of octahedral crystals of calcium oxalate in the luminal colloid. Later, Podach (1892) observed similar crystals while Gunther (1896) described crystalloids of a proteinaceous nature, different from calcium oxalate, within the luminal colloid. In 1914, Bensley described "needle-like" crystals in the follicular cells of the opossum thyroid. Uhlenhuth ('29) was able to induce experimentally the formation of similar "needle-like" crystals in salamander larvae. Bargmann ('39) gives an account of these "needle-like" crystals in so-called "chief cells" of the follicular epithelium of the opossum. Richter ('40) and Richter and McCarty ('54) reported again the finding of the octahedral crystals originally reported by Zeiss. The latest extensive report on crystals in the thyroid gland was made by Yoshimura and Irie ('61) who showed crystal-like structures in the follicular cells of both normal and stimulated rat and chicken thyroid glands. They correlated their crystals with those seen by Bensley ('14) and Bargmann ('39). In the light microscope, they appeared as periodic acid-Schiff-positive inclusions measuring 1.0-7.0 μ in length and 0.3-0.5 μ in width. They were membrane-bound but often were contained within a sac or vacuole. Fujita et al. ('63) have also reported seeing similar crystals in the thyroid follicular cells of stimulated rats.

The crystals under observation in the present study are similar to those described by Yoshimura and Irie ('61). However, there are some features of these crystals which they did not describe. First, in contrast to their observations, these crystals did not appear to be periodic acid-Schiff-positive. Second, there is present in almost

all of these crystalline inclusions, droplets or vacuoles of 0.02-0.4 μ in diameter (figs. 9, 10, 12). Third, there is generally an accumulation of a dense particulate material on the inner surface of the membrane delimiting the structure (figs. 9, 13, H). Fourth, some of these structures contain patchy irregular spaces giving the crystal a mottled appearance (figs. 10, 12, 13, H). Finally, all crystals contain striations running either obliquely or transversely through the matrix of the inclusion (figs. 12, 13, H).

Since their crystals were periodic acid-Schiff-positive, Yoshimura and Irie suggests that they are probably derived from colloid droplets. However, in the present study, it is seen that the crystals have morphological similarities to some of the dense granules. These morphological similarities are the presence of droplets within their matrix and a dense particulate material at the level of the membrane. It is believed therefore that these crystals may be derived from dense granules. This hypothesis is supported by the fact that very few dense granules are seen within follicular cells containing crystals (figs. 1, 11). No explanation can be given to account for the change in shape and size of these crystals, for if they are derived from granules they would have to elongate and in some cases become square in outline. The elongated structure may be the result of fusion of a number of granules, for it is noted that the granules sometimes appear aligned in an organized fashion (fig. 1). In general, the width of the crystals is smaller than the diameters of the granules and therefore a change in shape would be accompanied by a decrease in size. The shrinkage may be due to dehydration. As Wetzel et al. ('65) suggested, possibly some of the dense granules are derived from colloid droplets. If such is the case, then the view of Yoshimura and Irie ('61) that these crystals are derived from colloid droplets may indeed be a correct observation. The significance of the presence of the crystals within the follicular cell is not known. They may represent the accumulation of a secretory product which cannot be liberated from the cell and the possibility of viral particles cannot be ruled out. The findings indicate, however, that these crystals are only pre-

('67) noted that these granules stained with periodic acid-Schiff (a conclusion which was not confirmed in the present investigation, perhaps because of different fixation conditions). In the electron microscope, van Heyningen ('65), Youson ('66) and Rambourg and Leblond ('67) stained these granules with the periodic acid-silver methenamine technique. These results suggest the presence of periodic acid-reactive carbohydrates, probably of a glycoprotein nature, within the granules. In the electron microscope, the dense granules appear as single membrane-bound structures containing a halo and 70 Å particles resembling ferritin (figs. 6, 7). They resemble the structures originally isolated from liver fractions by DeDuve et al. ('55) and characterized morphologically by Novikoff ('61). Since then, many investigators have shown that these isolated structures contain acid phosphatase (DeMan, '60; Essner and Novikoff, '60, '61; Novikoff, '60, '61; Holt and Hicks, '61; Novikoff and Essner, '62; Ericsson and Trump, '64; and others) by employing Gomori's ('52) lead phosphate technique. This led Essner and Novikoff ('60) to suggest that all single membrane-bound bodies containing acid phosphatase should be termed "lysosomes." Fawcett ('66) and others state that, because lysosomes are heterogeneous, it is impossible to identify them on a morphological basis alone. According to these views, the investigator would be restricted in using the term "lysosome" in describing and discussing experimental data, and lysosomes should be identified through enzyme reactions such as acid phosphatase.

Lysosomes have been identified in the thyroid gland through enzyme reactions (Lever, '58; Sobel, '62; Novikoff and Vrobrodt, '63; Wollman et al., '64; Wetzel et al., '65; Seljelid, '67). A comparison of these granules showing enzyme activity with the dense granules described here, shows a number of interesting morphological similarities. They are all bound by a single, usually discontinuous membrane, and contain a halo, a similar relative density and granularity of their matrix and usually 70 Å particles. It seems reasonable therefore to suggest that dense granules are probably lysosomes, even though there

is insufficient evidence of enzyme activity within these granules at present.

The next question to be discussed is the role played by these granules within the follicular cell. At present, the best explanation has been provided by Wollman et al. ('64) and Wetzel et al. ('65). Wollman and coworkers showed in the light microscope a localization of esterase and acid phosphatase within these granules and droplets in the follicular cell. Wetzel et al. were then able to show in the electron microscope that, in hypophysectomized unstimulated animals, the acid phosphatase reaction is initially localized in dense granules occurring in clusters at the base of the cell. In animals given thyroid stimulating hormone (TSH), there is an increase in colloid droplets within the follicular cell, and eventually a nonspecific acid phosphatase localization is seen over the colloid droplets as well as the dense granules. It was therefore suggested that there is a possible transfer of enzymatic activity from dense granules to colloid droplets, either through fusion of granules and colloid droplets or through transfer across opposed intact membranes. Therefore, they suggest that one of the roles of these granules within the follicular cell is to provide enzymes necessary for the breakdown of colloid droplets. According to Nadler et al. ('62, '64), Wollman et al. ('64), colloid droplets represent a mechanism for the resorption and degradation of follicular colloid, and may be the site of thyroxine release.

The dense granules appeared in many diverse forms in the animals over 14 months of age (fig. 13, A-G). Wetzel et al. ('65) suggested that a large number of dense granules seen in the follicular cells of their hypophysectomized TSH-stimulated animals were probably aged colloid droplets. Colloid droplets when they first appear in the follicular cell are of low electron density, but with time they eventually become more electron-dense and may take on membrane fragments such as are seen in dense granules. The decreased density and size suggested to them a process of dehydration and concentration of droplet contents. Such an explanation if true could explain the many diverse forms of dense granules seen in the thyroid follicular cells

- protein-containing globules in the follicular cells of the thyroid gland of the rat. *J. Histochem. Cytochem.*, 13: 286-296.
- Watson, M. L. 1958 Staining of tissue sections for electron microscopy with heavy metals. *J. Biophys. Biochem. Cytol.*, 4: 475-478.
- Wetzel, B. K., S. S. Spicer and S. H. Wollman 1965 Changes in fine structure and acid phosphatase localization in rat thyroid cells following thyrotropin administration. *J. Cell Biol.*, 25: 593-618.
- Wissig, S. L. 1963 The anatomy of secretion in the follicular cells of the thyroid gland. *J. Cell Biol.*, 16: 93-117.
- Wollman, S. H., S. S. Spicer and M. S. Burstone 1964 Localization of esterase and acid phosphatase in granules and colloid droplets in rat thyroid epithelium. *J. Cell Biol.*, 21: 191-201.
- Yoshimura, F., and M. Irie 1961 Licht- und Elektronenmikroskopische Studie an den Kristalloiden in der Schilddrüsenzelle. *Z. Zellforsch.*, 55: 204-219.
- Youson, J. H. 1966 M.Sc. Thesis, Department of Anatomy, McGill University, Montreal.
- Zeiss, A. 1877 Inaugural Dissertation, Strassburg. (Cited by Richter and McCarty, 1954).

sent in the follicular cells of old animals. The animals used by Yoshimura and Irie ('61) and Fujita et al. ('63) were relatively young animals but in the majority of cases they were found in thyroid-stimulated animals. Their presence, therefore, may represent a certain level of activity within the follicular cell.

ACKNOWLEDGMENTS

This work was supported by a grant of the Medical Research Council of Canada to Dr. C. P. Leblond.

LITERATURE CITED

- Axelrad, A. A., and C. P. Leblond 1955 Induction of thyroid tumors in rats by a low iodine diet. *Cancer*, 8: 339-367.
- Bargmann, W. 1939 *Handbuch der Mikroskopischen Anatomie des Menschen*. Ed. by W. von Möllendorf. Julius Springer, Berlin, Vol. 6, part 2, 47.
- Bensley, R. R. 1914 The thyroid gland of the opossum. *Anat. Rec.*, 8: 431-440.
- DeDuve, C., B. C. Pressman, R. Gianetto, R. Wattiaux and F. Appelmans 1955 Tissue fractionation studies. *Biochem. J.*, 60: 604-617.
- DeMan, J. C. H. 1960 Observations, with the aid of the electron microscope, on the mitochondrial structure of experimental liver tumors in the rat. *J. Nat. Cancer Inst.*, 24: 795-819.
- Dogliotti, G. C., and G. Nizzi-Nuti 1935 Thyroid and senescence. *Endocrinol.*, 19: 289-292.
- Essner, E., and A. B. Novikoff 1960 Human hepatocellular pigments and lysosomes. *J. Ultrastructure Res.*, 3: 374-391.
- 1961 Localization of acid phosphatase activity in hepatic lysosomes by means of electron microscopy. *J. Biophys. Biochem. Cytol.*, 9: 773-798.
- Erdheim, J. 1903 Zur normalen und pathologischen Histologie der Glandula thyroidea, parathyroidea und Hypophysis. *Beitr. path. Anat.*, 33: 158-234.
- Ericsson, J. L. E., and B. F. Trump 1964 Electron microscopic studies of the epithelium of the proximal tubule of the rat kidney. *Lab. Invest.*, 13: 1427-1456.
- Fawcett, D. W. 1966 *The Cell*. W. B. Saunders, Philadelphia.
- Fujita, H., M. Machino and K. Nakagami 1963 Electron microscopic studies on the rat thyroid gland following administration of propylthiouracil and thyradin, with special reference to the inclusion body in the follicular cell. *Okajima Folia, anat. jap.*, 39: 157-177.
- Gomori, G. 1958 *Microscopic Histochemistry; Principles and Practice*. University of Chicago Press, Chicago.
- Günther, G. 1896 Über ein Kristalloid der menschlichen Schilddrüse. *S. B. Akad. Wiss. Wien, Math.-Naturw. Abt.*, 105: 341-346.
- Holt, S. J., and R. M. Hicks 1961 The localization of acid phosphatase in rat liver cells as revealed by combined cytochemical staining and electron microscopy. *J. Biophys. Biochem. Cytol.*, 11: 47-66.
- Karnovsky, M. J. 1961 Simple methods for "staining with lead" at high pH in electron microscopy. *J. Biophys. Biochem. Cytol.*, 11: 729-732.
- Korenchevsky, V. 1961 *Physiological and Pathological Ageing*. Hofner, New York.
- Lever, J. D. 1958 In: *Fourth International Conference on Electron Microscopy*. Julius Springer, Berlin.
- Luft, J. H. 1961 Improvements in epoxy resin embedding methods. *J. Biophys. Biochem. Cytol.*, 9: 409-414.
- Nadler, N. J., S. K. Sarkar and C. P. Leblond 1962 Origin of intracellular colloid droplets in the rat thyroid. *Endocrinol.*, 71: 120-129.
- Nadler, N. J., B. A. Young, C. P. Leblond and B. Mitmaker 1964 Elaboration of thyroglobulin in the thyroid follicle. *Endocrinol.*, 74: 333-354.
- Novikoff, A. B. 1960 *Developing Cell Systems and Their Control*. Ed. by D. Rudnick. Ronald Press, New York, 123.
- 1961 *Lysosomes and Related Particles in the Cell*. Ed. by J. Brachet and A. E. Mirsky. Academic Press, New York, 423.
- Novikoff, A. B., and E. Essner 1962 Cytolysosomes and mitochondrial degeneration. *J. Cell Biol.*, 15: 140-146.
- Novikoff, A. B., and A. Vorbrodt 1963 Lysosomes and thyroid function. *J. Cell Biol.*, 19: 53A.
- Palade, G. E. 1952 A study of fixation for electron microscopy. *J. Exp. Med.*, 95: 285-298.
- Payne, F. 1948 Changes in the endocrine glands of the fowl with age. *J. Gerontol.*, 4: 193-199.
- 1952 *Cowdry's Problems of Aging*. Ed. by A. I. Lansing. Williams and Wilkins Co., Baltimore.
- Podach, M. 1892 *Dissertation*. Königsberg. (Cited by Richter and McCarty)
- Rambourg, A., and C. P. Leblond 1967 Electron microscope observations on the carbohydrate-rich cell coat present at the surface of cells in the rat. *J. Cell Biol.*, 32: 27-53.
- Reynolds, E. S. 1963 The use of lead citrate at high pH as an electron-opaque stain in electron microscopy. *J. Cell Biol.*, 17: 208-212.
- Richter, M. N. 1940 Anisotropic crystalloids in the human thyroid gland. *Am. J. Pathol.*, 16: 654-655.
- Richter, M. N., and K. S. McCarty 1954 Anisotropic crystals in the human thyroid gland. *Am. J. Pathol.*, 30: 545-553.
- Seljelid, R. 1967 Endocytosis in thyroid follicle cells. *J. Ultrastruct. Res.*, 17: 195-219.
- Sobel, H. J. 1962 Relationship of three lysosomal enzymes to the Golgi zone and secretory activity in the rat pituitary and thyroid glands. *Anat. Rec.*, 143: 389-397.
- Uhlenhuth, E. 1927 Die Morphologie und Physiologie der Salamander-Schilddrüse. *Arch. Entw. Mech. Org.*, 109: 611-749.
- Van Heyningen, H. E. 1965 Correlated light and electron microscope observations on glyco-

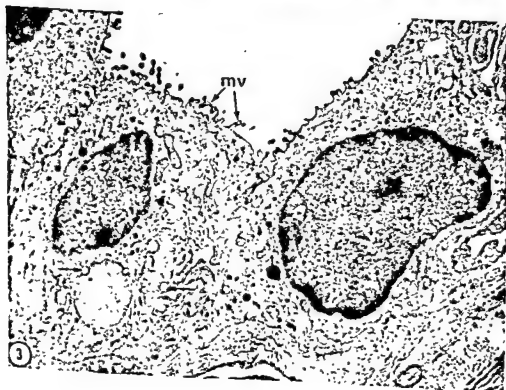


PLATE 1

EXPLANATION OF FIGURES

Low-magnification electron micrographs of the epithelium of a 24-month-old rat thyroid follicle. Osmium-fixation, Epon-embedding, uranyl acetate-lead stain. $\times 10,000$.

- 2 Oblique section through a thyroid follicle showing a number of follicular cells (FC) and a light cell (LC) at the base of the follicle. The follicular cells contain numerous dense granules of $0.1-1.0 \mu$.
- 3 Follicular cell with two dense granules of $1.0-2.5 \mu$ diameter. One of these granules appears spherical while the other is elongated and "torpedo-shaped." Both granules contain droplets of $0.02-0.04 \mu$ diameters within their matrix (arrows). The microvilli (mv) are highly irregular in their shape, number and distribution.

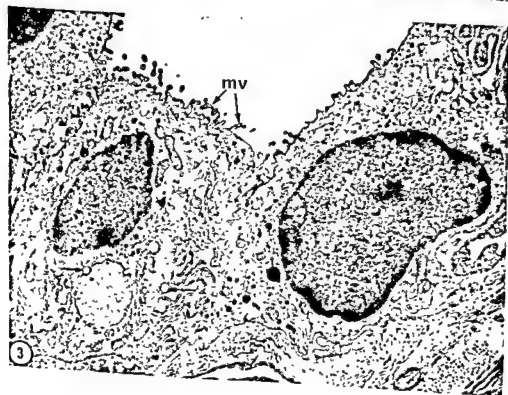


PLATE 2

EXPLANATION OF FIGURES

Follicular cells of 14-16-month-old rat thyroid gland. Osmium-fixation, Epon-embedding.

- 4 A follicular cell showing a group of dense granules in close proximity to a Golgi body (G). Also seen are lipid-like droplets (L). Note the accumulation of a dense hazy material abutting against the halo (arrows). Karnovsky's stain. $\times 30,000$.
- 5 A small portion of a follicular cell, showing a group of dense granules containing membrane fragments. One granule contains a small droplet within its matrix (arrow). Reynold's lead stain. $\times 35,000$.

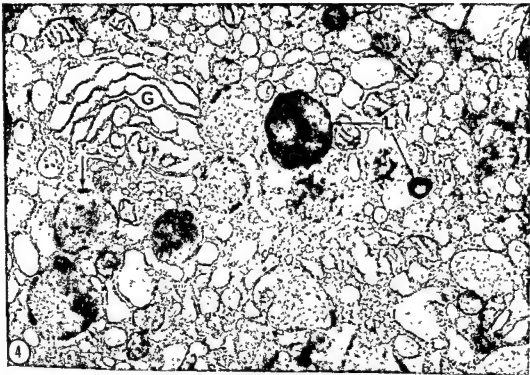


PLATE 2

EXPLANATION OF FIGURES

Follicular cells of 14-16-month-old rat thyroid gland. Osmium-fixation, Epon-embedding.

- 4 A follicular cell showing a group of dense granules in close proximity to a Golgi body (G). Also seen are lipid-like droplets (L). Note the accumulation of a dense hazy material abutting against the halo (arrows). Karnovsky's stain. $\times 30,000$.
- 5 A small portion of a follicular cell, showing a group of dense granules containing membrane fragments. One granule contains a small droplet within its matrix (arrow). Reynold's lead stain. $\times 35,000$.

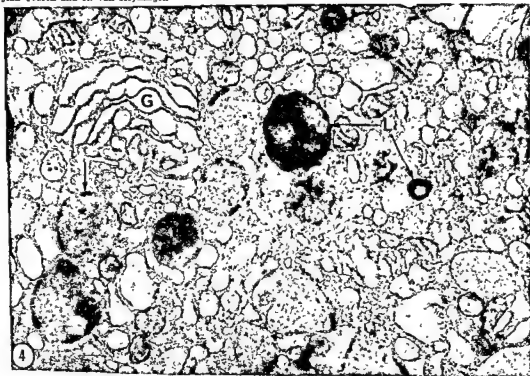


PLATE 3

EXPLANATION OF FIGURES

Follicular cells of 14-16-month-old rats. Osmium-fixation, Epon-embedding, Karnovsky's stain.

- 6 Large dense granules in the follicular cell containing droplets of 0.02-0.08 μ diameter (d). These granules also contain 70 Å particles (arrows). $\times 40,000$.
- 7 High magnification of a portion of a dense granule showing a single unit membrane (su) and halo (h). A fine, dense material is seen on the inner surface of the halo (arrow). $\times 100,000$.
- 8 High magnification of a group of dense granules showing 70 Å particles (arrows). One granule shows a distinctive halo (h) although it is almost obscured by a droplet. $\times 80,000$.

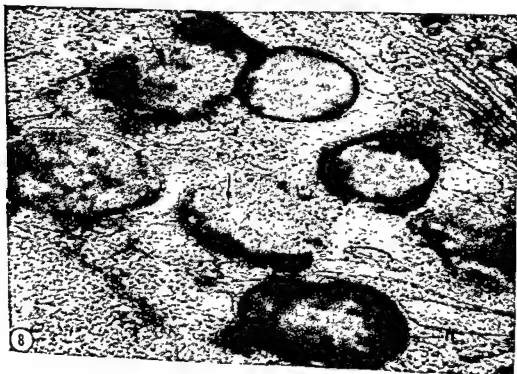


PLATE 3

EXPLANATION OF FIGURES

Follicular cells of 14-16-month-old rats. Osmium-fixation, Epon-embedding, Karnovsky's stain.

- 6 Large dense granules in the follicular cell containing droplets of 0.02-0.08 μ diameter (d). These granules also contain 70 Å particles (arrows). $\times 40,000$.
- 7 High magnification of a portion of a dense granule showing a single unit membrane (su) and halo (h). A fine, dense material is seen on the inner surface of the halo (arrow). $\times 100,000$.
- 8 High magnification of a group of dense granules showing 70 Å particles (arrows). One granule shows a distinctive halo (h) although it is almost obscured by a droplet. $\times 80,000$.

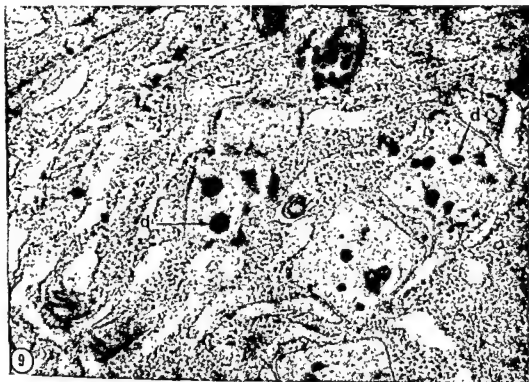


PLATE 4

EXPLANATION OF FIGURES

- 9 Crystalline inclusions within the follicular cell of a 14-16-month-old rat. Osmium-fixation, Epon-embedding, Karnovsky's stain. $\times 60,000$. Square- and oblong-shaped crystals appear to be within the cytoplasmic matrix and not within the cisternae. The matrix of the crystals is not homogeneous but contains droplets of $0.02-0.2 \mu$ (d).
- 10 Crystalline inclusion in the follicular cell of a 24-month-old rat. Osmium-fixation, Epon-embedding, uranyl acetate-lead stain. $\times 43,000$. Crystals are enclosed within a single membrane (s). Sometimes the membrane is absent giving the appearance of a vacuole-enclosed crystal (va). This "torpedo-shaped" crystal contains striations and small droplets (d) within its matrix. The matrix is not homogeneous but contains some clear areas (arrow).

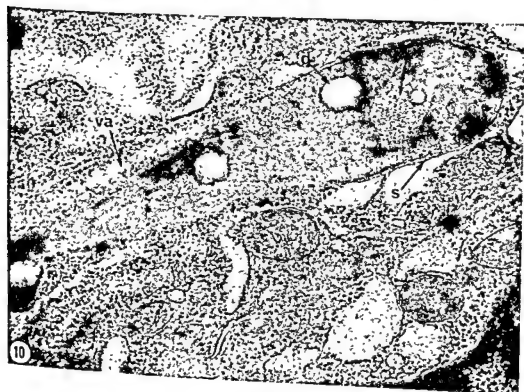


PLATE 5

EXPLANATION OF FIGURES

- 11 Vacuole-enclosed crystal within the follicular cell of a 24-month-old rat. Osmium fixation, Epon-embedding, uranyl acetate-lead stain. $\times 16,000$. A group of three short crystals are enclosed within a vacuole near the base of a follicular cell. At certain points (arrows) the crystals are still attached to a membrane.
- 12 Crystalline inclusion from a thyroid follicular cell of a 14-16-month-old rat. $\times 60,000$. These crystals show striations (st), droplets (d) and blotchy areas free of any crystalline matrix (arrows).

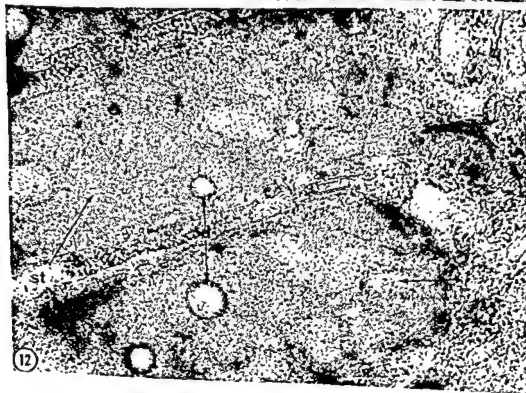


PLATE 5

EXPLANATION OF FIGURES

- 11 Vacuole-enclosed crystal within the follicular cell of a 24-month-old rat. Osmium fixation, Epon-embedding, uranyl acetate-lead stain. $\times 16,000$. A group of three short crystals are enclosed within a vacuole near the base of a follicular cell. At certain points (arrows) the crystals are still attached to a membrane.
- 12 Crystalline inclusion from a thyroid follicular cell of a 14-16-month-old rat. $\times 60,000$. These crystals show striations (st), droplets (d) and blotchy areas free of any crystalline matrix (arrows).

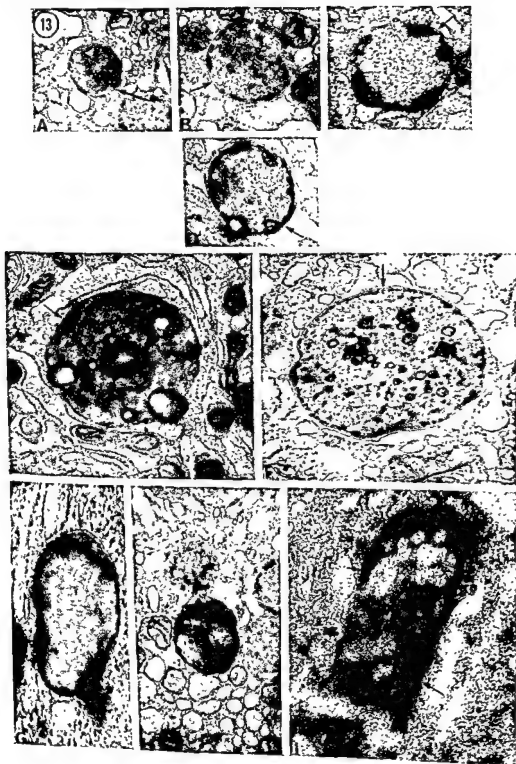


PLATE 6

EXPLANATION OF FIGURES

- 13 Types of inclusions found in the thyroid follicular cells of rats over 14 months of age. Osmium-fixation, Epon-embedding. A-G, dense granules. Close examination reveals the presence of a single unit membrane and "halo" (arrows) in all granule types.

H, lipid-like droplet.

I, crystalline inclusion. Note the presence of halo in this structure (arrows).

A, Karnovsky's lead stain. $\times 30,000$.

B, Karnovsky's lead stain. $\times 40,000$.

C, Karnovsky's lead stain. $\times 40,000$.

D, Karnovsky's lead stain. $\times 40,000$.

E, Reynold's lead stain. $\times 20,000$.

F, Karnovsky's lead stain. $\times 20,000$.

G, Karnovsky's lead stain. $\times 80,000$.

H, Karnovsky's lead stain. $\times 30,000$.

I, Reynold's lead and uranyl-acetate stain. $\times 52,500$

Articular and Internal Remodeling in the Human Otic Capsule¹

RUTH GUSSEN

Department of Pathology and the Department of Surgery, Division of Head and Neck Surgery, Otolaryngology Section, University of California School of Medicine, Los Angeles, California

ABSTRACT A comprehensive histologic study of the human otic capsule is presented demonstrating the interrelations between cartilage, bone, blood vessels and soft tissue throughout life. Remodeling occurs through continual degeneration of chondrocytes within the uncalcified articular surfaces of the stapediovestibular joint and through continual degeneration of cartilage about the cochlea and semicircular canals. Degenerated chondrocytes are removed by macrophages and new endochondral bone forms from adjacent osteogenically active blood vessels. The cartilage surfaces of the footplate and oval window are constantly replenished by new cartilage formed by mesenchymal cells of the annular ligament. Within the otic capsule, new cartilage forms from mesenchymal cells lining the labyrinth. Cartilage foci continually undergo partial replacement by endochondral bone with remnants of uncalcified cartilage matrix remaining, forming globuli ossei and interglobular spaces. In addition to continual endochondral bone formation partially replacing the continually forming and degenerating cartilage, chondroid bone forms by direct transformation of some cartilage to bone. These chondroid bone areas are cellular in young age groups, but become pale and relatively acellular with age. These processes occur throughout life, regardless of age or sex.

Before pathological processes can be adequately recognized and their pathogenesis determined, it is essential that there be a clear recognition of the normal processes occurring throughout the life of a tissue. Only then can deviations from the normal be recognized and explained. The bone and cartilage of the temporal bone have been an enigma. So many different types of cartilage and matrix and bone have been described, all apparently unrelated, that no comprehensive understanding of the otic capsule as a single entity with interrelated physiological mechanisms has seemed possible. The usual concepts have involved consideration of the bone and cartilage as virtually inert, with little, if any, internal reconstruction after the first few years of life. Until a clearer concept of the normal mechanisms inherent in the bone and cartilage of the temporal bone is evolved, it will not be possible to recognize the changes leading to otosclerosis, or the changes involving the temporal bone in systemic disease.

The present study presents an overall histologic picture of the human otic cap-

sule, including the stapediovestibular joint, from birth to old age, demonstrating the interrelations between cartilage, bone, blood vessels and soft tissue.

METHODS AND MATERIALS

Human temporal bones from 21 patients (42 specimens) were studied, ranging in age from one day to 82 years of age. Eleven of the patients were males from one day to 79 years of age, and ten of the patients were females ranging in age from three years to 82 years. Thirteen of the patients had normal temporal bones; the remaining eight had pathological changes which in no way involved the bone or cartilage of the otic capsule or footplate. In all 42 specimens, the appearance of the bone and cartilage was consistent with what has been considered normal. No case of otosclerosis was included.

The temporal bones were vacuum fixed in 10% neutral buffered formalin, demin-

¹Supported by grants from USPHS NB-06606, Central Bureau of Research of the American Otolaryngological Society, Inc., Boston, Mass., and the Deafness Research Foundation, New York, N. Y.

dral bone formation progressing into the deeper portions of the cartilage adjacent to bone, the cartilage surfaces were replenished by new cartilage formed by apposition of mesenchymal cells of the annular ligament and its fibrous extensions. These mesenchymal cells could be demonstrated partially enclosed by new matrix at the cartilage surfaces (figs. 3, 4). At times, small surface cartilage erosions were noted and clusters of mesenchymal cells could be demonstrated at these sites, filling in the defect with new cartilage (fig. 4). This process of continual cartilage degeneration and bone formation, with new cartilage forming by apposition, occurred at all ages, varying in degree after the active growth years from specimen to specimen rather than with age, and appears to represent physiological repair and remodeling.

Otic capsule. The otic capsule refers to the bone surrounding the soft membranous inner ear structures. This bone is usually described as occurring in three more or less distinct layers: an inner endosteal layer bordering the membranous cochlea and vestibular organs, a middle endochondral bone layer containing cartilage foci and cartilage matrix remnants, as well as foci of immature fibrous or woven bone, and an irregular outer periosteal layer, varying in thickness and containing scattered Haversian systems.

Cartilage foci containing cartilage cells were seen in all specimens in the bone about the membranous cochlea and semicircular canals. They appeared to be least numerous at birth where the endochondral layer was narrow. Although some of the older temporal bones seemed to show decreased numbers of cartilage foci, other older specimens contained increased numbers, so that variation occurred from specimen to specimen rather than with age. The most prominent and consistently present cartilage was in the bony septum between the basal and middle turns of the cochlea (fig. 2). However, cartilage foci were present in the bone about the entire cochlea, including the apical turn, to varying degrees in the different specimens. Few cartilage foci were seen about the semicircular canals in comparison to the

cochlea. Again, the cartilage matrix was always uncalcified.

The chondrocytes within these foci all showed essentially the same processes from birth to old age. Many of the chondrocytes were degenerating and undergoing phagocytosis by macrophages, exactly analogous to the situation described in the cartilage of the stapediostapedial joint. The thin matrix bars between the degenerating, phagocytized cells were uncalcified. However, as these involved cartilage lacunae were excavated by the macrophages, those lacunae closest to the surrounding bone occasionally revealed calcification of their thin matrix bars. This involved only two, three, or four lacunar walls at a time, rather than massive calcification of all the matrix bars present. Often, the thin matrix bars appeared to break down without calcification. Vascular osteogenic buds extended from the adjacent bone into the "prepared," opened, empty cartilage lacunae. There was deep basophilic staining of the blood vessel walls and the immediately surrounding perivascular tissue. These vessels appeared "active" osteogenically in all the specimens, supplying the osteogenic buds for endochondral bone formation and appeared to be in a continual state of stimulation. This process of cartilage degeneration with phagocytosis of the altered chondrocyte and endochondral ossification extending from osteogenic vascular buds in the surrounding bone could be demonstrated in every temporal bone, regardless of age or sex, and appeared to be a continuing process throughout life (fig. 6).

At times, the entire cartilaginous focus appeared to be replaced by new bone. More often, the new endochondral bone only partially filled the degenerated cartilage focus, with varying amounts of uncalcified cartilage matrix remaining. These areas have been termed globuli ossei. The uncalcified cartilage matrix within the interglobular spaces represents remaining remnants of matrix from the partially replaced cartilage focus and remains as such indefinitely throughout life (fig. 5).

In addition, cartilage foci were seen which seemed to follow different courses, all of which occurred without the presence

eralized by chelation with a 0.7 M solution of the tetrasodium salt of EDTA at pH 7.4 and 37°C (Gussen and Donahue, '65) and vacuum embedded in parlodion (Donahue and Gussen, '66). Sections were cut at 20 μ and stained with hematoxylin and eosin.

RESULTS

Stapediovestibular joint. The stapes footplate is a flat, oval bone with a peripheral circumferential cartilage rim. It fits into a similarly shaped opening, the oval window, in the bony wall between the middle ear and the inner ear. The footplate circumference is firmly attached to the cartilage surface of the oval window by means of the annular ligament, thus forming the stapediovestibular joint. This joint permits limited vibratory movements of the stapes footplate in the oval window in response to sound waves which, in this way, are transmitted to the fluid system of the inner ear. The joint is a specialized form of symphysis where the bony surfaces of the apposing bones are capped with cartilage and held together by fibrous tissue. No synovium or synovial cavity is present. A thin fibrous extension of the joint annular ligament continues into the anterior margin of the oval window (the fissula ante fenestram), and a similar, smaller fibrous extension of the joint annular ligament sometimes continues into the posterior margin of the oval window (the fossula post fenestram). Both the fissula and fossula are lined by cartilage continuous with that of the oval window (fig. 1).

In all the specimens from age one day to 82 years, the cartilage lining the footplate, the oval window, the fissula ante fenestram, and the fossula post fenestram was normally uncalcified. However, after about the age of 25 to 30 years, the surface cartilage matrix next to the ligament appeared to be calcified in virtually every case, but was separated from the underlying subchondral bone by varying amounts of uncalcified cartilage. Unlike most other joints, the deeper part of the articular cartilage at the bone-cartilage junction was never calcified. When, occasionally, calcified cartilage matrix was seen in more abundance, it was considered to be abnormal.

In all specimens, regardless of age or sex, varying degrees of degeneration of the chondrocytes within the uncalcified cartilage was evident. The chondrocyte degeneration was quite widespread, but even more striking was the presence of varying numbers of macrophages within the involved cartilage lacunae. When seen, there was usually one macrophage to a lacuna. The macrophages, themselves, often appeared to be undergoing degeneration. Uninvolved cartilage cells were present scattered among the degenerating cells within the articular cartilage. The degeneration of the chondrocytes was usually furthest advanced directly adjacent to the bone of the footplate and the oval window and the bone deep to the fibrous extensions of the joint. In these areas, directly adjacent to the bone, the cartilage septa of the degenerated, excavated lacunae were breaking down. At times, a few calcified septa were seen, three or four at the most, rather than any massive type of matrix calcification. Osteogenic vascular buds extended into the opened, excavated, "prepared" cartilage lacunae. This endochondral ossification occurred in varying degrees throughout all the specimens from one day to 82 years of age in these areas, and appeared to be most prominent during the actively growing years (figs. 3, 4).

Examination of the surface of the cartilage of the footplate, oval window, fissula ante fenestram and fossula post fenestram revealed new cartilage cells present at the cartilage surfaces and scattered sporadically throughout the uncalcified cartilage. These cells had medium-sized, basophilic, oval or round vesicular nuclei with prominent, rather delicate chromatin material, and stained clearly as compared to the pale, hardly discernible older chondrocytes. Varying numbers of mesenchymal cells within the annular ligament and thin fibrous extensions of the ligament appeared to be lined up alongside the surfaces of the cartilage in all these areas, becoming incorporated into new cartilage matrix. This varied from place to place and from specimen to specimen. In other words, while degeneration of cartilage cells and their removal by phagocytes was occurring within the bulk of the cartilage, with endochon-

dral bone formation progressing into the deeper portions of the cartilage adjacent to bone, the cartilage surfaces were replenished by new cartilage formed by apposition of mesenchymal cells of the annular ligament and its fibrous extensions. These mesenchymal cells could be demonstrated partially enclosed by new matrix at the cartilage surfaces (figs. 3, 4). At times, small surface cartilage erosions were noted and clusters of mesenchymal cells could be demonstrated at these sites, filling in the defect with new cartilage (fig. 4). This process of continual cartilage degeneration and bone formation, with new cartilage forming by apposition, occurred at all ages, varying in degree after the active growth years from specimen to specimen rather than with age, and appears to represent physiological repair and remodeling.

Otic capsule. The otic capsule refers to the bone surrounding the soft membranous inner ear structures. This bone is usually described as occurring in three more or less distinct layers: an inner endosteal layer bordering the membranous cochlea and vestibular organs, a middle endochondral bone layer containing cartilage foci and cartilage matrix remnants, as well as foci of immature fibrous or woven bone, and an irregular outer periosteal layer, varying in thickness and containing scattered Haversian systems.

Cartilage foci containing cartilage cells were seen in all specimens in the bone about the membranous cochlea and semicircular canals. They appeared to be least numerous at birth where the endochondral layer was narrow. Although some of the older temporal bones seemed to show decreased numbers of cartilage foci, other older specimens contained increased numbers, so that variation occurred from specimen to specimen rather than with age. The most prominent and consistently present cartilage was in the bony septum between the basal and middle turns of the cochlea (fig. 2). However, cartilage foci were present in the bone about the entire cochlea, including the apical turn, to varying degrees in the different specimens. Few cartilage foci were seen about the semicircular canals in comparison to the

cochlea. Again, the cartilage matrix was always uncalcified.

The chondrocytes within these foci all showed essentially the same processes from birth to old age. Many of the chondrocytes were degenerating and undergoing phagocytosis by macrophages, exactly analogous to the situation described in the cartilage of the stapediovestibular joint. The thin matrix bars between the degenerating, phagocytized cells were uncalcified. However, as these involved cartilage lacunae were excavated by the macrophages, those lacunae closest to the surrounding bone occasionally revealed calcification of their thin matrix bars. This involved only two, three, or four lacunar walls at a time, rather than massive calcification of all the matrix bars present. Often, the thin matrix bars appeared to break down without calcification. Vascular osteogenic buds extended from the adjacent bone into the "prepared," opened, empty cartilage lacunae. There was deep basophilic staining of the blood vessel walls and the immediately surrounding perivascular tissue. These vessels appeared "active" osteogenically in all the specimens, supplying the osteogenic buds for endochondral bone formation and appeared to be in a continual state of stimulation. This process of cartilage degeneration with phagocytosis of the altered chondrocyte and endochondral ossification extending from osteogenic vascular buds in the surrounding bone could be demonstrated in every temporal bone, regardless of age or sex, and appeared to be a continuing process throughout life (fig. 6).

At times, the entire cartilaginous focus appeared to be replaced by new bone. More often, the new endochondral bone only partially filled the degenerated cartilage focus, with varying amounts of uncalcified cartilage matrix remaining. These areas have been termed globuli ossei. The uncalcified cartilage matrix within the interglobular spaces represents remaining remnants of matrix from the partially replaced cartilage focus and remains as such indefinitely throughout life (fig. 5).

In addition, cartilage foci were seen which seemed to follow different courses, all of which occurred without the presence

of macrophages or endochondral bone replacement. Some of the cartilage foci lost their chondrocytes and remained as small, localized areas of uncalcified cartilage matrix with large, empty lacunae. At times, varying numbers of new cartilage cells similar to the new cartilage cells described in the footplate area were seen in cartilage matrix. Occasionally, cartilage foci appeared to transform into bone without prior resorption. The chondrocytes became more stellate in shape, and the thin, uncalcified matrix bars took on an eosinophilic stain. The focus was then indistinguishable from bone, although retaining the honeycomb structure of the previous cartilage. Cartilage matrix with large empty lacunae was also seen undergoing direct transformation to bone with small numbers of individual bone cells entering some of the empty lacunae (fig. 7A). In the younger specimens, this new chondroid bone was often very cellular. Bone cells appeared to arise from the adjacent perivascular tissue and enter the empty cartilage lacunae individually rather than as an osteogenic vascular bud. The thin cartilage matrix bars then became eosinophilic and were indistinguishable from bone. In figure 7B is seen formation of cellular chondroid bone in a three-year old female. With increasing age, cellular chondroid bone loses many of its osteocytes, and those remaining are very pale and seen with difficulty. This older, relatively acellular chondroid bone retains an appearance of pale basophilic sheaths or mantles surrounding the blood vessels (fig. 7C).

To sum up: The cartilage foci appear to undergo varying degrees of degeneration, with removal of the degenerated chondrocytes by macrophages. This is followed by ingrowth of osteogenic vascular buds which partially replace the cartilage focus with immature, woven endochondral bone, leaving globuli ossei with uncalcified cartilage matrix remnants. Those areas where chondrocytes degenerate without the appearance of macrophages apparently do not stimulate the formation of endochondral bone from adjacent vascular osteogenic buds, but either remain as uncalcified cartilage matrix with empty lacunae or else stimulate the appearance of new car-

tilage cells. At times, the cartilage matrix and cells transform directly to a chondroid type of bone. When the cartilage foci are completely filled in with new bone, this new bone usually appears to be a combination of endochondral bone and chondroid bone. With increasing age, the originally cellular chondroid bone areas lose many of their osteocytes and remain as very pale, basophilic-staining sheaths or mantles surrounding the blood vessels.

The soft tissue lining the inner endosteal surfaces of the otic capsule (including the spiral ligaments) contained mesenchymal cells which appeared to have both osteogenic and chondrogenic ability. In some specimens, a continuous uncalcified cartilage lining could be demonstrated along portions of the bony cochlea, which appeared to be undergoing transition to chondroid bone. When present, this was usually along the upper basal and lower middle cochlear turns (fig. 8A). This lining cartilage usually contained empty lacunae and appeared to merge with adjacent lining areas of chondroid bone. At times, the cartilage was separated from the soft tissue structures by a thin rim of chondroid bone (fig. 8B). Rare mesenchymal cells were seen along the inner surfaces of the cartilage and bone, appearing to enter into both cartilage and chondroid bone defects. This was far less prevalent than in the footplate area and was found with difficulty. More commonly, the inner lining of the bony cochlea consisted of patchy foci of cartilage or their partial replacement by endochondral bone (globuli ossei) and chondroid bone. The chondroid bone seen here usually had empty lacunae and was very pale staining.

The endosteal surface of the semicircular canals also consisted of pale-staining chondroid bone (fig. 9). Here again, rare mesenchymal cells could be seen within the uneven surface of the chondroid bone. However, numerous globuli ossei with uncalcified cartilage matrix remnants were present about the canals, attesting to the previous presence of numerous cartilage foci which had been partially replaced by endochondral bone. In addition, pale basophilic sheaths were prevalent about the blood vessels in these areas.

DISCUSSION

The fetal development of the human otic capsule has been very excellently described in detail by Bast ('30, '32, '33, '36, '38, '40, '42). The bone is preceded by a cartilaginous model with successive ossification centers appearing at specific locations within the capsule. Calcification of the cartilage matrix occurs with resorption, and osteogenic vascular buds then grow into the resorbed areas to form endochondral bone. During this process, foci of cartilage matrix remain, upon which the new bone forms. Bast ('32) noted certain features which he considered peculiar to the region about the semicircular canals. He described the removal of degenerating chondrocytes by phagocytes, with the subsequent deposition of bone by osteoblasts when sufficient excavation was accomplished. There was apparently just sufficient cartilage destroyed to permit the blood vessels to penetrate, rather than any massive destruction of cartilage.

The ability of macrophages to resorb matrix has also been described by Goldhaber ('61). He induced bone resorption in tissue cultures of mouse calvariae and demonstrated by time-lapse films the presence of very motile macrophages attacking bone spicules and participating directly in the resorption process.

Anderson and Parker ('66), in an electron microscopic study of endochondral ossification in the femur of newborn rats, showed areas where macrophages preceded the capillary endothelium. The cartilage matrix was calcified only for a distance of one to three chondrocyte capsules in advance of the invading capillary complex. Some matrix septa were very thin and did not actually calcify. The degree of calcification of the matrix walls was very variable, only about one-third of the septa actually showing complete calcification. Anderson and Parker also described intracytoplasmic clusters of mineralized matrix within many of the macrophages, and only occasionally mineralized clusters within osteoclasts.

The presence of degenerating cartilage cells and their removal by phagocytes has been shown in this present study to be a continuous process throughout life. With

the removal of the altered chondrocytes by macrophages, new endochondral bone forms from the vascular buds in the underlying bone and constitutes the physiological repair and remodeling of the otic capsule, whether it be in the stapediostibular joint or about the cochlea and semicircular canals. As the degenerating cartilage is replaced in the manner described, new cartilage cells form by apposition at the joint surfaces from chondrogenically active mesenchymal cells in the annular ligament. These mesenchymal cells retain this ability throughout life.

Anson and Martin ('35) and Bast ('36) described this chondrogenic ability of otic capsule mesenchymal tissue in some fetal and infant ears where cartilaginous and osteoid masses occurred within the fissula ante fenestram. They considered that the new cartilage formed from the fissular tissue by metamorphosis of the connective tissue cells to cartilage cells.

Within the otic capsule, globuli ossei with their interglobular uncalcified cartilage remnants represent the partially resorbed cartilage foci. In a previous study, the author (Gussen, '67) demonstrated the presence of bone canaliculi within the cartilage remnants about the globuli ossei. They were interpreted at that time as evidence of bone resorption because of their fragmented and particulate nature. This is now believed to be an incorrect interpretation. The fragments of bone canaliculi demonstrated in the previous study represent early endochondral bone formation partially replacing the degenerating cartilage focus.

Trueta ('63) has studied extensively the role of blood vessels in osteogenesis. He believes that degenerating chondrocytes, osteocytes, and endothelial cells are responsible for the liberation of osteogenic-inducing substances, and that such local substances act directly on the vascular system of the bone, stimulating the formation of osteoblasts or their precursors. Autoradiographic studies by Young ('63) and by Tonna and Cronkite ('61), using tritiated thymidine, clearly demonstrate the evolution of bone-forming cells from undifferentiated mesenchymal elements. It is logical to assume that the constantly

of macrophages or endochondral bone replacement. Some of the cartilage foci lost their chondrocytes and remained as small, localized areas of uncalcified cartilage matrix with large, empty lacunae. At times, varying numbers of new cartilage cells similar to the new cartilage cells described in the footplate area were seen in cartilage matrix. Occasionally, cartilage foci appeared to transform into bone without prior resorption. The chondrocytes became more stellate in shape, and the thin, uncalcified matrix bars took on an eosinophilic stain. The focus was then indistinguishable from bone, although retaining the honeycomb structure of the previous cartilage. Cartilage matrix with large empty lacunae was also seen undergoing direct transformation to bone with small numbers of individual bone cells entering some of the empty lacunae (fig. 7A). In the younger specimens, this new chondroid bone was often very cellular. Bone cells appeared to arise from the adjacent perivascular tissue and enter the empty cartilage lacunae individually rather than as an osteogenic vascular bud. The thin cartilage matrix bars then became eosinophilic and were indistinguishable from bone. In figure 7B is seen formation of cellular chondroid bone in a three-year old female. With increasing age, cellular chondroid bone loses many of its osteocytes, and those remaining are very pale and seen with difficulty. This older, relatively acellular chondroid bone retains an appearance of pale basophilic sheaths or mantles surrounding the blood vessels (fig. 7C).

To sum up: The cartilage foci appear to undergo varying degrees of degeneration, with removal of the degenerated chondrocytes by macrophages. This is followed by ingrowth of osteogenic vascular buds which partially replace the cartilage focus with immature, woven endochondral bone, leaving globuli ossei with uncalcified cartilage matrix remnants. Those areas where chondrocytes degenerate without the appearance of macrophages apparently do not stimulate the formation of endochondral bone from adjacent vascular osteogenic buds, but either remain as uncalcified cartilage matrix with empty lacunae or else stimulate the appearance of new car-

tilage cells. At times, the cartilage matrix and cells transform directly to a chondroid type of bone. When the cartilage foci are completely filled in with new bone, this new bone usually appears to be a combination of endochondral bone and chondroid bone. With increasing age, the originally cellular chondroid bone areas lose many of their osteocytes and remain as very pale, basophilic-staining sheaths or mantles surrounding the blood vessels.

The soft tissue lining the inner endosteal surfaces of the otic capsule (including the spiral ligaments) contained mesenchymal cells which appeared to have both osteogenic and chondrogenic ability. In some specimens, a continuous uncalcified cartilage lining could be demonstrated along portions of the bony cochlea, which appeared to be undergoing transition to chondroid bone. When present, this was usually along the upper basal and lower middle cochlear turns (fig. 8A). This lining cartilage usually contained empty lacunae and appeared to merge with adjacent lining areas of chondroid bone. At times, the cartilage was separated from the soft tissue structures by a thin rim of chondroid bone (fig. 8B). Rare mesenchymal cells were seen along the inner surfaces of the cartilage and bone, appearing to enter into both cartilage and chondroid bone defects. This was far less prevalent than in the footplate area and was found with difficulty. More commonly, the inner lining of the bony cochlea consisted of patchy foci of cartilage or their partial replacement by endochondral bone (globuli ossei) and chondroid bone. The chondroid bone seen here usually had empty lacunae and was very pale staining.

The endosteal surface of the semicircular canals also consisted of pale-staining chondroid bone (fig. 9). Here again, rare mesenchymal cells could be seen within the uneven surface of the chondroid bone. However, numerous globuli ossei with uncalcified cartilage matrix remnants were present about the canals, attesting to the previous presence of numerous cartilage foci which had been partially replaced by endochondral bone. In addition, pale basophilic sheaths were prevalent about the blood vessels in these areas.

remnants to typical hyaline cartilage. He considered chondroid an intermediate form of cartilaginous tissue. The concept of chondroid has particular significance, because chondroid grows, not like hyaline cartilage from an epiphyseal center but from mesenchyme, and, in osteogenesis, is not resorbed, but becomes bone by direct transformation. Moss believed that chondroid was unique to the articular areas of the lower jaw of fish, and described similar cartilaginous tissue in rat cranial sutures, which he called "secondary cartilage." Secondary cartilage has been defined as arising independently of primary cartilage and forming after the onset of ossification. De Beer ('37) found secondary cartilage (or chondroid) to be commonly associated with membrane bones, which are subjected to "precocious strains and stresses." He raised the possibility that periosteal cells might be capable of forming nodules of secondary cartilage or chondroid.

Enlow ('62) described chondroid bone as normally present at the crest of bone tubercles and bony processes in rapidly growing bones. He described it as similar or identical to the tissue on the growing alveolar crests surrounding teeth. Enlow felt that chondroid bone provided anchorage and perhaps resistance to pressure. He stated that although the fibrous matrix in bony processes is subject to tensile forces, the individual chondroid cells are resistant to the pressure exerted on them by surrounding fibrous matrix.

Symons ('52), in his discussion of the fetal development of the human mandibular joint, described secondary cartilage developing on the surface of the condyle, which is covered by a thick, fibrous layer. The deeper cells of this fibrous layer continually add new cartilage, in a manner analogous to that described above in the stapediovestibular joint. Symons described the bone in the temporal element of the joint as having "almost the appearance of an area of secondary cartilage."

Moffett et al. ('64) describe similar cartilage growth by apposition on the articular surfaces of the adult human temporomandibular joint. They describe alterations in the contour of the joint as a result of progressive and regressive remodeling

of the articular surfaces and believe that these changes are brought about as an adaptation to mechanical stresses. Such similarities between the temporomandibular joint and the joints of the temporal bone should not be surprising in view of the close association phylogenetically between this bone and the auditory ossicles. Preliminary studies indicate bone and cartilage mechanisms within the malleus and incus similar to those described in the stapediovestibular joint and the otic capsule, and will be presented in a separate study.

Mendoza and Rius ('66) have described the presence of fat droplets in the endochondral bone layer of normal otic capsules ranging in age from eighteen to eighty years. In contrast, no fat droplets were seen in the periosteal layer of the otic capsule. The authors considered these fat droplets as evidence of fatty degeneration associated with extensive areas of bone necrosis within the endochondral bone layer.

It has been known for some time that not only osteoblasts, but chondrocytes, as well, contain fat droplets. Fawcett ('54) has described the presence of large droplets of lipid as a common occurrence in mature, healthy chondrocytes. In a light microscopy and electron microscopy study of the intracellular lipids of cartilage, Collins et al. ('65) demonstrated intracellular lipid as an almost constant feature of chondrocytes and found it to be more prominent in ages beyond the active growth period. They, too, believed the chondrocytes to be healthy, since, with electron microscopy, the involved cartilage cells exhibited normal organelles. A study of the extracellular lipids of cartilage (Ghadially et al., '65) revealed the presence of lipid in adult articular cartilage matrix near the articular surface. The authors considered that the matrix lipid was originally formed within the chondrocytes and was extruded by the healthy cells into the matrix. They also suggest the possibility of lipid deposited in the matrix as a result of disintegration of cartilage cells.

Enlow et al. ('65) describe fine, granular, homogeneous deposits of lipid in bone

degenerating cartilage foci within the otic capsule, in some way, induce the formation of bone from the mesenchymal cells about the adjacent surrounding blood vessels. As mentioned before, the appearance of the blood vessels in the otic capsule is one of continued activity. Their perivascular structure is deeply basophilic, due presumably to increased or concentrated amounts of acid mucopolysaccharide in a state readily available for continual endochondral bone formation. The mucopolysaccharides in these areas, by virtue of their ion exchange ability, may well hold calcium ions in readiness for the ossification procedure.

It seems probable that cells arising from the perivascular tissues have the ability to form chondrocytes, as well as osteocytes. The new cartilage foci within the otic capsule appear to arise in this manner as well as from the soft tissue mesenchymal cells lining the inner portions of the otic capsule next to the membranous cochlea and semicircular canals. This dual ability does appear to be present within this mesenchymal lining (to a slight degree, at least), since, at times, mesenchymal cells are seen lying within pit-like depressions at the cartilage or chondroid bone surface. The chondrogenic ability of these mesenchymal cells is, however, extremely active during fetal life. Streeter ('18) has described the unusual embryological development of the semicircular canal portion of the otic capsule with its constantly changing cartilaginous character for accommodation of the enlarging semicircular canals. The new cartilage that forms and degenerates repeatedly during this process has been described by Streeter as arising from reticular tissue about the membranous canals. This is appositional growth of cartilage from the mesenchyme, which in postnatal life appears to decline in this area, but which is analogous to the appositional cartilage growth and formation that occurs in other portions of the otic capsule throughout life.

The ability of matrix-forming cells to produce bone or cartilage (or fibrous tissue) has been proven experimentally. It is believed that the local environment of these cells controls, to a very great extent,

which form the new tissue will take. It was Ham ('30) originally who suggested that cartilage formation, rather than bone formation, might occur in healing fractures if the oxygen tension was decreased. Fell ('32) showed that cultures of endosteal cells produced both bone and cartilage. Endosteal cells (like periosteal cells) form as membrane bone and do not normally pass through a cartilage stage. These cells were shown by Fell to have the capacity to form cartilage in an environment conducive to its formation.

More recently, studies by Bassett ('64) and by Shaw and Bassett ('67) have shown that not only can an inadequate supply of oxygen produce chondrogenesis by cells usually forming bone, but that variations in the concentration of oxygen produced different results. Utilizing organ cultures of embryonic tibiae and subjecting these growing tissues to varying concentrations of oxygen, Shaw and Bassett demonstrated that with intermediate oxygen concentrations, there was degeneration of chondrocytes, as well as transformation of chondrocytes directly into osteoblasts.

It is intriguing to speculate on the different changes occurring in the cartilage of the otic capsule and to suggest a relationship to the oxygen concentration (vascularity) in these areas. The direct transformation of cartilage foci to chondroid bone within the otic capsule may be related to the vascularity in the environment of the particular cartilage foci. Since there is new endochondral bone forming constantly throughout the otic capsule, there is also, then, a constant alteration in vascularity. It would seem logical that cartilage foci in the vicinity of areas increasing in vascularity might show changes related to the degree of altered oxygen concentration. Although other local environmental factors must be of importance, the amount of available oxygen appears to be of major importance in the determination of cartilage or bone formation by precursor mesenchymal cells.

The concept of the ability of cartilage, or of certain cartilages, to transform directly into bone is not a new one. Moss ('61) has described cartilaginous tissues varying from "chordoid" in notochordal

- Symons, N. B. B. 1952 The development of the human mandibular joint *J. Anat. (Lond.)*, 86: 326-332.
- Tonna, E. A., and E. P. Cronkite 1961 Cellular response to fracture studied with tritiated thymidine. *J. Bone and Joint Surg.*, 43A: 352-362.
- Trueta, J. 1963 The role of the vessels in osteogenesis. *J. Bone and Joint Surg.*, 45B: 402-418.
- Young, R. W. 1963 Nucleic acids, protein synthesis and bone. *Clin. Orthopaed.*, 26: 147-160.

Addendum

Work in progress since this study was submitted has shown that the perivascular bone does not form by direct transformation of chondroid cartilage, but rather undergoes alternating depolymerization (with loss of bone cells and mineral) and repolymerization (with remineralization and new bone cells arising from the perivascular soft tissue). This constitutes an unusual form of "remodeling" where no actual resorption space is formed and where the newly repolymerized bone is of the same structural immaturity as before. In the depolymerizing phase, the perivascular bone may resemble cartilage matrix by virtue of its lower polymerized state and closely spaced lacunae. This work is now in press as Supplement 235 of the *Acta Otolaryngologica*, entitled, "The Labyrinthine Capsule. Normal Structure and Pathogenesis of Otosclerosis."

matrix, as well as infrequently in osteocytes throughout the bone cortex of dog and Rhesus monkey femurs. They describe these lipid droplets as similar in appearance, size, and dispersal to the droplets found in hypertrophic chondrocytes. The authors state that no correlation has yet been seen between osteocyte necrosis and the presence of lipid deposition. They state that the homogeneous deposits of lipid present in the bone matrix appear to have been incorporated in the bone tissue at the time of its original formation, and they suggest a possible relationship between the occurrence of lipid in the matrix and the process of ossification.

The presence of lipid droplets within the endochondral bone layer of the adult otic capsule appears to be largely related to the continual degeneration of lipid-containing cartilage cells with release of their lipid content and incorporation of the lipid into the new bone matrix that continually forms.

ACKNOWLEDGMENTS

The author is indebted to Miss Doris Donahue and Mrs. Helen Shuck for their invaluable technical assistance, and to Mr. Frank Poynter for photography.

LITERATURE CITED

- Anderson, C. A., and J. Parker 1966 Invasion and resorption in enchondral ossification. *J. Bone and Joint Surg.*, 48A: 899-914.
- Anson, B. J. and J. Martin, Jr. 1935 Fissula ante fenestram. Its form and contents in early life. *Arch. Otolaryng.* (Chicago), 21: 303-323.
- Bassett, C. A. 1964 Environmental and cellular factors regulating osteogenesis. In: *Bone Dynamics*. H. Frost, ed. Little, Brown and Co., Boston, Massachusetts.
- Bast, T. H. 1930 Ossification of the otic capsule in human fetuses. *Contrib. to Embryology*, Carnegie Institute, 21: 53-82.
- 1932 Development of the otic capsule. I. Resorption of the cartilage in the canal portion of the otic capsule in human fetuses and its relation to the growth of the semicircular canals. *Arch. Otolaryng.* (Chicago), 16: 19-38.
- 1933 Development of the otic capsule. II. The origin, development and significance of the fissula ante fenestram and its relation to otosclerotic foci. *Arch. Otolaryng.* (Chicago), 18: 1-20.
- 1936 Development of the otic capsule. III. Fetal and infantile changes in the fissular region and their probable relationship to the formation of otosclerotic foci. *Arch. Otolaryng.* (Chicago), 23: 509-525.
- 1938 Development of the otic capsule. IV. The fissula post fenestram. *Arch. Otolaryng.* (Chicago), 27: 402-412.
- 1940 Development of the otic capsule V. Residual cartilages and defective ossification and their relation to otosclerotic foci. *Arch. Otolaryng.* (Chicago), 32: 771-782.
- 1942 Development of the otic capsule. VI. Histological changes and variations in the growing bony capsule of the vestibule and cochlea. *Annals of Otology, Rhinology and Laryngology*, 51: 343-357.
- Collins, D. H., F. N. Ghadially and G. Meschim 1965 Intra-cellular lipids of cartilage. *Ann. Rheum. Dis.*, 24: 123-135.
- De Beer, G. R. 1937 *The Development of the Vertebrate Skull*. Oxford University Press.
- Donahue, D., and R. Gussen 1966 Rapid parlodion embedding of temporal bones. *Arch. Otolaryng.* (Chicago), 83: 28.
- Enlow, D. H. 1962 A study of the postnatal growth and remodeling of bone. *Am. J. Anat.*, 110: 79-102.
- Enlow, D. H., J. L. Conklin and S. Bang 1965 Observations on the occurrence and the distribution of lipids in compact bone. *Clin. Orthopaed.*, 38: 157-169.
- Fawcett, D. W. 1954 In: *Histology*, R. O. Greep, ed. Chapt. 8, p. 124, Churchill, London.
- Fell, H. B. 1932 Chondrogenesis in cultures of endosteum. *Proc. Roy. Soc. London, Ser. B*, 112: 417-427.
- Ghadially, F. N., G. Meschim and D. H. Collins 1965 Extra-cellular lipid in the matrix of human articular cartilage. *Ann. Rheum. Dis.*, 24: 136-146.
- Goldhaber, P. 1961 Oxygen-dependent bone resorption in tissue culture. In: *The Parathyroids*. R. O. Greep and R. V. Talmage, ed. Charles C Thomas, Springfield, Ill.
- Gussen, R. 1967 Globuli Interossei as a manifestation of bone resorption. *Acta Otolaryng.* (Stockholm), 63: 411-422.
- Gussen, R., and D. Donahue 1965 Decalcification of temporal bones with tetrasodium edetate. *Arch. Otolaryng.* (Chicago), 82: 110-114.
- Ham, A. W. 1930 A histological study of the early phases of bone repair. *J. Bone and Joint Surg.*, 12: 827-844.
- Mendoza, D., and M. Rius 1966 Histology of the enchondral layer of the human otic capsule. *Acta Otolaryng.* (Stockholm), 62: 93-100, fasc. 2.
- Moffett, B. C., Jr., L. C. Johnson, J. B. McCabe and H. C. Askew 1964 Articular remodeling in the adult human temporomandibular joint. *Am. J. Anat.*, 115: 119-142.
- Moss, M. L. 1961 Osteogenesis of acellular teleost fish bone. *Am. J. Anat.*, 108: 99-109.
- Shaw, J. L., and C. A. Bassett 1967 The effects of varying oxygen concentration on osteogenesis and embryonic cartilage in vitro. *J. Bone and Joint Surg.*, 49A: 73-80.
- Streeter, G. L. 1918 The histogenesis and growth of the otic capsule and its contained periotic tissue-spaces in the human embryo. *Contrib. to Embryology*, Carnegie Institute, 7: 7-54.



PLATE 1

EXPLANATION OF FIGURES

- 1 Stapes footplate in oval window. Note thin fibrous fissula ante fenestram on left, continuous with the annular ligament and with fibrous tissue on the middle ear surface of the oval window. Middle ear lumen is above, and inner ear vestibule below, the footplate. seventy-nine year old male. (H&E \times 15)
- 2 Portion of basal and middle turns of cochlea. Note prominent cartilage layer in the septum between the basal and middle cochlear turns. sixty-nine year old female. (H&E \times 30)



PLATE I

EXPLANATION OF FIGURES

- 1 Stapes footplate in oval window. Note thin fibrous fissula ante fenestram on left, continuous with the annular ligament and with fibrous tissue on the middle ear surface of the oval window. Middle ear lumen is above, and inner ear vestibule below, the footplate. seventy-nine year old male. (H&E \times 15)
- 2 Portion of basal and middle turns of cochlea. Note prominent cartilage layer in the septum between the basal and middle cochlear turns. sixty-nine year old female. (H&E \times 30)



PLATE 2

EXPLANATION OF FIGURES

- 3A Posterior margin of oval window. Note pale, degenerating chondrocytes and scattered smaller, irregularly shaped macrophages (m) within the cartilage layer, and newly formed chondrocytes at the cartilage surface. Endochondral bone formation progresses from about the prominent blood vessel above center of photograph. One day old male (H&E $\times 280$)
- 3B Anterior margin of footplate (above) and oval window (below) with annular ligament between. Note uneven cartilage surfaces with mesenchymal cells lining up alongside forming new chondrocytes. Degenerating cartilage cells and scattered macrophages (m) are present within the cartilage. six year old male. (H&E $\times 280$)
- 3C Posterior margin of footplate (right) and oval window (left). Note newly forming cartilage cells from mesenchymal cells of annular ligament, and degenerating paler cartilage cells. Forty-seven year old female. (H&E $\times 280$)
- 3D Anterior margin of footplate (left lower field) and oval window (above). Note uneven cartilage surface with degenerating cartilage cells, occasional macrophages (m), and new endochondral bone formation (B). Calcification in the surface cartilage is noted in a few areas, as well as occasional new cartilage cells at the surface. Seventy-nine year old male. (H&E $\times 450$)



PLATE 3

EXPLANATION OF FIGURES

- 4 Anterior margin of footplate (left) and oval window (right). Note defect in cartilage of oval window with mesenchymal cells lined up forming new cartilage. Note new endochondral bone forming in footplate and oval window. Three year old female. (H&E \times 320)
- 5 Globuli ossei near basal cochlear turn with remaining remnants of uncalcified cartilage matrix. Note deeply staining blood vessels. Seventy-nine year old male. (H&E \times 130)



PLATE 4

EXPLANATION OF FIGURES

- 6A Cartilage focus near middle coil of cochlea. Note degenerated chondrocytes (C) and occasional macrophages (m) as well as prominent blood vessels and endochondral bone formation. Thirty-one year old male. (H&E \times 280)
- 6B Cartilage focus adjacent to middle cochlear coil. Note degenerated chondrocytes (C) and macrophages (m) within some lacunae. Calcification of individual matrix walls (H) is present with endochondral bone formation. Thirty-one year old male. (H&E \times 450)
- 6C Cartilage focus near basal coil of cochlea. Note degeneration of cartilage cells with ingrowth of osteogenic vascular buds and endochondral bone formation. Individual cartilage lacunar walls are calcified. Pale-staining macrophages are present. Fifty-six year old female. (H&E \times 450)
- 6D Cartilage in septum between basal and middle cochlear turns. Note degenerating chondrocytes with macrophages present in scattered lacunae. Endochondral bone formation is prominent. Seventy-nine year old male. (H&E \times 450)

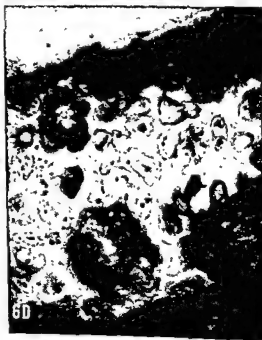


PLATE 4

EXPLANATION OF FIGURES

- 6A Cartilage focus near middle coil of cochlea. Note degenerated chondrocytes (C) and occasional macrophages (m) as well as prominent blood vessels and endochondral bone formation. Thirty-one year old male. (H&E \times 280)
- 6B Cartilage focus adjacent to middle cochlear coil. Note degenerated chondrocytes (C) and macrophages (m) within some lacunae. Calcification of individual matrix walls (H) is present with endochondral bone formation. Thirty-one year old male. (H&E \times 450)
- 6C Cartilage focus near basal coil of cochlea. Note degeneration of cartilage cells with ingrowth of osteogenic vascular buds and endochondral bone formation. Individual cartilage lacunar walls are calcified. Pale-staining macrophages are present. Fifty-six year old female. (H&E \times 450)
- 6D Cartilage in septum between basal and middle cochlear turns. Note degenerating chondrocytes with macrophages present in scattered lacunae. Endochondral bone formation is prominent. Seventy-nine year old male. (H&E \times 450)



PLATE 5

EXPLANATION OF FIGURES

- 7A Direct transformation of cartilage matrix to bone with ingrowth of individual deeply-staining bone cells. Otic capsule of 47 year old female. (H&E \times 320)
- 7B Cellular chondroid bone (CB) in otic capsule of three year old female. Note deeply staining basophilic bone matrix about central blood vessel and large dark-staining cells arising from about the vessel. Surrounding this bone, similar cells are seen entering empty cartilage lacunae within ossifying cartilage matrix. (H&E \times 280)
- 7C Combination of endochondral and old, relatively acellular chondroid bone (CB). Otic capsule near semicircular canal. Fifty-one year old male. (H&E \times 130)

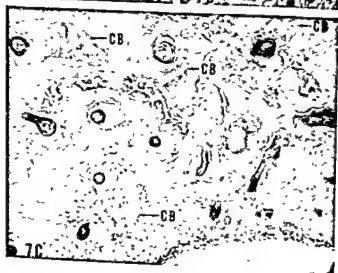


PLATE 5

EXPLANATION OF FIGURES

- 7A Direct transformation of cartilage matrix to bone with ingrowth of individual deeply-staining bone cells. Otic capsule of 47 year old female. (H&E \times 320)
- 7B Cellular chondroid bone (CB) in otic capsule of three year old female. Note deeply staining basophilic bone matrix about central blood vessel and large dark-staining cells arising from about the vessel. Surrounding this bone, similar cells are seen entering empty cartilage lacunae within ossifying cartilage matrix. (H&E \times 280)
- 7C Combination of endochondral and old, relatively acellular chondroid bone (CB). Otic capsule near semicircular canal. Fifty-one year old male. (H&E \times 130)

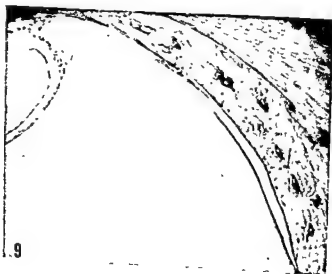


PLATE 6

EXPLANATION OF FIGURES

- 8A Otic capsule bordering basal cochlear turn. Note cartilage surface which appears to be transforming into chondroid bone. Note rare mesenchymal cells in superficial lacunae and depressions. One day old male. (H&E \times 130)
- 8B Cartilage lining portion of septum between basal and middle cochlear turns. Note degeneration of cartilage cells with occasional newer cartilage cells near surface. Surface of cartilage is covered by a rim of acellular chondroid bone. Note rare mesenchymal cell in small depression at surface in lower field. Sixty-nine year old female (H&E \times 280)
- 9 Portion of wall of semicircular canal. Note pale-staining chondroid bone adjacent to the membranous canal. Sixty-nine year old female. (H&E \times 130)

Fine Structure of Anchoring Villi of the Human Placenta¹

ALLEN C. ENDERS

Department of Anatomy, Washington University School of Medicine,
St. Louis, Missouri

ABSTRACT Anchoring villi from the first trimester, early second trimester, and term were examined with the electron microscope. It was found that the small anchoring villi of the third and fourth month were particularly informative, since at this stage the cytotrophoblast is still proliferating, yet these cells form a compact discoidal region at the surface of the basal plate. Transitions from relatively undifferentiated cytotrophoblast cells adjacent to the stroma of the villus to large isolated cells surrounded by fibrinoid could readily be followed. These highly differentiated cytotrophoblast cells were found to have extensive regions of fine filaments, in addition to their pronounced endoplasmic reticulum, and were designated fibrous cytotrophoblast cells. The nature of the frequently incomplete epithelium covering anchoring villi at term was described, and some of the functions of the cytotrophoblast are discussed in relation to the observations of their fine structure.

Study of anchoring villi of the human placenta and their relationship to the basal plate is complicated not only by the changes that occur in the villi as pregnancy progresses, but also by the heterogeneity of structure of the basal plate itself. Despite excellent discussions of this region by Wislocki and Bennett ('43), Wislocki and Padykula ('61), Hamilton and Boyd ('60), and Boyd and Hamilton ('67), the structural relationships are sufficiently confusing that divergent opinions are still found on such questions as the fate of the cells in the cytotrophoblastic shell and the source of the extracellular material loosely referred to as fibrinoid. An example of the unsettled state of our knowledge of this area is the continued use of the term "X" cells (Wilkin, '65; Wynn, '67; Benirschke and Driscoll, '67) for one of the prominent cell types of the junctional region.

Despite the wealth of studies with the electron microscope on the free villi of the placenta, relatively few observations have been made concerning anchoring villi. Boyd and Hamilton ('67) include a number of original observations in their extensive review of the development of the human placenta from the end of the third month of gestation, and Wynn ('67) briefly describes some aspects of the cytology of anchoring villi in association with the basal plate in term placentas.

In this study of the fine structure of anchoring villi, special attention was paid to the third and fourth month, at which time the anchoring villi are compact but still show extensive proliferation of the cytotrophoblast. The compact size of these villi was found helpful, since sections through the entire junctional area could be made, and the orientation consequently preserved.

MATERIALS AND METHODS

Placentas were collected at the time of hysterectomy, Casarian section, and normal delivery. Portions of the maternal face of the placentas were fixed in 3% glutaraldehyde in 0.1 N phosphate buffer, rinsed in buffer, and post fixed in 2% osmium tetroxide. Following dehydration in alcohol and embedding in araldite (Durcupan), sections were made for both light microscopic and electron microscopic observation. Thick sections of the plastic embedded material were stained with Azure B. The sections for electron microscopic examination were stained with lead citrate (Reynolds, '63). In a few instances, phos-

¹I would like to thank Dr. Frederick Kraus, Associate Pathologist, St. Luke's Hospital, and the Department of Obstetrics and Gynecology, Washington University School of Medicine, especially Dr. Ernst Friedrich, for aid in getting the early placental stages. This work was supported by grants GB-5024 from the National Science Foundation, and 1 RO1 HD 02613 from the National Institute of Child Health and Human Development.

Fine Structure of Anchoring Villi of the Human Placenta¹

ALLEN C. ENDERS

Department of Anatomy, Washington University School of Medicine,
St. Louis, Missouri

ABSTRACT Anchoring villi from the first trimester, early second trimester, and term were examined with the electron microscope. It was found that the small anchoring villi of the third and fourth month were particularly informative, since at this stage the cytotrophoblast is still proliferating, yet these cells form a compact discoidal region at the surface of the basal plate. Transitions from relatively undifferentiated cytotrophoblast cells adjacent to the stroma of the villus to large isolated cells surrounded by fibrinoid could readily be followed. These highly differentiated cytotrophoblast cells were found to have extensive regions of fine filaments, in addition to their pronounced endoplasmic reticulum, and were designated fibrous cytotrophoblast cells. The nature of the frequently incomplete epithelium covering anchoring villi at term was described, and some of the functions of the cytotrophoblast are discussed in relation to the observations of their fine structure.

Study of anchoring villi of the human placenta and their relationship to the basal plate is complicated not only by the changes that occur in the villi as pregnancy progresses, but also by the heterogeneity of structure of the basal plate itself. Despite excellent discussions of this region by Wislocki and Bennett ('43), Wislocki and Padykula ('61), Hamilton and Boyd ('60), and Boyd and Hamilton ('67), the structural relationships are sufficiently confusing that divergent opinions are still found on such questions as the fate of the cells in the cytotrophoblastic shell and the source of the extracellular material loosely referred to as fibrinoid. An example of the unsettled state of our knowledge of this area is the continued use of the term "X" cells (Wilkin, '65; Wynn, '67; Benirschke and Driscoll, '67) for one of the prominent cell types of the junctional region.

Despite the wealth of studies with the electron microscope on the free villi of the placenta, relatively few observations have been made concerning anchoring villi. Boyd and Hamilton ('67) include a number of original observations in their extensive review of the development of the human placenta from the end of the third month of gestation, and Wynn ('67) briefly describes some aspects of the cytology of anchoring villi in association with the basal plate in term placentas.

In this study of the fine structure of anchoring villi, special attention was paid to the third and fourth month, at which time the anchoring villi are compact but still show extensive proliferation of the cytotrophoblast. The compact size of these villi was found helpful, since sections through the entire junctional area could be made, and the orientation consequently preserved.

MATERIALS AND METHODS

Placentas were collected at the time of hysterectomy, Casarian section, and normal delivery. Portions of the maternal face of the placentas were fixed in 3% glutaraldehyde in 0.1 N phosphate buffer, rinsed in buffer, and post fixed in 2% osmium tetroxide. Following dehydration in alcohol and embedding in araldite (Durcupan), sections were made for both light microscopic and electron microscopic observation. Thick sections of the plastic embedded material were stained with Azure B. The sections for electron microscopic examination were stained with lead citrate (Reynolds, '63). In a few instances, phos-

¹ I would like to thank Dr. Frederick Kraus, Associate Pathologist, St. Luke's Hospital, and the Department of Obstetrics and Gynecology, Washington University School of Medicine, especially Dr. Ernst Friedrich, for aid in getting the early placental stages. This work was supported by grants GB-5024 from the National Science Foundation, and 1 R01 HD 02613 from the National Institute of Child Health and Human Development.

photungstic acid was added to the dehydrating alcohols to aid in the visualization of collagen. In addition, blocks of placenta fixed in Bouins were stained with either a tetrachrome stain (Hematoxylin, Chromotrope 2R, Orange G, Fast Green) or a modified silver reticular connective tissue stain.

Placentas were collected from the following stages: two in the first month, two in the second month, two at the end of the third month, two in the fourth month, and eight at term. Several blocks from each of the 16 placentas were studied.

DESCRIPTION

Anchoring villi have a number of different forms. When first established (as tertiary villi), the anchoring villi are characterized by the presence of cell columns. These cell columns, which are just distal to the mesenchymal core of the villus, are generally connected by a tenuous region of more dispersed cells to the compact cytotrophoblast at the primitive basal plate. A proximal to distal section (fetal to maternal) of the cytotrophoblast reveals, in order, basement membrane, compact proliferative cytotrophoblast, dispersed cytotrophoblast, then again compact cytotrophoblast. The syncytium covering the villus is discontinuous only at the latter group of cytotrophoblast cells. The period during which these elongate anchoring villi are characteristic ends before the end of the first trimester.

The anchoring villi of early second trimester are compact structures associated more directly with the basal plate. These villi are characterized by the presence of a thick basement membrane beneath the cytotrophoblast, a region of cell proliferation, then a region of more dispersed cytotrophoblast directly associated with the basal plate (the Umlagerungszone of Ortman, '60; or basaler Trophoblast of Strauss, '66). In some instances, fibrin and other extracellular materials may sharply delimit the distal extent of the anchoring villus. In still other instances the anchoring villus is associated with the persistent cytotrophoblastic shell of the previous stage. Because of the compact arrangement of the villi and diversity of relationships to the basal plate, this stage is par-

ticularly informative and has been given special emphasis in this study.

Later in the second trimester, many of the villi already show indications of maturation. The transitional forms of villi lack the abundant mitotic figures of the proliferative villi and even at their proximal ends exhibit modification of the cytotrophoblast cells into more fibrous cells.

The mature anchoring villi of term placentas show quite a range in structure, but all are characterized by an absence of proliferation. Some of the anchoring villi have entirely fibrotic stroma, and are completely embedded in the surrounding extracellular substances. Other anchoring villi may have patent vessels, but both syncytial and cytotrophoblastic coverings are incomplete, so that the stroma of the villus is exposed to the perivillous environment. Still other villi have patches of syncytium and large basophilic fibrous cytotrophoblastic cells associated with them. Almost invariably the anchoring villi of this stage are in contact with extracellular material, including fibrin, cellular debris, and the less readily identifiable extracellular materials generally grouped under the term fibrinoid.²

Anchoring villi in the first and second months. A partial indication of some of the subsequent forms the cytotrophoblast will take is indicated by the structure of the cytotrophoblast cells of the cell columns in early anchoring villi. Proximal to the basement membrane the cells are relatively similar to the Langhans cells within the rest of the villi. Extending more peripherally, the space between the cells increases, as does the amount of glycogen within the cells. Many of the more dispersed cells have extensive regions containing only glycogen granules. Desmosomes are numerous between the cytotrophoblast

² Grosser ('25) used the term fibrinoid to denote the extracellular material in the human placenta that was histologically distinguishable from both fibrin and connective tissue. He thus included both amorphous material and cellular debris. Considerable controversy exists over the source of fibrinoid and its chemical composition (see Boyd and Hamilton, '67, for a historical review of this subject). The meaning of the term is further complicated by its different use in pathology, particularly in describing fibrinoid changes of the connective tissue in collagen diseases. Recently Kirby *et al.* ('61) and Bradbury *et al.* ('65) have used the term fibrinoid to describe the acellular materials which are interposed between some of the maternal and fetal cells in the mouse placenta and have suggested that this material may constitute part of the immunological barrier.

cells, but have only a few associated filaments. Polyribosomes are common in the cytoplasm, and cisternae of the endoplasmic reticulum are elongate and tend to be associated with the round mitochondria. Irregular membrane-bound inclusions are frequently found, especially near the compact Golgi zone.

These anchoring villi are essentially attaching to other cytotrophoblast cells and only in a few instances is there a direct transition from the cell columns to cellular debris and decidua. Our material from this stage did not include enough decidua for adequate study of the relationship of the anchoring villi to the basal plate.

Anchoring villi of the third and fourth months. Sufficient material was obtained from late in the first trimester and the early second trimester to thoroughly investigate the anchoring villi of this particularly informative stage. At this point in development, the numerous small anchoring villi (up to 1-2 mm across) are centers of proliferation of the cytotrophoblast (fig. 1). It is customary to continue to refer to these regions of cytotrophoblast proliferation as cell columns. However, it should be noted that they no longer constitute columnar connections between the villi and the cytotrophoblast, but are flattened disc-shaped structures.

The stromal core of the anchoring portion of the villus shows little modification from other portions. There is usually a loose network of fibroblasts and occasionally a cluster of mesenchymal cells near the terminal end of the villus. Hofbauer cells are abundant, and the fetal vessels at this stage are deep within the stroma. The basement membrane is continuous and is particularly thick underlying the proliferating cytotrophoblast at the tip of the villus.

Along the margins of the anchoring villi, the normal relationships of trophoblast are found. The syncytial trophoblast overlies a single layer of cytotrophoblast (Langhans cells). As the terminal end of the villus is approached, the syncytium becomes more irregular and masses of this trophoblast frequently extend irregularly lateral to the anchoring villus, where they terminate in various shaped clumps.

The cytotrophoblast of the Langhans layer is directly continuous with the multi-

cellular disc of cytotrophoblast constituting the terminal end of the anchoring villus. This terminal group of cytotrophoblast cells shows definite zonation as it radiates out from the stromal surface into the basal plate. The innermost cells form a continuous basal epithelial layer on the stroma, but the amount of intercellular space increases and the cells become more irregular in outline towards the basal plate. Clumps of syncytium, which are isolated and therefore can be considered giant cells, are frequently found at the periphery of this cytotrophoblast and at isolated spots along the disc, but at no time is there a complete syncytial covering and many of the anchoring villi have syncytium only at the margins.

In some instances, masses of fibrin separate the trophoblast cells from the underlying decidua. In other instances there is relatively less fibrin, and only cellular debris and other intercellular substances (fibrinoid) are interposed between the two tissues. In a number of places, however, there is a further layer of dispersed cytotrophoblast cells. These cells are surrounded by large amounts of intercellular material, are rounded, and do not show a direct relationship to any specific villus.

Cytology. The vessels within the stroma of the villus are generally thick-walled capillaries, with no tendency for pore formation. Even in the earlier placenta numerous collagen filaments are present within the villi. Large Hofbauer cells are common and most typically are surrounded in part by an area devoid of collagen or visible ground substance. The basement membrane underlying the cytotrophoblast is thick and relatively smooth on its stromal side. However, projections of the cytotrophoblast cells extend into this thick membrane in numerous places. In addition to the relatively amorphous material and the fine reticulin filaments in the basement membrane, occasional granules are present (fig. 2).

The inner few layers of cytotrophoblast cells show many mitotic figures. The basal layer itself constitutes a continuous layer with little or no intercellular space (fig. 2). Numerous desmosomes are found between the cytotrophoblast cells, and usually some form of junctional complex can be dis-

photungstic acid was added to the dehydrating alcohols to aid in the visualization of collagen. In addition, blocks of placenta fixed in Bouins were stained with either a tetrachrome stain (Hematoxylin, Chromotrope 2R, Orange G, Fast Green) or a modified silver reticular connective tissue stain.

Placentas were collected from the following stages: two in the first month, two in the second month, two at the end of the third month, two in the fourth month, and eight at term. Several blocks from each of the 16 placentas were studied.

DESCRIPTION

Anchoring villi have a number of different forms. When first established (as tertiary villi), the anchoring villi are characterized by the presence of cell columns. These cell columns, which are just distal to the mesenchymal core of the villus, are generally connected by a tenuous region of more dispersed cells to the compact cytotrophoblast at the primitive basal plate. A proximal to distal section (fetal to maternal) of the cytotrophoblast reveals, in order, basement membrane, compact proliferative cytotrophoblast, dispersed cytotrophoblast, then again compact cytotrophoblast. The syncytium covering the villus is discontinuous only at the latter group of cytotrophoblast cells. The period during which these elongate anchoring villi are characteristic ends before the end of the first trimester.

The anchoring villi of early second trimester are compact structures associated more directly with the basal plate. These villi are characterized by the presence of a thick basement membrane beneath the cytotrophoblast, a region of cell proliferation, then a region of more dispersed cytotrophoblast directly associated with the basal plate (the Umlagerungszone of Ortman, '60; or basaler Trophoblast of Strauss, '66). In some instances, fibrin and other extracellular materials may sharply delimit the distal extent of the anchoring villus. In still other instances the anchoring villus is associated with the persistent cytotrophoblastic shell of the previous stage. Because of the compact arrangement of the villi and diversity of relationships to the basal plate, this stage is par-

ticularly informative and has been given special emphasis in this study.

Later in the second trimester, many of the villi already show indications of maturation. The transitional forms of villi lack the abundant mitotic figures of the proliferative villi and even at their proximal ends exhibit modification of the cytotrophoblast cells into more fibrous cells.

The mature anchoring villi of term placentas show quite a range in structure, but all are characterized by an absence of proliferation. Some of the anchoring villi have entirely fibrotic stroma, and are completely embedded in the surrounding extracellular substances. Other anchoring villi may have patent vessels, but both syncytial and cytotrophoblastic coverings are incomplete, so that the stroma of the villus is exposed to the perivillous environment. Still other villi have patches of syncytium and large basophilic fibrous cytotrophoblastic cells associated with them. Almost invariably the anchoring villi of this stage are in contact with extracellular material, including fibrin, cellular debris, and the less readily identifiable extracellular materials generally grouped under the term fibrinoid.²

Anchoring villi in the first and second months. A partial indication of some of the subsequent forms the cytotrophoblast will take is indicated by the structure of the cytotrophoblast cells of the cell columns in early anchoring villi. Proximal to the basement membrane the cells are relatively similar to the Langhans cells within the rest of the villi. Extending more peripherally, the space between the cells increases, as does the amount of glycogen within the cells. Many of the more dispersed cells have extensive regions containing only glycogen granules. Desmosomes are numerous between the cytotrophoblast

² Grosser ('25) used the term fibrinoid to denote the extracellular material in the human placenta that was histologically distinguished from both fibrin and connective tissue. He thus included both amorphous material and cellular debris. Considerable controversy exists over the source of fibrinoid and its chemical composition (see Boyd and Hamilton, '67, for a historical review of this subject). The meaning of the term is further complicated by its different use in pathology, particularly in describing fibrinoid changes of the connective tissue in collagen diseases. Recently Kirby *et al.* ('64) and Bradbury *et al.* ('65) have used the term fibrinoid to describe the acellular materials which are interposed between some of the maternal and fetal cells in the mouse placenta and have suggested that this material may constitute part of the immunological barrier.

anchoring villi which are separated from the underlying decidua by masses of fibrin and in which cell proliferation and accumulations of fibrinoid are present. Moreover, fibrous cells are common wherever fibrinoid is abundant, and are the cellular elements of the cytotrophoblastic shell that persist in the later stages (fig. 8).

Decidual cells. The decidual cells underlying the anchoring villi vary appreciably in cytology. The most common type of decidual cell is a large pale cell with scalloped margins (fig. 12). The cytoplasm of these cells has numerous cisternae of granular endoplasmic reticulum. The cisternae of the endoplasmic reticulum are less dilated and have fewer associated ribosomes than do those of the endoplasmic reticulum in the cytotrophoblast cells. The mitochondria are quite small and frequently rod-shaped. Much of the cytoplasm is occupied by fine filaments. Golgi zones are composed of small clusters of membranes and vesicles with membrane-coated granules and multivesicular bodies occasionally associated. Typically only a small amount of glycogen is present within these cells. At the free surface of these cells granular amorphous material which cannot be distinguished from the fibrinoid surrounding cytotrophoblast cells is found in abundance, and a filamentous layer is present usually underlying microvilli. Fibrin is often interspersed between these cells, but is usually not as close to the cell surface as the amorphous material. Collagen is only rarely seen between the cells near the fetal tissue, but is more abundant a few cells deeper into the decidua basalis (fig. 11).

Occasionally several decidual cells will constitute an assorted mass with wide areas of apposed membranes and occasionally a few desmosomes, but they appear to remain distinct cells rather than forming a symplasma. A few smaller decidual cells are more irregular in shape and have a highly dilated endoplasmic reticulum.

Often where decidual cells and cytotrophoblast cells are closely associated, individual cells cannot be positively identified if they are in a degenerating state. In a few places, however, such as where the cytotrophoblast reaches the endothelium of

a maternal vessel, close association between maternal and fetal elements can be seen. Cytotrophoblast cells can frequently be observed several cells deep within the decidua. However, it is not always clear whether such cells degenerate or persist in an altered form in subsequent stages.

Anchoring villi of the term placenta. Most of the anchoring villi at term are fibrotic, and many of them constitute a relatively inert portion of the basal plate. Even those anchoring villi which have patent vessels are characterized by an absence of proliferative cytotrophoblast, an increase in collagen deposits in the stroma of the villus, an increase in associated extracellular substances, especially fibrin, and a lack of integrity of surrounding trophoblast (fig. 13). The basement membrane of the anchoring villi is even thicker than at previous stages. In some instances, both the syncytium and a cytotrophoblastic layer persist, but the cytotrophoblast cells often show transition to the fibrous type and amorphous granular substance is found between such cells, even where the overlying syncytial membrane is complete (fig. 10). The fibrous cells in this period are larger than those of the previous period but can nevertheless be identified by the same characteristics (large amounts of granular endoplasmic reticulum and regions of intracellular filaments).

Some of the anchoring villi have patent vessels only a few microns removed from regions where both cytotrophoblast and syncytial trophoblast are incomplete. However, such villi are always embedded in extracellular materials. In some regions massive areas of fibrous cytotrophoblast cells constitute a portion of the basal plate. Both the fibrous cytotrophoblast cells and the decidual cells show a considerable increase in number of inclusion bodies (lysosomes, pigment, etc.) from midgestation.

The lack of a series of differentiating cytotrophoblast cells, the increase in extracellular deposits and the degenerative changes in both the cytotrophoblast and decidual cells makes identification of cell source more difficult at this stage. Juxtaposition of cells of obvious maternal origin (ex. glandular epithelium, endothelium) and cytotrophoblast cells is uncommon.

cerned near the apical ends of the lateral borders of these cells. Caveolae are frequently encountered along the basal portions of the lateral borders. In the earlier stages of pregnancy the cytoplasm of these cells has numerous polyribosomes and elongate branched cisternae of granular endoplasmic reticulum. By mid gestation the number of polyribosomes has diminished, although they are still common. The mitochondria are relatively short with lamelliform cristae, and frequently seem to be in close association with the granular endoplasmic reticulum. In the cells of the middle zone particularly the endoplasmic reticulum is dilated and surrounds many of the mitochondria, forming a single compound intracellular region (fig. 3). Golgi zones are compact, consisting of many vesicles, both smooth and rough-surfaced, with relatively few larger cisternae. Membrane-bound granules are occasionally associated with these regions.

The more dispersed cells radiating out from the basal layers have fewer mitotic figures, and show an increased accumulation of glycogen and occasionally a few lipid droplets (fig. 4). With progressive increase in intercellular space, the area of close association between the cells decreases progressively until in the outer layers the cells are associated principally at large desmosomes. Many fine filaments are associated with these desmosomes and extend some distance into the cytoplasm. Irregular microvilli project occasionally from the lateral borders of the cytotrophoblast cells, and caveolae are present in small numbers. Microtubules are more abundant in the outermost cells.

The most common intercellular substance encountered between these cells is a granular, somewhat flocculent, homogeneous, extracellular substance. From the great abundance of this material, its position, and a comparison with light micrographs, it is clear that this material constitutes the greatest part of the substance that is usually called fibrinoid. Often strands of dense, finely filamentous material are also found between some of the outermost cytotrophoblast cells. The resemblance of this material to previous illustrations of fibrin (Wyllie, '64), its position, and the periodicity (c. 230 Å)

discernible in many of the strands at high magnification make it readily identifiable as fibrin. No collagen filaments are found in this region.

Where the cytotrophoblast is in contact with isolated masses of syncytium (giant cells), it is usually attached by desmosomes. The syncytium at these positions is highly irregular, with numerous microvilli, large folds enclosing extracellular material and dilated irregular endoplasmic reticulum (fig. 5). In some of the isolated masses of syncytium, individual desmosomes completely surrounded by cytoplasm and lacking communicating membranes are seen, possibly indicating the origin of this material from cytotrophoblast. Fine filaments are also characteristic of this syncytium.

Stages of degeneration of both the syncytium and of the cytotrophoblast cells can be found, but degenerating syncytium is much more commonly encountered.

Fibrous cytotrophoblast cell. In some regions, as previously mentioned, the cytotrophoblast cells are isolated from the underlying decidua. (In most of the villi observed in this study, the isolating layer [Nitabuch's stria] included fibrin deposits as well as fibrinoid and cellular debris.) The more peripheral cytotrophoblast cells of some anchoring villi are dispersed, rounded, and surrounded almost completely by fibrinoid (fig. 7). The cells in this position are larger than more proximal cytotrophoblast cells, and smaller than many of the decidual cells. They have prominent microvilli, numerous cisternae of the granular endoplasmic reticulum, regions of fine filaments, and relatively little glycogen (fig. 9). Curved bundles of filaments separate the regions of endoplasmic reticulum and as a result these cells frequently have concentric basophilic areas in light microscope preparations. Often short dense oval bodies are found within the groups of filaments, which resemble very small engulfed desmosomes. (It should be pointed out, however, that these bodies do not have remnants of cell membranes associated with them, the way desmosomes do in newly formed syncytium [Enders, '65].)

The transition to these fibrous cells (fig. 6) can be traced most readily in those

(for example, by precipitation from the surrounding milieu) is produced by these cells. Lesser amounts of amorphous material are also found in relation to the decidual cells.

Dallenbach-Hellweg and Nette ('64) have recently suggested that the cytotrophoblast cells are functional in glycoprotein hormone production, even at the end of pregnancy. They base their suggestion not only on the basophilia of these cells but also on the presence of inclusions and assessment of activity of several hydrolytic and oxidative enzymes, and on the presence of protein-bound SH groups. However, it seems likely that the protein-bound SH groups are associated with the filamentous regions of the cytoplasm of the cytotrophoblast cells. Indeed the relative isolation of the fibrous cytotrophoblast cells, not only by the fibrinoid previously mentioned but also in many instances by surrounding areas of fibrin, plus the lack of granules within the cells, argue strongly against a function of production of gonadotropic hormone.

Tighe and Curran ('66) recently reported in a brief communication that villi could be found in the term placenta which altogether lacked epithelium, so that fibrin was deposited directly on the basement membrane of the villus. In confirmation of this report, villi were frequently found in which both the syncytium and the cytotrophoblast cells were discontinuous. Both fibrin and fibrinoid could be found in relation to the residual thick basement membrane of these villi. Although apparently patent vessels are found when only a small portion of the epithelium is discontinuous, only fibrotic villi completely lack epithelium. In no instance did we observe a villus lacking epithelium in direct contact with maternal blood. Rather extensive acellular coats, of which only the basement membrane shows much organization, always intervened.

LITERATURE CITED

- Anderson, W. R., and D. G. McKay 1966 Electron microscope study of the trophoblast in normal and toxemic placentas. *Am. J. Ob. Gyn.*, 95: 1134-1148.
- Benirschke, K., and S. G. Driscoll 1967 *The Pathology of the Human Placenta*. Springer-Verlag, New York.
- Boyd, J. D., and W. J. Hamilton 1967 Development and structure of the human placenta from the end of the third month of gestation. *J. Ob. Gyn. Brit. Comm.*, 74: 161-226.
- Bradbury, S., W. D. Billington and D. R. S. Kirby 1965 A histochemical and electron microscopical study of the fibrinoid of the mouse placenta. *J. Roy. Micr. Soc.*, 84: 199-211.
- Dallenbach-Hellweg, G., and G. Nette 1964 Morphological and histochemical observations on trophoblast and decidua of the basal plate of the human placenta at term. *Am. J. Anat.*, 115: 309-326.
- Enders, A. C. 1965 Formation of syncytium from cytotrophoblast in the human placenta. *Ob. Gyn.*, 25: 378-386.
- Grosser, O. 1925 Über Fibrin und Fibrinoid in der Placenta. *Zeit. Anat. Entwickl. Gesch.*, 76: 304-314.
- Hamilton, W. J., and J. D. Boyd 1960 Development of the human placenta in the first three months of gestation. *J. Anat.*, 94: 297-328.
- Kirby, D. R. S., W. D. Billington, S. Bradbury and D. J. Goldstein 1964 Antigen barrier of the mouse placenta. *Nature, Lond.*, 204: 548-549.
- Ortmann, R. 1960 Morphologie der menschlichen Placenta. *Verh. Anat. Gesell.* 106: 27-56.
- Reynolds, E. S. 1963 The use of lead citrate at high pH as an electron-opaque stain in electron microscopy. *J. Cell Biol.*, 17: 208-212.
- Reynolds, S. R. M. 1966 Formation of fetal cotyledons in the hemochorial placenta. *Am. J. Ob. Gyn.*, 94: 425-439.
- Strauss, F. 1966 Die normale Anatomie der menschlichen Placenta. In *Handbuch der speziellen pathologischen Anatomie und Histologie*, Springer-Verlag, Berlin.
- Tighe, J. R., and R. C. Curran 1966 Ultrastructure of the placenta. *J. Clin. Path.*, 19: 98.
- Walkin, P. 1965 *Pathologie du Placenta*. Masson, Paris.
- Wislocki, G. B., and H. S. Bennett 1943 The histology and cytology of the human and monkey placenta, with special reference to the trophoblast. *Am. J. Anat.*, 73: 335-449.
- Wislocki, G. B., and H. A. Padykula 1961 Histochemistry and electron microscopy of the placenta. In *Sex and Internal Secretions*. W. C. Young, ed., Williams and Wilkins Co., Baltimore.
- Wyllie, J. C. 1964 Identification of fibrin with ferritin-conjugated antifibrinogen. *Exp. Mol. Path.*, 3: 468-474.
- Wynn, R. M. 1967 Fetomaternal cellular relations in the human basal plate: an ultrastructural study of the placenta. *Am. J. Ob. Gyn.*, 87: 832-850.

DISCUSSION AND CONCLUSIONS

Electron microscopy offers a number of advantages in studying anchoring villi. Fibrin can be directly visualized, and the amorphous component of fibrinoid distinguished from cellular debris. The extent of differentiation of the cytotrophoblast cells is also more readily followed when the organelles and inclusions of the cell are clearly visualized. It is not surprising, however, that many of the observations recorded here with the electron microscope have been described previously with light microscopy by such careful students of the placenta as Wislocki, Padykula, Boyd, and Hamilton.

Differentiation of the cytotrophoblast cells from their juxtastromal position to the more peripheral position, as described by Wislocki and Padykula ('61), can readily be confirmed by electron microscopy. The origin of giant cells from the margins of the anchoring villi and from various points along the proliferating cytotrophoblast, as suggested by Hamilton and Boyd ('60), is confirmed not only by the location of these cells, but also by the presence of desmosomes within them and desmosomal contacts with surrounding cytotrophoblast. Wynn ('67), in his study of the basal plate, and Anderson and McKay ('66) have reported similar observations on giant cells.

The finding of numerous filaments within the cytoplasm of the more highly differentiated cytotrophoblast cells has added another characteristic feature to the previously known basophilia of these cells, and makes it possible to give these highly developed cytotrophoblast cells the more meaningful designation "fibrous cytotrophoblast cells" rather than using the term "X cell" (Wilkin, '65; Wynn, '67).

Several functions have been suggested for the cytotrophoblast cells in anchoring villi: (a) They are a center of cell proliferation. (b) They function in erosion of the decidua. (c) They act as mechanical attachment. (d) They participate in the production of fibrinoid or in the secretion of hormones.

(a) Mitotic figures are much more abundant in the anchoring villi than they are in general in the Langhans layer. These villi thus clearly show a specific proliferative activity, as suggested by Boyd and Ham-

ilton ('67). Although the resulting cells could in theory migrate in either the fetal or maternal direction, or both, it appears from the restriction of the mitotic figures to the inner layers and the progressive differentiation towards the maternal surface that the cells migrating in the latter direction lose their proliferative capacity.

(b) No direct evidence of lytic activity of the cytotrophoblast was observed. Necrotic decidual cells were found abundantly, particularly in relation to the giant cells. In many instances the cytotrophoblast cells were adjacent but not in contact with apparently viable glandular epithelial cells and endothelial cells. In such instances, no collagen was interposed, but the basement membrane of the epithelial cells was often thickened. (More observations on earlier stages would be most useful in determining the extent of lytic activity. In addition, more *in situ* material is desirable since areas of lysis may also be areas of disruption on removal of the placenta from the uterus.)

(c) As might be expected from small blocks of fixed tissue, little evidence of the stress that might be present on the anchoring villi could be obtained. In those regions where the anchoring villi were embedded in fibrin or fibrinoid, no particular directional effects could be seen in the surrounding substance. It was apparent, however, that where the proliferative anchoring villi were directly invading the decidua, the radiating groups of cytotrophoblast cells, adhering to one another by desmosomes, were very thoroughly attached to the underlying decidua and could not be expected to be displaced by ordinary vascular pressures (as for example those that Reynolds ['66] suggests contribute to enlargement of the intervillous spaces).

(d) Because of the basophilia of the more differentiated cytotrophoblast cells, secretory activity has often been postulated for them. Cytologically these cells have large amounts of granular endoplasmic reticulum. Somewhat paradoxically they also have large regions of filaments and relatively few granules. The abundance of fibrinoid surrounding these cells makes it clear that either this material is produced by the cytotrophoblast cells, or a substance which results in the deposition of fibrinoid



PLATE 1

EXPLANATION OF FIGURE

- 1 Anchoring villus from the fourth month of gestation. In this and all subsequent pictures the fetal side is in the upper part of the picture, and the maternal side in the lower portion. The fibrin deposits are a red-orange and fibrinoid is gray-green. Note the mass of cytotrophoblast cells just above the fibrin and fibrinoid, and the two mitotic figures on the right side of this mass. There is a uterine gland in the lower right surrounded by decidual cells. The insert shows a region where fibrin separates decidual cells from large cytotrophoblast cells. Note that vacuolated pale greenish-staining fibrinoid surrounds the cytotrophoblast cells, whereas the sharply outlined decidual cells form a compact mass with little intercellular space. Hematoxylin, Orange G, Chromotrope 2 R, Fast Green. $\times 500$. Insert $\times 700$.

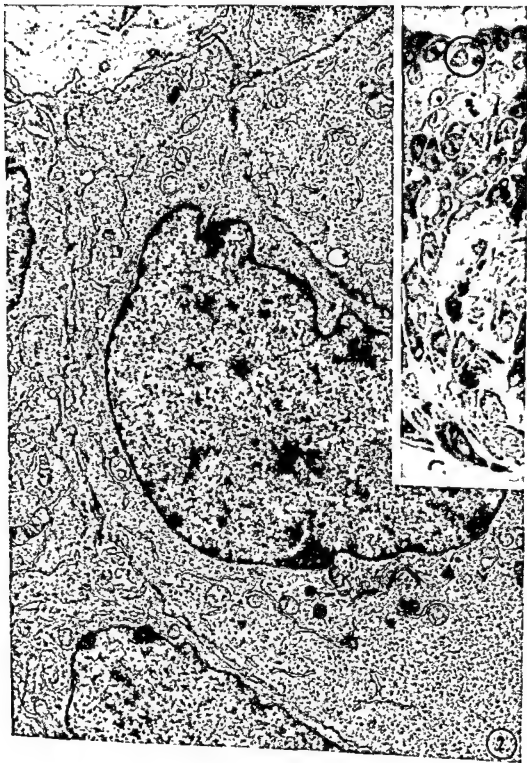


PLATE 2

EXPLANATION OF FIGURE

- 2 The insert in this figure and the next five figures is a photomicrograph of an Azure B stained section of a plastic embedded anchoring villus. The dark cytotrophoblast cells extend from the zone of proliferation at the top down into the maternal tissues. The circled area indicates the type of region of the anchoring villi depicted in the electron micrograph. The cytotrophoblast cells bordering the stroma of the villus form a compact mass with little intercellular space. Note the thickness of the basement membrane and the relatively sparse distribution of organelles. Beginning of fourth month. $\times 13,000$. Insert $\times 725$.



PLATE 2

EXPLANATION OF FIGURE

- 2 The insert in this figure and the next five figures is a photomicrograph of an Azure B stained section of a plastic embedded anchoring villus. The dark cytotrophoblast cells extend from the zone of proliferation at the top down into the maternal tissues. The circled area indicates the type of region of the anchoring villi depicted in the electron micrograph. The cytotrophoblast cells bordering the stroma of the villus form a compact mass with little intercellular space. Note the thickness of the basement membrane and the relatively sparse distribution of organelles. Beginning of fourth month. $\times 13,000$. Insert $\times 725$.

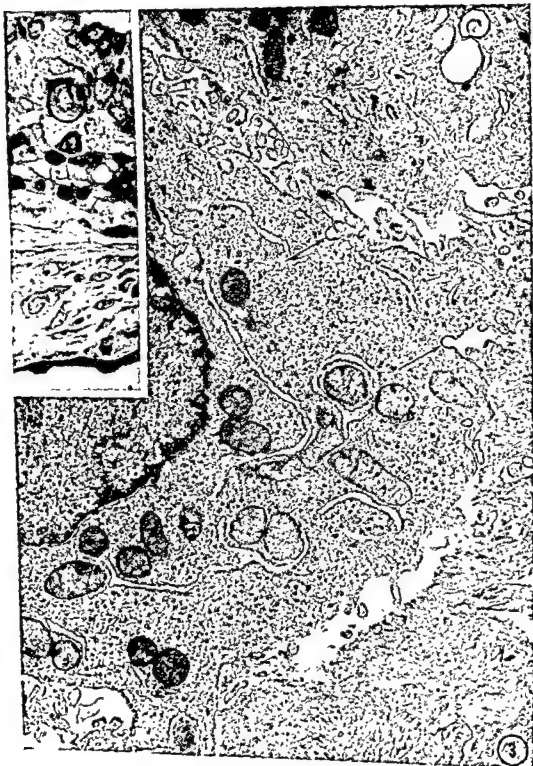


PLATE 3

EXPLANATION OF FIGURE

- 3 Cytotrophoblast cells near the maternal side of the proliferative zone of the anchoring villi have more intercellular space than those near the fetal stroma. Note also the infiltrated fibrin in the lower right. Several caveoli (arrows) give evidence of absorptive activity. The close association of the endoplasmic reticulum with the mitochondria is typical of these cells. The insert, in addition to depicting the region from which the electron micrograph was taken, shows an anchoring villus in which a mass of syncytium is interposed between the cytotrophoblast and the decidua. Several cells from a dilated uterine gland can be seen at the bottom of the insert. From the third month. $\times 20,000$. Insert $\times 675$.



PLATE 4

EXPLANATION OF FIGURE

- 4 In this micrograph, a series of cytotrophoblast cells extends down to a maternal vessel (MV). Note that these cells are heavily laden with glycogen, have elongate cisternae of the endoplasmic reticulum, and several partly extracted lipid droplets. A dense, apparently *necrotic* cytotrophoblast cell is interposed between the rest of the cytotrophoblast cells and the maternal endothelial cells. End of third month. $\times 11,000$. Insert $\times 725$.



PLATE 5

EXPLANATION OF FIGURE

- 5 A portion of a syncytial mass (giant cell) underlying an anchoring villus. The cytoplasm contains numerous tonofilaments and residual desmosomes (arrows). The amorphous material largely filling the extracellular space is fibrinoid. End of third month, $\times 30,000$. Insert $\times 850$.



PLATE 5

EXPLANATION OF FIGURE

- 5 A portion of a syncytial mass (giant cell) underlying an anchoring villus. The cytoplasm contains numerous tonofilaments and residual desmosomes (arrows). The amorphous material largely filling the extracellular space is fibrinoid. End of third month. $\times 30,000$. Insert $\times 850$.



PLATE 6

EXPLANATION OF FIGURE

- 6 These cytotrophoblast cells at the margin of an anchoring villus are illustrative of differentiation into the fibrous-type cell. Numerous filaments appear in the cytoplasm and separate the regions rich in endoplasmic reticulum. Note that some of these filaments are directly associated with desmosomes. In the upper right corner dense strands of fibrin are surrounded by amorphous fibrinoid. Beginning of fourth month. $\times 17,000$. Insert $\times 725$.

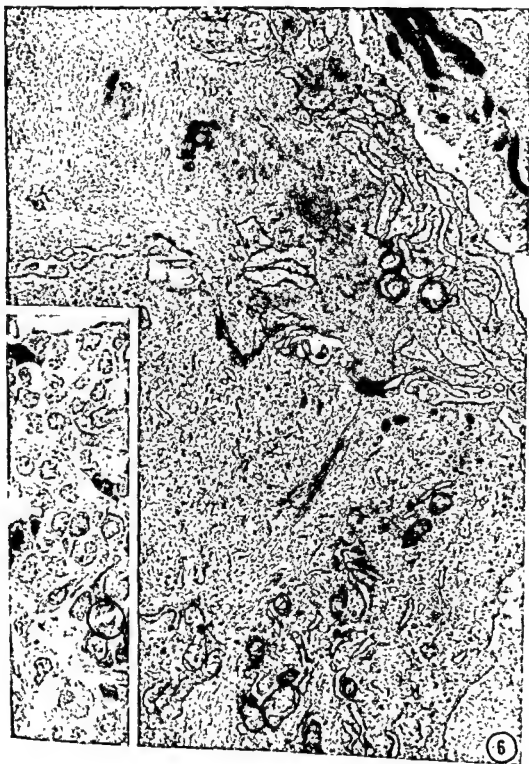


PLATE 7

EXPLANATION OF FIGURE

- 7 A fibrous cytotrophoblast cell completely surrounded by fibrinoid. These cells typically contain numerous bundles of filaments and extensive regions of granular endoplasmic reticulum. End of third month. $\times 9,700$. Insert $\times 725$.



PLATE 7

EXPLANATION OF FIGURE

- 7 A fibrous cytotrophoblast cell completely surrounded by fibrinoid. These cells typically contain numerous bundles of filaments and extensive regions of granular endoplasmic reticulum. End of third month. $\times 9,700$. Insert $\times 725$.



PLATE 8

EXPLANATION OF FIGURE

- 8 An isolated cytotrophoblast cell from a term placenta. Regions of filaments and granular endoplasmic reticulum are still abundant. However, there is an increase in lipid and pigment and some of the endoplasmic reticulum is dilated. This cell type is sometimes referred to in light micrographs as an "X cell". $\times 12,000$.

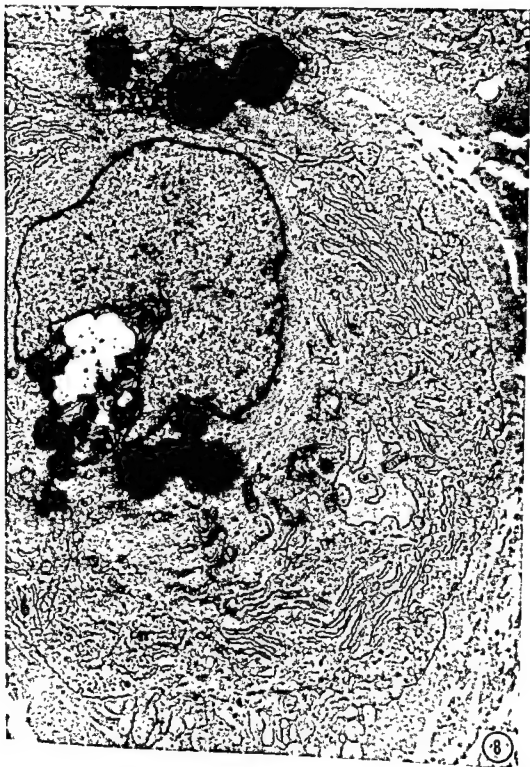


PLATE 8

EXPLANATION OF FIGURE

- 8 An isolated cytotrophoblast cell from a term placenta. Regions of filaments and granular endoplasmic reticulum are still abundant. However, there is an increase in lipid and pigment and some of the endoplasmic reticulum is dilated. This cell type is sometimes referred to in light micrographs as an "X cell". $\times 12,000$.

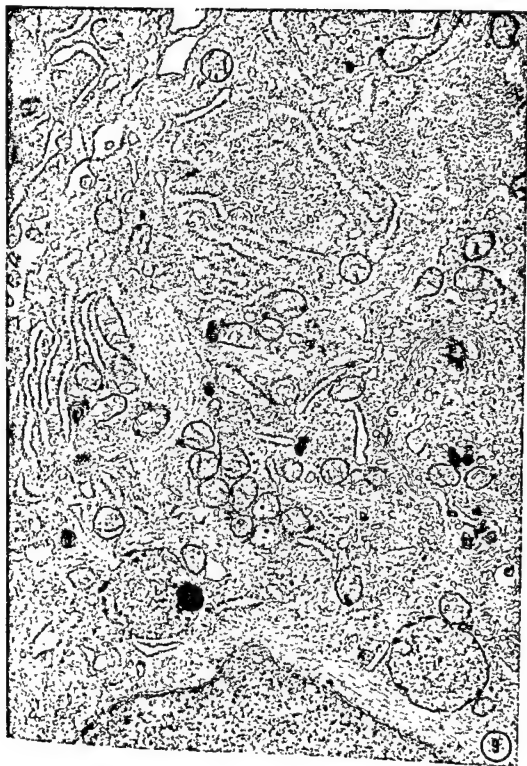


PLATE 9

EXPLANATION OF FIGURE

- 9 A fibrous cytotrophoblast cell from early in the fourth month, showing typical organelles. In addition to the granular endoplasmic reticulum and groups of filaments numerous small mitochondria are present. A well defined Golgi zone (G) and two structures (L) which are probably lysosomes are seen. $\times 27,000$.

PLACENTAL ANCHORING VILLI
Allen C. Enders

PLATE 10

EXPLANATION OF FIGURE

- 10 Conversion of cytotrophoblast cells to the fibrous type can frequently be seen to occur even when these cells are overlain by typical syncytial trophoblast. Note the presence of fibrinoid (arrows) between the two converting cytotrophoblast cells and the thickness of the basement membrane. Term placenta. $\times 11,7000$.



PLATE 10

EXPLANATION OF FIGURE

- 10 Conversion of cytotrophoblast cells to the fibrous type can frequently be seen to occur even when these cells are overlain by typical syncytial trophoblast. Note the presence of fibrinoid (arrows) between the two converting cytotrophoblast cells and the thickness of the basement membrane. Term placenta. $\times 11,7000$.



PLATE 11

EXPLANATION OF FIGURE

- 11 This micrograph of the decidual basalis at term illustrates the three types of extracellular substances consistently found in this region. At the right of the micrograph is collagen. The gray amorphous material in the center of the picture is fibrinoid and the dark filamentous substance is fibrin. A portion of a decidual cell is at the left of the picture, and cellular debris is seen in the center. The insert shows the periodicity of the strands of fibrin. $\times 24,500$. Insert $\times 47,200$.

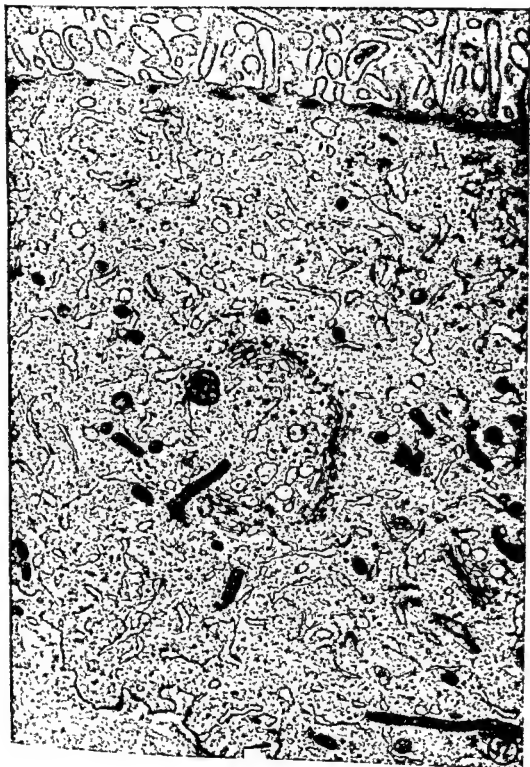


PLATE 12

EXPLANATION OF FIGURE

- 12 Cytoplasm of a typical decidual cell from the decidua basalis at the end of the third month. The mitochondria are small, dense and largely rod-shaped. The endoplasmic reticulum, although abundant, has relatively few associated ribosomes and is not highly dilated. Note the presence of a filamentous region with periodic densities underlying the microvilli at the top of the picture. Numerous fine filaments are also found throughout the cytoplasm, but they do not form bundles as they do in the fibrous cytotrophoblast cells. The fine filaments in the lower left corner are probably reticulin and are less common than collagen *per se*. Granules of glycogen are seen throughout the cytoplasm but are not accumulated. $\times 22,400$.

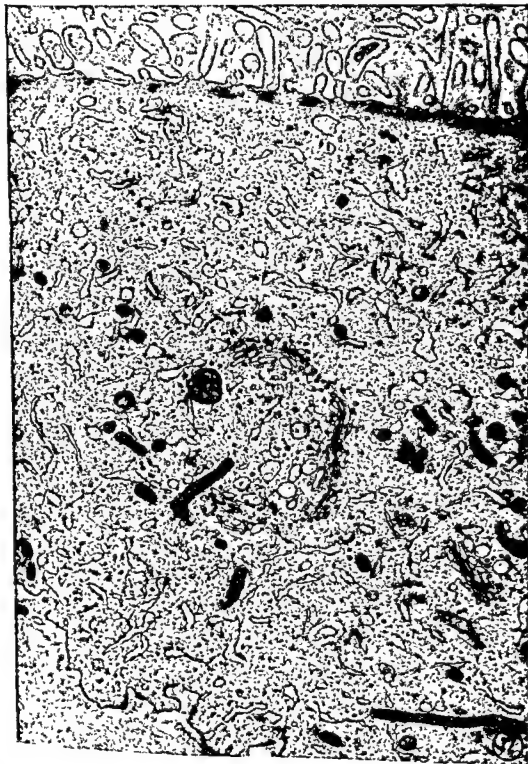


PLATE 13

EXPLANATION OF FIGURE

- 13 Villi such as this one, where the trophoblast is incomplete yet the stroma has not become completely fibrotic, are particularly common in term placentas. Note that the fibrin comes in direct contact with the thick basement membrane in the region (arrows) between the two decidual cells in the upper half of the picture. Note also the abundance of cellular debris in the lower left and the enlargement of the cytotrophoblast cell on the right. $\times 12,400$.



PLATE 13

EXPLANATION OF FIGURE

- 13 Villi such as this one, where the trophoblast is incomplete yet the stroma has not become completely fibrotic, are particularly common in term placentas. Note that the fibrin comes in direct contact with the thick basement membrane in the region (arrows) between the two decidual cells in the upper half of the picture. Note also the abundance of cellular debris in the lower left and the enlargement of the cytotrophoblast cell on the right. $\times 12,400$.



PLATE 13

EXPLANATION OF FIGURE

- 13 Villi such as this one, where the trophoblast is incomplete yet the stroma has not become completely fibrotic, are particularly common in term placentas. Note that the fibrin comes in direct contact with the thick basement membrane in the region (arrows) between the two decidual cells in the upper half of the picture. Note also the abundance of cellular debris in the lower left and the enlargement of the cytotrophoblast cell on the right. $\times 12,400$.



Formation and Structure of the Hemodichorial Chorio-allantoic Placenta of the Bat (*Myotis lucifugus lucifugus*)¹

ALLEN C. ENDERS AND WILLIAM A. WIMSATT

Department of Anatomy, Washington University, St. Louis, Missouri, and
Division of Biological Sciences, Cornell University, Ithaca, New York

ABSTRACT The definitive chorio-allantoic placenta of the bat is hemodichorial, since the cytotrophoblast layer persists to term. The syncytium contains intrasyntical lacunae in which there is a continuous lamina interrupted only where portions of the syncytium communicate with the thin ectoplasmic layer at the surface of the maternal blood spaces.

The future cytotrophoblast and syncytial trophoblast layers can be distinguished shortly after implantation. The future syncytial layer is not syncytial until after it invests most of the anastomotic vessels of the vascular tuft. The resulting labyrinth is converted from the vaso-chorial to the hemodichorial condition as processes of syncytium pass through the basement membrane of the maternal vessels and spread out under the endothelial cells. The basement membrane is then included within the syncytium as the intrasyntical lamina, and the maternal endothelial cells are lost. The numerous communications of the maternal vessels with the labyrinth seen early in gestation are reduced through occlusion of many of the efferent channels, which process also contributes areas of necrosis to the decidua basalis. The peculiarity of a maternal extracellular membrane being incorporated into the fetal portion of the placenta is discussed.

The cellular transformations that take place during implantation, and the general tendency for reduction in thickness of the layers interposed between the fetal and maternal circulations during gestation combine to make observation of the relationship between the fetal and maternal elements difficult to resolve in many of the placental types. It is not surprising therefore that electron microscopy has proved particularly useful in determining the layering of trophoblast and persistence or absence of various of the maternal elements at the fetal-maternal junction (Wislocki and Dempsey, '55; Wislocki and Padykula, '61; Bjorkman, '65a, b, c; Enders, '65; Wynn and Davies, '65; Davies and Wimsatt, '66). Since the complex relationship between the trophoblast and the maternal blood in the chorio-allantoic placenta of vespertilionid bats has been variously interpreted by different authors and lacks a definitive resolution, this study of its fine structure was initiated.

In the labyrinth of the chorio-allantoic placenta of most higher bats, the syncytial trophoblast can be seen to be encompassing channels containing maternal blood. How-

ever, even with the methods of light microscopy, there is clearly an interposed layer or layers between the actual maternal blood and the typical syncytial cytoplasm. Some authors have interpreted the layer closest to the maternal blood as a specialized region of the syncytium (Wimsatt, '45), others as an enucleate maternal endothelium (Branca, '27; Gerard, '28, Wimsatt, '58).

Wimsatt ('58) pointed out that in the vast majority of bats there is a second distinct and apparently continuous layer that is present throughout gestation and is formed of an acellular material that is revealed by eosin and by a variety of histochemical methods. He demonstrated that this layer was consistently periodic acid-Schiff positive, and he designated it the "interstitial membrane." In many species of higher bats, such as *Myotis lucifugus*, this membrane is overlain in later stages of gestation by only a thin anuclear layer

¹This study was supported by grant 1 RO1 HD-02613 from the National Institutes of Child Health and Human Development, and grants G-24043, GB-6435X, and GB-5024 from the National Science Foundation.

of cytoplasm. Because of the persistence of the "interstitial membrane" in this species, its structural and histochemical resemblance to a basement membrane, and the obvious presence of maternal endothelial cells upon this layer at earlier stages in *Myotis* and throughout gestation in more primitive species, Wimsatt ('58) suggested (as had Branch, '27) that the residual surface cytoplasmic layer was an enucleated endothelium. It became apparent in the course of the present study that this interpretation was not correct, and that the overlying thin cytoplasmic layer, rather than being maternal in origin, is actually a specialized component of the syncytial trophoblast. The persistence within the syncytium of an acellular layer that had its origin as a basement membrane of endometrial vessels is a perplexing feature of the *Myotis* placenta, and perhaps has singular physiologic importance.

MATERIALS AND METHODS

Little brown bats (*Myotis lucifugus lucifugus*) from a wild population in the vicinity of Ithaca, New York, were brought into the laboratory, where they were killed within one or two days of capture. The uteri were removed and portions of the placenta were fixed in 3% glutaraldehyde, followed by a rinse in buffer, and post-fixed in 2% osmium tetroxide. The tissues were dehydrated in ethyl alcohol, passed through propylene oxide, and embedded in either Araldite (Durcupan) or Epon epoxy resin. The sections were stained with the lead citrate method of Reynolds ('63) and were studied using an RCA EMU 3G electron microscope. In all instances, thick sections of the plastic-embedded material were stained with Azure B. These sections were used both for orientation purposes and for study by light microscopy of some of the interrelationships.

In several instances a colloidal solution of thorium dioxide (thorotrast) was injected into the wing vein of the maternal animal 15 minutes to one hour prior to fixation of the placental tissues. Placentas from a total of 40 bats in all stages from blastocyst implantation to term (approximately 22 mm CRL) were examined.

OBSERVATIONS

Establishment of the placenta

The histological features of implantation in *Myotis* have been described by Wimsatt ('44), and our current observations are largely confirmatory of that report. The only features that will be mentioned here are those that must be repeated in order to understand the relationships of the placenta, and cytological aspects which could not be determined in the previous study.

Implantation in *Myotis*, as in most other bats, is central. However, the uterine epithelium first disappears on the distended antimesometrial side, and the discoidal chorio-allantoic placenta later is established in this position (Wimsatt, '44).

In the first stage examined in our series, the implanting blastocyst occupies a distinct chamber, but the trophoblast is still unilaminar, and loss of the uterine epithelium in the antimesometrial region is just beginning. A few rounded free cells with pycnotic nuclei can be seen between the basement membrane (basal lamina) of the epithelium and the trophoblast cells, and many of the antimesometrial trophoblast cells contain accumulations of material that appears to have been phagocytized. The remaining luminal epithelium (mesometrially) is flattened but otherwise little altered. Immediately beneath the basement membrane on the maternal side is a series of anastomotic vessels which form a complete antimesometrial tuft. The endothelium of these vessels is relatively thick, especially away from the epithelial surface, and there is very little connective tissue between the vessels (fig. 1). Deep to this vascular tuft, the stroma is richly cellular, being composed of elongate cells circularly disposed. These are the cells that give the fibrous appearance to the "fibrous triangle" at the antimesometrial side of the endometrium (Wimsatt, '44). Little of the swelling which is generally characterized as a decidual reaction in the stroma is present at this stage.

In the next stage in development, there is further loss of luminal epithelium, but otherwise little change in the endometrium. However, the trophoblast, particularly at the margins of the embryonic disc (hence antimesometrially), has become distinctly bilaminar. Both layers of tropho-

blast at this stage are characterized cytologically by an abundance of polyribosomes and a relative sparsity of other organelles. The outer layer of trophoblast faces the inner layer, in that it exhibits rounding of cell surfaces on this side and most of the microvilli along its free surface face either laterally or towards the inner layer of trophoblast. Just as the inner layer of trophoblast has a smooth surface toward the cavity of the implanting blastocyst, so also the outer layer of trophoblast exhibits a relatively smooth continuous front facing the residual basement membrane remaining after loss of the luminal epithelium. In a few places, an occasional epithelial cell is still interposed between this basement membrane and the overlying outer trophoblastic layer. The bilaminar portions of the trophoblast are confined to the embryonic hemisphere of the implanting blastocyst.

With continued proliferation of both elements, the outer trophoblast layer, which still remains cellular, begins to come into contact with the vessels of the vascular tuft. At this stage the residual basement membrane of the luminal epithelium can no longer be discerned, but the thin basement membrane of the maternal vessels remains interposed between the outer trophoblast layer and the endothelial cells, and thus becomes an "interstitial membrane." Both the inner and outer layers of trophoblast continue to be characterized by their many polyribosomes and large nuclei. However, the inner trophoblast layer, the persistent cytotrophoblast of the later placenta, is composed of more regularly arranged distinctly denser cells, whereas the outer trophoblast layer, destined to become the syncytial trophoblast, has an irregular arrangement and is less dense. The cells of both layers contain large vacuoles filled with apparent cellular debris, and in a number of instances glycogen granules and lipid droplets can be seen in some of them.

The next stage in development of the chorio-allantoic placenta is the conversion of the outer trophoblast layer to syncytial trophoblast. Since this conversion coincides with the complete investment of the maternal vessels composing the vascular tuft, it results in the establishment of a

temporary placenta of the vaso-chorial or endothelio-chorial type.

The trophoblastic tissue at this stage is distinctly different from the previous stage. The cytotrophoblast cells show the least alteration. They are arranged as a layer from one to three cells thick over most of the now distinctly cup-like (presumptively discoidal) chorio-allantoic placenta. The proximal cells form a continuous layer underlain by a basement membrane bordering the cavity of the blastocyst. Distally these cells constitute a loose meshwork with prominent intercellular clefts, and rounded apical ends fronting on the syncytium. There are numerous points of adhesion between the individual cytotrophoblast cells, and extensive junctional complexes are found at the apical ends of their lateral borders. The cytotrophoblast and syncytium come in contact at irregular intervals. Well-formed desmosomes unite these epithelia at many of the points of contact. Between these adherent regions, and especially at their margins, the cytotrophoblast cells display groups of short microvilli which project into the spaces between cells. Furthermore solid cords of cytotrophoblast cells now extend in several places down into the syncytium, constituting the so-called primary villi (Wimsatt, '45). The cytotrophoblast is densely filled with polyribosomes, and mitotic figures are numerous. There are a few strands of granular endoplasmic reticulum, and several large mitochondria with lamelliform cristae are characteristic of these cells. Their Golgi zones are inconspicuous.

The outer trophoblast is now syncytial and consequently forms a continuum which extends from the cytotrophoblast outward around the vessels of the vascular tuft, which it invests, to the underlying endometrial stroma (fig. 2). In the syncytium at its surface fronting on the cytotrophoblast, in addition to desmosomes and microvilli, are found numerous dense tubular structures resembling the absorption tubules characteristic of the proximal convoluted tubule and of yolk sac epithelium. At the opposite side of the forming placental disc where the syncytium fronts on the fusiform decidua cells, the surface of the syncytium is relatively smooth, and the superficial cytoplasm contains numerous

of cytoplasm. Because of the persistence of the "interstitial membrane" in this species, its structural and histochemical resemblance to a basement membrane, and the obvious presence of maternal endothelial cells upon this layer at earlier stages in *Myotis* and throughout gestation in more primitive species, Wimsatt ('58) suggested (as had Branca, '27) that the residual surface cytoplasmic layer was an enucleated endothelium. It became apparent in the course of the present study that this interpretation was not correct, and that the overlying thin cytoplasmic layer, rather than being maternal in origin, is actually a specialized component of the syncytial trophoblast. The persistence within the syncytium of an acellular layer that had its origin as a basement membrane of endometrial vessels is a perplexing feature of the *Myotis* placenta, and perhaps has singular physiologic importance.

MATERIALS AND METHODS

Little brown bats (*Myotis lucifugus lucifugus*) from a wild population in the vicinity of Ithaca, New York, were brought into the laboratory, where they were killed within one or two days of capture. The uteri were removed and portions of the placenta were fixed in 3% glutaraldehyde, followed by a rinse in buffer, and post-fixed in 2% osmium tetroxide. The tissues were dehydrated in ethyl alcohol, passed through propylene oxide, and embedded in either Araldite (Durcupan) or Epon epoxy resin. The sections were stained with the lead citrate method of Reynolds ('63) and were studied using an RCA EMU 3G electron microscope. In all instances, thick sections of the plastic-embedded material were stained with Azure B. These sections were used both for orientation purposes and for study by light microscopy of some of the interrelationships.

In several instances a colloidal solution of thorium dioxide (thorotrast) was injected into the wing vein of the maternal animal 15 minutes to one hour prior to fixation of the placental tissues. Placentas from a total of 40 bats in all stages from blastocyst implantation to term (approximately 22 mm CRL) were examined.

OBSERVATIONS

Establishment of the placenta

The histological features of implantation in *Myotis* have been described by Wimsatt ('44), and our current observations are largely confirmatory of that report. The only features that will be mentioned here are those that must be repeated in order to understand the relationships of the placenta, and cytological aspects which could not be determined in the previous study.

Implantation in *Myotis*, as in most other bats, is central. However, the uterine epithelium first disappears on the distended antimesometrial side, and the discoidal chorio-allantoic placenta later is established in this position (Wimsatt, '44).

In the first stage examined in our series, the implanting blastocyst occupies a distinct chamber, but the trophoblast is still unilaminar, and loss of the uterine epithelium in the antimesometrial region is just beginning. A few rounded free cells with pycnotic nuclei can be seen between the basement membrane (basal lamina) of the epithelium and the trophoblast cells, and many of the antimesometrial trophoblast cells contain accumulations of material that appears to have been phagocytized. The remaining luminal epithelium (mesometrially) is flattened but otherwise little altered. Immediately beneath the basement membrane on the maternal side is a series of anastomotic vessels which form a complete antimesometrial tuft. The endothelium of these vessels is relatively thick, especially away from the epithelial surface, and there is very little connective tissue between the vessels (fig. 1). Deep to this vascular tuft, the stroma is richly cellular, being composed of elongate cells circularly disposed. These are the cells that give the fibrous appearance to the "fibrous triangle" at the antimesometrial side of the endometrium (Wimsatt, '44). Little of the swelling which is generally characterized as a decidual reaction in the stroma is present at this stage.

In the next stage in development, there is further loss of luminal epithelium, but otherwise little change in the endometrium. However, the trophoblast, particularly at the margins of the embryonic disc (hence antimesometrially), has become distinctly bilaminar. Both layers of tropho-

spread out, eventually loosening the endothelium from the interstitial membrane. As the endothelium loses contact with the membrane, the continuity of the endothelial layer is disrupted. Subsequently the endothelial cells are sloughed, those remnants lodging in the labyrinth being phagocytized by the syncytium along with leukocytes and other cellular debris.

In the decidua basalis, the vessels passing into the labyrinth are of two types, one with relatively low endothelium (arteries) and the other with an endothelium of markedly hypertrophied cells that at this stage may be more than one cell layer thick (veins). At about the time that loss of endothelium is occurring within the labyrinth, many of these venous channels emerging from the intralabyrinthine network become occluded and undergo massive necrosis, leaving relatively few definitive penetrating and emergent channels within the endometrium. In addition to limiting the vessels connecting the labyrinth with the endometrium, the extensive degeneration of the hypertrophied venous channels contributes areas of epithelial cell islands, symplasma, and necrosis to the decidua basalis in an irregular pattern that greatly increases the complexity and heterogeneity of this region.

Shortly after loss of the maternal endothelium in the labyrinth, fetal connective tissue and vessels begin to invade the solid cytotrophoblastic cell cords (primary villi), and the placental disc becomes fully vascularized. Thus by the time the embryo reaches the early limb bud stage, the major components of the placenta are in place.

Definitive placenta

The definitive chorio-allantoic placenta of *Myotis* is a discoidal structure. Marginally the disc is deeply undercut by the membranous chorion, restricting the region of contact between the decidua basalis and the labyrinth to a broad pedicle through which the maternal blood enters and leaves the placenta. Maternal blood entering the placenta courses to the fetal surface in moderately large channels whence it enters the numerous smaller passages of the labyrinth, proceeding through these structures back to the junc-

tional zone with the decidua, which is itself a complex region composed of several different zones (see Wimsatt, '45, '48, '49).

Labyrinth

The placental barrier in the labyrinth of the definitive placenta is essentially of the hemodichorial type (fig. 6). Proceeding from the fetal to the maternal blood, the following layers are encountered: fetal endothelium, sparse connective tissue, a continuous cytotrophoblastic cell layer, a covering layer of syncytial trophoblast containing near its surface the intrasyncytial lamina, and an overlying thin layer of cytoplasm continuous with the syncytium through perforations in the intrasyncytial lamina.

Cytologically the fetal endothelium is unremarkable, being composed of squamous cells exhibiting the usual features of endothelium, including an abundance of micropinocytotic vesicles, especially on the outer surface. The endothelium becomes quite thin in places but does not seem to have pore areas. In later stages these vessels partially indent the overlying trophoblast. The underlying basement membrane is thin, and relatively few collagen filaments are found around the vessels. From about midgestation on, small round bodies composed of individual dense particles with the image characteristics of ferritin are found in many areas of the fetal connective tissue (cf. Wimsatt, '49, for account of iron distribution in the placenta of *Myotis*, and Salazar, '67, for a similar type of body in the human placenta).

The cytotrophoblast is composed of a single layer of cells which is closely apposed to the overlying syncytium, to which it is associated by abundant desmosomes and occasional close junctions. In the early stages, the cytotrophoblast cells are roughly cuboidal (fig. 7). As pregnancy advances, they become more elongate, and their basal surface, which was smooth in the early stages, develops a series of small concavities into which microvilli project. Polyribosomes are present in the cytotrophoblast, but only a few strands of endoplasmic reticulum are found. At first the endoplasmic reticulum has associated ribosomes, but in the later stages, most of the endoplasmic reticulum is smooth. Glycogen in

fine filaments with periodic short spindle-shaped dense spots. This front of the syncytium on the decidua marks the boundary of penetration of the trophoblast into the endometrial tissue. (By the end of this stage the vascular tuft is completely enveloped. Apparently all subsequent development of the labyrinth and elongation of its vascular channels takes place within this region already enclosed by syncytium.)

The most irregular and most extensive surface of the syncytium is that associated with the anastomotic vessels of the original vascular tuft which, together with the surrounding syncytium, now constitute the placental labyrinth. The enclosed vessels retain at this stage a thin basement membrane, except, curiously, for a few spots along the vessel walls where stubby tongues of endothelial cytoplasm protrude through the basement membrane. Only an occasional stromal cell is found in this region, and such cells are usually undergoing necrosis. The surface of the syncytium contains numerous indentations, most of which front on the basement membrane of the maternal endothelial cells. Microvilli of the syncytium project into these spaces formed by the indentations. Large elongate desmosomes join the processes of the syncytium surrounding these areas. In most instances, very little extracellular material can be seen between the numerous microvilli, but in some instances small amounts of amorphous material with a density characteristic of the substances of basement membrane can be seen. The arrangements of the cell membranes and desmosomes are quite irregular. At this surface, caveolae of the coated vesicle type are common within the syncytium.

The cytoplasm of the syncytium is now more highly differentiated than in the previous stage. Although polyribosomes are still abundant, strands of granular endoplasmic reticulum are now a characteristic feature of this layer. The mitochondria too are more numerous than in the previous stage, and tend to be somewhat smaller and denser than those of the cytotrophoblast. Although centrioles are occasionally seen next to the maternal side of the syncytium, no mitotic figures are seen in this layer. The Golgi regions are still somewhat sparsely distributed, but the membranes

are more extensive and encompass larger regions than formerly. The most striking type of inclusion within the syncytium is a series of irregularly distributed vacuoles containing large paracrystalline bodies.

Establishment of the hemochorial condition

The placenta now undergoes a rapid change in character, during which it converts from the vasochorial to the hemochorial condition. The first indication of the conversion in a given stretch of vessel is the presence of a tongue of syncytium which protrudes through the basement membrane and spreads out underneath the maternal endothelium, in effect loosening its attachment to the basement membrane (figs. 3, 4). At other areas along the vessels, short stretches of endothelial cells may be actually displaced, resting solely on the microvilli of the syncytium. In still other places, the endothelium has disappeared entirely, yet the basement membrane in between the areas penetrated by the trophoblast remains, although it now has a covering of syncytial cytoplasm rather than endothelium. Thus the "interstitial membrane" interposed between maternal endothelium and the syncytium at the start of this stage becomes converted into an *intrasyncytial* lamina, perforated only at irregular intervals by syncytial tongues which spread out over its upper surface forming a nearly continuous layer (fig. 5). The layer of syncytium overlying the intrasyncytial membrane is largely devoid of organelles and, except for the presence of numerous, frequently elongate microvilli which, especially in earlier placentae, often display distinct tree-like projections is typically "ectoplasmic." At the close of this period, endothelial cells are no longer found within the labyrinth. However, numerous inclusions including nuclear remnants and fragments of maternal leukocytes and endothelial cells, are found within the superficial syncytium.

The observed morphological features suggest the following sequence. Tongues of syncytium extend through the basement membrane of the vessels (possibly at the places where there were penetrating endothelial cell processes originally). On reaching the maternal side of the membrane, the ectoplasmic syncytial processes

pread out, eventually loosening the endothelium from the interstitial membrane. As the endothelium loses contact with the membrane, the continuity of the endothelial layer is disrupted. Subsequently the endothelial cells are sloughed, those remnants lodging in the labyrinth being phagocytized by the syncytium along with leukocytes and other cellular debris.

In the decidua basalis, the vessels passing into the labyrinth are of two types, one with relatively low endothelium (arteries) and the other with an endothelium of markedly hypertrophied cells that at this stage may be more than one cell layer thick (veins). At about the time that loss of endothelium is occurring within the labyrinth, many of these venous channels emerging from the intralabyrinthine network become occluded and undergo massive necrosis, leaving relatively few definitive penetrating and emergent channels within the endometrium. In addition to limiting the vessels connecting the labyrinth with the endometrium, the extensive degeneration of the hypertrophied venous channels contributes areas of epithelial cell islands, symplasma, and necrosis to the decidua basalis in an irregular pattern that greatly increases the complexity and heterogeneity of this region.

Shortly after loss of the maternal endothelium in the labyrinth, fetal connective tissue and vessels begin to invade the solid cytotrophoblastic cell cords (primary villi), and the placental disc becomes fully vascularized. Thus by the time the embryo reaches the early limb bud stage, the major components of the placenta are in place.

Definitive placenta

The definitive chorio-allantoic placenta of *Myotis* is a discoidal structure. Marginally the disc is deeply undercut by the membranous chorion, restricting the region of contact between the decidua basalis and the labyrinth to a broad pedicle through which the maternal blood enters and leaves the placenta. Maternal blood entering the placenta courses to the fetal surface in moderately large channels whence it enters the numerous smaller passages of the labyrinth, proceeding through these structures back to the junc-

tional zone with the decidua, which is itself a complex region composed of several different zones (see Wimsatt, '45, '48, '49).

Labyrinth

The placental barrier in the labyrinth of the definitive placenta is essentially of the hemodichorial type (fig. 6). Proceeding from the fetal to the maternal blood, the following layers are encountered: fetal endothelium, sparse connective tissue, a continuous cytotrophoblastic cell layer, a covering layer of syncytial trophoblast containing near its surface the intrasyntactial lamina, and an overlying thin layer of cytoplasm continuous with the syncytium through perforations in the intrasyntactial lamina.

Cytologically the fetal endothelium is unremarkable, being composed of squamous cells exhibiting the usual features of endothelium, including an abundance of micropinocytotic vesicles, especially on the outer surface. The endothelium becomes quite thin in places but does not seem to have pore areas. In later stages these vessels partially indent the overlying trophoblast. The underlying basement membrane is thin, and relatively few collagen filaments are found around the vessels. From about midgestation on, small round bodies composed of individual dense particles with the image characteristics of ferritin are found in many areas of the fetal connective tissue (cf. Wimsatt, '49, for account of iron distribution in the placenta of *Myotis*, and Salazar, '67, for a similar type of body in the human placenta).

The cytotrophoblast is composed of a single layer of cells which is closely apposed to the overlying syncytium, to which it is associated by abundant desmosomes and occasional close junctions. In the early stages, the cytotrophoblast cells are roughly cuboidal (fig. 7). As pregnancy advances, they become more elongate, and their basal surface, which was smooth in the early stages, develops a series of small concavities into which microvilli project. Polyribosomes are present in the cytotrophoblast, but only a few strands of endoplasmic reticulum are found. At first the endoplasmic reticulum has associated ribosomes, but in the later stages, most of the endoplasmic reticulum is smooth. Glycogen in

the form of large areas of alpha particles is abundant in the cytotrophoblast cells in early stages of gestation, but is largely absent from midgestation on. Mitochondria are sparse and are round with lamelliform cristae at all stages, and the Golgi zones comprise small aggregates of cisternae with only a few associated vesicles. A distinct basement membrane underlies the cytotrophoblast.

The syncytial trophoblast is a thick, well organized layer with evenly spaced nuclei. As mentioned previously, numerous desmosomes are found in connection with the cytotrophoblastic border of the syncytium. Fine filaments are often apparent in the associated cytoplasm. The most conspicuous organelle within the syncytium is the granular endoplasmic reticulum, which is arranged in a series of cisternae extending in parallel array at right angles to the free and basal surface (figs. 7, 8). A flocculent material can be seen within the cisternae of the endoplasmic reticulum. At the ends of the cisternae dilations are found, many of which have a relatively sparse distribution of ribosomes on their surface. These cisternae are so numerous that in stained thick sections they impart a distinct striation to the syncytium.

The Golgi zones are large areas consisting of circularly arranged cisternae with numerous associated vesicles of both the smooth and rough surfaced varieties (fig. 9). The Golgi zones are generally situated towards the base of the syncytium, that is, from the level of the nuclei to a basal position. Frequently several microtubules are associated with the Golgi zone. The mitochondria are for the most part short rod-shaped structures with lamellar cristae and a dense matrix. They are not especially abundant.

Near the maternal surface is a complex of irregularly shaped linearly arranged bays or lacunae, which evidently forms a confluent space that is frequently interrupted by the projection of syncytial cytoplasm through to the surface of the maternal blood spaces. Caveolae of the rough-surfaced variety are found in association with the complex (fig. 11). In the center of the lacunae lies the homogeneous, acellular, intrasyncytial lamina, the "interstitial membrane" of early stages. In

the later stages of pregnancy, small membranous vesicles are frequently found within the lacunae, particularly in association with the maternal side. The surface of the maternal blood space is formed by a thin layer of syncytial cytoplasm which is relatively devoid of organelles (ectoplasm). Numerous microvilli project from it and rough surfaced caveolae are almost as frequent here as in the lacunae. Where adjacent processes of syncytium are contiguous, desmosomes are frequently present, but no evidence of tight junctions is seen. It consequently appears that spaces through which material can diffuse from maternal blood space into the intrasyncytial lacuna system are present (fig. 10). It was a surprising finding therefore that injected thorotrast does not pass directly from the maternal blood space into the lacunae.

During much of the gestation period, large multivesicular bodies are found within the ectoplasmic layer of the syncytium and more rarely in the deeper portion. Later, when small vesicles are common within the lacunae, such multivesicular bodies are less common. When thorotrast is found in the syncytium, it is usually contained within the multivesicular bodies. Large ovoid granules, many of which contain paracrystalline bodies, are a prominent inclusion of the midgestation period within the thicker portion of the syncytium. Later such granules disappear, and smaller more homogeneous granules and scattered lipid droplets are the major inclusions.

Junctional zone

Along the junction between the labyrinth and the decidua basalis, the syncytium forms a smooth front except at the relatively few places where the labyrinth is supplied by maternal vessels. The surface of the syncytial front is modified by the presence of a zone of cytoplasm underlying the surface membrane which contains numerous fine filaments and associated dense bodies (fig. 13). Large venous sinuses are present at regular intervals along this front, and form a prominent feature of the older placentas. In many of these sinuses the syncytium with its associated intrasyncytial membrane lines only

part of the sinus, and is contiguous with hypertrophied maternal vascular cells on the decidual side. In favorable sections near the center of the placental pedicle, direct continuity between the maternal blood spaces of the labyrinth and the maternal veins of the decidua is seen (fig. 12). In the best of these examples, the maternal vascular cells can be seen to stop abruptly at the junction of the decidua with the labyrinth, and the syncytium tends to overlap slightly the adjacent maternal vascular cells.

The maternal arteries at the center of the pedicle have a thick cellular sheath and, in contradistinction to the veins, are distinctly separated from the surrounding decidua. At the point of junction with the labyrinth, these maternal arteries are lined with large irregular endothelial cells containing numerous lipid droplets. The sheath of the artery ends relatively abruptly at the junction, but the endothelial cells may extend for some distance into the placenta. In this position they are underlain by syncytial trophoblast whose maternal face is highly irregular (figs. 14, 15). Processes from this syncytium extend to and make contact with the endothelial cells. However, this contact is irregular, and in a typical field there is a wide space containing processes from the endothelial cells, associated extracellular substance, processes from the syncytium, and a somewhat irregular distribution of the amorphous intrasyncytial lamina. Further along the labyrinth towards the fetal surface, the endothelium ceases and the lacunae of the syncytium become smaller and more regular in shape.

Decidua basalis

Within the decidua basalis are a number of different components, not all of which are present in all areas. Immediately adjacent to the syncytium is a region of relatively compact decidual cells. The small interstitial spaces between these cells are devoid of any connective tissue elements. The cells themselves are rather generalized in appearance, relatively small, with a few scattered strands of granular endoplasmic reticulum, small mitochondria, and occasional desmosomal connections. Beneath this layer are larger glycogen-rich decidual

cells in which large portions of the cytoplasm contain only alpha glycogen granules, and the other components occupy a narrow zone around the nucleus and margin of the cell. Among these cells are other cells with less glycogen and more abundant dilated granular endoplasmic reticulum (fig. 16). The two cell types are similar to the decidual cells of myomorph rodents, and seem to represent two aspects of a single population of cells. Regions of necrosis and associated multinucleate masses are also found in the decidua basalis especially in the earlier stages. Directly overlying the muscularis is a compact cellular region of fusiform cells exhibiting only partial decidualization.

DISCUSSION

Our electron microscopic observations require some modification of earlier ideas concerning the organization of the definitive placental barrier in *Myotis lucifugus* based on light microscopic and histochemical studies (cf. Wimsatt, '58). Clearly what was formerly interpreted as an "enucleate maternal endothelium" adjoining the maternal blood spaces turns out to be in fact an "ectoplasmic" layer of syncytiotrophoblast generously provided with microvilli. Thus throughout gestation (except for the early post-implantation stages) the placenta is truly hemochorial rather than endotheliochorial as formerly proposed. Prior to this study it was also thought that the cytotrophoblast layer was lost in the latter half of pregnancy. This misconception is not surprising insofar as the cytotrophoblast cells become highly attenuated in many places and in general indent the syncytium in such a way that the two layers form one relatively smooth unit. Nevertheless the definitive chorio-allantoic placenta of *Myotis* retains two distinct layers of trophoblast to term, and should therefore be classified as hemodichorial. In light of these findings in *Myotis* it is not at all improbable that similar conditions prevail in the placenta of other vespertilionids, for those examined by light microscopy show identical structural organization of the placental barrier to *Myotis* (Wimsatt, '45, '58, '62). Furthermore, Wimsatt ('58) has described and figured the placentas of several Phyllostomatidae, and these also re-

the form of large areas of alpha particles is abundant in the cytotrophoblast cells in early stages of gestation, but is largely absent from midgestation on. Mitochondria are sparse and are round with lamelliform cristae at all stages, and the Golgi zones comprise small aggregates of cisternae with only a few associated vesicles. A distinct basement membrane underlies the cytotrophoblast.

The syncytial trophoblast is a thick, well organized layer with evenly spaced nuclei. As mentioned previously, numerous desmosomes are found in connection with the cytotrophoblastic border of the syncytium. Fine filaments are often apparent in the associated cytoplasm. The most conspicuous organelle within the syncytium is the granular endoplasmic reticulum, which is arranged in a series of cisternae extending in parallel array at right angles to the free and basal surface (figs. 7, 8). A flocculent material can be seen within the cisternae of the endoplasmic reticulum. At the ends of the cisternae dilations are found, many of which have a relatively sparse distribution of ribosomes on their surface. These cisternae are so numerous that in stained thick sections they impart a distinct striation to the syncytium.

The Golgi zones are large areas consisting of circularly arranged cisternae with numerous associated vesicles of both the smooth and rough surfaced varieties (fig. 9). The Golgi zones are generally situated towards the base of the syncytium, that is, from the level of the nuclei to a basal position. Frequently several microtubules are associated with the Golgi zone. The mitochondria are for the most part short rod-shaped structures with lamellar cristae and a dense matrix. They are not especially abundant.

Near the maternal surface is a complex of irregularly shaped linearly arranged bays or lacunae, which evidently forms a confluent space that is frequently interrupted by the projection of syncytial cytoplasm through to the surface of the maternal blood spaces. Caveolae of the rough-surfaced variety are found in association with the complex (fig. 11). In the center of the lacunae lies the homogeneous, acellular, intrasyncytial lamina, the "interstitial membrane" of early stages. In

the later stages of pregnancy, small membranous vesicles are frequently found within the lacunae, particularly in association with the maternal side. The surface of the maternal blood space is formed by a thin layer of syncytial cytoplasm which is relatively devoid of organelles (ectoplasm). Numerous microvilli project from it and rough surfaced caveolae are almost as frequent here as in the lacunae. Where adjacent processes of syncytium are contiguous, desmosomes are frequently present, but no evidence of tight junctions is seen. It consequently appears that spaces through which material can diffuse from maternal blood space into the intrasyncytial lacuna system are present (fig. 10). It was a surprising finding therefore that injected thorotrast does not pass directly from the maternal blood space into the lacunae.

During much of the gestation period, large multivesicular bodies are found within the ectoplasmic layer of the syncytium and more rarely in the deeper portion. Later, when small vesicles are common within the lacunae, such multivesicular bodies are less common. When thorotrast is found in the syncytium, it is usually contained within the multivesicular bodies. Large ovoid granules, many of which contain paracrystalline bodies, are a prominent inclusion of the midgestation period within the thicker portion of the syncytium. Later such granules disappear, and smaller more homogeneous granules and scattered lipid droplets are the major inclusions.

Junctional zone

Along the junction between the labyrinth and the decidua basalis, the syncytium forms a smooth front except at the relatively few places where the labyrinth is supplied by maternal vessels. The surface of the syncytial front is modified by the presence of a zone of cytoplasm underlying the surface membrane which contains numerous fine filaments and associated dense bodies (fig. 13). Large venous sinuses are present at regular intervals along this front, and form a prominent feature of the older placentas. In many of these sinuses the syncytium with its associated intrasyncytial membrane lines only

the maternal blood spaces. Presumably the caveolae are also involved with exchanges at the surface of the syncytium, yet no direct interrelationship between these structures and the multivesicular bodies was observed.

Tillach ('66) used the intravascular injection of ferritin as a means of determining that pores existed in the outer layer of trophoblast in the rat placenta, permitting direct access of large molecules to the second layer of trophoblast. In a similar fashion Sinha ('67) used thorotrast to demonstrate that the intertubular clefts in the rabbit placenta were in communication with the maternal blood spaces. Despite the pore-like structures seen in the ectoplasmic layer in the *Myotis* placenta, thorotrast was virtually absent from the intrasyncytial lamina. Consequently thorotrast either does not penetrate directly or at any rate does not accumulate in the intrasyncytial lamina. Consequently the apparent openings in the ectoplasmic layer are probably effectively closed.

The small size of the little brown bat, its ready availability, and the wealth of cytological features associated with transport activities makes this species an excellent one for further studies on the passage of substances from the maternal blood spaces into the fetal tissues.

LITERATURE CITED

- Bjorkman, N. 1965a Fine structure of the ovine placenta. *J. Anat.*, 99: 283-297.
- 1965b The fine morphology of the area of foetal-maternal apposition in the equine placenta. *Z. Zellforsch.*, 65: 285-289.
- 1965c On the fine structure of the porcine placental barrier. *Acta anat.*, 62: 334-342.
- Branca, A. 1927 Recherches sur la placentation des Chiropteres. *Arch. de Zool. exper. et gen.*, 66: 291-450.
- Davies, J., and W. A. Wimsatt 1966 Observations on the fine structure of the sheep placenta. *Acta anat.*, 65: 182-223.
- Ender, A. C. 1965 A comparative study of the fine structure of the trophoblast in several hemochorial placentas. *Am. J. Anat.*, 116: 29-68.
- Friend, D. S. 1965 The fine structure of Brunner's glands in the mouse. *J. Cell Biol.*, 25: 563-576.
- Gerard, P. 1928 Recherches histophysiologiques sur les annexes foetales des chiropteres (*Vesperugo noctula* Schreb.). *Arch. Biol.*, 38: 327-354.
- Kirby, D. R. S., W. D. Billington, S. Bradbury, and D. J. Goldstein 1964 Antigen barrier of the mouse placenta. *Nature, Lond.*, 204: 548-549.
- Reynolds, E. S. 1963 The use of lead citrate at high pH as an electron-opaque stain in electron microscopy. *J. Cell Biol.*, 17: 208-212.
- Salazar, H., and A. Gonzalez-Angulo 1967 The fine structure of human chorionic villi and placental transfer of iron in late pregnancy. *Am. J. Ob. Gyn.*, 97: 851-865.
- Sinha, A. A. 1967 The intertubular cleft and thorotrast permeability in the rabbit placenta. *Anat. Rec.*, 157: 322.
- Tillack, T. W. 1966 The transport of ferritin across the placenta of the rat. *Lab. Invest.*, 15: 896-909.
- Wimsatt, W. A. 1944 An analysis of implantation in the bat, *Myotis lucifugus lucifugus*. *Am. J. Anat.*, 74: 355-411.
- 1945 The placentation of a vespertilionid bat, *Myotis lucifugus lucifugus*. *Am. J. Anat.*, 77: 1-51.
- 1948 The nature and distribution of lipoids in the placenta of the bat (*Myotis lucifugus lucifugus*), with observations on the mitochondria and Golgi apparatus. *Am. J. Anat.*, 82: 393-467.
- 1949 Cytochemical observations on the fetal membranes and placenta of the bat, *Myotis lucifugus lucifugus*. *Am. J. Anat.*, 84: 63-141.
- 1958 The allantoic placental barrier in Chiroptera: a new concept of its organization and histochemistry. *Acta Anat.*, 32: 141-186.
- 1962 Some aspects of the comparative anatomy of the mammalian placenta. *Am. J. Ob. Gyn.*, 84: 1568-1594.
- Wislocki, G. B., and E. W. Dempsey 1955 Electron microscopy of the human placenta. *Anat. Rec.*, 123: 133-168.
- Wislocki, G. B., and H. Padykula 1961 Histochemistry and electron microscopy of the placenta. In: *Sex and Internal Secretions*, W. C. Young, ed., Williams and Wilkins Co., Baltimore.
- Wynn, R. M., and J. Davies 1965 Comparative electron microscopy of the hemochorial placenta. *Am. J. Ob. Gyn.*, 91: 533-549.

semble at the light microscopic level the placenta of *Myotis*. When subjected to electron microscopic examination, perhaps these placentas also will be found to be hemodichorial and to be characterized by the unusual intrasyncytial lamina of acellular material that served initially as the basement membrane of the maternal endothelium, for the PAS-positive "interstitial membrane" is as characteristic of the placenta in phyllostomids as it is in vespertilionids.

Certainly the most striking feature of the placenta of *Myotis* is the presence of the continuous intrasyncytial lacuna system and contained lamina. This system is not only consistently present but is startlingly uniform in its distribution and position. The contained lamina is initially a product of the maternal organism, yet throughout most of gestation it is completely embedded within the syncytium. Both the displacement of the maternal endothelium and the subsequent enlargement of the labyrinth occur without destruction of this intrasyncytial lamina. However, the enlargement of the labyrinth, with its subsequent elongation of the maternal blood spaces, implies that during this stage the lamina must be formed at least in part by material synthesized by the syncytium.

This striking feature of the *Myotis* placenta is not entirely unique, since in *Eutamias* (chipmunk) also there is a sub-surface lacuna system within the syncytium that contains an extracellular material and is overlain by an ectoplasmic layer (Enders, '65). Indeed the analagous arrangement in these two divergent forms leads to the supposition that such an arrangement must have very distinct functional advantages. We have little evidence indicating what these advantages might be. However, it may be particularly significant that only an ectoplasmic layer overlies the intrasyncytial lamina. This acellular lamina consequently separates the maternal blood from not only the majority of fetal tissues but also the endoplasmic reticulum and other synthetic apparatus of the syncytium itself. It is tempting to speculate that this isolation serves as a portion of the immunological mechanism by which antigenic substances are kept

from entering the maternal organism from the fetal tissues. It is interesting to note that Kirby et al. ('64) has recently obtained evidence that acellular material may facilitate immunological isolation of ectopic implants from maternal tissues in the mouse.

A number of cytological features of the *Myotis* placenta are common to the hemodichorial placenta of the rabbit as well as other hemochorial placentas. The relatively thick syncytium with extensive granular endoplasmic reticulum and the orientation of the large Golgi zones towards the fetal side of the syncytium are features also found in the rabbit, human, armadillo and guinea pig. Thinning of the trophoblast in later stages of pregnancy, a basal layer of trophoblast (cytotrophoblast) cytologically less active in appearance than the overlying syncytium, and infoldings increasing the surface on the fetal side of the basal layer are all features that the chorio-allantoic placenta of the bat shares with the placenta of other species.

On the other hand, the granular endoplasmic reticulum within the syncytium becomes oriented to an extraordinary extent in the *Myotis* placenta. The organization of the cisternae in parallel array at right angles to the free surface results in pronounced striae in light microscope preparations. Such striae are ordinarily characteristic of glands with a high rate of protein granule production.

The relationships among the smooth and rough surfaced vesicles associated with the Golgi, the protein granules in the cytoplasm, the multivesicular bodies and the rough surfaced caveolae at both the maternal surface and in the intrasyncytial lacunae are complex and could not be fully discerned from this study. However, some evidence of interrelationships is seen. The presence of hemivesicular profiles at the margins of the Golgi membranes and continuous with adjacent endoplasmic reticulum is probably indicative of exchange between these two organelles, resembling as it does the observations of Friend ('65) in Brunner's glands. The presence of thorotrast within the multivesicular bodies (but not within the vesicles *per se*) is an indication that these compound structures are involved in absorption of material from



PLATE 1

EXPLANATION OF FIGURE

- 1** Section through a vessel in the maternal vascular tuft. Note the large size of the endothelial cells of these anastomotic vessels. $\times 6,800$.



PLATE 2

EXPLANATION OF FIGURE

- 2 Section through the labyrinth just after the outer layer of trophoblast has become syncytial, and before the maternal endothelial cells disappear. Note the basement membrane (arrows) surrounding the maternal blood vessel (MBV). The insert is an enlargement of the region in the central portion of the picture where the syncytium abuts on the cytotrophoblast. The small arrows in the insert point to absorption tubules within the syncytium. $\times 10,100$. Insert $\times 19,800$.



PLATE 2

EXPLANATION OF FIGURE

- 2 Section through the labyrinth just after the outer layer of trophoblast has become syncytial, and before the maternal endothelial cells disappear. Note the basement membrane (arrows) surrounding the maternal blood vessel (MBV). The insert is an enlargement of the region in the central portion of the picture where the syncytium abuts on the cytotrophoblast. The small arrows in the insert point to absorption tubules within the syncytium. $\times 10,100$. Insert $\times 19,800$.



PLATE 2

EXPLANATION OF FIGURE

- 2 Section through the labyrinth just after the outer layer of trophoblast has become syncytial, and before the maternal endothelial cells disappear. Note the basement membrane (arrows) surrounding the maternal blood vessel (MBV). The insert is an enlargement of the region in the central portion of the picture where the syncytium abuts on the cytotrophoblast. The small arrows in the insert point to absorption tubules within the syncytium. $\times 10,100$. Insert $\times 19,800$.



PLATE 3

EXPLANATION OF FIGURE

- 3 Labyrinth at the stage when the syncytial trophoblast is penetrating through the basement membrane of the maternal blood vessels and replacing endothelial cells. Note the projection of the syncytium through the basement membrane between the arrows, and that the maternal blood space (MBS) is already bordered by syncytium at the top of the micrograph. $\times 20,400$.



PLATE 4

EXPLANATION OF FIGURES

- 4 Another illustration of the syncytial trophoblast penetrating through the basement membrane (arrows) of the maternal blood vessel. Note that desmosomes are present where two of the several different projections of the syncytium abut. $\times 15,000$.
- 5 Syncytial trophoblast after conversion of the labyrinth to the hemodichorial state. Note that the syncytium lying above the basement membrane (now the intrasyncytial lamina) is an ectoplasm in that it is largely devoid of organelles. Note also the extensive cisternae of the granular endoplasmic reticulum. MBS, maternal blood space. $\times 16,200$.

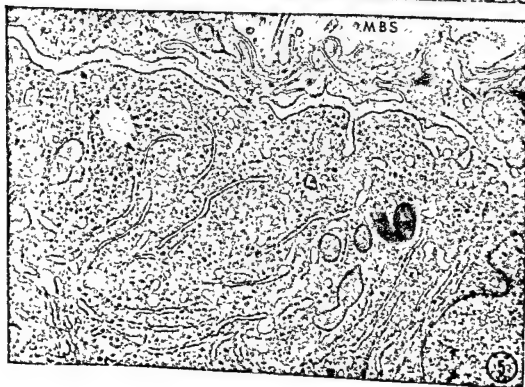


PLATE 4

EXPLANATION OF FIGURES

- 4 Another illustration of the syncytial trophoblast penetrating through the basement membrane (arrows) of the maternal blood vessel. Note that desmosomes are present where two of the several different projections of the syncytium abut. $\times 15,000$.
- 5 Syncytial trophoblast after conversion of the labyrinth to the hemodichorial state. Note that the syncytium lying above the basement membrane (now the intrasyncytial lamina) is an ectoplasm in that it is largely devoid of organelles. Note also the extensive cisternae of the granular endoplasmic reticulum. MBS, maternal blood space. $\times 16,200$.

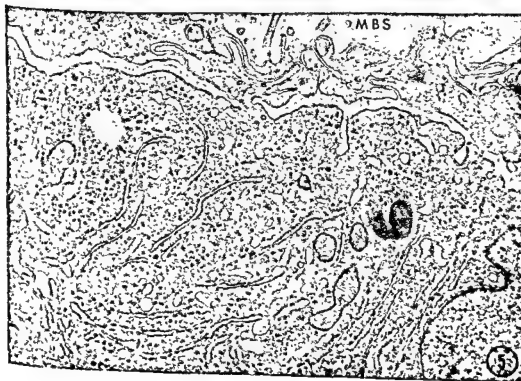
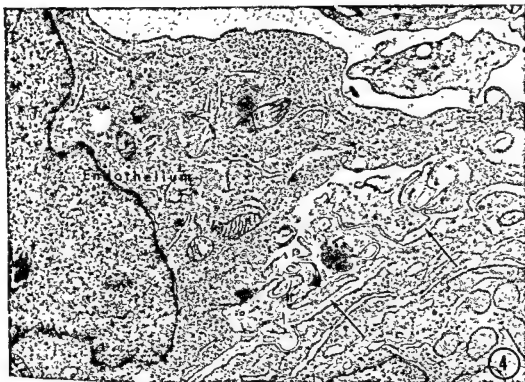


PLATE 5

EXPLANATION OF FIGURE

- 6 Micrograph of the fully established labyrinth (8.5 mm CRL fetus). The fetal capillary (FC) is separated from the maternal blood space (MBS) by its endothelium, a basement membrane, a thin connective tissue space, the basement membrane of the trophoblast, a continuous layer of cytotrophoblast, the organelle-containing layer of the syncytial trophoblast, the intrasyncytial lamina, and the ectoplasmic layer of the syncytium. Thus the only part of the syncytium bathed directly in maternal blood is the ectoplasmic layer. The dense circular structures in the lower left correspond to regions giving a positive Perl's reaction for iron in light microscopy, and appear in electron microscopy to be a combination of ferritin and basement membrane-like material. $\times 11,800$.



PLATE 5

EXPLANATION OF FIGURE

- 6 Micrograph of the fully established labyrinth (8.5 mm CRL fetus). The fetal capillary (FC) is separated from the maternal blood space (MBS) by its endothelium, a basement membrane, a thin connective tissue space, the basement membrane of the trophoblast, a continuous layer of cytotrophoblast, the organelle-containing layer of the syncytial trophoblast, the intrasyncytial lamina, and the ectoplasmic layer of the syncytium. Thus the only part of the syncytium bathed directly in maternal blood is the ectoplasmic layer. The dense circular structures in the lower left correspond to regions giving a positive Perl's reaction for iron in light microscopy, and appear in electron microscopy to be a combination of ferritin and basement membrane-like material. $\times 11,800$.



PLATE 6

EXPLANATION OF FIGURE

- 7 Typical labyrinth shortly after establishment of the hemodichorial condition (5 mm CRL fetus). The relatively thick cytotrophoblast layer is a characteristic feature of the earlier placenta as is the presence in the syncytium of large inclusions containing crystalloids. The parallel arrangement of the cisternae of the granular endoplasmic reticulum, the multivesicular bodies in the ectoplasmic layer, and the basally situated Golgi are all general characteristics of the syncytial trophoblast in this species. A portion of a fetal capillary appears in the lower left. $\times 15,500$.



PLATE 6

EXPLANATION OF FIGURE

- 7 Typical labyrinth shortly after establishment of the hemodichorial condition (5 mm CRL fetus). The relatively thick cytotrophoblast layer is a characteristic feature of the earlier placenta as is the presence in the syncytium of large inclusions containing crystalloids. The parallel arrangement of the cisternae of the granular endoplasmic reticulum, the multivesicular bodies in the ectoplasmic layer, and the basally situated Golgi are all general characteristics of the syncytial trophoblast in this species. A portion of a fetal capillary appears in the lower left. $\times 15,500$.

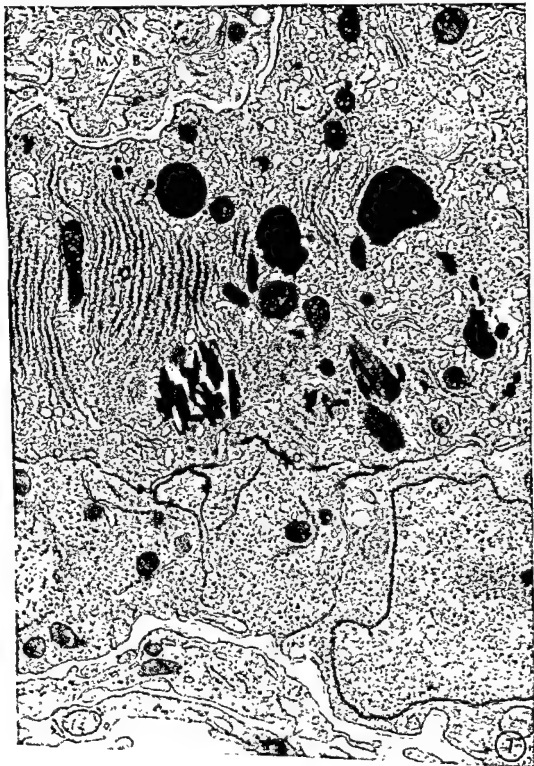


PLATE 6

EXPLANATION OF FIGURE

- 7 Typical labyrinth shortly after establishment of the hemodichorial condition (5 mm CRL fetus). The relatively thick cytotrophoblast layer is a characteristic feature of the earlier placenta as is the presence in the syncytium of large inclusions containing crystalloids. The parallel arrangement of the cisternae of the granular endoplasmic reticulum, the multivesicular bodies in the ectoplasmic layer, and the basally situated Golgi are all general characteristics of the syncytial trophoblast in this species. A portion of a fetal capillary appears in the lower left. $\times 15,500$.

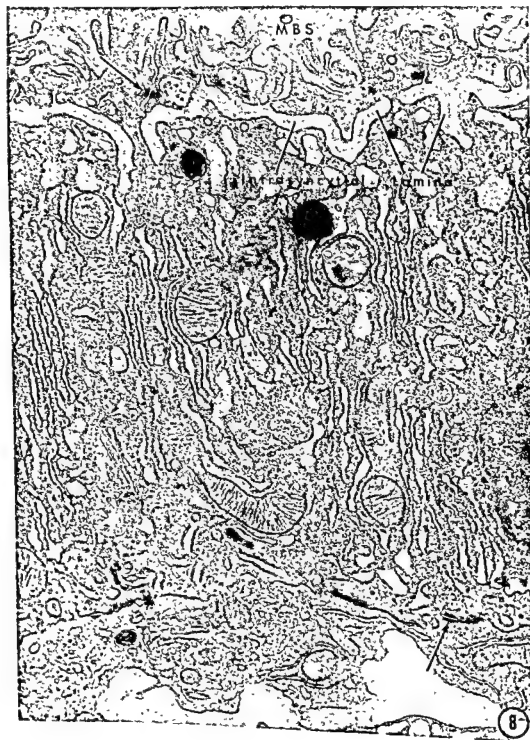


PLATE 7

EXPLANATION OF FIGURE

- 8 Labyrinth of the mature placenta (12 mm CRL fetus). The cytotrophoblast layer is now thinner, but is still closely associated with the syncytium. Note the communications of the syncytium with its ectoplasmic layer *through the intrasyncytial lamina*. *Desmosomes (arrows)* are seen both where different portions of the ectoplasmic layer abut and at the junction of the syncytium with the cytotrophoblast layer. $\times 20,800$.

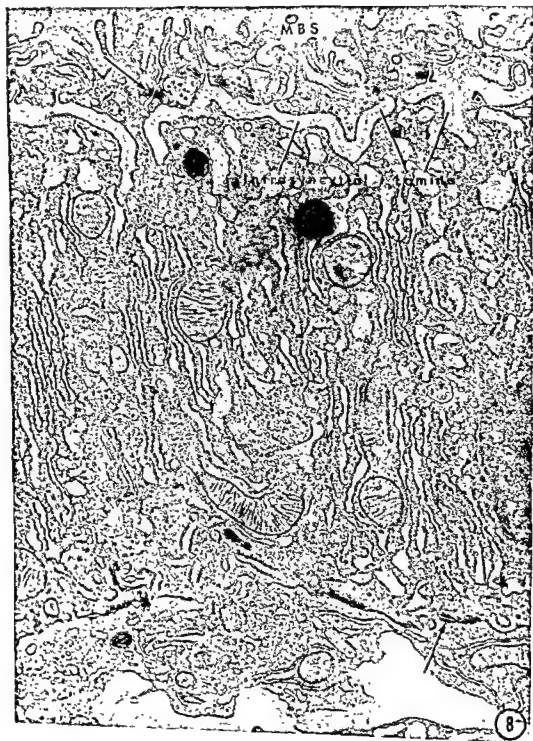


PLATE 8

EXPLANATION OF FIGURE

- 9 This tangential view of the junction of the syncytial trophoblast with the cytotrophoblast illustrates the basal position of the numerous Golgi zones within the syncytium. $\times 22,600$.

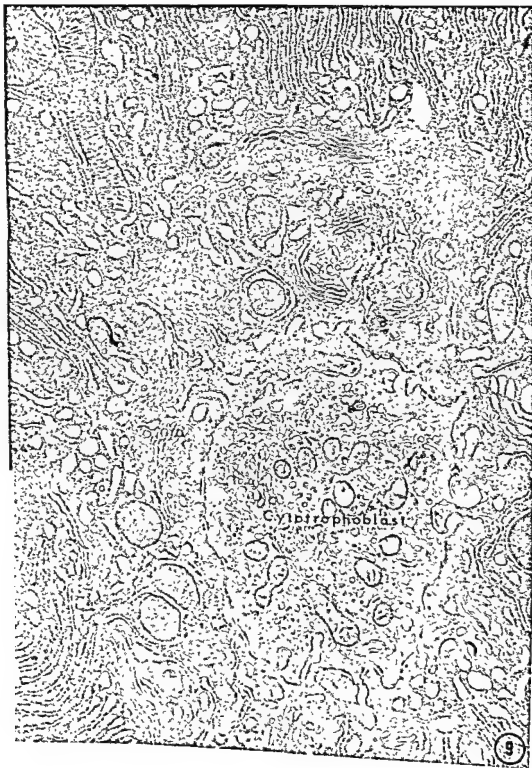


PLATE 8

EXPLANATION OF FIGURE

- 9 *This tangential view of the junction of the syncytial trophoblast with the cytotrophoblast illustrates the basal position of the numerous Golgi zones within the syncytium. $\times 22,600$.*



PLATE 8

EXPLANATION OF FIGURE

- 9 This tangential view of the junction of the syncytial trophoblast with the cytotrophoblast illustrates the basal position of the numerous Golgi zones within the syncytium. $\times 22,600$.

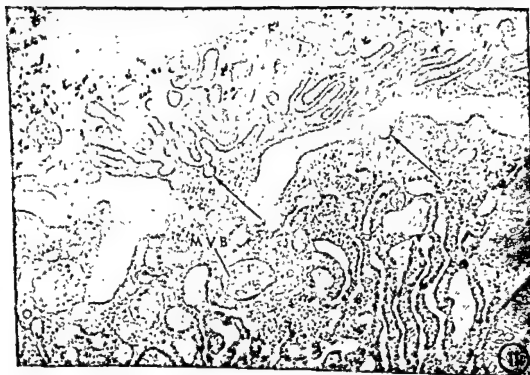


PLATE 9

EXPLANATION OF FIGURES

- 10 Surface of the syncytium from a bat (12 mm CRL fetus) injected with thorotrast five minutes before fixing the placenta. Note that small vesicles or granules (small arrows), of a size similar to those within the multivesicular bodies (MVB), are found in the intrasyncytial lacunar system. Note also the caveolae (large arrows). Little or no thorotrast has penetrated into the space occupied by the intrasyncytial lamina. This observation suggests that the apparent spaces between ectoplasmic projections of the syncytium (*ex*: upper left) are not sufficiently large to permit passage of the thorotrast, or that they are blocked by a coating substance. $\times 32,300$.
- 11 Surface of the syncytium of an animal injected with thorotrast five minutes before fixing the placenta. Caveolae (arrows) are seen both at the free surface and underlying the intrasyncytial lamina. As in figure 10, little or no thorotrast is in the intrasyncytial lacunar system, but particles of thorotrast are seen in a multivesicular body (MVB) within the syncytial trophoblast. This observation suggests bulk transport of the particles by engulfment at the free surface. $\times 32,300$.



PLATE 10

EXPLANATION OF FIGURE

- 12 Junction of the labyrinth with maternal tissue where a maternal blood space (MBS) of the labyrinth is broadly confluent with a venous channel in the decidua basalis. The syncytial trophoblast (left) characteristically shows filaments and densities along its border (arrows) with the maternal tissues. There is a relatively abrupt transition to the peculiar enlarged cells (right) of the maternal venous channels. Note also the characteristic irregularity of the intrasyncytial lamina in this region. $\times 8,700$.



PLATE 10

EXPLANATION OF FIGURE

- 12 Junction of the labyrinth with maternal tissue where a maternal blood space (MBS) of the labyrinth is broadly confluent with a venous channel in the decidua basalis. The syncytial trophoblast (left) characteristically shows filaments and densities along its border (arrows) with the maternal tissues. There is a relatively abrupt transition to the peculiar enlarged cells (right) of the maternal venous channels. Note also the characteristic irregularity of the intrasyncytial lamina in this region. $\times 8,700$.



PLATE 11

EXPLANATION OF FIGURE

- 13** Junctional zone illustrating the filaments and dense bodies (arrows) in the syncytium where it borders the decidual cells. $\times 13,200$.



PLATE 12

EXPLANATION OF FIGURE

- 14 This figure, combined with figure 15, illustrates the relationships at the junction of a maternal artery with the labyrinth. At such junctions, the endothelial cells ride over the syncytium for a short distance into the maternal blood spaces of the labyrinth. In this figure the cytotrophoblast and the syncytium are illustrated. Note the irregularity of the intrasyncytial lamina (ISL), and that the projections of the syncytium around this substance are not only irregular but also are not strictly ectoplasmic. The asterisk marks a vesicle which appears at the bottom of figure 15. FCT, fetal connective tissue. $\times 13,400$.



PLATE 12

EXPLANATION OF FIGURE

- 14 This figure, combined with figure 15, illustrates the relationships at the junction of a maternal artery with the labyrinth. At such junctions, the endothelial cells ride over the syncytium for a short distance into the maternal blood spaces of the labyrinth. In this figure the cytotrophoblast and the syncytium are illustrated. Note the irregularity of the intrasyncytial lamina (ISL), and that the projections of the syncytium around this substance are not only irregular but also are not strictly ectoplasmic. The asterisk marks a vesicle which appears at the bottom of figure 15. FCT, fetal connective tissue. $\times 13,400$.



PLATE 13

EXPLANATION OF FIGURE

- 15 In this micrograph, the maternal endothelium overlying the syncytial trophoblast at the junction of a maternal artery with the labyrinth is seen. The micrograph is at a slightly lower magnification than the previous micrograph. Note the irregular arrangements of the endothelial cells that border the blood space (upper right). Projections of the syncytium, including the one with the asterisk-marked vacuole, extend irregularly under the endothelial cells. $\times 9,600$.



PLATE 13

EXPLANATION OF FIGURE

- 15 In this micrograph, the maternal endothelium overlying the syncytial trophoblast at the junction of a maternal artery with the labyrinth is seen. The micrograph is at a slightly lower magnification than the previous micrograph. Note the irregular arrangements of the endothelial cells that border the blood space (upper right). Projections of the syncytium, including the one with the asterisk-marked vacuole, extend irregularly under the endothelial cells. $\times 9,600$.



PLATE 14

EXPLANATION OF FIGURE

- 16 Decidual cells of the glycogen-containing type within the decidua basalis. A number of other cell types are also found within the complex decidua basalis of the bat. ICS, intercellular space. Gly, glycogen; G, Golgi zone. $\times 18,000$.



16

Embryonic Origin of the Abdominal (Ventrolateral) Musculature in the Albino Rat ^{1,2}

WILLIAM PARRY

Department of Zoology, Indiana University, Bloomington, Indiana

ABSTRACT A study comprising both descriptive and experimental data was undertaken. The descriptive portion utilizes transverse, sagittal, and frontal serial sections of 10 through 20 day old rat embryos.

As development proceeds, the somites lengthen along their dorsoventral dimension, and epithelial-lined "buds" (ventral somite buds) extend into the lateral plate somatopleure. Concomitantly epithelium lining the somite "body" is converted to a loosely associated mass of mesenchyme, beginning at the deep medial border and extending around the cephalic and caudal faces of the somite to involve the superficial surface. Lastly, this process transforms the epithelium covering the ventral somite buds into a mesenchymal aggregation. Anlagen of the abdominal ventrolateral muscles arise in the precise position of the mesenchymal aggregation derived from the ventral somite buds.

The experimental section tests the development capacities of isolated portions of the trunk body wall when implanted in the anterior chamber of the eye. Grafts of somite material are highly proficient in forming striated muscle, while grafts of somite-free somatopleure have little ability to form striated muscle. Grafts of ventral body wall become more proficient in forming striated muscle with age. The increase in muscle-forming ability correlates directly with the invasion of material from the ventral somite buds into the ventral body wall. It is concluded that the ventrolateral (abdominal) musculature is of somitic origin.

Early 100 years ago His held that the lateral plate did not contribute to the formation of the ventrolateral musculature and that the probable source was the lateral plate somatopleure. This viewpoint, however, was not supported by other workers and by the turn of the century, it has been generally accepted that the musculature of the abdominal wall is derived from the lateral somites (Bardeen, '00; Butcher, Nicholas, '50). Recently evidence has been presented which suggests lateral plate involvement in the formation of the ventrolateral musculature.

Working with the chick embryo, the animal investigated by His, and utilizing a carbon-marking technique, Straus Rawles ('53) reported that the lateral somatopleure did, in fact, contribute to the ventrolateral musculature. The carbon marks were placed either on the lateral body wall or a portion thereof (medial or lateral), the proximal lateral plate, or the lateral plate. Analyses of the carbon marks in their final location showed that the somatic layer of the lateral plate contributed the ventral half of the trunk musculature, and the somites formed the dor-

sal third. The intermediate one-sixth of the abdominal wall musculature was formed by both the somites and the lateral plate. Intracoelemic grafts of lateral plate confirmed that the somatopleure was competent to form skeletal muscle, as well as "rib-like" cartilage.

The issue was reopened when Seno ('61) concluded from a similar series of experiments on the chick that the lateral plate did not contribute to the formation of the ventrolateral musculature. After "pinpoint" carbon-marking, i.e., marking by a single thrust of the needle, of the "boundary line" of the somites, Seno was able to recover carbon particles from both the dorsal and ventral body wall. Presumably the particles were carried to all parts of the abdominal wall by ventrally migrating somite cells, and were included in the

¹ This investigation was supported in part by Public Health Service fellowship GPM 18,959 from the Division of General Medical Sciences, Public Health Service.

² Submitted in partial fulfillment of the requirements for the Degree of Doctor of Philosophy in the Graduate School, Indiana University, Bloomington, Indiana, 1965. This paper appeared in abstract form in *American Zoologist*, 6: 356, 1966.

³ Present address: Department of Pediatrics, Indiana University Medical Center, Indianapolis, Indiana.

muscle of the abdominal wall as these cells differentiated into muscle. Carbon particles placed in the proximal lateral plate were seen to be pushed aside by ventrally migrating somite cells. Carbon particles placed in the distal lateral plate were recovered along the ventral midline and occasionally within the pectoralis major muscle and also in the tip of the sternum, a known somatopleural derivative (Fell, '39), but never within the muscles of the ventrolateral series. In agreement with Straus and Rawles, Seno reported that intracoelomic grafts of lateral plate differentiated into cartilage. No statement was made concerning the presence of striated muscle in the grafts. Seno concluded, therefore, that cells from the somites formed all of the abdominal musculature and ribs and that the lateral plate served only as a matrix into which the cells migrate.

Seno viewed the discrepancy between his results and those of Straus and Rawles as due to the difference in the application of the carbon marks. He felt that in marking the somite itself Straus and Rawles missed the lateral cells that migrate farthest ventrad while a mark on the "boundary" between the somite and lateral plate insured detection of those same cells. Furthermore, he interpreted the results of Straus and Rawles which showed a contribution by the lateral plate as being due to the migration of somite cells into the somatopleure, rather than an actual incorporation of marked somatopleure cells into the muscle of the abdominal wall. Straus and Rawles, on the other hand, claimed to find carbon particles within myotubes in the ventral portion of the body wall after marking the lateral plate. Seno suspected that the cartilage which differentiated in the intracoelomic grafts was appendicular in origin, arising from the influence of the limb "field" or sternal "field," rather than being axial in origin.

Inasmuch as Straus and Rawles point to the lack of comparable data for the other classes of vertebrates, Detwiler ('55) responded with a study of the ventrolateral musculature in *Amblystoma*. His evidence was derived from a comprehensive series of defect and transplantation experiments.

The series included extirpation of somites, extirpation and inversion of somites, and extirpation of the lateral plate. Also, heteroplastic grafts of somites or lateral plate were made between *A. punctatum* and *A. tigrinum*. Furthermore, tissue (e.g. eye cup) was inserted between the somites and lateral plate to act as a mechanical block to any migration of somitic cells into the lateral plate. Cumulative evidence was acquired from these experiments which showed that the somites were the sole source of the abdominal wall musculature and that the lateral plate played no role in its formation.

Liedke ('58) reported an investigation of the situation in the *Anura* involving both defect and transplantation experiments similar to those of Detwiler. The results indicated that the myotomes played the decisive role in the origin of the ventrolateral series.

Theiler ('57) studied sections of 26 human embryos with regard to the origin of the ventrolateral musculature and also surveyed sections of chick, pig, guinea pig, and mouse embryos. He reported the existence of "somite buds" which extended into the lateral plate in all of these animals. Other workers also have seen these buds (Bardeen, '00; Butcher, '29; Danilova, '63). Somite buds are ventral extensions of the somites and, being capped by an epithelial border, are easily recognized. They are especially prominent in the 9 mm (crown-rump) human embryo between the eighth cervical somite and the third lumbar somite. The ventral somite buds were seen by Theiler to move beyond the level of the Wolffian duct and ventrally into the lateral plate. The buds lost their distinctness by the time the embryo reached 10 mm and could not be distinguished from cells of the somatopleuric mesenchyme. Shortly thereafter, in the 11 mm human embryo, the outline of the abdominal wall muscles could be recognized as dense aggregations of "mesenchymal" cells. Using the Wolffian duct as a landmark, Theiler stated that the "blastema" of the rectus abdominis muscle condensed from the "mesenchyme" in the precise position from which the somite buds had disappeared. Thus, ac-

cording to Theiler, the rectus is originally formed in a lateral position.

Danilova ('63) reported that somite buds in Karakul sheep extend into the lateral plate but that their ventral limits remain in the dorsal half of the embryonic body. This finding was correlated with that of Straus and Rawles in which the carbon particles of marked somites remained in the dorsal half of the abdominal wall. Since the further development of the musculature was not reported, it is not known whether the most ventral muscles are somatopleuric in origin as Danilova implies, or if they arise in a lateral position from somitic material as Theiler proposes.

Although the preponderance of the evidence seems to support the contention that the somites are the source of the ventrolateral musculature, uncertainty has arisen as a result of recent studies. For this reason and since no experimental evidence is available for mammals, it was thought that an analysis of the situation in a mammal would be in order. Therefore, it is the purpose of this paper to report a descriptive and experimental study of the origin of the ventrolateral musculature in the albino rat.

SECTION I. DESCRIPTIVE

Methods and materials

The rat embryos for the descriptive portion of the study were supplied in part by Dr. T. W. Torrey, Indiana University, from his collection. Additional specimens for supplemental study were prepared by the author. Use was made of serial sections cut in transverse, sagittal, and frontal planes. The sections were stained with hematoxylin, Azan, or Mallory's triple stain (Gray, '58). A total of 52 embryos ranging in age from ten days to 20 days were examined. The bulk of the material (45 embryos) consisted of specimens ranging in age from 10.5 days to 14 days, with at least four embryos being included in each half-day interval. The age of the embryos was reckoned from the discovery of a copulation plug in the vagina. Embryos were considered to be one-half day old the morning of the discovery of the copulation plug.

OBSERVATIONS

The ventrolateral musculature consists of the rectus abdominis muscle plus a lateral group of three overlapping muscle sheets, the external oblique, internal oblique, and transverse muscles.

As in any biological system, individual variation was exhibited by the embryos included in this study. The following account of the development of the ventrolateral musculature, therefore, represents the typical state of the embryo at the age under consideration. The most advanced specimen at any time interval frequently would equal in development the least advanced in the succeeding half-day interval.

The 10 day embryo is a convenient beginning point for the study of the embryology of the ventrolateral musculature. Readily apparent at this age, along the length of the embryo, is a gradation of somite differentiation, the more cephalad and earlier formed somites demonstrate more advanced development. Newly formed somites appear only as compact cell masses, whereas the cells of somewhat older somites are arranged as an epithelium about a hollow somite center (the myocoel) which in still older somites is filled with cells. A typical mid-trunk somite has the latter appearance, i.e., a pseudostratified columnar epithelial border surrounding a core of small rounded cells. Although there is an initial developmental lag on the part of the caudal somites, their differentiation proceeds at a relatively more rapid pace, enabling them to attain the same degree of development as the more cephalad somites by 10.5 days.

Whereas the epithelium covers all surfaces of the earlier somites, at 10.5 days the epithelium of the deep ventral and medial borders begins to break down and its cells, together with the cells of the central core appear to stream toward the notochord (fig. 4). The breakdown of the epithelial borders continues until, at 11 days, the somite is an aggregation of loosely associated cells (sclerotome) lying deep to a prominent superficial epithelial border (dermomyotome). The epithelial border turns in at all edges to partially cover the adjacent surfaces (fig. 5). An overall lengthening of the somite along its dorso-ventral axis is evident.

The epithelium continue to disappear along the cephalic and caudal edges. Eventually (at 12 days) the superficial surface is also involved. Rather than streaming toward the notochord, as do the cells of the deep epithelium and central core, the cells of the superficial epithelium become reoriented parallel to the cephalo-caudal axis of the body. At this time, however, the "dissolution" of the superficial epithelium does not involve its dorsal and ventral edges. In fact, the "turning-in" of the epithelium at these edges is more obvious. The epithelium-covered tips of the somite constitute the dorsal and ventral "somite buds." The ventral somite bud is markedly larger than the dorsal somite bud and resembles a tall, narrow cup of pseudostratified epithelium filled with "mesenchymal" cells. It is distinct from the material of the somatopleure (fig. 6). During the period from 11 to 12 days of age, the somites continue to lengthen along the dorso-ventral axis. From a position dorsal to the lateral plate the ventral somite buds extend into the lateral plate, reach the level of the Wolfian duct, and occasionally push beyond.

Since the somatopleure must enclose a great visceral mass in the heart and liver region, the ventral somite buds at this level must traverse a greater overall distance in their migration to the ventral midline than do the more caudal somite buds. As a consequence, the distance from the ventral edge of the somites to the ventral midline varies along the length of the embryonic body. This gives the impression that the caudal trunk somites (immediately cephalad to the hind limb buds) have migrated farther into the lateral plate than the more cephalic somites (in the region of the heart and liver) but in reality all trunk somites are approximately the same length and have migrated the same distance.

The process of dissolution of the superficial epithelium and reorientation of cells along the cephalo-caudal axis which had been initiated at 12 days is complete at 12.5 days of age. There is blending of the cephalic and caudal edges of adjacent somites at this time. Dense condensations of cells in the intersomitic spaces are the first indication of rib formation (fig. 7).

The only epithelium remaining at 12.5 days is that covering the somite buds. The breakdown of the epithelium now extends to the medial surface of the buds. This process will continue around the side of the somite buds until there is no epithelium remaining. The lower edge of the ventral somite bud has progressed to a level beyond that of the Wolfian duct in all cases.

At 13 days the epithelium of the somite buds has completely disappeared, and boundaries of the buds cannot be determined, except by means of the gradation of cell density from obvious somite material to obvious somatopleure. Dorsally the adjacent somites are confluent and ventrally the buds have the appearance of a dense cord of cells (figs. 8-10).

Transverse sections of somite buds demonstrate the gradation of cell density from somite to somatopleure (fig. 8). Discernible boundaries do not exist. The somite buds are particularly hard to follow in cross section because of the blending of the borders of adjacent somites. The buds are most easily located and enumerated by following the ventral rami of the spinal nerves.

Figure 9 is a frontal section of the tips of the ventral somite buds, demonstrating the rearrangement in architecture. The tips are distinguished from the somatopleure only because the tips form a denser aggregation of cells. There is no distinctive cellular feature, no distinguishing arrangement or orientation of cells. Sagittal sections also demonstrate these features (fig. 10). The tips of the somite buds show no cellular orientation, although immediately dorsal to the tips the cells are aligned in the cephalo-caudal direction. Rib anlagen are well formed at this stage.

Further ventral elongation occurs. The ventral processes of the more caudal somites have nearly reached the ventral midline. The ventral borders of the more cephalic somite buds are still located a considerable distance from the ventral midline because of the greater distance to the ventral midline in the heart-liver region.

The boundaries of adjacent ventral tips of somites blended together and soon become confluent, erasing any evidence of segmentation except that of the ribs and

nerve rami. The ventral edge of the somite mass is discernible only because it comprises a denser cell mass than does the lateral plate somatopleure.

Cells of the somite mass gradually condense into aggregations which can be identified as the anlagen of the ventrolateral series of muscles. The initial morphological appearance of the anlagen cannot be pinpointed. The anlage of the rectus abdominis is the first formed and is occasionally recognizable in 13.5 day embryos. The anlagen of the entire ventrolateral series have clearly been formed by 14 days (figs. 11-13).

Due to the greater overall distance to the ventral midline in the area of the heart and liver, the muscle anlagen must necessarily form in a lateral position in the anterior abdomen if they are to arise from the somite buds. The path of the rectus muscle clearly follows the former path of the ventral margins of the somites (fig. 11). It lies very close to the ventral midline at its posterior limit and swings up to a lateral position as it travels anteriorly, terminating in a position lateral and dorsal to the rib anlagen at the anterior border of the liver (fig. 12). The other muscles of the ventrolateral series can be identified as irregular condensations of mesenchymal cells formed dorsal to the rectus anlage. The transverse anlage can be seen as a thin layer of cells in contact with the parietal peritoneum. The internal oblique anlage is a rather diffuse layer of cells in contact with the rectus ventrally and the rib anlagen dorsally. The most superficial of the three lamina is the external oblique which has no apparent dorsal connections but is in contact with the rectus anlage ventrally (fig. 13).

The muscles of the ventrolateral series are plainly outlined at 15 days (fig. 14). The rectus muscle has migrated ventrad and the other muscles have followed. Whereas the anlagen consisted of condensed cells at 14 days, now the cells have become aligned in directions which correspond to the directions of the fibers in the adult muscles. The cells of the rectus anlage are oriented in a cephalo-caudal direction, the transverse arranged dorso-ventrally, the external oblique aligned from

cephalo-dorsal to caudo-ventral in direction, and the internal oblique distributed from caudo-dorsal to cephalo-ventral.

Myotube formation has been initiated by 17 days. The rectus muscle has reached the midline along the length of the abdomen except in the region of the anterior liver. The definitive relationships of the insertions of the three lateral muscle sheets to the rectus muscle are now apparent (fig. 15). The external and internal oblique muscles unite in a common aponeurosis superficial to the rectus muscle whereas the transverse muscle passes deep to the rectus. The fibers of the aponeurosis of the oblique muscles and the transverse muscle unite and decussate to form the linea alba, a dense fibrous band, the anlage of which is now evident.

At no time was there any evidence for the migration of individual cells from the somite buds into the somatopleure. No cells were ever seen to delaminate from the epithelium covering the somites or their processes. The continuity of the epithelium dissociated in the manner described, and the cells reoriented along the cephalo-caudal axis, but no ventral migration was observed. Even after the epithelium had completely disappeared from the tips of the ventral somite buds, there was no discernible ventral migration of individual cells. Indeed, by this time none was necessary because the somite buds themselves had entered into the somatopleure, and the anlagen of the rectus muscles were precisely aligned with the former lower border of the ventral somite buds.

SECTION II. EXPERIMENTAL

The somatopleure must be competent to form striated muscle if the lateral plate is to contribute materially to the formation of the ventrolateral musculature. Portions of the trunk of rat embryos ranging in age from 12 through 15 days were tested for competency to differentiate into striated muscle by implantation into the anterior chamber of the eye.

MATERIALS AND METHODS

Young adult Sprague-Dawley rats (approximately 90 days old) were obtained from the Holtzman Company, Madison,

The epithelium continue to disappear along the cephalic and caudal edges. Eventually (at 12 days) the superficial surface is also involved. Rather than streaming toward the notochord, as do the cells of the deep epithelium and central core, the cells of the superficial epithelium become reoriented parallel to the cephalo-caudal axis of the body. At this time, however, the "dissolution" of the superficial epithelium does not involve its dorsal and ventral edges. In fact, the "turning-in" of the epithelium at these edges is more obvious. The epithelium-covered tips of the somite constitute the dorsal and ventral "somite buds." The ventral somite bud is markedly larger than the dorsal somite bud and resembles a tall, narrow cup of pseudostratified epithelium filled with "mesenchymal" cells. It is distinct from the material of the somatopleure (fig. 6). During the period from 11 to 12 days of age, the somites continue to lengthen along the dorso-ventral axis. From a position dorsal to the lateral plate the ventral somite buds extend into the lateral plate, reach the level of the Wolffian duct, and occasionally push beyond.

Since the somatopleure must enclose a great visceral mass in the heart and liver region, the ventral somite buds at this level must traverse a greater overall distance in their migration to the ventral midline than do the more caudal somite buds. As a consequence, the distance from the ventral edge of the somites to the ventral midline varies along the length of the embryonic body. This gives the impression that the caudal trunk somites (immediately cephalad to the hind limb buds) have migrated farther into the lateral plate than the more cephalic somites (in the region of the heart and liver) but in reality all trunk somites are approximately the same length and have migrated the same distance.

The process of dissolution of the superficial epithelium and reorientation of cells along the cephalo-caudal axis which had been initiated at 12 days is complete at 12.5 days of age. There is blending of the cephalic and caudal edges of adjacent somites at this time. Dense condensations of cells in the intersomitic spaces are the first indication of rib formation (fig. 7).

The only epithelium remaining at 12.5 days is that covering the somite buds. The breakdown of the epithelium now extends to the medial surface of the buds. This process will continue around the side of the somite buds until there is no epithelium remaining. The lower edge of the ventral somite bud has progressed to a level beyond that of the Wolffian duct in all cases.

At 13 days the epithelium of the somite buds has completely disappeared, and boundaries of the buds cannot be determined, except by means of the gradation of cell density from obvious somite material to obvious somatopleure. Dorsally the adjacent somites are confluent and ventrally the buds have the appearance of a dense cord of cells (figs. 8-10).

Transverse sections of somite buds demonstrate the gradation of cell density from somite to somatopleure (fig. 8). Discernible boundaries do not exist. The somite buds are particularly hard to follow in cross section because of the blending of the borders of adjacent somites. The buds are most easily located and enumerated by following the ventral rami of the spinal nerves.

Figure 9 is a frontal section of the tips of the ventral somite buds, demonstrating the rearrangement in architecture. The tips are distinguished from the somatopleure only because the tips form a denser aggregation of cells. There is no distinctive cellular feature, no distinguishing arrangement or orientation of cells. Sagittal sections also demonstrate these features (fig. 10). The tips of the somite buds show no cellular orientation, although immediately dorsal to the tips the cells are aligned in the cephalo-caudal direction. Rib anlagen are well formed at this stage.

Further ventral elongation occurs. The ventral processes of the more caudal somites have nearly reached the ventral midline. The ventral borders of the more cephalic somite buds are still located a considerable distance from the ventral midline because of the greater distance to the ventral midline in the heart-liver region.

The boundaries of adjacent ventral tips of somites blended together and soon become confluent, erasing any evidence of segmentation except that of the ribs and

nerve rami. The ventral edge of the somite mass is discernible only because it comprises a denser cell mass than does the lateral plate somatopleure.

Cells of the somite mass gradually condense into aggregations which can be identified as the anlagen of the ventrolateral series of muscles. The initial morphological appearance of the anlagen cannot be pinpointed. The anlage of the rectus abdominis is the first formed and is occasionally recognizable in 13.5 day embryos. The anlagen of the entire ventrolateral series have clearly been formed by 14 days (figs. 11-13).

Due to the greater overall distance to the ventral midline in the area of the heart and liver, the muscle anlagen must necessarily form in a lateral position in the anterior abdomen if they are to arise from the somite buds. The path of the rectus muscle clearly follows the former path of the ventral margins of the somites (fig. 11). It lies very close to the ventral midline at its posterior limit and swings up to a lateral position as it travels anteriorly, terminating in a position lateral and dorsal to the rib anlagen at the anterior border of the liver (fig. 12). The other muscles of the ventrolateral series can be identified as irregular condensations of mesenchymal cells formed dorsal to the rectus anlage. The transverse anlage can be seen as a thin layer of cells in contact with the parietal peritoneum. The internal oblique anlage is a rather diffuse layer of cells in contact with the rectus ventrally and the rib anlagen dorsally. The most superficial of the three lamina is the external oblique which has no apparent dorsal connections but is in contact with the rectus anlage ventrally (fig. 13).

The muscles of the ventrolateral series are plainly outlined at 15 days (fig. 14). The rectus muscle has migrated ventrad and the other muscles have followed. Whereas the anlagen consisted of condensed cells at 14 days, now the cells have become aligned in directions which correspond to the directions of the fibers in the adult muscles. The cells of the rectus anlage are oriented in a cephalo-caudal direction, the transverse arranged dorso-ventrally, the external oblique aligned from

cephalo-dorsal to caudo-ventral in direction, and the internal oblique distributed from caudo-dorsal to cephalo-ventral.

Myotube formation has been initiated by 17 days. The rectus muscle has reached the midline along the length of the abdomen except in the region of the anterior liver. The definitive relationships of the insertions of the three lateral muscle sheets to the rectus muscle are now apparent (fig. 15). The external and internal oblique muscles unite in a common aponeurosis superficial to the rectus muscle whereas the transverse muscle passes deep to the rectus. The fibers of the aponeurosis of the oblique muscles and the transverse muscle unite and decussate to form the linea alba, a dense fibrous band, the anlage of which is now evident.

At no time was there any evidence for the migration of individual cells from the somite buds into the somatopleure. No cells were ever seen to delaminate from the epithelium covering the somites or their processes. The continuity of the epithelium dissociated in the manner described, and the cells reoriented along the cephalo-caudal axis, but no ventral migration was observed. Even after the epithelium had completely disappeared from the tips of the ventral somite buds, there was no discernible ventral migration of individual cells. Indeed, by this time none was necessary because the somite buds themselves had entered into the somatopleure, and the anlagen of the rectus muscles were precisely aligned with the former lower border of the ventral somite buds.

SECTION II. EXPERIMENTAL

The somatopleure must be competent to form striated muscle if the lateral plate is to contribute materially to the formation of the ventrolateral musculature. Portions of the trunk of rat embryos ranging in age from 12 through 15 days were tested for competency to differentiate into striated muscle by implantation into the anterior chamber of the eye.

MATERIALS AND METHODS

Young adult Sprague-Dawley rats (approximately 90 days old) were obtained from the Holtzman Company, Madison,

The epithelium continue to disappear along the cephalic and caudal edges. Eventually (at 12 days) the superficial surface is also involved. Rather than streaming toward the notochord, as do the cells of the deep epithelium and central core, the cells of the superficial epithelium become reoriented parallel to the cephalo-caudal axis of the body. At this time, however, the "dissolution" of the superficial epithelium does not involve its dorsal and ventral edges. In fact, the "turning-in" of the epithelium at these edges is more obvious. The epithelium-covered tips of the somite constitute the dorsal and ventral "somite buds." The ventral somite bud is markedly larger than the dorsal somite bud and resembles a tall, narrow cup of pseudostratified epithelium filled with "mesenchymal" cells. It is distinct from the material of the somatopleure (fig. 6). During the period from 11 to 12 days of age, the somites continue to lengthen along the dorso-ventral axis. From a position dorsal to the lateral plate the ventral somite buds extend into the lateral plate, reach the level of the Wolffian duct, and occasionally push beyond.

Since the somatopleure must enclose a great visceral mass in the heart and liver region, the ventral somite buds at this level must traverse a greater overall distance in their migration to the ventral midline than do the more caudal somite buds. As a consequence, the distance from the ventral edge of the somites to the ventral midline varies along the length of the embryonic body. This gives the impression that the caudal trunk somites (immediately cephalad to the hind limb buds) have migrated farther into the lateral plate than the more cephalic somites (in the region of the heart and liver) but in reality all trunk somites are approximately the same length and have migrated the same distance.

The process of dissolution of the superficial epithelium and reorientation of cells along the cephalo-caudal axis which had been initiated at 12 days is complete at 12.5 days of age. There is blending of the cephalic and caudal edges of adjacent somites at this time. Dense condensations of cells in the intersomitic spaces are the first indication of rib formation (fig. 7).

The only epithelium remaining at 12.5 days is that covering the somite buds. The breakdown of the epithelium now extends to the medial surface of the buds. This process will continue around the side of the somite buds until there is no epithelium remaining. The lower edge of the ventral somite bud has progressed to a level beyond that of the Wolffian duct in all cases.

At 13 days the epithelium of the somite buds has completely disappeared, and boundaries of the buds cannot be determined, except by means of the gradation of cell density from obvious somite material to obvious somatopleure. Dorsally the adjacent somites are confluent and ventrally the buds have the appearance of a dense cord of cells (figs. 8-10).

Transverse sections of somite buds demonstrate the gradation of cell density from somite to somatopleure (fig. 8). Discernible boundaries do not exist. The somite buds are particularly hard to follow in cross section because of the blending of the borders of adjacent somites. The buds are most easily located and enumerated by following the ventral rami of the spinal nerves.

Figure 9 is a frontal section of the tips of the ventral somite buds, demonstrating the rearrangement in architecture. The tips are distinguished from the somatopleure only because the tips form a denser aggregation of cells. There is no distinctive cellular feature, no distinguishing arrangement or orientation of cells. Sagittal sections also demonstrate these features (fig. 10). The tips of the somite buds show no cellular orientation, although immediately dorsal to the tips the cells are aligned in the cephalo-caudal direction. Rib anlagen are well formed at this stage.

Further ventral elongation occurs. The ventral processes of the more caudal somites have nearly reached the ventral midline. The ventral borders of the more cephalic somite buds are still located a considerable distance from the ventral midline because of the greater distance to the ventral midline in the heart-liver region.

The boundaries of adjacent ventral tips of somites blended together and soon become confluent, erasing any evidence of segmentation except that of the ribs and

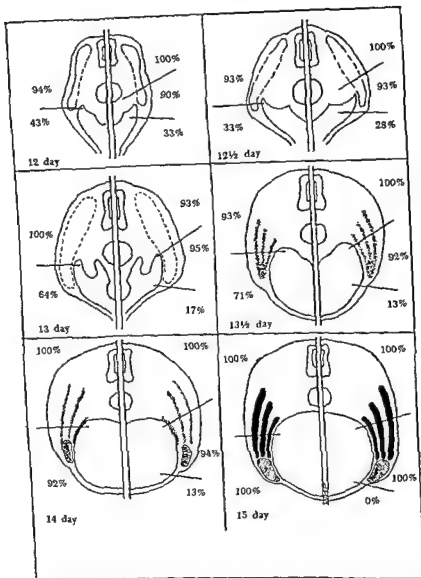


Fig. 1 A diagrammatic representation of the operational procedure and results of Series I (left half at each age) and Series II (right half). Percentages indicate the per cent of recovered grafts containing striated muscle.

was inserted into the anterior chamber through the slit and the tissue deposited as the pipette was slowly withdrawn. The cornea was allowed to heal spontaneously.

The graft was allowed to differentiate in the anterior chamber for a chosen number of days (tables 1, 2), whereupon the animal was sacrificed. The whole eyeball was removed and fixed in Bouin's solution or

10% buffered formalin (MacManus and Mowry, '60). After at least twenty-four hours of fixation, the eyeball was opened and the graft recovered. The graft was then serially sectioned and stained with Mallory's triple stain (Gray, '58).

Presence of epidermal structures in the graft material was the criterion for con-

Wisconsin. Males were paired with females and each morning the females were examined for the presence of the vaginal "plug of coagulated semen indicative of a mating. Embryos were arbitrarily considered to be one-half day old the morning of the discovery of the copulation plug. Pregnant females were placed in individual cages until the embryos had attained the desired age whereupon the operations were performed.

Dissection of the embryos was performed beneath an operating hood which consisted of a sheet of flexible plastic stretched over a plywood frame. Centrally located in the plastic sheet were holes large enough to accommodate the oculars of a dissecting microscope. The operating hood prevented dust and other air-borne contaminants from reaching the operating dishes. Moreover, the air beneath the hood was sterilized prior to the operations by exposing it to ultraviolet light from a portable U-V source. All glassware and solutions were autoclaved. Metal instruments were sterilized in 70% alcohol.

After the gravid female had been anesthetized with ether, her abdomen was shaved and washed with 70% alcohol. A midline incision in the caudal abdomen exposed the uterus which was removed and immediately placed in a covered sterile Petri dish and then transferred to the operating hood.

The uterus was opened along its length with fine pointed scissors. The embryos were detached from their placentae and transferred to another Petri dish which contained enough mammalian Ringer's saline (22°-25°C) to cover them. Here the extra-embryonic membranes were removed and discarded. Next the embryos were dissected with watchmaker's forceps and iridectomy scissors under the dissecting microscope. The area of trunk employed was that portion of body wall covering the liver and intestinal loop, the cephalic boundary being just caudal to the forelimb buds and heart, and the caudal boundary being just cephalic to the hindlimb buds and genital tubercle. Care was taken not to include in the graft tissue any limb bud material nor any of the septum transversum because these materials could

contribute striated muscle to the grafts (Saunders, '48; Wells, '54). Also trimmed from the body wall were the liver, intestine, urogenital ridge, and neural tube. The body wall was divided into appropriate parts according to the series and the parts were set aside according to category in saline-filled Petri dishes until the dissection of the litter was completed.

Two series of experiments were employed (fig. 1). In the first series the body wall was divided into two parts; the portion covering the coelomic cavity, designated as ventral half, and the portion dorsal to the coelom, the dorsal half. The second series consisted of subdividing the body wall into a dorsal component containing the somite buds, and a ventral component consisting only of lateral plate somatopleure. The boundaries of the somites and their buds were easily visualized in the earlier stages and even after the somite buds were no longer distinct, the boundary between the thin somite-free somatopleure could be distinguished from the thicker mass of somite-derived tissue by illuminating the tissue from an oblique angle.

The size of the grafts was at least 1.5 mm². Since the somatopleure is thin and fragile and the somite material is thick and firm, the size of the somite graft was matched with the size of the somatopleure graft obtained in order to avoid problems of "critical mass" (Grobstein, '59). This usually necessitated that the somite portion be trimmed until its mass was approximately equivalent to the somatopleure graft.

Each portion of the trunk was tested for its competency to form striated muscle by transplantation into the anterior chamber of the eye. The host was anesthetized with ether and the iris of the eye was dilated with 2% atropine sulfate in order to preclude bleeding through accidental cutting of the iris during the grafting procedure. The eyeball was extruded by pressing the blunt end of a forceps into the orbit ventral to the eyeball. A slit approximately 2 mm long was made in the cornea with the edge of a razor blade which had been broken so that a sharp point was formed. A Spemann pipette containing the tissue

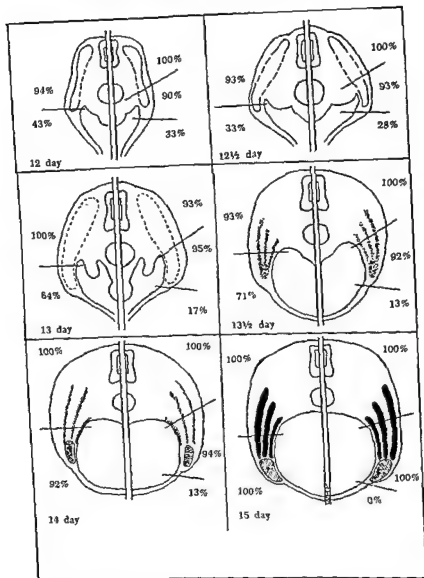


Fig. 1 A diagrammatic representation of the operational procedure and results of Series I (left half at each age) and Series II (right half). Percentages indicate the per cent of recovered grafts containing striated muscle.

was inserted into the anterior chamber through the slit and the tissue deposited as the pipette was slowly withdrawn. The cornea was allowed to heal spontaneously.

The graft was allowed to differentiate in the anterior chamber for a chosen number of days (tables 1, 2), whereupon the animal was sacrificed. The whole eyeball was removed and fixed in Bouin's solution or

10% buffered formalin (MacManus and Mowry, '60). After at least twenty-four hours of fixation, the eyeball was opened and the graft recovered. The graft was then serially sectioned and stained with Mallory's triple stain (Gray, '58).

Presence of epidermal structures in the graft material was the criterion for con-

sidering the graft to have survived and differentiated. Those grafts consisting of only a vascular stroma were classified as resorbed since the stroma could have developed as a result of the inflammatory reaction of the cornea. Visible cross-striations were required to be present in order for a tissue to be classified as muscle.

RESULTS AND DISCUSSIONS

Both the dorsal and ventral halves of the body wall have the capacity to form striated muscle as shown by the results of Series I (figs. 1, 2; table 1). The dorsal half formed muscle in at least 90% of the recovered grafts at all ages tested. In contrast, muscle was found in the ventral

TABLE 1
Summary of the results of Series I

Age	Portion of body wall	Operations attempted	Duration	Grafts lost ¹	Grafts recovered	
					Muscle present	Muscle absent
<i>days</i>			<i>days</i>	(%)	(%)	(%)
12	dorsal	21	10	5(24)	15(94)	1(6)
	ventral	21	10	7(33)	6(43)	8(57)
12.5	dorsal	18	10	4(22)	13(93)	1(7)
	ventral	20	10	5(25)	5(33)	10(67)
13	dorsal	17	9	5(29)	12(100)	0
	ventral	21	9	7(33)	9(64)	5(36)
13.5	dorsal	19	9	4(21)	14(93)	1(7)
	ventral	19	9	5(26)	10(71)	4(29)
14	dorsal	17	8	3(18)	14(100)	0
	ventral	17	8	5(29)	11(92)	1(8)
15	dorsal	14	7	3(22)	11(100)	0
	ventral	14	7	4(29)	10(100)	0

¹ Due to infection, resorption, or death of host.

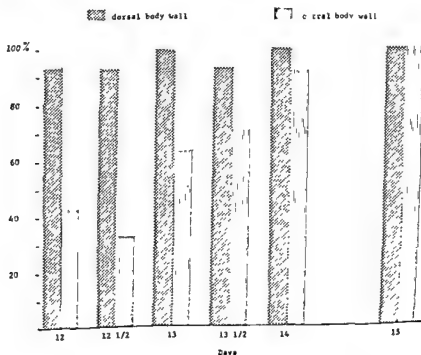


Fig. 2 Series I. A graph of the per cent of recovered grafts containing striated muscle.

half grafts at all ages tested but there was a wide range (33% to 100%) in the per cent of grafts which contained muscle at the various ages. In general, among the ventral-half grafts, the lower percentage of muscle-containing grafts occurred in the earlier ages and the percentage increased as the embryos grew older, until 100% of the recovered grafts contained muscle (at 15 days).

Thus, the ventral half appears at first to be less proficient than the dorsal half and becomes more proficient to form muscle with age. Is this a real or only apparent difference in muscle-forming proficiency of the two groups? Due to the small size and the variations in size of the samples, percentages are not a valid measurement of comparison. Accordingly, the two groups were compared by means of a statistical test, the Chi-square "exact test" (Baily, '59).

The results of the statistical comparison confirm that the ventral-half grafts do increase in muscle-forming ability with age. There is no statistical difference between the performance of the two portions of body wall at 13.5 days and thereafter, indicating that the ventral half is as proficient in forming muscle as the dorsal half at these ages. Earlier, however, there is a statistical difference in muscle-forming ability indicating the ventral half is less proficient in muscle formation and, moreover, the younger the embryo, the more statistically significant the difference becomes. At 13 days the difference is significant beyond the 5% confidence level ($p = 0.030$), and at 12 and 12.5 days it is beyond the 1% confidence level ($p = 0.003$, $p = 0.0012$, respectively).

Even though the ventral half of the body wall is not as proficient as the dorsal half in muscle formation at the earlier ages, Series I does demonstrate that the ventral half has the potentiality to form muscle and thus could be a source of the ventrolateral musculature. If the ventral half of the body wall is the source of the ventrolateral musculature, why is there this difference in developmental ability when compared with muscle-forming material of the dorsal half of the body wall? Recall that somite material in the form of the

somite buds invades the lateral plate. Could the difference be due to competent material (the somite buds) migrating into an incompetent area (lateral plate somatopleure)? Series I does not distinguish between the respective capacities for muscle formation of the somite material and the somatopleure. To test the somatopleure free of material from the somite buds and to compare it with the ability of the somite buds to form muscle was the intent of the second series of experiments of experiments. The dorsal portion of the somite served as control.

The difference in muscle-forming ability between the somite-free ventral portion of the body wall and the somite-derived portions is readily apparent (figs. 1, 3; table 2). In both the dorsal (dorsal somite) and lateral (somite bud) portions of the body wall at least 90% of the recovered grafts contained striated muscle. The somite-free ventral portion was capable of differentiating into muscle in a small per cent of the grafts, the percentage decreasing with the increased age of the embryo. Thirty-three per cent of the grafts contained muscle at 12 days, but only 28% at 12.5 days, 17% at 13 days, 13% at 13.5 and 14 days, and no grafts contained muscle at 15 days. The statistical difference between the muscle-forming ability of the ventral and lateral portions was highly significant at all ages tested, attaining the 0.1% confidence level at all ages except 12 days which was significant at the 5% level. Thus, grafts that contained somite material were highly proficient in forming muscle whereas the somite-free somatopleure had little ability to differentiate into muscle. These results are compatible with an interpretation that the somites are the source of the ventrolateral musculature.

Even though, as indicated by the descriptive and experimental evidence, muscle formation is not its normal role, the somite-free somatopleure can to a limited extent differentiate into striated muscle when implanted into the anterior chamber of the eye. Grobstein ('55) demonstrated that the anterior chamber of the eye is not a truly neutral culture medium, as had previously been supposed. Metanephrogenic mesenchyme *in vitro* spreads out into

sidering the graft to have survived and differentiated. Those grafts consisting of only a vascular stroma were classified as resorbed since the stroma could have developed as a result of the inflammatory reaction of the cornea. Visible cross-striations were required to be present in order for a tissue to be classified as muscle.

RESULTS AND DISCUSSIONS

Both the dorsal and ventral halves of the body wall have the capacity to form striated muscle as shown by the results of Series I (figs. 1, 2; table 1). The dorsal half formed muscle in at least 90% of the recovered grafts at all ages tested. In contrast, muscle was found in the ventral-

TABLE 1
Summary of the results of Series I

Age	Portion of body wall	Operations attempted	Duration	Grafts lost ¹	Grafts recovered	
					Muscle present	Muscle absent
days			days	(%)	(%)	(%)
12	dorsal	21	10	5(24)	15(94)	1(6)
	ventral	21	10	7(33)	6(43)	8(57)
12.5	dorsal	18	10	4(22)	13(93)	1(7)
	ventral	20	10	5(25)	5(33)	10(67)
13	dorsal	17	9	5(29)	12(100)	0
	ventral	21	9	7(33)	9(64)	5(36)
13.5	dorsal	19	9	4(21)	14(93)	1(7)
	ventral	19	9	5(26)	10(71)	4(29)
14	dorsal	17	8	3(18)	14(100)	0
	ventral	17	8	5(29)	11(92)	1(8)
15	dorsal	14	7	3(22)	11(100)	0
	ventral	14	7	4(29)	10(100)	0

¹ Due to infection, resorption, or death of host.

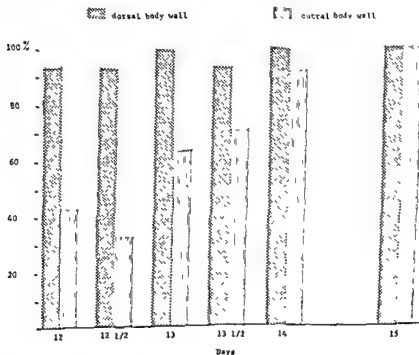


Fig. 2 Series I. A graph of the per cent of recovered grafts containing striated muscle.

half grafts at all ages tested but there was a wide range (33% to 100%) in the per cent of grafts which contained muscle at the various ages. In general, among the ventral-half grafts, the lower percentage of muscle-containing grafts occurred in the earlier ages and the percentage increased as the embryos grew older, until 100% of the recovered grafts contained muscle (at 15 days).

Thus, the ventral half appears at first to be less proficient than the dorsal half and becomes more proficient to form muscle with age. Is this a real or only apparent difference in muscle-forming proficiency of the two groups? Due to the small size and the variations in size of the samples, percentages are not a valid measurement of comparison. Accordingly, the two groups were compared by means of a statistical test, the Chi-square "exact test" (Baily, '59).

The results of the statistical comparison confirm that the ventral-half grafts do increase in muscle-forming ability with age. There is no statistical difference between the performance of the two portions of body wall at 13.5 days and thereafter, indicating that the ventral half is as proficient in forming muscle as the dorsal half at these ages. Earlier, however, there is a statistical difference in muscle-forming ability indicating the ventral half is less proficient in muscle formation and, moreover, the younger the embryo, the more statistically significant the difference becomes. At 13 days the difference is significant beyond the 5% confidence level ($p = 0.030$), and at 12 and 12.5 days it is beyond the 1% confidence level ($p = 0.003$, $p = 0.0012$, respectively).

Even though the ventral half of the body wall is not as proficient as the dorsal half in muscle formation at the earlier ages, Series I does demonstrate that the ventral half has the potentiality to form muscle and thus could be a source of the ventrolateral musculature. If the ventral half of the body wall is the source of the ventrolateral musculature, why is there this difference in developmental ability when compared with muscle-forming material of the dorsal half of the body wall? Recall that somite material in the form of the

somite buds invades the lateral plate. Could the difference be due to competent material (the somite buds) migrating into an incompetent area (lateral plate somatopleure)? Series I does not distinguish between the respective capacities for muscle formation of the somite material and the somatopleure. To test the somatopleure free of material from the somite buds and to compare it with the ability of the somite buds to form muscle was the intent of the second series of experiments of experiments. The dorsal portion of the somite served as control.

The difference in muscle-forming ability between the somite-free ventral portion of the body wall and the somite-derived portions is readily apparent (figs. 1, 3; table 2). In both the dorsal (dorsal somite) and lateral (somite bud) portions of the body wall at least 90% of the recovered grafts contained striated muscle. The somite-free ventral portion was capable of differentiating into muscle in a small per cent of the grafts, the percentage decreasing with the increased age of the embryo. Thirty-three per cent of the grafts contained muscle at 12 days, but only 28% at 12.5 days, 17% at 13 days, 13% at 13.5 and 14 days, and no grafts contained muscle at 15 days. The statistical difference between the muscle-forming ability of the ventral and lateral portions was highly significant at all ages tested, attaining the 0.1% confidence level at all ages except 12 days which was significant at the 5% level. Thus, grafts that contained somite material were highly proficient in forming muscle whereas the somite-free somatopleure had little ability to differentiate into muscle. These results are compatible with an interpretation that the somites are the source of the ventrolateral musculature.

Even though, as indicated by the descriptive and experimental evidence, muscle formation is not its normal role, the somite-free somatopleure can to a limited extent differentiate into striated muscle when implanted into the anterior chamber of the eye. Grobstein ('55) demonstrated that the anterior chamber of the eye is not a truly neutral culture medium, as had previously been supposed. Metanephrogenic mesenchyme *in vitro* spreads out into

sidering the graft to have survived and differentiated. Those grafts consisting of only a vascular stroma were classified as resorbed since the stroma could have developed as a result of the inflammatory reaction of the cornea. Visible cross-striations were required to be present in order for a tissue to be classified as muscle.

RESULTS AND DISCUSSIONS

Both the dorsal and ventral halves of the body wall have the capacity to form striated muscle as shown by the results of Series I (figs. 1, 2; table 1). The dorsal half formed muscle in at least 90% of the recovered grafts at all ages tested. In contrast, muscle was found in the ventral-

TABLE 1
Summary of the results of Series I

Age	Portion of body wall	Operations attempted	Duration	Grafts lost ¹	Grafts recovered	
					Muscle present	Muscle absent
<i>days</i>			<i>days</i>	(%)	(%)	(%)
12	dorsal	21	10	5(24)	15(94)	1(6)
	ventral	21	10	7(33)	6(43)	8(57)
12.5	dorsal	18	10	4(22)	13(93)	1(7)
	ventral	20	10	5(25)	5(33)	10(67)
13	dorsal	17	9	5(29)	12(100)	0
	ventral	21	9	7(33)	9(64)	5(36)
13.5	dorsal	19	9	4(21)	14(93)	1(7)
	ventral	19	9	5(26)	10(71)	4(29)
14	dorsal	17	8	3(18)	14(100)	0
	ventral	17	8	5(29)	11(92)	1(8)
15	dorsal	14	7	3(22)	11(100)	0
	ventral	14	7	4(29)	10(100)	0

¹ Due to infection, resorption, or death of host.

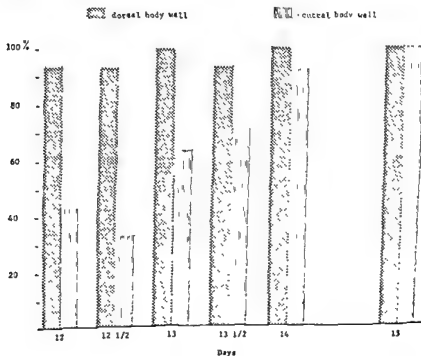


Fig. 2 Series I. A graph of the per cent of recovered grafts containing striated muscle.

half grafts at all ages tested but there was a wide range (33% to 100%) in the per cent of grafts which contained muscle at the various ages. In general, among the ventral-half grafts, the lower percentage of muscle-containing grafts occurred in the earlier ages and the percentage increased as the embryos grew older, until 100% of the recovered grafts contained muscle (at 15 days).

Thus, the ventral half appears at first to be less proficient than the dorsal half and becomes more proficient to form muscle with age. Is this a real or only apparent difference in muscle-forming proficiency of the two groups? Due to the small size and the variations in size of the samples, percentages are not a valid measurement of comparison. Accordingly, the two groups were compared by means of a statistical test, the Chi-square "exact test" (Baily, '59).

The results of the statistical comparison confirm that the ventral-half grafts do increase in muscle-forming ability with age. There is no statistical difference between the performance of the two portions of body wall at 13.5 days and thereafter, indicating that the ventral half is as proficient in forming muscle as the dorsal half at these ages. Earlier, however, there is a statistical difference in muscle-forming ability indicating the ventral half is less proficient in muscle formation and, moreover, the younger the embryo, the more statistically significant the difference becomes. At 13 days the difference is significant beyond the 5% confidence level ($p = 0.030$), and at 12 and 12.5 days it is beyond the 1% confidence level ($p = 0.003$, $p = 0.0012$, respectively).

Even though the ventral half of the body wall is not as proficient as the dorsal half in muscle formation at the earlier ages, Series I does demonstrate that the ventral half has the potentiality to form muscle and thus could be a source of the ventrolateral musculature. If the ventral half of the body wall is the source of the ventrolateral musculature, why is there this difference in developmental ability when compared with muscle-forming material of the dorsal half of the body wall? Recall that somite material in the form of the

somite buds invades the lateral plate. Could the difference be due to competent material (the somite buds) migrating into an incompetent area (lateral plate somatopleure)? Series I does not distinguish between the respective capacities for muscle formation of the somite material and the somatopleure. To test the somatopleure free of material from the somite buds and to compare it with the ability of the somite buds to form muscle was the intent of the second series of experiments of experiments. The dorsal portion of the somite served as control.

The difference in muscle-forming ability between the somite-free ventral portion of the body wall and the somite-derived portions is readily apparent (figs. 1, 3; table 2). In both the dorsal (dorsal somite) and lateral (somite bud) portions of the body wall as least 90% of the recovered grafts contained striated muscle. The somite-free ventral portion was capable of differentiating into muscle in a small per cent of the grafts, the percentage decreasing with the increased age of the embryo. Thirty-three per cent of the grafts contained muscle at 12 days, but only 28% at 12.5 days, 17% at 13 days, 13% at 13.5 and 14 days, and no grafts contained muscle at 15 days. The statistical difference between the muscle-forming ability of the ventral and lateral portions was highly significant at all ages tested, attaining the 0.1% confidence level at all ages except 12 days which was significant at the 5% level. Thus, grafts that contained somite material were highly proficient in forming muscle whereas the somite-free somatopleure had little ability to differentiate into muscle. These results are compatible with an interpretation that the somites are the source of the ventrolateral musculature.

Even though, as indicated by the descriptive and experimental evidence, muscle formation is not its normal role, the somite-free somatopleure can to a limited extent differentiate into striated muscle when implanted into the anterior chamber of the eye. Grobstein ('55) demonstrated that the anterior chamber of the eye is not a truly neutral culture medium, as had previously been supposed. Metanephrogenic mesenchyme *in vitro* spreads out into

TABLE 2
Summary of the results of Series II

Age	Portion of body wall	Operations attempted	Duration	Grafts lost ¹	Grafts recovered	
					Muscle present	Muscle absent
days			days	(%)	(%)	(%)
12	dorsal	8	10	2(25)	6(100)	0
	lateral	14	10	4(29)	9(90)	1(10)
	ventral	14	10	5(36)	3(33)	6(67)
12.5	dorsal	14	10	2(14)	12(100)	0
	lateral	16	10	2(12)	13(93)	1(7)
	ventral	18	10	4(22)	4(28)	10(72)
13	dorsal	14	9	0	13(93)	1(7)
	lateral	24	9	5(21)	18(95)	1(5)
	ventral	24	9	6(25)	3(17)	15(83)
13.5	dorsal	16	9	2(12)	14(100)	0
	lateral	31	9	6(19)	23(92)	2(8)
	ventral	31	9	8(26)	3(13)	20(87)
14	dorsal	12	8	2(17)	10(100)	0
	lateral	22	8	5(23)	16(94)	1(6)
	ventral	22	8	7(32)	2(13)	13(87)
15	dorsal	8	7	1(12)	7(100)	0
	lateral	11	7	2(18)	9(100)	0
	ventral	11	7	5(45)	0	6(100)

¹ Due to infection, resorption, or death of host.

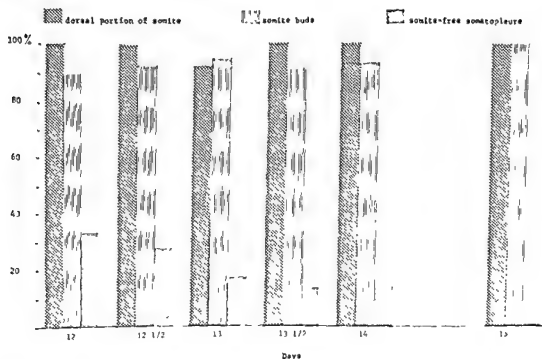


Fig. 3 Series II. A graph of the per cent of recovered grafts containing striated muscle.

a cellular sheet unless placed under the influence of an appropriate inductor. In the anterior chamber of the eye, however, the same metanephrogenic mesenchyme

differentiates into ducts and tubules, without having been exposed to any known inductor. The ocular tissues were tested *in vitro* and none showed inductive activity.

TABLE 3
Statistical comparison of groups (p values)

Age	Series I dorsal vs Series I ventral	Series II lateral vs Series II ventral	Series I ventral vs Series II ventral	Series I ventral vs Series II lateral
days				
12	p=0.003 ³	p=0.017 ³	p=0.31 ¹	p=0.023 ³
12.5	0.0012 ³	0.0007 ⁴	0.30 ¹	0.0012 ³
13	0.03 ²	0.0001 ⁴	0.007 ³	0.034 ²
13.5	0.30 ¹	0.0001 ⁴	0.0005 ⁴	0.92 ¹
14	0.46 ¹	0.0001 ⁴	0.0001 ⁴	0.50 ¹
15	1.0 ¹	0.0002 ⁴	0.0001 ⁴	0.0 ¹

¹ Not significant.

² Significant, 5% confidence level.

³ Highly significant, 1% confidence level.

⁴ Very highly significant, 0.1% confidence level.

ity. The influence of the anterior chamber of the eye does not seem to be "directive," but to be "permissive," i.e., allowing complete expression of a tissue's embryonic potential. This apparent action of the anterior chamber may have some influence on the results of this experiment, in particular, enabling the somatopleure to consistently differentiate into muscle even though the evidence disposes against the somatopleure playing a role *in vivo* in the development of the ventrolateral musculature.

Thus, the presence of muscle in the somite-free somatopleure grafts may be the expression of the self-differentiating capacity of the somatopleure. Embryonic cells possess an "intrinsic latent repertoire of potencies" (Weiss, '39). That is, there are a number of discrete histological differentiations which a cell may undergo. The different developmental directions available to a cell or tissue are more easily demonstrated if the tissue is isolated from whatever factors normally influence it.

In addition, the muscle formed by the somite-free somatopleure could have differentiated from cells under the influence of the limb "fields," or from cells actually destined to become part of the appendicular musculature. It is unlikely that the cells of the grafts could have been destined to take part in the actual formation of limb muscle since care was taken not to include any limb bud tissue. It is not as easy to rule out the influence of the limb fields.

The limb buds are discrete but still rudimentary at the ages when the somite-free somatopleure is most capable of forming

muscle (12 and 12.5 days). Presumably there would still be a wide area of the trunk under the influence of the limb buds. This area would be capable of responding to an appropriate stimulus, e.g., removal from the vicinity of the limb, by forming muscle. Some of this area could have included in the grafts. As the embryos age, the influence of the limb field declines. Consequently the ability to respond lessens which would result in a decreased incidence of muscle in the grafts. This interpretation is in harmony with the results in this experiment.

LITERATURE CITED

- Baily, N. T. J. 1959 Statistical Methods of Biology. English University Press, London.
- Bardeen, C. R. 1900 The development of the musculature of the body wall in the pig, including its histogenesis and its relations to the myotomes and to the skeletal and nervous apparatus. Johns Hopkins Hospital Report, 9: 367-399.
- Butcher, E. O. 1929 The development of the somites in the white rat (*Mus norvegicus albinus*) and the fate of the myotomes, neural tube, and gut in the tail. Am. J. Anat., 44: 381-440.
- Danilova, L. V. 1963 Somite differentiation in the Karakul sheep embryo. Federation Proceedings Translation Supplement, 22: 667-683; translated from Izvestiya Akademii Nauk SSSR, Seriya Biologicheskaya, 1: 70, 1962.
- Detwiler, S. R. 1955 Experiments on the origin of the ventrolateral trunk musculature in the urodele (*Amblystoma*). J. Exp. Zool., 129: 45-76.
- Fell, H. B. 1939 The origin and developmental mechanics of the avian sternum. Phil. Trans., Series B, Royal Society, 229: 407-463.
- Gray, Peter 1958 Handbook of Basic Microtechnique. 2nd Ed. McGraw-Hill, New York.

- Grobstein, Clifford 1955 Inductive interaction in development of mouse metanephrosis. *J. Exp. Zool.*, 130: 319-339.
- 1959 *The Cell*. Vol. 1. J. Brachet and A. Mirsky, eds. Academic Press, New York.
- Liedke, K. B. 1958 Experiments on the development of trunk muscles in anura (*Rana pipiens*). *Anat. Rec.*, 131: 97-118.
- MacManus, J. F. A., and W. Mowry 1960 *Staining Methods — Histologic and Histochemical*. Hoeber, New York.
- Nicholas, J. S. 1950 Development of contractility. *Proc. Am. Phil. Soc.*, 94: 175-183.
- Saunders, J. W. 1948 Do the somites contribute to the formation of the chick wing? *Anat. Rec.*, 100: 756.
- Seno, T. 1961 An experimental study on the formation of the body wall in the chick. *Acta Anat.*, 45: 60-82.
- Straus, W. L., Jr., and M. E. Rawles 1953 An experimental study of the origin of the trunk musculature and ribs in the chick. *Am. J. Anat.*, 92: 471-509.
- Theiler, K. 1957 Über die Differenzierung der Rumpfmotome beim Menschen und die Herkunft der Bauchwandmuskeln. *Acta Anat.*, 30: 842-864.
- Weiss, Paul 1939 *Principles of Development*. Henry Holt and Co., New York.
- Wells, L. J. 1954 Development of the human diaphragm and pleural sacs. *Contr. to Embryol.*, Carnegie Instit. Wash., 35: 107-134.

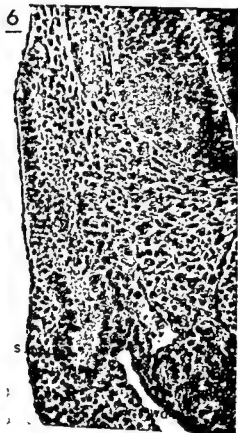
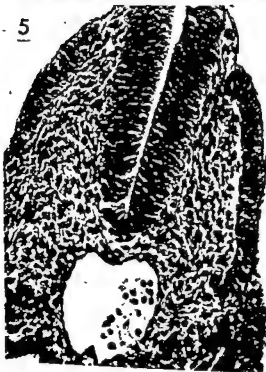
Abbreviations

s, somite bud	RA, rectus abdominis
r, rib anlage	EO, external oblique
wd, Wolffian duct	IO, internal oblique
v, ventral ramus of spinal nerve	T, transverse abdominis
ii, internal intercostal m.	LA, linea alba
ei, external intercostal m.	

PLATE 1

EXPLANATION OF FIGURES

- Somite 19 of a ten and one-half day embryo. On the left is the posterior border of the somite; on the right the section is midway between the anterior and posterior borders of the somite. Note the epithelial border and the central core of cells. $\times 400$.
- Somite 20 of an 11 day embryo. The somite on the right is sectioned midway between the anterior and posterior somite borders. Note the lack of medial epithelium. On the left, the section is oblique, revealing adjacent borders of two somites. $\times 240$.
- Somite 21 of a 12 day embryo. The somite can be seen extending into the lateral plate somatopleure. $\times 180$.



- Grobstein, Clifford 1955 Inductive interaction in development of mouse metanephrosis. *J. Exp. Zool.*, 130: 319-339.
- 1959 *The Cell*. Vol. 1. J. Brachet and A. Mirsky, eds. Academic Press, New York.
- Liedke, K. B. 1958 Experiments on the development of trunk muscles in anura (*Rana pipiens*). *Anat. Rec.*, 131: 97-118.
- MacManus, J. F. A., and W. Mowry 1960 *Staining Methods—Histologic and Histochemical*. Hoeber, New York.
- Nicholas, J. S. 1950 Development of contractility. *Proc. Am. Phil. Soc.*, 94: 175-183.
- Saunders, J. W. 1948 Do the somites contribute to the formation of the chick wing? *Anat. Rec.*, 100: 756.
- Seno, T. 1961 An experimental study on the formation of the body wall in the chick. *Acta Anat.*, 45: 60-82.
- Straus, W. L., Jr., and M. E. Rawles 1953 An experimental study of the origin of the trunk musculature and ribs in the chick. *Am. J. Anat.*, 92: 471-509.
- Theiler, K. 1957 Über die Differenzierung der Rumpfmotome beim Menschen und die Herkunft der Bauchwandmuskeln. *Acta Anat.*, 30: 842-864.
- Weiss, Paul 1939 *Principles of Development*. Henry Holt and Co., New York.
- Wells, L. J. 1954 Development of the human diaphragm and pleural sacs. *Contr. to Embryol.*, Carnegie Instit. Wash., 35: 107-134.

Abbreviations

s, somite bud	RA, rectus abdominis
r, rib anlage	EO, external oblique
wd, Wolffian duct	IO, internal oblique
v, ventral ramus of spinal nerve	T, transverse abdominis
li, internal intercostal m.	LA, linea alba
ei, external intercostal m.	

PLATE 1

EXPLANATION OF FIGURES

- 4 Somite 19 of a ten and one-half day embryo. On the left is the posterior border of the somite; on the right the section is midway between the anterior and posterior borders of the somite. Note the epithelial border and the central core of cells. $\times 400$.
- 5 Somite 20 of an 11 day embryo. The somite on the right is sectioned midway between the anterior and posterior somite borders. Note the lack of medial epithelium. On the left, the section is oblique, revealing adjacent borders of two somites. $\times 240$.
- 6 Somite 21 of a 12 day embryo. The somite can be seen extending into the lateral plate somatopleure. $\times 180$.

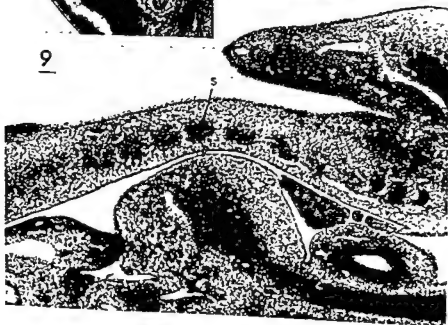


PLATE 2

EXPLANATION OF FIGURES

- 7 Parasagittal section of a 12.5 day embryo. Note the prominent epithelium of the ventral somite bud. Rib anlagen are visible. $\times 60$.
- 8 Cross section of mid-trunk region of a 13 day embryo. Note the dense aggregation of cells which is the only indication of the ventral extent of somite material. Epithelium has completely disappeared. The arrow locates the apparent boundary between somite and somatopleure. $\times 45$.
- 9 Frontal section of the tips of the ventral somite buds of a 13 day embryo. Note that the epithelial border separating the somite from the somatopleure has disappeared. $\times 40$.

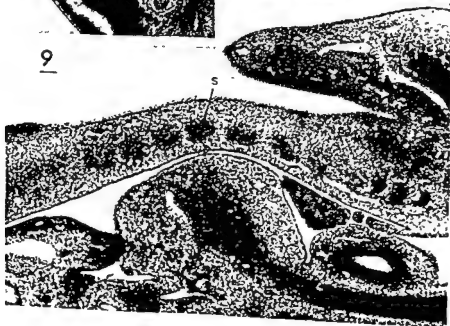
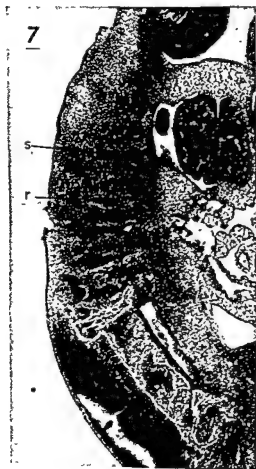


PLATE 3

EXPLANATION OF FIGURES

- 10 Parasagittal sections of a 13 day embryo. Note again the lack of epithelium covering the tips of the somite bud (Cf. fig. 7). Note the confluence of somite material dorsal to the somite buds. $\times 45$.
- 11 Parasagittal section of a 14 day embryo. Note the path of the rectus abdominis muscle corresponding to the former path of the ventral edge of the somite buds (Cf. fig. 10). $\times 30$.



PLATE 3

EXPLANATION OF FIGURES

- 10 Parasagittal sections of a 13 day embryo. Note again the lack of epithelium covering the tips of the somite bud (Cf. fig. 7). Note the confluence of somite material dorsal to the somite buds. $\times 45$.
- 11 Parasagittal section of a 14 day embryo. Note the path of the rectus abdominis muscle corresponding to the former path of the ventral edge of the somite buds (Cf. fig. 10). $\times 30$.

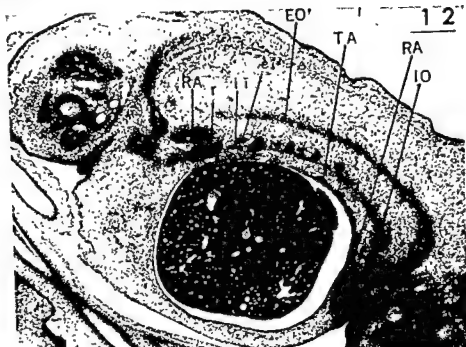


PLATE 4

EXPLANATION OF FIGURES

- 12 Parasagittal section of a 14 day embryo. Note the presence of the anlagen of all the muscles of the abdominal (ventrolateral) series as well as several ribs. $\times 40$.
- 13 Transverse section of a 14 day embryo revealing the anlagen of the abdominal (ventrolateral) series of muscles. Note the lateral position of the rectus abdominis. $\times 45$.

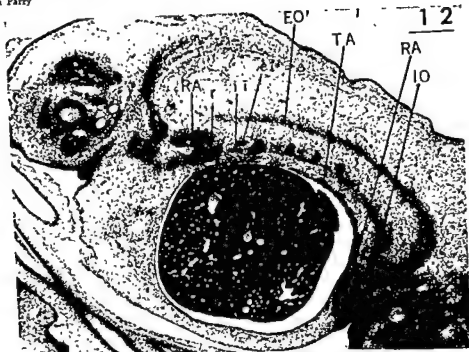


PLATE 4

EXPLANATION OF FIGURES

- 12 Parasagittal section of a 14 day embryo. Note the presence of the anlagen of all the muscles of the abdominal (ventrolateral) series as well as several ribs. $\times 40$.
- 13 Transverse section of a 14 day embryo revealing the anlagen of the abdominal (ventrolateral) series of muscles. Note the lateral position of the rectus abdominis. $\times 45$.

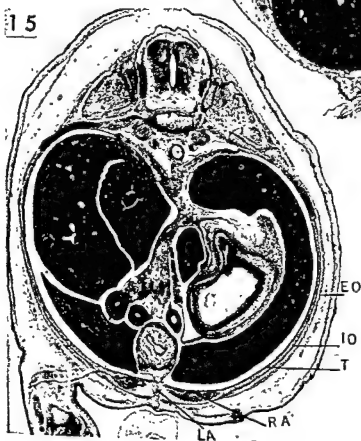
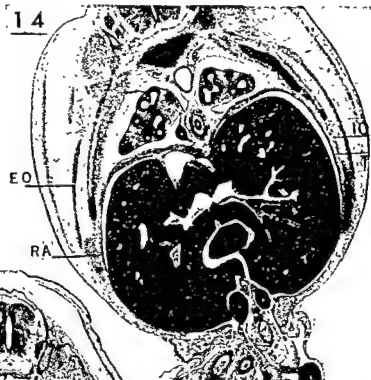


PLATE 5

EXPLANATION OF FIGURES

- 14 Transverse section of a 15 day embryo demonstrating the positions of the abdominal muscle series. Note that the rectus muscle is still lateral in position. $\times 20$.
- 15 Transverse section of a 17 day embryo demonstrating the final disposition of the muscles of the abdominal (ventrolateral) series. $\times 20$.

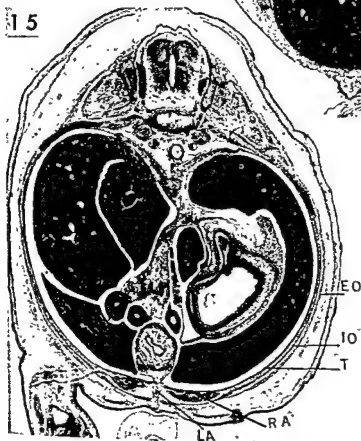
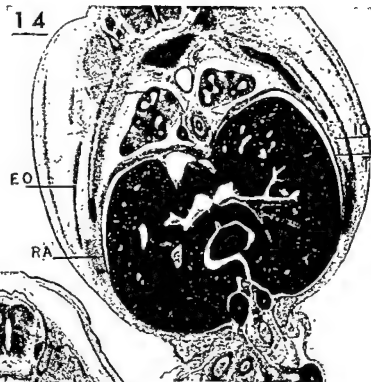
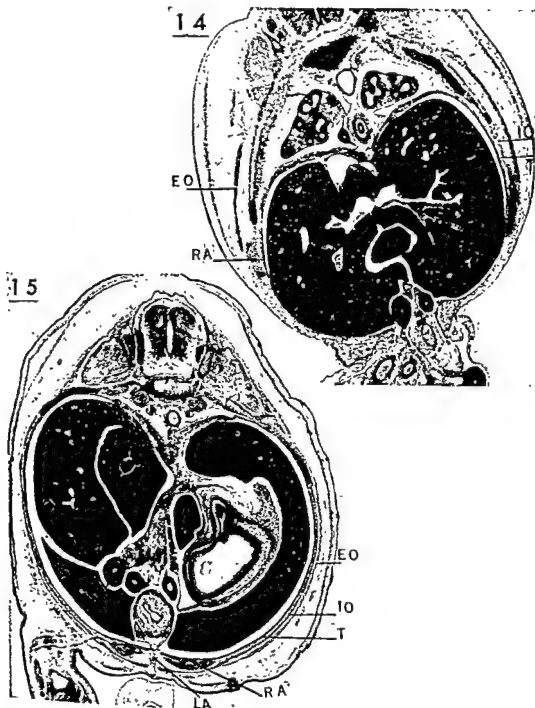


PLATE 5

EXPLANATION OF FIGURES

- 14 Transverse section of a 15 day embryo demonstrating the positions of the abdominal muscle series. Note that the rectus muscle is still lateral in position. $\times 20$.
- 15 Transverse section of a 17 day embryo demonstrating the final disposition of the muscles of the abdominal (ventrolateral) series. $\times 20$.



Changes in the Fine Structure of the Parietal Yolk Sac of the Rat Placenta with Increasing Gestational Age¹

WILLIAM F. JOLLIE

Tulane University School of Medicine, New Orleans, Louisiana

ABSTRACT The fine structure of the portion of the parietal yolk sac which extends across the fetal surface of the rat placenta (which is the only portion of the parietal yolk sac which persists after the sixteenth day of pregnancy) was examined sequentially on the even numbered days during the second half of gestation. The placental parietal yolk sac was seen to consist of two cellular layers, trophoblast and endodermal epithelium, which were separated by a thick, amorphous membrane (of Reichert). The trophoblast attenuated with increasing gestational age and, on day 18, became perforated by fenestrations which were closed by diaphragmata. By day 22, the attenuated trophoblast was patently perforate, and maternal blood was exposed to Reichert's membrane. Since throughout gestation, the cells of the parietal endoderm formed a discontinuous layer, at all stages Reichert's membrane was exposed to the vitelline cavity. When ferritin and thorotrast were injected i.v., both separately and together, the former passed readily from maternal blood through Reichert's membrane and was phagocytosed by cells of the parietal endoderm. Thorotrast, however, did not cross Reichert's membrane. Since the rodent yolk-sac complex is known to serve as a placental route, selective permeability of Reichert's membrane may help regulate maternofetal exchange.

During late implantation stages in rodents, a relatively thick sheet of amorphous material appears between extraembryonic endoderm and trophoblast (Snell, '41). Termed Reichert's membrane, the sheet forms a tough reinforcement for the trophoblast and endoderm. Together these three layers form a parietal yolk sac. With enlargement of the yolk-sac cavity, the parietal yolk sac and its related Reichert's membrane invest both the embryo and, save the chorionallantoic placenta, the embryonic adnexa. By the time the embryo attains definitive form (11-12 days of gestational age in the rat), the only discontinuity in the parietal membrane is at the root of the umbilical cord. At this point, allantoic blood vessels emerge from the chorionic vesicle to vascularize the chorionallantoic labyrinth. In peripheral relation to the root of the cord, parietal and visceral layers of the yolk sac meet. Here Reichert's membrane first delimits circumvallate reflections into the fetal placental surface (the endodermal sinuses of Duval, 1892) and then terminates in direct continuity with two basement membranes which reinforce the vascularized visceral yolk sac².

The visceral yolk sac of rodents has been shown to serve a placental function

(Everett, '35; Mossman, '37; Noer and Mossman, '47; Wislocki and Padykula, '53; Brambell and Hemmings, '54; Brambell and Halliday, '56; Fedinec, '62; Lambson, '66; Padykula, Deren and Wilson, '66; Jollie and Jollie, '67). In the rat, in order to reach the peripheral vitelline circulation of this membrane, materials from maternal blood must cross both the parietal yolk sac (i.e., trophoblast, Reichert's membrane and parietal endoderm) and the cavity (yolk-sac cavity) which separates parietal and visceral layers. Late on the sixteenth day, placental relations are altered. Reichert's membrane along the parietal wall ruptures. The membrane, its related endoderm and trophoblast, and the decidua capsularis retract to the peripheral margins of the chorionallantoic placenta (Bridgman, '46). Upon such rupture and retraction, uterine and vitelline cavities become confluent. Over the fetal surface of the placenta,

¹ Supported by Research grants numbered HD 00369 and HD 02279 from the National Institutes of Health.

² Occasionally, the basement membranes of the visceral yolk sac also are considered as part of Reichert's membrane (Everett, '35; Remus, '65a); more commonly however, the term Reichert's membrane is reserved for that portion of the membrane complex which separates endoderm from trophoblast within the parietal yolk sac (Grosser, '27; Mossman, '37; Bridgman, '46; Wislocki and Padykula, '53), a terminological convention which is followed here.

constant. It was composed of ill-defined fibrils which precisely paralleled both each other and the plane of the entire membrane (figs. 1, 2, 3, 6, 12). In certain sections a striated appearance of the membrane was replaced by a stippled appearance (figs. 7, 8, 10). Since the former is characteristic of fibrils which are cut in longitudinal section and the latter of fibrils which are cut in oblique or cross section, the membrane can be regarded as being composed indeed of parallel fibrils, rather than of parallel lamellae. On the trophoblastic side of Reichert's membrane, however, in many sections, there appeared to be a more dense layer about 750 Å wide which delimited this edge of the membrane (figs. 3, 6, 7, 8, 9, 10). Regardless of the orientation of the fibrillar components of the membrane, this layer appeared as a line. Consequently it represented a lamina, or sheet in contradistinction to the rest of the membrane. This lamina appeared consistently to be separated from the plasmalemmata of adjacent trophoblast cells by a layer which was quite uniformly wide at about 500 Å. No comparable dense and light layers were identified adjacent to the parietal endoderm on the opposite side of Reichert's membrane.

In all stages of pregnancy which were examined, i.e., from 12 to 22 days post coitum, the epithelial cells of the parietal yolk-sac endoderm were cuboidal and often were widely separated from each other. Consequently, in many regions, Reichert's membrane was directly exposed to the space which in life was yolk-sac cavity (figs. 2, 3, 6, 8). Where endodermal cells occasionally adjoined, the intercellular junctions were not modified into desmosomes (figs. 1, 4, 9). Cytologically, the endodermal cells exhibited differentiation in association with gestational aging. In the 12-day yolk sacs, endodermal epithelial cells contained both cisterns of rough endoplasmic reticulum which delimited a material of moderate electron density and an abundance of both free ribosomes and of rosettes of ribosomes (fig. 1). The cells were rich in lipid droplets. By the fourteenth day, rough endoplasmic reticulum had increased; lipid droplets were still abundant (fig. 2). At later stages, lipid was not identified, and rough endoplasmic

reticulum was increasingly abundant. In placentas which were taken on the twentieth and twenty-second days of pregnancy, (i.e., shortly before term) within the parietal endodermal cells, the cisterns of endoplasmic reticulum were markedly dilated and contained a flocculent material of little electron density (figs. 6, 9).

In all of the placentas which were examined from 12 to 20 days of pregnancy, the subsurface placental labyrinthine sinuses, through which in life maternal blood circulated, were lined by trophoblastic cells. At these stages, the sinuses and Reichert's membrane were separated by a layer of trophoblast which was variably thick. This trophoblastic layer was discretely cellular; and where intertrophoblastic junctional complexes were identified, attachments were desmosomal (figs. 2, 3, 4, 9, 10). A cytological differentiation with increasing gestational age was apparent in these cellular elements. From day 12 through day 20, there appeared to be an attenuation of the trophoblastic cytoplasm which was related to Reichert's membrane. By day 18 and in later stages, fenestrations in this cytoplasm were evident (figs. 3, 4, 5, 9). The fenestrations which were in direct relation to the Reichert's membrane measured 700–800 Å in diameter; and each was closed by a diaphragm. Often similarly fenestrated wisps of trophoblastic cytoplasm bore no direct relationship to Reichert's membrane (fig. 4). Occasionally, the trophoblastic cytoplasm on the far side of the subsurface maternal blood sinuses appeared fenestrated (fig. 5). In 22-day placentas, the fenestrae were often enlarged, lacked diaphragmata, and appeared to be completely patent (fig. 6).

The placental yolk sac of injected animals. In animals which were given an i.v. injection of cadmium-free ferritin 15 minutes before autopsy, electron dense particles which measured 50–60 Å in diameter were identified within phagosomal profiles in the cytoplasm of the trophoblast which lined the maternal blood sinuses subjacent to Reichert's membrane (fig. 7). Phagocytosed particles which were interpreted as ferritin were also identified within some of the cells of the endodermal epithelium on the side of Reichert's mem-

however, Reichert's membrane remains intact. Since maternal blood sinuses within the labyrinth extend to a position just beneath the placental surface, maternal blood remains separated from the uterine-yolk-sac cavity by the trophoblast-Reichert's membrane-endoderm complex, i.e., a residual portion of the parietal yolk sac.

Investigations on selective maternofetal interchange by the yolk-sac placental route have concentrated on the vascularized visceral yolk sac. Here the "placental barrier" is considered to be composed collectively of the tissues which separate the yolk-sac cavity from fetal blood within vitelline capillaries at the villous cores of the visceral yolk sac. However, as has been explained, from days 10 through 16 of pregnancy, both portions of the parietal yolk sac—viz., that which is related to the capsularis ("capsular yolk sac") and that which is related to the fetal surface of the placenta ("placental yolk sac")—also are interposed in the exchange route from maternal to fetal bloods. And from day 17 through to term at day 23, the persisting portion of the parietal membrane, or placental yolk sac, still affords the most direct route for placental exchange between maternal blood in the subsurface, labyrinthine sinuses and fetal blood in the vitelline capillaries. Consequently, at all stages of pregnancy in the rat, this membrane remains an integral part of the yolk-sac placental route.

It has become well established that both selectivity for maternofetal transport and transport rates by the yolk-sac placental route vary with gestational age (Brambell and Halliday, '56; Mayersbach, '58; Hemmings and Brambell, '61; Lambson, '66; Padykula, Deren and Wilson, '66; Jollie and Jollie, '67). We have examined the parietal yolk sac at the fetal surface of the chorioallantoic placenta at increasing gestational ages and have attempted to correlate changes in the fine structure of this membrane with changes in transport function. Further, by injecting electron opaque colloids intravenously into pregnant animals and subsequently examining fetal tissues, we have attempted to visualize selective transport of materials across this portion of the yolk-sac placenta.

MATERIALS AND METHODS

By a breeding method which has been described elsewhere (Jollie, '64), gestational ages in days were reckoned within an hour of coition. An initial series of animals consisted of two specimens at each even-numbered day from day 12 to day 22. Additionally three series of 12- to 22-day pregnant animals were treated as follows: in the animals of the first series, 100 mg ferritin in 1.0 cm³ physiological saline³ was injected i.v. into the tail 15 minutes before autopsy; in the second series, 1.0 cm³ thorotrast⁴ similarly was injected; and in the third, 1.0 cm³ ferritin was followed by a 1.0 cm³ injection of thorotrast.

At autopsy, the rats were anesthetized with an i.p. injection of 5 mg/100 gm body weight sodium pentobarbital. By ventral laparotomy and uterine incision, the chorioallantoic placentas were extirpated and transferred immediately to several drops of phosphate buffered 3% glutaraldehyde at pH 7.3. Under a stereoscopic microscope, blocks of tissue approximately 1 × 1 × 3 mm were cut perpendicular to the fetal surface so that in each case this surface was at one end of the block and normal to its long axis. The blocks were fixed in the glutaraldehyde fixative at 4°C for two hours, post-fixed in phosphate buffered 1% osmium tetroxide, dehydrated in ethanol, and embedded in Durcupan epoxy resin⁵. Thin sections were cut on an MT-1 Porter-Blum ultramicrotome, mounted on naked 200 mesh copper grids, stained with lead hydroxide (Millonig, '61), and examined with an RCA EMU-3G electron microscope.

OBSERVATIONS

The placental yolk sac of uninjected animals. In normal section, Reichert's membrane appeared as a band of moderate electron density at all stages of pregnancy. With increasing gestational age, it widened considerably, viz., from about 3 μ at 12 days *post coitum* (figs. 1, 2) to about 8 μ at 22 days (fig. 6). Throughout gestation, the fine structure of the membrane was

³ Horse-spleen ferritin which was purchased from Nutritional Biochemicals Corporation was first rendered cadmium-free by dialysis against EDTA (Farquhar and Palade, '63).

⁴ "Thorotrast," a colloidal suspension of 25% thorium dioxide, stabilized with dextrin, Tessier and Co., Inc., Detroit, Michigan.

⁵ Durcupan Fluka AC, Buchs SG, Switzerland.

constant. It was composed of ill-defined fibrils which precisely paralleled both each other and the plane of the entire membrane (figs. 1, 2, 3, 6, 12). In certain sections a striated appearance of the membrane was replaced by a stippled appearance (figs. 7, 8, 10). Since the former is characteristic of fibrils which are cut in longitudinal section and the latter of fibrils which are cut in oblique or cross section, the membrane can be regarded as being composed indeed of parallel fibrils, rather than of parallel lamellae. On the trophoblastic side of Reichert's membrane, however, in many sections, there appeared to be a more dense layer about 750 Å wide which delimited this edge of the membrane (figs. 3, 6, 7, 8, 9, 10). Regardless of the orientation of the fibrillar components of the membrane, this layer appeared as a line. Consequently it represented a lamina, or sheet in contradistinction to the rest of the membrane. This lamina appeared consistently to be separated from the plasmalemmata of adjacent trophoblast cells by a layer which was quite uniformly wide at about 500 Å. No comparable dense and light layers were identified adjacent to the parietal endoderm on the opposite side of Reichert's membrane.

In all stages of pregnancy which were examined, i.e., from 12 to 22 days post coitum, the epithelial cells of the parietal yolk-sac endoderm were cuboidal and often were widely separated from each other. Consequently, in many regions, Reichert's membrane was directly exposed to the space which in life was yolk-sac cavity (figs. 2, 3, 6, 8). Where endodermal cells occasionally adjoined, the intercellular junctions were not modified into desmosomes (figs. 1, 4, 9). Cytologically, the endodermal cells exhibited differentiation in association with gestational aging. In the 12-day yolk sacs, endodermal epithelial cells contained both cisterns of rough endoplasmic reticulum which delimited a material of moderate electron density and an abundance of both free ribosomes and of rosettes of ribosomes (fig. 1). The cells were rich in lipid droplets. By the fourteenth day, rough endoplasmic reticulum had increased; lipid droplets were still abundant (fig. 2). At later stages, lipid was not identified, and rough endoplasmic

reticulum was increasingly abundant. In placentas which were taken on the twentieth and twenty-second days of pregnancy, (i.e., shortly before term) within the parietal endodermal cells, the cisterns of endoplasmic reticulum were markedly dilated and contained a flocculent material of little electron density (figs. 6, 9).

In all of the placentas which were examined from 12 to 20 days of pregnancy, the subsurface placental labyrinthine sinuses, through which in life maternal blood circulated, were lined by trophoblastic cells. At these stages, the sinuses and Reichert's membrane were separated by a layer of trophoblast which was variably thick. This trophoblastic layer was discretely cellular; and where intertrophoblastic junctional complexes were identified, attachments were desmosomal (figs. 2, 3, 4, 9, 10). A cytological differentiation with increasing gestational age was apparent in these cellular elements. From day 12 through day 20, there appeared to be an attenuation of the trophoblastic cytoplasm which was related to Reichert's membrane. By day 18 and in later stages, fenestrations in this cytoplasm were evident (figs. 3, 4, 5, 9). The fenestrations which were in direct relation to the Reichert's membrane measured 700–800 Å in diameter; and each was closed by a diaphragm. Often similarly fenestrated wisps of trophoblastic cytoplasm bore no direct relationship to Reichert's membrane (fig. 4). Occasionally, the trophoblastic cytoplasm on the far side of the subsurface maternal blood sinuses appeared fenestrated (fig. 5). In 22-day placentas, the fenestrae were often enlarged, lacked diaphragmata, and appeared to be completely patent (fig. 6).

The placental yolk sac of injected animals. In animals which were given an i.v. injection of cadmium-free ferritin 15 minutes before autopsy, electron dense particles which measured 50–60 Å in diameter were identified within phagosomal profiles in the cytoplasm of the trophoblast which lined the maternal blood sinuses subjacent to Reichert's membrane (fig. 7). Phagocytosed particles which were interpreted as ferritin were also identified within some of the cells of the endodermal epithelium on the side of Reichert's mem-

brane opposite from maternal blood (figs. 8, 9). Occasionally free particles of ferritin were seen within the substance of the membrane itself (fig. 8). There was no apparent variation in the distribution of the particles at different gestational ages. At all stages which were examined, ferritin appeared readily to become incorporated into the trophoblast which was related to Reichert's membrane, to traverse Reichert's membrane and to penetrate the endodermal epithelial cells of the parietal yolk sac.

In animals which 15 minutes prior to autopsy were given an i.v. injection of thorotrast, electron dense shadows which measured 150-300 Å in diameter and which were regarded as representing particles of thorium dioxide were localized both in relation to the plasma membranes of the trophoblast and within phagosomes in the cytoplasm of these cells (figs. 10, 11). In no instance at the stages of gestation which were examined, were thorotrast particles seen to have penetrated Reichert's membrane, nor were they identified within phagosomes of the endodermal epithelium of the parietal yolk-sac.

In animals which were given i.v. injections of both ferritin and thorotrast, again, ferritin was identified in all three layers of the placental parietal yolk sac (i.e., trophoblast, Reichert's membrane and yolk-sac endodermal epithelium). The distribution of thorotrast was restricted to the trophoblastic side of the membrane. Particles of this latter injectate were seen in relation to the plasmalemma of the trophoblast, to trophoblastic phagosomes and occasionally to the trophoblastic side of Reichert's membrane. Occasionally both electron opaque colloids were identified in a given field, often with the particles segregated so that ferritin appeared on the "fetal" (endodermal) side of Reichert's membrane and thorotrast on the "maternal" (blood-trophoblast) side of the membrane (fig. 12).

CONCLUSIONS AND DISCUSSION

Reichert's membrane. Of the three layers of the placental parietal yolk sac, Reichert's membrane appeared to change least during the stages of pregnancy which were examined. It increased in width with increasing age, an observation which,

on the basis of light microscopy, has previously been reported (Wislocki and Padykula, '53). At the light microscopic level, Reichert's membrane has been described as both fibrinous (Kolster, '03) and hyaline (Mossman, '37; Pierce et al., '62). It has been likened to a basement membrane (Grosser, '27). In support of these observations, on the basis of an affinity for PAS, Wislocki and Padykula ('53) found that, like various basement membranes, it contained a glycoprotein, or mucopolysaccharide. However, since toluidine blue did not stain it metachromatically, nor was it basophilic (as it would be, were it acidic), they concluded that it was not composed of sulfated acid mucopolysaccharide. Histochemically it was found to resemble the ocular lens capsule and Decemet's membrane (Wislocki, '52), and to contrast markedly with both of the "basement membranes" of the visceral yolk sac with which it is continuous, viz., the serosal basement membrane and the visceral basement membrane (Wislocki and Padykula, '53).

In its fine structure, Reichert's membrane has been shown also to be unlike either of the basement membranes of the visceral yolk sac. It is less discretely fibrillar than is the serosal basement membrane, which is composed of fine fibrils which exhibit a periodicity which is typical of collagen (Lambson, '66). The visceral basement membrane, on the other hand, like most basement membranes of the light microscopists, is divisible into a thin, amorphous basal lamina and an ill-defined thicker area of closely associated collagen fibrils (Jollie and Jollie, '67). At an electron microscopic level, Reichert's membrane has been described as finely fibrillar, or lamellar, and of uniform appearance throughout its width, both in the rat (Wislocki and Dempsey, '55) and in the mouse (Pierce, Midgley, Sri Ram and Feldman, '62). From the observation that Reichert's membrane appeared fibrillar in some sections and stippled in others, it can be concluded that the membrane is fibrillar, rather than lamellar in organization. Despite histochemical similarities with Decemet's membrane, we have not seen in Reichert's membrane any indication of tropocollagen or of collagen in

ordered arrays of hexagonal figures, as has been described in aging Decemet's membrane (Fawcett, '65).

The origin of Reichert's membrane has long been disputed. Duval (1892) regarded it as an ectodermal (trophoblastic) derivative. Because of the close adherence of the membrane to the surface of trophoblast cells, Wislocki and Padykula ('53) also suggested an ectodermal derivation. On the other hand, the observations of Fawcett ('50) and Fawcett, Wislocki and Waldo ('47) that in primary ectopic implantations in mice a material like Reichert's membrane occasionally differentiated among isolated parietal epithelial cells suggested an endodermal origin. Along the same line, from the observation that a hyaline material which both electron microscopically and immunohistochemically resembled Reichert's membrane was synthesized within cells of a mouse parietal yolk-sac endoderm carcinoma, Pierce, and his co-workers ('62) also concluded that the membrane is derived from endoderm. Although the origin of the membrane can hardly be ascertained by observing its fine structure when already differentiated, it seems pertinent to the controversy to point out that the external, or trophoblastic, edge of the Reichert's membrane consistently exhibited a more dense layer about 750 Å wide which was separated from the plasmalemma of the trophoblast cells by an electron light area which was uniformly wide at about 500 Å. This much of the membrane resembled the basal laminae (viz., lamina densa and lamina lucida) of other epithelia. From its intimate association with the trophoblast, one can conclude that this portion represents a trophoblastic adepthelial laminar complex. The remainder, and greater bulk, of Reichert's membrane undoubtedly is derived from parietal endoderm and may well represent a basal laminar complex of this epithelium, one which lacks a lamina lucida. As a consequence, Reichert's membrane may well represent the fused adepthelial basal laminae of the two germ layers between which it arises.

Recently several workers have investigated the permeability of placental tissues to the electron opaque tracers, ferritin and thorotrast. Both have been identified

within the placental barrier of the chorioallantoic labyrinth; and passage of both appeared to be arrested at the same level (Jollie, '65a). It has also been shown that when ferritin was injected into the maternal circulation, it was as readily incorporated into the apical cytoplasm of the visceral yolk-sac endoderm as when it was injected directly into the uterine lumen (to which the visceral endoderm directly is exposed) (Lambson, '66). Thorotrast, however, has been shown not to be incorporated into the visceral endoderm when injected into the maternal circulation (Jollie and Jollie, '66). It has been shown, however, that thorotrast was picked up rapidly by the visceral endoderm of hamsters when introduced into the uterine lumen, (Carpenter and Ferm, '66). This latter observation was made in animals which were 13, 14, and 15 days pregnant; but in each case the colloid was introduced so that the apices of the visceral cells were directly exposed to the injectate. From these several lines of evidence, one can make the following conclusions. (1) Neither ferritin nor thorotrast traverses the chorioallantoic placental route. (2) When injected into the yolk-sac cavity or *in utero* in late pregnancy, both colloids are incorporated into visceral yolk-sac endodermal epithelium. (3) When injected i.v. into pregnant animals, only ferritin reaches this epithelium.

Our present observations strongly suggest that ferritin is transferred readily across Reichert's membrane, but that thorotrast is not. These results are in accord with the above conclusions; furthermore they lend support to an early realization that this membrane is selective for maternofetal interchange by the yolk-sac placental route (Everett, '35), a realization which was made on the basis of the observation that trypan blue crossed Reichert's membrane, but iron ammonium citrate did not. More recently it has similarly been demonstrated that lithium carmine particles traverse the membrane, but that lampblack does not (Al-Abbass and Schultz, '66).

Parietal yolk-sac trophoblast. Throughout most of pregnancy, the trophoblast which lined the subsurface sinuses of the placental labyrinth intervened between

brane opposite from maternal blood (figs. 8, 9). Occasionally free particles of ferritin were seen within the substance of the membrane itself (fig. 8). There was no apparent variation in the distribution of the particles at different gestational ages. At all stages which were examined, ferritin appeared readily to become incorporated into the trophoblast which was related to Reichert's membrane, to traverse Reichert's membrane and to penetrate the endodermal epithelial cells of the parietal yolk sac.

In animals which 15 minutes prior to autopsy were given an i.v. injection of thorotrast, electron dense shadows which measured 150–300 Å in diameter and which were regarded as representing particles of thorium dioxide were localized both in relation to the plasma membranes of the trophoblast and within phagosomes in the cytoplasm of these cells (figs. 10, 11). In no instance at the stages of gestation which were examined, were thorotrast particles seen to have penetrated Reichert's membrane, nor were they identified within phagosomes of the endodermal epithelium of the parietal yolk-sac.

In animals which were given i.v. injections of both ferritin and thorotrast, again, ferritin was identified in all three layers of the placental parietal yolk sac (i.e., trophoblast, Reichert's membrane and yolk-sac endodermal epithelium). The distribution of thorotrast was restricted to the trophoblastic side of the membrane. Particles of this latter injectate were seen in relation to the plasmalemma of the trophoblast, to trophoblastic phagosomes and occasionally to the trophoblastic side of Reichert's membrane. Occasionally both electron opaque colloids were identified in a given field, often with the particles segregated so that ferritin appeared on the "fetal" (endodermal) side of Reichert's membrane and thorotrast on the "maternal" (blood-trophoblast) side of the membrane (fig. 12).

CONCLUSIONS AND DISCUSSION

Reichert's membrane. Of the three layers of the placental parietal yolk sac, Reichert's membrane appeared to change least during the stages of pregnancy which were examined. It increased in width with increasing age, an observation which,

on the basis of light microscopy, has previously been reported (Wislocki and Padykula, '53). At the light microscopic level, Reichert's membrane has been described as both fibrinous (Kolster, '03) and hyaline (Mossman, '37; Pierce et al., '62). It has been likened to a basement membrane (Grosser, '27). In support of these observations, on the basis of an affinity for PAS, Wislocki and Padykula ('53) found that, like various basement membranes, it contained a glycoprotein, or mucopolysaccharide. However, since toluidine blue did not stain it metachromatically, nor was it basophilic (as it would be, were it acidic), they concluded that it was not composed of sulfated acid mucopolysaccharide. Histochemically it was found to resemble the ocular lens capsule and Decemet's membrane (Wislocki, '52), and to contrast markedly with both of the "basement membranes" of the visceral yolk sac with which it is continuous, viz., the serosal basement membrane and the visceral basement membrane (Wislocki and Padykula, '53).

In its fine structure, Reichert's membrane has been shown also to be unlike either of the basement membranes of the visceral yolk sac. It is less discretely fibrillar than is the serosal basement membrane, which is composed of fine fibrils which exhibit a periodicity which is typical of collagen (Lambson, '66). The visceral basement membrane, on the other hand, like most basement membranes of the light microscopists, is divisible into a thin, amorphous basal lamina and an ill-defined thicker area of closely associated collagen fibrils (Jollie and Jollie, '67). At an electron microscopic level, Reichert's membrane has been described as finely fibrillar, or lamellar, and of uniform appearance throughout its width, both in the rat (Wislocki and Dempsey, '55) and in the mouse (Pierce, Midgley, Sri Ram and Feldman, '62). From the observation that Reichert's membrane appeared fibrillar in some sections and stippled in others, it can be concluded that the membrane is fibrillar, rather than lamellar in organization. Despite histochemical similarities with Decmet's membrane, we have not seen in Reichert's membrane any indication of tropocollagen or of collagen in

brane. Often the cisternal contents appeared finely filamentous.

By light microscopy, it has been observed that cells of parietal endoderm contain numerous PAS positive droplets (Wislocki and Padykula, '53; Pierce et al., '62). Since at the fine structural level, granules which would correspond to these PAS positive bodies have not been identified, and since the cisterns of endoplasmic reticulum often virtually fill the cytoplasm of these cells, it has been suggested that the cisternal content is responsible for the pronounced intracytoplasmic PAS reaction. Since Reichert's membrane, also is strongly positive for PAS (*vide supra*), the suggestion has been made that the cisternal content is a precursor of the membrane (Pierce et al., '62, '63). By immunohistochemistry Pierce and his co-workers ('62) were able to demonstrate specific staining, both of Reichert's membrane and of intracytoplasmic granules which they interpreted to be the cisternal contents of endoplasmic reticulum. This observation they regarded as further evidence that the hyaline of which the membrane is composed is synthesized in the cisterns of parietal cell endoplasmic reticulum. If this is correct, the marked dilatation and focal rarification of the endodermal cisterns which we have observed in 20- and 22-day placentas may indicate a cessation of the synthesis of Reichert's membrane toward the end of pregnancy.

The endodermal cells readily phagocytosed the material (ferritin) which passed through Reichert's membrane from maternal blood. The functional significance of phagocytic activity by these cells is obscure. Since they do not form a continuous layer in relation to Reichert's membrane at any time during pregnancy from day 12 through day 22, they do not afford a pathway for transport by this route. The discontinuity of this layer of cells and the structural isolation, one cell from another, also renders unlikely the suggestion that passage of materials by the yolk-sac placental route is by a "diffusion" directly through the cells of the parietal layer to the cells of the visceral layer with which they are contiguous (Al-Abbass and Schultz, '66). As a consequence of the discontinuity of the parietal cells, passage to

the visceral cells most probably is by diffusion from Reichert's membrane directly across the vitelline cavity.

It appeared that the overall function of the three-layered parietal yolk sac is to regulate passage of materials between maternal blood and yolk-sac cavity. Since in the latest stage of pregnancy which was examined the trophoblastic layer was discontinuous over the external aspect of Reichert's membrane and at all stages appeared readily permeable to both of the tracers which were tested, and since at no stage of pregnancy which was examined did the parietal endoderm present a continuous layer over the internal aspect of the membrane, the only barrier to a free exchange of materials between maternal blood and fetal yolk-sac cavity was Reichert's membrane itself. A comparable direct exposure of the external aspect of Reichert's membrane in the capsular portion of the parietal yolk sac to the maternal blood which circulates within intertrophoblast-giant-cell sinuses of the mouse recently has been described (Reinius, '65b, '67). At late implantation stages in the rat, by virtue of discontinuities of the parietal endoderm of the capsular yolk sac, the internal aspect of Reichert's membrane is comparably naked to the yolk-sac cavity (Enders and Schlafke, '67). Consequently, even at very early stages, Reichert's membrane in its capsular portion apparently serves as the only barrier to an interchange between maternal blood and the contents of the yolk-sac cavity. The data which are presented here indicate that at the placental fetal surface this membrane continues to function as a selectively permeable barrier to such interchange throughout later stages of gestation.

LITERATURE CITED

- Al-Abbass, A. H., and R. L. Schultz 1966 Phagocytic activity of the rat placenta. *J. Anat.*, 100: 349-359.
- Anderson, J. W. 1959 The placental barrier to gamma-globulins in the rat. *Am. J. Anat.*, 104: 403-429.
- Brambell, F. R., and R. Halliday 1956 The route by which passive immunity is transmitted from mother to foetus in the rat. *Proc. Roy. Soc.*, 145: 179-185.
- Brambell, F. R., and W. A. Hemmings 1954 Active transport through embryonic membranes. *Sympos. Soc. Exp. Biol.*, 8: 476-489.

tween maternal blood and Reichert's membrane. The cells of this layer appeared similar to and were contiguous with the outermost trophoblastic investment over the labyrinthine trabeculae, which are considered the structural and functional units of the chorioallantoic placenta of rodents (Jollie, '64; Enders, '65). Like the elements of trabecular trophoblast, the trophoblast which is related to Reichert's membrane in the placental parietal yolk sac is distinctly cellular, attenuates with increasing gestational age, and becomes fenestrated. In both cases, trophoblast cells are contiguous at true desmosomes. Additionally, the cytoplasmic architecture of the trophoblast which anatomically was related to Reichert's membrane more closely resembled that of labyrinthine trophoblast than it did any of the trophoblastic elements within the so-called junctional zone at the maternal surface of the placenta (Jollie, '65b).

Differences between the two types of trophoblast cells can be cited. Most noticeable was the presence of aepithelial basal laminae (lamina lucida and lamina densa) in relation to the trophoblast cells which lined Reichert's membrane; comparable related laminae are lacking from the external trophoblast of the trabeculae. Cells of this latter trophoblast show relatively greater evidence of micropinocytotic activity; although, in experimentally injected animals, phagosomal profiles were often seen in the cytoplasm of the parietal yolk-sac trophoblast cells, relatively few smooth-membrane microvesicular profiles were identified in these cells in uninjected specimens. Trabecular trophoblast cells have been seen to persist as an unbroken lining within the intertrabecular blood sinuses until term (Jollie, '64); in the present study, however, the trophoblast cells of the placental parietal yolk sac were seen to be perforate on the day before term. The evidence which is presented suggests that maternal blood becomes exposed to Reichert's membrane by rupture of the diaphragmata and enlargement of the fenestrae between the twentieth and twenty-second days of pregnancy. Since these patent openings consistently were present in 22-day placentas but were absent in placentas at earlier stages, it is as-

sumed that they are not artifacts which were introduced during preparation of the tissues. This observation is in accord with the conclusion, which was based on light microscopic observations, that maternal blood in the subsurface placental sinuses probably becomes exposed to Reichert's membrane (Anderson, '59).

A progressive thinning of the cytoplasm from days 12 through 18, the appearance, on day 18, of fenestrations which are closed by diaphragmata, and the rupture of the diaphragmata and enlargement of the pores by day 22 all suggest increasing facility for material transport by this route. The results with electron dense tracers, however, do not indicate a greater rate of transport at later stages. As was the case with the outermost trophoblast of the chorioallantoic labyrinthine placental barrier (Jollie, '65a), the trophoblast of the placental parietal yolk sac appeared to offer little resistance to the passage across it of either ferritin or thorotrast. Although thorotrast was blocked from crossing Reichert's membrane, it appeared readily to traverse the thickness of the related trophoblast at all stages of pregnancy.

Parietal endoderm. In none of the placentas which were examined were epithelial cells of the parietal yolk sac at the placental surface seen to form a continuous layer. Where adjacent cells infrequently met, interendodermal junctional complexes were unmodified. In this they are in marked contrast to the cells of the visceral yolk-sac endodermal epithelium which are columnar and contiguous, and which exhibit well-developed terminal bars (Wislocki and Dempsey, '55; Padykula, Deren and Wilson, '66; Lambson, '66).

Our observations indicate that the parietal cells undergo progressive differentiation with increasing gestational age. At the earliest stage which was examined (12 days), although rosettes of free ribosomes were abundant, rough-surfaced endoplasmic reticulum was moderately well developed. Droplets of lipid were present in large numbers until day 16, after which time they were not identified. The cisterns of endoplasmic reticulum which increased in abundance enclosed a material of a density similar to the material of Reichert's mem-

brane. Often the cisternal contents appeared finely filamentous.

By light microscopy, it has been observed that cells of parietal endoderm contain numerous PAS positive droplets (Wislocki and Padykula, '53; Pierce et al., '62). Since at the fine structural level, granules which would correspond to these PAS positive bodies have not been identified, and since the cisterns of endoplasmic reticulum often virtually fill the cytoplasm of these cells, it has been suggested that the cisternal content is responsible for the pronounced intracytoplasmic PAS reaction. Since Reichert's membrane, also is strongly positive for PAS (*vide supra*), the suggestion has been made that the cisternal content is a precursor of the membrane (Pierce et al., '62, '63). By immunohistochemistry Pierce and his co-workers ('62) were able to demonstrate specific staining, both of Reichert's membrane and of intracytoplasmic granules which they interpreted to be the cisternal contents of endoplasmic reticulum. This observation they regarded as further evidence that the hyaline of which the membrane is composed is synthesized in the cisterns of parietal cell endoplasmic reticulum. If this is correct, the marked dilatation and focal rarification of the endodermal cisterns which we have observed in 20- and 22-day placentas may indicate a cessation of the synthesis of Reichert's membrane toward the end of pregnancy.

The endodermal cells readily phagocytosed the material (ferritin) which passed through Reichert's membrane from maternal blood. The functional significance of phagocytic activity by these cells is obscure. Since they do not form a continuous layer in relation to Reichert's membrane at any time during pregnancy from day 12 through day 22, they do not afford a pathway for transport by this route. The discontinuity of this layer of cells and the structural isolation, one cell from another, also renders unlikely the suggestion that passage of materials by the yolk-sac placental route is by a "diffusion" directly through the cells of the parietal layer to the cells of the visceral layer with which they are contiguous (Al-Abbass and Schultz, '66). As a consequence of the discontinuity of the parietal cells, passage to

the visceral cells most probably is by diffusion from Reichert's membrane directly across the vitelline cavity.

It appeared that the overall function of the three-layered parietal yolk sac is to regulate passage of materials between maternal blood and yolk-sac cavity. Since in the latest stage of pregnancy which was examined the trophoblastic layer was discontinuous over the external aspect of Reichert's membrane and at all stages appeared readily permeable to both of the tracers which were tested, and since at no stage of pregnancy which was examined did the parietal endoderm present a continuous layer over the internal aspect of the membrane, the only barrier to a free exchange of materials between maternal blood and fetal yolk-sac cavity was Reichert's membrane itself. A comparable direct exposure of the external aspect of Reichert's membrane in the capsular portion of the parietal yolk sac to the maternal blood which circulates within intertrophoblast-giant-cell sinuses of the mouse recently has been described (Reinius, '65b, '67). At late implantation stages in the rat, by virtue of discontinuities of the parietal endoderm of the capsular yolk sac, the internal aspect of Reichert's membrane is comparably naked to the yolk-sac cavity (Enders and Schlafke, '67). Consequently, even at very early stages, Reichert's membrane in its capsular portion apparently serves as the only barrier to an interchange between maternal blood and the contents of the yolk-sac cavity. The data which are presented here indicate that at the placental fetal surface this membrane continues to function as a selectively permeable barrier to such interchange throughout later stages of gestation.

LITERATURE CITED

- Al-Abbass, A. H., and R. L. Schultz 1966 Phagocytic activity of the rat placenta. *J. Anat.*, 100: 349-359.
- Anderson, J. W. 1959 The placental barrier to gamma-globulins in the rat. *Am. J. Anat.*, 104: 403-429.
- Brambell, F. R., and R. Halliday 1956 The route by which passive immunity is transmitted from mother to foetus in the rat. *Proc. Roy. Soc.*, 145: 179-185.
- Brambell, F. R., and W. A. Hemmings 1954 Active transport through embryonic membranes. *Sympos. Soc. Exp. Biol.*, 8: 476-489.

tween maternal blood and Reichert's membrane. The cells of this layer appeared similar to and were contiguous with the outermost trophoblastic investment over the labyrinthine trabeculae, which are considered the structural and functional units of the chorioallantoic placentas of rodents (Jollie, '64; Enders, '65). Like the elements of trabecular trophoblast, the trophoblast which is related to Reichert's membrane in the placental parietal yolk sac is distinctly cellular, attenuates with increasing gestational age, and becomes fenestrated. In both cases, trophoblast cells are contiguous at true desmosomes. Additionally, the cytoplasmic architecture of the trophoblast which anatomically was related to Reichert's membrane more closely resembled that of labyrinthine trophoblast than it did any of the trophoblastic elements within the so-called junctional zone at the maternal surface of the placenta (Jollie, '65b).

Differences between the two types of trophoblast cells can be cited. Most noticeable was the presence of aepithelial basal laminae (lamina lucida and lamina densa) in relation to the trophoblast cells which lined Reichert's membrane; comparable related laminae are lacking from the external trophoblast of the trabeculae. Cells of this latter trophoblast show relatively greater evidence of micropinocytotic activity; although, in experimentally injected animals, phagosomal profiles were often seen in the cytoplasm of the parietal yolk-sac trophoblast cells, relatively few smooth-membrane microvesicular profiles were identified in these cells in uninjected specimens. Trabecular trophoblast cells have been seen to persist as an unbroken lining within the intertrabecular blood sinuses until term (Jollie, '64); in the present study, however, the trophoblast cells of the placental parietal yolk sac were seen to be perforate on the day before term. The evidence which is presented suggests that maternal blood becomes exposed to Reichert's membrane by rupture of the diaphragmata and enlargement of the fenestrae between the twentieth and twenty-second days of pregnancy. Since these patent openings consistently were present in 22-day placentas but were absent in placentas at earlier stages, it is as-

sumed that they are not artifacts which were introduced during preparation of the tissues. This observation is in accord with the conclusion, which was based on light microscopic observations, that maternal blood in the subsurface placental sinuses probably becomes exposed to Reichert's membrane (Anderson, '59).

A progressive thinning of the cytoplasm from days 12 through 18, the appearance, on day 18, of fenestrations which are closed by diaphragmata, and the rupture of the diaphragmata and enlargement of the pores by day 22 all suggest increasing facility for material transport by this route. The results with electron dense tracers, however, do not indicate a greater rate of transport at later stages. As was the case with the outermost trophoblast of the chorioallantoic labyrinthine placental barrier (Jollie, '65a), the trophoblast of the placental parietal yolk sac appeared to offer little resistance to the passage across it of either ferritin or thorotrast. Although thorotrast was blocked from crossing Reichert's membrane, it appeared readily to traverse the thickness of the related trophoblast at all stages of pregnancy.

Parietal endoderm. In none of the placentas which were examined were epithelial cells of the parietal yolk sac at the placental surface seen to form a continuous layer. Where adjacent cells infrequently met, interendodermal junctional complexes were unmodified. In this they are in marked contrast to the cells of the visceral yolk-sac endodermal epithelium which are columnar and contiguous, and which exhibit well-developed terminal bars (Wislocki and Dempsey, '55; Padykula, Deren and Wilson, '66; Lambson, '66).

Our observations indicate that the parietal cells undergo progressive differentiation with increasing gestational age. At the earliest stage which was examined (12 days), although rosettes of free ribosomes were abundant, rough-surfaced endoplasmic reticulum was moderately well developed. Droplets of lipid were present in large numbers until day 16, after which time they were not identified. The cisterns of endoplasmic reticulum which increased in abundance enclosed a material of a density similar to the material of Reichert's mem-

PLATES

- Bridgman, J. 1948 A morphological study of the development of the placenta of the rat. 1. An outline of the development of the placenta of the white rat. *J. Morph.*, 83: 179-185.
- Carpenter, S. J., and V. H. Ferm 1966 Electron microscopic observations on the uptake and storage of Thorotrast by rodent yolk sac epithelial cells. *Anat. Rec.*, 154: 327-328. (Abstract).
- Deren, J. J., H. A. Padykula and T. H. Wilson 1966 Development of structure and function in the mammalian yolk sac. III. The development of amino acid transport by rabbit yolk sac. *Devel. Biol.*, 13: 370-384.
- Duval, M. 1892 *Le placenta des rongeurs*. 2 vol. Alcan, Paris.
- Enders, A. C. 1965 A comparative study of the fine structure of the trophoblast in several hemochorial placentas. *Am. J. Anat.*, 116: 29-68.
- Enders, A. C., and S. Schlafke 1967 A morphological analysis of the early implantation stages in the rat. *Am. J. Anat.*, 120: 185-226.
- Everett, J. W. 1935 Morphological and physiological studies on the placenta of the albino rat. *J. Exp. Zool.*, 70: 243-284.
- Farquhar, M. G., and G. E. Palade 1961 Glomerular permeability. II. Ferritin transfer across the glomerular capillary wall in nephrotic rats. *J. Exp. Med.*, 114: 699-716.
- Fawcett, D. H. 1950 Development of mouse ova under the capsule of the kidney. *Anat. Rec.*, 108: 71-91.
- 1965 *The Cell: An Atlas of Fine Structure*. Saunders, Philadelphia.
- Fawcett, D. H., G. B. Wislocki and C. M. Waldo 1947 The development of mouse ova in the anterior chamber of the eye and in the abdominal cavity. *Am. J. Anat.*, 81: 413-444.
- Fedinec, A. A. 1962 Observations on the passage of tetanus toxin through the placenta and fetal membranes of the rat. *Lab. Invest.*, 11: 536-543.
- Grosser, O. 1927 *Frühentwicklung, Eihautbildung und Placentation des Menschen und der Säugetiere*. In: *Deutsche Frauenheilkunde*, 5: 1-454. Bergmann, München.
- Jollie, W. P. 1964 Fine structural changes in placental labyrinth of the rat with increasing gestational age. *J. Ultrastruct. Res.*, 10: 27-47.
- 1965a Visualization of a block to placental transport of protein and dextrin in the rat. *Tulane Med. Bull.*, 24: 213-224.
- 1965b Fine structural changes in the junctional zone of the rat placenta with increasing gestational age. *J. Ultrastruct. Res.*, 12: 420-438.
- Jollie, W. P., and L. G. Jollie 1966 Visualization of transport of electron opaque colloids in placental membranes of the rat. In: *Electron Microscopy 1966* (R. Uyeda, editor) Maruzen, Tokyo.
- 1967 Variations in fine structural localization of exogenous peroxidase in rat visceral yolk sac with increasing gestational age. *Anat. Rec.*, 157: 267 (abstract).
- Kolster, R. 1903 *Zur Kenntnis der Embryotrophe beim Vorhandensein einer Decidua Capsularis*. *Anat. Hefte*, 22: 1-58.
- Lambson, R. O. 1966 An electron microscopic visualization of transport across rat visceral yolk sac. *Am. J. Anat.*, 118: 21-32.
- Mayersbach, H. 1958 *Zur Frage des Proteinüberganges von der Mutter zum Foeten. I. Befunde an Ratten am ende der Schwangerschaft*. *Z. Zellforsch.*, 48: 479-504.
- Millonig, G. 1961 A modified procedure for lead staining of thin sections. *J. Biophys. Biochem. Cytol.*, 11: 736-739.
- Mossman, H. W. 1937 Comparative morphogenesis of the fetal membranes and accessory uterine structures. *Carnegie Contrib. to Embryol.*, 26: 129-246.
- Noer, H. R., and H. W. Mossman 1947 Surgical investigation of the function of the inverted yolk sac placenta in the rat. *Anat. Rec.*, 98: 31-37.
- Padykula, H. A., J. J. Deren and T. H. Wilson 1966 Development of structure and function in the mammalian yolk sac. I. Developmental morphology and vitamin B₁₂ uptake of the rat yolk sac. *Devel. Biol.*, 13: 311-348.
- Pierce, G. B., A. R. Midgley and J. Sri Ram 1963 The histogenesis of basement membranes. *J. Exp. Med.*, 117: 339-348.
- Pierce, G. B., A. R. Midgley, J. Sri Ram and J. D. Feldman 1962 Parietal yolk sac carcinoma: a clue to the histogenesis of Reichert's membrane of the mouse embryo. *Am. J. Path.*, 41: 549-566.
- Reinius, S. 1965a Morphology of the mouse embryo from the time of implantation to mesoderm formation. *Z. Zellforsch.*, 68: 711-723.
- 1965b Light and electron microscopy of Reichert's membrane, endoderm and trophoblast during early egg implantation in the mouse. (*Proc. Scandinavian Electr. Micro. Soc. J. Ultrastruct. Res.*, 12: 242 (abstract).
- 1967 Ultrastructure of blastocyst attachment in the mouse. *Z. Zellforsch.*, 77: 257-266.
- Snell, G. D. 1941 In: *Biology of the Laboratory Mouse* (G. D. Snell, editor) Dover, New York.
- Wislocki, G. B. 1952 The anterior segment of the eye of the rhesus monkey investigated by histochemical means. *Am. J. Anat.*, 81: 233-262.
- Wislocki, G. B., and E. W. Dempsey 1955 Electron microscopy of the placenta of the rat. *Anat. Rec.*, 123: 33-63.
- Wislocki, G. B., E. W. Dempsey and H. A. Padykula 1953 Reichert's membrane and the yolk sac of the rat investigated by histochemical means. *Am. J. Anat.*, 92: 117-151.

PLATES

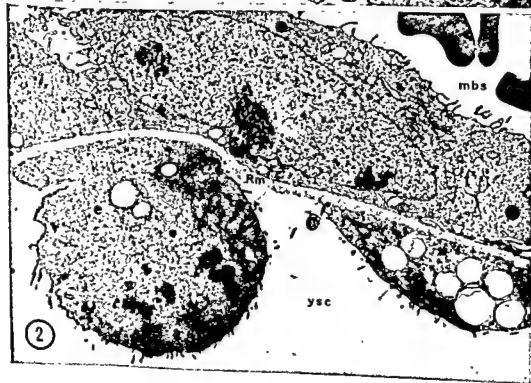
Abbreviations

e, parietal endoderm	t, trophoblast
mbs, maternal blood sinus	ysc, yolk-sac cavity
Rm, Reichert's membrane	

PLATE I

EXPLANATION OF FIGURES

- 1 The parietal yolk sac from a 12-day placenta. In this field, Reichert's membrane appears covered externally by trophoblast and internally by parietal endoderm. At all stages of pregnancy, however, discontinuities in the latter are common. Note that the cisterns of endoplasmic reticulum in the endodermal cells contain a material of a density similar to that of Reichert's membrane. $\times 16,000$.
- 2 Placental parietal yolk sac at 14 days. Note the elaborate development of endoplasmic reticulum within the parietal endoderm, particularly in the cell toward the left which is undergoing mitosis. Lipid droplets, which are still abundant at this stage, are largely leached out during tissue preparation. $\times 4,500$.



Abbreviations

e, parietal endoderm	t, trophoblast
mbs, maternal blood sinus	ysc, yolk-sac cavity
Rm, Reichert's membrane	

PLATE 1

EXPLANATION OF FIGURES

- 1 The parietal yolk sac from a 12-day placenta. In this field, Reichert's membrane appears covered externally by trophoblast and internally by parietal endoderm. At all stages of pregnancy, however, discontinuities in the latter are common. Note that the cisterns of endoplasmic reticulum in the endodermal cells contain a material of a density similar to that of Reichert's membrane. $\times 16,000$.
- 2 Placental parietal yolk sac at 14 days. Note the elaborate development of endoplasmic reticulum within the parietal endoderm, particularly in the cell toward the left which is undergoing mitosis. Lipid droplets, which are still abundant at this stage, are largely leached out during tissue preparation. $\times 4,500$.

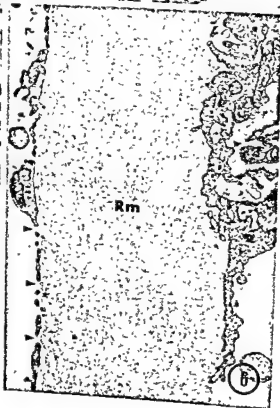
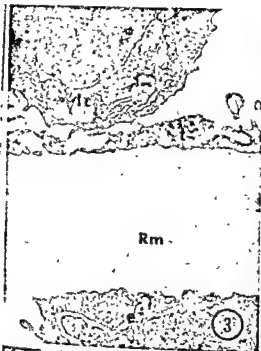


PLATE 2

EXPLANATION OF FIGURES

- 3 18-day placental parietal yolk sac. Note the reduction in thickness of the trophoblast which covers Reichert's membrane. Toward the left, it is seen to be fenestrated. The trophoblastic basal laminar complex (laminae lucida and densa) are seen to advantage in this figure. The cell in the subsurface blood sinus is a maternal lymphocyte (1c). $\times 16,000$.
- 4 In this field of an 18-day placenta, fenestrated cytoplasmic extensions of trophoblast project into the maternal blood sinus. They appear unrelated to Reichert's membrane. $\times 18,000$.
- 5 In another field of an 18-day placenta, the trophoblast on the deep side of the maternal blood sinus appears fenestrated. The fenestrae are cut both in normal and in surface views (arrows). Within the sinus, portions of both a leucocyte (at left) and an erythrocyte (at right) are visible. $\times 16,000$.
- 6 In a 22-day placental parietal yolk sac (the day before term) cisterns of endoplasmic reticulum in the endodermal cells appear focally rarified and markedly dilated. Note also that the parietal yolk-sac trophoblast appears discontinuous over Reichert's membrane at patent pores (arrows). $\times 10,000$.

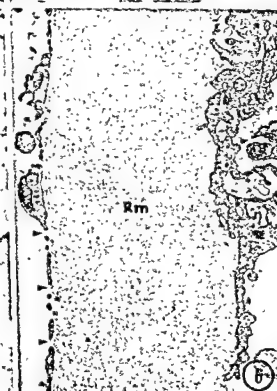
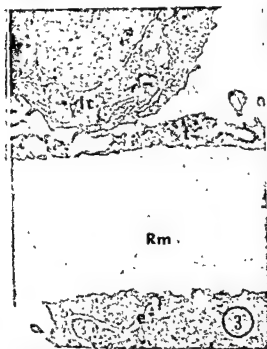


PLATE 3

EXPLANATION OF FIGURES

- 7 A portion of a 16-day placental parietal yolk sac. Two trophoblast cells and the adjacent Reichert's membrane are featured. Fifteen minutes before autopsy, the pregnant animal was injected with ferritin. Ferritin particles can be seen within trophoblastic phagosomal profiles (arrows). $\times 48,000$.
- 8 In another area of the same yolk sac as depicted in figure 7, ferritin particles are seen to be both enclosed within endodermal phagosomes (long arrow) and scattered within Reichert's membrane (short arrows). $\times 30,000$.



PLATE 3

EXPLANATION OF FIGURES

- 7 A portion of a 16-day placental parietal yolk sac. Two trophoblast cells and the adjacent Reichert's membrane are featured. Fifteen minutes before autopsy, the pregnant animal was injected with ferritin. Ferritin particles can be seen within trophoblastic phagosomal profiles (*arrows*). $\times 48,000$.
- 8 In another area of the same yolk sac as depicted in figure 7, ferritin particles are seen to be both enclosed within endodermal phagosomes (*long arrow*) and scattered within Reichert's membrane (*short arrows*). $\times 30,000$.

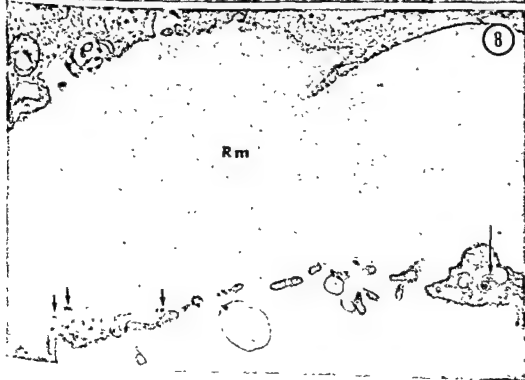


PLATE 4

EXPLANATION OF FIGURES

- 9 A 20-day placental parietal yolk sac from an animal which had been injected with ferritin. Note the abundance of phagosomal ferritin (arrows) in the parietal endodermal cell. At this late stage of pregnancy, although the trophoblast which is related to Reichert's membrane is attenuated and highly fenestrated, it is still intact. Cisterns of endodermal cell endoplasmic reticulum are dilated and focally rarified. Note that interendodermal junctions are unmodified and that intertrophoblastic junctions are made by desmosomal attachments. $\times 18,000$.

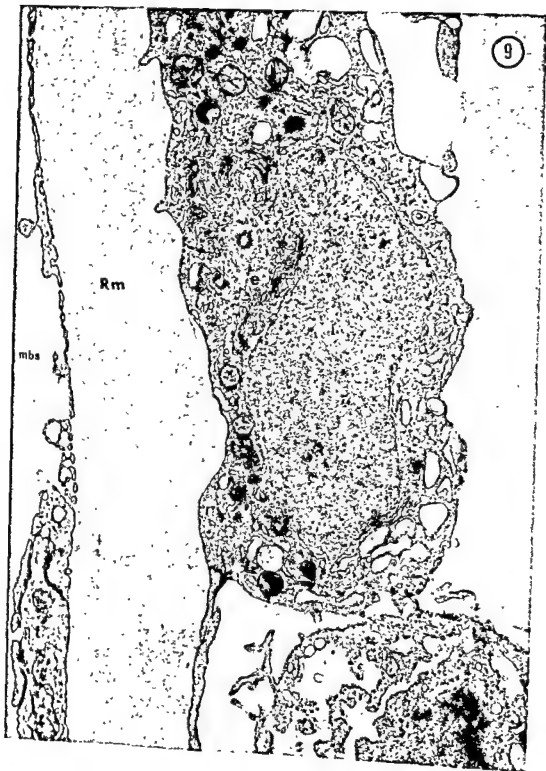


PLATE 5

EXPLANATION OF FIGURES

- 10 A portion of the parietal yolk-sac trophoblastic layer and adjacent Reichert's membrane in a 22-day placenta 15 minutes after thorotrast injection. Particles of thorotrast are seen enclosed within a trophoblastic phagosome. $\times 60,000$.
- 11 A portion of a 14-day placental parietal yolk sac 15 minutes after thorotrast injection. Thorotrast particles can be identified in relation to the trophoblastic plasmalemma. $\times 65,000$.
- 12 A portion of a 12-day placental parietal yolk sac from an animal which was doubly injected before autopsy. Thorotrast particles are in relation to the plasma membrane of the trophoblast cell and within trophoblastic phagosomes. Ferritin particles, on the other hand, have crossed Reichert's membrane and are enclosed within phagosomes (arrows) of the parietal endoderm. $\times 54,000$.

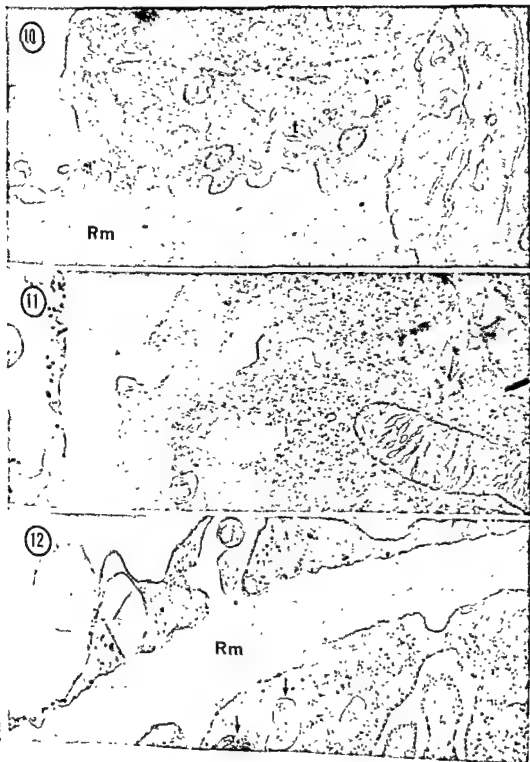


PLATE 5

EXPLANATION OF FIGURES

- 10 A portion of the parietal yolk-sac trophoblastic layer and adjacent Reichert's membrane in a 22-day placenta 15 minutes after thorotrast injection. Particles of thorotrast are seen enclosed within a trophoblastic phagosome. $\times 60,000$.
- 11 A portion of a 14-day placental parietal yolk sac 15 minutes after thorotrast injection. Thorotrast particles can be identified in relation to the trophoblastic plasmalemma. $\times 65,000$.
- 12 A portion of a 12-day placental parietal yolk sac from an animal which was doubly injected before autopsy. Thorotrast particles are in relation to the plasma membrane of the trophoblast cell and within trophoblastic phagosomes. Ferritin particles, on the other hand, have crossed Reichert's membrane and are enclosed within phagosomes (arrows) of the parietal endoderm. $\times 54,000$.

A Comparative Morphologic Study of the Cardiac Innervation in Domestic Animals

I. THE CANINE

JOHN SCOTT McKIBBEN AND ROBERT GETTY

Department of Veterinary Anatomy, Iowa State University, Ames, Iowa

ABSTRACT Cardiac nerves arising from the cervical and thoracic sympathetic chain, the vagi, and the recurrent laryngeal nerves of the dog were described. The findings are correlated with the nomenclature of the NA ('66) and proposals of the NAV ('67), and additional suggestions are made when appropriate. Although individual cardiac nerves were followed to specific areas of the heart, additional supplies to these areas were noted from the cardiac plexus. Sympathetic cardiac innervation arose primarily from the vertebral ganglion. Cranial vagal cardiac nerves on the left and caudal vagal cardiac nerves on the right contributed the majority of the parasympathetic cardiac innervation. Right cardiac nerves ramified primarily along the right coronary artery, left descending branch of the left coronary artery, circumflex branch of the left coronary artery on the left surface of the heart, and onto the right atrium. Left heart nerves, in addition to their direct contributions to all but the last area, proceeded along the circumflex branch of the left coronary artery on the caudal and right surfaces of the heart. Right nerves contributed more in the area of the S.A. node, while left nerves formed a network in the area of the coronary sinus and A.V. node. Both sympathetic and parasympathetic nerves were followed to each area. It was noted that pulmonary innervation via the cardiac plexus would be disturbed by the technique of cardiac denervation referred to as regional neural ablations.

This investigation was undertaken to compare the extrinsic cardiac innervation of the canine, feline, equine, porcine, bovine, ovine, and caprine. In addition, the findings are correlated with the nomenclature of the 1966 *Nomina Anatomica*, that explained by Wreite ('59a,b), the proposed nomenclature for the *Nomina Anatomica Veterinaria* by Schreiber, Frewein, and Walter ('63) and McClure, Schreiber, Walter, Frewein, and DiDio ('67) and the additional suggestions of the present authors and others.

Many investigations on the innervation of the dog heart have been undertaken in the past century. Most studies have been concerned with the intrinsic innervation. Schmiedeberg (1871) first described extrinsic cardiac nerves in the dog. Later Lim Boon Keng (1893) provided a more detailed description of this species, but not until the investigations of Perman ('24), Schurawlew ('28), Nonidez ('39), and Mizeres ('55a,b, '57, '58) were comprehensive studies undertaken in the dog. Veterinary textbooks, with one exception (Miller, Christensen and Evans, '64), have considered the cardiac innervation only very

superficially. The lack of compatibility of the nomenclature between texts and between species leads to confusion.

MATERIAL AND METHODS

Five large lean dogs were embalmed using the formula of the Department of Veterinary Anatomy, Iowa State University. The staining techniques of Perman ('24) and of Saccomano ('43) were tried, but the senior investigator preferred unstained well embalmed cadavers.

The portion of the body caudal to the diaphragm was removed, as were the ribs near their vertebral articulations, using a Stryker autopsy saw and a scalpel. Excess fat, the pericardium, and the lungs were carefully removed. Further dissection proceeded with thumb forceps. Extremely fine nerves were followed with the aid of a Dazor (2), floating arm fluorescent illuminated magnifier or a magna-sighter 3-D binocular eye loupe.

RESULTS

A. *Thoracic ganglia and cardiac nerves.* Independent THORACIC GANGLIA were present bilaterally in each intercostal space

A Comparative Morphologic Study of the Cardiac Innervation in Domestic Animals

1. THE CANINE

JOHN SCOTT McKIBBEN and ROBERT GETTY

Department of Veterinary Anatomy, Iowa State University, Ames, Iowa

ABSTRACT Cardiac nerves arising from the cervical and thoracic sympathetic chain, the vagi, and the recurrent laryngeal nerves of the dog were described. The findings are correlated with the nomenclature of the NA ('66) and proposals of the NAV ('67), and additional suggestions are made when appropriate. Although individual cardiac nerves were followed to specific areas of the heart, additional supplies to these areas were noted from the cardiac plexus. Sympathetic cardiac innervation arose primarily from the vertebral ganglion. Cranial vagal cardiac nerves on the left and caudal vagal cardiac nerves on the right contributed the majority of the parasympathetic cardiac innervation. Right cardiac nerves ramified primarily along the right coronary artery, left descending branch of the left coronary artery, circumflex branch of the left coronary artery on the left surface of the heart, and onto the right atrium. Left heart nerves, in addition to their direct contributions to all but the last area, proceeded along the circumflex branch of the left coronary artery on the caudal and right surfaces of the heart. Right nerves contributed more in the area of the SA node, while left nerves formed a network in the area of the coronary sinus and A.V. node. Both sympathetic and parasympathetic nerves were followed to each area. It was noted that pulmonary innervation via the cardiac plexus would be disturbed by the technique of cardiac denervation referred to as regional neural ablations.

This investigation was undertaken to compare the extrinsic cardiac innervation of the canine, feline, equine, porcine, bovine, ovine, and caprine. In addition, the findings are correlated with the nomenclature of the 1966 *Nomina Anatomica*, that explained by Wrete ('59a,b), the proposed nomenclature for the *Nomina Anatomica Veterinaria* by Schreiber, Frewein, and Walter ('63) and McClure, Schreiber, Walter, Frewein, and DiDio ('67) and the additional suggestions of the present authors and others.

Many investigations on the innervation of the dog heart have been undertaken in the past century. Most studies have been concerned with the intrinsic innervation. Schmiedeberg (1871) first described extrinsic cardiac nerves in the dog. Later Lim Boon Keng (1893) provided a more detailed description of this species, but not until the investigations of Perman ('24), Schurawlew ('28), Nonidez ('39), and Mizceres ('55a,b, '57, '58) were comprehensive studies undertaken in the dog. Veterinary textbooks, with one exception (Miller, Christensen and Evans, '64), have considered the cardiac innervation only very

superficially. The lack of compatibility of the nomenclature between texts and between species leads to confusion.

MATERIAL AND METHODS

Five large lean dogs were embalmed using the formula of the Department of Veterinary Anatomy, Iowa State University. The staining techniques of Perman ('24) and of Saccomano ('43) were tried, but the senior investigator preferred unstained well embalmed cadavers.

The portion of the body caudal to the diaphragm was removed, as were the ribs near their vertebral articulations, using a Stryker autopsy saw and a scalpel. Excess fat, the pericardium, and the lungs were carefully removed. Further dissection proceeded with thumb forceps. Extremely fine nerves were followed with the aid of a Dazor (2), floating arm fluorescent illuminated magnifier or a magna-sighter 3-D binocular eye loupe.

RESULTS

A. Thoracic ganglia and cardiac nerves. Independent THORACIC GANGLIA were present bilaterally in each intercostal space

caudal to and including the third or fourth intercostal space. They were quite uniform in size, measuring about 3 mm craniocaudal by 2 mm dorsoventral by 1 mm mediolateral. In the majority of the specimens nerves could be followed from these ganglia to the great vessels, esophagus, and lungs, but not directly to the heart. In two specimens, however, *thoracic cardiac nerves* arose from the LEFT third through eighth thoracic ganglia, joined, and followed the bronchoesophageal artery cranioventral between the esophagus and aorta. They continued over the left primary bronchus and entered the cardiac plexus. In one specimen thoracic cardiac nerves arose from the right third through fifth thoracic ganglia, and followed the right vena azygos, then the cranial vena cava, to the lateral face of the right atrium where they ramified.

B. Cervicothoracic ganglia and cardiac nerves. On each side the CAUDAL CERVICAL GANGLION and first two or three THORACIC GANGLIA fused to form the CERVICO-THORACIC (stellate) GANGLION. This lay on the lateral surface of the longus colli muscle, extending from the cranial border of the first intercostal space to the caudal border of the second intercostal space.

Rami communicantes were present between this ganglion and at least the first four thoracic spinal nerves. Cranially, rami, extended via the vertebral nerve (*nervus transversarius*) to join the seventh through the second cervical spinal nerves. A ramus communicans to the eighth cervical spinal nerve arose independently from this ganglion. The cervicothoracic ganglia were approximately the same size (table 1). Cervicothoracic cardiac nerves arose from the cranial and caudal portions of this ganglion. A LEFT cranial cervicothoracic cardiac nerve followed the cranial limb of the ansa subclavia, then joined the left craniomedial vertebral cardiac nerve with which it passed to the heart as described for the latter nerve. Between two and six LEFT caudal cervicothoracic cardiac nerves were noted. One sometimes joined the left thoracic cardiac nerves. The others passed caudally on the brachiocephalic artery, across the left lateral face of the aorta to supply the foregoing vessels and then entered the cardiac plexus. RIGHT cranial cervicothoracic cardiac nerves were not observed. RIGHT caudal cervicothoracic cardiac nerves usually followed the caudal limb of the ansa subclavia to its ventral limit. Here they branched, joining the

TABLE 1
Canine: dimensions of the ansa subclavia and of the ganglia of origin for cardiac nerves in millimeters

Canine number	Approximate canine weight in pounds	Cervicothoracic ganglion						Vertebral ganglion					
		Left			Right			Left			Right		
		C-C	D-V	M-L	C-C	D-V	M-L	C-C	D-V	M-L	C-C	D-V	M-L
1	90	30	7	3	35	6	2	15	4	3	10	3	2
2	60	25	4	2	25	3	1	15	4	3	10	3	2
3	30	20	4	3	20	4	3	10	5	2	5	3	2
4	35	20	3	2	25	4	1	10	3	2	7	3	2
5	35	15	4	2	20	4	2	6	3	2	7	3	2

Canine number	Approximate canine weight in pounds	Ansa subclavia							
		Left				Right			
		Length		Width		Length		Width	
		Cranial limb	Caudal limb	Cranial limb	Caudal limb	Cranial limb	Caudal limb	Cranial limb	Caudal limb
1	90	25	25	2	2	45	50	2	2
2	60	30	30	1	2	45	55	1	1
3	30	21	24	2	1	30	35	2	2
4	35	15	18	3	1	20	33	2	2
5	35	23	25	1	1	25	40	1	2

C-C, Craniocaudal; D-V, Dorsoventral; M-L, Mediolateral.

TABLE 2
Distribution of cardiac nerves in the canine

Nerves	Side	Along right coronary artery	Along the descending and circumflex branches of the left coronary artery on the left side ¹	Along the circumflex branch of the left coronary artery caudally and on the right side ²	Between the cranial and caudal venae cavae ³	Between the caudal vena cava and left atrium ⁴	Cardiac plexus
Thoracic cardiac nerves	left	—	—	—	—	—	+
	right	—	—	—	+	—	—
Cervicothoracic cardiac nerves	left	+	+	+	—	+	+
	right	+	+	+	—	—	—
Intermediate cardiac nerves	left	—	—	—	—	—	—
	right	—	—	—	—	—	—
Vertebral cardiac nerves	left	+	+	+	+	+	+
	right	+	+	+	+	+	+
Middle cervical cardiac nerves	left	—	—	—	—	—	—
	right	—	—	—	—	—	—
Cranial cervical cardiac nerves	left	—	—	—	—	—	—
	right	—	—	—	—	—	—
Cranial vagal cardiac nerves	left	+	+	+	—	+	+
	right	+	+	+	+	+	+
Caudal vagal cardiac nerves	left	—	—	—	—	—	—
	right	—	—	—	—	—	—
Recurrent cardiac nerves	left	+	+	+	+	+	+
	right	+	+	+	+	+	+

—, not followed to this area; +, some may supply this area; ++, moderate supply to the area; +++, major supply to the area.

¹ Main distribution includes the right auricle, atrium, and ventricle.

² Main distribution includes the left auricle, left ventricle on the left side, left interventricular septum and the left cranial portion of the right ventricle.

³ Main distribution includes the dorsum of the left auricle, ventrum of the left atrium, caudal and right sides of the left ventricle, right interatrial and interventricular septa and caudal right surface of the right ventricle.

⁴ Main distribution includes the lateral right atrial wall towards the sinoatrial node and sometimes the extension across the coronary groove into the right longitudinal sulcus.

⁵ Main distribution may include the left atrium, right atrium, right side of the left ventricle, interatrial and interventricular septa on the right side, and the right caudal portion of the right ventricle.

⁶ Main distribution to the dorsal atrial walls, great vessels, and intermingling of incoming branches which may then pass with major branches to the other five areas.

caudal to and including the third or fourth intercostal space. They were quite uniform in size, measuring about 3 mm craniocaudal by 2 mm dorsoventral by 1 mm mediolateral. In the majority of the specimens nerves could be followed from these ganglia to the great vessels, esophagus, and lungs, but not directly to the heart. In two specimens, however, *thoracic cardiac nerves* arose from the LEFT third through eighth thoracic ganglia, joined, and followed the bronchoesophageal artery cranioventral between the esophagus and aorta. They continued over the left primary bronchus and entered the cardiac plexus. In one specimen thoracic cardiac nerves arose from the right third through fifth thoracic ganglia, and followed the right vena azygos, then the cranial vena cava, to the lateral face of the right atrium where they ramified.

B. Cervicothoracic ganglia and cardiac nerves. On each side the CAUDAL CERVICAL GANGLION and first two or three THORACIC GANGLIA fused to form the CERVICO-THORACIC (stellate) GANGLION. This lay on the lateral surface of the longus colli muscle, extending from the cranial border of the first intercostal space to the caudal border of the second intercostal space.

Rami communicantes were present between this ganglion and at least the first four thoracic spinal nerves. Cranially, rami, extended via the vertebral nerve (*nervus transversarius*) to join the seventh through the second cervical spinal nerves. A ramus communicans to the eighth cervical spinal nerve arose independently from this ganglion. The cervicothoracic ganglia were approximately the same size (table 1). Cervicothoracic cardiac nerves arose from the cranial and caudal portions of this ganglion. A LEFT cranial cervicothoracic cardiac nerve followed the cranial limb of the ansa subclavia, then joined the left craniomedial vertebral cardiac nerve with which it passed to the heart as described for the latter nerve. Between two and six LEFT caudal cervicothoracic cardiac nerves were noted. One sometimes joined the left thoracic cardiac nerves. The others passed caudally on the brachiocephalic artery, across the left lateral face of the aorta to supply the foregoing vessels and then entered the cardiac plexus. RIGHT cranial cervicothoracic cardiac nerves were not observed. RIGHT caudal cervicothoracic cardiac nerves usually followed the caudal limb of the ansa subclavia to its ventral limit. Here they branched, joining the

TABLE 1
Canine: dimensions of the ansa subclavia and of the ganglia of origin for cardiac nerves in millimeters

Canine number	Approximate canine weight in pounds	Cervicothoracic ganglion									Vertebral ganglion					
		Left						Right			Left			Right		
		C-C	D-V	M-L	C-C	D-V	M-L	C-C	D-V	M-L	C-C	D-V	M-L	C-C	D-V	M-L
1	90	30	7	3	35	6	2	15	4	3	10	3	2			
2	60	25	4	2	25	3	1	15	4	3	10	3	2			
3	30	20	4	3	20	4	3	10	5	2	5	3	2			
4	35	20	3	2	25	4	1	10	3	2	7	3	2			
5	35	15	4	2	20	4	2	6	3	2	7	3	2			

Canine number	Approximate canine weight in pounds	Ansa subclavia							
		Left				Right			
		Length		Width		Length		Width	
		Cranial limb	Caudal limb	Cranial limb	Caudal limb	Cranial limb	Caudal limb	Cranial limb	Caudal limb
1	90	25	25	2	2	45	50	2	2
2	60	30	30	1	2	45	55	1	1
3	30	21	24	2	1	30	35	2	2
4	35	15	18	3	1	20	33	2	2
5	35	23	25	1	1	25	40	1	2

C-C, Craniocaudal; D-V, Dorsoventral; M-L, Mediolateral.

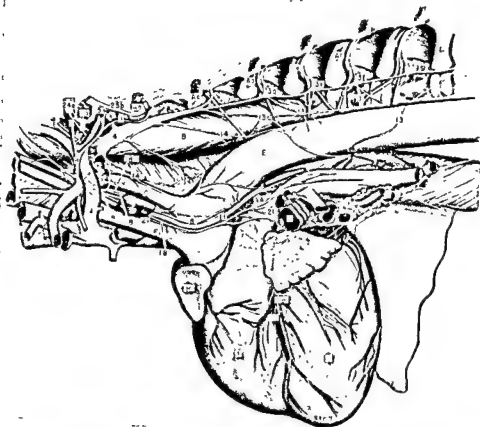


Fig 1 Canine Left lateral view of the cardiac nerves and related ganglia.

the aorta and pulmonary trunk, and continued mainly between the left auricle and left pulmonary veins to the coronary groove caudally. Branches continued to the right side and cranially along the circumflex branch of the left coronary artery into the right longitudinal sulcus. Along this course it gave twigs to the caudodorsal portion of the left auricle, ventrum of the left atrium, caudal and right sides of the left ventricle, interatrial and interventricular septa and right caudal portion of the right ventricle. Branches of the left caudolateral vertebral cardiac nerve, which did not continue along this main course, in addition to sending twigs to the aorta and pulmonary artery, primarily entered the cardiac plexus near the ligamentum arteriosum. The LEFT caudomedial vertebral cardiac nerve passed over the lateral face of the aorta to the area of the

ligamentum arteriosum and ramified around this structure onto the aorta and pulmonary artery as well as into the cardiac plexus. Another twig from this nerve was followed to the origin of the right and left coronary arteries and along their courses with the more important combined right cardiac nerves. The LEFT cranio-medial vertebral cardiac nerve coursed caudally, ventral to the esophagus and trachea and continued between the left subclavian artery and brachiocephalic trunk to the right side, after combining with the left dorsal vertebral cardiac nerve, and ramified in the cardiac plexus. The largest branch was followed through the plexus and back to the left side caudal to the aorta. It continued between the aorta and pulmonary artery just caudal to the ligamentum arteriosum and ventrally into the left coronary groove and left longi-

right vertebral, vagal, and recurrent cardiac nerves as well as passing directly to the cranial vena cava and extending into the cardiac plexus.

On each side the cranial and caudal limbs of the ANSA SUBCLAVIA arose singly from the cervicothoracic ganglion, passed on the respective sides of the subclavian artery and joined the vertebral ganglion. The right limbs were longer than the left ones and the caudal limb longer than the cranial one on the right side (table 1). Cervicothoracic cardiac nerves often followed these limbs a variable distance before passing to the heart.

C. Cervical ganglia and cardiac nerves. Each VERTEBRAL GANGLION lay bilaterally cranioventral to the origin of the vertebral artery from the subclavian artery on the dorsolateral surface of the carotid artery in an intimate association with the vagus nerve. The left ganglion measured slightly larger than the right (table 1). Nerves arising from the vertebral ganglia contribute the greatest sympathetic innervation to the dog's heart. Four LEFT vertebral cardiac nerves were generally present.

The LEFT caudolateral vertebral cardiac nerve coursed caudally with the left vagus nerve, passed over the left lateral face of

Abbreviations

- | | |
|--|---|
| 1: Ramus communicans | 26: Vascular nerve |
| 2: Sympathetic trunk | 28: Cardiac plexus |
| 3c: Third thoracic ganglion | 29: Inferior (nodose) ganglion of the vagus nerve |
| 3d: Fourth thoracic ganglion | Aa: First rib |
| 3e: Fifth thoracic ganglion | Ab: Second rib |
| 3f: Sixth thoracic ganglion | Ac: Third rib |
| 3g: Seventh thoracic ganglion | Ad: Fourth rib |
| 3h: Eighth thoracic ganglion | Ae: Fifth rib |
| 4: Cervicothoracic ganglion | Af: Sixth rib |
| 5: Ansa subclavia (caudal limb) | Ag: Seventh rib |
| 5': Ansa subclavia (cranial limb) | B: Longus colli muscle |
| 8: Vertebral ganglion | C: Esophagus |
| 10: Cranial cervical ganglion | D: Intercostal artery |
| 11: Vagus nerve | D': Intercostal vein |
| 12: Right recurrent laryngeal nerve | E: Aorta |
| 12': Left recurrent laryngeal nerve | F: Brachiocephalic artery |
| 13: Thoracic cardiac nerve | G': Left subclavian artery |
| 14: Cranial cervicothoracic cardiac nerve | G'': Right subclavian artery |
| 14': Caudodorsal cervicothoracic cardiac nerve | H: Costocervical artery |
| 14'': Caudovertral cervicothoracic cardiac nerve | I: Transverse colli artery (dorsal artery) |
| 16: Vertebral nerve | J: Supreme intercostal artery (subcostal artery) |
| 18: Cranial vertebral cardiac nerve | K: Vertebral artery |
| 18': Caudal vertebral cardiac nerve | L: Deep cervical artery |
| 18'': Caudomedial vertebral cardiac nerve | M': Costocervico-vertebral vein |
| 18''': Caudolateral vertebral cardiac nerve | N': Left common carotid artery |
| 18''': Dorsal vertebral cardiac nerve | N'': Right common carotid artery |
| 21: Cranial vagal cardiac nerve | O: Right vena azygos |
| 21': Caudal vagal cardiac nerve | P: Cranial vena cava |
| 22: Recurrent cardiac nerve | Q: Caudal vena cava |
| 24a: Eighth cervical spinal nerve | R: Right atrium |
| 24b: Seventh cervical spinal nerve | R': Right auricle |
| 24c: Sixth cervical spinal nerve | S': Left auricle |
| 24d: Fifth cervical spinal nerve | T: Right ventricle |
| 24e: Fourth cervical spinal nerve | U: Left ventricle |
| 24f: Third cervical spinal nerve | W: Trachea |
| 24g: Second cervical spinal nerve | X: Bronchus |
| 25a: First thoracic spinal nerve | Y: Pulmonary artery |
| 25b: Second thoracic spinal nerve | Y': Pulmonary vein |
| 25c: Third thoracic spinal nerve | Z: Lung |
| 25d: Fourth thoracic spinal nerve | AA: Ligamentum arteriosum |
| 25e: Fifth thoracic spinal nerve | BB: Right coronary artery |
| 25f: Sixth thoracic spinal nerve | BB': Descending branch of left coronary artery |
| 25g: Seventh thoracic spinal nerve | BB'': Circumflex branch of left coronary artery |
| 25h: Eighth thoracic spinal nerve | CC: Great cardiac vein |

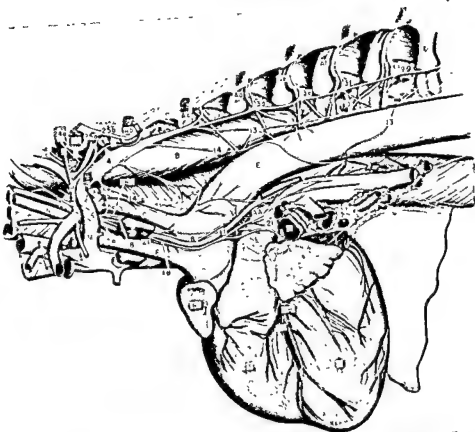


Fig. 1 Canine: Left lateral view of the cardiac nerves and related ganglia.

the aorta and pulmonary trunk, and continued mainly between the left auricle and left pulmonary veins to the coronary groove caudally. Branches continued to the right side and cranially along the circumflex branch of the left coronary artery into the right longitudinal sulcus. Along this course it gave twigs to the caudodorsal portion of the left auricle, ventrum of the left atrium, caudal and right sides of the left ventricle, interatrial and interventricular septa and right caudal portion of the right ventricle. Branches of the left caudolateral vertebral cardiac nerve, which did not continue along this main course, in addition to sending twigs to the aorta and pulmonary artery, primarily entered the cardiac plexus near the ligamentum arteriosum. The **LEFT caudomedial vertebral cardiac nerve** passed over the lateral face of the aorta to the area of the

ligamentum arteriosum and ramified around this structure onto the aorta and pulmonary artery as well as into the cardiac plexus. Another twig from this nerve was followed to the origin of the right and left coronary arteries and along their courses with the more important combined right cardiac nerves. The **LEFT cranio-medial vertebral cardiac nerve** coursed caudally, ventral to the esophagus and trachea and continued between the left subclavian artery and brachiocephalic trunk to the right side, after combining with the left dorsal vertebral cardiac nerve, and ramified in the cardiac plexus. The largest branch was followed through the plexus and back to the left side caudal to the aorta. It continued between the aorta and pulmonary artery just caudal to the ligamentum arteriosum and ventrally into the left coronary groove and left longi-

right vertebral, vagal, and recurrent cardiac nerves as well as passing directly to the cranial vena cava and extending into the cardiac plexus.

On each side the cranial and caudal limbs of the ANSA SUBCLAVIA arose singly from the cervicothoracic ganglion, passed on the respective sides of the subclavian artery and joined the vertebral ganglion. The right limbs were longer than the left ones and the caudal limb longer than the cranial one on the right side (table 1). Cervicothoracic cardiac nerves often followed these limbs a variable distance before passing to the heart.

C. Cervical ganglia and cardiac nerves. Each VERTEBRAL GANGLION lay bilaterally cranioventral to the origin of the vertebral artery from the subclavian artery on the dorsolateral surface of the carotid artery in an intimate association with the vagus nerve. The left ganglion measured slightly larger than the right (table 1). Nerves arising from the vertebral ganglia contribute the greatest sympathetic innervation to the dog's heart. Four LEFT vertebral cardiac nerves were generally present.

The LEFT caudolateral vertebral cardiac nerve coursed caudally with the left vagus nerve, passed over the left lateral face of

Abbreviations

- | | |
|--|---|
| 1: Ramus communicans | 26: Vascular nerve |
| 2: Sympathetic trunk | 28: Cardiac plexus |
| 3c: Third thoracic ganglion | 29: Inferior (nodose) ganglion of the vagus nerve |
| 3d: Fourth thoracic ganglion | Aa: First rib |
| 3e: Fifth thoracic ganglion | Ab: Second rib |
| 3f: Sixth thoracic ganglion | Ac: Third rib |
| 3g: Seventh thoracic ganglion | Ad: Fourth rib |
| 3h: Eighth thoracic ganglion | Ae: Fifth rib |
| 4: Cervicothoracic ganglion | Af: Sixth rib |
| 5: Ansa subclavia (caudal limb) | Ag: Seventh rib |
| 5': Ansa subclavia (cranial limb) | B: Longus colli muscle |
| 8: Vertebral ganglion | C: Esophagus |
| 10: Cranial cervical ganglion | D: Intercostal artery |
| 11: Vagus nerve | D': Intercostal vein |
| 12: Right recurrent laryngeal nerve | E: Aorta |
| 12': Left recurrent laryngeal nerve | F: Brachiocephalic artery |
| 13: Thoracic cardiac nerve | G': Left subclavian artery |
| 14: Cranial cervicothoracic cardiac nerve | G'': Right subclavian artery |
| 14': Caudodorsal cervicothoracic cardiac nerve | H: Costocervical artery |
| 14'': Caudoventral cervicothoracic cardiac nerve | I: Transverse colli artery (dorsal artery) |
| 16: Vertebral nerve | J: Supreme intercostal artery (subcostal artery) |
| 18: Cranial vertebral cardiac nerve | K: Vertebral artery |
| 18': Caudal vertebral cardiac nerve | L: Deep cervical artery |
| 18'': Caudomedial vertebral cardiac nerve | M': Costocervico-vertebral vein |
| 18''': Caudolateral vertebral cardiac nerve | N: Left common carotid artery |
| 18''': Dorsal vertebral cardiac nerve | N': Right common carotid artery |
| 21: Cranial vagal cardiac nerve | O: Right vena azygos |
| 21': Caudal vagal cardiac nerve | P: Cranial vena cava |
| 22: Recurrent cardiac nerve | Q: Caudal vena cava |
| 24a: Eighth cervical spinal nerve | R: Right atrium |
| 24b: Seventh cervical spinal nerve | R': Right auricle |
| 24c: Sixth cervical spinal nerve | S': Left auricle |
| 24d: Fifth cervical spinal nerve | T: Right ventricle |
| 24e: Fourth cervical spinal nerve | U: Left ventricle |
| 24f: Third cervical spinal nerve | V: Trachea |
| 24g: Second cervical spinal nerve | X: Bronchus |
| 25a: First thoracic spinal nerve | Y: Pulmonary artery |
| 25b: Second thoracic spinal nerve | Y': Pulmonary vein |
| 25c: Third thoracic spinal nerve | Z: Lung |
| 25d: Fourth thoracic spinal nerve | AA: Ligamentum arteriosum |
| 25e: Fifth thoracic spinal nerve | BB: Right coronary artery |
| 25f: Sixth thoracic spinal nerve | BB': Descending branch of left coronary artery |
| 25g: Seventh thoracic spinal nerve | BB'': Circumflex branch of left coronary artery |
| 25h: Eighth thoracic spinal nerve | CC: Great cardiac vein |

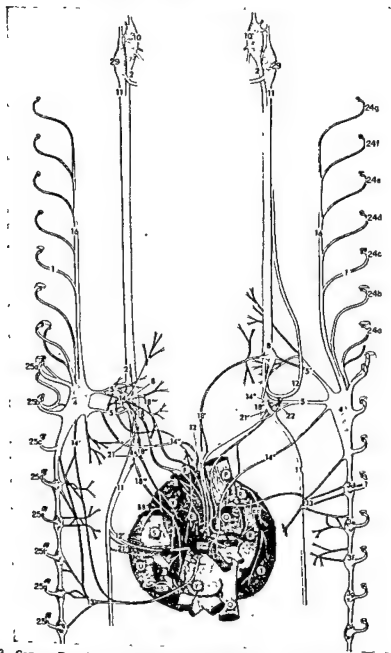


Fig. 3 Canine Dorsal view of the cardiac innervation. The sympathetic trunks and vagi are reflected laterally.

lowed the right vagus nerve to the caudal surface of the subclavian artery where it was joined by the right recurrent, right cervicothoracic, and the right caudal vagal cardiac nerves. The combined trunk passed

between the cranial vena cava and aorta and entered the cardiac plexus. The main continuation through the plexus passed around the caudal border of the aorta to the left side where it joined and followed the

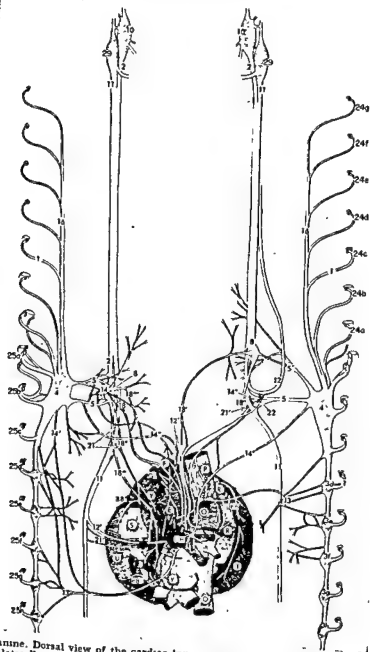


Fig 3 Canine. Dorsal view of the cardiac innervation. The sympathetic trunks and vagi are reflected laterally.

lowed the right vagus nerve to the caudal surface of the subclavian artery where it was joined by the right recurrent, right cervicothoracic, and the right caudal cardiac nerves. The combined trunk passed

between the cranial vena cava and aorta and entered the cardiac plexus. The main continuation through the plexus passed around the caudal border of the aorta to the left side where it joined and followed the

coronary arteries. Areas of distribution included the right ventral portion of the right atrium, right ventricle, left side of the left ventricle, ventrum of the left auricle, and interventricular septum. Another branch of the combined right cardiac nerves passed between the venae cavae to the right atrium where it radiated toward the terminal sulcus. Twigs also extended between the caudal vena cava and left atrium to the coronary groove as well as cranially onto the right atrium.

No independent MIDDLE CERVICAL or INTERMEDIATE GANGLIA were noted grossly in the canine. Each CRANIAL CERVICAL GANGLION lay in close apposition to the vagus nerves ventral to the tympanic bulla. They appeared fusiform, averaging about 13 mm in length by 4 mm in diameter. In the cervical region between the vertebral and cranial cervical ganglia each vagus nerve and respective sympathetic trunk were bound in a common connective tissue sheath forming vagosympathetic trunks approximately 5 mm in width.

D. Vagal cardiac nerves. Fine cranial vagal cardiac nerves arose from the LEFT vagus nerve near the left vertebral ganglion and joined the left vertebral cardiac nerves. The largest passed with the left caudomedial vertebral cardiac nerve. Two or three additional cranial vagal cardiac nerves which originated between the left vertebral ganglion and the origin of the left recurrent laryngeal nerve also joined this nerve. From this latter area another nerve joined the left caudolateral vertebral cardiac nerve passing with it to the caudal portion of the left auricle, caudal and right surfaces of the left ventricle, ventrum of the left atrium, interatrial and interventricular septa, and caudal portion of the right ventricle. With the other left vertebral cardiac nerves and the left cervicothoracic nerves, left cranial vagal cardiac nerves passed to the cardiac plexus, with main branches extending to the left side of the right and left ventricles, right side of the right ventricle and ventrum of the right auricle. Near the origin of the right vertebral cardiac nerves small RIGHT cranial vagal cardiac nerves joined the former and accompanied them to their destinations along the coronary arteries or between the venae cavae onto the right atrium.

Usually one or two LEFT caudal vagal cardiac nerves passed cranioventral between the pulmonary artery and left primary bronchus to the cardiac plexus. Between two and five RIGHT caudal vagal cardiac nerves arose from the right vagus nerve within 3 cm caudal to the right subclavian artery. One immediately combined with the more dorsal right caudal vertebral cardiac nerve and right recurrent cardiac nerve which it accompanied along the coronary arteries and between the venae cavae, or around the caudal vena cava to ramify in the coronary groove and onto the right atrium. The remaining nerves joined the more ventral right cardiac nerve or passed directly to the cardiac plexus.

E. Recurrent cardiac nerves. The left recurrent laryngeal nerve gave several small LEFT recurrent cardiac nerves to the cardiac plexus, after reaching the right caudal surface of the aorta. One passed caudomedial between the left branch of the pulmonary artery and the left pulmonary veins, then between the latter and the left auricle to the caudal coronary groove. It then accompanied the other autonomic nerves to the right side and cranially along the course of the circumflex branch of the left coronary artery. On entering the cardiac plexus, the left recurrent laryngeal nerve often lost its identity, but reformed into a single trunk cranial to the plexus. It communicated with the right vertebral, caudal vagal, and recurrent cardiac nerves after reforming. One or two RIGHT recurrent cardiac nerves arose from the right recurrent laryngeal nerve. They coursed caudoventrally and united after a short distance with the right vertebral or caudal vagal cardiac nerves which they accompanied along the coronary arteries and between the venae cavae to supply the right atrium. Some twigs passed around the caudal vena cava to the coronary groove and cranially onto the right atrium.

DISCUSSION

Variations in the thoracic cardiac nerves occur in the dog. Perman ('24), and Mizeres ('55a) found no thoracic cardiac nerves. Schurawlew ('28) and Nonidez ('39) reported them as being from the left side only. The present findings, like

those of Ionescu and Enachescu ('28), were that though inconsistent morphologically, both right and left thoracic cardiac nerves occur in the dog.

The cervicothoracic ganglion was formerly called the stellate ganglion by most authors; however, Mannu ('14) referred to the vertebral ganglion as the stellate ganglion. Because this descriptive term does not apply uniformly in all species the term cervicothoracic, used first by Hardesty ('33), is the most useful for describing the united caudal cervical and a variable number of thoracic ganglia. Rami communicantes from the cervicothoracic ganglia were found passing, via the vertebral nerve, cranially as far as the second cervical spinal nerve. Silverman ('63) indicated that the vertebral nerve terminated at the sixth cervical spinal nerve. Fukuyama and Abuki ('58) demonstrated its extension cranially as far as the third cervical spinal nerve. Cervicothoracic cardiac nerves generally were small, contributing a smaller proportion of the sympathetic cardiac innervation than vertebral cardiac nerves. The former generally passed along the ansa subclavia for a variable distance before passing to the heart, but passed directly to the heart occasionally. According to Mizeres ('58), right cervicothoracic cardiac nerves carry most, if not all of the right accelerator fibers. He followed these nerves to the cardiac plexus and right atrium. Perman ('24) found that they passed along the right coronary artery and descending branch of the left coronary artery. Schurawlew ('28) indicated that right vertebral cardiac nerves supply the areas Perman ('24) described. In the present investigation the right cervicothoracic cardiac nerves were found to enter the cardiac plexus independently or extend with other right vertebral, recurrent, and caudal vagal cardiac nerves to the cardiac plexus, the right atrium, along the course of the right coronary artery, along the descending branch of the left coronary artery, and with the circumflex branch of the left coronary artery on the left side of the heart. Left cervicothoracic cardiac nerves passed to the cardiac plexus, followed other heart nerves along the vessels just described as accompanied by right cervicothoracic cardiac nerves, and additionally

accompanied the circumflex branch of the left coronary artery on the caudal and right side with a branch of the right cranio-medial vertebral cardiac nerve which joined the caudolateral vertebral cardiac nerve. Perman ('24), Schurawlew ('28), and Mizeres ('55a) followed left cervicothoracic cardiac nerves to the latter area. In addition, Mizeres ('55a) indicated that they pass to the cardiac plexus and Perman ('24) followed some to the left longitudinal sulcus.

In the dog the vertebral ganglion has been designated as the caudal cervical ganglion by Schurawlew ('28), Nonidez ('37a,b), Mizeres ('55a,b, '57, '58), Sisson and Grossman ('53), and Stromberg ('64). It is called the middle cervical ganglion by Lim Boon Keng (1893), Perman ('24), Nonidez ('39), and Ellenberger and Baum ('43). In man this ganglion has been designated as the intermediate ganglion by Kuntz ('49, '53), Jonnesco ('23), and White and Smithwick ('52). In the horse, Usenik ('57) called it the intermediate ganglion. Mannu ('14) called it the stellate ganglion in the dog. Laubmann ('31), Mitchell ('53), Grant ('58), Wreite ('59a, b), Gardner, Gray and O'Rahilly ('63), and Davies and Davies ('64) in man have noted that this ganglion should be called the vertebral ganglion, as has Mizeres ('55a) in the dog. The present authors are in agreement, after dissecting seven domestic species of animals, that the ganglion should be designated the vertebral ganglion.

Vertebral cardiac nerves morphologically comprised the greatest sympathetic supply to the heart in the dog. In agreement with Schurawlew ('28) the senior author followed vertebral cardiac nerves on each side to the same areas described in the present investigation for cervicothoracic cardiac nerves. The number and origin of these nerves was generally in agreement with Mizeres ('55a).

The middle cervical ganglion, as described by Wreite ('59) and often considered absent in man (Kuntz, '49, '53), was not grossly, independently demonstrated in the dog. Further embryological and physiological studies should be undertaken to ascertain whether it is incorporated into the vertebral ganglion, diffusely dis-

tributed along the cervical sympathetic trunk, included in the cranial cervical ganglion, or is absent in the dog.

Intermediate ganglia, distributed constantly between the sympathetic trunk ganglia in the internodal rami were not grossly identified in the dog. Cranial cervical cardiac nerves arising from the cranial cervical ganglion were not noted in the dog.

The present morphologic study of the vagal cardiac nerves substantiated the microscopic conclusions of Tcheng ('51) and Hirsch ('65) that parasympathetic fibers passed to both the atria and ventricles. To distinguish between vagal cardiac nerves they were divided into cranial vagal and caudal vagal cardiac nerves based upon their respective cranial and caudal relationship to the origin of the recurrent laryngeal nerve. Stromberg ('64) described vagal cardiac nerves arising from each of the portions of the vagi, similar to those described by Nonidez ('39) and Mizeres ('55a), however, the areas of distribution were not completely described. Recurrent cardiac nerves were reported as arising from each recurrent laryngeal nerve by Stromberg ('64), however, the designation recurrent cardiac nerve was reserved for a large nerve from the right recurrent cardiac nerve. The senior author observed a large trunk formed by right cranial and caudal vagal, right vertebral, right cervicothoracic, and right recurrent cardiac nerves. This combined trunk, as illustrated by Mizeres ('55a,b, '57), should not be designated as the recurrent cardiac nerve since right recurrent cardiac nerves form only a small portion of this trunk.

Branches arising from the cardiac nerves may enter the cardiac plexus, located ventral to the bifurcation of the trachea, caudal and lateral to the arch of the aorta, and around the bifurcation of the pulmonary artery. It appeared that from the cardiac plexus, twigs may follow larger continuing cardiac nerves to any area of the heart. Major contributions to various areas, however, were assumed by specific cardiac nerves. Cooper ('61) has presented an improved method of regional ablation for cardiac denervation which was designed to eliminate sequella on other thoracic viscera. The present authors, however,

found a continuation of nerves to the lungs from the artificially separate cardiac and pulmonary plexuses. Therefore, probably all sequella are not eliminated.

ACKNOWLEDGMENT

The appreciation of the authors is extended to R. L. Hamm for the illustrations and to Dr. D. J. Hillmann for the photography.

LITERATURE CITED

- Cooper, T., J. W. Gilbert, R. D. Bloodwell and J. R. Crout 1961 Chronic extrinsic cardiac denervation by regional neural ablation: description of the operation, verification of the denervation and its effects on myocardial catecholamines. *Circ. Res.*, 9: 275-281.
- Davies, D. V., and F. Davies 1961 Gray's anatomy. Thirty-third ed. Longmans, Green and Co., Ltd., London, England.
- Ellenberger, W., and H. Baum 1943 Handbuch der vergleichenden Anatomie der Haustiere. Eighteenth ed. Springer Verlag, Berlin, Germany.
- Fukuyama, U., and M. Yabuki 1958 On the vertebral nerve and the communicating rami connecting with the inferior cervical ganglion in dog. *Fukushima J. Med. Sci.*, 5: 63-68.
- Gardner, E., D. J. Gray and R. O'Rahilly 1963 Anatomy: a regional study of human structure. Second ed. W. B. Saunders Co., Philadelphia, Penna.
- Grant, J. C. B. 1958 A method of anatomy. Sixth ed. The Williams and Wilkins Co., Baltimore, Maryland.
- Hardesty, I. 1933 The nervous system. In: Morris' human anatomy Ninth ed. C. M. Jackson, ed. W. B. Saunders Co., Philadelphia, Penna., pp. 825-1127.
- Hirsch, E. F., G. C. Kaiser and T. Cooper 1965 Experimental heart block in the dog. II. Injuries of the septal nerves. *Arch. Pathol.*, 79: 86-107.
- Ionescu, D., and M. Enachescu 1928 Untersuchungen bei Säugetieren und beim Menschen über die aus dem Brustganglion des Sympathicus unterhalb des Ganglion stellatum entspringenden Herznerven. *Ztschr. f. Anat. u. Entw.*, 85: 470-489.
- Jonnisco, T. 1923 Le sympathique cervico-thoracique. Masson, Paris, France. Original not available; cited in Wreite, M. 1959 The anatomy of the sympathetic trunks in man. *J. Anat.*, 93: 451.
- Kuntz, A. 1949 The neuroanatomic basis of the autonomic nervous system. First ed. Charles C Thomas, Springfield, Illinois.
- 1953 The autonomic nervous system. Fourth ed. Lea and Febiger, Philadelphia, Penna.
- Laubmann, W. 1931 Anatomische studie über den Halsympathicus des Menschen. *Ztschr. f. Anat. u. Entw.*, 96: 787-805.

- Lim Boon Keng, M. B. 1893 On the nervous supply of the dog's heart. *J. Physiol.*, 14: 467-483.
- Manno, A. 1914 Ricerche anatomo-comperative sul simpatico cervicale nei mammiferi. *Intern. Monatsschr. f. Anat. u. Physiol.*, 30: 49-168.
- McClure, R. C., J. Schreiber, P. Walter, J. Frewein and L. A. DiDio 1967 Systems nervosum autonomicum. Unpublished typewritten report proposed to the International Commission for Veterinary anatomical nomenclature. Area VI^a Columbia, Missouri.
- Miller, M. E., G. C. Christensen and H. E. Evans 1964 Anatomy of the dog. W. B. Saunders Co., Philadelphia, Penna.
- Mitchell, C. A. G. 1953 Anatomy of the autonomic nervous system. E. and S. Livingstone, Edinburgh, Scotland.
- Mizes, N. J. 1955a The anatomy of the autonomic nervous system in the dog. *J. Anat.*, 95: 285-318.
- 1955b Isolation of the cardioinhibitory branches of the right vagus nerve in the dog. *Anat. Rec.*, 123: 437-446.
- 1957 The course of the left cardioinhibitory fibers in the dog. *Anat. Rec.*, 127: 109-116.
- 1958 The origin and course of the cardioaccelerator fibers in the dog. *Anat. Rec.*, 132: 261-280.
- Monina Anatomica 1966 Third ed. Excerpta Medica Foundation, Amsterdam, Holland.
- Conder, J. F. 1937a Identification of the receptor areas in the vena cavae and pulmonary veins which initiate reflex cardiac acceleration (Bainbridge's reflex). *Am. J. Anat.*, 61: 203-232.
- 1937b Distribution of the aortic nerve fibers and the epitheloid bodies (supracardial 'paraganglia') in the dog. *Anat. Rec.*, 69: 299-318.
- 1939 Studies on the innervation of the heart. I. Distribution of the cardiac nerves, with special reference to the identification of the sympathetic and parasympathetic postganglionics. *Am. J. Anat.*, 65: 361-401.
- 1924 Anatomische untersuchung über die Herznerven bei den höheren Säugetieren und bei Menschen. *Ztschr. f. Anat. u. Entw.*, 71: 382-457.
- Saccomanno, G. 1943 The components of the upper thoracic sympathetic nerves. *J. Comp. Neurol.*, 79: 355-378.
- Schmiedeberg, O. 1871 Über die Innervationsverhältnisse des Hundeherzens. *Ber. sächs. Akad. Wiss. Math-phys. Klasse.*, 23: 148-170.
- Schreiber, J., J. Frewein and P. Walter 1963 Systema nervosum autonomicum. Unpublished typewritten report proposed to the International Commission for Veterinary Anatomical Nomenclature. Area VI, Hannover, Germany.
- Schurawlew, A. N. 1928 Die Herznerven des Hundes. *Ztschr. f. Anat. u. Entw.*, 86: 655-697.
- Silverman, E. H. 1963 Zur Topographie des Nervus vertebralis bei Wiederkäuer und Fleischfresser. Inaugural dissertation, Ludwig-Maximilians-Universität Munich, Germany.
- Sisson, S., and J. D. Grossman 1953 The anatomy of the domesticated animals. Fourth ed. W. B. Saunders Co., Philadelphia, Penna.
- Stromberg, M. W. 1964 The autonomic nervous system. In: Miller, M. E., G. C. Christensen and H. E. Evans 1964 Anatomy of the dog. W. B. Saunders Co., Philadelphia, Penna., pp. 626-644.
- Tcheng, K. T. 1951 Innervation of the dog's heart. *Am. Heart J.*, 41: 512-523.
- Usenik, E. A. 1957 Sympathetic innervation of the head and neck of the horse. neuropharmacological studies of sweating in the horse. Unpublished Ph.D. thesis, Library, University of Minnesota, Minneapolis, Minnesota.
- Waites, G. M. H. 1957 The course of the efferent cardiac nerves of the sheep. *J. Physiol.*, 139: 417-433.
- White, J. C., and R. H. Smithwick 1952 The autonomic nervous system. Third ed. Macmillan, New York, New York.
- Wrote, M. 1959a The anatomy of the sympathetic trunks in man. *J. Anat.*, 93: 448-459.
- 1959b Die Anatomie der sympathischen Grenzstränge beim Menschen und bei Säugetieren mit spezieller Rücksicht auf die Nomenklatur. *Anat. Anz.*, 106: 304-322.

tributed along the cervical sympathetic trunk, included in the cranial cervical ganglion, or is absent in the dog.

Intermediate ganglia, distributed constantly between the sympathetic trunk ganglia in the internodal rami were not grossly identified in the dog. Cranial cervical cardiac nerves arising from the cranial cervical ganglion were not noted in the dog.

The present morphologic study of the vagal cardiac nerves substantiated the microscopic conclusions of Tcheng ('51) and Hirsch ('65) that parasympathetic fibers passed to both the atria and ventricles. To distinguish between vagal cardiac nerves they were divided into cranial vagal and caudal vagal cardiac nerves based upon their respective cranial and caudal relationship to the origin of the recurrent laryngeal nerve. Stromberg ('64) described vagal cardiac nerves arising from each of the portions of the vagi, similar to those described by Nonidez ('39) and Mizeres ('55a), however, the areas of distribution were not completely described. Recurrent cardiac nerves were reported as arising from each recurrent laryngeal nerve by Stromberg ('64), however, the designation recurrent cardiac nerve was reserved for a large nerve from the right recurrent cardiac nerve. The senior author observed a large trunk formed by right cranial and caudal vagal, right vertebral, right cervicothoracic, and right recurrent cardiac nerves. This combined trunk, as illustrated by Mizeres ('55a,b, '57), should not be designated as the recurrent cardiac nerve since right recurrent cardiac nerves form only a small portion of this trunk.

Branches arising from the cardiac nerves may enter the cardiac plexus, located ventral to the bifurcation of the trachea, caudal and lateral to the arch of the aorta, and around the bifurcation of the pulmonary artery. It appeared that from the cardiac plexus, twigs may follow larger continuing cardiac nerves to any area of the heart. Major contributions to various areas, however, were assumed by specific cardiac nerves. Cooper ('61) has presented an improved method of regional ablation for cardiac denervation which was designed to eliminate sequella on other thoracic viscera. The present authors, however,

found a continuation of nerves to the lungs from the artificially separate cardiac and pulmonary plexuses. Therefore, probably all sequella are not eliminated.

ACKNOWLEDGMENT

The appreciation of the authors is extended to R. L. Hamm for the illustrations and to Dr. D. J. Hillmann for the photography.

LITERATURE CITED

- Cooper, T., J. W. Gilbert, R. D. Bloodwell and J. R. Crout 1961 Chronic extrinsic cardiac denervation by regional neural ablation: description of the operation, verification of the denervation and its effects on myocardial catecholamines. *Circ. Res.*, 9: 275-281.
- Davies, D. V., and F. Davies 1964 *Gray's anatomy*. Thirty-third ed. Longmans, Green and Co., Ltd., London, England.
- Ellenberger, W., and H. Baum 1943 *Handbuch der vergleichenden Anatomie der Haustiere*. Eighteenth ed. Springer Verlag, Berlin, Germany.
- Fukuyama, U., and M. Yabuki 1958 On the vertebral nerve and the communicating ramus connecting with the inferior cervical ganglion in dog. *Fukushima J. Med. Sci.*, 5: 63-88.
- Gardner, E., D. J. Gray and R. O'Rahilly 1963 *Anatomy: a regional study of human structure*. Second ed. W. B. Saunders Co., Philadelphia, Penna.
- Grant, J. C. B. 1958 *A method of anatomy*. Sixth ed. The Williams and Wilkins Co., Baltimore, Maryland.
- Hardesty, I. 1933 *The nervous system*. In: *Morris' human anatomy* Ninth ed. C. M. Jackson, ed. W. B. Saunders Co., Philadelphia, Penna., pp. 825-1127.
- Hirsch, E. F., G. C. Kaiser and T. Cooper 1965 Experimental heart block in the dog. II. Injuries of the septal nerves. *Arch. Path.*, 79: 86-107.
- Ionescu, D., and M. Enachescu 1928 Untersuchungen bei Säugetieren und beim Menschen über die aus dem Brustganglion des Sympathicus unterhalb des Ganglion stellatum entspringenden Herznerven. *Ztschr. f. Anat. u. Entw.*, 85: 476-489.
- Jonnasco, T. 1923 *Le sympathique cervico-thoracique*. Masson, Paris, France. Original not available; cited in Wretling, M. 1959 *The anatomy of the sympathetic trunks in man*. *J. Anat.*, 93: 451.
- Kuntz, A. 1949 *The neuroanatomic basis of the autonomic nervous system*. First ed. Charles C Thomas, Springfield, Illinois.
- 1953 *The autonomic nervous system*. Fourth ed. Lea and Febiger, Philadelphia, Penna.
- Laubmann, W. 1931 *Anatomische studie über den Halssympathicus des Menschen*. *Ztschr. f. Anat. u. Entw.*, 96: 787-805.

- Lim Boon Keng, M. B. 1893 On the nervous supply of the dog's heart. *J. Physiol.*, 14: 467-483.
- Manno, A. 1914 Ricerche anatomo-comperative sul simpatico cervicale nei mammiferi. *Intern. Monatsschr. f. Anat. u. Physiol.*, 30: 49-168.
- McClure, R. C., J. Schreiber, P. Walter, J. Frewein and L. A. DiDio 1967 Systems nervosum autonomicum. Unpublished typewritten report proposed to the International Commission for Veterinary anatomical nomenclature. Area VI^a Columbia, Missouri.
- Miller, M. E., G. C. Christensen and H. E. Evans 1964 Anatomy of the dog. W. B. Saunders Co., Philadelphia, Penna.
- Mitchell, G. A. G. 1953 Anatomy of the autonomic nervous system. E. and S. Livingstone, Edinburgh, Scotland.
- Muertes, N. J. 1955a The anatomy of the autonomic nervous system in the dog. *J. Anat.*, 96: 283-318.
- 1955b Isolation of the cardioinhibitory branches of the right vagus nerve in the dog. *Anat. Rec.*, 123: 437-446.
- 1957 The course of the left cardioinhibitory fibers in the dog. *Anat. Rec.*, 127: 109-116.
- 1958 The origin and course of the cardioaccelerator fibers in the dog. *Anat. Rec.*, 132: 261-280.
- Nomina Anatomica 1966 Third ed. Excerpta Medica Foundation, Amsterdam, Holland.
- Nomidez, J. F. 1937a Identification of the receptor areas in the vena cavae and pulmonary veins which initiate reflex cardiac acceleration (Bainbridge's reflex). *Am. J. Anat.*, 61: 203-232.
- 1937b Distribution of the aortic nerve fibers and the epitheloid bodies (supracardial "paraganglia") in the dog. *Anat. Rec.*, 69: 299-318.
- 1939 Studies on the innervation of the heart. I. Distribution of the cardiac nerves, with special reference to the identification of the sympathetic and parasympathetic postganglionics. *Am. J. Anat.*, 65: 361-401.
- Perrnan, E. 1924 Anatomische untersuchung über die Herznerven bei den hohsten Säugtieren und bei Menschen. *Ztschr. f. Anat. u. Entw.*, 71: 382-457.
- Saccomanno, G. 1943 The components of the upper thoracic sympathetic nerves. *J. Comp. Neurol.*, 79: 355-378.
- Schmiedeberg, O. 1871 Über die Innervationsverhältnisse des Hundeherzens. *Ber. sächs. Akad. Wiss. Math-phys. Klasse.*, 23: 148-170.
- Schreiber, J., J. Frewein and P. Walter 1963 Systema nervosum autonomicum. Unpublished typewritten report proposed to the International Commission for Veterinary Anatomical Nomenclature. Area VI, Hannover, Germany.
- Schurawlew, A. N. 1928 Die Herznerven des Hundes. *Ztschr. f. Anat. u. Entw.*, 86: 655-697.
- Silverman, E. H. 1963 Zur Topographie des Nervus vertebralis bei Wiederkäuer und Fleischfresser. Inaugural dissertation, Ludwig-Maximilians-Universität Munich, Germany.
- Sisson, S., and J. D. Grossman 1953 The anatomy of the domesticated animals. Fourth ed. W. B. Saunders Co., Philadelphia, Penna.
- Stromberg, M. W. 1964 The autonomic nervous system. In: Miller, M. E., G. C. Christensen and H. E. Evans 1964 Anatomy of the dog. W. B. Saunders Co., Philadelphia, Penna., pp. 626-644.
- Tcheng, K. T. 1951 Innervation of the dog's heart. *Am. Heart J.*, 41: 512-523.
- Usenik, E. A. 1957 Sympathetic innervation of the head and neck of the horse; neuropharmacological studies of sweating in the horse. Unpublished Ph.D. thesis, Library, University of Minnesota, Minneapolis, Minnesota.
- Waites, G. M. H. 1957 The course of the efferent cardiac nerves of the sheep. *J. Physiol.*, 139: 417-433.
- White, J. C., and R. H. Smithwick 1952 The autonomic nervous system. Thurd ed. Macmillan, New York, New York.
- Wrete, M. 1959a The anatomy of the sympathetic trunks in man. *J. Anat.*, 93: 448-459.
- 1959b Die Anatomie der sympathischen Grenzstränge beim Menschen und bei Säugtieren mit spezieller Rücksicht auf die Nomenklatur. *Anat. Anz.*, 106: 304-322.

A Comparative Morphologic Study of the Cardiac Innervation in Domestic Animals

II. THE FELINE

JOHN SCOTT MCKIBBEN AND ROBERT GETTY

Department of Veterinary Anatomy, Iowa State University, Ames, Iowa

ABSTRACT Detailed morphological studies of the cardiac innervation of the cat were reported. Sympathetic cardiac nerves arose from the thoracic, cervicothoracic, vertebral, and intermediate ganglia. Parasympathetic cardiac nerves arose from the vagi, both cranial and caudal to the origin of the recurrent laryngeal nerves, and from the right recurrent laryngeal nerve. Left cardiac nerves passed primarily to the caudal and right surfaces of the left chambers while right ones ramified on the right chambers and left portion of the left chambers. Left cardiac nerves are more prominent around the coronary sinus and atrioventricular node, while right ones contribute more to the area of the sinoatrial node. Both sympathetic and parasympathetic nerves were followed to each chamber. Interconnections through the cardiac plexus facilitated overlapping of nerve distributions.

The cat, although having an early history as an animal for various laboratory investigations, has not enjoyed the attention of cardiologists which the dog has received. Anatomical descriptions of the cardiac innervation are limited. Bernhardt (1868), Boehm (1875), and Kazem Beck (1888) described the depressor nerve and its relationship to the heart. Mannu ('14) reported on the cardiac nerves of one cat. Perman ('24), Nonidez ('39), and Saccomanno ('43) contributed further information regarding the cardiac innervation of the cat. Only Anufriew ('28), however, has morphologically described the innervation of the feline heart in detail.

Current veterinary anatomical textbooks do not include the morphological description of these cardiac nerves in the cat. The present investigation includes further morphological observations relevant to the proper understanding of cardiac function as well as for specialized procedures such as cardiac denervation studies.

MATERIAL AND METHODS

Ten adult cats were embalmed using the Iowa State University, Department of Veterinary Anatomy embalming formula. Direct morphologic dissection proceeded, exposing and tracing the cardiac nerves, as previously described (McKibben and Getty, '68).

RESULTS

A. Thoracic ganglia and cardiac nerves

Independent THORACIC GANGLIA were present along the thoracic sympathetic trunks bilaterally in each intercostal space from the third or fourth space caudally. They maintained a fairly uniform size of 2 mm craniocaudal, 1 mm dorsoventral, and 1 mm mediolateral. LEFT thoracic cardiac nerves arose from the third to fifth thoracic ganglia, joined the dorsal cervicothoracic cardiac nerve and entered the cardiac plexus. RIGHT thoracic cardiac nerves passing directly to the heart were not observed grossly; however, nerves arising from the third and fourth thoracic ganglia joined the right vagus nerve and potentially could reach the right atrium with the right caudal vagal cardiac nerves.

B. Cervicothoracic ganglia and cardiac nerves

On each side the CAUDAL CERVICAL and first two or three THORACIC GANGLIA combined to form the CERVICOTHORACIC GANGLION. This ganglion lies on the lateral surface of the longus colli muscle in the first intercostal space on the right side, and extends between the first and second intercostal spaces on the left side. Rami communicantes extend caudally at least to the third thoracic spinal nerve and cranially

TABLE 2
Distribution of cardiac nerves in the Feline

Nerves	Side	Along right coronary artery ¹	Along the descending and circumflex branches of the left coronary artery on the left side ²	Along the circumflex branch of the left coronary artery caudally and on the right side ³	Between the cranial and caudal veins ⁴	Between the caudal vena cava and left atrium ⁵	Cardiac plexus ⁶
Thoracic cardiac nerves	Left	+	+	++	-	+	+
	Right	+	-	++	+	+	+
Cervicothoracic cardiac nerves	Left	+	+	+	+	+	+
	Right	++	++	-	+	+	+
Intermediate cardiac nerves	Left	+	+	+	-	-	+
	Right	-	-	-	-	-	-
Vertebral cardiac nerves	Left	+	+	++	+	+	++
	Right	++	++	-	-	-	++
Middle cervical cardiac nerves	Left	-	-	-	-	-	-
	Right	-	-	-	-	-	-
Cranial cervical cardiac nerves	Left	-	-	-	-	-	-
	Right	-	-	-	-	-	-
Cranial vagal cardiac nerves	Left	+	+	++	-	-	++
	Right	+	+	+	-	-	+
Caudal vagal cardiac nerves	Left	++	++	+	++	++	++
	Right	-	-	-	-	-	-
Recurrent cardiac nerves	Left	+	+	-	-	-	+
	Right	+	+	+	-	-	+

¹ not followed to this area, +, some may supply this area, ++, moderate supply to the area, +++, major supply to the area

² Main distribution includes the right auricle, atrium, and ventricle.

³ Main distribution includes the left auricle, left ventricle on the left side, left interventricular septum and the left cranial portion of the right ventricle.

⁴ Main distribution includes the dorsum of the left auricle, ventrum of the left atrium, caudal and right sides of the left ventricle, right interatrial and interventricular septa and caudal right surface of the right ventricle.

⁵ Main distribution includes the lateral right atrial wall towards the sinoatrial node and sometimes the extension across the coronary groove into the right longitudinal sulcus.

⁶ Main distribution may include the left atrium, right side of the left ventricle, interatrial and interventricular septa on the right side, and the right caudal portion of the right ventricle.

⁷ Main distribution to the dorsal atrial walls, great vessels, and intermingling of incoming branches which may then pass with major branches to the other (ve) areas.

at least to the sixth, seventh, and eighth cervical spinal nerves, grossly. The ganglia bilaterally were approximately the same size (table 1).

Typically two or three cardiac nerves arose from the caudal portion of the LEFT cervicothoracic ganglion. A *caudodorsal cervicothoracic cardiac nerve* passed caudally along the dorsolateral border of the left subclavian artery and near this vessel's origin joined a left caudoventral cervicothoracic nerve. The LEFT *caudoventral cervicothoracic cardiac nerves* followed the caudal limb of the ansa subclavia, then the

left vagus towards the heart. The combined nerves passed over the left lateral surface of the aorta and ramified near the caudal border of the aortic arch. Here left cranial vagal cardiac nerves and left vertebral cardiac nerves also joined them. Principal branches passed caudoventrally, lateral to the pulmonary artery, and continued between the left auricle and pulmonary veins to the caudal portion of the coronary groove. They continued along the course of the circumflex branch of the left coronary artery to the right side of the left ventricle and into the right longitudinal sulcus. Branches

Abbreviations

1	Ramus communicans	29	Inferior (nodose) ganglion of the vagus nerve
2	Sympathetic trunk	Aa	First rib
3c	Third thoracic ganglion	Ab	Second rib
3d	Fourth thoracic ganglion	Ac	Third rib
3e	Fifth thoracic ganglion	Ad	Fourth rib
3f	Sixth thoracic ganglion	Ae	Fifth rib
3g	Seventh thoracic ganglion	Af	Sixth rib
3h	Eighth thoracic ganglion	Ag	Seventh rib
3j	Ninth thoracic ganglion	Ah	Eighth rib
4	Cervicothoracic ganglion	Aj	Ninth rib
5	Ansa subclavia (caudal limb)	B	Longus colli muscle
5'	Ansa subclavia (cranial limb)	C	Esophagus
7	Intermediate ganglion	D	Intercostal artery
8	Vertebral ganglion	D'	Intercostal vein
10	Cranial cervical ganglion	E	Aorta
11	Vagus nerve	F	Brachiocephalic artery
12	Right recurrent laryngeal nerve	G'	Left subclavian artery
12'	Left recurrent laryngeal nerve	G"	Right subclavian artery
13	Thoracic cardiac nerve	H	Costocervical artery
14'	Caudodorsal cervicothoracic cardiac nerve	I	Transverse colli artery (dorsal artery)
14"	Caudoventral cervicothoracic cardiac nerve	J	Supreme intercostal artery (subcostal artery)
16	Vertebral nerve	K	Vertebral artery
17	Intermediate cardiac nerve	L	Deep cervical artery
18'	Caudal vertebral cardiac nerve	M'	Costocervico-vertebral vein
20	Cranial cervical nerve	N'	Left common carotid artery
21	Cranial vagal cardiac nerve	N"	Right common carotid artery
21'	Caudal vagal cardiac nerve	O	Right vena azygos
22	Recurrent cardiac nerve	P	Cranial vena cava
24a	Eighth cervical spinal nerve	Q	Caudal vena cava
24b	Seventh cervical spinal nerve	R	Right atrium
24c	Sixth cervical spinal nerve	R'	Right auricle
24d	Fifth cervical spinal nerve	S'	Left auricle
24e	Fourth cervical spinal nerve	T	Right ventricle
24f	Third cervical spinal nerve	U	Left ventricle
25a	First thoracic spinal nerve	W	Trachea
25b	Second thoracic spinal nerve	X	Bronchus
25c	Third thoracic spinal nerve	Y	Pulmonary artery
25d	Fourth thoracic spinal nerve	Y'	Pulmonary vein
25e	Fifth thoracic spinal nerve	Z	Lung
25f	Sixth thoracic spinal nerve	AA	Ligamentum arteriosum
25g	Seventh thoracic spinal nerve	BB	Right coronary artery
25h	Eighth thoracic spinal nerve	BB'	Descending branch of left coronary artery
25j	Ninth thoracic spinal nerve	BB"	Circumflex branch of left coronary artery
26	Vascular nerve	CC	Great cardiac vein
28	Cardiac plexus	FF	Middle cardiac vein

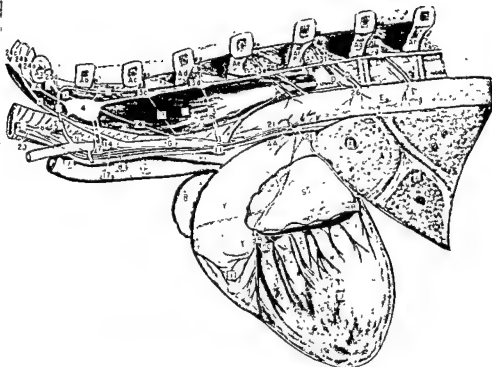


Fig. 1 Feline Left lateral view of the cardiac nerves and related ganglia.

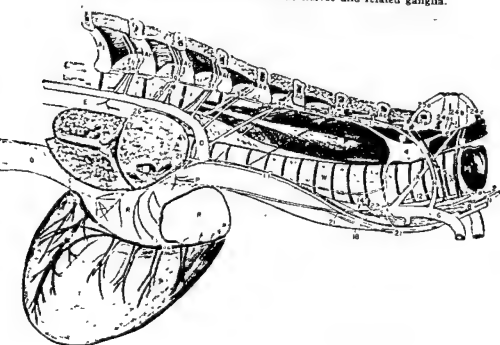


Fig. 2 Feline. Right lateral view of the cardiac nerves and related ganglia.

at least to the sixth, seventh, and eighth cervical spinal nerves, grossly. The ganglia bilaterally were approximately the same size (table 1).

Typically two or three cardiac nerves arose from the caudal portion of the LEFT cervicothoracic ganglion. A *caudodorsal cervicothoracic cardiac nerve* passed caudally along the dorsolateral border of the left subclavian artery and near this vessel's origin joined a left caudoventral cervicothoracic nerve. The LEFT *caudoventral cervicothoracic cardiac nerves* followed the caudal limb of the ansa subclavia, then the

left vagus towards the heart. The combined nerves passed over the left lateral surface of the aorta and ramified near the caudal border of the aortic arch. Here left cranial vagal cardiac nerves and left vertebral cardiac nerves also joined them. Principal branches passed caudoventrally, lateral to the pulmonary artery, and continued between the left auricle and pulmonary veins to the caudal portion of the coronary groove. They continued along the course of the circumflex branch of the left coronary artery to the right side of the left ventricle and into the right longitudinal sulcus. Branches

Abbreviations

1	Ramus communicans	29	Inferior (nodose) ganglion of the vagus nerve
2	Sympathetic trunk	Aa	First rib
3c	Third thoracic ganglion	Ab	Second rib
3d	Fourth thoracic ganglion	Ac	Third rib
3e	Fifth thoracic ganglion	Ad	Fourth rib
3f	Sixth thoracic ganglion	Ae	Fifth rib
3g	Seventh thoracic ganglion	Af	Sixth rib
3h	Eighth thoracic ganglion	Ag	Seventh rib
3j	Ninth thoracic ganglion	Ah	Eighth rib
4	Cervicothoracic ganglion	Aj	Ninth rib
5	Ansa subclavia (caudal limb)	B	Longus colli muscle
5'	Ansa subclavia (cranial limb)	C	Esophagus
7	Intermediate ganglion	D	Intercostal artery
8	Vertebral ganglion	D'	Intercostal vein
10	Cranial cervical ganglion	E	Aorta
11	Vagus nerve	F	Brachiocephalic artery
12	Right recurrent laryngeal nerve	G'	Left subclavian artery
12'	Left recurrent laryngeal nerve	G"	Right subclavian artery
13	Thoracic cardiac nerve	H	Costocervical artery
14'	Caudodorsal cervicothoracic cardiac nerve	I	Transverse colli artery (dorsal artery)
14"	Cauoventral cervicothoracic cardiac nerve	J	Supreme intercostal artery (subcostal artery)
16	Vertebral nerve	K	Vertebral artery
17	Intermediate cardiac nerve	L	Deep cervical artery
18'	Caudal vertebral cardiac nerve	M'	Costocervico-vertebral vein
20	Cranial cervical nerve	N'	Left common carotid artery
21	Cranial vagal cardiac nerve	N"	Right common carotid artery
21'	Caudal vagal cardiac nerve	O	Right vena azygos
22	Recurrent cardiac nerve	P	Cranial vena cava
24a	Eighth cervical spinal nerve	Q	Caudal vena cava
24b	Seventh cervical spinal nerve	R	Right atrium
24c	Sixth cervical spinal nerve	R'	Right auricle
24d	Fifth cervical spinal nerve	S'	Left auricle
24e	Fourth cervical spinal nerve	T	Right ventricle
24f	Third cervical spinal nerve	U	Left ventricle
25a	First thoracic spinal nerve	W	Trachea
25b	Second thoracic spinal nerve	X	Bronchus
25c	Third thoracic spinal nerve	Y	Pulmonary artery
25d	Fourth thoracic spinal nerve	Y'	Pulmonary vein
25e	Fifth thoracic spinal nerve	Z	Lung
25f	Sixth thoracic spinal nerve	AA	Ligamentum arteriosum
25g	Seventh thoracic spinal nerve	BB	Right coronary artery
25h	Eighth thoracic spinal nerve	BB'	Descending branch of left coronary artery
25j	Ninth thoracic spinal nerve	BB"	Circumflex branch of left coronary artery
26	Vascular nerve	CC	Great cardiac vein
28	Cardiac plexus	FF	Middle cardiac vein

cardiac plexus and between the aorta and pulmonary artery to join the trunk of combined right cardiac nerves. Together these nerves followed the right and left coronary arteries from near their origins to their ramifications on the right ventricle, left cranial portion of the left ventricle, and the cranial and ventral portions of the right and left auricles.

RIGHT cervicothoracic cardiac nerves passed with the caudal limb of the ansa subclavia to its junction with the right vagus nerve just caudal to the subclavian artery. Here they joined right vertebral, recurrent, and caudal vagal cardiac nerves, passed caudally on the ventral surface of the trachea, continued between the cranial vena cava and aorta and entered the cardiac plexus. The main continuation through the plexus was followed around the caudal surface of the aorta to the left side of the heart. On the left side it proceeded cranially around either side of the pulmonary artery, then along the right and left coronary arteries. Branches along these arteries passed to the right ventricular wall, cranial left portions of the left ventricle, interventricular septum and the cranial and ventral portions of the right and left auricles. Other right cervicothoracic cardiac nerves arising from the caudal limb of the ansa subclavia passed caudally with the right vagus nerve to the area of the right apical bronchus. Here, together with caudal vagal cardiac nerves, they left the vagus and proceeded between the right branch of the pulmonary artery and the cranial vena cava to ramify on the dorsolateral surface of the right atrium. Their course onto the right atrium was between the venae cavae or between the caudal vena cava and left atrium. Twigs may extend to the area of the coronary sinus. Occasionally, independent right cervicothoracic cardiac nerves passed directly from the right cervicothoracic ganglion to the area of the right apical bronchus. Here they joined caudal vagal cardiac nerves and passed to the right atrium. Twigs from right cervicothoracic cardiac nerves also passed to the cardiac plexus, right pulmonary artery and veins, and cranial and caudal vena cava.

C. Cervical ganglia and cardiac nerves

An inconstant **INTERMEDIATE GANGLION** of variable size (table 1) was noted on the

more caudal of the paired left caudal limbs of the ansa subclavia in three cats. *Intermediate cardiac nerves* arising from this ganglion passed with the left caudoventral cervicothoracic cardiac nerves to the heart. No homologous ganglion or nerves were noted grossly on the **RIGHT** side.

Each **VERTEBRAL GANGLION** was located at the cranial ends of each ansa subclavia, directly craniomedial to the vertebral artery, and just dorsal to the vagus nerve. Each was approximately the same size (table 1).

Two to four *vertebral cardiac nerves* arose from the **LEFT** vertebral ganglion, joined into one trunk after passing caudally for a few millimeters, and continued caudally in close apposition to the left vagus nerve. Near the caudal border of the aortic arch it joined the other left cardiac nerves and passed to areas along the circumflex branch of the left coronary artery on the caudal and right sides of the heart, as previously described. Nerves from the left vertebral ganglion may join a nerve from the cranial cervical ganglion, and continue between the brachiocephalic and left subclavian arteries to reach the aorta. **RIGHT vertebral cardiac nerves**, generally three or four in number, joined the other right cardiac nerves and passed with them to the heart, as previously described under the right cervicothoracic cardiac nerves.

No independent **MIDDLE CERVICAL GANGLION** was noted grossly in the cat.

The **CRANIAL CERVICAL GANGLION** lay in close apposition to the nodose ganglion ventromedial to the tympanic bulla. It measured approximately 8 mm craniocaudal, 3 mm dorsoventral, and 2 mm mediolateral. No cranial cervical cardiac nerves were noted; however, on the left side a completely separable nerve arising from the cranial cervical ganglion, left cranial laryngeal nerve, and left vagus accompanied the vagosympathetic trunk caudally. It passed ventral to the left subclavian artery and between the left subclavian artery and brachiocephalic trunk and ramified on the aorta.

D. Vagal cardiac nerves

In addition to the vagal fibers passing in the previously described nerve, **LEFT cranial vagal cardiac nerves** arose from the

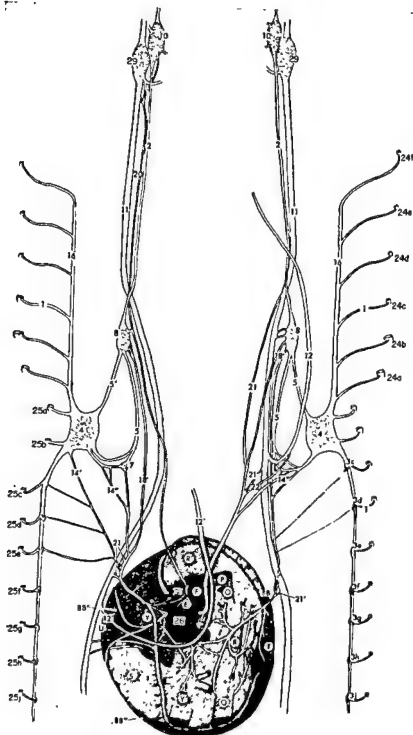


Fig. 3 Feline: Dorsal view of the cardiac innervation. The sympathetic trunks and vagi are reflected laterally.

passed to the dorsum of the left auricle, ventrum of the left atrium, caudal and right walls of the left ventricle, interatrial and interventricular septa from the right, and the caudal right portion of the right

ventricle. Other branches of the left caudo-ventral cervicothoracic cardiac nerves passed to the aorta, pulmonary artery, left pulmonary veins and into the cardiac plexus. Some twigs continued through the

cardiac plexus and between the aorta and pulmonary artery to join the trunk of combined right cardiac nerves. Together these nerves followed the right and left coronary arteries from near their origins to their ramifications on the right ventricle, left cranial portion of the left ventricle, and the cranial and ventral portions of the right and left auricles.

RIGHT cervicothoracic cardiac nerves passed with the caudal limb of the ansa subclavia to its junction with the right vagus nerve just caudal to the subclavian artery. Here they joined right vertebral, recurrent, and caudal vagal cardiac nerves, passed caudally on the ventral surface of the trachea, continued between the cranial vena cava and aorta and entered the cardiac plexus. The main continuation through the plexus was followed around the caudal surface of the aorta to the left side of the heart. On the left side it proceeded cranially around either side of the pulmonary artery, then along the right and left coronary arteries. Branches along these arteries passed to the right ventricular wall, cranial left portions of the left ventricle, interventricular septum and the cranial and ventral portions of the right and left auricles. Other right cervicothoracic cardiac nerves arising from the caudal limb of the ansa subclavia passed caudally with the right vagus nerve to the area of the right apical bronchus. Here, together with caudal vagal cardiac nerves, they left the vagus and proceeded between the right branch of the pulmonary artery and the cranial vena cava to ramify on the dorsolateral surface of the right atrium. Their course onto the right atrium was between the venae cavae or between the caudal vena cava and left atrium. Twigs may extend to the area of the coronary sinus. Occasionally, independent right cervicothoracic cardiac nerves passed directly from the right cervicothoracic ganglion to the area of the right apical bronchus. Here they joined caudal vagal cardiac nerves and passed to the right atrium. Twigs from right cervicothoracic cardiac nerves also passed to the cardiac plexus, right pulmonary artery and veins, and cranial and caudal vena cava.

C Cervical ganglia and cardiac nerves

An INCONSTANT INTERMEDIATE GANGLION of variable size (table 1) was noted on the

more caudal of the paired left caudal limbs of the ansa subclavia in three cats. *Intermediate cardiac nerves* arising from this ganglion passed with the left caudoventral cervicothoracic cardiac nerves to the heart. No homologous ganglion or nerves were noted grossly on the RIGHT side.

Each VERTEBRAL GANGLION was located at the cranial ends of each ansa subclavia, directly craniomedial to the vertebral artery, and just dorsal to the vagus nerve. Each was approximately the same size (table 1).

Two to four *vertebral cardiac nerves* arose from the LEFT vertebral ganglion, joined into one trunk after passing caudally for a few millimeters, and continued caudally in close apposition to the left vagus nerve. Near the caudal border of the aortic arch it joined the other left cardiac nerves and passed to areas along the circumflex branch of the left coronary artery on the caudal and right sides of the heart, as previously described. Nerves from the left vertebral ganglion may join a nerve from the cranial cervical ganglion, and continue between the brachiocephalic and left subclavian arteries to reach the aorta. **RIGHT vertebral cardiac nerves**, generally three or four in number, joined the other right cardiac nerves and passed with them to the heart, as previously described under the right cervicothoracic cardiac nerves.

No independent MIDDLE CERVICAL GANGLION was noted grossly in the cat.

The CRANIAL CERVICAL GANGLION lay in close apposition to the nodose ganglion ventromedial to the tympanic bulla. It measured approximately 8 mm craniocaudal, 3 mm dorsoventral, and 2 mm mediolateral. No cranial cervical cardiac nerves were noted; however, on the left side a completely separable nerve arising from the cranial cervical ganglion, left cranial laryngeal nerve, and left vagus accompanied the vagosympathetic trunk caudally. It passed ventral to the left subclavian artery and between the left subclavian artery and brachiocephalic trunk and ramified on the aorta.

D. Vagal cardiac nerves

In addition to the vagal fibers passing in the previously described nerve, LEFT cranial vagal cardiac nerves arose from the

intimately interwoven association of the left vagus with the sympathetic nerves at the junction of the aorta, pulmonary artery, and left bronchus. These nerves followed the sympathetic nerves from this side into the cardiac plexus, to the aorta and pulmonary artery, to the caudal and right aspects of the left ventricle, ventrum of the left atrium, interventricular and interatrial septa, and caudal portion of the right ventricle. Twigs may indirectly reach the left longitudinal sulcus and cranial coronary groove along the coronary arteries. A *RIGHT cranial vagal cardiac nerve* passed with other right cardiac nerves as described previously for the right cervicothoracic cardiac nerves.

Two or three *caudal vagal cardiac nerves* arose from the *LEFT* vagus nerve about 5 mm caudal to the origin of the left recurrent laryngeal nerve from the vagus and passed cranioventrally between the pulmonary veins and left auricle into the coronary groove. The left auricle received twigs as the nerves passed it. They also ramified along the circumflex branch of the left coronary artery onto the caudal and right surfaces of the left ventricle, ventrum of the left atrium, interatrial and interventricular septa, and caudal wall of the right ventricle. Fine twigs sometimes also passed to the cardiac plexus, the left longitudinal sulcus, and along the right coronary artery. From the intimate association of the right vagus with the right sympathetic nerves, as the caudal limb of the ansa subclavia approximates the vagus, *RIGHT caudal vagal cardiac nerves* combined with sympathetic and right recurrent cardiac nerves and passed caudoventrally, ventral to the trachea. Their distribution included the right ventricle, left and cranial portions of the left ventricle, and the cranial and ventral portions of the auricles. Two or three additional caudal vagal cardiac nerves arose. These accompanied the right cervicothoracic cardiac nerves to the dorsolateral portion of the right atrium, the cardiac plexus, right pulmonary vessels, venae cavae and sometimes extended into the coronary groove in the area of the coronary sinus.

E. Recurrent cardiac nerves

Twigs arising from the *LEFT* recurrent laryngeal nerves were not followed to the

heart grossly. Some ramified, however, on the caudal border of the aorta. One or two fine *RIGHT recurrent cardiac nerves* joined the sympathetic and vagal cardiac nerve trunk which originated near the caudal limb of the ansa subclavia. They passed together, as previously described, to the right ventricle, left caudal portion of the left ventricle, and the cranial and ventral portions of the auricles.

DISCUSSION

In the present morphologic investigation thoracic cardiac nerves were found to arise from the sympathetic trunk between the cervicothoracic ganglia and fourth or fifth thoracic ganglia on the right and left sides, respectively. Perman ('24) and investigators previous to him, did not report thoracic cardiac nerves in the cat. Anufriew ('28) noted their presence as far caudal as the second thoracic ganglion only on the left side. Saccomanno ('43), supporting gross findings with histologic observations, followed them bilaterally from the upper five or six thoracic sympathetic ganglia to the cardiac plexus. Thoracic cardiac nerves are variable in number and origin between specimens.

Cervicothoracic cardiac nerves have been traced to the cardiac plexus from each side by Saccomanno ('43). Perman ('24) indicated that they passed to the atria, dorsal walls of both ventricles, and the lateral wall of the left ventricle from the left side. In agreement with Anufriew ('28), the present authors found that left cervicothoracic cardiac nerves passed primarily to the dorsum of the left auricle, ventrum of the left atrium, caudal and right walls of the left ventricle, interatrial and interventricular septa from the right side, and the caudal right portion of the right ventricle. In addition, the present investigators found branches which continued through the cardiac plexus to join the combined trunk of right heart nerves. Both Perman ('24) and Anufriew ('28) found right cervicothoracic cardiac nerves passing to the ventral portion of the right ventricle and along the left longitudinal sulcus to both ventricles. In addition, Anufriew ('28) noted branches to the right auricles and atrium. The findings of the present authors are in agreement with Anufriew ('28).

The inconstant intermediate ganglion and intermediate cardiac nerves in the cat were not reported previous to the present investigation. Their prominence varied considerably between specimens and they were similarly located only in one other species, the porcine.

In accordance with Wrete ('59) the term intermediate ganglion is reserved for small inconstant ganglia situated in internodal rami between constant ganglia, as well as in communicating rami or in the main trunk or roots of spinal nerves.

Though somewhat less than in the canine, the vertebral cardiac nerves contribute a large portion of the sympathetic cardiac innervation in the feline. Mannu ('14) and Saccomanno ('43) noted cardiac nerves from the vertebral ganglia but followed them only to the cardiac plexus. Perman ('24) noted their distribution from each side to the cranial portion of the right ventricle. Anufriew ('28) did not recognize these nerves. The present authors found that vertebral cardiac nerves passed to each of the major areas of distribution (table 2).

Cervical cardiac nerves were not noted from the cranial cervical ganglion, nor was a middle cervical ganglion noted grossly.

Vagal cardiac nerves, in agreement with Anufriew ('28), were followed to each of the major areas of distribution (table 2). Both the atria and ventricles received fibers. Left recurrent cardiac nerves were not observed, though submacroscopic communications are suspected. Right recurrent cardiac nerves joined and were distributed with other right cardiac nerves.

Though the origin, course, and distribution of cardiac nerves of the feline re-

semble those of the canine, generally, they combined on each side in the cat resulting in large trunks to specific areas. However, through communication with the cardiac plexus several areas could be supplied by a single trunk.

ACKNOWLEDGMENT

The appreciation of the authors is extended to Dr. D. J. Hillman for the photography.

LITERATURE CITED

- Anufriew, W. N. 1928 Die Herznerven des Katze. *Ztschr. f. Anat. u. Entw.*, 86: 639-654.
- Bernhardt, E. 1868 Anatomische und physiologische Untersuchungen über den Nerve depressor bei der Katze. Dissertation Dorpat. Original not available; cited in Anufriew, W. N. 1928 Die Herznerven des Katze. *Ztschr. f. Anat. u. Entw.*, 86: 639-654.
- Boehm, R. 1875 Untersuchungen über den Nervus accelerator cordis der Katze. *Arch. f. Exp. Path. u. Pharm.*, 4: 255-279.
- Kazem Beck, A. 1888 Beitrag zur Innervation des Herzens. *Arch. f. Anat. u. Phys.*, 12: 325-349.
- Mannu, A. 1914 Ricerche anatomocomperative sul simpatico cervicale nei mammiferi. *Intern. Monatsschr. f. Anat. u. Physiol.*, 30: 49-168.
- McKibben, J., and R. Getty 1968 A comparative morphologic study of the cardiac innervation in domestic animals. I. The canine. *Am. J. Anat.*, 122: 533-544.
- Nonidez, J. F. 1939 Studies on the innervation of the heart. I. Distribution of the cardiac nerves, with special reference to the identification of the sympathetic and parasympathetic postganglionics. *Am. J. Anat.*, 65: 361-401.
- Perman, E. 1924 Anatomische Untersuchung über die Herznerven bei den höheren Säugtieren und bei Menschen. *Ztschr. f. Anat. u. Entw.*, 71: 382-457.
- Saccomanno, G. 1943 The components of the upper thoracic sympathetic nerves. *J. Comp. Neur.*, 79: 355-379.
- Wrete, M. 1959 The anatomy of the sympathetic trunks in man. *J. Anat.*, 93: 448-459.

intimately interwoven association of the left vagus with the sympathetic nerves at the junction of the aorta, pulmonary artery, and left bronchus. These nerves followed the sympathetic nerves from this side into the cardiac plexus, to the aorta and pulmonary artery, to the caudal and right aspects of the left ventricle, ventrum of the left atrium, interventricular and interatrial septa, and caudal portion of the right ventricle. Twigs may indirectly reach the left longitudinal sulcus and cranial coronary groove along the coronary arteries. A *RIGHT cranial vagal cardiac nerve* passed with other right cardiac nerves as described previously for the right cervicothoracic cardiac nerves.

Two or three *caudal vagal cardiac nerves* arose from the *LEFT* vagus nerve about 5 mm caudal to the origin of the left recurrent laryngeal nerve from the vagus and passed cranioventrally between the pulmonary veins and left auricle into the coronary groove. The left auricle received twigs as the nerves passed it. They also ramified along the circumflex branch of the left coronary artery onto the caudal and right surfaces of the left ventricle, ventrum of the left atrium, interatrial and interventricular septa, and caudal wall of the right ventricle. Fine twigs sometimes also passed to the cardiac plexus, the left longitudinal sulcus, and along the right coronary artery. From the intimate association of the right vagus with the right sympathetic nerves, as the caudal limb of the ansa subclavia approximates the vagus, *RIGHT caudal vagal cardiac nerves* combined with sympathetic and right recurrent cardiac nerves and passed caudoventrally, ventral to the trachea. Their distribution included the right ventricle, left and cranial portions of the left ventricle, and the cranial and ventral portions of the auricles. Two or three additional *caudal vagal cardiac nerves* arose. These accompanied the right cervicothoracic cardiac nerves to the dorsolateral portion of the right atrium, the cardiac plexus, right pulmonary vessels, venae cavae and sometimes extended into the coronary groove in the area of the coronary sinus.

E. Recurrent cardiac nerves

Twigs arising from the *LEFT* recurrent laryngeal nerves were not followed to the

heart grossly. Some ramified, however, on the caudal border of the aorta. One or two fine *RIGHT recurrent cardiac nerves* joined the sympathetic and vagal cardiac nerve trunk which originated near the caudal limb of the ansa subclavia. They passed together, as previously described, to the right ventricle, left caudal portion of the left ventricle, and the cranial and ventral portions of the auricles.

DISCUSSION

In the present morphologic investigation thoracic cardiac nerves were found to arise from the sympathetic trunk between the cervicothoracic ganglia and fourth or fifth thoracic ganglia on the right and left sides, respectively. Perman ('24) and investigators previous to him, did not report thoracic cardiac nerves in the cat. Anufriew ('28) noted their presence as far caudal as the second thoracic ganglion only on the left side. Saccomanno ('43), supporting gross findings with histologic observations, followed them bilaterally from the upper five or six thoracic sympathetic ganglia to the cardiac plexus. Thoracic cardiac nerves are variable in number and origin between specimens.

Cervicothoracic cardiac nerves have been traced to the cardiac plexus from each side by Saccomanno ('43). Perman ('24) indicated that they passed to the atria, dorsal walls of both ventricles, and the lateral wall of the left ventricle from the left side. In agreement with Anufriew ('28), the present authors found that left cervicothoracic cardiac nerves passed primarily to the dorsum of the left auricle, ventrum of the left atrium, caudal and right walls of the left ventricle, interatrial and interventricular septa from the right side, and the caudal right portion of the right ventricle. In addition, the present investigators found branches which continued through the cardiac plexus to join the combined trunk of right heart nerves. Both Perman ('24) and Anufriew ('28) found right cervicothoracic cardiac nerves passing to the ventral portion of the right ventricle and along the left longitudinal sulcus to both ventricles. In addition, Anufriew ('28) noted branches to the right auricles and atrium. The findings of the present authors are in agreement with Anufriew ('28).

The Relationship between the Dimensions of the Fibres and the Number of Nuclei during Normal Growth of Skeletal Muscle in the Domestic Fowl

F. P. MOSS

Department of Animal Husbandry, University of Sydney,
Sydney, N.S.W., Australia

ABSTRACT Between 0 and 266 days of age the weight of the pectoral and gastrocnemius muscles of chickens increased 300-600- and 40-90-fold respectively depending on the breed and sex. In both muscles the mean cross-sectional area of the fibres and the total number of nuclei (estimated from DNA determination) maintained a constant ratio during growth. This suggests that for individual fibres the cross-sectional area increased in proportion to the number of nuclei. This phenomenon is discussed in relation to current knowledge concerning the mode of growth and multinucleation of skeletal muscle fibres.

In the pectoral muscle, between 0 and 266 days, the cross-sectional area of the fibres increased in proportion to the two-thirds power of the muscle weight, which suggests that the length and diameter of the fibres maintained a constant ratio. The same relationship existed for the gastrocnemius for two months, after which the fibre cross-sectional area increased in proportion to the muscle weight, which suggests that the fibre length was then constant.

An increase during growth of the number of nuclei in the skeletal muscles of the rat has been reported by Enesco and Leblond ('62) and by Enesco and Puddy ('64). Similar studies of the pectoral muscle of the chicken have been undertaken in this laboratory, and a mathematical relationship between the weight of the muscle and the total number of nuclei has been reported by Moss, Summons and McNary ('64). It was found that between hatching and 28 days of age, while the weight of the muscle increased some 50- to 80-fold depending on the breed and sex, the number of nuclei increased in proportion to the two-thirds power of the weight of the muscle. Since growth of skeletal muscle is very largely the result of hypertrophy of the constituent fibres, it seems reasonable to suppose that this relationship may indicate an underlying relationship between the number of nuclei and the dimensions of the fibres.

In order to test this hypothesis, a study was made of the growth of the pectoral and gastrocnemius muscles of the chicken from hatching to maturity. Animals were sacrificed at various ages, the total number of nuclei in the muscles estimated

from their DNA content and the mean diameter of their fibres determined histometrically.

MATERIALS AND METHODS

Five male and five female chickens of each of two breeds, New Hampshire and White Leghorn, were sacrificed at each of eight ages: 0, 4, 8, 16, 32, 66, 128 and 266 days. The system of management was designed to promote the maximum rate of growth of the chickens and to minimise the variation between them due to environmental factors.

The first group of chickens received neither food nor water and was sacrificed within a few hours of hatching. The remainder were placed in electrically-heated battery brooders in a totally enclosed air-conditioned room which was maintained at approximately 25°C. Lighting was continuous for two days and 14 hours per day thereafter. The temperature of the brooders was maintained at 35°C for the first week, 32°C for the second and 29°C for the third, after which heating was discontinued. At 33 days of age the chickens were transferred to unheated "follow-on cages" in the same room, and at ten weeks of age the pullets were transferred to

The Relationship between the Dimensions of the Fibres and the Number of Nuclei during Normal Growth of Skeletal Muscle in the Domestic Fowl

F. P. MOSS

*Department of Animal Husbandry, University of Sydney,
Sydney, N.S.W., Australia*

ABSTRACT Between 0 and 266 days of age the weight of the pectoral and gastrocnemius muscles of chickens increased 300-600- and 40-90-fold respectively depending on the breed and sex. In both muscles the mean cross-sectional area of the fibres and the total number of nuclei (estimated from DNA determination) maintained a constant ratio during growth. This suggests that for individual fibres the cross-sectional area increased in proportion to the number of nuclei. This phenomenon is discussed in relation to current knowledge concerning the mode of growth and multinucleation of skeletal muscle fibres.

In the pectoral muscle, between 0 and 266 days, the cross-sectional area of the fibres increased in proportion to the two-thirds power of the muscle weight, which suggests that the length and diameter of the fibres maintained a constant ratio. The same relationship existed for the gastrocnemius for two months, after which the fibre cross-sectional area increased in proportion to the muscle weight, which suggests that the fibre length was then constant.

An increase during growth of the number of nuclei in the skeletal muscles of the rat has been reported by Enesco and Leblond ('62) and by Enesco and Puddy ('64). Similar studies of the pectoral muscle of the chicken have been undertaken in this laboratory, and a mathematical relationship between the weight of the muscle and the total number of nuclei has been reported by Moss, Sammonds and McNary ('64). It was found that between hatching and 28 days of age, while the weight of the muscle increased some 50- to 80-fold depending on the breed and sex, the number of nuclei increased in proportion to the two-thirds power of the weight of the muscle. Since growth of skeletal muscle is very largely the result of *hypertrophy* of the constituent fibres, it seems reasonable to suppose that this relationship may indicate an underlying relationship between the number of nuclei and the dimensions of the fibres.

In order to test this hypothesis, a study was made of the growth of the pectoral and gastrocnemius muscles of the chicken from hatching to maturity. Animals were sacrificed at various ages, the total number of nuclei in the muscles estimated

from their DNA content and the mean diameter of their fibres determined histometrically.

MATERIALS AND METHODS

Five male and five female chickens of each of two breeds, New Hampshire and White Leghorn, were sacrificed at each of eight ages: 0, 4, 8, 16, 32, 66, 128 and 266 days. The system of management was designed to promote the maximum rate of growth of the chickens and to minimise the variation between them due to environmental factors.

The first group of chickens received neither food nor water and was sacrificed within a few hours of hatching. The remainder were placed in electrically-heated battery brooders in a totally enclosed air-conditioned room which was maintained at approximately 25°C. Lighting was continuous for two days and 14 hours per day thereafter. The temperature of the brooders was maintained at 35°C for the first week, 32°C for the second and 29°C for the third, after which heating was discontinued. At 33 days of age the chickens were transferred to unheated "follow-on cages" in the same room, and at ten weeks of age the pullets were transferred to

single bird laying cages in a conventional building. The cockerels were transferred at the same time to single bird cockerel cages in the same building.

The chickens were fed commercial feeds appropriate to their age, change of ration being made at 10 and 20 weeks of age. The feeds, which were in crumble form, were fed *ad libitum* and water was provided at all times. Care was taken to ensure that all chickens commenced to eat and drink within a few hours of being placed in the brooders.

The chickens were killed by decapitation. The whole of the pectoral muscle was removed from the sternum, dissected free of visible fat and tendon and weighed. Since the muscle is bilaterally symmetrical, one side was used for DNA determination and the other for histometry. Both gastrocnemii were removed, freed from visible tendon and individually weighed. The muscle from the right leg was used for DNA determination and that from the left leg for histometry.

The usual procedure was for samples intended for DNA estimation to be minced, either in the apparatus described by Seevers and Shideman ('41) or, for the larger samples, in a culinary mincer; but when the sample weighed less than about 2 gm, it was finely cut up with scissors. The minced muscle was then thoroughly mixed and samples, 1 gm if available, were weighed into capped plastic tubes, rapidly frozen and stored at -20°C . The samples for histometry were taken from the centre of one side of the pectoral muscle and from the thickest part of the gastrocnemius of the left leg. They were fixed in formol saline and remained in the fixative until required.

After thawing, the samples were homogenized in distilled water in a Servall Omnimixer, and DNA was determined by the indole colorimetric reaction described by Ceriotti ('52). This was carried out on the complete homogenate as it had been found that prior extraction with perchloric acid according to the method of Paul ('56) resulted in the destruction of some of the DNA and trichloroacetic acid inhibits colour formation (Ceriotti, '55). The method used was as follows. Two ml of

homogenate containing 20–40 mg of muscle were pipetted into a 10 ml centrifuge tube and 1 ml of 0.04% indole plus 1 ml of 6N HCl were added. The tube was stoppered with a glass marble and heated in a boiling water bath for 12 minutes then rapidly cooled in cold water. After centrifugation at 3,000 G for five minutes, the supernatant was decanted into another centrifuge tube and extracted three times with 4 ml of chloroform. The coloured solution was centrifuged for one minute to clear the emulsion and its absorbance measured at 490 m μ . Calibration was by means of standard solutions of DNA containing 10 μg and 20 μg per ml, treated in the same way. Ceriotti ('52) carried out exhaustive tests of the specificity of the indole reaction. He found that only arabinose, arabofuranosyladenine and deoxyribose yielded the same colour as DNA and, even then, at a much lower intensity. The possibility of increased colour yield due to substances other than DNA in the homogenate therefore seems remote. The absence of interfering substances which might reduce the colour yield was demonstrated by means of recovery tests, carried out by adding standard DNA solutions to muscle homogenates.

Since the mean quantity of DNA per diploid nucleus is constant for individual species (Vendrelly, '55), the total number of nuclei in an organ or tissue may be estimated from its DNA content. Although this method has a number of limitations, which are discussed by Enesco and Leblond ('62), it is considered to be satisfactory for skeletal muscle. Davidson ('60) gives a value of 2.5×10^{-9} mg DNA per diploid nucleus for the chicken and this value has been used in the present studies.

The histometric technique was that described by Joubert ('56). Free-hand shavings, made across the grain of the muscle, were teased apart in dilute glycerine on a microscope slide, and a coverslip was gently applied. Measurements of the cross-diameter of 100 fibres per sample were made using an ocular micrometer at a magnification of 300. The ocular micrometer was calibrated using a stage micrometer. The mean cross-sectional area of the fibres was calculated from the

mean of the measured diameters, assuming the fibres to be of circular cross-section.

RESULTS

The increase with age of the weight of the muscles, their total number of nuclei and the mean diameter of their constituent fibres is shown in table 1. Between hatching and 266 days of age the weight of the pectoral muscle increased between 300- and 600-fold, depending on the breed and sex. In the same period, the number of nuclei increased between 40- and 90-fold and the mean cross-sectional area of the fibres increased between 60- and 90-fold. The growth of the gastrocnemius muscle was considerably less than that of the pectoral, the increase of

weight being between 80- and 170-fold, depending on breed and sex. The corresponding increases of the number of nuclei and of the fibre diameter were 20- to 50-fold and 30- to 70-fold respectively.

It had been shown previously (Moss et al., '64) that, between hatching and 28 days of age, the number of nuclei in the pectoral muscle increased in proportion to the two-thirds power of the weight of the muscle. The results of the present experiment were therefore analysed to determine whether this relationship was maintained until 266 days of age and whether the same relationship existed for the gastrocnemius. This was most conveniently accomplished by plotting the logarithm of the number of nuclei against

TABLE 1
Variation with age of the weight of the muscle, total number of nuclei and mean cross-sectional area of the fibres of the pectoral and gastrocnemius muscles of New Hampshire (N.H.) and White Leghorn (W.L.) chickens
(Means of five animals)

Age (days)	0	4	8	16	32	66	128	266
Weight of pectoral muscle (g)								
NH. ♂	0.72	1.5	5.2	13	35	130	270	450
NH. ♀	0.63	1.9	5.6	13	32	100	270	290
W.L. ♂	0.66	1.2	5.0	14	32	100	200	260
W.L. ♀	0.68	1.5	3.8	11	30	87	200	220
Number of nuclei in whole pectoral muscle (10 ³)								
NH. ♂	0.79	1.3	2.8	5.0	9.8	28	46	76
NH. ♀	0.68	1.6	3.2	4.8	8.9	24	39	44
W.L. ♂	0.72	1.3	2.8	4.8	9.1	25	36	43
W.L. ♀	0.78	1.3	1.9	4.1	8.5	18	32	32
Cross-sectional area of pectoral muscle fibres (μ ²)								
NH. ♂	41	79	200	380	740	2100	3200	3500
NH. ♀	43	87	200	400	790	1900	3200	3500
W.L. ♂	40	76	180	350	760	1700	2600	3000
W.L. ♀	44	79	190	360	690	1700	2900	2800
Weight of gastrocnemius muscle (g)								
NH. ♂	0.63	0.87	1.2	2.5	9.6	33	76	120
NH. ♀	0.59	0.87	1.2	2.4	7.1	26	52	63
W.L. ♂	0.48	0.76	1.1	2.4	7.2	27	50	64
W.L. ♀	0.54	0.68	0.96	1.9	6.6	19	34	44
Number of nuclei in whole gastrocnemius muscle (10 ³)								
NH. ♂	0.50	0.60	0.87	1.4	3.0	9.3	15	27
NH. ♀	0.44	0.60	0.76	1.1	2.2	7.1	11	11
W.L. ♂	0.39	0.52	0.64	1.1	2.5	7.2	11	13
W.L. ♀	0.40	0.41	0.51	0.91	2.1	4.7	6.6	7.2
Cross-sectional area of gastrocnemius muscle fibres (μ ²)								
NH. ♂	100	130	170	290	680	1500	4600	7300
NH. ♀	120	130	170	300	700	1500	3600	4900
W.L. ♂	100	120	150	280	600	1500	3200	5000
W.L. ♀	100	130	160	290	630	1500	2700	3400

single bird laying cages in a conventional building. The cockerels were transferred at the same time to single bird cockerel cages in the same building.

The chickens were fed commercial feeds appropriate to their age, change of ration being made at 10 and 20 weeks of age. The feeds, which were in crumble form, were fed *ad libitum* and water was provided at all times. Care was taken to ensure that all chickens commenced to eat and drink within a few hours of being placed in the brooders.

The chickens were killed by decapitation. The whole of the pectoral muscle was removed from the sternum, dissected free of visible fat and tendon and weighed. Since the muscle is bilaterally symmetrical, one side was used for DNA determination and the other for histometry. Both gastrocnemii were removed, freed from visible tendon and individually weighed. The muscle from the right leg was used for DNA determination and that from the left leg for histometry.

The usual procedure was for samples intended for DNA estimation to be minced, either in the apparatus described by Seevers and Shideman ('41) or, for the larger samples, in a culinary mincer; but when the sample weighed less than about 2 gm, it was finely cut up with scissors. The minced muscle was then thoroughly mixed and samples, 1 gm if available, were weighed into capped plastic tubes, rapidly frozen and stored at -20°C . The samples for histometry were taken from the centre of one side of the pectoral muscle and from the thickest part of the gastrocnemius of the left leg. They were fixed in formol saline and remained in the fixative until required.

After thawing, the samples were homogenized in distilled water in a Servall Omnimixer, and DNA was determined by the indole colorimetric reaction described by Ceriotti ('52). This was carried out on the complete homogenate as it had been found that prior extraction with perchloric acid according to the method of Paul ('56) resulted in the destruction of some of the DNA and trichloroacetic acid inhibits colour formation (Ceriotti, '55). The method used was as follows. Two ml of

homogenate containing 20–40 mg of muscle were pipetted into a 10 ml centrifuge tube and 1 ml of 0.04% indole plus 1 ml of 6N HCl were added. The tube was stoppered with a glass marble and heated in a boiling water bath for 12 minutes then rapidly cooled in cold water. After centrifugation at 3,000 G for five minutes, the supernatant was decanted into another centrifuge tube and extracted three times with 4 ml of chloroform. The coloured solution was centrifuged for one minute to clear the emulsion and its absorbance measured at 490 m μ . Calibration was by means of standard solutions of DNA containing 10 μg and 20 μg per ml, treated in the same way. Ceriotti ('52) carried out exhaustive tests of the specificity of the indole reaction. He found that only arabinose, arabofuranosyladenine and deoxyribose yielded the same colour as DNA and, even then, at a much lower intensity. The possibility of increased colour yield due to substances other than DNA in the homogenate therefore seems remote. The absence of interfering substances which might reduce the colour yield was demonstrated by means of recovery tests, carried out by adding standard DNA solutions to muscle homogenates.

Since the mean quantity of DNA per diploid nucleus is constant for individual species (Vendrelly, '55), the total number of nuclei in an organ or tissue may be estimated from its DNA content. Although this method has a number of limitations, which are discussed by Enesco and Leblond ('62), it is considered to be satisfactory for skeletal muscle. Davidson ('60) gives a value of 2.5×10^{-3} mg DNA per diploid nucleus for the chicken and this value has been used in the present studies.

The histometric technique was that described by Joubert ('56). Free-hand shavings, made across the grain of the muscle, were teased apart in dilute glycerine on a microscope slide, and a coverslip was gently applied. Measurements of the cross-diameter of 100 fibres per sample were made using an ocular micrometer at a magnification of 300. The ocular micrometer was calibrated using a stage micrometer. The mean cross-sectional area of the fibres was calculated from the

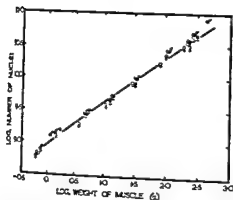


Fig. 1 Relationship between the number of nuclei and the weight of the pectoral muscle during growth (0-266 days). Open circles, White Leghorn; closed circles, New Hampshire.

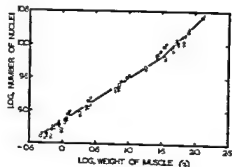


Fig. 2 Relationship between the number of nuclei and the weight of the gastrocnemius muscle during growth (0-266 days). Open circles, White Leghorn; closed circles, New Hampshire.

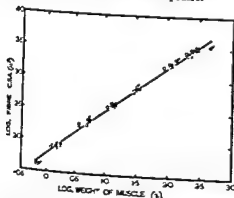


Fig. 3 Relationship between the cross-sectional area of the fibres and the weight of the pectoral muscle during growth (0-266 days). Open circles, White Leghorn; closed circles, New Hampshire.

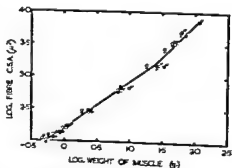


Fig. 4 Relationship between the cross-sectional area of the fibres and the weight of the gastrocnemius muscle during growth (0-266 days). Open circles, White Leghorn; closed circles, New Hampshire.

ficients, shown in table 3, are close to unity, it follows that during the growth of the gastrocnemius muscle, like that of the pectoral, the mean cross-sectional area of the fibres increased in proportion to the total number of nuclei.

DISCUSSION

The results show that during normal muscle growth mathematical relationships exist between the weight of the muscle, the mean cross-sectional area of the fibres and the total number of nuclei. In the pectoral muscle during the entire period studied (0-9 months) the mean cross-sectional area of the fibres is proportional

to the two-thirds power of the weight of the muscle. This is also valid for the gastrocnemius muscle until about two months of age, after which the fibre cross-sectional area increases directly in proportion to the weight of the muscle. In both muscles during the entire period studied the mean cross-sectional area of the fibres is proportional to the total number of nuclei in the muscle.

It is reasonable to suppose that these findings are indicative of underlying relationships between the number of nuclei and the dimensions of individual fibres. This hypothesis will now be discussed in the light of our present knowledge of the

the logarithm of the weight of the muscle, since a straight line of gradient 0.67 would signify the relationship. Figure 1 shows that for the pectoral muscle, irrespective of breed or sex, such a relationship did exist throughout the whole growth period. The regression coefficients of the logarithm of the number of nuclei on the logarithm of the weight of the muscle were calculated for each breed and sex. They ranged from 0.70 ± 0.04 for the New Hampshire males to 0.66 ± 0.04 for the White Leghorn females and are not significantly different from 0.67 (table 2).

The graph of the logarithm of the number of nuclei against the logarithm of the weight of the gastrocnemius muscle is shown in figure 2. It is seen that for this muscle a linear relationship did not exist for the whole of the growth period, but that the curve approximates to two straight lines. It is also evident that, whereas the gradient of the line relating to early growth is approximately 0.67, the gradient of the line relating to late growth is close to unity, indicating that at that stage the number of nuclei were increasing in direct proportion to the weight of the muscle.

To study the relationship between the growth of the muscles and the growth of their constituent fibres, graphs were plotted of the logarithm of the cross-sectional area of the fibres against the logarithm of the weight of the muscles. For the pectoral muscle, the relationship was linear (fig. 3), the regression coefficients being approximately 0.72 irrespective of breed or sex (table 2). The curve for the gastrocnemius muscle approximates to two straight lines (fig. 4). The gradient of the line relating to muscle weights of less than about 30 gm

is approximately 0.7, while the gradient of the line relating to muscle weights in excess of this is close to unity.

It has been shown above that for the pectoral muscle there were linear relationships between log number of nuclei and log weight of muscle and between log fibre cross-sectional area and log weight of muscle. It therefore follows that there must also be a linear relationship between log fibre cross-sectional area and log number of nuclei. Consequently, the four regression equations, one for each breed and sex, were calculated and compared by the appropriate statistical tests (Brownlee, '60). These showed that the four regression lines were coincident and the regression equation to the coincident line was calculated. The regression equations relating to the four individual lines, as well as that relating to the coincident line, are shown in table 3 and the coincident line is plotted in figure 5. It is seen that the regression coefficients are close to unity, which indicates that during the growth of the pectoral muscle the mean cross-sectional area of the fibres increased in proportion to the total number of nuclei.

Comparison of figures 2 and 4 shows that for the gastrocnemius muscle the curves of log number of nuclei on log weight of muscle and of log fibre cross-sectional area on log weight of muscle are very similar. Both approximate to two straight lines, one of gradient approximately 0.7, for values of log muscle weight less than 1.5 (approximately 30 gm) and the other of gradient approximately 1.0, for values of log muscle weight greater than 1.5. This suggests that there is a simple relationship between the number of nuclei and the cross-sectional area of the fibres. Consequently, the regression equations of log number of nuclei on log fibre cross-sectional area were calculated for each breed and sex, and compared by the appropriate statistical tests. The regression lines, which were shown to be parallel but not coincident are plotted in figure 6. For the same cross-sectional area, the number of nuclei tended to be higher in the New Hampshires than in the White Leghorns and higher in the males than in the females. Since the regression coef-

TABLE 2

Regression coefficients (b) of the mean values at different ages (0, 4, 8, 16, 32, 66, 128 and 266 days) of the logarithm of the number of nuclei (N) and the logarithm of the fibre cross-sectional area (C) on the logarithm of the weight of the pectoral muscle (W).

(Five animals at each age)

	b _{NW}	b _{CW}
New Hampshire ♂	0.70 ± 0.04	0.71 ± 0.05
New Hampshire ♀	0.68 ± 0.03	0.73 ± 0.04
White Leghorn ♂	0.67 ± 0.04	0.72 ± 0.03
White Leghorn ♀	0.66 ± 0.04	0.72 ± 0.04

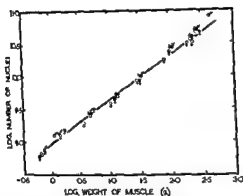


Fig. 1 Relationship between the number of nuclei and the weight of the pectoral muscle during growth (0-266 days). Open circles, White Leghorn; closed circles, New Hampshire.

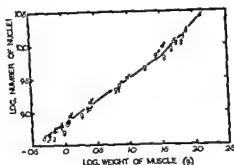


Fig. 2 Relationship between the number of nuclei and the weight of the gastrocnemius muscle during growth (0-266 days). Open circles, White Leghorn; closed circles, New Hampshire.

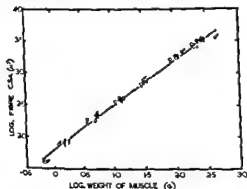


Fig. 3 Relationship between the cross-sectional area of the fibres and the weight of the pectoral muscle during growth (0-266 days). Open circles, White Leghorn, closed circles, New Hampshire.

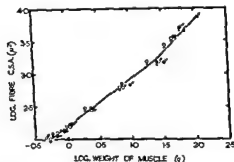


Fig. 4 Relationship between the cross-sectional area of the fibres and the weight of the gastrocnemius muscle during growth (0-266 days). Open circles, White Leghorn; closed circles, New Hampshire.

ficants, shown in table 3, are close to unity, it follows that during the growth of the gastrocnemius muscle, like that of the pectoral, the mean cross-sectional area of the fibres increased in proportion to the total number of nuclei.

DISCUSSION

The results show that during normal muscle growth mathematical relationships exist between the weight of the muscle, the mean cross-sectional area of the fibres and the total number of nuclei. In the pectoral muscle during the entire period studied (0-9 months) the mean cross-sectional area of the fibres is proportional

to the two-thirds power of the weight of the muscle. This is also valid for the gastrocnemius muscle until about two months of age, after which the fibre cross-sectional area increases directly in proportion to the weight of the muscle. In both muscles during the entire period studied the mean cross-sectional area of the fibres is proportional to the total number of nuclei in the muscle.

It is reasonable to suppose that these findings are indicative of underlying relationships between the number of nuclei and the dimensions of individual fibres. This hypothesis will now be discussed in the light of our present knowledge of the

TABLE 3

Regression coefficients of the mean values at different ages (0, 4, 8, 16, 32, 66, 128 and 266 days) of logarithm of the cross-sectional area of the fibres on the logarithm of the number of nuclei.

(Five animals at each age)

	Pectoral	Gastrocnemius
New Hampshire ♂	1.01 ± 0.12	1.05 ± 0.11
New Hampshire ♀	1.07 ± 0.08	1.11 ± 0.16
White Leghorn ♂	1.09 ± 0.10	1.12 ± 0.10
White Leghorn ♀	1.05 ± 0.04	1.08 ± 0.06
Coincident or parallel lines (see text)	1.05 ± 0.04	1.08 ± 0.06

structure and growth of skeletal muscle. Three postulates are necessary:

(a) The post-embryonic growth of skeletal muscle is almost entirely the result of hypertrophy of existing fibres, accompanied by an increase in the amount of extracellular material. Hyperplasia plays a very minor role in the process.

In the following mammalian species it is believed that the number of fibres is fixed at birth: man (MacCallum, 1898; Montgomery, '62), rabbit (Meara, '47), sheep (Joubert, '56) and pig (McMeekan, '40). Eliot, Wiggington and Corbin ('43) believed that this was also so for the rat, but other workers, Morpurgo (1898), Enesco and Puddy ('64) and Chiakulas and Pauly ('65), were of the opinion that hyperplasia continued to occur for a few weeks after birth. However, the results of these workers indicate that, even during this period, hypertrophy of the existing fibres is the major cause of muscle growth. Goldspink ('62) believed that in the mouse an increase of cross-sectional area of the fibres was the main cause of growth of the biceps brachia, but that there was an increase in the number of fibres until eight weeks of age.

Smith ('63) found that in the chicken between hatching and ten weeks of age the cross-sectional area of the sartorius muscle increased 14-fold and that of its constituent fibres 15-fold which suggests that the number of fibres did not increase. Montgomery, Dickerson and McCance ('64), however, found an increase of the number of fibres seen in muscle cross-section but they point out that this may

have been due to a lengthening of the existing fibres and not an increase of their number.

(b) The weight of the fibres is a relatively fixed proportion of the total weight of a muscle. Therefore, by weighing the whole muscle we can obtain an estimate of the total weight of the fibres.

Enesco and Puddy ('64) studied the growth of four muscles of the rat and estimated the fraction of the muscle tissue occupied by the fibres, endomycium and perimycium, at 16, 36 and 86 days of age. Their results showed that the fibres oc-

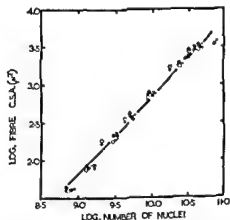


Fig. 5 Relationship between the cross-sectional area of the fibres and the number of nuclei in the pectoral muscle during growth (0-266 days). Open circles, White Leghorns; closed circles, New Hampshire.

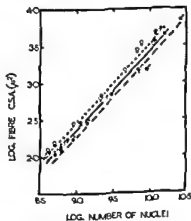


Fig. 6 Relationship between the cross-sectional area of the fibres and the number of nuclei of the gastrocnemius muscle during growth (0-266 days). Open circles, White Leghorn; closed circles, New Hampshire.

cupied between 70% and 90% of the total muscle volume, depending on the age.

(c) The nuclei of the muscle fibres are a relatively fixed proportion of the total number of nuclei within a muscle.

Enesco and Puddy ('64) estimated the percentage of the total number of nuclei which were within the fibres, endomycium and perimycium. The fraction of the nuclei within the fibres was approximately 65% and showed little variation with age.

If postulates (a) and (b) are valid, it follows that the growth (change in weight) of a muscle is a measure, in arbitrary units, of the mean growth (change in weight or volume) of its constituent fibres. If postulates (a) and (c) are valid, it follows that the change with age in the total number of nuclei in a muscle is a measure of the change in the mean number of nuclei per fibre.

Assuming these relationships, an attempt will be made to explain the relationships between the weight of the muscle, the mean cross-sectional area of its fibres and the number of nuclei. The muscle fibres are essentially cylindrical structures. If they grow in such a way that their length and diameter maintain a constant ratio, their volume will increase in proportion to the cube of their diameter. Since their cross-sectional area is proportional to the square of their diameter, it follows that their cross-sectional area would be proportional to the two-thirds power of their volume (or weight) and roughly proportional to the two thirds power of the total weight of the muscle. If, however, the length of the fibres is constant, their cross-sectional area will increase in proportion to their volume and, therefore, roughly in proportion to the total weight of the muscle.

The results of the present studies, therefore, suggest that during the entire period of growth of the pectoral muscle and the first two months of growth of the gastrocnemius, the length and diameter of the muscle fibres maintain a constant ratio, but that there is no increase of length of the gastrocnemius muscle fibres after that age. It is of interest to note that Meara ('47) found that the fibres of the gastrocnemius muscle of the rabbit attained

their maximum length at two months of age. Analysis of the results of Mehner ('38) showed that in the gracilis and sartorius muscles of the chicken the cross-sectional area of the fibres increased roughly in proportion to the two-thirds power of the muscle weight between hatching and six months of age. It would appear, therefore, that in these two muscles also the length and diameter of the fibres maintain a constant ratio during growth.

The results of the present work also suggest that, during growth of the muscle fibres, their cross-sectional area and their number of nuclei maintain a constant ratio. This would explain the fact that the mean cross-sectional area of the fibres was roughly proportional to the total number of nuclei in the muscle. An explanation of this phenomenon is possible in the light of recent work concerning the mode of increase in the number of nuclei of skeletal muscle fibres.

There are three theories explaining the multinucleation of muscle fibres (Stockdale and Holtzer, '61; MacConnachie, Enesco and Leblond, '64). They are: (1) mitotic division of the nuclei without cytoplasmic division, (2) amitotic division of the nuclei without cytoplasmic division, (3) cell fusion. Mitotic figures are rarely, if ever, seen in the nuclei of muscle fibres and, in the past, amitosis has been the accepted explanation. However, in the light of present knowledge concerning the function of DNA and its replication during nuclear division, one is led to the conclusion expressed by Ris ('55), Leblond and Walker ('56) and Bucher ('63) that mitosis is the only means of nuclear proliferation and that amitosis is merely fragmentation.

In vitro studies, using a variety of techniques, all indicate that multinucleation is the result of cell fusion. Numerous workers (Holtzer, Abbot and Lash, '58; Capers, '60; Stockdale and Holtzer, '61; Cooper and Konigsberg, '61) confirm the absence of mitotic (or amitotic) division of myotube nuclei but report that the mononucleated myoblasts exhibit mitosis and fuse with the existing myotubes. Firket ('58) and Strehler, Konigsberg and

TABLE 3

Regression coefficients of the mean values at different ages (0, 4, 8, 16, 32, 68, 128 and 266 days) of logarithm of the cross-sectional area of the fibres on the logarithm of the number of nuclei.

(Five animals at each age)

	Pectoral	Gastrocnemius
New Hampshire ♂	1.01 ± 0.12	1.05 ± 0.11
New Hampshire ♀	1.07 ± 0.08	1.11 ± 0.16
White Leghorn ♂	1.09 ± 0.10	1.12 ± 0.10
White Leghorn ♀	1.05 ± 0.04	1.08 ± 0.06
Coincident or parallel lines (see text)	1.05 ± 0.04	1.08 ± 0.06

structure and growth of skeletal muscle. Three postulates are necessary:

(a) The post-embryonic growth of skeletal muscle is almost entirely the result of hypertrophy of existing fibres, accompanied by an increase in the amount of extracellular material. Hyperplasia plays a very minor role in the process.

In the following mammalian species it is believed that the number of fibres is fixed at birth: man (MacCallum, 1898; Montgomery, '62), rabbit (Meara, '47), sheep (Joubert, '56) and pig (McMeekan, '40). Elliot, Wiggington and Corbin ('43) believed that this was also so for the rat, but other workers, Morpurgo (1898), Enesco and Puddy ('64) and Chiakulas and Pauly ('65), were of the opinion that hyperplasia continued to occur for a few weeks after birth. However, the results of these workers indicate that, even during this period, hypertrophy of the existing fibres is the major cause of muscle growth. Goldspink ('62) believed that in the mouse an increase of cross-sectional area of the fibres was the main cause of growth of the biceps brachia, but that there was an increase in the number of fibres until eight weeks of age.

Smith ('63) found that in the chicken between hatching and ten weeks of age the cross-sectional area of the sartorius muscle increased 14-fold and that of its constituent fibres 15-fold which suggests that the number of fibres did not increase. Montgomery, Dickerson and McCance ('64), however, found an increase of the number of fibres seen in muscle cross-section but they point out that this may

have been due to a lengthening of the existing fibres and not an increase of their number.

(b) The weight of the fibres is a relatively fixed proportion of the total weight of a muscle. Therefore, by weighing the whole muscle we can obtain an estimate of the total weight of the fibres.

Enesco and Puddy ('64) studied the growth of four muscles of the rat and estimated the fraction of the muscle tissue occupied by the fibres, endomycium and perimycium, at 16, 36 and 86 days of age. Their results showed that the fibres oc-

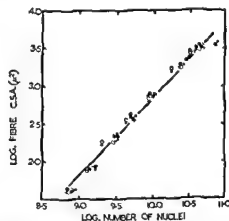


Fig. 5 Relationship between the cross-sectional area of the fibres and the number of nuclei in the pectoral muscle during growth (0-266 days). Open circles, White Leghorns; closed circles, New Hampshire.

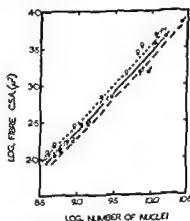


Fig. 6 Relationship between the cross-sectional area of the fibres and the number of nuclei of the gastrocnemius muscle during growth (0-266 days). Open circles, White Leghorn; closed circles, New Hampshire.

cupied between 70% and 90% of the total muscle volume, depending on the age.

(c) The nuclei of the muscle fibres are a relatively fixed proportion of the total number of nuclei within a muscle.

Enesco and Puddy ('64) estimated the percentage of the total number of nuclei which were within the fibres, endomycium and perimycium. The fraction of the nuclei within the fibres was approximately 65% and showed little variation with age.

If postulates (a) and (b) are valid, it follows that the growth (change in weight) of a muscle is a measure, in arbitrary units, of the mean growth (change in weight or volume) of its constituent fibres. If postulates (a) and (c) are valid, it follows that the change with age in the total number of nuclei in a muscle is a measure of the change in the mean number of nuclei per fibre.

Assuming these relationships, an attempt will be made to explain the relationships between the weight of the muscle, the mean cross-sectional area of its fibres and the number of nuclei. The muscle fibres are essentially cylindrical structures. If they grow in such a way that their length and diameter maintain a constant ratio, their volume will increase in proportion to the cube of their diameter. Since their cross-sectional area is proportional to the square of their diameter, it follows that their cross-sectional area would be proportional to the two-thirds power of their volume (or weight) and roughly proportional to the two thirds power of the total weight of the muscle. If, however, the length of the fibres is constant, their cross-sectional area will increase in proportion to their volume and, therefore, roughly in proportion to the total weight of the muscle.

The results of the present studies, therefore, suggest that during the entire period of growth of the pectoral muscle and the first two months of growth of the gastrocnemius, the length and diameter of the muscle fibres maintain a constant ratio, but that there is no increase of length of the gastrocnemius muscle fibres after that age. It is of interest to note that Mears ('47) found that the fibres of the gastrocnemius muscle of the rabbit attained

their maximum length at two months of age. Analysis of the results of Mehner ('38) showed that in the gracilis and sartorius muscles of the chicken the cross-sectional area of the fibres increased roughly in proportion to the two-thirds power of the muscle weight between hatching and six months of age. It would appear, therefore, that in these two muscles also the length and diameter of the fibres maintain a constant ratio during growth.

The results of the present work also suggest that, during growth of the muscle fibres, their cross-sectional area and their number of nuclei maintain a constant ratio. This would explain the fact that the mean cross-sectional area of the fibres was roughly proportional to the total number of nuclei in the muscle. An explanation of this phenomenon is possible in the light of recent work concerning the mode of increase in the number of nuclei of skeletal muscle fibres.

There are three theories explaining the multinucleation of muscle fibres (Stockdale and Holtzer, '61; MacConnachie, Enesco and Leblond, '64). They are: (1) mitotic division of the nuclei without cytoplasmic division, (2) amitotic division of the nuclei without cytoplasmic division, (3) cell fusion. Mitotic figures are rarely, if ever, seen in the nuclei of muscle fibres and, in the past, amitosis has been the accepted explanation. However, in the light of present knowledge concerning the function of DNA and its replication during nuclear division, one is led to the conclusion expressed by Ris ('55), Leblond and Walker ('56) and Bucher ('63) that mitosis is the only means of nuclear proliferation and that amitosis is merely fragmentation.

In vitro studies, using a variety of techniques, all indicate that multinucleation is the result of cell fusion. Numerous workers (Holtzer, Abbot and Lash, '58; Capers, '60; Stockdale and Holtzer, '61; Cooper and Konigsberg, '61) confirm the absence of mitotic (or amitotic) division of myotube nuclei but report that the mononucleated myoblasts exhibit mitosis and fuse with the existing myotubes. Firke ('58) and Strehler, Konigsberg and

Kelly ('63) showed that the myotube nuclei are invariably diploid but that a small proportion of the myoblast nuclei are tetraploid, as would be expected in cells preparing to divide. By using tritiated thymidine, Stockdale and Holtzer ('61) and Bassleer ('62, '63) showed that whereas myoblast nuclei synthesize DNA, myotube nuclei do not. The delayed appearance within the myotubes of labelled nuclei, presumably derived from the myoblasts, is further evidence that multinucleation is the result of cell fusion.

The results of the present studies suggest that the fusion of a myoblast with an existing muscle fibre, results in the increase of its cross-sectional area by a fixed amount as well as the addition of a single nucleus. There is also evidence (Goldspink, '65) that during growth of muscle fibres, their number of myofibrils is proportional to their cross-sectional area which suggests that the number of nuclei and the number of myofibrils maintain a constant ratio. This would occur if each myoblast supplied the same number of myofibrils in addition to a single nucleus.

Dreyfus, Kruh and Shapira ('60) showed that muscles of adult rats synthesize myosin. This indicates the existence of an active DNA-RNA system and of functional nuclei. It is, therefore, tentatively suggested that there may be a functional, as well as a numerical, relationship between the nuclei and the myofibrils.

ACKNOWLEDGMENTS

The author expresses his thanks to Dr. H. W. McNary for his advice during the course of this work and to Dr. R. K. Ryan for constructive criticism of the manuscript.

Financial support for this study was provided by the Poultry Husbandry Research Foundation, University of Sydney.

LITERATURE CITED

- Bassleer, R. 1962 Etude de l'augmentation du nombre de noyaux dans des bourgeons musculaires cultivés *in vitro*. Observations sur le vivant, dosages cytophotométriques et histautoradiographies. *Z. Anat. EntwGesch.*, 123: 184-205.
- 1963 Application de techniques cyto- logiques modernes à l'étude du problème des amitoses dans les bourgeons musculaires. In: *Cell Growth and Cell Division*. R.J.C. Harris, ed. Academic Press, New York, pp. 299-312.
- Brownlee, K. A. 1960 Statistical theory and methodology in science and engineering. Academic Press, New York, pp. 288-290.
- Bucher, O. 1963 Le problème de l'amitose. In: *Cell Growth and Cell Division*. R.J.C. Harris, ed. Academic Press, New York, pp. 313-321.
- Capers, C. R. 1960 Multinucleation of skeletal muscle *in vitro*. *J. biophys. biochem. Cytol.*, 7: 559-566.
- Cerioti, G. 1952 A microchemical determina- tion of deoxyribonucleic acid. *J. biol. Chem.*, 198: 297-303.
- 1955 Determination of nucleic acids in animal tissues. *J. biol. Chem.*, 214: 59-70.
- Chiakulas, J. J., and J. E. Pauly 1965 A study of postnatal growth of skeletal muscle in the rat. *Anat. Rec.*, 152: 55-62.
- Cooper, W. G., and I. R. Konigsberg 1961 Dy- namics of myogenesis *in vitro*. *Anat. Rec.*, 140: 195-205.
- Davidson, J. N. 1960 The biochemistry of the nucleic acids. Methuen and Co. Ltd. London, p. 142.
- Dreyfus, J. C., J. Kruh and G. Shapira 1960 Metabolism of myosin and life time of myo- fibrils. *Biochem. J.*, 75: 574-578.
- Eliot, T. S., R. C. Wiggington and K. C. Corbin 1943 The number and size of muscle fibres in the rat soleus in relation to age, sex and exercise. *Anat. Rec.*, 85: 307-308.
- Enesco, M., and C. P. Leblond 1962 Increase in cell number as a factor in the growth of the organs and tissues of the young male rat. *J. Embryol. exp. Morph.*, 10: 530-562.
- Enesco, M., and D. Puddy 1964 Increase in the number of nuclei and weight in skeletal muscle of rats of various ages. *Am. J. Anat.*, 114: 235-244.
- Firket, H. 1958 Recherches sur la synthèse des acides désoxyribonucleiques et la prépara- tion à la mitose dans des cellules cultivées *in vitro*. *Archs. Biol., Liège.*, 69: 1-166.
- Goldspink, G. 1962 Studies on post-embryonic growth and development of skeletal muscle. 1. Evidence of two phases in which striated muscle fibres are able to exist. *Proc. R. Ir. Acad.*, 62: 135-150.
- 1965 Cytological basis of decrease in muscle strength during starvation. *Am. J. Physiol.*, 209: 100-104.
- Holtzer, H., J. Abbot and J. Lash 1958 On the formation of multinucleated myotubes. *Anat. Rec.*, 131: 567.
- Joubert, D. M. 1956 An analysis of factors influencing post-natal growth and development of the muscle fibre. *J. agric. Sci., Camb.*, 47: 59-102.
- Leblond, C. P., and B. E. Walker 1956 Re- newal of cell populations. *Physiol. Rev.*, 36: 255-275.
- MacCallum, J. B. 1898 On the histogenesis of the striated muscle fibre and the growth of the human sartorius muscle. *Johns Hopkins Hosp. Bull.*, 9: 208-215.

- MacConnachie, H. F., M. Enesco and C. P. Leblond 1964 The mode of increase in the number of skeletal muscle nuclei in the post-natal rat. *Am. J. Anat.*, 114: 245-253.
- McMeekan, C. P. 1940 Growth and development in the pig, with special reference to carcass quality characters. 1. *J. Agric. Sci.*, 30: 276-343.
- Meara, P. J. 1947 Meat studies No. 1. Post-natal growth and development of muscle, as exemplified by the gastrocnemius and psoas muscles of the rabbit. Onderstepoort J. vet. Sci. Anim. Ind., 21: 329-466.
- Mehner, A. 1938 Beziehungen zwischen Zellgrösse und Körpergrösse. *Z. Zücht. Reithe B. Tierzücht. ZüchtBiol.*, 40: 1-48.
- Montgomery, R. D. 1962 Growth of human striated muscle. *Nature, Lond.*, 195: 194-195.
- Montgomery, R. D., J. W. T. Dickerson and R. A. McCance 1964 Severe undernutrition in growing and adult animals. 13. The morphology and chemistry of development and undernutrition in the sartorius muscle of the fowl. *Br. J. Nutr.*, 18: 587-593.
- Morpurgo, B. 1893 Ueber die postembryonale Entwicklung der quergestriefen Muskeln von weissen Ratten. *Anat. Anz.*, 15: 200-206.
- Moss, F. P., R. A. Simmonds and H. W. McNary 1964 The growth and composition of skeletal muscle in the chicken. 2. The relationship between muscle weight and the number of nuclei. *Poult. Sci.*, 43: 1086-1091.
- Paul, J. 1956 The chemical determination of DNA in tissue cultures. *J. biochem biophys. Cytol.*, 2: 797-798.
- Ris, H. 1955 Cell division. In: *Analysis of Development*. B. H. Willier, P. A. Weiss and V. Hamburger, ed. W. B. Saunders Company, Philadelphia and London, p. 119.
- SeEVERS, M. H., and F. E. Shideman 1941 A mincer adaptable to small quantities of tissue. *Science, N.Y.*, 94: 351-352.
- Smith, J. H. 1963 Relation of body size to muscle cell size and number in the chicken. *Poult. Sci.*, 42: 283-290.
- Stockdale, F. E., and H. Holtzer 1961 DNA synthesis and myogenesis. *Expl. Cell Res.*, 24: 508-520.
- Strehler, B. L., I. R. Konigsberg and J. E. T. Kelly 1963 Floidy of myotube nuclei developing in vitro as determined with a recording double beam microspectrophotometer. *Expl. Cell Res.*, 32: 232-241.
- Vendrel, R. 1955 The desoxyribonucleic acid content of the nucleus. In: *The nucleic acids*, Vol. 2. E. C. Chargaff and J. N. Davidson, eds. Academic Press, New York, pp. 155-180.

Kelly ('63) showed that the myotube nuclei are invariably diploid but that a small proportion of the myoblast nuclei are tetraploid, as would be expected in cells preparing to divide. By using tritiated thymidine, Stockdale and Holtzer ('61) and Bassleer ('62, '63) showed that whereas myoblast nuclei synthesize DNA, myotube nuclei do not. The delayed appearance within the myotubes of labelled nuclei, presumably derived from the myoblasts, is further evidence that multinucleation is the result of cell fusion.

The results of the present studies suggest that the fusion of a myoblast with an existing muscle fibre, results in the increase of its cross-sectional area by a fixed amount as well as the addition of a single nucleus. There is also evidence (Goldspink, '65) that during growth of muscle fibres, their number of myofibrils is proportional to their cross-sectional area which suggests that the number of nuclei and the number of myofibrils maintain a constant ratio. This would occur if each myoblast supplied the same number of myofibrils in addition to a single nucleus.

Dreyfus, Kruh and Shapira ('60) showed that muscles of adult rats synthesize myosin. This indicates the existence of an active DNA-RNA system and of functional nuclei. It is, therefore, tentatively suggested that there may be a functional, as well as a numerical, relationship between the nuclei and the myofibrils.

ACKNOWLEDGMENTS

The author expresses his thanks to Dr. H. W. McNary for his advice during the course of this work and to Dr. R. K. Ryan for constructive criticism of the manuscript.

Financial support for this study was provided by the Poultry Husbandry Research Foundation, University of Sydney.

LITERATURE CITED

- Bassleer, R. 1962 Étude de l'augmentation du nombre de noyaux dans des bourgeons musculaires cultivés *in vitro*. Observations sur le vivant, dosages cytophotométriques et historadiographies. *Z. Anat. EntwGesch.*, 123: 184-205.
- 1963 Application de techniques cytologiques modernes à l'étude du problème des amitoses dans les bourgeons musculaires. In: *Cell Growth and Cell Division*. R.J.C. Harris, ed. Academic Press, New York, pp. 299-312.
- Brownlee, K. A. 1960 Statistical theory and methodology in science and engineering. Academic Press, New York, pp. 288-290.
- Bucher, O. 1963 Le problème de l'amitose. In: *Cell Growth and Cell Division*. R.J.C. Harris, ed. Academic Press, New York, pp. 313-321.
- Capers, C. R. 1960 Multinucleation of skeletal muscle *in vitro*. *J. biophys. biochem. Cytol.*, 7: 559-566.
- Cerriotti, G. 1952 A microchemical determination of desoxyribonucleic acid. *J. biol. Chem.*, 198: 297-303.
- 1955 Determination of nucleic acids in animal tissues. *J. biol. Chem.*, 214: 59-70.
- Chiakulas, J. J., and J. E. Pauly 1965 A study of postnatal growth of skeletal muscle in the rat. *Anat. Rec.*, 152: 55-62.
- Cooper, W. G., and I. R. Konigsberg 1961 Dynamics of myogenesis *in vitro*. *Anat. Rec.*, 140: 195-205.
- Davidson, J. N. 1960 The biochemistry of the nucleic acids. Methuen and Co. Ltd. London, p. 142.
- Dreyfus, J. C., J. Kruh and G. Shapira 1960 Metabolism of myosin and life time of myofibrils. *Biochem. J.*, 75: 574-578.
- Eliot, T. S., R. C. Wigginton and K. C. Corbin 1943 The number and size of muscle fibres in the rat soleus in relation to age, sex and exercise. *Anat. Rec.*, 85: 307-308.
- Enesco, M., and C. P. Leblond 1962 Increase in cell number as a factor in the growth of the organs and tissues of the young male rat. *J. Embryol. exp. Morph.*, 10: 530-562.
- Enesco, M., and D. Puddy 1964 Increase in the number of nuclei and weight in skeletal muscle of rats of various ages. *Am. J. Anat.*, 114: 235-244.
- Firket, H. 1958 Recherches sur la synthèse des acides désoxyribonucleiques et la préparation à la mitose dans des cellules cultivées *in vitro*. *Archs. Biol.*, Liège, 69: 1-166.
- Goldspink, G. 1962 Studies on post-embryonic growth and development of skeletal muscle. 1. Evidence of two phases in which striated muscle fibres are able to exist. *Proc. R. Ir. Acad.*, 62: 135-150.
- 1965 Cytological basis of decrease in muscle strength during starvation. *Am. J. Physiol.*, 209: 100-104.
- Holtzer, H., J. Abbot and J. Lash 1958 On the formation of multinucleated myotubes. *Anat. Rec.*, 131: 567.
- Joubert, D. M. 1956 An analysis of factors influencing post-natal growth and development of the muscle fibre. *J. agric. Sci., Camb.*, 47: 59-102.
- Leblond, C. P., and B. E. Walker 1956 Renewal of cell populations. *Physiol. Rev.*, 36: 255-275.
- MacCallum, J. B. 1898 On the histogenesis of the striated muscle fibre and the growth of the human sartorius muscle. *Johns Hopkins Hosp. Bull.*, 9: 208-215.

The Relationship between the Dimensions of the Fibres and the Number of Nuclei during Restricted Growth, Degrowth and Compensatory Growth of Skeletal Muscle

F. P. MOSS

Department of Animal Husbandry, University of Sydney,
Sydney, N.S.W., Australia

ABSTRACT During unrestricted growth of the pectoral muscle of chickens, the mean cross-sectional area of the fibres increased in proportion to the total number of nuclei and in proportion to the two thirds power of the weight of the muscle. Continuous restricted feeding from 0 day, which limited the weight of the muscle at 16 days to 44% or 69% of that of chickens fed *ad libitum*, did not affect these relationships.

A sudden restriction of feed from eight days of age retarded growth of the muscle to approximately 70% of the weight of the controls at 16 days. It did not affect the relationship between the number of nuclei and the fibre cross-sectional area, both of which were also limited to about 70% of those of the controls; but it did disrupt the relationship of these two variates to the weight of the muscle. Subsequent *ad libitum* feeding caused compensatory growth and restored the relationship.

Starvation or severe undernutrition for a few days, which reduced weight of the muscle and the fibre cross-sectional area by approximately 25%, caused no loss of nuclei, thereby disrupting both relationships. Subsequent *ad libitum* feeding initially caused an increase of muscle weight and fibre cross-sectional area but no increase in the number of nuclei. This restored the relationships, which were then maintained during subsequent compensatory growth.

It has been shown (Moss, '68) that, during normal growth of skeletal muscles in the chicken, there are mathematical relationships between the weight of the muscle, the mean cross-sectional area of its fibres and its total number of nuclei. An explanation of this phenomenon has been offered in terms of contemporary theories of the anatomy and mode of growth of skeletal muscle and of the mechanism of multinucleation of the muscle fibres.

This report describes three experiments, which were conducted to determine to what extent these relationships were modified under various conditions of abnormal growth caused by different feeding regimes.

The total number of nuclei in the muscle was estimated from the DNA content, assuming a value of 2.5×10^{-9} mg DNA per diploid nucleus (Davidson, '60). The average amount of material associated with each nucleus was calculated by dividing the weight of the muscle by the number of nuclei. Following the nomenclature of Enesco and Leblond ('62), it has been termed the "weight per nucleus." If, as suggested previously (Moss, '68), the total

weight of a muscle provides an estimate of the average weight of the fibres (in arbitrary units), the weight divided by the mean fibre cross-sectional area provides an estimate of their average length (in arbitrary units).

MATERIALS AND METHODS

The nutritional regimes appertaining to the three experiments are described below. In other respects, the management of the chickens, as well as the laboratory techniques, were generally as described previously (Moss, '68). However, in all experiments a Potter Elvehjem tissue homogenizer was used in place of the Servall Omnimix, and in the first experiment DNA estimation was by the method of Paul ('56).

Experiment 1

Broiler chickens were fed a commercial mash *ad libitum* from hatching until eight days of age. One group was then fed a limited quantity ($2\frac{1}{2}$ –3 g per capita) of the same food four times daily until 16 days of age, after which they were again

The Relationship between the Dimensions of the Fibres and the Number of Nuclei during Restricted Growth, Degrowth and Compensatory Growth of Skeletal Muscle

F. P. MOSS

Department of Animal Husbandry, University of Sydney,
Sydney, N.S.W., Australia

ABSTRACT During unrestricted growth of the pectoral muscle of chickens, the mean cross-sectional area of the fibres increased in proportion to the total number of nuclei and in proportion to the two thirds power of the weight of the muscle. Continuous restricted feeding from 0 day, which limited the weight of the muscle at 16 days to 44% or 68% of that of chickens fed *ad libitum*, did not affect these relationships.

A sudden restriction of feed from eight days of age retarded growth of the muscle to approximately 70% of the weight of the controls at 16 days. It did not affect the relationship between the number of nuclei and the fibre cross-sectional area, both of which were also limited to about 70% of those of the controls; but it did disrupt the relationship of these two variates to the weight of the muscle. Subsequent *ad libitum* feeding caused compensatory growth and restored the relationship.

Starvation or severe undernutrition for a few days, which reduced weight of the muscle and the fibre cross-sectional area by approximately 25%, caused no loss of nuclei, thereby disrupting both relationships. Subsequent *ad libitum* feeding initially caused an increase of muscle weight and fibre cross-sectional area but no increase in the number of nuclei. This restored the relationships, which were then maintained during subsequent compensatory growth.

It has been shown (Moss, '68) that, during normal growth of skeletal muscles in the chicken, there are mathematical relationships between the weight of the muscle, the mean cross-sectional area of its fibres and its total number of nuclei. An explanation of this phenomenon has been offered in terms of contemporary theories of the anatomy and mode of growth of skeletal muscle and of the mechanism of multinucleation of the muscle fibres.

This report describes three experiments, which were conducted to determine to what extent these relationships were modified under various conditions of abnormal growth caused by different feeding regimes.

The total number of nuclei in the muscle was estimated from the DNA content, assuming a value of 2.5×10^{-9} mg DNA per diploid nucleus (Davidson, '60). The average amount of material associated with each nucleus was calculated by dividing the weight of the muscle by the number of nuclei. Following the nomenclature of Enesco and Leblond ('62), it has been termed the "weight per nucleus." If, as suggested previously (Moss, '68), the total

weight of a muscle provides an estimate of the average weight of the fibres (in arbitrary units), the weight divided by the mean fibre cross-sectional area provides an estimate of their average length (in arbitrary units).

MATERIALS AND METHODS

The nutritional regimes appertaining to the three experiments are described below. In other respects, the management of the chickens, as well as the laboratory techniques, were generally as described previously (Moss, '68). However, in all experiments a Potter Elvehjem tissue homogenizer was used in place of the Servall Omnimix, and in the first experiment DNA estimation was by the method of Paul ('56).

Experiment 1

Broiler chickens were fed a commercial mash *ad libitum* from hatching until eight days of age. One group was then fed a limited quantity ($2\frac{1}{2}$ –3 g per capita) of the same food four times daily until 16 days of age, after which they were again

fed *ad libitum*. This restriction of feed limited the growth of the muscle at 16 days to 70% of that of the controls, which were fed *ad libitum* throughout the entire period. Four chickens were sacrificed at eight days of age and eight from each group at 16 and 26 days. The weight and DNA content of the pectoral muscle were determined.

Experiment 2

New Hampshire chickens were fed a commercial ration *ad libitum* from hatching until seven days of age. One group was deprived of food for 48 hours, after which they were again fed *ad libitum*; the other group was fed *ad libitum* throughout the entire period. Chickens were sacrificed at 7, 8, 9, 10, 11, 13, 16, 20 and 27 days of age. At seven days (before starvation) eight chickens were sacrificed, but at the other ages 12 from the starved group and four from the control group were used. The smaller number of controls was considered sufficient, since the growth relationships during *ad libitum* feeding had already been established in previous experiments. The weight and DNA content of the pectoral muscle were determined.

Experiment 3

As in the previous two experiments, the number of nuclei in the muscle was estimated by DNA determination, but, in addition, the mean diameter of the fibres was determined histometrically. This enabled the relationship between the number of nuclei and the cross-sectional area of the fibres to be established. Restriction of nutrient intake was effected by adding

various proportions of cellulose to the mash and the mixtures were fed *ad libitum*. Three mash-cellulose mixtures were used, containing 90%, 60% and 40% mash, and were designated 90%, 60% and 40% feed, respectively. The chickens were New Hampshire pullets.

The experiment was conducted in two parts, the first of which, like the previous experiments, was to study the effect of sudden changes in nutrient intake. The organisation of this part of the experiment is outlined in table 3. The second part of the experiment was to study the effect of continuous restricted feeding from the time of hatching. Groups of chickens were fed pure mash (100% feed), 90% feed and 60% feed. Five individuals were sacrificed immediately after hatching (0 day) and five from each group at 4, 8 and 16 days of age.

RESULTS

Experiment 1

After eight days of feed restriction the weight of the muscle and its number of nuclei were significantly less than for the controls, but there was no difference in weight per nucleus. However, after ten days *ad libitum* feeding the differences had disappeared (table 1).

It is seen from figure 1 that for the controls there was a linear relationship between the logarithm of the weight of the muscle and the logarithm of its number of nuclei. The regression coefficient of log. number of nuclei on log. weight of muscle was 0.72 ± 0.24 , which is similar to the values obtained in previous experiments,

TABLE 1

Experiment 1. The effect of a sudden reduction of feed intake from 8 to 16 days of age and subsequent *ad libitum* feeding to 26 days on the growth of the pectoral muscle, its number of nuclei and the weight of muscle per nucleus

Age	Treatment group Nutritional status	Number of chickens	Weight of muscle	Number of nuclei	Weight per nucleus
(days)			(gm)	(10 ⁹)	(10 ⁻⁹ g)
8	Pre-treatment	4	6.2	3.3	1.8
16	Undernourished	8	10.6	4.2	2.5
16	Controls	8	15.0	6.2	2.4
26	Re-fed	8	31.0	10.8	2.9
26	Controls	8	29.2	10.1	2.9

{ Not significantly different ($P < 0.05$).

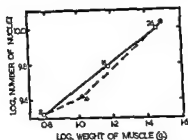


Fig. 1 Experiment 1. The effect of a sudden reduction of food intake from 8 to 16 days of age, followed by *ad libitum* feeding to 26 days, on the relationship between the number of nuclei and the weight of the pectoral muscle. Controls O; Restricted feed ●. Figures indicate age.

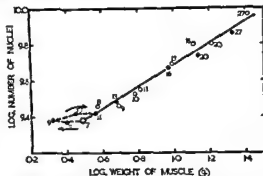


Fig. 2 Experiment 2. The effect of starvation from 7 to 9 days of age, followed by *ad libitum* feeding to 27 days, on the relationship between the number of nuclei and the weight of the pectoral muscle. Controls O; Starved, re-fed ●. Figures indicate age.

and confirms that during growth of the muscle the number of nuclei increased in proportion to the two thirds power of the weight. It is evident from figure 1 that a sudden restriction of feed intake upsets this relationship, but that it is restored after a period of *ad libitum* feeding.

Experiment 2

After 48 hours starvation the weight of the muscle had fallen to 70% of its original value, and this was reflected in a similar reduction of the weight per nucleus. There was no loss of nuclei (table 2).

Graphs of the logarithm of the number of nuclei (N) against the logarithm of the weight of the muscle (W) were plotted for the two treatments, starved-re-fed and controls, (fig. 2). It is seen that for the latter the usual linear relationship existed for the entire period, 7 to 27 days, and that after two days of re-feeding (11 days of age) the relationship for the former appeared to be the same. The two regression

lines were shown to be coincident (Brownlee, '60b). Their equations are shown below:

Controls, 7-27 days $\log N = 9.06 + 0.63 \log W$
 Re-fed, 11-27 days $\log N = 9.09 + 0.57 \log W$

Experiment 3

The effect of a sudden reduction of food intake, followed by *ad libitum* feeding is shown in table 3. In order that the results could be subjected to statistical analysis, the data (with the exception of R, the ratio of fibre cross-sectional area to number of nuclei) were subjected to logarithmic transformation to stabilize the variances (Brownlee, '60a). Comparisons between relevant pairs of means were made and the results are summarised in table 4.

As in experiment 2, starvation for two days caused a reduction in the weight of the muscle and the weight per nucleus but was without effect on the number of nuclei.

TABLE 2
 Experiment 2. The effect of starvation from seven to nine days of age and subsequent re-feeding on the growth of the pectoral muscle, its number of nuclei and the weight of muscle per nucleus.

Age	Weight of muscle		Number of nuclei		Weight per nucleus	
(days)	Starved	Controls	Starved	Controls	Starved	Controls
		(gm.)			(10 ⁻⁸ gm)	
		3.11			1.29	
7	2.60	3.75	2.34	2.88	1.07	1.32
8	2.17	4.89	2.40	2.88	0.93	1.74
9	2.86	6.11	2.63	3.39	1.10	1.82
10	3.75	6.49	2.63	3.55	1.38	1.82
11	4.86	9.72	3.02	4.90	1.58	2.00
12	9.38	12.9	4.68	6.31	2.00	2.09
13	13.8	16.2	5.50	6.31	2.51	2.51
14	21.4	25.9	7.24	9.12	2.88	2.82

(Pre-treatment: means of 8 chickens. Starved, means of 12 chickens. Controls: means of 4 chickens)

fed *ad libitum*. This restriction of feed limited the growth of the muscle at 16 days to 70% of that of the controls, which were fed *ad libitum* throughout the entire period. Four chickens were sacrificed at eight days of age and eight from each group at 16 and 26 days. The weight and DNA content of the pectoral muscle were determined.

Experiment 2

New Hampshire chickens were fed a commercial ration *ad libitum* from hatching until seven days of age. One group was deprived of food for 48 hours, after which they were again fed *ad libitum*; the other group was fed *ad libitum* throughout the entire period. Chickens were sacrificed at 7, 8, 9, 10, 11, 13, 16, 20 and 27 days of age. At seven days (before starvation) eight chickens were sacrificed, but at the other ages 12 from the starved group and four from the control group were used. The smaller number of controls was considered sufficient, since the growth relationships during *ad libitum* feeding had already been established in previous experiments. The weight and DNA content of the pectoral muscle were determined.

Experiment 3

As in the previous two experiments, the number of nuclei in the muscle was estimated by DNA determination, but, in addition, the mean diameter of the fibres was determined histometrically. This enabled the relationship between the number of nuclei and the cross-sectional area of the fibres to be established. Restriction of nutrient intake was effected by adding

various proportions of cellulose to the mash and the mixtures were fed *ad libitum*. Three mash-cellulose mixtures were used, containing 90%, 60% and 40% mash, and were designated 90%, 60% and 40% feed, respectively. The chickens were New Hampshire pullets.

The experiment was conducted in two parts, the first of which, like the previous experiments, was to study the effect of sudden changes in nutrient intake. The organisation of this part of the experiment is outlined in table 3. The second part of the experiment was to study the effect of continuous restricted feeding from the time of hatching. Groups of chickens were fed pure mash (100% feed), 90% feed and 60% feed. Five individuals were sacrificed immediately after hatching (0 day) and five from each group at 4, 8 and 16 days of age.

RESULTS

Experiment 1

After eight days of feed restriction the weight of the muscle and its number of nuclei were significantly less than for the controls, but there was no difference in weight per nucleus. However, after ten days *ad libitum* feeding the differences had disappeared (table 1).

It is seen from figure 1 that for the controls there was a linear relationship between the logarithm of the weight of the muscle and the logarithm of its number of nuclei. The regression coefficient of log. number of nuclei on log. weight of muscle was 0.72 ± 0.24 , which is similar to the values obtained in previous experiments,

TABLE 1

Experiment 1. The effect of a sudden reduction of feed intake from 8 to 16 days of age and subsequent *ad libitum* feeding to 26 days on the growth of the pectoral muscle, its number of nuclei and the weight of muscle per nucleus

Age	Treatment group Nutritional status	Number of chickens	Weight of muscle	Number of nuclei	Weight per nucleus
(days)			(gm)	(10^9)	(10^{-9} g)
8	Pre-treatment	4	6.2	3.3	1.8
16	Undernourished	8	10.6	4.2	2.5
16	Controls	8	15.0	6.2	2.4
26	Re-fed	8	31.0	10.8	2.9
26	Controls	8	29.2	10.1	2.9

{ Not significantly different ($P < 0.05$).

maintenance ration, since there was no change in any of the variates.

Ninety percent feed for a period of eight days permitted muscle growth, but at a slower rate than the controls. As in experiment 1, it is seen that the retardation of growth was associated with reduced nuclear proliferation, but that the weight per nucleus increased to the same extent as in the controls. The rate of increase of fibre diameter was also reduced but the increase of their estimated length was not significantly different from the controls. There was no significant difference in the ratio of the cross-sectional area of the fibres to the number of nuclei.

Subsequent *ad libitum* feeding resulted in compensatory growth, and at 24 days of age there were no significant differences between any of the feeding regimes.

The effect of continuous restricted feeding is shown in table 5. It is seen that the slower growth of the muscle is associated

with a slower rate of nuclear proliferation and with a reduced rate of increase of both the cross-sectional area and estimated length of the fibres.

In order to determine whether continuous restricted feeding affected the mathematical relationships between the weight of the muscle, the number of nuclei and the cross-sectional area of the fibres, two regression equations were calculated for each of the three nutritional regimes (table 6). The first equation related the logarithm of the fibre cross-sectional area to the logarithm of the number of nuclei and the second related the logarithm of the number of nuclei to the logarithm of the weight of the muscle. In both cases, comparison of the regression equations (Brownlee, '60b) showed that the regression lines were coincident (figs. 3, 4), which indicates that the mathematical relationships were independent of the nutritional regime.

TABLE 5

Experiment 3, part 2. The effect of continuous restricted feeding on the weight of the pectoral muscle (W), the number of nuclei (N), weight per nucleus (V), fibre cross-sectional area (C) and estimated fibre length (L)

Nutritional regime	Age	W	N	V	C	L	$R = \frac{C}{N}$
	(days)	(gm)	(10 ³)	(10 ⁻³ gm)	(μ^2)	(Units)	
Before feeding	0	0.63	0.68	0.95	71	8.9	102
Controls	4	1.26	1.05	1.20	123	10.0	117
90% feed	4	1.07	0.93	1.18	112	9.6	120
60% feed	4	0.89	0.81	1.10	91	9.8	113
Controls	8	4.2	2.51	1.66	246	17	98
90% feed	8	3.4	2.09	1.62	209	16	99
60% feed	8	1.4	0.96	1.41	123	11	129
Controls	16	14.4	4.9	3.0	480	30	97
90% feed	16	9.8	3.5	2.8	340	29	94
60% feed	16	6.3	2.7	2.3	270	23	100

(Means of five chickens)

TABLE 6

Experiment 3, part 2 Regression equations relating the mean value at different ages (0, 4, 8 and 16 days) of the logarithm of the cross-sectional area of the muscle fibres (C) to the logarithm of the number of nuclei (N) and of the logarithm of the number of nuclei (N) to the logarithm of the weight of the muscle (W)

Ration (fed continuously)	Regression equations
Controls (100% feed)	$\log. C \approx -6.37 + 0.93 \log. N$
90% feed	$\log. C \approx -6.12 + 0.91 \log. N$
60% feed	$\log. C \approx -6.25 + 0.92 \log. N$
Coincident lines (see text)	$\log. C \approx -6.21 + 0.92 \log. N$
Controls (100% feed)	$\log. N = 8.96 + 0.64 \log. W$
90% feed	$\log. N = 8.96 + 0.62 \log. W$
60% feed	$\log. N = 8.94 + 0.61 \log. W$
Coincident lines (see text)	$\log. N = 8.95 + 0.63 \log. W$

The diameter of the fibres decreased, and consequently the ratio of the fibre cross-sectional area to the number of nuclei was reduced. There was no change in weight of the muscle divided by fibre cross-sectional area, that is, in the estimated length of the fibres. These changes were reversed during two days re-feeding, there being an increase in the weight of muscle, the weight per nucleus and the diameter of the

fibres but no change in the number of nuclei or estimated fibre length. The ratio of the fibre cross-sectional area to the number of nuclei increased.

The effect of 40% feed for four days was similar to that of starvation, there being a reduction of muscle weight and fibre diameter but not of estimated fibre length or number of nuclei. Sixty percent feed for a period of six days acted as a

TABLE 3

Experiment 3, part 1. The effect of a sudden reduction of feed intake and subsequent ad libitum feeding on the weight of the pectoral muscle (W), number of nuclei (N), weight of muscle per nucleus (V), fibre cross-sectional area (C) and estimated fibre length (L)

Nutritional regime ¹	Age	W	N	V	C	L	$R = \frac{C}{N}$
	(days)	(gm)	(10 ³)	(10 ⁻⁹ gm)	(μ^2)	(Units)	
Controls (100%)	8	4.2	2.5	1.6	240	17	98
Controls (100%)	10	6.7	3.1	2.2	290	23	96
Starved 8-10 days	10	3.1	2.8	1.1	170	19	62
Controls (100%)	12	8.8	3.8	2.3	360	25	93
Starved 8-10 days	12	4.7	2.5	1.8	230	20	90
40% 8-12 days	12	3.2	2.2	1.4	190	17	87
Controls (100%)	14	10.6	3.8	2.8	400	27	105
60% 8-14 days	14	4.3	2.4	1.8	210	21	87
Controls (100%)	16	14.5	4.9	3.0	350	27	97
90% 8-16 days	16	10.0	3.4	3.0	350	27	104
Controls (100%)	24	21.5	6.6	3.3	570	37	91
Starved 8-10 days	24	22.5	6.8	3.3	590	38	89
40% 8-12 days	24	20.1	6.2	3.2	520	39	85
60% 8-14 days	24	20.0	6.0	3.3	540	37	92
90% 8-16 days	24	19.2	5.6	3.4	540	36	96

(Means of five chickens)

¹ All groups received 100% feed ad libitum except during the period of feed restriction.

TABLE 4

Experiment 3, part 1. The effect of a sudden reduction of feed intake on the weight of the pectoral muscle (W), the number of nuclei (N), weight per nucleus (V), fibre cross-sectional area (C) and estimated fibre length (L)

Diet ¹	A ₁	A ₂	W	N	V	C	L	$R = \frac{C}{N}$
	(days)	(days)	(gm)	(10 ³)	(10 ⁻⁹ gm)	(μ^2)	(Units)	
100%	8	10	160	122	136	121	134	(98)
Starved	8	10	76	(110)	68	69	(110)	(63)
100% ²	10	12	150	(92)	164	137	(109)	(146)
3	8	12	(114)	(101)	(112)	(94)	(120)	(92)
100%	8	12	213	153	139	147	145	(96)
40%	8	12	77	(88)	(91)	78	(98)	(89)
100%	8	14	255	149	171	163	156	(108)
60%	8	14	(105)	(96)	(109)	(86)	(122)	(90)
100%	8	16	350	195	180	196	179	(99)
100%	8	16	242	135	180	144	161	(107)
90%	8	16	69	69	(100)	74	(90)	(108)
90% : 100% at 16 days								

This table, which summarises the results of table 3, shows the value at age A₂ as a percentage of the value at age A₁. The parentheses indicate that the relevant pairs of values are not significantly different.

¹ All groups fed 100% feed to eight days of age.

² Previously starved from eight to ten days of age.

³ Starved from eight to ten days, 100% feed ten to twelve days of age.

maintenance ration, since there was no change in any of the variates.

Ninety percent feed for a period of eight days permitted muscle growth, but at a slower rate than the controls. As in experiment 1, it is seen that the retardation of growth was associated with reduced nuclear proliferation, but that the weight per nucleus increased to the same extent as in the controls. The rate of increase of fibre diameter was also reduced but the increase of their estimated length was not significantly different from the controls. There was no significant difference in the ratio of the cross-sectional area of the fibres to the number of nuclei.

Subsequent *ad libitum* feeding resulted in compensatory growth, and at 24 days of age there were no significant differences between any of the feeding regimes.

The effect of continuous restricted feeding is shown in table 5. It is seen that the slower growth of the muscle is associated

with a slower rate of nuclear proliferation and with a reduced rate of increase of both the cross-sectional area and estimated length of the fibres.

In order to determine whether continuous restricted feeding affected the mathematical relationships between the weight of the muscle, the number of nuclei and the cross-sectional area of the fibres, two regression equations were calculated for each of the three nutritional regimes (table 6). The first equation related the logarithm of the fibre cross-sectional area to the logarithm of the number of nuclei and the second related the logarithm of the number of nuclei to the logarithm of the weight of the muscle. In both cases, comparison of the regression equations (Brownlee, '60b) showed that the regression lines were co-incident (figs. 3, 4), which indicates that the mathematical relationships were independent of the nutritional regime.

TABLE 5

Experiment 3, part 2. The effect of continuous restricted feeding on the weight of the pectoral muscle (W), the number of nuclei (N), weight per nucleus (V), fibre cross-sectional area (C) and estimated fibre length (L)

Nutritional regime	Age (days)	W (gm)	N (10 ²)	V (10 ⁻⁹ gm)	C (μ ²)	L (Units)	R = $\frac{C}{N}$
Before feeding	0	0.63	0.68	0.95	71	8.9	102
Controls	4	1.26	1.05	1.20	123	10.0	117
90% feed	4	1.07	0.93	1.18	112	9.6	120
60% feed	4	0.89	0.81	1.10	91	9.8	113
Controls	8	4.2	2.51	1.66	246	17	98
90% feed	8	3.4	2.09	1.62	209	16	99
60% feed	8	1.4	0.96	1.41	123	11	129
Controls	16	14.4	4.9	3.0	480	30	97
90% feed	16	9.8	3.5	2.8	340	29	94
60% feed	16	6.3	2.7	2.3	270	23	100

(Means of five chickens)

TABLE 6

Experiment 3, part 2. Regression equations relating the mean value at different ages (0, 4, 8 and 16 days) of the logarithm of the cross-sectional area of the muscle fibres (C) to the logarithm of the number of nuclei (N) and of the logarithm of the number of nuclei (N) to the logarithm of the weight of the muscle (W)

Ration (fed continuously)	Regression equations
Controls (100% feed)	log. C = -6.37 + 0.93 log. N
90% feed	log. C = -6.12 + 0.91 log. N
60% feed	log. C = -6.25 + 0.92 log. N
Coincident lines (see text)	log. C = -6.21 + 0.92 log. N
Controls (100% feed)	log. N = 8.96 + 0.64 log. W
90% feed	log. N = 8.96 + 0.62 log. W
60% feed	log. N = 8.94 + 0.61 log. W
Coincident lines (see text)	log. N = 8.95 + 0.63 log. W

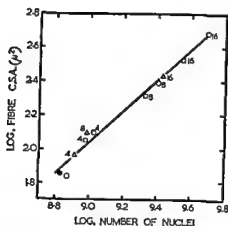


Fig. 3 Experiment 3, part 2. Relationship between the cross-sectional area of the fibres and the number of nuclei in the pectoral muscle during growth on different planes of nutrition, 100% O, 90% □ and 60% Δ feed. Figures indicate age in days.

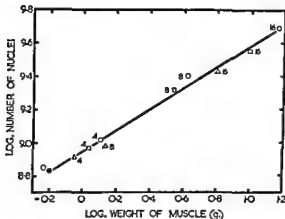


Fig. 4 Experiment 3, part 2. Relationship between the number of nuclei and the weight of the pectoral muscle during growth on different planes of nutrition, 100% O, 90% □ and 60% Δ feed. Figures indicate age in days.

DISCUSSION

It has been shown previously (Moss, '68) that during normal growth of the pectoral muscle of the chicken there were three mathematical relationships. (1) The mean cross-sectional area of the muscle fibres was proportional to the total number of nuclei in the muscle. This was interpreted as indicating that the cross-sectional area of the fibres was proportional to their number of nuclei. (2) The mean cross-sectional area of the fibres was proportional to the two thirds power of the weight of the muscle. This was interpreted as indicating that the length and diameter of individual fibres maintained a constant ratio. (3) The

total number of nuclei in the muscle was proportional to the two thirds power of its weight. This relationship is the result of the other two.

The results of the present work show that during steady, retarded growth, caused by restricted feeding, the above relationships were maintained. However, an abrupt reduction in growth rate, due to a sudden restriction of feed intake, disrupted the relationship between the number of nuclei and the weight of the muscle but not that between the number of nuclei and the cross-sectional area of the fibres. It follows therefore that the relationship between the fibre cross-sectional area and the weight of the muscle was also upset, which implies that the ratio of the length to the diameter of the fibres was abnormal. In fact, the results show that, although the cross-sectional area of the fibres of the retarded muscle was less than that of the controls, there was no difference in estimated length. It is also evident that during compensatory growth, nuclear proliferation and the increase of fibre diameter were accelerated, but that the rate of increase of estimated fibre length was the same as the controls. By this means, the normal ratio between the length and diameter of the fibres was restored.

When, as a result of starvation or severe undernutrition, degrowth of the muscle occurred, all three mathematical relationships were disrupted. There was a diminution of the diameter of the fibres but not of their estimated length. This was not unexpected. A reduction of the length of the fibres would result in them tearing out of their *tendinous insertions*, unless the tendons themselves lengthened. This would not be expected to occur. The results also showed that, during the initial period of regrowth after starvation, the fibres regained their original diameter. However, during this phase there was no increase in their estimated length, nor did nuclear proliferation resume, until the normal relationships between the dimensions of the fibres and the number of nuclei had been restored.

Goldspink ('65) presented evidence that during growth of muscle fibres, their number of myofibrils is proportional to their cross-sectional area. It was therefore suggested (Moss, '68) that the number of

myofibrils in a fibre is proportional to its number of nuclei. During muscle degrowth there was no loss of nuclei, but a reduction in cross-sectional area of the fibres occurred. However, it is possible that this was a result of the reduction of thickness of the myofibrils and not a reduction of their number. If this is so, the normal relationship between the number of nuclei and the number of myofibrils would not appear to be modified during muscle degrowth or regrowth.

ACKNOWLEDGEMENTS

The author expresses his thanks to Dr. H.W. McNary for his advice during the course of this work and to Dr. R.K. Ryan for constructive criticism of the manuscript. The technical assistance of Mr. B.J. Harris is gratefully acknowledged.

Financial support for this study was provided by the Poultry Husbandry Research Foundation, University of Sydney.

LITERATURE CITED

- Brownlee, K. A. 1960a Statistical theory and methodology in science and engineering. Academic Press. New York and London, pp. 113-115.
- 1960b Statistical theory and methodology in science and engineering. Academic Press. New York and London, pp. 289-290.
- Davidson, J. N. 1960 The biochemistry of the nucleic acids. Methuen and Co. Ltd., London, p. 142.
- Enesco, M., and C. P. Leblond 1962 Increase of cell number as a factor in the growth of the tissues and organs of the young male rat. *J. Embryol. exp. Morph.*, 10: 530-562.
- Goldspink, G. 1955 Cytological basis of decrease in muscle strength during starvation. *Am. J. Physiol.*, 209, 100-101.
- Moss, F. P. 1958 The relationship between the dimensions of the fibres and the number of nuclei during normal growth of skeletal muscle in the domestic fowl. *Am. J. Anat.*, 122: 555-564.
- Paul, J. 1956 The chemical determination of DNA in tissue cultures. *J. biochem. biophys. Cytol.*, 2: 797-798.

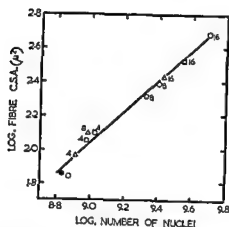


Fig. 3 Experiment 3, part 2. Relationship between the cross-sectional area of the fibres and the number of nuclei in the pectoral muscle during growth on different planes of nutrition, 100% O, 90% □ and 60% Δ feed. Figures indicate age in days.

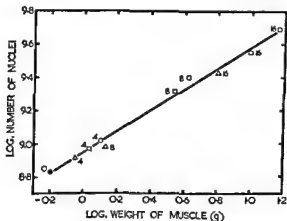


Fig. 4 Experiment 3, part 2. Relationship between the number of nuclei and the weight of the pectoral muscle during growth on different planes of nutrition, 100% O, 90% □ and 60% Δ feed. Figures indicate age in days.

DISCUSSION

It has been shown previously (Moss, '68) that during normal growth of the pectoral muscle of the chicken there were three mathematical relationships. (1) The mean cross-sectional area of the muscle fibres was proportional to the total number of nuclei in the muscle. This was interpreted as indicating that the cross-sectional area of the fibres was proportional to their number of nuclei. (2) The mean cross-sectional area of the fibres was proportional to the two thirds power of the weight of the muscle. This was interpreted as indicating that the length and diameter of individual fibres maintained a constant ratio. (3) The

total number of nuclei in the muscle was proportional to the two thirds power of its weight. This relationship is the result of the other two.

The results of the present work show that during steady, retarded growth, caused by restricted feeding, the above relationships were maintained. However, an abrupt reduction in growth rate, due to a sudden restriction of feed intake, disrupted the relationship between the number of nuclei and the weight of the muscle but not that between the number of nuclei and the cross-sectional area of the fibres. It follows therefore that the relationship between the fibre cross-sectional area and the weight of the muscle was also upset, which implies that the ratio of the length to the diameter of the fibres was abnormal. In fact, the results show that, although the cross-sectional area of the fibres of the retarded muscle was less than that of the controls, there was no difference in estimated length. It is also evident that during compensatory growth, nuclear proliferation and the increase of fibre diameter were accelerated, but that the rate of increase of estimated fibre length was the same as the controls. By this means, the normal ratio between the length and diameter of the fibres was restored.

When, as a result of starvation or severe undernutrition, degrowth of the muscle occurred, all three mathematical relationships were disrupted. There was a diminution of the diameter of the fibres but not of their estimated length. This was not unexpected. A reduction of the length of the fibres would result in them tearing out of their tendinous insertions, unless the tendons themselves lengthened. This would not be expected to occur. The results also showed that, during the initial period of regrowth after starvation, the fibres regained their original diameter. However, during this phase there was no increase in their estimated length, nor did nuclear proliferation resume, until the normal relationships between the dimensions of the fibres and the number of nuclei had been restored.

Goldspink ('65) presented evidence that during growth of muscle fibres, their number of myofibrils is proportional to their cross-sectional area. It was therefore suggested (Moss, '68) that the number of

Involution and Regeneration of the Thymus in Mice, Induced by Bacterial Endotoxin and Studied by Quantitative Histology and Electron Microscopy¹

PALLE GAD² AND SAM L. CLARK, Jr.³

Department of Anatomy, Washington University School of Medicine,
St. Louis, Missouri

ABSTRACT Lipopolysaccharide from *S. typhosa*, injected intraperitoneally into Swiss albino mice, produced acute thymic involution—maximal at 48 hours after injection, followed by regeneration that was complete within 5 to 7 days. Using tissues fixed and embedded for electron microscopy, cell counts were made with the light microscope and cytological details were examined in electron micrographs. The cellular events of involution and regeneration were similar to those produced by injection of adrenal glucocorticoids, but it remains to be determined whether or not endotoxin acts on the thymus by inciting adrenal cortical secretion.

Involution appeared to be the result of both the death of small lymphocytes and reduced lymphopoiesis in the thymus. Within 48 hours, macrophages had cleared away the cellular debris and medullary epithelial cells showed signs of hypertrophy and increased putative secretory activity. Subsequently, large lymphocytes proliferated at an accelerated rate in the subcapsular cortex, the cortex grew in width by the accumulation of small lymphocytes, and regeneration ceased when the thymus had reached its former size.

These observations provide circumstantial evidence for the hypothesis that in regeneration, medullary epithelial cells increase their production of a lymphopoietic hormone which stimulates mitotic proliferation of cortical lymphocytes.

The thymus involutes—by sudden depletion of its population of small lymphocytes—in response to a wide variety of stimuli, such as adrenocorticotrophic hormone, adrenal and gonadal steroids, colloidal substances, Freund's adjuvant (Svet-Moldavsky and Raffkina, '63), reserpine (Draskoči and Janković, '64), ionizing irradiation, acidified serum, vitamin-deficient diets and, in fact, almost any severe stress (reviewed by Bargmann, '43; Cowan and Sorenson, '64). Thymic involution has also been described as a normal accompaniment of pregnancy and weaning (Ito and Hoshino, '62a). Adrenocorticotrophin fails to produce involution in adrenalectomized animals (Simpson et al., '43), and it has been suspected that many of the other thymolytic agents act by virtue of being stressful stimuli, inducing the secretion of adrenal glucocorticoids, which are the direct cause of thymic involution. Recently, bacterial endotoxins have been added to the list of provoking factors (Landy et al., '65; Rowlands et al., '65).

Acute thymic involution, in response to many different inducing agents, entails a

common pattern of events. The thymus diminishes in size and weight for 2 or 3 days, reaching a minimum that is quantitatively proportional to the stimulus—at least in the case of adrenal steroids (Ringertz et al., '52; Stephenson, '54; Ishidate and Metcalf, '63). Small lymphocytes disappear from the cortex to such an extent that this alone can probably account for the shrinkage of the thymus that occurs. Medullary lymphocytes are less severely affected, so that the relative cellular densities of the two regions may be reversed (Dustin, '29; Ringertz et al., '52; Kaplan and Brown, '57; Ito and Hoshino, '62b; Rowlands et al., '65). Pycnotic cells accumulate and macrophages become filled with cellular debris. These have been taken

¹Supported in part by grants GM 3784 and GM AM 7176 from the National Institutes of Health, United States Public Health Service, grant GB 4788 from the National Science Foundation, and a grant from P. Carl Petersen's Foundation, Denmark.

²Present address: Division of Electron Microscopy, Institute of Anatomy, University of Aarhus, Aarhus C, Denmark.

³Career Development Awardee of the National Institutes of Health, United States Public Health Service. Present address: Department of Anatomy, University of Massachusetts School of Medicine, 100 Arlington Street, Boston, Massachusetts 02116.

Involution and Regeneration of the Thymus in Mice, Induced by Bacterial Endotoxin and Studied by Quantitative Histology and Electron Microscopy¹

PALLE GAD² AND SAM L. CLARK, Jr.³

Department of Anatomy, Washington University School of Medicine,
St. Louis, Missouri

ABSTRACT Lipopolysaccharide from *S. typhosa*, injected intraperitoneally into Swiss albino mice, produced acute thymic involution—maximal at 48 hours after injection, followed by regeneration that was complete within 5 to 7 days. Using tissues fixed and embedded for electron microscopy, cell counts were made with the light microscope and cytological details were examined in electron micrographs. The cellular events of involution and regeneration were similar to those produced by injection of adrenal glucocorticoids, but it remains to be determined whether or not endotoxin acts on the thymus by inciting adrenal cortical secretion.

Involution appeared to be the result of both the death of small lymphocytes and reduced lymphopoiesis in the thymus. Within 48 hours, macrophages had cleared away the cellular debris and medullary epithelial cells showed signs of hypertrophy and increased putative secretory activity. Subsequently, large lymphocytes proliferated at an accelerated rate in the subcapsular cortex, the cortex grew in width by the accumulation of small lymphocytes, and regeneration ceased when the thymus had reached its former size.

These observations provide circumstantial evidence for the hypothesis that in regeneration, medullary epithelial cells increase their production of a lymphopoietic hormone which stimulates mitotic proliferation of cortical lymphocytes.

The thymus involutes—by sudden depletion of its population of small lymphocytes—in response to a wide variety of stimuli, such as adrenocorticotrophic hormone, adrenal and gonadal steroids, colloidal substances, Freund's adjuvant (Svet-Moldavsky and Raffkina, '63), reserpine (Draskoči and Janković, '64), ionizing irradiation, acidified serum, vitamin-deficient diets and, in fact, almost any severe stress (reviewed by Bargmann, '43; Cowan and Sorenson, '64). Thymic involution has also been described as a normal accompaniment of pregnancy and weaning (Ito and Hoshino, '62a). Adrenocorticotrophin fails to produce involution in adrenalectomized animals (Simpson et al., '43), and it has been suspected that many of the other thymolytic agents act by virtue of being stressful stimuli, inducing the secretion of adrenal glucocorticoids, which are the direct cause of thymic involution. Recently, bacterial endotoxins have been added to the list of provoking factors (Landy et al., '65; Rowlands et al., '65).

Acute thymic involution, in response to many different inducing agents, entails a

common pattern of events. The thymus diminishes in size and weight for 2 or 3 days, reaching a minimum that is quantitatively proportional to the stimulus—at least in the case of adrenal steroids (Ringertz et al., '52; Stephenson, '54; Ishidate and Metcalf, '63). Small lymphocytes disappear from the cortex to such an extent that this alone can probably account for the shrinkage of the thymus that occurs. Medullary lymphocytes are less severely affected, so that the relative cellular densities of the two regions may be reversed (Dustin, '29; Ringertz et al., '52; Kaplar and Brown, '57; Ito and Hoshino, '62b; Rowlands et al., '65). Pycnotic cells accumulate and macrophages become filled with cellular debris. These have been taken

¹Supported in part by grants GM 3784 and GM 1176 from the National Institutes of Health, United States Public Health Service, grant GB 478 from the National Science Foundation, and a grant from P. Carl Petersen's Foundation, Denmark.

²Present address: Division of Electron Microscopy, Institute of Anatomy, University of Aarhus, Aarhus, Denmark.

³Career Development Awardee of the National Institutes of Health, United States Public Health Service. Present address: Department of Anatomy, University of Massachusetts School of Medicine, 1 Arlington Street, Boston, Massachusetts 02116.

as indications that cellular depletion is due to the death of small lymphocytes (Ringertz et al., '52; Weaver, '55; Kaplan and Brown, '57; Ishidate and Metcalf, '63; Cowan and Sorenson, '64), although Fiore-Donati and Kaye ('64) have reported that urethan produces thymic involution without evidence of dying cells. On the other hand, mitotic activity also is said to be reduced during the early stages of involution and might be instrumental in failing to maintain the normal size of the cellular population (Ito and Hoshino, '62a, b; Ishidate and Metcalf, '63). Puck ('66) has proposed that thymic involution induced by irradiation can be accounted for entirely by cessation of cell division, but he did not use histological techniques to rule out cellular death. The roles of cellular birth and death have not been examined critically in involution produced by other agents, and much remains to be learned concerning the mechanisms involved.

Acute involution is followed by regeneration. There is intense mitotic activity among large and medium-sized lymphocytes, particularly in the periphery of the cortex, where a pale subcapsular zone of lymphopoiesis can be delineated (Kaplan and Brown, '57; Axelrad and van der Gaag, '62; Hinrichsen, '65; von Gaudecker, '66). After a week or two, when the thymus has almost regained its former size, lymphopoiesis abates and a steady state is reached (Ringertz et al., '52; Kaplan and Brown, '57; Ito and Hoshino, '62a, b; Cowan and Sorenson, '64; Rowlands et al., '65). Neither the stimulus for this proliferation nor the source of the proliferating lymphocytes is known.

Metcalf ('56) has proposed that the thymus produces a lymphopoietic factor, and some epithelial cells in the thymic medulla appear to be secretory (Clark, '66). They possess rough-surfaced endoplasmic reticulum, a well-developed Golgi complex and clusters of cytoplasmic vacuoles containing an amorphous material with the staining characteristics of an acid polysaccharide. Furthermore, these cells rapidly incorporate radioactive sulfate and glucosamine into this putative secretory product. Similar material accumulates in

the lumens of epithelial cysts. If this mucoid material is a lymphopoietic hormone, then an increase in its secretion might account for the increased mitotic activity of thymic regeneration. Ito and Hoshino ('62b) have reported that the PAS-positive epithelial cells of the thymic medulla increase in number during regeneration following hydrocortisone, but this reaction has not been examined by electron microscopy.

In the present investigation, quantitative histological techniques and electron microscopy were used to study the thymic involution and regeneration produced by bacterial endotoxin. An endotoxin was chosen for study because, as natural products of the intestinal flora, these substances may be important both in the normal function of the thymus and in pathological conditions (Landy and Braun, '64). Particular attention was paid to the birth and death of lymphocytes and to putative secretion by epithelial cells.

MATERIALS AND METHODS

Experimental animals. A total of 65 male inbred Swiss mice, 4 to 8 weeks old and weighing 14.7 to 32.0 gm, were studied in detail. They were fed Ralston Purina Laboratory Chow and tap water *ad libitum*, and were caged in litters or singly, although some had been kept as mixed groups prior to the beginning of the experiment. Animals that showed evidence of fighting or that had been allowed to exhaust their supply of food or water were not included in this number. Littermates were distributed randomly between experimental and control groups and were weighed daily at about 9:00 A.M.

Treatment. Forty-eight mice received a single intraperitoneal injection of endotoxin (Lipopolysaccharide B from *Salmonella typhosa* 0901, Difco Laboratories) in a dose ranging from 15 to 200 μ g suspended in 0.1 ml pyrogen-free 0.9% NaCl. Thirteen of the littermate-control mice received an injection of 0.1 ml of pyrogen-free 0.9% NaCl, and the remaining four were not injected. The needle was inserted through the unprepared skin of the inguinal region and passed subcutaneously as far cranially as possible before entering the abdominal cavity; using this technique,

no leakage of injected material was observed.

Cell counts were made on 34 mice injected with 25 μ g of endotoxin and on seven littermate controls. Endotoxin-treated mice were injected at the beginning of each experiment and killed at intervals from 3–120 hours thereafter. Control mice were injected with saline at 48 hours and killed at 120 hours after the injection of endotoxin into their littermates.

Tissue preparation. At intervals from 3 to 120 hours after injection, mice were weighed, anesthetized with ether and bled by transsection of the throat. Within four minutes from the time each animal was removed from its cage, the thymus had been dissected free from other tissues and dropped *in toto* into the glutaraldehyde fixative to be described below. The thymus was weighed to the nearest 0.1 mg on a torsion balance, immersed in fixative in a tared vial. The spleen and mesenteric lymph node were treated similarly.

Initial fixation was accomplished in glutaraldehyde that had been filtered through charcoal, diluted to a concentration of 6.25% in 0.08 M sodium phosphate, adjusted to a pH of 7.2 to 7.4 and nearly saturated with calcium by the addition of one drop of 1% CaCl per ml. Immediately after weighing, the tissues were cut into blocks approximately 1 mm³, fixed in glutaraldehyde at 0° C for 3–4 hours, washed over-night in cold phosphate buffer, post-fixed for two hours at room temperature in 1% osmium tetroxide in a balanced salt solution containing added calcium (Clark, '63), dehydrated in ethanol and embedded in epoxy resin—either Epon 812 (Luft, '61) or a mixture of Dow resins (Lockwood and Langston, '64). Sections were cut with glass knives on Porter-Blum (Servall) ultramicrotomes.

Thin sections for electron microscopy were stained either with saturated uranyl acetate in 50% ethanol for 15 minutes, with lead hydroxide (Millonig, '61) or both RCA 2D, 3F and 3H electron microscopes were used.

Quantitative histology. Sections approximately 2 μ thick were stained with hot 1% azure-B bromide. Micrographs were made on 24 \times 36 mm film (Pana-

tomic-X, Kodak), using a Leitz Orthomat photomicroscope with monochromatic green filter, oiled condenser and dry 40 power apochromatic objective (NA:0.95). For each animal, at least one micrograph was taken for each of three regions: the outer cortex just within the capsule, the inner cortex and the medulla. Micrographs of outer and inner cortex were taken only where the cortex was broad enough to allow the two micrographs to be made without overlapping. Except for avoiding large blood vessels, the selection of fields for photography was random.

Cell counts were made on micrographs enlarged photographically to a final magnification of 1,070 \times . A sheet of transparent plastic, ruled with a rectangular grid containing 40 rectangles, was placed over each micrograph to subdivide it into areas for counting (fig. 11). Each rectangle represented an area of 30.4 \times 28.1 μ in the original section. In order to avoid bias, micrographs were counted in random order, without knowledge of the source of the sections. A few micrographs were counted in a similar way by a second observer, and in each case, agreement between the two observers was close.

Cells were classified as small or large lymphocytes, pycnotic cells, phagocytes, epithelial cells and mitotic cells. Hassall's corpuscles, small blood vessels and clusters of vacuoles within epithelial cells were counted also. Small lymphocytes were distinguishable from large lymphocytes not only by their small size, but also by their dense nuclear chromatin and scanty cytoplasm. However, in making cell counts, size was the criterion used. Sections of lymphocytes wider than approximately 10 μ were counted as large; therefore most medium-sized lymphocytes were counted as small, reducing the sensitivity with which immature lymphocytes were detected, but simplifying the problem of classifying cells by size in thin sections.

Cell counts were recorded for each rectangle, and averages were calculated successively for each micrograph, each block of tissue, each animal and each experimental group. Averages were unweighted except where counts of zero occurred. For statistical comparisons, the average counts for each mouse were used as single data.

as indications that cellular depletion is due to the death of small lymphocytes (Ringertz et al., '52; Weaver, '55; Kaplan and Brown, '57; Ishidate and Metcalf, '63; Cowan and Sorenson, '64), although Fiore-Donati and Kaye ('64) have reported that urethan produces thymic involution without evidence of dying cells. On the other hand, mitotic activity also is said to be reduced during the early stages of involution and might be instrumental in failing to maintain the normal size of the cellular population (Ito and Hoshino, '62a, b; Ishidate and Metcalf, '63). Puck ('66) has proposed that thymic involution induced by irradiation can be accounted for entirely *be cessation of cell division, but he did not use histological techniques to rule out cellular death. The roles of cellular birth and death have not been examined critically in involution produced by other agents, and much remains to be learned concerning the mechanisms involved.*

Acute involution is followed by regeneration. There is intense mitotic activity among large and medium-sized lymphocytes, particularly in the periphery of the cortex, where a pale subcapsular zone of lymphopoiesis can be delineated (Kaplan and Brown, '57; Axelrad and van der Gaag, '62; Hinrichsen, '65; von Gaudecker, '66). After a week or two, when the thymus has almost regained its former size, lymphopoiesis abates and a steady state is reached (Ringertz et al., '52; Kaplan and Brown, '57; Ito and Hoshino, '62a, b; Cowan and Sorenson, '64; Rowlands et al., '65). Neither the stimulus for this proliferation nor the source of the proliferating lymphocytes is known.

Metcalf ('56) has proposed that the thymus produces a lymphopoietic factor, and some epithelial cells in the thymic medulla appear to be secretory (Clark, '66). They possess rough-surfaced endoplasmic reticulum, a well-developed Golgi complex and clusters of cytoplasmic vacuoles containing an amorphous material with the staining characteristics of an acid polysaccharide. Furthermore, these cells rapidly incorporate radioactive sulfate and glucosamine into this putative secretory product. Similar material accumulates in

the lumens of epithelial cysts. If this mucoid material is a lymphopoietic hormone, then an increase in its secretion might account for the increased mitotic activity of thymic regeneration. Ito and Hoshino ('62b) have reported that the PAS-positive epithelial cells of the thymic medulla increase in number during regeneration following hydrocortisone, but this reaction has not been examined by electron microscopy.

In the present investigation, quantitative histological techniques and electron microscopy were used to study the thymic involution and regeneration produced by bacterial endotoxin. An endotoxin was chosen for study because, as natural products of the intestinal flora, these substances may be important both in the normal function of the thymus and in pathological conditions (Landy and Braun, '64). Particular attention was paid to the birth and death of lymphocytes and to putative secretion by epithelial cells.

MATERIALS AND METHODS

Experimental animals. A total of 65 male inbred Swiss mice, 4 to 8 weeks old and weighing 14.7 to 32.0 gm, were studied in detail. They were fed Ralston Purina Laboratory Chow and tap water *ad libitum*, and were caged in litters or singly, although some had been kept as mixed groups prior to the beginning of the experiment. Animals that showed evidence of fighting or that had been allowed to exhaust their supply of food or water were not included in this number. Littermates were distributed randomly between experimental and control groups and were weighed daily at about 9:00 A.M.

Treatment. Forty-eight mice received a single intraperitoneal injection of endotoxin (Lipopolysaccharide B from *Salmonella typhosa* 0901, Difco Laboratories) in a dose ranging from 15 to 200 μ g suspended in 0.1 ml pyrogen-free 0.9% NaCl. Thirteen of the littermate-control mice received an injection of 0.1 ml of pyrogen-free 0.9% NaCl, and the remaining four were not injected. The needle was inserted through the unprepared skin of the inguinal region and passed subcutaneously as far cranially as possible before entering the abdominal cavity; using this technique,

not common (Cowan and Sorenson, '64). Hassall's corpuscles, similar to those described by Kohnen and Weiss ('64), were more numerous than in mice of strain 129/J (Clark, '63). They consisted of concentric nests of epithelial cells rich in tonofibrils and desmosomes, surrounding a central heterogenous mass that appeared to consist of mucoid material and cellular debris. No evidence of phagocytosis by epithelial cells was observed.

Macrophages containing osmiophilic inclusions and cellular debris could be distinguished from epithelial cells by their lack of tonofibrils and desmosomes. They were smaller than those giant cells seen in mice of strain 129/J (Clark, '63) and were scattered randomly throughout the thymus (fig. 16).

A few plasma cells and eosinophilic leucocytes were seen, both within the thymic parenchyma and in the perivascular connective tissue, but mast cells were rare.

Endotoxin-treated mice

Within a few minutes after injection of endotoxin, mice became inactive, assumed a huddled posture with ruffled fur, and showed little interest in food or drink. By 12 hours after injection, they had lost more weight than was to be expected during the diurnal cycle, and weight loss was maximal 16–24 hours after injection (figs. 1–3). The severity of the clinical illness was roughly proportional to the dose of endo-

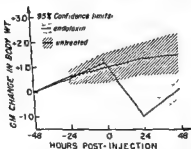


Fig 2 Changes in body weight of 32 mice injected with endotoxin, and of 17 littermate controls. Doses of endotoxin injected were: 15 μ g (2 mice), 25 μ g (20 mice) and 50–200 μ g (10 mice). At 24 hours after injection, endotoxin-treated mice weighed approximately 2 gm less than controls. By 48 hours after injection, they were regaining lost weight at an accelerated pace, but still weighed significantly less than controls.

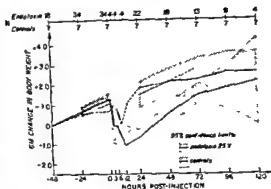


Fig. 3 Changes in body weight of 34 mice injected with 25 μ g of endotoxin and of seven littermate controls injected with 0.9% NaCl. These were the mice examined by quantitative histological methods (figs. 7–9). The diurnal cycle in body weight taken from figure 1 is superimposed (broken line). Weights were obtained at the hours indicated on the abscissa, and the numbers at the top of the graph (N) represent the number of animals weighed at each interval. The seven control mice were weighed daily, injected with saline at 72 hours and killed at 120 hours. Endotoxin-treated mice were killed at intervals after injection, and the diminishing numbers weighed at successive times represent all those not yet killed. The four mice weighed at 3, 6 and 12 hours after injection included only those killed at each of these intervals.

During the first six hours after injection (at 9 A.M.) endotoxin-treated mice lost no more weight than would be expected during the normal diurnal cycle, but they continued to lose weight during the next six hours. Subsequently, recovery was rapid, and body weight reached normal levels by 72 hours after injection.

toxin, within the range of 15–200 μ g. No mice died from the effects of endotoxin. Within 10–30 hours after injection, the mice looked healthy again, and they regained lost body weight within 72–120 hours.

Thymic involution was produced by as little as 15 μ g of endotoxin but the response was minimal and inconsistent at this dosage. Twenty-five μ g of endotoxin consistently produced moderate involution and was relatively non-toxic. Therefore, this dose was adopted for intensive study, in order to examine thymic involution and regeneration in mice that were not seriously ill. The remainder of this paper will deal with the 34 mice that received 25 μ g of endotoxin, and with their seven littermate controls (fig. 3).

to estimate 95% confidence limits for the means of each experimental group as: [group mean $\pm t_{0.05} \times$ standard error of the mean], using two-tailed values for t .

RESULTS

Control mice

The four mice that received no injections were similar, in all parameters measured, to those injected with saline. Therefore, all were considered together as controls. These young adult mice gained approximately 0.5 gm per day in body weight, but this was accomplished through a diurnal cycle in which weight was lost during the day and regained at night (fig. 1). The lymphoid organs varied little in weight (figs. 4-6). Control mice were killed at the end of these experiments, and it has been assumed, for the sake of comparison, that weights of the organs did not

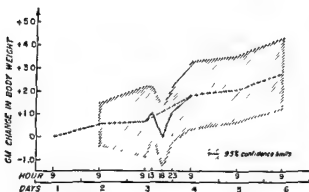


Fig. 1 Rate of growth and diurnal variation in body weight of seven control mice, 30 days old and weighing approximately 18 gm. Weights were obtained only at the hours indicated on the abscissa; therefore the diurnal cycle in weight can be seen only during the third day. These mice gained approximately 0.5 gm per day, but this was accomplished in the face of a loss of approximately 1 gm during the daylight hours.

change during the several days occupied by each experiment.

The histological and submicroscopic appearance of the thymus was similar, in most respects, to that described by others (Clark, '63; Hoshino, '63; Weiss, '63; Cowan and Sorenson, '64; Kohnen and Weiss, '64; van Haelst, '67). Small lymphocytes predominated (Table 1), but were only half as concentrated in the medulla as in the cortex. They appeared indistinguishable from those in other lymphoid organs (Murray et al., '65a). Large lymphocytes were most numerous in the outer cortex. Mitotic cells, which appeared to be large lymphocytes (Murray et al., '65b), were distributed similarly. In some control mice, a pale subcapsular zone of lymphopoiesis could be recognized, but this was variable in thickness and prominence (figs. 10, 12-15). No mitotic epithelial cells or macrophages were seen.

Epithelial cells were twice as concentrated in the medulla as in the cortex (table 1). Some of the attenuated cortical epithelial cells contained vacuoles filled with a fluffy or filamentous material, similar to those depicted by Hoshino ('63), Weiss ('63), Cowan and Sorenson ('64) and van Haelst ('67), but there was little other evidence of secretory activity in these cells. Among the more voluminous medullary epithelial cells, a minority contained mucoid vacuoles, together with variable quantities of rough-surfaced endoplasmic reticulum and Golgi complex (figs. 16, 17). The cytoplasm surrounding the mucoid vacuoles was scanty, in most cases. The remaining medullary epithelial cells contained varying quantities of ribosomes and rough-surfaced endoplasmic reticulum, but the Golgi complex was inconspicuous. Epithelial cysts, some lined with cilia, were

TABLE 1

Cell counts in thymus of seven control mice (Number of cells per 0.1 mm² of section)

	Outer cortex		Inner cortex		Medulla	
	Mean	\pm S.E.	Mean	\pm S.E.	Mean	\pm S.E.
Small lymphocytes	3630.1	70.3	3501.3	152.2	1873.6	82.0
Large lymphocytes	52.1	18.2	20.8	6.4	3.5	—
Mitotic cells	16.7	2.8	3.9	0.5	0.7	—
Pycnotic cells	11.8	2.0	10.7	3.2	7.4	2.3
Phagocytic cells	8.2	2.0	2.9	8.4	8.9	1.9
Pycnotic plus phagocytic cells	17.0	2.1	19.3	3.9	15.9	2.9
Epithelial cells	168.5	3.6	177.3	5.2	409.0	20.6

not common (Cowan and Sorenson, '64). Hassall's corpuscles, similar to those described by Kohnen and Weiss ('64), were more numerous than in mice of strain 129/J (Clark, '63). They consisted of concentric nests of epithelial cells rich in tonofibrils and desmosomes, surrounding a central heterogeneous mass that appeared to consist of mucoid material and cellular debris. No evidence of phagocytosis by epithelial cells was observed.

Macrophages containing osmiophilic inclusions and cellular debris could be distinguished from epithelial cells by their lack of tonofibrils and desmosomes. They were smaller than those giant cells seen in mice of strain 129/J (Clark, '63) and were scattered randomly throughout the thymus (fig. 16).

A few plasma cells and eosinophilic leukocytes were seen, both within the thymic parenchyma and in the perivascular connective tissue, but mast cells were rare.

Endotoxin-treated mice

Within a few minutes after injection of endotoxin, mice became inactive, assumed a huddled posture with ruffled fur, and showed little interest in food or drink. By 12 hours after injection, they had lost more weight than was to be expected during the diurnal cycle, and weight loss was maximal 16–24 hours after injection (figs. 1–3). The severity of the clinical illness was roughly proportional to the dose of endo-

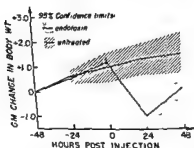


Fig 2 Changes in body weight of 32 mice injected with endotoxin, and of 17 littermate controls. Doses of endotoxin injected were: 15 μ g (2 mice), 25 μ g (20 mice) and 50–200 μ g (10 mice). At 24 hours after injection, endotoxin-treated mice weighed approximately 2 gm less than controls. By 48 hours after injection, they were regaining lost weight at an accelerated pace, but still weighed significantly less than controls.

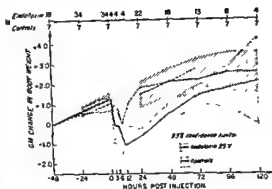


Fig. 3 Changes in body weight of 34 mice injected with 25 μ g of endotoxin and of seven littermate controls injected with 0.9% NaCl. These were the mice examined by quantitative histological methods (figs. 7–9). The diurnal cycle in body weight taken from figure 1 is superimposed (broken line). Weights were obtained at the hours indicated on the abscissa, and the numbers at the top of the graph (N) represent the number of animals weighed at each interval. The seven control mice were weighed daily, injected with saline at 72 hours and killed at 120 hours. Endotoxin-treated mice were killed at intervals after injection, and the diminishing numbers weighed at successive times represent all those not yet killed. The four mice weighed at 3, 6 and 12 hours after injection included only those killed at each of these intervals.

During the first six hours after injection (at 9 A.M.) endotoxin-treated mice lost no more weight than would be expected during the normal diurnal cycle, but they continued to lose weight during the next six hours. Subsequently, recovery was rapid, and body weight reached normal levels by 72 hours after injection.

toxin, within the range of 15–200 μ g. No mice died from the effects of endotoxin. Within 10–30 hours after injection, the mice looked healthy again, and they regained lost body weight within 72–120 hours.

Thymic involution was produced by as little as 15 μ g of endotoxin but the response was minimal and inconsistent at this dosage. Twenty-five μ g of endotoxin consistently produced moderate involution and was relatively non-toxic. Therefore, this dose was adopted for intensive study, in order to examine thymic involution and regeneration in mice that were not seriously ill. The remainder of this paper will deal with the 34 mice that received 25 μ g of endotoxin, and with their seven littermate controls (fig. 3).

The weight of the thymus appeared to diminish within six hours after injection of 25 μ g of endotoxin, but this evidence of involution did not reach statistically significant proportions until 48–72 hours after injection, when thymuses of injected mice weighed 70–75% of control values (fig. 4). By 96 hours after injection, most of the lost thymic weight had been regained. The mesenteric lymph node lost weight slightly but significantly during this same period (fig. 6), but the spleen seemed to respond only by an increase in weight 96 hours after injection (fig. 5).

Involution. During the first 24 hours after endotoxin, the most obvious histological change was an accumulation of pycnotic cells and macrophages laden with cellular debris (figs. 7–9, 11). In electron micrographs, the pycnotic cells appeared to be small lymphocytes, similar to those seen in the involution produced by hydrocortisone (Cowan and Sorenson, '64). However, it is not known whether pycnosis of large lymphocytes could produce a similar appearance. Some pycnotic lymphocytes lay free in the intercellular spaces of the thymic parenchyma, but most had been ingested by macrophages, which lay either between the epithelial cells or in perivascular connective tissue. No pycnotic cells were recognized within epithelial cells.

The concentration of small lymphocytes did not diminish during this period of involution (figs. 7–9), in contrast to what other investigators have described (Dustin, '29; Ringertz et al., '52; Kaplan and Brown, '57; Ito and Hoshino, '62b; Rowlands et al., '65). This probably is an indication of the mildness of the involution produced by 25 μ g of endotoxin, but in any case, the thymus lost a quarter of its mass during

this time. Therefore, many small lymphocytes must have disappeared, either by death or emigration.

WEIGHT OF THYMUS

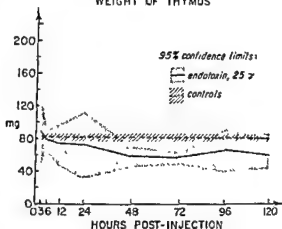


Figure 4

WEIGHT OF SPLEEN

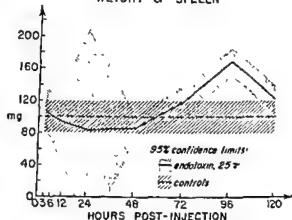


Figure 5

WEIGHT OF MESENTERIC LYMPH NODE

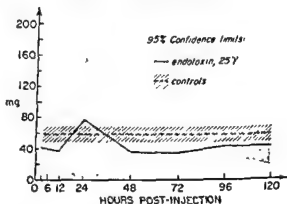
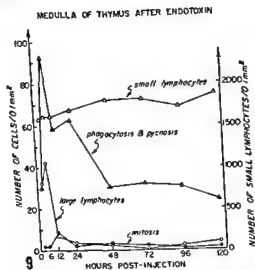
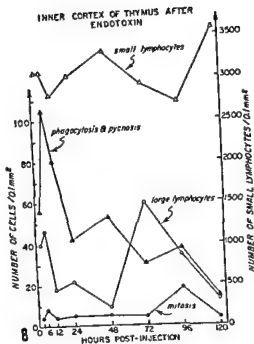
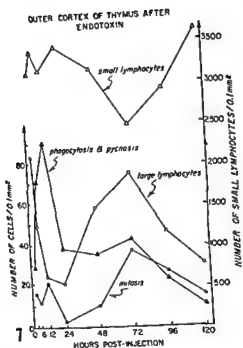


Figure 6

Figs. 4–6 Weights of thymus, spleen and mesenteric lymph node in the mice of figure 3, killed after injection of 25 μ g of endotoxin or 0.9% NaCl. The seven control mice were killed at 120 hours; mean weights and 95% confidence limits are extended across the graphs to facilitate comparison with endotoxin-treated mice. Four endotoxin-treated mice were killed at each interval indicated on the abscissa, except at 48 and 72 hours, when five mice were killed. The weight of the thymus was significantly decreased 48 and 72 hours after injection (fig. 4) and the mesenteric lymph node was significantly low in weight at 6, 48 and 72 hours after injection (fig. 6). The spleen had increased in weight at 96 hours after injection (fig. 5).



Figs. 7-9 Mean cell counts in the thymuses of 34 mice injected with 25 μ g of endotoxin, whose numbers and body weights are shown in figure 3. Counts were made on light micrographs, using the grid shown in figure 11, and results are expressed as cells per 0.1 mm² of section. Numbers of small lymphocytes are indicated by the right hand ordinate, and all other cells by the left-hand ordinate. Counts labeled "phagocytosis and pycnosis" are the sums of counts of phagocytic and pycnotic cells, which varied in close parallel. Values for littermate control mice, killed at 120 hours after injection, are shown in table 1. Counts were compared by t-test at the 95%

confidence interval, and the statistically significant results are as follows:

Outer cortex (fig. 7)

- Phagocytosis and pycnosis at 48 hours > control.
- Mitotic cells at 24 hours < control.
- at 72 hours > control.
- 6, 24 and 48 hours.
- Small lymphocytes at 72 hours < control.
- 6 and 24 hours.

Inner cortex (fig. 8)

- Phagocytosis and pycnosis at 3, 6 and 48 hours > control.

Medulla (fig. 9)

- Phagocytosis and pycnosis at 6 hours > control and 96 hours.

The weight of the thymus appeared to diminish within six hours after injection of 25 μ g of endotoxin, but this evidence of involution did not reach statistically significant proportions until 48–72 hours after injection, when thymuses of injected mice weighed 70–75% of control values (fig. 4). By 96 hours after injection, most of the lost thymic weight had been regained. The mesenteric lymph node lost weight slightly but significantly during this same period (fig. 6), but the spleen seemed to respond only by an increase in weight 96 hours after injection (fig. 5).

Involution. During the first 24 hours after endotoxin, the most obvious histological change was an accumulation of pycnotic cells and macrophages laden with cellular debris (figs. 7–9, 11). In electron micrographs, the pycnotic cells appeared to be small lymphocytes, similar to those seen in the involution produced by hydrocortisone (Cowan and Sorenson, '64). However, it is not known whether pycnosis of large lymphocytes could produce a similar appearance. Some pycnotic lymphocytes lay free in the intercellular spaces of the thymic parenchyma, but most had been ingested by macrophages, which lay either between the epithelial cells or in perivascular connective tissue. No pycnotic cells were recognized within epithelial cells.

The concentration of small lymphocytes did not diminish during this period of involution (figs. 7–9), in contrast to what other investigators have described (Dustin, '29; Ringertz et al., '52; Kaplan and Brown, '57; Ito and Hoshino, '62b; Rowlands et al., '65). This probably is an indication of the mildness of the involution produced by 25 μ g of endotoxin, but in any case, the thymus lost a quarter of its mass during

this time. Therefore, many small lymphocytes must have disappeared, either by death or emigration.

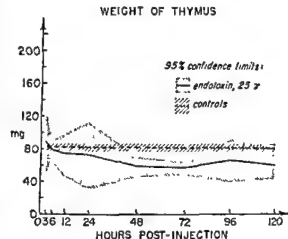


Figure 4

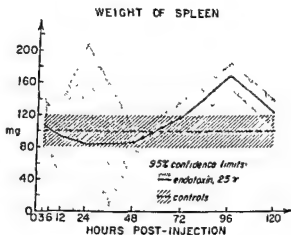


Figure 5

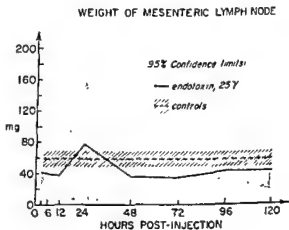
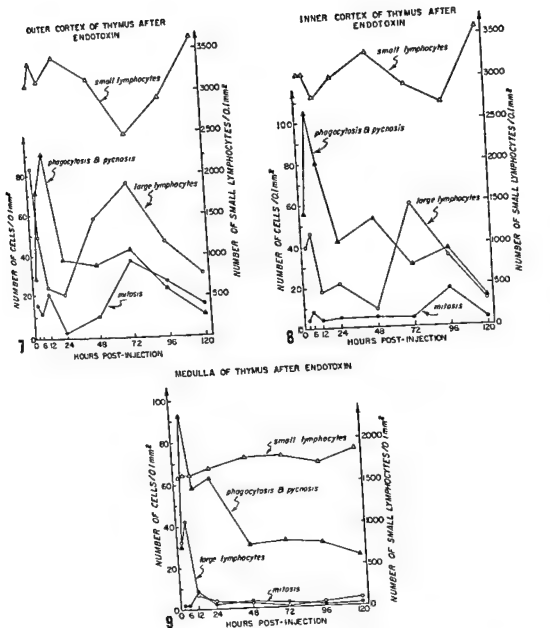


Figure 6

Figs. 4–6 Weights of thymus, spleen and mesenteric lymph node in the mice of figure 3, killed after injection of 25 μ g of endotoxin or 0.9% NaCl. The seven control mice were killed at 120 hours; mean weights and 95% confidence limits are extended across the graphs to facilitate comparison with endotoxin-treated mice. Four endotoxin-treated mice were killed at each interval indicated on the abscissa, except at 48 and 72 hours, when five mice were killed. The weight of the thymus was significantly decreased 48 and 72 hours after injection (fig. 4) and the mesenteric lymph node was significantly low in weight at 6, 48 and 72 hours after injection (fig. 6). The spleen had increased in weight at 96 hours after injection (fig. 5).



Figs. 7-9 Mean cell counts in the thymuses of 34 mice injected with 25 μ g of endotoxin, whose numbers and body weights are shown in figure 3. Counts were made on light micrographs, using the grid shown in figure 11, and results are expressed as cells per 0.1 mm² of section. Numbers of small lymphocytes are indicated by the right hand ordinate, and all other cells by the left-hand ordinate. Counts labeled "phagocytosis and pycnosis" are the sums of counts of phagocytic and pycnotic cells, which varied in close parallel. Values for littermate control mice, killed at 120 hours after injection, are shown in table 1. Counts were compared by t-test at the 95%

confidence interval, and the statistically significant results are as follows:

- Outer cortex (fig. 7)**
 Phagocytosis and pycnosis at 48 hours > control.
 at 24 hours < control.
 Mitotic cells at 72 hours > control,
 6, 24 and 48 hours.
 Small lymphocytes at 72 hours < control,
 6 and 24 hours.
- Inner cortex (fig. 8)**
 Phagocytosis and pycnosis at 3, 6 and 48 hours > control.
- Medulla (fig. 9)**
 Phagocytosis and pycnosis at 6 hours > control
 and 96 hours.

Although large lymphocytes appeared to diminish in number, samples were not large enough to demonstrate statistically significant changes.

Mitotic activity in the outer cortex diminished significantly within 24 hours after injection, and a pale subcapsular zone could no longer be detected (figs. 10, 14).

Epithelial cells changed in appearance early in involution. During the first 24 hours, their borders became highly convoluted, presumably as a result of the loss of intervening small lymphocytes. Some cells contained dilated vacuolar spaces, myelin figures and lipid droplets; these may be indications of toxic degeneration, or they may represent the results of phagocytosis, but no pycnotic cells or recognizable cellular debris were found within epithelial cells. Signs of secretory activity were not greatly different in number or kind from those observed in controls.

No changes were observed in blood vessels or Hassall's corpuscles.

Regeneration. Between 48 and 120 hours after injection of 25 μ g of endotoxin, pycnotic cells and laden macrophages waned to control levels, indicating the end of the involutional phase of the response (figs. 7-9). Large lymphocytes and mitotic

cells increased in number, particularly in the outer cortex, and the pale subcapsular zone broadened to include most of the cortex (figs. 10, 12-15). As the thymus regained its lost weight, 48-72 hours after injection, the surviving small lymphocytes were transiently reduced in concentration, apparently diluted by the proliferating population of large lymphocytes. Eventually, small lymphocytes increased in concentration, lymphopoiesis subsided, and regeneration ceased.

During the regenerative phase, epithelial cells lost some of the signs of degeneration seen earlier, and secretory activity appeared to be increased. Most medullary epithelial cells, and some cortical ones as well, grew large with prominent nucleoli and voluminous cytoplasm (figs. 18-22). Ribosomes were numerous, the Golgi complex was large, and in most cells there were clusters of mucoid vacuoles (figs. 19-22). However, these mucoid vacuoles were generally smaller in size and in some cases fewer in number than those seen in control mice. In addition, some epithelial cells in regenerating thymuses were filled with rough-surfaced endoplasmic reticulum in varying states of engorgement (fig. 21). In a few cells, dilatation of the endoplasmic reticulum was extreme, but no other signs suggestive of degeneration were observed (figs. 23, 24).

Thus, thymic regeneration appeared to be characterized by hypertrophy of medullary epithelial cells and the development of mucoid vacuoles. In addition, the medulla appeared to occupy a larger volume in regenerating than in control thymuses. However, these indications of enhanced secretory activity are based on qualitative and subjective judgements; the cytological details were too difficult to detect by light microscopy to allow statistical evaluation. Therefore, in order to achieve an unbiased judgement, a blind comparison of electron micrographs was made, in which each animal was classified as demonstrating "high," "medium" or "low" activity on the basis of the features described above, without knowledge of the treatment it had received. The distribution shown in table 2 was obtained, indicating that "high activity" was associated almost exclusively with endo-

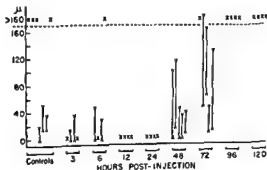


Fig. 10 Width of subcapsular lymphopoietic zone in the mice injected with 25 μ g of endotoxin and their littermate controls (fig. 3). Sections with ample portions of medulla were chosen for measurement, to avoid obliquity in the subcapsular region, and sections were evaluated in random order without knowledge of the treatment received by each mouse. Representative appearances of the subcapsular zone are shown in figures 12-15. Each X or vertical line in the graph represents a single mouse; maximum and minimum thickness of the subcapsular zone in each animal are plotted as V and A, respectively.

TABLE 2

Morphological signs of activity in thymus, as judged in electron micrographs

Treatment	Number of mice	Estimated activity		
		High	Medium	Low
Endotoxin	9	5	3	0
Control	8	1	3	4

Endotoxin-treated mice each received a single injection of 15-200 μ g endotoxin and were killed 24-72 hours after injection.

toxin-treated mice and "low activity" only with control mice.

Mitotic activity was not observed in epithelial cells or macrophages during regeneration.

DISCUSSION

Quantitative histology

Before the results can be interpreted in biological terms, the resolution, reproducibility and appropriateness of the quantitative techniques need to be assessed.

Cell counts. The use of osmium-fixed, plastic-embedded tissue offered higher optical resolution than is available with classical histological methods. Sections could be cut thinner—minimizing overlap of cells, and the superior preservation of cytological structure allowed more precise identification of cells than is possible in paraffin sections. In addition, tissues viewed by light microscopy could be compared directly with electron micrographs of thin sections taken from the same blocks. Thus cells could be classified with almost the precision of electron microscopy.

Cell counts were highly reproducible when repeated upon the same micrographs, even when two observers counted them independently—indicating that cells could be classified with consistency and counted accurately. The greatest non-biological source of variation in cell counts probably was variation in thickness of sections, but because the sections were thin in relation to the thickness of the cells being counted, variation from this source presumably was not great.

The sensitivity with which differences between cell counts could be detected depended upon the size of the samples that could be obtained in relation to the variability in counts among experimental animals. As indicated by standard errors of

means (table 1), and the significance of differences stated in the legends to figures 7-9, statistical significance could be assigned to most of the changes observed. However, this was true only for the extremes of cellular fluctuation, and greater sensitivity would have been desirable. This might have been achieved by obtaining more data, or by using more elaborate statistical techniques to assess variability among the counts from a single animal—rather than using the mean for each animal as a single datum. Nevertheless, significant changes were detected by the methods used.

The estimates of cellular concentration can not be accepted in absolute terms, because there is a bias inherent in counting sections of spheres. This bias is due partly to the difficulty in detecting tangential sections of cells, and it varies with the size of the cell in relation to the thickness of the section. Therefore, the cell counts are useful only in relative terms. For this reason counts are recorded per unit area of section, rather than per volume of tissue.

The choice of the assay method was based on the need to know what happens to whole populations of cells during involution and regeneration. However, cell counts are expressed as concentrations of cells rather than as total numbers of cells. Therefore, appearance and disappearance of cells can be detected accurately, only if changes in volume occupied by the cellular population are taken into account. Changes in the mass of the thymus were measured by weighing, but relative changes in the volumes of the several regions of the thymus could only be guessed at. Therefore, conclusions concerning changes in cellular populations can be semiquantitative at best.

Semiquantitative comparisons. The comparisons presented in table 2 and figure 10 must be viewed with circumspection because they were based on subjective estimates and relatively small samples. However, the material was examined without knowledge of its source, and two observers reached similar, independent conclusions concerning the criteria for morphological classification and the segregation of experimental material into groups. Therefore, these estimates do serve

Although large lymphocytes appeared to diminish in number, samples were not large enough to demonstrate statistically significant changes.

Mitotic activity in the outer cortex diminished significantly within 24 hours after injection, and a pale subcapsular zone could no longer be detected (figs. 10, 14).

Epithelial cells changed in appearance early in involution. During the first 24 hours, their borders became highly convoluted, presumably as a result of the loss of intervening small lymphocytes. Some cells contained dilated vacuolar spaces, myelin figures and lipid droplets; these may be indications of toxic degeneration, or they may represent the results of phagocytosis, but no pycnotic cells or recognizable cellular debris were found within epithelial cells. Signs of secretory activity were not greatly different in number or kind from those observed in controls.

No changes were observed in blood vessels or Hassall's corpuscles.

Regeneration. Between 48 and 120 hours after injection of 25 μ g of endotoxin, pycnotic cells and laden macrophages waned to control levels, indicating the end of the involutional phase of the response (figs. 7-9). Large lymphocytes and mitotic

cells increased in number, particularly in the outer cortex, and the pale subcapsular zone broadened to include most of the cortex (figs. 10, 12-15). As the thymus regained its lost weight, 48-72 hours after injection, the surviving small lymphocytes were transiently reduced in concentration, apparently diluted by the proliferating population of large lymphocytes. Eventually, small lymphocytes increased in concentration, lymphopoiesis subsided, and regeneration ceased.

During the regenerative phase, epithelial cells lost some of the signs of degeneration seen earlier, and secretory activity appeared to be increased. Most medullary epithelial cells, and some cortical ones as well, grew large with prominent nucleoli and voluminous cytoplasm (figs. 18-22). Ribosomes were numerous, the Golgi complex was large, and in most cells there were clusters of mucoid vacuoles (figs. 19-22). However, these mucoid vacuoles were generally smaller in size and in some cases fewer in number than those seen in control mice. In addition, some epithelial cells in regenerating thymuses were filled with rough-surfaced endoplasmic reticulum in varying states of engorgement (fig. 21). In a few cells, dilatation of the endoplasmic reticulum was extreme, but no other signs suggestive of degeneration were observed (figs. 23, 24).

Thus, thymic regeneration appeared to be characterized by hypertrophy of medullary epithelial cells and the development of mucoid vacuoles. In addition, the medulla appeared to occupy a larger volume in regenerating than in control thymuses. However, these indications of enhanced secretory activity are based on qualitative and subjective judgements; the cytological details were too difficult to detect by light microscopy to allow statistical evaluation. Therefore, in order to achieve an unbiased judgement, a blind comparison of electron micrographs was made, in which each animal was classified as demonstrating "high," "medium" or "low" activity on the basis of the features described above, without knowledge of the treatment it had received. The distribution shown in table 2 was obtained, indicating that "high activity" was associated almost exclusively with endo-

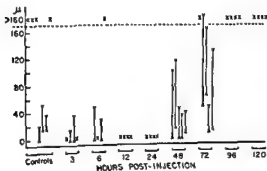


Fig. 10 Width of subcapsular lymphopoietic zone in the mice injected with 25 μ g of endotoxin and their littermate controls (fig. 3). Sections with ample portions of medulla were chosen for measurement, to avoid obliquity in the subcapsular region, and sections were evaluated in random order without knowledge of the treatment received by each mouse. Representative appearances of the subcapsular zone are shown in figures 12-15. Each X or vertical line in the graph represents a single mouse; maximum and minimum thickness of the subcapsular zone in each animal are plotted as V and A, respectively.

may be suggested that during involution, post-mitotic growth of lymphocytes is interrupted by inhibition of RNA synthesis preventing the regeneration of large lymphocytes and, secondarily, preventing their preparation for subsequent mitosis.

Regeneration. Regeneration appears to be more than the cessation of involution. The regenerating thymus grows at a rate exceeding that in control mice, small lymphocytes in the cortex are at first diluted in concentration by increasing numbers of large lymphocytes and mitotic cells, the cortex grows in width as small lymphocytes reaccumulate, and regeneration is a self-limiting process. Therefore regeneration needs to be explained by accounting for the rapidly proliferating large lymphocytes that accumulate in the subcapsular region.

The origin of these proliferating lymphocytes is not certain. No evidence of mitosis or transformation of epithelial cells was seen to suggest that they become large lymphocytes. Some large lymphocytes did appear to survive involution, and others may have immigrated from distant sites (Ford, '66; Bumbry and Metcalf, '67). In any case, it is their accelerated proliferation that needs to be explained. In control mice, approximately one fourth of subcapsular large lymphocytes were found in mitosis, whereas during regeneration the proportion exceeded 35% (at 96 hours after injection of endotoxin). These proportions would have more meaning if the durations of the cellular reproductive cycles in the two situations were known, but it appears likely that some lymphopoietic stimulus acts during regeneration. Perhaps this stimulus is the putative medullary epithelial secretory product.

The proportion of medullary epithelial cells showing signs of secretory activity increased early in regeneration by what appeared to be a process of cellular differentiation. Cells were found with prominent nucleoli, numerous ribosomes and rudimentary mucoid vacuoles or none at all. Even some cortical epithelial cells assumed the appearance of medullary secretory cells. These observations are consistent with the increased secretion of a lymphopoietic hormone suggested in the previous paragraph.

Thus these experiments provide additional circumstantial evidence that medullary epithelial cells secrete a lymphopoietic hormone, which is active in normal mice and secreted at an accelerated rate during thymic regeneration. However, it is difficult to explain how a hormone produced in the medulla should stimulate lymphopoiesis confined chiefly to the subcapsular region. More direct evidence is needed.

The variability in the appearance of the subcapsular zone in control mice (figs. 10, 13-15) may be taken to indicate that lymphopoiesis does not proceed at a constant rate. Perhaps there are physiological cycles of lymphopoietic activity in the thymus of adult mice, or perhaps the thymus undergoes minor degrees of involution and regeneration in apparently healthy animals.

The other lymphoid organs have not been examined in detail. The slight loss of weight of the mesenteric lymph node probably represents the toxic effect of endotoxin or adrenal cortical hormones on the lymphocytes there. The increase in the weight of the spleen four days after injection of endotoxin may be an early sign of the accelerated splenic hemopoiesis produced by endotoxin and other thymolytic agents (Fruhman, '66a,b).

This work demonstrates some of the possibilities and pitfalls of quantitative histology. The use of tissues prepared for electron microscopy appears to offer important advantages. Morphological methods provide a unique opportunity to view the organism as an entity—as a complex community of cells, each influencing its neighbors; but if students of morphology are to advance beyond the stage of description, they will need to rely more and more upon quantitative methods.

LITERATURE CITED

- Axelrad, A. A., and H. van der Gaag 1962 Susceptibility to lymphoma induction by Gross passage A virus in C3H/BI mice of different ages: Relation to thymus cell multiplication and differentiation. *J. Nat. Cancer Inst.*, 28: 1065-1093.
- Bargmann, W. 1943 *Der Thymus. Handbuch der Mikroskopischen Anatomie des Menschen*. Vol. 6, Teil IV: 1-172, ed. by W. von Möllendorff, Springer-Verlag, Berlin.
- Brumby, M., and D. Metcalf 1967 Migration of cells to the thymus demonstrated by parabiosis. *Proc. Soc. Exp. Biol. Med.*, 124: 99-103.

to reinforce the conclusions drawn by simple inspection.

Biological Interpretation

In confirmation of previous reports (Landy et al., '65; Rowlands et al., '65), endotoxin from *S. typhosa* 0901 induced thymic involution in doses of 15 to 200 μ g per mouse. Many of the toxic effects of endotoxin seem to depend upon the participation of antibodies against endotoxin (Schaedler and Dubos, '64), but it remains to be determined whether or not this is true for thymic involution.

The involution observed after injection of 25 μ g of endotoxin was less severe than that described by Rowlands and his colleagues ('65), who used a larger dose. For instance, small lymphocytes did not decrease in concentration in our experiments. The mice also showed little evidence of illness and none died. Therefore the changes that were observed probably represent the progress of involution and regeneration uncomplicated by debilitating illness.

The effects of endotoxin on the mouse thymus appear to be similar to those ascribed to adrenal glucocorticoids. In electron micrographs, the pycnosis and phagocytosis of small lymphocytes produced by endotoxin is indistinguishable from that produced by hydrocortisone (Cowan and Sorenson, '64). The quantitative data obtained by Ito and Hoshino ('62b) after injection of hydrocortisone are comparable to the results of the present experiments, in spite of differences in methodology. They used paraffin sections and related their data to arbitrary "phases of regeneration," rather than to the interval after injection, but they reported fluctuations in lymphopoiesis similar to those produced by endotoxin. Mitotic activity was depressed during involution, and although it rose only to normal levels during regeneration, they averaged their counts over the whole cortex and therefore may have overlooked the localized hyperplasia which we observed in the subcapsular region after endotoxin. PAS-positive inclusions in medullary epithelial cells have been demonstrated to correspond with the mucoid vacuoles and contents of epithelial cysts seen in electron micrographs (Hoshino,

'63; Clark, '66). Therefore the increase in number of PAS-positive epithelial cells reported by Ito and Hoshino ('62b) presumably corresponds to the increased signs of secretory activity seen after endotoxin.

In view of the similarities in response of the thymus to endotoxin and to glucocorticoids, it may be supposed that endotoxin produces involution by eliciting adrenal cortical secretion, rather than by acting directly upon the thymus, but evidence is not yet available to test this hypothesis. We attempted to administer endotoxin to adrenalectomized mice, but even the smallest doses were rapidly fatal (unpublished experiments).

The cellular mechanisms which may be involved in involution and regeneration will be discussed in light of the observed cellular changes.

Involution. The destruction of small lymphocytes and reduced lymphopoiesis both appear to contribute.

Pycnotic cells were found lying in the intercellular spaces and there were no indications that macrophages had ingested viable lymphocytes. Therefore it seems likely that pycnosis of small lymphocytes is one of the primary events in involution, and that macrophages play a secondary role by ingesting lymphocytes that are already degenerate. Adrenal hormones have been reported to be toxic to lymphocytes *in vitro* (Makman et al., '66), but little is known concerning the toxicity of endotoxin for lymphocytes.

Both the number of large lymphocytes and the number undergoing mitosis appeared to decrease during involution—the decrease in mitotic activity in the outer cortex was statistically significant. It is uncertain whether large lymphocytes degenerated, because it is not known whether pycnotic large lymphocytes look different from pycnotic small lymphocytes, but in any event, the reduction in the number of mitotic cells seems greater than can be accounted for by the decrease in total number of large lymphocytes. The effects of endotoxin on mitotic activity are not known. Adrenal glucocorticoids seem to act primarily by interfering with the synthesis of RNA, rather than by inhibiting synthesis of DNA directly (Haynes and Sutherland, '67; Kidson, '67). Therefore it

may be suggested that during involution, post-mitotic growth of lymphocytes is interrupted by inhibition of RNA synthesis preventing the regeneration of large lymphocytes and, secondarily, preventing their preparation for subsequent mitosis.

Regeneration. Regeneration appears to be more than the cessation of involution. The regenerating thymus grows at a rate exceeding that in control mice, small lymphocytes in the cortex are at first diluted in concentration by increasing numbers of large lymphocytes and mitotic cells, the cortex grows in width as small lymphocytes reaccumulate, and regeneration is a self-limiting process. Therefore regeneration needs to be explained by accounting for the rapidly proliferating large lymphocytes that accumulate in the subcapsular region.

The origin of these proliferating lymphocytes is not certain. No evidence of mitosis or transformation of epithelial cells was seen to suggest that they become large lymphocytes. Some large lymphocytes did appear to survive involution, and others may have immigrated from distant sites (Ford, '66; Burnby and Metcalf, '67). In any case, it is their accelerated proliferation that needs to be explained. In control mice, approximately one fourth of subcapsular large lymphocytes were found in mitosis, whereas during regeneration the proportion exceeded 35% (at 96 hours after injection of endotoxin). These proportions would have more meaning if the durations of the cellular reproductive cycles in the two situations were known, but it appears likely that some lymphopoietic stimulus acts during regeneration. Perhaps this stimulus is the putative medullary epithelial secretory product.

The proportion of medullary epithelial cells showing signs of secretory activity increased early in regeneration by what appeared to be a process of cellular differentiation. Cells were found with prominent nucleoli, numerous ribosomes and rudimentary mucoid vacuoles or none at all. Even some cortical epithelial cells assumed the appearance of medullary secretory cells. These observations are consistent with the increased secretion of a lymphopoietic hormone suggested in the previous paragraph.

Thus these experiments provide additional circumstantial evidence that medullary epithelial cells secrete a lymphopoietic hormone, which is active in normal mice and secreted at an accelerated rate during thymic regeneration. However, it is difficult to explain how a hormone produced in the medulla should stimulate lymphopoiesis confined chiefly to the subcapsular region. More direct evidence is needed.

The variability in the appearance of the subcapsular zone in control mice (figs. 10, 13-15) may be taken to indicate that lymphopoiesis does not proceed at a constant rate. Perhaps there are physiological cycles of lymphopoietic activity in the thymus of adult mice, or perhaps the thymus undergoes minor degrees of involution and regeneration in apparently healthy animals.

The other lymphoid organs have not been examined in detail. The slight loss of weight of the mesenteric lymph node probably represents the toxic effect of endotoxin or adrenal cortical hormones on the lymphocytes there. The increase in the weight of the spleen four days after injection of endotoxin may be an early sign of the accelerated splenic hemopoiesis produced by endotoxin and other thymolytic agents (Fruhman, '66a,b).

This work demonstrates some of the possibilities and pitfalls of quantitative histology. The use of tissues prepared for electron microscopy appears to offer important advantages. Morphological methods provide a unique opportunity to view the organism as an entity—as a complex community of cells, each influencing its neighbors; but if students of morphology are to advance beyond the stage of description, they will need to rely more and more upon quantitative methods.

LITERATURE CITED

- Axelrad, A. A., and H. van der Gaag 1962 Susceptibility to lymphoma induction by Gross passage A virus in C3Hf/BI mice of different ages: Relation to thymus cell multiplication and differentiation. *J. Nat. Cancer Inst.*, 28: 1065-1093.
- Bergmann, W. 1943 *Der Thymus. Handbuch der Mikroskopischen Anatomie des Menschen*. Vol. 6, Teil IV: 1-172, ed. by W. von Möllendorff, Springer-Verlag, Berlin.
- Burnby, M., and D. Metcalf 1967 Migration of cells to the thymus demonstrated by parabiosis. *Proc. Soc. Exp. Biol. Med.*, 124: 99-103.

- Clark, S. L., Jr. 1963 The thymus in mice of strain 129/J, studied with the electron microscope. *Am. J. Anat.*, 112: 1-34.
- 1966 Cytological evidences of secretion in the thymus. Ciba Foundation Symposium, The Thymus: Experimental and Clinical Studies, ed. by G. E. W. Wolstenholme and R. Porter, J. & A. Churchill, Ltd., London, pp. 3-30.
- Cowan, W. K., and G. Sorenson 1964 Electron microscopic observations of acute thymic involution produced by hydrocortisone. *Lab. Invest.*, 13: 353-370.
- Draskoči, M., and B. D. Janković 1964 Involution of thymus and suppression of immune responses in rats treated with reserpine. *Nature, Lond.*, 202: 408-409.
- Dustin, A. P. 1929 Les poisons caryoclastiques moyens d'analyse cytophysiologique. *Arch. Anat. Micr.*, 25: 37-48.
- Fiore-Donati, L., and A. M. Kaye 1964 Kinetics of changes, in thymus and other lymphopoietic organs of adult mice, induced by single doses of urethan. *J. Nat. Cancer Inst.*, 33: 907-920.
- Ford, C. E. 1966 Traffic of lymphoid cells in the body. Ciba Foundation Symposium, The Thymus: Experimental and Clinical Studies, ed. by G. E. W. Wolstenholme and R. Porter, J. & A. Churchill, Ltd., London, pp. 131-152.
- Fruhman, G. J. 1966a Bacterial endotoxin: Effects on erythropoiesis. *Blood*, 27: 363-370.
- 1966b Effects of starvation and refeeding on erythropoiesis in mice. *Z. Zellforsch.*, 75: 258-271.
- Haynes, R. C., Jr., and E. W. Sutherland, III 1967 Altered metabolism of DNA in rat thymus, an early response to cortisol. *Endocrinology*, 80: 297-301.
- Hilrichsen, K. 1965 Zellteilungen und Zellwanderungen im Thymus der erwachsenen Maus. *Z. Zellforsch.*, 68: 427-444.
- Hoshino, T. 1963 Electron microscopic studies of the epithelial reticular cells of the mouse thymus. *Z. Zellforsch.*, 59: 513-529.
- Ishidate, M., Jr., and D. Metcalf 1963 The pattern of lymphopoiesis in the mouse thymus after cortisone administration or adrenalectomy. *Austr. J. Exp. Biol.*, 41: 637-649.
- Ito, T., and T. Hoshino 1962a Studies of the influences of pregnancy and lactation on the thymus in the mouse. *Z. Zellforsch.*, 57: 667-678.
- 1962b Histological changes of the mouse thymus during involution and regeneration following administration of hydrocortisone. *Z. Zellforsch.*, 56: 445-464.
- Kaplan, H. S., and M. B. Brown 1967 Radiation injury and regeneration in lymphoid tissues. The Leukemias: Etiology, Pathophysiology and Treatment, ed. by J. W. Rebusck and others, Academic Press, New York, pp. 163-175.
- Kidson, C. 1967 Cortisol in the regulation of RNA and protein synthesis. *Nature*, 213: 779-782.
- Kohnen, P., and L. Weiss 1964 An electron microscopic study of thymic corpuscles in the guinea pig and the mouse. *Anat. Rec.*, 143: 29-57.
- Landy, M., and W. Braun, eds. 1964 Bacterial Endotoxins. Institute of Microbiology, New Brunswick, N. J.
- Landy, M., R. P. Sanderson, M. T. Bernstein and E. M. Lerner, II 1965 Involvement of thymus in immune response of rabbits to somatic polysaccharides of Gram-negative bacteria. *Science*, 147: 1591-1592.
- Lockwood, W. R., and L. L. Langston, Jr. 1964 A reliable and easily sectioned epoxy embedding medium. *Anat. Rec.*, 150: 129-140.
- Luft, J. H. 1961 Improvements in epoxy resin embedding methods. *J. Biophys. Biochem. Cytol.*, 9: 409-414.
- Makman, M. H., B. Dvorkin and A. White 1966 Alterations in protein and nucleic acid metabolism of thymocytes produced by adrenal steroids *in vitro*. *J. Biol. Chem.*, 241: 1646-1648.
- Metcalf, D. 1956 The thymic origin of the plasma lymphocytosis stimulating factor. *Brit. J. Cancer*, 10: 442-457.
- Millonig, G. 1961 A modified procedure for lead staining of thin sections. *J. Biophys. Biochem. Cytol.*, 11: 736-739.
- Murray, R. G., A. Murray and A. Pizzo 1965a The fine structure of the thymocytes of young rats. *Anat. Rec.*, 151: 17-40.
- 1965b The fine structure of mitosis in rat thymic lymphocytes. *J. Cell Biol.*, 26: 601-619.
- Puck, T. T. 1966 Cellular aspects of mammalian radiation syndrome. II. Cell depletion in bone marrow, spleen and thymus of young mice. *Radiation Res.*, 27: 272-283.
- Ringertz, N., A. Fagraeus and K. Berglund 1952 On the action of cortisone on the thymus and lymph nodes in mice. *Acta Path. Microbiol. Scand.*, Suppl. 93, 30: 44-51.
- Rowlands, D. T., H. N. Claman and P. D. Kind 1965 The effect of endotoxin on the thymus of young mice. *Am. J. Path.*, 46: 165-176.
- Schaedler, R. W., and R. Dubos 1964 Relationship of intestinal flora to resistance. Bacterial Endotoxins, ed. by M. Landy and W. Braun, Institute of Microbiology, New Brunswick, N. J., pp. 390-396.
- Schedel, J. 1985 Zellvermehrung in der Thymusdrüse. *Arch. Mikr. Anat.*, 24: 352-354.
- Simpson, M. E., C. H. Li, W. O. Reinhardt and H. M. Evans 1943 Similarity of response of thymus and lymph node to administration of adrenocorticotrophic hormone in the rat. *Proc. Soc. Exp. Biol. Med.*, 54: 135-137.
- Stephenson, N. R. 1954 Assay of adrenocortical hormones on the thymus of the weanling rat. *Canad. J. Biochem. Physiol.*, 32: 689-702.
- Svet-Moldavsky, G. J., and L. I. Raffkina 1963 Thymus-lymphatic nodes interrelations following injection of Freund's adjuvant. *Nature, Lond.*, 197: 52-53.
- Van Haelst, U. 1967 Light and electron microscopic study of the normal and pathological thymus of the rat. I. The normal thymus. *Z. Zellforsch.*, 77: 534-553.

Von Gaudecker, B. 1966 Elektronenmikroskopische Autoradiographie mit H^3 -Thymidin an der Thymusrinde der Maus. *Z. Zellforsch.*, 72: 281-294.

Weiss, L. 1963 Electron microscopic observations on the vascular barrier in the cortex of

the thymus of the mouse. *Anat. Rec.*, 145: 413-437.

Weaver, J. A. 1955 Changes induced in the thymus and lymph nodes of the rat by the administration of cortisone and sex hormones and by other procedures. *J. Path. Bact.*, 69: 133-139.

PLATE 1

EXPLANATION OF FIGURE

- 11 Light micrograph of thymic cortex, fixed 3 hours after injection of 25 μ g of endotoxin. This magnification ($\times 1072$) was used to make cell counts, and the superimposed lines represent the grid, ruled on transparent plastic, which was placed over each micrograph to subdivide it for counting. Most of the cells in this field are small lymphocytes, but in addition there are pycnotic cells (pyc) and phagocytic cells laden with debris (ph), which were increased in number 3 hours after injection of endotoxin. There are also a few large lymphocytes (L), mitotic cells (arrows) and a small blood vessel (bv). $\times 1072$.

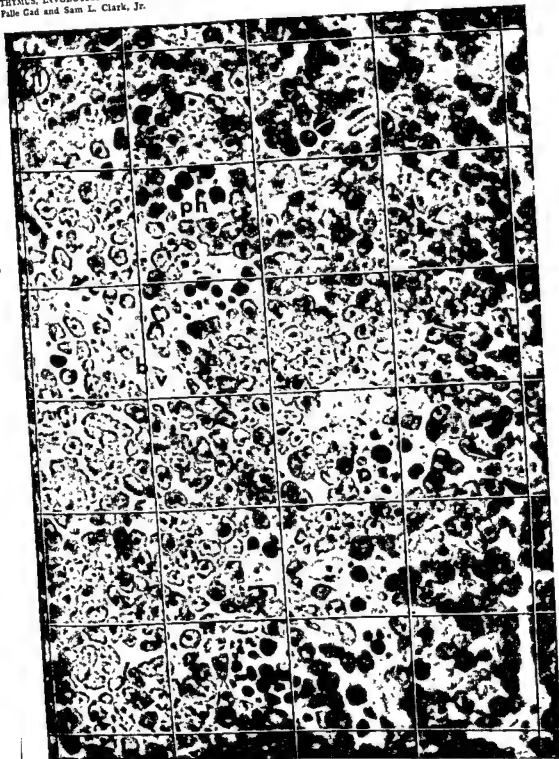
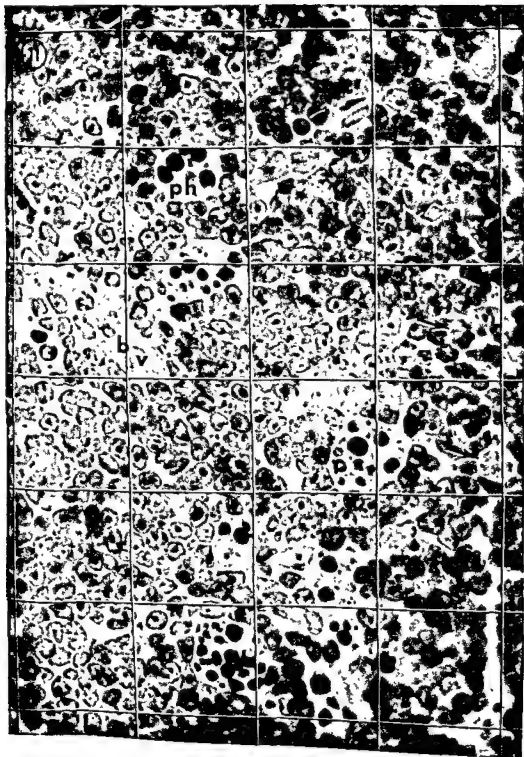
THYMUS, INVOLUTION AND REGENERATION
Folde Gad and Sam L. Clark, Jr.

PLATE 1

EXPLANATION OF FIGURE

- 11 Light micrograph of thymic cortex, fixed 3 hours after injection of 25 μ g of endotoxin. This magnification ($\times 1072$) was used to make cell counts, and the superimposed lines represent the grid, ruled on transparent plastic, which was placed over each micrograph to subdivide it for counting. Most of the cells in this field are small lymphocytes, but in addition there are pycnotic cells (pyc) and phagocytic cells laden with debris (ph), which were increased in number 3 hours after injection of endotoxin. There are also a few large lymphocytes (L), mitotic cells (arrows) and a small blood vessel (bv). $\times 1072$.

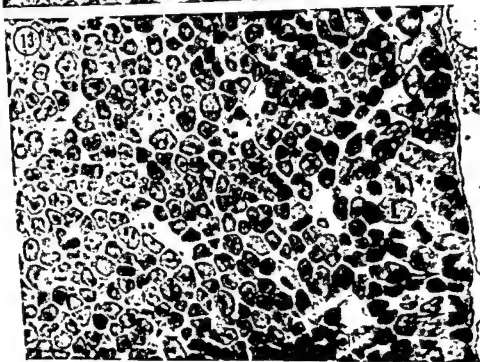
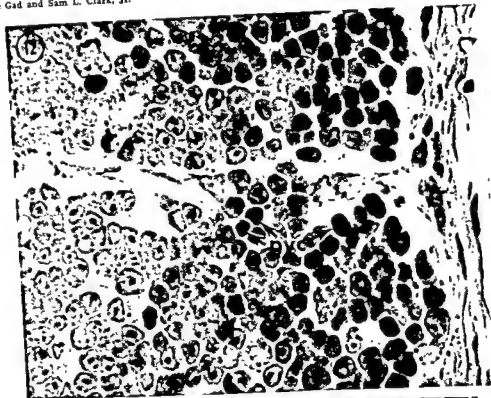


Figs. 12-15 Light micrographs of the outer cortex, all from control mice, demonstrating representative appearances of the subcapsular zone. The capsule is on the right in each micrograph. $\times 1072$.

PLATE 2

EXPLANATION OF FIGURES

- 12 *Inactive subcapsular zone.* This region is filled with small lymphocytes but contains few large lymphocytes and no visible mitotic cells. There are several pycnotic cells (pyc). This would be classified as a zone of zero width in figure 10.
- 13 *Narrow lymphopoietic zone.* In this region there is a subcapsular zone approximately $30\ \mu$ wide containing few small lymphocytes, but filled with large lymphocytes (L) and mitotic cells (arrows).

THYMUS, INVOLUTION AND REGENERATION
Palle Gad and Sam L. Clark, Jr.

Figs. 12-15 Light micrographs of the outer cortex, all from control mice, demonstrating representative appearances of the subcapsular zone. The capsule is on the right in each micrograph. $\times 1072$.

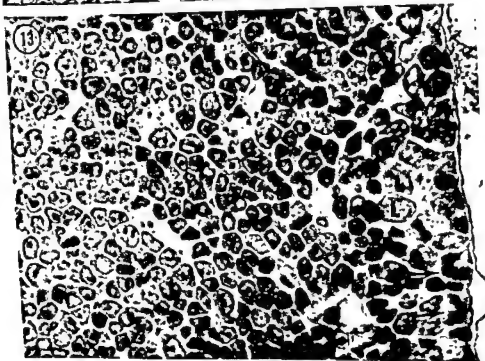
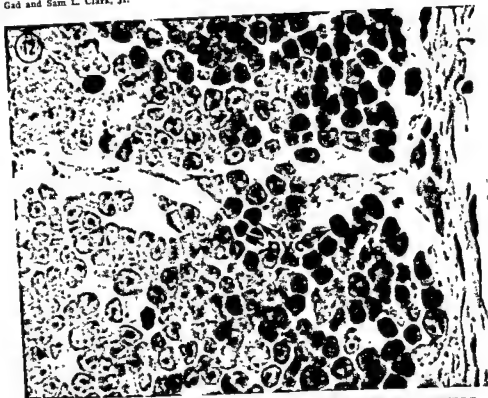
PLATE 2

EXPLANATION OF FIGURES

- 12 *Inactive subcapsular zone.* This region is filled with small lymphocytes but contains few large lymphocytes and no visible mitotic cells. There are several pycnotic cells (pyc). This would be classified as a zone of zero width in figure 10.
- 13 *Narrow lymphopoietic zone.* In this region there is a subcapsular zone approximately $30\ \mu$ wide containing few small lymphocytes, but filled with large lymphocytes (L) and mitotic cells (arrows).

THYMUS, INVOLUTION AND REGENERATION

Palle Gad and Sam L. Clark, Jr.



Figs. 12-15 Light micrographs of the outer cortex, all from control mice, demonstrating representative appearances of the subcapsular zone. The capsule is on the right in each micrograph. $\times 1072$.

PLATE 2

EXPLANATION OF FIGURES

- 12 *Inactive subcapsular zone.* This region is filled with small lymphocytes but contains few large lymphocytes and no visible mitotic cells. There are several pycnotic cells (pyc). This would be classified as a zone of zero width in figure 10.
- 13 *Narrow lymphopoietic zone.* In this region there is a subcapsular zone approximately $30\ \mu$ wide containing few small lymphocytes, but filled with large lymphocytes (L) and mitotic cells (arrows).

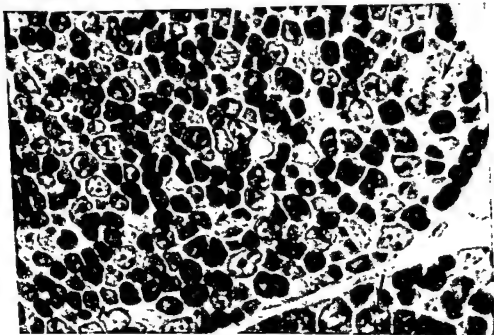
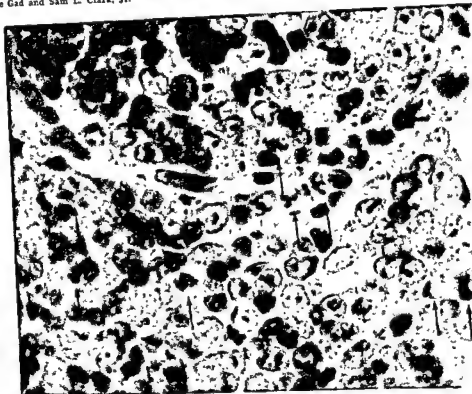
THYMUS, INVOLUTION AND REGENERATION
Palle Gad and Sam L. Clark, Jr.

PLATE 3

EXPLANATION OF FIGURES

- 14 *Wide lymphopoietic zone.* In this mouse, the entire outer cortex is filled with large lymphocytes and mitotic cells (arrows) but contains few small lymphocytes. This would be classified as a zone wider than $160\ \mu$ in figure 10; it is characteristic of regenerating thymus and was also found in some control mice.
- 15 *Wide subcapsular zone containing small lymphocytes.* The entire outer cortex in this region contains numerous large lymphocytes (L) and mitotic cells (arrows), but in addition there are moderate numbers of small lymphocytes. This zone was classified as wider than $160\ \mu$ in figure 10; perhaps it represents a more advanced stage of regeneration than that in figure 14.

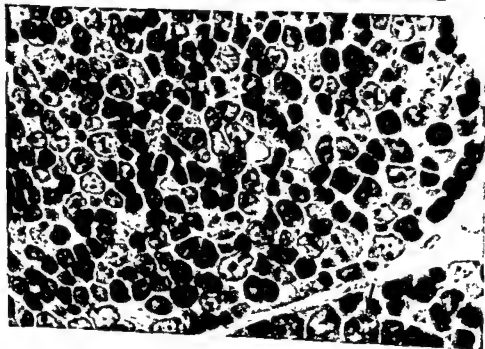
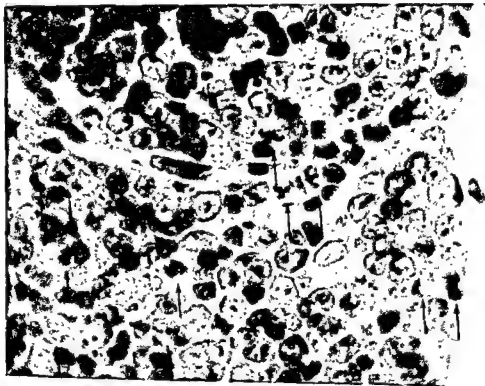


PLATE 3

EXPLANATION OF FIGURES

- 14 *Wide lymphopoietic zone.* In this mouse, the entire outer cortex is filled with large lymphocytes and mitotic cells (arrows) but contains few small lymphocytes. This would be classified as a zone wider than $160\ \mu$ in figure 10; it is characteristic of regenerating thymus and was also found in some control mice.
- 15 *Wide subcapsular zone containing small lymphocytes.* The entire outer cortex in this region contains numerous large lymphocytes (L) and mitotic cells (arrows), but in addition there are moderate numbers of small lymphocytes. This zone was classified as wider than $160\ \mu$ in figure 10; perhaps it represents a more advanced stage of regeneration than that in figure 14.

THYMUS, INVOLUTION AND REGENERATION
Palle Gad and Sam L. Clark, Jr

PLATE 4

EXPLANATION OF FIGURE

- 16 Low power electron micrograph of thymic medulla from a control mouse. The upper half of the field is almost filled with a nest of epithelial cells (nuclei labeled: E), in which there are two clusters of cytoplasmic vacuoles (V). The vacuoles contain varying quantities of an amorphous material, presumed to be a secretory product. In the lower part of the field is a macrophage (M) containing condensed debris, and the remainder of the space is occupied by small lymphocytes. $\times 9,000$.

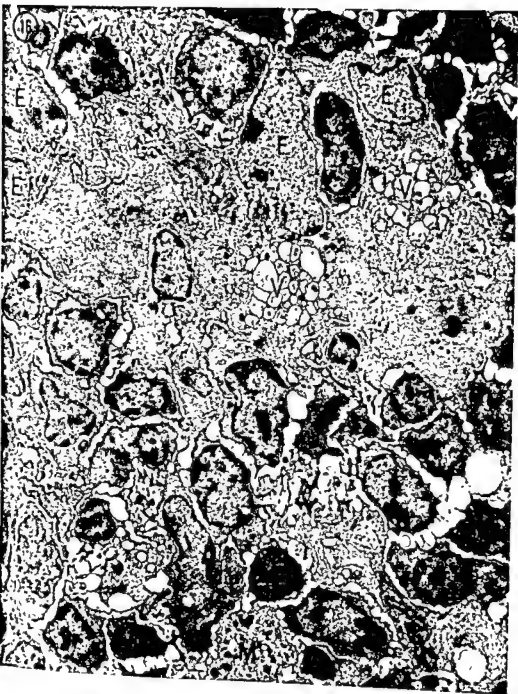


PLATE 4

EXPLANATION OF FIGURE

- 16 Low power electron micrograph of thymic medulla from a control mouse. The upper half of the field is almost filled with a nest of epithelial cells (nuclei labeled: E), in which there are two clusters of cytoplasmic vacuoles (V). The vacuoles contain varying quantities of an amorphous material, presumed to be a secretory product. In the lower part of the field is a macrophage (M) containing condensed debris, and the remainder of the space is occupied by small lymphocytes. $\times 9,000$.



PLATE 5

EXPLANATION OF FIGURE

- 17 An epithelial cell (E) from the medulla of a control mouse, surrounded by small and medium-sized lymphocytes. The cytoplasm contains a cluster of mucoid vacuoles (V), elements of a Golgi complex (G), ribosomes and some rough-surfaced endoplasmic reticulum. Desmosomes (arrow) attach it to a neighboring epithelial cell. The volume of the cytoplasm external to the vacuoles is relatively scanty. In the lower left, there is another epithelial cell containing cytoplasmic tonofibrils (t). $\times 13,000$.

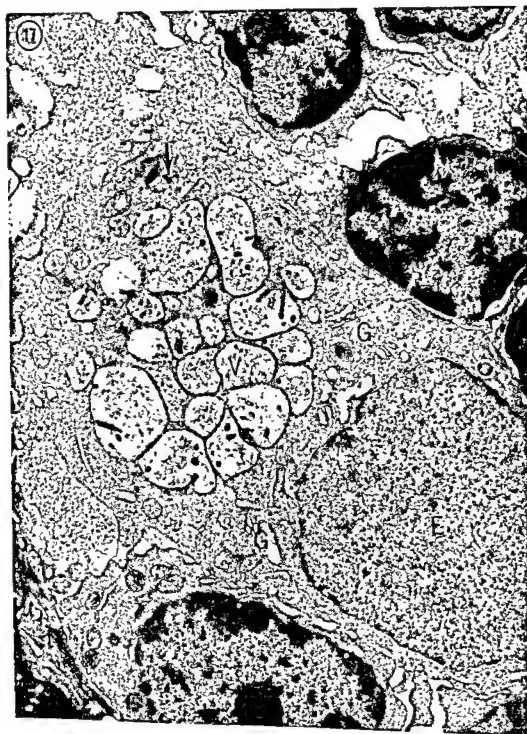


PLATE 5

EXPLANATION OF FIGURE

- 17 An epithelial cell (E) from the medulla of a control mouse, surrounded by small and medium-sized lymphocytes. The cytoplasm contains a cluster of mucoïd vacuoles (V), elements of a Golgi complex (G), ribosomes and some rough-surfaced endoplasmic reticulum. *Desmosomes* (arrow) attach it to a neighboring epithelial cell. The volume of the cytoplasm external to the vacuoles is relatively scanty. In the lower left, there is another epithelial cell containing cytoplasmic tonofibrils (t). $\times 13,000$.

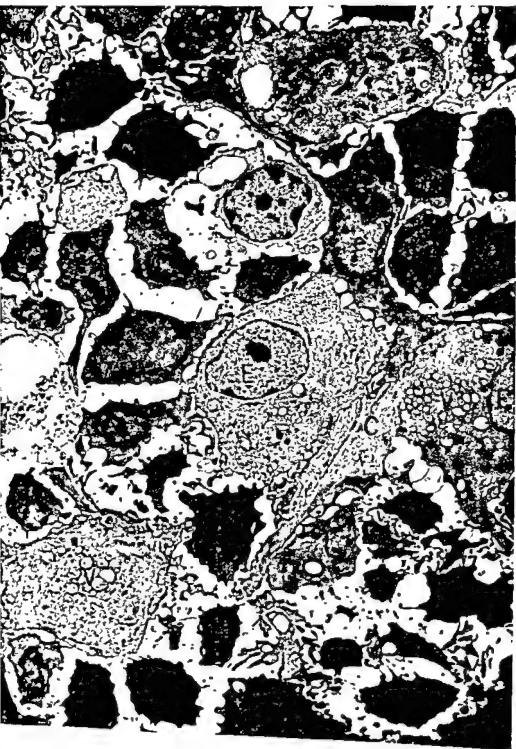


PLATE 6

EXPLANATION OF FIGURE

- 18 Low power electron micrograph of thymic medulla from a mouse injected 38 hours previously with 25 μ g of endotoxin. Small lymphocytes are relatively depleted in number, leaving large intercellular spaces. Two types of epithelial cells are in evidence: (1) dense, attenuated cells (nuclei labeled: e) that are rich in tonofibrils (t) and form thin investments around connective tissue fibers (C), and (2) large, less dense cells (nuclei labeled: E). The first type of epithelial cell is found in both cortex and medulla, whereas cells of the second type are characteristic of the medulla. Their nuclei have dispersed chromatin and prominent nucleoli, as seen in the cell in the center of the field, and clusters of vacuoles can be found in the cytoplasm of most of them (V). In contrast to the large medullary epithelial cells of control animals (figs. 16, 17), these cells are more numerous, and their cytoplasmic vacuoles tend to be smaller. $\times 9,000$.



PLATE 7

EXPLANATION OF FIGURE

- 19 Medulla from a mouse injected 38 hours previously with 25 μ g of endotoxin. In the upper part of the field there is a macrophage (M) filled with dense debris, presumably the digestion products of dead lymphocytes. In the lower half of the field is a nest of epithelial cells (E) two of which contain clustered vacuoles (V). The vacuoles on the left are large, and the cytoplasm surrounding them is relatively sparse, as in control mice. In contrast, the vacuoles on the right are small and rudimentary. They are surrounded by a voluminous cytoplasm containing many mitochondria and elements of the Golgi complex (G)—this appearance is typical of epithelial cells in regenerating thymus. Between the two nuclei labeled E, there are remnants of what appears to be an epithelial cell with prominent Golgi complex (G) and rough-surfaced endoplasmic reticulum (R); it may have been degenerating or undergoing some kind of hypertrophy. The redundancy of plasma membranes seen in this micrograph is typical of involuted thymus and probably is the result of the depletion of small lymphocytes. (C: connective tissue fiber surrounded by a basement membrane and attenuated epithelial cells.) $\times 9,000$.

THYMUS, INVOLUTION AND REGENERATION
Falle Gad and Sam L. Clark, Jr.

PLATE 7

EXPLANATION OF FIGURE

- 19 Medulla from a mouse injected 38 hours previously with 25 μ g of endotoxin. In the upper part of the field there is a macrophage (M) filled with dense debris, presumably the digestion products of dead lymphocytes. In the lower half of the field is a nest of epithelial cells (E) two of which contain clustered vacuoles (V). The vacuoles on the left are large, and the cytoplasm surrounding them is relatively sparse, as in control mice. In contrast, the vacuoles on the right are small and rudimentary. They are surrounded by a voluminous cytoplasm containing many mitochondria and elements of the Golgi complex (G)—this appearance is typical of epithelial cells in regenerating thymus. Between the two nuclei labeled E, there are remnants of what appears to be an epithelial cell with prominent Golgi complex (G) and rough-surfaced endoplasmic reticulum (R); it may have been degenerating or undergoing some kind of hypertrophy. The redundancy of plasma membranes seen in this micrograph is typical of involuted thymus and probably is the result of the depletion of small lymphocytes. (C: connective tissue fiber surrounded by a basement membrane and attenuated epithelial cells.) $\times 9,000$.



PLATE 8

EXPLANATION OF FIGURE

- 20 A nest of epithelial cells (nuclei labeled: E), from the thymic medulla of a mouse injected 38 hours previously with 25 μ g of endotoxin. In the cell to the right, there is a prominent nucleolus and a cluster of cytoplasmic vacuoles (V). Adjacent cells contain well-developed elements of the Golgi complex (G), numerous ribosomes, and some rough-surfaced endoplasmic reticulum (R). These signs of heightened synthetic activity are typical of epithelial cells observed during the phase of regeneration. (Arrow: centriole; t: tonofibrils). $\times 17,000$.

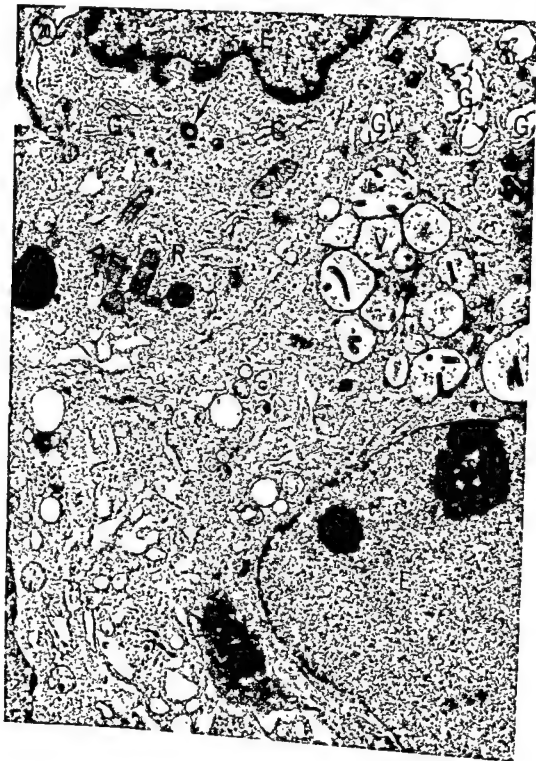


PLATE 8

EXPLANATION OF FIGURE

- 20 A nest of epithelial cells (nuclei labeled: E), from the thymic medulla of a mouse injected 38 hours previously with 25 μ g of endotoxin. In the cell to the right, there is a prominent nucleolus and a cluster of cytoplasmic vacuoles (V). Adjacent cells contain well-developed elements of the Golgi complex (G), numerous ribosomes, and some rough-surfaced endoplasmic reticulum (R). These signs of heightened synthetic activity are typical of epithelial cells observed during the phase of regeneration. (Arrow. centriole; t: tonofibrils). $\times 17,000$.

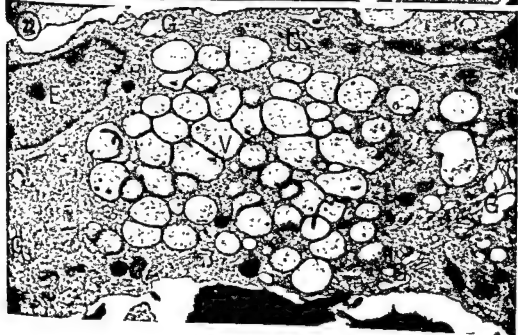
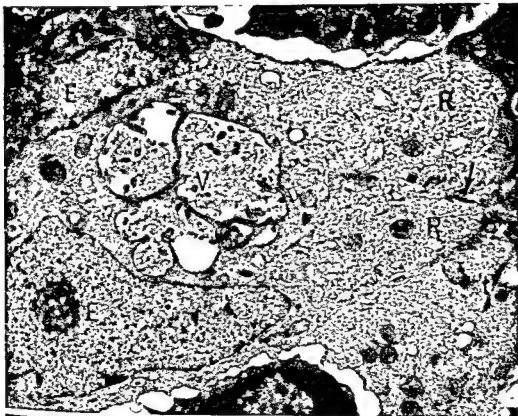


PLATE 9

EXPLANATION OF FIGURES

- 21 A nest of medullary epithelial cells (E) from a mouse injected with 25 μ g of endotoxin 38 hours previously. The lower of the two nuclei contains a prominent nucleolus, and in its cytoplasm is a cluster of large vacuoles containing an amorphous material and microvillous extensions of the membranes that enclose the vacuoles. The cytoplasm is rich in rough-surfaced endoplasmic reticulum (R), whereas the cell in the lower right is rich in ribosomes but contains little endoplasmic reticulum. A desmosome (arrow) connects adjacent cells. (t: tonofibrils). $\times 11,000$.
- 22 Part of an epithelial cell (E) from the thymic medulla of a mouse injected 38 hours previously with 25 μ g of endotoxin. There is a large cluster of vacuoles (V) surrounded by well-developed elements of the Golgi complex (G). $\times 11,000$.

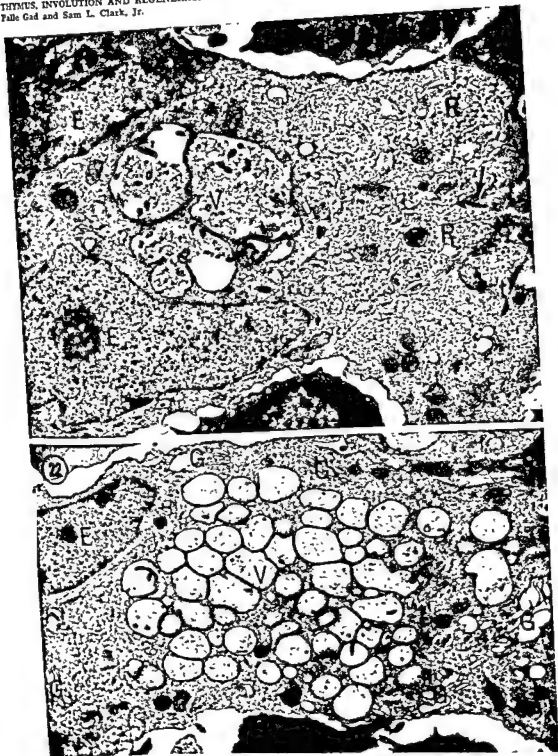
THYMUS, INVOLUTION AND REGENERATION
Falls Gad and Sam L. Clark, Jr.

PLATE 9

EXPLANATION OF FIGURES

- 21 A nest of medullary epithelial cells (E) from a mouse injected with 25 μ g of endotoxin 38 hours previously. The lower of the two nuclei contains a prominent nucleolus, and in its cytoplasm is a cluster of large vacuoles containing an amorphous material and microvillous extensions of the membranes that enclose the vacuoles. The cytoplasm is rich in rough-surfaced endoplasmic reticulum (R), whereas the cell in the lower right is rich in ribosomes but contains little endoplasmic reticulum. A desmosome (arrow) connects adjacent cells. (t: tonofibrils). $\times 11,000$.
- 22 Part of an epithelial cell (E) from the thymic medulla of a mouse injected 38 hours previously with 25 μ g of endotoxin. There is a large cluster of vacuoles (V) surrounded by well-developed elements of the Golgi complex (G). $\times 11,000$.

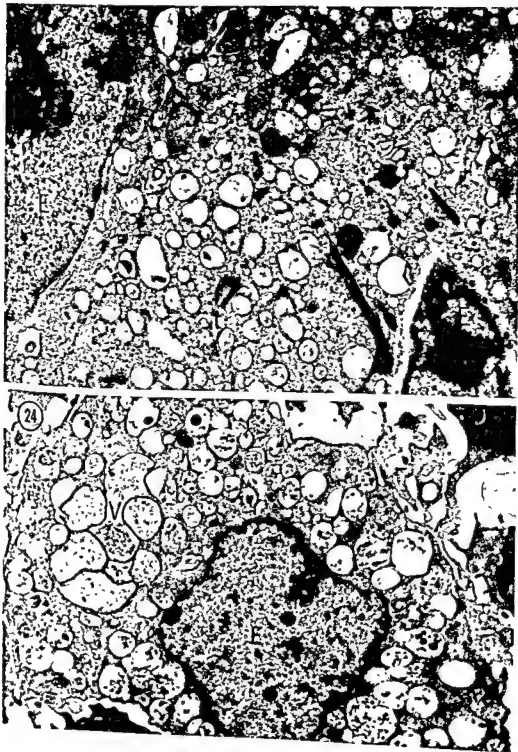


PLATE 10

EXPLANATION OF FIGURES

- 23 A nest of epithelial cells (E) from the thymic medulla of a mouse injected 38 hours previously with 25 μ g of endotoxin. The cytoplasm is filled with vacuoles, most of which represent dilated rough-surfaced endoplasmic reticulum. The perinuclear space around the lower nucleus (E) is also dilated. The nucleus to the left (E) contains a prominent nucleolus and there are no signs of extensive degeneration in these cells. (t: tonofibrils). $\times 17,000$.
- 24 An epithelial cell (E) from the thymic medulla of a mouse injected 38 hours previously with 25 μ g of endotoxin. Most of the vacuoles filling the cytoplasm of this cell are dilated elements of the rough-surfaced endoplasmic reticulum, more evident at higher magnification than in this print. There is also a typical cluster of cytoplasmic vacuoles (V), filled with an amorphous material—presumably secretory. Both the clustered vacuoles and the dilated endoplasmic reticulum contain small rods and spheres. $\times 7,700$.

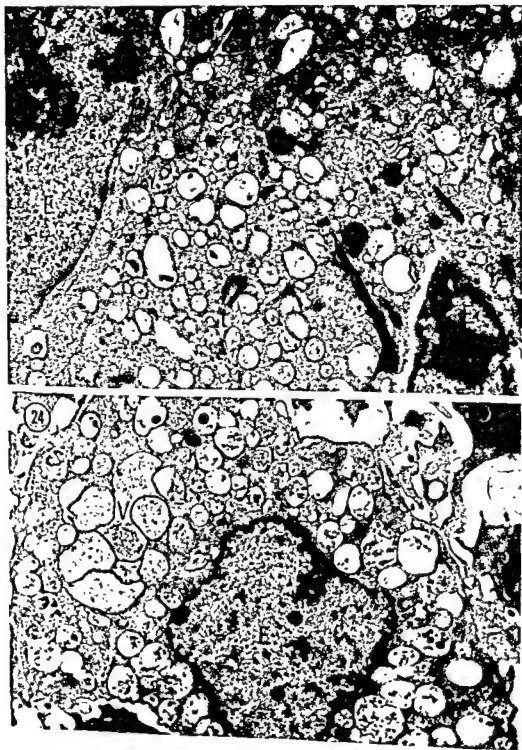
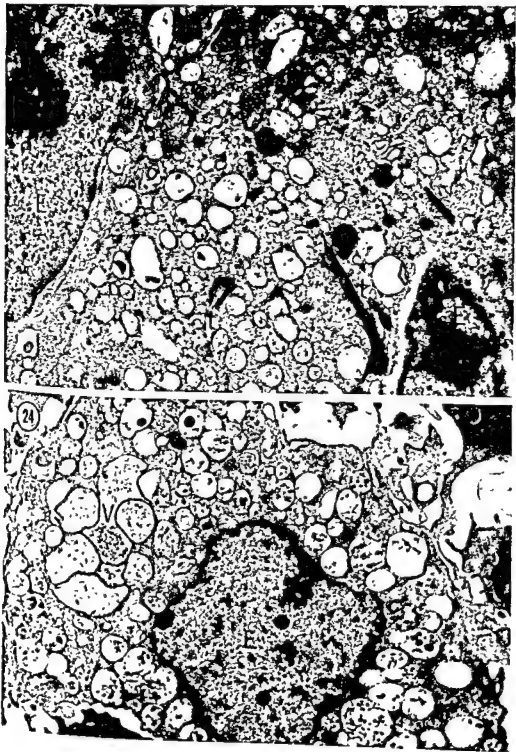


PLATE 10

EXPLANATION OF FIGURES

- 23 A nest of epithelial cells (E) from the thymic medulla of a mouse injected 38 hours previously with 25 μ g of endotoxin. The cytoplasm is filled with vacuoles, most of which represent dilated rough-surfaced endoplasmic reticulum. The perinuclear space around the lower nucleus (E) is also dilated. The nucleus to the left (E) contains a prominent nucleolus and there are no signs of extensive degeneration in these cells. (t: tonofibrils). $\times 17,000$.
- 24 An epithelial cell (E) from the thymic medulla of a mouse injected 38 hours previously with 25 μ g of endotoxin. Most of the vacuoles filling the cytoplasm of this cell are dilated elements of the rough-surfaced endoplasmic reticulum, more evident at higher magnification than in this print. There is also a typical cluster of cytoplasmic vacuoles (V), filled with an amorphous material—presumably secretory. *Both the clustered vacuoles and the dilated endoplasmic reticulum contain small rods and spheres.* $\times 7,700$.



Histochemical and Autoradiographic Studies of the Formation of the Metrial Gland in the Pregnant Rat¹

LYNN H. LARKIN² AND RICHARD L. SCHULTZ³

Department of Anatomy, University of Colorado School of Medicine,
Denver, Colorado

ABSTRACT It is shown in this study that cells of the mesometrial triangle proliferate at a high rate in the early formative period of the metrial gland. This, plus observations of sequential appearance of specific cell types during growth of this tissue, indicate that the metrial cells are formed *in situ*.

Support for the hypothesis of *in situ* formation of metrial gland tissue also was obtained by observation of apparent differentiation of metrial cells from a precursor cell type. The precursor cells appear to arise from fibroblast-like cells located in the mesometrial triangle throughout the formative period of the metrial gland. Quantitative autoradiographic studies indicate that the precursor cells accumulate glycogen, undergo division, and subsequently produce diastase-resistant, PAS-positive granules that are characteristic of metrial cells. These cells, which contain specific granules and glycogen, are an individual cell type and are referred to as mononucleate metrial cells. The experiments suggest that the mononucleate metrial cells undergo karyokinesis without cytokinesis resulting in typical binucleate metrial cells. Binucleate metrial cells synthesize DNA and appear to become polyploid rather than forming multinucleated cells or binucleate daughter cells. Some nuclei apparently attain a high ploidy, but the majority of binucleates are not highly polyploid.

The metrial gland of the rat is regarded as a component of the maternal placenta (Selye and McKeown, '35; Gerard, '25) and is present in the mesometrial triangle of the rat uterus from day 9 of pregnancy through the twenty-second day of lactation (Baker, '48). This structure is also found in deciduoma formation in the rat and displays morphological and cellular components nearly identical to the metrial gland of true pregnancy (Ellis, '57; Wislocki et al., '57; Velardo et al., '53).

The report that relaxin is localized in metrial cells of the pregnant rat (Dallenbach-Hellweg et al., '65) has renewed interest in the metrial gland. The typical or mature metrial cell is a large binucleate cell that contains cytoplasmic aggregations of acidophilic, diastase-fast, PAS-positive granules (specific granules) surrounded by a rim of clear cytoplasm. The intense reaction of this clear area with the PAS technique in tissue not subjected to diastase digestion implies a high content of glycogen. The metrial cells of the rat, although generally described as being located in the metrial gland, are present also in the mesometrial decidua from day 7 through day 14 of pregnancy. Metrial cells are found not only in the uterus of the

gravid rat but have also been described in uteri of pregnant mice (Smith, '66), guinea pigs, and rabbits (Asplund et al., '40). Cells histochemically and morphologically similar to the metrial cells of the rat have been found in human (Dallenbach-Hellweg et al., '65) and monkey uteri (Dallenbach-Hellweg et al., '66).

Dickson and Bulmer ('61) suggested that the metrial cells in maternal vessels are products of the trophoblast and eventually migrate into tissue of the mesometrial triangle. They also suspect that the endovascular plasmodium, which generally is regarded to be of fetal origin (Bridgman, '48b), is a precursor for some of the metrial gland cells. Most investigators suggest that these cells arise from maternal cellular elements, particularly the fibroblast-like cells in the mesometrial triangle (Dallenbach-Hellwig et al., '65; Ellis, '57; Baker, '48; Selye and McKeown, '35). This latter belief is well supported by deciduoma studies that prove that at least some

¹Supported by U.S. Public Health Service grant 5-F1-GM-24,733-02, and National Science Foundation grant GB-2923.

²Current address: Institute for Developmental Biology, University of Colorado, Boulder, Colorado.

³Career Development Awardee, K3-HD-7680.

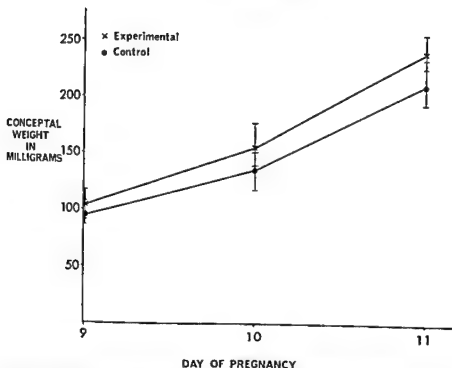


Fig. 1 Viability of conceptual tissue as shown by comparison of experimental and control (first operation) weights over a two day period (three operations). Consecutive operations were performed at days 9, 10, and 11 on five animals. Conceptuses from four control animals were weighed on each day.

these animals at specific periods ranging from one hour to five days after administration of the labeled precursor. Removal of most of the conceptuses was performed with the laparotomy technique described by Schultz, Reger, and Schultz ('66). Figure 1 illustrates the viability of conceptual tissues taken using this procedure. No more than normal resorption was noted. Three animals that were allowed to go to term after successive operations on days 9, 10, and 11 delivered the apparently normal, although slightly smaller, remaining young. The higher dosage of the tritiated compound was given to animals used in the four and five day periods. A minimum of four conceptuses, two from each of two maternal animals, were used for each period of the project.

Two sets of slides were prepared from each of the conceptuses. One set was treated with diastase before PAS staining while the other was subjected to the PAS technique alone. Both sets of slides were

counterstained with Harris hematoxylin. At least 1000 labeled cells were counted in each mesometrial triangle studied. Labeled mononucleate cells were divided into the following groups; PAS-negative, PAS-positive without diastase digestion, and PAS-positive with diastase digestion. Labeled binucleate cells were divided into the following groups: PAS-positive without prior diastase digestion, PAS-positive with prior diastase digestion. Counts of identical cell types were made on day 12 metrial gland tissue taken from four animals not injected with H^3 -thymidine and these counts served as controls.

Measurement of nuclear diameter. Nuclear measurements were performed on four conceptuses at day 12 and at day 14. A technique similar to that of Carriere and Patterson ('62) was employed to measure the diameter of nuclei in the mesometrial triangle. At least 1000 nuclei of mononucleate cells were measured in each of the day 12 conceptuses and the nuclei

of the metrial cells arise from maternal tissue (Ellis, '57; Selye and McKeown, '35).

Periods of cytoplasmic basophilia, glycogen accumulation, and granule formation in cells of the mesometrial triangle of the rat in deciduoma formation (Ellis, '57) and pregnancy (Baker, '48) offer additional evidence for maternal origin. More recently Smith ('66) has suggested that metrial cells in the decidua of mice arise from cells of the lymphocytic series, thus indicating a maternal, extrauterine origin.

Although metrial cells of the rat appear to be of maternal origin, the possibility of metrial cells of fetal origin has not been eliminated. Studies concerned with cell proliferation in the fetal and maternal rat placenta (Jollie, '64; Jones, '61; Bridgman, '48a,b) have given little information to indicate whether the cells which constitute the mature metrial gland migrate into the mesometrial triangle (Selye and McKeown, '35) or are formed *in situ*.

The work reported in this article describes the formation of the metrial gland within the mesometrial triangle. Experiments were conducted to determine the turnover of cells in the mesometrial triangle during the formative period of the metrial gland and to demonstrate more conclusively the origin and differentiation of typical metrial cells.

MATERIALS AND METHODS

Holtzman rats ranging in weight from 200 to 270 gm were used. The day in which sperm were noted in an early morning vaginal lavage from estrus females caged overnight with males was considered to be day zero of pregnancy.

Histological and histochemical preparations. Conceptuses used in all of the following experiments were fixed in alcoholic formalin, embedded in paraplast, and sectioned transversely with a Spencer microtome at an average thickness of 4 μ . Sections from conceptuses of days 8 through 14 of pregnancy were used for histological and histochemical study and were stained with Harris hematoxylin, orange G, and eosin Y; with PAS, with and without prior diastase digestion and Harris hematoxylin; or with Feulgen reaction and orange G.

Autoradiographic studies. Two separate studies were performed using H^3 -thymidine (sp. act. 15c/mmole). Tritiated thymidine was administered intraperitoneally in all animals between 11:00 and 12:00 AM to avoid the complications of diurnal fluctuations of DNA synthetic activity (Pilgrim and Maurer, '65). The technique of applying and processing the liquid photographic emulsion (Prescott, '64) was identical in both studies. Kodak NTB3 or NTB emulsion was used. The PAS technique was utilized before application of the photographic emulsion, whereas all other stains were employed after photographic processing. Cells exhibiting at least four silver grains over their nuclei were considered labeled. Background was determined by counting the number of silver grains per unit area in a portion of the autoradiogram where no tissue was present (Thrasher, '66). In order to obtain adequate sampling of the cells in the mesometrial triangle in the quantitative studies, sections of the conceptuses were traversed with the microscope from one external muscle layer of the uterus to the external muscle layer of the opposite side of the so-called "triangle." The first traverse was always made immediately adjacent to the circular muscle layer and each succeeding traverse was made one microscope field mesometrially.

In the first study each pregnant rat was administered 0.5 μ Cl of H^3 -thymidine per gram body weight. The labeled DNA precursor was injected into three rats per day on days 8 through 14 of gestation. Conceptuses were removed five hours after injection in two animals and one hour after injection in the third animal for each day of gestation studied. At least two conceptuses from each animal were examined to determine the per cent of labeled cells. A minimum of 1000 labeled cells were counted in each mesometrial triangle. The tissues used in this study were stained with Harris hematoxylin, eosin Y, and orange G. Tissues from the one hour samples on days 8 and 9 were stained with toluidine blue.

In the subsequent autoradiographic study, animals were injected with 0.5 or 1.0 μ Cl of H^3 -thymidine per gm body weight. Conceptuses were removed from

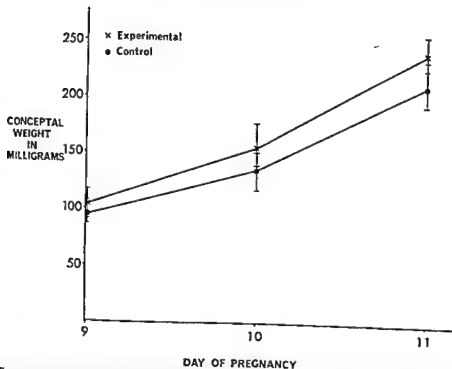


Fig. 1 Viability of conceptual tissue as shown by comparison of experimental and control (first operation) weights over a two day period (three operations). Consecutive operations were performed at days 9, 10, and 11 on five animals. Conceptuses from four control animals were weighed on each day.

these animals at specific periods ranging from one hour to five days after administration of the labeled precursor. Removal of most of the conceptuses was performed with the laparotomy technique described by Schultz, Reger, and Schultz ('66). Figure 1 illustrates the viability of conceptual tissues taken using this procedure. No more than normal resorption was noted. Three animals that were allowed to go to term after successive operations on days 9, 10, and 11 delivered the apparently normal, although slightly smaller, remaining young. The higher dosage of the tritiated compound was given to animals used in the four and five day periods. A minimum of four conceptuses, two from each of two maternal animals, were used for each period of the project.

Two sets of slides were prepared from each of the conceptuses. One set was treated with diastase before PAS staining while the other was subjected to the PAS technique alone. Both sets of slides were

counterstained with Harris hematoxylin. At least 1000 labeled cells were counted in each mesometrial triangle studied. Labeled mononucleate cells were divided into the following groups; PAS-negative, PAS-positive without diastase digestion, and PAS-positive with diastase digestion. Labeled binucleate cells were divided into the following groups: PAS-positive without prior diastase digestion, PAS-positive with prior diastase digestion. Counts of identical cell types were made on day 12 metrial gland tissue taken from four animals not injected with H^3 -thymidine and these counts served as controls.

Measurement of nuclear diameter. Nuclear measurements were performed on four conceptuses at day 12 and at day 14. A technique similar to that of Carriere and Patterson ('62) was employed to measure the diameter of nuclei in the mesometrial triangle. At least 1000 nuclei of mononucleate cells were measured in each of the day 12 conceptuses and the nuclei

of the metrial cells arise from maternal tissue (Ellis, '57; Selye and McKeown, '35).

Periods of cytoplasmic basophilia, glycogen accumulation, and granule formation in cells of the mesometrial triangle of the rat in deciduoma formation (Ellis, '57) and pregnancy (Baker, '48) offer additional evidence for maternal origin. More recently Smith ('66) has suggested that metrial cells in the decidua of mice arise from cells of the lymphocytic series, thus indicating a maternal, extrauterine origin.

Although metrial cells of the rat appear to be of maternal origin, the possibility of metrial cells of fetal origin has not been eliminated. Studies concerned with cell proliferation in the fetal and maternal rat placenta (Jollie, '64; Jones, '61; Bridgman, '48a,b) have given little information to indicate whether the cells which constitute the mature metrial gland migrate into the mesometrial triangle (Selye and McKeown, '35) or are formed *in situ*.

The work reported in this article describes the formation of the metrial gland within the mesometrial triangle. Experiments were conducted to determine the turnover of cells in the mesometrial triangle during the formative period of the metrial gland and to demonstrate more conclusively the origin and differentiation of typical metrial cells.

MATERIALS AND METHODS

Holtzman rats ranging in weight from 200 to 270 gm were used. The day in which sperm were noted in an early morning vaginal lavage from estrus females caged overnight with males was considered to be day zero of pregnancy.

Histological and histochemical preparations. Conceptuses used in all of the following experiments were fixed in alcoholic formalin, embedded in paraplast, and sectioned transversely with a Spencer microtome at an average thickness of 4 μ . Sections from conceptuses of days 8 through 14 of pregnancy were used for histological and histochemical study and were stained with Harris hematoxylin, orange G, and eosin Y; with PAS, with and without prior diastase digestion and Harris hematoxylin; or with Feulgen reaction and orange G.

Autoradiographic studies. Two separate studies were performed using H^3 -thymidine (sp. act. 15c/mmole). Tritiated thymidine was administered intraperitoneally in all animals between 11:00 and 12:00 AM to avoid the complications of diurnal fluctuations of DNA synthetic activity (Pilgrim and Maurer, '65). The technique of applying and processing the liquid photographic emulsion (Prescott, '64) was identical in both studies. Kodak NTB3 or NTB emulsion was used. The PAS technique was utilized before application of the photographic emulsion, whereas all other stains were employed after photographic processing. Cells exhibiting at least four silver grains over their nuclei were considered labeled. Background was determined by counting the number of silver grains per unit area in a portion of the autoradiogram where no tissue was present (Thrasher, '66). In order to obtain adequate sampling of the cells in the mesometrial triangle in the quantitative studies, sections of the conceptuses were traversed with the microscope from one external muscle layer of the uterus to the external muscle layer of the opposite side of the so-called "triangle." The first traverse was always made immediately adjacent to the circular muscle layer and each succeeding traverse was made one microscope field mesometrially.

In the first study each pregnant rat was administered 0.5 μ Ci of H^3 -thymidine per gram body weight. The labeled DNA precursor was injected into three rats per day on days 8 through 14 of gestation. Conceptuses were removed five hours after injection in two animals and one hour after injection in the third animal for each day of gestation studied. At least two conceptuses from each animal were examined to determine the per cent of labeled cells. A minimum of 1000 labeled cells were counted in each mesometrial triangle. The tissues used in this study were stained with Harris hematoxylin, eosin Y, and orange G. Tissues from the one hour samples on days 8 and 9 were stained with toluidine blue.

In the subsequent autoradiographic study, animals were injected with 0.5 or 1.0 μ Ci of H^3 -thymidine per gm body weight. Conceptuses were removed from

two nuclei. Cells with pyknotic nuclei are found in considerable numbers in the metrial gland on day 13. These cells exhibit PAS-positive, diastase-resistant granules in the immediate vicinity of their nuclear remnants. The association of PAS-positive, diastase-resistant material with the nuclear fragments suggests that the dying cells may be metrial cells. At day 14 areas containing cell debris and metrial cells with pyknotic nuclei are found in the metrial gland.

At days 12, 13, and 14, metrial cells are noted that contain unusually large nuclei (fig. 9). These large nuclei stain with approximately the same intensity as the smaller, more normal sized nuclei and contain two or more large nucleoli. Cells in various stages of division are seen quite regularly on days 8 through 11. By day 12, however, the number is reduced and by day 14 mitotic figures are infrequent. Mitoses are noted in undifferentiated cells and cells that contain specific granules and/or glycogen. Occasionally, large mitotic figures are present in cells that contain specific granules (fig. 10).

Autoradiographic studies. In the first autoradiographic study H^3 -thymidine was

administered to animals on days 8 through 14 of gestation to determine the number of cells that were synthesizing DNA, i.e., proliferating. The percent of labeled cells in the mesometrial triangle varied greatly from day 8 to day 14 (fig. 2). A high proliferative rate was noted before day 12. At day 12, the rate had definitely decreased and by day 14 the number of cells synthesizing DNA was extremely low. At day 8 the cells synthesizing DNA were undifferentiated. On later days mono- and binucleate metrial cells of animals labeled one hour with H^3 -thymidine exhibited silver grains over their nuclei (fig. 11).

The autoradiograms stained with toluidine blue revealed metachromatically staining mast cells in the myometrium and mesometrium. Few mast cells were found within the mesometrial triangle and none of the mast cells were labeled at day 8 or 9 of pregnancy.

Figure 3 illustrates results of the study in which H^3 -thymidine was administered to rats on day 9 and conceptuses taken at specific periods. The percent of labeled mononucleate cells containing glycogen was quite low on day 9. The relative number of these cells increased progressively

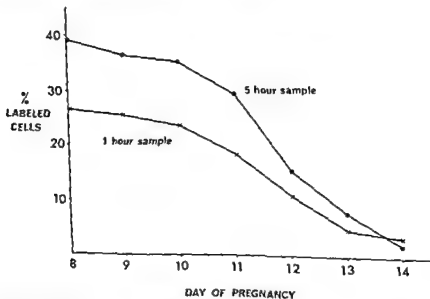


FIG. 2 Percent of cells synthesizing DNA in the mesometrial triangle on days 8 through 14 of pregnancy.

of at least 500 binucleate cells were measured from each of the day 12 and 14 samples. The tissue used in this study was stained with either Harris hematoxylin, eosin Y, and orange G or PAS after diastase digestion and Harris hematoxylin.

OBSERVATIONS

Morphology of the developing metrial gland. The tissue within the mesometrial triangle enlarges greatly from day 8 to day 14 of pregnancy. The growth is easily noted on days 8 through 13. It is difficult to judge the relative growth of the metrial gland from day 13 to 14 due to the great increase in size of the fetal tissues at this time.

The cells that constitute the tissue within the mesometrial triangle on day 8 of pregnancy do not contain any characteristic cytoplasm granules or material that permits identifying them as metrial cells. The cells are mononucleate and are present as two distinct morphological types. One type resembles the fibroblast or mesenchymal cell to the extent that it is a long, slender spindle shaped cell (figs. 4, 6, 7). The fibroblast-like cells have elongate nuclei that contain numerous, small chromatin bodies and at least one nucleolus. The second type of cell is rounded and contains an oval nucleus (fig. 4). The nuclei of the second cell type appear similar to nuclei of decidua basalis cells since they stain lightly with nuclear dyes and contain a large nucleolus. These spherical cells within the mesometrial triangle on day 8 appear identical to cells described by Ellis ('57) and Baker ('48) as precursor cells of the metrial cells. Therefore, the second type cells will be referred to as precursor cells.

At day 9, cells morphologically similar in size, shape, and nuclear structure to precursor cells are found that contain a diastase-sensitive cytoplasmic material (glycogen) (fig. 5). Occasionally, similar cells are noted that contain specific granules characteristic of metrial cells (fig. 6). This latter cell type is considered a mononucleate metrial cell because it contains specific granules. It is unlikely to be a fragment of a binucleate cell since binucleate metrial cells are extremely rare in day 9 mesometrial triangle tissue. In con-

trast to the mature binucleate metrial cell, the mononucleate metrial cells are small and contain only few specific granules. The fibroblast-like cells and precursor cells are present in the mesometrial triangle in abundance on day 9 of pregnancy.

At ten days typical metrial cells first make their appearance in the mesometrial triangle. Generally, they are situated close to the mesometrial surface of the inner circular muscle layer. These metrial cells are binucleate and contain large amounts of glycogen (fig. 7). With diastase digestion, the metrial cells also exhibit numerous specific granules that are well localized in close proximity to the two nuclei (fig. 8). The cells most frequently noted on day 10 are precursor cells and mononucleate cells that contain glycogen. Fibroblast-like cells are present throughout the tissue but seem to be concentrated peripherally, adjacent to the external muscle layer of the uterus.

The many mono- and binucleate metrial cells present on day 11 give the tissue of the mesometrial triangle a glandular appearance. The binucleate metrial cells are found throughout the mesometrial triangle, but the heaviest concentration of the cells is observed immediately adjacent to the circular muscle layer. Considerable numbers of mononucleate metrial cells and precursor cells are located throughout the metrial gland. The areas adjacent to the external muscle layer are sparsely populated with metrial cells. These lateral areas of the metrial gland, however, do contain fibroblast-like cells.

The metrial gland becomes more tightly packed with metrial cells on days 12, 13, and 14. At day 14 fibroblast-like cells, precursor cells, and mononucleate cells containing specific granules and/or glycogen can be noted throughout the metrial gland, but, as noted on earlier days the fibroblast-like cells are localized laterally in the gland. In sections not treated with diastase no cells were noted that contained specific granules alone. It is assumed that cells which contained specific granules also contained glycogen. Although Ellis ('57) reports that metrial cells containing three or four nuclei are not uncommon, examination of the 4 μ sections revealed extremely few metrial cells that contain more than

two nuclei. Cells with pyknotic nuclei are found in considerable numbers in the metrial gland on day 13. These cells exhibit PAS-positive, diastase-resistant granules in the immediate vicinity of their nuclear remnants. The association of PAS-positive, diastase-resistant material with the nuclear fragments suggests that the dying cells may be metrial cells. At day 14 areas containing cell debris and metrial cells with pyknotic nuclei are found in the metrial gland.

At days 12, 13, and 14, metrial cells are noted that contain unusually large nuclei (fig. 9). These large nuclei stain with approximately the same intensity as the smaller, more normal sized nuclei and contain two or more large nucleoli. Cells in various stages of division are seen quite regularly on days 8 through 11. By day 12, however, the number is reduced and by day 14 mitotic figures are infrequent. Mitoses are noted in undifferentiated cells and cells that contain specific granules and/or glycogen. Occasionally, large mitotic figures are present in cells that contain specific granules (fig. 10).

Autoradiographic studies. In the first autoradiographic study H^3 -thymidine was

administered to animals on days 8 through 14 of gestation to determine the number of cells that were synthesizing DNA, i.e., proliferating. The percent of labeled cells in the mesometrial triangle varied greatly from day 8 to day 14 (fig. 2). A high proliferative rate was noted before day 12. At day 12, the rate had definitely decreased and by day 14 the number of cells synthesizing DNA was extremely low. At day 8 the cells synthesizing DNA were undifferentiated. On later days mono- and binucleate metrial cells of animals labeled one hour with H^3 -thymidine exhibited silver grains over their nuclei (fig. 11).

The autoradiograms stained with toluidine blue revealed metachromatically staining mast cells in the myometrium and mesometrium. Few mast cells were found within the mesometrial triangle and none of the mast cells were labeled at day 8 or 9 of pregnancy.

Figure 3 illustrates results of the study in which H^3 -thymidine was administered to rats on day 9 and conceptuses taken at specific periods. The percent of labeled mononucleate cells containing glycogen was quite low on day 9. The relative number of these cells increased progressively

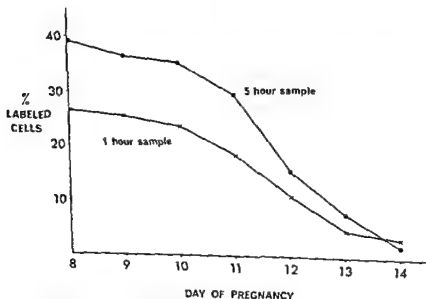


Fig. 2. Percent of cells synthesizing DNA in the mesometrial triangle on days 8 through 14 of pregnancy.

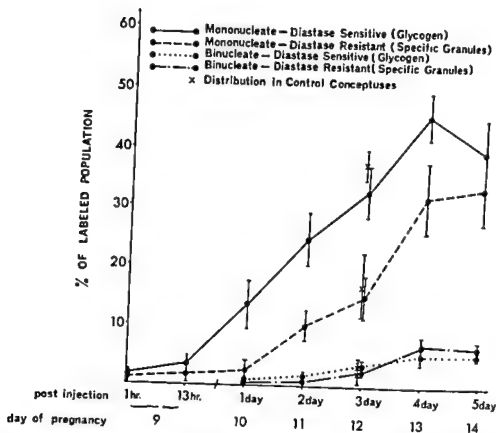


Fig. 3 Relative number of differentiated, labeled cells at various periods after injection of H^3 -thymidine at day 9 of pregnancy.

through days 10, 11, 12, and 13. The percent of labeled mononucleate cells containing specific granules was similar to the percent of labeled mononucleate cells containing glycogen on day 9. The percent of mononucleate metrial cells in the total labeled population began to increase by day 11 and reached a maximum at day 13. All mononucleate cells that contained glycogen did not contain specific granules. This is illustrated by the difference in percent of these two cell types on days 10 through 13. As stated previously, all cells that contained specific granules did contain glycogen. It follows that the population of mononucleates containing glycogen included the population of mononucleate metrial cells.

The binucleates represented a small percent of the total labeled population on days 9, 10, and 11. The percent of binucleate metrial cells began to increase by day 12 and reached a maximum at day 13; this level was maintained through day 14. Since the percent of labeled binucleate cells

that contain glycogen is similar to the percent of those that contain specific granules on all days of this study, the binucleate cells that exhibit glycogen and specific granules in the two different preparations are assumed to be one and the same cell type.

Labeled pyknotic nuclei were noted in the mesometrial triangle of the day 13 and 14 conceptuses that were subjected to H^3 -thymidine on day 9. The majority of these cells exhibited a diastase resistant, PAS-positive material in the immediate vicinity of their nuclear remnants and thus were considered to be degenerating metrial cells.

Nuclear diameters. Although the mean diameter of the binucleate metrial cells are similar on both days 12 and 14, the binucleate population has a higher percent of large nuclei on day 14 than on day 12 (table 1). Moreover, binucleate cells on both days 12 and 14 have a higher percent of large nuclei than mononucleate cells at day 12.

TABLE 1
Per cents of large and small nuclei of cells in the metrial gland

	Mean	Nuclear diameter 6 μ and smaller	Nuclear diameter larger than 6 μ
		%	%
Day 12 mononucleate	5.9	58.6	41.4
Day 12 binucleate	6.1	51.9	48.1
Day 14 binucleate	6.2	46.7	53.3

DISCUSSION

Proliferation of cells in the mesometrial triangle. One of our objectives was to determine if proliferation of cells in the mesometrial triangle of the rat was sufficiently high to indicate that the tissue of the metrial gland was formed *in situ*. Accordingly, we determined the number of cells synthesizing DNA in the mesometrial triangle during the formative period of the metrial gland. Autoradiograms of tissues from animals that received daily injections of H³-thymidine on days 8 through 14 illustrate that the tissue was proliferating at a high rate on days 8 through 11. By day 14, however, the rate was quite low. These findings, plus morphological studies that illustrated an orderly sequence of growth and cell differentiation, indicated that the metrial gland (as seen on day 14 of gestation in the rat) was indeed formed by proliferation of cells in the mesometrial triangle. The results seem to negate the suggestion that decidual tissue migrates into the mesometrial triangle to form the metrial gland (Selye and McKeown, '35). This study, though, does not exclude the possibility that some of the metrial cells may be of fetal origin.

Differentiation of metrial cells. Previous histological and histochemical studies, although in dispute with respect to stages in differentiation of the metrial cells, indicated that undifferentiated cells first occupy the mesometrial triangle (Ellis, '57, Baker, '48). Mononucleate cells containing specific cytoplasmic granules (Baker, '48) or glycogen (Ellis, '57) next appeared in the mesometrial triangle. Subsequently, binucleate metrial cells began to appear in significant numbers and reached a maximum on day 14 of pregnancy (Baker, '48) and decidualoma forma-

tion (Ellis, '57). Our observations generally agree with Ellis ('57) and Baker ('48) but specifically support the work of Ellis ('57) in that cells containing glycogen were noted earlier in pregnancy than cells containing specific granules.

Histological and histochemical studies can at best only give information about the tissue at the time of fixation. To study the sequence of differentiation of metrial cells a population of cells in the mesometrial triangle was labeled at day 9 and subsequently scored for periods up to five days. Since the mature metrial cell is binucleate and contains both cytoplasmic glycogen and diastase-resistant PAS-positive granules, one can observe the sequential appearance of these three morphological characteristics in the differentiation of the metrial gland cell.

The initial morphological event of metrial cell differentiation appears to be the accumulation of glycogen. This is indicated by the observation that only glycogen is present in a significant number of the labeled cells of the mesometrial triangle at a time when this tissue is made up of precursor and fibroblast-like cells. Subsequently specific granules accompanying the glycogen were found in a substantial number of labeled cells. Thereafter, the labeled cells containing specific granules and glycogen apparently became binucleate.

Since the glycogen-containing cells exhibit mitoses, their increase in number presumably results from division of existing glycogen cells and accumulation of glycogen in precursor cells. Two observations indicate that the binucleate metrial cells arise from the mononucleate metrial cells: (1) the binucleate cells contain glycogen and specific granules; (2) the labeled

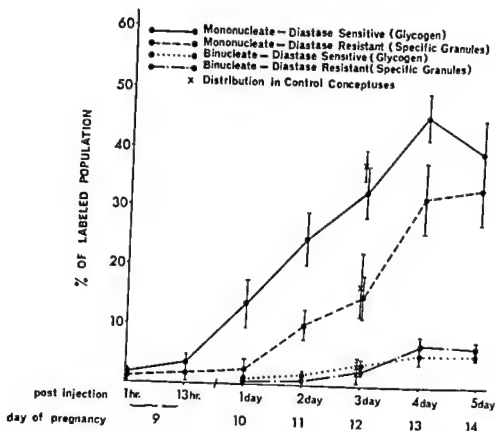


Fig. 3 Relative number of differentiated, labeled cells at various periods after injection of H^3 -thymidine at day 9 of pregnancy.

through days 10, 11, 12, and 13. The percent of labeled mononucleate cells containing specific granules was similar to the percent of labeled mononucleate cells containing glycogen on day 9. The percent of mononucleate metrial cells in the total labeled population began to increase by day 11 and reached a maximum at day 13. All mononucleate cells that contained glycogen did not contain specific granules. This is illustrated by the difference in percent of these two cell types on days 10 through 13. As stated previously, all cells that contained specific granules did contain glycogen. It follows that the population of mononucleates containing glycogen included the population of mononucleate metrial cells.

The binucleates represented a small percent of the total labeled population on days 9, 10, and 11. The percent of binucleate metrial cells began to increase by day 12 and reached a maximum at day 13; this level was maintained through day 14. Since the percent of labeled binucleate cells

that contain glycogen is similar to the percent of those that contain specific granules on all days of this study, the binucleate cells that exhibit glycogen and specific granules in the two different preparations are assumed to be one and the same cell type.

Labeled pyknotic nuclei were noted in the mesometrial triangle of the day 13 and 14 conceptuses that were subjected to H^3 -thymidine on day 9. The majority of these cells exhibited a diastase resistant, PAS-positive material in the immediate vicinity of their nuclear remnants and thus were considered to be degenerating metrial cells.

Nuclear diameters. Although the mean diameter of the binucleate metrial cells are similar on both days 12 and 14, the binucleate population has a higher percent of large nuclei on day 14 than on day 12 (table 1). Moreover, binucleate cells on both days 12 and 14 have a higher percent of large nuclei than mononucleate cells at day 12.

hibition of cleavage furrow formation by the specific granules, then these granules for the same reason would inhibit formation of polyploid mononucleate cells.

The large or polyploid metrial cell nuclei appear in significant numbers on day 12. No polyploid cells were noted that were undifferentiated; that is, large nuclei were only observed in the metrial gland in cells that contained specific granules. Since signs of differentiation appear before polyploidy, differentiation does not seem to result from polyploidy; however, polyploidy may result from differentiation. The observation that metrial cells synthesize DNA and exhibit mitotic figures is in disagreement with the proposition that differentiation and mitotic activity exclude each other.

LITERATURE CITED

- Asplund, J., V. Borell and H. Holmgren 1940 In der Unterwand während Gravidität auf auftretende metachromatische granuläre Zellen und ihre Stellung zur "Glandula myometrialis." *Z. Mikr.-anat. Forsch.*, 48: 478-528.
- Baker, B. L. 1948 Histochemical variations in the metrial gland of the rat during pregnancy and lactation. *Proc. Soc. Exp. Biol. and Med.*, 68: 492-496.
- Beams, H. W., and R. L. King 1942 The origin of binucleate and large mononucleate cells in the liver of the rat. *Anat. Rec.*, 83: 281-297.
- Bridgman, J. 1948a A morphological study of the development of the placenta of the rat. I. An outline of the development of the placenta of the white rat. *J. Morph.*, 83: 61-85.
- 1948b A morphological study of the development of the placenta of the rat. II. A histological and cytological study of the development of the chorioallantoic placenta of the white rat. *J. Morph.*, 83: 195-223.
- Carriere, R. 1962 Role of the thyroid gland in the control of polyploid cell formation in the rat liver. *Endocrinology*, 70: 761-773.
- Carriere, R., and D. Patterson 1962 The counting of mono- and binucleated cells in tissue sections. *Anat. Rec.*, 142: 443-456.
- Dallenbach-Hellweg, G., J. V. Battista and F. D. Dallenbach 1965 Immunohistological and histochemical localization of relaxin in the metrial gland of the pregnant rat. *Am. J. Anat.*, 117: 433-450.
- Dallenbach-Hellweg, G., A. B. Dawson and F. L. Hisaw 1966 The effect of relaxin on the endometrium of monkeys. *Histological and histochemical studies*. *Am. J. Anat.*, 119: 61-78.
- Dickson, A. D., and D. Bulmer 1961 Observations on the origin of metrial gland cells in the rat placenta. *J. Anat.*, 95: 262-273.
- Ellis, R. A. 1957 Histochemistry of the cellular components of the metrial gland of the rat during prolonged pseudopregnancy. *Anat. Rec.*, 129: 39-52.
- Gerard, P. 1925 Sur un gland myometrial de la souris et du rat. *C. R. Soc. Biol.*, 93: 457-459.
- Haskins, C. L. 1952 Nuclear reproduction. *Int. Rev. Cytol.*, 1: 9-26.
- Jollie, W. P. 1964 Radioautographic observations on variations in desoxyribonucleic acid synthesis in rat placenta with increasing gestational age. *Am. J. Anat.*, 114: 161-171.
- Jones, L. A. 1961 A study of the formation of the placenta in the rat. Master's Thesis, Connecticut College, New London, Conn., 1-132.
- Pilgrim, C., and W. Maurer 1965 Autoradiographische untersuchung ubes die konstanz der DNS-Kerndopplungs dauer bei Zellarten von Maus und Ratte durch doppelmarkierung mit ^3H - und ^{14}C -thymidin. *Exp. Cell Res.*, 37: 183-199.
- Prescott, D. M. 1964 Autoradiography with liquid emulsion. In: *Methods in Cell Physiology*. I. D. M. Prescott, ed. Academic Press, New York, pp. 365-370.
- Sachs, L. 1953 Simple methods for mammalian chromosomes. *Stain Tech.*, 28: 169-172.
- Sachs, L., and M. C. Shelesnyak 1955 The development and suppression of polyploidy in the developing and suppressed deciduomas in the rat. *J. Endocrin.*, 12: 146-151.
- Schultz, P. W., J. F. Reger and R. L. Schultz 1966 Effects of Triton WR-1339 on the rat yolk sac placenta. *Am. J. Anat.*, 119: 199-233.
- Selye, H., and T. McKeown 1935 Studies on the physiology of the maternal placenta in the rat. *Proc. Roy. Soc. London*, 119: 1-31.
- Smith, L. J. 1966 Metrial gland and other glycolytic containing cells in the mouse uterus following mating and through implantation of the embryo. *Am. J. Anat.*, 119: 15-23.
- Swift, H. 1950 The desoxyribose nucleic acid content of animal nuclei. *Physiol. Zool.*, 23: 169-199.
- Thrasher, J. D. 1966 Analysis of renewing epithelial cell populations. In: *Methods in Cell Physiology*. II. D. M. Prescott, ed. Academic Press, New York, pp. 323-357.
- Velardo, J. T., A. B. Dawson, A. G. Olson and F. L. Hisaw 1953 Sequence of histological changes in the uterus and vagina of the rat during prolongation of pseudopregnancy associated with the presence of deciduomata. *Am. J. Anat.*, 93: 273-305.
- Wilson, J. W., and E. H. Leduc 1948 The occurrence and formation of binucleate and multinucleated cells and polyploid nuclei in the mouse liver. *Am. J. Anat.*, 82: 353-391.
- Wislocki, G. B., L. P. Weiss, M. H. Burgos and Richard A. Ellis 1957 The cytology, histochemistry and electron microscopy of the granular cells of the metrial gland of the gravid rat. *J. Anat.*, 91: 130-140.

binucleate metrial cells appear subsequent to the labeled mononucleate metrial cells. Although mononucleate metrial cells appear to give rise to binucleate metrial cells, the number of mononucleate metrial cells continues to increase. This increase is presumed to occur from the accumulation of specific granules in mononucleate cells that contain glycogen. The latter suggestion is made because no cells were found that contained only specific granules, i.e., all cells that contained specific granules must have had glycogen prior to the granules.

The labeled binucleate cells increase in number during periods of fairly high cell proliferation (days 10, 11, and 12). The number of binucleate cells does not increase from day 13 to 14 when the proliferation of cells is extremely low. The finding that binucleates increase in number during high proliferative periods and not during low proliferative periods indicates that the binucleates are being formed by a process involving division. This general observation would suggest that binucleation stems from mitosis without cytokinesis and that fusion of mononucleate metrial cells is not involved. The former mechanism of binucleation has been described in rat liver cells (Wilson and Leduc, '48; Beams and King, '42). Binucleation in liver cells may result when a large amount of inert material in the cell inhibits formation of the normal cleavage furrow (Beams and King, '42). Similarly, Ellis ('57) has suggested that binucleation of metrial cells may be due to a physical interference with cytokinesis by the specific granules that occupy the central portion of the interphase cytoplasm. This could easily be the case since cells were noted that exhibited metaphase plates in the presence of specific granules.

Ploidy of the metrial cells. One aspect of the metrial gland cells that has not been investigated previously is their ploidy. Various mammalian tissues contain cells that have two or more times their normal G-1 diploid amount of DNA. Mouse liver, pancreas, thymus, lymphocytes, and Sertoli cells all exhibit polyploidy to some extent (Swift, '50). In nuclei of each of these tissues there is a direct relationship between nuclear volume and DNA content (Swift, '50). The relationship of greater

nuclear volume with increased DNA content also has been found in rat liver cells (Carriere, '62) and decidual cells in rat deciduoma (Sachs and Shelesnyak, '55; Sachs, '53). When nuclei of different tissues of the same animal are compared, however, there is no correlation between nuclear size and DNA content (Haskins, '52; Swift, '50). Visual observation of increased numbers of chromosomes also indicates polyploidy. Sachs and Shelesnyak ('55), for example, determined ploidy of decidual cells by correlating high chromosome numbers and large metaphase plates with enlarged nuclei.

Extremely large nuclei in typical metrial cells indicate that some binucleate metrial cells are polyploid. Two types of mechanisms for polyploidy of individual metrial cell nuclei can be proposed. The process may be similar to that described by Beams and King ('42) and by Wilson and Leduc ('48) in rat liver cells. Beams and King ('42) suggest that "the two nuclei prepare for the next division synchronously, but usually only one spindle is formed at metaphase so that either two tetraploid daughter cells result from a complete mitosis, or cytokinesis may be suppressed again thus giving rise to a binucleate cell with tetraploid nuclei." In contrast to this theory, the metrial cells that were synthesizing DNA might undergo endoduplication. The process apparently occurs in trophoblastic giant cells of the fetal rat placenta (Jollie, '64). The trophoblastic giant cells synthesize DNA but do not undergo mitosis; therefore, they are assumed to be highly polyploid (Jollie, '64). The polyploidization of metrial cells may be the same as that suggested for liver cells. Both nuclei of the binucleate metrial cells synthesize DNA synchronously and appear morphologically similar. The large metaphase plates associated with specific granules suggests that polyploid metrial cells are undergoing mitosis.

The ploidy of metrial cells apparently increases with gestational age since more large nuclei are noted on day 14 than day 12 in the binucleates. Few cells are found with more than two nuclei, thus suggesting that the nuclei become polyploid rather than producing multinucleate cells. If binucleation originally results from the in-

hibition of cleavage furrow formation by the specific granules, then these granules for the same reason would inhibit formation of polyploid mononucleate cells.

The large or polyploid metrial cell nuclei appear in significant numbers on day 12. No polyploid cells were noted that were undifferentiated; that is, large nuclei were only observed in the metrial gland in cells that contained specific granules. Since signs of differentiation appear before polyploidy, differentiation does not seem to result from polyploidy; however, polyploidy may result from differentiation. The observation that metrial cells synthesize DNA and exhibit mitotic figures is in disagreement with the proposition that differentiation and mitotic activity exclude each other.

LITERATURE CITED

- Asplund, J., V. Borell and H. Holmgren 1940 In der Untersuchung während Gravidität auf auftretende metachromatische granulierte Zellenbänder und ihre Stellung zur "Glandula myometrialis." *Z. Mikr.-anat. Forsch.*, 48: 478-528.
- Baker, B. L. 1948 Histochemical variations in the metrial gland of the rat during pregnancy and lactation. *Proc. Soc. Exp. Biol. and Med.*, 68: 492-496.
- Beams, H. W., and R. L. King 1942 The origin of binucleate and large mononucleate cells in the liver of the rat. *Anat. Rec.*, 83: 281-297.
- Bridgman, J. 1948a A morphological study of the development of the placenta of the rat. I. An outline of the development of the placenta of the white rat. *J. Morph.*, 83: 61-85.
- 1948b A morphological study of the development of the placenta of the rat. II. A histological and cytological study of the development of the chorioallantoic placenta of the white rat. *J. Morph.*, 83: 195-223.
- Arner, R. 1962 Role of the thyroid gland in the control of polyploid cell formation in the rat liver. *Endocrinology*, 70: 761-773.
- Arner, R., and D. Patterson 1962 The counting of mono- and binucleated cells in tissue sections. *Anat. Rec.*, 142: 443-456.
- Allenbach-Hellweg, G., J. V. Battista and F. D. Dallenbach 1965 Immunohistological and histochemical localization of relaxin in the metrial gland of the pregnant rat. *Am. J. Anat.*, 117: 433-450.
- Allenbach-Hellweg, G., A. B. Dawson and F. L. Hisaw 1966 The effect of relaxin on the endometrium of monkeys. Histological and histochemical studies. *Am. J. Anat.*, 119: 61-78.
- Dickson, A. D., and D. Bulmer 1961 Observations on the origin of metrial gland cells in the rat placenta. *J. Anat.*, 95: 262-273.
- Ellis, R. A. 1957 Histochemistry of the cellular components of the metrial gland of the rat during prolonged pseudopregnancy. *Anat. Rec.*, 129: 39-52.
- Gerard, P. 1925 Sur un gland myometrial de la souris et du rat. *C. R. Soc. Biol.*, 93: 457-459.
- Haskins, C. L. 1932 Nuclear reproduction. *Int. Rev. Cytol.*, 1: 9-26.
- Jollie, W. P. 1964 Radioautographic observations on variations in desoxyribonucleic acid synthesis in rat placenta with increasing gestational age. *Am. J. Anat.*, 114: 161-171.
- Jones, L. A. 1961 A study of the formation of the placenta in the rat. Master's Thesis, Connecticut College, New London, Conn., 1-132.
- Pilgrim, C., and W. Maurer 1965 Autoradiographische untersuchung ueber die konstanz der DNS-Kerndopplungs dauer bei Zellarten von Maus und Ratte durch doppelmarkierung mit ^3H - und ^{14}C -thymidin. *Exp. Cell Res.*, 37: 183-199.
- Prescott, D. M. 1964 Autoradiography with liquid emulsion. In: *Methods in Cell Physiology*, L. D. M. Prescott, ed. Academic Press, New York, pp. 365-370.
- Sachs, L. 1953 Simple methods for mammalian chromosomes. *Stain Tech.*, 28: 169-172.
- Sachs, L., and M. C. Shelesnyak 1955 The development and suppression of polyploidy in the developing and suppressed deciduas in the rat. *J. Endocrin.*, 12: 146-151.
- Schultz, P. W., J. F. Reger and R. L. Schultz 1966 Effects of Triton WR-1339 on the rat yolk sac placenta. *Am. J. Anat.*, 119: 199-233.
- Selye, H., and T. McKeown 1935 Studies on the physiology of the maternal placenta in the rat. *Proc. Roy. Soc. London*, 119: 1-31.
- Smith, L. J. 1966 Metrial gland and other glycogen containing cells in the mouse uterus following mating and through implantation of the embryo. *Am. J. Anat.*, 119: 15-23.
- Swift, H. 1950 The desoxyribose nucleic acid content of animal nuclei. *Physiol. Zool.*, 23: 169-199.
- Thrasher, J. D. 1966 Analysis of renewing epithelial cell populations. In: *Methods in Cell Physiology*, H. D. M. Prescott, ed. Academic Press, New York, pp. 323-357.
- Velardo, J. T., A. B. Dawson, A. G. Olson and F. L. Hisaw 1953 Sequence of histological changes in the uterus and vagina of the rat during prolongation of pseudopregnancy associated with the presence of deciduomata. *Am. J. Anat.*, 93: 273-305.
- Wilson, J. W., and E. H. Leduc 1948 The occurrence and formation of binucleate and multinucleated cells and polyploid nuclei in the mouse liver. *Am. J. Anat.*, 82: 353-391.
- Wislocki, G. B., L. P. Weiss, M. H. Burgos and Richard A. Ellis 1957 The cytology, histochemistry and electron microscopy of the granular cells of the metrial gland of the gravid rat. *J. Anat.*, 91: 130-140.

binucleate metrial cells appear subsequent to the labeled mononucleate metrial cells. Although mononucleate metrial cells appear to give rise to binucleate metrial cells, the number of mononucleate metrial cells continues to increase. This increase is presumed to occur from the accumulation of specific granules in mononucleate cells that contain glycogen. The latter suggestion is made because no cells were found that contained only specific granules, i.e., all cells that contained specific granules must have had glycogen prior to the granules.

The labeled binucleate cells increase in number during periods of fairly high cell proliferation (days 10, 11, and 12). The number of binucleate cells does not increase from day 13 to 14 when the proliferation of cells is extremely low. The finding that binucleates increase in number during high proliferative periods and not during low proliferative periods indicates that the binucleates are being formed by a process involving division. This general observation would suggest that binucleation stems from mitosis without cytokinesis and that fusion of mononucleate metrial cells is not involved. The former mechanism of binucleation has been described in rat liver cells (Wilson and Leduc, '48; Beams and King, '42). Binucleation in liver cells may result when a large amount of inert material in the cell inhibits formation of the normal cleavage furrow (Beams and King, '42). Similarly, Ellis ('57) has suggested that binucleation of metrial cells may be due to a physical interference with cytokinesis by the specific granules that occupy the central portion of the interphase cytoplasm. This could easily be the case since cells were noted that exhibited metaphase plates in the presence of specific granules.

Ploidy of the metrial cells. One aspect of the metrial gland cells that has not been investigated previously is their ploidy. Various mammalian tissues contain cells that have two or more times their normal G-1 diploid amount of DNA. Mouse liver, pancreas, thymus, lymphocytes, and Sertoli cells all exhibit polyploidy to some extent (Swift, '50). In nuclei of each of these tissues there is a direct relationship between nuclear volume and DNA content (Swift, '50). The relationship of greater

nuclear volume with increased DNA content also has been found in rat liver cells (Carriere, '62) and decidual cells in rat deciduoma (Sachs and Shelesnyak, '55; Sachs, '53). When nuclei of different tissues of the same animal are compared, however, there is no correlation between nuclear size and DNA content (Haskins, '52; Swift, '50). Visual observation of increased numbers of chromosomes also indicates polyploidy. Sachs and Shelesnyak ('55), for example, determined ploidy of decidual cells by correlating high chromosome numbers and large metaphase plates with enlarged nuclei.

Extremely large nuclei in typical metrial cells indicate that some binucleate metrial cells are polyploid. Two types of mechanisms for polyploidy of individual metrial cell nuclei can be proposed. The process may be similar to that described by Beams and King ('42) and by Wilson and Leduc ('48) in rat liver cells. Beams and King ('42) suggest that "the two nuclei prepare for the next division synchronously, but usually only one spindle is formed at metaphase so that either two tetraploid daughter cells result from a complete mitosis, or cytokinesis may be suppressed again thus giving rise to a binucleate cell with tetraploid nuclei." In contrast to this theory, the metrial cells that were synthesizing DNA might undergo endoduplication. The process apparently occurs in trophoblastic giant cells of the fetal rat placenta (Jollie, '64). The trophoblastic giant cells synthesize DNA but do not undergo mitosis; therefore, they are assumed to be highly polyploid (Jollie, '64). The polyploidization of metrial cells may be the same as that suggested for liver cells. Both nuclei of the binucleate metrial cells synthesize DNA synchronously and appear morphologically similar. The large metaphase plates associated with specific granules suggests that polyploid metrial cells are undergoing mitosis.

The ploidy of metrial cells apparently increases with gestational age since more large nuclei are noted on day 14 than day 12 in the binucleates. Few cells are found with more than two nuclei, thus suggesting that the nuclei become polyploid rather than producing multinucleate cells. If binucleation originally results from the in-

hibition of cleavage furrow formation by the specific granules, then these granules for the same reason would inhibit formation of polyploid mononucleate cells.

The large or polyploid metrial cell nuclei appear in significant numbers on day 12. No polyploid cells were noted that were undifferentiated; that is, large nuclei were only observed in the metrial gland in cells that contained specific granules. Since signs of differentiation appear before polyploidy, differentiation does not seem to result from polyploidy; however, polyploidy may result from differentiation. The observation that metrial cells synthesize DNA and exhibit mitotic figures is in disagreement with the proposition that differentiation and mitotic activity exclude each other.

LITERATURE CITED

- Asplund, J., V. Borell and H. Holmgren 1940 In der Unterwand während der Gravidität auf tretende metachromatische granulierte Zellen und ihre Stellung zur "Glandula myometrialis" Z. Mikr.-anat. Forsch., 48: 478-528.
- Baker, B. L. 1948 Histochemical variations in the metrial gland of the rat during pregnancy and lactation Proc. Soc. Exp. Biol. and Med., 68: 492-496.
- Beams, H. W., and R. L. King 1942 The origin of binucleate and large mononucleate cells in the liver of the rat. Anat. Rec., 83: 281-297.
- Endgman, J. 1948a A morphological study of the development of the placenta of the rat. I. An outline of the development of the placenta of the white rat. J. Morph., 83: 61-85.
- 1948b A morphological study of the development of the placenta of the rat. II. A histological and cytological study of the development of the chorioallantoic placenta of the white rat J. Morph., 83: 195-223.
- Carnere, R. 1962 Role of the thyroid gland in the control of polyploid cell formation in the rat liver. Endocrinology, 70: 761-773.
- Carnere, R., and D. Patterson 1962 The counting of mono- and binucleated cells in tissue sections Anat. Rec., 142: 443-456.
- Dallenbach Hellweg, G., J. V. Battista and F. D. Daßenbach 1965 Immunohistological and histochemical localization of relaxin in the metrial gland of the pregnant rat Am. J. Anat., 117: 433-450.
- Dallenbach Hellweg, G., A. B. Dawson and F. L. Hisaw 1966 The effect of relaxin on the endometrium of monkeys. Histological and histochemical studies Am. J. Anat., 119: 61-78.
- Dakson, A. D., and D. Bulmer 1961 Observations on the origin of metrial gland cells in the rat placenta. J. Anat., 95: 262-273.
- Ellis, R. A. 1957 Histochemistry of the cellular components of the metrial gland of the rat during prolonged pseudopregnancy. Anat. Rec., 129: 39-52.
- Gerard, P. 1925 Sur un gland myometrial de la souris et du rat. C. R. Soc. Biol., 93: 457-459.
- Haskins, C. L. 1952 Nuclear reproduction. Int. Rev. Cytol., 1: 9-26.
- Jollie, W. P. 1964 Radioautographic observations on variations in desoxyribonucleic acid synthesis in rat placenta with increasing gestational age. Am. J. Anat., 114: 161-171.
- Jones, L. A. 1961 A study of the formation of the placenta in the rat. Master's Thesis, Connecticut College, New London, Conn., 1-132.
- Pilgrim, C., and W. Maurer 1965 Autoradiographische untersuchung über die konstanz der DNS-Kerndopplung dauer bei Zellarten von Maus und Ratte durch doppelmarkierung mit ^3H - und ^{14}C -thymidin. Exp. Cell Res., 37: 183-199.
- Prescott, D. M. 1964 Autoradiography with liquid emulsion. In: Methods in Cell Physiology. L. D. M. Prescott, ed. Academic Press, New York, pp. 365-370.
- Sachs, L. 1953 Simple methods for mammalian chromosomes. Stain Tech., 28: 169-172.
- Sachs, L., and M. C. Shelesnyak 1955 The development and suppression of polyploidy in the developing and suppressed deciduomas in the rat J. Endocrin., 12: 146-151.
- Schultz, P. W., J. F. Reger and R. L. Schultz 1966 Effects of Triton WR-1339 on the rat yolk sac placenta. Am. J. Anat., 119: 199-233.
- Selye, H., and T. McKeown 1935 Studies on the physiology of the maternal placenta in the rat. Proc. Roy. Soc. London, 119: 1-31.
- Smith, L. J. 1966 Metrial gland and other glycogen containing cells in the mouse uterus following mating and through implantation of the embryo. Am. J. Anat., 119: 15-23.
- Swift, H. 1950 The desoxyribose nucleic acid content of animal nuclei. Physiol. Zool., 23: 169-199.
- Thrasher, J. D. 1966 Analysis of renewing epithelial cell populations. In: Methods in Cell Physiology. II. D. M. Prescott, ed. Academic Press, New York, pp. 323-357.
- Velardo, J. T., A. B. Dawson, A. G. Olson and F. L. Hisaw 1953 Sequence of histological changes in the uterus and vagina of the rat during prolongation of pseudopregnancy associated with the presence of deciduomata. Am. J. Anat., 93: 273-305.
- Wilson, J. W., and E. H. Leduc 1948 The occurrence and formation of binucleate and multinucleated cells and polyploid nuclei in the mouse liver. Am. J. Anat., 82: 353-391.
- Wislocki, G. B., L. P. Weiss, M. H. Burgos and Richard A. Ellis 1957 The cytology, histochemistry and electron microscopy of the granular cells of the metrial gland of the gravid rat. J. Anat., 91: 130-140.

PLATE 1

EXPLANATION OF FIGURES

- 4 Cell types found in mesometrial triangle at day 8. P, precursor cell; F, fibroblast-like cell. PAS and Harris hematoxylin. $\times 1000$.
- 5 Cell morphologically similar to precursor cells, but contains glycogen (arrow). This cell type first seen at day 9. S, smooth muscle fibers. PAS and Harris hematoxylin. $\times 1000$.
- 6 Mononucleate cells, which contain specific granules, occasionally seen at day 9 (arrow). F, fibroblast-like cells; S, smooth muscle fibers. PAS after diastase digestion and Harris hematoxylin. $\times 1000$.
- 7 Typical binucleate metrial cell first seen in mesometrial triangle at day 10 (arrow). F, fibroblast-like cells. $\times 1000$.



PLATE 2

EXPLANATION OF FIGURES

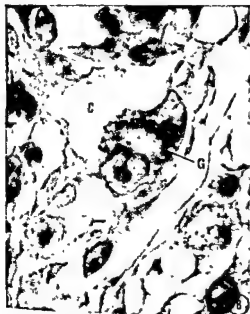
- 8 Micrograph of section from same conceptus as figure 7 illustrating that binucleate metrial cells first seen at day 10 contain specific granules (G). C, area of cell that normally contains glycogen. PAS after diastase digestion and Harris hematoxylin. $\times 1000$.
- 9 Metrial cell with large nuclei (arrow). G, specific granules. Feulgen and orange G. $\times 1000$.
- 10 Large metaphase plate in day 12 metrial gland tissue (arrow). A smaller, more normal sized, mitotic figure (N) is indicated. G, specific granules. PAS after diastase digestion and Harris hematoxylin. $\times 1000$.
- 11 Labeled binucleate metrial cell in day 12 metrial gland tissue taken one hour after administration of H^3 -thymidine (arrow). M, labeled mononucleate metrial cell. Emulsion exposure time three weeks. Harris hematoxylin, orange G, and eosin Y. $\times 1000$.



PLATE 2

EXPLANATION OF FIGURES

- 8 Micrograph of section from same conceptus as figure 7 illustrating that binucleate metrial cells first seen at day 10 contain specific granules (G). C, area of cell that normally contains glycogen. PAS after diastase digestion and Harris hematoxylin. $\times 1000$.
- 9 Metrial cell with large nuclei (arrow). G, specific granules. Feulgen and orange G. $\times 1000$.
- 10 Large metaphase plate in day 12 metrial gland tissue (arrow). A smaller, more normal sized, mitotic figure (N) is indicated. G, specific granules. PAS after diastase digestion and Harris hematoxylin. $\times 1000$.
- 11 Labeled binucleate metrial cell in day 12 metrial gland tissue taken one hour after administration of H^3 -thymidine (arrow). M, labeled mononucleate metrial cell. Emulsion exposure time three weeks. Harris hematoxylin, orange G, and eosin Y. $\times 1000$.



Nerve Endings in the Human Endocardium¹

BRIAN D. JOHNSTON

Department of Anatomy, University of California School of Medicine,
San Francisco, California

ABSTRACT The endocardium of 12 human hearts was studied following methylene blue perfusion and immersion within eight hours after death. Photomicrographs presented show two major types of endings: complex unencapsulated endings, and end-nets. Complex unencapsulated endings are discrete, much branched, highly variable "bush-like" endings, which originate from myelinated fibers. These structures were found only in the atria, and particularly at atrio-venous junctions. The close resemblance of complex unencapsulated endings to stretch receptors seen in other tissues suggests that they serve as "baroreceptors" in the heart. End-nets are composed of repeatedly branching and anastomosing fine beaded fibers. The fine, beaded fibers originate from myelinated fibers, but the number and origin of the parent fibers is not known. In this study, end-nets were found in the atria, on the atrioventricular valves, and in the ventricular endocardium. The function of the end-net is unknown, and while most evidence suggests that it is sensory, motor function cannot be ruled out.

Despite numerous studies of the sensory nerve endings in the mammalian heart, there still remains some disagreement concerning the types and distribution of these structures. In part, differences in histological technique probably account for much of the variation in observations and interpretation. It is also unfortunate that few of the numerous published reports include photomicrographs of the described material.

Afferent nerve endings in the mammalian heart were first described and figured by Berkley (1895), Smirnow (1895) and Dogiel (1898). Later studies have been reported by Michailow ('08), Wollard ('26), Nettleship ('36), Nonidez ('39), Meyling ('53), Mitchell ('56), Holmes ('57a,b), Khabarova ('62), Semenov ('63), Abraham ('64), Miller ('64), Voloshchenko ('64), Williams ('64a) and Chervova ('65).

In general, most workers recognize the presence of complex unencapsulated nerve endings (e.g., "bush-like," stretch-receptor-like) in both the epicardium and the atrial endocardium. Only Meyling ('53) and Mitchell ('56), who used both methylene blue and silver techniques, did not report the presence of discrete bush-like endings.

Less generally recognized and less well understood, however, is the so-called endocardial "end-net." This structure was first reported by Michailow ('08), and later described by Meyling ('53), Mitchell ('56),

Holmes ('57a,b), Miller ('64), and Williams ('64a).

While the hearts of many mammalian species have been studied, very little information has been published concerning the sensory innervation of the human heart. Only Khabarova ('62) has published on a large series of human hearts (40), but in her study no photomicrographs were presented. She also did not mention the endocardial end-net.

Since the sensory innervation of the human heart has not been well studied, and there are no published photographs of receptors in the human heart, the present study was undertaken.

MATERIALS AND METHODS

Clearly discernible nerve endings could be demonstrated by methylene blue perfusion or immersion in human hearts up to eight hours after death. In material from persons deceased as long as 15 hours some neural structures could be stained, but the results were generally poor.

The present report is based on a study of 12 human hearts, the freshest stained two hours and 55 minutes after death, and the least fresh, eight hours post mortem.

When the entire heart was available for study, the coronary arteries were perfused with 20-40 ml of 0.01% methylene blue

¹ This investigation was supported by USPHS grants 1 SO 2 FR 03355-05 and 06.

Nerve Endings in the Human Endocardium¹

BRIAN D. JOHNSTON

Department of Anatomy, University of California School of Medicine,
San Francisco, California

ABSTRACT The endocardium of 12 human hearts was studied following methylene blue perfusion and immersion within eight hours after death. Photomicrographs presented show two major types of endings: complex unencapsulated endings, and end-nets. Complex unencapsulated endings are discrete, much branched, highly variable "bush-like" endings, which originate from myelinated fibers. These structures were found only in the atria, and particularly at atrio-venous junctions. The close resemblance of complex unencapsulated endings to stretch receptors seen in other tissues suggests that they serve as "baroreceptors" in the heart. End-nets are composed of repeatedly branching and anastomosing fine beaded fibers. The fine, beaded fibers originate from myelinated fibers, but the number and origin of the parent fibers is not known. In this study, end-nets were found in the atria, on the atrioventricular valves, and in the ventricular endocardium. The function of the end-net is unknown, and while most evidence suggests that it is sensory, motor function cannot be ruled out.

Despite numerous studies of the sensory nerve endings in the mammalian heart, there still remains some disagreement concerning the types and distribution of these structures. In part, differences in histological technique probably account for much of the variation in observations and interpretation. It is also unfortunate that few of the numerous published reports include photomicrographs of the described material.

Afferent nerve endings in the mammalian heart were first described and figured by Berkley (1895), Smirnow (1895) and Dogiel (1898). Later studies have been reported by Michailow ('08), Wollard ('26), Nettleship ('36), Nonidez ('39), Meyling ('53), Mitchell ('56), Holmes ('57a,b), Khabarova ('62), Semenov ('63), Abraham ('64), Miller ('64), Voloshchenko ('64), Williams ('64a) and Chervova ('65).

In general, most workers recognize the presence of complex unencapsulated nerve endings (e.g., "bush-like," stretch-receptor-like) in both the epicardium and the atrial endocardium. Only Meyling ('53) and Mitchell ('56), who used both methylene blue and silver techniques, did not report the presence of discrete bush-like endings.

Less generally recognized and less well understood, however, is the so-called endocardial "end-net." This structure was first reported by Michailow ('08), and later described by Meyling ('53), Mitchell ('56),

Holmes ('57a,b), Miller ('64), and Williams ('64a).

While the hearts of many mammalian species have been studied, very little information has been published concerning the sensory innervation of the human heart. Only Khabarova ('62) has published on a large series of human hearts (40), but in her study no photomicrographs were presented. She also did not mention the endocardial end-net.

Since the sensory innervation of the human heart has not been well studied, and there are no published photographs of receptors in the human heart, the present study was undertaken.

MATERIALS AND METHODS

Clearly discernible nerve endings could be demonstrated by methylene blue perfusion or immersion in human hearts up to eight hours after death. In material from persons deceased as long as 15 hours some neural structures could be stained, but the results were generally poor.

The present report is based on a study of 12 human hearts, the freshest stained two hours and 55 minutes after death, and the least fresh, eight hours *post mortem*.

When the entire heart was available for study, the coronary arteries were perfused with 20-40 ml of 0.01% methylene blue

¹ This investigation was supported by USPHS grants 1 SO 1 FR 05355-05 and 06.

in physiologic saline. In addition, the chambers were opened, and the heart was immersed in 0.01% methylene blue for 15 to 20 minutes. When the whole organ could not be obtained, the parts available for study were removed and immersed in 0.01% methylene blue for 15 to 20 minutes. Following immersion, the tissue was rinsed in normal saline, and exposed to air for approximately five minutes. After staining, an entire heart was dissected into appropriate-sized segments for fixation. Tissues were fixed in chilled (approximately 5° C) 8% ammonium molybdate in distilled water for up to 16 hours. Following fixation, tissue pieces were trimmed to approximately 2 mm thickness, thoroughly washed with iced distilled water, dehydrated in alcohol, cleared in xylene, and stored in benzyl benzoate for study.

In tissues prepared in this way, it is possible to focus through the entire thickness of the subendocardial connective tissue to determine the three-dimensional distribution of the neural structures.

The intercaval portion of the right atrium and the left atrial wall, particularly in the vicinity of the entrance of the pulmonary veins, were the parts most frequently taken for study. The endocardium of the atrioventricular valves, the pulmonic and aortic valves, and the ventricles were also stained and studied.

OBSERVATIONS

The nerve endings described in this report are classified according to the system of Miller and Kasahara ('64), who studied the sensory innervation of the heart and other tissues. Sensory endings are arbitrarily categorized by them as follows: "1. Free fiber endings which are little branched or unbranched terminations of small myelinated or unmyelinated fibers. 2. Complex unencapsulated endings, resulting from the repeated branching of terminal fibers and which are distinctly discrete but unencapsulated structures (e.g., Ruffini, Ruffini-like, or Golgi-like endings). 3. Encapsulated endings, characteristically discrete and surrounded by a capsule of modified Schwann cells or connective tissue elements (e.g., Meissner's corpuscles, Krause end bulbs, Golgi Mazzoni ends, or

the various sized Vater-Pacinian corpuscles." To these three categories was added a new one, the end-net. It was proposed that the end-net might represent a specialized form of free fiber ending unique to the cardiovascular system.

When the term "end-net" is used, it denotes a structure composed of repeatedly branching and anastomosing "dendrites" of several myelinated fibers, which may or may not originate as collaterals of a single parent fiber.

In this study two basic types of neural structures were found: complex unencapsulated endings (figs. 1, 2, 3, 4), and end-nets (figs. 5, 6, 7, 8). The complex unencapsulated endings are subdivided into diffuse (figs. 1, 2) and compact (figs. 3, 4) varieties, and a distinction is made between dense end-nets (fig. 6) and sparse end-nets (figs. 5, 7, 8).

Atria

More nerve endings are found in the atrial endocardium than in the endocardium of any other part of the heart. Complex unencapsulated endings of both compact and diffuse varieties are always present, and in some hearts end-nets are found. It is only in the atria that both complex unencapsulated endings and end-nets are seen. Moreover, the end-nets of the atria generally tend to be more extensive, and to be composed of more fibers.

Complex unencapsulated endings and end-nets may occur in close proximity, or in widely separated portions of the endocardium. No consistent association of these two types of nerve endings was observed. While no counts of endings were made, end-nets and complex unencapsulated endings seemed to be present in approximately equal numbers in both atria.

Complex unencapsulated endings are consistently found at atrio-venous junctions. In particular, they are almost invariably seen at the entrances into the heart of the venae cavae, the pulmonary veins, and the coronary sinus. They are also found in other locations, but much less consistently than at the atrio-venous junctions. These large brush-like endings are occasionally seen on the interatrial septum, and on the posterior walls of the

atria. They were not observed in the auricular appendage, in any portion of the ventricular endocardium, or on any of the valve leaflets.

Complex unencapsulated endings originate invariably from myelinated fibers which lose their sheaths immediately before arborizing to form the typical receptor. The bush-like endings seen in this study are similar to those drawn and photographed by previous workers.

Occasionally a diffuse complex unencapsulated ending was seen to give rise to a secondary myelinated fiber, clearly distinct from the primary fiber which gave rise to the ending. If the secondary fiber was followed, it could sometimes be seen to give rise to a new diffuse complex unencapsulated ending some distance from the original bush-like ending. Thus, in some instances diffuse complex unencapsulated endings may be connected to each other as in a series electric circuit.

The complex unencapsulated endings closely resemble "stretch" receptors found in tendons, fasciae, joint capsules and other tissues, and are probably the "baroreceptors" of which the physiologists speak. As can be seen in the photomicrographs, (figs 1, 2, 3, 4), their structures and size vary considerably.

While the complex unencapsulated endings stain with reassuring ease, and show little degeneration as many as 15 hours post mortem, the end-net is not consistently demonstrable. In our experience it is never seen in hearts stained more than five hours post mortem, and is not consistently demonstrable even in hearts stained less than five hours after death. Whether the end-net is not always present, or is sometimes difficult to stain is not known.

In some well-stained preparations, the end-net appears very dense (fig. 6) and consists of many repeatedly branching and anastomosing fine beaded fibers. Myelinated fibers are seen in and around the end-net, and fine beaded fibers may be seen to leave the myelinated fibers to participate in the end-net formation. Because of the diffuse nature of the end-net, and because of its complex three-dimensional disposition in the subendocardial space, it is impossible to be certain of the number and origin of the nerve fibers which give

rise to the end-net. In markedly dense nets, the fibers have many fine beads at short intervals, and often run roughly parallel to each other as they branch and re-join (fig. 6).

In other well-stained preparations, sparse end-nets (figs. 5, 7, 8) are seen. In these sparse nets far fewer fibers participate; there are fewer, larger beads on the fibers, and the fibers are often not generally parallel to each other. They tend, instead, to divide the endocardial surface into polygons. The sparse nets are seen more frequently than the markedly dense end-nets, and they are observed over broader areas of endocardium. They are located most frequently along the base of the interatrial septum (fig. 7), and near the atrioventricular valves. Myelinated fibers contribute fine beaded fibers to the sparse end-nets, but as in the dense end-nets, it has not been possible to determine the numbers or source of the parent fibers which give rise to the end-net.

Valvular structures

In preparations in which the atrium and the atrioventricular valve are not separated, it is possible to trace a sparse end-net from the atrium onto the valvular endocardial surface. The sparse end-net is the only neural element seen on the atrioventricular valve, and its organization in that structure is entirely comparable to that of the sparse end-net of the atrial endocardium.

The pulmonary valve possesses a sparse end-net (fig. 5), and like the atrioventricular valve, no other endings are found. The aortic valve leaflets show no fibers or receptors of any sort.

No complex unencapsulated endings and no myelinated fibers were found on any valvular structures.

Ventricles

The ventricular endocardium shows very few, thin, sparsely beaded anastomosing fibers. The ventricular end-net is similar to the sparse end-nets of the atrium and the valves, but even fewer fibers make up this structure.

The ventricular end-net is best seen in the outflow tract of the right ventricle. No

in physiologic saline. In addition, the chambers were opened, and the heart was immersed in 0.01% methylene blue for 15 to 20 minutes. When the whole organ could not be obtained, the parts available for study were removed and immersed in 0.01% methylene blue for 15 to 20 minutes. Following immersion, the tissue was rinsed in normal saline, and exposed to air for approximately five minutes. After staining, an entire heart was dissected into appropriate-sized segments for fixation. Tissues were fixed in chilled (approximately 5° C) 8% ammonium molybdate in distilled water for up to 16 hours. Following fixation, tissue pieces were trimmed to approximately 2 mm thickness, thoroughly washed with iced distilled water, dehydrated in alcohol, cleared in xylene, and stored in benzyl benzoate for study.

In tissues prepared in this way, it is possible to focus through the entire thickness of the subendocardial connective tissue to determine the three-dimensional distribution of the neural structures.

The intercaval portion of the right atrium and the left atrial wall, particularly in the vicinity of the entrance of the pulmonary veins, were the parts most frequently taken for study. The endocardium of the atrioventricular valves, the pulmonic and aortic valves, and the ventricles were also stained and studied.

OBSERVATIONS

The nerve endings described in this report are classified according to the system of Miller and Kasahara ('64), who studied the sensory innervation of the heart and other tissues. Sensory endings are arbitrarily categorized by them as follows: "1. Free fiber endings which are little branched or unbranched terminations of small myelinated or unmyelinated fibers. 2. Complex unencapsulated endings, resulting from the repeated branching of terminal fibers and which are distinctly discrete but unencapsulated structures (e.g., Ruffini, Ruffini-like, or Golgi-like endings). 3. Encapsulated endings, characteristically discrete and surrounded by a capsule of modified Schwann cells or connective tissue elements (e.g., Meissner's corpuscles, Krause end bulbs, Golgi Mazzoni ends, or

the various sized Vater-Pacinian corpuscles." To these three categories was added a new one, the end-net. It was proposed that the end-net might represent a specialized form of free fiber ending unique to the cardiovascular system.

When the term "end-net" is used, it denotes a structure composed of repeatedly branching and anastomosing "dendrites" of several myelinated fibers, which may or may not originate as collaterals of a single parent fiber.

In this study two basic types of neural structures were found: complex unencapsulated endings (figs. 1, 2, 3, 4), and end-nets (figs. 5, 6, 7, 8). The complex unencapsulated endings are subdivided into diffuse (figs. 1, 2) and compact (figs. 3, 4) varieties, and a distinction is made between dense end-nets (fig. 6) and sparse end-nets (figs. 5, 7, 8).

Atria

More nerve endings are found in the atrial endocardium than in the endocardium of any other part of the heart. Complex unencapsulated endings of both compact and diffuse varieties are always present, and in some hearts end-nets are found. It is only in the atria that both complex unencapsulated endings and end-nets are seen. Moreover, the end-nets of the atria generally tend to be more extensive, and to be composed of more fibers.

Complex unencapsulated endings and end-nets may occur in close proximity, or in widely separated portions of the endocardium. No consistent association of these two types of nerve endings was observed. While no counts of endings were made, end-nets and complex unencapsulated endings seemed to be present in approximately equal numbers in both atria.

Complex unencapsulated endings are consistently found at atrio-venous junctions. In particular, they are almost invariably seen at the entrances into the heart of the venae cavae, the pulmonary veins, and the coronary sinus. They are also found in other locations, but much less consistently than at the atrio-venous junctions. These large brush-like endings are occasionally seen on the interatrial septum, and on the posterior walls of the

are probably motor in function, it is not certain that these same fibers are part of the end-net. If one were to grant that the end-net innervated cardiac muscle fibers in the mitral valve, however, one would still have to propose still other functions for the end-nets found elsewhere in the heart, where there are no demonstrable cardiac muscle cells.

Electron microscopic studies by Rogers and Burnstock ('66), and Bennett and Rogers ('67) show in detail how monoaminergic fibers which appear finely beaded in methylene blue preparations may innervate smooth muscle. Thus, the end-net may innervate smooth cells in the atrial endocardium (Lannigan, '66), even though the paucity of smooth muscle cells in the endocardium make that function seem unlikely.

Until it is clearly established what the end-net does, it will be necessary to consider such unlikely possibilities as that it may be a neurohumoral transducer.

It is also possible that the end-net may be nothing more than a highly diffuse stretch or baroreceptor. Further studies, particularly histochemical and ultrastructural, are needed to help clarify the nature of this neural structure, which is seemingly unique to cardiovascular tissue.

ACKNOWLEDGMENTS

The author wishes to express his deep appreciation for the kind guidance, encouragement, and material support of Dr. M. R. Miller, and Miss M. Kasahara. The author also wishes to acknowledge gratefully the generous cooperation of Dr. J. Carr, Pathologist, St. Francis Hospital, San Francisco; and Drs. O. Rambo, C. Montgomery, and R. Wisner, Dept. of Pathology, University of California Medical Center, San Francisco.

LITERATURE CITED

- Abraham, A. 1964 Die mikroskopische Innervation des Herzens und der Blutgefäße von von Vertebraten Akadémiai Kiadó, Budapest.
- Bennett, M. R. and D. C. Rogers 1967 A study of the taenia coli. *J. Cell Biol.*, Vol. 33, No. 3, pp. 573-596.
- Berkley, H. J. 1895 The intrinsic nerve supply of the cardiac ventricles in certain vertebrates. The Johns Hopkins Hospital Reports. Report in Neurology II, 4: 248-275.
- Chabarov, A. J. 1959 (Same authoress listed below as Khabarova, A. I.) Die afferente Innervation des Herzens. *Z. Mikr-anat. Forsch.*, 66: 236-250.
- Chervova, I. A. 1965 Structural organization of the intra-cardiac nervous apparatus. *Arkh. Anat.*, 48: 60-66, February.
- Cooper, T. L. M. Napolitano, M. J. T. Fitzgerald, K. E. Moore, W. M. Daggett, V. C. Willman, E. H. Sonnenblick and C. R. Hanlon 1966 Structural basis of cardiac valvular function. *Arch. Surg.*, 93: 767-771.
- Dogiel, A. S. 1898 Die sensiblen Nervenendigungen im Herzen und in dem Blutgefäße der Säugethiere. *Arch. mikr. Anat.*, 52: 44-68.
- Holmes, R. L. 1957a Structures in the atrial endocardium of dog, which stain with methylene blue and the effect of unilateral vagotomy. *J. Anat.*, 91: 259-266.
- 1957b Cholinesterase activity in the atrial wall of the dog and cat heart. *J. Physiol.*, 137: 421-426.
- Khabarova, A. I. 1962 The Afferent Innervation of the Heart. Consultant's Bureau, New York.
- Kuleshova, T. F. 1964 Afferent innervation of the cardiac nerve structures in monkey. *Arkh. Anat.*, 47: 58-63, December.
- Lannigan, R. A. 1966 Ultrastructure of the Normal Atrial Endocardium. *Brit. Heart J.*, 28: 785-796.
- Meyling, H. A. 1953 Structure and significance of the peripheral extension of the autonomic nervous system. *J. Comp. Neur.*, 99: 495-543.
- Michailow, S. 1908 Die Nerven des Endocardiums. *Anat. Anz.*, 32: 87-101.
- Miller, M. R., and M. Kasahara 1964 Studies on the nerve endings in the heart. *Am. J. Anat.*, Vol. 115, No. 2, pp. 217-234.
- Mitchell, C. A. G. 1956 Cardiovascular Innervation. E. and S. Livingstone, Ltd., Edinburgh.
- Nonidez, J. F. 1939 Studies on the innervation of the heart. *Am. J. Anat.*, 65: 361-413.
- Ralston, H. J., III, M. R. Miller and M. Kasahara 1960 Nerve endings in human fasciae, tendons, ligaments, periosteum, and joint synovial membranes. *Anat. Rec.*, 136: 137-148.
- Rogers, D. C., and G. Burnstock 1966 Multi-axonal autonomic junctions in intestinal smooth muscle of the toad (*Bufo marinus*). *J. Comp. Neur.*, 126: 625-651.
- Semenov, S. P. 1963 Experimental and morphological study of cardiac afferents. *Arkh. Anat.*, 45: 72-83, September.
- Smurnow, A. 1895 Ueber die sensiblen Nervenendigungen im Herzen bei Amphibien und Säugetieren. *Anat. Anz.*, 10: 737-748.
- Sonnenblick, E. H., L. M. Napolitano, W. M. Daggett and T. Cooper 1967 An intrinsic neuromuscular basis for mitral valve motion in the dog. *Circ. Res.*, 21: 9-15.
- Voloshchenko, A. A. 1964 Afferent innervation of the atrioventricular valve. *Arkh. Anat.*, 47: 81-86, August.
- Williams, T. H. 1964a Mitral and tricuspid valve innervation. *Brit. Heart J.*, 26: 105-115.
- 1964b Fast-conducting fibers in the mitral valve. *Brit. Heart J.*, 26: 554-557.
- Woodward, H. H. 1926 The innervation of the heart. *J. Anat.*, 60: 345-373.

complex unencapsulated endings and no myelinated fibers were seen in the ventricular endocardium.

DISCUSSION

The findings of this study of the human heart are largely consistent with those of Michailow ('08), Holmes ('57a), and Miller and Kasahara ('64), who studied the hearts of other mammalian species. Both the discrete complex unencapsulated endings and the end-nets reported by these authors in other mammals were found in much the same distribution in the human heart.

Khabarova ('62), in her studies of the human heart, describes the bush-like endings reported here, but she does not describe or illustrate an end-net. Evaluation of her studies and those of other Russian workers (Semenov, '63; Kuleshova, '64; Voloshchenko, '64; Chervova, '65) is difficult because exact procedural details are not given, and most structures are illustrated with drawings, rather than photographs.

Failure to demonstrate the endocardial end-net is probably related to staining technique and to the freshness of the tissue. As a rule, only methylene blue used in fairly fresh material will stain the end-net. Silver techniques in general do not stain the fine, multibranched and anastomosing terminals of the end-net formation.

Miller and Kasahara ('64) and Williams ('64a) found myelinated fibers giving rise to complex unencapsulated endings on the atrioventricular valves of mammals. Using an osmium tetroxide-zinc iodine technique, Williams ('64a) also demonstrated other myelinated fibers crossing the mitral valve and travelling down the chordae tendineae. These large fibers subsequently became the object of another study (Williams, '64b).

While not doubting these well-documented reports (Miller and Kasahara, '64; Williams, '64a,b), it can only be said that in the material examined in this series of human hearts, no myelinated fibers and no complex unencapsulated endings were found on any valvular structures.

The close structural similarity of the complex unencapsulated endings of the

endocardium to stretch receptors found in other tissues (Ralston et al., '60) suggests that these receptors have similar functions. Thus, the complex unencapsulated endings, or "baroreceptors" are probably stimulated by stretching or deformation of the subendocardial connective tissue of the atrial wall. Sympathetic and vagal section studies by Woollard ('26), Nettlehip ('36), Nonidez ('39), Holmes ('57a), and Chaharowa ('59) indicate that fibers from the baroreceptors travel mainly with the vagus, and terminate in the medulla. Some baroreceptors may terminate in the upper thoracic spinal cord according to later studies by Khabarova ('62) and Semenov ('63).

The exact structure and function of the end-net has not been clearly determined, and there are several opinions concerning its nature. The majority of workers who have described this structure consider it sensory, but there is some evidence to support the contention that it may innervate muscle.

Holmes ('57a) found that the end-net was unaffected by vagal section, and concluded that it was probably sympathetic in origin. Holmes ('57b) and Williams ('64a) stained the end-nets to show cholinesterase activity. These two workers, along with Miller and Kasahara ('64) concluded that the end-net was sensory. Williams ('64a) went further, speculating on the type of information reported by the end-net: "It seems unlikely, therefore, that the main network is concerned with the measurement of any bulk property of the blood, such as temperature or sodium concentration, since these properties being virtually the same throughout each chamber, would require relatively small sensory zones for their evaluation. On the other hand, extensive plexuses such as have been described in the valves would be appropriate for the measurement of flow characteristics, namely the recording of blood movements across different portions of each cusp."

Recent ultrastructural, physiologic, and pharmacologic studies by Cooper et al. ('66) and Sonnenblick et al. ('67), indicate that beaded monoaminergic fibers innervate cardiac muscle fibers in the mitral valve of the dog. While such fibers

are probably motor in function, it is not certain that these same fibers are part of the end-net. If one were to grant that the end-net innervated cardiac muscle fibers in the mitral valve, however, one would still have to propose still other functions for the end-nets found elsewhere in the heart, where there are no demonstrable cardiac muscle cells.

Electron microscopic studies by Rogers and Burnstock ('66), and Bennett and Rogers ('67) show in detail how monoaminergic fibers which appear finely beaded in methylene blue preparations may innervate smooth muscle. Thus, the end-net may innervate smooth cells in the atrial endocardium (Lannigan, '66), even though the paucity of smooth muscle cells in the endocardium make that function seem unlikely.

Until it is clearly established what the end-net does, it will be necessary to consider such unlikely possibilities as that it may be a neurohumoral transducer.

It is also possible that the end-net may be nothing more than a highly diffuse stretch or baroreceptor. Further studies, particularly histochemical and ultrastructural, are needed to help clarify the nature of this neural structure, which is seemingly unique to cardiovascular tissue.

ACKNOWLEDGMENTS

The author wishes to express his deep appreciation for the kind guidance, encouragement, and material support of Dr. M. R. Miller, and Miss M. Kasahara. The author also wishes to acknowledge gratefully the generous cooperation of Dr. J. Carr, Pathologist, St. Francis Hospital, San Francisco; and Drs. O. Rambo, C. Montgomery, and R. Wisner, Dept. of Pathology, University of California Medical Center, San Francisco.

LITERATURE CITED

- Abraham, A. 1964 Die mikroskopische Innervation des Herzens und der Blutgefäße von von Vertebraten. Akadémiai Kiadó, Budapest.
- Bennett, M. R., and D. C. Rogers 1967 A study of the taenia coli. *J. Cell Biol.*, Vol. 33, No. 3, pp. 573-596.
- Berkley, H. J. 1895 The intrinsic nerve supply of the cardiac ventricles in certain vertebrates. *The Johns Hopkins Hospital Reports. Report in Neurology* 11, 4 248-275.
- Chabarov, A. J. 1959 (Same authoress listed below as Khabarova, A. I.) Die afferente Innervation des Herzens. *Z. Mikr-anat. Forsch.*, 66: 236-250.
- Chervova, I. A. 1965 Structural organization of the intra-cardiac nervous apparatus. *Ark. Anat.*, 48: 60-66, February.
- Cooper, T., L. M. Napolitano, M. J. T. Fitzgerald, K. E. Moore, W. M. Daggett, V. C. Willman, E. H. Sonnenblick and C. R. Hanlon 1966 Structural basis of cardiac valvular function. *Arch. Surg.*, 93: 767-771.
- Dogiel, A. S. 1898 Die sensiblen Nervenendigungen im Herzen und in dem Blutgefäße der Säugethiere. *Arch. mikr. Anat.*, 52: 44-68.
- Holmes, R. L. 1957a Structures in the atrial endocardium of dog, which stain with methylene blue and the effect of unilateral vagotomy. *J. Anat.*, 91: 259-266.
- 1957b Cholinesterase activity in the atrial wall of the dog and cat heart. *J. Physiol.*, 137: 421-426.
- Khabarova, A. I. 1962 The Afferent Innervation of the Heart. Consultant's Bureau, New York.
- Kuleshova, T. F. 1964 Afferent innervation of the cardiac nerve structures in monkey. *Ark. Anat.*, 47: 58-63, December.
- Lannigan, R. A. 1966 Ultrastructure of the Normal Atrial Endocardium. *Brit. Heart J.*, 28: 785-796.
- Meyling, H. A. 1953 Structure and significance of the peripheral extension of the autonomic nervous system. *J. Comp. Neur.*, 99: 495-543.
- Michailow, S. 1908 Die Nerven des Endocardiums. *Anat. Anz.*, 32: 87-101.
- Miller, M. R., and M. Kasahara 1964 Studies on the nerve endings in the heart. *Am. J. Anat.*, Vol. 115, No. 2, pp. 217-234.
- Mitchell, G. A. G. 1936 Cardiovascular Innervation. E. and S. Livingstone, Ltd., Edinburgh.
- Nonidez, J. F. 1939 Studies on the innervation of the heart. *Am. J. Anat.*, 65: 361-413.
- Ralston, H. J., III, M. R. Miller and M. Kasahara 1960 Nerve endings in human fascia, tendons, ligaments, periosteum, and joint synovial membranes. *Anat. Rec.*, 136: 137-148.
- Rogers, D. C., and G. Burnstock 1966 Multi-axonal autonomic junctions in intestinal smooth muscle of the toad (*Bufo marinus*). *J. Comp. Neur.*, 126: 625-651.
- Semenov, S. P. 1963 Experimental and morphological study of cardiac afferents. *Ark. Anat.*, 45 72-83, September.
- Smirnow, A. 1895 Ueber die sensiblen Nervenendigungen im Herzen bei Amphibien und Säugetieren. *Anat. Anz.*, 10: 737-748.
- Sonnenblick, E. H., L. M. Napolitano, W. M. Daggett and T. Cooper 1967 An intrinsic neuromuscular basis for mitral valve motion in the dog. *Circ. Res.*, 21: 9-15.
- Voloschenko, A. A. 1964 Afferent innervation of the atrioventricular valve. *Ark. Anat.*, 47: 81-86, August.
- Williams, T. H. 1964a Mitral and tricuspid valve innervation. *Brit. Heart J.*, 26: 105-115.
- 1964b Fast-conducting fibers in the mitral valve. *Brit. Heart J.*, 26: 554-557.
- Woollard, H. H. 1926 The innervation of the heart. *J. Anat.*, 60 345-373.

The nerve endings demonstrated in all figures were stained by methylene blue immersion or perfusion.

The straight black line in each photograph represents a distance of 100 μ .

In the explanation of figures "C.U.E." is the abbreviation for complex unencapsulated ending.

PLATE 1

EXPLANATION OF FIGURES

- 1 Large, diffuse C.U.E., on the interatrial septum, left atrium of a human heart. Endings similar to this are most often seen at atrio-venous junctions.
- 2 Diffuse C.U.E. near the entrance of one of the right pulmonary veins into the left atrium of a human heart. This ending, like all other complex unencapsulated endings seen in this study, originated from myelinated fibers, seen entering at the top of the figure.
- 3 Compact type of C.U.E. seen on the interatrial septum, left atrium of a human heart.
- 4 Compact type of C.U.E. found at the entrance of the superior vena cava into the right atrium of a human heart.



The nerve endings demonstrated in all figures were stained by methylene blue immersion or perfusion.

The straight black line in each photograph represents a distance of 100 μ .

In the explanation of figures "C.U.E." is the abbreviation for complex unencapsulated ending.

PLATE 1

EXPLANATION OF FIGURES

- 1 Large, diffuse C.U.E., on the interatrial septum, left atrium of a human heart. Endings similar to this are most often seen at atrio-venous junctions.
- 2 Diffuse C.U.E. near the entrance of one of the right pulmonary veins into the left atrium of a human heart. This ending, like all other complex unencapsulated endings seen in this study, originated from myelinated fibers, seen entering at the top of the figure.
- 3 Compact type of C.U.E. seen on the interatrial septum, left atrium of a human heart.
- 4 Compact type of C.U.E. found at the entrance of the superior vena cava into the right atrium of a human heart.

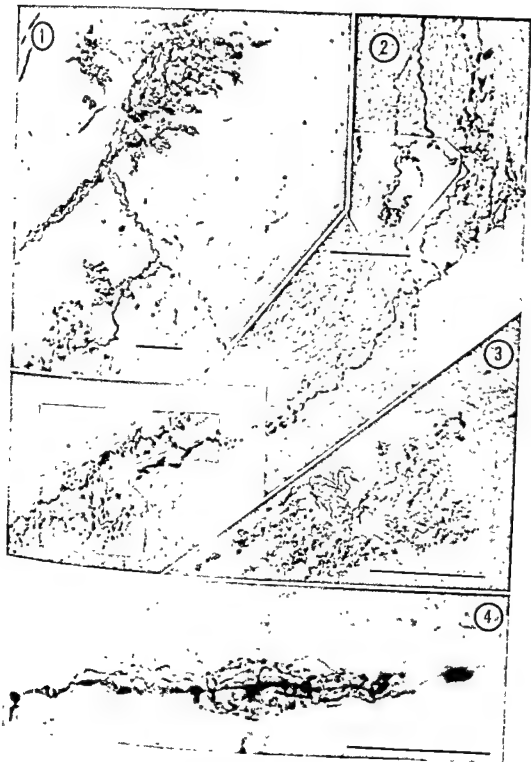
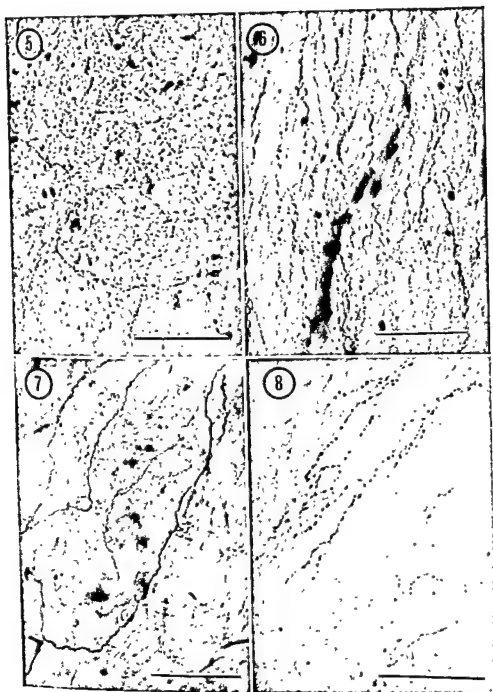


PLATE 2

EXPLANATION OF FIGURES

- 5 Sparse type of end-net seen on the leaflets of the pulmonic valve of a human heart. Sparse end-nets were the only neural structures found on valves in this study.
- 6 Dense end-net found in the intercaval portion of the right atrium of a human heart. Note that the fine beaded fibers forming this end-net run roughly parallel to each other.
- 7 Sparse type of end-net at the base of the interatrial septum of the right atrium of a human heart. End-nets of this type, continuous with those of the atria, are found on the atrioventricular valve.
- 8 Typical sparse end-net in the atrial endocardium of a human heart.

HUMAN ENDOCARDIAL INNERVATION
Brian D. Johnston

Ultrastructure of the Lung of the Goose and its Lining of Surface Material¹

ROGER O. LAMBSON AND JEROME E. COHN²

Departments of Anatomy and Medicine, University of Kentucky School of Medicine, Lexington, Kentucky

ABSTRACT As the primary bronchus passes through the goose lung it gives rise to two sets of secondary bronchi. One set is located on the dorsal surface of the lung and the other on the ventral surface. These two sets of bronchi are connected by numerous parabronchi which run parallel to one another through the lung. Each parabronchus is the center of and supplies air to a cylindrical lung lobule. Numerous outpocketings of the parabronchial wall, which are called atria, connect with the finest air spaces of the lung parenchyma.

The epithelium lining the parabronchi is continuous with flattened epithelial cells which line the atria and the finest air spaces. The air-blood barrier is composed of endothelium, a basal lamina, an attenuated pulmonary epithelium, and an 80-120 Å thick osmophilic layer which covers the attenuated epithelium. Multiple layers of a unit membrane-like material similar to that lining each fine air space is found covering and invaginating the epithelial cells lining the atria and parabronchi. Within many of these atrial and parabronchial cells, laminated osmophilic material is found within cisternae of rough-surfaced endoplasmic reticulum, and inclusion bodies which may contain both laminations and a granular matrix similar to that within adjacent Golgi vesicles. It is suggested that the endoplasmic reticulum may be involved in the synthesis of the surface material found lining the goose lung.

Studies of the avian lung have shown that its smaller airways are arranged in series in a fashion reminiscent of the artery-capillary-vein pattern of vascular channels (Bradley, '15; Locy and Larsell, '16; Bremer, '39; Akester, '60). This particular arrangement provides a basis for circulation of air through the bird lung (Hazelhoff, '51) which is quite different from the ebb-and-flow pattern of air movement through the tree-like bronchial branches in mammalian lungs. Ultrastructural examinations of bird lung parenchyma (Schultz, '59; Chase, '59; Tyler, Pangborn, and Julian, '61; Tyler and Pangborn, '64; Nagaishi, Okada, Ishiko and Daido, '64; and others) have shown that the air-blood barrier is similar to that found in mammalian lungs and is composed of a continuous epithelial covering, a basal lamina, and endothelium.

While the presence of surface-active materials in lungs of various mammals has been demonstrated with a variety of techniques (Pattle, '55; Klaus, Clements and Havel, '61; Miller and Bondurant, '61; Buckingham and Avery, '62; Mendenhall and Sun, '64; and others), there is no established agreement as to the intracellu-

lar origin of this material (Klaus, Clements and Havel, '61; Buckingham, McNary and Sommers, '64; Sorokin, '67; and others). The question as to whether a surface-active material is present in bird lungs is controversial (Miller and Bondurant, '61; Pattle and Hopkinson, '63).

The purposes of this paper are: (1) to describe the structure of the goose lung as it is seen with the electron microscope; (2) to present morphologic evidence that surface material is present in the goose lung as a covering of the epithelium of the air-blood barrier and the atrial and parabronchial epithelium; and (3) to present morphological evidence indicating that the surface material is produced, in part at least, within cisternae of rough-surfaced endoplasmic reticulum of the lining cells of the tertiary bronchi and atria of the goose lung.

MATERIAL AND METHODS

Six white-fronted geese (*Anser*) purchased from local farmers were used in

¹ Supported in part by U. S. Public Health Service grant HE08932 and National Science Foundation grant GB3030.

² Deceased April 3, 1967.

respiratory epithelium lining the smallest air spaces in the lung parenchyma proper.

Figure 5 is a low-magnification electron micrograph of a small segment of the lung parenchyma distal to the atria. This figure shows the general relationships between the fine air spaces and the numerous blood capillaries which surround them. As can be seen in figure 5, a single capillary may be shared by more than one air space. Higher magnification (fig. 6) shows that the pulmonary barrier, which separates blood and air, is composed of endothelium, a basal lamina, and an attenuated pulmonary epithelium. At still higher magnification (figs. 7-12), the capillary wall is seen to be a relatively thick portion of the pulmonary barrier. The endothelial cell has a surface similar to that found in smooth muscle cells (Fawcett, '63) in that micropinocytotic vesicles are the prominent structural specializations seen (figs. 10-12). Goose pulmonary endothelium does not appear to have specialized pores or fenestrations such as those found in the capillaries of intestine, endocrine glands, and kidney (Fawcett, '63).

The basal lamina which separates endothelium and pulmonary epithelium is an apparently homogeneous material on which these cells rest (figs. 6-11). The pulmonary epithelium of the goose lung is attenuated but appears to be continuous. Unlike the relatively thick endothelium with its numerous vesicles, the pulmonary epithelial lining of the smallest air spaces appears to consist of little more than two apposed cell membranes in many regions (figs. 7-12). The relatively small number of pulmonary epithelial cell nuclei which are seen even after viewing many sections indicates that the cytoplasm of these cells is spread over large areas.

In addition to endothelium, a basal lamina, and pulmonary epithelium, there appears to be a fourth component to the blood-air barrier of the goose lung. This component is a layer of electron-dense material 8-12 $m\mu$ thick which separates the pulmonary epithelium from air. In some sections (figs. 6, 7, 8, 11) it appears as a single thickness and in others (figs. 9, 10, 12) as a trilaminar unit membrane-like structure with 30 Å laminations. In some air spaces (fig. 11), the surface material

is clearly seen sandwiched between folds of epithelium. Material similar to that found covering the respiratory surfaces of the finest air spaces is found as a relatively compact multilayered covering (figs. 13-14) or as whorls of material (fig. 4) loosely attached to the surfaces of the alveolar and parabronchial lining cells. This material is also found within deep surface invaginations (fig. 14) and complicated infoldings of cell surfaces (fig. 15), and as tightly packed intracellular accumulations (figs. 18-20) in lining cells of the parabronchi and alveoli which connect with the lung parenchyma. In addition to these relatively large intracellular accumulations, similar laminated material is located within cisternae of rough surfaced endoplasmic reticulum (figs. 16, 17). Within some parts of the endoplasmic reticulum, single strands of the laminated material are found oriented parallel to the cisternal walls (fig. 16). In other parts, stacks of short lamellae are found oriented perpendicular to the cisternal membranes (figs. 16, 17). Other small membrane-enclosed inclusions of lamellae are sometimes associated with the Golgi apparatus; these sometimes contain only laminated material (fig. 18) but in other cases contain a fine granular material in addition to lamellae (figs. 19, 20). Multivesicular bodies, which are a characteristic feature of the Golgi apparatus of granular pneumocytes in several mammals (Sorokin, '67), were not commonly found in parabronchial or atrial lining cells in the goose lung.

DISCUSSION

The observations presented in this study of the lung of the goose offer several new additions to descriptions of avian lungs. The finding of a continuous epithelial lining in the finest air spaces of the goose lung reveals in another species the basic plan of a continuous tripartite air-blood barrier. The present study also supports the recent finding that, in birds, the pulmonary epithelial component of the blood-air barrier is very thin, and the total air-blood barrier is two to three times thinner than that found in man (Schulz, '62).

The question of surface materials in lungs raises several points germane to the present discussion of the bird lung. In

this study. They were housed in individual cages and fed a commercial ration and water *ad libitum*. Several different fixation procedures were tried, using osmium tetroxide or glutaraldehyde in varying osmotic concentrations of phosphate buffers. The following procedure yielded uniform, good fixation. Five hundred ml of 3% glutaraldehyde in 0.1 M phosphate buffer at pH 7.1 (Harkin, '65) was slowly infused into the trachea of the goose which had been anesthetized with sodium pentobarbital. The lungs were exposed as soon as possible after the infusion, and small pieces of lung tissue were removed and placed in 0.1 M phosphate-buffered 3% glutaraldehyde at 4° C. for 2-5 hours. The tissues were then rinsed for 24-36 hours in several changes of 0.1 M phosphate buffer containing 5% sucrose (Harkin, '65). The tissues were post-fixed in 2% osmium tetroxide in 0.1 phosphate buffer for two hours at room temperature. Following post-fixation, the tissues were divided into 2 groups for further processing. One group of tissues was rinsed in water, dehydrated in ethanol and embedded in Durcupan.³ The second group of tissues was washed in water and stained for two hours in 0.5% uranyl acetate buffered to pH 5.0 in Michaelis Buffer (Farquhar and Palade, '64). The stained tissues were subsequently rinsed in water, dehydrated, and embedded as above.

Sections were cut with a Sorval MT-2 ultramicrotome with glass and diamond knives. Sections 0.5-1 μ thick were mounted on glass slides, stained with toluidine blue-borate and studied with the light microscope. Pale gold to silver sections were mounted unsupported on 300 mesh copper grids, stained with lead hydroxide (Millonig, '61), and viewed in a Siemens Elmiskop I at 60 KV.

OBSERVATIONS

In the lung of the goose, a caudally-directed primary bronchus pierces the ventral surface of each lung and passes laterally and dorsally to terminate at the caudal margin of the lung. Near the point where the primary bronchus pierces the ventral surface of the lung, it gives rise to several branches which subdivide three to four times. These branches and their sub-

branches, which together form the ventral surface of the lung, are collectively called "ventral secondary bronchi." Near its termination, the primary bronchus gives rise to a branch which passes to an abdominal air sac and a second set of branches which divide several times as they course along the dorsal surface of the lung. These branches and their sub-branches, which lie on the dorsal surface of the lung, are collectively termed "dorsal secondary bronchi." The dorsal bronchial branches are connected with their ventral counterparts by means of numerous small tubules (0.5 mm in diameter) called parabronchi. These run roughly parallel to one another through the substance of the lung and occasionally anastomose (fig. 1). In a magnified view of the surface of a dried lung, with the secondary bronchi removed (fig. 2), one can see the openings of numerous parabronchi and the branching courses of blood vessels. The blood vessels indistinctly outline the periphery of each lung lobule while the parabronchi serve as the central axes of the columnar lobules. As is seen in the inset of figure 2, incomplete circular septa project into each parabronchial lumen. Between these septa, the parabronchial walls are closely beset with, and open into, thin-walled chambers, called atria, from which numerous, smaller irregularly-shaped air spaces arise and intermingle with blood capillaries (figs. 2, 3). These blood capillaries originate from larger vessels, many of which course within the connective tissue separating adjacent lobules (fig. 3). In the electron microscope, at higher magnification, sections passing through the parabronchial septa show that these structures contain a core of somewhat specialized smooth muscle cells (fig. 4). The myofilaments of these cells appear in two sizes but lack the organization seen in striated muscle cells. As seen in figure 4 and its inset, a thin sheath of flattened epithelial cells covers the muscular core of the parabronchial septa. This epithelium is continuous with other squamous epithelial cells (figs. 13, 14, 18) which line the atrial walls and become continuous with the extremely attenuated

³ Durcupan ACM was obtained from Fluka AG, Buchs SG, Switzerland.

respiratory epithelium lining the smallest air spaces in the lung parenchyma proper.

Figure 5 is a low-magnification electron micrograph of a small segment of the lung parenchyma distal to the atria. This figure shows the general relationships between the fine air spaces and the numerous blood capillaries which surround them. As can be seen in figure 5, a single capillary may be shared by more than one air space. Higher magnification (fig. 6) shows that the pulmonary barrier, which separates blood and air, is composed of endothelium, a basal lamina, and an attenuated pulmonary epithelium. At still higher magnification (figs. 7-12), the capillary wall is seen to be a relatively thick portion of the pulmonary barrier. The endothelial cell has a surface similar to that found in smooth muscle cells (Fawcett, '63) in that micropinocytotic vesicles are the prominent structural specializations seen (figs. 10-12). Goose pulmonary endothelium does not appear to have specialized pores or fenestrations such as those found in the capillaries of intestine, endocrine glands, and kidney (Fawcett, '63).

The basal lamina which separates endothelium and pulmonary epithelium is an apparently homogeneous material on which these cells rest (figs. 6-11). The pulmonary epithelium of the goose lung is attenuated but appears to be continuous. Unlike the relatively thick endothelium with its numerous vesicles, the pulmonary epithelial lining of the smallest air spaces appears to consist of little more than two apposed cell membranes in many regions (figs. 7-12). The relatively small number of pulmonary epithelial cell nuclei which are seen even after viewing many sections indicates that the cytoplasm of these cells is spread over large areas.

In addition to endothelium, a basal lamina, and pulmonary epithelium, there appears to be a fourth component to the blood-air barrier of the goose lung. This component is a layer of electron-dense material 8-12 m μ thick which separates the pulmonary epithelium from air. In some sections (figs. 6, 7, 8, 11) it appears as a single thickness and in others (figs. 9, 10, 12) as a trilaminar unit membrane-like structure with 30 Å laminations. In some air spaces (fig. 11), the surface material

is clearly seen sandwiched between folds of epithelium. Material similar to that found covering the respiratory surfaces of the finest air spaces is found as a relatively compact multilayered covering (figs. 13-14) or as whorls of material (fig. 4) loosely attached to the surfaces of the alveolar and parabronchial lining cells. This material is also found within deep surface invaginations (fig. 14) and complicated infoldings of cell surfaces (fig. 15), and as tightly packed intracellular accumulations (figs. 18-20) in lining cells of the parabronchi and alveoli which connect with the lung parenchyma. In addition to these relatively large intracellular accumulations, similar laminated material is located within cisternae of rough surfaced endoplasmic reticulum (figs. 16, 17). Within some parts of the endoplasmic reticulum, single strands of the laminated material are found oriented parallel to the cisternal walls (fig. 16). In other parts, stacks of short lamellae are found oriented perpendicular to the cisternal membranes (figs. 16, 17). Other small membrane-enclosed inclusions of lamellae are sometimes associated with the Golgi apparatus; these sometimes contain only laminated material (fig. 18) but in other cases contain a fine granular material in addition to lamellae (figs. 19, 20). Multivesicular bodies, which are a characteristic feature of the Golgi apparatus of granular pneumocytes in several mammals (Sorokin, '67), were not commonly found in parabronchial or atrial lining cells in the goose lung.

DISCUSSION

The observations presented in this study of the lung of the goose offer several new additions to descriptions of avian lungs. The finding of a continuous epithelial lining in the finest air spaces of the goose lung reveals in another species the basic plan of a continuous tripartite air-blood barrier. The present study also supports the recent finding that, in birds, the pulmonary epithelial component of the blood-air barrier is very thin, and the total air-blood barrier is two to three times thinner than that found in man (Schulz, '62).

The question of surface materials in lungs raises several points germane to the present discussion of the bird lung. In

1954, Macklin divided mammalian alveolar cells (pneumocytes) into a granular type, a phagocytic type, and a membranous type. He argued that the granular pneumocytes in the mammalian lung contribute some substance to the alveolar fluid which assist in the following: (1) removal of particulate matter; (2) maintenance of the correct surface tension within the alveoli; (3) facilitation of gaseous exchange; (4) prevention of desiccation; and (5) suppression of invasion by microorganisms. Considerable interest developed in this remarkable alveolar substance which could be washed or expressed from the lungs of several species. Studies on the physicochemical behavior and chemical composition of this alveolar material revealed a lipoprotein composition and marked surface-active properties (Klaus, Clements and Havel, '61; Miller and Bondurant, '61; Pattle and Thomas, '61). Pattle ('63) stated that without this surface-active agent the surface tension created by the curved mammalian alveolar walls would cause the alveoli to collapse or to withdraw fluids from the adjacent capillaries. Although the question of surface agents in bird lungs had received less attention than in mammalian lungs, Pattle ('63) argued that even though the more rigid structure of the tubular bird lung would probably prevent the collapse of its fine air spaces, the extremely small radii of these air spaces would create even greater surface tensions than the larger alveoli of mammals and that the bird lung would therefore require a surface-active film to prevent transudation of plasma fluids. In a study of extracts from the lungs of several species, Miller and Bondurant ('61) concluded that surface-active lining materials were not present in bird lungs. However, Pattle and Hopkinson ('63) used a different physicochemical technique and succeeded in demonstrating the presence of surface-active material in the avian lung.

The successful morphological demonstration of surface materials with the electron microscope has no doubt been hindered by standard techniques of fixation followed by ethanol dehydration (Morgan and Huber, '67). Although Chase in 1959 utilized a freeze-dry technique for electron microscopy and demonstrated a

rather thick covering over the alveolar walls in mammals and in a thin covering in the bird lung, it wasn't until other fixatives were used that surface materials were observed by many investigators (Mendenhall and Sun, '64; Bowden, Ganham and Thomas, '66; Ladman and Finlay, '66, and others). These successful demonstrations of surface films have perhaps been a result of better preservation of lipids during tissue processing for electron microscopy.

Despite the demonstration of some sort of surface materials in lungs of several animals, the evidence relating these surface materials to surfactant is largely circumstantial. However, strong support of this correlation came in 1964 from work by Mendenhall and Sun. Utilizing a combination of techniques, they showed that surface-active material had a chemical composition and physicochemical attributes which are similar to cellular unit-membranes. They also suggested that, in the pig lung at least, surface-active material existed "as a complex lamellar structured unit much the same as internal and external cellular membranes." This important finding also gave support to the idea that the laminated osmiophilic inclusions found in Macklin's granular pneumocytes by many investigators were closely related to surfactant (Buckingham and Avery, '62; Buckingham, McNary, and Sommers, '64; Ladman and Finlay, '66).

The intracellular origin of surface materials has not been established. Until recently it was generally believed that transformed mitochondria were the source of the osmiophilic inclusions within granular pneumocytes (Woodside and Dalton, '58; Klaus, Reiss, Tooley, Peil and Clements, '62; Nagaiishi, Okada, Ishiko and Diado, '64; Tyler and Pearce, '66; and others). However, recent studies by Baylis and Conen ('64), Buckingham, McNary and Sommers ('64), Ladman and Finlay ('66), and Sorokin ('67) suggest a non-mitochondrial origin of the surface material. In particular, Baylis and Conen ('64) suggest that "alteration of all cytoplasmic membranes may be involved in the process of inclusion body formation." Sorokin ('67), on the other hand, suggests that alveolar cell cytosomal-lipid is produced in multi-

vesicular bodies derived from the Golgi apparatus. Although the observations made in this study are purely morphological and do not identify the chemical composition or the physicochemical behavior of the different laminated structures described within the goose lung, the morphology which has been found does offer three suggestions which are consistent with the observations of others: (1) The laminated material found within the goose lung has structure and dimensions similar to that of the surfactant described by Mendenhall and Sun ('64). This laminated material therefore probably represents for the goose the same surface-active materials which Pattle and Hopkinson ('63) have been able to express from other bird lungs. (2) The thick layers of material on the surfaces of the parabronchial and atrial lining cells as well as the large intracellular accumulations of laminated materials within these same cells could suggest their involvement either in this material's synthesis or degradation. However, intracellular laminated inclusions in these lining cells have structurally similar counterparts within Macklin's granular pneumocytes which have long been suspected of producing surfactant. Although the lining cells of the goose lung are in a location slightly different from that of the mammalian granular pneumocytes, a recent histochemical study of Tyler and Pearse ('66) has demonstrated that the atrial and parabronchial lining cells are also histochemically similar to Macklin's granular pneumocytes (Said, Klein, Norrell, and Maddox, '66). Tyler and Pearse also showed that the atrial and parabronchial lining cells in the chicken lung possess the required metabolic machinery to produce the quantities of laminated phospholipids found there. (3) The presence of laminated materials within cisternae of rough-surfaced endoplasmic reticulum and the close approximation between some of the larger laminated inclusion bodies and small Golgi vesicles which contain granular material of similar appearance to that found in the laminated inclusions, suggests that both organelles may participate in the elaboration of the laminated surface material. An autoradiographic study at the ultrastructural level utilizing radioactive-

labeled precursors is underway to further test this hypothesis.

ACKNOWLEDGMENT

I should like to acknowledge Mrs. Merle Wekstein for contributing technical assistance to this work.

LITERATURE CITED

- Akester, A. R. 1960 The comparative anatomy of the respiratory pathways in the domestic fowl (*Gallus Domesticus*), pigeon (*Columba Livia*) and domestic duck (*Anas Platyrhynchos*). *J. Anat.*, 94: 487-506.
- Baylis, J. U., and P. E. Conen 1964 The role of alveolar inclusion bodies in the developing lung. *Lab. Invest.*, 13: 1215-1229.
- Bowden, D. H., W. G. Grantham and C. E. Thomas 1966 Cellular morphogenesis of the alveolar surface lining (Abstract). *Fed. Proc.*, 25: 603.
- Bradley, O. C. 1915 The Structure of the Fowl. A. C. Black, Ltd., London.
- Bremer, J. L. 1939 Evidence of an epithelial lining in the labyrinth of the avian lung. *Anat. Rec.*, 73: 497-513.
- Buckingham, S., and M. E. Avery 1962 Time of appearance of lung surfactant in the foetal mouse. *Nature*, 193: 688-689.
- Buckingham, S., W. F. McNary and S. C. Sommers 1964 Morphologic and functional studies of alveolar cells and lung surfactant in fetal rats (Abstract). *Fed. Proc.*, 23: 333.
- Chase, W. H. 1959 The surface membrane of pulmonary alveolar walls. *Exp. Cell Res.*, 18: 15-28.
- Farquhar, M. G., and G. E. Palade 1965 Cell junctions in amphibian skin. *J. Cell Biol.*, 26: 263-291.
- Fawcett, D. W. 1963 Comparative observations on the fine structure of blood capillaries. In: *The Peripheral Blood Vessels*. (J. L. Orbinson and D. E. Smith, Ed.) Williams and Wilkins Co., Baltimore, pp. 17-44.
- Harkin, J. C. 1964 A series of desmosomal attachments in the Schwann sheath of myelinated nerves. *Z. Zellforsch.*, 64: 189-196.
- Hazelhoff, E. H. 1951 Structure and function of the lung of birds. *Poul. Sci.*, 30: 3-10.
- Klaus, M., O. K. Reiss, W. H. Tooley, C. Piel and J. A. Clements 1962 Alveolar epithelial cell mitochondria as source of the surface-active lung lining. *Science*, 137: 750-751.
- Ladman, A. J., and T. N. Finley 1966 Electron microscopic observations of pulmonary surfactant and the cells which produce it (Abstract). *Anat. Rec.*, 154: 372.
- Locy, W. A., and O. Larsell 1916a The embryology of the birds lung. Based on observations of the domestic fowl. Part I. *Am. J. Anat.*, 19: 447-504.
- 1916b The embryology of the birds lung. Based on observations of the domestic fowl. Part II. *Am. J. Anat.*, 20: 1-44.
- Mendenhall, R. M., and C. N. Sun 1964 Surface lining of lung alveoli as a structure. *Nature*, 201: 713-714.

1954, Macklin divided mammalian alveolar cells (pneumocytes) into a granular type, a phagocytic type, and a membranous type. He argued that the granular pneumocytes in the mammalian lung contribute some substance to the alveolar fluid which assist in the following: (1) removal of particulate matter; (2) maintenance of the correct surface tension within the alveoli; (3) facilitation of gaseous exchange; (4) prevention of desiccation; and (5) suppression of invasion by microorganisms. Considerable interest developed in this remarkable alveolar substance which could be washed or expressed from the lungs of several species. Studies on the physicochemical behavior and chemical composition of this alveolar material revealed a lipoprotein composition and marked surface-active properties (Klaus, Clements and Havel, '61; Miller and Bondurant, '61; Pattle and Thomas, '61). Pattle ('63) stated that without this surface-active agent the surface tension created by the curved mammalian alveolar walls would cause the alveoli to collapse or to withdraw fluids from the adjacent capillaries. Although the question of surface agents in bird lungs had received less attention than in mammalian lungs, Pattle ('63) argued that even though the more rigid structure of the tubular bird lung would probably prevent the collapse of its fine air spaces, the extremely small radii of these air spaces would create even greater surface tensions than the larger alveoli of mammals and that the bird lung would therefore require a surface-active film to prevent transudation of plasma fluids. In a study of extracts from the lungs of several species, Miller and Bondurant ('61) concluded that surface-active lining materials were not present in bird lungs. However, Pattle and Hopkinson ('63) used a different physicochemical technique and succeeded in demonstrating the presence of surface-active material in the avian lung.

The successful morphological demonstration of surface materials with the electron microscope has no doubt been hindered by standard techniques of fixation followed by ethanol dehydration (Morgan and Huber, '67). Although Chase in 1959 utilized a freeze-dry technique for electron microscopy and demonstrated a

rather thick covering over the alveolar walls in mammals and in a thin covering in the bird lung, it wasn't until other fixatives were used that surface materials were observed by many investigators (Mendenhall and Sun, '64; Bowden, Gantham and Thomas, '66; Ladman and Finlay, '66, and others). These successful demonstrations of surface films have perhaps been a result of better preservation of lipids during tissue processing for electron microscopy.

Despite the demonstration of some sort of surface materials in lungs of several animals, the evidence relating these surface materials to surfactant is largely circumstantial. However, strong support of this correlation came in 1964 from work by Mendenhall and Sun. Utilizing a combination of techniques, they showed that surface-active material had a chemical composition and physicochemical attributes which are similar to cellular unit-membranes. They also suggested that, in the pig lung at least, surface-active material existed "as a complex lamellar structured unit much the same as internal and external cellular membranes." This important finding also gave support to the idea that the laminated osmiophilic inclusions found in Macklin's granular pneumocytes by many investigators were closely related to surfactant (Buckingham and Avery, '62; Buckingham, McNary, and Sommers, '64; Ladman and Finley, '66).

The intracellular origin of surface materials has not been established. Until recently it was generally believed that transformed mitochondria were the source of the osmiophilic inclusions within granular pneumocytes (Woodside and Dalton, '58; Klaus, Reiss, Tooley, Peil and Clements, '62; Nagaishi, Okada, Ishiko and Diado, '64; Tyler and Pearce, '66; and others). However, recent studies by Baylis and Conen ('64), Buckingham, McNary and Sommers ('64), Ladman and Finley ('66), and Sorokin ('67) suggest a non-mitochondrial origin of the surface material. In particular, Baylis and Conen ('64) suggest that "alteration of all cytoplasmic membranes may be involved in the process of inclusion body formation." Sorokin ('67), on the other hand, suggests that alveolar cell cytosomal-lipid is produced in multi-



- Miller, D. A., and S. Bondurant 1961 Surface characteristics of vertebrate lung extracts. *J. Appl. Physiol.*, 16: 1075-1077.
- Millonig, G. 1961 A modified procedure for lead staining of thin sections. *J. Biophys. Biochem. Cytol.*, 11: 736-739.
- Morgan, T. E., and G. L. Huber 1967 Loss of lipid during fixation for electron microscopy. *J. Cell Biol.*, 32: 757-760.
- Nagaishi, C., V. Okada, S. Ishiko and S. Daido 1964 Electron microscopic observations of the pulmonary alveoli. *Exp. Med. Surg.*, 22: 81-117.
- Pattle, R. E. 1963 The lining layer of the lung alveoli. *Brit. Med. Bull.*, 19: 41-44.
- Pattle, R. E., and D. A. W. Hopkinson 1963 Lung lining in bird, reptile and amphibian. *Nature*, 200: 894.
- Pattle, R. E., and L. C. Thomas 1961 Lipoprotein composition of the film lining the lung. *Nature*, 189: 844.
- Said, S. I., R. M. Klein, L. W. Norrell and Y. T. Maddox 1966 Metabolism of alveolar cells: Histochemical evidence and relation to pulmonary surfactant. *Science*, 152: 657-659.
- Schultz, H. 1962 Some remarks on the sub-microscopic anatomy and pathology of the blood-air pathway in the lung. In: *Ciba Foundation Symposium on Pulmonary Structure and Function*. (A. V. S. DeReuck and M. O'Connor, Ed.), Little Brown & Co., Boston, pp. 203-210.
- Sorokin, S. P. 1967 A morphologic and cytochemical study on the great alveolar cell. *J. Histochem. Cytochem.*, 14: 884-897.
- Tyler, W. S., and J. Pangborn 1961 Laminated membrane surface and osmophilic inclusions in avian lung epithelium. *J. Cell Biol.*, 20: 157-164.
- Tyler, W. S., W. S. Pangborn and L. M. Julian 1961 Fine structure of the air capillaries of the avian lung (Abstract). *Am. Zool.*, 1: 394.
- Tyler, W. S., and A. G. E. Pearse 1966 Functional and analytical histochemistry of the chicken lung lobule with particular reference to surfactant. *Poul. Sci.*, 45: 501-511.
- Woodside, G. L., and A. J. Dalton 1958 The ultrastructure of the lung tissue from newborn and embryo mice. *J. Ultrastruct. Res.*, 2: 28-54.

Abbreviations

A, atrium	L, lipid droplet
air, smallest air space	m, mitochondrion
C, blood capillary	PBL, parabronchial lumen
DB, dorsal secondary bronchus	pe, pulmonary epithelium
E, endothelium	RBC, red blood cell
G, Golgi apparatus	VB, ventral secondary
I, inclusions	bronchus
I, basal lamina	

PLATE 1

EXPLANATION OF FIGURES

- 1 Medial aspect of a Wood's Metal cast of a goose lung. The branching dorsal secondary bronchi (DB) can be seen passing medially over the dorsal surface of the lung. Numerous parabronchi (arrows) can be seen passing ventrally, roughly parallel to one another, to connect with a ventral set of secondary bronchi (VB). Adjacent parabronchi sometimes anastomose (circles). $\times 3$.
- 2 Dorsal view of a dried lung with the secondary bronchi removed. Between many of the parabronchial openings (arrows) branching blood vessels are seen indistinctly outlining the periphery of each cylindrical lung lobule whose central axis is a parabronchus. $\times 8$. Inset. A parabronchus at higher magnification. Incomplete circular septa project into the parabronchial lumen. Atria open into the parabronchus between these septa (arrows). $\times 60$.
- 3 Photomicrograph of a histological section cut in a plane parallel to the longitudinal axis of a parabronchus. Septa (arrows) project into the parabronchial lumen (PBL). Atria (A) open into the parabronchial lumen between these septa. Numerous fine air spaces and channels surrounded by a rich capillary network open into the atria (arrow heads). An arteriole is seen in the interlobular connective tissue. Hematoxylin and eosin stain. $\times 300$.



PLATE 2

EXPLANATION OF FIGURE

Inset. Photomicrograph of a 1 μ -thick toluidine blue-stained plastic embedded section of a parabronchial septum. A filamentous material can be seen projecting from some of the squamous cells (arrows) which surround a dense apical core. $\times 500$.

- 4** Electron micrograph of the apical end of a projection similar to the inset showing the flattened epithelium covering the core of muscle cells. The muscle cells contain mitochondria, micropinocytotic vesicles, electron-dense spots along the cell membrane, and apparently two sizes of myofilaments. A relatively large accumulation of laminated surface material is seen loosely attached to long microvilli projecting from the lining cells. Uranyl acetate and lead hydroxide stain. $\times 16,000$.

GOOSE LUNG ULTRASTRUCTURE
Roger O. Lambson and Jerome E. Cohn

PLATE 3

EXPLANATION OF FIGURES

- 5 Low magnification electron micrograph showing the general organization of the fine air spaces (air) and numerous blood capillaries (C) of goose lung parenchyma. Several spindle-shaped nucleated red blood cells (RBC) are seen in the capillaries. Uranyl acetate and lead hydroxide stain. $\times 4,000$.
- 6 Section through a partition separating two adjacent air spaces. The components of the air-blood barrier are the attenuated pulmonary epithelial cells (pe), a basal lamina (l), and capillary endothelium (E). Microtubules (arrows) are present in the red blood cell (RBC). The two outlined areas are shown at higher magnification in figures 7 and 8. Lead hydroxide stain. $\times 28,000$.

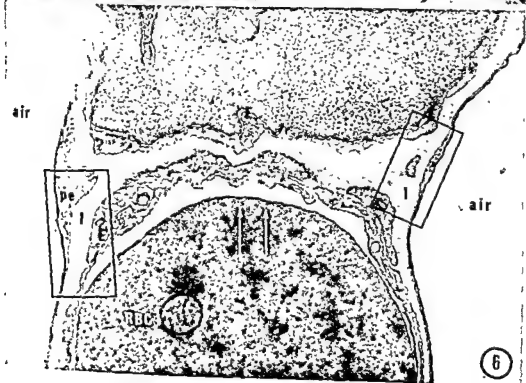
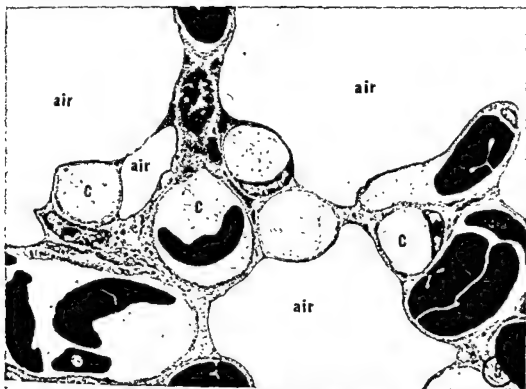


PLATE 4

EXPLANATION OF FIGURES

- 7 Detail of field shown in figure 6 magnified to show the surface material situated between the outer plasma membrane of the pulmonary epithelial cell and the air space. A single layer of material may be found either closely applied to the surface (single arrows) or detached from it (arrow head). $\times 65,000$.
- 8 Detail of a field shown in figure 6 showing surface material (arrows) attached to the outer plasma lamina appearing as a thickened "unit membrane." Lead hydroxide stain. $\times 65,000$.
- 9 Detail of blood-air barrier in which a 90 Å layer of surface material resembles a unit membrane (arrows). Lead hydroxide stain. $\times 71,000$.
- 10 Detail of blood-air barrier showing layered surface material (arrows), some of which appears to be partially detached (arrow heads). Lead hydroxide stain. $\times 70,500$.
- 11 Air space in which the surface material is seen sandwiched between two overlapping flaps of epithelial cytoplasm (arrows). Lead hydroxide stain. $\times 51,000$.
- 12 Detail of pulmonary epithelium and its surface covering. The layered surface material (arrows) is strikingly similar to the underlying epithelial cell membranes (pe). It is not known whether the cell interposed between the epithelium and endothelium represents cytoplasm of a cell lining an adjacent air space, a capillary, or some interstitial cell. Uranyl acetate and lead hydroxide stain. $\times 50,000$.

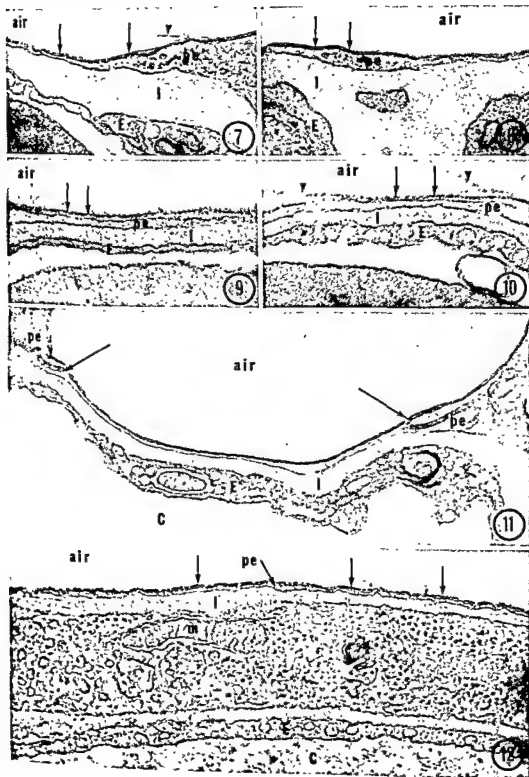


PLATE 4

EXPLANATION OF FIGURES

- 7 Detail of field shown in figure 6 magnified to show the surface material situated between the outer plasma membrane of the pulmonary epithelial cell and the air space. A single layer of material may be found either closely applied to the surface (single arrows) or detached from it (arrow head). $\times 65,000$.
- 8 Detail of a field shown in figure 6 showing surface material (arrows) attached to the outer plasma lamina appearing as a thickened "unit membrane." Lead hydroxide stain. $\times 65,000$.
- 9 Detail of blood-air barrier in which a 90 \AA layer of surface material resembles a unit membrane (arrows). Lead hydroxide stain. $\times 71,000$.
- 10 Detail of blood-air barrier showing layered surface material (arrows), some of which appears to be partially detached (arrow heads). Lead hydroxide stain. $\times 70,500$.
- 11 Air space in which the surface material is seen sandwiched between two overlapping flaps of epithelial cytoplasm (arrows). Lead hydroxide stain. $\times 51,000$.
- 12 Detail of pulmonary epithelium and its surface covering. The layered surface material (arrows) is strikingly similar to the underlying epithelial cell membranes (pc). It is not known whether the cell interposed between the epithelium and endothelium represents cytoplasm of a cell lining an adjacent air space, a capillary, or some interstitial cell. Uranyl acetate and lead hydroxide stain. $\times 50,000$.

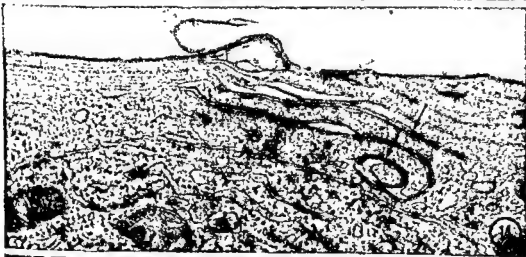
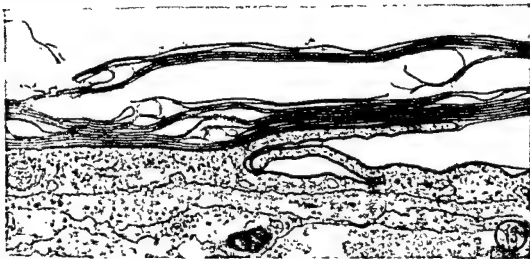


PLATE 5

EXPLANATION OF FIGURES

- 13 Atrial lining cell with several layers of laminated material. One layer is seen intimately following the outlines of microvilli. Uranyl acetate and lead hydroxide stain. $\times 26,000$.
- 14 Lining cell with the surface material appearing to follow infoldings of the surface (arrows). Uranyl acetate and lead hydroxide stain. $\times 41,000$.
- 15 Basal part of lining cell with complex folds containing laminated material. It is not known whether these structures represent intricate surface infoldings as in figure 14 or intracellular accumulations of this material. Uranyl acetate and lead hydroxide stain. $\times 31,000$.

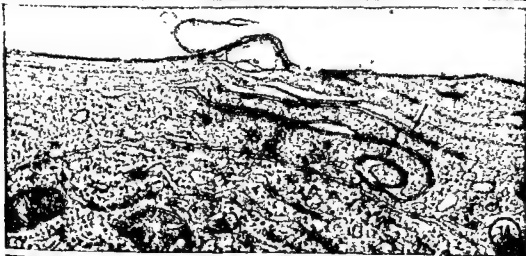


PLATE 6

EXPLANATION OF FIGURES

- 16 Parabronchial lining cell with large lipid droplet (L), laminated inclusion (I), and laminations within the rough-surfaced endoplasmic reticulum (arrows). Although the endoplasmic reticulum laminations are similar in structure to those seen on the surface, they do not have the same electron density or crispness as the surface laminations seen in figure 13. Uranyl acetate and lead hydroxide stain. $\times 41,000$.
Inset. Inset shows a small area of ergastoplasm at higher magnification. $\times 80,000$.
- 17 Lining cell demonstrating that the laminations are also occasionally found as aggregations oriented perpendicular to the cisternal walls (arrows). Uranyl acetate and lead hydroxide stain. $\times 42,000$.

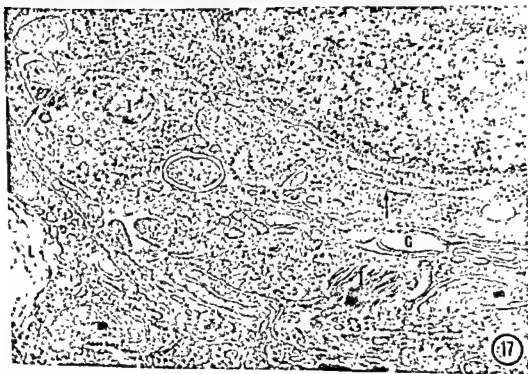


PLATE 6

EXPLANATION OF FIGURES

- 16 Parabronchial lining cell with large lipid droplet (L), laminated inclusion (I), and laminations within the rough-surfaced endoplasmic reticulum (arrows). Although the endoplasmic reticulum laminations are similar in structure to those seen on the surface, they do not have the same electron density or crispness as the surface laminations seen in figure 13. Uranyl acetate and lead hydroxide stain. $\times 41,000$.
Inset. Inset shows a small area of ergastoplasm at higher magnification. $\times 80,000$.
- 17 Lining cell demonstrating that the laminations are also occasionally found as aggregations oriented perpendicular to the cisternal walls (arrows). Uranyl acetate and lead hydroxide stain. $\times 42,000$.

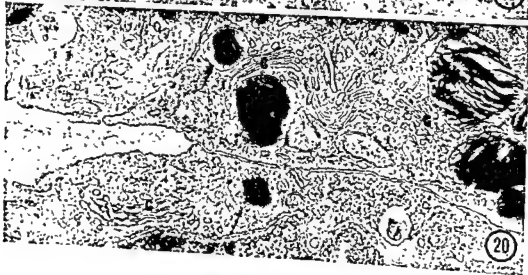
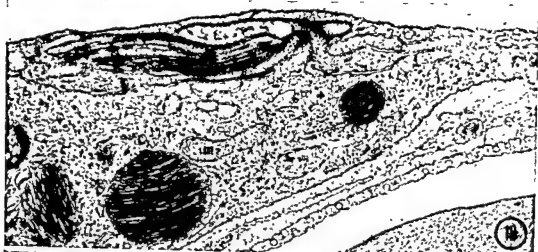
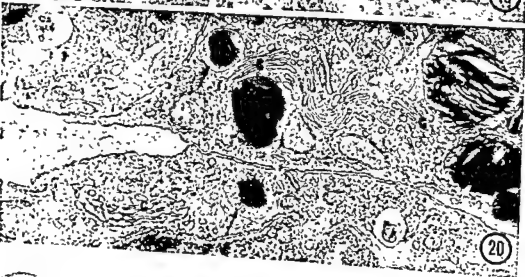


PLATE 7

EXPLANATION OF FIGURES

- 18 Atrial lining cell with three laminated inclusions (I) as well a a linear accumulation of material. Uranyl acetate and lead hydroxide stain. $\times 24,000$.
- 19 Lining cell with several inclusions. One inclusion contains a fine granular material in addition to laminations (arrow). Uranyl acetate and lead hydroxide stain. $\times 40,000$.
- 20 Adjacent lining cells showing laminated inclusions (arrows) located near the Golgi apparatus. Uranyl acetate and lead hydroxide stain. $\times 28,000$.



Index

A

- Abdominal (ventrolateral) musculature in the albino rat, the embryonic origin of the acid deficiency on the skin of the mouse, the effects of essential fatty 491
- Albino rat, the embryonic origin of the abdominal (ventrolateral) musculature in the 491
- Anastomosis and its homologue in other vertebrates, the avian intercarotid 1
- Anchoring villi of the human placenta, fine structure of 419
- Animals, a comparative morphologic study of the cardiac innervation in domestic. I. The canine 533
- Animals, a comparative morphologic study of the cardiac innervation in domestic. II. The feline 545
- Annulate lamellae, the primary human oocyte: Some observations on the fine structure of Balbiani's vitelline body and the origin of the 107
- Articular and internal remodeling in the human otic capsule 397
- ATERNAN, KURT. See Corrin, Brian 57
- ATP-ASE reaction in normal and denervated skeletal muscles of guinea pig, histochemical investigation of fiber type ratios with the myofibrillar 145
- Autoradiographic studies of the formation of the metrial gland in the pregnant rat, histochemical and 607
- Autoradiographic study of their origin in the mouse brain, subcommissural organ and adjacent ependyma: 317
- Autoradiography in the epidermis of different species, protein synthesis studied by 269
- Avian intercarotid anastomosis and its homologue in other vertebrates, the 1

B

- Bacterial endotoxin and studied by quantitative histology and electron microscopy, involution and regeneration of the thymus in mice, induced by 573
- Balbians's vitelline body and the origin of the annulate lamellae, the primary human oocyte. Some observations on the fine structure of 107
- Bat (*Myotis lucifugus lucifugus*), formation and structure of the hemodichorial chorio-allantoic placenta of the 453
- BAUMEL, JULIAN J., AND LEBOY GERSHMAN. The avian intercarotid anastomosis and its homologue in other vertebrates 1
- BRANSTEN, MAURICE H. See Elwood, William K. 73
- Binding of tritiated norepinephrine in pigmented nuclei of human brain, tissue 139
- Blood brain barrier to peroxidase in capillaries surrounded by perivascular spaces, 249

- Blood in the sheep, origin and distribution of portal 95
- BODENHEIMER, THOMAS S. See Long, Don M. 209
- BODENHEIMER, T. S., AND M. W. BRIGHTMAN. A blood-brain barrier to peroxidase in capillaries surrounded by perivascular spaces 249
- Body and the origin of the annulate lamellae, the primary human oocyte: Some observations on the fine structure of Balbiani's vitelline 107
- Brain, subcommissural organ and adjacent ependyma: Autoradiographic study of their origin in the mouse 317
- Brain, tissue binding of tritiated norepinephrine in pigmented nuclei of human 139
- Brain, ultrastructural features of the shark 209
- BRIGHTMAN, M. W. See Bodenheimer, T. S. 249
- BROWNING, HENRY C. See Crisp, Thomas M. 169
- Bufo arenarum Hensel, dense-core microtubules in neurons and glial cells of the toad 157
- BUSTOS-OREGON, E. See Clermont, Y. 237

C

- Canine, a comparative morphologic study of the cardiac innervation in domestic animals. I. The 533
- Capillaries surrounded by perivascular spaces, a blood-brain barrier to peroxidase in 249
- Capsule, articular and internal remodeling in the human otic 397
- Cardiac innervation in domestic animals, a comparative morphologic study of the. I. The canine 533
- Cardiac innervation in domestic animals, a comparative morphologic study of the. II. The feline 545
- Cells in the ferret, the relationship between the transverse tubular system and other tubules at the Z disc levels of myocardial 193
- Changes in the fine structure of the parietal yolk sac of the rat placenta with increasing gestational age 513
- Chorio-allantoic placenta of the bat (*Myotis lucifugus lucifugus*), formation and structure of the hemodichorial 453
- Ciliogenesis in developing epidermis and trachea in the embryo of *Xenopus laevis*, an electron microscopic study of 19
- CLARK, SAM L., JR. See Gad, Palle 573
- CLERMONT, Y., AND E. BUSTOS-OREGON. Re-examination of spermatogonial renewal in the rat by means of semitiferous tubules mounted "in toto" 237
- COHN, JEROME E. See Lambson, Roger O. 631
- Comparative morphologic study of the cardiac innervation in domestic animals, a. I. The canine 533
- Comparative morphologic study of the cardiac innervation in domestic animals, a. II. The feline 545

- Compensatory growth of skeletal muscle, the relationship between the dimensions of the fibres and the number of nuclei during restricted growth, degrowth and 565
- Corpora lutea in ovarian transplants of mice following luteotrophin stimulation, the fine structure of 169
- CORRIN, BRIAN, AND KURT ATERMAN. The pattern of glycogen distribution in the liver 57
- CRISP, THOMAS M., AND HENRY C. BROWN-ING. The fine structure of corpora lutea in ovarian transplants of mice following luteotrophin stimulation 169
- Crystals in the thyroids of senile rats, dense granules (lysosomes?) and 377
- ### D
- Degrowth and compensatory growth of skeletal muscle, the relationship between the dimensions of the fibres and the number of nuclei during restricted growth .. 565
- Denervated skeletal muscles of guinea pig, histochemical investigation of fiber type ratios with the myofibrillar ATP-ASE reaction in normal and 145
- Dense-core microtubules in neurons and gliocytes of the toad *Bufo arenarum* Hensel 157
- Dense granules (lysosomes?) and crystals in the thyroids of senile rats 377
- Developing epidermis and trachea in the embryo of *Xenopus laevis*, an electron microscopic study of ciliogenesis in 19
- Distribution in the liver, the pattern of glycogen 57
- Distribution of portal blood in the sheep, origin and 95
- Domestic animals, a comparative morphological study of the cardiac innervation in. I. The canine 533
- Domestic animals, a comparative morphological study of the cardiac innervation in. II. The feline 545
- Domestic fowl, the relationship between the dimensions of the fibres and the number of nuclei during normal growth of skeletal muscle in the .. 555
- ### E
- Effects of essential fatty acid deficiency on the skin of the mouse, the 337
- Electron microscopy, involution and regeneration of the thymus in mice, induced by bacterial endotoxin and studied by quantitative histology and 573
- Electron microscopic study of ciliogenesis in developing epidermis and trachea in the embryo of *Xenopus laevis*, an 19
- ELWOOD, WILLIAM K., AND MAURICE H. BERNSTEIN. The ultrastructure of the enamel organ related to enamel formation Embryo of *Xenopus laevis*, an electron microscopic study of ciliogenesis in developing epidermis and trachea in the 73
- Embryonic origin of the abdominal (ventrolateral) musculature in the albino rat, the 491
- Enamel organ related to enamel formation, the ultrastructure of the 73
- ENDERS, ALLEN C., AND WILLIAM A. WIM-SATT. Formation and structure of the hemodichorial chorio-allantoic placenta of the bat (*Myotis lucifugus lucifugus*) 453
- ENDERS, ALLEN C. Fine structure of anchoring villi of the human placenta 419
- Endocardium, nerve endings in the human 621
- Endotoxin and studied by quantitative histology and electron microscopy, involution and regeneration of the thymus in mice, induced by bacterial 573
- ENGEL, W. KING. See Karpatis, G. 145
- Ependyma, subcommissural organ and adjacent: Autoradiographic study of their origin in the mouse brain 317
- Epidermis and trachea in the embryo of *Xenopus laevis*, an electron microscopic study of ciliogenesis in developing 19
- Epidermis of different species, protein synthesis studied by autoradiography in the 269
- EPSTEIN, WILLIAM L. See Fukuyama, Kimie. 269
- Essential fatty acid deficiency on the skin of the mouse, the effects of 337
- ### F
- Fatty acid deficiency on the skin of the mouse, the effects of essential 337
- Feline, a comparative morphologic study of the cardiac innervation in domestic animals. II. The 545
- Ferret, the relationship between the transverse tubular system and other tubules at the Z disc levels of myocardial cells in the Fiber type ratios with the myofibrillar ATP-ASE reaction in normal and denervated skeletal muscles of guinea pig, histochemical investigation of 145
- Fibres and the number of nuclei during normal growth of skeletal muscle in the domestic fowl, the relationship between the dimensions of the 555
- Fibres and the number of nuclei during restricted growth, degrowth and compensatory growth of skeletal muscle 565
- Fine structure of anchoring villi of the human placenta 419
- Fine structure of Balbiani's vitelline body and the origin of the annulate lamellae, the primary human oocyte: Some observations on the 107
- Fine structure of corpora lutea in ovarian transplants of mice following luteotrophin stimulation, the 169
- Fine structure of the hamster pineal gland, the 357
- Formation and structure of the hemodichorial chorio-allantoic placenta of the bat (*Myotis lucifugus lucifugus*) 453
- Formation, the ultrastructure of the enamel organ related to enamel 73

- Fowl, the relationship between the dimensions of the fibres and the number of nuclei during normal growth of skeletal muscle in the domestic 555
- FRIEDE, REINHARD L. See Ishii Tsuyoshi ... 139
- FUKUYAMA, KIMIE, AND WILLIAM L. EPSTEIN. Protein synthesis studied by autoradiography in the epidermis of different species 269

G

- GAD, PAUL, AND SAM L. CLARK, JR. Involution and regeneration of the thymus in mice, induced by bacterial endotoxin and studied by quantitative histology and electron microscopy 573
- GERCHMAN, LEBOY. See Baumel, Julian J. Gestational age, changes in the fine structure of the parietal yolk sac of the rat placenta with increasing 513
- GEITY, ROBERT. See McKibben, John Scott 533, 545
- Gland in the pregnant rat, histochemical and autoradiographic studies of the formation of the metrial 607
- Gland, the fine structure of the hamster pineal 357
- Gliocytes of the toad *Bufo arenarum* Hensel, dense-core microtubules in neurons and Glycogen distribution in the liver, the pattern of 157
- Gonocyte degeneration in the postnatal male rat 275
- Goose and its lining of surface material, ultrastructure of the lung of the 631
- Granules (lysosomes?) and crystals in the thyroids of senile rats, dense 377
- Growth, degrowth and compensatory growth of skeletal muscle, the relationship between the dimensions of the fibres and the number of nuclei during restricted 565
- Growth of skeletal muscle in the domestic fowl, the relationship between the dimensions of the fibres and the number of nuclei during normal 555
- Guinea pig, histochemical investigation of fiber type ratios with the myofibrillar ATP-ASE reaction in normal and denervated skeletal muscles of 145
- GUSSEN, RUTH Articular and internal remodeling in the human otic capsule ... 397

H

- Hamster pineal gland, the fine structure of the 357
- HARTMANN, J. FRANCIS. See Long, Don M. 209
- HEATH, TREVOR Origin and distribution of portal blood in the sheep 95
- Hemodichorial chorio-allantoic placenta of the bat (*Myotis lucifugus lucifugus*), formation and structure of the 453
- HENDERSON, NANCY E. See Hill, Joanna Jensen 301
- HIRTIG, ARTHUR T. The primary human oocyte. Some observations on the fine structure of Balbiani's vitelline body and the origin of the annulate lamellae 107

- HILL, JOANNA JENSEN, AND NANCY E. HENDERSON. The vascularization of the hypothalamic-hypophyseal region of the Eastern brook trout, *Salvelinus fontinalis* 301
- Histochemical and autoradiographic studies of the formation of the metrial gland in the pregnant rat 607
- Histochemical investigation of fiber type ratios with the myofibrillar ATP-ASE reaction in normal and denervated skeletal muscles of guinea pig 145
- Histology and electron microscopy, involution and regeneration of the thymus in mice, induced by bacterial endotoxin and studied by quantitative 573
- Homologue in other vertebrates, the avian intercarotid anastomosis and its 1
- Human brain, tissue binding of tritiated norepinephrine in pigmented nuclei of 139
- Human endocardium, nerve endings in the 621
- Human oocyte, the primary: Some observations on the fine structure of Balbiani's vitelline body and the origin of the annulate lamellae 107
- Human otic capsule, articular and internal remodeling in the 397
- Human placenta, fine structure of anchoring villi of the 419
- Hypothalamic-hypophyseal region of the Eastern brook trout, *Salvelinus fontinalis*, the vascularization of the 301

I

- Intercarotid anastomosis and its homologue in other vertebrates, the avian 1
- Internal remodeling in the human otic capsule, articular and 397
- Involution and regeneration of the thymus in mice, induced by bacterial endotoxin and studied by quantitative histology and electron microscopy 573
- ISHII, TSUYOSHI, AND REINHARD L. FRIEDE. Tissue binding of tritiated norepinephrine in pigmented nuclei of human brain ... 139

J

- JOHNSTON, BRIAN D. Nerve endings in the human endocardium 621
- JOLLIE, WILLIAM P. Changes in the fine structure of the parietal yolk sac of the rat placenta with increasing gestational age 513

K

- KARPATI, G., AND W. KING ENGEL. Histochemical investigation of fiber type ratios with the myofibrillar ATP-ASE reaction in normal and denervated skeletal muscles of guinea pig 145
- KLATZO, IGOR. See Long, Don M. ... 209

- Compensatory growth of skeletal muscle, the relationship between the dimensions of the fibres and the number of nuclei during restricted growth, degrowth and 565
- Corpora lutea in ovarian transplants of mice following luteotrophin stimulation, the fine structure of 169
- CORRIN, BRIAN, AND KURT ATERMAN. The pattern of glycogen distribution in the liver 57
- CRISP, THOMAS M., AND HENRY C. BROWNING. The fine structure of corpora lutea in ovarian transplants of mice following luteotrophin stimulation 169
- Crystals in the thyroids of senile rats, dense granules (lysosomes?) and 377
- ### D
- Degrowth and compensatory growth of skeletal muscle, the relationship between the dimensions of the fibres and the number of nuclei during restricted growth .. 565
- Denervated skeletal muscles of guinea pig, histochemical investigation of fiber type ratios with the myofibrillar ATP-ASE reaction in normal and 145
- Dense-core microtubules in neurons and gliocytes of the toad *Bufo arenarum* Hensel 157
- Dense granules (lysosomes?) and crystals in the thyroids of senile rats 377
- Developing epidermis and trachea in the embryo of *Xenopus laevis*, an electron microscopic study of ciliogenesis in 19
- Distribution in the liver, the pattern of glycogen 57
- Distribution of portal blood in the sheep, origin and 95
- Domestic animals, a comparative morphologic study of the cardiac innervation in. I. The canine 533
- Domestic animals, a comparative morphologic study of the cardiac innervation in. II. The feline 545
- Domestic fowl, the relationship between the dimensions of the fibres and the number of nuclei during normal growth of skeletal muscle in the 555
- ### E
- Effects of essential fatty acid deficiency on the skin of the mouse, the 337
- Electron microscopy, involution and regeneration of the thymus in mice, induced by bacterial endotoxin and studied by quantitative histology and 573
- Electron microscopic study of ciliogenesis in developing epidermis and trachea in the embryo of *Xenopus laevis*, an 19
- ELWOOD, WILLIAM K., AND MAURICE H. BERNSTEIN. The ultrastructure of the enamel organ related to enamel formation Embryo of *Xenopus laevis*, an electron microscopic study of ciliogenesis in developing epidermis and trachea in the 19
- Embryonic origin of the abdominal (ventrolateral) musculature in the albino rat, the 491
- Enamel organ related to enamel formation, the ultrastructure of the 73
- ENDERS, ALLEN C., AND WILLIAM A. WIM-SATT. Formation and structure of the hemodichorial chorio-allantoic placenta of the bat (*Myotis lucifugus lucifugus*) 453
- ENDERS, ALLEN C. Fine structure of anchoring villi of the human placenta 419
- Endocardium, nerve endings in the human 621
- Endotoxin and studied by quantitative histology and electron microscopy, involution and regeneration of the thymus in mice, induced by bacterial 573
- ENGL, W. KING. See Karpatl, G. 145
- Ependyma, subcommissural organ and adjacent: Autoradiographic study of their origin in the mouse brain 317
- Epidermis and trachea in the embryo of *Xenopus laevis*, an electron microscopic study of ciliogenesis in developing 19
- Epidermis of different species, protein synthesis studied by autoradiography in the 269
- EPSTEIN, WILLIAM L. See Fukuyama, Kimie. Essential fatty acid deficiency on the skin of the mouse, the effects of 337
- ### F
- Fatty acid deficiency on the skin of the mouse, the effects of essential 337
- Feline, a comparative morphologic study of the cardiac innervation in domestic animals. II. The 545
- Ferret, the relationship between the transverse tubular system and other tubules at the Z disc levels of myocardial cells in the 193
- Fiber type ratios with the myofibrillar ATP-ASE reaction in normal and denervated skeletal muscles of guinea pig, histochemical investigation of 145
- Fibres and the number of nuclei during normal growth of skeletal muscle in the domestic fowl, the relationship between the dimensions of the 555
- Fibres and the number of nuclei during restricted growth, degrowth and compensatory growth of skeletal muscle 565
- Fine structure of anchoring villi of the human placenta 419
- Fine structure of Balbiani's vitelline body and the origin of the annulate lamellae, the primary human oocyte: Some observations on the 107
- Fine structure of corpora lutea in ovarian transplants of mice following luteotrophin stimulation, the 169
- Fine structure of the hamster pineal gland, the 357
- Formation and structure of the hemodichorial chorio-allantoic placenta of the bat (*Myotis lucifugus lucifugus*) 453
- Formation, the ultrastructure of the enamel organ related to enamel 73

L

- LAMBSON, ROGER O., AND JEROME E. COHN.
Ultrastructure of the lung of the goose
and its lining of surface material 631
- Lamellae, the primary human oocyte: Some
observations on the fine structure of
Balbiani's vitelline body and the origin of
the annulate 107
- LARKIN, LYNN H., AND RICHARD L. SCHULTZ.
Histochemical and autoradiographic studies
of the formation of the metrial gland
in the pregnant rat 607
- LEIK, JEAN. See Roosen-Runge, Edward C.
Liver, the pattern of glycogen distribution
in the 275
- LONG, DON M., THOMAS S. BODENHEIMER, J.
FRANCIS HARTMANN AND IGOR KLATZO.
Ultrastructural features of the shark brain
Lung of the goose and its lining of surface
material, ultrastructure of the 209
- Lutea in ovarian transplants of mice following
luteotrophin stimulation, the fine
structure of corpora 631
- Luteotrophin stimulation, the fine structure
of corpora lutea in ovarian transplants
of mice following 169
- (Lysosomes?) and crystals in the thyroids
of senile rats, dense granules 377

M

- Male rat, gonocyte degeneration in the post-
natal 275
- McKIBBEN, JOHN SCOTT, AND ROBERT GETTY.
A comparative morphologic study of the
cardiac innervation in domestic animals.
I. The canine 533
- McKIBBEN, JOHN SCOTT, AND ROBERT GETTY.
A comparative morphologic study of the
cardiac innervation in domestic animals.
II. The feline 545
- MENTON, DAVID N. The effects of essential
fatty acid deficiency on the skin of the
mouse 337
- Metrial gland in the pregnant rat, histochem-
ical and autoradiographic studies of the
formation of the 607
- Mice following luteotrophin stimulation, the
fine structure of corpora lutea in ovarian
transplants of 169
- Mice, induced by bacterial endotoxin and
studied by quantitative histology and
electron microscopy, involution and regen-
eration of the thymus in 573
- Microscopic study of ciliogenesis in devel-
oping epidermis and trachea in the em-
bryo of *Xenopus laevis*, an electron 19
- Microscopy, involution and regeneration of
the thymus in mice, induced by bacterial
endotoxin and studied by quantitative
histology and electron 573
- Microtubules in neurons and gliocytes of
the toad *Bufo arenarum* Hensel, dense-
core 157
- Morphologic study of the cardiac innervation
in domestic animals, a comparative. I.
The canine 533

- Morphologic study of the cardiac innerva-
tion in domestic animals, a comparative.
II. The feline 545
- Moss, F. P. The relationship between the
dimensions of the fibres and the number
of nuclei during normal growth of skeletal
muscle in the domestic fowl 555
- Moss, F. P. The relationship between the
dimensions of the fibres and the number
of nuclei during restricted growth, de-
growth and compensatory growth of
skeletal muscle 565
- Mouse brain, subcommissural organ and ad-
jacent ependyma: Autoradiographic study
of their origin in the 317
- Mouse, the effects of essential fatty acid de-
ficiency on the skin of the 337
- Musculature in the albino rat, the em-
bryonic origin of the abdominal (ventro-
lateral) 491
- Muscle in the domestic fowl, the relation-
ship between the dimensions of the fibres
and the number of nuclei during normal
growth of skeletal 555
- Muscle, the relationship between the dimen-
sions of the fibres and the number of
nuclei during restricted growth, de-
growth and compensatory growth of
skeletal 565
- Muscles of guinea pig, histochemical invest-
igation of fiber type ratios with the myo-
fibrillar ATP-ASE reaction in normal and
denervated skeletal 145
- Myocardial cells in the ferret, the relation-
ship between the transverse tubular sys-
tem and other tubules at the Z disc levels
of 193
- Myofibrillar ATP-ASE reaction in normal
and denervated skeletal muscles of guinea
pig, histochemical investigation of fiber
type ratios with the 145
- (*Myotis lucifugus lucifugus*), formation and
structure of the hemodichorial chorio-
allantoic placenta of the bat 453

N

- Neurons and gliocytes of the toad *Bufo
arenarum* Hensel, dense-core micro-
tubules in 157
- Nerve endings in the human endocardium
Normal and denervated skeletal muscles of
guinea pig, histochemical investigation
of fiber type ratios with the myofibrillar
ATP-ASE reaction in 145
- Norepinephrine in pigmented nuclei of
human brain, tissue binding of tritiated
Nuclei during normal growth of skeletal
muscle in the domestic fowl, the relation-
ship between the dimensions of the fibres
and the number of 555
- Nuclei during restricted growth, degrowth
and compensatory growth of skeletal mus-
cle, the relationship between the dimen-
sions of the fibres and the number of ..
Nuclei of human brain, tissue binding of
tritiated norepinephrine in pigmented .. 139

Q

Observations on the fine structure of Balbiani's vitelline body and the origin of the annulate lamellae, the primary human oocyte: Some	107
Oocyte, the primary human: Some observations on the fine structure of Balbiani's vitelline body and the origin of the annulate lamellae	107
Organ related to enamel formation, the ultrastructure of the enamel	73
Origin and distribution of portal blood in the sheep	95
Origin of the annulate lamellae, the primary human oocyte: Some observations on the fine structure of Balbiani's vitelline body and the	107
Otic capsule, articular and internal remodeling in the human	397
Ovarian transplants of mice following luteotrophin stimulation, the fine structure of corpora lutea in ..	169

P

Parietal yolk sac of the rat placenta with increasing gestational age, changes in the fine structure of the	513
ARRY, WILLIAMS. The embryonic origin of the abdominal (ventrolateral) musculature in the albino rat	491
'attern of glycogen distribution in the liver, the	57
'erivascular spaces, a blood-brain barrier to peroxidase in capillaries surrounded by peroxidase in capillaries surrounded by perivascular spaces, a blood-brain barrier to	249
PIZZI, R. S. See Rodríguez Echandia, E. L.	157
Pigmented nuclei of human brain, tissue binding of tritiated norepinephrine in ...	139
Pineal gland, the fine structure of the hamster	357
Placenta, fine structure of anchoring villi of the human	419
Placenta of the bat (<i>Myotis lucifugus lucifugus</i>), formation and structure of the hemodichorial chorio-allantoic	453
Placenta with increasing gestational age, changes in the fine structure of the parietal yolk sac of the rat	513
Portal blood in the sheep, origin and distribution of	95
Postnatal male rat, gonocyte degeneration in the	275
Pregnant rat, histochemical and autoradiographic studies of the formation of the metrial gland in the	607
Primary human oocyte, the. Some observations on the fine structure of Balbiani's vitelline body and the origin of the annulate lamellae ..	107
Protein synthesis studied by autoradiography in the epidermis of different species ...	269

R

	RABIK, PASKO, AND RICHARD L. SIDMAN.	
	Subcommissural organ and adjacent ependyma: Autoradiographic study of their origin in the mouse brain	31
	Ratios with the myofibrillar ATP-ASE reaction in normal and denervated skeletal muscles of guinea pig, histochemical investigation of fiber type	14
	Rat by means of seminiferous tubules mounted "in toto," re-examination of spermatogonial renewal in the	23
	Rat, gonocyte degeneration in the post-natal male	27
	Rat, histochemical and autoradiographic studies of the formation of the metrial gland in the pregnant.	60
	Rat placenta with increasing gestational age, changes in the fine structure of the parietal yolk sac of the ..	5
	Rat, the embryonic origin of the abdominal (ventrolateral) musculature in the albino ..	4
	Rats, dense granules (lysosomes?) and crystals in the thyroids of senile	3
	RAYNS, D. G. See Simpson, F. O.	1
	Reaction in normal and denervated skeletal muscles of guinea pig, histochemical investigation of fiber type ratios with the myofibrillar ATP-ASE	1
3	Re-examination of spermatogonial renewal in the rat by means of seminiferous tubules mounted "in toto"	
1	Regeneration of the thymus in mice, induced by bacterial endotoxin and studied by quantitative histology and electron microscopy, involution and	
57	REITER, RUSSEL J. See Sheridan, Michael N.	
49	Relationship between the dimensions of the fibres and the number of nuclei during normal growth of skeletal muscle in the domestic fowl, the	
49	Relationship between the dimensions of the fibres and the number of nuclei during restricted growth, degrowth and compensatory growth of skeletal muscle, the	
57	Relationship between transverse tubular system and other tubules at the Z disc levels of myocardial cells in the ferret, the	
39	Restricted growth, degrowth and compensatory growth of skeletal muscle, the relationship between the dimensions of the fibres and the number of nuclei during	
357	RODRÍGUEZ ECHANDÍA, E. L., R. S. PIEZZI AND E. M. RODRÍGUEZ. Dense-core microtubules in neurons and gliocytes of the toad <i>Bufo arenarum</i> Hensel	
419	RODRÍGUEZ, E. M. See Rodríguez Echandia, E. L.	
453	ROOSEN-RUNGE, EDWARD C., AND JEAN LEIK. Gonocyte degeneration in the postnatal male rat	
513		
95		
275		
607		

2

Salvelinus fontinalis, the vascularization of the hypothalamic-hypophyseal region of the Eastern brook trout
SCHULTZ, RICHARD L. See Larkin, Lynn H.

L

- LAMBSON, ROGER O., AND JEROME E. COHN.
Ultrastructure of the lung of the goose
and its lining of surface material 631
- Lamellae, the primary human oocyte: Some
observations on the fine structure of
Balbani's vitelline body and the origin of
the annulate 107
- LARKIN, LYNN H., AND RICHARD L. SCHULTZ.
Histochemical and autoradiographic stud-
ies of the formation of the metrial gland
in the pregnant rat 607
- LEIK, JEAN. See Roosen-Runge, Edward C.
Liver, the pattern of glycogen distribution
in the 57
- LONG, DON M., THOMAS S. BODENHEIMER, J.
FRANCIS HARTMANN AND IGOR KLATZO.
Ultrastructural features of the shark brain
Lung of the goose and its lining of surface
material, ultrastructure of the 209
- Lutea in ovarian transplants of mice follow-
ing luteotrophin stimulation, the fine
structure of corpora 631
- Luteotrophin stimulation, the fine structure
of corpora lutea in ovarian transplants
of mice following 169
- (Lysosomes?) and crystals in the thyroids
of senile rats, dense granules 169
- 377

M

- Male rat, gonocyte degeneration in the post-
natal 275
- McKIBBEN, JOHN SCOTT, AND ROBERT GETTY.
A comparative morphologic study of the
cardiac innervation in domestic animals.
I. The canine 533
- McKIBBEN, JOHN SCOTT, AND ROBERT GETTY.
A comparative morphologic study of the
cardiac innervation in domestic animals.
II. The feline 545
- MENTON, DAVID N. The effects of essential
fatty acid deficiency on the skin of the
mouse 337
- Metrial gland in the pregnant rat, histochem-
ical and autoradiographic studies of the
formation of the 607
- Mice following luteotrophin stimulation, the
fine structure of corpora lutea in ovarian
transplants of 169
- Mice, induced by bacterial endotoxin and
studied by quantitative histology and
electron microscopy, involution and regen-
eration of the thymus in 573
- Microscopic study of ciliogenesis in develop-
ing epidermis and trachea in the em-
bryo of *Xenopus laevis*, an electron 19
- Microscopy, involution and regeneration of
the thymus in mice, induced by bacterial
endotoxin and studied by quantitative
histology and electron 573
- Microtubules in neurons and gliocytes of
the toad *Bufo arenarum* Hensel, dense-
core 157
- Morphologic study of the cardiac innervation
in domestic animals, a comparative. I.
The canine 533

- Morphologic study of the cardiac innerva-
tion in domestic animals, a comparative.
II. The feline 5
- Moss, F. P. The relationship between the
dimensions of the fibres and the number
of nuclei during normal growth of skeletal
muscle in the domestic fowl 5
- Moss, F. P. The relationship between the
dimensions of the fibres and the number
of nuclei during restricted growth, de-
growth and compensatory growth of
skeletal muscle 5
- Mouse brain, subcommissural organ and ad-
jacent ependyma: Autoradiographic study
of their origin in the 3
- Mouse, the effects of essential fatty acid de-
ficiency on the skin of the 3
- Musculature in the albino rat, the em-
bryonic origin of the abdominal (ventro-
lateral) 4
- Muscle in the domestic fowl, the relation-
ship between the dimensions of the fibres
and the number of nuclei during normal
growth of skeletal 5
- Muscle, the relationship between the dimen-
sions of the fibres and the number of
nuclei during restricted growth, de-
growth and compensatory growth of
skeletal 5
- Muscles of guinea pig, histochemical investi-
gation of fiber type ratios with the myo-
fibrillar ATP-ASE reaction in normal and
denervated skeletal 1
- Myocardial cells in the ferret, the relation-
ship between the transverse tubular sys-
tem and other tubules at the Z disc levels
of 1
- Myofibrillar ATP-ASE reaction in normal
and denervated skeletal muscles of guinea
pig, histochemical investigation of fiber
type ratios with the 1
- (*Myotis lucifugus lucifugus*), formation and
structure of the hemodichorial chorio-
allantoic placenta of the bat 4

N

- Neurons and gliocytes of the toad *Bufo
arenarum* Hensel, dense-core micro-
tubules in 1
- Nerve endings in the human endocardium 6
- Normal and denervated skeletal muscles of
guinea pig, histochemical investigation
of fiber type ratios with the myofibrillar
ATP-ASE reaction in 14
- Norepinephrine in pigmented nuclei of
human brain, tissue binding of tritiated
Nuclei during normal growth of skeletal
muscle in the domestic fowl, the relation-
ship between the dimensions of the fibres
and the number of 55
- Nuclei during restricted growth, degrowth
and compensatory growth of skeletal mus-
cle, the relationship between the dimen-
sions of the fibres and the number of .. 56
- Nuclei of human brain, tissue binding of
tritiated norepinephrine in pigmented .. 13

- Seminiferous tubules mounted "in toto," re-examination of spermatogonial renewal in the rat by means of 237
- Senile rats, dense granules (lysosomes?) and crystals in the thyroids of 377
- Shark brain, ultrastructural features of the Sheep, origin and distribution of portal blood in the 209
- SHERIDAN, MICHAEL N., AND RUSSEL J. REITER. The fine structure of the hamster pineal gland 95
- SIDMAN, RICHARD L. See Rakic, Pasko 357
- SIMPSON, F. O., AND D. G. RAYNS. The relationship between the transverse tubular system and other tubules at the Z disc levels of myocardial cells in the ferret 301
- Skeletal muscle in the domestic fowl, the relationship between the dimensions of the fibres and the number of nuclei during normal growth of 193
- Skeletal muscle, the relationship between the dimensions of the fibres and the number of nuclei during restricted growth, degrowth and compensatory growth of 555
- Skeletal muscles of guinea pig, histochemical investigation of fiber type ratios with the myofibrillar ATP-ASE reaction in normal and denervated 565
- Skin of the mouse, the effects of essential fatty acid deficiency on the 145
- Species, protein synthesis studied by autoradiography in the epidermis of different 337
- Spermatogonial renewal in the rat by means of seminiferous tubules mounted "in toto," re-examination of 269
- STEINMAN, RALPH M. An electron microscopic study of cillogenesis in developing epidermis and trachea in the embryo of *Xenopus laevis* 237
- Structure of Balbiani's vitelline body and the origin of the annulate lamellae, the primary human oocyte: Some observations on the fine 19
- Subcommissural organ, and adjacent lamina tertia: Autoradiographic study of their origin in the mouse brain 107
- Synthesis studied by autoradiography in the epidermis of different 317
- Transverse tubular system and other tubules at the Z disc levels of myocardial cells in the ferret, the relationship between the transverse 237
- Tritiated norepinephrine in pigmented nuclei of human brain, tissue binding of Trout, *Salvelinus fontinalis*, the vascularization of the hypothalamic-hypophyseal region of the Eastern brook 377
- Tubules mounted "in toto," re-examination of spermatogonial renewal in the rat by means of seminiferous 209
- Tubular system and other tubules at the Z disc levels of myocardial cells in the ferret, the relationship between the transverse 95
- U
- Ultrastructural features of the shark brain 555
- Ultrastructure of the lung of the goose and its lining of surface material 565
- V
- VAN HEYNINGEN, H. See Youson, John 145
- Vascularization of the hypothalamic-hypophyseal region of the Eastern brook trout, *Salvelinus fontinalis*, the (Ventrolateral) musculature in the albino rat, the embryonic origin of the abdominal 337
- Vertebrates, the avian intercarotid anastomosis and its homologue in other 269
- Villi of the human placenta, fine structure of anchoring 237
- Vitelline body and the origin of the annulate lamellae, the primary human oocyte: Some observations on the fine structure of Balbiani's 19
- W
- WEISSAT, WILLIAM A. See Enders, Allen C. 317
- X
- Xenopus laevis*, an electron microscopic study of cillogenesis in developing epidermis and trachea in the embryo of 107
- Y
- Yolk sac of the rat placenta with increasing gestational age, changes in the fine structure of the parietal 573
- YOUSON, JOHN, AND H. VAN HEYNINGEN. Dense granules (lysosomes?) and crystals in the thyroids of senile rats 377
- Z
- Z disc levels of myocardial cells in the ferret, the relationship between the transverse tubular system and other tubules at the 139
- Thymus in mice, induced by bacterial endotoxin and studied by quantitative histology and electron microscopy, stimulation and regeneration of the 157
- Thyroids of senile rats, dense granules (lysosomes?) and crystals in the 169
- Tissue binding of tritiated norepinephrine in pigmented nuclei of human brain 139
- Toad *Bufo arenarum* Hensel, dense-core microtubules in neurons and gliocytes of the Trachea in the embryo of *Xenopus laevis*, an electron microscopic study of cillogenesis in developing epidermis and 157
- Transplants of mice following luteotrophin stimulation, the fine structure of corpora lutea in ovarian 169

